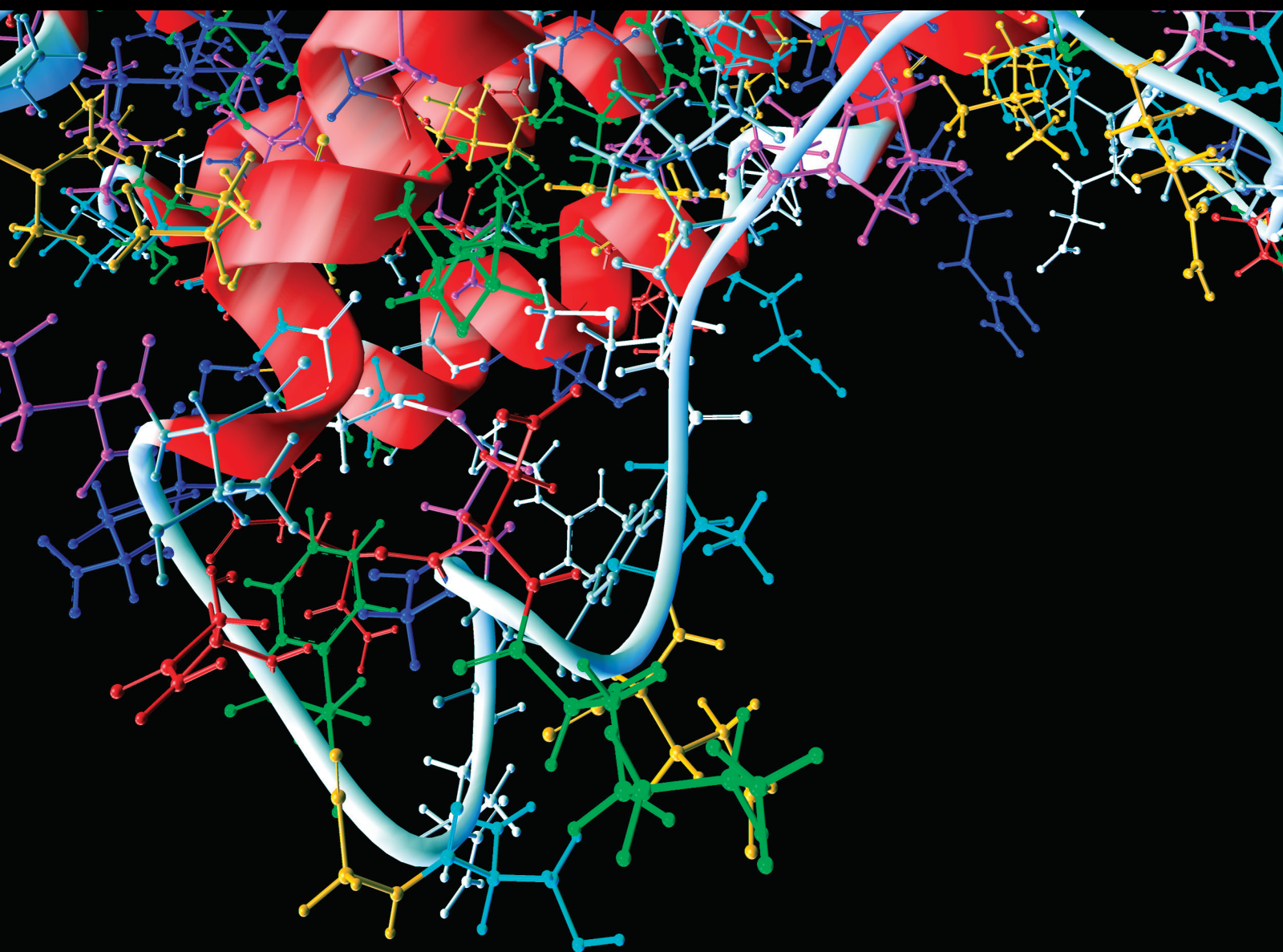


# Knowledge Discovery-Based Computational Technologies for Medical Big Data

Lead Guest Editor: Hangjun Che

Guest Editors: Cheng Liu and Shimin Wang





---

# **Knowledge Discovery-Based Computational Technologies for Medical Big Data**



Computational and Mathematical Methods in Medicine

---

**Knowledge Discovery-Based  
Computational Technologies for  
Medical Big Data**

Lead Guest Editor: Hangjun Che



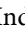
Guest Editors: Cheng Liu and Shimin Wang



Copyright © 2023 Hindawi Limited. All rights reserved.

This is a special issue published in “Computational and Mathematical Methods in Medicine.” All articles are open access articles distributed under the Creative Commons Attribution License, which permits unrestricted use, distribution, and reproduction in any medium, provided the original work is properly cited.

## Associate Editors

Ahmed Albahri, Iraq  
Konstantin Blyuss , United Kingdom  
Chuangyin Dang, Hong Kong  
Farai Nyabadza , South Africa  
Kathiravan Srinivasan , India

## Academic Editors

Laith Abualigah , Jordan  
Yaser Ahangari Nanekaran , China  
Mubashir Ahmad, Pakistan  
Sultan Ahmad , Saudi Arabia  
Akif Akgul , Turkey  
Karthick Alagar, India  
Shadab Alam, Saudi Arabia  
Raul Alcaraz , Spain  
Emil Alexov, USA  
Enrique Baca-Garcia , Spain  
Sweta Bhattacharya , India  
Junguo Bian, USA  
Elia Biganzoli , Italy  
Antonio Boccaccio, Italy  
Hans A. Braun , Germany  
Zhicheng Cao, China  
Guy Carrault, France  
Sadaruddin Chachar , Pakistan  
Prem Chapagain , USA  
Huiling Chen , China  
Mengxin Chen , China  
Haruna Chiroma, Saudi Arabia  
Watcharaporn Cholanjiak , Thailand  
Maria N. D.S. Cordeiro , Portugal  
Cristiana Corsi , Italy  
Qi Dai , China  
Nagarajan Deivanayagam Pillai, India  
Didier Delignières , France  
Thomas Desaive , Belgium  
David Diller , USA  
Qamar Din, Pakistan  
Irina Doytchinova, Bulgaria  
Sheng Du , China  
D. Easwaramoorthy , India

Esmaeil Ebrahimie , Australia  
Issam El Naqa , USA  
Ilias Elmouki , Morocco  
Angelo Facchiano , Italy  
Luca Faes , Italy  
Maria E. Fantacci , Italy  
Giancarlo Ferrigno , Italy  
Marc Thilo Figge , Germany  
Giulia Fiscon , Italy  
Bapan Ghosh , India  
Igor I. Goryanin, Japan  
Marko Gosak , Slovenia  
Damien Hall, Australia  
Abdulsattar Hamad, Iraq  
Khalid Hattaf , Morocco  
Tingjun Hou , China  
Seiya Imoto , Japan  
Martti Juhola , Finland  
Rajesh Kaluri , India  
Karthick Kanagarathinam, India  
Rafik Karaman , Palestinian Authority  
Chandan Karmakar , Australia  
Kwang Gi Kim , Republic of Korea  
Andrzej Kloczkowski, USA  
Andrei Korobeinikov , China  
Sakthidasan Sankaran Krishnan, India  
Rajesh Kumar, India  
Kuruva Lakshmanan , India  
Peng Li , USA  
Chung-Min Liao , Taiwan  
Pinyi Lu , USA  
Reinoud Maex, United Kingdom  
Valeri Makarov , Spain  
Juan Pablo Martínez , Spain  
Richard J. Maude, Thailand  
Zahid Mehmood , Pakistan  
John Mitchell , United Kingdom  
Fazal Ijaz Muhammad , Republic of Korea  
Vishal Nayak , USA  
Tongguang Ni, China  
Michele Nichelatti, Italy  
Kazuhisa Nishizawa , Japan  
Bing Niu , China

Hyuntae Park , Japan  
Jovana Paunovic , Serbia  
Manuel F. G. Penedo , Spain  
Riccardo Pernice , Italy  
Kemal Polat , Turkey  
Alberto Policriti, Italy  
Giuseppe Pontrelli , Italy  
Jesús Poza , Spain  
Maciej Przybyłek , Poland  
Bhanwar Lal Puniya , USA  
Mihai V. Putz , Romania  
Suresh Rasappan, Oman  
Jose Joaquin Rieta , Spain  
Fathalla Rihan , United Arab Emirates  
Sidheswar Routray, India  
Sudipta Roy , India  
Jan Rychtar , USA  
Mario Sansone , Italy  
Murat Sari , Turkey  
Shahzad Sarwar, Saudi Arabia  
Kamal Shah, Saudi Arabia  
Bhisham Sharma , India  
Simon A. Sherman, USA  
Mingsong Shi, China  
Mohammed Shuaib , Malaysia  
Prabhishek Singh , India  
Neelakandan Subramani, India  
Junwei Sun, China  
Yung-Shin Sun , Taiwan  
Min Tang , China  
Hongxun Tao, China  
Alireza Tavakkoli , USA  
João M. Tavares , Portugal  
Jlenia Toppi , Italy  
Anna Tsantili-Kakoulidou , Greece  
Markos G. Tsipouras, North Macedonia  
Po-Hsiang Tsui , Taiwan  
Sathishkumar V E , Republic of Korea  
Durai Raj Vincent P M , India  
Gajendra Kumar Vishwakarma, India  
Liangjiang Wang, USA  
Ruisheng Wang , USA  
Zhouchao Wei, China  
Gabriel Wittum, Germany  
Xiang Wu, China

KI Yanover , Israel  
Xiaojun Yao , China  
Kaan Yetilmezsoy, Turkey  
Hiro Yoshida, USA  
Yuhai Zhao , China

## Contents

### **Retracted: A Retrospective Analysis of Internet-Based Sharing Nursing Service Appointment Data**

Computational and Mathematical Methods in Medicine


Retraction (1 page), Article ID 9851706, Volume 2023 (2023)

### **Dynamic Monitoring of Serum Protein in Acute Respiratory Distress Syndrome Based on Artificial Neural Network**

Zhihui Zhou  and Yi Long 


Research Article (10 pages), Article ID 3542942, Volume 2022 (2022)

### **Effect of Nursing Intervention on Promoting Healing of RW in Patients with Diabetic Foot: A Systematic Review and Meta-Analysis**

Huan Chen, Xiaoxia Lv, and Yingying Zhang 


Research Article (10 pages), Article ID 8284870, Volume 2022 (2022)

### **Preliminary Investigation on the Relationship between Raman Spectra of Beef and Metmyoglobin and Metmyoglobin Reductase Activity**

Tonggang Zhang, Yalei Li, Ruiming Luo , and Shuang Bo


Research Article (8 pages), Article ID 4117261, Volume 2022 (2022)

### **The Value of Macrogen Second-Generation Sequencing in the Diagnosis, Guidance of Drug Use, and Efficacy Monitoring of Infectious Pneumonia in Premature Infants**

LiLi Wang, Ping Zha, YuJuan Wang, Ying Kong, Yu Su, LiYing Dai, and Yang Wang 


Research Article (8 pages), Article ID 4398614, Volume 2022 (2022)

### **Study on Antidepressant Emotion Regulation Based on Feedback Analysis of Music Therapy with Brain-Computer Interface**

Mengru Sun 


Research Article (14 pages), Article ID 7200678, Volume 2022 (2022)

### **Analysis of Diabetes Disease Risk Prediction and Diabetes Medication Pattern Based on Data Mining**

Lindong Zhang and Min Liu 


Research Article (9 pages), Article ID 2665339, Volume 2022 (2022)

### **Early Clinical Outcomes of ACL Reconstruction Using Semitendinosus Tendon Combined with LARS Synthetic**

Baocai Zhang, Peng Xiang , Shuai Bian, Yibo Wang, Yu Wang, and Yuzhuo Ma

Research Article (7 pages), Article ID 2845114, Volume 2022 (2022)

### **The Effects of Combuxil and Leizumab on Retinal Function and Serum Interleukin-17A in Premature Infants with Retinopathy**

Huixuan Ren, Gang Su, Shunian Xu, Li Zhou, and Shanjun Cai 


Research Article (7 pages), Article ID 6371994, Volume 2022 (2022)



**Three Acupuncture Methods for Postoperative Pain in Mixed Hemorrhoids: A Systematic Review and Network Meta-Analysis**

Sunsong Ye, Jianhua Zhou, Xiutian Guo, and Xiaoxue Jiang   
Research Article (25 pages), Article ID 5627550, Volume 2022 (2022)

**Clinical Intervention Effect of a Predictive Model Constructed Based on Risk Factors for Falls in Elderly Patients during Hospitalization**

Lizhi Wu and Lin Zhou   
Research Article (7 pages), Article ID 4983254, Volume 2022 (2022)

**Application Effect of Laparoscopic Myomectomy and Comprehensive Rehabilitation Nursing on Patients with Uterine Fibroids**

Zhihong Liu, Zhiwen Gao , Fangwei Li, Lifan Xu, and Xinghua Liu  
Research Article (8 pages), Article ID 4018803, Volume 2022 (2022)

**Meta-Analysis and Data Mining-Based Study on the Expression Characteristics of Inflammatory Factors and Causes of Recurrence in Spinal Tuberculosis**

Jun Wang and Shaoning Jiang   
Research Article (9 pages), Article ID 8246510, Volume 2022 (2022)





**Unilateral Biportal Endoscopic Discectomy versus Microendoscopic Discectomy for the Treatment of Lumbar Spinal Stenosis: A Systematic Review and Meta-Analysis**

Yufei Niu, Zhen Shen, and Haoyang Li   
Research Article (11 pages), Article ID 7667463, Volume 2022 (2022)

**Context Aware Convolutional Neural Network for Children Caries Diagnosis on Dental Panoramic Radiographs**

Xiaojie Zhou , Guoxia Yu , Qiyue Yin, Yan Liu, Zhiling Zhang, and Jie Sun  
Research Article (8 pages), Article ID 6029245, Volume 2022 (2022)

**Investigation of Applying Machine Learning and Hyperparameter Tuned Deep Learning Approaches for Arrhythmia Detection in ECG Images**

Kogilavani Shanmugavadivel , V. E. Sathishkumar , M. Sandeep Kumar, V. Maheshwari, J. Prabhu , and Shaikh Muhammad Allayear   
Research Article (12 pages), Article ID 8571970, Volume 2022 (2022)

**Medical Data Classification Assisted by Machine Learning Strategy**


Lei Wang and Keqiang Zuo   
Research Article (8 pages), Article ID 9699612, Volume 2022 (2022)

**Effect of Enhanced Recovery after Surgery (ERAS) Concept and Cluster Nursing on Psychological State and Pain of Oral Outpatients Undergoing Root Canal Therapy**

Bei Liu, Mao Xiong, Feng Liu, Wenyu Chen, Shumei Jiang, Meixiang Qu, Lixiang Mao, Genyun Yi, Xiongwei Liu, and Yuehui Wang   
Research Article (7 pages), Article ID 4868569, Volume 2022 (2022)


## Contents

### **Research on Medical Big Data Analysis and Disease Prediction Method Based on Artificial Intelligence**

Fang Zhang, Zhen Zhang, and Hui Xiao 




Research Article (10 pages), Article ID 4224287, Volume 2022 (2022)

### **Analysis of Risk Factors and Surgical Strategy of Knee Traumatic Arthritis after Internal Plate Fixation in the Treatment of Tibial Plateau Fracture**

Xingming Jin , Dengying Li, Lei Yang, Fuyuan Han, and Pinwu Jia


Research Article (7 pages), Article ID 9146227, Volume 2022 (2022)

### **Analysis of the Application Effect of Exercise Rehabilitation Therapy Based on Data Mining in the Prevention and Treatment of Knee Osteoarthritis**

Wei Liu , Congan Wang, Gongchang Yu , Bin Shi , and Jingwen Wang


Research Article (8 pages), Article ID 2109528, Volume 2022 (2022)

### **Survey on Mental Health Status and Quality of Life and Correlation among Patients with Permanent Stoma of Colorectal Tumor**

Yanlei Zou, Qiu Yang, Bi Guan, Xiaoyu Fu, Jia Wang, and Yan Li 

Research Article (6 pages), Article ID 5792312, Volume 2022 (2022)


### **Detection Method of Athlete Joint Injury Based on Deep Learning Model**

Jianjia Liu, Xin Yang , Tiannan Liao, and Yong Huang

Research Article (11 pages), Article ID 8165580, Volume 2022 (2022)


### **Effect of Multichannel Convolutional Neural Network-Based Model on the Repair and Aesthetic Effect of Eye Plastic Surgery Patients**

YixinQu, BingyingLin, ShuilingLi, XianchaiLin, ZhenMao, XingyiLi, RongxinChen , and

DanpingHuang 


Research Article (8 pages), Article ID 5315146, Volume 2022 (2022)

### **Correlation Analysis and Application of Respiratory and Lung Diseases in Pediatrics of Traditional Chinese Medicine Based on Factor Analysis Method**

Shengnan Sun, Lingling Zhuang , and Ming Cao


Research Article (9 pages), Article ID 4550039, Volume 2022 (2022)

### **Efficacy and Mechanisms of Oleuropein in Postmenopausal Osteoporosis**

Huilan Liu, Aiguo Zhao, Yulu Huang, Anli Hou, Wenbin Miao, Lu Hong, Nina Deng, and Yujuan Fan 


Research Article (9 pages), Article ID 9767113, Volume 2022 (2022)

### **Design of Association Application System of Face Recognition and Test-Tube Barcode Based on CNN**



Zhangning Zhou, He Shi, and Xuemin Niu 

Research Article (11 pages), Article ID 1987857, Volume 2022 (2022)


**A Cohort Study of the Effects of Integrated Medical and Nursing Rounds Combined with AIDET Communication Mode on Recovery and Quality of Life in Patients Undergoing Percutaneous Coronary Intervention**

Lan Li, Yongheng Li, Tao Yin, Jinglin Chen, and Fengjiao Shi   
Research Article (9 pages), Article ID 9489203, Volume 2022 (2022)


**Clinical Efficacy, Survival, and Adverse Reaction Evaluation of Immune Checkpoint Inhibitor in Advanced Gastric Cancer: A Systematic Review and Meta-Analysis**

Ping Zhang, Xiaomeng Zhang, Na Zhu, Feifei Zhuang, Dongmei Zhou , and Ping Wang   
Research Article (9 pages), Article ID 6998090, Volume 2022 (2022)


**Effect of Psychological Nursing Intervention on Abnormal-Induced Labor of Fetus during Puerperium: Study on the Effects of Anxiety, Depression, and Life Events**

Yanjuan He, Huiwen He, and Cai Tang   
Research Article (7 pages), Article ID 6206851, Volume 2022 (2022)



**MRI Evaluation of Indomethacin Suppositories in the Prevention of Complications of Pancreatitis and Hyperamylasemia after Choledocholithiasis ERCP Based on Image Denoising Algorithm**

Fusheng Gao, Chuan Zhang, Yue Feng, and Yutao Zhan   
Research Article (7 pages), Article ID 4805185, Volume 2022 (2022)

**Effects of Different Surgical Procedures on the Therapeutic Effects, Prognosis, and Major Complications of Acetabular Fractures in the Elderly of China: A Systematic Review and Meta-Analysis**

Lei Wen, Kun Liu , Ge Chen, Jianhua Ji, Changshun Chen, and Zhong Chen  
Research Article (8 pages), Article ID 9249920, Volume 2022 (2022)


**[Retracted] A Retrospective Analysis of Internet-Based Sharing Nursing Service Appointment Data**

Yuchen Fan , Yuezheng Ma, Yong Zhang, and Changjian Sun   
Research Article (7 pages), Article ID 8735099, Volume 2022 (2022)


**Big Data Analysis and Application of Liver Cancer Gene Sequence Based on Second-Generation Sequencing Technology**

Chaohui Xiao, Fuchuan Wang, Tianye Jia, Liru Pan, and Zhaohai Wang   
Research Article (9 pages), Article ID 4004130, Volume 2022 (2022)

**Effect of Multimedia Health Education on Psychological Burden, Quality of Life Ability, and Self-Efficacy of Congenital Microtia**


Yanni Zhou, Xiaoxia Li, Meiyi Zhang, Guifen Lv, Bing Duan, and Zhujun Tang   
Research Article (8 pages), Article ID 1482865, Volume 2022 (2022)

**Diagnostic Value and Prognostic Significance of Procalcitonin Combined with C-Reactive Protein in Patients with Bacterial Bloodstream Infection**

Yan Zhang, Mei La , Jihong Sun, Mimi Chen, Dandan Liu, Xiaolin Liu, and Yating Kang  
Research Article (7 pages), Article ID 6989229, Volume 2022 (2022)


## Contents

### **Extraction and Analysis of Foot Bone Shape Features Based on Deep Learning**

Yue Ma and Zhuangzhi Zhi 


Research Article (11 pages), Article ID 2372160, Volume 2022 (2022)

### **A Case Study of Multiple Maintenance Efficacy in Gynaecological Surgery Assessed by Deep Learning**

Yanmei Zheng and Qi Yuan 

Research Article (6 pages), Article ID 8574000, Volume 2022 (2022)

### **Study on the Effect of Positive Psychological Intervention Based on PERMA Model on Perioperative Patients with AIDS Complicated with Breast Cancer**

Lingmei Luo , Ying Li, Zhou Zhou, Saifen Yang, Yao Qin, Hua Peng, Yirong Wang, Zhe Li, and Tianqin Yin


Research Article (8 pages), Article ID 9788122, Volume 2022 (2022)

### **Expression of TNF- $\alpha$ and IL-1 $\beta$ in Peripheral Blood of Patients with T2DM Retinopathy**

Jin Qian and Ying Huang 



Research Article (7 pages), Article ID 9073372, Volume 2022 (2022)

### **Antistroke Network Pharmacological Prediction of Xiaoshuan Tongluo Recipe Based on Drug-Target Interaction Based on Deep Learning**

Yongfu Zhou 

Research Article (10 pages), Article ID 6095964, Volume 2022 (2022)

### **Analysis and Recognition of Clinical Features of Diabetes Based on Convolutional Neural Network**

Rui Wang , Ping Li, and Zhengfei Yang 


Research Article (9 pages), Article ID 7902786, Volume 2022 (2022)

### **Humanistic Spirit Training of Medical Students Based on Multisource Medical Data Fusion**

Jie Bai 


Research Article (12 pages), Article ID 7896367, Volume 2022 (2022)

### **Health Effects of Probiotics on Nonalcoholic Fatty Liver in the Life Cycle Based on Data Analysis**

Jia Wang, Yanfei Hao , Xiao Jin, Xiaoyue Li, Yi Liu, Li Zhang, Jing Wang, and Mingxin Hu



Research Article (6 pages), Article ID 2123162, Volume 2022 (2022)

### **Expression and Clinical Significance of Serum Krüppel-Like Factor 7 (KLF7) in NSCLC Patients**

Huigai Song, Jingjing Sun, Zhiming Xu, Xinru Liu, and Na Liu 




Research Article (6 pages), Article ID 9270789, Volume 2022 (2022)

### **Prediction of Metabolic Characteristics of Cardiovascular and Cerebrovascular Diseases Based on Convolutional Neural Network**

Zhengfei Yang , Ping Li, and Rui Wang 






Research Article (13 pages), Article ID 3206378, Volume 2022 (2022)

**Study on the Mechanism of Action of Different Acupuncture Regimens on Premature Ovarian Failure Model Rats**

Yonghao Yuan, Qingchang Xia, Wenzhe Cui, Wen Cao, Ziyang Zhou , Jian Peng, Hailiang Huang , Zhifei Song, Shuying Xie, Runjie Geng, Ran Li, Xiaohua Yu, and Jing Zhang 

Research Article (10 pages), Article ID 5254628, Volume 2022 (2022)

**Expression of DNA Helicase Genes Was Correlated with Homologous Recombination Deficiency in Breast Cancer**

Mengping Long , Hongjun Liu, Jinbo Wu, Shu Wang , Xin Liao , Yiqiang Liu , and Taobo Hu 

Research Article (7 pages), Article ID 5508301, Volume 2022 (2022)



## Retraction

# Retracted: A Retrospective Analysis of Internet-Based Sharing Nursing Service Appointment Data

### Computational and Mathematical Methods in Medicine

Received 19 September 2023; Accepted 19 September 2023; Published 20 September 2023

Copyright © 2023 Computational and Mathematical Methods in Medicine. This is an open access article distributed under the Creative Commons Attribution License, which permits unrestricted use, distribution, and reproduction in any medium, provided the original work is properly cited.

This article has been retracted by Hindawi following an investigation undertaken by the publisher [1]. This investigation has uncovered evidence of one or more of the following indicators of systematic manipulation of the publication process:

- (1) Discrepancies in scope
- (2) Discrepancies in the description of the research reported
- (3) Discrepancies between the availability of data and the research described
- (4) Inappropriate citations
- (5) Incoherent, meaningless and/or irrelevant content included in the article
- (6) Peer-review manipulation

The presence of these indicators undermines our confidence in the integrity of the article's content and we cannot, therefore, vouch for its reliability. Please note that this notice is intended solely to alert readers that the content of this article is unreliable. We have not investigated whether authors were aware of or involved in the systematic manipulation of the publication process.

Wiley and Hindawi regrets that the usual quality checks did not identify these issues before publication and have since put additional measures in place to safeguard research integrity.

We wish to credit our own Research Integrity and Research Publishing teams and anonymous and named external researchers and research integrity experts for contributing to this investigation.

The corresponding author, as the representative of all authors, has been given the opportunity to register their agreement or disagreement to this retraction. We have kept a record of any response received.

### References

- [1] Y. Fan, Y. Ma, Y. Zhang, and C. Sun, "A Retrospective Analysis of Internet-Based Sharing Nursing Service Appointment Data," *Computational and Mathematical Methods in Medicine*, vol. 2022, Article ID 8735099, 7 pages, 2022.

## Research Article

# Dynamic Monitoring of Serum Protein in Acute Respiratory Distress Syndrome Based on Artificial Neural Network

Zhihui Zhou<sup>1</sup> and Yi Long<sup>2</sup>

<sup>1</sup>Department of Critical Care Medicine, Chongqing General Hospital, Chongqing 401120, China

<sup>2</sup>Department of Critical Care Medicine, Chongqing University Cancer Hospital, Chongqing 400030, China

Correspondence should be addressed to Yi Long; longyizmd@126.com

Received 19 July 2022; Accepted 11 August 2022; Published 17 October 2022

Academic Editor: Hangjun Che

Copyright © 2022 Zhihui Zhou and Yi Long. This is an open access article distributed under the Creative Commons Attribution License, which permits unrestricted use, distribution, and reproduction in any medium, provided the original work is properly cited.

Acute respiratory distress syndrome (ARDS) is one of the more serious diseases in human lung disease. Reducing its incidence rate is an important task in current clinical research. Dynamic monitoring of serum protein in patients will help to achieve the early diagnosis and treatment of ARDS. In this study, a protein monitoring model based on artificial neural network is proposed. First, surface enhanced laser desorption ionization time-of-flight mass spectrometry is used for protein detection, and then BP neural network is used for protein classification and content analysis. In the experimental analysis, serum samples from patients with acute respiratory distress syndrome in our hospital from November 2020 to August 2021 were selected for experimental testing. The experimental results show that the serum protein monitoring model based on BP neural network has low error and high convergence ability and can monitor individual protein in protein monitoring, and the area under the ROC curve in diagnostic performance reaches 0.854. The above results show that the artificial neural network has a good effect on the dynamic monitoring of serum protein in acute respiratory distress syndrome, and the diagnostic performance evaluation can reach 0.854, which has the ability to significantly improve the clinical diagnosis and treatment of acute respiratory distress syndrome.

## 1. Introduction

Acute respiratory distress syndrome (ARDS) is an acute inflammation of the lungs. The mortality of patients with severe ARDS can be as high as 50%. After years of clinical research and practice, the known causes of severe acute respiratory distress syndrome are complex and diverse. In clinical practice, severe infection and trauma are the main causes of the disease. Therefore, acute respiratory distress syndrome is the main factor causing respiratory failure [1–3]. Acute respiratory distress syndrome will show rapid deterioration at the initial stage of onset, and its deterioration will cause severe damage to patients. Therefore, it is an important research content to target acute respiratory distress syndrome in clinical practice [4, 5]. It is of great significance to treat and block respiratory distress syndrome at

the stage of disease development. At present, acute physiology and chronic health scoring tools are generally used for clinical diagnosis of respiratory distress syndrome. However, the complexity of clinical diagnosis and the impact of subjective operation make it difficult to meet clinical needs [6–8]. On this basis, with the continuous development of medical technology, for patients with acute respiratory distress syndrome, serum protein detection has gradually become the main means of clinical diagnosis of acute respiratory distress syndrome [9].

In recent years, with the increasing incidence rate of acute respiratory distress syndrome, improving the clinical diagnostic effect of acute respiratory distress syndrome has become an important means to alleviate the disease. Among them, serum protein monitoring through proteomics technology is a more effective method [10, 11]. Clinical

proteomics technology is a medical technology to study the changes of human protein. In clinical proteomics technology, surface enhanced laser desorption ionization technology can directly detect blood, urine, and other samples [12, 13]. In protein detection, surface enhanced laser analytic ionization can analyze the dynamic changes of disease-specific proteins, show the content of proteins in the test samples and the molecular weight information, and compare the protein differences between the disease samples and the normal samples, so as to obtain the early disease indicators and symptoms [14, 15]. In order to improve the clinical diagnostic effect of acute respiratory distress syndrome, most studies have proposed a serum protein monitoring scheme for patients with acute respiratory distress syndrome. However, from the current application status, in the information age, a large number of serum protein monitoring methods are slightly backward. How to realize intelligent monitoring is a problem that needs to be solved in clinic [16].

With the continuous development of the information age, intelligent medicine has gradually attracted people's attention, and artificial intelligence technology has also been widely used in medical diagnosis and treatment. In the application of artificial intelligence technology, deep learning is particularly widely used because it can continuously improve the self-detection performance by using the adaptive learning ability in disease diagnosis and greatly improve the disease diagnosis ability in intelligent medicine [17–19]. In medical diagnosis and treatment, as an advanced computer network algorithm, artificial neural network (ANN) can effectively analyze complex data by simulating biological intelligent processing ability [20]. At the same time, in the process of in-depth learning, the use of artificial intelligence algorithms to achieve human physiological indicators has gradually become an important technology in the current intelligent medicine [21]. However, the application and effect of most artificial intelligence algorithms in intelligent medical treatment are still difficult to meet the needs of medical treatment. Therefore, the application of artificial neural network in medical diagnosis is deeply discussed in this research.

In the diagnosis of acute respiratory distress syndrome, artificial neural network technology will be used to realize the dynamic monitoring of serum protein. In order to monitor the acute respiratory distress syndrome accurately and dynamically, BP neural network of artificial neural network was used to realize the dynamic monitoring of serum protein. BP neural network uses direction propagation to process information. In the process of direction propagation, BP neural network can minimize the error between the actual output and the expected value. Therefore, in this study, the dynamic monitoring of serum protein was carried out by surface enhanced laser desorption ionization, and the diagnostic model of acute respiratory distress syndrome was established by using the low error ability of BP audit network.

## 2. Related Work

*2.1. Acute Respiratory Distress Syndrome Protein Monitoring.* Due to the serious consequences of acute respiratory distress syndrome, in order to understand its pathogenesis, a large

number of studies have given monitoring results for the protein changes in the course of its pathogenesis. Cui et al. analyzed the influence mechanism of death-related protein kinase 1 in acute respiratory distress syndrome, monitored the change of death related protein kinase 1 under 5-Aza-2'-deoxycytidine, and evaluated the effect of related protein change on acute respiratory distress syndrome [22]. Ortolan et al. found through research that the change of endothelial protein C receptor is an important risk factor in the pathogenesis of acute respiratory distress syndrome. Using protein monitoring technology, they learned that the change of endothelial protein C receptor will increase cell adhesion, and the improvement of cell adhesion is the main influencing factor of acute respiratory distress syndrome [23]. In order to understand the pathogenesis of acute respiratory distress syndrome, Dahmer et al. found that the increase of surfactant protein D is a relatively specific indicator of lung injury through protein monitoring and proved that the increase of surfactant protein D is related to the poor prognosis of children with acute respiratory failure through the design of relevant experiments [24]. Svenja et al. developed Luminex binding analysis to realize high-throughput and rapid serum protein monitoring in patients with acute respiratory distress syndrome and rapidly detected circulating antibodies to coronavirus type 2s protein in patients with acute respiratory distress syndrome, which facilitated the prognosis of acute respiratory distress syndrome [25].

In the early diagnosis of acute respiratory distress syndrome, dynamic monitoring of protein can effectively predict the onset of acute respiratory distress syndrome. However, it can be found from the existing studies that few studies can monitor multiple proteins at one time in the dynamic monitoring of proteins, and the monitoring results of existing studies are difficult to meet the clinical needs.

*2.2. BP Neural Network.* As a traditional artificial neural network, BP neural network has a good computing ability and classification ability. With the development of society, its application field is gradually expanding. In order to improve the effect of information processing and reduce the loan and storage resources of information in the transmission process, Yang et al. proposed an image compression and encryption algorithm based on BP neural network, which uses the information processing technology of BP neural network to compress the information and increase the security of information in transmission [26]. Ghosh et al. used the artificial neural network to diagnose cardiovascular diseases, estimated the characteristics of cardiac health monitoring parameters for patients, realized the screening of cardiac disease precursors, and combined the artificial neural network with impedance cardiogram to check individual cardiovascular health [27]. Li et al. proposed a small sample learning method based on data expansion and a GA based method for fault diagnosis of high pressure common rail diesel engine. The fault diagnosis method of BP neural network uses the data processing ability of neural network for fault diagnosis. The results show that the overall accuracy of the fault diagnosis model based on the improved BP neural network is as high as 98.3% [28]. In order to realize the

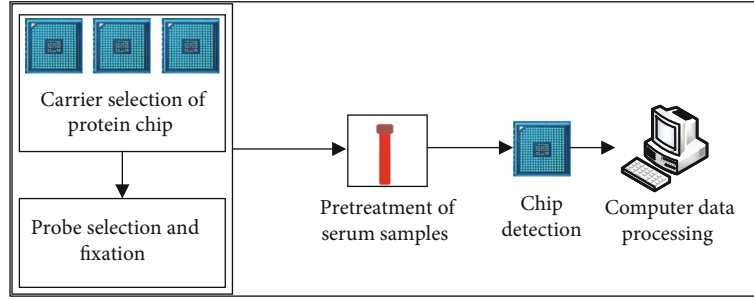


FIGURE 1: Technical process of surface enhanced laser desorption ionization time of flight mass spectrometry.

intelligent classification of loess deposits in tunnel engineering, Zhang and others proposed an evaluation system based on BP neural network, which was applied to practical analysis and showed that the model output results were consistent with the actual results [29].

Artificial neural network has been gradually applied in many fields, but it is rarely used in medical assistance. Therefore, BP neural network of artificial neural network is applied to the dynamic monitoring of protein in acute respiratory distress syndrome in order to improve the early diagnosis effect of acute respiratory distress syndrome.

### 3. Method

**3.1. Dynamic Monitoring Technique of Surface Enhanced Laser Analytical Ionization.** Surface enhanced laser desorption ionization is a rising technology in the development of proteomics. It is often combined with time-flight mass spectrometry in application and has a good dynamic detection effect on specific proteins in serum samples. The whole technical process of surface enhanced laser desorption ionization time-flight mass spectrometry is shown in Figure 1.

As shown in Figure 1, surface enhanced laser desorption ionization time-of-flight mass spectrometry is a combination of chip technology and mass spectrometry technology. Its technical process includes selecting protein chip carrier, selecting and fixing probe, preprocessing of serum samples, chip detection, and computer data processing [30]. Surface enhanced laser desorption ionization time-of-flight mass spectrometry has the characteristics of strong specificity and high resolution in protein detection and can detect low abundance and small molecular weight proteins, as well as disease-related protein changes.

In the diagnosis and treatment of lung diseases, surface enhanced laser desorption ionization time-of-flight mass spectrometry has been gradually applied to the classification and prediction of lung cancer tissues and the diagnosis of lung cancer. Some studies have confirmed that surface enhanced laser desorption ionization time-of-flight mass spectrometry can effectively detect the malignant protein signal of lung epithelial cells and has important value in the diagnosis and screening of lung cancer [31, 32]. However, the application of surface enhanced laser desorption ionization time-of-flight mass spectrometry still needs to be improved. First, surface enhanced laser desorption ionization time-of-flight mass spectrometry is a semiquantitative

technology, and the difference in protein properties and serum concentration shown in the detection cannot be shown [33]. Second, the protein sequence cannot be classified and analyzed, that is, the protein sequence cannot be determined, resulting in the inability to obtain important information such as protein configuration in protein detection [34].

**3.2. A Diagnosis Model Based on BP Neural Network.** After protein detection by surface enhanced laser desorption ionization time-of-flight mass spectrometry, BP neural network model was constructed and trained by using the detection results. Each node of BP neural network represents a specific function, and the connection between the two nodes represents the weight. It is worth noting that BP neural network will continuously adjust the weight during long-term learning to optimize the data processing performance of the model [35, 36]. In order to improve the data processing performance of BP neural network, a three-layer BP neural network model is constructed as shown in Figure 2.

It can be seen from Figure 2 that the number of input neurons and output neurons of the three-layer BP neural network model used in the study is set as  $m$  and  $p$  in turn, and the number of hidden layer neurons is  $n$ . At this time, the  $m$ -th neuron in the existing input layer is expressed as  $x_m$ , and the  $n$ -th neuron in the hidden layer and the  $p$ -th neuron in the output layer are expressed as  $z_n$  and  $y_p$  in turn.  $W_{mn}$  represents the connection weight from the input layer to the hidden layer, and  $W_{np}$  represents the connection weight from the hidden layer to the output layer. The selection of hidden layer neurons is shown in the following formula.

$$n < \sqrt{m + p} + a. \quad (1)$$

Equation (1) is the empirical formula for selecting the reference of the number of neurons in the hidden layer  $n$ , where  $m$  represents the number of nodes in the input layer,  $p$  represents the number of nodes in the output layer, and  $a$  represents any constant in the interval (0, 10). Second, sigmoid function in BP neural network is analyzed, as shown in the following formula.

$$f(x) = \frac{1}{(1 + e^{-x})}. \quad (2)$$

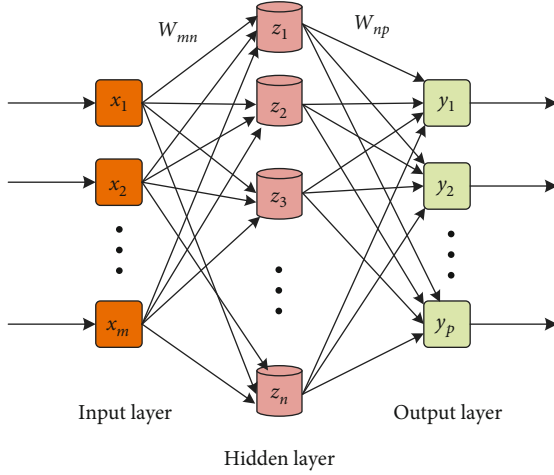


FIGURE 2: Schematic diagram of BP neural network.

Equation (2) is the sigmoid type nonlinear function  $f(x)$  acting on each neuron, and  $x$  is the input function value. Through the hidden layer, the output of BP neural network is obtained, as shown in the following formula.

$$\begin{cases} \text{net}_k = \sum_j \omega_{kj} O_j + \theta_k, \\ O_k = f(\text{net}_k). \end{cases} \quad (3)$$

In formula (3),  $\omega_{kj}$  represents the connection weight value between neuron  $U_k$  and upper layer neuron  $U_j$ ;  $O_j$  represents the output of neuron  $U_j$ . The input value, output value, and threshold value of neuron  $U_k$  are represented by  $\text{net}_k$ ,  $O_k$ , and  $\theta_k$  in turn. When BP neural network is used as a weak learning model, and the loss function is  $\psi(y, f) = 1/2 \cdot (y - f(x))^2$  at the same time, the residual error is  $(y - f(x))$ , where  $f(x)$  is the model fitting value. Continue to fit the residuals, and train the next BP neural network along the descending direction of the gradient.

$$\hat{f}(x) = f_0(x) + \sum_{i=1}^M \rho_i \cdot h(x, \theta_i). \quad (4)$$

Equation (4) is the calculation formula of the model fitting value of the test data, where  $\rho_i$  represents the optimal reduction step,  $h(x, \theta_i)$  represents the weak learning model,  $\theta$  represents the model parameters, and  $M$  represents the number of iterations.

**3.3. Experimental Design.** All data in the study are from November 2020 to August 2021, and all samples are from inpatients in our hospital. Inclusion criteria: (1) meet the diagnostic criteria of acute respiratory distress syndrome; (2) complete clinical data. Exclusion criteria: (1) patients with chronic obstructive pulmonary disease; (2) liver and kidney dysfunction; (3) used glucocorticoids.

Collect 3 ml of fasting venous blood of the subjects, store the serum samples in a 4°C refrigerator, and centrifuge the

serum samples for 5 min after standing for 1 h. The centrifuged serum was centrifuged again for 5 min, and the serum was subpacked and stored in a -80°C refrigerator. At the same time, the sera of normal people were collected and mixed. They were used as the mixed control group and stored in the refrigerator at -80°C.

The serum samples were detected by surface enhanced laser desorption ionization time-of-flight mass spectrometry chip. The serum protein mass spectra of acute respiratory distress syndrome and normal control group were detected, respectively. The serum protein on the surface of the serum protein chip was detected. The mass charge ratio range of the chip was optimized to be 2000~20000 m/z, and the laser intensity was 210. Baseline reduction and homogenization were used to preprocess the obtained serum protein mass spectra. The BP neural network is used to build the diagnosis model. In the diagnosis model, the nodes of the input layer, hidden layer, and output layer of the BP neural network model are set as 5, 4, and 1, respectively. The tangent S-shaped transfer function is used in the operation of BP neural network, and the operation results are initialized randomly in the calculation. In the input node, the peak intensity of the screened differential protein is used as the input.

## 4. Results

**4.1. Repeatability Test Results.** The obtained serum protein mass spectrum data are shown in Figure 3. It can be seen from Figure 3 that in order to avoid the interference of matrix peaks on the repeatability test results, the peaks below 2000 m/z are filtered. In the expression of serum protein mass spectrometry data, the protein peaks with strong expression were 2735 m/z, 4080 m/z, 6970 m/z, and 7010 m/z, respectively. The average coefficient of variation of the four peaks was 13.64%, which was below 15%, indicating a high repeatability. At the same time, it can be seen that 2735 m/z appears in each map, and the average coefficient of variation is 14.32%, which is less than 15%.

**4.2. Detection of Differential Protein Peaks.** The sera of patients with acute respiratory distress syndrome and the control group were analyzed by surface enhanced laser desorption ionization time-of-flight mass spectrometry. A total of 794 protein peaks were detected, as shown in Figure 4. As can be seen from Figure 4, in the difference analysis between the two groups, the statistical analysis results showed that there were significant differences in 118 protein peaks between the two groups, and the test results showed that the differences were statistically significant ( $p < 0.05$ ). It can be seen that the peak of serum protein mass charge ratio in patients with acute respiratory distress syndrome and the control group is mainly distributed between 2000~15000 m/z.

It can be seen from Figure 4 that in the comparison of serum differences between patients with acute respiratory distress syndrome and the control group, 15 protein peaks are distributed between 2000 and 8000 m/z. Through statistical analysis, it can be found that in the expression of serum



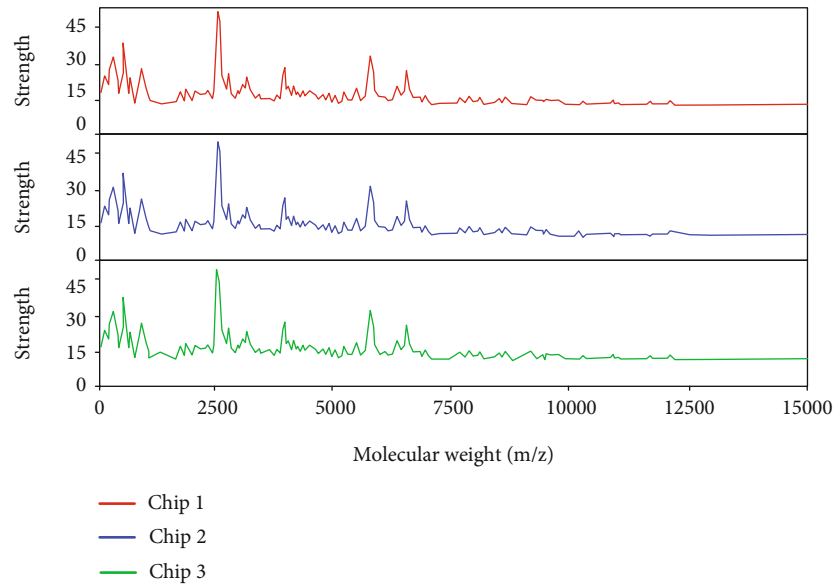


FIGURE 3: Detection of protein fingerprints in serum samples.

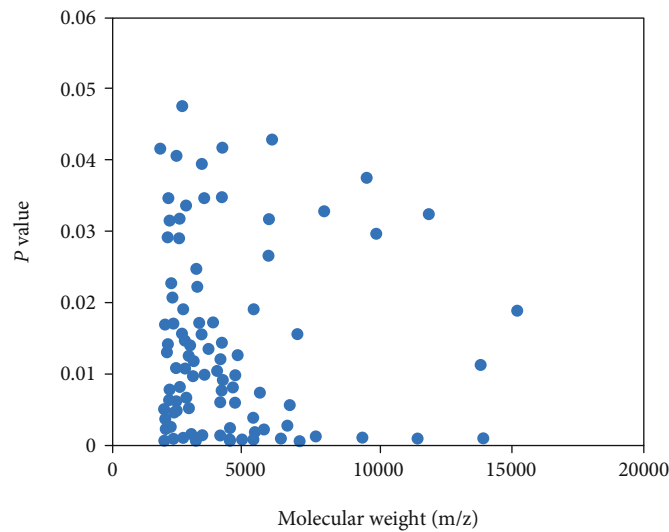


FIGURE 4: Differential expression of serum protein fingerprints in patients with acute respiratory distress syndrome and control group.

proteins in patients with acute respiratory distress syndrome and the control group, the differences of 15 protein peaks in the classification cluster are particularly obvious. The comparison results are shown in Figure 5.

**4.3. Performance Analysis of BP Neural Network.** The 15 protein peaks with significant differential expression are used for combination processing, and the BP neural network protein monitoring model is constructed. The performance of the constructed protein monitoring model based on BP neural network is analyzed. First, the mean square error (MSE) of BP neural network in the training process is analyzed, as shown in Figure 6. As can be seen from Figure 6, with the increasing number of iterations, the mean

square error of BP neural network protein monitoring model shows a decreasing trend. After the number of iterations reaches 20, the curve decreasing speed gradually decreases. After the number of iterations reaches 80, the mean square error of the model approaches the target value and begins to remain stable.

Figure 7 shows the change results of the fitness values of the BP neural network protein monitoring model. From Figure 7, it can be seen that the BP neural network and the convolution neural network are compared and analyzed. With the increase of iteration times, the number of iterations required to reach the optimal fitness of the BP neural network model is significantly less than that of the convolution neural network. The above results show that compared with

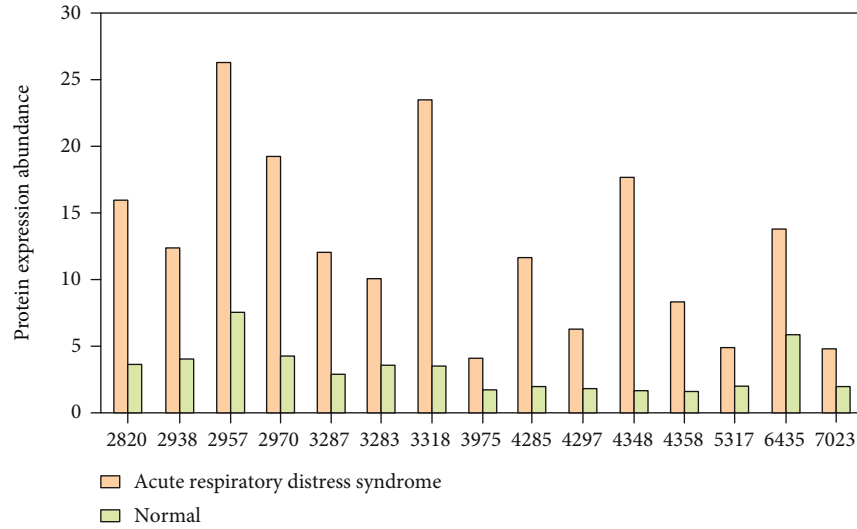


FIGURE 5: Difference in expression intensity of 15 protein peaks.

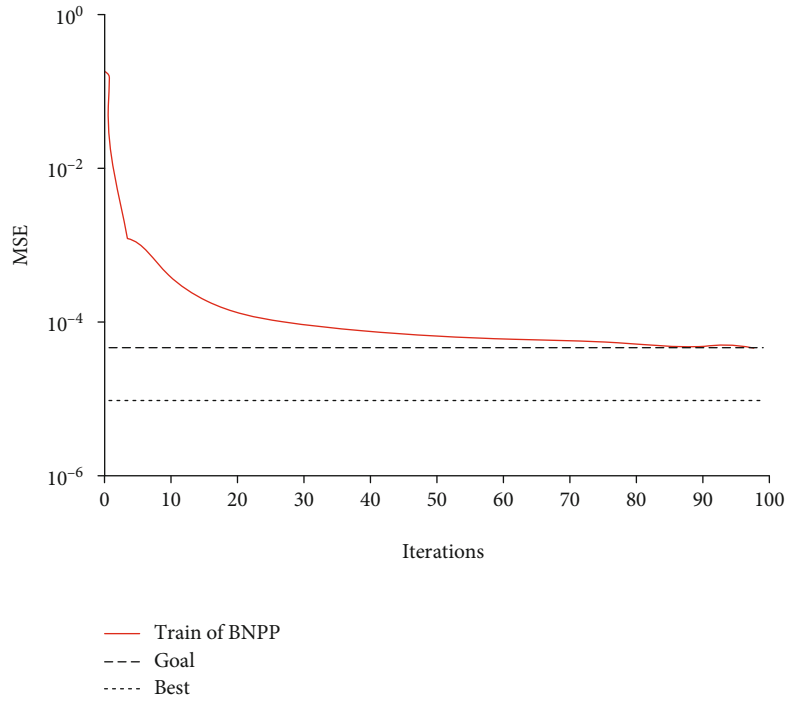


FIGURE 6: Training results of mean square error of BP neural network.

convolution neural network, BP neural network can reach the best fitness faster in data processing and has better convergence.

**4.4. Effect Analysis of BP Neural Network Protein Monitoring Model.** Select 10 patients with acute respiratory distress syndrome and 10 normal people for BP model monitoring, diagnosis, and test analysis, as shown in Table 1. It can be seen from Table 1 that the BP neural network protein monitoring model can be used to calculate the output value for patients with acute respiratory distress syndrome and the

normal population, and the difference between the output value and the target output value is not obvious, indicating that the status of acute respiratory distress syndrome of the tested population can be accurately judged.

BP neural network was used to monitor the protein of the subjects. During the monitoring process, the difference between the serum protein of patients with mild, moderate and moderate acute respiratory distress syndrome, and the normal population was compared, as shown in Table 2. It can be seen from Table 2 that the monitoring includes C-reactive protein (CRP) and albumin (ALB). Table 2 shows

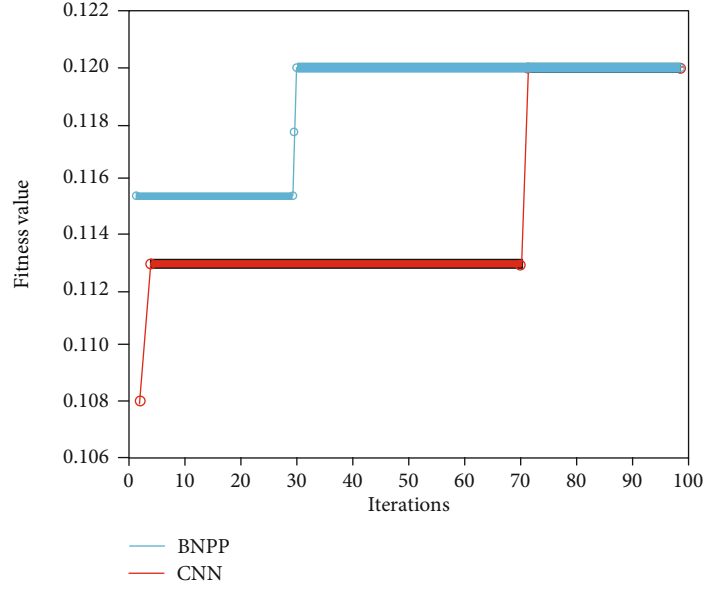


FIGURE 7: Comparison of fitness of different neural network models.

TABLE 1: Comparison of model experiment results.

Target number	Acute respiratory distress syndrome		Normal	
	Target output value	BP output value	Target output value	BP output value
0	1	0.935642	0	0.027464
1	1	0.975358	0	0.018971
2	1	0.973150	0	0.038612
3	1	1.054531	0	0.027431
4	1	1.131256	0	0.013472
5	1	0.972101	0	0.039412
6	1	0.892345	0	0.019418
7	1	0.987982	0	-0.015646
8	1	0.948542	0	0.223763
9	1	0.963165	0	0.026429
10	1	1.078321	0	0.013494

that under the BP neural network protein monitoring model, the serum protein content of patients with acute respiratory distress syndrome can be clearly displayed and can be significantly distinguished from the normal population.

Finally, the diagnostic performance of BP neural network protein monitoring model in the diagnosis of acute respiratory distress syndrome is analyzed, as shown in Figure 8. As can be seen from Figure 8, the offline area of BP neural network model is 0.854, significantly larger than 0.5, with good diagnostic performance.

## 5. Discussion

In order to diagnose acute respiratory distress syndrome, according to the changes of physiological characteristics of patients with acute respiratory distress syndrome, artificial neural network was used to monitor the serum protein of

patients. In the research, first, the protein of the research object is detected by surface enhanced laser desorption ionization time-of-flight mass spectrometry. Second, the BP neural network model is used to realize protein classification and protein level content analysis. Finally, the effectiveness of the proposed model is obtained through experimental tests.

In the study, aiming at the application effect of surface enhanced laser desorption ionization time-of-flight mass spectrometry, the effectiveness of surface enhanced laser desorption ionization time-of-flight mass spectrometry was analyzed through repeatability test and differential protein peak detection. The results show that in the repeatability test, the average coefficient of variation between multiple chips is 13.64%, which has high repeatability; The detection of differential protein peak shows that there is a significant difference in serum protein expression between patients with

TABLE 2: Protein detection of BPNN monitoring model.

Group	Acute respiratory distress syndrome			Normal
	Light	Moderate	Severe	
CRP (mg/L)	$86.03 \pm 12.97$	$121.39 \pm 25.72$	$152.92 \pm 33.01$	$6.31 \pm 1.21$
ALB (g/L)	$27.83 \pm 1.01$	$26.91 \pm 1.04$	$24.51 \pm 2.03$	$37.31 \pm 1.42$
CRP/ALB	$3.09 \pm 0.43$	$4.69 \pm 1.01$	$6.72 \pm 0.42$	$0.18 \pm 0.03$

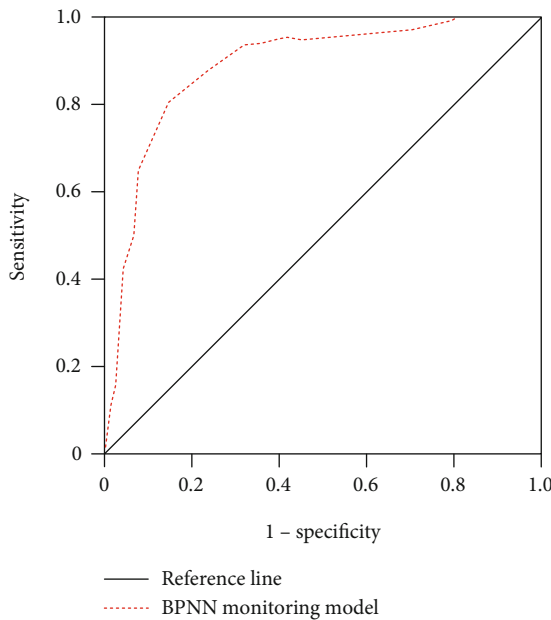


FIGURE 8: ROC curve of BPNN monitoring model.

acute respiratory distress syndrome and normal people, and the above results are consistent with the results of previous studies [37].

The performance analysis of BP neural network model shows that its error value continues to decrease with the increase of iteration times and can reach the target value after fewer iterations, indicating that it has high convergence and can improve the efficiency of the diagnostic model. The comparative analysis of model fitness shows that compared with convolutional neural network, BP neural network can reach the best fitness faster, indicating that BP neural network has better convergence and higher adaptability. The current research results are consistent with previous studies [38]. The protein monitoring model based on BP neural network model is applied to clinical practice. The results show that the BP neural network protein monitoring model can clearly show the numerical difference between patients with acute respiratory distress syndrome and normal people, that is, it can accurately distinguish the two and achieve the effect of preoperative diagnosis. Analyzing the diagnostic performance of BP neural network protein monitoring model, the ROC curve shows that the area under the curve of BP neural network protein monitoring model is as high as 0.854, indicating that this model has a significant effect in diagnosing acute respiratory distress syndrome by monitoring serum protein content [39].

In conclusion, it is effective to use artificial neural network to monitor the serum protein of patients with acute respiratory distress syndrome, and it can make early diagnosis of acute respiratory distress syndrome. However, there are still some limitations in the study. The proteome in serum is complex and diverse, and the protein types monitored in the study are still few. In the follow-up work, it is necessary to monitor other serum protein types.

### Data Availability

The dataset can be accessed upon request.

### Conflicts of Interest

The authors declare that there are no conflicts of interest.

### References

- [1] F. Weidemann, S. Decker, J. Epping et al., "Analysis of extracorporeal membrane oxygenation in trauma patients with acute respiratory distress syndrome: a case series," *The International Journal of Artificial Organs*, vol. 45, no. 1, pp. 81–88, 2022.
- [2] H. Yi, X. Li, Z. Mao et al., "Higher PEEP versus lower PEEP strategies for patients in ICU without acute respiratory distress syndrome: a systematic review and meta-analysis," *Journal of Critical Care*, vol. 67, pp. 72–78, 2022.
- [3] M. S. Buckley, S. K. Agarwal, R. Garcia-Orr, R. Saggat, and R. MacLaren, "Comparison of fixed-dose inhaled epoprostenol and inhaled nitric oxide for acute respiratory distress syndrome in critically ill adults," *Journal of Intensive Care Medicine*, vol. 36, no. 4, pp. 466–476, 2021.
- [4] R. Li, H. Liu, H. Qi et al., "Lung ultrasound assessment of acute respiratory distress syndrome caused by coronavirus disease 2019: an observational study," *Hong Kong Journal of Emergency Medicine*, vol. 28, no. 1, pp. 8–14, 2021.
- [5] T. Wang, L. Wang, X. Zhu, and G. Liu, "Correlation between TLR4 gene polymorphism and acute respiratory distress syndrome after esophageal cancer surgery," *American Journal of Translational Research*, vol. 13, no. 4, pp. 3337–3343, 2021.
- [6] P. Buonanno, A. Marra, M. Vargas, C. Iacovazzo, and G. Servillo, "Is the Pao 2:Fio 2 ratio the best marker to monitor the blood-air barrier function in acute respiratory distress syndrome?," *Critical Care Medicine*, vol. 49, no. 7, pp. e726–e727, 2021.
- [7] Y. Zhao, Y. Yue, Y. Wang, W. Zhao, and G. Feng, "The risk factors for postoperative acute respiratory distress syndrome in Stanford type a acute aortic dissection patients," *American Journal of Translational Research*, vol. 13, no. 6, pp. 7318–7326, 2021.


- [8] Y. Liu, H. Peng, and F. Gui, "Long noncoding plasmacytoma variant translocation 1 facilitates the surveillance of acute respiratory distress syndrome and mortality prediction in sepsis," *Biomarkers in Medicine*, vol. 15, no. 6, pp. 401–412, 2021.
- [9] K. Ho, J. Gordon, K. T. Litzenberg, M. C. Exline, J. A. Englert, and D. D. Herman, "Cancer is an independent risk factor for acute respiratory distress syndrome in critically ill patients: a single center retrospective cohort study," *Journal of Intensive Care Medicine*, vol. 37, no. 3, pp. 385–392, 2022.
- [10] C. G. Cornelissen, I. Bergs, A. G. Müller et al., "Broncho-alveolar lavage in patients with acute respiratory distress syndrome due to COVID-19," *Internal Medicine Journal*, vol. 51, no. 6, pp. 965–967, 2021.
- [11] S. S. Medar, S. Villacres, S. Kaushik, R. Eisenberg, and M. E. Stone Jr., "Pediatric acute respiratory distress syndrome (PARDS) in children with pulmonary contusion," *Journal of Intensive Care Medicine*, vol. 36, no. 1, pp. 107–114, 2021.
- [12] L. Huang, M. Song, Y. Liu et al., "Acute respiratory distress syndrome prediction score: derivation and validation," *American Journal of Critical Care*, vol. 30, no. 1, pp. 64–71, 2021.
- [13] K. O. Dong, "Corticosteroids in acute respiratory distress syndrome: outcomes obscured by mortality," *The Korean Journal of Internal Medicine*, vol. 36, no. 1, pp. 65–66, 2021.
- [14] S. M. Fernando, B. L. Ferreyro, M. Urner, L. Munshi, and E. Fan, "Diagnosis and management of acute respiratory distress syndrome," *Canadian Medical Association Journal*, vol. 193, no. 21, pp. E761–E768, 2021.
- [15] A. M. Adams, R. B. Laverty, P. M. McCarthy et al., "Tracheostomy placement in patients with acute respiratory distress syndrome requiring extracorporeal membrane oxygenation: did COVID-19 change our practice?," *Journal of the American College of Surgeons*, vol. 233, no. 5, pp. e210–e211, 2021.
- [16] L. A. Materne, O. Hunsicker, M. Menk, and J. A. Graw, "Hemolysis in patients with extracorporeal membrane oxygenation therapy for severe acute respiratory distress syndrome - a systematic review of the literature," *International Journal of Medical Sciences*, vol. 18, no. 8, pp. 1730–1738, 2021.
- [17] C. Hartmann, D. Opritescu, and W. Volk, "An artificial neural network approach for tool path generation in incremental sheet metal free-forming," *Journal of Intelligent Manufacturing*, vol. 30, no. 2, pp. 757–770, 2019.
- [18] M. Faezirad, A. Pooya, Z. Naji-Azimi, and M. Amir Haeri, "Preventing food waste in subsidy-based university dining systems: an artificial neural network-aided model under uncertainty," *Waste Management & Research*, vol. 39, no. 8, pp. 1027–1038, 2021.
- [19] R. Kuc, "Artificial neural network classification of surface reflectors and volume scatterers using sequential echoes acquired with a biomimetic audible sonar," *The Journal of the Acoustical Society of America*, vol. 147, no. 4, pp. 2357–2364, 2020.
- [20] B. Lagesse, S. Wang, T. V. Larson, and A. A. Kim, "Predicting PM<sub>2.5</sub> in well-mixed indoor air for a large office building using regression and artificial neural network models," *Environmental Science & Technology*, vol. 54, no. 23, pp. 15320–15328, 2020.
- [21] C. Wei, T. Quan, K. Y. Wang et al., "Artificial neural network prediction of same-day discharge following primary total knee arthroplasty based on preoperative and intraoperative variables," *Bone and Joint Journal*, vol. 103-B, no. 8, pp. 1358–1366, 2021.
- [22] S. N. Cui, L. Chen, Y. Y. Yang et al., "Activation of death-associated protein kinase 1 promotes neutrophil apoptosis to accelerate inflammatory resolution in acute respiratory distress syndrome," *Laboratory Investigation*, vol. 99, no. 8, pp. 1143–1156, 2019.
- [23] L. dos Santos Ortolan, M. K. Sercundes, G. C. Moura et al., "Endothelial protein C receptor could contribute to experimental malaria-associated acute respiratory distress syndrome," *Journal of Immunology Research*, vol. 2019, Article ID 3105817, 18 pages, 2019.
- [24] M. K. Dahmer, H. Flori, A. Sapru et al., "Surfactant protein D is associated with severe pediatric ARDS, prolonged ventilation, and death in children with acute respiratory failure," *Chest*, vol. 158, no. 3, pp. 1027–1035, 2020.
- [25] S. Weiss, J. Klingler, C. Hioe et al., "A high-throughput assay for circulating antibodies directed against the S protein of severe acute respiratory syndrome coronavirus 2," *The Journal of Infectious Diseases*, vol. 222, no. 110, pp. 1–6, 2020.
- [26] F. Yang, J. Mou, Y. Cao, and R. Chu, "An image encryption algorithm based on BP neural network and hyperchaotic system," *China Communications*, vol. 17, no. 5, pp. 21–28, 2020.
- [27] S. Ghosh, B. P. Chattopadhyay, R. M. Roy, J. Mukherjee, and M. Mahadevappa, "Estimation of echocardiogram parameters with the aid of impedance cardiography and artificial neural networks," *Artificial Intelligence in Medicine*, vol. 96, pp. 45–58, 2019.
- [28] L. Li, S. Tiexiong, F. Ma, and Y. Pu, "Research on a small sample fault diagnosis method for a high-pressure common rail system," *Advances in Mechanical Engineering*, vol. 13, no. 9, Article ID 168781402110461, 2021.
- [29] X. L. Zhang, Y. G. Xue, D. H. Qiu et al., "Multi-index classification model for loess deposits based on rough set and BP neural network," *Polish Journal of Environmental Studies*, vol. 28, no. 2, pp. 953–963, 2019.
- [30] T. Rahmel, K. Rump, J. Peters, and M. Adamzik, "Aquaporin 5-1364A/C promoter polymorphism is associated with pulmonary inflammation and survival in acute respiratory distress syndrome," *Anesthesiology*, vol. 130, no. 3, pp. 404–413, 2020.
- [31] J. Liu, J. Du, X. Chen et al., "The effects of mitogen-activated protein kinase signaling pathways on lipopolysaccharide-mediated osteo/odontogenic differentiation of stem cells from the apical papilla," *Journal of Endodontics*, vol. 45, no. 2, pp. 161–167, 2019.
- [32] J. E. Whitney, B. Zhang, N. Koterba et al., "Systemic endothelial activation is associated with early acute respiratory distress syndrome in children with extrapulmonary sepsis\*," *Critical Care Medicine*, vol. 48, no. 3, pp. 344–352, 2020.
- [33] J. C. Mercier, N. Ouldali, I. Melki et al., "Severe acute respiratory syndrome coronavirus 2-related multisystem inflammatory syndrome in children mimicking Kawasaki disease," *Archives of Cardiovascular Diseases*, vol. 114, no. 5, pp. 426–433, 2021.
- [34] K. Liu, L. Chen, J. Xiong, S. Xie, Y. Hu, and Y. Shi, "HFOV vs CMV for neonates with moderate-to-severe perinatal onset acute respiratory distress syndrome (NARDS): a propensity score analysis," *European Journal of Pediatrics*, vol. 180, no. 7, pp. 2155–2164, 2021.
- [35] A. Bansal, A. D. Singh, V. Jain et al., "The association of D-dimers with mortality, intensive care unit admission or acute respiratory distress syndrome in patients hospitalized with coronavirus disease 2019 (COVID-19): a systematic review and meta-analysis," *Heart & Lung*, vol. 50, no. 1, pp. 9–12, 2021.



- [36] A. Cyh, C. Yltb, and A. Ckl, “The prone position ventilation (PPV) as an approach in pregnancy with acute respiratory distress syndrome (ARDS),” *Taiwanese Journal of Obstetrics and Gynecology*, vol. 60, no. 3, pp. 574–576, 2021.
- [37] J. A. Choreño-Parra, L. A. Jiménez-Álvarez, G. Ramírez-Martínez et al., “Expression of surfactant protein D distinguishes severe pandemic influenza A(H1N1) from coronavirus disease 2019,” *The Journal of Infectious Diseases*, vol. 224, no. 1, pp. 21–30, 2021.
- [38] J. Z. Ahlström, F. Massaro, P. Mikolka et al., “Synthetic surfactant with a recombinant surfactant protein C analogue improves lung function and attenuates inflammation in a model of acute respiratory distress syndrome in adult rabbits,” *Respiratory Research*, vol. 20, no. 1, pp. 245–245, 2019.
- [39] M. Li, Y. Zhao, J. He et al., “Protein kinase C theta inhibition attenuates lipopolysaccharide-induced acute lung injury through notch signaling pathway via suppressing Th17 cell response in mice,” *Inflammation*, vol. 42, no. 6, pp. 1980–1989, 2019.

## Research Article

# Effect of Nursing Intervention on Promoting Healing of RW in Patients with Diabetic Foot: A Systematic Review and Meta-Analysis

Huan Chen,<sup>1</sup> Xiaoxia Lv,<sup>1</sup> and Yingying Zhang<sup>2</sup> 

<sup>1</sup>Department of Neurology, Huzhou Central Hospital, Affiliated Central Hospital Huzhou University, Huzhou, 313000 Zhejiang, China

<sup>2</sup>Orthopedics Department, Huzhou Central Hospital, Affiliated Central Hospital Huzhou University, Huzhou, 313000 Zhejiang, China

Correspondence should be addressed to Yingying Zhang; 1417421207@st.usst.edu.cn

Received 21 July 2022; Revised 11 August 2022; Accepted 6 September 2022; Published 14 October 2022

Academic Editor: Hangjun Che

Copyright © 2022 Huan Chen et al. This is an open access article distributed under the Creative Commons Attribution License, which permits unrestricted use, distribution, and reproduction in any medium, provided the original work is properly cited.

**Objective.** To systematically assess the effect of nursing intervention on promoting the healing of refractory wounds (RW) in patients with diabetic foot (DF). **Methods.** A computer search of PubMed, EMBASE, ScienceDirect, CochraneLibrary, China knowledge Network Database (CNKI), China VIP Database, Wanfang Database, and China Biomedical Literature Database (CBM) online database was conducted in a randomized controlled trial (RCT) of traditional Chinese and western medicine nursing intervention on patients with RW of DF. Retrieval time was limited to the period from the date the database was established to present. Separately, two researchers gathered the data. RevMan5.3 statistical software was used to analyze the collected data by meta-analysis according to Cochrane Handbook 5.3. **Results.** Finally, 8 articles were included with a total sample size of 772 cases. The meta-analysis of the wound healing time after intervention indicated that the wound healing time of the study group was notably shorter, and the difference was statistically significant ( $P < 0.05$ ). Qualitative, fixed-effect model analysis indicated that the nursing effective rate after treatment in the study group was notably higher, and the difference was statistically significant ( $P < 0.05$ ). Fasting blood glucose level in the study group after treatment was notably lower, and the difference was statistically significant ( $P < 0.05$ ). The life quality in the study group was notably higher, and the difference was statistically significant ( $P < 0.05$ ). Further subgroup analysis indicated that the score of physical function (PF), emotional function (RE), social function (SF), physical pain (BP), general health (GH), vitality (VT), and mental health (MH) in the study group were higher, and the difference was statistically significant ( $P < 0.05$ ). A publication bias analysis was conducted using the inverted funnel chart as the outcome indicator for this study. The results indicated that most of the funnel maps were symmetrical and a few were asymmetrical, suggesting that there exhibited a certain publication bias in the included literature. **Conclusion.** The application of traditional Chinese and western medicine nursing intervention when treating DF patients clinically can effectively promote the healing of foot ulcer wounds. Traditional Chinese and western medicine nursing can help patients heal wounds faster and enhance their life quality compared to simplistic western medicine nursing. According to the original literature, the conclusion deserves to be popularized in clinic.

## 1. Introduction

Refractory wounds (RW) are wounds that have failed to heal after more than one month of treatment for various reasons and have no tendency to heal [1]. Diabetes, varicose veins of lower extremities, burns, frostbite, postoperative radiotherapy of cancer, orthopedic postoperative infection, and so

on are easy to cause wound nonhealing. Clinical common RW include diabetic foot (DF), traumatic ulcer, compression ulcer, radiation ulcer, venous congestion ulcer, arterial ischemic ulcer, infectious ulcer, and malignant ulcer [2, 3]. DF patients generally have a long course of treatment. This disease is easy to repeat. Long-term failure will lead to excessive consumption, poor nutritional status, decline of physical

function, forming a vicious circle, which will not only bring about the decline of the life quality of patients with diabetes, but also cause huge social and economic burden. Wound infections in DF tend to spread to the subcutaneous fat layer and deep tendons. Untimely or improperly treated, the patient's condition can rapidly worsen and eventually lead to amputation, which can be life-threatening in severe cases. Up to now, the use of more advanced molecular biology technology to provide favorable conditions for wound healing, nursing intervention has attached importance to promoting the healing of RW and enhancing the life quality of patients.

The treatment and care of RW such as DF, pressure ulcers, and venous leg ulcers has always been a clinical problem to be overcome. Among various forms of local reflection, foot ulcer is the most common form of manifestation [4]. The clinical features of DF are early extremity numbness, accompanied by pain or no sensation, chills or intermittent claudication, and rest pain [5]. DF refers to patients diagnosed with DM or with a history of DM. Foot infections and severe ulcers can manifest as gangrene, which are often accompanied by diabetic neuropathy or lower extremity vascular disease [6].

Foot ulcers mostly occur 10 years after the onset of diabetes. The longer the course of the disease, the more patients will have neurological disorders of the foot. About 45% of the patients with a course of more than 20 years have neurological disorders of the foot. Recent studies have shown that diabetes people have a 15–40 times higher risk of amputation than nondiabetic patients. Based on the 9th edition of the Global Diabetes Map published by the International Diabetes Federation in 2019, there are currently about 463 million people with diabetes in the world, among which the 20–79-year-old age group, one in every 11 people is a patient. By 2030, 578.4 million people are expected to suffer from DM; by 2045, 700.2 million are expected to suffer from DM [7, 8]. Ninety-two million Chinese people suffer from diabetes today. And there are still 148.2 million adults in the impaired period of glucose regulation, which continues to grow [9]. About 14% of the diabetic patients in China are complicated with DF, among which the risk population of DF is mainly the elderly. One of the vital causes of disability and even death of diabetic patients is DF [10]. 70% of amputations occur in diabetic patients, accounting for more than 50% of all nontraumatic amputations. The mortality rate within 30 days after amputation is about 10%, and the median survival time is 22 months, which is extremely harmful to patients [11].

The clinical value of traditional Chinese and western medicine nursing intervention is explained by the effectiveness of a certain literature or the improvement of a certain evaluation index, which the results are unconvincing. A large number of clinical data have confirmed that integrated traditional Chinese and western medicine nursing has obvious enhancing effect in the healing of ulcer wounds in diabetic group, which has the advantages of less adverse reactions and high patient acceptance [12, 13]. The effect of promoting wound healing in group ulcers has not been internationally recognized and still needs to be supported by high-

quality research evidence. In addition, there are large differences between different research designs and many evaluation indicators. There is a great need for more and more authoritative scientific studies to demonstrate the role of Chinese and western nursing interventions in the wound healing of DF ulcers in order to supply a theoretical basis to apply this nursing protocol. Therefore, this study systematically, quantitatively, and comprehensively analyzed the results of multiple independent studies of the same type through meta-analysis.

## 2. Research Contents and Methods

*2.1. The Sources and Retrieval Methods of Documents.* PubMed, EMBASE, ScienceDirect, Cochrane Library, China Journal full-text Database (CNKI), VIP full-text Database (VIP), Wanfang Database, Chinese Biomedical Literature data (CBM), relevant Chinese journals, conference papers, and degree papers were collected. Relevant data was about the nursing effect of traditional Chinese and western medicine nursing intervention on DF patients with difficult wound healing. The literature was searched by the way of free words and subject words, with the key words of nursing intervention, difficult wound healing, traditional Chinese and western medicine nursing, DF, healing effect, meta-analysis, refractory wound, and healing effect from January 2010 to March 2022.

*2.2. Literature Inclusion Criteria and Exclusion Criteria.* The following are the literature inclusion criteria:

- (1) *Research Type.* All RCT on the effect of nursing intervention of traditional Chinese and western medicine on patients with DF which is difficult to heal
- (2) *Subjects.* Patients with DF with difficult wound healing were clearly diagnosed. And the diagnostic criteria referred to the relevant diagnostic criteria in the 2010 edition (interpretation of Chinese guidelines to diagnose and treat DF) [14]
- (3) *Intervention.* The study group received integrated traditional Chinese and western medicine nursing, while the control group only received routine western medicine nursing

The following are the literature exclusion standard:

- (1) It was not a randomized controlled study
- (2) There was an incomplete data report, so the data could not be used
- (3) The content of the study was repeated, and the latest study was taken
- (4) The assessment of the efficacy of the study was not notable

### 2.3. Quality Evaluation and Data Extraction

- (1) *Bias Risk Assessment Included in the Study.* For the evaluation, a bias risk assessment tool recommended by Cochrane System Review Manual 5.3 was used
- (2) *Literature Screening and Data Extraction.* Independently, two researchers screened literature, gathered data, assessed quality, and cross-checked results. When there are differences in opinion, discuss and resolve them or ask the third researcher for help. Research data was managed and extracted using Note Express document management software and Excel office software. A request for additional data would be sent to the author of this article if the data included in the literature were incomplete. The contents of data extraction included (1) basic information as follows: author, publication time, and number of cases; (2) intervention measures as follows: scheme and course of treatment; (3) outcome indicators as follows: nursing effective rate, fasting blood glucose level, wound healing time, and life quality score

**2.4. Statistical Processing.** The standardized mean difference (SMD) with Hedges'  $g$  was chosen as the measure of the effect. The effect size was calculated using a random-effects model with a restricted maximum-likelihood (REML) and considered a large, moderate, and small effect with respect to the SMD values of 0.8, 0.5, and 0.2, respectively. The heterogeneity among the studies included in a meta-analysis was assessed using Cochrane's  $Q$ , tau-squared, and  $I^2$ -squared ( $I^2$ ). Cochrane's  $Q$  test quantifies total variance and generates a  $P$  value that determines the heterogeneity is present. Tau-squared indicates the true variance that is the between-study variance, while  $I^2$  represents the percentage of the total variance that is due to the true variance. The degree of heterogeneity is said to be low, moderate, and high, with  $I^2$  values of 25%, 50%, and 75%. RevMan 5.4 software was adopted for meta-analysis. HR and its 95% CI were employed as effect analysis statistics for OS and PFS, and risk ratio and 95% CI were employed as effect analysis statistics for binary variables.  $P$  and  $I^2$  values in heterogeneity test results were adopted to determine whether there was statistical heterogeneity among the results.  $P > 0.10$  and  $I^2 < 50\%$  indicated that there was no statistical heterogeneity among the research results, and a fixed effect model was used for combined analysis.  $P \leq 0.10$  and  $I^2 \geq 50\%$  indicated statistical heterogeneity among the research results, and a random effects model was adopted for combined analysis. The test level of meta-analysis was set as  $\alpha = 0.05$ . Eggers' test was used to examine the funnel plot asymmetry. Whenever this test was significant with a  $P$  value of less than 0.1, we used the trim and fill method to correct the funnel plot and adjust the effect size for potential publication bias.

### 3. Results and Analysis

**3.1. The Results of Literature Retrieval and the Basic Situation of Literature Inclusion.** The computer database retrieved 1642 articles, and 528 articles were eliminated

when repeated studies were removed. After screening the titles and abstracts of 113 articles, 96 articles were included after eliminating irrelevant studies, reviews, case reports, and no control literature. After carefully reading 88 studies with insufficient data and no major outcome markers, 8 RCTs were eventually included [15–20]. The meta-analysis covered 772 samples in total. All results were shown in Figure 1 and Table 1.

**3.2. Evaluation of the Quality of the Methodology Included in the Literature.** The eight CT articles included in this meta-analysis reported the baseline health status of the patients. All RCT mentioned "random allocation", of which 6 articles did not describe the randomized method in detail. All gave detailed intervention measures, and only one RCT explained the course of treatment. The number and reasons of blind method and loss of follow-up or withdrawal were not described in detail in 8 RCT articles. According to the Jadad scale, it was found that all the 8 articles had  $RCT \leq 2$  points (Figures 2 and 3).

### 3.3. Meta-Analysis Result

**3.3.1. Wound Healing Time.** There were 8 RCTs included in this study with 772 samples. Meta-analysis was conducted on the wound healing time after intervention. The results of the heterogeneity test indicated that  $\text{Chi}^2 = 60.01$ ,  $df = 2$ ,  $P < 0.00001$  and  $I^2 = 97\%$ , indicating that the research data contained in the study showed distinct heterogeneity. The random effect model was used to analyze (Figure 4) the wound healing time after intervention, indicated that the wound healing time of the study group was notably shorter than that in control group, and the difference was statistically significant ( $P < 0.05$ ), suggesting that traditional Chinese and western medicine nursing interventions can effectively shorten the healing time of promoting the healing of DF ulcer wounds.

**3.3.2. Effective Rate of Nursing.** A meta-analysis was conducted on the nursing effectiveness. The results of the heterogeneity test indicated that  $\text{Chi}^2 = 3.49$ ,  $df = 4$ ,  $P = 0.48$ , and  $I^2 = 0\%$ , indicating that the research data contained in the study showed distinct heterogeneity. The fixed effect model analysis indicated that the nursing effective rate in the study group after treatment was notably higher, and the difference was statistically significant ( $P < 0.05$ , Figure 5). It suggested the effectiveness of traditional Chinese and western medicine nursing interventions on wound healing of DF ulcers.

**3.3.3. Fasting Blood Glucose Level.** A meta-analysis of fasting blood glucose levels after intervention indicated that  $\text{Chi}^2 = 0.01$ ,  $df = 1$ ,  $P = 0.92$ , and  $I^2 = 0\%$ , indicating that the research data contained in the study showed distinct heterogeneity. It can be seen from the fixed effect model analysis (Figure 6), that the level of fasting blood glucose in the study group after treatment was notably lower, and the difference was statistically significant ( $P < 0.05$ ). It suggested that the nursing intervention of traditional Chinese and western

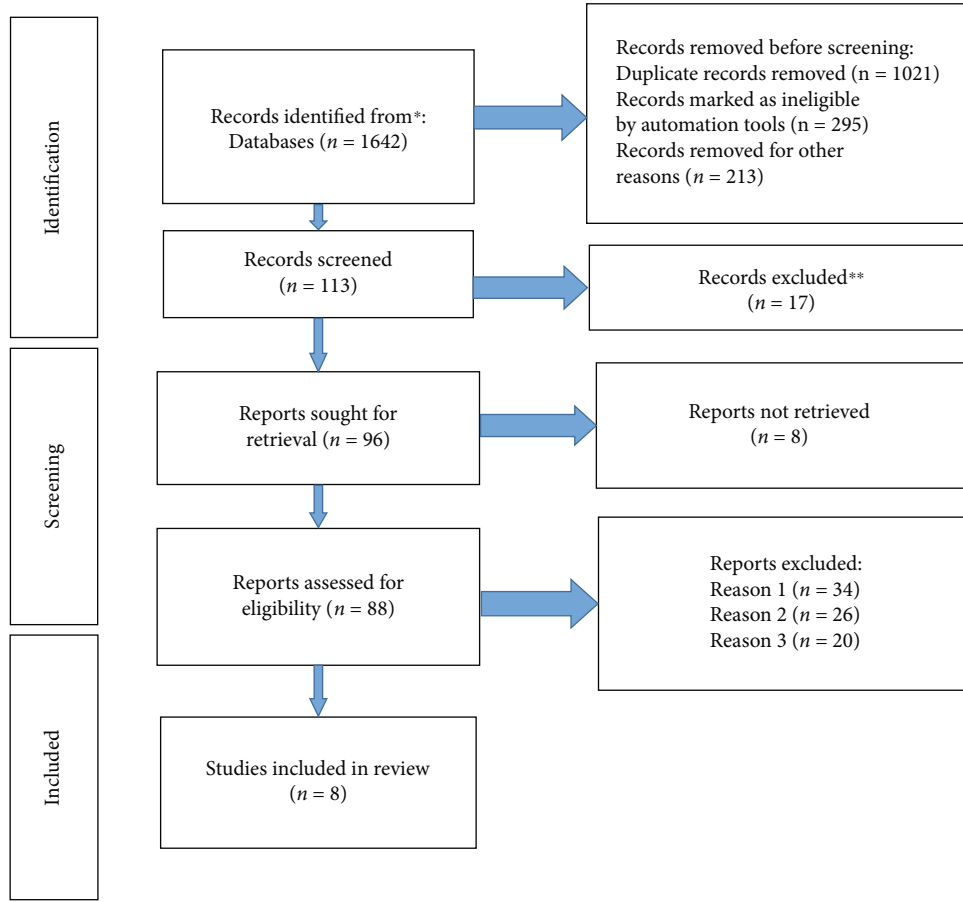


FIGURE 1: Illustration of literature screening.

TABLE 1: Basic characteristics of literature.

Include the literature	Year of publication	N(C/T)	C	Intervention method T	Outcome index	Course of treatment	Stochastic method	Blind or not
Chen [15]	2021	41/41	Routine western medicine nursing	Routine western medicine nursing + TCM nursing	(1)	Unknown	Computer random method	No
Zhong et al. [16]	2018	68/68	Routine western medicine nursing	Routine western medicine nursing + TCM nursing	(1) (4)	6 months	Random number table	No
Luo [17]	2021	45/45	Routine western medicine nursing	Routine western medicine nursing + TCM nursing	(2) (4)	Unknown	Not specified	No
Xiao [18]	2013	35/35	Comprehensive treatment scheme	Comprehensive treatment plus TCM nursing	(1)	Unknown	Not specified	No
Zhong et al. [19]	2019	112/112	Routine western medicine nursing	Routine western medicine nursing + TCM nursing	(1) (3)	Unknown	Not specified	No
Zhong [20]	2019	35/35	Routine nursing intervention	Routine nursing + traditional Chinese and western medicine nursing	(1) (3) (4)	Unknown	Different nursing methods	No
Hu [21]	2016	40/40	Routine western medicine nursing	Routine western medicine nursing + TCM nursing	(1)	Unknown	Not specified	No
Gao and Wang [22]	2019	45/45	Routine western medicine nursing	Routine western medicine nursing + TCM nursing	(2)	Unknown	Not specified	No

Note: C: control group; T: research group. (1) Effective rate of nursing; (2) wound healing time; (3) fasting blood glucose level; (4) life quality score.



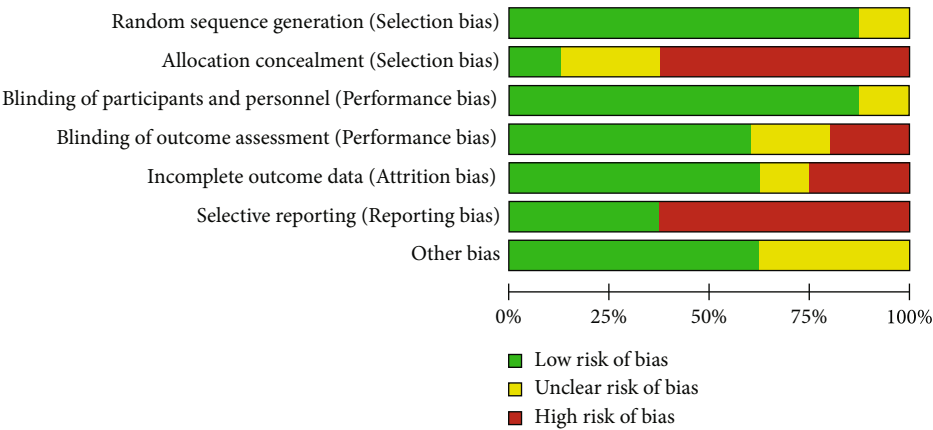


FIGURE 2: Risk bias chart.

	Random sequence generation (Selection bias)	Allocation concealment (Selection bias)	Blinding of participants and personnel (Performance bias)	Blinding of outcome assessment (Detection bias)	Incomplete outcome data (Attrition bias)	Selective reporting (Reporting bias)	Other bias
Jing Hu2016	+	?	+	-	+	-	+
Limin Zhong2019	?	+	+	?	+	+	-
Liqiong Zhong2018	+	?	+	-	+	-	+
Na Chen2021	+	-	+	-	?	-	?
Qing Luo2021	+	-	+	+	+	-	+
Shuzhen Xiao2013	+	-	+	-	+	-	+
Tingting Zhong2019	+	-	+	+	-	+	+
Yinghong Goa2019	+	-	?	+	-	+	?

FIGURE 3: Summary chart of risk bias.

medicine could successfully enhance the blood glucose control level of patients with DF.

3.3.4. Life Quality Score. A meta-analysis was conducted on the quality-of-life scores of the patients after intervention. The results of the heterogeneity test indicated that  $\text{Chi}^2 = 98.07$ ,  $\text{df} = 20$ ,  $P < 0.00001$ , and  $I^2 = 80\%$ . The research data contained in the study showed distinct heterogeneity. It could be seen by random effect model analysis (Figure 7)

that the life quality of the research group after intervention was notably higher, and the difference was statistically significant ( $P < 0.05$ ). Further subgroup analysis indicated that the scores of PF, RE, SF, BP, GH, VT, and MH in the study group were higher, and the difference was statistically significant ( $P < 0.05$ ).

3.3.5. Publication Bias Analysis. The inverted funnel chart was adopted to measure the publication bias of the study with nursing efficiency as the outcome index (see Figure 8). The results indicated that most of the funnel charts were symmetrical and a few were asymmetrical, suggesting that there was a certain publication bias in the included literature. This may be relevant to the heterogeneity of the study and the small number of included literatures.

4. Analysis and Discussion

RW not only seriously affect the life and work of patients, but also an important cause of more serious complications, such as DF has become the primary cause of clinical non-traumatic amputation. Because the mechanism of wound healing is complex and the treatment is difficult, the treatment and nursing of this kind of wound has become a recognized clinical problem. Wound nursing has changed from letting it heal naturally in the past to using bandages, new dressings, creating an environment conducive to wound healing, and nurses' attention to wound exudation, smell, and the progress of wound healing [23]. In recent years, the combination of wound bed theory and wet healing theory has guided a new direction and made a great contribution to the wound treatment of DF. However, the damage to the nerves, blood vessels, muscles, and tendons of the DF caused by high blood sugar, and the changes in the local microenvironment make the wound extremely susceptible to infection and difficult to heal. Even if the wound heals, it is still easy to occur repeatedly [24]. Therefore, patients with DF should go to specialist hospitals for all-round treatment, so as to reduce the disability caused by the continuous deterioration of the disease. At the same time, it is necessary to educate the patients on the knowledge of diabetes and local braking, to change the dressing of the wound regularly in

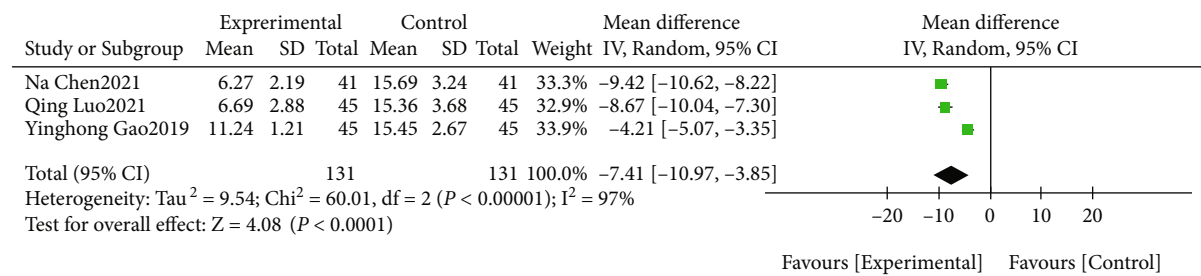


FIGURE 4: Wound healing time.

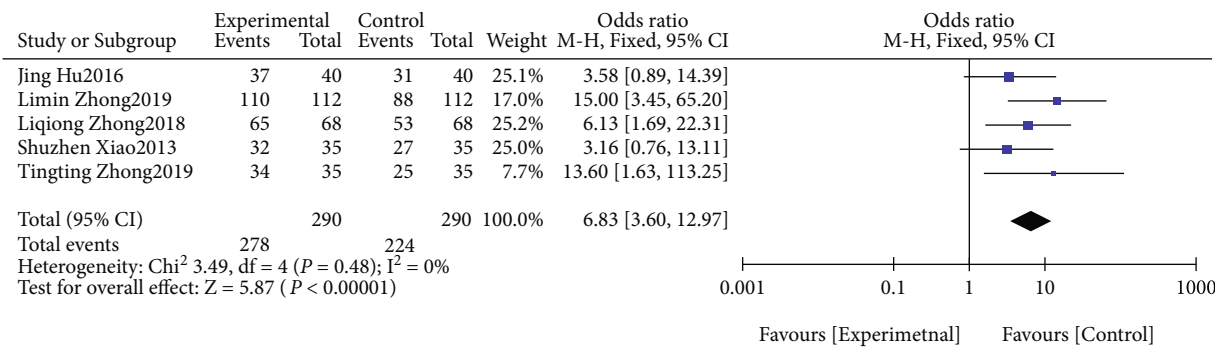


FIGURE 5: Nursing efficiency.

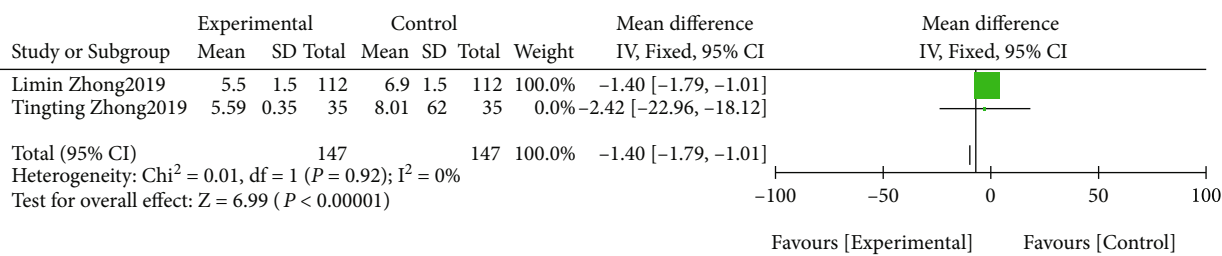


FIGURE 6: Fasting blood glucose level.

the process of nursing, to avoid friction and weight-bearing, to control the patient’s diet, and to take careful care of the patient. It can effectively promote the rehabilitation of patients [25]. This study systematically, quantitatively, and comprehensively analyzed the results of multiple independent studies of the same type through meta-analysis.

Modern medical treatment of DF has a certain effect in controlling blood sugar, improving circulation, nourishing nerve, debridement, and dressing change. Patients have long hospitalization time, long treatment cycle, and high cost, which not only bring great economic pressure to patients but also brings greater burden to society and families. For DF with infection, long-term use of antibiotics will have drug resistance and other problems, which is very difficult. There are also some western medicines when treating digestive tract adverse reactions or other adverse reactions, clinical treatment is faced with many challenges. At the present stage, nursing for patients with DF is the whole treatment process of integrated traditional Chinese and western medicine nursing patients. Flexible application of massage techniques in TCM can greatly reduce the risk of amputation and successfully enhance the survival rate and life quality

of patients. According to Chinese medicine, DF belongs to the category of “gangrene”, which is a result of prolonged thirst, resulting in deficiency of both Qi and Yin. If Qi deficiency cannot stimulate the flow of blood, then blood flow is not smooth, meridians are obstructed and limbs cannot be nourished; damp heat is injected and heat toxins accumulate, resulting in pulsatile joint pain and gangrene. Improper treatment and care can lead to aggravation of foot ulcer infection, gangrene and even amputation [26, 27]. Judging from the literature screened and included in this study, a large number of related studies on Chinese and western medicine nursing intervention when treating DF patients have been conducted in China, among which there are many randomized control groups, double-blind, and multicenter high-level studies. It has high clinical application value in patients with DF. There were 8 RCTs included with 772 samples. Qualitative, fixed-effect model analysis indicated that the nursing effective rate after treatment in the study group was notably higher. Traditional Chinese and western medicine nursing interventions are found to enhance the wound healing effect of DF ulcers. The meta-analysis indicated that the nursing intervention of traditional Chinese

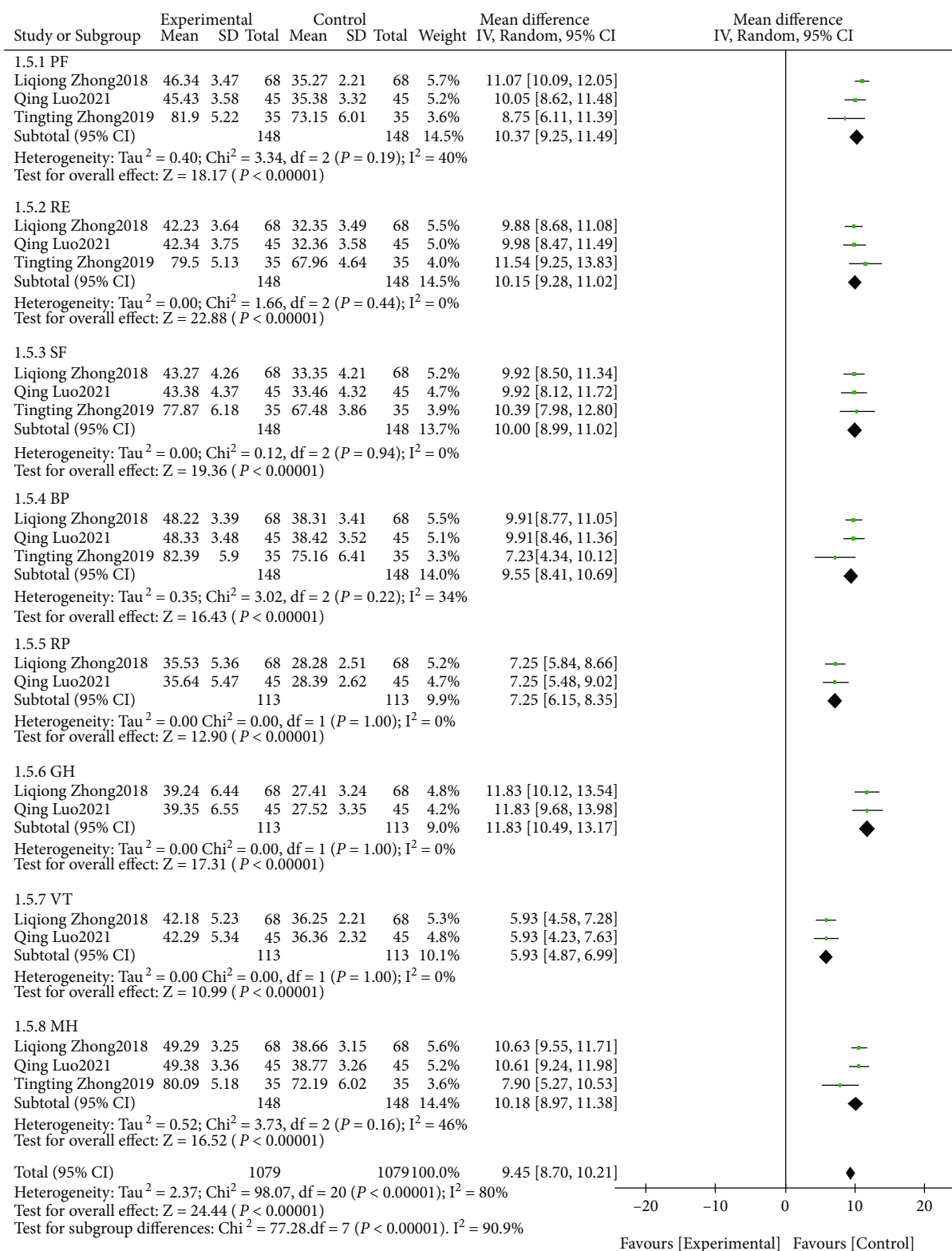


FIGURE 7: Life quality score.

and western medicine could effectively enhance the blood glucose control level of patients with DF. In the nursing model of traditional Chinese and western medicine, we should pay more attention to the treatment of patients with

primary diseases. We can start from the root, take measures such as hypoglycemia and nutritional support to control the blood glucose level of patients with diabetes. The reason why the nursing intervention of traditional Chinese and western



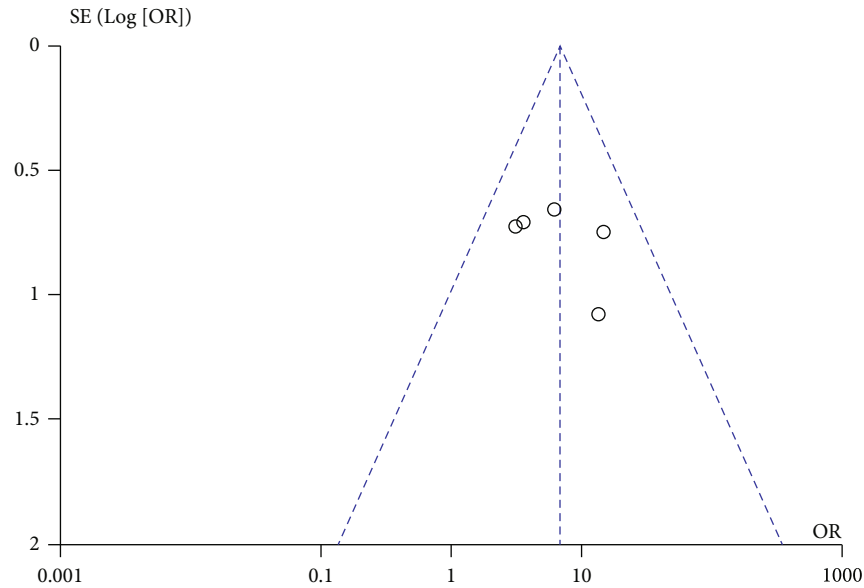


FIGURE 8: Funnel chart of nursing efficiency.

medicine can improve the wound healing effect of DF ulcer is that the nursing model can control the blood glucose level of patients through multidimensional nursing intervention, improve local blood circulation and inhibit inflammatory reaction, prevent the occurrence of infection, enhance its body immunity, and then notably improve the effect of ulcer wound healing. The treatment and control of the primary disease are the prerequisites for the treatment of RW. Stabilizing blood sugar, nutritional support, improving blood circulation, nourishing nerves, and enhancing resistance can promote the healing of wounds to a certain extent.

In the aspect of western medicine, psychological nursing, diet nursing, and exercise nursing intervention are the main contents of western medicine nursing work. On the one hand, effective psychological interventions are used to help patients cope with their negative emotions and improve them. The meta-analysis of the wound healing time after intervention indicated wound healing time of the study group was longer. The shortened healing time of ulcer wounds in patients is mainly because the primary disease (diabetes) is controlled. Moreover, targeted measures are taken to inhibit the inflammatory response and nutritional status of the wound, which can effectively enhance the patient's health status and accelerate the recovery of the disease. At the same time, it can effectively control the phenomenon of elevated blood sugar caused by excitement and finally improve the matching degree of patients in the process of treatment. A fair and scientific diet plan can be created by diet nursing taking into account the dietary taboos that patients should be aware of. In addition, exercise nursing can promote the blood circulation of patients and effectively enhance the effect of ulcer healing [28].

In terms of herbal medicine, the absorption of herbs through the patient's acupuncture points by means of foot baths, application, and moxibustion can effectively promote smooth blood circulation. Eliminating the inflammation of

the wound to avoid infection of the ulcerated area, thus further promoting the regrowth and development of the tissues and ultimately achieving the therapeutic goal of foot wound healing [29]. In addition, scientific massage on patients' acupoints can effectively stimulate the regulating function of patients themselves through acupoint stimulation, which greatly improve their own immunity and finally effectively promote the speed of wound healing of patients [30]. A meta-analysis was conducted on the quality-of-life scores of the patients after the intervention. The results of the heterogeneity test indicated that the research data contained in the study showed distinct heterogeneity. The random effect model was adopted to analyze the results of the study group. The quality-of-life score was notably higher compared to the control group. It is suggested that the application of traditional Chinese and western medicine nursing in the clinical treatment of diabetic patients can notably enhance the quality of their prognosis. Nursing interventions of integrated traditional Chinese and western medicine are potentially effective to relieve the symptoms of patients. The traditional Chinese medicine nursing techniques are relatively safe and easy to use in prevention and treatment of patients. The main reason why the patient's life quality has been greatly improved is that the disease has been notably relieved. The patient's self-care ability has been notably improved, and the psychological state has also been improved, enabling him to gradually return to normal life. Moreover, nursing interventions have been identified as paramount in managing other relevant chronic conditions, reducing other available risk factors, and establishing physiological condition conducive to greater healing. The monitoring of DF profile, patient activities, and nutritious diet contributes to healing and improves quality of life. Continuous and up-to-date education for nurses caring for patients with DF is another area positively correlated with the efficacy and superiority of the interventions carried out.

Research limitations included that the inclusion and exclusion criteria were relatively strict, and the final number of documents included was relatively small. The result of meta-analysis is not immutable, it is only the result of comprehensive analysis of the existing data. It is considered that with the continuous inclusion and enrichment of new research data, its conclusions should be updated. In the future, it is necessary to conduct more related randomized controlled trials to verify the efficacy. Therefore, it is recommended to carry out more large-sample, multicenter, and high-quality randomized blind studies in strict accordance with the CONSORT statement, to ensure that the follow-up period is long enough and to provide high-quality research evidence for the secondary evaluation with internationally recognized, objective, and transmissible criteria, so as to better evaluate its clinical efficacy, and show the value of promotion.

## 5. Conclusion

To sum up, traditional Chinese and western medicine nursing intervention has a notable effect on enhancing the condition of DF patients with difficult wound healing, which can successfully reduce the blood glucose level of patients, shorten the healing time of DF ulcer wound, and improve their life quality. This intervention method is suitable for clinical application. It is worth popularizing in clinical practice.

## Data Availability

The datasets used and analyzed during the current study are available from the corresponding author upon reasonable request.

## Conflicts of Interest

The authors declare that they have no conflict of interest.

## References

- [1] F. HuangDe, G. E. Bin, and T. Qianli, "Influencing factors of chronic refractory wound and research progress of traditional Chinese and western medicine treatment," *Chinese Journal of Burn Wounds and Ulcers*, vol. 30, no. 2, pp. 77–81, 2018.
- [2] B. Cheng and X. Fu, "The focus and target: angiogenesis in refractory wound healing," *The International Journal of Lower Extremity Wounds*, vol. 17, no. 4, pp. 301–303, 2018.
- [3] L. Qiuxiang, Z. Huixia, and Z. Zhifang, "Observation and nursing of RW treated by continuous closed negative pressure drainage," *Medical Aesthetic Cosmetology*, vol. 28, no. 24, pp. 149–150, 2019.
- [4] G. M. Virador, L. de Marcos, and V. M. Virador, "Skin wound healing: RW and novel solutions," *Methods in Molecular Biology*, vol. 2018, pp. 221–241, 2019.
- [5] E. Everett and N. Mathioudakis, "Update on management of diabetic foot ulcers," *Annals of the New York Academy of Sciences*, vol. 1411, no. 1, pp. 153–165, 2018.
- [6] L. Coffey, C. Mahon, and P. Gallagher, "Perceptions and experiences of diabetic foot ulceration and foot care in people with diabetes: a qualitative meta-synthesis," *International Wound Journal*, vol. 16, no. 1, pp. 183–210, 2019.
- [7] R. Sorber and C. J. Abularrage, "Diabetic foot ulcers: epidemiology and the role of multidisciplinary care teams," *Seminars in Vascular Surgery*, vol. 34, no. 1, pp. 47–53, 2021.
- [8] C. A. Chastain, N. Klopfenstein, C. H. Serezani, and D. M. Aronoff, "A clinical review of diabetic foot infections," *Clinics in Podiatric Medicine and Surgery*, vol. 36, no. 3, pp. 381–395, 2019.
- [9] H. Haoyi, "Research progress on influencing factors and treatment of DF ulcer," *Enterprise Health in Urban and Rural Areas of China*, vol. 37, no. 6, pp. 30–32, 2022.
- [10] X. Long Danfeng, W. X. Zhiwei, and W. Jinsheng, "Epidemiological investigation and risk factors of complications in type 2 diabetes mellitus," *Medical Information*, vol. 33, no. 21, pp. 128–130, 2020.
- [11] D. Jiale, N. Shuo, H. Wei, and J. Zhili, "Advances when treating DF ulcer [J/OL]," *Medical Review*, vol. 6, pp. 1198–1204, 2022.
- [12] S. Ziran and H. H. Zhiqi, "Meta analysis of therapeutic effect of integrated traditional Chinese and western medicine nursing on DF," *Evidence-Based Nursing*, vol. 7, no. 8, pp. 1011–1016, 2021.
- [13] M. Xiuqin, "Nursing care of diabetic peripheral neuropathy with traditional Chinese and western medicine," *Occupation and Health*, vol. 34, no. 10, pp. 1438–1440, 2018.
- [14] Z. Chenxu and Z. Huimin, "Interpretation of guidelines for diagnosis and treatment of DF in China," *Chinese Journal of Clinicians*, vol. 49, no. 12, pp. 1405–1408, 2010.
- [15] C. Na, "To explore the effect of nursing intervention of traditional Chinese and western medicine on the outcome of DF and promoting wound healing of DF ulcer," *Drugstore Weekly*, vol. 30, no. 25, p. 159, 2021.
- [16] Z. Liqiong, Z. Qingping, W. Qiuqin, and L. Siping, "Effect of integrated traditional Chinese and western medicine nursing on wound healing and life quality in patients with type 2 DF," *Inner Mongolia Medical Journal*, vol. 50, no. 9, pp. 1141–1142, 2018.
- [17] L. Qing, "Study on the effect of traditional Chinese and western medicine nursing intervention on the outcome of DF and promoting wound healing of DF ulcer," *Chinese Community Physician*, vol. 37, no. 18, pp. 163–164, 2021.
- [18] X. Shuzhen, "Effect of integrated traditional Chinese and western medicine nursing on healing and amputation rate of DF ulcer," *When Zhenguo Medicine*, vol. 24, no. 7, pp. 1757–1758, 2013.
- [19] Z. Limin, X. Fina, and C. Qixin, "Observation on the effect of traditional Chinese and western medicine nursing intervention on the outcome of DF," *Clinical Medical Engineering*, vol. 23, no. 10, pp. 1415–1416, 2016.
- [20] Z. Tingting, "Observation on the effect of integrated traditional Chinese and western medicine nursing on patients with DF," *Clinical Research of TCM*, vol. 11, no. 25, pp. 130–132, 2019.
- [21] H. Jing, "Observation on the clinical effect of integrated traditional Chinese and western medicine nursing DF," *Journal of Liaoning University of TCM*, vol. 18, no. 11, pp. 190–192, 2016.
- [22] G. Yinghong and W. Hua, "Evaluation of clinical effect of nursing DF with integrated traditional Chinese and western medicine," *Jilin Medicine*, vol. 40, no. 6, pp. 1411–1412, 2019.

- [23] A. Altoijry, H. AlGhofli, S. N. Alanazi et al., "Diabetic foot and peripheral arterial disease. Single centre experience," *Saudi Medical Journal*, vol. 42, no. 1, pp. 49–55, 2021.
- [24] S. Lixia, Q. Hongsong, Y. Xuesong, and H. Qingzhi, "Research progress on wound repair of DF ulcer infection," *Journal of Vascular and Endovascular Surgery*, vol. 7, no. 9, pp. 1084–1088, 2021.
- [25] A. A. Wahbi, "Operative versus non-operative treatment in diabetic dry toe gangrene," *Diabetes & Metabolic Syndrome: Clinical Research & Reviews*, vol. 13, no. 2, pp. 959–963, 2019.
- [26] Z. Xiaoke, S. Hongxia, and D. Yuhong, "Interpretation of TCM treatment in Chinese guidelines for prevention and treatment of DF (2019 edition)," *Modern TCM*, vol. 42, no. 2, pp. 17–19, 2022.
- [27] F. S. Ejagwulu, K. E. Amaefule, Y. Z. Lawal, I. M. Maitama, S. S. Audu, and T. Delia, "Peripheral gangrene and extremity amputations-painful preventable sequelae of meningococcal septicaemia: case series reports," *West African Journal of Medicine*, vol. 37, no. 2, pp. 189–196, 2020.
- [28] Professional Committee of Peripheral Vascular Diseases of Chinese Society of Integrated traditional Chinese and Western Medicine, "Chinese expert consensus on Prevention and treatment of DF with integrated traditional Chinese and western medicine (1st edition)," *Journal of Vascular and Endovascular Surgery*, vol. 5, no. 5, pp. 379–402, 2019.
- [29] L. Xueling, "Analysis on the efficacy of combination of traditional Chinese and western medicine when treating DF gangrene," *Bipedal and Health Care*, vol. 28, no. 15, pp. 56–57, 2019.
- [30] L. Wei, C. Zhuangli, and L. Jiehui, "Application status and research progress of TCM external treatment of DF," *Chinese Journal of Burn wounds and ulcers*, vol. 33, no. 4, 2021233–236+250.

## Research Article

# Preliminary Investigation on the Relationship between Raman Spectra of Beef and Metmyoglobin and Metmyoglobin Reductase Activity

Tonggang Zhang,<sup>1</sup> Yalei Li,<sup>2</sup> Ruiming Luo ,<sup>2</sup> and Shuang Bo<sup>2</sup>

<sup>1</sup>School of Biology and Brewing Engineering, Taishan University, Shandong 271000, China

<sup>2</sup>School of Agriculture, Ningxia University, Ningxia 750021, China

Correspondence should be addressed to Ruiming Luo; ruimingluo.nx@tsu.edu.cn

Received 2 August 2022; Revised 7 September 2022; Accepted 19 September 2022; Published 13 October 2022

Academic Editor: Hangjun Che

Copyright © 2022 Tonggang Zhang et al. This is an open access article distributed under the Creative Commons Attribution License, which permits unrestricted use, distribution, and reproduction in any medium, provided the original work is properly cited.

A hand-held Raman spectroscopic device was used as a rapid nondestructive testing device to predict the metmyoglobin (MetMb) and metmyoglobin reductase activity (MRA) values on the surface layer of fresh beef. Longissimus dorsi muscles were from 10 young bulls (Holstein-Friesian) from two different cattle farms (group A = 5 and B = 5). The Raman spectra of 100 samples were correlated with the MetMb and MRA values using partial least squares regression (PLSR). Two groups could be discriminated, and the separate correlation models were better than the joint correlation model for the fresh beef. The coefficients of determination are  $R^2 = 0.81$  (group A) and  $R^2 = 0.87$  (group B) for MetMb and  $R^2 = 0.80$  (group A) and  $R^2 = 0.85$  (group B) for MRA. The results show the usefulness of Raman spectra in predicting the inner traits such as MetMb and MRA during meat storage. In conclusion, it is feasible to determine the MetMb and MRA values by Raman spectroscopy. Color is an important indicator of beef freshness and can vary depending on the age, sex, and breed of the cow. They play a very important role in human nutrition. The color of meat is an important indicator of meat freshness, and many researchers are already investigating the causes of color changes. The research was conducted in this environment.

## 1. Introduction

The color is an important indicator of the freshness of beef, which could be changed due to ages, sex, and breeds of cows (Delgado et al., 2002; [21]). They play a very significant part in human diet. The meat color is an important marker of the meat's freshness, and many researches have been done to search for the causes of the color variability. The metmyoglobin accumulation rate is based on the rate of autoxidation of the iron (II) of the protein, myoglobin. Oxymyoglobin, carboxymyoglobin, and metmyoglobin [17] can be used, and metmyoglobin reductase activity is affected [18]; Mikelsen et al., 1992). Both the nonenzymatic and enzyme reductions have been well studied [22]. Other researchers have studied the metmyoglobin reductase activity of beef with different color stability, and some researchers have found that the MRA of beef with poor color stability is the

largest [8]. Though many studies have focused on the key of metmyoglobin reductase in fresh beef meat, the measured method is too time-consuming to be suitable for fast testing. A novel testing method for the metmyoglobin and metmyoglobin reductase activity measurement is rapidly changing this picture.

Raman spectroscopy is one of the technologies that has become more and more popular [2, 3], because it is noninvasive, requires nearly no sample preparation, and is not influenced by the amount water in the sample. The Raman signals come from the inelastic scattering of the incident light from a sample, and the frequency shift of the scattered light shifts in a manner of feature molecular vibrations [14]. Therefore, the Raman spectrum is a vibrational spectrum and may be regarded as a "personal ID" of the scattering material providing quantitative and qualitative information about the molecular structure and composition. Nowadays,

the Raman spectroscopy is used as an analytical technique for the evaluation of food quality and safety. In the past, researchers have demonstrated the potential of Raman spectroscopy to predict certain meat quality characteristics such as drip loss, pH, and water holding capacity of pork (Pedersen, Morel, Andersen, & Balling Engelsen, 2003; Scheier, Bauer, & Schmidt, 2014; Scheier, Köhler, & Schmidt, 2014) shear and cooking losses in beef. [2, 25]. Combining chemometric methods with Raman spectroscopy has enabled huge progression for both qualitative and quantitative measurements of food components [27]. Thus, Raman spectroscopy is a nondestructive tool which is potentially suited to predict some meat quality characteristics fast [7].

This is the scattering spectrum. Raman spectroscopy Indian scientist K.V. He invented an analytical method based on the Raman effect to study the scattering spectra of incident light of different frequencies to obtain information about the vibration and rotation of molecules and apply them to the analysis of molecular structure research. Inelastic scattering caused by excitation interactions such as molecular vibrations, optical phonons in solids, and laser light is called Raman scattering. This is an analytical method used to study the molecular structure by analyzing the scattering spectra of light at different frequencies to obtain information about molecular vibrations and rotations.

However, there are no reports on the application of Raman to predict the MetMb and MRA values of fresh beef. The paper reports on a research, which uses 100 samples, to compare whether the measurement of fresh meat by Raman spectra could be used to predict the MetMb and MRA values. In the second part of the paper, the determination of myoglobin reductase activity in the surface layer of fresh beef, Raman spectroscopy processing methods, and processing techniques were described; in the third part, the application of MetMb and MRA values in beef quality identification was analyzed in the spectral processing results; in the fourth part, the parameters of beef quality were analyzed.

## 2. Materials and Methods

**2.1. Sample Preparation.** Longissimus dorsi muscles from 12 young cattle (bulls and cow half, Holstein-Friesian), of approximately 16 months of age, from two different cattle farms (group A = 6 and B = 6, bulls and cow half), Ningxia University, were slaughtered at a commercial slaughter plant (Ningxia Laoheqiao Halal Meat Ware Co. Ltd., China). The mean hot carcass weight was  $250.8 \pm 25.3$  kg (ranging from 225.1 to 297.4 kg). After slaughter, hemoglobin is depleted with blood loss. Then, the color of meat was mainly determined by myoglobin. With the change of myoglobin concentration, the color of the meat change was also obvious. It had a relationship with the spectra [26]. At 24 h postmortem, the meat was cut into slices (20 mm thickness) using a scalpel. And all meat samples were individually vacuum packed and stored at 4°C in the dark. Each group had 50 muscle samples. In there, twenty-five muscle samples were tested without any treatment immediately. The rest of the samples were vacuum packed and stored at 4°C in the dark until preparation on day 5.

24 hours after death, the meat was cut into thin slices with a scalpel. All meat samples were individually vacuum packed and stored at 4°C in the dark. There were 50 muscle samples in each group, and the rest of the samples were discarded. There is no need for direct processing and packaging. Condition at 4°C and store in the dark until day 5 of the preparation date.

**2.2. Measurement of Metmyoglobin Concentration on the Surface Layer of Fresh Beef.** Take the fresh beef topping, mix the fresh beef topping with the fresh beef topping salt buffer solution, and homogenize it with an ultrafine homogenizer and a centrifuge for 20 minutes. The supernatant was filtered through filter paper, and the absorbance of NM was measured at different points with a spectrophotometer. Take the average of the formula to calculate the concentration.

According to the method of Krzywicki et al., [15], a 5 g sample from the surface layer of fresh beef was mixed with 25 mL phosphate buffer (0.04 mol/L, pH = 6.8) and homogenized with an ultrafine homogenizer (FLUKO F6/10, Germany; 10000 rpm, 25 s). After standing for 60 min at 4°C in the dark, the mixture was centrifuged at  $4500 \times g$  for 20 min at 4°C. The supernatant was filtered through filter paper, and the absorbance was measured at 525, 545, 565, and 572 nm separately with a spectrophotometer. Each sample was measured three times, and the average value was taken for the further statistical data analysis with the following formula:

$$\text{MetMb}(\%) = (-2.514R1 + 0.777R2 + 0.800R3 + 1.098) \times 100,$$

$$R1 = \frac{A572}{A525},$$

$$R2 = \frac{A565}{A525},$$

$$R3 = \frac{A545}{A525}.$$

(1)

**2.3. Measurement of Metmyoglobin Reductase Activity on the Surface Layer of Fresh Beef.** Methemoglobin reductase extract was obtained from the skin of fresh beef with minor modifications. Muscle and phosphate-buffered saline were mixed and centrifuged, and fat was removed from the supernatant through a filter paper. Excessive oxidized hemoglobin was added, the solution was dialyzed as a phosphate buffer, and the methemoglobin reductase activity of the extract was measured by spectrophotometry, and the final result was the amount of enzyme activity.

Metmyoglobin reductase extracts were obtained from the surface layer of fresh beef by the Reddy and Carpenter method with slight modifications [22]: 12 g muscle and 20 mL 2.0 mM phosphate buffer (pH = 7.0) were mixed and homogenized with an ULTRA-TURRAX (30 s, 12,000 rpm, 4°C). The homogenate was centrifuged (30 min,  $35000 \times g$ , 4°C), and the fat was removed from the supernatant by a paper filter. Excessive  $K_3Fe(CN)_6$  was added to





FIGURE 1: Portable Raman system for on-line measurements of meat consisting of a hand-held Raman device.

oxidize the oxyhemoproteins, and the solution was dialyzed (14000 MW) against 2 mM phosphate buffer (pH = 7.0). The filtrate was centrifuged (20 min,  $15000 \times g$ ,  $4^\circ\text{C}$ ), and the volume of the filtrate was adjusted to 20 mL with 2.0 mM phosphate buffer (pH = 7.0).

Metmyoglobin reductase activity of the extract was measured spectrophotometrically: the standard assay mixture included 0.1 mL water, 0.10 mL 50 mM phosphate buffer (pH = 7.0), 0.10 mL 5.0 mM EDTA (pH = 6.4), 0.1 mL 3.0 mM  $\text{K}_4\text{Fe}(\text{CN})_6$ , 0.2 mL 0.75 mM MbFe (III) in 2.0 mM phosphate buffer (pH = 7.0), 0.3 mL extract, and 0.1 mL 2.0 mM NADH. Addition of NADH initiated the reaction. Metmyoglobin reductase activity was calculated as nanomole metmyoglobin reduced per min per g of beef meat during the initial linear phase of the assay, using a difference in molar absorptivity of  $12 \times 10^3/\text{mol} \cdot \text{cm}$  at 580 nm. The effects of storage ( $4^\circ\text{C}$ ) time of the beef meat prior to extraction as well as the effect of storage time of enzyme extracts were also investigated. Metmyoglobin reductase activities are expressed as the means.

**2.4. Raman Spectroscopy.** An Inspector 300 Raman microscope (SciAps, USA) with a 785 nm laser source, a motorized microscope stage sample holder, and a CCD detector (SciAps, USA) were used. The instrument was used at 10 mW laser power with 8 s acquisition. Each sample was placed on the translation stage and scanned. The spectra were obtained in the range of  $400\text{--}1700\text{ cm}^{-1}$  at a resolution of  $6\text{ cm}^{-1}$  (Figure 1) after calibration using the spectra of polystyrene. Each sample was manipulated with the built-in “automatic baseline correct” function of the software. Five replicate analyses were performed on each sample.

**2.5. Spectral Processing.** In the Raman shift ( $400\text{--}1700\text{ cm}^{-1}$ ), chemical bonds cause vibrational and rotational transitions, resulting in absorption bands in spectral curves [6]. There are many combination bands that overlap the absorption bands, which make the spectrum highly convoluted and dif-

TABLE 1: Mean  $\pm$  s.d., minimum and maximum for the measured traits: carcass weight (kg), MetMb (%), and MAR (nmol/min-g) according to the group (50 samples per group).

	Group	Minimum	Maximum	Mean $\pm$ s.d.
MetMb (%)	A	13.52	31.08	$22.30 \pm 4.78$
	B	16.95	38.16	$27.56 \pm 5.61$
MRA (nmol/min-g)	A	10.48	29.08	$19.78 \pm 3.72$
	B	9.73	31.26	$20.49 \pm 4.99$

ficult to be interpreted. In addition, other factors, such as the natural light, may also make the spectrum more complex. Therefore, chemometric methods of spectral processing are used to interpret the spectrum. The spectral processing includes spectral pretreatment, modeling, and model evaluation.

In the Raman shift ( $400\text{--}1700\text{ cm}^{-1}$ ), the compounds induce vibrational and rotational changes, and then, absorption bands appear on the spectral curve, while several combined bands dominate on the d-band. Absorption makes a spectral complex and is difficult to interpret, so spectra can be interpreted using stoichiometric methods of spectral processing.

Raman spectral data across the full wavenumber range were treated by multivariate analysis to find out key information related to the reference MetMb and MRA values. There are a lot of multivariate algorithms for building quantitative models, such as PCA, MLR, and PLS [4]. In this study, PLS and PCR were used to establish predictive models [12]. Prediction of MetMb and MRA values in the models was attained by a group of latent variables, which were statistically uncorrelated and got the most information in  $X$  (Raman spectral data) and  $Y$  (reference values of MetMb and MRA values).

Chemical properties of samples and influences in instrument response may cause light scattering effects, and these elements may influence the real responses and the robustness of later multivariate calibration models [24]. In order to decrease or even remove these undesirable elements, pretreatment of the spectral data is necessary, such as multiplicative scatter correction, smoothing, and standard normal variate [20]. In this study, there are four spectral pretreatment methods (Savitzky-Golay smoothing, derivatives, MSC, and Nor). The optimal pretreatment method was chosen by comparing the best performance.

Multivariate data analysis was carried out to predict MetMb and MRA values of samples using their corresponding spectral information. The same Raman spectral dataset can be used together with MetMb and MRA values to build a predictive partial PLS model. Thus, the measured spectra can be used to predicted MetMb and MRA values for the new sample directly. PLSs were carried out to perform linear models of prediction between spectral data and the values of one of the quality parameters obtained from the traditional measurement.

TABLE 2: PLS models for predicting MetMb and MRA values on the surface layer of fresh beef with raw and pretreated spectral data.

	Pretreatment	Number of latent number	Calibration		Crossvalidation		Prediction	
			$R^2_c$	RMSE <sub>c</sub>	$R^2_{cv}$	RMSE <sub>cv</sub>	$R^2_p$	RMSE <sub>p</sub>
MetMb	Raw	6	0.827	1.169	0.804	0.985	0.885	1.387
	SGS	5	0.856	0.815	0.832	0.693	0.916	0.983
	MSC	6	0.837	0.911	0.815	0.741	0.908	1.157
	Nor	5	0.846	0.894	0.797	0.733	0.911	0.9981
MAR	Raw	4	0.762	1.416	0.801	0.857	0.806	1.514
	SGS	5	0.801	1.325	0.853	1.215	0.845	1.502
	MSC	6	0.818	0.993	0.862	0.819	0.853	1.361
	Nor	6	0.836	0.869	0.887	0.786	0.871	0.908

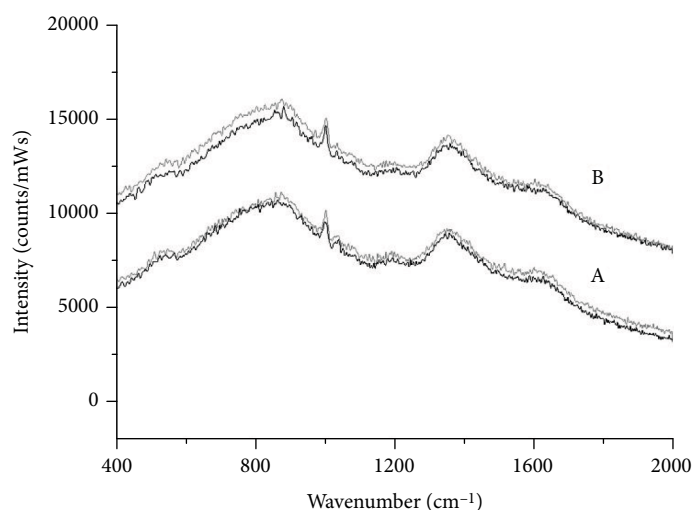


FIGURE 2: Averaged Raman spectra on the surface layer of fresh beef for A samples and B samples grouped according to their storage time, 0 d (gray curves) and 5 d (black curves).

TABLE 3: Raman modes useful in interpretation of the protein structure adapted from the works of Li-Chan [19] and Beattie et al. [3].

Origin	Wavenumber (cm <sup>-1</sup> )	Assignment	Structural information obtained
Phenylalanine	1006	Breathing ring	Conformation insensitive; useful as an internal intensity standard
Histidine	1409	N-Diimidazole	Probe of ionization state, metalloprotein structure, and proton transfer in deuterated solution
Tryptophan	760, 880, 1360	Indole ring	Sharp intense band indicates buried residues; sensitive to environment polarity
Aspartic acid, glutamic acid	1400–1430	C=O stretch of COO <sup>-</sup>	Ionized carboxyl groups
Amide III	1230–1240	N-H in-plane bend, C-N stretch	Antiparallel g-sheet
Amide I	1650–1660	Amide C=O stretch, N-H wag	$\alpha$ -Helix
Aliphatic amino acids	1450, 1465	C-H bending	Microenvironment, polarity



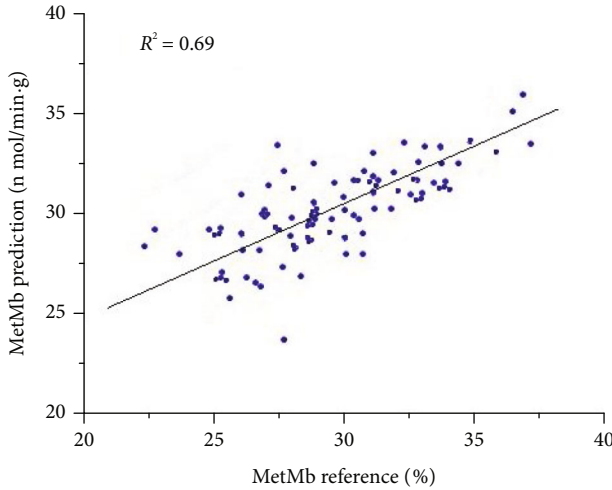


FIGURE 3: PLS correlation model of Raman data for MetMb on the surface layer of fresh beef and coefficient of determination.

The accuracy of the PLS model was identified based on the coefficient of determination in calibration ( $R^2_C$ ), coefficient of determination in crossvalidation ( $R^2_{CV}$ ), root mean square error of calibration ( $RMSE_C$ ), and root mean square error by crossvalidation ( $RMSE_{CV}$ ). Usually, a useful model should have high values of  $R^2$  and low values of 4.

**2.6. Statistical Analysis.** The spectral data and computation analyses were operated and completed with the aid of chemometric software MATLABR2011a (The MathWorks Inc., Natick, MA, USA) and Unscrambler X 10.3 (CAMO, Trondheim, Norway).

### 3. Results and Discussion

**3.1. MetMb and MRA Values.** The MetMb and MRA values on the surface layer of beef samples determined by a spectrophotometer are listed in Table 1 (groups A and B). Three replicate analyses were performed on each beef sample. There are 100 beef samples in total. Earlier studies have shown that the fresh meat color should keep bright and stable during storage to maximize consumer acceptance [22].

**3.2. Spectral Processing.** The stoichiometric method of spectral processing is used to interpret the spectra. Spectral processing includes preliminary spectral processing, simulation, and model analysis. Raman spectral data across the entire wavenumber range was processed using multivariate analysis to find key information related to MetMb and MRA reference values.

The Raman spectra were normalized by dividing the intensity using integration time and laser power to compare the two groups A and B. Firstly, the PCA method was used to identify the remaining spectra of fat in the data which had not been removed during data collection. Raman spectra with scores associated to the fat pattern over a threshold value were removed before the next step. The threshold

was determined repeatedly by decreasing the value and then making a new PCA model with the rest of the data until the Raman fat pattern was removed from the first 4 loading of the PCA model. By this way, 47 of 1038 Raman spectra of group A and 34 of 1015 spectra of group B were removed. To the next step analysis, the beef Raman spectra were normalized to the baseline intensity at  $1517\text{ cm}^{-1}$  to make the PCA and PLS models better. For each sample, the rest of the 12–15 different spectra were averaged and preprocessed using four spectral pretreatment methods (Savitzky-Golay smoothing, derivatives, MSC, and Nor) and mean centering.

PCA, principal component analysis, is an unsupervised machine learning algorithm. It is a method of studying multidimensional data structures. It is mainly used to reduce the dimensionality of data. Downsizing can be used to find features that are easier to understand. It speeds up the processing of valuable information from samples and can also be used for visualization (up to 2D) and noise reduction. And the PCA algorithm simplifies the data and does not depend on parameters.

The performance of PLS models based on three spectral pretreatment methods (MSC, Nor, and Savitzky-Golay smoothing) is shown in Table 2. As shown in Table 2, compared with the model of the original spectral data, the detection effect of the model of the processed spectral data is improved more or less, which indicates that the pretreatment methods can eliminate the noise in the spectral data effectively. For the different detection parameters, the pretreatment methods are also different.

Compared with the results of raw spectra ( $R^2_p$  of 0.885,  $RMSE_p$  of 1.387), both of the MSC, Nor, and Savitzky-Golay smoothing methods provided some improvement in model robustness because of higher  $R^2_p$  and lower  $RMSE_p$ . In the models, the Nor-PLSR model showed the highest values:  $R^2_p$  of 0.916 and  $RMSE_p$  of 0.983. So, SGS was chosen as the optimal pretreatment method to build the model of the MetMb values. Similarly, the Nor was chosen for the MAR values.

Spectra show typical Raman signals of muscle tissue. The difference between the Raman spectra of the two sites is a 35% higher broadband spectral background for group B. This may be related to the gender of group B, but the sample or environmental factors cannot be omitted.

The samples were put into two storage groups randomly to find out whether the Raman spectra could distinguish two groups. Figure 2 shows the averaged raw spectra from all beef samples from groups A (lower curves) and B (upper curves) with storage 0 d (gray curves) and 5 d (black curves). For comparison, the Raman spectra were divided by integration time and laser power. The number of samples per group is as follows: 25 storage 0 d and 25 storage 5 d samples for group A and 25 storage 0 d and 25 storage 5 d samples for group B. The spectra exhibited the typical Raman signals of muscle tissue [23]. The difference between the Raman spectra of both sites is a 35% higher broadband spectral background of group B. That could be due to the sex of group B, but the sample or environment elements cannot be ignored. For example, the oxygen content of the

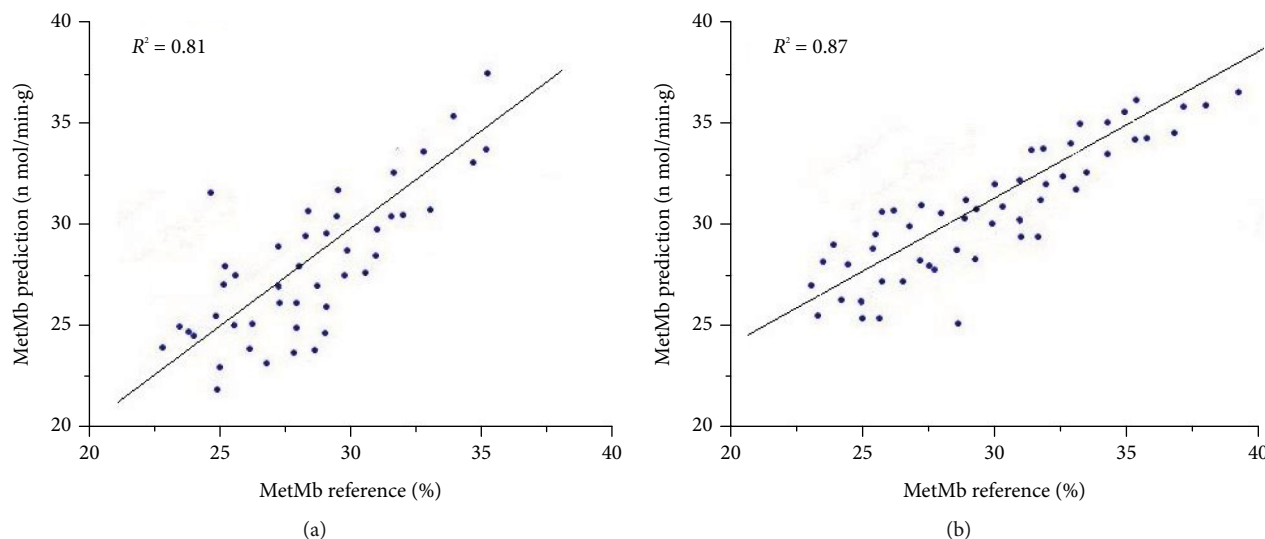


FIGURE 4: PLS correlation models of Raman data for MetMb on the surface layer of fresh beef and coefficient of determination((a) A samples; (b)B samples).

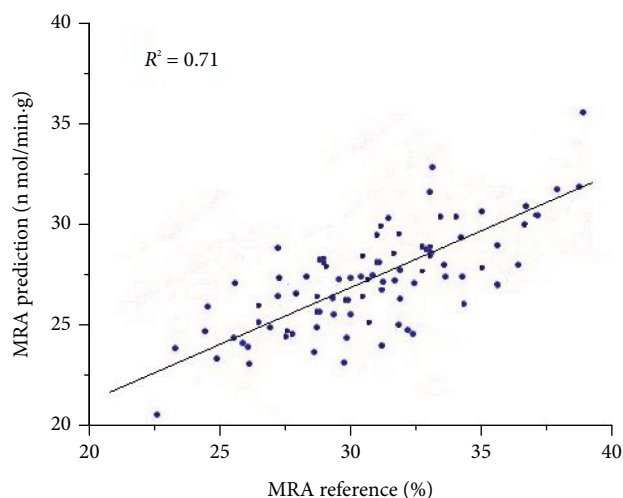


FIGURE 5: PLS correlation model of Raman data for MRA on the surface layer of fresh beef and coefficient of determination.

vacuum-packaged beef can lead to a variation of the fluorescence level because of the fluorescence quenching effect [16]. So, to reduce the minimum bias, discharge the air as much as possible prior to the Raman measurement. An off-set of the spectral background is also shown between the different storage groups (0 d and 5 d) (Figure 2).

Raw spectra of beef samples were background corrected, showing changes and intensities of protein vibrations (Table 3) at around 930, 1006, 1019, 1230, 1360, and 1655  $\text{cm}^{-1}$ . The Raman spectra can show the typical Raman signals of muscle [23]. Hydroxyproline, a typical component of connective tissue, may show a signal at 877  $\text{cm}^{-1}$ , so the corresponding moderately strong band in connective tissue is not found in the amide III region and is removed [5, 11, 13]. The Raman spectra of the samples seemed to be similar; however, there were spectral data differences due to intensity differences in the same band intensity. The band positioned

at 1265  $\text{cm}^{-1}$  belongs to  $\delta(\text{C-H})$  bending at the cis double bond in  $\text{R-HC=CH-R}$  [9]. The bands at 800–900 and 1000–1100  $\text{cm}^{-1}$  are due to the vibration of skeletal C-C bonds in  $-(\text{CH}_2)_n-$  molecules [1]. The band at 1213  $\text{cm}^{-1}$  is due to antisymmetric phosphoryl stretching corresponding to the vibrations of fatty acid and phospholipid chains [10]. Lu (2014) determined the relative amounts of hemoglobin by Raman spectral and found that the spectral differences between the three hemoglobin derivatives were exhibited in several relevant peaks in 1210–1230  $\text{cm}^{-1}$ , 1375–1379  $\text{cm}^{-1}$ , and 1550–1650  $\text{cm}^{-1}$ . Compared to oxyhemoglobin, a number of changes were apparent in the range of 1550–1650  $\text{cm}^{-1}$  in the Raman spectra of carboxyhemoglobin. Compared to oxyhemoglobin, in the spectra of carboxyhemoglobin, the band at 1559  $\text{cm}^{-1}$  appears to be more intense, while the 1589  $\text{cm}^{-1}$  and 1645  $\text{cm}^{-1}$  bands were less intense. In the spectra of methemoglobin, a number of changes were exhibited in the range of 1210–1230  $\text{cm}^{-1}$ , 1375–1379  $\text{cm}^{-1}$ , and 1550–1650  $\text{cm}^{-1}$ , by comparing with oxyhemoglobin (Lu et al. 2013). Along with the spectral differences, the peaks show signals of structural traits that can help in the Raman detection of MetMb and MRA. The result show that Raman spectroscopy could be a useful method instead of the time-consuming and destructive mechanical method in the measurement of MetMb and MRA in fresh beef.

The analysis of A and B groups of the PLS model is showed in Figure 3. In the PLS model, the correlation is moderate with a coefficient of determination of  $R^2 = 0.79$ , a root mean square error of calibration ( $\text{RMSE}_C$ ) of 1.493, and a root mean square error of validation ( $\text{RMSE}_{CV}$ ) of 1.203. Further analysis was showed for A and B groups.

PLS regression analysis correlating the Raman spectra with the MetMb values for the subsets of samples shows a coefficient of determination of  $R^2 = 0.81$  (A) and  $R^2 = 0.87$  (B). The result of the analysis is showed in Figure 4. The  $\text{RMSE}_{CS}$  are computed to be 1.276 (A) and 1.218 (B). It

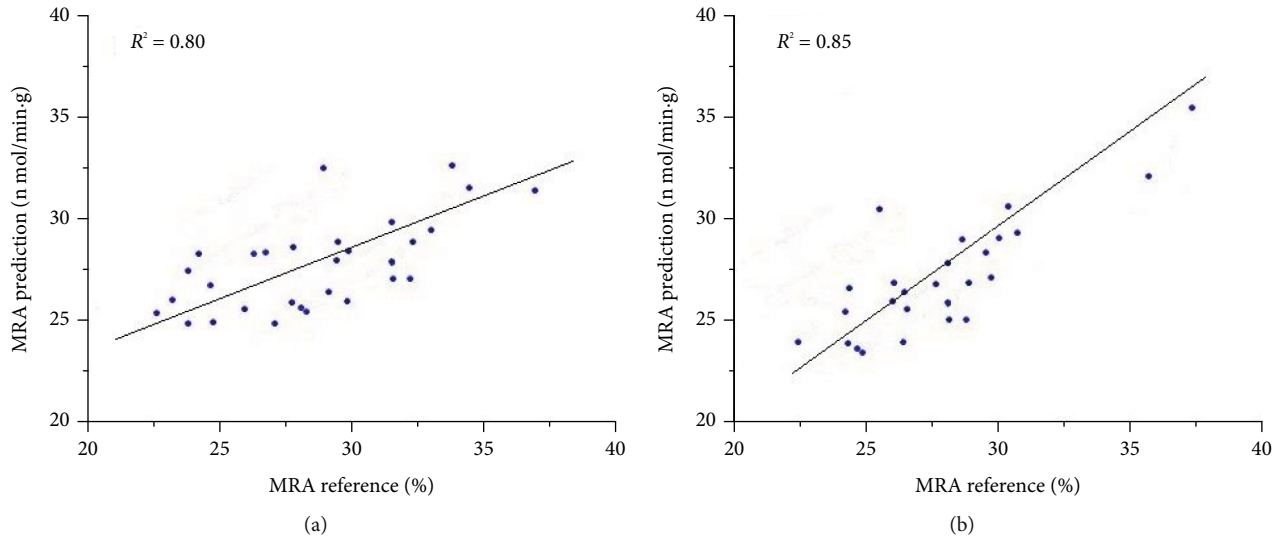


FIGURE 6: PLS correlation models of Raman data for MRA on the surface layer of fresh beef and coefficient of determination((a) A samples; (b) B samples).

can evaluate the validity of the PLS model. The values were not satisfactory because of the MetMb values being distributed unevenly, i.e., rather few samples with low MetMb values were measured. The more evenly distributed of MetMb data making the coefficient of determination was better than the A subset.

The Raman spectra was correlated with the MRA reference measurements. The joint treatment of A and B subsets brought about a less good enough model (Figure 5). The coefficient of determination of  $R^2 = 0.71$ ,  $RMSE_C = 1.626\%$ , and  $RMSE_{CV} = 1.395$  yield reasonable values for the model, respectively.

The distribution of MetMb values is not the same, i.e., few models with low MetMb values are measured, so these values are not satisfactory. The MetMb data distribution of the coefficient of determination is better than that of subset A. The Raman spectrum is related to the ARM reference measurement, and the coefficients for each setting provide reasonable values for the model.

The separate treatment of the A and B groups improves the results (Figure 6).  $R^2 = 0.80$  for A samples and  $R^2 = 0.85$  for B samples.  $RMSE_C = 1.193$  and  $RMSE_{CV} = 0.947$  for A samples and  $RMSE_C = 1.063$  and  $RMSE_{CV} = 0.802$  for B samples. Therefore, for the MetMb measurements, the correlation of the B group was slightly better than that of the A group. To be used in meat production accurately and widely, the samples must be more diverse and also have strong predictions of the characteristics of measurement after a period of storage. These problems will be studied in the future research.

#### 4. Conclusion

PLS regression uses the principle of principal component analysis to combine multiple  $X$  and multiple  $Y$  components ( $X$  is the principal component of  $U$ ,  $Y$  is the principal component of  $V$ ) and then uses the principle of canonical corre-

lation to determine the relationship between  $X$  to analyze the  $Y$  relationship between  $X$  and  $V$ , combined with the principle of multiple linear regression, analyze the relationship between  $X$  and  $V$ , and explore the relationship between  $X$  and  $Y$ .

The Raman spectra of samples of two different cattle farms A and B could be correlated with the values of MetMb and MRA on the surface layer of fresh beef using PLS regression analysis. Groups and B group could be significantly distinguished by the different Raman spectra. And the distinction is based on spectral broadband differences. But the reasons of the broadband differences was not unclear. In the Raman spectra of beef samples in different storage time and sources, it can recognize signals that come from  $\alpha$ -helical protein structures, the aromatic amino acid side chain of tryptophan and phenylalanine. The correlation models of separate correlation of Raman spectra subsets A and B were better than the joint correlation for the all data. The result show that Raman spectroscopy could be a useful method instead of the time-consuming and destructive mechanical method for the prediction of quality traits such as MetMb and MRA values in fresh beef meat. The future study should research the prediction ability of Raman spectra for the quality traits of fresh beef when the spectra are collected on meat during the full storage time. Considering the application of new technologies in the future, intelligent computing combined with the PLSR algorithm is used for parameter optimization and application. Further, the beef quality of different varieties was classified and the key factors of beef quality were discussed and analyzed in depth under the influence of various factors.

#### Data Availability

The experimental data used to support the findings of this study are available from the corresponding author upon request.

## Conflicts of Interest

The authors declared that they have no conflicts of interest regarding this work.

## Acknowledgments

This work has been financially supported by the National Natural Science Foundation of China (no. 3166100446).

## References

- [1] V. Baeten, P. Hourant, M. T. Morales, and R. Aparicio, "Oil and fat classification by FT-Raman spectroscopy," *Journal of Agricultural and Food Chemistry*, vol. 46, no. 7, pp. 2638–2646, 1998.
- [2] R. J. Beattie, S. J. Bell, L. J. Farmer, B. W. Moss, and D. Patterson, "Preliminary investigation of the application of Raman spectroscopy to the prediction of the sensory quality of beef silverside," *Meat Science*, vol. 66, no. 4, pp. 903–913, 2004.
- [3] J. R. Beattie, S. J. Bell, C. Borggaard, A. Fearon, and B. Moss, "Classification of adipose tissue species using Raman spectroscopy," *Lipids*, vol. 42, no. 7, pp. 679–685, 2007.
- [4] P. Blanco, C. Sieiro, and T. G. Villa, "Production of pectic enzymes in yeasts," *FEMS Microbiology Letters*, vol. 175, no. 1, pp. 1–9, 1999.
- [5] E. B. Carew, H. E. Stanley, J. C. Seidel, and J. Gergely, "Studies of myosin and its proteolytic fragments by laser Raman spectroscopy," *Biophysical Journal*, vol. 44, no. 2, pp. 219–224, 1983.
- [6] H. Cen and Y. He, "Theory and application of near infrared reflectance spectroscopy in determination of food quality," *Trends in Food Science and Technology*, vol. 18, no. 2, pp. 72–83, 2007.
- [7] J. L. Damez and S. Clerjon, "Meat quality assessment using biophysical methods related to meat structure," *Meat Science*, vol. 80, no. 1, pp. 132–149, 2008.
- [8] R. Michardiere and D. B. Salem, "Comparison of MRA and arteriography in the monitoring of intracranial aneurysms treated with gdc," *Journal of Neuroradiology*, vol. 48, no. 1, 2021.
- [9] R. El-Abassy, P. Eravuchira, P. Donfack, B. Von der Kammer, and A. Materny, "Fast determination of milk fat content using Raman spectroscopy," *Vibrational Spectroscopy*, vol. 56, no. 1, pp. 3–8, 2011.
- [10] S. Gallier, K. C. Gordon, R. Jiménez-Flores, and D. W. Everett, "Composition of bovine milk fat globules by confocal Raman microscopy," *International Dairy Journal*, vol. 21, no. 6, pp. 402–412, 2011.
- [11] A. M. Herrero, "Raman spectroscopy for monitoring protein structure in muscle food systems," *Critical Reviews in Food Science and Nutrition*, vol. 48, no. 6, pp. 512–523, 2008.
- [12] H.-J. He, D. Wu, and D.-W. Sun, "Potential of hyperspectral imaging combined with chemometric analysis for assessing and visualising tenderness distribution in raw farmed salmon fillets," *Journal of Food Engineering*, vol. 126, pp. 156–164, 2014.
- [13] T. Ikoma, H. Kobayashi, J. Tanaka, D. Walsh, and S. Mann, "Physical properties of type I collagen extracted from fish scales of *Pagrus major* and *Oreochromis niloticus*," *International Journal of Biological Macromolecules*, vol. 32, no. 3–5, pp. 199–204, 2003.
- [14] K. Kneipp, H. Kneipp, I. Itzkan, R. R. Dasari, and M. S. Feld, "Ultrasensitive chemical analysis by Raman spectroscopy," *Chemical Reviews*, vol. 99, no. 10, pp. 2957–2976, 1999.
- [15] K. Krzywicki, "The determination of haem pigments in meat," *Meat Science*, vol. 7, no. 1, pp. 29–36, 1982.
- [16] J. R. Lakowicz and G. Weber, "Quenching of protein fluorescence by oxygen. Detection of structural fluctuations in proteins on the nanosecond time scale," *Biochemistry*, vol. 12, no. 21, pp. 4171–4179, 1973.
- [17] D. A. Ledward, "Colour of raw and cooked meat," *Special Publication-Royal Society of Chemistry*, vol. 106, pp. 128–128, 1992.
- [18] Y. Chen, H. Cheng, K. Tram et al., "A paper-based surface-enhanced resonance Raman spectroscopic (SERRS) immunoassay using magnetic separation and enzyme-catalyzed reaction," *Analyst*, vol. 138, no. 9, p. 2624, 2013.
- [19] E. C. Y. Li-Chan, "The applications of Raman spectroscopy in food science," *Trends in Food Science & Technology*, vol. 7, no. 11, pp. 361–370, 1996.
- [20] J. Luybaert, S. Heuerding, Y. V. Heyden, and D. L. Massart, "The effect of preprocessing methods in reducing interfering variability from near-infrared measurements of creams," *Journal of Pharmaceutical and Biomedical Analysis*, vol. 36, no. 3, pp. 495–503, 2004.
- [21] A. J. McAfee, E. M. McSorley, G. J. Cuskelly et al., "Red meat consumption: an overview of the risks and benefits," *Meat Science*, vol. 84, no. 1, pp. 1–13, 2010.
- [22] A. Mikkelsen, D. Juncher, and L. H. Skibsted, "Metmyoglobin reductase activity in porcine m. longissimus dorsi muscle," *Meat Science*, vol. 51, no. 2, pp. 155–161, 1999.
- [23] M. Pezolet, M. Pigeon-Gosselin, and J. P. Caille, "Laser Raman investigation of intact single muscle fibers," *Biochimica et Biophysica Acta (BBA)-Protein Structure*, vol. 533, no. 1, pp. 263–269, 1978.
- [24] A. Rinnan, F. V. D. Berg, and S. B. Engelsen, "Review of the most common preprocessing techniques for near-infrared spectra," *TrAC Trends in Analytical Chemistry*, vol. 28, no. 10, pp. 1201–1222, 2009.
- [25] H. Schmidt, R. Scheier, and D. L. Hopkins, "Preliminary investigation on the relationship of Raman spectra of sheep meat with shear force and cooking loss," *Meat Science*, vol. 93, no. 1, pp. 138–143, 2013.
- [26] Z. Xiong, D. W. Sun, H. Pu, A. Xie, Z. Han, and M. Luo, "Non-destructive prediction of thiobarbituric acid reactive substances (TBARS) value for freshness evaluation of chicken meat using hyperspectral imaging," *Food Chemistry*, vol. 179, pp. 175–181, 2015.
- [27] H. Yang, J. Irudayaraj, and M. M. Paradkar, "Discriminant analysis of edible oils and fats by FTIR, FT-NIR and FT-Raman spectroscopy," *Food Chemistry*, vol. 93, no. 1, pp. 25–32, 2005.



## Research Article

# The Value of MacroGene Second-Generation Sequencing in the Diagnosis, Guidance of Drug Use, and Efficacy Monitoring of Infectious Pneumonia in Premature Infants

LiLi Wang, Ping Zha, YuJuan Wang, Ying Kong, Yu Su, LiYing Dai, and Yang Wang 

Department of Pediatrics, The First Affiliated Hospital of Anhui Medical University, Hefei, Anhui 230000, China

Correspondence should be addressed to Yang Wang; 15040140348@xs.hnit.edu.cn

Received 15 July 2022; Revised 2 August 2022; Accepted 13 September 2022; Published 12 October 2022

Academic Editor: Hangjun Che

Copyright © 2022 LiLi Wang et al. This is an open access article distributed under the Creative Commons Attribution License, which permits unrestricted use, distribution, and reproduction in any medium, provided the original work is properly cited.

**Objective.** A group-controlled trial was conducted to explore the value of macrogene second-generation sequencing in the diagnosis, drug use, and efficacy monitoring of infectious pneumonia in premature infants. **Methods.** One hundred and thirty-eight premature infants with suspected infectious pneumonia treated in our hospital from March 2019 to June 2022 were selected as subjects. All patients underwent deep phlegm extraction and were randomly divided into two groups. 69 cases of control group were treated with general bacterial and fungal culture. The lavage fluid of the remaining 69 cases of observation group were detected by metagenomic next-generation sequencing (mNGS). The number of diagnosed preterm infants with infectious pneumonia was compared between the two groups, and the diagnostic value of the two methods was analyzed by the receiver operator characteristic (ROC) curve. Then, the differences in clinical efficacy, antimicrobial neonatal intensive care unit (NICU) use time, antimicrobial adjustment frequency, NICU stay time, hospital stay, and serum inflammatory factors were compared between the two groups. **Results.** The positive rate of mNGS pathogen detection in the lavage fluid of the observation group was 92.75% (64/69). The positive rate of the culture of the lavage fluid of the control group was 52.17% (36/69). The ROC curve analysis showed that the ROC AUC of traditional culture was 0.752 (95%CI = 0.610-0.894), and that of mNCS was 0.934 (95%CI = 0.854-0.999). In the observation group, there were 35 cases of bacterial infection, 20 cases of fungi, 4 cases of virus, and 5 cases of Chlamydia psittaci. In the control group, 26 cases of bacterial infection and 9 cases of fungi were detected; but viruses and other mycoplasmas could not be detected. After 2 weeks of treatment, the effective rate of the observation group was 95.31%, while that of the control group was 69.44%. The NICU use time, adjustment frequency, NICU stay time, and hospitalization time of antibiotics in the observation group were significantly less than those in the control group, and the difference was statistically significant ( $P < 0.05$ ). After treatment, the levels of serum interleukin-6 (IL-6), procalcitonin (PCT), and hypersensitivity-C-reactive protein (hs-CRP) in observation group were significantly higher than those in control group, and the difference was statistically significant ( $P < 0.05$ ). **Conclusion.** mNGS can improve the efficiency of clinical diagnosis of infectious pneumonia in premature infants, effectively improve the detection rate of pathogens and the clinical efficacy of premature infants. At the same time, it can also assist the clinical efficacy monitoring and adjust the treatment plan at any time.

## 1. Introduction

Infectious diseases are currently the diseases with the highest morbidity and mortality in the world. According to epidemiological studies, the most common type of infectious diseases is pulmonary infection (21.8%) [1], which is the main cause of death of infectious diseases. However, patho-

genic microorganisms can also be detected by conventional pathogen detection methods, and the two pulmonary imaging findings are also similar, mostly exudative changes. If clinicians cannot correctly differentiate and diagnose infected/noninfectious lung diseases, they will miss the best time for diagnosis and treatment, resulting in the abuse of antibiotics. Therefore, it is very important to guide clinicians to correctly

and timely differential diagnosis of pulmonary infection/noninfectious diseases and to formulate a reasonable treatment plan. There are many influencing factors of pulmonary infection in premature infants, which have great complexity and difficulty in clinical prevention and treatment. It has been reported that the younger the gestational age and the lower the body mass of premature infants, the worse the development of premature infants. More tissues and organs are underdeveloped [2].

At present, there are the following detection methods for the diagnosis of pulmonary infectious diseases, including etiology-based detection methods, molecular biology-based detection methods, and immunology-based detection methods [2, 3]. In order to ensure the health and safety of premature infants, nursing or treatment procedures that increase the risk of infection should be avoided [4]. Although these methods have their own obvious advantages, they often expose some weaknesses when dealing with complex infectious diseases, such as tedious detection process, time-consuming, and narrow detection range. As a result, the accuracy of conventional pathogen detection methods is limited [5]. Due to the imperfect development of physiological function and poor immune ability, premature infants have a high risk of pulmonary infection when carrying out protection and treatment measures such as invasive examination and mechanical ventilation. It will have a great adverse impact on the healthy development and life safety of premature infants [6] and cannot be diagnosed and treated in time [7]. Therefore, the application of correct detection methods will help to reduce the misdiagnosis and missed diagnosis rate of clinicians and effectively carry out symptomatic treatment.

Metagenomic next-generation sequencing (mNGS) can directly detect all potential pathogens—bacteria, viruses, fungi, and parasites—in clinical samples without isolation and culture [8]. NGS has the following procedures in detecting pathogens, including sample collection and input: sample types include sputum, nasopharyngeal swabs, airway suction secretions, bronchoalveolar lavage fluid, blood, and tissue. The database should have a complete microbial genome sequence, and the analysis process includes data quality control [9–12]. With the continuous progress of NGS technology, this technology is realizing faster and more comprehensive macrogenomic analysis at lower cost. It is more and more widely used in clinic. However, there are few reports on the application value of macrogene second-generation sequencing technology in the diagnosis, guidance of drug use, and efficacy monitoring of infectious pneumonia in premature infants. This study focused on 138 premature infants with suspected infectious pneumonia treated in our hospital. A group-controlled trial was conducted to explore the value of macrogene second-generation sequencing in the diagnosis, drug use, and efficacy monitoring of infectious pneumonia in premature infants.

## 2. Materials and Methods

**2.1. General Information.** One hundred and thirty-eight premature infants with suspected infectious pneumonia treated in our hospital from March 2019 to June 2022 were selected

as subjects. All patients underwent deep phlegm extraction and were randomly divided into two groups. 69 cases of them were treated with general bacterial and fungal culture (control group) and the deep phlegm extraction of the remaining 69 cases were detected by mNGS (observation group). There was no significant difference in the general data between the two groups ( $P > 0.05$ ), as shown in Table 1. All legal guardians of premature infant representatives signed informed consent.

The following are the selection criteria: (1) regardless of sex, all patients who were accompanied by persistent hypothermia or high fever, with apnea or lung moist rales, dyspnea and lung auscultation with wet rales, abnormal leukocyte, and other clinical symptoms; (2) gestational age  $< 37$  weeks; (3) diagnosis gold standard: blood culture and pharyngeal swab smear and culture indicating infection and chest X-ray examination showing patchy infiltration shadow; and (4) complete clinical data.

The following are the exclusion criteria: (1) premature infants with severe heart, liver, renal insufficiency, and malignant tumors; (2) premature infants with pulmonary tuberculosis, congenital bronchial asthma, and other diseases; (3) guardians who refused to have their infants participate; (4) premature infants with other severe infections; (5) premature infants who could not be treated because of drug allergy; and (6) premature infants with serious cardiovascular diseases, arrhythmias, heart failure, and other diseases.

## 2.2. Methods

**2.2.1. Diagnostic Method.** All patients underwent bronchoalveolar lavage with fiberoptic bronchoscope with more than 5 years of experience. Midazolam was selected for intravenous sedation (instead of midazolam 0.1 mg/kg), endotracheal intubation or nasal endoscopy was performed, and 2% lidocaine was used to topical anesthetize the airway mucosa and segmental bronchi. The top of the bronchoscope was embedded in the branch of the bronchus tree. Inject normal saline at 37°C into the bronchial tree under the following conditions: 1 mL/kg/time,  $\leq 20$  mL/time, total volume  $\leq 5$ –10 mL/kg, and suction at 100 mmHg negative pressure. The recovery rate was 40%–60%, and the recovered lavage solution was packed into a sterilized container with a culture sample (sputum 1 mL, bronchoalveolar lavage fluid 5 mL).

For sputum sample detection, at least 2–3 mL sputum was collected and sent to a sterile container for mNGS testing. 600  $\mu$ L sputum samples and 12  $\mu$ L sputum IC were collected and mixed in a 2 mL centrifuge tube. After mixing, the wall was broken by biological sample homogenizer (BioPrep-24, Hangzhou Jieyi Technology Co., Ltd., China). After that, 3 min was centrifuged by 12000 rpm centrifuge (LX-200, Haimen Kirin Bell instrument, China), and 400  $\mu$ L of the supernatant was absorbed into the genomic nucleic acid extraction or purification kit (MD013, Hangzhou Jieyi Biotechnology Co., Ltd., China). After that, reagents were added to the cartridge and finally put into the nucleic acid automatic detection reaction system construction system (NGSmaster™ library preparation, MAR002, Hangzhou Jieyi Biotechnology Co., Ltd.). In the

TABLE 1: The clinical data of 138 premature infants [n/%].

Basic data	Research group (n = 69)	Control group (n = 69)	$\chi^2/t$	P
Gender			0.727	0.394
Male	30 (43.48)	35 (50.72)		
Female	39 (56.52)	34 (49.28)		
Gestational age (weeks)	30.81 $\pm$ 3.16	30.93 $\pm$ 3.26	0.220	0.827
Body weight (kg)	1.91 $\pm$ 0.68	1.85 $\pm$ 0.62	0.542	0.589
Mode of production			0.267	0.606
Cesarean section	41 (59.42)	38 (55.07)		
Natural delivery	28 (40.58)	31 (44.93)		
Premature rupture of membranes			1.451	0.228
Yes	43 (62.32)	36 (52.17)		
No	26 (37.68)	33 (47.83)		
1 min Apgar scoring			0.116	0.733
$\leq 7$ points	35 (50.72)	37 (53.62)		
$> 7$ points	34 (49.28)	32 (46.38)		
Coma			0.038	0.845
Yes	17 (24.64)	18 (26.09)		
No	52 (75.36)	51 (73.91)		

abovementioned construction system, the DNA library is established after automatic nucleic acid extraction, endonuclease digestion, end repair, end adenylation, node ligation, and other procedures. The established library was quantitatively analyzed and summarized by real-time PCR (KAPA). The quantitative DNA library is sequenced in the illumina Nextseq system (Inman Inc., USA) with high throughput. The original data obtained by sequencing first filtered the low-quality sequences, then filtered the human-derived sequences (GRCh38.p13), and compared the remaining sequences with the reference microbial Gene Database (NCBINt, GenBank, and in-house curated genomic database) to determine the microbial species and sequence count.

For the detection of bronchoalveolar lavage fluid samples, respiratory physicians lavaged the focus under bronchoscope according to the lung imaging findings of the patients and obtained at least 2-3 mL bronchoalveolar lavage fluid (BALF) into aseptic containers for mNGS testing. Samples of lavage fluid and brush were sent to the laboratory for microbiological detection at the same time. In addition, the bacterial and fungal smears and culture of sputum were routinely detected in patients with pulmonary infection. 1.2 mL bronchoalveolar lavage fluid samples and 12  $\mu$ L bronchoalveolar lavage fluid IC were mixed in a 2 mL centrifuge tube, and then, the wall was broken by a biological sample homogenizer (BioPrep-24, Hangzhou Ausheng, China). After that, 12000 rpm was centrifuged for 3 min (LX-200, Haimen Qilin Bell instrument, China); absorb 400  $\mu$ L of the supernatant to the genomic nucleic acid extraction or purification kit (MD013, Hangzhou Jieyi Biotechnology Co., Ltd., China), and add other corresponding reagents to the card box as required, and finally put it into the automatic nucleic acid detection reaction system construction system (NGSmaster™ library preparation, MAR002, Hangzhou Jieyi Biotechnology

Co., Ltd., China). In the above-mentioned construction system, the DNA library is established after automatic nucleic acid extraction, endonuclease digestion, end repair, end adenylation, node ligation, and other procedures. The established library was quantitatively analyzed and summarized by real-time PCR (KAPA). The quantitative DNA library is sequenced in the illumina Nextseq system (Inman Inc., USA) with high throughput. The original data obtained by sequencing first filtered the low-quality sequences, then filtered the human-derived sequences (GRCh38.p13), and compared the remaining sequences with the reference microbial Gene Database (NCBINt, GenBank, and in-house curated genomic database) to determine the microbial species and sequence count.

**2.2.2. Treatment Scheme.** The patients in the control group were treated with routine treatment, including warmth, oxygen inhalation, sputum suction, and anti-infection. Cefotaxime sodium was mainly selected for anti-infection. The dose of cefotaxime sodium was 50 mg/kg each time, and the dose of cefotaxime sodium could be increased to 200 mg/(kg·d) by intravenous drip 3 times a day for patients with severe infection. The curative effect was evaluated after continuous treatment for 2-3 weeks. The medication regimen could be adjusted continuously according to the patient's condition.

On the basis of the control group, the patients in the observation group adjusted the anti-infective regimen according to the mNGS results of bronchoalveolar lavage fluid. Patients with pneumonia caused by bacteria can be treated with antibiotics, such as cefaclor, amoxicillin, azithromycin, meropenem, and cefuroxime. Patients with pneumonia caused by virus can be treated with detoxification and antiviral drugs. Patients with pneumonia caused by mycoplasma and chlamydia can be treated with erythromycin, meropenem, and azithromycin. The specific medication plan of the patients in the observation group should be



adjusted according to the severity of the patient's condition, body weight, drug allergy, and other indexes. The curative effect was evaluated after continuous treatment for 2-3 weeks. The medication plan could be adjusted continuously according to the changes of the patient's condition during the treatment period.

### 2.3. Observation Index

**2.3.1. Physical Examination of Pathogen.** The detection rate and distribution of pathogens were compared between the two groups. Pathogen physical examination rate = (number of pathogen positive cases/total number of cases in this group)  $\times 100\%$ .

**2.3.2. Clinical Curative Effect.** The third-grade standard was used to evaluate the clinical curative effect. Two weeks after treatment, according to the standard published by Jing [13], it was divided into three levels, consisting of markedly effective, effective, and ineffective, and the total effective was the total effective. Effective rate = (number of significantly effective cases + number of effective cases)/total number of cases  $\times 100\%$ . The 28-day mortality of the patients was calculated.

**2.3.3. The Antimicrobial NICU Use Time, Adjustment Frequency, NICU Stay Time, and Hospital Stay between the Two Groups.** At the end of treatment, the neonatal intensive care unit (NICU) use time, adjustment frequency, NICU stay time, and hospitalization time of the two groups were compared.

**2.3.4. Cytokine Level.** IMMULITE/IMMULIE1000 analyzer, immune scattering turbidimetry, sandwich, and chemiluminescence methods were used to detect serum cytokines (hs-CRP, PCT, and IL-6). The detection process was strictly in accordance with the instructions, before treatment and 2 weeks after treatment. All the kits were purchased from SIE-MENS company in Germany. According to the operation flow of the manufacturer's instructions, the processed samples were sent to the analyzer for detection. The corresponding cytokine concentration was recorded.

**2.4. Statistical Analysis.** The data were analyzed by SPSS23.0 software. The normal distribution of measurement data was expressed by the mean  $\pm$  standard deviation, a *t*-test was used for the comparison between groups, a frequency method was used for counting data, a  $\chi^2$  test was used for comparison between groups, and a bilateral test was used for all statistical tests. The ROC curve of the measurement index is drawn, the AUC value is calculated, and the prediction performance of each parameter is analyzed and evaluated. According to statistics, the actual range of AUC value is 0.5-1. The diagnostic value of AUC was lower when 0.5~0.7, moderate when AUC was 0.7~0.9, and higher when AUC > 0.9. The Youden index was used to determine the best predictive standard value of each parameter and its accuracy, sensitivity, specificity, PPV, NPV, and  $P < 0.05$ . There were significant differences in statistics.

## 3. Results

**3.1. Analysis of Clinical Data of Two Groups of Premature Infants.** First, we analyzed the clinical data of 138 premature infants. The comparison of clinical data between the two groups is shown in Table 1. There was no significant difference in clinical data between the two groups ( $P > 0.05$ ).

**3.2. Diagnostic Value of Traditional Culture and mGCS Detection in Preterm Infants with Infectious Pneumonia.** The positive rate of mNGS pathogens in lavage fluid was 92.75% (64/69) in the observation group and 52.17% (36/69) in the control group. We further analyzed the diagnostic value of traditional culture and mNCS detection in preterm infants with infectious pneumonia by ROC curve. The results showed that the ROC AUC of traditional culture was 0.752 (95%CI = 0.610~0.894) and the ROC AUC of mNCS was 0.934 (95%CI = 0.854~0.999). All results are shown in Figure 1.

**3.3. Application Effect of Traditional Culture and mGCS Detection in Pathogen Detection of Infectious Pneumonia in Premature Infants.** The application effect of traditional culture and mGCS detection in pathogen detection of infectious pneumonia in premature infants was analyzed. 35 cases of bacteria were detected in the observation group, of which *Klebsiella pneumoniae* (15.63%) and *Acinetobacter baumannii* (12.50%) were the highest. There were 20 cases of fungi, of which the detection rate of *Pneumocystis carinii* was the highest (12.50%). The detection rate of *Candida albicans* and *Aspergillus fumigatus* was 7.81%. There were 4 cases of virus, of which human sporovirus 5 was the main type of virus with a detection rate of 3.13%. There were 5 cases of *Chlamydia psittaci*, 1 case of *Mycobacterium tuberculosis*, and 1 case of *Mycobacterium Kansas*. A total of 26 cases of bacteria were detected in the control group, of which *Acinetobacter baumannii* was the highest, followed by *Klebsiella pneumoniae*, *Pseudomonas aeruginosa*, *Staphylococcus aureus*, *Streptococcus pneumoniae*, and *Serratia marcescens*. Nine cases of fungi, *Candida albicans* (13.89%), and *Aspergillus fumigatus* (11.11%) failed to detect virus and other mycoplasma. All results are shown in Table 2.

**3.4. Comparison of Clinical Efficacy between the Two Groups.** The clinical effects of the two groups were compared. After 2 weeks of treatment, 27 cases were significantly effective, 30 cases were effective, and 3 cases were ineffective in the observation group. The effective rate was 95.31%. The control group was significantly effective in 10 cases, effective in 15 cases, and ineffective in 11 cases. The treatment effective rate was 69.44%, and the difference was statistically significant ( $P < 0.05$ ). All results are shown in Figure 2.

**3.5. The Antimicrobial NICU Use Time, Adjustment Frequency, NICU Stay Time, and Hospital Stay between the Two Groups.** Comparing the NICU use time, adjusted frequency, NICU stay time, and hospitalization time of the two groups of patients, the observation group was significantly shorter than the control group in terms of antibiotic NICU use time, adjusted frequency, NICU stay time, and

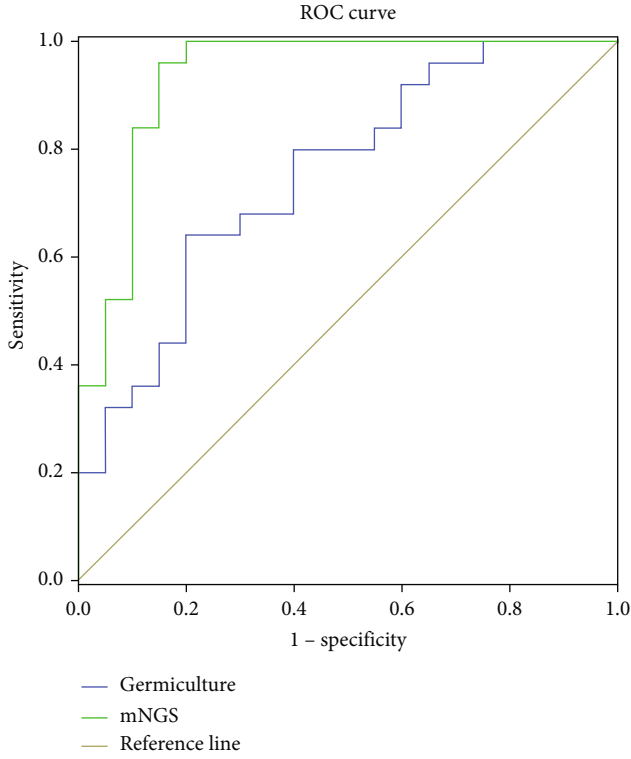


FIGURE 1: ROC curve of traditional culture and mGCS detection in the diagnosis of infectious pneumonia in premature infants.

hospital stay, and the difference was statistically significant ( $P < 0.05$ ). All results are shown in Table 3.

**3.6. Comparison of Cytokine Levels between the Two Groups after Treatment.** After treatment, the serum levels of IL-6, PCT and hs-CRP in both groups decreased significantly, and the difference was statistically significant ( $P < 0.05$ ). The observation group was significantly lower than the control group, and the difference was statistically significant ( $P < 0.05$ ). All the results are shown in Table 4.

#### 4. Discussion

As the normal physiological mechanism of premature infants cannot play an effective role, the sensitivity to the external environment is high. It is difficult to adjust and adapt, and the immune ability to bacteria is poor [14]. Respiratory function is in the tubule stage with low secretion of active substances on the lung surface, poor pulmonary compliance, and imperfect independent breathing [15, 16]. The need for the establishment of artificial channels and mechanical ventilation and other invasive means greatly increases the risk of respiratory infection in premature infants but also have the risk of inhibiting lung development, leading to chronic respiratory sequelae [17, 18].

Early identification of infectious pathogens and targeted anti-infection is the key to the treatment of infectious pneumonia. Traditional pathogen culture requires high conditions, long cycle, and low positive rate, and the use of antibiotics affects its culture. A large number of clinical data

TABLE 2: Analysis and comparison of pathogen physical examination between the two groups ( $n/\%$ ).

Pathogen	Observation group ( $n = 64$ )	Control group ( $n = 36$ )
Bacteria		
Pseudomonas aeruginosa	5 (7.81)	5 (13.89)
Klebsiella pneumoniae	10 (15.63)	6 (16.67)
Acinetobacter baumannii	8 (12.50)	8 (22.22)
Streptococcus pneumoniae	2 (3.13)	2 (5.56)
Staphylococcus aureus	5 (7.81)	5 (13.89)
Legionella pneumophila	2 (3.13)	—
Nocardia	1 (1.56)	—
Serratia marcescens	1 (1.56)	1 (2.78)
Burkholderia cepacia	1 (1.56)	—
Fungus		
Candida albicans	5 (7.81)	5 (13.89)
Pneumocystis	8 (12.50)	—
Yersini		
Aspergillus fumigatus	5 (7.81)	4 (11.11)
Virus		
Human spore virus type 1	1 (1.56)	—
Human sporrash virus 5	2 (3.13)	—
Cytomegalovirus	1 (1.56)	—
Chlamydia psittaci	5 (7.81)	—
Mycobacterium tuberculosis	1 (1.56)	—
Mycobacterium Kansas	1 (1.56)	—

show that the inability to identify the infectious pathogen of infectious pneumonia as soon as possible is one of the important reasons for the high mortality of this kind of disease [19]. The unknown pathogen of infection has seriously affected the effect of empirical anti-infective treatment [20]. Therefore, there is an urgent need for new detection techniques to quickly and accurately find infectious pathogens and give accurate anti-infective treatment.

In this study, the detection rate of mNGS pathogens in lavage fluid of the observation group was 92.75%, which was significantly higher than that of the control group (52.17%). This study systematically compared mNGS and traditional culture methods and found that mNGS has advantages in many aspects. First, mGCS has higher diagnostic value for infectious pneumonia in premature infants. The ROC curve analysis showed that the traditional culture ROCAUC was 0.752, which was significantly lower ROCAUC0.934 which was detected in mNCS. In addition,

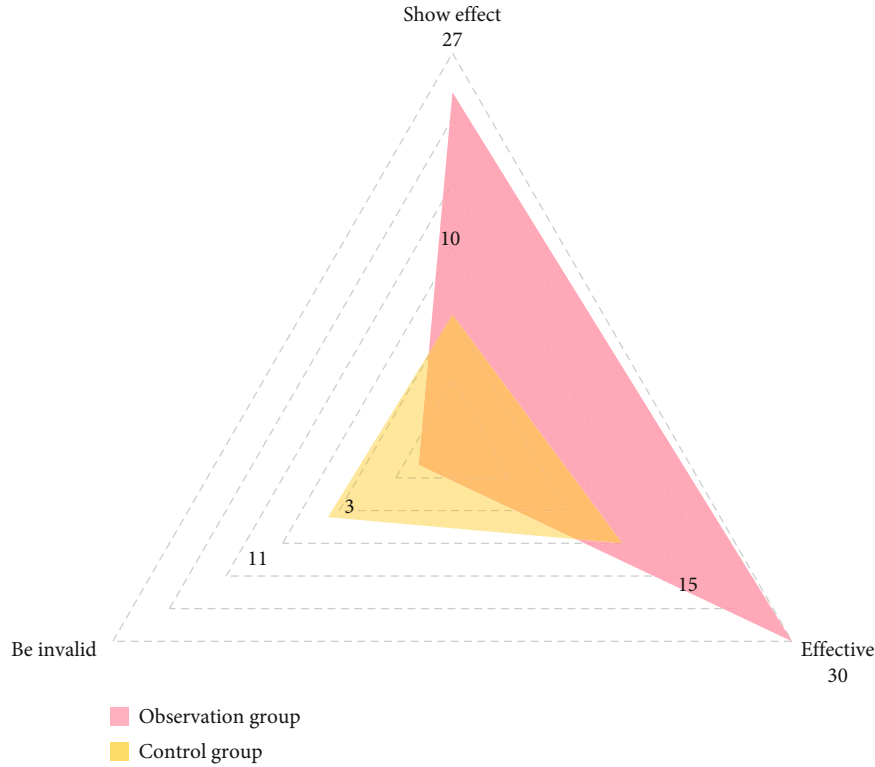


FIGURE 2: Comparison of clinical efficacy between the two groups.

TABLE 3: The antimicrobial NICU use time, adjustment frequency, NICU stay time, and hospital stay between the two groups  $[\bar{x} \pm s]$ .

Grouping	$N$	Antimicrobial NICU use time (d)	Adjustment frequency of antibiotics (times)	NICU residence time (d)	Hospitalization time (d)
Observation group	64	$16.47 \pm 2.68$	$2.41 \pm 0.51$	$10.65 \pm 4.46$	$18.58 \pm 2.66$
Control group	36	$19.43 \pm 3.62$	$3.77 \pm 0.62$	$14.78 \pm 5.51$	$21.96 \pm 4.43$
$t$		4.659	11.830	4.078	4.772
$P$		<0.05	<0.05	<0.05	<0.05

TABLE 4: Cytokine levels between the two groups after treatment  $[\bar{x} \pm s]$ .

Grouping	$N$	IL-6 (ng/mL)		PCT (ng/mL)		hs-CRP (mg/L)	
		Before treatment	After treatment	Before treatment	After treatment	Before treatment	After Treatment
Observation group	64	$95.22 \pm 15.06$	$73.76 \pm 7.01^*$	$25.27 \pm 1.93$	$12.62 \pm 1.88^*$	$29.96 \pm 6.66$	$18.42 \pm 4.12^*$
Control group	36	$95.39 \pm 15.33$	$80.97 \pm 14.32^*$	$25.36 \pm 2.01$	$20.24 \pm 0.84^*$	$30.10 \pm 6.74$	$25.18 \pm 6.74^*$
$t$		0.054	3.380	0.221	27.922	0.100	6229
$P$		>0.05	<0.05	>0.05	<0.05	0.920	<0.05

\*Compared with that before treatment, the difference was statistically significant ( $P < 0.05$ ).

mNGS has a clear advantage in detecting pathogens such as *Klebsiella*, anaerobes, *Pseudomonas*, viruses, and *Mycoplasma*. The results of this study showed that the proportion of pathogens in the observation group was bacteria, fungi, viruses, and other pathogens from high to low. And most of the bacteria were gram-negative bacteria. *Pseudomonas aeruginosa*, *Acinetobacter baumannii*, and *Klebsiella pneumoniae* were the main gram-negative bacteria. *Staphylococcus aureus* was the main gram-positive bacteria. Therefore,

anti-*Pseudomonas aeruginosa*  $\beta$ -lactam drugs should be considered in the empirical anti-infection of infectious pneumonia in premature infants and vancomycin should be added if necessary. 20 cases of fungi were detected in the observation group. We found that most of these premature infants had a history of hormone treatment, so we should routinely improve G test and GM test and experience antifungal therapy as soon as possible. In addition, the observation group also detected rare pathogens such as

Nucasmella, Mycobacterium tuberculosis, and Mycobacterium Kansas. MNGS can sequence hundreds of thousands to millions of DNA molecules at one time and can detect the gene sequences of culturable and unculturable microorganisms, bypassing the process of microbial isolation and culture. It has the characteristics of high positive rate, high speed, and high sensitivity in pathogen detection [21–23]. The traditional culture conditions of these pathogens are very high, which generally need to be cultivated in tuberculosis hospitals, suggesting that mNGS can improve the detection rate of rare pathogens.

In this study, 5 premature infants with severe pneumonia were finally diagnosed with Chlamydia psittaci infection by mNGS. It is reported that Chlamydia psittaci pneumonia accounts for about 1% of community-acquired pneumonia [24]. The sensitivity and specificity of traditional serological test or PCR test are not high, and the pathogen is extremely difficult to culture. In the past, most patients were missed or misdiagnosed due to the limitation of detection conditions. With the popularization of mNGS technology, the disease is reported more and more [25, 26]. The virus is extremely difficult to cultivate in the ordinary laboratory of the hospital, and the diagnosis of viral pneumonia has always been a clinical problem. Clinical diagnosis combined with medical history and chest CT manifestations for empirical diagnosis, the accurate diagnosis, and treatment of patients are seriously lagging behind [27–30]. In this study, no virus was detected in the control group, indicating that mNGS has a good effect in the diagnosis of virus infection.

Most of the pathogenic bacteria in patients with pneumonia are unknown. Patients with severe pneumonia often require long-term, high-dose broad-spectrum antibiotics. This phenomenon has led to the rising rate of antibiotic resistance of pathogenic bacteria, which is an urgent problem to be solved globally. Our findings showed that early identification of pathogens and timely adjustment of treatment plan through mNGS could reduce the adjustment frequency and NICU use time of antibiotics, which will provide a new direction for the management of antibiotics. With the progress of technology, we expect that mNGS can detect drug resistance genes and better guide clinical anti-infective treatment. At the same time, it was found that the effective rate of clinical treatment in the experimental group was higher. The length of stay and the cost of hospitalization were lower, which improved the prognosis of patients and reduced their economic burden. The above data analysis suggested that mNGS played a positive role in guiding the choice of treatment for premature infants with infectious pneumonia. The limitation of the mNGS method for the diagnosis of infectious pneumonia is that this technology is affected by the equipment of the hospital, because some hospitals do not routinely use the mNGS method in the diagnosis of infectious pneumonia. This study still has some shortcomings. Firstly, the quality of this study is limited due to the small sample size we included in the study. Secondly, this research is a single-center study, and our findings are subject to some degree of bias. Therefore, our results may differ from those of large-scale multicenter studies from other academic institutes. This research is still clinically sig-

nificant, and further in-depth investigations will be carried out in the future.

To sum up, mNGS is of high value in the diagnosis of infectious pneumonia in premature infants. It can significantly improve the detection rate of pathogens in severe pneumonia and can adjust the treatment plan according to the pathogen detection results of mNGS. It can shorten the time of use of antibiotics and adjust frequency and hospital stay.

## Data Availability

The datasets used and analyzed during the current study are available from the corresponding author upon reasonable request.

## Conflicts of Interest

The authors declare that they have no conflicts of interest.

## References

- [1] D. B. McArthur, “Emerging infectious diseases,” *Nursing Clinics*, vol. 54, no. 2, pp. 297–311, 2019.
- [2] J. Yang, N. Rejiafu, and L. Yongqiao, “Incidence and related factors of bronchopulmonary dysplasia in premature infants from 2015 to 2018,” *Chinese Journal of Child Health*, vol. 27, no. 10, 2019.
- [3] Z. Min, L. Yujiang, and C. Xiaoxia, “Analysis of influencing factors of bronchopulmonary dysplasia in premature infants,” *Journal of Guizhou Medical University*, vol. 44, no. 2, pp. 213–217, 2019.
- [4] S. Kadambari, E. Whittaker, and H. Lyall, “Postnatally acquired cytomegalovirus infection in extremely premature infants: how best to manage?,” *Archives of Disease in Childhood. Fetal and Neonatal Edition*, vol. 105, no. 3, pp. 334–339, 2020.
- [5] J. Xueyang, R. Hongyu, N. Xudong, Q. Tian, and L. Jianguo, “Research progress on detection methods of pathogens in lower respiratory tract infection,” *Chinese Journal of Zoonoses*, vol. 35, no. 3, pp. 263–270, 2019.
- [6] H. A. Mbunkah, A. Marzel, S. Schmutz et al., “Low prevalence of transmitted HIV-1 drug resistance detected by a dried blood spot (DBS)-based next-generation sequencing (NGS) method in newly diagnosed individuals in Cameroon in the years 2015–16,” *Journal of Antimicrobial Chemotherapy*, vol. 73, no. 7, pp. 1917–1929, 2018.
- [7] D. Ou, B. Chen, T. A. Hadi, W. Niu, and Y. R. Alfiansah, “Next-generation sequencing revealed specific microbial symbionts in *Porites lutea* with pigment abnormalities in North Sulawesi, Indonesia,” *Acta Oceanologica Sinica*, vol. 37, no. 12, pp. 78–84, 2018.
- [8] X. L. Wang, Y. Ma, S. H. Wang, W. B. Dong, and X. P. Lei, “A meta-analysis of fluconazole for the prevention of invasive fungal infection in preterm infants,” *American Journal of Translational Research*, vol. 13, no. 2, pp. 434–447, 2021.
- [9] K. R. Kumar, M. J. Cowley, and R. L. Davis, “Next-generation sequencing and emerging technologies,” *Seminars in Thrombosis and Hemostasis*, vol. 45, no. 7, pp. 661–673, 2019.
- [10] P. Chen, W. Sun, and Y. He, “Comparison of the next-generation sequencing (NGS) technology with culture



- methods in the diagnosis of bacterial and fungal infections,” *Journal of Thoracic Disease*, vol. 12, no. 9, pp. 4924–4929, 2020.
- [11] T. Hu, N. Chitnis, D. Monos, and A. Dinh, “Next-generation sequencing technologies: an overview,” *Human Immunology*, vol. 82, no. 11, pp. 801–811, 2021.
  - [12] Y. D. Liu and L. Q. Wu, “Application of next-generation sequencing technology in prenatal screening and diagnosis,” *Zhonghua Yu Fang Yi Xue Za Zhi*, vol. 55, no. 9, pp. 1037–1042, 2021.
  - [13] C. Jing, “Clinical efficacy and safety of fiberoptic bronchoscopic bronchoalveolar lavage in the treatment of refractory pneumonia,” *Chinese practical medicine*, vol. 15, no. 3, pp. 41–42, 2020.
  - [14] R. Lu, L. Hongju, and X. Yang, “Analysis of risk factors of pulmonary infection in premature infants,” *Journal of community medicine*, vol. 18, no. 21, pp. 1479–1482, 2020.
  - [15] Y. Xie, S. Ying, C. Qiang, D. Yuannan, and S. Rubing, “Study on the relationship between chorioamnionitis, umbilical cord inflammation and lung injury in premature infants,” *Chinese journal of neonatal pediatrics*, vol. 33, no. 2, pp. 109–112, 2018.
  - [16] J. Pan, C. Zhan, T. Yuan et al., “Effects and molecular mechanisms of intrauterine infection/inflammation on lung development,” *Respiratory Research*, vol. 19, no. 1, p. 93, 2018.
  - [17] K. Qiong, P. Yi, and J. Xiaorong, “Analysis of risk factors and nursing countermeasures of pulmonary infection in premature infants in intensive care,” *Practical Journal of Cardiac, Cerebrovascular and Vascular Diseases*, vol. 28, no. S1, pp. 197–199, 2020.
  - [18] X. Li, Z. Lianhong, and S. Ting, “Analysis of risk factors and preventive measures of pulmonary infection in premature infants in pediatric intensive care unit,” *Anhui medicine*, vol. 21, no. 7, pp. 1266–1269, 2017.
  - [19] D. Senol Cali, J. S. Kim, S. Ghose, C. Alkan, and O. Mutlu, “Nanopore sequencing technology and tools for genome assembly: computational analysis of the current state, bottlenecks and future directions,” *Briefings in Bioinformatics*, vol. 20, no. 4, pp. 1542–1559, 2019.
  - [20] W. J. Guan, J. C. Li, F. Liu et al., “Next-generation sequencing for identifying genetic mutations in adults with bronchiectasis,” *Journal of Thoracic Disease*, vol. 10, no. 5, pp. 2618–2630, 2018.
  - [21] S. Wenwen, G. Jin, and F. Lin, “Diagnostic value of metagenome second-generation sequencing in different types of tuberculosis,” *Chinese journal of tuberculosis and respiration*, vol. 44, no. 2, pp. 96–100, 2021.
  - [22] A. S. Handel, W. J. Muller, and P. J. Planet, “Metagenomic next-generation sequencing (mNGS): SARS-CoV-2 as an example of the technology’s potential pediatric infectious disease applications,” *Journal of the Pediatric Infectious Diseases Society*, vol. 10, Supplement\_4, pp. S69–S70, 2021.
  - [23] D. Guldemir, S. Usluca, and A. S. Nalbantoglu, “Genome sequencing of *Leishmania infantum* causing cutaneous leishmaniasis from a Turkish isolate with next-generation sequencing technology,” *Acta Parasitologica*, vol. 66, no. 1, pp. 75–80, 2021.
  - [24] S. L. Gough, J. Carrick, S. L. Raidal et al., “Chlamydia psittaci infection as a cause of respiratory disease in neonatal foals,” *Equine Veterinary Journal*, vol. 52, no. 2, pp. 244–249, 2020.
  - [25] E. S. Klochikhina, V. E. Shershov, V. E. Kuznetsova, S. A. Lapa, and A. V. Chudinov, “Specificities of multi-primer polymerase chain reaction optimization for the detection of infectious pneumonia agents in human,” *Fine Chemical Technologies*, vol. 16, no. 3, pp. 225–231, 2021.
  - [26] S. A. Lapa, E. S. Klochikhina, R. A. Miftakhov, A. M. Zolotov, A. S. Zasedatelev, and A. V. Chudinov, “Multiplex PCR for identification of bacterial pathogens of infectious pneumonia,” *Russian Journal of Bioorganic Chemistry*, vol. 46, no. 5, pp. 859–861, 2020.
  - [27] B. Allen, C. Cheng, and V. Chan, “Association of noninfectious pneumonia with ustekinumab use,” *JAMA Dermatology*, vol. 155, no. 2, pp. 1–4, 2019.
  - [28] Z. Zainudin, Z. Kassim, and N. Othman, “Congenital pneumonia,” *Journal of Pediatric Infectious Diseases*, vol. 13, no. 4, pp. 255–267, 2018.
  - [29] N. V. Saarinen, V. M. Stone, M. M. Hankaniemi et al., “Antibody responses against enterovirus proteases are potential markers for an acute infection,” *Viruses*, vol. 12, no. 1, p. 78, 2020.
  - [30] Y. Bastidas-Legarda Leidy and S. I. Khakoo, “Conserved and variable natural killer cell receptors: diverse approaches to viral infections,” *Immunology*, vol. 156, no. 4, pp. 319–328, 2019.

## Research Article

# Study on Antidepressant Emotion Regulation Based on Feedback Analysis of Music Therapy with Brain-Computer Interface

Mengru Sun 

*School of Sookmyung Women's University, Seoul 04310, Republic of Korea*

Correspondence should be addressed to Mengru Sun; 15211010306@stu.cpu.edu.cn

Received 3 August 2022; Revised 25 August 2022; Accepted 6 September 2022; Published 5 October 2022

Academic Editor: Hangjun Che

Copyright © 2022 Mengru Sun. This is an open access article distributed under the Creative Commons Attribution License, which permits unrestricted use, distribution, and reproduction in any medium, provided the original work is properly cited.

In today's society, people with poor mental ability are prone to neuropsychiatric diseases such as anxiety, ADHD, and depression due to long-term negative emotions. Although conventional Western medicine has certain curative effect, these drugs have significant anticholinergic side effects central toxicity as well as cardiovascular and gastrointestinal side effects which limit their application in the elderly. At present, several antidepressants used in clinic have certain limitations. According to the symptoms of depression, this paper proposes a feedback emotion regulation method of brain-computer interface music therapy. This method uses special music stimulation to regulate the release of inhibiting sex hormones in the body, reduce the influence of negative emotions on the internal environment of the body, and maintain the steady state of the body. In this method, EEG is used as the emotional control signal of depressed patients, and this biological signal is transformed into music that depressed patients can understand, so as to clarify their physiological and psychological state and realize emotional self-regulation by feedback.

## 1. Introduction

In this review, music therapy is examined as evidence of a treatment. To evaluate the effect of music therapy on behavioral, social, cognitive, and emotional problems in Alzheimer's patients, a randomized controlled trial was conducted to report the clinical outcomes of music therapy for behavioral, social, cognitive, and emotional problems in Alzheimer's patients [1]. Music, as a specific stimulus, combines motion and stimulation through different sensory pathways to obtain motor and emotional responses. In this study, a prospective, randomized, controlled, and single blind method was used to study the effects of music therapy on motor and emotional function of Parkinson's patients. MT is effective for motor, emotional, and behavioral functions. We propose active MT as a new method to be included in PD rehabilitation program [2]. Many studies have shown that listening to music activates many brain structures involved in cognition, sensorimotor, and emotional processing. This paper briefly summarizes the factors affecting the effect of music therapy. Then, neuroscience research uses music to investigate emotions, perceptual-action intermedi-

aries, and social cognition, including illustrative correlations in these areas of music therapy [3]. There is evidence that music therapy can improve the mental health of patients with depression. Therefore, the possible mechanism of this complex intervention is studied, and it is considered that music therapy is partially effective, because active music production within the therapeutic framework provides patients with new opportunities for aesthetic, physical, and relational experiences [4]. Music therapy is a potential nondrug treatment for the behavioral and psychological symptoms of dementia, and while some studies have found it helpful, most are small and uncontrollable. Music therapy is a safe and effective method to treat anxiety and restlessness in patients with moderate and severe Alzheimer's disease. This is consistent with the results of some noncontrol studies on music therapy for dementia [5]. The field of brain-computer interface represents a more interesting field in neurophysiology research, because it studies the development of machines that transform the brain's "thoughts" into certain predefined behaviors. The research shows that the EEG data measured in complex dynamic visual motion tasks carry enough information about the current motion, which can be successfully

extracted by appropriate signal processing and recognition methods [6]. The idea of brain-computer interface based on EEG is to help those who are unable to communicate ideas due to neuromuscular diseases and thus affected by motor disorders. Wavelet transform and other techniques are used to preprocess the data, and linear predictive coding is used to determine autoregressive coefficients as feature vectors, and neural networks are trained for classification. Then, the data of 140 random experiments are tested on the trained network, and the efficiency of this method is determined to be 71.5% [7]. The application of steady-state visual evoked potential (SSVEP) in brain-computer interface (BCI) system has attracted more and more attention. An online multichannel brain-computer interface system based on SSVEP is proposed, which uses canonical correlation analysis (CCA) to extract frequency information related to SSVEP. Experimental results show that the BCI system has high performance, with an average accuracy of 95.3% [8]. People can learn to control the EEG characteristics composed of sensorimotor rhythm amplitudes and can use this control to move the cursor to the target on the screen in one or two dimensions. The results show that the order selection of autoregressive model is an important determinant of BCI performance, which should be based on the criteria reflecting system performance [9]. A time-frequency (TF) method for extracting features from electroencephalogram (EEG) images of left and right hand movements is studied in this paper. Feature extraction process (FEP) extracts frequency domain information to form features, and at the same time, time-frequency resolution is obtained by localizing the fast Fourier transform (FFTs) of the signal to a specific window of time localization. This method is quantified by classification accuracy (CA), information transmission rate (IT), and mutual information (MI) and achieves good performance [10]. Common space mode (CSP) is one of the most widely used methods in brain-computer interface (BCI), which can enhance the separability of multichannel electroencephalogram (EEG) and other brain signals. This paper proposes to divide each class into many subclasses and describes this problem in a redesigned graph embedding framework with vertices as cluster centers. We have also redefined the traditional FLDA in our diagram embedding framework, which is helpful to develop and understand the proposed method. Experimental results show the superiority of this method [11]. Whether successful antidepressant therapy is associated with changes in psycho-behavioral strategies used to regulate mood is unclear. We examined depressive symptoms and emotion regulation strategies before and after antidepressants. Since we evaluated acute outcomes, it is not clear whether the effects of antidepressants on mood regulation will persist over time [12]. As we all know, serotonin can regulate mood, sleep, and appetite systematically, so it is related to the control of many behaviors and physiological functions. This paper reviews the latest progress in this field and discusses the mechanism of antidepressant acting on this target and its possible interaction with other components of serotonergic neurotransmission [13]. Emotional regulation and impulse are the core aspects of borderline personality disorder (BPD) pathology. Although these two problems may be particularly com-

bined in BPD, so far, few studies have studied impulsive emotion regulation in BPD. The results of this study are consistent with the view that the disorder of amygdala-prefrontal neural network in BPD patients is compensated by the subcortical loop involving subthalamic nucleus, which leads to the inhibition of normal behavior in these patients [14]. There is a great deal of evidence that stress response and stress adaptation dysfunction are in the pathophysiological mechanism of human depression (MDD). Endogenous opioid neurotransmission activates mu-opioid receptors to participate in stress and emotion regulation and is further related to MDD [15].

## 2. Music Therapy

**2.1. Mechanism of Music Therapy.** Music therapy is a process of healing wounds, regulating emotions and physical functions by using melody, rhythm, and unique language and movements of music. In the limbic system, the amygdala is the central hub of neural circuit, which is deeply involved in the initiation, generation, detection, maintenance, regulation, and termination of emotions. Among them, blood level-dependent fMRI signals were relatively enhanced in ventral striatum and anterior insular lobe, while the amygdala, hippocampus, parahippocampal gyrus, and temporal polar region were relatively enhanced in musician's happy music stimulation. The fMRI-dependent signals from the amygdala, hippocampus, parahippocampal gyrus, and temporal polar regions were proportionally enhanced by randomly played discordant musical stimuli. These findings indicate that the center near the hippocampus plays an important role in the processing of acoustic roughness.

Balli et al.'s music research reveals for the first time that different regions of human amygdala have different functional characteristics in response to musical stimuli. In this study, harmonic piano music and sharp piano music were used as positive and negative stimuli, respectively, and the effects of two types of music on the dependence intensity of blood samples in the amygdala were examined. The results showed that under two different types of music stimulation, the dependent signal of blood samples in basolateral region increased, while the level-dependent signal of blood samples on amygdala surface decreased. The sample was weakened and the level-dependent signal from the blood sample was amplified in the superficial region of the amygdala. The functional network between brain structures involved in emotional processing is shown in Figure 1.

**2.2. Social Functions of Music.** Society is a living space where people can maintain each other and live together for a long time. People constantly participate in various social functions, and music activities are one of the comprehensive functions involving various social functions.

The early form of music is to express personal communication information through sound level and volume. With the development of human society, music activities greatly enrich the ways and means of expressing emotions, and



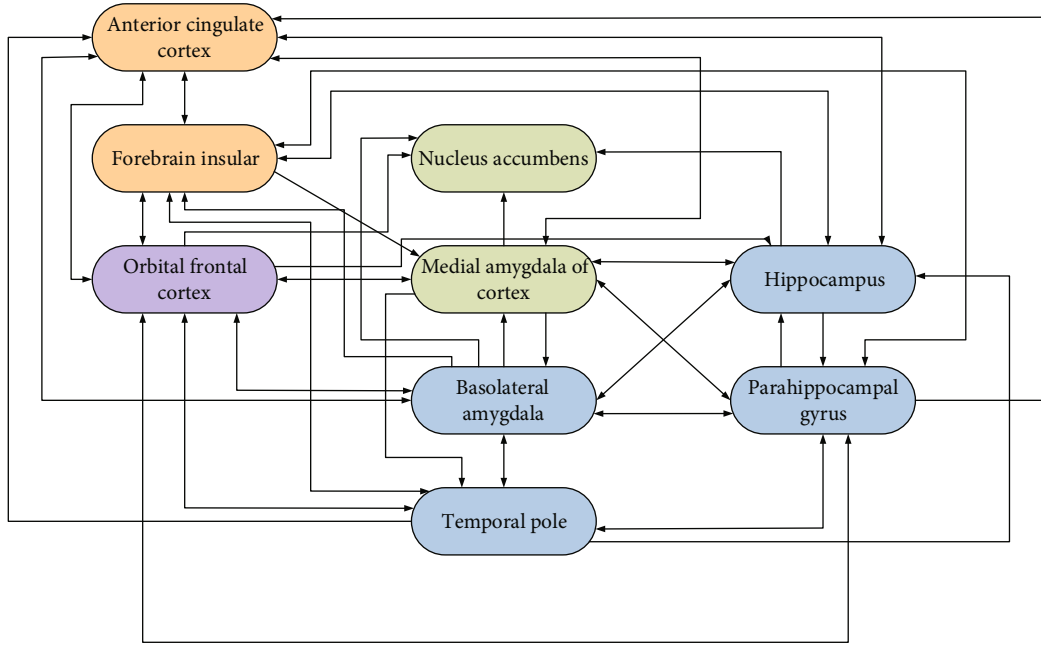


FIGURE 1: Functional network diagram of brain structure involved in emotional processing.

people also integrate national culture and social environment into music. The reason why music can evolve from simple thought expression to contemporary music functions such as concert, recital, and drama is the result of the interaction between music and society. Examples of the influence of music creation on social individuals include the following:

Close communication of thoughts and emotions strengthens social skills, builds mutual trust, and effectively prevents social isolation. Compared with traditional medical methods, it is more helpful to cure mental diseases. Therefore, involving depressed patients in making music is usually more beneficial to treat depression than listening to music, because it can improve expression and communication skills, improve social relations, and prevent social isolation of depressed patients. In addition, making music involves changes in social cognitive skills. Social cognition is a process of analyzing and understanding the external environment.

In a word, different music activities are often accompanied by changes in different social activities. These social activities can affect the external performance of depressed patients, for example, improve social skills, improve emotional state, and improve cognitive level. This provides theoretical support for the follow-up use of music activities as a means to regulate depression.

**2.3. Methods of Music Therapy Feedback to Regulate Depression.** According to the above theoretical knowledge, this paper proposes a brain-computer interface music therapy feedback analysis of depression emotion regulation method. The flow is shown in Figure 2.

Long-term depression is the main symptom of depression. When patients with depression are stimulated by external pressure, they will process the stimulus through the structure of limbic system and produce corresponding nega-

tive emotions. One way to regulate depression through music feedback is to use EEG signals to monitor patients' emotions and convert this signal into music signals that patients can understand.

### 3. Algorithm of EEG Signal Processing by CNN

**3.1. Basic Network of Convolution Neural Network.** CNN network is an important part of deep learning algorithm research. Its essence can be regarded as an artificial neural network that transmits feedback, inspired by the abstract process of human vision. Every neuron in CNN network can be considered as a neuron corresponding to human visual field, which is simulated and does not need much manual processing to train. The CNN model is not as popular as it used to be in the EEG classification of movie tasks. A very important reason is that until now, it is difficult to find an effective transformation method to represent EEG signals, so that the EEG shape of signals can better match the way CNN processes data. Figure 3 shows the basic structure of CNN network.

As shown in Figure 3, the basic structure of CNN network is mainly composed of input layer, convolution layer, pooling layer, FC layer, and other network structure layers.

The important network layers are explained below.

**3.1.1. Convolution Layer.** Convolution layer is related to the performance of the whole network when assembling and decomposing data. The convolution calculation of the input data of the previous layer through convolution adjustment is essentially a weight matrix, and the characteristics of the convolution layer can be finally determined after the offset value is processed by a certain trigger function.

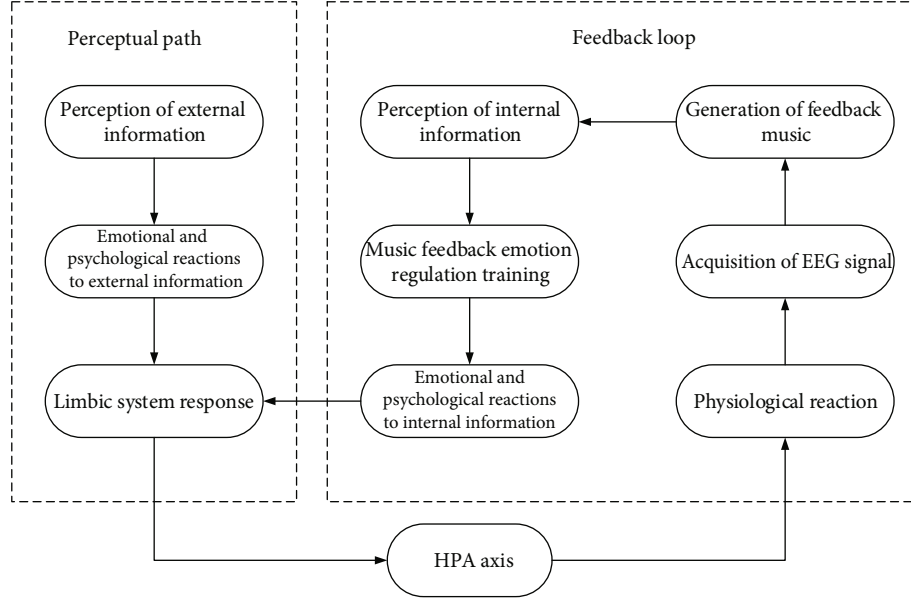


FIGURE 2: Description diagram of music feedback control method for depression based on EEG.

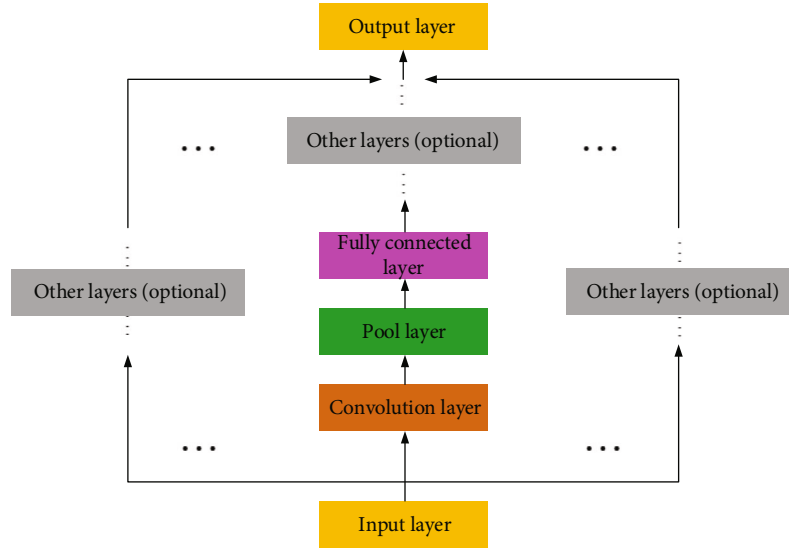


FIGURE 3: Basic structure diagram of CNN network.

Convolution transport can be expressed mathematically by

$$k * g = \int_{-\infty}^{+\infty} k(\tau)g(\tau - t)dt. \quad (1)$$

In this way, the convolution editing process of convolution layer can be expressed as

$$C_j^L = f\left(\sum_{i \in N^{L-1}} C_i^{L-1} * W_j^L + b_j^L\right), \quad (2)$$

where  $C_j^L$  represents the  $J$ th feature map of the  $L$ th convolution layer,  $C_i^{L-1}$  represents the  $L - 1$  layer, that is, the feature map of the previous layer, which is also the input of the  $L$ th layer, and  $W_j^L$  is the feature layer of the  $J$ th layer.

It should be noted that the connection weights between different neurons on the same layer are universal, so this design is beneficial to the convergence of the model. In order to improve the performance of network architecture, functions such as ReLU, sigmoid, and tanh are often used. Formulas (3), (4), and (5), respectively, express different mathematical expressions of the above joint activation function:

$$\text{ReLU} : f(x) = \max(0, x), \quad (3)$$

$$\text{sigmoid} : f(x) = \frac{1}{1 + e^{-x}}, \quad (4)$$

$$\text{tanh} : f(x) = \frac{1 - e^{-2x}}{1 + e^{-2x}}. \quad (5)$$

**3.1.2. Pooling Layer.** The neurons in the pooling layer are the same as those in the convolution layer. Generally speaking, there are two commonly used pooling methods: maximum pooling and average pooling. For comparison, the maximum value is selected as the output of this range, and the merging process can be simplified to

$$P_j^K = \text{down} = \left( \sum_{i \in N^{K-1}} C_i^K \beta_j^K + b_j^K \right), \quad (6)$$

where  $P_j^K$  represents the  $J$ th feature map of the  $K$ th pooled layer,  $\beta_j^K$  is the multiplier deviation of the  $J$ th pooled core of the  $K$ th layer,  $b_j^K$  is the corresponding additional deviation, and  $\text{down}(\cdot)$  represents different collections.

Generally, convolution layer and pooling layer appear alternately. As shown in Figure 4, the data set is represented by convolution layer with convolution size of  $2 \times 2$  and pooling layer with size of  $2 \times 2$ . Examples of average pooling and maximum pooling are given.

**3.1.3. Full Connection Layer.** Generally speaking, the whole CNN network has one or more FC layers. At present, the activation functions commonly used in FC layers are ReLU and sigmoid.

### 3.2. EEG Classification Model Based on CNN Network

**3.2.1. Network Topology.** In this section, we build a multi-layer network model to analyze data. The whole identification process is shown in Figure 5.

(1) *Build a CNN Model for ECoG Data.* The CNN model structure is shown in Figure 6.

**Input layer:** in the input layer, each original signal is a tensor matrix, and the sample data is transformed into a tensor matrix with dimension  $[N_e, N_s, 1]$ , so that EEG data can be regarded as gray images, which is

$$a_j^0(m) = x_i(m), \quad (7)$$

wherein  $x_i(m)$  represents the data of the  $m$ th sampling point of the  $i$ th electrode channel,  $1 \leq i \leq N_e$ ,  $1 \leq m \leq N_s$ .

**Conv1 layer:** according to the characteristics of convolution layer, ECoG data is processed by

$$a_j^{(L)}(m) = \text{ReLU} \left( \sum_{i=1}^{N_s} a_i^{(L-1)}(m) * W_j^{(L-1)}(m) + b_j^{(L-1)} \right), \quad (8)$$

where  $L$  is the number of convolution layers, there are four convolution layers, and each convolution layer is followed by a pooling layer.

**Pool 1 layer:** it can speed up the processing speed of the algorithm without losing data, and the calculation formula is shown in

$$a_j^{(K)}(m) = \max \left( \sum_{i=1}^{N_e} a_i^{(K-1)}(m) \cdot \beta_j^{(L-1)}(m) + b_j^K \right), \quad (9)$$

where  $K$  is the number of pooled layers and there are four pooled layers, so the values of  $K$  are 2, 4, 6, and 8.  $\beta_j^K$  is the coefficient bias and  $b_j^K$  is the additional bias.

**FC1:** FC1 is the first fully connected layer to properly increase network depth.

**Output layer:** the output layer can use softmax function to classify the previously extracted high-level data, and the calculation expression is shown in

$$a^{(11)} = \text{soft max} \left( \sum_i^{N_s} a^{(10)} W^{(11)} + b^{(11)} \right). \quad (10)$$

The expression for softmax is shown in

$$\text{soft max}(x_i) = \frac{e^{x_i}}{\sum_{n=1}^N e^{x_n}}. \quad (11)$$

Finally, a vector  $a^{(11)} = [a_0^{(11)}, a_1^{(11)}]^T$  is output,  $a_0^{(11)}$  represents the probability of belonging to a fictitious task, and  $a_1^{(11)}$  represents the probability of not belonging to a fictitious task.

(2) *Constructing CNN Model from EEG Data.* The CNN network topology based on EEG data is similar to the network topology based on ECoGEEG signal. The difference is that the number of network layers used is different.

It should be noted that in order to improve the efficiency of the algorithm, Dropout and L1 adjustment are also used to prevent overfitting as much as possible. In order to promote the complex cooperation between neurons and improve the learning ability of the model, the weights of neurons are randomly reset with a certain probability. The above two methods are widely used in neural network training to reduce overfitting. This article is also based on CNN mechanism to suppress the influence of overfitting.

**3.2.2. Network Parameter Training.** The CNN model is based on ECoG and EEG-EEG data. As you can see from the previous section, using the input data vector  $x$ , the output of the model is  $a^{(11)} = [a_0^{(11)}, a_1^{(11)}]^T$ , where  $a_i^{(11)}$  represents the prediction probability of each class, giving a new result. If the actual title of the sample is  $y = [y_0, y_1]^T$ , then when  $N$  samples are taught, the loss function is shown in

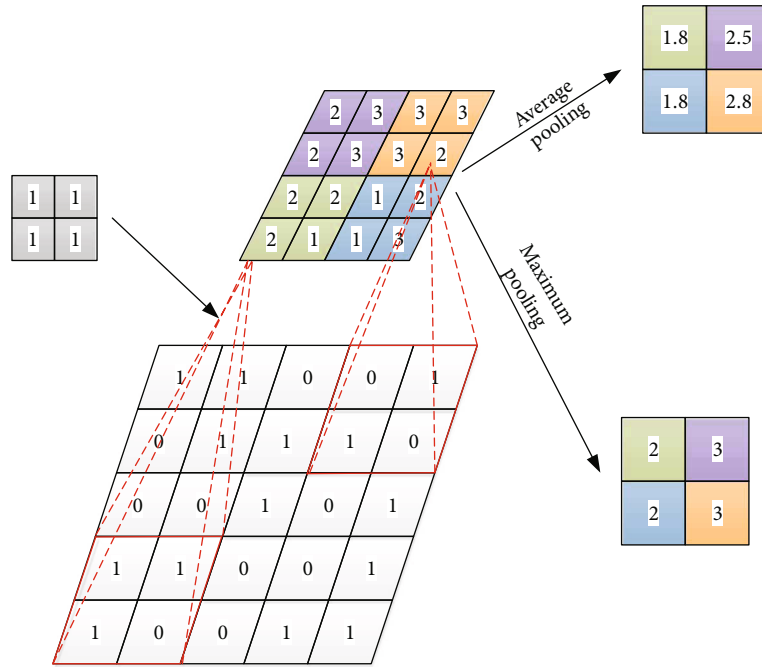


FIGURE 4: Example of convolution and pooling.

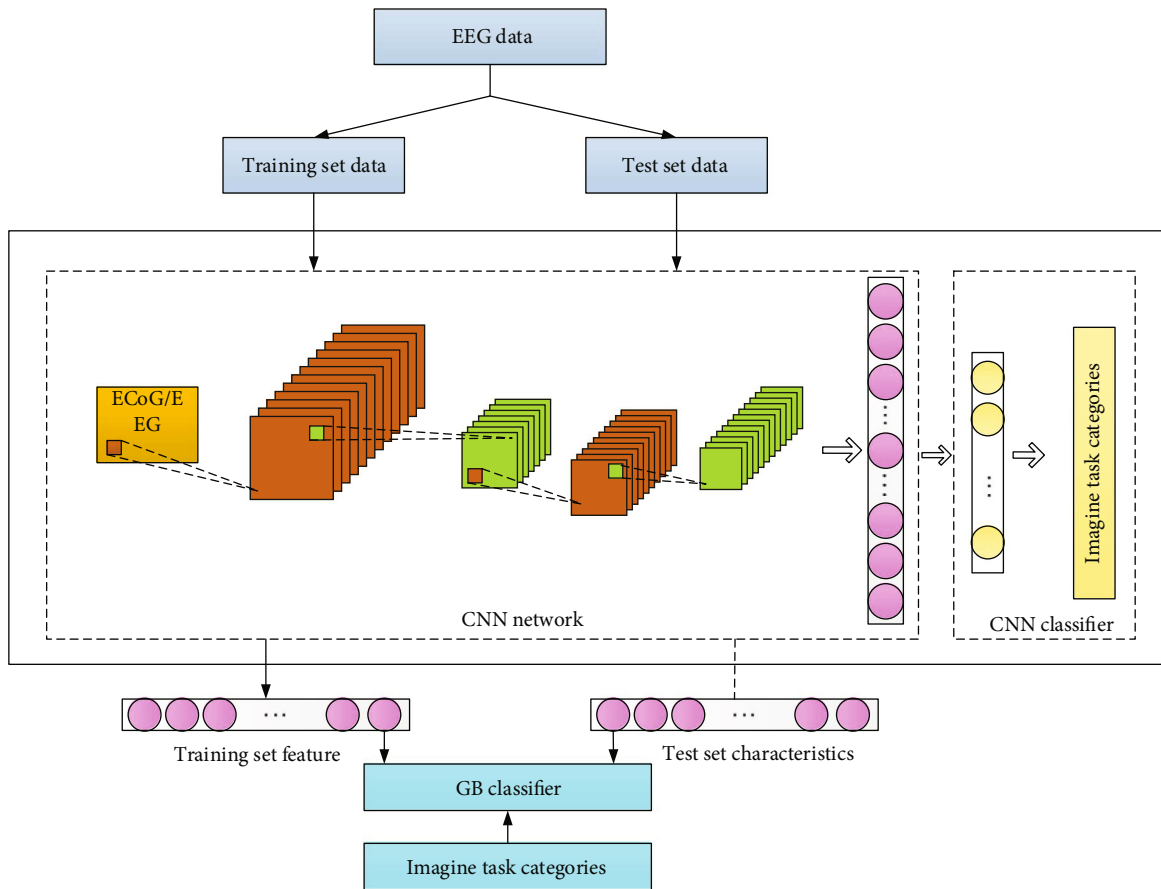


FIGURE 5: Flow chart of moving image classification task recognition based on CNN model.

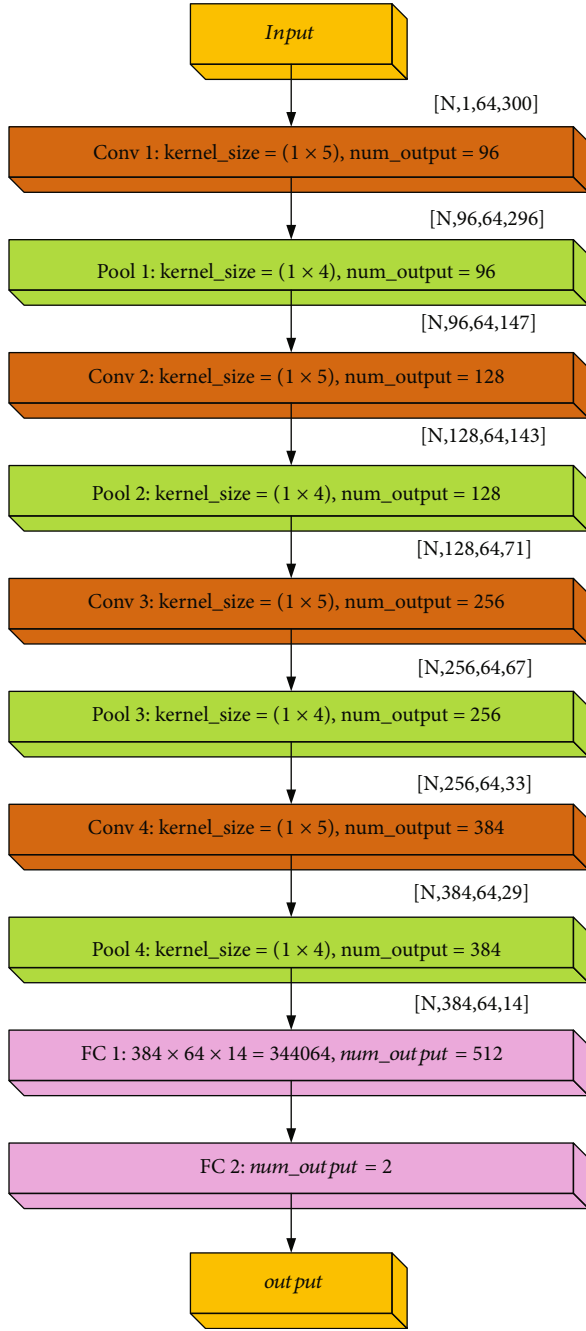


FIGURE 6: Network topology diagram of CNN.

$$E = -\frac{1}{N} \sum_{n=1}^N \sum_{i=1}^1 y_i \log(a_i^{(11)}). \quad (12)$$

The formulas for calculating the weights and deviation gradients of the network are shown in

$$\frac{\partial E}{\partial W^{(11)}} = -\frac{1}{N} \sum_{n=1}^N \left[ \frac{y_0}{a_0^{(11)}} \frac{\partial a_0^{(11)}}{\partial W^{(l)}} + \frac{y_1}{a_1^{(11)}} \frac{\partial a_1^{(11)}}{\partial W^{(l)}} \right], \quad (13)$$

$$\frac{\partial E}{\partial b^{(l)}} = -\frac{1}{N} \sum_{n=1}^N \left[ \frac{y_0}{a_0^{(11)}} \frac{\partial a_0^{(11)}}{\partial b^{(l)}} + \frac{y_1}{a_1^{(11)}} \frac{\partial a_1^{(11)}}{\partial b^{(l)}} \right]. \quad (14)$$

Once the gradient is obtained, the parameters are updated according to the gradient descent method, as shown in

$$W_{t+1} = W_t - \eta \frac{\partial E(W, b)}{\partial W_t}, \quad (15)$$

$$b_{t+1} = b_t - \eta \frac{\partial E(W, b)}{\partial b_t}. \quad (16)$$

High speed means that it takes less time for the model to reach the convergence point. At high speed, the model jumps too much and cannot find the optimal center of gravity.

**3.2.3. Classification Algorithm.** As a machine learning algorithm, GB classifier is used to get a strong classifier from many classifications. Its basic idea is to continuously optimize the loss function of the model in order to obtain stronger prediction or classification ability. The power of the model is constantly increasing. According to mathematical theory, when the loss function follows the direction of its data gradient, it can achieve the best and fastest decline.

If the function data performed by the CNN network is  $o_i$ , the mathematical representation is shown in

$$L(F_m; O; Y) = \log \left( \prod_{i=1}^N p_m(y_i = 1|o_i)^{y_i} p_m(y_i = 0|o_i)^{1-y_i} \right), \quad (17)$$

where the logarithmic regression model is defined as shown in

$$p_m(y_i = 1|o_i) = \frac{e^{F_m(o_i)}}{e^{F_m(o_i)} + e^{-F_m(o_i)}}. \quad (18)$$

The initial value of logarithmic regression model is preset as  $p_0(y_i = 1|o_i) = 0.5$ .

Taking ordinary least square regression as the minimum loss function, GB algorithm based on OLS regression can be expressed as the following process:

- (1) Calculate the gradient of the loss function in the direction of gradient descent, as shown in

$$\bar{y}_i = \left[ \frac{\partial L(F(o_i))}{\partial F(o_i)} \right]_{F=F_{m-1}} = 2(y_i - p_{m-1}(y_i = 1|o_i)) \quad (19)$$

- (2) Based on the OLS, select the appropriate gradient, as shown in

$$f_m = \arg \min_f \sum_{i=1}^N (\bar{y} - f(o_i))^2 \quad (20)$$

The result of the weak classifier is that the vector  $o_i(t)$  of the EKoG sample is projected onto the regression coefficient  $a$  at time  $t$ , as shown by

$$f(o_i, a, t) = a^T o_i(t). \quad (21)$$

$(a_m, t_m)$  when the error is minimized, it is then selected as the parameter of the weak classification, as shown by

$$f_m(o_i) = f(o_i, a, t). \quad (22)$$

(3) Then, calculate its weight, as shown in

$$\gamma_m = \arg \max_{\gamma} L(F_{m-1} + \gamma f_m; O, Y) \quad (23)$$

(4) Multiply a small number  $\varepsilon$  in each step, reduce the value of  $\gamma_m$ , and then get a strong classification through iteration, which can improve the generalization ability of the algorithm as shown in

$$F_m = F_{m-1} + \varepsilon \gamma_m f_m \quad (24)$$

(5) Finally, a new logarithmic regression value is obtained, as shown in

$$p_m(y_i = 1 | o_i) = \frac{e^{F_m(o_i)}}{e^{F_m(o_i)} + e^{-F_m(o_i)}} \quad (25)$$

Among them, in order to find the optimal iteration times and achieve fast classification, we use logarithmic regression model, which is not limited by the predicted value of the model.

## 4. Experimental Research and Analysis

**4.1. Selection of Preprocessing Algorithm for EEG Signal.** In the preprocessing of EEG signal, there are short-time Fourier transform, wavelet transform, Gunner distribution, EMD, and other methods. In order to process the signal more intuitively and efficiently, we compare these algorithms in self-adaptation, high-efficiency deep mining ability of data and decomposition signal. Five comparative experiments are carried out, and the results are shown in Figures 7, 8, and 9.

Looking at the figure above, we can see that in the aspect of self-adaptation, the performance of data efficient deep mining ability and signal decomposition ability is compared. EMD algorithm has more advantages, so we can draw that EMD algorithm is intuitive, efficient, self-adaptive, hindsight, and other advantages.

**4.2. Optimal Selection of Pretreatment Methods.** This section describes SNIR, average energy, and MAPE to measure the system's ability to suppress noise. See formula (26) for SNIR calculation formula:

$$\text{SNIR} = \frac{\text{SNR}_o}{\text{SNR}_i}, \quad (26)$$

where  $\text{SNR}_o$  is the signal-to-noise ratio of the system output and  $\text{SNR}_i$  is the signal-to-noise ratio of the system input. SNR is the average power ratio of signal to noise. The calculation formula is shown in

$$\text{SNR} = \frac{S}{N}. \quad (27)$$

In decibels (dB), as shown in

$$\text{SNR(dB)} = 10 \times \log_{10} \left( \frac{S}{N} \right) (\text{dB}). \quad (28)$$

The calculation formula of energy mean value is shown in

$$\bar{E} = \frac{1}{n} \sum_{i=1}^n x^2(i), \quad (29)$$

where  $x(i)$  is the discrete amplitude of EEG signal after noise suppression and  $N$  is the number of sampling points.

The calculation formula for MAPE is shown in

$$M = \sum_{t=1}^n \left| \frac{A_t - F_t}{A_t} \right| \times \frac{100\%}{n}. \quad (30)$$

Among them, the smaller the MAPE, the smaller the error.

SNIR, energy average, and MAPE are calculated for the original EEG signal after the above-mentioned "tenfold reduction" by three denoising methods, and the results are shown in Table 1.

Table 2 shows the comparison results of Deap data set and self-collected data set, including 1152 EEG signal data sets, which have been processed by three noise reduction methods. Due to the large amount of data, the results are presented in the form of data sets.

In Table 1, the results show that EMD+FastICA algorithm has the highest SNIR, the lowest MAPE, and the lowest average energy value of EEG signals. Table 2 also clearly shows that better results can be obtained by mute calculation of three indexes for EEG signal data through EMD+FastICA algorithm.

**4.3. Subjects.** All the subjects selected in this experiment are graduate students. Four, eight, and four graduate students were selected as normal control group, depression control group, and feedback training group. Evaluation and feedback training are conducted once a week for a total of six weeks. The initial grouping criteria are shown in Table 3.

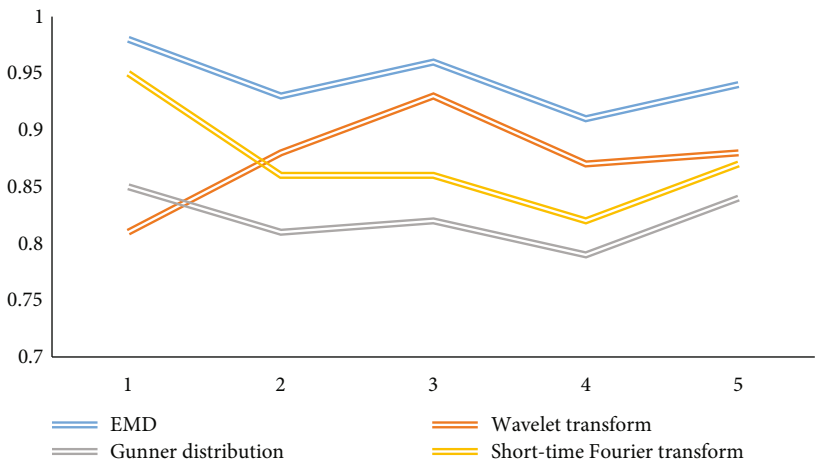


FIGURE 7: Comparison of adaptability.

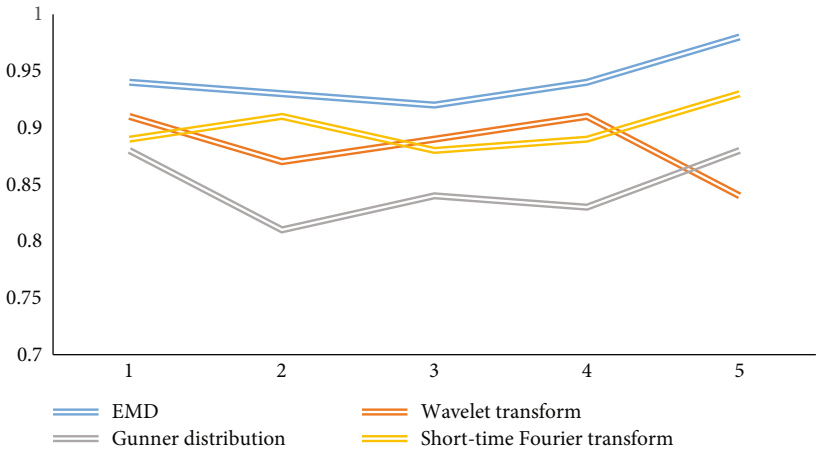


FIGURE 8: Comparison of signal decomposition ability.

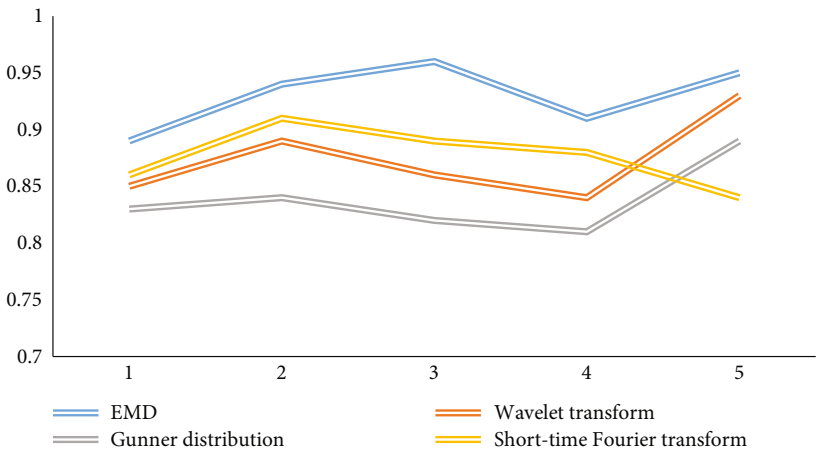


FIGURE 9: Comparison of data mining capabilities.



TABLE 1: Three noise reduction methods.

EEG signal classification	SNIR (dB)	Average energy ( $\mu V$ )	MAPE (%)
After EMD algorithm denoising	-4.5609	1.2826	2.3974
After denoising by FastICA algorithm	-3.6278	0.977	1.9444
After EMD+FastICA algorithm denoising	0.1866	0.6227	1.5044

TABLE 2: Comparison of denoising effects of three methods based on all EEG data.

EEG signal classification	SNIR (dB)	Average energy ( $\mu V$ )	MAPE (%)
After EMD algorithm denoising	$-4.5039 \pm 0.6057$	$1.4549 \pm 0.1447$	$2.4473 \pm 0.5843$
After denoising by FastICA algorithm	$-2.9835 \pm 0.9539$	$1.1311 \pm 0.1781$	$1.7389 \pm 0.6545$
After EMD+FastICA algorithm denoising	$1.0123 \pm 0.2012$	$0.7501 \pm 0.2398$	$1.1326 \pm 0.3794$

TABLE 3: Subject grouping criteria.

Group name	SCL-90 score	SDS score	PHQ-9 score	Feedback training times	Scale evaluation times
Normal control group	<8	<53	<5	0	6
Depression control group	>26	53-62	5-9	0	6
Feedback training group	>26	53-62	5-9	6	6

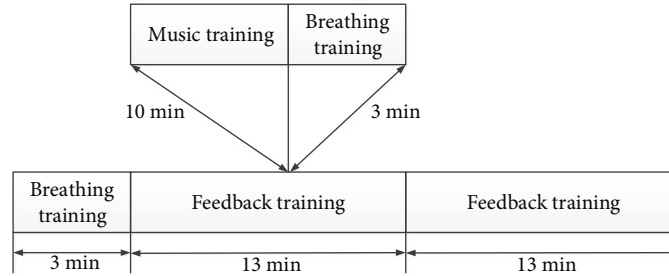


FIGURE 10: Flow chart of feedback training.

**4.4. Experimental Flow.** In order to make the experimental results more accurate, our test site was chosen in a relatively undisturbed room. And the test time is strictly controlled within 45 minutes. The specific experimental process is as follows:

- (1) Rating stage scale: before each test, the user asked the subjects to complete three scales, SCL-90, SDS, and PHQ-9, so that the subjects could evaluate the degree of depression before the test. This step takes about 10 minutes
- (2) Experimental preparation stage: first, determine whether the subject can complete the test. After that, the operator explains the working principle of the system to the subject, feeds back the test process, matters needing attention in the test process, etc. Finally, the operator sticks electrode stickers on the positions of FP1, FP2, and FPZ electrodes on the forehead to ensure the normal acquisition of EEG signals. This step takes about 3 minutes

The feedback exercise stage includes one breathing exercise and two feedback exercises. Before the feedback training, the operator organized the subjects to practice breathing for 3 minutes. The purpose of this is to help the subjects relax and concentrate, so that the subjects can quickly adapt to feedback training. After that, the instructor guided the subjects through a series of two feedback exercises, each lasting 13 minutes. This step takes about 29 minutes.

- (3) Training stage: in the previous article, we designed two feedback training methods: breathing and music. The specific feedback training process is shown in Figure 10
- (4) Communication stage: in this stage, the experimenter communicates with the tester to understand whether the feedback music is effective and check whether the subjects can manage their physical condition skillfully. At the same time, the subjects are

TABLE 4: Scoring standards of SCL-90, SDS, and PHQ-9.

Degree of depression	SCL-90	SDS	PHQ-9
Normal	0-26	0-52	0-4
Mild		53-62	5-9
Moderate		63-72	10-14
Moderate and severe	>26		15-29
Severe		>72	20-27

TABLE 5: SCL-90 scale evaluation statistics.

Number of experiments	Mean and standard deviation of SCL-90 scale			T-test		
	Feedback training group I	Depression control group II	Normal control group III	I and II	I and III	II and III
Baseline	31.40 $\pm$ 5.10	31.53 $\pm$ 5.66	2.74 $\pm$ 3.19	0.9482	0.0000	0.0000
2	29.75 $\pm$ 2.33	31.83 $\pm$ 6.30	2.37 $\pm$ 2.96	0.4065	0.0000	0.0000
3	28.04 $\pm$ 1.60	31.14 $\pm$ 4.52	2.75 $\pm$ 3.18	0.0025	0.0000	0.0000
4	24.30 $\pm$ 1.75	31.23 $\pm$ 5.09	2.60 $\pm$ 3.16	0.0000	0.0000	0.0000
6	17.20 $\pm$ 2.87	30.82 $\pm$ 3.16	2.12 $\pm$ 2.12	0.0000	0.0000	0.0000

TABLE 6: Evaluation statistics of SDS scale.

Number of experiments	Mean and standard deviation of SDS scale			T-test		
	Feedback training group I	Depression control group II	Normal control group III	I and II	I and III	II and III
Baseline	56.75 $\pm$ 2.41	56.77 $\pm$ 2.58	34.37 $\pm$ 5.92	0.9703	0.0000	0.0000
2	55.42 $\pm$ 2.48	56.42 $\pm$ 2.12	33.91 $\pm$ 5.72	0.1734	0.0000	0.0000
3	50.59 $\pm$ 3.57	56.64 $\pm$ 2.55	34.00 $\pm$ 5.93	0.0000	0.0000	0.0000
4	46.50 $\pm$ 2.14	56.79 $\pm$ 2.54	34.19 $\pm$ 5.75	0.0000	0.0000	0.0000
6	37.54 $\pm$ 5.79	56.30 $\pm$ 2.58	34.30 $\pm$ 5.91	0.0000	0.0742	0.0000

encouraged to listen to sober and exciting music when they are depressed and adjust their emotions through feedback training

#### 4.5. Statistical Analysis

**4.5.1. Scoring Analysis of Scale.** Three scales, SCL-90, SDS, and PHQ-9, were selected to measure the degree of symptoms. Patient health questionnaire is used in the study. See Table 4 for the criteria of patients with depression. During the 6-week follow-up test, we selected the data measured at the first time as the baseline data.

SCL-90, SDS, and PHQ-9 were averaged among the three groups, and independent *T*-test was performed. The results are shown in Tables 5, 6, and 7. It can be seen from the table that before feedback training, there is little difference in scale scores between the feedback training group and depression control group. With the progress of feedback training, the difference between the feedback training group and the depression control group became larger and larger. In the sixth test evaluated by SDS and PHQ-9, it was found that there were significant differences between the feedback training group and some correlations between

the normal controls. Obviously, the method designed in this paper can effectively improve the condition of patients with mild depression.

Figures 11, 12, and 13 show the changes in the scores of the three corresponding SCL-90, SDS, and PHQ-9 scales over a six-week period. It can be observed that the scale evaluation scores of the feedback training group showed a downward trend, indicating that music feedback has a positive effect on emotional regulation. When the two control groups did not participate in feedback training, the scores of individual subjects were different, and there was no obvious trend in the overall scale scores. In addition, with the passage of time, the evaluation scores in the feedback training group decreased more and more obviously, especially in the third to sixth tests. This shows that the emotion regulation method with music feedback proposed in this paper is always effective in regulating the depression of patients with mild depression. At the same time, after the first three music feedback experiments, the negative emotions were improved, and the performance was further improved with the help. Music regulates itself. During the follow-up period, emotional regulation and depressive symptoms improved.

TABLE 7: Evaluation statistics of PHQ-9 scale.

Number of experiments	Mean and standard deviation of PHQ-9 scale			T-test		
	Feedback training group I	Depression control group II	Normal control group III	I and II	I and III	II and III
Baseline	6.37 $\pm$ 1.09	6.38 $\pm$ 1.26	1.25 $\pm$ 1.37	0.9580	0.0000	0.0000
2	6.00 $\pm$ 1.22	6.39 $\pm$ 1.21	1.27 $\pm$ 1.36	0.1923	0.0000	0.0000
3	4.72 $\pm$ 1.59	6.39 $\pm$ 1.33	1.29 $\pm$ 1.38	0.0000	0.0000	0.0000
4	3.79 $\pm$ 0.80	6.44 $\pm$ 1.14	1.14 $\pm$ 1.31	0.0000	0.0000	0.0000
6	2.24 $\pm$ 1.08	6.38 $\pm$ 1.21	1.25 $\pm$ 1.37	0.0000	0.0202	0.0000

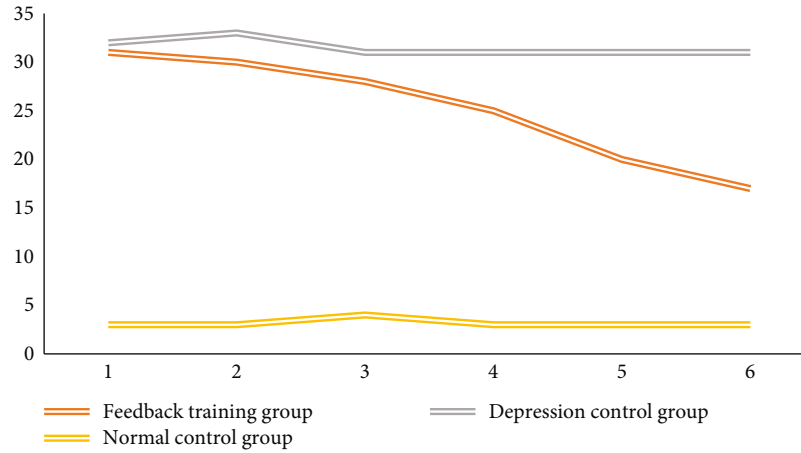


FIGURE 11: The change trend of SCL-90 scale score.

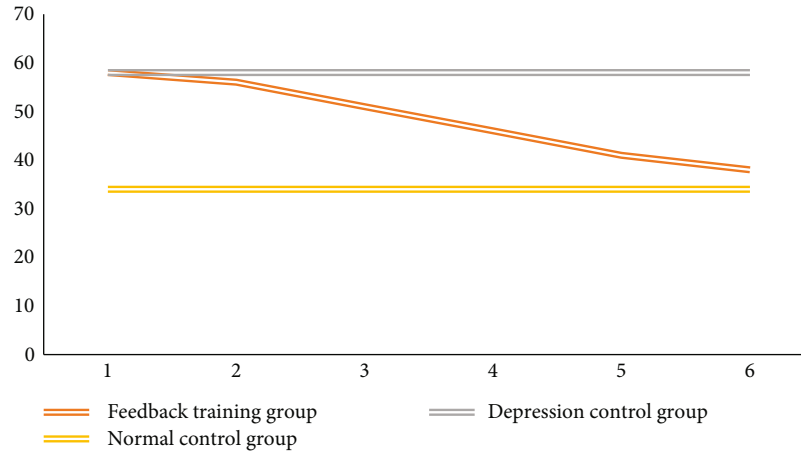


FIGURE 12: Change trend of SDS scale score.

In addition, because the subjects of this study are educated graduate students, during the experiment, the subjects are more or less aware of the treatment of depression and receive some degree of cognitive behavioral therapy. This may also be the reason why the subjects can quickly adapt to music therapy and adjust themselves in the experiment.

**4.5.2. Quantity Analysis of Emotional Fragments.** This paper also analyzes the changes of emotional fragments of EEG

signals in music experiments. The EEG character sequences obtained by us are divided into three types: active state, passive state, and normal state. The length of each type of EEG character sequence is 0.5 s. For each music feedback test, we conducted two feedback trainings. For each music feedback test, we need to calculate the emotional state within 6 seconds. During the experiment, the system needs to convert 399 segments, about 4788 EEG markers. Among them, the number of strings in each EEG signal is too much, which

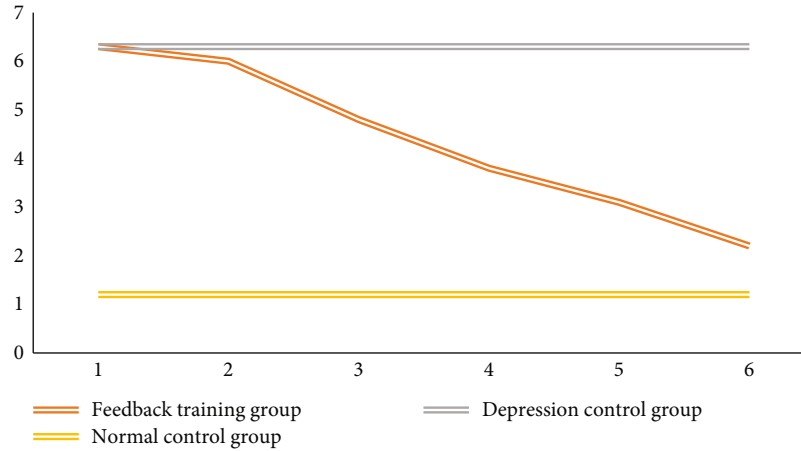


FIGURE 13: Change trend of PHQ-9 scale score.

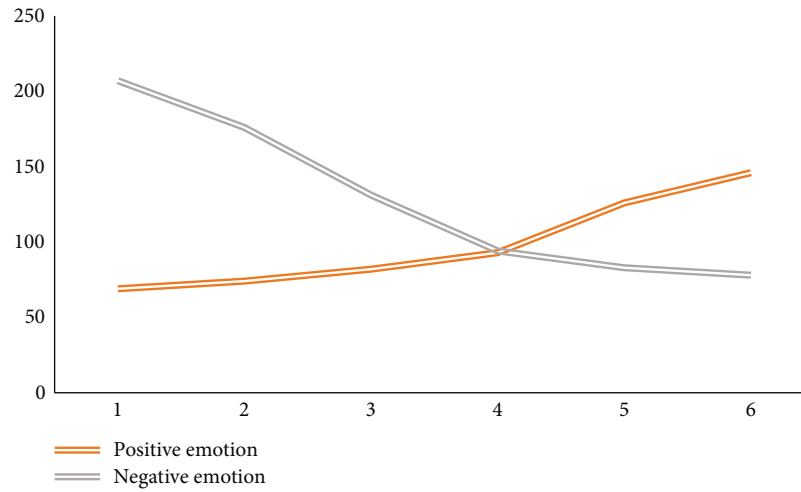


FIGURE 14: The change trend of the number of feedback music clips corresponding to positive and negative emotions.

is not intuitive. Therefore, this section selects the feedback music segments that change during the experiment to reflect the changes of subjects' emotions.

The change trend of the number of feedback music segments in the feedback training group is shown in Figure 14. Observation shows that feedback music representing positive emotions is increasing. Among them, the changes of feedback music fragments from the first trial to the third trial are obviously different from those from the third trial to the sixth trial. The reason may be that during the first and third experiments, the emotional state of the subjects changed from negative to normal due to music feedback training. Therefore, the number of music fragments representing negative emotions first decreased and then increased slowly, while the number of music fragments representing positive emotions first increased slowly and then increased rapidly.

In the experiment of converting EEG into music, the signal sequence of EEG signals obtained by music stimulation will be affected by the characteristics of depressed patients. The test strictly screens the characteristics of depressed

patients such as age, education level, and medical history, so the application range of EEG signal feature set obtained in the test is limited. In addition, in the EEG conversion music experiment, there are only three kinds of music stimuli (positive, medium, and negative), so there is less emotional feedback. Future research should consider the differences of different target groups and individual knowledge and increase the types of music stimulation in the experiment, so that the system can be applied to the treatment of a wider range of mental health disorders.

## 5. Concluding Remarks

Depression has become a very common disease in people's daily life. Modern people are under increasing pressure in life, work, and study. Contradictions and setbacks make people exhausted. Music therapy is a new interdisciplinary subject, which combines the essence of music, medicine, and psychology. It is a process in which music therapists help patients break through psychological barriers and recover their physical and mental health through specially designed

music models. Music therapy is mainly based on the theory and method of psychotherapy, which makes use of the unique psychological and physiological effects of music. The results of this study show that the quality of life and anxiety symptoms of depressed patients have been improved after music therapy, especially music therapy combined with EEG feedback training. If it can be popularized in the treatment of depressed patients, it will be a great boon for patients.

## Data Availability

The experimental data used to support the findings of this study are available from the corresponding author upon request.

## Conflicts of Interest

The author declares no conflicts of interest regarding this work.

## References

- [1] A. C. Vink, J. S. Birks, and M. S. Bruinsma, "Music therapy for people with dementia," *Cochrane Database of Systematic Reviews (Online)*, vol. 4, no. 3, article CD003477, 2003.
- [2] F. Mancini, "Active music therapy in Parkinson's disease: an integrative method for motor and emotional rehabilitation," *Psychosomatic Medicine*, vol. 62, no. 3, p. 386, 2005.
- [3] S. Koelsch, "A neuroscientific perspective on music therapy," *Annals of the New York Academy of Sciences*, vol. 1169, no. 1, pp. 374–384, 2009.
- [4] A. Maratos, M. J. Crawford, and S. Procter, "Music therapy for depression: it seems to work, but how?," *The British Journal of Psychiatry*, vol. 199, no. 2, pp. 92–93, 2011.
- [5] H. B. Svansdottir and J. Snaedal, "Music therapy in moderate and severe dementia of Alzheimer's type: a case-control study," *International Psychogeriatrics*, vol. 18, no. 4, pp. 613–621, 2006.
- [6] V. Logar and A. Belic, "Brain-computer interface analysis of a dynamic visuo-motor task," *Artificial Intelligence in Medicine*, vol. 51, no. 1, pp. 43–51, 2011.
- [7] E. S. Gopi, R. S. Vijay, and V. Rangarajan, "Brain computer interface analysis using wavelet transforms and autoregressive coefficients," in *2006 International Conference on Electrical and Computer Engineering*, pp. 169–172, Dhaka, Bangladesh, 2007.
- [8] G. Bin, X. Gao, and Y. Zheng, "An online multi-channel SSVEP-based brain-computer interface using a canonical correlation analysis method," *Journal of Neural Engineering*, vol. 6, no. 4, article 046002, 2009.
- [9] D. J. Mcfarland and J. R. Wolpaw, "Sensorimotor rhythm-based brain-computer interface (BCI): model order selection for autoregressive spectral analysis," *Journal of Neural Engineering*, vol. 5, no. 2, pp. 155–162, 2008.
- [10] D. Coyle, G. Prasad, and T. M. McGinnity, "A time-frequency approach to feature extraction for a brain-computer interface with a comparative analysis of performance measures," *Eurasip Journal on Advances in Signal Processing*, vol. 2005, Article ID 861614, 11 pages, 2005.
- [11] Y. Pang, Y. Yuan, and K. Wang, "Learning optimal spatial filters by discriminant analysis for brain-computer-interface," *Neurocomputing*, vol. 77, no. 1, pp. 20–27, 2012.
- [12] E. Hayakawa, "Effects of antidepressant medication on emotion regulation in depressed patients: an iSPOT-D report," *Journal of Affective Disorders*, vol. 159, no. 3, pp. 127–132, 2014.
- [13] P. Schloss and D. C. Williams, "The serotonin transporter: a primary target for antidepressant drugs," *Journal of Psychopharmacology*, vol. 12, no. 2, pp. 115–121, 1998.
- [14] G. Jacob, K. Zvonik, S. Kamphausen et al., "Emotional modulation of motor response inhibition in women with borderline personality disorder: an fMRI study," *Journal of Psychiatry & Neuroscience*, vol. 38, no. 3, pp. 164–172, 2013.
- [15] S. E. Kennedy, R. A. Koeppe, E. A. Young, and J. K. Zubieta, "Dysregulation of endogenous opioid emotion regulation circuitry in major depression in women," *Archives of General Psychiatry*, vol. 63, no. 11, pp. 1199–1208, 2006.

## Research Article

# Analysis of Diabetes Disease Risk Prediction and Diabetes Medication Pattern Based on Data Mining

Lindong Zhang and Min Liu 

*The First School of Clinical Medical Sciences, Guangzhou University of Chinese Medicine, Guangzhou, Guangdong 510000, China*

Correspondence should be addressed to Min Liu; 20201120112@stu.gzucm.edu.cn

Received 13 July 2022; Revised 25 August 2022; Accepted 14 September 2022; Published 3 October 2022

Academic Editor: Hangjun Che

Copyright © 2022 Lindong Zhang and Min Liu. This is an open access article distributed under the Creative Commons Attribution License, which permits unrestricted use, distribution, and reproduction in any medium, provided the original work is properly cited.

Diabetes mellitus is the second most common disease after cardiovascular diseases and malignant tumors. With the continuous acceleration of people's living standards and life rhythm, the number of diabetic patients is rapidly increasing and showing a trend of youthfulness. A recent study found that 114 million adults in China have diabetes and have a high prevalence rate, but the awareness rate, treatment rate, and compliance rate are low. If diabetes is not treated and controlled in time, various complications will occur, such as cardiovascular, cerebrovascular, and diabetic foot, which will not only have a great impact on the survival of the patient, but also cause a lot of pressure on the family and society. Therefore, prevention and control of diabetes is an important strategy to save medical resources and reduce medical costs. In this paper, we mainly read a lot of literature and accumulate some important theoretical knowledge to clarify the basic principles and methods of data mining and refer to the research results of other scholars to select a new combined algorithm model combining K-means algorithm and logistic regression algorithm to construct a prediction model of diabetes and explore the law of medication for diabetic patients based on this analysis.

## 1. Introduction

Diabetes mellitus (DM) is a metabolic abnormality syndrome caused by the interaction of genetic and environmental factors, mainly characterized by chronic hyperglycemia. As the standard of living of our people continues to improve, diabetes has had a significant impact on their quality of life, and its dangers have become a major public health issue. At the World Diabetes Conference 2015, the International Diabetes Federation recently published a report on diabetes, which mentioned that 415 million adults worldwide have diabetes, or 1 in 11. 110 million people in China have diabetes, the most common disease in the world [1]. Without intervention, the number of diabetics will increase geometrically by 2040. In the last 30 years, the prevalence of diabetes in China has increased from 0.67% to 11.6%. In Preventing Type 2 Diabetes in China (2013 Edition) [3], it is stated that the main incidence group in China today is type 2 diabetes, 90% of which are middle-aged and elderly people. According to studies with relevant information, the prevalence of diabetes is more than

20% among patients aged 60 years and above. Its incidence is 10 times higher than that of the young population aged 20-30. Moderated by other factors, the incidence of diabetes rises by 68% for every 10 years of growth. The rapid increase in the incidence of diabetes in our country is mainly due to the following factors [2]. Firstly, changes in lifestyle. The decreasing availability of manual labour in society and the high utilisation of medical resources have led to an increasing incidence of diabetes. Secondly, changes in diet. As people's standard of living increases, the incidence of diabetes increases along with the prevalence of obesity. Thirdly, the ageing of the population and genetic factors etc. [3].

According to the latest data from the International Diabetes Federation, the worldwide prevalence of diabetes reached 8.3% in 2013 [4], and the number is growing rapidly [2]. It is estimated that by 2035, approximately 592 million people worldwide will have diabetes, and approximately 46% of these people will be undiagnosed. Data show that the number of deaths from diabetes complications worldwide is approximately 5.1 million, with medical costs of



\$548 billion, or 11% of total world health spending, and is projected to reach \$627.3 billion in 2035. Currently, there are 114 million people with diabetes in the country, and 50.1% of them are “reservists” with diabetes. The potential incidence of diabetes is as high as 15.5%, and 60.7% of diabetic patients do not receive timely treatment and preventive education [5].

According to the China Statistical Yearbook, the share of health care in per capita consumption was 6.9% in 2013, an increase of 4.2% from 1990 [6]. This indicates that in addition to the rising cost of health care, the importance of health management is also increasing, which is an important reason for increasing health care spending. Health management is a subject of increasing interest in recent years, and its development will be more promising. Tertiary prevention is implemented to spread health knowledge and transform poor lifestyles in order to prevent and control risks [7].

At present, the prevention and treatment of diabetes in China has established the policy of “government-led, universal participation, prevention-oriented, combined with control, active initiation, and steady progress,” but the prevalence and mortality of diabetes are still high. The reason for this is that the early diagnosis and screening techniques for diabetes are not yet perfect [8], so many patients are already in the middle or late stage when they are diagnosed; in addition, the efficacy and prognosis of diabetes are very poor, and the domestic investment in primary and secondary prevention of diabetes is obviously insufficient, and there is also a lack of effective prevention and intervention means; finally, due to its complications, the quality of life of diabetic patients decreases [9], causing a great medical burden to families and society. Finally, due to its complications, the quality of life of diabetic patients decreases, causing a great medical burden to families and society. Therefore, risk prediction for diabetic patients can provide both early warning and comprehensive, continuous and proactive management to promote health and improve quality of life [10].

Most current healthcare information systems are limited to one-way data collection and statistics, lacking methods to summarize medical and health data, acquire knowledge and information, and proactively manage [11], feedback, and intervene on the information already available [5]. Data mining is an important technical tool that can extract the needed data from the massive amount of data. Therefore, the research in this thesis focuses on the use of various data mining techniques to develop diabetes risk prediction models and analyze their drug use patterns for the purpose of preventing and controlling the development of diabetes [12].

## 2. Introduction to Related Technologies

**2.1. Data Mining Techniques.** The concept of data mining was first introduced at the 11th International Joint Conference on Artificial Intelligence (IJCAI) in August 1989. Data mining is a technique to transform data into knowledge; it will collect data in a targeted way and analyze it and transform it into useful knowledge. Among these rules, data mining needs to follow the following rules:

- (1) The data mining target is large and high-dimensional data
- (2) The result of data mining is understandable and useful knowledge
- (3) Data mining is data-based and provides support for decision making

**2.1.1. Processes Underlying Data Mining.** The usual data mining includes the following: target understanding, data collection, data pre-processing, model building, model evaluation, and execution [13]. The flow chart of data mining is shown in Figure 1.

- (1) Objective understanding. The initial work focuses on understanding the target needs of the project and translating the knowledge learned into data mining problems
- (2) Data acquisition. Based on this, the data objects to be performed are collected, and the required data are stored in a database or data warehouse [14]
- (3) Data preprocessing. This includes data integration, data attribution, data cleaning, and data conversion
- (4) Modeling. Depending on the data and mining objectives, appropriate analytical tools such as SPSS

Clementine, Wika, etc. are identified. Bayesian networks, association rules, decision trees, networks, cluster analysis and other relevant models can be built for the needs of data mining.

- (5) Model evaluation. By comparing the existing accurate results or confirming them by experts
- (6) Model implementation. The obtained knowledge is stored in a knowledge base for use by other applications

Data mining can be thought of as a cyclical process of operation, where if each step fails to achieve the goals set before mining, then you will go back to the previous step, make adjustments again, and execute again [15].

**2.2. K-Means Algorithm.** Clustering is the effective classification of similarities between different data items in a collection of data; each resulting set is called a cluster [16]. Clustering is an unsupervised learning method that provides only the attribute values of the data items without giving the classification values of the data items and its main goal is to put other types of data items into a cluster. The original data was analyzed and studied in depth using the clustering algorithm, and it was possible to discover the specific location of each data item and to compare the attributes in the dataset based on the experimental results [17].

The K-means algorithm is a typical distance-based clustering method, which uses distance as a measure of similarity, meaning that the shorter the given distance, the more similar it is.

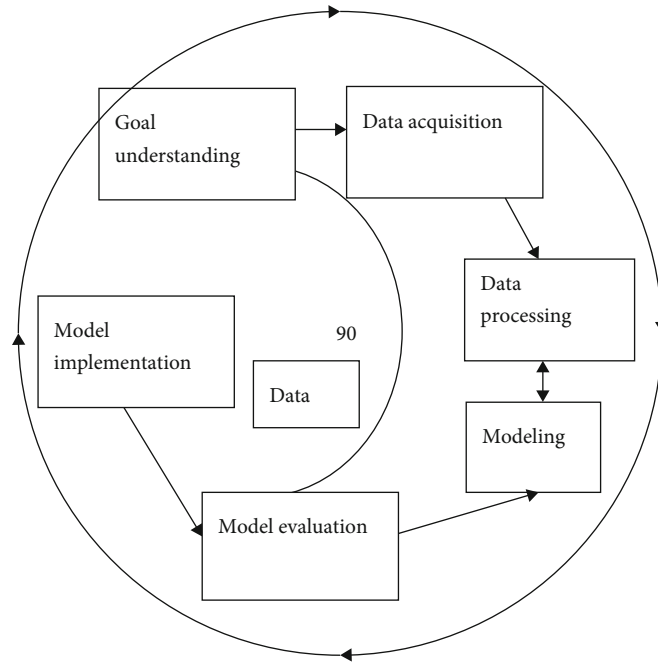


FIGURE 1: Flow chart of data mining.

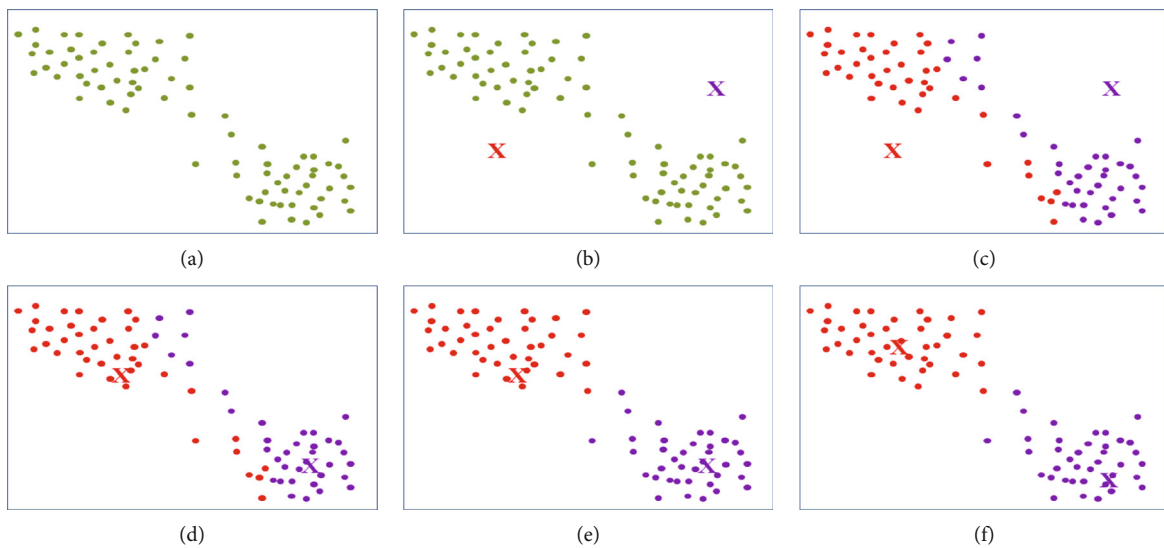


FIGURE 2: Illustration of the K-means algorithm process.

The key to the K-means algorithm is to choose the  $K$ -value, which is an unsupervised learning algorithm that requires the experimenter to choose the  $K$ -value based on experience.

The algorithm proceeds as follows, and a simple diagram is shown in Figure 2.

- (1) Set  $K$  (assuming  $K = 2$ ) as the initial cluster center of the algorithm, and choose  $K$  (assuming  $K = 2$ ) arbitrarily in that original dataset
- (2) Compute each of the remaining data items separately, and classify them into clusters represented

by the nearest centers according to the computed distances

- (3) Recalculate the centers of the clusters, and determine whether the centers have changed
- (4) Cycle 2-3 steps until the new cluster centers are equal to or less than the initial critical points, and the method is completed

**2.3. Logistic Regression Algorithm.** In the clinical application of diabetes, a dichotomous approach is generally used to classify the independent variables of patients into two categories [18]. Logistic regression algorithm models are divided

into two types, quadratic and multiple, depending on the variable. The case of binary dependent variables is more common, that is, the output may have only two values, “0” and “1,” which represent meanings such as pass or fail, win or lose, live or die, and healthy or sick. Multiple logistic regression analysis occurs when there are more than two outcome types for the attribute values of a variable [19].

Logistic regression methods predict a finite number of dependent variables (two factors in Bernoulli’s experiment) rather than a continuous one, compared to conventional linear regression methods. Moreover, linear regression is not meaningful for predicting binary variables. What we want to do is to transform the binary variables into variables that can withstand all the true values (positive or negative) [20]. To achieve this, binomial logistic regression first divides the probability of an event into individual independent variables at each level, scales them (continuously but not negatively), and establishes a continuous criterion for their logarithm (i.e., logit or log-odds) as a transformed version of the by variable.

The analytical study conducted in this thesis for diabetes focuses on a binary logistic regression algorithm model, which is based on a linear regression algorithm model of the following formula:

$$P = \alpha + \beta_1 x_1 + \beta_2 x_2 + \dots + \beta_m x_m, \quad (1)$$

where  $m$  is the number of independent variables.

The formula for the logistic regression algorithm model is defined as follows, where Figure 3 shows a simple example of the Sigmoid function transformation curve.

$$\begin{aligned} \Pr = \{Y = +1 | X_1, X_2 \dots X_d\} \\ = \sigma \left( \sum_{1 \leq i \leq d} \beta_{i1} X_i + \sum_{1 \leq j < d} \beta_{ij} X_i X_j \right), \\ \Pr(Y = +1 | X) \sim \beta \cdot X, \end{aligned} \quad (2)$$

$$\Pr(Y = -1 | X) = 1 - \Pr(Y = +1 | X),$$

$$\sigma(x) := \frac{1}{1 + e^{-x}} \in [0, 1],$$

where Sigmoid function transformation is shown in Figure 3.

$$\Pr(Y = +1 | X) \sim \sigma(\beta \cdot X) \text{ and } \Pr(Y = -1 | X) = 1 - \Pr(Y = +1 | X). \quad (3)$$

### 3. Application Method Design

**3.1. Combined K-Means and Logistic Regression Algorithm Model.** Data mining technology has a broad application prospect in the diagnosis of diabetic patients, whether it is classification, clustering, or association analysis, which can provide relevant research basis for diabetic patients [21]. The correct use of data mining techniques can uncover the hidden information from the massive data. In this paper, an improved method based on K-means and logistic regression has been used to predict the combination, and the cor-

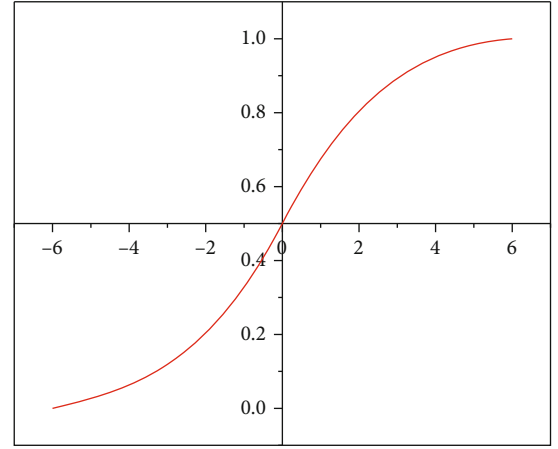


FIGURE 3: Sigmoid function transformation curve.

responding model is given. Its model flow chart is shown in Figure 4.

The application of this combined K-means and logistic regression algorithm model consists of the following 7 steps:

- (1) A test based on information from the UCI to obtain possible factors for diabetes
- (2) Screening of certain inappropriate and inconsistent data in the data preprocessing stage
- (3) The original data with categorical markers were eliminated using the K-means clustering algorithm
- (4) Determining the ratio of the remaining data volume to the total original data, and using new seed values if the ratio is less than 75%
- (5) Using supervised logistic regression algorithm to classify the remaining data
- (6) Validated the test results by accuracy, safety, and specification
- (7) Compared with the existing model and proved that this model outperforms the existing model

**3.2. Experimental Data Pre-Processing.** Data preprocessing is a key part of data mining, because data mining is a data-driven experiment. From the analysis of data characteristics and systems in the previous section, we can see that complete, accurate, adequate, and valid data is the basis of data mining; otherwise, it will inevitably lead to the failure of data mining “rubbish in, rubbish out.”

The preprocessing of medical data for diabetic patients is similar to the preprocessing of centralized mining, but also has its own characteristics, and is generally divided into the following steps:

- (1) Data selection: Irrelevant and redundant information is eliminated. For example, some information of the patient that is not related to the changing pattern of the condition can be eliminated

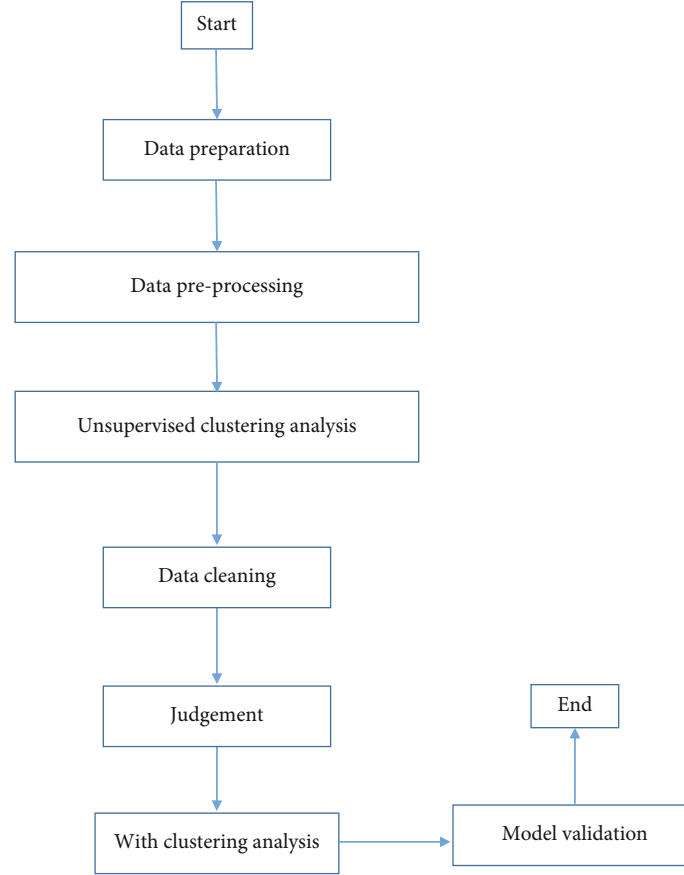


FIGURE 4: Combination algorithm model flow chart.

- (2) Data removal: This mainly includes the following: excluding noise, excluding abnormal data, correcting inconsistent data, making up for missing data, removing missing data, deleting missing data, replacing missing values with constants, means, and predicted values. This step is an important part of the data preprocessing process, which will directly affect the modelling and analysis of data mining
- (3) Data transformation: It transforms the integrated data into a data format that meets the requirements of data mining, including data formatting and digitization of text data, etc.
- (4) Simplicity of data: If the data has too many attributes or variables, not only will it not be able to construct models effectively, but it will also generate noise, so it must be processed with simple data
- (5) Processing of anomalous data (outliers): Mathematical methods, anomaly detection, cluster analysis, and other algorithms are used to process anomalous data

**3.3. Analysis of the Implementation Process of the Combined Model Algorithm.** The original data that cannot be correctly clustered are first filtered using the improved K-means method [22], and the remaining optimized data are used as

TABLE 1: Result of the 2-means cluster of the initial dataset.

Number	Label	Quantity
1	cluster 0	458
2	cluster 1	310

input for the next layer. Then, the logistic regression method is used to classify the remaining data, and the final conclusion is the classification effect of the whole model.

In the experiment of applying the method to Pima Indian Diabetes data, it was also necessary to optimize the quality of the raw data using data preprocessing techniques to improve the efficiency of data mining [23]. First, the definition of each attribute and its relationship with diabetes were compared in detail, and a conclusion was drawn that 0 indicates no pregnancy and 1 indicates pregnancy experience. This arithmetic process reduces the complexity of the information and increases the processing speed of arithmetic operations.

When collecting information, various records are often lost, and statistical items are not standardized. For example, the values of diastolic blood pressure, fat thickness, and serum insulin are not likely to be zero, which indicates that some of them are true. In order to reduce the impact of missing values and nonsense values on the prediction results, this paper uses the "ReplaceMissingValues" filtering method, which replaces all missing values with the most common

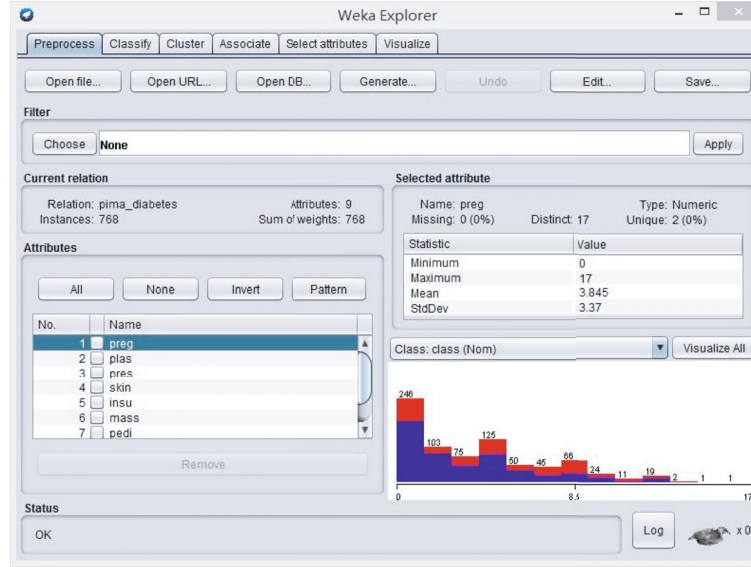


FIGURE 5: WEKA experiment tool interface.

method or average. Here, the 0 values in the previously processed pregnancy count items do not have to be replaced.

One of the biggest drawbacks of the K-means algorithm on the WEKA tool platform is that the initial seed values are generated randomly, so the experimenter must determine the initial seed values based on his or her own project experience. The initial seed value of the K-means algorithm often has a direct impact on the clustering effect of the experimental data. To prevent random errors in the initial seed values, a number of effective methods were used in the experiment. The first step is to record the resulting values and arrange them in order, where each value corresponds to a value called “within cluster sum of squared errors,” and the smaller the value, the better the clustering effect. The experiment recorded all 10,000 values of “within cluster sum of squared errors,” which corresponded to 1-10,000 subvalues. The obtained high quality primary seed values will be used in the next stage. The second part is that at the end of the K-means algorithm, a cycle must be added. The data that could not be correctly clustered were excluded from the experiment, and the following formula was used to find the scale values. If the ratio exceeds 75%, the next level will be performed using the correct grouped data. If not, this algorithm will exit the loop and reset a new seed value. If after 10,000 uses, or after 10 seconds of use, a suitable initial seed value has not been found and that value is greater than 75%, the largest initial seed value, and the corresponding seed value will be selected. Based on initial experience and preliminary judgments, the initial value of the seed selected for this test was 100.

In Table 1, the final cluster results of the above processing are shown, where 458 were clustered into cluster0 to represent negative items, while the other 310 were clustered into cluster 1 to represent positive items. By comparing the distribution of the 768 data items in the original dataset (500 negative and 268 positive), 179 incorrectly clustered and 589 correctly clustered examples were finally obtained, with

TABLE 2: Sample of Pima Indian Dataset.

Preg	Plas	Pres	Skin	Insu	Mass	Pedi	Age	Class
1	89	66	23	94	28.1	0.167	21	tested_negative
0	137	40	35	168	43.1	2.288	33	tested_positive
3	78	50	32	88	31	0.248	26	tested_positive
2	197	70	45	543	30.5	0.158	53	tested_positive
1	189	60	23	846	30.1	0.398	59	tested_positive
5	166	72	19	175	25.8	0.587	51	tested_positive
0	118	84	47	230	45.8	0.551	31	tested_positive
1	103	30	38	83	43.3	0.183	33	tested_negative
1	115	70	30	96	34.6	0.529	32	tested_positive
3	126	88	41	235	39.3	0.704	27	tested_negative

the correct clustering examples accounting for 76.69% of the total initial dataset.

In this paper, the K-means clustering method is used to classify the data into positive and negative categories with an initial seed number of 100. By this method, the data with classification errors can be classified as noise, which results in more accurate data. The initial set of data had 500 negative and 268 positive numbers. Classifying them with the clustering algorithm yielded 458 negative and 310 positive messages, which means that there were 200 incorrectly clustered data. After eliminating these messages, the number of instances in the remaining dataset reached 568, and this part of the data occupied 74% of the total dataset.

In the secondary stage, the logistic regression algorithm was used for classification analysis. As with the independent variable information items in the original dataset, there were two categories of positive and negative classification result attributes. The logistic regression algorithm in which  $Y$  is whether the subject is diabetic or not and  $X$  is the value of the eight attributes of the original dataset. Each factor  $X$  is assigned a coefficient value, called  $\beta$ , which represents the weight. The data were effectively analyzed by a logistic



```

=== Stratified cross-validation ===
=== Summary ===

Correctly Classified Instances      562      95.416 %
Incorrectly Classified Instances    27      4.584 %
Kappa statistic                    0.8975
Mean absolute error                0.0947
Root mean squared error            0.2093
Relative absolute error            20.8655 %
Root relative squared error        43.9386 %
Total Number of Instances         589

=== Detailed Accuracy By Class ===

          TP Rate  FP Rate  Precision  Recall  F-Measure  MCC      ROC Area  PRC Area  Class
          0.982    0.098    0.950     0.982    0.965     0.899    0.979    0.990    tested_negative
          0.902    0.018    0.964     0.902    0.932     0.899    0.979    0.933    tested_positive
Weighted Avg.   0.954    0.070    0.954     0.954    0.954     0.899    0.979    0.970

=== Confusion Matrix ===
      a    b  <-- classified as
377    7 |  a = tested_negative
20 185 |  b = tested_positive

```

FIGURE 6: Graph of experimental results.

regression algorithm to obtain the weights of the variables, and the magnitude of each weight indicates the difference between  $X$  and  $Y$ . After completing the algorithmic model, new data were entered and the results were predicted for both positive and negative outcomes.

#### 4. Experimental Analysis of Application Practice

**4.1. Experimental Environment Setup.** The tool used in this paper is the WEKA Waikato Intelligent Analysis Environment (WEKA), which contains a large number of preprocessing, classification, clustering and related classical classification, clustering and correlation algorithms. The visualization interface developed using WEKA makes the experimental subject data available for quick and easy experimentation. At the same time, using the basic information provided by WEKA, one can quickly master the operation of the platform and use WEKA's interface files to easily complete one's own calculations. Its interface diagram is shown in Figure 5.

The WEKA platform combines a large number of core models and visualization tools to provide the experimenter with a convenient human-machine interface for a wide range of different data collection. The original version of WEKA consisted of a Tcl/Tk front-end model algorithm and Makefile system to run machine learning and data mining experiments. Nowadays, this fully Java-based version is widely used in many ways, especially in teaching and research. Its main advantages are as follows:

- (1) Freedom of access to this tool platform for all interested parties
- (2) Portability: The Java-based development tool platform can be easily ported on other platforms
- (3) Combination of most effective data preprocessing and data modelling techniques
- (4) Easy-to-use graphical user interface

TABLE 3: Result of the new dataset.

Item	Value (%)
Prediction accuracy	90.7
Precision	91.6
Recall	96.4
MCC	75.2
ROC area	95.7
Kappa statistic	75.2

**4.2. Dataset Preparation.** The first dataset used in this paper is from the Pima Indian Diabetes data in the UCI (UCI) machine learning database, with a total of 768 items. The 768 subjects are a general public in the state of Arizona, USA, and the National Institute of Diabetes and Kidney Diseases will conduct ongoing research on the population in this region. Each data item includes eight basic attributes, all of which are numeric in type, including the individual's basic health status and health care screening. For each attribute value, some examples of this dataset are shown in Table 2.

**4.3. Analysis of Experimental Results for Diabetes Prediction.** The improved K-means and logistic regression combined prediction model was proposed in the previous chapter, and after applying it to the dataset and conducting related experiments, it was finally concluded that the combined K-means and logistic regression prediction model is very good. The experimental results presented on the WEKA tool platform are shown in Figure 6.

Tested on a dataset, this paper presents an improved combined K-Min-Logistic regression forecasting model and compares its performance with other models.

The improved K-means and logistic regression methods were used to analyze the experimental data, and the corresponding experimental results were obtained, as shown in Tables 3 and 4. The Kappa statistic value was 0.752, which exceeded 0.75 indicating that the method had good similarity. The prediction accuracies were 0.916, 0.964, 0.964, 0.752,



TABLE 4: Comparison of the experiment.

Algorithm	Accuracy rate (%)
Our model	90.7
Random forest	79
MLP	78
Bayes net	77
J48	72
Logistic	72

and 0.957, respectively. The results showed an accuracy of 90.7%. The analysis of the experimental data showed the validity of this method.

**4.4. Experimental Analysis of Medication Use Patterns in Diabetic Patients.** According to the modified K-means and logistic regression prediction model, the drug use pattern of diabetic patients was studied. The experimental results showed that there were 283 T2DM patients with 187 herbal medicines, with *Salvia divinorum* being the highest with 243 cases, accounting for 85.87%.

The analysis of the medication use in T2DM patients revealed 21 clinically significant drug combinations, including 10 types of Dan Shen, Xuan Shen, Cang Zhu, Ge Ge Ge, Bai Zhu, Huang Lian, Huang Qi, Sang Zhi, Gui Yao, and Lycium.

In particular, two drugs were identified in the trial, pioglitazone and chlorosulfopropylurea. To verify this conclusion, we reviewed a large amount of literature, and based on the available studies, pioglitazone was indeed a risk factor for increased hospitalization rates. As the combination of pioglitazone and chlorosulfopropurea has been associated with some adverse effects in diabetic patients, it can be assumed that the above effects of pioglitazone and chlorosulfopropurea may increase the risk of re-hospitalization in hospitalized patients.

Drug rule data mining trials not only consider single data, but also do not act as a vertical dataset and may contain incomplete data. For example, many of the underlying data items are ignored because they have small variance and missing values. Also, the information does not distinguish type 1 from type 2 diabetes, so the results of the above trial do not reflect the differences in medication use rules between the two. This trial represents an attempt to use data mining techniques in this area. Therefore, future studies should use the same approach to analyze this electronic medical record in Virginia to further test and improve the existing medication rules.

## 5. Conclusion

The rapid growth of medical data and the development of data mining techniques have made the effective use of medical data a focus of attention. This paper combines data mining models with medical data features to analyze the disease and drug use of diabetic patients in clinical data and proposes a set of reasonable and appropriate prediction models for the risk of diabetes in high-risk groups based on the

experience of a large number of researchers. The model has been analyzed through the WEKA platform, and its predictive accuracy has been found to be significantly improved over previous studies. The Pima Indian Diabetes dataset used in this paper is the standard for many studies on diabetes-related data mining, and these data were compared with other researchers. The strengths and weaknesses of the trial data were preprocessed in detail to ensure that they were correct, reasonable, and standardized. Finally, after comparing the improved K-means and Logistic regression methods, which have a prediction accuracy of up to 95.42% and a conclusion of better results in terms of average prediction, the analysis of diabetes medication patterns can be carried out by keyword design during the model experiments, yielding the highest frequency of Danshen, occurrence.

## Data Availability

The dataset used in this paper are available from the corresponding author upon request.

## Conflicts of Interest

The authors declared that they have no conflicts of interest regarding this work.

## References

- [1] W. Yao, *Methods and applications of diabetes health data analysis*, [M.S. thesis], Harbin Institute of Technology, 2017.
- [2] H. Ye, *Research on diabetes prediction model based on machine learning algorithm*, [M.S. thesis], Harbin Institute of Technology, 2016.
- [3] G. Shi, S. Liu, and D. Ye, "Design and implementation of diabetes risk assessment model based on mobile things," in *2015 7th International Conference on Information Technology in Medicine and Education*, Huangshan, China, November 2015.
- [4] C. Liao, "Current epidemiology of diabetes in China and its outlook," *Journal of Chongqing Medical University*, vol. 40, no. 7, 2015.
- [5] *Diabetes Atlas*, International Diabetes Federation (IDF), 8th edition, 2017.
- [6] Y. D. He, *Analysis of diabetes clinical data based on data mining technology*, [M.S. thesis], Changchun University of Technology, 2016.
- [7] N. Chetty, "An improved method for disease prediction using fuzzy approach," in *2015 Second International Conference on Advances in Computing and Communication Engineering*, Dehradun, India, May 2015.
- [8] S. M. Butt, K. F. Navarro, M. Shorab, S. M. Butt, and A. Onn, "Using mobile technology to improve nutritional information of diabetic patients," in *New Advances in Information Systems and Technologies*, Springer Cham, 2016.
- [9] Y. Luo, C. Ling, J. Schuurman, and R. Petrella, "GlucoGuide. An intelligent type-2 diabetes solution using data mining and mobile computing," in *2014 IEEE International Conference on Data Mining Workshop*, Shenzhen, China, December 2014.
- [10] I. Kavakiotis, O. Tsave, A. Salifoglou, N. Maglaveras, I. Vlahavas, and I. Chouvarda, "Machine learning and data

- mining methods in diabetes research,” *Computational and Structural Biotechnology Journal*, vol. 15, pp. 104–116, 2017.
- [11] J. Roski, G. W. Bo-Linn, and T. A. Andrews, “Creating value in health care through big data: opportunities and policy implications,” *Health Affairs*, vol. 33, no. 7, pp. 1115–1122, 2014.
  - [12] N. V. Chawla and D. A. Davis, “Bringing big data to personalized healthcare: a patient-centered framework,” *Journal of General Internal Medicine*, vol. 28, no. S3, pp. 660–665, 2013.
  - [13] S. E. Dilsizian and E. L. Siegel, “Artificial intelligence in medicine and cardiac imaging: harnessing big data and advanced computing to provide personalized medical diagnosis and treatment,” *Current Cardiology Reports*, vol. 16, no. 1, pp. 1–8, 2014.
  - [14] W. Xueyan and Y. J. Sun, “Cloud computing and big data for healthcare collaboration,” *Communication World*, vol. 10, pp. 15–15, 2013.
  - [15] W. Hequan, “The value of big data is comparable to oil: the primary application is intelligent medical care,” *Golden Card Project*, vol. 12, p. 2, 2012.
  - [16] Z. Guanghua, X. Ying, and Z. Yajie, “Exploring the application of big data in health care,” *Chinese Journal of Health Information Management*, vol. 4, pp. 296–300, 2013.
  - [17] C. Jiahui, Z. Tao, and Z. Wenhong, “Challenges and considerations of big data in healthcare,” *Chinese Journal of Health Information Management*, vol. 4, pp. 292–295, 2013.
  - [18] L. Ying, “A preliminary exploration of the application of big data analysis in the medical industry,” *Decoration*, vol. 6, pp. 40–43, 2014.
  - [19] Z. Beiji, “Big data analytics and its application in the medical field,” *Computer Education*, vol. 7, pp. 8–9, 2014.
  - [20] Y. Zhang, H. Zhang, Y. Zhancan, L. Ming, and Z. Wen, “Early warning of severe acute pancreatitis as an example of disease prediction model based on electronic medical records using support vector institutions,” *Modern Library and Information Technology*, vol. 2, pp. 83–89, 2016.
  - [21] W. Shu, C. Min, Y. Guangjun, Y. Guo, and Z. Ling, “Research on clinical decision support system for typical childhood respiratory infectious diseases based on data mining technology,” *China Digital Medicine*, vol. 12, pp. 40–43, 2015.
  - [22] K. Luo and H. Caiwang, “An improved association rule extraction algorithm based on APriori algorithm,” *Computers and Digital Engineering*, no. 4, pp. 55–57, 2016.
  - [23] Y. X. Jing, Z. Wang, and Y. Du, “A new improved APriori algorithm,” *Journal of Changchun University of Technology*, vol. 30, no. 2, p. 72 I 74, 2017.

## Research Article

# Early Clinical Outcomes of ACL Reconstruction Using Semitendinosus Tendon Combined with LARS Synthetic

Baocai Zhang,<sup>1</sup> Peng Xiang<sup>2</sup>,<sup>3</sup> Shuai Bian,<sup>2</sup> Yibo Wang,<sup>2</sup> Yu Wang,<sup>1</sup> and Yuzhuo Ma<sup>3</sup>

<sup>1</sup>The First Operating Room, The First Hospital of Jilin University, Changchun City, Jilin Province 130021, China

<sup>2</sup>Department of Sports Medicine and Arthroscopic Surgery, The First Hospital of Jilin University, Changchun City, Jilin Province 130021, China

<sup>3</sup>Nursing Platform of Stroke Center, The First Hospital of Jilin University, Changchun City, Jilin Province 130021, China

Correspondence should be addressed to Peng Xiang; [xiangpeng@jlu.edu.cn](mailto:xiangpeng@jlu.edu.cn)

Received 24 June 2022; Revised 26 August 2022; Accepted 27 August 2022; Published 30 September 2022

Academic Editor: Hangjun Che

Copyright © 2022 Baocai Zhang et al. This is an open access article distributed under the Creative Commons Attribution License, which permits unrestricted use, distribution, and reproduction in any medium, provided the original work is properly cited.

**Objective.** To compare the early clinical outcomes of ACL reconstruction using the augmented semitendinosus tendon combined with LARS synthetic material and the autologous hamstring tendons. **Methods.** A total of 68 eligible patients with ACL rupture were reconstructed using either 4-strand autologous hamstring tendons, representing the control group, or the LARS synthetic material augmented grafts. The duration of postoperative swelling and recovery exercise was recorded. Lysholm and IKDC scores were used for evaluation of knee joint function. Lachman and pivot shift tests were conducted to evaluate stability. **Results.** The scores of the three knee functions in cases of the augmentation group were significantly higher than those of the control group 6 months after surgery ( $P < 0.05$ ). There were no significant differences in Tegner score in the two groups 12 months after surgery ( $P > 0.05$ ). In general, the augmentation group returned to exercise 12 weeks after surgery, while the control group required 30 weeks. **Conclusions.** The present study indicates that synthetic material augmentation grafts allow earlier return to exercise and display more satisfactory results compared with the control group.

## 1. Introduction

Anterior cruciate ligament (ACL) is essential for maintaining stability in the knee joint. It has been established that ACL-deficient knees exhibit damage to intra-articular structures such as the meniscus and cartilage, eventually resulting in serious joint degeneration. Arthroscopic ACL reconstruction is the best therapeutic option in young and active population, while the controversy continues over the choice of the graft tissue. In the past, the BPTB autograft has been considered the gold standard in ACL reconstruction because of its osseous fixation mode. Increasingly, the hamstring tendon autografts have been used as an alternative to the BPTB graft due to the reduced donor site morbidity and significantly improved fixation technique and are currently considered as one of the most common grafts. However, regardless the graft type, autograft requires a long time of maturity following implantation, limiting early exercise postoperation, which may negatively affect recovery. Synthetic ligaments for ACL reconstruction have

been widely used since the 1980s. The initial enthusiasm about the introduction of synthetic materials stemmed from lack of donor morbidity, abundant supply, and significant strength. The strength of a synthetic material can be applied to share tension during the process of autologous tendon remodeling, protecting potential weak areas and reducing the risk of secondary injury during rehabilitation training, which can help patients return to activity earlier. The aim of the present study was to compare the early outcome of ACL reconstruction using augmentation of semitendinosus tendons with synthetic material versus 4-strand autologous semitendinosus and gracilis tendons (ST/G) to assess the effectiveness of the two groups regarding knee function. Our hypothesis was that postoperative knee stability was better in the augmented group.

## 2. Patients and Methods

**2.1. Clinical Data.** A total of 68 patients with a torn ACL from June 2018 to February 2019 were included in the

TABLE 1: Demographics of the augmented and control groups.

Group	M/FM	Age	Time to surgery	Lysholm score	Tegner score	IKDC score
Enhance	30/6	27 (17-37)	2.2 (1-6)	46.7 $\pm$ 3.4	2.1 $\pm$ 0.6	49.2 $\pm$ 3.8
Control	24/8	33 (21-42)	3.6 (1-8)	45.1 $\pm$ 3.0	2.1 $\pm$ 0.5	47.5 $\pm$ 3.5

present study (Table 1). Patients were diagnosed using a pivot shift test and magnetic resonance imaging. Each patient was informed in detail of the nature of their injury and the possible surgical procedures. Each received either an augmented semitendinosus tendon with synthetic material (LARS, L130605B) or 4-strand ST/G, representing the control group, as a graft. The patients were assigned by a single-blind quasirandomization. After passing the inclusion/exclusion criteria and giving consent for the study, they were numbered serially, and alternate numbers were assigned to the two groups. The surgeon was not informed of the group to which a patient was assigned until before surgery. There were 36 cases in the augmentation group, of which 5 cases were complicated by a posterior horn tear of the medial meniscus and 4 with posterior horn tear of the lateral meniscus. There were 32 cases in the control group, of which 4 cases were complicated by posterior horn tear of the medial meniscus and 6 with posterior horn tear of the lateral meniscus. The two groups were comparable in terms of gender, age, period between injury and surgery, and preoperative knee joint function score. All procedures were approved by the local ethical committee and performed by a single senior surgeon. All subjects provided signed informed consent.

**2.2. Inclusion and Exclusion Criteria.** Inclusion criteria: patients suffering their first ACL injury, with no history of knee surgery; professional sports injuries, requiring surgery to continue a sports career; pursuing high quality of life, hoping to return to exercise quickly.

Exclusion criteria: patients with complicated medial or lateral collateral ligament injury, complicated posterior cruciate ligament injury, complicated joint cartilage injury requiring microfracture or osteochondral transplantation, ACL reconstruction adopting an alternative fixation method were excluded. Patients with incomplete clinical information or cognitive impairment and mental abnormalities were also excluded.

### 2.3. Surgical Technique

**2.3.1. Graft Preparation of the Augmentation Group.** The semitendinosus tendon of the affected limb was excised using conventional methods. LARS synthetic material of an appropriate length and width and a single semitendinosus tendon were laminated and woven together and then folded into two strands, with synthetic material completely wrapping around the semitendinosus tendon, the two edges closed with high-strength sutures to complete preparation of the graft, which had a diameter of 8 mm, and so was the control group. The graft was then soaked in vancomycin saline solution for 10 minutes (Figure 1).

**2.3.2. Arthroscopic Graft Installation.** Arthroscopic examination was performed using standard anteromedial and anterolateral approaches. Any remaining ACL with synovial covering was preserved as far as possible. All patients underwent arthroscopic single bundle ACL reconstruction. An appropriate femoral offset guide was placed at a 2 or 10 o'clock position for the left or right knees to cover the footprint zone of the anteromedial bundle. The tibial tunnel was positioned as forward as possible, to ensure it did not conflict with the intercondylar fossa. The femoral end of the graft was suspended and fixed with a tight cord (Arthrex, 3.5 mm), while the tibial end was fixed with a bioresorbable screw (Arthrex, 8 mm) combined with an anchor (Arthrex, SwiveLock, 4.75 mm).

### 2.4. Postoperative Rehabilitation

**2.4.1. Augmentation Group.** Isometric contraction of the quadriceps femoris and ankle pump exercises were conducted immediately following recovery from anesthesia. Knee flexion increased gradually to complete flexion and extension and full weight bearing using a brace within the first 2 weeks. Cycling and jogging were permitted 4 weeks postoperatively. Return to full exercise occurred 3 months after surgery.

**2.4.2. Control Group.** Isometric contraction of the quadriceps femoris and ankle pump exercise were conducted immediately following recovery from anesthesia. Knees were bent to 90 degrees, and partial weight bearing was permitted using crutches during the first week. Static stepping for balance was allowed for 2 weeks followed by full weight bearing after 4 weeks postoperatively, and cycling and swimming 3 months postoperatively. A gradual return to exercise occurred 6-9 months after surgery.

**2.5. Follow-Up and Evaluation.** All cases were followed up for at least 12 months in strict accordance with the advice from a clinician. The duration of postoperative knee joint swelling evaluated by floating patella test, the duration of the period before return to exercise, and complications such as joint stiffness, infection, and re-tear were recorded for each patient. The Lysholm score [1], Tegner activity score [2], and IKDC scores [3] were recorded on 4 occasions: preoperatively and after 3, 6, and 12 months. At the final follow-up examination, Lachman and pivot shift tests were conducted for knee stability evaluation.

**2.6. Statistical Analysis.** Prism 6 (GraphPad) statistical software was used to analyze patient data. Measurement data are expressed as means  $\pm$  SDs and functional score values recorded during follow-up examinations analyzed statistically using a one-way ANOVA and observation results by  $t$



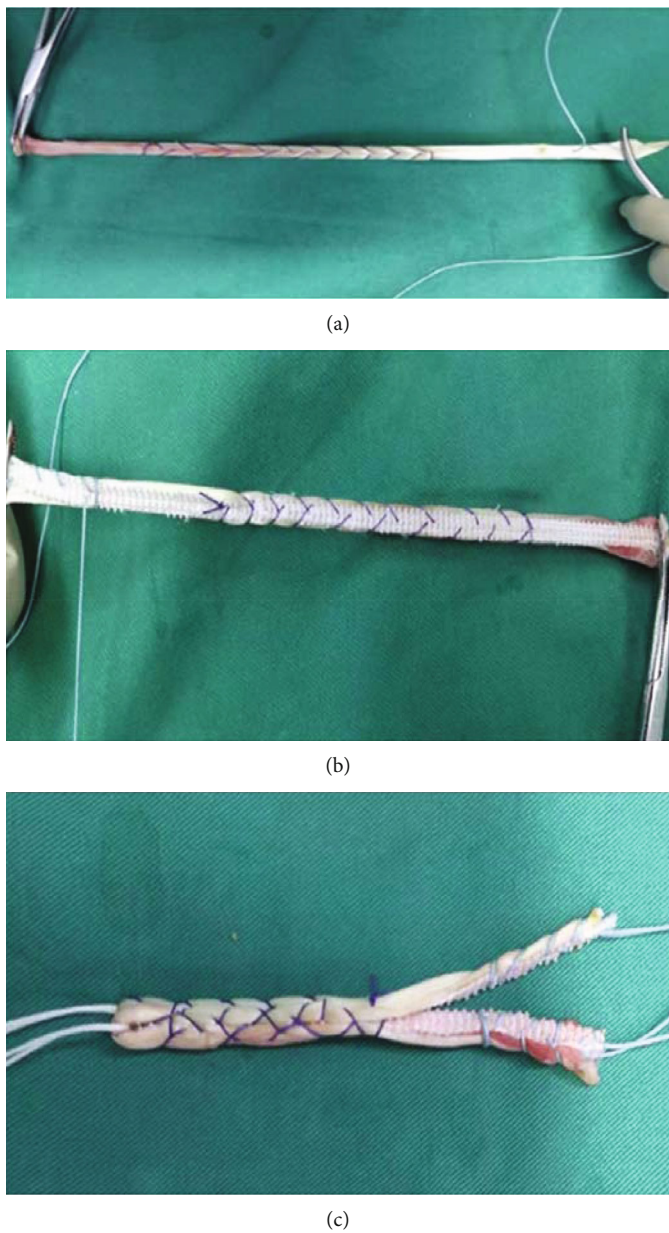


FIGURE 1: The preparation process of augmented graft: (a) graft was woven; (b) the reverse side; (c) final appearance of the augmented graft.

-tests. A chi-square test was used to compare count data. Differences in which  $P < 0.05$  were considered statistically significant.

3. Results

3.1. Postsurgical Follow-Up. All patients completed a successful follow-up plan. The mean duration of postoperative swelling was 8 days (range: 3-22 days) in the augmentation group and 14 days (range: 10-30 days) in the control group. The augmentation group began to return to exercise 12 weeks (range: 8-20 weeks) after surgery, while the control group was fully exercising 20 weeks (range: 24-40 weeks) after surgery. No patients experienced subjective instability of the knee joint. Objective examination (Table 2) indicated that stability of the knee joint within the augmentation

TABLE 2: Lachman and pivot shift test 12 months after surgery.

Group	Lachman			Pivot shift		
	0	1+	2+	0	I	II
Enhance ( $n = 36$ )	34	2	0	36	0	0
Control ( $n = 32$ )	26	4	2	29	3	0

group was greater than that of the control group one year after surgery. At the final follow-up examination, 2 cases underwent arthroscopic secondary exploration for removal of tibial screws (Figure 2).

3.2. Knee Joint Functional Score

3.2.1. Comparative Analysis between Groups. There was no significant difference in three knee joint functional scores



FIGURE 2: Magnified observation: augmented graft with synovial sheath and infiltrating vessels during the 12-month follow-up examination.

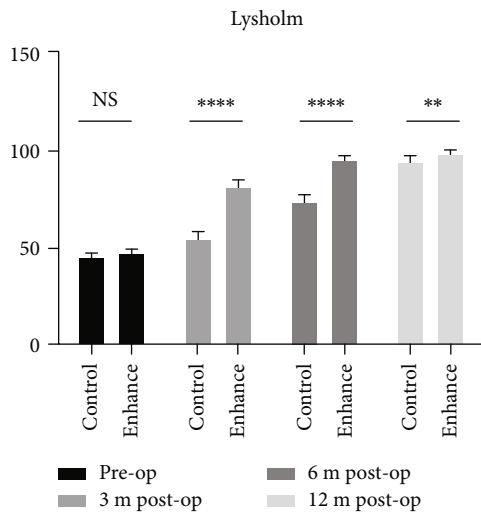


FIGURE 3: Lysholm scoring of the two groups was compared pre- and postoperatively (\* stands for  $P < 0.05$ , \*\* stands for  $P < 0.01$ , and \*\*\* stands for  $P < 0.001$ , ns = not significant).

between the two groups preoperatively ( $P > 0.05$ ). All scores in the augmentation group were significantly higher than those in the control group 3 and 6 months postoperatively ( $P < 0.05$ ). There was no significant difference in Tegner score between the two groups 12 months after surgery ( $P > 0.05$ ), while the Lysholm and IKDC scores in the augmentation group were  $97.9 \pm 1.9$  and  $96.9 \pm 2.5$ , respectively, higher than the scores in the control group, at  $94.6 \pm 1.7$  and  $93.7 \pm 2.1$ , respectively ( $P < 0.05$ ), although the differences were substantially smaller than at earlier time points. This demonstrates that differences in functional scores in the two groups gradually narrowed as recovery time progressed, being closest at 12 months postoperatively.

**3.2.2. Comparative Analysis Intragroup.** The increase in the three knee joint functional scores in the augmentation group was the largest in the first 3 months after surgery and lower

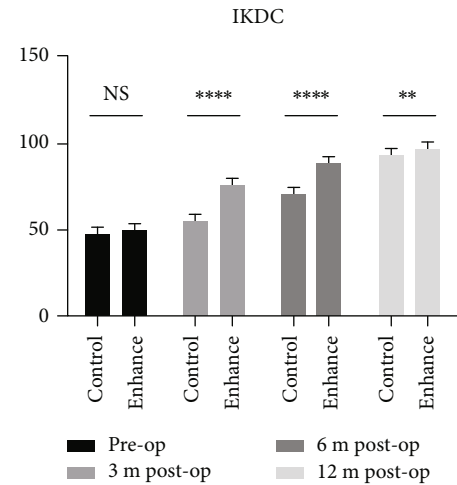


FIGURE 4: IKDC scoring of the two groups was compared pre- and postoperatively (\* stands for  $P < 0.05$ , \*\* stands for  $P < 0.01$ , and \*\*\* stands for  $P < 0.001$ , ns = not significant).

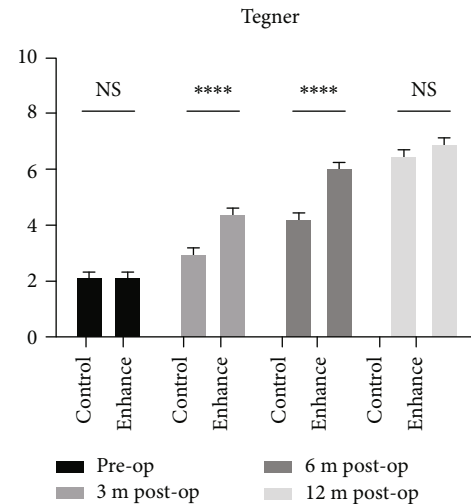


FIGURE 5: Tegner scoring of the two groups were compared pre- and postoperatively (\* stands for  $P < 0.05$ , \*\* stands for  $P < 0.01$ , and \*\*\* stands for  $P < 0.001$ , ns = not significant).

in the second 3 months, while being the lowest from 6 to 12 months postoperatively. Conversely, in the control group, the increase in knee joint functional scores was the smallest in the first 3 months, while the largest in the period from 6 to 12 months postoperatively (Figures 3–5).

**3.3. Postoperative Complications.** There were 2 cases suffering knee crepitus, following surgery in the augmentation group and 6 cases in the control group. One patient in the augmentation group developed fever after surgery. The infection was eliminated and bacterial culture of the joint fluid was negative. In the control group, 2 cases still had limitations in bending of their knees 3 months after surgery, which were improved by manipulation during outpatient visits. No complications were observed, such as screw



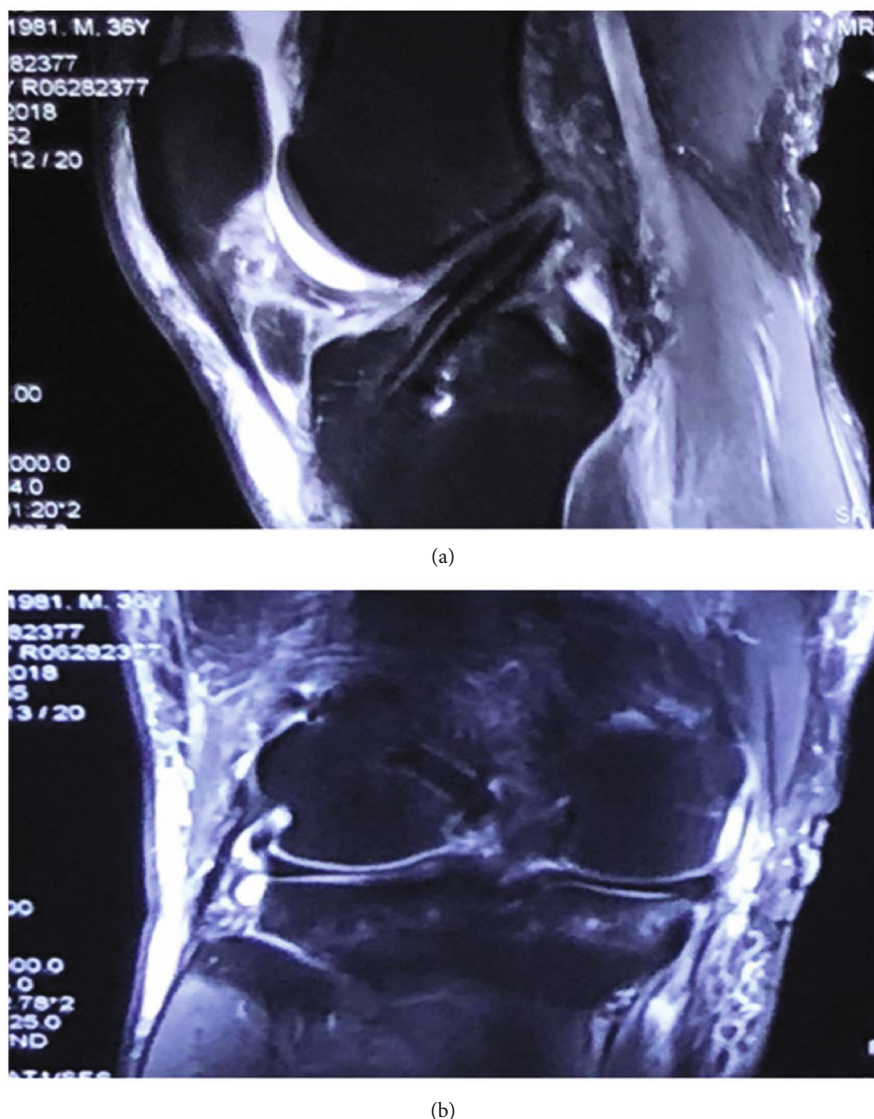


FIGURE 6: MRI evaluation following ACL reconstruction using an augmented graft. Sagittal view: normal shape of the graft in the joint and synthetic material wrapped around the autogenous tendon. Coronal view: femoral tunnel is completely filled with the graft.

loosening, infection, reactive synovitis, bone tunnel enlargement, or retear.

#### 4. Discussion

Over recent years, ST/G has become a common autologous grafting procedure for reconstruction of the ACL. However, postoperative ligament relaxation and retear are not uncommon. Literature reports indicate these are related to gender, age, level of exercise, and graft diameter [4]. A cohort study indicated that for every 0.5 mm increase in graft diameter, postoperative revision rate decreased by 14% [5]. Park et al. [6] followed up 296 patients with ST/G ACL reconstruction and found that recovery of knee joint function in grafts with a diameter greater than or equal to 8 mm was significantly greater than that smaller than 8 mm. However, the diameter of an autologous graft is related to the patient's native tendon, which surgeons cannot control. Autologous

tendons undergo necrosis, revascularization, and replacement of collagen fibers and finally become shaped and reconstructed into a substitute ligament close to the biological characteristics of an ACL following implantation, its strength correspondingly changing from strong to weak and then gradually increasing. The process lasts for 6 to 9 months or even longer [7, 8]. The high risk of ligament laxity during this period limits the recovery of early activity. Aboalata et al. [9] believed that grafts augmented by high strength sutures could reduce the ligament laxity ratio in patients with a high body mass index and narrow graft (diameter 7 or 7.5 mm).

Synthetic ligaments, in which no revascularization process is required, can exert large mechanical effects immediately following implantation. However, they cannot achieve the biomechanical characteristics of ACL due to the lack of viscoelasticity and occurrence of abrasion [10]. The combination of a synthetic ligament and autogenous tendon can

ensure sufficient thickness and length of the graft, and the use of high-strength artificial materials to maintain the initial stability of the joint can protect an autogenous tendon so that the creep period is endured uneventfully, ensuring that early postoperative functional exercise can be safely undertaken, while autogenous tendons can compensate for the deficiency of fatigue decay of the synthetic materials following remodeling. In the present study, standard 4-strand ST/G reconstruction was used as a control, and functional recovery of the knee following augmented reconstruction was evaluated in terms of the subjective assessment of patients, evaluation of clinicians and objective motor capability. The results indicate that the patients in the augmentation group began to return to exercise 12 weeks after surgery, significantly earlier than the 30 weeks in the control group. The three knee joint scores of patients in the augmented group were higher than those in the control group 3 and 6 months after surgery, indicating that knee joint function had recovered more quickly. The Tegner score in particular, which reflects motor capability, improved most significantly 3 months after surgery but was not significantly different in either group after 12 months, indicating that the advantage of this technique is functional improvement during the early stages of recovery.

As early as the 1980s, Kennedy et al. [11] first proposed a ligament augmentation device (LAD), used mainly for *in situ* repair of partial ACL laceration. Kdolsky et al. [12] utilized the Kennedy-LAD technique to treat 66 patients with ACL laceration and followed up for 5-8 years, finding that 75% of the patients recovered preinjury levels of movement following surgery. Nakayama et al. [13] reported that 92% of 50 athletes returned to sporting activities one year after ACL reconstructive surgery using Leeds-Keio augmented autologous ligaments. However, due to limitations in the development of materials science, many negative reports have been published.

With the extensive use of LARS ligament products in France, good therapeutic effects have been achieved. Some researchers [14] have recommended the use of a hollow LARS ligament combined with autologous tendon for ACL reconstruction in patients with poor donor ligament quality, but this method uses only a simple overlap of synthetic material of the two types of graft, which is entirely exposed in the joint cavity and with the same risk of complications as the standard LARS ligament. The maximum load for strips of LARS synthetic material selected in the present study was 3600 N, satisfying the requirements of the mechanical strength of an ACL ( $1730 \pm 270$  N). Postoperative nuclear magnetic resonance imaging clearly displayed the structure of the graft, completely wrapped around an autologous tendon (Figure 6), which was able to exert mechanical effects while avoiding the inherent complications of the synthetic material, the incidence of ligament relaxation significantly lower than that of the control group assessed during the one-year follow-up examination. In addition, we used suspension fixation technology, which did not require strict use of absolutely equal graft lengths during surgery, providing excellent fault tolerance compared with conventional LARS reconstruction.

Although removal of any remaining ACL assists in locating the intra-articular bone tunnel and improves the accuracy of surgical procedure, histological studies have confirmed that an abundant blood supply and proprioceptors are present in ligaments and the synovium [15]. In the present study, all patients underwent reconstruction with remnant preservation [16]. The remnant ACL was as far as possible pulled into the bone tunnel or tunnel portal when the graft was installed. The synovium attached to the edge of femoral intercondylar fossa was retained to promote recovery of proprioception following surgery. In addition, only the semitendinosus tendon was excised in the augmentation group, preserving the function of the gracilis muscle.

The sample size of this study was limited and the duration of follow-up not extensive. The clinical value of the study is to some degree compromised, and in the future, a larger sample size and longer duration of follow-up observation are required.

## 5. Conclusions

Compared with standard 4-strand ST/G, LARS synthetic material augmentation of the semitendinosus tendon for ACL reconstruction was able to achieve greater knee joint stability and more satisfactory results, especially in patients who require early recovery of high-level exercise.

## Data Availability

The datasets used and analyzed during the current study are available from the corresponding author upon reasonable request.

## Conflicts of Interest

The authors declare that they have no conflicts of interest.

## Authors' Contributions

Baocai Zhang and Yuzhuo Ma have contributed equally to this work and share first authorship.

## References

- [1] J. Lysholm and J. Gillquist, "Evaluation of knee ligament surgery results with special emphasis on use of a scoring scale," *The American Journal of Sports Medicine*, vol. 10, no. 3, pp. 150-154, 1982.
- [2] Y. Tegner and J. Lysholm, "Rating systems in the evaluation of knee ligament injuries," *Clinical Orthopaedics and Related Research*, vol. 198, pp. 42-49, 1985.
- [3] F. Hefti and W. Muller, "Current state of evaluation of knee ligament lesions. The new IKDC knee evaluation form," *Orthopade*, vol. 22, no. 6, pp. 351-362, 1993.
- [4] P. M. Kamien, J. M. Hydrick, W. H. Replogle, L. T. Go, and G. R. Barrett, "Age, graft size, and Tegner activity level as predictors of failure in anterior cruciate ligament reconstruction with hamstring autograft," *The American Journal of Sports Medicine*, vol. 41, no. 8, 2013.

- [5] T. Snaebjornsson, E. Hamrin Senorski, O. R. Ayeni et al., "Graft diameter as a predictor for revision anterior cruciate ligament reconstruction and KOOS and EQ-5D values: a cohort study from the Swedish National Knee Ligament Register Based on 2240 patients," *The American Journal of Sports Medicine*, vol. 45, no. 9, pp. 2092–2097, 2017.
- [6] S. Y. Park, H. Oh, S. Park, J. H. Lee, S. H. Lee, and K. H. Yoon, "Factors predicting hamstring tendon autograft diameters and resulting failure rates after anterior cruciate ligament reconstruction," *Knee Surgery, Sports Traumatology, Arthroscopy*, vol. 21, no. 5, pp. 1111–1118, 2013.
- [7] A. Weiler, R. F. Hoffmann, H. J. Bail, O. Rehm, and N. P. Sudkamp, "Tendon healing in a bone tunnel. Part II: histologic analysis after biodegradable interference fit fixation in a model of anterior cruciate ligament reconstruction in sheep," *Arthroscopy*, vol. 18, no. 2, pp. 124–135, 2002.
- [8] A. Weiler, R. Peine, A. Pashmineh-Azar, C. Abel, N. P. Sudkamp, and R. F. Hoffmann, "Tendon healing in a bone tunnel. Part I: biomechanical results after biodegradable interference fit fixation in a model of anterior cruciate ligament reconstruction in sheep," *Arthroscopy*, vol. 18, no. 2, pp. 113–123, 2002.
- [9] M. Aboalata, A. Elazab, A. Halawa, A. B. Imhoff, and Y. Bassiouny, "Internal suture augmentation technique to protect the anterior cruciate ligament reconstruction graft," *Arthroscopy Techniques*, vol. 6, no. 5, pp. e1633–e1638, 2017.
- [10] L. M. Batty, C. J. Norsworthy, N. J. Lash, J. Wasiak, A. K. Richmond, and J. A. Feller, "Synthetic devices for reconstructive surgery of the cruciate ligaments: a systematic review," *Arthroscopy*, vol. 31, no. 5, pp. 957–968, 2015.
- [11] J. C. Kennedy, J. H. Roth, H. V. Mendenhall, and J. B. Sanford, "Presidential address: intraarticular replacement in the anterior cruciate ligament-deficient knee," *The American Journal of Sports Medicine*, vol. 8, no. 1, pp. 1–8, 1980.
- [12] R. Kdolsky, O. Kwasny, and R. Schabus, "Synthetic augmented repair of proximal ruptures of the anterior cruciate ligament," *Clinical Orthopaedics and Related Research*, vol. 295, pp. 183–189, 1993.
- [13] Y. Nakayama, Y. Shirai, T. Narita, A. Mori, and K. Kobayashi, "Knee functions and a return to sports activity in competitive athletes following anterior cruciate ligament reconstruction," *Journal of Nippon Medical School*, vol. 67, no. 3, pp. 172–176, 2000.
- [14] F. Hamido, H. Al Harran, A. R. Al Misfer et al., "Augmented short undersized hamstring tendon graft with LARS® artificial ligament versus four-strand hamstring tendon in anterior cruciate ligament reconstruction: preliminary results," *Orthopaedics & Traumatology, Surgery & Research*, vol. 101, no. 5, pp. 535–538, 2015.
- [15] L. Guo, H. Chen, J. M. Luo, L. Yang, L. C. Gu, and D. J. Fu, "An arthroscopic second-look study on the effect of remnant preservation on synovialization of bone-patellar tendon-bone allograft in anterior cruciate ligament reconstruction," *Arthroscopy*, vol. 32, no. 5, pp. 868–877, 2016.
- [16] H. L. Nag and H. Gupta, "Anterior cruciate ligament reconstruction with preservation of femoral anterior cruciate ligament stump," *Arthroscopy Techniques*, vol. 3, no. 5, pp. e575–e577, 2014.

## Research Article

# The Effects of Combuxil and Leizumab on Retinal Function and Serum Interleukin-17A in Premature Infants with Retinopathy

Huixuan Ren,<sup>1</sup> Gang Su,<sup>2</sup> Shunian Xu,<sup>2</sup> Li Zhou,<sup>2</sup> and Shanjun Cai<sup>2</sup> 

<sup>1</sup>Ophthalmology, Department of Ophthalmology, Affiliated Hospital of Zunyi Medical University, Guizhou Provincial Eye Hospital, Guizhou Branch Center of National Clinical Research Center for Eye Diseases, Guizhou Provincial Key Laboratory of Characteristic Eye Diseases Characteristics, Zunyi, Guizhou 563003, China

<sup>2</sup>Ophthalmology, Affiliated Hospital of Zunyi Medical University, Zunyi, Guizhou 563003, China

Correspondence should be addressed to Shanjun Cai; [csj123@zcmu.edu.cn](mailto:csj123@zcmu.edu.cn)

Received 20 June 2022; Revised 16 August 2022; Accepted 23 August 2022; Published 26 September 2022

Academic Editor: Hangjun Che

Copyright © 2022 Huixuan Ren et al. This is an open access article distributed under the Creative Commons Attribution License, which permits unrestricted use, distribution, and reproduction in any medium, provided the original work is properly cited.

**Objective.** To investigate the effects of Compaximab and raizumab on retinal function and serum interleukin-17A level in retinopathy of prematurity. **Methods.** Sixty cases of retinopathy of prematurity treated in our hospital from February 2019 to April 2021 were selected. The patients were randomly divided into control group ( $n = 30$ ) and research group ( $n = 30$ ). The control group was treated with Compaq and the research group was treated with razumab. The curative effect, retinal function, incidence of complications, intraocular pressure at different time, and the level of serum interleukin-17A were compared. **Results.** Compared with the two groups, the curative effect of the research group 93.33% (28/30) was greater than that of the control group 66.67% (20/30), and the difference was statistically significant ( $P < 0.05$ ). Compared with the incidence of complications, the incidence of corneal opacity, lens opacity, preretinal and vitreous hemorrhage, endophthalmitis, and traction retinal detachment in the research group was greatly lower, and the difference was statistically significant ( $P < 0.05$ ). Following the therapy, the IOP of the two groups decreased at different times. The IOP of 1 min, 10 min, and 30 min in the research group was obviously lower, and the difference was statistically significant ( $P < 0.05$ ). Following treatments, the levels of serum IL-17A were decreased. Compared with the control group, the level of serum IL-17A in the research group was greatly downregulated, and the difference was statistically significant ( $P < 0.05$ ). **Conclusion.** Intravitreal injection of razumab is an effective treatment for retinopathy of prematurity, which can effectively improve the retinal function of infants. The level of serum interleukin-17A can be reduced and intraocular pressure can be regulated, which is safe and effective.

## 1. Introduction

Retinopathy of prematurity (ROP), formerly known as posterior lens fibroplasia, was first proposed by Terry. It is characterized by abnormal growth of retinal vessels at the junction of vascularized and nonvascularized areas of the retina [1, 2]. According to a retrospective analysis of the causes of visual impairment in children abroad, the blindness rate caused by ROP is as high as 8%. The rate of blindness can be reduced through early detection and timely treatment of ROP. The rate of blindness is high, so it has attracted more and more attention of pediatricians all over the world. Globally, there were about 184700 new ROP patients in 2010. About 20000 patients became blind or developed severe visual impairment

as a result of ROP, and 12300 developed mild to moderate visual impairment [3]. ROP is a blindness disease. The main cause of blindness is retinal detachment caused by retinal vascular abnormality and scar formation. At present, hyperoxia exposure, small gestational age and low birth weight have been confirmed to be the main risk factors for retinopathy of prematurity [4, 5].

The main pathological changes of ROP are the arrest of normal retinal vascular development and pathological neovascularization, which can lead to blindness of retinal detachment in severe cases. In addition, the duration of mechanical ventilation, blood transfusion, use of caffeine, and serious complications such as respiratory distress syndrome (NRDS), bronchopulmonary dysplasia (BPD), maternal



pregnancy induced hypertension, and prenatal hormone use were also confirmed to be related to the occurrence of ROP [6]. The pathogenesis of ROP is still unclear. It is generally believed that postnatal hyperoxia exposure on the one hand stops the development of normal retinal vessels. On the other hand, with the development of the disease, hypoxia causes excessive production of angiogenic factors in the body, which leads to pathological angiogenesis. It is suggested that inflammatory factors play an important role in blocking normal retinal vascular development, inducing pathological neovascularization, and promoting the occurrence of ROP. Some studies have shown that the levels of endothelial nitric oxide synthase, dicarboxylic acid carnitine (C3DC), glycine, and serine are significantly increased in children with ROP. Other biomarkers such as brain-derived neurotrophic factor and matrix metalloproteinase-9 (MMP-9) are still being studied. At present, a few foreign studies have confirmed that IL-17A is related to ocular neovascularization [7] and IL-17-related cytokines have also been confirmed to be involved in the pathological process of ROP [8], but its underlying mechanism is still unclear.

Previous studies at home and abroad have found that VEGF has been well explained in many animal models and humans [9–11]. Both razumab and bevacizumab are humanized monoclonal VEGF antibody fragments against retinal vascular diseases. Comperxil is a recombinant fusion protein with fully humanized amino acid sequence, which has become another choice for ROP therapy. Combuxil showed higher VEGF binding ability because it binds to the second Ig domain of VEGF receptor-1 [12]. Prospective study follow-up for 1 year found good anatomical structure and functional outcome of retina can be obtained after Compaq treatment of ROP [13]. Previously, some scholars have conducted a small sample study on the treatment of ROP by intravitreal injection of Combuxil. The results show that Compaq has less effect on intraocular pressure, but the efficacy and safety of larger samples after treatment, especially the effect on growth and development after treatment with Combuxil is still unclear [14]. The common dose of anti-VEGF of ROP is half that of adults, but VEGF is very important for neonatal development, especially for the development of brain, kidney, lung, and other important organs. The half-life of Compaximab is longer and its molecular weight is larger than that of razumab, which may have a greater negative effect on the growth and development of premature infants [15]. Therefore, Compaximab and raizumab were used to treat ROP, and the efficacy, safety, growth, and development parameters were evaluated and compared in order to delivery effective references for the follow-up of ROP. This study was to investigate the effects of Compaximab and raizumab on retinal function and serum interleukin-17A level in retinopathy of prematurity.

## 2. Materials and Methods

**2.1. General Information.** Sixty cases of retinopathy of prematurity from February 2019 to June 2021 were enrolled. The control group ( $n = 30$ ) were treated with Compaq, and the study participants were treated with razumab. The con-

trolled gestational age was 25–33 weeks, including 18 males and 12 females. In the research group ( $n = 30$ ), the gestational age was 25–33 weeks, including 16 males and 14 females. This study was approved by the ethics committee of the hospital. All the guardians of the participants consent with the study.

Selection criteria: (1) according to the 2014 Chinese guidelines for screening retinopathy of prematurity [16], after the diagnosis of threshold lesion or type 1 prethreshold lesion, treatment should be received within 72 hours as far as possible. Threshold disease: Stage 3 + in area I or II and the adjacent lesions lasted for at least 5 hours or accumulate up to 8 hours, it was a disease that must be treated. Prethreshold disease: referred to the severity of ROP lesions that were obvious but have not reached the threshold, it can be divided into “type 1 pre-threshold lesion” and “type 2 pre-threshold lesion”. Type 1 prethreshold lesions included any stage lesions in area I with additional lesions, stage 3. Aggressive posterior ROP (AP-ROP): it occurs in the posterior pole, usually in area I, with rapid progress and often involving four quadrants. The disease may not progress according to the typical development law of stage 1 to 3, and the severe “additional lesion” was once called “Rush” disease; it often occurred in very low-weight premature infants. The condition was often more serious and needs to be treated as soon as possible. (2) Good compliance and can cooperate with the examiner during the follow-up period.

Exclusion criteria: (1) premature infants with ROP4 and stage 5 retinal detachment, and other retinal choroidopathy, those with congenital cataract or corneal leukoplakia and other serious ocular diseases, could not observe the fundus condition, and those with severe systemic diseases had no history of other eye surgery and external injuries. (2) Uncooperative treatment and lost patients during follow-up. (3) It did not meet the treatment standard of China’s guidelines for screening retinopathy of prematurity.

**2.2. Methods.** All the children were treated with vitreous injection under surface anesthesia in the aseptic laminar flow operating room of our hospital. The infants were fasted for 2 hours before operation, and compound tropicamide eye drop was used for 3 times (10 min/times). After 3 times (5 min/times) of surface anesthesia with promeacaine hydrochloride eye drops, 5% povidone iodine solution was used to disinfect the eyes. The eyelid was opened with special eyelid opener for children, and the eyeball was fixed with ophthalmic micro tweezers. The 30G injection needle was injected into the 1 mm parallel optic axis behind the temporal limbus of the eyes. The control cases were injected by Compaq 0.25 mg. The research group received injection of 0.25 mg tobramycin dexamethasone eye ointment. Three days after operation, routine antibiotic eye drops were used.

### 2.3. Observation Indicators

**2.3.1. Curative Effect.** The curative effect was judged by observing the anatomical outcome [17]. Effective: retrogression of additional lesions, tortuosity of retinal vessels, disappearance or decrease of neovascularization, and growth of

normal retinal vessels around; ineffective: during the follow-up period, the recurrence of the disease requires reinjection or laser treatment, abnormal lesions such as crest and additional lesions relapse. Total effective rate = number of valid cases/total number of cases  $\times$  100%.

**2.3.2. Incidence of Adverse Reactions.** The adverse reactions were compared during treatment, including ocular complications, corneal haze implantation, lens opacity, preretinal and intravitreous hemorrhage, endophthalmitis, and traction retinal detachment.

**2.3.3. Intraocular Pressure at Different Time.** Intraocular pressure (IOP) was measured and recorded with Icare magnetic rebound tonometer (Icare, Finland) 1 minute before treatment and 1, 10, and 30 minutes after treatment.

**2.3.4. Serum IL-17A Level.** Venous blood 1 ml was collected before treatment, on the 1st day and 15th day after treatment. The content of IL-17A in serum was determined by ELISA (ebioscience, USA). The content was determined according to the instructions of the kit.

**2.4. Statistical Analysis.** IBMSPSS24.0 software was applied for statistical analysis. The measurement data were expressed by mean  $\pm$  standard deviation. The counting data were expressed by frequency or rate. *T*-test was used when measurement data obey normal distribution, and rank sum test was used when it did not obey normal distribution.  $\chi^2$  test was used to compare the classified counting data. Repeated measurement data were analyzed by repeated measurement analysis of variance. Main effect test results were used when there was no interaction, and simple effect analysis was carried out when there was interaction.  $P < 0.05$  indicated that the difference between groups is statistically significant.

### 3. Results

**3.1. Comparison of Curative Effect between Two Groups.** Comparing the curative effect, the curative effect of the research cohort was 93.33% (28/30), which was upregulated remarkably than that of the control group 66.67% (20/30), and the difference was statistically significant ( $P < 0.05$ ). All results were shown in Figure 1.

**3.2. Comparison of the Incidence of Complications.** The incidence of corneal opacity, lens opacity, preretinal and vitreous hemorrhage, endophthalmitis, and traction retinal detachment in the research group was greatly lower than the control group, and the difference was statistically significant ( $P < 0.05$ ). All results were shown in Figure 2.

**3.3. Comparison of Intraocular Pressure at Different Time.** Following treatment, the IOP of the two groups decreased at different times, and the IOP of 1 min, 10 min, and 30 min in the research group was considerably lower than that of the control. All results were shown in Table 1.

**3.4. Comparison of Serum IL-17A Levels.** After treatment, the level of serum IL-17A in both groups decreased, and the

level of serum IL-17A in the research group was remarkably downregulated than control group. All results were shown in Table 2.

### 4. Discussion

Epidemiological survey results show that more than 1300 million premature infants born worldwide survived through infancy in 2010 [18]. It is estimated that more than 1.8 million premature infants suffer from varying degrees of ROP, of which more than 50000 may cause visual impairment [19–22]. The “first ROP blindness epidemic” occurred in industrialized countries in the 1940s and 1950s, mainly affecting premature infants in the United States. Unmonitored oxygen supplementation is a major risk factor for premature infants [18]. At that time, it has been carried out for 6 years since 1940 for the presence of bilateral eye-related lesions (the growth of embryonic connective tissue behind the lens, only a few retinal vessels full of blood flow, the presence of intravitreous arteries, abnormal iris color, retinal folds, and retinal detachment. The investigation of the project with different severity (only a few traces after the lens to the extent of extensive involvement) found that extremely premature infants were abnormally common. At that time, many eye signs were considered to be caused by such important and abnormal eye development, such as retinal retardation or lack, early shallowness of the anterior chamber, corneal lens adhesion, corneal opacity, and congenital glaucoma. ROP is not only the leading cause of sexual blindness in children but also one of the important eye diseases leading to white pupil sign [19, 20]. However, premature infants have no choice but to use the auxiliary oxygen therapy of inhaling high concentration oxygen. It is an important measure to save the lives of premature infants, but it is a risk factor for retinopathy of premature infants [21–23]. This study was to investigate the effects of Compaximab and raizumab on retinal function and serum interleukin-17A level in retinopathy of prematurity.

Compared with after birth, the fetus is in a state of hypoxia in the womb. When babies are born prematurely, relative oxygen levels sometimes will increase even if oxygenation is at normal environmental levels. Supplementary oxygen therapy with high supplementation of oxygen may damage capillaries and make the development of retina in an environment of high oxygen concentration, which leads to the delay of normal retinal growth and development. However, once the auxiliary system of oxygen therapy is removed, the retina of children will immediately be in a relatively anoxic concentration environment. The pathological neovascularization will grow excessively in order to balance oxygen supply and demand. Therefore, the mismatch of oxygen demand in the developing retina, coupled with preterm delivery and other factors can affect normal retinal angiogenesis, leading to the occurrence of ROP [24].

Retinal vessels first proliferate and differentiate from fusiform cells to endothelial cells in the inner layer of the retina, while the inner vessels develop into outer vessels by budding. Angiogenesis is regulated by many factors, and there are many regulatory factors that promote angiogenesis.



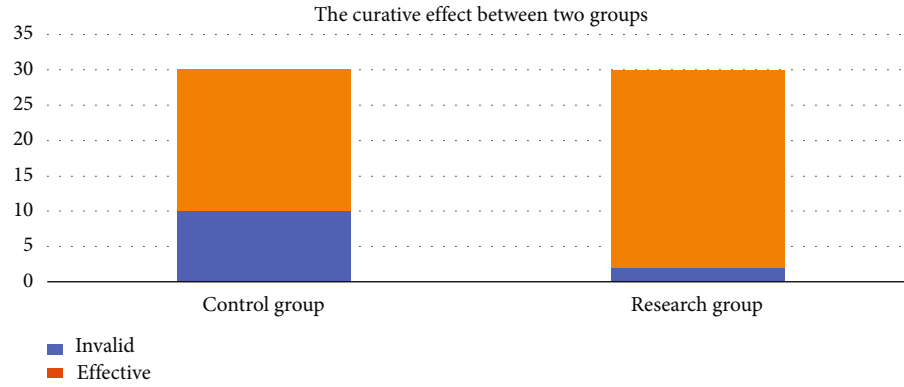


FIGURE 1: The comparison of the curative effect between two groups. The blue bar is indicating the invalid cases following treatment; the orange bar is indicating the effective cases after therapy.

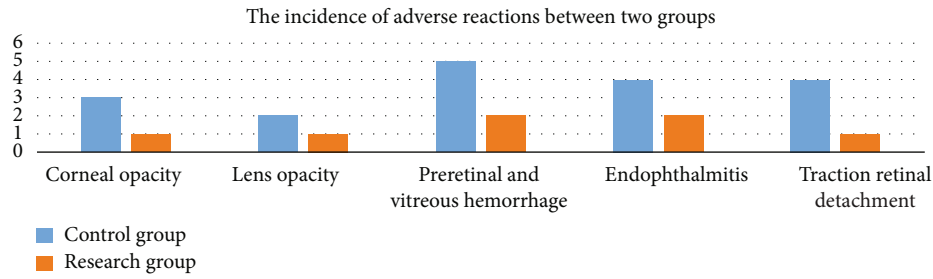


FIGURE 2: The comparison of the incidence of adverse reactions between two groups. The blue bar is indicating the control group; the orange bar is indicating the research group.

TABLE 1: Intraocular pressure between the two groups at different times  $[\bar{x} \pm s]$ .

Grouping	N	Before treatment	After treatment 1 min	After treatment 10 min	After treatment 30 min
Control group	30	$16.59 \pm 2.21$	$25.96 \pm 3.37$	$18.39 \pm 3.45$	$16.59 \pm 3.31$
Research group	30	$16.53 \pm 2.34$	$20.39 \pm 2.21$	$16.49 \pm 2.29$	$14.34 \pm 1.21$
T value		0.102	7.570	2.513	3.496
P value		>0.05	<0.05	<0.05	<0.05

TABLE 2: Serum IL-17A levels between the two groups  $[\bar{x} \pm s, \text{pg/ml}]$ .

Grouping	N	Before treatment	After treatment 1d	After treatment 15d
Control group	30	$473.95 \pm 54.22$	$406.29 \pm 16.34$	$379.59 \pm 24.94$
Research group	30	$476.39 \pm 50.91$	$363.94 \pm 43.42$	$324.01 \pm 31.56$
t value		0.179	4.999	7.568
P value		>0.05	<0.05	<0.05

So far, vascular endothelial growth factor (VEGF) is the strongest growth factor found to promote angiogenesis [25]. It can induce angiogenesis, increase vascular permeability, degenerate extracellular matrix, and proliferate vascular endothelial cells. At the same time, it is also the main cytokine that leads to abnormal vascular and fibrous vascular proliferation of ROP [26, 27], which can promote retinal neovascularization. In recent years, more and more studies have found the importance of development and pathogenesis of ROP [28]. Vitreous injection of anti-VEGF is also used more and more to treat ROP [29–31].

Among these anti-VEGF drugs, razumab is a specific, recombinant humanized IgG1kappa homologous monoclonal antibody fragment with molecular weight 48kD, which has a strong affinity for all subtypes of VEGF [32]. Razumab can block VEGF-A quickly and for a long time, thus reducing vascular endothelial cell proliferation and vascular permeability, inhibiting angiogenesis and repairing the blood-retinal barrier [33]. The drug has been approved for market in many countries at home and abroad and has been approved for clinical application in wet (neovascular) ARMD in China [34]. In the related ROP treatment studies,

the RAINBOW study has proved the efficacies and safeties of intravitreal razumab, which makes intravitreal injection of anti-VEGF drug razumab gradually become an important means. Many studies have reported that vitreous injection of anti-VEGF razumab is generally effective [35]. Chandra treated 52 eyes with razumab, and 8 eyes (15.38%) in the razumab group needed additional retinal laser photocoagulation, anti-VEGF, external scleral ligation, or vitrectomy [36]. The study of Biju et al. included 283 eyes of 145 patients [37]. Vascular lesions disappeared in 266 eyes (94.0%) after intravitreal injection of razumab, and another 152 eyes received additional laser or surgical treatment.

Interleukin 17A (IL-17A) is a cytokine marker produced by T helper cell 17 (Th17) and a cytokine marker of the IL-17 family. There is increasing evidence that IL-17 mediates neovascularization in ophthalmopathy, but the specific mechanism is still controversial [38]. The possible role of IL-17A in neovascularization is realized through the regulatory network of cytoskeleton remodeling, VEGF-related cytokines and complement components. IL-17A may be an indirect angiogenic factor. On the one hand, its angiogenic effect involves the enhancement of cell migration and angiogenesis, which depends on the cytoskeleton remodeling mediated by PI3K-Rac1 and RhoA. On the other hand, IL-17A can increase the capillary formation of vascular endothelial cells by enhancing the migration, proliferation, and expression of VEGF, IL-6, and IL-8.

Conbercept, is a fusion protein containing extracellular domain of VEGF receptor 1 and 2 independently developed in China, which can bind to VEGF with high affinity and exert its effect. Conbercept can block all homo-types of VEGF with high binding affinity for VEGF-An and a longer half-life in the vitreous cavity [39]. It is necessary to add other differences that may exist in the treatment of ROP as mentioned in the introduction.

VEGF is a protein that can cause macular edema [20]. Many studies have shown that the expression of VEGF in vitreous cavity of patients with RVO is higher than that of normal people [21, 22]. Therefore, suppressing or reducing the expression of VEGF should be a good strategy for the treatment of ROP. Vitreous injection of anti-VEGF drugs has become the main measure for the treatment of ROP at home and abroad. The most widely used anti-VEGF drugs in China are razumab and Combuxil. Razumab has been approved for the treatment of ROP by FDA for many years since 2007 and 2010, showing its good efficacy.

With the widespread use of razumab and Compaximab, adverse reactions of razumab and Compaximab include accelerated cataract formation, thrombosis, and vitreous hemorrhage [23, 24]. The analysis shows that compared with Combuxil, razumab can attenuate neovascularization retinopathy by inhibiting the expression of IL-17A and act on RORIL-17A axis to reduce the production of VEGF by reducing the proliferation of microglia and Muller glial cells. At the same time, it can prevent the loss of ganglion cells, further regulate intraocular pressure, and improve the prognosis of patients [40]. This study still has some shortcomings. Firstly, the quality of this study is limited due to the small sample size we included in the study. Secondly, this

research is a single-center study, and our findings are subject to some degree of bias. Therefore, our results may differ from those of large-scale multicenter studies from other academic institutes. This research is still clinically significant and further in-depth investigations will be carried out in the future.

To sum up, intravitreal injection of razumab is an effective treatment for retinopathy of prematurity, which can effectively improve the retinal function of infants. The level of serum interleukin-17A can be reduced and intraocular pressure can be regulated, which is safe and effective.

## Data Availability

The datasets used and analyzed during the current study are available from the corresponding author upon reasonable request.

## Conflicts of Interest

The authors declare that they have no conflicts of interest.

## Acknowledgments

Explore the application of multidisciplinary diagnosis and treatment mode to the prevention and control of retinal disease of prematurity Project No.: Zunhua Kehua Tech, HZ Zi (2019), No. 111. Screening and treatment of retinopathy of prematurity, source: Science and Technology Department of Guizhou Province, No.: Qianke and NY Word [2006], 3054.

## References

- [1] "Eye diseases and conditions-retinopathy of prematurity; recent studies from Stanford University add new data to retinopathy of prematurity (current management of retinopathy of prematurity in sub-saharan Africa)," *Journal of Technology & Science*, vol. 31, no. 52, pp. 394–398, 2020.
- [2] "Eye diseases and conditions-retinopathy of prematurity; new retinopathy of prematurity study findings have been reported by investigators at University of Ataturk (determination and comparison of the urinary iodine levels of premature infants with and without retinopathy of prematurity)," *Chemicals & Chemistry*, vol. 45, no. 62, pp. 395–397, 2020.
- [3] "Eye diseases and conditions-retinopathy of prematurity; findings in retinopathy of prematurity reported from Korea University (incidence, long-term visual outcomes, and mortality in retinopathy of prematurity in Korea: a nationwide population-based study)," *Biotech Week*, vol. 45, no. 52, pp. 67–69, 2020.
- [4] "Eye diseases and conditions-retinopathy of prematurity; findings from Royal Children's Hospital update understanding of retinopathy of prematurity (anaesthesia management of laser photocoagulation for retinopathy of prematurity. A retrospective review of perioperative adverse events)," *Biotech Week*, vol. 452, no. 53, pp. 494–497, 2020.
- [5] "Eye diseases and conditions-retinopathy of prematurity; report summarizes retinopathy of prematurity study findings from Peking University (foveal structure, function and

- microvascular morphology in school-age children with laser-treated retinopathy of prematurity),” *Journal of Engineering*, 2021.
- [6] “Eye diseases and conditions-retinopathy of prematurity; researchers at Indian Institute of Technology (IIT) Hyderabad have reported new data on retinopathy of prematurity (a fully convolutional neural network approach for the localization of optic disc in retinopathy of prematurity diagnosis),” *Network Weekly News*, vol. 42, no. 664, pp. 4921–4926, 2020.
  - [7] “Eye diseases and conditions - retinopathy of prematurity; reports from R. Schade and co-researchers add new data to findings in retinopathy of prematurity (update in the treatment of retinopathy of prematurity),” *Biotech Week*, vol. 31, no. 75, pp. 547–548, 2020.
  - [8] Y. Lin Lisa, K. Jensen Anne, E. Quinn Graham et al., “Symmetry of disease in retinopathy of prematurity in the postnatal growth and retinopathy of prematurity (G-ROP) study.[J],” *Ophthalmic Epidemiology*, vol. 13, no. 41, pp. 448–449, 2020.
  - [9] “Voriconazole,” *Reactions Weekly*, vol. 1806, no. 1, pp. 265–488, 2020.
  - [10] S. Parveen, B. Pramod, R. Ekta, G. Lingam, and J. Smriti, “Anatomical and visual outcomes in stage 5 retinopathy of prematurity with microincision vitrectomy surgery,” *Retina*, vol. 55, no. 42, pp. 3931–3937, 2020.
  - [11] T. R. Padhi, T. Das, P. Kaur et al., “Characteristics of ‘sawtooth shunt’ following anti-vascular endothelial growth factor for aggressive posterior retinopathy of prematurity,” *International Ophthalmology*, vol. 40, no. 4, pp. 491–499, 2020.
  - [12] G. Binenbaum and G.-s. Ying, “Inquiries on the validation of a model to reduce retinopathy of prematurity testing reply,” *JAMA Ophthalmology*, vol. 138, no. 6, p. 711, 2020.
  - [13] A. Sahin, “Mydriatics in retinopathy of prematurity,” *Southern African Journal of Anaesthesia and Analgesia*, vol. 26, no. 2, pp. 966–969, 2020.
  - [14] “Artificial intelligence; study data from Oregon Health & Science University (OHSU) update understanding of artificial intelligence (artificial intelligence in retinopathy of prematurity diagnosis),” *Journal of Robotics & Machine Learning*, vol. 55, no. 63, pp. 393–399, 2020.
  - [15] “Eye diseases and conditions - retinopathy of prematurity; researchers from Heidelberg University Hospital report on findings in retinopathy of prematurity (antenatal exposure to fenoterol is not associated with the development of retinopathy of prematurity in infants born before 32 weeks of gestation),” *Chemicals & Chemistry*, vol. 44, no. 64, pp. 942–948, 2020.
  - [16] J. M. Kang, M. A. Flores Pimentel, and A. G. de Alba Campomanes, “Peripheral retinal changes in regressed retinopathy of prematurity,” *Journal Of Pediatric Ophthalmology And Strabismus*, vol. 57, no. 2, pp. 96–99, 2020.
  - [17] “Eye diseases and conditions-retinopathy of prematurity; findings on retinopathy of prematurity described by researchers at Aravind Eye Hospital (aggressive posterior retinopathy of prematurity in two cohorts of patients in South India: implications for primary, secondary, and tertiary prevention),” *Biotech Week*, vol. 44, no. 63, pp. 494–498, 2020.
  - [18] “Eye diseases and conditions-retinopathy of prematurity; reports summarize retinopathy of prematurity findings from Baskent University (evaluation of iridocorneal angle, choroidal thickness and retinal nerve fiber layer thickness in children with a history of retinopathy of prematurity),” *Journal of Engineering*, vol. 92, no. 35, p. 497, 2020.
  - [19] “Eye diseases and conditions-retinopathy of prematurity; investigators from Duke University have reported new data on retinopathy of prematurity (differentiating retinal detachment and retinoschisis using handheld optical coherence tomography in stage 4 retinopathy of prematurity),” *Journal of Engineering*, vol. 42, no. 65, p. 449, 2020.
  - [20] C. Yen-Ting, L. Laura, L. Chi-Chun, C. Kuan-Jen, H. Yih-Shiou, and W.-C. Wu, “Anatomical and functional results of intravitreal aflibercept monotherapy for type 1 retinopathy of prematurity: one-year outcomes,” *Retina (Philadelphia, Pa.)*, vol. 844, no. 63, pp. 84–89, 2020.
  - [21] D. Anna, D. Maria, Z. Nikolaos, and M. Asimina, Eds., “OCT angiography of the choroid in children with spontaneously regressed retinopathy of prematurity and children born preterm,” *Graefes’s archive for clinical and experimental ophthalmology = Albrecht von Graefes Archiv fur klinische und experimentelle Ophthalmologie*, vol. 258, no. 1, pp. 496–499, 2020.
  - [22] V. Anand, D. M. Ram, and S. Bhujang, “Imaging the ora serrata with the 3nethra neo camera - importance in screening and treatment in retinopathy of prematurity,” *Indian Journal of Ophthalmology*, vol. 68, no. 1, pp. 913–918, 2020.
  - [23] “Eye diseases and conditions-retinopathy of prematurity; research from Qingdao University School of Medicine in retinopathy of prematurity provides new insights (recent treatment advances in aggressive posterior retinopathy of prematurity),” *Biotech Week*, vol. 42, no. 53, pp. 4849–4856, 2020.
  - [24] H. Hannes, B. Thomas, P. Johannes, S. Thomas, and R.-J. Kuon, “Antenatal exposure to fenoterol is not associated with the development of retinopathy of prematurity in infants born before 32 weeks of gestation,” *Archives Of Gynecology And Obstetrics*, vol. 301, no. 3, pp. 966–969, 2020.
  - [25] J. Singh, V. Bhardwar, H. Singh, I. Bhardwaj, S. Choudhary, and A. Toora, “Evaluation of risk factors for retinopathy of prematurity in premature born infants in Tertiary Care Centre in Punjab,” *International Journal of Medical and Dental Sciences*, vol. 9, no. 1, pp. 1–5, 2020.
  - [26] S. Anin, S. Brar Anand, D. Rebika, A. Dewang, and S. Rohit, “Association of pseudo-exotropia with true esotropia in cicatricial retinopathy of prematurity,” *Indian Journal of Ophthalmology*, vol. 68, no. 5, pp. 946–949, 2020.
  - [27] L. Malheiro, I. Falcao, L. Neiva et al., “Application of the WINROP model in retinopathy of prematurity (ROP) screening in a Portuguese cohort of premature infants,” *Revista Brasileira de Oftalmologia*, vol. 78, no. 1, pp. 686–689, 2019.
  - [28] C. T. Okamoto, R. Assman, C. Olderburg, and R. Nisihara, “Retinopathy of prematurity: analysis of a damage reduction attempt,” *Revista Brasileira de Oftalmologia*, vol. 78, no. 2, pp. 034–038, 2019.
  - [29] E. C. Ingolfssland, J. L. Haapala, L. A. Buckley, E. W. Demarath, S. F. Guiang, and S. E. Ramel, “Late growth and changes in body composition influence odds of developing retinopathy of prematurity among preterm infants[J],” *Nutrients*, vol. 12, no. 1, pp. 402–406, 2020.
  - [30] O. Shumpei, H. Tomoaki, I. Taku et al., “Short-term changes in intraocular pressure after intravitreal injection of bevacizumab for the treatment of retinopathy of prematurity,” *Clinical*

- ophthalmology* (Auckland, N.Z.), vol. 13, no. 53, pp. 494–497, 2019.
- [31] S. Singh, M. Dogra, D. Katoch, and M. Dogra, “Bilateral iris cysts in an infant with retinopathy of prematurity,” *Indian Journal of Ophthalmology*, vol. 67, no. 12, p. 2062, 2019.
  - [32] E. Gilbert Clare, D. Lisa, W. Michelle, and B. A. Darlow, “Obstetric strategies to reduce blindness from retinopathy of prematurity in infants born preterm,” *Acta Obstetricia et Gynecologica Scandinavica*, vol. 98, no. 12, pp. 955–959, 2019.
  - [33] “Eye diseases and conditions-retinopathy of prematurity; reports from Chang Gung University add new data to findings in retinopathy of prematurity (prediction of visual outcomes by an artificial neural network following intravitreal injection and laser therapy for retinopathy of prematurity),” *Robotics & Machine Learning*, vol. 93, no. 52, pp. 391–396, 2019.
  - [34] V. P. Kaur, J. Shaikh, P. Manchanda, and S. Chiva-Razavi, “Pro59 literature review on the epidemiology of retinopathy of prematurity in Europe,” *Value in Health*, vol. 22, Supplement 3, pp. 491–496, 2019.
  - [35] G. Mishra, M. Modi, S. Saluja, A. Soni, and A. Khosla, “Incidence and risk factors of retinopathy of prematurity among very-low-birth- weight neonates,” *Current Medicine Research and Practice*, vol. 9, no. 6, pp. 215–217, 2019.
  - [36] P. Chandra, “Retinopathy of prematurity: challenges of a growing epidemic in India,” *Current Medicine Research and Practice*, vol. 9, no. 6, pp. 211–212, 2019.
  - [37] R. Biju, N. S. D. Raju, J. D. Akkara, and A. Pathengay, “Smart-phone-based fundus documentation in retinopathy of prematurity,” *Indian Journal of Ophthalmology*, vol. 67, no. 11, pp. 192–196, 2019.
  - [38] G. Anubhav, G. Mahesh, A. Giridhar, D. P. Chandrashekhara, T. Thachil, and A. Sharma, “Response to comments on: smartphone-based fundus documentation in retinopathy of prematurity,” *Indian Journal Of Ophthalmology*, vol. 67, no. 11, pp. 4904–4906, 2019.
  - [39] “Eye diseases and conditions-retinopathy of prematurity; new findings from University of Toronto in retinopathy of prematurity provides new insights (late erythropoiesis-stimulating agents to prevent red blood cell transfusion in preterm or low birth weight infants),” *Information Technology News-weekly*, vol. 55, no. 63, pp. 9243–9247, 2019.
  - [40] “Effects of congenital ocular toxoplasmosis on peripheral retinal vascular development in premature infants at low risk for retinopathy of prematurity,” *Journal of Ophthalmology*, vol. 49, no. 4, p. 234, 2019.
  - [41] S. Z. Khair, A. S. Ismail, Z. Embong, and A. A. Yusoff, “Detection of FZD4, LRP5 and TSPAN12 genes variants in Malay premature babies with retinopathy of prematurity,” *Journal of Ophthalmic & Vision Research*, vol. 14, no. 2, pp. 394–398, 2019.
  - [42] “Eye diseases and conditions-retinopathy of prematurity; study findings from university Children’s Hospital broaden understanding of retinopathy of prematurity [effects of closed-loop automatic control of the inspiratory fraction of oxygen (FiO2-C) on outcome of extremely preterm infants study],” *Chemicals & Chemistry*, vol. 66, no. 54, pp. 925–928, 2019.
  - [43] “Eye diseases and conditions-retinopathy of prematurity; new findings from Shenzhen People’s Hospital describe advances in retinopathy of prematurity (clinical effect of laser photocoagulation combined with minimal doses of intravitreal ranibizumab for aggressive posterior retinopathy of prematurity),” *Biotech Week*, vol. 33, no. 32, pp. 303–305, 2019.
  - [44] “Eye diseases and conditions-retinopathy of prematurity; recent findings from University of Toronto advance knowledge in retinopathy of prematurity (effect of eye masks on neonatal stress following dilated retinal examination: the MASK-ROP randomized clinical trial),” *Biotech Week*, vol. 193, no. 23, pp. 193–196, 2019.
  - [45] “Eye diseases and conditions-retinopathy of prematurity; new retinopathy of prematurity findings from Nagoya University outlined (optical coherence tomography angiography of the foveal avascular zone in children with a history of treatment-requiring retinopathy of prematurity),” *Journal of Technology*, vol. 67, no. 53, pp. 3934–3936, 2019.
  - [46] “Eye diseases and conditions - retinopathy of prematurity; National Center for Child Health and Development reports findings in retinopathy of prematurity (severe recurrent fibrovascular proliferation after combined intravitreal bevacizumab injection and laser photocoagulation for aggressive posterior),” *Biotech Week*, vol. 44, no. 53, pp. 319–324, 2019.



## Research Article

# Three Acupuncture Methods for Postoperative Pain in Mixed Hemorrhoids: A Systematic Review and Network Meta-Analysis

Sunsong Ye,<sup>1</sup> Jianhua Zhou,<sup>2</sup> Xiutian Guo,<sup>3</sup> and Xiaoxue Jiang<sup>ib</sup><sup>2</sup>

<sup>1</sup>Department of Anorectology, Wenzhou Hospital of Traditional Chinese Medicine Affiliated to Zhejiang Chinese Medicine University, Wenzhou 325000, China

<sup>2</sup>Department of Traditional Chinese Medicine, Shanghai Eighth People's Hospital, Shanghai 200235, China

<sup>3</sup>Department of Anorectology, Shanghai Municipal Hospital of Traditional Chinese Medicine, Affiliated Shanghai University of Traditional Chinese Medicine, Shanghai 200071, China

Correspondence should be addressed to Xiaoxue Jiang; [jiangxxvip@163.com](mailto:jiangxxvip@163.com)

Received 5 July 2022; Revised 18 July 2022; Accepted 4 August 2022; Published 26 September 2022

Academic Editor: Hangjun Che

Copyright © 2022 Sunsong Ye et al. This is an open access article distributed under the Creative Commons Attribution License, which permits unrestricted use, distribution, and reproduction in any medium, provided the original work is properly cited.

**Background.** Mixed hemorrhoids are a common anorectal disorder, surgery is the most effective means of eradicating hemorrhoids, and pain is the most common postoperative complication of mixed hemorrhoids. **Objective.** To compare the clinical efficacy of auricular plaster, acupoint application, and acupoint catgut embedding for treating postoperative pain in mixed hemorrhoids. **Method.** PubMed, Embase, The Cochrane Library, Web of Science, CNKI, Wanfang, VIP, and CBM databases were searched for randomized controlled trials (RCTs) of three acupuncture-related therapies for postoperative pain in mixed hemorrhoids from the time of database creation to October 2021. After screening the literature, extracting information, and evaluating the risk of bias of included studies, statistical analysis was performed using RevMan 5.3 and Stata 15.0. **Result.** Forty-seven RCTs with a total of 5121 patients were included. Network meta-analysis (NMA) showed that auricular plaster (OR = 5.90, 95% CI = (2.02, 17.21)) and acupoint catgut embedding therapy (OR = 5.55, 95% CI = (1.01, 30.40)) were more effective than analgesics in the treatment of postoperative pain in mixed hemorrhoids. The cumulative ranking probability (SUCRA) showed that acupoint application (73.6%) had the best overall efficacy and the rest were auricular plaster (68.7%), acupoint catgut embedding therapy (64.6%), auricular plaster combined with acupoint application (63.4%), and pain medication (8.9%) in that order. Secondly, auricular plaster (OR = -0.93, 95% CI = (-1.66, -0.20)), acupoint catgut embedding (OR = -0.8, 95% CI = (-1.50, -0.10)), and acupoint application (OR = -1.4, 95% CI = (-2.50, -0.31)) all led to a significant decrease in pain scores and were all more effective than analgesics. As ranked by SUCRA, the results showed that the efficacy of acupoint application (73.5%) was optimal and the rest were auricular plaster (56.1%), acupoint catgut embedding (50.2%), and pain medication (15.3%) in that order. In terms of pain degree, acupoint application (OR = 3.83, 95% CI = (1.25, 11.74)) was significantly better than pain medication. **Conclusion.** Acupoint application can improve the overall efficiency, reduce pain scores, and relieve the degree of postoperative pain in mixed hemorrhoids.

## 1. Introduction

Mixed hemorrhoids are a common anorectal disease [1], surgery is the most effective means of eradicating hemorrhoids [2], and pain is the most frequent postoperative complication of mixed hemorrhoids. Postoperative pain in hemorrhoids is a thorny problem that has troubled patients and physicians for a long time; it makes patients extremely nervous psychologically and fearful of defecation after sur-

gery, which seriously affects the quality of surgery [3]. Pain arises for various reasons: (1) the innervation of the spinal nerve below the dentate line makes the pain response sensitive, (2) there is release of inflammatory mediators after surgery, and (3) there is postoperative stimulation of the wound surface by activities such as defecation and dressing changes, resulting in persistent spasm of the sphincter muscle [4].

In clinical practice, drug therapy is mostly used for postoperative pain in hemorrhoids but it requires multiple doses

TABLE 1: Search strategy in PubMed.

Search	Query
#1 Search:	("Acupuncture"[Mesh]) OR (Auricular point[Title/Abstract]) OR (Auricular plaster therapy[Title/Abstract]) OR (acupoint catgut embedding[Title/Abstract]) OR (acupoint application therapy[Title/Abstract])
#2 Search:	("hemorrhoidectomy" [Mesh]) OR ((postoperative pain of mixed hemorrhoids [Title/Abstract]) OR (hemorrhoid excision[Title/Abstract]) OR (hemorrhoid surgery acupuncture [Title/Abstract])
#3 Search:	randomized controlled trial[Publication Type] OR randomized[Title/Abstract] OR placebo[Title/Abstract]
#4 Search:	#1 and #2 and #3

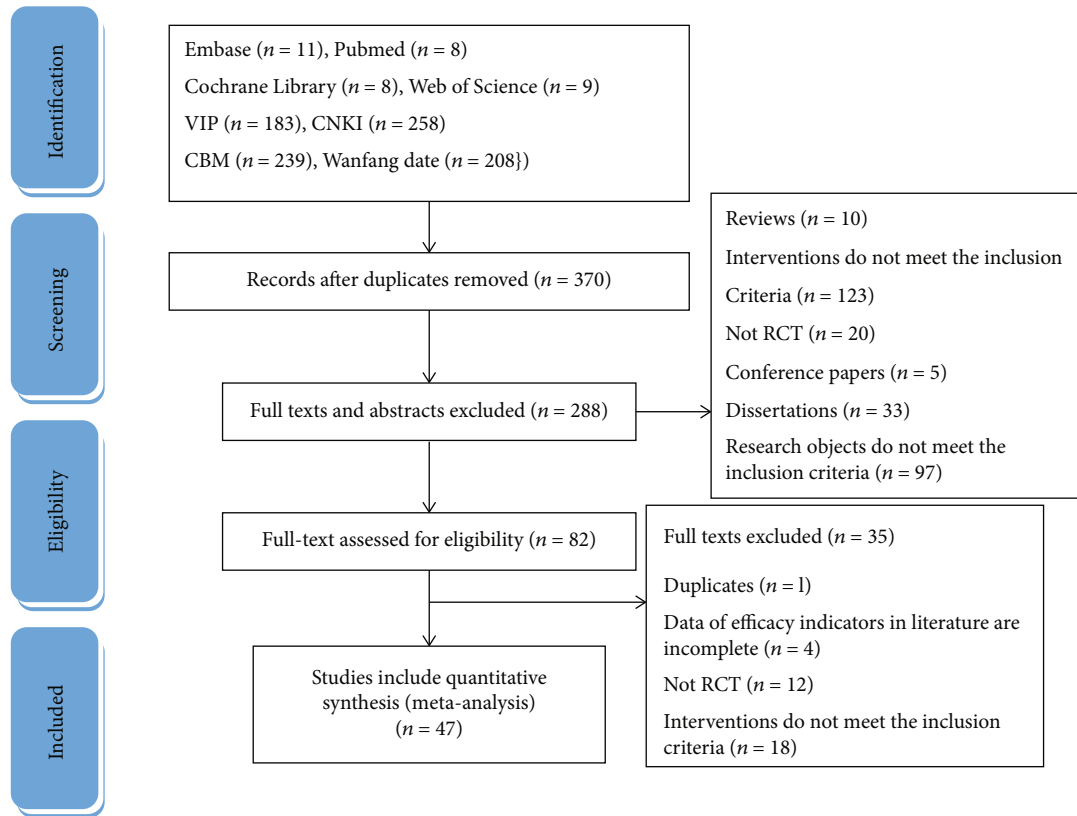


FIGURE 1: Flow chart literature screening.

within a short period of time, which easily causes adverse reactions in the gastrointestinal tract and central nervous system, often resulting in dizziness, nausea, vomiting, dry mouth, and itchy skin [5–7], and the high cost of drugs increases the economic burden of patients. Therefore, the basic principle of pain management is to effectively relieve pain while minimizing the adverse effects of drugs and the cost of treatment. This has led to an urgent clinical need for nonpharmacological approaches to alleviate patients' pain and improve their quality of life.

Acupuncture is an important part of Traditional Chinese medicine, and acupuncture mainly includes auricular plaster, acupoint application, and acupoint catgut embedding, compared with conventional acupuncture, which is simple to operate, saves consumables and time cost, and can avoid the pain caused by applying regular acupuncture to patients. However, there is a lack of comparative studies on the efficacy of the three treatment methods and it is difficult to

obtain a clear comparison by traditional meta-analysis. In this study, NMA was used to screen the best therapeutic measures based on ranking efficacy indexes for postoperative pain in hemorrhoid treatment in acupuncture to provide a reliable evidence-based reference for the clinic.

## 2. Methods and Analysis

**2.1. Search Strategy.** PubMed, Embase, The Cochrane Library, Web of Science, CNKI, Wanfang, VIP, and CBM databases were searched from the establishment to October 2021 to find clinical randomized controlled trials about 3 acupuncture therapies, auricular plaster, acupoint application, and acupoint catgut embedding, for the postoperation pain of mixed hemorrhoids. PubMed was used as an example, and a combination of subject terms and free words were used for the search. The search strategy is shown in Table 1.



TABLE 2: The basic characteristics of the included studies.

Author year	Sample size	Treatment group 1 Intervention age (year)/course (year)	Treatment group 2 Intervention age (year)/course (year)	Anesthetic mode	Operation method	Outcome	Adverse reactions and complications
Xiong and Xie [9]	63	Acupoint catgut embedding therapy 41.1 ± 13.5/9.7 ± 4.1	Analgesic 43.1 ± 13.7/10.3 ± 4.6	NA	NA	1, 2	NA
Chen and Deng [10]	40	Auricular plaster 45.5 ± 23.5/NA	Regular treatment 45.0 ± 22.0/NA	NA	NA	2	NA
Fang et al. [11]	66	Auricular plaster 38.7 ± 10.5/NA	Regular treatment 40.8 ± 11.8/NA	NA	NA	3	Treatment group 1: none; treatment group 2: 1 case of perianal skin pruritus and wound bleeding, 1 case of asthma, and 1 case of abnormal liver function and urinary tract infection
Zhu et al. [12]	120	Auricular plaster 37.4/NA	Regular treatment 37.8/NA	Lumbar anesthesia	MM	1	NA
Huang et al. [13]	120	Auricular plaster 38/NA	Regular treatment 38/NA	Lumbar anesthesia	MM	1, 2	NA
Di et al. [14]	60	Auricular plaster 42.93 ± 10.94/NA	Regular treatment 45.69 ± 9.07/NA	Lumbar anesthesia	PPH	2	Treatment group 1: 1 case of dizziness and 2 cases of dry mouth, 3 cases of dizziness; treatment group 2: 2 cases of nausea, 1 case of vomiting, and 3 cases of dry mouth
Gao and Liu [15]	90	Auricular plaster 44.58 ± 10.98/NA	Analgesic 42.17 ± 11.5/NA	NA	MM	3	NA
Liu and Zheng [16]	601	Auricular plaster NA/NA	Regular treatment NA/NA	Local anesthesia	MM	1	NA
Di et al. [17]	120	Auricular plaster 45.15 ± 2.53/NA	Analgesic 47.08 ± 3.09/NA	Lumbar anesthesia	PPH	1	Treatment group 1: none; treatment group 2: 2 cases of dizziness, 3 cases of nausea, 1 case of vomiting, 1 case of drowsiness, and 1 case of dry mouth
Yan [18]	120	Auricular plaster NA/NA	Regular treatment NA/NA	Local anesthesia	MM	2	NA
Yang et al. [19]	100	Auricular plaster combined with acupoint application 41.5 ± 3.5/15.1 ± 5.6	Regular treatment 40.2 ± 2.6/14.9 ± 6.8	NA	NA	1, 2	NA
Hu [20]	120	Auricular plaster 34/NA	Regular treatment 33/NA	NA	NA	1	NA
Liu et al. [21]	140	Auricular plaster 47.5 ± 5.6/NA	Regular treatment 48.8 ± 6.4/NA	NA	NA	2	NA
Beilei et al. [22]	66	Auricular plaster 46.52 ± 3.71/4.03 ± 2.87	Analgesic 45.92 ± 3.63/4.06 ± 2.91	NA	NA	1, 2, 3	NA

TABLE 2: Continued.

Author year	Sample size	Treatment group 1 Intervention age (year)/course (year)	Treatment group 2 Intervention age (year)/course (year)	Anesthetic mode	Operation method	Outcome	Adverse reactions and complications
Chen et al. [23]	224	Auricular plaster $50.1 \pm 8.2/\text{NA}$	Regular treatment $51.6 \pm 9.0/\text{NA}$	NA	MM	3	NA
Gan [24]	271	Auricular plaster NA/NA	Regular treatment NA/NA	Lumbar anesthesia	MM	1	NA
Tang and Hu [25]	40	Auricular plaster 31/NA	Analgesic 31/NA	Lumbar anesthesia	MM	1	NA
Hong et al. [26]	100	Auricular plaster 60/NA	Analgesic 58/NA	Local anesthesia	MM	1, 3	NA
Chai and Feng [27]	140	Auricular plaster $41.87/\text{NA}$	Analgesic 42.13/NA	NA	NA	1	NA
Yang [28]	60	Auricular plaster $38.06 \pm 3.52/\text{NA}$	Regular treatment $37.52 \pm 3.64/\text{NA}$	NA	NA	2	Treatment group 1: none; treatment group 2: 2 cases of dizziness, 1 case of chest tightness, and 1 case of urticaria
Zhang [29]	60	Auricular plaster $34.55 \pm 3.63/10.48 \pm 1.35$	Regular treatment $39.22 \pm 1.56/11.12 \pm 1.82$	NA	NA	3	None
Li [30]	106	Auricular plaster $42.9 \pm 7.0/\text{NA}$	Analgesic 42.7 $\pm$ 7.1/NA	NA	NA	1	NA
Pan [31]	80	Auricular plaster $48.50 \pm 5.75/3.68 \pm 0.55$	Analgesic $47.50 \pm 5.63/3.50 \pm 0.68$	NA	NA	2	Treatment group 1: 2 cases with irregular defecation and 1 case with edema; treatment group 2: 4 cases of urinary retention, 1 case of bleeding, 2 cases of irregular defecation, and 3 cases of edema
Zheng and Yv [32]	120	Auricular plaster combined with acupoint application $37.2 \pm 7.2/\text{NA}$	Analgesic 35.3 $\pm$ 8.5/NA	NA	NA	3	Treatment group 1: none; treatment group 2: 7 cases with mild stomach pain and other stomach upset symptoms
Wang and Chen [33]	80	Acupoint application $32.15 \pm 10.12/\text{NA}$	Analgesic $33.85 \pm 9.96/\text{NA}$	NA	MM	2	Treatment group 1: none; treatment group 2: postoperative urinary retention in 3 cases, local trauma tissue edema in 2 cases; postoperative stomachache was relieved spontaneously in 1 case
Huang et al. [34]	60	Acupoint catgut embedding therapy $41.2 \pm 10.05/\text{NA}$	Regular treatment $42.3 \pm 11.7/\text{NA}$	Local anesthesia	MM	2	NA
Li et al. [35]	120	Acupoint catgut embedding therapy $41.2 \pm 10.5/10.1 \pm 0.5$	Regular treatment $42.3 \pm 11.7/9.2 \pm 0.4$	Caudal anesthesia	MM	3	NA
Yang et al. [36]	120	Acupoint catgut embedding therapy	Analgesic 43.6 $\pm$ 12.1/NA	Local anesthesia	MM	2	Treatment group 1: 2 cases of urinary retention, 7 cases of edema, and 1 case of

TABLE 2: Continued.

Author year	Sample size	Treatment group 1 Intervention age (year)/course (year)	Treatment group 2 Intervention age (year)/course (year)	Anesthetic mode	Operation method	Outcome	Adverse reactions and complications
		42.1 ± 11.5/NA					nausea; treatment group 2: 8 cases of urinary retention, 17 cases of edema, 6 cases of nausea, 4 cases of vomiting, and 5 cases of vertigo
Sheng et al. [37]	60	Acupoint catgut embedding therapy 43 ± 16/NA	Regular treatment 44 ± 15/NA	Lumbar anesthesia	MM	2	Treatment group 1: 3 cases of irregular defecation and 2 cases of anal edema; treatment group 2: 10 cases of irregular defecation and 8 cases of anal edema
Yue and Li [38]	200	Acupoint catgut embedding therapy 46.5/NA	Analgesic 47.3/NA	NA	MM	1	NA
Zhang [39]	70	Acupoint catgut embedding therapy 35 ± 10/2.9 ± 1.4	Analgesic 34 ± 12/13.1 ± 1.2	NA	NA	2	NA
Liang et al. [40]	60	Acupoint application	Regular treatment	NA	MM	2	NA
Li [41]	30	Acupoint application	Regular treatment	NA	NA	3	NA
Meng et al. [42]	160	Acupoint application	Regular treatment	NA	NA	1, 2, 3	NA
Zhou et al. [43]	90	Acupoint catgut embedding therapy 36 ± 4/7.8 ± 2.1	Analgesic 35 ± 7/7.3 ± 2.00	CSEA	MM	2	Treatment group 1: 1 case of nausea and vomiting, 1 case of localized skin discomfort; treatment group 2: 8 cases of dizziness and headache, 13 cases of nausea and vomiting, 6 cases of being flustered, and 4 cases of local skin discomfort
Li et al. [44]	90	Acupoint catgut embedding therapy 44.9 ± 5.7/9.3 ± 0.2	Analgesic 46.4 ± 4.9/10.5 ± 0.4	Local anesthesia	MM	3	Treatment group 1: 7 cases had difficulty urinating and 4 cases had edema; treatment group 2: 15 cases had difficulty urinating and 9 cases had edema
Du [45]	60	Acupoint catgut embedding therapy 41.3 ± 12.08/4.88 ± 3.12	Analgesic 42.88 ± 11.93/5.79 ± 2.64	Local anesthesia	MM	2	Treatment group 1: none; treatment group 2: 3 cases of nausea and vomiting
Wang [46]	68	Auricular plaster combined with acupoint application 45.58 ± 11.98/NA	Regular treatment 43.17 ± 12.5/NA	Lumbar anesthesia	MM	2	Treatment group 1: 2 cases of nausea, 1 case of vomiting; treatment group 2: 5 cases of nausea, 3 cases of vomiting, 1 case of stomatitis, 1 case of allergic dermatitis
Liang and Wen [47]	96	Acupoint application 60.10 ± 8.23/NA	Regular treatment 58.23 ± 8.97/NA	Intravertebral canal anesthesia	MM	1	NA
Wang et al. [48]	90	Acupoint application 48.8 ± 12.6/NA	Regular treatment 43.2 ± 14.0/NA	NA	NA	1	NA

TABLE 2: Continued.

Author year	Sample size	Treatment group 1 Intervention age (year)/course (year)	Treatment group 2 Intervention age (year)/course (year)	Anesthetic mode	Operation method	Outcome	Adverse reactions and complications
Xie and Huang [49]	60	Acupoint application $47.1 \pm 4.6/\text{NA}$	Regular treatment $46.2 \pm 4.3/\text{NA}$	Local anesthesia	MM	2	NA
Huang et al. [50]	60	Auricular plaster $42.1 \pm 8.52/\text{NA}$	Regular treatment $41.3 \pm 10.37/\text{NA}$	Local anesthesia	MM	2	None
Ma [51]	150	Auricular plaster $41.7 \pm 0.7/3.2 \pm 0.3$	Regular treatment $42.6 \pm 0.5/3.1 \pm 0.5$	NA	NA	1	NA
Sun and Chen [52]	100	Auricular plaster	Regular treatment	NA	MM	2	NA
Wang et al. [53]	60	Acupoint catgut embedding therapy $40 \pm 6.64/\text{NA}$	Regular treatment $38 \pm 7.02/\text{NA}$	Intravertebral canal anesthesia	NA	3	Treatment group 1: 3 cases of voiding difficulties and 2 cases of edema; treatment group 2: 10 cases of voiding difficulties, 8 cases of edema
Yan et al. [54]	80	Auricular plaster $41.39 \pm 9.4/\text{NA}$	Regular treatment $46.18 \pm 13.18/\text{NA}$	NA	NA	3	NA
Pei et al. [7]	130	Acupoint catgut embedding therapy	Regular treatment	NA	MM	2	NA

Outcome indicators: 1: total effective rate; 2: pain score; 3: pain degree; NA: not available; MM: Milligan-Morgan; PPH: procedure for prolapse and hemorrhoids; CSEA: combined spinal-epidural anesthesia.

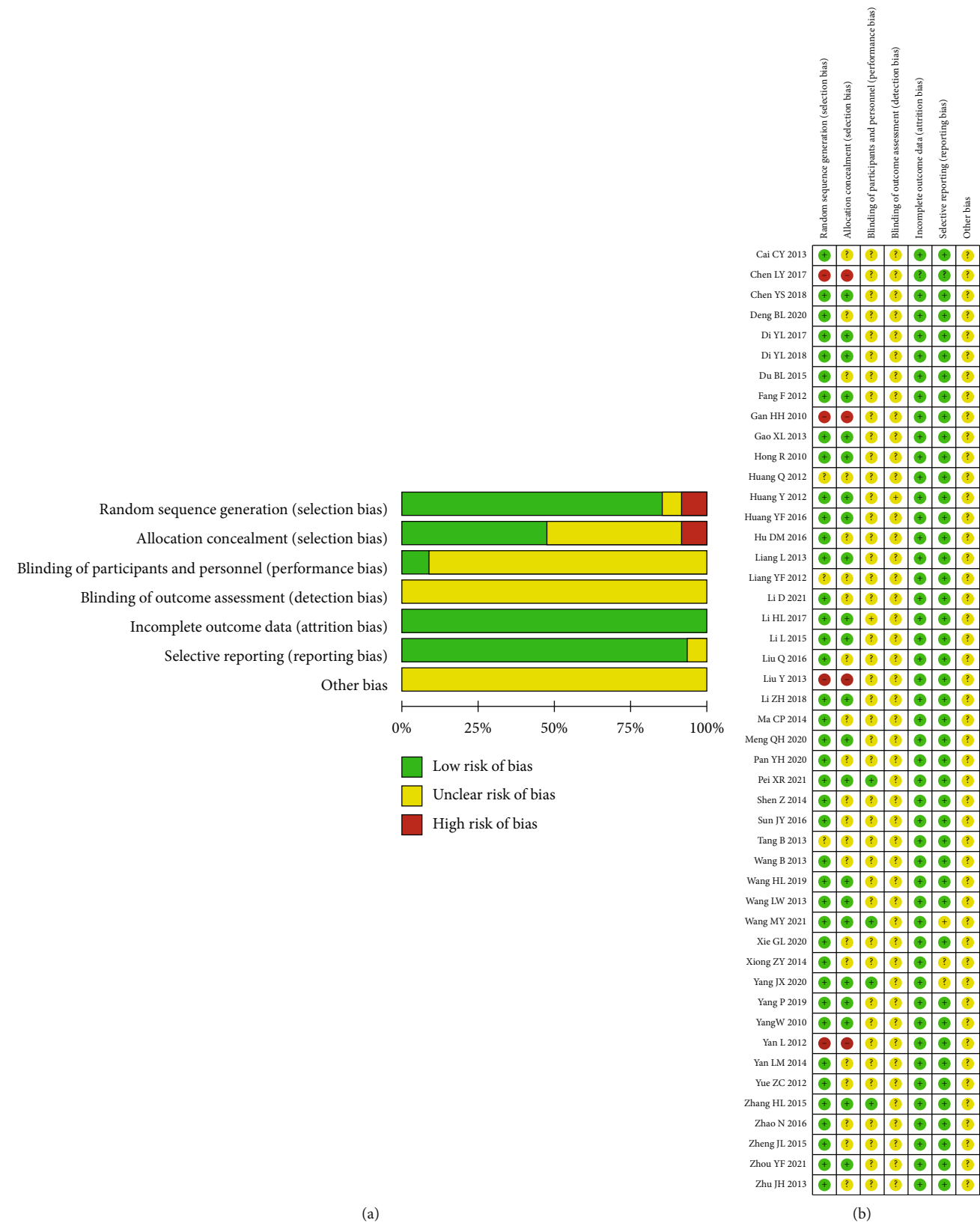


FIGURE 2: Results of basic characteristics of included studies and risk of bias evaluation. (a) Risk of bias graph. (b) Risk of bias summary.

2.1.1. Inclusion Criteria. To be eligible for inclusion, the following criteria had to be fulfilled: (1) study design: RCTs; (2) study population: patients with postoperative pain in mixed

hemorrhoids. Gender, age, and source of disease cases were not limited, and the mode of surgery and the degree of disease were not limited; (3) interventions: auricular plaster,

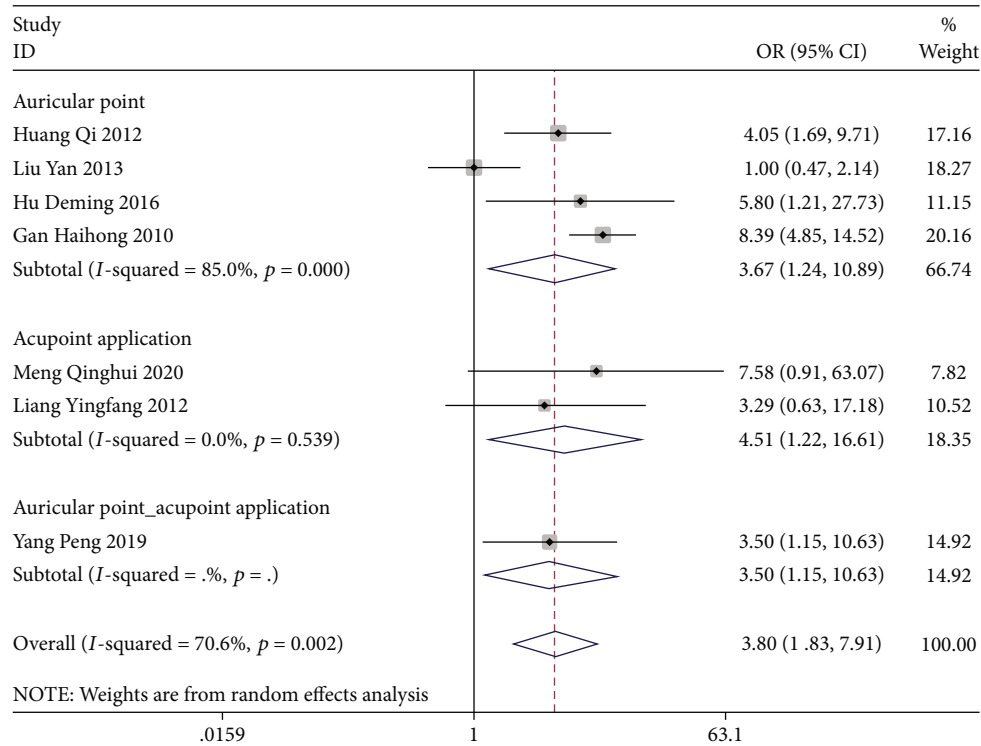


FIGURE 3: Forest plot of meta-analysis of the overall efficacy of three different acupuncture methods for postoperative pain relief of mixed hemorrhoids (compared with conventional treatment).

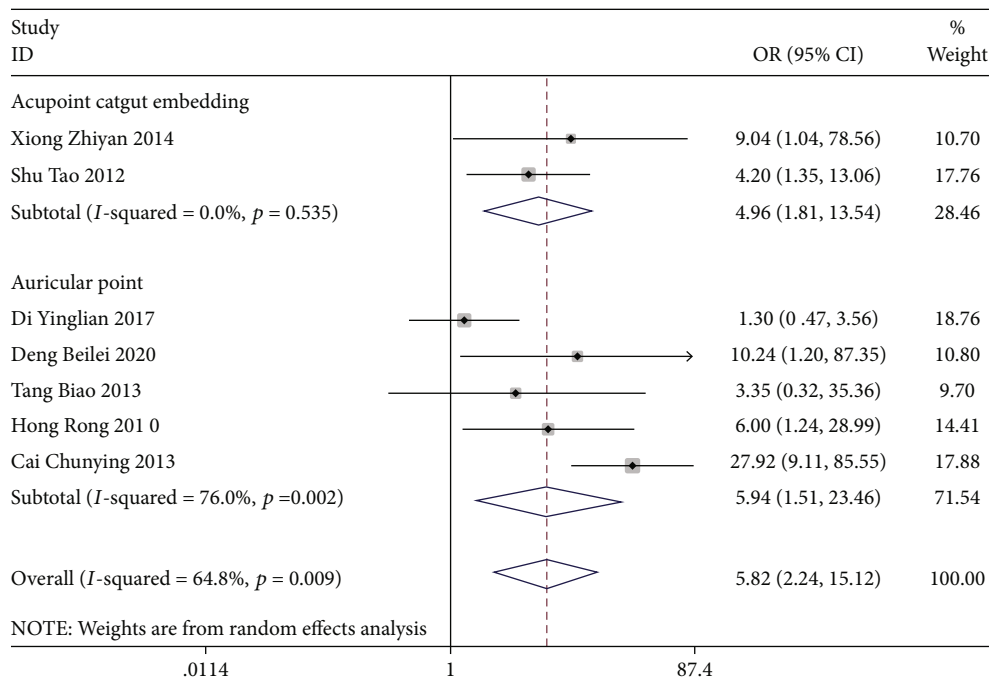


FIGURE 4: Forest plot of meta-analysis of the overall efficacy of three different acupuncture methods for postoperative pain relief of mixed hemorrhoids (compared with analgesics).

acupoint application, and acupoint catgut embedding (can be one or more therapies combined) for the observation group and analgesic drugs or conventional treatment for the control group; (4) outcome indicators: the main indica-

tors: (i) total effective rate, (ii) pain score, and (iii) pain degree; secondary indicators: (i) complications and (ii) adverse reactions; (5) efficacy evaluation criteria: (i) visual analog scoring VAS score, (ii) international standard pain



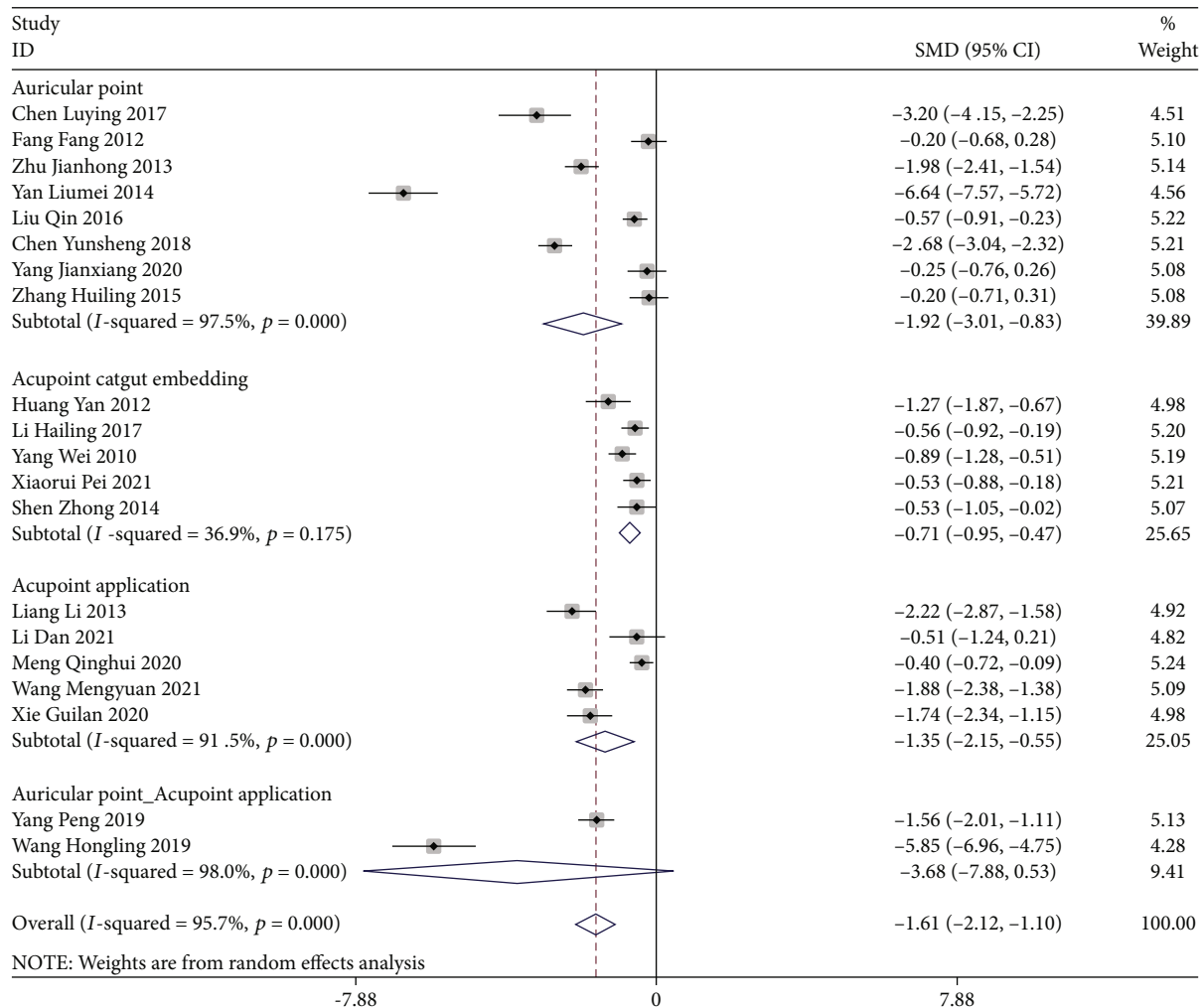


FIGURE 5: Forest map of meta-analysis of three acupuncture methods for postoperative pain scores of mixed hemorrhoids (compared with conventional treatment).

assessment numerical grading method NRS, (iii) Changhai Pain Scale, (iv) WHO pain degree grading standard, divided into 0—III, and (v) numerical rating scale NRS score; and (6) Chinese Pain Society Han Jisheng recommended VAS.

**2.1.2. Exclusion Criteria.** The following are the exclusion criteria: (1) study subjects: patients with combined postoperative pain from perianal diseases other than mixed hemorrhoids; (2) intervention: patients with combined herbal or proprietary Chinese medicine treatment; (3) experience, case reports, reviews, animal experiments, and case retrospective studies; (4) conference papers or dissertations, etc.; (5) repeatedly published literature; (6) outcome indicators: none or imperfect; and (7) the original text of the study not being obtained

**2.2. Literature Screening.** The retrieved literature records were managed using reference management software NoteExpress (version3.2). Based on the inclusion and exclusion criteria, two independent researchers conducted a detailed screening of titles and abstracts of reference records identified through database searching. All potential articles that meet the eligibil-

ity criteria and controversial literature were required for a full-text review. The third researcher will conduct the arbitration, who was responsible for resolving the conflict between the two researchers. A total of 924 relevant papers were obtained from the initial review, and 47 RCT studies were finally included after the stratified screening (Figure 1).

**2.3. Quality Evaluation.** Two investigators assessed the quality of the included studies according to the Cochrane Risk of Bias Assessment Tool recommended in the Cochrane Systematic Assessment Manual, version 5.1. The Cochrane Risk of Bias Assessment included seven aspects: randomization methods, blinding of participants and investigators, blinding of evaluators, allocation concealment, completeness of outcomes, selective reporting of outcomes, and other sources of bias. Bias was assessed for each of the included RCTs in terms of low risk, high risk, and unclear [8]. Any inconsistency was resolved through joint discussions with third-party investigators.

**2.4. Data Information Collection.** An Excel sheet database was set up to extract study information, including authors, year of publication, gender of study subjects, age, sample size,

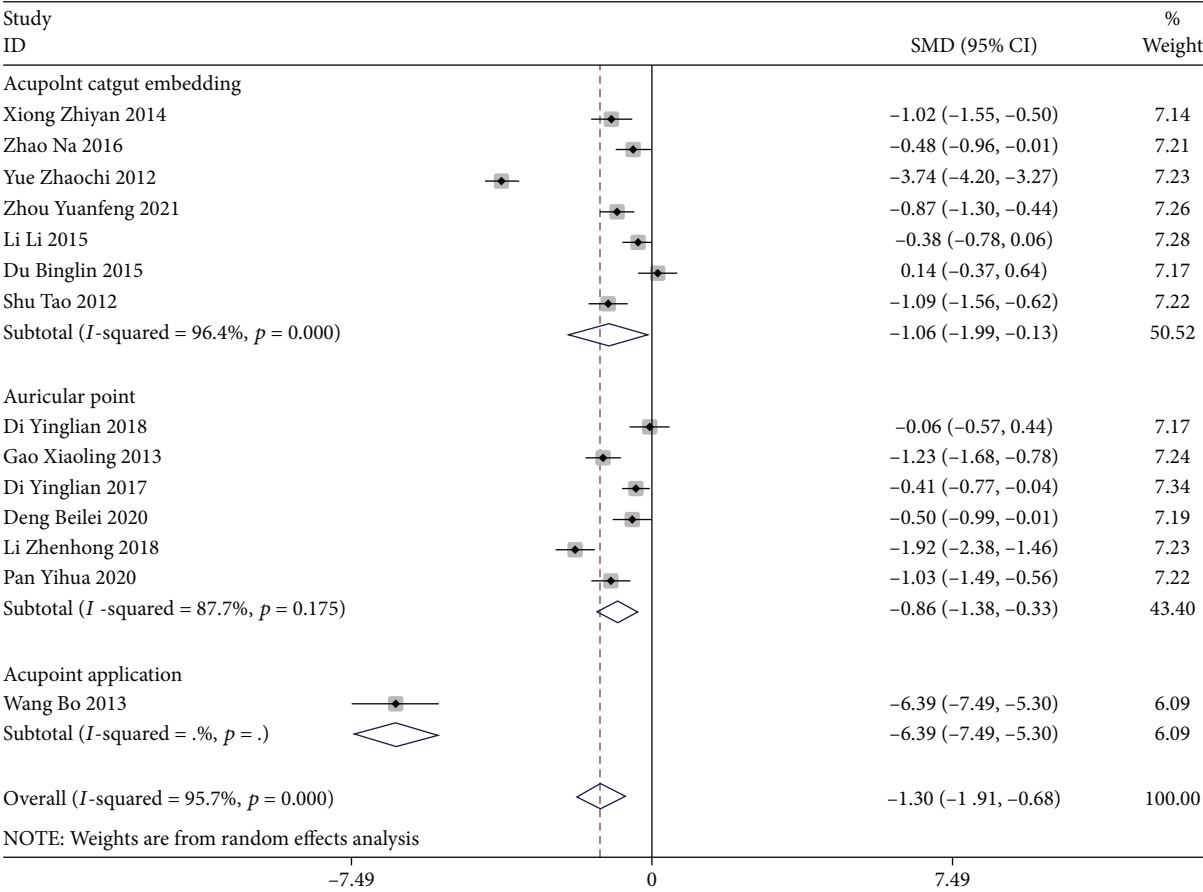


FIGURE 6: Forest map of meta-analysis of three acupuncture methods for postoperative pain scores of mixed hemorrhoids (compared with analgesics).

intervention measures, outcome indicators, complications, adverse events, surgical methods, and anesthesia methods.

**2.5. Statistical Analysis.** The risk bias was evaluated using RevMan 5.3 software. The included literature was compared directly using Stata 15.0 software,  $I^2 \leq 50\%$ ,  $P \geq 0.05$  was considered as no statistical heterogeneity in the included literature, and the meta-analysis was performed using the fixed-effect model;  $I^2 > 50\%$  or  $P < 0.05$ , the included literature was statistically heterogeneous, and a random-effects model was used for meta-analysis.

The ranking between interventions was obtained by direct and indirect comparisons using Stata 15.0 software, with odd ratios (OR) for dichotomous variables and standardized mean difference (SMD) and 95% credible intervals (CI) for continuous variables. The closed loop formed by studies with both direct and indirect evidence was performed to test inconsistency, the surface under the cumulative ranking curves (SUCRA) closer to 100%, the better the efficacy of the intervention, and the difference is considered statistically significant at  $P < 0.05$ .

3. Results

**3.1. Results of Basic Characteristics of Included Studies and Risk of Bias Evaluation.** A total of 5121 cases were included

in 47 [7, 9–54] studies. A total of 47 RCTs were included in this study, of which 17 evaluated auricular plaster versus common treatment [10–14, 16, 18, 20, 21, 23, 24, 28, 29, 50–52, 54], 8 evaluated auricular plaster versus painkillers [15, 17, 22, 25–27, 30, 31], 5 evaluated acupoint catgut embedding versus common treatment [7, 34, 35, 37, 53], 7 evaluated acupoint catgut embedding versus painkillers [9, 36, 38, 39, 43–45], 6 evaluated acupoint application point versus common treatment [40–42, 47–49], 1 evaluated acupoint application point versus painkillers [33], 1 evaluated auricular plaster and acupoint application point versus painkillers [32], and 2 evaluated auricular plaster and acupoint application point versus common treatment [19, 46].

47 literature were all two-arm studies. 34 studies [7, 9–15, 17–19, 21–23, 28–31, 33–46, 48, 49] reported pain scores, 14 studies [9, 13, 16, 17, 19, 20, 22, 24–27, 39, 42, 47] reported the total efficiency, 9 studies [22, 26, 32, 42, 50–54] reported postoperative pain degree, and in terms of study design, 11 studies [11, 14, 17, 28, 29, 32, 33, 36, 43, 45, 46] reported adverse effects and detail management measures, 14 studies [11, 15, 17, 19, 34–36, 40, 42, 43, 46, 47, 52, 54] used random number tables, and 20 studies [9, 12, 18, 20–22, 26, 27, 29, 31–33, 37–39, 41, 45, 48, 50, 51] mentioned only the word random without details; 1 study [49] used randomization by lottery, 2 studies [23, 44] gave

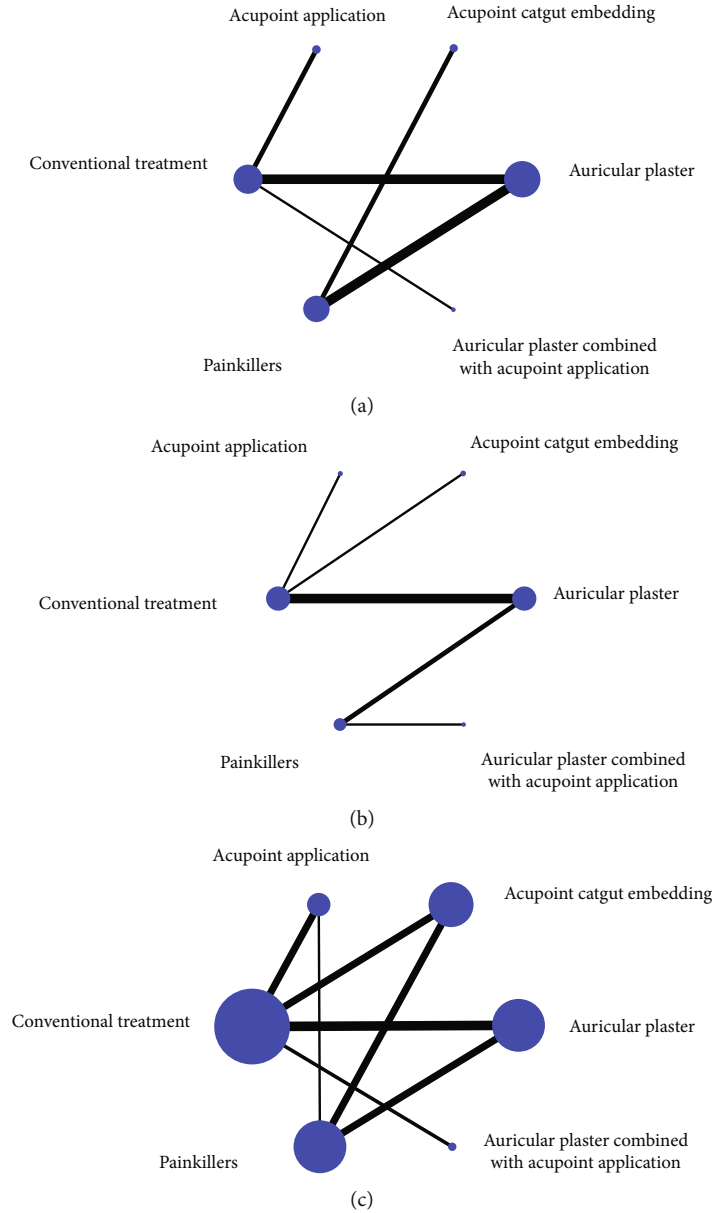


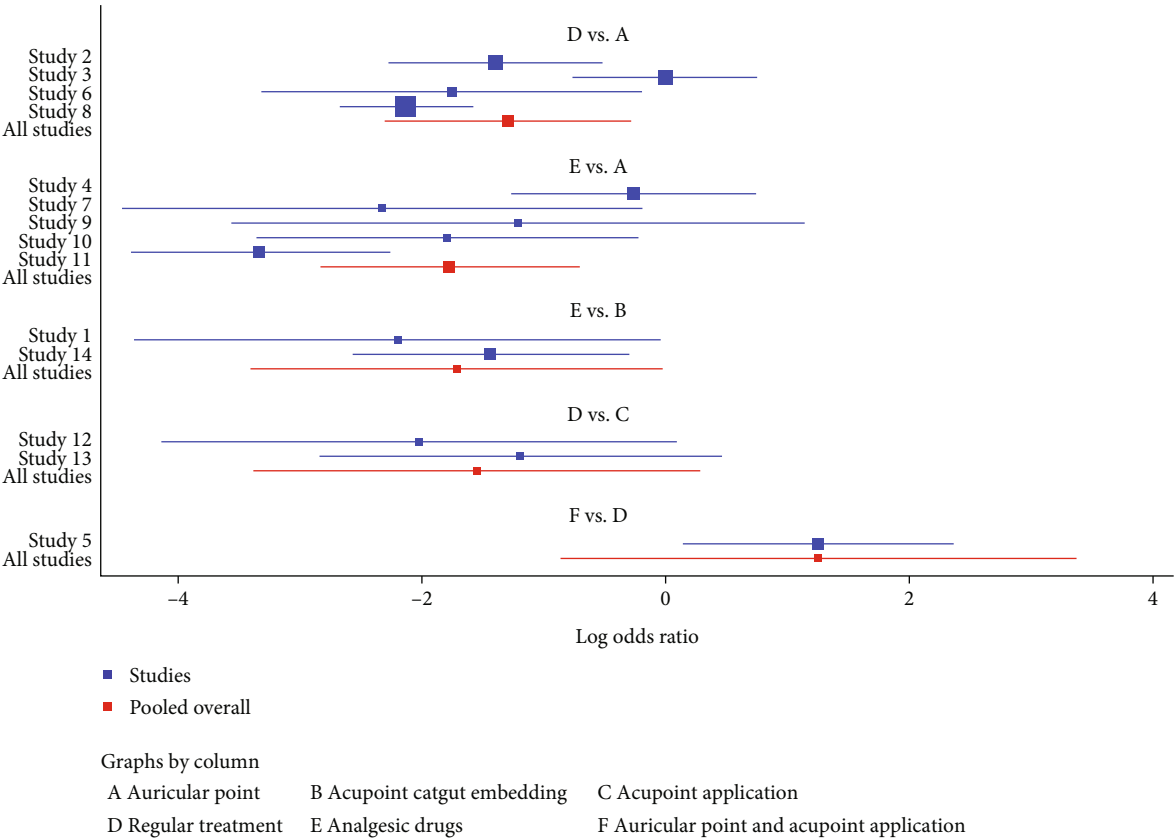
FIGURE 7: Network evidence diagram for the total effective rate, pain score, and pain degree. (a) Total effective rate evidence network diagram. (b) Network diagram of evidence of the pain degree. (c) Pain score evidence network diagram.

TABLE 3: Network meta-analysis of the overall efficacy of different treatment therapies (OR (95% CI)).

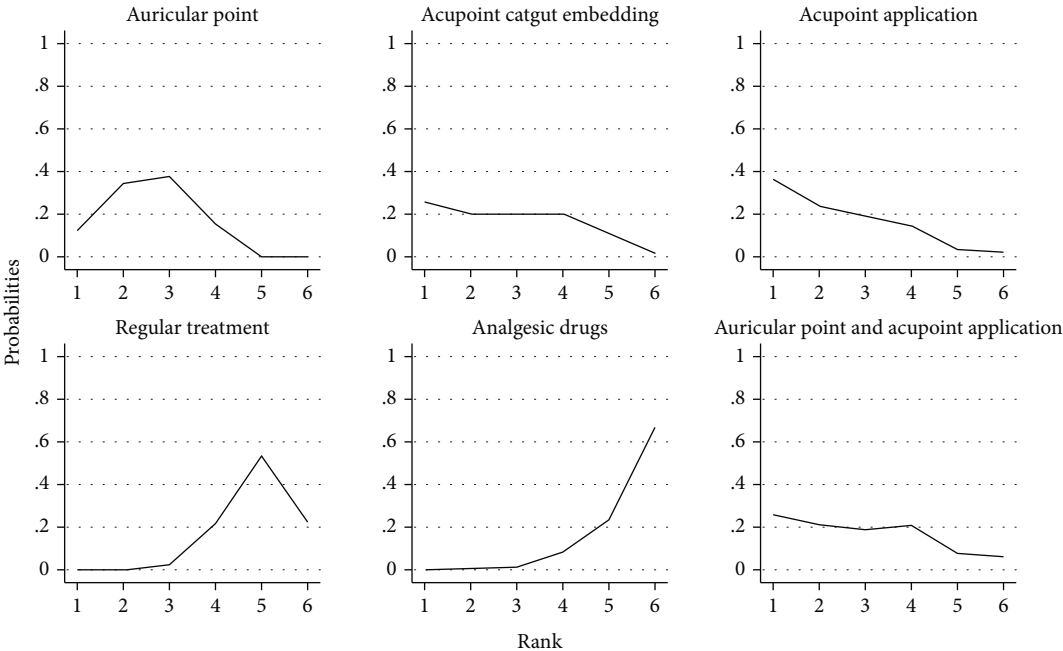
Acupoint application	0.77 (0.09, 6.33)	0.73 (0.04, 13.34)	0.74 (0.04, 12.22)	0.21 (0.03, 1.33)	0.13 (0.01, 1.39)
1.29 (0.16, 10.54)	Auricular	Point 0.94 (0.13, 7.02)	0.96 (0.09, 10.01)	0.27 (0.10, 0.75)	0.17 (0.06, 0.49)
1.37 (0.07, 25.04)	1.06 (0.14, 7.91)	Acupoint catgut embedding	1.01 (0.05, 22.31)	0.29 (0.03, 2.75)	0.18 (0.03, 0.99)
1.35 (0.08, 22.31)	1.05 (0.10, 10.97)	0.99 (0.04, 21.69)	Auricular point and acupoint application	0.29 (0.03, 2.38)	0.18 (0.01, 2.35)
4.73 (0.75, 29.71)	3.66 (1.33, 10.13)	3.45 (0.36, 32.79)	3.50 (0.42, 29.10)	Regular treatment	0.62 (0.14, 2.72)
7.61 (0.72, 80.39)	5.90 (2.02, 17.21)	5.55 (1.01, 30.40)	5.63 (0.43, 74.46)	1.61 (0.37, 7.04)	Analgesic drugs

computerized random sequence, 2 studies [14, 30] used randomized block group design grouping, 3 studies [34, 36, 44] described case shedding, and 3 studies [7, 29, 48] used a

blinded method. The basic characteristics of the included studies are shown in Table 2, and the results of the risk of bias evaluation are shown in Figures 2(a) and 2(b).



(a)



(b)

FIGURE 8: Total efficiency. (a) Forest map of different treatment methods of the total effective rate for mixed hemorrhoids. (b) Sucre diagram of the total effective rate of different methods for postoperative pain.

TABLE 4: Sucra ratio of total effective rate of different treatment methods.

Treatment	SUCRA	PrBest	MeanRank
Auricular point	68.7	12.5	2.6
Acupoint catgut embedding	64.6	25.6	2.8
Acupoint application	73.6	36.1	2.3
Regular treatment	20.9	0.0	5.0
Analgesic drugs	8.9	0.0	5.6
Auricular point and acupoint application	63.4	25.9	2.8

TABLE 5: Network meta-analysis of the pain score of different treatment therapies (SMD (95% CI)).

Auricular point and acupoint application	2.80 (0.33, 5.28)	3.27 (0.84, 5.70)	3.41 (0.95, 5.86)	4.20 (1.74, 6.67)	4.48 (2.15, 6.81)
-2.80 (-5.28, -0.33)	Acupoint application	0.47 (-0.59, 1.53)	0.60 (-0.52, 1.73)	1.40 (0.31, 2.50)	1.68 (0.79, 2.56)
-3.27 (-5.70, -0.84)	-0.47 (-1.53, 0.59)	Auricular point	0.13 (-0.72, 0.98)	0.93 (0.20, 1.66)	1.20 (0.55, 1.86)
-3.41 (-5.86, -0.95)	-0.60 (-1.73, 0.52)	-0.13 (-0.98, 0.72)	Acupoint catgut embedding	0.80 (0.10, 1.50)	1.07 (0.29, 1.85)
-4.20 (-6.67, -1.74)	-1.40 (-2.50, -0.31)	-0.93 (-1.66, -0.20)	-0.80 (-1.50, -0.10)	Analgesic drugs	0.27 (-0.52, 1.07)
-4.48 (-6.81, -2.15)	-1.68 (-2.56, -0.79)	-1.20 (-1.86, -0.55)	-1.07 (-1.85, -0.29)	-0.27 (-1.07, 0.52)	Regular treatment

### 3.2. Direct Comparison Results of Meta-Analysis

**3.2.1. Total Effective Rate.** A total of 14 studies reported the total effective rate, and the results of the meta-analysis showed that in terms of improving the total effective rate, auricular plaster combined with acupoint application (OR = 3.50, 95% CI (1.15, 10.63)), auricular plaster (OR = 8.06, 95% CI (4.80, 13.52)), and acupoint application (OR = 4.51, 95% CI (1.22, 16.61)) were superior to conventional treatment. Among the three, the efficacy of acupoint application was more significant ( $P < 0.05$ ) (Figure 3). Acupoint catgut embedding (OR = 4.96, 95% CI (1.81, 13.54)) and auricular plaster (OR = 5.94, 95% CI (1.51, 23.46)) were superior to painkillers, and auricular plaster was more effective, with statistically significant differences ( $P < 0.05$ ) (Figure 4).

**3.2.2. Pain Scoring.** Auricular plaster (SMD = -1.92, 95%CI (-3.01, -0.83)), acupoint catgut embedding (SMD = -0.71, 95%CI (-0.95, -0.47)), and acupoint application (SMD = -1.35, 95%CI (-2.15, -0.55)) were better than conventional treatment, and auricular plaster was more effective ( $P < 0.05$ ) (Figure 5). Acupoint catgut embedding (SMD = -1.06, 95%CI (-1.99, -0.13)), auricular plaster (SMD = -0.86, 95%CI (-1.38, -0.33)), and acupoint application (SMD = -6.39, 95%CI (-7.49, -5.30)) were all superior to pain medication, and the efficacy of acupoint application was statistically significant ( $P < 0.05$ ) (Figure 6).

### 3.3. Results of Network Meta-Analysis (NMA)

**3.3.1. Network Evidence Diagram for Total Effective Rate, Pain Score, and Pain Degree.** The total effective rate was included in 14 studies [9, 13, 16, 17, 19, 20, 22, 24–27, 39, 42, 47] and pain degree in 9 studies [22, 26, 32, 42, 50–54], both without closed loop formation (Figures 7(a) and 7(b)).

A total of 34 papers [7, 9–15, 17–19, 21–23, 28–31, 33–46, 48, 49] were included in the pain score, involving 6 treatment

measures (auricular plaster, acupoint catgut embedding, acupoint application, conventional treatment, and pain medication), forming a total of 3 closed loops, namely, conventional treatment-acupoint application-painkiller-acupoint catgut embedding, conventional treatment-acupoint application-painkiller-auricular plaster, and conventional treatment-acupoint catgut embedding-painkiller-auricular plaster (Figure 7(c)).

**3.3.2. Total Efficiency.** In terms of improving the total effective rate, auricular plaster (OR = 5.90, 95%CI = (2.02, 17.21)) and acupoint catgut embedding (OR = 5.55, 95%CI = (1.01, 30.40)) had higher total efficiency than painkillers. Auricular plaster (OR = 3.66, 95%CI = (1.33, 10.13)) was superior than conventional treatment, and the differences were all statistically significant,  $P < 0.05$  (Table 3 and Figure 8(a)).

The efficacy ranking was based on cumulative SUCRA, and the larger the area, the better the efficacy. The results of SUCRA ranking showed that acupoint application (73.6%) > auricular plaster (68.7%) > acupoint catgut embedding (64.6%) > auricular plaster combined with acupoint application (63.4%) > conventional treatment (20.9%) > painkillers (8.9%) (Table 4 and Figure 8(b)).

**3.3.3. Pain Scoring.** In terms of pain score reduction, auricular plaster (OR = -0.93, 95%CI = (-1.66, -0.20)), acupoint catgut embedding (OR = -0.8, 95%CI = (-1.50, -0.10)), and acupoint application (OR = -1.4, 95%CI = (-2.50, -0.31)) were superior to painkillers. Auricular plaster (OR = -1.20, 95%CI = (-1.86, -0.55)), acupoint catgut embedding (OR = -1.07, 95%CI = (-1.85, -0.29)), and acupoint application (OR = -1.68, 95%CI = (-2.56, -0.79)) were superior to conventional treatment.

Auricular plaster combined with acupoint application was superior to auricular plaster (OR = -3.27, 95%CI = (-5.70, -0.84)), acupoint catgut embedding (OR = -3.41, 95%

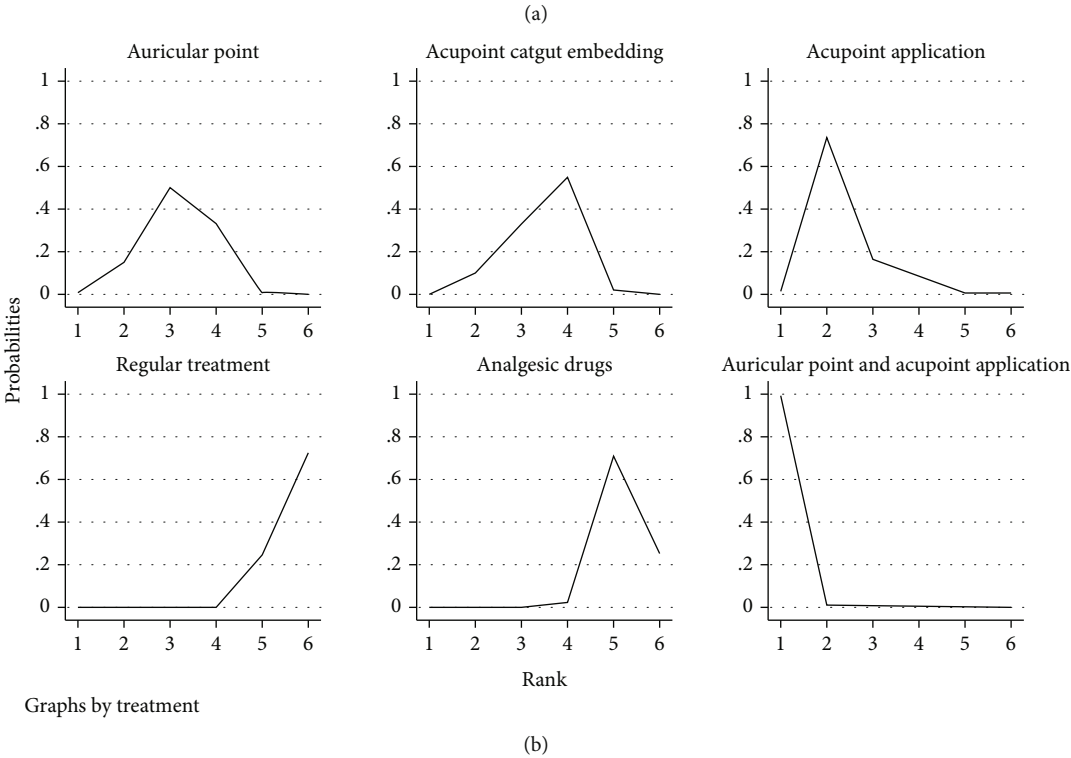
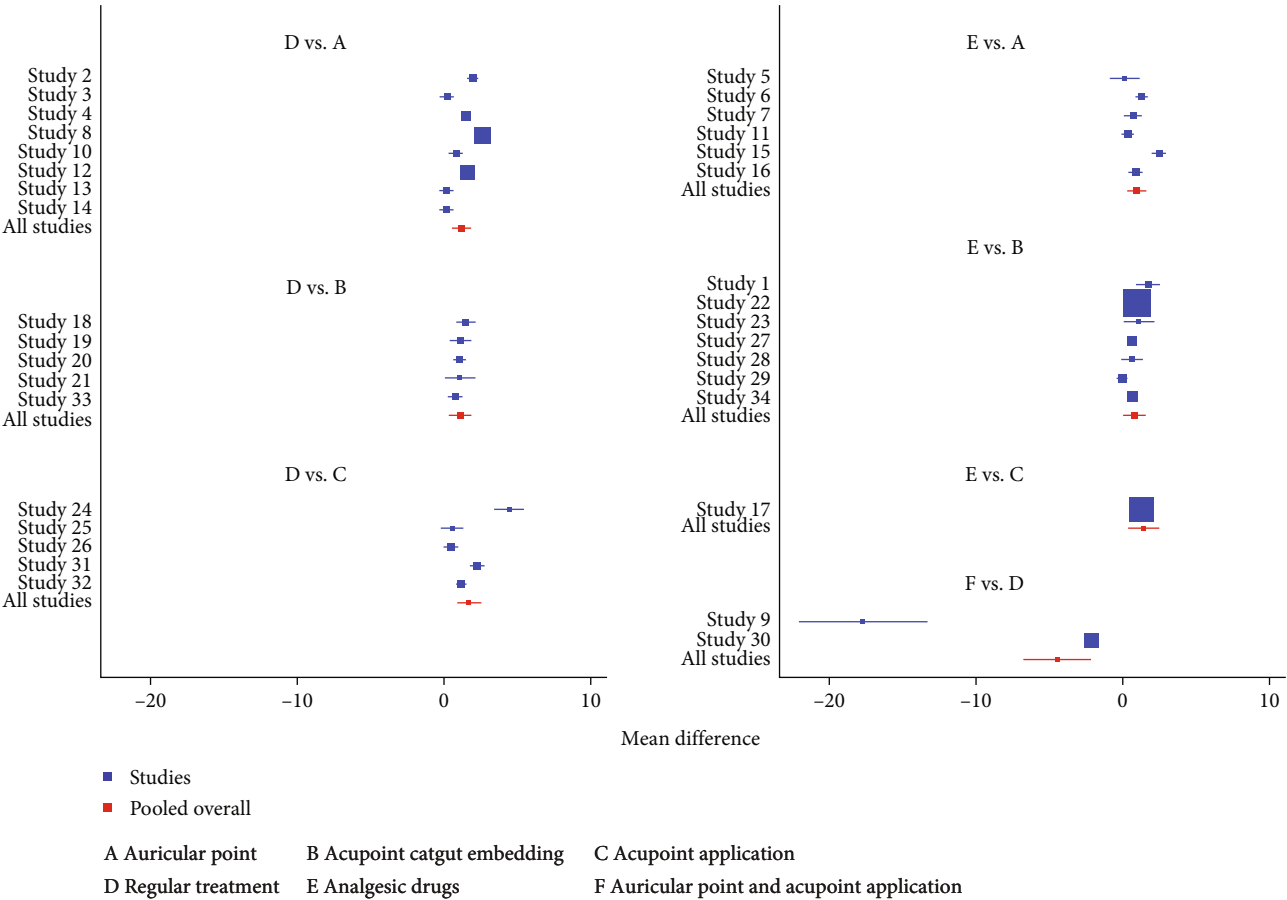


FIGURE 9: Pain scoring. (a) Forest map of the pain score after different treatment methods. (b) Sucra plot of the pain score after different treatment methods.



TABLE 6: Sucra proportion table of the pain score of different treatment methods.

Treatment	SUCRA	PrBest	MeanRank
Auricular point	56.1	0.1	3.2
Acupoint catgut embedding	50.2	0.1	3.5
Acupoint application	73.5	1.3	2.3
Regular treatment	5.3	0.0	5.7
Analgesic drugs	15.3	0.0	5.2
Auricular point and acupoint application	99.5	98.5	1.0

TABLE 7: Network meta-analysis of the pain degree of patients with mixed hemorrhoids treated by different methods (OR (95% CI)).

Acupoint application	0.51 (0.22, 1.15)	0.40 (0.05, 3.40)	0.26 (0.09, 0.80)	0.16 (0.00, 8.93)	0.16 (0.08, 0.32)
1.98 (0.87, 4.48)	Auricular point	0.79 (0.11, 5.71)	0.52 (0.24, 1.11)	0.32 (0.01, 17.06)	0.32 (0.20, 0.50)
2.51 (0.29, 21.36)	1.27 (0.18, 9.18)	Auricular point and acupoint application	0.66 (0.11, 4.07)	0.41 (0.00, 34.47)	0.41 (0.05, 3.09)
3.83 (1.25, 11.74)	1.94 (0.90, 4.16)	1.53 (0.25, 9.48)	Analgesic drugs	0.62 (0.01, 35.52)	0.62 (0.26, 1.50)
6.18 (0.11, 340.82)	3.13 (0.06, 166.63)	2.46 (0.03, 209.31)	1.61 (0.03, 92.59)	Acupoint catgut embedding	1.00 (0.02, 51.97)
6.18 (3.11, 12.28)	3.13 (2.00, 4.89)	2.47 (0.32, 18.76)	1.62 (0.67, 3.92)	1.00 (0.02, 52.02)	Regular treatment

CI = (-5.86, -0.95)), acupoint application (OR = -2.80, 95%CI = (-5.28, -0.33)), conventional treatment (OR = -4.48, 95%CI = (-6.81, -2.15)), and painkillers (OR = -4.20, 95%CI = (-6.67, -1.74)); all differences were statistically significant,  $P < 0.05$  (Table 5 and Figure 9(a)).

The results of the area under the curve (SUCRA) ranking showed that auricular plaster combined with acupoint application (99.5%) > acupoint application (73.5%) > auricular plaster (56.1%) > acupoint catgut embedding therapy (50.2%) > pain medication (15.3%) > conventional treatment (5.3%) (Table 6 and Figure 9(b)).

**3.3.4. Pain Degree.** After treatment, patients with no pain and mild pain were significantly relieved but there was no significant effect on the symptoms of patients with moderate and severe pain. The results showed that auricular plaster (OR = 3.13, 95%CI = (2.00, 4.89)) and acupoint application (OR = 6.18, 95%CI = (3.11, 12.28)) were better than conventional treatment and acupoint application (OR = 3.83, 95%CI = (1.25, 11.74)) was better than painkillers; all differences were statistically significant,  $P < 0.05$  (Table 7 and Figure 10(a)).

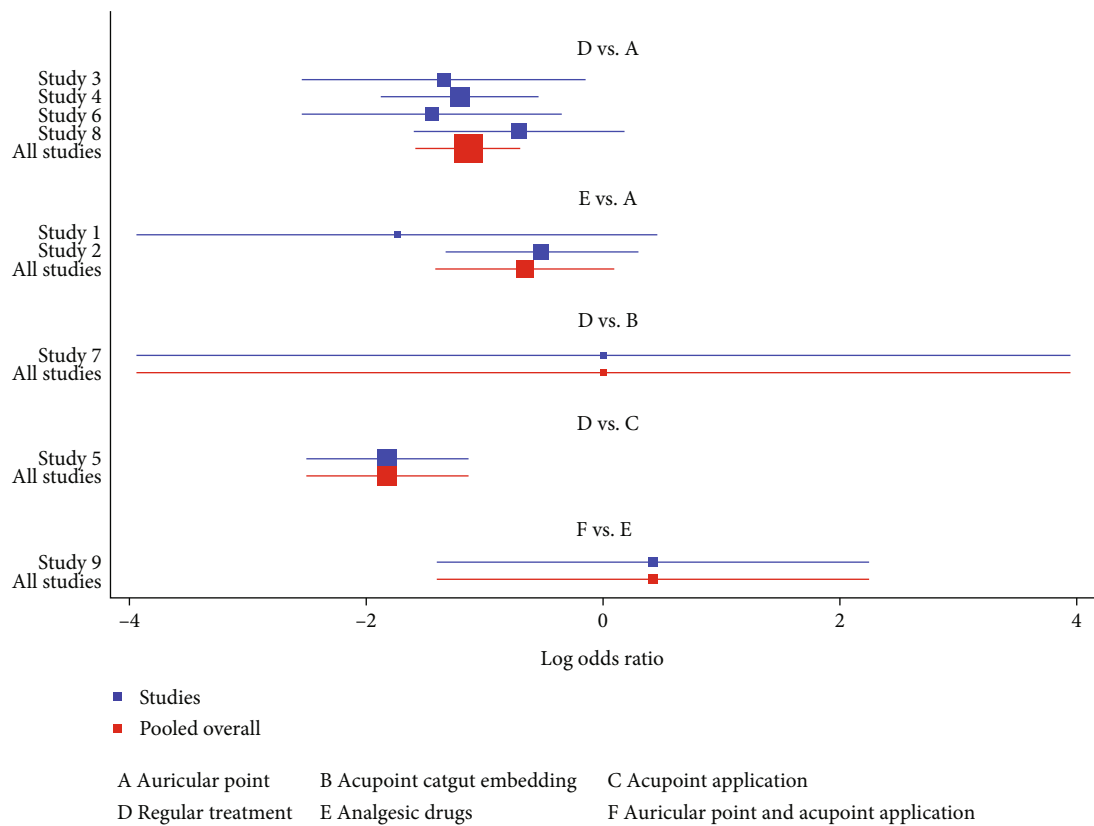
The results of the area under the curve (SUCRA) ranking showed that acupoint application (91.2%) > auricular plaster (66.1%) > auricular plaster combined with acupoint application (54.6%) > painkillers (36.6%) > acupoint catgut embedding (34.8%) > conventional treatment (16.8%); all differences were statistically significant,  $P < 0.05$  (Table 8 and Figure 10(b)).

**3.3.5. Complications and Adverse Reactions.** Six publications reported complications [31, 33, 36, 37, 44, 53] in a total of 490 patients, of which 133 patients developed complications. In terms of reducing postoperative complications, auricular plaster (RR = 0.24, 95%CI = (0.06, 0.96)) and acupoint catgut embedding (RR = 0.28, 95%CI = (0.12, 0.69)) were superior to painkillers and auricular plaster (RR = 0.15, 95%

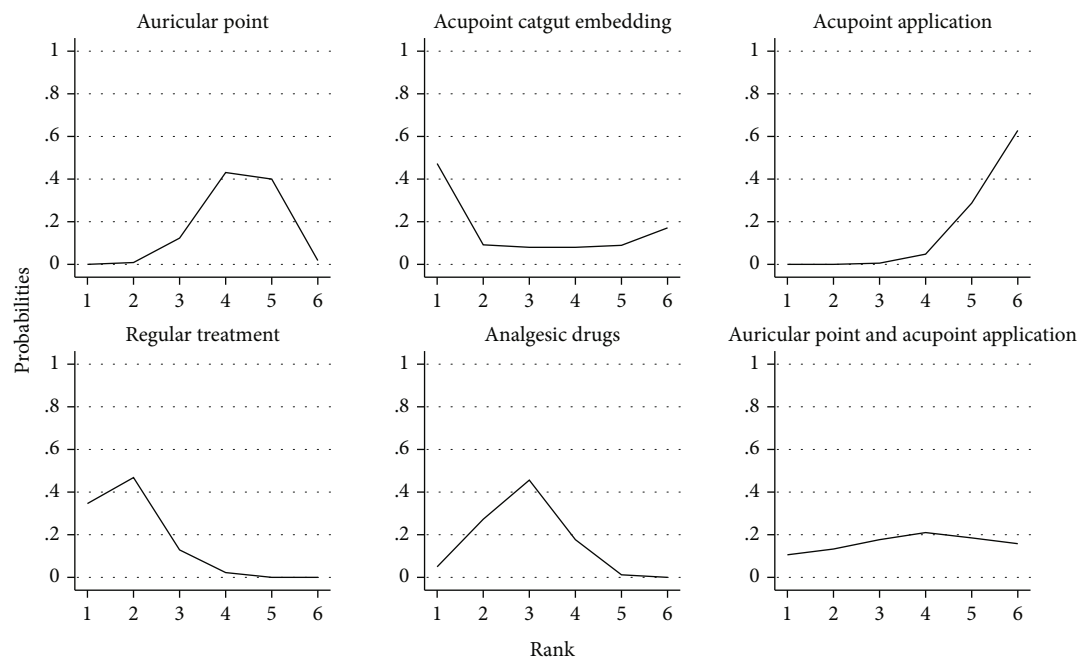
%CI = (0.03, 0.89)) and acupoint catgut embedding (RR = 0.18, 95%CI = (0.10, 0.33)) were superior to conventional treatment and the differences were statistically significant,  $P < 0.05$  (Table 9 and Figure 11(a)).

The results of SUCRA ranking showed that acupoint application (86.5%) > auricular plaster (69.6%) > acupoint catgut embedding (65.8%) > painkillers (21.5%) > conventional treatment (6.6%) (Figure 11(b)). Regarding adverse reactions, a total of 10 publications reported [11, 14, 17, 28, 29, 32, 33, 36, 43, 45, 46] a total of 844 patients, of which 100 patients experienced adverse reactions. In terms of reducing patients' adverse reactions, auricular plaster (RR = 0.2, 95%CI = (0.04, 0.97)), acupoint catgut embedding (RR = 0.04, 95%CI = (0.01, 0.21)), and auricular plaster combined with acupoint application (RR = 0.19, 95%CI = (0.05, 0.69)) were superior to conventional treatment and auricular plaster (RR = 0.15, 95%CI = (0.05, 0.48)), acupoint catgut embedding (RR = 0.03, 95%CI = (0.01, 0.11)), and auricular plaster combined with acupoint application (RR = 0.14, 95%CI = (0.02, 0.83)) were superior to painkillers and the differences were statistically significant,  $P < 0.05$  (Table 10 and Figure 12(a)). The results of SUCRA ranking showed that acupoint catgut embedding (96.2%) > auricular plaster combined with acupoint application (64.9%) > auricular plaster (63%) > acupoint application (43.5%) > conventional treatment (20.3%) > painkillers (12.2%) (Figure 12(b)).

**3.3.6. Duration of Onset of Acupuncture Intervention.** Meta-analysis results showed that the control group was conventional treatment; 24 h after intervention treatment, SMD = -1.40, 95%CI = (-2.05, -0.74), 48 h, SMD = -1.14, 95%CI = (-1.55, -0.74), and 72 h, SMD = -1.80, 95%CI = (-2.48, -1.11) all played a pain relief effect, with the 72 h efficacy being more effective. In the control group with analgesics, 24 h, SMD = -1.33, 95%CI = (-2.07, -0.60), 48 h, SMD = -1.33, 95%CI = (-2.27, -0.40), and 72 h, SMD = -2.12, 95%CI = (-3.21, -1.03) after the intervention had an analgesic



(a)



Graphs by treatment

(b)

FIGURE 10: Pain degree. (a) Forest map of the pain degree after different treatment methods. (b) Sucra diagram of the pain degree after different methods for postoperative pain.

TABLE 8: Sucra proportion table of the pain degree in patients with mixed hemorrhoids treated by different methods.

Treatment	SUCRA	PrBest	MeanRank
Auricular point	66.1	1.9	2.7
Acupoint catgut embedding	34.8	17.3	4.3
Acupoint catgut embedding	91.2	63.8	1.4
Regular treatment	16.8	0	5.2
Analgesic drugs	36.6	0.2	4.2
Auricular point and acupoint application	54.6	16.7	3.3

TABLE 9: Network meta-analysis of complications that occurred in patients with mixed hemorrhoids treated by different methods (RR (95% CI)).

Acupoint application	3.05 (0.12, 77.68)	3.55 (0.17, 76.05)	12.55 (0.67, 234.86)	19.72 (0.87, 448.52)
0.33 (0.01, 8.34)	Auricular point	1.16 (0.22, 6.02)	4.11 (1.04, 16.29)	6.46 (1.12, 37.31)
0.28 (0.01, 6.03)	0.86 (0.17, 4.44)	Acupoint catgut embedding	3.53 (1.44, 8.67)	5.55 (3.01, 10.23)
0.08 (0.00, 1.49)	0.24 (0.06, 0.96)	0.28 (0.12, 0.69)	Analgesic drugs	1.57 (0.53, 4.65)
0.05 (0.00, 1.15)	0.15 (0.03, 0.89)	0.18 (0.10, 0.33)	0.64 (0.21, 1.88)	Regular treatment

effect, the efficacy of 72 h was more visible, and all differences were statistically significant,  $P < 0.05$  (Figures 13(a) and 13(b)).

#### 4. Publication Bias Analysis and Small Sample Effect Assessment

Because 34 of the 47 publications reported pain scores, this study used pain scores as an outcome indicator to test for small sample effects or publication bias and the funnel plot showed that most of the study scatters were located between the funnel plot and were more symmetrical, suggesting that there may be a small publication bias (Figure 14).

#### 5. Discussion

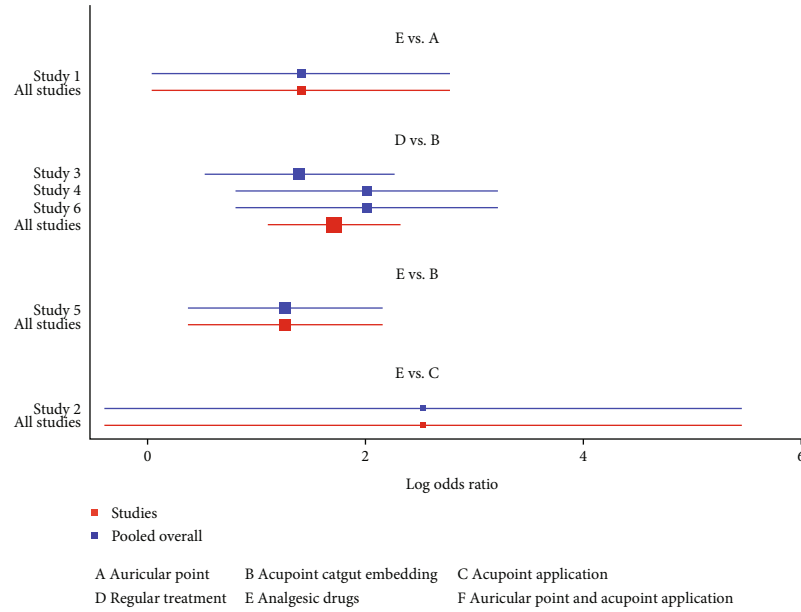
This study is aimed at discussing the efficacy of three different acupuncture therapies (auricular plaster, acupoint application, and acupoint catgut embedding) for postoperative pain in mixed hemorrhoids. 47 RCTs involving 5121 patients were included in this study. The results of the NMA showed that auricular plaster, acupoint application, and acupoint catgut embedding were superior to pain medication and conventional treatment in improving the overall efficiency and the ranking results showed that acupoint application was the most effective. Reducing postoperative pain scores, auricular plaster, acupoint application, and acupoint catgut embedding were superior to pain medication and conventional treatment. Auricular plaster combined with acupoint application was probably the most effective, followed by acupoint application.

However, of the 47 studies included in this study, only 3 [19, 32, 46] had auricular plaster combined with acupoint application, which is a small sample size, and more studies need to be included to confirm the efficacy of the combined therapy. In terms of reducing postoperative complications, auricular plaster, acupoint application, and acupoint catgut embedding were superior to pain medication and conven-

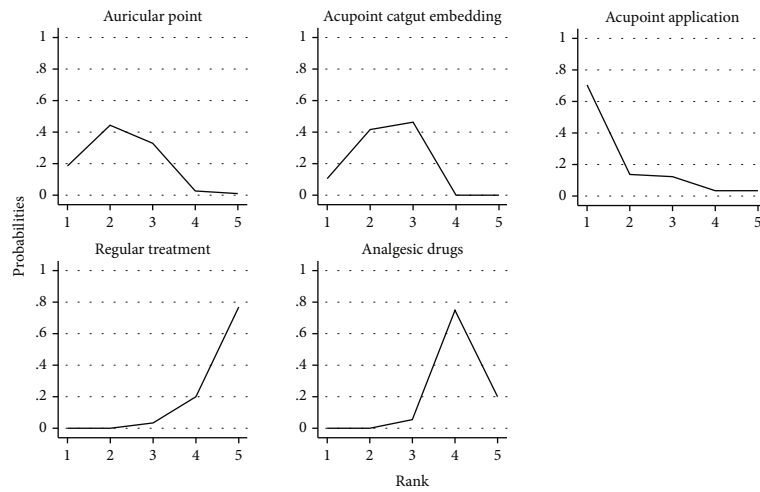
tional treatment and acupoint application was the most effective, significantly reducing postoperative edema, urinary retention, and other complications; in terms of safety, auricular plaster, acupoint application, and acupoint catgut embedding were superior to pain medication. Acupoint catgut embedding was the most effective for the onset of effect of the three acupuncture interventions; it was found that the analgesic effect was superior to that of analgesics at different time periods of 24 h, 48 h, and 72 h postoperatively. The perianal area is a concentrated area of nerve endings and is more sensitive to nociception. As the effects of anesthesia wear off, patients have a painful process that lasts 24 h to 48 h [55]. This study found that it still has a better analgesic effect at 72 h postoperatively, indicating that the effect of acupuncture for postoperative pain on mixed hemorrhoids is long lasting and stable, guiding that the treatment course of the three acupuncture therapies for postoperative pain in mixed hemorrhoids should last at least until 72 h for better therapeutic effect.

Nowadays, medical treatment of postoperative pain in mixed hemorrhoids mostly uses opioid analgesics, nonsteroidal anti-inflammatory drugs, central analgesics, etc. Although the pain relief effect is good, drug side effects such as nausea, dizziness, vomiting, and sweating can easily occur [56, 57], with adverse reactions as high as 37% [58]. Acupuncture therapy, as a green complementary alternative therapy, has better clinical efficacy for postoperative pain in mixed hemorrhoids.

This study showed that the efficacy of acupoint application for postoperative pain in mixed hemorrhoids was more advantageous compared with other therapies. In fact, the mechanism of acupoint application for postoperative pain in mixed hemorrhoids is more widely studied, which may be related to its good efficacy. Acupoint application is based on the guidance of Chinese medicine meridian science, and the drug is applied to specific points on the body surface, both for acupuncture point stimulation and for absorbing the active ingredients of the drug through the skin tissue, producing a local concentration of the drug and playing



(a)



(b)

FIGURE 11: Complications. (a) Forest map of complications after the treatment of postoperative pain by different methods. (b) Sucra diagram of complication after the treatment of postoperative pain by different methods.

TABLE 10: Network meta-analysis of adverse reaction that occurred in patients with mixed hemorrhoids treated by different methods (RR (95% CI)).

Acupoint catgut embedding	4.30 (0.67, 27.82)	4.57 (0.94, 22.30)	9.91 (0.31, 315.19)	22.72 (4.77, 108.27)	30.48 (8.81, 105.38)
0.23 (0.04, 1.50)	Auricular point and acupoint application	1.06 (0.17, 6.84)	2.30 (0.06, 91.53)	5.28 (1.45, 19.18)	7.08 (1.21, 41.53)
0.22 (0.04, 1.07)	0.94 (0.15, 6.06)	Auricular point	2.17 (0.07, 67.20)	4.97 (1.04, 23.82)	6.67 (2.07, 21.43)
0.10 (0.00, 3.21)	0.43 (0.01, 17.26)	0.46 (0.01, 14.32)	Acupoint application	2.29 (0.06, 81.97)	3.08 (0.12, 77.78)
0.04 (0.01, 0.21)	0.19 (0.05, 0.69)	0.20 (0.04, 0.97)	0.44 (0.01, 15.59)	Regular treatment	1.34 (0.29, 6.23)
0.03 (0.01, 0.11)	0.14 (0.02, 0.83)	0.15 (0.05, 0.48)	0.33 (0.01, 8.22)	0.75 (0.16, 3.46)	Analgesic drugs

the dual role of Chinese medicine and meridian regulation at the same time. Medical research has shown that trans-acupoint application drugs have permeability, exosensitivity, and amplification effects [59].

This study showed that the efficacy of acupoint application for postoperative pain in mixed hemorrhoids was more advantageous compared with other therapies. In fact, the mechanism of acupoint application for postoperative pain

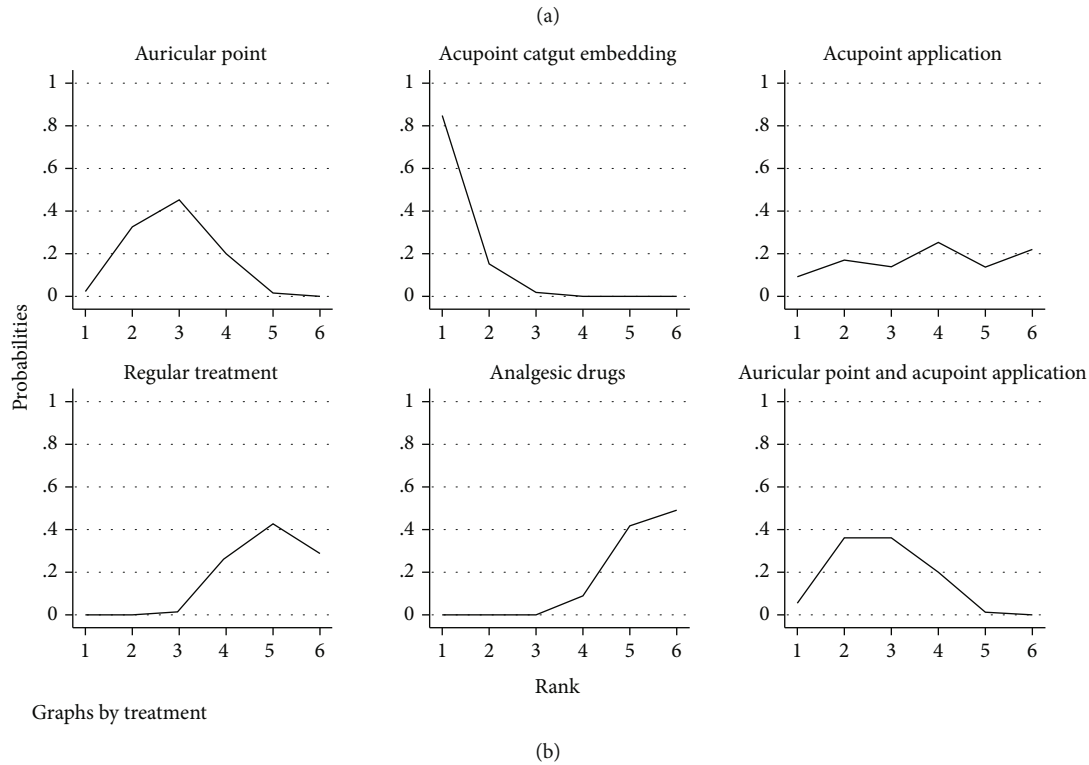
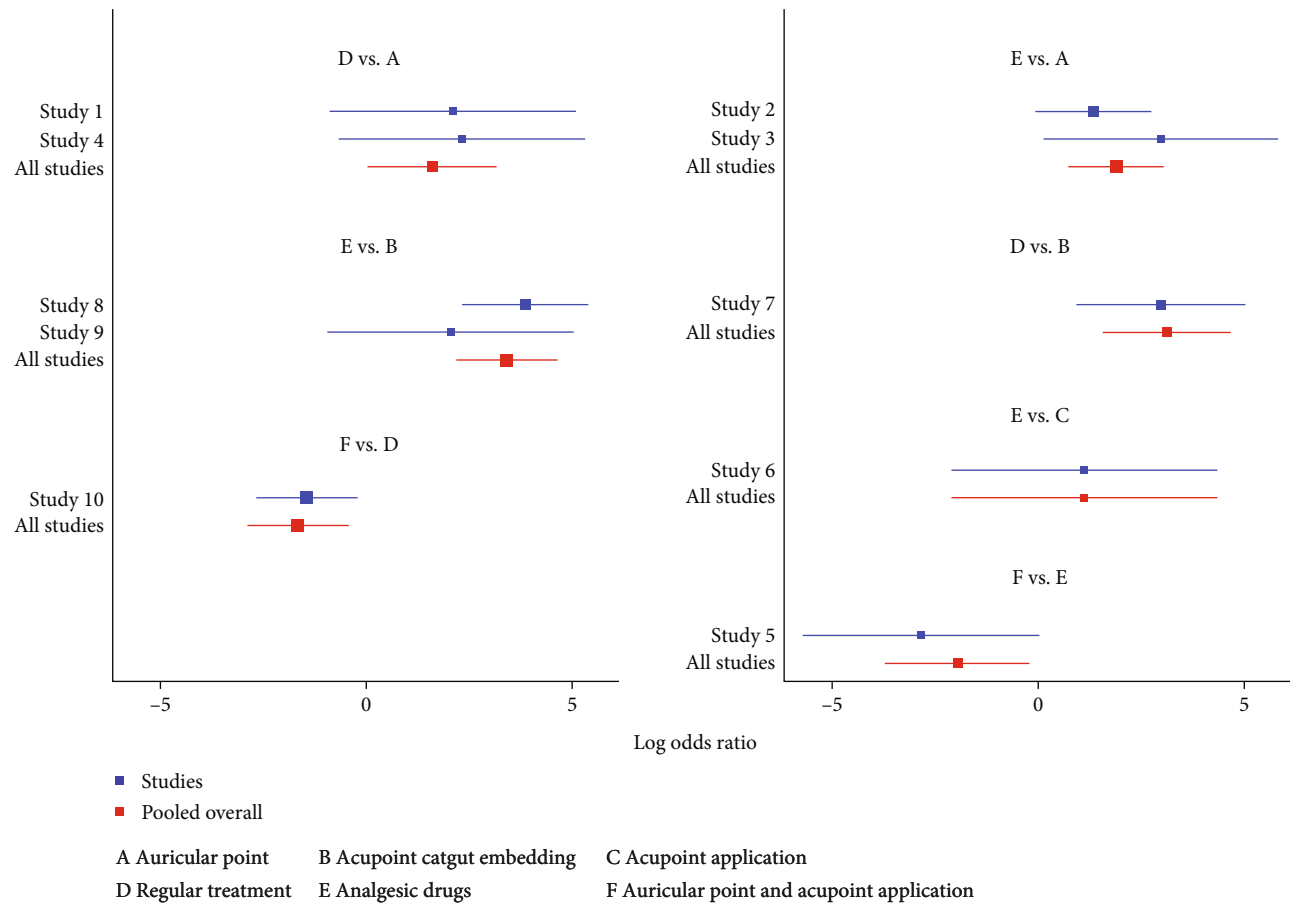


FIGURE 12: Adverse reactions. (a) Forest map of adverse reactions after the treatment of postoperative pain by different methods. (b) Sucra diagram of adverse reactions after the treatment of postoperative pain by different methods.

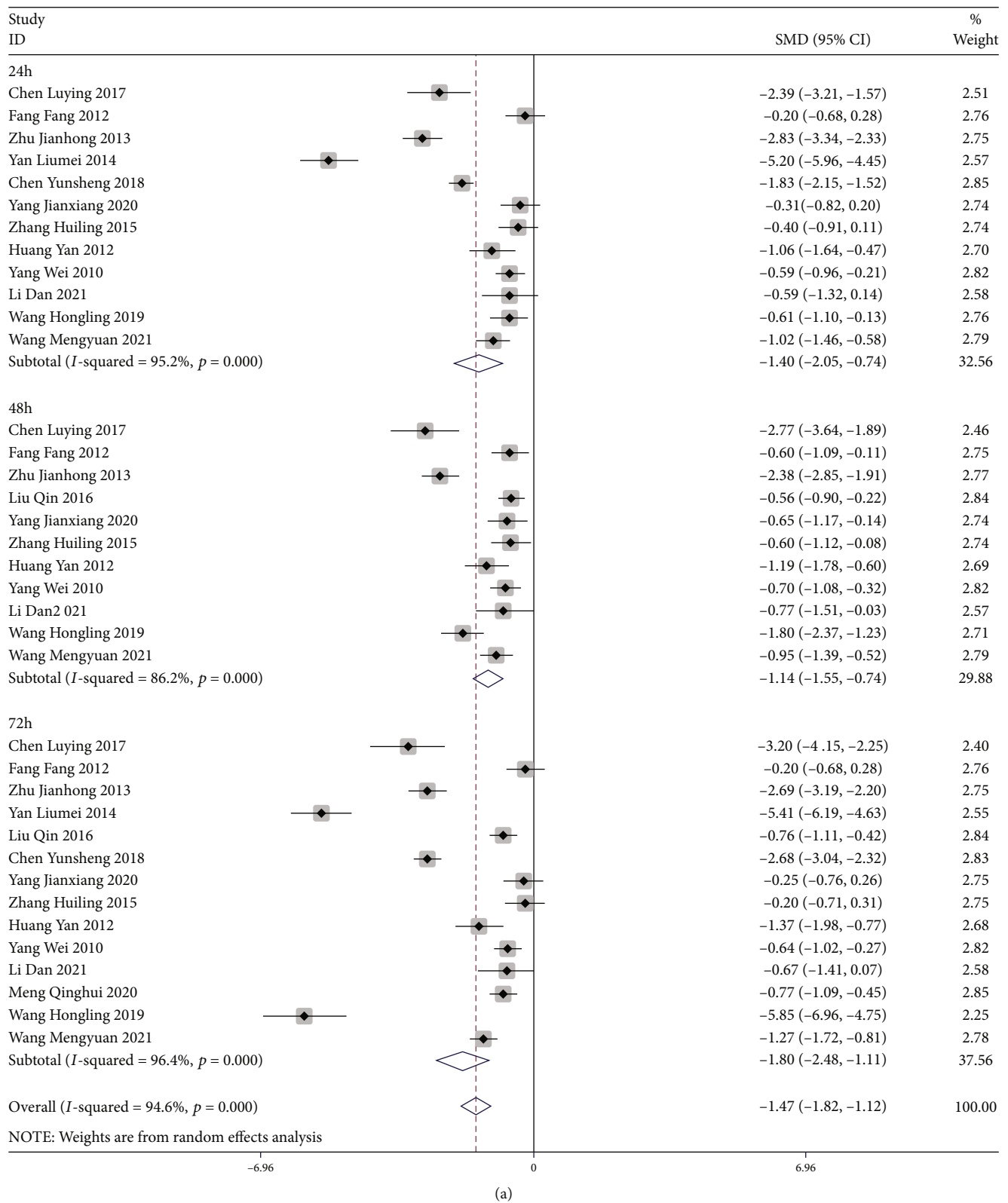


FIGURE 13: Continued.



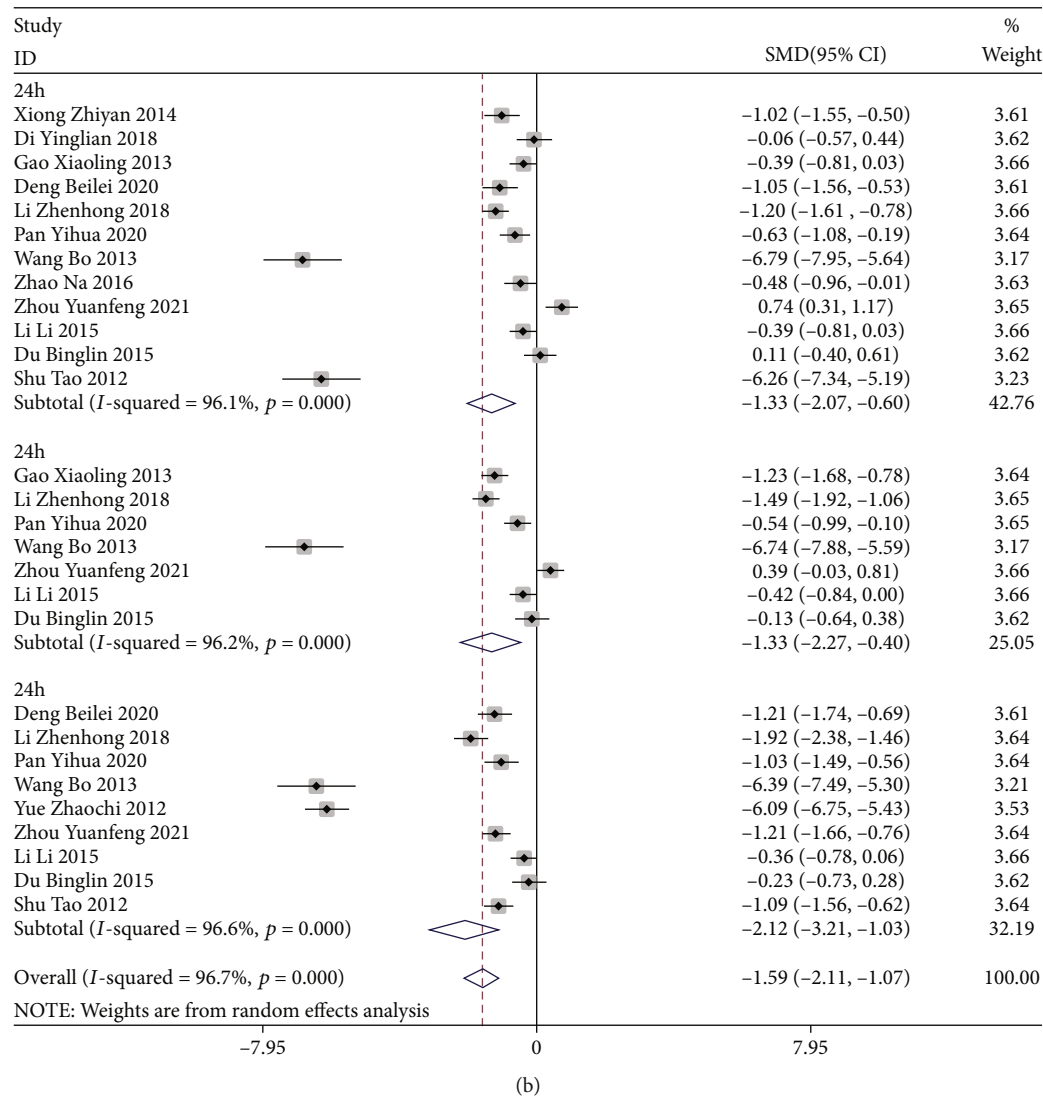


FIGURE 13: Duration of onset of acupuncture intervention. (a, b) Meta-analysis of postoperative pain scores of mixed hemorrhoids treated with acupuncture at different times.

in mixed hemorrhoids is more widely studied, which may be related to its good efficacy. Acupoint application is based on the guidance of Chinese medicine meridian science. The drug is applied to specific points on the body surface, both for acupuncture point stimulation and for absorbing the active ingredients of the drug through the skin tissue, producing a local concentration of the drug and playing the dual role of Chinese medicine and meridian regulation at the same time. Medical research has shown that trans-acupoint-applied drugs have permeability, exosensitivity, and amplification effects [47]. Another study showed that acupoint application could produce the effect of biological function through biological wave meridian points, through the process of absorption, transmission, and reflection, to activate blood and remove blood stasis, unblock meridians, and achieve pain relief [59]. The local absorption of drugs in the skin reduces the adverse reactions in the gastrointestinal tract [60]. In modern medicine, acupoint application therapy is classified as TDS, the transdermal drug delivery

system of Chinese medicine [61]. 90% of the human dermis is a vascular-rich connective tissue, and the drug is absorbed into the blood through keratin transit, and the keratin layer is the main barrier for transdermal absorption, which forms a dense state locally after acupoint application, causing the cells of the keratin layer to swell into a porous state and make its tight structure lose, letting it easy for the drug to penetrate [62].

As a part of Chinese traditional medicine, acupuncture therapy has the advantages of precise efficacy, low toxic side effects, and easy acceptance by patients. In recent years, acupuncture therapy has gradually become the mainstream of global medicine as a green alternative or complementary treatment [63, 64]. Compared with conventional drug therapy, it can effectively reduce drug side effects and postoperative complications such as urinary retention and traumatic edema, as well as reduce the economic burden of patients [65, 66], and even if it cannot completely replace analgesics, it can participate in the synergistic use of drugs and reduce

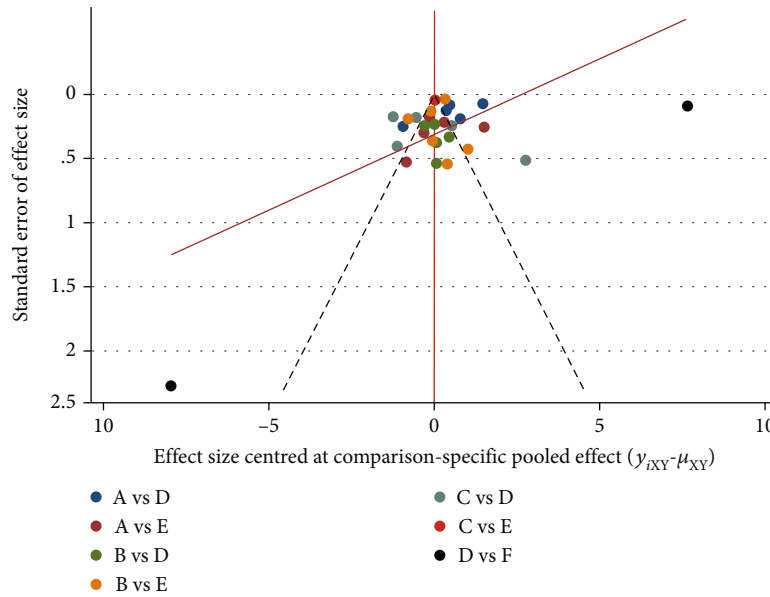


FIGURE 14: Comparison of different acupuncture in treating postoperative pain of mixed hemorrhoids by adjusting the funnel plot.

the number and dose of analgesic drugs taken by patients, thus reducing the occurrence of adverse reactions in patients. Compared to ordinary acupuncture, the three acupuncture treatments avoid the pain caused to patients by multiple needle sticks, reduce the workload of medical personnel, and make up for the short duration of the curative effect of ordinary acupuncture and the large arbitrariness of the operation. More importantly, there is no need to change the needles daily, which helps improve patient compliance and promote the clinical grassroot application.

This study still has shortcomings, such as the lack of systematic and standardized methods for making homemade acupoint-applied plasters and the need to further standardize the methods for making acupoint-applied plasters. The methodological quality of the included studies was low, most of the studies did not mention the distribution concealment method, and due to the specificity of acupuncture therapy, most of the studies were not implemented blinded, which may produce implementation bias; in order to reduce bias and make the results more reliable, in the future, researchers should follow the CONSORT reporting standards [67]. The control group has drug interventions which did not consider the drug dose and duration and frequency, and the specific content of the acupuncture protocol was not explored, such as TCM identification, treatment frequency, and duration; the details of acupuncture therapy were reported unclear, which to some extent caused the bias of the study results and decreased the guiding effect on TCM clinical practice, and in future studies, clinical trials of acupuncture therapy should follow STRICTA standards [68]. For combination therapy, there are fewer clinical research trials, which can be a focus of future research to provide more possibilities for the selection of analgesic methods and provide evidence-based medical evidence reference for the use of this method in clinical practice. In a word, given the very low methodological quality of the included systematic evalua-

tions and the risk bias of poor reporting of randomized controlled trials, a more rigorous design and standardized reporting are needed in the future to demonstrate the reliability of this study further.

## 6. Conclusion

Current evidence suggests that acupoint application therapy for the treatment of postoperative pain in mixed hemorrhoids has better efficacy in improving overall effectiveness and reducing pain scores as well as relieving pain levels.

## Data Availability

The datasets used and/or analyzed during the current study are available from the corresponding author upon reasonable request.

## Conflicts of Interest

The authors have no conflicts of interest.

## Authors' Contributions

Sunsong Ye extracted data for statistical analysis and wrote the paper; Xiaoxue Jiang conducted the conception and design of the article, implementation and feasibility analysis of the study, and revision of the paper and was responsible for the quality control and review of the article; Xiutian Guo and Jianhua Zhou were responsible for the overall article and supervision and management.

## Acknowledgments

The study is supported by the Shanghai Municipal Health Care Commission Scientific Research Project: clinical standardization study on the treatment of mixed hemorrhoids

by modified elastic thread ligation, Project no: 202140158, and the Three Year Action Plan for Further Acceleration of the Development of Traditional Chinese Medicine in Shanghai (2018–2020), Project no: ZY (2018–2020)-RCPY-1028.

## References

- [1] A. Medina-Gallardo, Y. Curbelo-Pena, X. De Castro, P. Roura-Poch, J. Roca-Closa, and E. De Caralt-Mestres, "Is the severe pain after Milligan-Morgan hemorrhoidectomy still currently remaining a major postoperative problem despite being one of the oldest surgical techniques described? A case series of 117 consecutive patients," *International Journal of Surgery Case Reports*, vol. 30, pp. 73–75, 2017.
- [2] A. G. Acheson and J. H. Scholefield, "Management of haemorrhoids," *BMJ*, vol. 336, no. 7640, pp. 380–383, 2008.
- [3] D. Yeo and K. Y. Tan, "Hemorrhoidectomy - making sense of the surgical options," *World Journal of Gastroenterology*, vol. 20, no. 45, pp. 16976–16983, 2014.
- [4] Z. T. Yang, J. T. Zhang, and D. X. Wang, "Changes of serum levels of IL-17, IL-6 and TNF-alpha in hemorrhoids treated by internal and external treatment of traditional Chinese medicine," *Chinese Archives of Traditional Chinese Medicine*, vol. 36, no. 8, pp. 1933–1935, 2018.
- [5] M. A. Al Mamun, K. Islam, M. J. Alam et al., "Flavonoids isolated from *Tridax procumbens* (TPF) inhibit osteoclasts differentiation and bone resorption," *Biological Research*, vol. 48, no. 1, p. 51, 2015.
- [6] H. Fu, W. Guo, B. Zhou, Y. Liu, Y. Gao, and M. Li, "Efficacy and safety of micronized purified flavonoid fractions for the treatment of postoperative hemorrhoid complications: a systematic review and meta-analysis," *Phytomedicine*, vol. 104, p. 154244, 2022.
- [7] X. Pei, S. Song, H. Li, and D. Lu, "Efficacy and safety of acupoint catgut embedding in treating postoperative pain of mixed hemorrhoids: a randomized controlled trial protocol," *Medicine (Baltimore)*, vol. 100, no. 19, article e25948, 2021.
- [8] J. P. Higgins, D. G. Altman, P. C. Gøtzsche et al., "The Cochrane Collaboration's Tool for assessing risk of bias in randomised trials," *BMJ*, vol. 343, p. d5928, 2011.
- [9] Z. Y. Xiong and W. J. Xie, "Clinical observation of 32 cases of anal pain after mixed hemorrhoid surgery treated with acupoint catgut embedding therapy (in Chinese)," *Guiding Journal of Traditional Chinese Medicine and Pharmacy*, vol. 20, no. 1, pp. 68–69, 2014.
- [10] L. Y. Cheng and X. F. Deng, "Effect of magnetic bead pressure on auricular points on postoperative pain relief in patients with mixed hemorrhoids (in Chinese)," *Journal of Cardiovascular Surgery*, vol. 6, no. 2, p. 170, 2017.
- [11] F. Fang, Q. A. Dai, S. K. Chen, and W. J. Zhou, "Application of pressing ear Acupoint with magnetic beads to pain after mixed hemorrhoid surgery," *Western Journal of Traditional Chinese Medicine*, vol. 25, no. 7, pp. 89–91, 2012.
- [12] J. H. Zhu, Q. A. Dai, W. J. Zhou, and F. Fang, "Application of magnetic beads to pressure ear points in postoperative pain relief of mixed hemorrhoids (in Chinese)," *Yunnan Journal of Traditional Chinese Medicine and Materia Medica*, vol. 34, no. 5, pp. 51–52, 2013.
- [13] Q. Huang, X. F. Du, M. Liu, and Q. A. Dai, "Application of magnetic bead pressure auricular therapy in the postoperative pain care of mixed hemorrhoids (in Chinese)," *Today Nurse*, vol. 6, pp. 128–129, 2012.
- [14] Y. L. Di, B. H. Yan, Y. Hu, and C. T. Zhang, "Study on the effectiveness of ear acupuncture in early postoperative analgesia in patients with mixed hemorrhoids (in Chinese)," *Journal of Nurses Training*, vol. 33, no. 5, pp. 438–440, 2018.
- [15] X. L. Gao and M. Z. Liu, "Efficacy of ear-acupuncture bean burial in relieving postoperative trauma pain of mixed hemorrhoids (in Chinese)," *Nursing Practice and Research*, vol. 10, no. 15, pp. 154–155, 2013.
- [16] Y. Liu and G. H. Zeng, "Clinical observation on relieving mixed hemorrhoids postoperative pain by ear buried beans," *Clinical Journal of Chinese Medicine*, vol. 5, no. 18, pp. 81–82, 2013.
- [17] Y. L. Di, B. H. Yan, and W. Hu, "Clinical observation on relieving mixed hemorrhoids postoperative pain by ear buried beans," *Nursing Research (in Chinese)*, vol. 31, no. 12, pp. 1504–1505, 2017.
- [18] L. M. Yan, "Application of ear acupuncture bean burial in postoperative analgesia of mixed hemorrhoids," *China Health Care Nutrition*, vol. 6, pp. 3869–3870, 2014.
- [19] P. Yang, X. P. Liu, T. R. Liu, D. R. Li, and L. J. Zeng, "Effect of auricular seed embedding combined with acupressure on pain and nursing cooperation in postoperative patients with mixed hemorrhoids (in Chinese)," *The Journal of Medical Theory and Practice*, vol. 32, no. 18, pp. 3008–3010, 2019.
- [20] D. M. Hu, "Clinical observation study of auricular acupressure on post-surgical pain and urination disorder of mixed hemorrhoids (in Chinese)," *Home Medicine*, vol. 7, pp. 11–12, 2016.
- [21] Q. Liu, J. Qian, C. H. Zhang, and H. Jiang, "Clinical observation study of auricular acupressure on post-surgical pain and urination disorder of mixed hemorrhoids (in Chinese)," *Hebei Journal of Traditional Chinese Medicine*, vol. 38, no. 3, 2016.
- [22] D. E. Beilei, Z. H. Ru, H. U. Xinsong, Z. H. Qin, and Z. H. Ying, "Efficiency of auricular point sticking therapy in treatment of perioperative pain of mixed hemorrhoids," *Journal of Clinical Medicine in Practice*, vol. 24, no. 10, p. 3, 2020.
- [23] Y. S. Chen, B. Yu, and Q. Lv, "Clinical observation of auricular acupressure intervention for pain after external and internal ligation of mixed hemorrhoids (in Chinese)," *Shanxi Journal of Traditional Chinese Medicine*, vol. 34, no. 4, pp. 32–33, 2018.
- [24] H. H. Gan, "Clinical observation of auricular acupressure for relieving postoperative pain of mixed hemorrhoids (in Chinese)," *Today Nurse (Comprehensive Version)*, vol. 8, p. 40, 2010.
- [25] B. Tang and J. C. Hu, "Efficacy of auricular acupressure in the treatment of post-surgical pain of mixed hemorrhoids (in Chinese)," *Journal of Practical Traditional Chinese Medicine*, vol. 29, no. 9, p. 758, 2013.
- [26] R. Hong, X. M. Ma, and W. Z. Qian, "50 cases of postoperative pain of mixed hemorrhoids treated with auricular acupressure (in Chinese)," *Zhejiang Journal of Traditional Chinese Medicine*, vol. 46, no. 5, p. 370, 2011.
- [27] C. R. Chai and Q. Feng, "Effectiveness of ear acupressure bean intervention for postoperative pain in mixed hemorrhoids (in Chinese)," *Journal of North Pharmacy*, vol. 10, no. 3, p. 181, 2013.
- [28] J. X. Yang, "A study on the effectiveness of ear acupressure bean intervention for postoperative pain in mixed hemorrhoids (in Chinese)," *Diabetes World*, vol. 17, no. 7, p. 286, 2020.
- [29] H. L. Zhang, "Effect of auricular pressure bean care on postoperative pain in mixed hemorrhoids (in Chinese)," *The Journal*

- of Medical Theory and Practice*, vol. 29, no. 7, pp. 954-955, 2016.
- [30] Z. H. Li, "Nursing experience of ear acupressing beans to reduce postoperative pain of mixed hemorrhoids(in Chinese)," *Capital Medicine*, vol. 25, no. 17, p. 121, 2018.
  - [31] Y. Y. Pan, "Application of ear point pressing bean combined with pain nursing in operation of patients with mixed hemorrhoids," *Nursing Practice and Research*, vol. 17, no. 12, pp. 149-150, 2020.
  - [32] J. L. Zheng and F. Yv, "Effect of auricular point pressure bean combined with herbal acupressure for postoperative pain of mixed hemorrhoids(in Chinese)," *Chinese Journal of Rural Medicine and Pharmacy*, vol. 22, no. 17, pp. 33-34, 2015.
  - [33] B. Wang and Y. P. Chen, "Clinical observation about different intervention at Erbai point in treatment of mixed hemorrhoids postoperative pain(in Chinese)," *Liaoning Journal of Traditional Chinese Medicine*, vol. 40, no. 3, pp. 484-486, 2013.
  - [34] Y. Huang, W. Yang, Y. Y. Ning, L. C. Zhang, and Y. Zhou, "Clinical study on the efficacy of acupuncture point sutures on intraoperative and postoperative analgesia in patients with mixed hemorrhoids (in Chinese)," *Yunnan Journal of Traditional Chinese Medicine and Materia Medica*, vol. 6, no. 6, pp. 52-53, 2012.
  - [35] H. L. Li, Y. X. Song, and Y. F. Hui, "Clinical observation on the prevention and treatment of postoperative complications of mixed hemorrhoids with acupoint catgut embedding therapy (in Chinese)," *Xinjiang Journal of Traditional Chinese Medicine*, vol. 35, no. 4, pp. 42-44, 2017.
  - [36] W. Yang, L. C. Zhang, and L. F. Wang, "The efficacy of postoperative pain intervention in patients with mixed hemorrhoids by acupoint catgut embedding therapy with over-the-top analgesia(in Chinese)," in *Chinese Anorectal Disease Research Insights Collection*, pp. 597-599, Acupuncture Research, 2011.
  - [37] Z. Sheng, Q. Deng, G. G. Yang et al., "Therapeutic observation of acupoint thread embedding in alleviating pain after Milligan-Morgan for mixed hemorrhoids," *Shanghai Journal of Acupuncture and Moxibustion*, vol. 33, no. 12, pp. 1129-1131, 2014.
  - [38] C. C. Yue and J. Li, "The efficacy of acupoint catgut embedding therapy in treating 102 cases of postoperative pain of mixed hemorrhoids (in Chinese)," *Journal of Frontiers of Medicine*, vol. 2, no. 9, pp. 333-334, 2012.
  - [39] N. Zhang, "Study on the effectiveness of acupoint catgut embedding therapy in treating postoperative pain of mixed hemorrhoids (in Chinese)," *China Health Care Nutrition*, vol. 26, no. 24, pp. 314-314, 2016.
  - [40] L. Liang, E. H. Zhang, J. L. Yue, and Z. J. Chen, "Effect of acupoint application on postoperative pain in patients with mixed hemorrhoids," *World Latest Medicine*, vol. 16, pp. 274-275, 2013.
  - [41] D. Li, "Observation on the therapeutic effect and nursing of acupoint application on postoperative pain of mixed hemorrhoids," *Chinese Medicine Modern Distance Education of China*, vol. 19, no. 1, pp. 169-171, 2021.
  - [42] Q. H. Meng, J. H. Li, and X. X. Zhu, "Effectiveness of acupoint application to improve postoperative pain in patients with mixed hemorrhoids," *Journal of Qilu Nursing*, vol. 27, no. 8, pp. 95-97, 2021.
  - [43] Y. F. Zhou, M. Li, and J. M. Wang, "Clinical study on the use of buried threads at lumbar and Chengshan points for postoperative analgesia of mixed hemorrhoids," *Journal of Shaanxi University of Chinese Medicine*, vol. 44, no. 3, pp. 109-113, 2021.
  - [44] L. Li, L. Y. Lu, Y. Zhu, and Q. Sun, "Clinical observation on therapeutic effect of preoperational catgut im-plantation at Changqiang(GV 1)acupoint for hemorrhoid operation - induced pain," *World Journal of Integrated Traditional and Western Medicine*, vol. 10, no. 10, pp. 1421-1423, 2015.
  - [45] B. L. Du, "Clinical study on the treatment of postoperative pain of mixed hemorrhoids with buried thread at Changqiang point," *Chinese Journal of Information on Traditional Chinese Medicine*, vol. 32, no. 1, pp. 87-88, 2015.
  - [46] H. L. Wang, "Effectiveness of Chinese herbal acupoint application combined with auricular seed embedding on relieving postoperative pain and edema of mixed hemorrhoids," *Journal of Frontiers of Medicine*, vol. 9, no. 33, pp. 221-222, 2019.
  - [47] Y. F. Liang and Y. Wen, "Observation of postoperative pain relief of mixed hemorrhoids by acupoint application," *Chinese Journal of Aesthetic Medicine*, vol. 21, no. 10, p. 242, 2012.
  - [48] M. Y. Wang, R. H. Liu, Q. Y. Hong, J. N. Li, and S. X. Zhang, "The efficacy of acupoint application for postoperative pain of mixed hemorrhoids," *Modern Journal of Integrated Traditional Chinese and Western Medicine*, vol. 30, no. 16, pp. 1766-1769, 2021.
  - [49] G. L. Xie and L. H. Huang, "Clinical application of self-made traditional Chinese medicine acupoint application in the treatment of postoperative pain of mixed hemorrhoids," *Clinical Journal of Chinese Medicine*, vol. 12, no. 30, pp. 99-100, 2020.
  - [50] Y. F. Huang, X. F. Liu, and F. Chen, "The effectiveness of auricular point sticking with vaccaria seeds on postoperative pain in patients after mixed hemorrhoid surgery," *Chinese Journal of Nursing Education*, vol. 13, no. 3, pp. 219-221, 2016.
  - [51] C. P. Ma, "The efficacy of auricular acupressure applied to postoperative pain of mixed hemorrhoids," *Hebei Journal of Traditional Chinese Medicine*, vol. 36, no. 4, pp. 615-616, 2014.
  - [52] J. Y. Sun and C. X. Chen, "The influence of auricular-plaster therapy on postoperative pain and urinary function of mixed hemorrhoid," *Journal of Guiyang College of Traditional Chinese Medicine*, vol. 38, no. 2, pp. 49-52, 2016.
  - [53] L. W. Wang, Z. Sheng, Q. Y. Yang et al., "Clinical observation on the use of acupoint catgut embedding therapy for postoperative analgesia of mixed hemorrhoids," *Journal of Chinese Physician*, vol. 1, pp. 77-79, 2013.
  - [54] L. Yan, J. C. Zhao, and J. F. Zhou, "Effectiveness of auricular acupressure in relieving postoperative pain of mixed hemorrhoids," *Journal of Nursing and Rehabilitation*, vol. 11, no. 2, pp. 185-186, 2012.
  - [55] G. Diaz and P. Flood, "Strategies for effective postoperative pain," *Minerva anesthesiologica*, vol. 72, no. 3, pp. 145-150, 2006.
  - [56] National Academies of Sciences Engineering and Medicine, *Pain Management and the Opioid Epidemic: Balancing Societal and Individual Benefits and Risks of Prescription Opioid Use*, The National Academies Press, Washington, DC, USA, 2017.
  - [57] G. Singh and G. Triadafilopoulos, "Epidemiology of NSAID induced gastrointestinal complications," *The Journal of Rheumatology. Supplement*, vol. 56, pp. 18-24, 1999.
  - [58] Y. Cao, W. W. Hao, M. Xie, and L. L. Jiang, "Analysis of pain intensity and influencing factors of adverse reactions in emergency department patients with dize-cine analgesia," *Evidence-Based Care*, vol. 5, no. 8, pp. 749-751, 2019.

- [59] H. Q. Pang, L. Pan, and H. M. Song, "Effect of fructus amomi ginger power acupoint application based on meridional flow method on hyperemesis in pregnancy," *Nursing Research*, vol. 34, no. 2, pp. 359–361, 2020.
- [60] H. Ma, "Effects of acupoint application combined with modified five birds play on bone density, pain level and quality of life of lumbar spine in patients with osteoporotic vertebral fractures," *International Journal of Nursing*, vol. 39, no. 21, pp. 3936–3939, 2020.
- [61] R. R. Zhao and S. Zhou, "Advances in the clinical application of acupoint application," *National Medical Forum*, vol. 32, no. 1, pp. 68–70, 2017.
- [62] L. H. Sun and J. M. Cao, "Introduction to acupressure," *Journal of Henan College of Traditional Chinese Medicine*, vol. 16, no. 2, pp. 45–46, 2001.
- [63] Z. Ning and L. Lao, "Acupuncture for pain management in evidence-based medicine," *Journal of Acupuncture and Meridian Studies*, vol. 8, no. 5, pp. 270–273, 2015.
- [64] X. Meng, S. Xu, and L. Lao, "Clinical acupuncture research in the West," *Frontiers in Medicine*, vol. 5, no. 2, pp. 134–140, 2011.
- [65] Y. Sun, T. J. Gan, J. W. Dubose, and A. S. Habib, "Acupuncture and related techniques for postoperative pain: a systematic review of randomized controlled trials," *British Journal of Anaesthesia*, vol. 101, no. 2, pp. 151–160, 2008.
- [66] T. I. Usichenko, C. Lehmann, and E. Ernst, "Auricular acupuncture for postoperative pain control: a systematic review of randomised clinical trials," *Anaesthesia*, vol. 63, no. 12, pp. 1343–1348, 2008.
- [67] K. F. Schulz, D. G. Altman, and D. Moher, "CONSORT 2010 statement: updated guidelines for reporting parallel group randomised trials," *Journal of Pharmacology and Pharmacotherapeutics*, vol. 1, no. 2, pp. 100–107, 2010.
- [68] H. MacPherson, A. White, M. Cummings, K. Jobst, K. Rose, and R. Niemtow, "Standards for reporting interventions in controlled trials of acupuncture: the STRICTA recommendations," *Complementary Therapies in Medicine*, vol. 9, no. 4, pp. 246–249, 2001.



## Research Article

# Clinical Intervention Effect of a Predictive Model Constructed Based on Risk Factors for Falls in Elderly Patients during Hospitalization

Lizhi Wu<sup>1</sup> and Lin Zhou<sup>2</sup> 

<sup>1</sup>Pharmacy Intravenous Admixture Services, Wenling First People's Hospital, Wenling, Zhejiang 317500, China

<sup>2</sup>Department of Integrated Traditional Chinese and Western Medicine, Department of Geriatrics, Wenling First People's Hospital, Wenling, Zhejiang 317500, China

Correspondence should be addressed to Lin Zhou; [nn201109@st.btbu.edu.cn](mailto:nn201109@st.btbu.edu.cn)

Received 21 June 2022; Revised 16 August 2022; Accepted 24 August 2022; Published 23 September 2022

Academic Editor: Hangjun Che

Copyright © 2022 Lizhi Wu and Lin Zhou. This is an open access article distributed under the Creative Commons Attribution License, which permits unrestricted use, distribution, and reproduction in any medium, provided the original work is properly cited.

Falls in elderly patients are an important cause of fractures, functional impairment, and mortality. In this paper, a questionnaire was used to collect information on fall history, balance function and sensory function from patients over 65 years of age. In the analysis, the presence or absence of falls was used as a factor, and a corresponding prediction model was constructed using methods such as univariate analysis and regression analysis. This survey found that in the past year, 60% of the patients had fallen, 16.67% had one fall, 33.33% had two falls, and 50% had three or more falls; model specificity is 61.54%, the sensitivity is 71.43%, and the misjudgment is 38.46%. The model has good specificity and sensitivity and a small misjudgment rate; so, the model is more reasonable. This paper selects several sensitivity indices that have a certain impact on the risk of falling and makes a satisfactory forecast, which can provide a theoretical basis for the prevention of the risk of falls in elderly patients during hospitalization.

## 1. Introduction

Since the 1950s, researches on falls of the elderly at home and abroad have been carried out in foreign countries, but due to their own reasons, there are a lot of literature in China [1, 2]. The mechanism of fall includes the central nervous system, musculoskeletal system, and proprioception. At present, there are many studies on the prevention and treatment of falls and injuries [3]. For example, the elderly are prone to fractures after a fall, among which hip fractures are the most common. Therefore, researchers in this area have developed protective measures in this area and have achieved good follow-up results [4]. Second, external factors have a certain impact on falls, such as the environment. Therefore, some scholars start with how to reduce the risk of falling from

the external environment, such as scientific planning of the home environment and the production of nonslip shoes. In terms of rehabilitation medicine, it is mainly necessary to start from the cause and take corresponding measures to reduce the risk of falling. Numerous interventional studies have shown that exercise can effectively reduce the risk of falls.

In the past literature, most researchers used different assessment methods to assess the risk of falling [5–7], for example, DGI assessment scale, Berg balance scale, etc., to evaluate the balance of the individual, and then to further reflect the risk of falling. The higher the score, the better the balance and the lower the risk of falling. In addition, TUGT is a standing walking test at a designated time to measure the balance state of the subjects. It is better to take less



TABLE 1: Subject's basic information.

Parameter	Minimum	Maximum	$\bar{X} \pm S$
Age	65.00	71.00	$67.08 \pm 2.19$
Height (cm)	149.50	170.50	$159.85 \pm 6.59$
Weight (kg)	41.20	76.05	$63.68 \pm 9.54$
BMI	18.43	27.96	$24.81 \pm 2.54$

than 20 seconds, and there is a risk of falling if more than 30 seconds. There are subjective factors in the above evaluation methods, and there is a lack of objective, reasonable, and comprehensive evaluation methods [8].

Recent years, there have been some nonlinear research methods such as local dynamic stabilization, which can reflect the changes of the gait of the elderly over time [9]. They can also track the elderly and people who have not fallen. Quandt et al. report that the Lyapunov index (LEE) derived from the upper body acceleration of the upper body shows that the local dynamic stability of the medial outer edge (ML) changes between different age groups [10]. It was found that its local stability decreased with aging. Similar findings were reported by Buz et al. The LEE was derived from the longitudinal movement time-course data of the lower extremities, and the LEE values were higher than in elderly patients. LEE shows age-related changes in gait control; so, LEE also has the potential to predict fall risk. Bisi et al. combined the timing of linear body acceleration in various directions to analyze and compare the LEE of children and adolescents. Children have higher levels of LEE, and it is certain that children's pace stability will be reduced.

Kukidome et al. reported that 20% of older adults at risk of falling at baseline improved after falling; meaning, their odds of falling increased as the risk of the problem increased reduce [11]. The Turkeli S system designed a suitable algorithm and a wearable electronic device for the elderly, a Tesodev-type drop detector [12]. Yanping et al. applied back-propagation multilevel neural networks to predict the risk of falling from a physiological perspective [13]. Peng developed a hazard and detection system and applied it to the homes of 19 elderly people. The system consists of Doppler radar, Microsoft Kinect, and 2 cameras [14]. By collecting data, comparing it with sensor data, and calculating and developing, it helps the elderly to maintain a normal life. At present, there are many monitoring instruments and means about falls of the elderly in my country, but the relevant literature on preventing falls is rare. Fall risk is a combination of multiple systems, but, whatever the reason, identifying specific factors that help increase risk can help adjust intervention strategies or change the situation to reduce the chance of falls.

At present, the relevant data on the risk of falls in elderly patients are relatively abundant, but from the point of view of biomechanics, there is no relevant data for reference. In this paper, various measurement methods are used to collect different viewing angle indices, a relatively complete analysis of the gait characteristics of the elderly and the correlation

between various parameters is carried out, and a prediction model is established using appropriate statistical methods, so as to provide a better understanding of the elderly. The in-depth study of the biological mechanism of patient falls has laid the foundation.

## 2. Research Objects and Methods

**2.1. Research Object.** 20 elderly patients, including 12 women and 8 men (65-75), were included in this study, and their height, weight, and BMI were measured [15]. Recruitment conditions have the ability to actively participate in the trial and have a clear willingness to know. Before the test, the operator explained the test process and operation points and completed the relevant operations. The following is the basic information of the subjects, see Table 1.

### 2.2. Research Methods

**2.2.1. Questionnaire Survey Method.** This paper adopts The Tinetti-style "balanced volume" developed by Tinetti et al. which serves as a general method for assessing fall risk in the elderly. The test is divided into gait and balance. The balance test includes 10 items such as standing balance, sitting balance, standing balance, turn-standing balance, and jogging response, all of which are 16 items, of which 8 items include starting, striding, swinging foot height, symmetry, and continuous width, a total of 12 a [16]. A score lower than 24 points indicates a risk of falling, walking path, and trunk sway, with a score of 0.70 and a specificity of 0.53.

#### 2.2.2. Experimental Method

(1) *Visual Test.* In order to reduce the measurement error and ensure the accuracy and reliability of the data, a vision meter based on a vision meter is used [17]. In the experiment, the distance between the experimental subject and the target was 5 meters, the left eye and the right eye were tested once, one side was blocked, and then the final vision was statistically processed by the binocular average.

(2) *Proprioceptive Test.* This paper adopts the Biodex isokinetic muscle strength measurement device measured the upper limb flexion of the subjects. During this period, in order to avoid the influence of vision and hearing, it needs to be performed under silent conditions.

Active position sense was as follows: the starting position of the isokinetic muscle force meter is 90 degrees of knee flexion, the end position is to extend the knee joint 45 degrees, and the movement is carried out at a rate of 5 degrees/s. In the test, participants started from the starting point, and the lower limbs first performed knee flexion activities until the posture was completed, held for 10 seconds, and then returned to the starting point. When you reach the starting point, press the button to complete your trial. The above experiment was repeated 3 times and averaged. The effect of active positioning is evaluated according to the difference between actual positioning and set

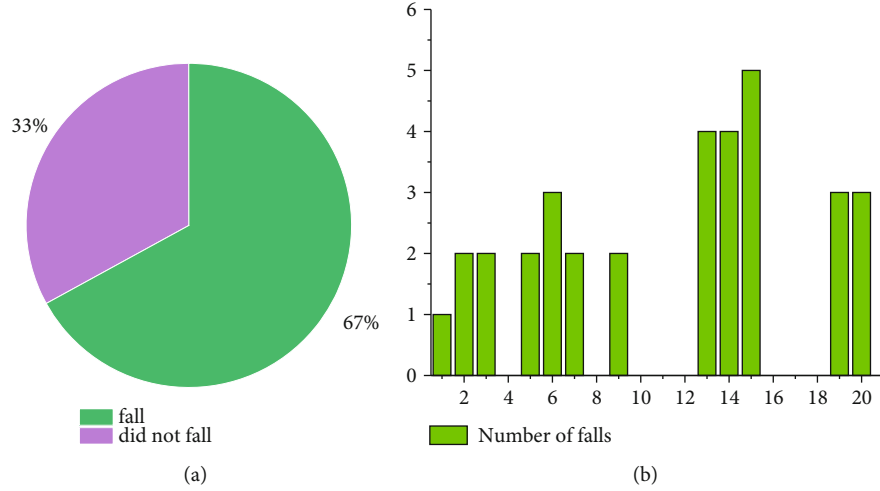


FIGURE 1: Fall time.

TABLE 2: Gender and age distribution of fall events.

Age	Female_			Male_		
	<i>n</i>	<i>N</i> number	Fall rate	<i>n</i>	<i>N</i> number	Fall rate
65-70	7	4	57%	3	1	33%
71-75	5	3	60%	5	1	80%

TABLE 3: Subject's basic information.

Project indicators	Fall group	No fall group	<i>P</i>
Age	70 ± 3.79	68.38 ± 2.72	0.31_
Height (cm)	162.8 ± 5.33	161.11 ± 7.14	0.55_
Weight (kg)	64.28 ± 6.43	60.51 ± 12.25	0.90_

positioning. During the test, the subject should concentrate and not be distracted.

Passive position sense was as follows: the device settings are the same as above. In the test procedure, when the subject is in a passive state, press the button to complete the test.

(3) *Static Balance Test*. This test uses the German Zeeblis capacitive foot pressure tester. In the test, when the subject is standing, the heels are separated by 3-4 cm, the toes are 25-30 degrees, and the hands are naturally placed on both sides. While sitting, the eyes are looking straight ahead; when standing on one foot, the experimenter is in the center of the test platform, one foot is off the ground, the knee is bent, and the eyes are looking straight ahead. When the subjects were standing upright, their eyes looked straight at the wall, their eyes looked straight at a fixed object on the wall, and then they put their hands on their side; when they closed their eyes, they were tested. The subject stood on the test platform with his hands by his side, eyes closed, and his face facing forward.

Note that the test is divided into bipedal and monopedic, and the subject's body is measured without external force.

TABLE 4: Basic index comparison.

Project indicators	Fall group	No fall group	<i>P</i>
BMI	24.25 ± 2.10	23.20 ± 3.81	0.44_
Lean body mass (kg)	42.57 ± 6.00	50.90 ± 11.16	0.4_
Sex (male)	71.40 ± 3.91	67.33 ± 3.21	0.01
Gender (female)	69.00 ± 3.65	65.00 ± 2.55	0.01

TABLE 5: Perceptual metric comparison.

Project indicators	Fall group	No fall group	<i>P</i>
Vision	4.59 ± 0.14	4.61 ± 0.09	0.73
Active position sense (°)	5.34 ± 1.31	6.78 ± 1.66	0.04
Passive position sense (°)	6.23 ± 1.65	5.68 ± 1.11	0.743

The test period of each method is 10 seconds, the test data is recorded in real time, and the data is counted.

(4) *Stability Limit Test*. This part of the test uses the Tecno-body balance test and training system. Before the test, the subject stood in the middle of the test platform, that is, on both sides of A1, with the heels of both feet together, the second toes of both feet corresponding to A2 and A8, respectively, and their hands on their chests. During the test, subjects were required to move as far as possible in the directions of A1, A3, A5, and A7. During the exercise, flexion of the hips, knees, and heels were not allowed. Observe the angle of inclination in 4 directions, and the smaller the angle, the higher the risk of falling.

(5) *Gait Test*. The study subjects wore experimental clothing, wearing their usual shoes, and no jewelry, while the women had their hair tied up. Before the test, the experimenter will guide the subjects to make adjustments on other treadmills to avoid results that do not match the treadmill. During the trial, walking trials were performed according to the

TABLE 6: Comparison of eye-opening and eye-closing indicators when standing on both feet.

Project indicators	Feet-eyes open			Feet-eyes closed		
	Fall group	No fall group	<i>P</i>	Fall group	No fall group	<i>P</i>
Envelope length (mm)	17.43 ± 3.32	13.47 ± 1.87	0.007	17.10 ± 4.03	14.42 ± 2.04	0.102
Envelope area (mm <sup>2</sup> )	170.28 ± 27.85	138.83 ± 39.08	0.049	166.94 ± 27.90	138.83 ± 39.08	0.076
Envelope angle (°)	59.50 ± 15.33	44.60 ± 23.67	0.103	47.84 ± 14.29	42.10 ± 25.08	0.521
Overall length of pressure center of gravity (mm)	303.85 ± 41.49	233.74 ± 43.64	0.002	287.19 ± 46.19	258.74 ± 20.38	0.121
Horizontal swing of pressure center of gravity (mm)	2.48 ± 0.99	3.42 ± 0.67	0.031	3.06 ± 0.87	3.42 ± 0.67	0.338
Pressure center of gravity vertical swing (mm)	4.07 ± 0.57	4.41 ± 0.30	0.142	4.40 ± 0.74	4.91 ± 0.48	0.107
Percentage of pressure on right foot (%)	46.19 ± 5.85	45.36 ± 3.47	0.725	46.52 ± 6.17	45.36 ± 3.47	0.637
Percentage of pressure on left foot (%)	51.06 ± 6.40	50.14 ± 5.00	0.738	51.06 ± 6.40	50.64 ± 4.78	0.878

TABLE 7: Comparison of eye-opening and eye-closing indicators when standing on one foot.

Project indicators	Feet-eyes open			Feet-eyes closed		
	Fall group	No fall group	<i>P</i>	Fall group	No fall group	<i>P</i>
Envelope length (mm)	18.02 ± 3.08	15.73 ± 2.02	0.082	19.68 ± 3.45	18.60 ± 1.89	0.432
Envelope area (mm <sup>2</sup> )	175.28 ± 25.92	163.83 ± 48.26	0.498	188.83 ± 25.80	179.44 ± 22.77	0.403
Envelope angle (°)	64.84 ± 12.91	50.85 ± 18.45	0.061	69.84 ± 14.27	59.60 ± 11.23	0.106
Overall length of pressure center of gravity (mm)	336.35 ± 36.03	311.24 ± 34.39	0.138	361.35 ± 49.99	336.24 ± 42.90	0.261
Horizontal swing of pressure center of gravity (mm)	3.06 ± 0.83	3.67 ± 0.31	0.065	3.56 ± 1.00	4.42 ± 1.01	0.078
Pressure center of gravity vertical swing (mm)	4.32 ± 0.46	4.66 ± 0.50	0.137	4.57 ± 0.44	5.04 ± 0.74	0.094
Percentage of pressure on right foot (%)	47.02 ± 7.01	50.24 ± 6.17	0.307	48.69 ± 6.28	52.74 ± 5.70	0.161
Percentage of pressure on left foot (%)	52.39 ± 6.50	57.02 ± 6.02	0.126	56.97 ± 8.41	63.89 ± 6.61	0.067

TABLE 8: Univariate logistic regression analysis of standing with eyes open.

Project indicators	Regression coefficients	Standard error	<i>P</i>
Envelope length (mm)	-0.792	0.407	0.009
Envelope area (mm <sup>2</sup> )	0.061	0.098	0.047
Envelope angle (°)	0.816	0.295	0.093
Overall length of pressure center of gravity (mm)	0.009	0.009	0.004
Pressure center of gravity horizontal swing (mm)	0.658	0.029	0.031
Pressure center of gravity vertical swing (mm)	2.315	0.741	0.128
Percentage of pressure on right foot (%)	0.141	0.173	0.707
Percentage of pressure on left foot (%)	0.027	0.680	0.870

TABLE 9: Univariate logistic regression analysis of standing with eyes closed.

Project indicators	Regression coefficients	Standard error	<i>P</i>
Envelope length (mm)	-0.005	-0.005	0.999
Envelope area (mm <sup>2</sup> )	0.006	0.006	0.511
Envelope angle (°)	0.001	0.025	0.218
Overall length of pressure center of gravity (mm)	-0.017	0.028	0.505
Pressure center of gravity horizontal swing (mm)	0.001	0.004	0.852
Pressure center of gravity vertical swing (mm)	-0.002	0.006	0.773
Percentage of pressure on right foot (%)	-0.030	0.089	0.801
Percentage of pressure on left foot (%)	0.031	0.091	0.702

TABLE 10: Univariate logistic regression analysis of standing on one foot with eyes open.

Project indicators	Regression coefficients	Standard error	P
Envelope length (mm)	-0.001	0.001	0.509
Envelope area (mm <sup>2</sup> )	0.000	0.002	0.421
Envelope angle (°)	0.002	0.005	0.408
Overall length of pressure center of gravity (mm)	0.007	0.018	0.545
Pressure center of gravity horizontal swing (mm)	0.005	0.011	0.531
Pressure center of gravity vertical swing (mm)	-0.001	0.003	0.796
Percentage of pressure on right foot (%)	-0.080	0.080	0.308
Percentage of pressure on left foot (%)	0.071	0.076	0.902

TABLE 11: Univariate logistic regression analysis of standing on one foot with eyes closed.

Project indicators	Regression coefficients	Standard error	P
Envelope length (mm)	0.001	0.001	0.845
Envelope area (mm <sup>2</sup> )	0.001	0.001	0.407
Envelope angle (°)	0.001	0.003	0.959
Overall length of pressure center of gravity (mm)	0.005	0.001	0.984
Pressure center of gravity horizontal swing (mm)	-0.006	0.010	0.425
Pressure center of gravity vertical swing (mm)	-0.006	0.005	0.648
Percentage of pressure on right foot (%)	0.079	0.065	0.102
Percentage of pressure on left foot (%)	-0.039	0.065	0.100

TABLE 12: Unconditional logistic regression analysis of risk factors for falls.

Project indicators	Regression coefficients	Standard error	P
Constant	-12.904	4.279	0.004
Gender	0.905	0.239	0.001
Active position sense of the knee joint (°)	0.034	0.021	0.043
Eye opening envelope area of both feet (mm <sup>2</sup> )	0.001	0.000	0.047
Full length of center of gravity with both feet open and eyes open (mm)	0.005	0.001	0.045
Pressure center of gravity swing horizontally with both feet open (mm)	.235	0.091	0.002

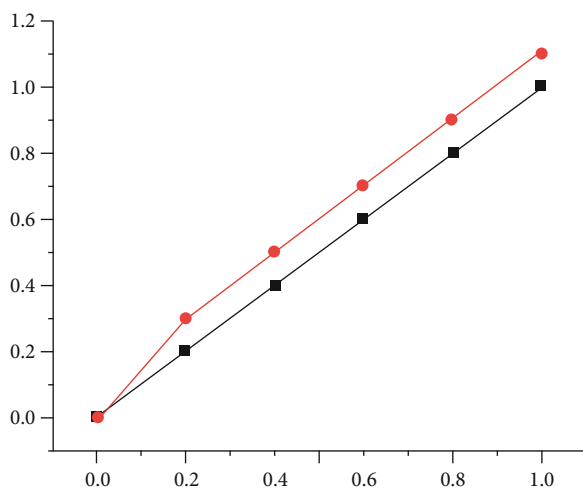


FIGURE 2: ROC curve.

participants' walking rate, with a staff member behind them to provide safety.

### 3. Research Result

The analysis discusses data comparisons between fallen and nonfalling patients, occurrence of falls, and screening predictors.

**3.1. Occurrence of Fall Events.** The subjects of the study were fall accidents. After the trial was completed, 15 older adults were followed. The study found no statistically significant difference in the subjects' falls before and after the trial. Therefore, before the experiment, we will still select the fall situation as the follow-up analysis. According to statistics, in the past year, 60% of the patients had fallen, 16.67% had one fall, 33.33% had two falls, and 50% had three or more falls, see Figure 1.

TABLE 13: Results of 3 back substitutions.

Model judgment	Whether there is a history of falls		Total
	Yes	No	
Yes	5	5	10
No	2	8	10
Total	7	13	20

In the past year, 12 women had a 60% chance of falling; 8 men had a 40% chance of falling. Statistical analysis based on underlying details found that falls were age-related and increased with age (see Table 2).

**3.2. Comparison of Related Indicators of Elderly Patients in the Fall Group and the Nonfall Group.** The elderly who fell or not within one year were surveyed and statistically processed. As shown in Table 3 below, there was no significant difference in height, age, and weight.

**3.2.1. Comparison of Basic Indicators.** An independent sample *t*-test was performed on the data of the falling group and the nonfalling group. The results showed that the lean body mass  $P = 0.043$ , the gender  $P = 0.000$ , and the difference were statistically significant, and there was a significant difference between the groups,  $P = 0.44$ , on the MBI index,  $P > 0.05$ , which is not statistically significant, see Table 4.

**3.2.2. Comparison of Perceptual Functions.** The observed sensory index data, using *t*-test and self-sampling, respectively, and statistical analysis, found that there is no obvious difference between the normal fall group and the normal fall group. Conclusion is as follows: the lower extremity activity sensation  $P < 0.05$  is statistically significant compared with the control group, see Table 5.

**3.2.3. Comparison of Balance Ability**

**(1) Standing on Both Feet-Eyes Open and Eyes Closed.** Legged stance index was calculated by single-case *t*-test. The analyzed data are shown in Table 6. When the eyes are closed, there is no significant difference in the indicators of falling and not falling; when the patient opens his eyes, the envelope length and the full length of the center of gravity pressure are significantly different. There was a significant difference between the patients who fell and those who did not fall.  $P < 0.05$  for the envelope area and the horizontal swing of the pressure center of gravity is as follows, and there was a significant difference between the patients who fell and those who did not fall.

**(2) Standing on One Foot-Eyes Open and Eyes Closed.** The purpose of this test was to compare the balance of eyes open and closed on one foot between those who had fallen and those who had not fallen, and the results showed no significant difference between the two indicators, see Table 7.

**3.2.4. Univariate Analysis of Balanced Indicators.** Taking the risk factors of falls in elderly patients as the main variable and whether or not falling was the main variable, the single

linear regression method was used to explore various factors related to falls.

**(1) Univariate Analysis of Static Balance Index.** Standing on Both Feet-Eyes Open and Eyes Closed

When standing on two feet or with eyes open, a preliminary analysis of three factors related to falls, including envelope area, length of pressure center of gravity, and lateral sway of pressure center of gravity, was carried out, while when standing on two feet, no findings were found. Factors were associated with falls (Tables 8 and 9).

**Standing on One Foot-Eyes Open and Eyes Closed**

When standing on one foot, using the data of eyes open and closed as independent variables, and the fall accident as the dependent variable, multiple linear regression was performed, and no factors related to falls were found (Tables 10 and 11).

## 4. Screening of Fall Risk-Sensitive Indicators and Establishment of Models

According to the above results, the multifactor unconditional logistic regression was used for statistical test, the probability of inclusion was 0.05, whether the elderly fell as the dependent variable, the possibility of exclusion was 0.1, and the statistical method was carried out by gradual regression. The five indicators in the statistical sensitivity index, gender, posture sense of knee joint activity, capsule area at foot opening, length of pressure center, and lateral shaking of pressure center, are the main causes of falls in the elderly, as shown in Table 12.

ROC is a typical measurement method of specificity and sensitivity. ROC is a working characteristic, which determines its specificity and sensitivity according to a certain threshold point, and expresses the specificity and sensitivity in the form of graphics. Figure 2 shows the ROC curve with 1-specificity on the abscissa and sensitivity on the ordinate, and the region consisting of the curve and the coordinate axis can be evaluated for the accuracy of the model. In the chart, from left to right, from left to right, and from left to right, as the area under the curve approaches 1, the prediction accuracy of the model is better, between 0.7 and 0.9, and the model is around 0.704, indicating that the pattern is correct.

After the goodness-of-fit test,  $X^2$  was 5.301, and  $P$  was 0.703, indicating that the formula can well explain the relationship between the five factors and the risk of falling. Therefore, the selection of the sensitivity index can well predict the risk of falling. Taking the fall accident as the benchmark, the samples of this pattern are grouped back and replaced, and the following data are obtained (see Table 13):

It can be concluded from the table that specificity =  $8/13 = 61.54\%$ , where sensitivity is  $5/7 = 71.43\%$ , and Error probability =  $1 - \text{specific} = 38.46\%$ .

It can be seen from the above results that the model has good specificity and sensitivity and has a small error prediction ability; so, the model is more reasonable.



## 5. Conclusion

In this study, through questionnaires, laboratory tests, and other methods, the correlation between different influencing factors and the risk of falling in the elderly was explored, the relevant factors were found out, and a corresponding prediction model was constructed accordingly, which is helpful for my country's entry into the aging society. Prevention work has laid a solid theoretical basis. From the above analysis, the following points are obtained:

- (1) The subjects in this paper are all 65 years old and the elderly. The survey data can be used as the basis for reducing falls in the elderly
- (2) The data statistics show that the selected predictors have a good forecasting effect, but there are differences in the scope of their influence, which can be used for targeted research
- (3) For the elderly who have fallen, the factors such as balance ability, active position sense function of the knee joint, eye opening envelope area, length of pressure center of gravity, and amplitude of lateral swaying of center of gravity are all risk factors for falling. The method has good accuracy and a good false positive rate and can be used for the effectiveness analysis of clinical treatment

## Data Availability

The dataset used in this paper are available from the corresponding author upon request.

## Conflicts of Interest

The authors declared that they have no conflicts of interest regarding this work.

## References

- [1] J. S. Yun, Y. M. Park, K. Han, S. A. Cha, Y. B. Ahn, and S. H. Ko, "Association between BMI and risk of severe hypoglycaemia in type 2 diabetes," *Diabetes & Metabolism*, vol. 45, no. 1, pp. 19–25, 2019.
- [2] R. T. Crews, S. V. Yalla, A. E. Fleischer, and S. C. Wu, "A growing troubling triad: diabetes, aging, and falls," *Journal of Aging Research*, vol. 2013, Article ID 342650, 6 pages, 2013.
- [3] M. Auais, B. E. Alvarado, C. L. Curcio, A. Garcia, A. Ylli, and N. Deshpande, "Fear of falling as a risk factor of mobility disability in older people at five diverse sites of the IMIAS study," *Archives of gerontology and geriatrics*, vol. 66, pp. 147–153, 2016.
- [4] P. Hewston, A. Garcia, B. Alvarado, and N. Deshpande, "Fear of falling in older adults with diabetes mellitus: the IMIAS study," *Canadian Journal on Aging*, vol. 37, no. 3, pp. 261–269, 2018.
- [5] K. Peng, M. Tian, M. Andersen et al., "Incidence, risk factors and economic burden of fall-related injuries in older Chinese people: a systematic review," *Injury Prevention*, vol. 25, no. 1, pp. 4–12, 2019.
- [6] W. D. Rinkel, S. van Nieuwkasteele, M. C. Cabezas, J. W. van Neck, E. Birnie, and J. H. Coert, "Balance, risk of falls, risk factors and fall-related costs in individuals with diabetes," *Diabetes Research and Clinical Practice*, vol. 158, article 107930, 2019.
- [7] E. Y. Hur, Y. Jin, T. Jin, and S. M. Lee, "Longitudinal evaluation of Johns Hopkins fall risk assessment tool and nurses' experience," *Journal of Nursing Care Quality*, vol. 32, no. 3, pp. 242–251, 2017.
- [8] A. Lazkani, T. Delespierre, B. Bauduceau et al., "Predicting falls in elderly patients with chronic pain and other chronic conditions," *Aging Clinical and Experimental Research*, vol. 27, no. 5, pp. 653–661, 2015.
- [9] R. K. Yau, E. S. Strotmeyer, H. E. Resnick et al., "Diabetes and risk of hospitalized fall injury among older adults," *Diabetes Care*, vol. 36, no. 12, pp. 3985–3991, 2013.
- [10] S. A. Quandt, J. M. Stafford, R. A. Bell, S. L. Smith, B. M. Snively, and T. A. Arcury, "Predictors of falls in a multiethnic population of older rural adults with diabetes," *The journals of gerontology Series A, Biological sciences and medical sciences*, vol. 61, no. 4, pp. 394–398, 2006.
- [11] D. Kukidome, T. Nishikawa, M. Sato et al., "Impaired balance is related to the progression of diabetic complications in both young and older adults," *Journal of diabetes and its complications*, vol. 31, no. 8, pp. 1275–1282, 2017.
- [12] Z. Jing, L. Qingping, H. Qiong, and B. Zhang, "Analysis of the current situation of literature research on fall assessment scale for elderly patients in China," *Qilu Nursing Journal*, vol. 11, pp. 66–68, 2016.
- [13] H. Yanping, L. Xueqin, and D. Shengping, "A test study on the fall risk assessment scale for the elderly," *Nursing Research*, vol. 20, pp. 1873–1876, 2007.
- [14] P. Yu, X. Ting, and L. Jie, "Technical guidelines for fall intervention in the elderly," *Chinese Journal of Practical Rural Doctors*, vol. 19, no. 8, pp. 1–13, 2012.
- [15] L. Ruihong, Y. Kefei, F. Ronglan, and J. Wang, "Development of a fall risk assessment scale for inpatients," *Journal of Nursing*, vol. 18, no. 5, pp. 23–25, 2011.
- [16] Y. Chen, J. Xiaoying, and Z. Xiulan, "Reliability and validity of the fall prevention knowledge, attitude and action questionnaire for the elderly in elderly care institutions," *Zhonghua Nursing Education*, vol. 13, no. 3, pp. 165–169, 2016.
- [17] L. Jing, *Study on the knowledge, attitude and action scale for inpatient fall prevention in elderly patients*, Beijing University of Traditional Chinese Medicine, 2016.



## Research Article

# Application Effect of Laparoscopic Myomectomy and Comprehensive Rehabilitation Nursing on Patients with Uterine Fibroids

Zhihong Liu,<sup>1</sup> Zhiwen Gao<sup>1</sup> ,<sup>1</sup> Fangwei Li,<sup>1</sup> Lifen Xu,<sup>2</sup> and Xinghua Liu<sup>3</sup>

<sup>1</sup>Department of Obstetrics and Gynecology, Zunhua People's Hospital, Hebei, China

<sup>2</sup>Department of Obstetrics and Gynecology, Zhengding Maternal and Child Health Hospital, Shijiazhuang, Hebei, China

<sup>3</sup>Department of Obstetrics and Gynecology, Anxin County Hospital, Xiguan Street, Anxin County, Baoding, Hebei, China

Correspondence should be addressed to Zhiwen Gao; gzw19800214@163.com

Received 21 July 2022; Accepted 30 August 2022; Published 22 September 2022

Academic Editor: Hangjun Che

Copyright © 2022 Zhihong Liu et al. This is an open access article distributed under the Creative Commons Attribution License, which permits unrestricted use, distribution, and reproduction in any medium, provided the original work is properly cited.

**Background.** Uterine fibroids are most common in women aged 30-50 and are the most common benign gynecological tumors. Relevant data suggest that about 25% of patients with uterine fibroids are at childbearing age. Uterine fibroids not only cause the discomfort symptoms, and affect the pregnancy, but also have certain malignant transformation risk, thus needed to be treated positively and promptly. **Aim.** This study is aimed at exploring the effect of laparoscopic myomectomy and comprehensive rehabilitation nursing on patients with uterine fibroids. **Methods.** The clinical data of 110 cases of uterine fibroids admitted to our hospital from August 2019 to December 2021 were analyzed retrospectively, and they were divided into two groups according to postoperative rehabilitation strategies. Both groups were treated with laparoscopic myomectomy. The A group was treated with routine rehabilitation strategy, while the B group was treated with comprehensive rehabilitation nursing strategy. The differences in operation-related indicators, stress factors, inflammatory factors, nutritional indicators, knowledge mastery, occurrence of adverse symptoms and pain scores, negative emotion scores, nursing satisfaction, and simplified comfort status scale (GCQ) scores between the two groups under nursing strategies were compared. **Results.** The postoperative exhaust time ( $13.14 \pm 2.03$  h), bed time ( $9.86 \pm 1.94$  h), postoperative hospital stay ( $4.37 \pm 1.31$  d), and total hospital stay ( $6.78 \pm 1.69$  d) in the B group were shorter than those in the A group, and the hospitalization expenses ( $0.74 \pm 0.25$  million) were less than those in the A group ( $P < 0.05$ ). Before operation, stress factors, inflammatory factors, and nutritional indexes were compared between the two groups ( $P > 0.05$ ). On the 3rd day after operation, tumor necrosis factor- $\alpha$  (TNF- $\alpha$ ), cortisol (Cor), norepinephrine (NE), and interleukin-1 $\beta$  (IL-1 $\beta$ ) in the two groups showed a significantly upward trend compared with those before operation, and albumin and transferrin were significantly fell compared with those before operation. However, the values of stress factor and inflammatory factor in the B group were significantly lower than those in the A group, and the values after the decrease of nutritional index were significantly higher than those in the A group ( $P < 0.05$ ). The pain scores at 24 h, 48 h, and 72 h after operation in the B group were significantly lower than those in the A group ( $P < 0.05$ ). Negative emotions, nursing satisfaction, and GCQ scores were compared between the two groups before intervention ( $P > 0.05$ ). After the intervention, the scores of Hamilton Depression Scale (HAMD) and Hamilton Anxiety Scale (HAMA) in the two groups were significantly lower than those before the intervention, and the scores of nursing satisfaction and GCQ were higher than those before the intervention. The values of negative emotions in the B group after the decline were significantly lower than those in the A group, while the values of nursing satisfaction and GCQ after the increase were higher than those in the A group ( $P < 0.05$ ). The excellent and good rate of knowledge acquisition in the B group was 94.55% (52/55), which was significantly higher than 78.18% (43/55) in the A group ( $P < 0.05$ ). The incidence of adverse symptoms in the B group was 9.09% (5/55), which was lower than 21.82% (12/55) in the A group, while the difference was not statistically significant ( $P > 0.05$ ). **Conclusion.** Laparoscopic myomectomy combined with comprehensive rehabilitation nursing can reduce the postoperative stress state of patients with uterine fibroids, improve patient satisfaction, reduce adverse emotions, and promote rehabilitation.

## 1. Introduction

Uterine fibroids are common benign tumors in the female reproductive system, which can give rise to abnormal uterine bleeding, abdominal mass, abdominal pain, bulge, leucorrhea, infertility, abortion, and other symptoms and signs [1]. The etiology and pathogenesis of uterine fibroids have not been fully clarified so far. Mutations in myometrium cells, disorder of sex hormones, and abnormal local growth factors are thought to be related to the occurrence of this disease [2]. At present, surgical treatment is generally used in clinical practice to cause myomectomy, and laparoscopic myomectomy is one of the common surgical methods [3]. However, due to the impact of uterine fibroids disease itself and surgical trauma, the patient's body is in a state of stress and cause negative emotions [4].

Nursing is an important supplement to clinical medical work. The implementation of high-quality nursing intervention after laparoscopic myomectomy helps to reduce the negative emotions of patients and actively cooperate with follow-up treatment [5]. Comprehensive rehabilitation nursing is a kind of comprehensive nursing intervention mode, starting from basic nursing, psychological counseling, health education, and other aspects to help patients recover better and return to normal work and life soon [6, 7]. This study explored the application effect of laparoscopic myomectomy and comprehensive rehabilitation nursing on patients with uterine fibroids, which is reported as follows.

Core tips were as follows: laparoscopic myomectomy is commonly used in the clinical treatment of uterine fibroids, and most patients can benefit from it. However, there are still a considerable number of patients with severe postoperative negative emotions, which is harmful to their recovery. In this study, patients with laparoscopic myomectomy were taken as the subjects to explore the impact of comprehensive rehabilitation nursing on their prognosis. It was found that laparoscopic myomectomy combined with comprehensive rehabilitation nursing can reduce the body stress state of patients with uterine fibroids after operation, improve patient satisfaction, reduce bad emotions, and promote rehabilitation.

## 2. Data and Methods

**2.1. General Information.** The data of 110 cases of uterine fibroids admitted to the hospital from August 2019 to December 2021 were analyzed retrospectively. The age was 22–43 years old, with an average of  $(35.45 \pm 3.88)$  years old. According to the postoperative rehabilitation strategy, they were divided into two groups. The control group (group A) accepted the conventional rehabilitation strategy, and the observation group (group B) accepted comprehensive rehabilitation nursing strategy. The data between the two groups were balanced ( $P > 0.05$ ), see Table 1

The inclusion criteria were as follows: (1) clinical diagnosis of uterine fibroids confirmed by enhanced MRI and ultrasonography [8]; (2) accompanied by menstrual abnormalities, abdominal pain, frequent urination, anemia, and other clinical symptoms; (3) The International Union of

Obstetrics and Gynecology is classified as 0–VI [8]; (4) patients have indications for surgery, laparoscopic myomectomy was performed under general anesthesia, and the pathological results were leiomyoma of uterus; (5) complete clinical data and follow-up data; and (6) ages 18–45 years old.

The exclusion criteria were as follows: (1) there were coagulation abnormalities, such as platelet 25s and prothrombin activity  $< 40\%$ ; (2) perimenopausal signs; (3) malignant lesions such as cervical cancer and endometrial cancer; (4) there is language communication disorder or cognitive dysfunction, unable to carry out effective communication or curative effect evaluation; (5) functional insufficiency of the liver and kidney; (6) self-injury, suicidal tendencies, or behavior; conversion to laparotomy; and (7) past history of abdominal and pelvic surgery.

**2.2. Method.** Patients in the two groups were treated with laparoscopic myomectomy and general anesthesia with tracheal intubation, and the patients were in supine position. A 10 mm incision was made at the upper edge of the umbilical wheel as the observation hole to establish pneumoperitoneum, and the pressure was maintained at about 12 mmHg. Laparoscopic exploration of abdominal cavity observes the number, size, and location of fibroids. Make a transverse incision on the toe joint and place the surgical instruments. The subserous myoma was ligated at the pedicle of the myoma, the myoma was removed at 5 mm above the ligation site, and the wound was electrocoagulation to stop bleeding. Intramyometrial myoma was injected with oxytocin at the most prominent part of the tumor. The myometrium of the uterus was cut to the fibroid capsule layer, and the fibroid nodules were stripped. The tumor cavity was closed by absorbable intestinal line. After determining no active bleeding, the abdominal cavity was washed, and sodium hyaluronate was injected to prevent intrauterine adhesions.

The A group accepted the conventional rehabilitation strategy. The patients were instructed to complete the preoperative examination before operation, and the operation precautions were informed by the visit. The patients were instructed to have reasonable diet, activities, and follow-up treatment according to the doctor's advice after operation.

The B group accepted comprehensive rehabilitation nursing strategy: preoperative psychological counseling, inform patients of the purpose of preoperative preparation, guide patients to pay attention to rest, and strengthen nutrition; according to the patient's educational level, use comprehensive language to introduce the advantages of laparoscopic myomectomy and perioperative cooperation points. Guide patients to bed position and deep breathing training. Patients were asked to stay in bed absolutely for at least 24 h, drink more water, and eat light and digestible food on the day after operation. If the symptoms of limb numbness, pain, nausea, vomiting, fever occurred, the nurse would tell them that these were normal reactions after operation to let them relaxed, and give symptomatic treatment. From the second day after operation, the patients were instructed to get out of bed properly, eat general food, and strengthen nutrition. Guide patients to take a comfortable

TABLE 1: Differences in general information between the two groups of patients.

Normal information	A group ( $n = 55$ )	B group ( $n = 55$ )	$\chi^2$ or $t$	$P$
Age ( $(\bar{x} \pm s)$ , age)	$35.27 \pm 4.55$	$35.52 \pm 4.18$	0.300	0.765
BMI ( $(\bar{x} \pm s)$ , $\text{kg/m}^2$ )	$22.56 \pm 2.47$	$22.49 \pm 2.51$	0.147	0.883
Course of disease ( $(\bar{x} \pm s)$ , month)	$11.25 \pm 3.75$	$11.09 \pm 3.82$	0.222	0.825
Pregnancy ( $(\bar{x} \pm s)$ , number)	$1.78 \pm 0.59$	$1.81 \pm 0.63$	0.258	0.797
Maximum fibroid diameter ( $(\bar{x} \pm s)$ , mm)	$5.46 \pm 0.31$	$5.51 \pm 0.36$	0.537	0.593
Disease type ( $n$ (%))				
Single shot	33 (60.00)	37 (67.27)	0.629	0.428
Multiple	22 (40.00)	18 (32.73)		
Tumor location ( $n$ (%))				
Uterine submucosal fibroids	30 (54.55)	29 (52.73)	0.037	0.848
Cervical fibroids	25 (45.45)	26 (47.27)		
Marital status ( $n$ (%))				
Married	35 (63.64)	38 (69.09)	0.367	0.545
Unmarried	20 (36.36)	17 (30.91)		
Educational level ( $n$ (%))				
Elementary school and below	14 (25.45)	12 (21.82)	0.607	0.738
Junior high school to high school	21 (38.18)	25 (45.45)		
College and above	20 (36.36)	18 (32.73)		

position and relax the abdominal muscles, through chat, watch TV, and other methods to distract attention, to relieve pain. Severe pain can be given analgesics according to the doctor's advice. Guide patients to rest after discharge, strengthen nutrition, maintain personal hygiene, avoid severe activity, and review on time. If the patients appeared abdominal pain, bleeding, etc., the nurse would give timely treatment.

**2.3. Observation Indicators and Detection Methods.** The differences in operation-related indicators, stress factors, inflammatory factors, nutritional indicators, knowledge mastery, occurrence of adverse symptoms and pain scores, negative emotion scores, nursing satisfaction, and simplified comfort status scale (GCQ) scores between the two groups under nursing strategies were compared.

5 mL fasting peripheral venous blood samples were collected before operation and 3 days after operation and were placed in vacuum to collect blood vessels. The blood was centrifuged within 1 hour, and the rotation speed was 3000 r/min. The centrifugal time was 10 min. Tumor necrosis factor- $\alpha$  (TNF- $\alpha$ ), serum cortisol (Cor), norepinephrine (NE), and interleukin-1 $\beta$  (IL-1 $\beta$ ) were detected by enzyme-linked immunosorbent assay. Albumin was detected by bromocresol green method; transferrin was detected by immunoturbidimetry. The kit is produced by Shanghai Enzyme Linked Biological Technology Co., Ltd., and the detection instrument is Merry RT-96A.

**2.4. Score Standard.** Degree of pain was as follows: according to the visual analogue scale (VAS) score [9], the score is 0-10 points, and the score range indicates no heavy pain.

Negative emotions were as follows: according to the evaluation of Hamilton Depression Scale (HAMD) and Hamilton Anxiety Scale (HAMA) [10], 17 items were used in the HAMD score in this study, with the score higher than 24 divided into severe depression and the score higher than 17 divided into moderate depression: more than 7 points for mild depression and the score below 7 points without depression. HAMA score more than 29 points of severe anxiety, more than 21 points for positive anxiety, and more than 14 points have anxiety, and more than 7 points may exist anxiety.

Nursing satisfaction was as follows: in the hospital self-made scale evaluation, covering the environment, medical staff business level, attitude, etc., score range is 0-100 points, and score range indicates the low-high nursing satisfaction.

GCQ score [11] was as follows: evaluation of comfort, including physiology, social culture, psychological spirit, and environment, covers 28 items, with a single score of 1-4 and a total score of 28-112. The score range indicates the low-high comfort.

The level of mastery of relevant knowledge was as follows: hospital self-made scale covers the pathophysiology of the disease, postoperative care, precautions, diet, etc. The score range is 0-100 points, of which over 90 points are excellent, over 80 points are good, over 60 points are general, and less than 60 points are poor.

**2.5. Statistical Method.** The data were processed by SPSS26.0. The normality and homogeneity of variance of measurement data were tested by  $K$ -S test and Levene test, respectively. The measurement data conforming to the standard were described by  $(\bar{x} \pm s)$ . The  $t$ -test was used for

TABLE 2: Differences in surgery-related indicators between the two groups ( $\bar{\chi} \pm s$ ).

Group	<i>n</i>	Postoperative exhaust time	Time to get out of bed	Hospital stay (d)		Hospital costs (ten thousand)
		(h)	(h)	Postoperative hospital stay	Total hospital stay	
A group	55	15.89 ± 2.11	12.88 ± 2.19	5.24 ± 1.56	8.46 ± 1.83	0.86 ± 0.29
B group	55	13.14 ± 2.03	9.86 ± 1.94	4.37 ± 1.31	6.78 ± 1.69	0.74 ± 0.25
<i>t</i>		6.965	7.655	3.167	5.002	2.324
<i>P</i>		0.000	0.000	0.002	0.000	0.022

TABLE 3: Differences in stress factors and inflammatory factors between the two groups ( $\chi \pm s$ ).

Group	<i>n</i>	Cor (ng/mL)		NE (ng/mL)		TNF- $\alpha$ (ng/mL)		IL-1 $\beta$ ( $\mu$ g/L)	
		Preoperative	3 d after surgery	Preoperative	3 d after surgery	Preoperative	3 d after surgery	Preoperative	3 d after surgery
A group	55	131.54 ± 38.85	182.56 ± 34.17	301.52 ± 37.85	369.89 ± 41.75*	13.52 ± 3.17	28.96 ± 4.52*	7.89 ± 2.17	13.89 ± 2.57
B group	55	128.74 ± 42.16	153.69 ± 29.99	289.76 ± 41.07	331.25 ± 34.51*	13.48 ± 3.69	22.54 ± 3.26*	8.02 ± 2.24	11.75 ± 2.26
<i>t</i>		0.362	4.709	1.562	5.290	0.061	8.543	0.309	4.637
<i>P</i>		0.718	0.000	0.121	0.000	0.951	0.000	0.758	0.000

\* represents the comparison with preoperative,  $P < 0.05$ .

TABLE 4: Differences in nutritional indicators between the two groups ( $\bar{\chi} \pm s$ ).

Group	<i>n</i>	Albumin (mg/L)		Transferrin (g/L)	
		Preoperative	3 d after surgery	Preoperative	3 d after surgery
A group	55	369.98 ± 41.17	228.59 ± 36.69*	2.25 ± 0.29	1.46 ± 0.25*
B group	55	372.45 ± 36.52	254.56 ± 38.52*	2.23 ± 0.31	1.68 ± 0.29*
<i>t</i>		0.333	3.620	0.349	4.261
<i>P</i>		0.740	0.000	0.727	0.000

\* represents the comparison with preoperative,  $P < 0.05$ .

TABLE 5: Differences in postoperative pain levels between the two groups ( $\bar{\chi} \pm s$ ).

Group	<i>n</i>	VAS score (point)			
		6 hours after surgery	24 hours after surgery	48 hours after surgery	72 hours after surgery
A group	55	2.89 ± 0.47	3.48 ± 0.45	3.96 ± 0.41	2.58 ± 0.56
B group	55	2.91 ± 0.44	3.06 ± 0.37	3.38 ± 0.38	2.17 ± 0.39
<i>t</i>		0.230	5.347	7.695	4.456
<i>P</i>		0.818	0.000	0.000	0.000

comparison. The enumeration data were compared by  $\chi^2$  test. The  $\chi^2$  test of four-grid table or row $\times$ list was used.

### 3. Results

**3.1. Differences in General Data between the Two Groups of Patients.** In terms of general information such as age, BMI, course of disease, pregnancy, maximum myoma diameter, disease type, tumor location, marital status, and educational

level, no statistical significance was found between the two groups after statistical test ( $P > 0.05$ ), see Table 1.

**3.2. Differences in Surgical-Related Indicators between the Two Groups.** The postoperative exhaust time ( $13.14 \pm 2.03$ ) h, ambulation time ( $9.86 \pm 1.94$ ) h, postoperative hospitalization time ( $4.37 \pm 1.31$ ) d, and total hospitalization time ( $6.78 \pm 1.69$ ) d in the B group were shorter than those in the A group, and the hospitalization cost ( $0.74 \pm 0.25$ ) ten

TABLE 6: Differences in negative emotions, nursing satisfaction, and GCQ scores between the two groups ( $(\bar{x} \pm s)$ , point).

Group	<i>n</i>	HAMD score		HAMA score		Nursing satisfaction score		GCQ score	
		Before intervention	After intervention	Before intervention	After intervention	Before intervention	After intervention	Before intervention	After intervention
A group	55	22.85 $\pm$ 4.15	16.96 $\pm$ 3.28*	22.15 $\pm$ 3.96	17.23 $\pm$ 3.41*	58.89 $\pm$ 7.47	74.88 $\pm$ 6.36*	54.85 $\pm$ 8.14	71.54 $\pm$ 7.56*
B group	55	23.03 $\pm$ 3.92	13.89 $\pm$ 3.11*	22.04 $\pm$ 4.05	14.58 $\pm$ 2.86*	60.75 $\pm$ 8.26	87.49 $\pm$ 6.17*	53.74 $\pm$ 7.67	86.32 $\pm$ 8.07*
<i>t</i>		0.234	5.037	0.144	4.416	1.239	10.554	0.736	9.912
<i>P</i>		0.816	0.000	0.886	0.000	0.218	0.000	0.463	0.000

\* represents the comparison with preoperative,  $P < 0.05$ .

TABLE 7: Differences in the level of related knowledge mastery between the two groups.

Group	<i>n</i>	Excellent	Good	Generally	Difference	Excellent and good rate
A group	55	30 (54.55)	13 (23.64)	7 (12.73)	5 (9.09)	43 (78.18)
B group	55	46 (83.64)	6 (10.91)	2 (3.64)	1 (1.82)	52 (94.55)
$\chi^2$						6.253
<i>P</i>						0.012

TABLE 8: Differences in the occurrence of adverse symptoms between the two groups.

Group	<i>n</i>	Urinary retention	Upset stomach	Urinary tract infection	Local edema	Wound infection	Total
A group	55	4 (7.27)	2 (3.64)	3 (5.45)	2 (3.64)	1 (1.82)	12 (21.82)
B group	55	1 (1.82)	1 (1.82)	2 (3.64)	1 (1.82)	0 (0.00)	5 (9.09)
$\chi^2$							3.409
<i>P</i>							0.065

thousand was less than that in the A group ( $P < 0.05$ ), see Table 2.

**3.3. Differences in Stress Factors and Inflammatory Factors between the Two Groups.** Before operation, the stress factors and inflammatory factors were not statistically different between the two groups ( $P > 0.05$ ). On the 3rd day after operation, the levels of Cor, NE, TNF- $\alpha$ , and IL-1 $\beta$  in the two groups were significantly higher than those before operation, while the values of the above factors in the B group were significantly lower than those in the A group ( $P < 0.05$ ), see Table 3.

**3.4. Differences in Nutritional Indicators between the Two Groups.** Before operation, the nutritional indexes were not statistically different between the two groups ( $P > 0.05$ ). Three days after operation, albumin and transferrin in both groups were significantly decreased compared with those before operation, while the nutritional indexes in the B group were higher than those in the A group ( $P < 0.05$ ), see Table 4.

**3.5. Difference in Postoperative Pain between the Two Groups.** The pain scores at 24h, 48h, and 72h after opera-

tion in the B group were significantly lower than those in the A group ( $P < 0.05$ ), see Table 5.

**3.6. Differences of Negative Emotion, Nursing Satisfaction, and GCQ Score between the Two Groups.** Before intervention, the negative emotion, nursing satisfaction, and GCQ score were not statistically different between the two groups ( $P > 0.05$ ). After the intervention, the HAMD score and HAMA score of the two groups were significantly lower than those before the intervention, and the nursing satisfaction score and GCQ score were higher than those before the intervention. The negative emotion of the B group was significantly lower than that of the A group, while the nursing satisfaction score and GCQ score were higher than those of the A group ( $P < 0.05$ ), see Table 6.

**3.7. Differences in Mastery of Relevant Knowledge between the Two Groups.** The excellent and good rate of knowledge acquisition in the B group was 94.55% (52/55), which was significantly higher than 78.18% (43/55) in the A group ( $P < 0.05$ ), see Table 7.

**3.8. Difference in Occurrence of Adverse Symptoms between the Two Groups.** The incidence of adverse symptoms in the B group was 9.09% (5/55), which was lower than 21.82%



(12/55) in the A group, while the difference was not statistically significant ( $P > 0.05$ ), see Table 8.

#### 4. Discussion

In recent years, minimally invasive techniques have been widely used in the treatment of gynecological diseases. Traditional open myomectomy has gradually been replaced by laparoscopic surgery [12]. Laparoscopic surgery has the advantages of small wound, light pain and rapid postoperative recovery, but there are also complications such as pelvic adhesions and cervical stump bleeding. Due to little knowledge of laparoscopic surgery and uterine fibroids, patients have obvious perioperative negative emotions and poor psychological resilience [13, 14]. Routine nursing often only pays attention to the treatment of diseases, but not to the negative emotions and rehabilitation quality of patients [15].

Comprehensive rehabilitation nursing is a comprehensive nursing intervention model, involving medication, diet, exercise, psychology and other aspects of patients [16]. This study found that the postoperative exhaust time, ambulation time, postoperative hospitalization time and total hospitalization time of the comprehensive rehabilitation nursing intervention group were shorter than those of the routine nursing intervention group, and the hospitalization expenses were less than those of the routine nursing intervention group. The incidence of adverse symptoms was apparently lower than that of routine nursing intervention. This result suggested that laparoscopic myomectomy combined with comprehensive rehabilitation nursing could accelerate the postoperative rehabilitation process of patients and reduce adverse symptoms medical costs. This is due to the comprehensive rehabilitation nursing mode could make patients understand the operation process and rise perioperative cooperation points by preoperative psychological counseling and health education, thus better cooperating with the operation of medical staff. By guiding patients with reasonable diet, comprehensive rehabilitation nursing mode could promote wound healing and gastrointestinal function recovery, so as to accelerate the recovery process [17, 18].

Postoperative pain is an adverse factor affecting the compliance of patients with rehabilitation treatment, and can aggravate negative emotions and sleep disorders. Negative emotions and sleep disorders can increase the sensitivity of pain and cause pain. Severe pain can cause irritability and raise the risk of nurse-patient disputes [19, 20]. In this study, the pain score of patients 24 h, 48 h, 72 h after the operation were analyzed, and it was found that the comprehensive rehabilitation nursing intervention VAS score at each time point were considerably lower than the conventional nursing intervention; after intervention, HAMD and HAMA scores were lower than those of routine nursing intervention, and nursing satisfaction score, GCQ score and excellent rate of related knowledge mastery were higher than those of routine nursing intervention. The above results suggested laparoscopic myomectomy combined with comprehensive rehabilitation nursing could increase the comfort and satisfaction of patients, and enhance the mastery of relevant knowledge and reduce adverse emotions. This is due to the comprehensive

rehabilitation nursing mode reduce the negative emotions of patients through psychological counseling, so that they can deal with the disease with a more optimistic and positive attitude. Health education deepens patients' understanding of disease-related knowledge and enhances their self-care ability. By guiding the patient to take a comfortable position, relax the abdominal muscle, chat, watch TV and other methods to distract attention, in order to alleviate pain. Severe pain can be given analgesics according to the doctor's advice, so that patients with postoperative pain greatly reduced [21–23].

Surgical trauma can lead to stress response and inflammatory response in the body. Cor and NE are common clinical stress indicators, and the change of serum level can reflect the degree of stress response in the body [24–26]. TNF- $\alpha$  and IL-1 $\beta$  are classical inflammatory factors, which can influence and promote each other, and cause the expansion of inflammatory response [27–29]. Good nutritional status is an important prerequisite for promoting wound healing and rehabilitation of patients. Albumin and transferrin are commonly used clinical nutritional indicators. Patients with uterine fibroids are often in malnutrition due to abnormal uterine bleeding and intraoperative bleeding [30–32]. In this study, through the detection of the above indicators, it was found that the Cor, NE, TNF- $\alpha$  and IL-1 $\beta$  of the comprehensive rehabilitation nursing intervention group were higher than those of the routine nursing intervention group at 3d after operation, and the albumin and transferrin were evidently higher than those of the routine nursing intervention group. These results suggested that laparoscopic myomectomy combined with comprehensive rehabilitation nursing could relieve stress state and inflammatory response state of patients with uterine fibroids after operation, and improve the nutritional state of the body, which was an important mechanism for promoting postoperative rehabilitation of patients. Under the comprehensive rehabilitation nursing mode, psychological counseling enables patients to have a psychological preparation for the operation process and possible symptoms such as limb numbness, pain, nausea, vomiting and fever after operation, so as to reduce the stress response. Early postoperative guidance of patients with reasonable activity, take comfortable position to reduce the stress response caused by pain. Guiding patients to take a reasonable rest, avoiding intensive activities and increasing nutritional intake can improve the nutritional status of the body [33–35].

In summary, laparoscopic myomectomy combined with comprehensive rehabilitation nursing can reduce the body stress state of patients with uterine fibroids after operation, improve patient satisfaction, reduce adverse emotions, and promote rehabilitation.

#### Data Availability

The datasets used and analyzed during the current study are available from the corresponding author upon reasonable request.

#### Conflicts of Interest

The authors declare that they have no conflicts of interest.



## Acknowledgments

This study was supported by the Project No. of Hebei Provincial Health Commission: 20211737.

## References

- [1] A. Nensi, P. Kennedy, and D. Small, "Successful antepartum myomectomy of a large pedunculated fibroid," *Journal of Gynecologic Surgery*, vol. 35, no. 6, pp. 395–397, 2019.
- [2] Z. Jin, Y. Chenghao, and P. Cheng, "Anticancer effect of tan-shinones on female breast cancer and gynecological cancer," *Frontiers in Pharmacology*, vol. 12, p. 824531, 2022.
- [3] M. J. Bray, L. K. Davis, E. S. Torstenson, S. H. Jones, T. L. Edwards, and D. R. Velez Edwards, "Estimating uterine fibroid SNP-based heritability in European American women with imaging-confirmed fibroids," *Human Heredity*, vol. 84, no. 2, pp. 73–81, 2019.
- [4] M. Bongers, J. Gupta, J. G. Garza-Leal, M. Brown, and R. Felberbaum, "The INTEGRITY trial: preservation of uterine-wall integrity 12 months after transcervical fibroid ablation with the sonata system," *Journal of Gynecologic Surgery*, vol. 35, no. 5, pp. 299–303, 2019.
- [5] K. Ota, T. Takahashi, N. Kamo, Y. Endo, S. Furukawa, and S. Soeda, "Successful management of a submucosal fibroid using a hysteroscopic morcellator system in a patient with a history of total proctocolectomy: a case report," *The Journal of Obstetrics and Gynaecology Research*, vol. 46, no. 11, pp. 2450–2453, 2020.
- [6] K. Anton, N. G. Rosenblum, P. Teefey, S. Dayaratna, and C. F. Gonsalves, "The enlarged fibroid uterus: aberrant arterial supply via the omental artery," *Cardiovascular and Interventional Radiology*, vol. 42, no. 4, pp. 615–619, 2019.
- [7] K. Yabumoto, F. Ito, H. Matsushima, T. Mori, I. Kusuki, and J. Kitawaki, "Massive prolapsed submucosal fibroid treated with laparoscopic surgery: a case report," *The Journal of Obstetrics and Gynaecology Research*, vol. 45, no. 4, pp. 942–946, 2019.
- [8] J. H. Lang, W. P. Bai, and C. L. Chen, "Chinese expert consensus expert group on the diagnosis and treatment of uterine fibroids," *Chinese Journal of Obstetrics and Gynecology*, vol. 52, no. 12, pp. 793–800, 2017.
- [9] S. Bing and C. Xiaoming, "Visual Analogue Scale (VAS)," *Chinese Journal of Neurosurgery*, vol. 28, no. 6, p. 645, 2012.
- [10] I. Helmreich, S. Wagner, R. Mergl et al., "The Inventory of Depressive Symptomatology (IDS-C28) is more sensitive to changes in depressive symptomatology than the Hamilton Depression Rating Scale (HAM-D17) in patients with mild major, minor or subsyndromal depression," *European Archives of Psychiatry and Clinical Neuroscience*, vol. 261, no. 5, pp. 357–367, 2011.
- [11] Z. Lixia, G. Fengli, L. Honghui, D. Haibo, and W. Qiuli, "Reliability and validity of the comfort status scale," *Chinese Journal of Practical Nursing*, vol. 22, no. 13, pp. 57–59, 2006.
- [12] G. Pschadka, M. Engelhardt, C. Niehoff, and D. Toub, "Term delivery in an infertile patient after transcervical radiofrequency fibroid ablation and assisted reproductive technology," *Journal of Gynecologic Surgery*, vol. 35, no. 4, pp. 253–255, 2019.
- [13] M. Bongers, S. D. Quinn, M. D. Mueller et al., "Evaluation of uterine patency following transcervical uterine fibroid ablation with the Sonata system (the OPEN clinical trial)," *International Journal*, vol. 242, no. 2, pp. 122–125, 2019.
- [14] D. Maclean, G. Vigneswaran, T. Bryant, S. Modi, and N. Hacking, "A retrospective cohort study comparing a novel, spherical, resorbable particle against five established embolic agents for uterine fibroid embolisation," *Clinical Radiology*, vol. 76, no. 6, pp. 452–457, 2021.
- [15] A. R. Zota, R. J. Geller, A. M. Calafat, C. Q. Marfori, A. A. Baccarelli, and G. N. Moawad, "Phthalates exposure and uterine fibroid burden among women undergoing surgical treatment for fibroids: a preliminary study," *Fertility and Sterility*, vol. 111, no. 1, pp. 112–121, 2019.
- [16] G. Shifrin, M. Engelhardt, P. Gee, and G. Pschadka, "Transcervical fibroid ablation with the Sonata™ system for treatment of submucous and large uterine fibroids," *International Journal of Gynecology & Obstetrics*, vol. 155, no. 1, pp. 79–85, 2021.
- [17] B. S. Mautz, S. H. Jones, E. S. Torstenson, J. N. Hellwege, T. L. Edwards, and D. R. Edwards, "Genetic correlations and exploration of uterine fibroid clinical phenotype in black and white women," *Genetic Epidemiology*, vol. 43, no. 7, p. 897, 2019.
- [18] W. Osorio, N. Posada, J. Cano, S. Tamayo, and J. Giraldo, "Hysteroscopic myomectomy for submucosal type 2 fibroids with cold enucleation technique and complete fibroid extraction using a double-lumen intracervical cannula," *Fertility and Sterility*, vol. 115, no. 2, pp. 522–524, 2021.
- [19] L. A. Learman, "Treatment of uterine fibroid symptoms with relugolix combination therapy," *Obstetrical and Gynecological Survey*, vol. 76, no. 6, pp. 334–336, 2021.
- [20] C. Rao, H. Hu, and R. Tan, "Comparative analysis of clinical effects of the cable-pin system and Kirschner wire tension band (TBW) internal fixation in the treatment of the olecranon fracture," *Contrast Media & Molecular Imaging*, vol. 2022, article 3073121, 7 pages, 2022.
- [21] C. Dillon, M. Rezvani, H. McLean et al., "A tissue preparation to characterize uterine fibroid tissue properties for thermal therapies," *Medical Physics*, vol. 46, no. 8, pp. 3344–3355, 2019.
- [22] A. Amoah, N. Joseph, S. Reap, and S. D. Quinn, "Appraisal of national and international uterine fibroid management guidelines: a systematic review," *BJOG*, vol. 129, no. 3, pp. 356–364, 2022.
- [23] Y. Watahiki, T. Hikichi, K. Watanabe et al., "A case of inflammatory fibroid polyp of the stomach with an "erect penis like appearance" successfully removed by endoscopic submucosal dissection," *Clinical Journal of Gastroenterology*, vol. 12, no. 3, pp. 279–284, 2019.
- [24] A. Netter, V. Pauly, P. Siles, A. Pivano, V. Vidal, and A. Agostini, "Predictors of uterine fibroid volume reduction under ulipristal acetate: a prospective MRI study," *Reproductive Biomedicine Online*, vol. 39, no. 5, pp. 795–801, 2019.
- [25] I. Szydlowska, A. Marciniak, and A. Starczewski, "Uterine endometrial stromal sarcoma revealed after treatment of uterine fibroid with ulipristal acetate: a case report," *European Journal of Gynaecological Oncology*, vol. 40, no. 3, pp. 494–497, 2019.
- [26] C. N. Mitchell, M. S. Islam, S. Afrin, J. Brennan, K. J. Psoter, and J. H. Segars, "Mechanical stiffness augments ligand-dependent progesterone receptor B activation via MEK 1/2 and Rho/ROCK-dependent signaling pathways in uterine fibroid cells," *Fertility and Sterility*, vol. 116, no. 1, pp. 255–265, 2021.
- [27] M. Ciebia, B. Męczekalski, K. Łukaszuk, and G. Jakiel, "Potential synergism between ulipristal acetate and vitamin

- D3 in uterine fibroid pharmacotherapy -2 case studies,” *Gynecological Endocrinology*, vol. 35, no. 6, pp. 473–477, 2019.
- [28] M. Frijlingh, I. de Milliano, W. J. K. Hehenkamp, and J. A. F. Huirne, “Differences in fibroid vascularity after three months of pre-treatment with leuprolide acetate or ulipristal acetate: A pilot study,” *European Journal of Obstetrics, Gynecology, and Reproductive Biology*, vol. 245, no. 5, pp. 186–192, 2020.
  - [29] R. K. Shaffer, A. D. Dobberfuhr, K. N. Vu et al., “Are fibroid and bony pelvis characteristics associated with urinary and pelvic symptom severity?,” *American Journal of Obstetrics and Gynecology*, vol. 220, no. 5, pp. 471.e1–471.e11, 2019.
  - [30] T. Kroencke and M. David, “Uterine artery embolization (UAE) for fibroid treatment - results of the 7th Radiological Gynecological Expert Meeting,” *Geburtshilfe und Frauenheilkunde*, vol. 79, no. 7, pp. 688–692, 2019.
  - [31] S. M. Toprani and V. Kelkar Mane, “Role of DNA damage and repair mechanisms in uterine fibroid/leiomyomas: a review,” *Biology of Reproduction*, vol. 104, no. 1, pp. 58–70, 2021.
  - [32] A. L. Patterson, J. W. George, A. Chatterjee et al., “Putative human myometrial and fibroid stem-like cells have mesenchymal stem cell and endometrial stromal cell properties,” *Trends in Ecology & Evolution*, vol. 35, no. 1, pp. 44–57, 2020.
  - [33] R. Sparić, D. Papoutsis, Z. Bukumirić et al., “The incidence of and risk factors for complications when removing a single uterine fibroid during cesarean section: a retrospective study with use of two comparison groups,” *The Journal of Maternal-Fetal & Neonatal Medicine*, vol. 33, no. 19, pp. 3258–3265, 2020.
  - [34] M. El Sabeh and M. A. Borahay, “The future of uterine fibroid management: a more preventive and personalized paradigm,” *Reproductive Sciences*, vol. 28, no. 11, pp. 3285–3288, 2021.
  - [35] J. Donnez, G. E. Courtoy, and M.-M. Dolmans, “Fibroid management in premenopausal women,” *Climacteric*, vol. 22, no. 1, pp. 27–33, 2019.

## Research Article

# Meta-Analysis and Data Mining-Based Study on the Expression Characteristics of Inflammatory Factors and Causes of Recurrence in Spinal Tuberculosis

Jun Wang and Shaoning Jiang 

*Orthopedics, Shanghai Public Health Clinical Center, Shanghai 250001, China*

Correspondence should be addressed to Shaoning Jiang; [jsnshgw@sina.com](mailto:jsnshgw@sina.com)

Received 19 July 2022; Revised 19 August 2022; Accepted 30 August 2022; Published 22 September 2022

Academic Editor: Hangjun Che

Copyright © 2022 Jun Wang and Shaoning Jiang. This is an open access article distributed under the Creative Commons Attribution License, which permits unrestricted use, distribution, and reproduction in any medium, provided the original work is properly cited.

With the rapid development of modern medical information technology, hospitals are accumulating huge amounts of clinical data while providing medical services to patients, and in the era of big data, how to mine valuable information from the huge amount of clinical data so as to make new contributions to future disease diagnosis and medical research. In order to solve this problem, more and more scholars have introduced data mining techniques into the medical field in recent years, and mining and analysing medical data is a hot topic at present. If spinal TB is detected and treated early, not only can spinal deformities be prevented and treated but also the course of treatment can be shortened, the financial burden on the patient can be reduced, spinal function can be maintained, and eradication can be achieved without the need for surgical intervention. Early detection of spinal tuberculosis is the key to preventing and treating it. Therefore, in this paper, we use meta-analysis and data mining techniques to process and analyse the medical data of spinal tuberculosis disease, its main inflammatory factors expression characteristics, and the causes of patient recurrence.

## 1. Introduction

Tuberculosis of the spine is an infectious disease caused by *Mycobacterium tuberculosis*. Of these tuberculosis diseases, spinal tuberculosis is the most prevalent. According to the World Health Organization [1, 2], there are now approximately 9 million new cases of spinal tuberculosis worldwide each year, and approximately 1.5 million deaths from spinal tuberculosis each year [3]. In China, TB of the spine is the second most prevalent infection in the world, with the highest incidence in the country. Bone and joint tuberculosis is the most common form of spinal tuberculosis secondary to spinal tuberculosis, accounting for about 5-10% of cases, with spinal tuberculosis being the most common at about 50%. Spinal TB is most common in young people and occurs mainly in the lumbar spine, thoracic, cervical, and sacral spine. TB of the spine is a bony injury to the vertebrae that can easily lead to lesions that, if not treated promptly, can easily lead to spinal deformities and, in severe cases, affects

the spine and compress the spinal cord [4]. Spinal nerve damage or paralysis occurs in 10% to 61% of patients with spinal TB.

There are four diagnostic bases for infectious spinal disease: symptoms, signs, specialist investigations, laboratory tests, imaging tests, and pathology [5]. The positive rate of blood cultures for brucella ranges from 10% to 74% (9), and the detection rate of *Mycobacterium tuberculosis* (TB) is 44.5% (10). Before the use of antimicrobial therapy, the positive rate of blood cultures is about 70%, and the positive rate of blood cultures is as high as 70%. The long cycle of blood cultures for brucella adds to the difficulty of early diagnosis [6-9]. The final diagnosis of spinal infection is established by puncture biopsy and surgical pathology, but surgical treatment is usually required. MRI is useful for the early diagnosis of infectious spinal lesions, assessing the extent of the lesion and the presence or absence of invasive intradural lesions, and visualising lesions in the spinal cord and nerve roots. It is currently the examination of choice

for infected spinal lesions due to its better soft tissue resolution, multidirectional [10], multiparametric imaging, noninvasiveness, and clear visualisation of structures within the spinal canal. Therefore, exploring the expression characteristics and etiology of inflammatory factors in spinal tuberculosis is a useful reference for diagnosis, treatment, and prognosis.

## 2. Introduction to Relevant Theories

**2.1. Medical Data Mining.** Data mining is an interdisciplinary discipline that encompasses database technology, pattern recognition, machine learning, artificial intelligence, parallel computing, statistics, and data visualisation [11]. In short, data mining is the extraction of potentially valuable information and knowledge from large, incomplete, noisy, fuzzy, and random data of practical application. Data mining is an important part of knowledge discovery, which is based on a full and deep understanding of data, a high degree of abstraction and summary of the intrinsic and essential nature of data, and the sublimation of data from perceptual to rational cognition. Since it was introduced in the late 20th century, it has been valued by many experts and scholars [12].

The development of medicine has evolved from empirical medicine and experimental medicine to the current evidence-based medicine, which has a huge amount of medical data with characteristics such as objectivity and experimentation.

The process of medical data mining includes: problem definition, data preparation, data mining, result analysis, and knowledge application [13].

- (1) *Defining the problem.* First, a thorough communication with medical professionals is necessary to analyse their needs, define their requirements, determine their purpose, and measure their success
- (2) *Data integration.* Data integration (integrating different types of data from multiple archives or multiple repository operating environments), data purging (removing noisy and irrelevant data from the original data set, missing data, and removing dirt), data transformation (basically finding the characteristic representation of data, using transformation methods to reduce the number of valid variables or discovering data invariants)
- (3) *Data mining.* The main components are: selection of data models, determination of training and experimental processes, model building, model evaluation, etc. In order to verify the validity of the data mining and the correctness of the data, it is also necessary to verify the validity of the data in conjunction with clinical practice
- (4) *Research results.* The knowledge and rules found in data mining need to be judged as correct and easy to understand from the user's perspective. It is also important to evaluate whether the knowledge mined

is medically meaningful, medically relevant, medically meaningful, and consistent with the original intent of data mining

- (5) *Use of theory.* The execution and control of the conclusions should be planned in detail, and a detailed summary of the whole project should be made and used in future medical practice

**2.2. Introduction to Association Rules.** The application of association rules in data mining is one of the most current concerns in data mining. Association rules are used to describe possible relationships between items of information in a database. The object of association rule mining is usually a transaction database, which was originally used in the retail industry, for example in supermarket sales management. The development of barcode technology has made it easier and better to collect data, so that huge amounts of transaction information can be stored, and association rules are used to identify customers based on their purchase behaviour. The information obtained through association rules can be used for catalogue design, merchandise layout, target marketing, etc.

The problem of association of item sets in customer transaction databases was first introduced by Agrawal et al. in 1993, and a typical Apriori mining method was introduced in 1994. Based on this, many scholars have explored association rules in depth. Their work is to optimise the existing Apriori algorithm, such as introducing random sampling, the idea of parallelism, and using hashing, in order to improve the mining efficiency of the algorithm; some have proposed a new method of association rule mining that is not related to Apriori, such as Jianwei et al.'s FP-Growth method and association rule mining based on association graph mining [14–17].

**2.3. Meta-Analysis Theory.** Meta-analysis is a statistical method for comparing and synthesising the same scientific questions. Combining all relevant studies allows for a more accurate assessment of the effectiveness of health care services compared to a single study and also helps to explore the consistency and differences between the results of different studies. And where different studies have different findings, meta-analysis can be used to produce a statistical analysis that is similar to the actual situation [18].

Meta-analysis mainly includes: (i) analysis of heterogeneity and statistical consistency tests on data from multiple independent experiments and (ii) evaluation of combined effects.

In meta-analysis, the test of heterogeneity is a very critical process, and the Q-test is mostly used to determine whether there is a significant difference in the heterogeneity of multiple independent studies, and it is usually considered that the results of each independent study are consistent at  $P > 0.1$ .

Effect values are generally selected based on the nature of the clinical study and the type of data. In meta-analysis [19], fixed-effects and random-effects models are usually used, with fixed-effects models being used where there is consistency across multiple studies, and random-effects models



may be used to calculate different effect factors where different studies exist, for example, where different subgroup analyses are conducted and satisfactory results are still not obtained after heterogeneous analysis and processing.

Meta-analysis, especially based on high quality randomised controlled trials (RCTs), is considered to be a high level of evidence-based evidence which serves: (i) to achieve quantification; (ii) to address the same issues in a systematic and reproducible manner; (iii) to synthesise the same topics from multiple small samples to improve the statistical efficiency of the original results; (iv) to resolve inconsistencies in study findings and improve assessment of effects; (v) provide answers to questions not asked in the original study; (vi) explore the extent of publication bias in the existing literature; (vii) provide new topics for future research.

**2.4. Theory of Spinal Tuberculosis.** Spinal tuberculosis is a chronic disease with systemic pathology. Nationally, spinal tuberculosis is the most common, with spinal tuberculosis predominating and adnexal tuberculosis being very rare. In terms of location, the lumbar spine is the largest, followed by the thoracic spine. As for tuberculosis of the sacral and caudal spine, it is even rarer.

Classification of spinal tuberculosis:

Depending on the location of the lesion, it can be divided into two categories: the central type and the marginal type.

- (1) The central type of spinal tuberculosis occurs mostly within 10 years of age, mainly in the thoracic spine. Due to the rapid development of the tumour, the entire vertebral body is wedge-shaped and usually invades only one vertebra
- (2) Marginal spinal tuberculosis is predominant in adults, with the lumbar spine predominating. The intervertebral discs are damaged and the vertebral space is reduced. Cold abscesses develop first and then compression leads to spinal cord injury

Clinical features of spinal tuberculosis:

- (1) Systemic clinical manifestations include fatigue and weakness, loss of appetite, physical wasting, low fever in the afternoon, and vegetative dysfunction. Fever is common in children, and they do not like to play and cry at night
- (2) The early manifestation of pain is usually a dull ache. It is aggravated by walking and exertion and relieved by rest; the pain is aggravated by sneezing and coughing. The pain is mainly localized and radiating. Localised pain usually occurs on both sides of the spine or between the spinous processes and the spines. Following an injury, radiating pain can develop in the corresponding segmental innervation areas [20]. Patients with lesions in the thoracolumbar segment often present with pain in the lumbosacral region. If the lesion compresses the spinal cord and nerve roots, it can produce very intense pain that radiates outwards along the nerve roots. The

pain is not very pronounced because of the distance between the spinal column and the spinous process: percussion is localised to the spinous process and there is pain

- (3) Disorders of posture. Due to differences in the location of the lesion, patients with cervical tuberculosis often hold their heads in their hands; patients with lumbar tuberculosis have back pain and are afraid to stoop when picking up objects
- (4) Spinal abnormalities, the most common being backward curvature of the spine. Posterior convexity is the most common type, with the spine bulging backwards at an angle. Children with thoracic spinal tuberculosis are prone to kyphosis because of the number of sites of their lesions
- (5) Myospasm, which is initially a reflex spasm of the muscles on the side of the spine due to pain, followed by spastic dystonia, leads to abnormalities in certain positions. Examples include cervical spondylosis in patients with tuberculosis of the spine and a self-expanding gait in patients with tuberculosis of the thoracolumbar segment. In children, the relaxation of the muscles after sleeping causes pain when turning over or changing position, resulting in “nocturnal crying in children”.

### 3. Application Method Design

**3.1. Data Mining Model Construction.** In the process of data mining, the expression characteristics of spinal tuberculosis inflammatory factor, the basic principles of relevance, feasibility, validity, and safety should be followed, and on the premise of satisfying the basic principles, the traditional method of generating the expression characteristics of spinal tuberculosis inflammatory factor is based on a simple inference system, while for multimorbidity users, this paper proposes that it is based on the original spinal tuberculosis inflammatory factor expression characteristics data. Based on the original spinal tuberculosis inflammatory factor expression characteristics data, this paper proposes to generate the final spinal tuberculosis inflammatory factor expression characteristics by data mining through association models to constitute an inference system for spinal tuberculosis inflammatory factors [21]. The model can also be used to mine the medical data of relapsed patients and to generate features on the causes of relapse. The model structure is illustrated in Figure 1.

One of the data mining processes is as follows:

- (1) *Stating the problem and clarifying the hypothesis.* In practical data mining, each project has its own area of expertise and application context, so it requires some understanding of the relevant expertise, business processes, etc. Thus, the analyst can understand the need and importance of the project. This process tests not only the analyst’s technical skills but also

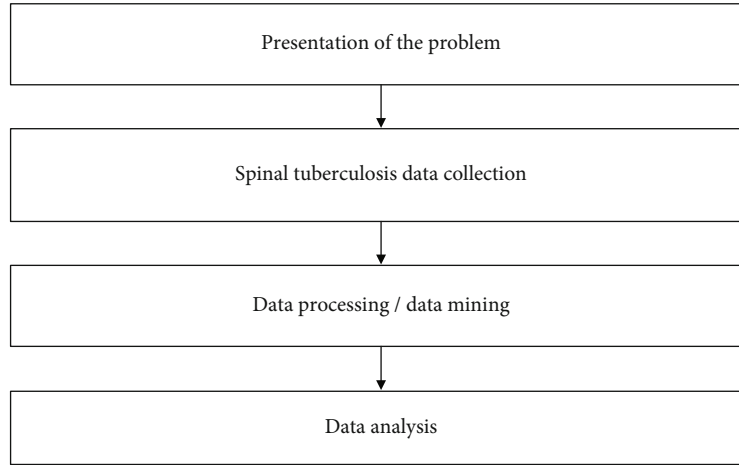


FIGURE 1: Simple reasoning flow chart.

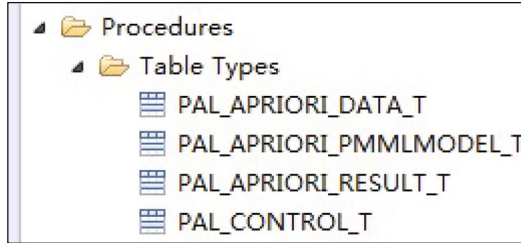


FIGURE 2: Stored procedure table.

TABLE 1: Parameter settings for PAL\_APRIORI\_PDATA\_TBL.

ID	Typename	Direction
1	DISEASE.PLA_APRIORI_DATA_T	In
2	DISEASE.PLA_CONTROL_T	In
3	DISEASE.PLA_APRIORI_RESULT_T	Out
4	DISEASE.PLA_APRIORI_PMMLMODEL_T	Out

TABLE 2: Structure of the implementation results data sheet.

Serial number	Field	Data type	Description
1	PRERULE	VARCHAR(500)	Frequent items
2	POSTRULE	VARCHAR(500)	Item ID
3	SUPPORT	DOUBLE	Support
4	CONFIDENCE	DOUBLE	Confidence

TABLE 3: Structure of the data sheet for the implementation result parameters.

Serial number	Field	Data type	Description
1	ID	INT	Frequent items
2	PMMLMODEL	VARCHAR(5000)	Item ID

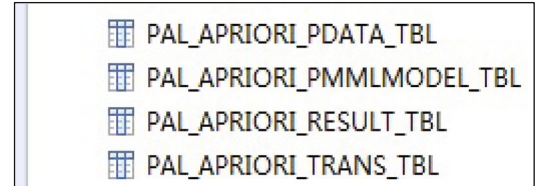


FIGURE 3: Table of implementation results.

the level of cooperation between the analyst and specific industry players [22]

- (2) *Data collection.* This step considers the generation and collection of data, and depending on the purpose of the data collection and the technical guidelines required, the extraction of data from the database is done to generate the data to be analysed. Usually, comprehensive, high quality, and accurate information is an important guarantee for data mining efforts. Mixed data and too much data will have a negative impact on the effectiveness and validity of data mining
- (3) *Data preprocessing.* After the appropriate information has been collected, it cannot be analysed directly. It must go through multiple stages of data preprocessing such as data cleaning, fusion, selection, and conversion. Since some problems are bound to arise during data collection, data cleaning is mainly to remove noise and inconsistency. Data integration is the process of bringing together various data resources, while data selection is the process of extracting relevant information from the data. Data conversion, on the other hand, is the process of merging and consolidating, making it possible to undergo conversion and uniform processing in order to form a format suitable for subsequent operations
- (4) *Data mining.* In practical engineering problems, methods more appropriate to the engineering context are used to solve them. This shows the role that



TABLE 4: Data mining results for the dataset.

Variables	BS( $n = 40$ cases)	NPS( $n = 1$ case)	TBS( $n = 6$ cases)	$\chi^2$	$P$
Epidural abscess-characteristic 1				2.790	0.248
Absent	39(36.11%)	16(14.81%)	53(49.07%)		
Yes	1(10.00%)	2(20.00%)	7(70.00%)		
Type of vertebral bone destruction-characteristic 2				38.856	0.001
Granuloma	28(63.64%) <sup>a</sup>	9(20.45%) <sup>a</sup>	7(15.91%) <sup>b</sup>		
Confined abscess	11(19.30%) <sup>a</sup>	8(14.04%) <sup>a,b</sup>	38(66.67%) <sup>b</sup>		
Lytic abscess	1(5.88%) <sup>a</sup>	1(5.88%) <sup>a,b</sup>	15(88.24%) <sup>b</sup>		
Paravertebral lesion-feature 3				45.630	0.001
Restricted granuloma	22(62.86%) <sup>a</sup>	7(20.00%) <sup>a</sup>	6(17.14%) <sup>b</sup>		
Spreading granuloma	2(66.67%) <sup>a</sup>	0(0.00%) <sup>a</sup>	1(33.33%) <sup>a</sup>		
Confined abscess	15(32.61%) <sup>a</sup>	10(21.74%) <sup>a</sup>	21(45.65%) <sup>a</sup>		
Spreading abscess	1(2.94%) <sup>a</sup>	1(2.94%) <sup>a</sup>	32(94.12%) <sup>b</sup>		

TABLE 5: The statistical results of the spinal tuberculosis inflammatory factor data mining model.

Main parameters	Slight inflammation		Significant inflammation	Severe inflammation	Early spinal tuberculosis			
	Point estimate	95% CI estimate	Point estimate	95% CI	Point estimate	95% CI estimate	Point estimate	95% CI
SEN	0.80	0.71-0.87	0.84	0.81-0.86	0.87	0.84-0.89	0.89	0.87-0.91
SPE	0.76	0.69-0.82	0.77	0.72-0.80	0.84	0.80-0.87	0.89	0.86-0.92
PLR	3.90	2.60-5.80	4.70	4.0-5.5	6.3	5.0-7.9	8.2	6.6-10.1
NLR	0.30	0.23-0.37	0.28	0.23-0.34	0.19	0.15-0.23	0.12	0.09-0.16
AUC	0.85	0.82-0.88	0.88	0.84-0.90	0.92	0.89-0.94	0.95	0.93-0.97
DOR	13.008.00-21.0017.00		12.00-23.0034.00		23.00-50.0067.00		44.00-101.00	

appropriate algorithms play in the mining process. Firstly, the model is tested by selecting an appropriate data set to ensure its correctness and quality. And the appropriate modifications are made according to the actual situation.

- (5) *Data analysis*. The process of data interpretation is important. One is the impact of the knowledge models found in the data mining process on the value of the business; another issue is how to visualise the results of data mining. In addition, depending on the needs of the industry, there is a need to compare and analyse the results and conclusions obtained with the relevant industry knowledge, a field of knowledge that covers a wide range of topics, from the experience of experts to industry regulations. The performance of the finalised or general indicators assesses their effectiveness prospects.

**3.2. Meta-Analysis Design.** Data analysis was performed using the ReviewManager 5.3 software package. In the statistical data, the two categories of effective and ineffective and cured and uncured were expressed in terms of dominance ratio, relative risk, risk difference, risk ratio and HR, and in terms of weighted mean difference (WMD).

- (1) *Mapping the forest*. Meta-analysis focuses on the mapping and analysis of the forest map
- (2) *Testing for heterogeneity*. The primary means of testing is for tests where an  $I$ -value of more than 50% and a  $P$  value of less than 0.1 indicate heterogeneity and a random-effects model should be used. In contrast, for studies with good homogeneity, a fixed-effect model is usually used
- (3) *Tests of bias*. The “inverted funnel plot” is the current main mode of presentation. When there is bias, the point-shaped data on the curve is uneven
- (4) *Sensitivity analysis*. According to the JADAD scale, low quality and bias-causing literature was excluded, the remaining high quality literature was statistically analysed, and the two were compared to determine their stability

## 4. Application of Experimental Analysis

**4.1. Introduction to the Data Set.** The data were obtained from a medical case database developed by Cerner in the USA [23], and included hospital admissions of spinal TB patients from 130 hospitals across the country (2010-2020) over a 10-year period, including 18 in the Midwest, 58 in

the Northeast, 28 in the South, and 16 in the West. This database contains 41 tables with 117 attributes. This database contains 740,366,643 medical records corresponding to 17,880,231 patients and 2,889,571 data provision sources.

The dataset includes more than 50 attributes, including the following characteristics:

- (1) This information is for inpatient cases
- (2) All are cases of spinal tuberculosis, which includes all types of spinal tuberculosis
- (3) The duration of hospitalisation ranged from 1 to 14 days
- (4) All tests performed in a laboratory setting
- (5) Details of all hospital medication administered were recorded
- (6) The dataset contains the following basic characteristics: patient number, race, sex, age, type of hospitalisation, length of stay, attending physician, number of clinical trials, glycated hemoglobin tests, diagnosis, number of drugs administered, number of treatments, number of hospitalisations, and number of emergency admissions in the year

**4.2. Preprocessing of Spinal Nodule Data.** ETL is a key part of the implementation of a data warehouse and undertakes the transformation from the data source to the destination data warehouse. The content of ETL focuses on the extraction, transformation, and loading of data to achieve structured data. The following are:

- (1) *Extraction.* The raw data is extracted from various commercial systems and used as a data source. Sixty-five tables with a total of over 800 fields were extracted from both clinical and research sources to construct a single disease-specific data marketplace for spinal tuberculosis.
- (2) *Transformation.* The extracted information was transformed according to preset rules, resulting in a consistent data format.
- (3) *Loading.* The transformed information is entered into the data warehouse as a source for later mining and analysis. In this paper, clinical information on spinal tuberculosis is processed based on the information process.

**4.3. Inflammatory Factor Expression Characteristics Mining Analysis Results.** The dataset includes medical records for each patient's length of stay in hospital, and changes in their attendance are important for the treatment of spinal tuberculosis. In this paper, we analyse the inflammatory response of patients in the context of hospital infection and look for the most common inflammatory expression factors in terms of inflammatory expression.

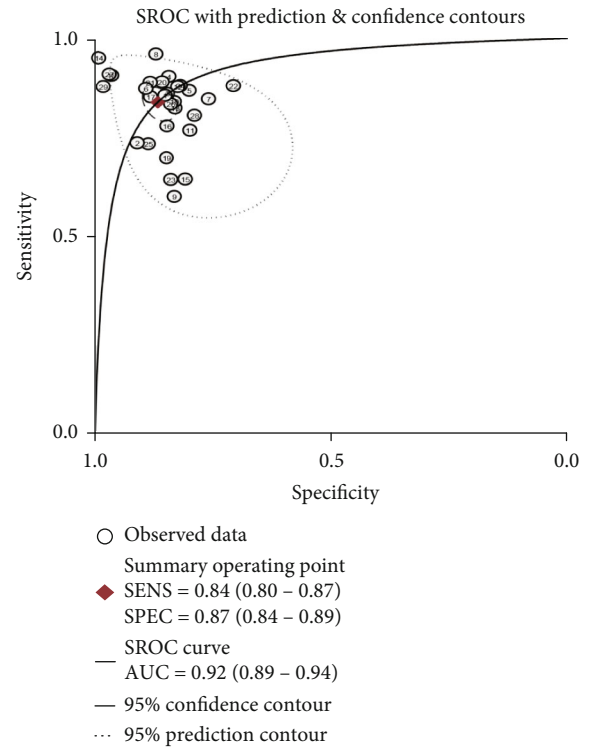


FIGURE 4: SROC Plot.

The following analysis of spinal TB coinfection will be completed using PAL, in the data preparation phase, as follows:

- (1) *Determine the storage procedure for the raw data to be analysed.* To temporarily store the results of all intermediate calculations, as opposed to the actual data tables that follow, create the table type storage procedure, see Figure 2.
- (2) *Definition of metadata.* In the metadata table PAL\_APRIORI\_PAL\_APRIORI\_, the properties of each stored procedure using the association rule algorithm.

In PDATA\_TBL, the inputs and outputs of the algorithm are identified in Table 1.

- (3) *Definition of the results of the implementation.* The results of the implementation of the algorithm are placed in the output tables of the implementation results in Table 2 and the implementation results in Table 3.

The SQL statement is as follows: (a) drop table PAL\_APRIORI\_RESULT\_TBL and (b) create column table PAL\_APRIORI\_RESULT\_TBL ("PRERULE" VARCHAR(5000), "POSTRULE" VARCHAR(5000), "SUPPORT" Double, "CONFIDENCE" Double, and "LIFT" DOUBLE).

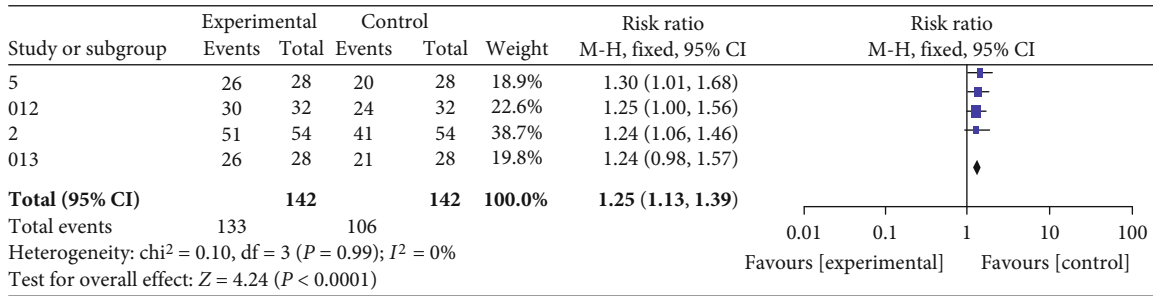


FIGURE 5: Forest map of recurrence.

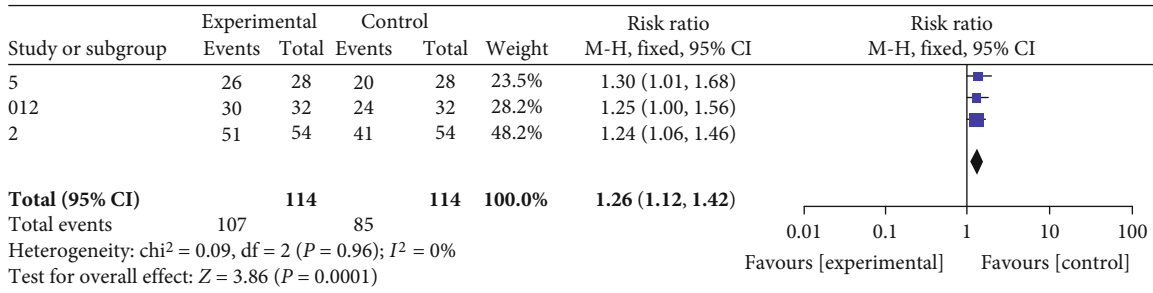


FIGURE 6: Medium sensitivity test.

This resulted in four tables as shown in Figure 3.

**4.3.1. Implementing the Apriori Algorithm.** Table 4 demonstrates the results of data mining for concurrent inflammation, which reveals a relationship between spinal TB and inflammation. The greatest proportion of granulomatous inflammatory factor expression features can be seen in the types of vertebral bone destruction and the greatest proportion of spreading granulomas in paravertebral lesions.

**4.4. Analysis of Recurrence Cause Data Mining Results.** Data mining of medical data revealed that 70.6% of patients had multiple spinal lesions which were extensive and jumpy and could not be completely removed. The patients were in poor physical condition with large spinal gaps, postoperative spinal instability, and poor circulation to the transplanted vertebrae, which can affect fusion and repair of the spine.

36.3% of relapsed patients relapse due to the unstable location of the spinal tuberculosis lesion. Postoperative fixation of the lesion is mainly internal and external to maintain the stability of the spine. The absence and destruction of the anterior midcolumn structures of the spinal cord during surgery for spinal TB lesion excision, bone graft fusion, and lesion removal results in poor spinal stability and severe retroconvex deformity, and spinal stability is a prerequisite for TB healing and bone graft fusion, and the final healing of spinal TB can only be achieved after the location of the spinal TB occurrence is stabilized.

In 40.7% of these relapses, irregular pre and postoperative chemotherapy caused the relapse, and irregular pre and postoperative chemotherapy is the main cause of spinal TB relapse. Therefore, appropriate chemotherapy before and after surgery is essential to prevent tumour recurrence and to ensure the success of surgery. Patients and families should

therefore be informed of how to administer regular antituberculosis chemotherapy to prevent recurrence.

**Conclusion:** nutritional support, complete intraoperative excision of the lesion, close postoperative bracing and pre and postoperative chemotherapy can effectively reduce and prevent postoperative recurrence.

**4.5. Meta-Analysis Results.** This meta-analysis was performed on 29 trials including 7,555 patients with a diagnostic threshold in the range of 7.0 to 14.2 Kpa. In data mining for inflammatory factors in spinal tuberculosis, a sensitivity of 0.84 (95% CI: 0.80 to 0.87), a combined specificity of 0.87 (95% CI: 0.84 to 0.89), a combined positive likelihood ratio of 6.3 (95% CI: 5.0 to 7.9), a combined negative likelihood ratio of 0.19 (95% CI: 0.15 to 0.23), SROC area under the curve was 34 (95% CI: 23 to 50), and SROC area under the curve was 0.92 (95% CI: 0.89 to 0.94). The statistical results of the spinal tuberculosis inflammatory factor data mining model are shown in Table 5.

(1) The SROC curve is plotted as shown in Figure 4

(2) Forest mapping

As shown in Figure 5, there is a clear advantage in reducing spinal TB recurrence in cases where inflammation is well controlled.

(3) Sensitivity tests

Excluding one trial with a low Jadad score and reanalysing, the test of heterogeneity was  $P = 0.96 > 0.1$ , with good

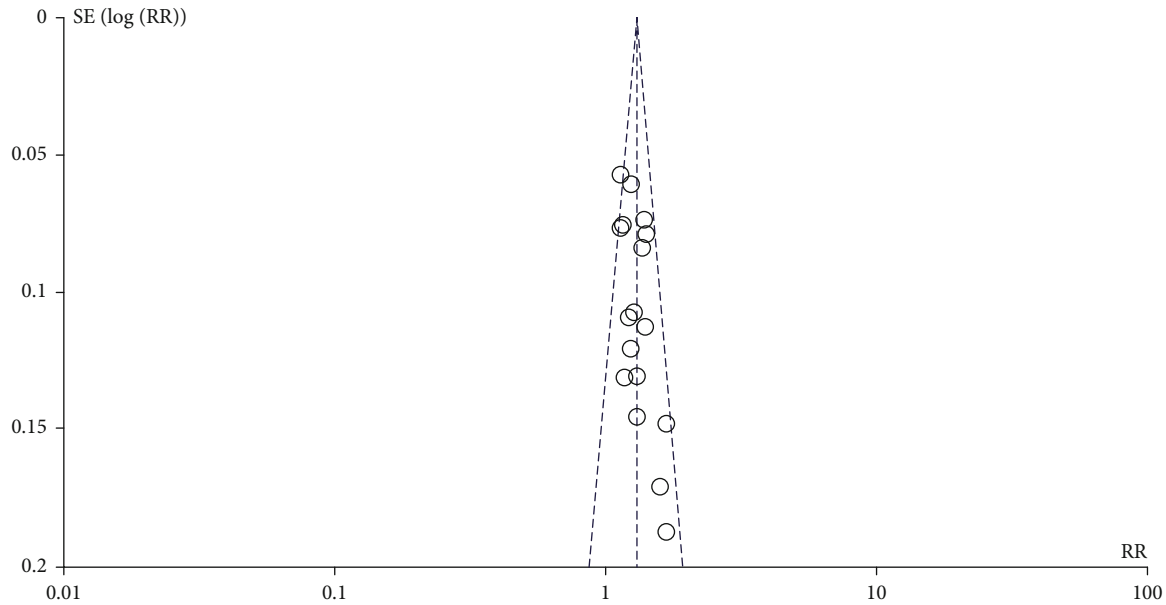


FIGURE 7: Inverted funnel diagram.

agreement, and using a fixed-effects model combined with effects analysis, 95% CI: 1.26 (1.12, 1.42),  $P = 0.0001$ , with no significant difference between the two, showing good stability. As shown in Figure 6.

## 5. Potential for Bias

An 'inverted funnel plot' was drawn to see if there was any bias. The graph shows that the dotted distribution is not very symmetrical, representing a degree of bias as shown in Figure 7.

## 6. Conclusion

Data mining is an emerging discipline that has emerged in recent years. It makes comprehensive use of various learning methods and approaches such as statistics, rough sets, and fuzzy mathematics to extract abstract knowledge from massive amounts of data, thereby revealing the intrinsic relationships and essential laws of the objective world hidden in the data, thus enabling the automatic extraction of knowledge.

Spinal tuberculosis is one of the most common forms of osteoarticular tuberculosis, accounting for about 50% of all tuberculosis in the body, and is also a major cause of spinal deformity and paralysis. Due to its high rate of disability, it seriously affects the quality of survival of patients. Currently, surgery is the mainstay, but the recurrence rate of TB remains high in spinal TB surgery. Therefore, in this paper, data mining techniques were used to mine medical data in depth, and the data were screened and analysed. The most significant of these was found to be the expression characteristics of granulomatous inflammatory factors, and based on the information mined, the causes of recurrence were analysed and the incidence of multiple spinal lesions was found to be 70.6%. Meta-analysis of the various inflammatory pro-

files revealed a significant reduction in the recurrence rate of spinal tuberculosis with control of inflammation.

## Data Availability

The dataset used in this paper are available from the corresponding author upon request.

## Conflicts of Interest

The authors declared that they have no conflicts of interest regarding this work.

## References

- [1] M. Pai and M. Schito, "Tuberculosis diagnostics in 2015: landscape, priorities, needs, and prospects," *Journal of Infectious Diseases*, vol. 211, suppl\_2, pp. S21–S28, 2015.
- [2] M. R. Rasouli, M. Mirkoochi, A. R. Vaccaro, K. K. Yarandi, and V. Rahimi-Movaghar, "Spinal tuberculosis: diagnosis and management," *Asian spine journal*, vol. 6, no. 4, pp. 294–308, 2012.
- [3] G.-P. Zhang, Q.-Q. Wu, H.-W. Guan, J. Zhang, and C. Wang, *Spinal Tuberculosis Pathology*, People's Military Medical Publishing House, Beijing, 2007.
- [4] S. H. Dong, H. T. Bai, Y. B. Li, and H. Yu, "Imaging manifestations of brucella spondylitis and its treatment," *Chinese gerontology*, vol. 34, no. 8, pp. 2310–2312, 2014.
- [5] J. D. Colmenero, J. D. Ruiz-Mesa, A. Plata et al., "Clinical findings, therapeutic approach, and outcome of brucellar vertebral osteomyelitis," *Clinical Infectious Diseases*, vol. 46, no. 3, pp. 426–433, 2008.
- [6] R. Bornemann, J. D. Müller-Broich, M. Deml, K. Sander, D. C. Wirtz, and R. Pflugmacher, "Diagnosis and treatment of spondylodiscitis/spondylitis in clinical practice," *Zeitschrift für Orthopädie und Unfallchirurgie*, vol. 153, no. 5, pp. 540–545, 2015.

- [7] J. Lianshun, "Emphasis on septic spondylitis and early diagnosis and treatment," *Chinese Journal of Orthopaedic Surgery*, vol. 18, no. 1, pp. 7-8, 2010.
- [8] J. Lianshun, *Modern Spine Surgery*, People's Military Medical Publishing House, Beijing, 2007.
- [9] M. Turgut, A. T. Turgut, and U. Koşar, "Spinal brucellosis: Turkish experience based on 452 cases published during the last century," *Acta neurochirurgica*, vol. 148, no. 10, pp. 1033-1044, 2006.
- [10] J. D. Shi and Z. L. Wang, "Early diagnosis of atypical spinal tuberculosis," *Chinese Journal of Spinal Cord*, vol. 5, pp. 432-434, 2010.
- [11] Q. F. Hua, J. J. Zheng, B. B. Hu, Z. Cui, and S. Gong, "Application of CT-guided percutaneous puncture biopsy technique in the diagnosis of spinal infection lesions," *Chinese Journal of Hospital Infection*, vol. 26, no. 12, pp. 2797-2799, 2016.
- [12] J. Guihua, T. Junzhang, Z. Liyin et al., "MRI manifestations of infectious spondylitis," *Ningxia Medical Journal*, vol. 9, pp. 618-620, 2005.
- [13] S. Wang and L. X. Qian, "Comparative analysis of magnetic resonance imaging features of brucellosis spondylitis and spinal tuberculosis," *China Drugs and Clinics*, vol. 14, no. 7, pp. 934-935, 2014.
- [14] L. Xu, J. He, H. Meng et al., "Application of information entropy-based decision trees to the identification of chronic gastritis in Chinese medicine," *Chinese Health Statistics*, vol. 6, pp. 10-12, 2004.
- [15] J. Junzhong, L. Chunnian, and Y. Jing, "A fast Bayesian network structure learning algorithm," *Computer Research and Development*, vol. 44, no. 3, pp. 412-419, 2007.
- [16] J. Junzhong, H. Renbing, Z. Hongxun, and L. Tsunnian, "A hybrid Bayesian net structure learning algorithm," *Computer Research and Development*, vol. 9, pp. 1498-1507, 2009.
- [17] Y. Tan, D. Q. Geng, and X. L. Huang, "Prediction model of ischemic stroke recurrence using artificial neural network," *China Health Statistics*, vol. 5, pp. 687-689, 2013.
- [18] W. Shuyan, G. Guohua, and L. Bingchun, "Application of decision tree algorithm in medical image data mining," *Journal of Northwestern University (Natural Science Edition)*, vol. 3, pp. 262-265, 2005.
- [19] X. Lei, H. Jia, M. Hong et al., "Application of information entropy-based decision trees to the identification of chronic gastritis in Chinese medicine," *China Health Statistics*, vol. 6, pp. 10-12, 2004.
- [20] L. Breidman, "Bagging predictors," *Machine Learning*, vol. 24, no. 2, pp. 123-140, 1996.
- [21] Z.-G. Liu, Z.-G. Li, C. Tang, R.-C. Wang, and H.-P. Huang, "Fuzzy multi-objective algorithm based on wavelet transform," in *Proceedings of the 13th International Conference on Machine Learning*, pp. 148-156, USA, 1996.
- [22] W. Shuyan and W. Xiaomei, "Research on the application of association rule mining algorithm in classification," *Computer and Digital Engineering*, vol. 8, pp. 46-49, 2009.
- [23] S. B. Wu and W. C. Xu, "Application of multi-support association rules in web usage mining," *Computer Engineering and Applications*, vol. 31, pp. 168-171, 2005.



## Research Article

# Unilateral Biportal Endoscopic Discectomy versus Microendoscopic Discectomy for the Treatment of Lumbar Spinal Stenosis: A Systematic Review and Meta-Analysis

Yufei Niu, Zhen Shen, and Haoyang Li 

Department of Orthopaedics, Jincheng people's Hospital, Jincheng, China

Correspondence should be addressed to Haoyang Li; 2016120362@jou.edu.cn

Received 19 July 2022; Revised 12 August 2022; Accepted 26 August 2022; Published 21 September 2022

Academic Editor: Hangjun Che

Copyright © 2022 Yufei Niu et al. This is an open access article distributed under the Creative Commons Attribution License, which permits unrestricted use, distribution, and reproduction in any medium, provided the original work is properly cited.

**Objective.** In minimally invasive spinal surgery, the treatment of lumbar spinal stenosis with microendoscopic discectomy (MED) or unilateral biportal endoscopic discectomy (UBED) shows effective results, but which is more effective is controversial. Our study aimed to evaluate the efficacy and safety of UBED versus MED in the treatment of lumbar spinal stenosis by a systematic review and meta-analysis, so as to provide reference for the promotion of UBED in clinical practice. **Methods.** The multiple databases like PubMed, EMBASE, Web of Science, Cochrane Library, Chinese National Knowledge Databases, Chinese BioMedical Database, and Wanfang Database were used to search for the relevant studies. Review Manager 5.4 was adopted to estimate the effects of the results among selected articles. Odds ratio (OR) and mean difference (MD) with 95% confidence intervals (CIs) were used to estimate the overall pooled effect. Subgroup analysis, forest plots, funnel plots and Egger's test for the articles included were also conducted. **Results.** Three randomized clinical trials and seven cohort studies were finally retrieved, these studies included 685 and 829 patients in the UBED and MED groups, respectively. There were no differences in terms of operation time (MD = -0.92,  $P = 0.72$ ), estimated blood loss (MD = -26.31,  $P = 0.08$ ), complications (MD = 0.81,  $P = 0.38$ ) and Oswestry Disability Index (ODI) score ( $P > 0.05$  in four subgroup) between the two groups. The visual analog scale (VAS) score of back pain in the UBED group was better than MED group only at 6 months (MD = -0.23,  $P = 0.006$ ) after operation, the VAS score of leg pain in the UBED group was better than that of MED group at 3 months (MD = -0.22,  $P = 0.002$ ) and 6 months (MD = -0.24,  $P = 0.006$ ) after operation, the UBED group had a less postoperative length of stay than the MED group (MD = -1.85,  $P < 0.001$ ). The bias analysis showed that there was no potential publication bias in the included literature. **Conclusion.** This study showed that compared with MED, UBED has the advantages of short hospital stay and good short-term curative effect, but there is no significant difference in long-term efficacy and safety, they can be replaced by each other in clinical application.

## 1. Introduction

Lumbar spinal stenosis is a common disease in spinal surgery, which tends to occur in middle-aged and elderly patients over 50 years old [1]. With the increase of age, the incidence rate also increases. It is considered to be the second largest cause of low back and leg pain in middle-aged and elderly people [2, 3]. Lumbar spinal stenosis refers to the changes in the morphology and tissue structure of lumbar bones and soft tissues (vertebral body, facet joint, lamina etc.) caused by various reasons, it usually results in stenosis of central spinal canal and lateral recess, causes nerve root

and/or cauda equina nerve to be stimulated or compressed, and results in clinical symptoms such as lower limb radiative pain and intermittent claudication, which seriously affects the quality of life of patients [4].

Traditional open laminectomy has a definite effect, but the operation extensively destroys the soft tissue structure, which will lead to long-term back heaviness and soreness, even some patients with poor physical conditions cannot tolerate spinal surgery [5]. At present, the clinical treatment of lumbar spinal stenosis is mainly single channel endoscopic surgery, including percutaneous foraminotomy endoscopic surgery and microendoscopic discectomy

(MED) [6, 7]. These methods can completely preserve the physiological structure of the lumbar spine with small surgical trauma and fast postoperative recovery [8, 9]. However, there are also defects such as small scope of visual field under the microscope, limited operation under the microscope, and it is difficult to expand the range of decompression when necessary [10, 11].

Unilateral biportal endoscopic discectomy (UBED) is a new minimally invasive surgery for the treatment of lumbar spinal stenosis in recent years [12]. In the past decade, UBED has received the attention of clinicians under the improvement of Korean scholars [13–16]. This surgical method constructs two channels, one is implanted into the endoscope to provide vision, and the other is implanted into the surgical instrument operation, which combines the advantages of traditional minimally invasive surgery and open surgery [17].

Compared with conventional surgery for lumbar spinal stenosis, minimally invasive spinal surgery using microscope or endoscopic approach shows more effective clinical results [18, 19]. However, in minimally invasive spinal surgery, there has been a controversy about which is more effective in the treatment of lumbar spinal stenosis with microscope or endoscope [20, 21]. Through the systematic review and meta-analysis, this paper evaluated and compared the effect results of UBED versus MED in minimally invasive spinal surgery, and evaluated the effectiveness and safety of the two methods.

## 2. Methods

**2.1. Literature Search Strategy.** We searched the PubMed, EMBASE, Web of Science, Cochrane Library, Chinese National Knowledge Databases, Chinese BioMedical Database, and Wanfang Database, which were assessed up to June 2022 with the following keywords: (“unilateral biportal endoscopic discectomy” or “unilateral biportal endoscopic spinal surgery” or “unilateral biportal endoscopic laminectomy”) and (“microendoscopic discectomy” or “microscopic lumbar decompression laminectomy” or “micro endoscopic spine surgery”) and (“lumbar spinal stenosis”). There were no restrictions on the language of publication in document retrieval. We retrieved potentially relevant articles and screened their reference lists to find studies that our search strategy may have missed.

**2.2. Study Selection.** The potential relevant studies identified were retrieved and the respective full text analyzed for their eligibility according the PICOS criteria: (P) Population: patients with the lumbar spinal stenosis. (I) Intervention: patients underwent surgical corrections using the surgical approaches of unilateral biportal endoscopic discectomy (UBED). (C) Comparison: microendoscopic discectomy (MED). (O) Outcomes: intraoperative and postoperative indexes (operation time, estimated blood loss, postoperative length of stay, postoperative complication rate) and effectiveness indicators, such as the visual analog scale (VAS) score of back pain and leg pain, the Oswestry Disability Index (ODI) score. (S) Study design: clinical human studies,

including randomized controlled trials (RCTs), retrospective cohort studies (RCSs), prospective cohort studies (PCSs) and case series.

**2.3. Data Extraction and Quality Assessment.** Two pairs of reviewers (Y Niu, Z Shen) independently screened titles, abstracts, and full-text articles of potentially eligible studies and resolved disagreement through discussion. The first author and the year of the study were extracted as general information. Parameters, such as country, study design, population number, gender, age, time of follow-up and study duration, were utilized to analyze the study characteristics.

The Newcastle Ottawa scale (NOS) and the Cochrane Collaboration’s tool were used to evaluate the methodological quality and bias risk of non randomized controlled trials (nRCTs) and RCTs, respectively.

**2.4. Statistical Analysis.** Meta analysis was performed by using Review Manager 5.4 (Nordic Cochrane Centre). Briefly, we utilized the odds ratio (OR) with 95% confidence intervals (CIs) for dichotomous variables and mean difference (MD) with 95% CIs for continuous variables to estimate the overall pooled effect. We conducted the subgroup analysis according to the different follow-up time. The heterogeneity among trials evaluated by the  $\chi^2$ -based Q testing (0.05 was set as the statistical significance cut-off for the test of heterogeneity) and  $I^2$  statistics ( $I^2 > 50\%$ ). In our analytical framework, fixed effect model or random-effect model was used depending on the absence ( $P > 0.05$  or  $I^2 < 50\%$ ) or presence of significant heterogeneity. Funnel plot and Egger’s test were used to show potential publication bias.

## 3. Results

**3.1. Search Process.** Figure 1 showed the process of screening articles for inclusion in the systematic review and meta-analysis. The search strategy resulted in a total of 820 articles from all databases. After duplicate elimination, 695 studies underwent titles and abstracts screening, leaving 96 articles for eligibility screening. After full-texts screening, 10 studies were finally included in our meta-analysis [22–31].

**3.2. Characteristics of the Included Studies.** The baseline characteristics of the patients included in the meta-analysis were reported in Table 1. This study included 3 RCTs [26, 29, 30], 5 RCSs [22, 23, 25, 27, 28] and 2 PCSs [24, 31], which included 685 patients treated with UBED and 829 patients treated with MED. The average age of each group was over 60. All the 10 articles were published from 2018 to 2021. The follow-up time were more than 6 months and the longest was more than 3 years.

**3.3. Results of Quality Assessment.** Finally, 3 RCTs and 7 cohort studies were included in this study. The Cochrane collaboration’s tool and NOS were used to carry out the quality assessment. The results were shown in Tables 2 and 3, respectively. The quality of the three RCTs was high, and there were no obvious risk of bias. The final scores of the seven cohort studies were higher than 7

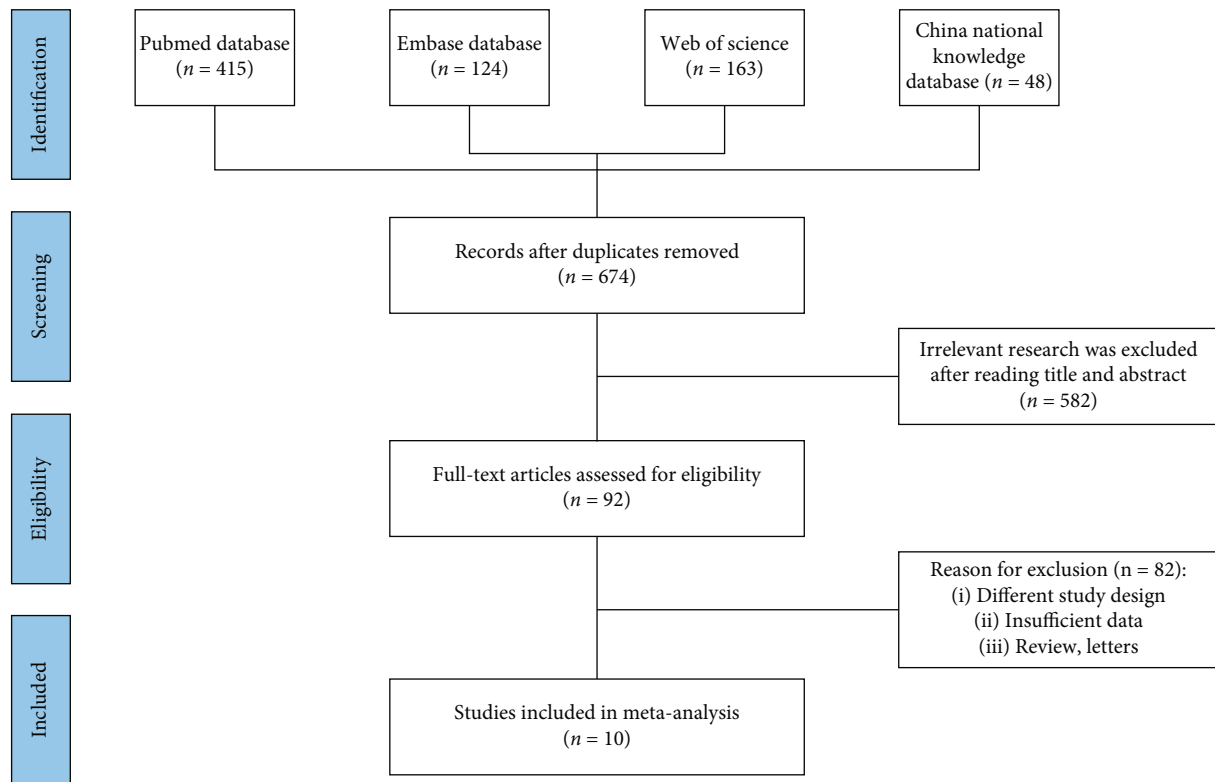


FIGURE 1: Schematic of the trial selection process.

TABLE 1: Characteristics of included studies.

Study	Country	Study design	No. of patients		Gender (M/F)		Age (years)		Follow-up (months)	Duration
			UBED	MED	UBED	MED	UBED	MED		
Heo [24]	Korea	PCS	46	42	18/28	16/26	65.8 ± 8.9	63.6 ± 10.5	>12	March 2016 to October 2017
Choi [22]	Korea	RCS	35	30	14/21	17/13	65.4 ± 11.8	65.2 ± 12.0	6	December 2013 to March 2015
Heo [23]	Korea	RCS	37	33	15/22	12/21	66.7 ± 9.4	63.4 ± 11.1	12	March 2016 to December 2017
Kang [26]	Korea	RCT	32	30	18/14	14/16	65.1 ± 8.6	67.2 ± 9.5	6	January 2015 to December 2016
McGrath [28]	USA	RCS	50	45	27/23	27/18	—	—	12	September 2014 to February 2017
Park [30]	Korea	RCT	32	32	13/19	18/14	66.2 (41 – 80)	67.1 (45 – 79)	12	November 2017 to June 2018
Rieger [31]	Germany	PCS	327	413	152/101	178/119	76 ± 10	78 ± 13	12~36	January 2012 to July 2017
Kim [27]	Korea	RCS	30	30	13/17	12/18	64.23 ± 5.26	66.20 ± 6.01	12	September 2015 to March 2017
Min [29]	Korea	RCT	54	35	27/27	19/16	65.74 ± 10.52	66.74 ± 7.96	>36	March 2015
Ito [25]	Japan	RCS	42	139	28/14	71/68	66.3 ± 12.3	65.0 ± 11.1	>6	November 2018 to June 2019

UBED, unilateral biportal endoscopic discectomy; MED, microendoscopic discectomy; PCS, prospective cohort study; RCS, retrospective cohort study; RCT, randomized controlled trial.

TABLE 2: Risk of bias of randomized controlled trials.

Study	Random allocation	Hidden distribution	Blind method	Incomplete outcome data	Selective reporting of results	Other bias	Quality level
Kang [26]	Low risk	Low risk	Low risk	Low risk	Low risk	Low risk	High
Park [30]	Low risk	Low risk	Low risk	Low risk	Low risk	Low risk	High
Min [29]	Low risk	Low risk	Low risk	Low risk	Low risk	Low risk	High

TABLE 3: Risk of bias of cohort studies.

Study	Representativeness of cohort	Selection Selection of nonexposed cohort	Ascertainment of exposure	Outcome lacking at the beginning	Comparability of cohorts	Outcome assessment	Outcomes Sufficient follow-up time	Follow up adequacy	Score*
Heo [24]	+	+	+	+	++	—	+	+	8
Choi [22]	+	+	+	+	++	+	+	+	9
Heo [23]	+	+	+	+	+	+	+	+	8
McGrath [28]	+	+	+	+	+	+	+	+	8
Rieger [31]	+	+	+	+	++	+	+	+	9
Kim [27]	+	+	+	+	+	—	+	+	7
Ito [25]	+	+	+	+	++	+	+	+	9

\*, The total score of NOS evaluation is 9 points; +, represents that the item has obtained the score; -, represents that the item has not been scored.

according to NOS, which represented that the bias of the 7 included literature was relatively small.

### 3.4. Primary Outcomes

**3.4.1. VAS (Back Pain).** Eight studies had data available to assess change in VAS of back pain. Although the overall combined effect showed that the VAS score (back pain) of UBED group was lower than that of MED group (MD = -0.36, 95% CI -0.66 to -0.05,  $P=0.02$ ) (Figure 2), according to the different follow-up time, the VAS score (back pain) in UBED group was significantly lower than that of MED group at 6 months (MD = -0.24, 95% CI -0.40 to -0.07,  $P=0.006$ ) after operation, but there was no difference between the two groups at 1 months (MD = -0.23, 95% CI -0.67 to 0.20,  $P=0.29$ ), 3 months (MD = -0.48, 95% CI -1.03 to 0.08,  $P=0.09$ ) and 1 year (MD = -0.31, 95% CI -1.01 to 0.39,  $P=0.38$ ) after operation.

**3.4.2. VAS (Leg Pain).** For VAS of leg pain, 7 studies reported it. Meta-analysis showed that there was no significant difference of VAS score (leg pain) between UBED group and MED group (MD = -0.31, 95% CI -0.74 to 0.12,  $P=0.15$ ) (Figure 3), however, after stratification according to the follow-up time, the subgroup meta-analysis showed that there was no significant difference of VAS score (leg pain) between the two group at 1 month (MD = -0.03, 95% CI -0.91 to 0.85,  $P=0.95$ ) and 1 year (MD = -0.37, 95% CI -1.35 to 0.61,  $P=0.45$ ) after operation, but the VAS score (leg pain) in UBED group was

lower than that in Med group at 3 months (MD = -0.22, 95% CI -0.35 to -0.08,  $P=0.002$ ) and 6 months (MD = -0.24, 95% CI -0.40 to -0.07,  $P=0.006$ ) after operation.

**3.4.3. ODI.** A total of 9 literature studies reported ODI. The overall combined effect showed that the ODI score of UBED group was lower than that of MED group (MD = -1.73, 95% CI -3.40 to -0.07,  $P=0.04$ ) (Figure 4). However, according to the hierarchical comparison of different follow-up times, it was found that there was no significant difference in ODI value between the two groups in 1 month (MD = -3.62, 95% CI -8.18 to 0.93,  $P=0.12$ ), 3 months (MD = -1.12, 95% CI -2.29 to 0.06,  $P=0.06$ ), 6 months (MD = -0.72, 95% CI -0.19 to 1.63,  $P=0.12$ ) and 1 year (MD = -2.59, 95% CI -6.92 to 1.75,  $P=0.24$ ) after operation.

### 3.5. Secondary Outcomes

**3.5.1. Operation Time.** Five studies comprising 1654 patients provided information regarding operative time. The UBED group showed no significant difference of operation time comparing to the MED group (MD = -0.92, 95% CI -5.97 to 4.13,  $P=0.72$ ) (Figure 5).

**3.5.2. Postoperative Length of Stay.** The postoperative length of stay was reported in 4 studies. The pooled data revealed that the postoperative length of stay was significantly shorter in the UBED group than the MED group (MD = -1.85, 95% CI -2.53 to -1.17,  $P<0.00001$ ) (Figure 6).

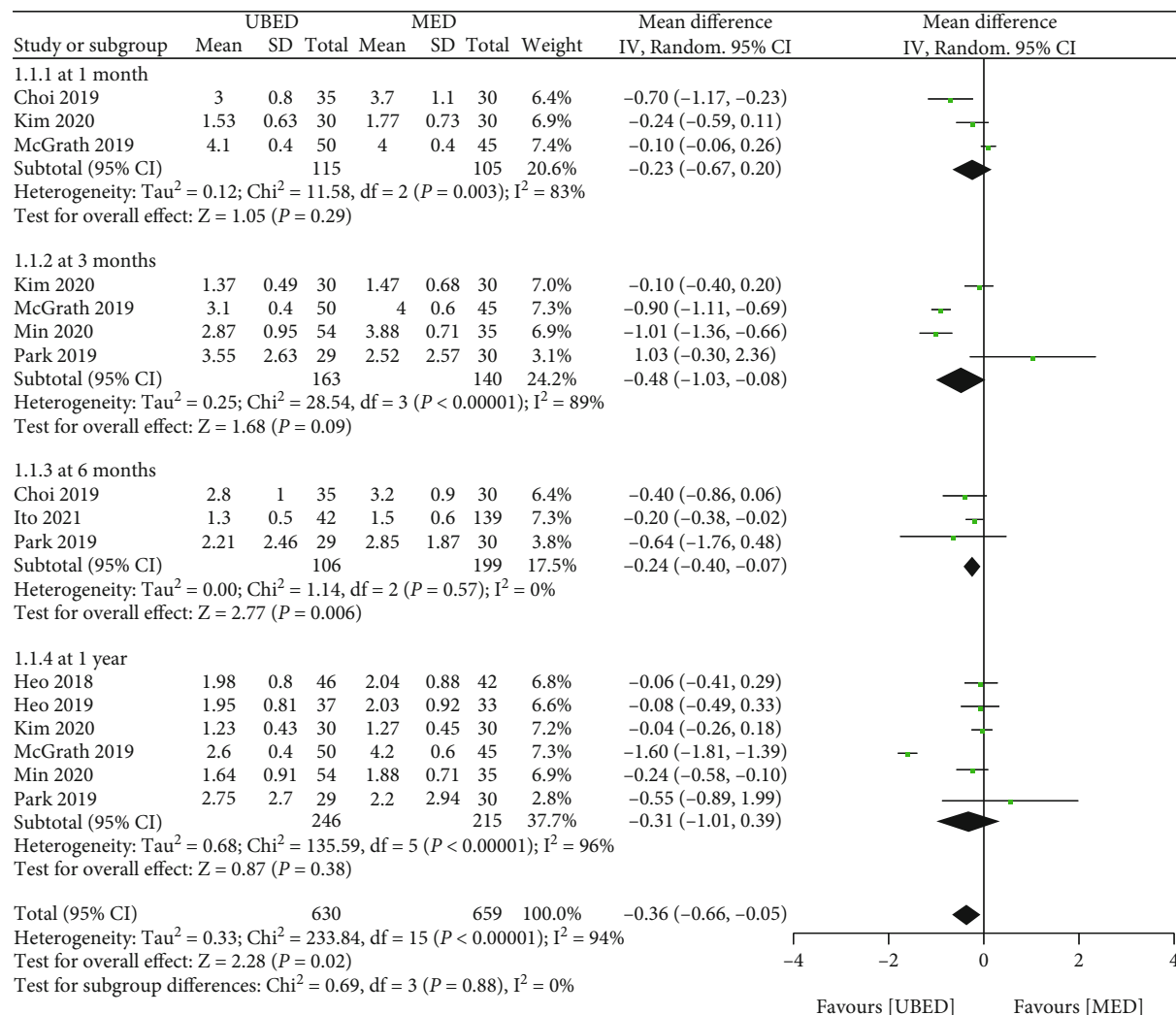


FIGURE 2: Forest plots of patient clinical outcomes: VAS of back pain. VAS, visual analog scale. UBED, unilateral biportal endoscopic discectomy; MED, microendoscopic discectomy.

**3.5.3. Estimated Blood Loss.** For the estimated blood loss, 4 included studies reported it. The pooled result showed that the UBED group had no significant difference of estimated blood loss than the MED group ( $MD = -26.31$ , 95% CI -55.47 to 2.85,  $P = 0.08$ ) (Figure 7).

**3.5.4. Complication.** The complication was reported in 6 studies. The pooled data revealed that no significant difference in the rate of complication was detected between the UBED group and the MED group ( $MD = 0.81$ , 95% CI 0.51 to 1.29,  $P = 0.38$ ) (Figure 8).

**3.6. Publication Bias.** Funnel plot was performed to qualitatively evaluate the publication bias for the complication rate. The funnel plot seemed to be asymmetric (Figure 9), but the  $P$  value of Egger's test of quantitative analysis was  $>0.05$ , indicating that there was no obvious publication bias.

## 4. Discussion

The purpose of surgical treatment of lumbar spinal stenosis is to completely decompress the "responsible segment", so that the compressed spinal cord and nerve roots can be effectively loosened, and at the same time, the overall stability of the spine can be destroyed as little as possible, so as to achieve the purpose of alleviating the symptoms of patients [32, 33]. Total laminectomy, which is commonly used in clinic, has the advantages of sufficient decompression, large operating space and clear vision, but it also has the disadvantages of large injury, long operation time and prone to lumbar instability or spondylolisthesis in the later stage [34]. Therefore, some patients need to perform spinal internal fixation and fusion at the same time, which prolongs the operation time and increases the cost of patients [35].

With the development of minimally invasive surgery, MED technology has gradually become a common method



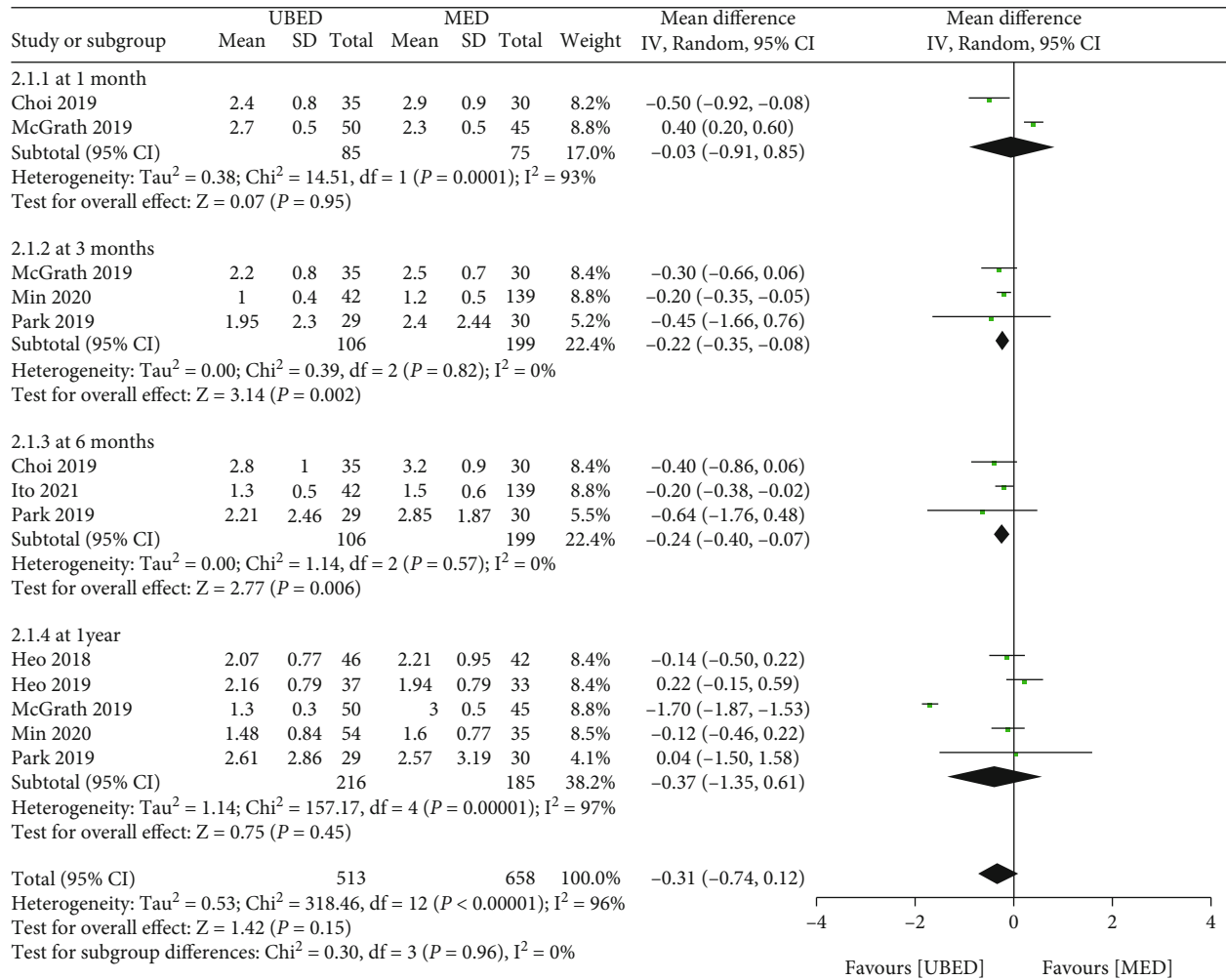


FIGURE 3: Forest plots of patient clinical outcomes: VAS of leg pain. VAS, visual analog scale. UBED, unilateral biportal endoscopic discectomy; MED, microendoscopic discectomy.

for the treatment of lumbar spinal stenosis [36]. It has the advantages of small incision, fast recovery, less bleeding, preservation of spinal soft tissue structure and so on [37]. However, the shortcomings of MED technology are also very obvious, such as the limited vision of surgery, and the limited range of motion of the instrument through a single channel. UBED combines the advantages of microscope and endoscope [38, 39]. UBED technology has two channels, one channel provides surgical field of vision and continuous flushing, and the other channel is used for instrument operation [40]. A separate operation channel increases the movable range of the operation, makes the operation easier, and also provides a good field of vision in the contralateral intervertebral foramen area [41, 42]. The continuous flushing function is conducive to controlling bleeding and providing a clearer surgical field of vision. UBED does not need a sleeve and will not restrict the use of instruments [43]. Conventional arthroscopic instruments and spinal open surgery instruments can be used, which can save costs [44].

In this study, the clinical outcome indicators of minimally invasive spinal surgery performed by UBED versus MED were combined analyzed, and a total of 10 literatures

were included. In terms of effectiveness, compared with MED group, the VAS score (leg pain) of UBED group was better than MED group only at 3 and 6 months after operation, while there was no difference in other follow-up time between the two groups; at 6 months after operation, the VAS score (back pain) of UBED group was better than that of the MED group, while there was no difference in other follow-up time between the two groups. At any follow-up time, there was no significant difference in ODI between the two groups. Among the surgery related indicators, the postoperative length of stay in the UBED group was significantly lower than that in the MED group, but there was no difference in operation time, estimated blood loss and complication rate. Tang's research specifically made a meta-analysis of the postoperative complications of minimally invasive spinal surgery performed by UBED and MED [45]. The results showed that there was no statistical difference in the total complications between the two groups, which was consistent with our research results. Moreover, Chen's study also made a grouping analysis of the detailed complications, the results showed that there was no difference in the incidence of related complications such as

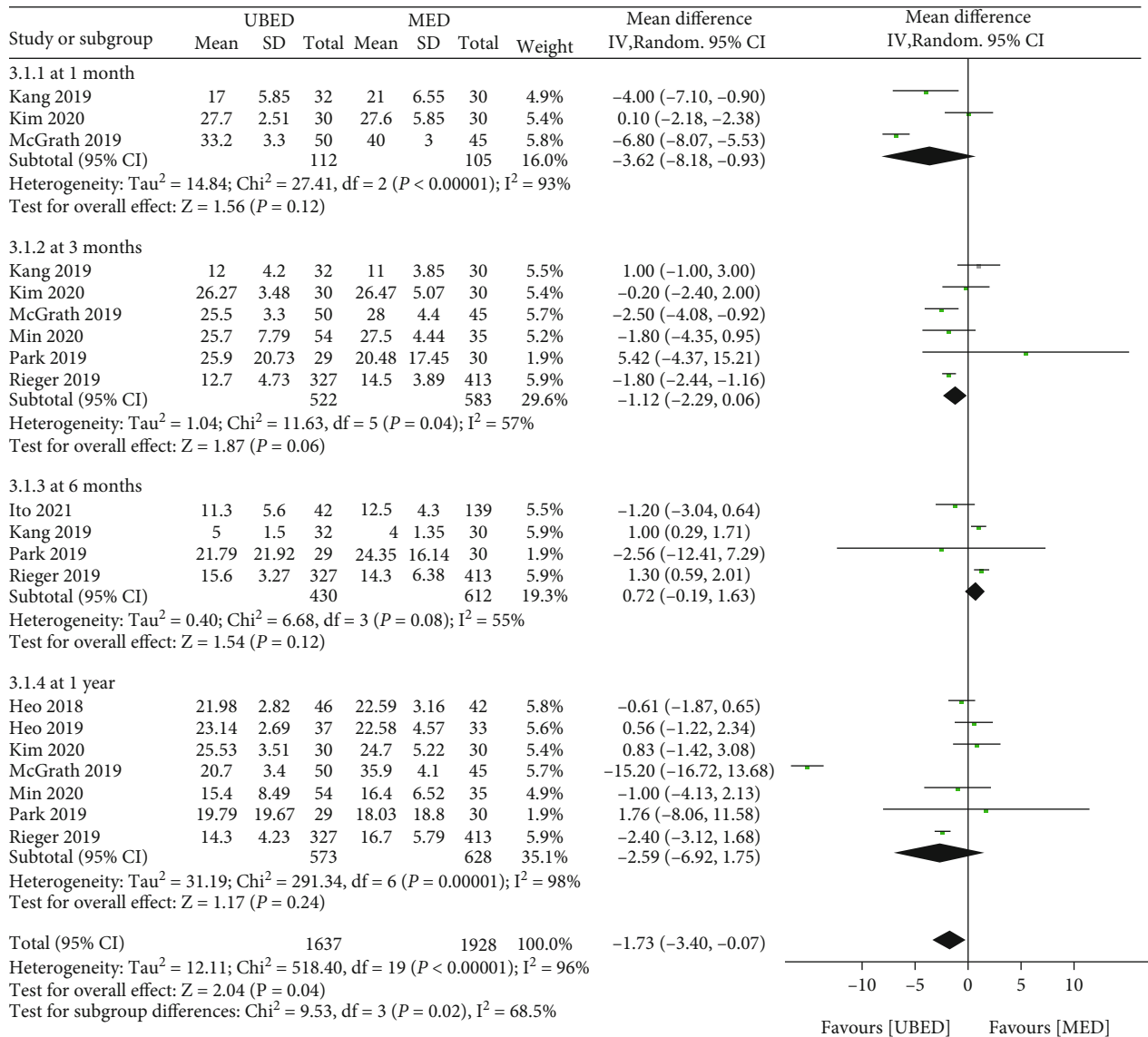


FIGURE 4: Forest plots of patient clinical outcomes: ODI. ODI, Oswestry Disability Index. UBED, unilateral biportal endoscopic discectomy; MED, microendoscopic discectomy.

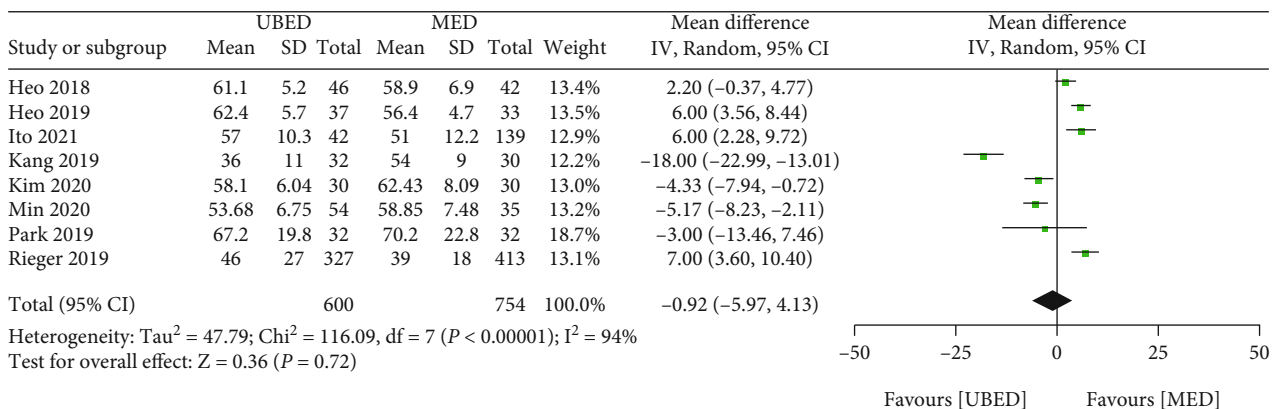


FIGURE 5: Forest plots of patient clinical outcomes: operation time. UBED, unilateral biportal endoscopic discectomy; MED, microendoscopic discectomy.

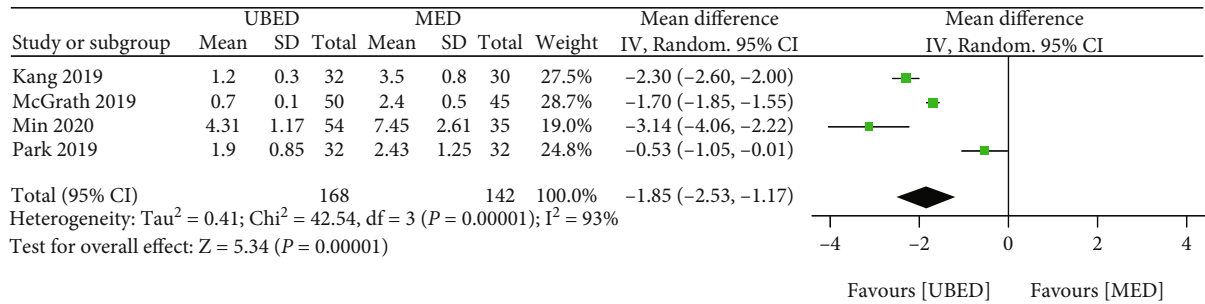


FIGURE 6: Forest plots of patient clinical outcomes: postoperative length of stay. UBED, unilateral biportal endoscopic discectomy; MED, microendoscopic discectomy.

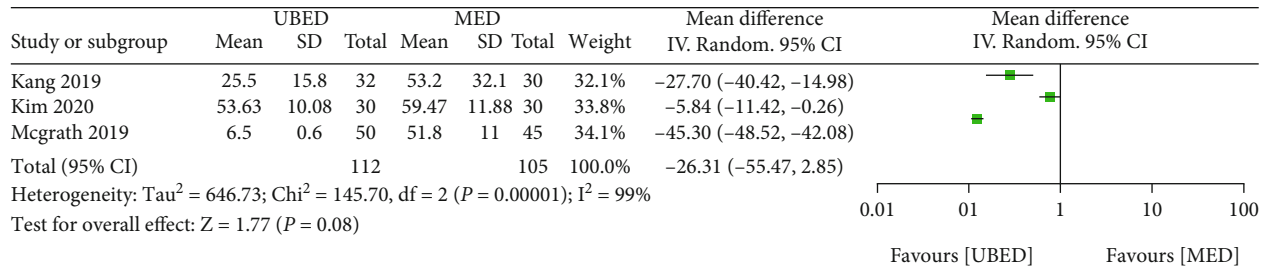


FIGURE 7: Forest plots of patient clinical outcomes: estimated blood loss.

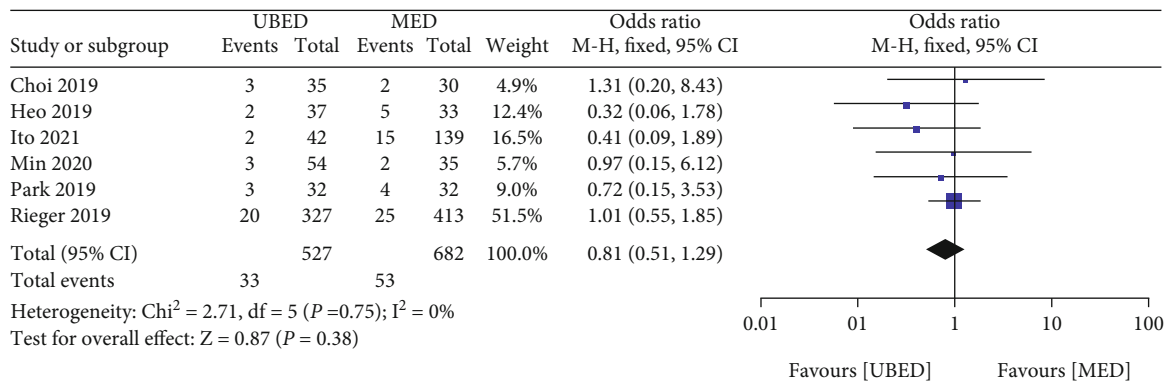


FIGURE 8: Forest plots of patient clinical outcomes: complication. UBED, unilateral biportal endoscopic discectomy; MED, microendoscopic discectomy.

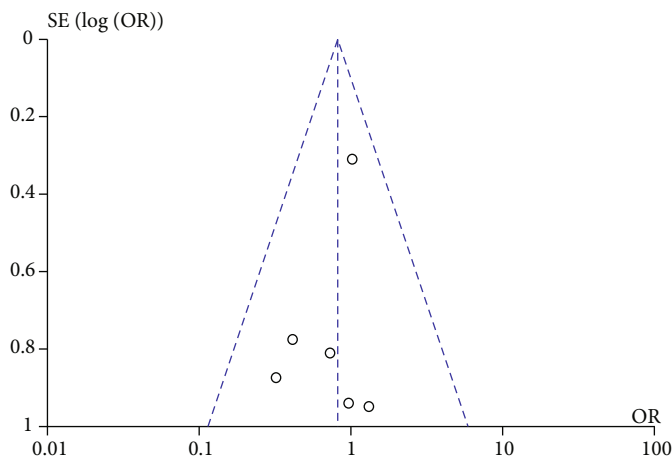


FIGURE 9: Funnel plot for potential publication bias of complication.

epidural hematoma, nerve root injury, dural sac injury and incomplete decompression [46].

There were some limitations in this meta-analysis. Firstly, the included literature included 3 RCTs and 7 cohort studies. More observational studies were included in this study, which will limit the quality of the meta-analysis. Secondly, among the 10 literatures included, 7 were from South Korea, which may lead to certain limitations in the extrapolation of results. In addition, due to the small number of included literatures, this study did not make a detailed analysis of different types of complications, and some outcome variables were included in fewer literatures, which will also affect the reliability of the final conclusion.

## 5. Conclusions

To sum up, UBED has a faster recovery time than MED in the treatment of lumbar spinal stenosis, and the short-term (3 months and 6 months after operation) surgical effect is better, but the follow-up of 1 month and 12 months after operation shows that there is no significant difference, indicating that UBED and MED have the same curative effect in the treatment of lumbar spinal stenosis. However, due to the limitations of the quantity and quality of the included studies, the above conclusions still need to be confirmed by more high-quality studies.

## Abbreviations

MED:	Microendoscopic discectomy
UBED:	Unilateral biportal endoscopic discectomy
OR:	Odds ratio
MD:	Mean difference
CIs:	Confidence intervals
ODI:	Oswestry disability index
VAS:	Visual analog scale
PICOS:	Population, intervention, comparison, outcomes, study design
RCTs:	Randomized controlled trials
RCs:	Retrospective cohort studies
PCs:	Prospective cohort studies
NOS:	Newcastle Ottawa scale.

## Data Availability

The datasets used and analyzed during the current study are available from the corresponding author upon reasonable request.

## Ethical Approval

The authors are accountable for all aspects of the work in ensuring that questions related to the accuracy or integrity of any part of the work are appropriately investigated and resolved.

## Conflicts of Interest

The author(s) declare(s) that they have no conflicts of interest.

## References

- [1] R. K. Jensen, T. S. Jensen, B. Koes, and J. Hartvigsen, "Prevalence of lumbar spinal stenosis in general and clinical populations: a systematic review and meta-analysis," *European Spine Journal*, vol. 29, no. 17, pp. 252–272, 2020.
- [2] G. X. Lin, P. Huang, V. Kotheraanurak et al., "A systematic review of unilateral Biportal endoscopic spinal surgery: preliminary clinical results and complications," *World Neurosurgery*, vol. 125, no. 18, pp. 425–432, 2019.
- [3] H. Ma, B. Hai, M. Yan, X. Liu, and B. Zhu, "Evaluation of effectiveness of treatment strategies for degenerative lumbar spinal stenosis: a systematic review and network meta-analysis of clinical studies," *World Neurosurgery*, vol. 152, no. 18, pp. 95–106, 2021.
- [4] Y. Torudom and T. Dilokhuttakarn, "Two portal percutaneous endoscopic decompression for lumbar spinal stenosis: preliminary study," *Asian Spine Journal*, vol. 10, no. 2, pp. 335–342, 2016.
- [5] W. Bing, G. Lu, and W. Liu, "Analysis of the causes of intraoperative conversion to open surgery for full endoscopic interlaminar discectomy," *Chinese Journal of Spine & Spinal Cord*, vol. 14, no. 8, pp. 123–128, 2011.
- [6] J. E. Kim and D. J. Choi, "Unilateral biportal endoscopic decompression by 30° endoscopy in lumbar spinal stenosis: technical note and preliminary report," *Journal of Orthopaedics*, vol. 15, no. 2, pp. 366–371, 2018.
- [7] W. C. Zhang, L. Z. Zhong, C. Yuan, X. G. Yang, and H. J. Liu, "Treatment of lumbar spinal stenosis in the elder by microendoscopic discectomy," *China Journal of Orthopaedics and Traumatology*, vol. 24, no. 5, pp. 408–410, 2011.
- [8] L. Rodrigues and J. Natour, "Surgical treatment for lumbar spinal stenosis: a single-blinded randomized controlled trial," *Advances in Rheumatology*, vol. 61, no. 1, pp. 25–34, 2021.
- [9] M. S. Kang, H. J. Park, J. H. Hwang, J. E. Kim, and H. J. Chung, "Safety evaluation of Biportal endoscopic lumbar discectomy: assessment of cervical epidural pressure during surgery," *Spine*, vol. 45, no. 20, pp. E1349–E1356, 2020.
- [10] H. Aygun and K. Abdulshafi, "Unilateral Biportal endoscopy versus tubular microendoscopy in Management of Single Level Degenerative Lumbar Canal Stenosis: a prospective study," *Clinical Spine Surgery*, vol. 34, no. 6, pp. E323–E328, 2021.
- [11] A. Eich-Krohm, J. Piel, D. Schrage, and B. P. Robra, "Middle-term surgical outcomes of microscopic posterior decompression for far-out syndrome," *Journal of Neurological Surgery*, vol. 75, no. 2, pp. 79–83, 2014.
- [12] K. Li, K. Gao, T. Zhang, and C. L. Lv, "Comparison of percutaneous transforaminal endoscopic lumbar discectomy through unilateral versus bilateral approach for L3/4 or L4/5 lumbar disc herniation with bilateral symptoms: technical notes and a prospective randomized study," *European Spine Journal*, vol. 29, no. 7, pp. 1724–1732, 2020.
- [13] K. C. Choi, H. K. Shim, J. S. Kim et al., "Cost-effectiveness of microdiscectomy versus endoscopic discectomy for lumbar disc herniation," *The Spine Journal*, vol. 12, no. 25, pp. 242–251, 2019.
- [14] J. Hwa Eum, D. Hwa Heo, S. K. Son, and C. K. Park, "Percutaneous biportal endoscopic decompression for lumbar spinal stenosis: a technical note and preliminary clinical results," *Journal of Neurosurgery: Spine*, vol. 24, no. 4, pp. 602–607, 2016.

- [15] J. Kim, J. Park, S. W. Kim, J. K. Oh, and T. H. Kim, "Prevalence of sleep disturbance in patients with lumbar spinal stenosis and analysis of the risk factors," *The Spine Journal*, vol. 20, no. 8, pp. 654–662, 2020.
- [16] H. Habibi, A. Suzuki, K. Hayashi, H. Salimi, and H. Nakamura, "Expression and function of FGF9 in the hypertrophied ligamentum flavum of lumbar spinal stenosis patients," *The Spine Journal*, vol. 21, no. 6, pp. 487–495, 2021.
- [17] K. Yoshikane, K. Kikuchi, and K. Okazaki, "Lumbar endoscopic unilateral Laminotomy for bilateral decompression for lumbar spinal stenosis provides comparable clinical outcomes in patients with and without degenerative spondylolisthesis," *World Neurosurgery*, vol. 150, no. 8, pp. 1208–1217, 2021.
- [18] J. Zhu, J. Sun, R. Li, Y. Yu, and L. Zhang, "Fully endoscopic versus microscopic vascular decompression for hemifacial spasm: a retrospective cohort study," *Acta Neurochirurgica*, vol. 163, no. 9, pp. 2417–2423, 2021.
- [19] S. Pairuchvej, J. A. Muljadi, J. C. Ho, A. Arirachakaran, and J. Kongtharvonskul, "Full-endoscopic (bi-portal or uni-portal) versus microscopic lumbar decompression laminectomy in patients with spinal stenosis: systematic review and meta-analysis," *European Journal of Orthopaedic Surgery & Traumatology*, vol. 30, no. 4, pp. 2604–2621, 2019.
- [20] A. Merter, O. Karaeminogullari, and M. Shibayama, "Comparison of radiation exposure among three different endoscopic discectomy techniques for lumbar disc herniation," *World Neurosurgery*, vol. 139, no. 2, pp. 2502–2510, 2020.
- [21] M. Balolu and Z. Hüseyin, "Comparison of physical therapy follow-up of patients with operated and non-operated lumbar spinal stenosis according to the Nottingham health profile-pain scale," *Open Journal of Modern Neurosurgery*, vol. 11, no. 4, pp. 234–241, 2021.
- [22] D. Choi and J. Kim, "Efficacy of Biportal endoscopic spine surgery for lumbar spinal stenosis," *Clinics in Orthopedic Surgery*, vol. 11, no. 1, pp. 82–88, 2019.
- [23] D. H. Heo, D. C. Lee, and C. K. Park, "Comparative analysis of three types of minimally invasive decompressive surgery for lumbar central stenosis: biportal endoscopy, uniportal endoscopy, and microsurgery," *Neurosurgical Focus*, vol. 46, no. 5, p. E9, 2019.
- [24] D. H. Heo, J. Quillo-Olvera, and C. K. Park, "Can Percutaneous Biportal Endoscopic Surgery Achieve Enough Canal Decompression for Degenerative Lumbar Stenosis? Prospective Case-Control Study," *World Neurosurgery*, vol. 120, pp. e684–e689, 2018.
- [25] Z. Ito, M. Shibayama, S. Nakamura et al., "Clinical comparison of unilateral Biportal endoscopic laminectomy versus microendoscopic laminectomy for single-level laminectomy: a single-center, retrospective analysis," *World Neurosurgery*, vol. 148, pp. e581–e588, 2021.
- [26] T. Kang, S. Y. Park, C. H. Kang, S. H. Lee, J. H. Park, and S. W. Suh, "Is biportal technique/endoscopic spinal surgery satisfactory for lumbar spinal stenosis patients?," *Medicine*, vol. 98, no. 18, article e15451, 2019.
- [27] H. Kim, S. Choi, D. Shim, I. Lee, Y. Oh, and Y. Woo, "Advantages of new endoscopic unilateral laminectomy for bilateral decompression (ULBD) over conventional microscopic ULBD," *Clinics in Orthopedic Surgery*, vol. 12, no. 3, pp. 330–336, 2020.
- [28] L. B. McGrath, G. A. White-Dzuro, and C. P. Hofstetter, "Comparison of clinical outcomes following minimally invasive or lumbar endoscopic unilateral laminotomy for bilateral decompression," *Journal of Neurosurgery: Spine*, vol. 30, no. 4, pp. 491–499, 2019.
- [29] W. Min, J. Kim, D. Choi, E. J. Park, and J. Heo, "Clinical and radiological outcomes between biportal endoscopic decompression and microscopic decompression in lumbar spinal stenosis," *Journal of Orthopaedic Science*, vol. 25, no. 3, pp. 371–378, 2020.
- [30] S. M. Park, J. Park, H. S. Jang, Y. W. Heo, and J. S. Yeom, "Biportal endoscopic versus microscopic lumbar decompressive laminectomy in patients with spinal stenosis: A randomized controlled trial," *The Spine Journal*, vol. 20, no. 2, article e1016, 2019.
- [31] B. Rieger, K. H. Sitoci-Ficici, C. Reinshagen et al., "Endoscopic and microscopic segmental decompression via translaminar crossover spinal approach in elderly patients," *World Neurosurgery*, vol. 125, pp. e361–e371, 2019.
- [32] Y. H. Huang, F. C. Lien, L. Y. Chao, C. H. Lin, and S. H. Chen, "Full Endoscopic Uniportal Unilateral Laminotomy for Bilateral Decompression in Degenerative Lumbar Spinal Stenosis: Highlight of Ligamentum Flavum Detachment and Survey of Efficacy and Safety in 2 Years of Follow-up," *World Neurosurgery*, vol. 134, no. 5, pp. e672–e681, 2020.
- [33] S. Ayoub, A. G. Rajamohan, J. Acharya, J. Gross, and V. Patel, "Chronic tophaceous gout causing lumbar spinal stenosis," *Radiology Case Reports*, vol. 16, no. 2, pp. 237–240, 2021.
- [34] S. Ruetten, M. Komp, H. Merk, and G. Godolias, "Surgical treatment for lumbar lateral recess stenosis with the full-endoscopic interlaminar approach versus conventional microsurgical technique: a prospective, randomized, controlled study," *Journal of Neurosurgery: Spine*, vol. 10, no. 5, pp. 476–485, 2009.
- [35] C. Li, F. Ju, W. Li et al., "Efficacy and safety of unilateral biportal endoscopy compared with microscopic decompression in the treatment of lumbar spinal stenosis," *Medicine*, vol. 100, no. 50, article e27970, 2021.
- [36] M. Piazza and J. Lee, "Endoscopic and microscopic microvascular decompression," *Neurosurgery Clinics of North America*, vol. 27, no. 3, pp. 305–313, 2016.
- [37] T. Aihara, K. Endo, H. Suzuki, A. Kojima, and K. Yamamoto, "Long-Term Outcomes Following Lumbar Microendoscopic Decompression for Lumbar Spinal Stenosis with and without Degenerative Spondylolisthesis: Minimum 10-Year Follow-Up," *World Neurosurgery*, vol. 146, no. 3, article e2308, 2020.
- [38] X. Fang, X. Q. Zhuang, L. U. Sheng-Lin, D. O. Orthopedics, and G. N. Hospital, "A clinical study about the treatment of degenerative spinal canal stenosis by the micro endoscopic discectomy," *Laboratory Medicine and Clinic*, vol. 12, no. 8, pp. 1084–1085, 2015.
- [39] M. Sasaki, M. Abekura, S. Morris et al., "Microscopic bilateral decompression through unilateral laminotomy for lumbar canal stenosis in patients undergoing hemodialysis," *Journal of Neurosurgery: Spine*, vol. 5, no. 6, pp. 494–499, 2006.
- [40] M. Komp, P. Hahn, S. Oezdemir et al., "Bilateral spinal decompression of lumbar central stenosis with the full-endoscopic interlaminar versus microsurgical laminotomy technique: a prospective, randomized, controlled study," *Pain Physician*, vol. 18, no. 1, pp. 61–70, 2015.
- [41] M. Teli, A. Lovi, M. Brayda-Bruno et al., "Higher risk of dural tears and recurrent herniation with lumbar micro-endoscopic discectomy," *European Spine Journal*, vol. 19, no. 3, pp. 443–450, 2010.



- [42] C. H. Kim, C. K. Chung, Y. Choi et al., “Direct medical costs after surgical or nonsurgical treatment for degenerative lumbar spinal disease: a nationwide matched cohort study with a 10-year follow-up,” *PLoS One*, vol. 16, no. 3, pp. 2541–2552, 2021.
- [43] S. K. Kim, S. W. Park, B. C. Lim, and S. C. Lee, “Comparison of reoperation after fusion and after decompression for degenerative lumbar spinal stenosis: a single-center experience of 987 cases,” *Journal of Neurological Surgery*, vol. 81, no. 5, pp. 392–398, 2020.
- [44] H. Wu, W. D. Yu, R. Jiang, and Z. L. Gao, “Treatment of multilevel degenerative lumbar spinal stenosis with spondylolisthesis using a combination of microendoscopic discectomy and minimally invasive transforaminal lumbar interbody fusion,” *Experimental & Therapeutic Medicine*, vol. 18, no. 3, pp. 843–851, 2013.
- [45] S. Tang, T. N. Mok, Q. He et al., “Comparison of clinical and radiological outcomes of full-endoscopic versus microscopic lumbar decompression laminectomy for the treatment of lumbar spinal stenosis: a systematic review and meta-analysis,” *Annals of Palliative Medicine*, vol. 10, no. 10, pp. 10130–10146, 2021.
- [46] T. Chen, G. Zhou, Z. Chen, X. Yao, and D. Liu, “Biportal endoscopic decompression vs. microscopic decompression for lumbar canal stenosis: a systematic review and metaanalysis,” *Experimental and Therapeutic Medicine*, vol. 20, no. 3, pp. 1536–1547, 2020.

## Research Article

# Context Aware Convolutional Neural Network for Children Caries Diagnosis on Dental Panoramic Radiographs

Xiaojie Zhou <sup>1</sup>, Guoxia Yu <sup>1</sup>, Qiyue Yin,<sup>2</sup> Yan Liu,<sup>1</sup> Zhiling Zhang,<sup>1</sup> and Jie Sun<sup>1</sup>

<sup>1</sup>Department of Stomatology, Beijing Children's Hospital, Capital Medical University, National Center for Children's Health, China

<sup>2</sup>Institute of Automation, Chinese Academy of Sciences, China

Correspondence should be addressed to Guoxia Yu; yuguoxia@bch.com.cn

Received 12 May 2022; Revised 10 August 2022; Accepted 23 August 2022; Published 21 September 2022

Academic Editor: Shimin Wang

Copyright © 2022 Xiaojie Zhou et al. This is an open access article distributed under the Creative Commons Attribution License, which permits unrestricted use, distribution, and reproduction in any medium, provided the original work is properly cited.

The objective of this study is to improve traditional convolutional neural networks for more accurate children dental caries diagnosis on panoramic radiographs. A context aware convolutional neural network (CNN) is proposed by considering information among adjacent teeth, based on the fact that caries of teeth often affects each other due to the same growing environment. Specifically, when performing caries diagnosis on a tooth, information from its adjacent teeth will be collected and adaptively fused for final classification. Children panoramic radiographs of 210 patients with one or more caries and 94 patients without caries are utilized, among which there are a total of 6028 teeth with 3039 to be caries. The proposed context aware CNN outperforms typical CNN baseline with the accuracy, precision, recall, F1 score, and area-under-the-curve (AUC) being 0.8272, 0.8538, 0.8770, 0.8652, and 0.9005, respectively, showing potential to improve typical CNN instead of just copying them in previous works. Specially, the proposed method performs better than two five-year attending doctors for the second primary molar caries diagnosis. Considering the results obtained, it is beneficial to promote CNN based deep learning methods for assisting dentists for caries diagnosis in hospitals.

## 1. Introduction

Dental caries or called tooth decay is a prevalent infectious chronic dental disease, which is caused by the interaction of bacteria and sugary foods on tooth enamel [1]. Usually, if a child suffers from dental caries in the primary dentition, the probability of infections in the permanent dentition increases [2]. Due to above immediate and potential long-time damage to oral health, dental caries should be given enough attention in children oral health [3]. Fortunately, dental caries is preventable and once detected can be cured and may be reversed in the early stages [4].

X-ray radiography is one of the most important approaches that help radiologists to diagnose caries, especially for teeth that are hard to be detected by visual inspection [5, 6]. Generally, there are several popular dental x-rays that can be utilized for children caries detection [7–9], e.g., bitewing, panoramic, and periapical. Recently, panoramic

radiography is widely utilized for dental caries diagnosis because of several advantages [10, 11]. Apart from a low radiation dose and high patient comfort, panoramic radiography consists of the entire patient dentition, based on which, caries can be diagnosed for each tooth in a single image [12].

However, panoramic radiographs of children are usually with primary or mixed dentition along with surrounding bones and jaw structure, making automatic caries diagnosis a hard problem [13]. To perform caries diagnosis on a panoramic radiography, there are often two possible steps [14, 15]: (1) extract all teeth to make a tooth isolate from others and (2) diagnose whether a tooth has decay. To extract teeth in panoramic radiographs, several works have been proposed based on conventional edge detection methods [16], genetic algorithms [17], and the most popular CNN networks [18–20]. The performance of tooth extraction is very important for caries recognition, and usually, a nurse or a

trained data annotation worker could accomplish such step, so we move our focus on step two, which requires experience from expert dentist.

To perform caries classification on each tooth image, early studies extract statistical characteristics from the caries and normal tooth images and make a decision by discovering differences between them or by training classifiers. For example, Saravanan et al. [21] found that pixel intensities of caries and normal tooth are concentrated in different ranges, and spectrum of a decayed tooth has high frequency components in the spectral components compared with that of normal tooth. Virupaiah and Sathyanarayana [22] utilized Gaussian low pass filter to preprocess dental images, based on which, statistical features are extracted and used by support vector machine classifier for caries classification. Recently, with the breakthrough of deep learning [23, 24], especially its outstanding performances of image analysis based on CNN technology [25, 26], several works have been proposed for panoramic radiography caries diagnosis based on CNN [12, 14, 27–29].

Overall, most of previous CNN based panoramic radiography caries detection methods just utilize popular CNN architectures and put their focus on testing CNN performance or achieving efficient parameters transfer. For example, Vinayahalingam et al. [27] verified MobileNet V2 network on classifying caries of third molar. Bui et al. [14] tested the performance of several typical CNN frameworks on panoramic radiography caries detection, including Alexnet, GoogLeNet, VGG16, VGG19, Resnet18, Resnet50, Resnet101, and Xception networks. Haghanifar et al. [12] utilized CapsNet for binary caries classification and used transfer learning for feature extraction. To the best of our knowledge, none of previous works consider a tooth caries predication using general knowledge of the field, e.g., information from its adjacent teeth, which we claim to be important because caries of teeth often affects each other due to the same growing environment.

Therefore, this study is aimed at proposing a novel context aware CNN for more accurate caries diagnosis of primary dentition on dental panoramic radiographs, by considering general knowledge of caries, i.e., collecting and adaptively fusing information from adjacent teeth to help diagnosis. Specifically, the proposed context aware CNN adopts a pooling strategy to collect information from adjacent teeth and utilizes an attention mechanism for current and adjacent teeth information fusion. Compared with conventional CNN frameworks, our method can be a plug-in component to improve those frameworks, based on which, those CNN frameworks can be enhanced to gather enough useful information for caries diagnosis. In summary, our method provides a framework to improve caries classification performance, which will be shown in the Results Section.

## 2. Materials and Methods

**2.1. Ethics Statement.** This study was conducted with the approval of the Institutional Review Board (IRB) of Beijing Children's Hospital, Capital Medical University, National

Center for Children's Health (IRB No.: [2022]-E-044-R). This study was a noninterventional study, and no-clinical trial was performed.

**2.2. Materials.** This study was performed on panoramic radiographs of patients in Beijing Children's Hospital, Capital Medical University, National Center for Children's Health from December 2015 to December 2021. Patients diagnosed with one or more caries (decided by the diagnostic report) via panoramic radiograph were selected as part of the database. Besides, dental age-matched patients without caries (decided by five-years attending doctors) were selected from the same hospital and time period to serve as reference data. In total, there are 210 panoramic radiographs with at least one tooth caries and 94 without caries. In the above 304 panoramic radiographs, there are 6028 teeth, among which there are 3039 and 2989 teeth with and without caries, respectively. Note that some teeth are missing, but we keep those panoramic radiographs and just ignore those teeth positions. All panoramic radiographs are JPEG format with size around  $2441 \times 1150$  pixels.

### 2.3. Methods

**2.3.1. Data Preprocessing.** A panoramic radiograph consists of all the teeth, which should be extracted because dental diagnosis is usually performed for each individual tooth. Teeth extraction is out of the scope of this study, which can be accomplished by dentist, nurse, or trained data annotation workers. Based on several mature annotation tools such as via (<https://www.robots.ox.ac.uk/vgg/software/via/>), extracting each tooth is easily performed as shown in Figure 1.

It should be noted that teeth are diverse in shape and size, so we do not use the same sized rectangular box for all the teeth, leading to various input sizes for CNN model (tooth image should be resized before fed into CNN). Specially, when a tooth is missing in a panoramic radiograph, we leave it out of our database. After the tooth extraction process, we obtain a database consisting of all the teeth, based on which, we split the database into training, validation, and test sets. More details are summarized in Table 1.

**2.3.2. A Typical CNN Baseline.** Resnet [30] is one of the most successful CNN architectures for image analysis, based on which, various computer vision tasks have reached state-of-the-art performance. Overall, Resnet utilizes residual block to alleviate gradient vanishing/exploding when increasing the number of layers, i.e., depth of the CNN. Recently, Resnet has been applied for caries diagnosis, and relatively good performance has been obtained [14]. In our model, Resnet (Resnet18 with 18 trainable layers) is utilized as a baseline method and a modular to form context aware CNN, which will be elaborated in the next subsection.

**2.3.3. Context Aware CNN.** The aim of our proposed method is to improve caries classification performance. Considering teeth in the same mouth share the same growing environment, it is natural that if one tooth has dental caries, the probability of being caries of its adjacent teeth will be greatly

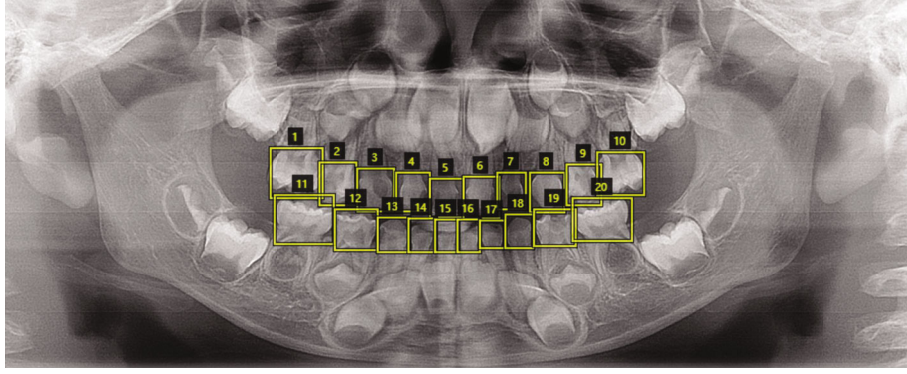


FIGURE 1: Extraction of each tooth on a panoramic radiograph.

TABLE 1: Data characteristics in this study.

Characteristics	Values
Total, with, and without caries panoramic radiograph numbers	304, 210, 94
Total, caries, and normal teeth numbers	6028, 3039, 2989
Training, validation, and test panoramic radiograph numbers	244, 30, 30
Training of total, caries, and normal teeth numbers	4833, 2432, 2401
Validation of total, caries, and normal teeth numbers	599, 320, 279
Test of total, caries, and normal teeth numbers	596, 287, 309

increased. Based on such intuitive assumption, an idea of promoting caries classification performance is to encode the above information when developing CNN models. Accordingly, we propose a context aware CNN, and the overall framework is shown in Figure 2.

In the proposed model, there are three key steps: (1) current tooth and its adjacent teeth are fed into the Resnet model for higher level representations extraction; (2) representations of the adjacent teeth are merged through pooling operation to obtain an adjacent representation; and (3) current and adjacent representations are adaptively fused through attention network for final representation learning, based on which a classifier layer is adopted for final caries predication. Noted that we leave out the classifier layer of Resnet for high level representations extraction, and pooling is selected as average pooling.

Mathematically, suppose the higher level representations of the current tooth and its  $k_{th}$  adjacent tooth (using the same Resnet for representation extraction) are  $r_c$  and  $r_{ak}$ ,  $k = 1, \dots, K$ , respectively, then, the adjacent representation  $r_a$  by merging all the  $K$  neighbors is calculated as

$$r_a = \text{pooling}(r_{a1}, \dots, r_{aK}). \quad (1)$$

By bringing in an extra multilayer perceptron network, we feed the network with concatenation of current and adjacent representations and obtain a weight  $\alpha$  for the current representation based on sigmoid activation function:

$$\alpha = \text{sigmoid}(W_2 \times \text{sigmoid}(W_1 \times ([r_c, r_a]) + b_1) + b_2), \quad (2)$$

where  $W_1$ ,  $W_2$ ,  $b_1$ , and  $b_2$  are parameters of the multilayer perceptron network. Then, the final representation  $r_f$  of the current tooth is calculated by:

$$r_f = \alpha \times r_c + (1 - \alpha) \times r_a. \quad (3)$$

$r_f$  will be fed into a softmax activated classifier layer for caries predication.

**2.4. Network Training.** In our database, there are 6028 teeth, which is big enough to train the deep neural networks, so we use no pretraining and just train the typical CNN baseline and our context aware CNN end to end. Contrast enhancement, adjusting the intensity of each pixel based on its relative magnitude with respect to the bilateral filter, is set to be 1.5 times, which we found is useful for caries classification. As for the data augmentation, we found no improvements can be obtained, so no data augmentation is utilized.

**2.5. Training Configuration.** The server used is configured with Intel(R) Xeon(R) Gold 6240R CPU and NVIDIA RTX 2080 Ti GPU (12GB ram), and the system is CentOS Linux release 7.8.2003. As for the hyperparameters, the network parameters are iterated for up to 10000 epochs using the Adam optimizer. The mini-batch size and the learning rate are set as 32 and  $10^{-3}$ , respectively. We select the model with the best performance on the validation set and then deployed to obtain the diagnosis results on the test set. Finally, the number of selected neighbors is set to be 3, and we will test the influence of varying numbers of neighbors in the following experiments.

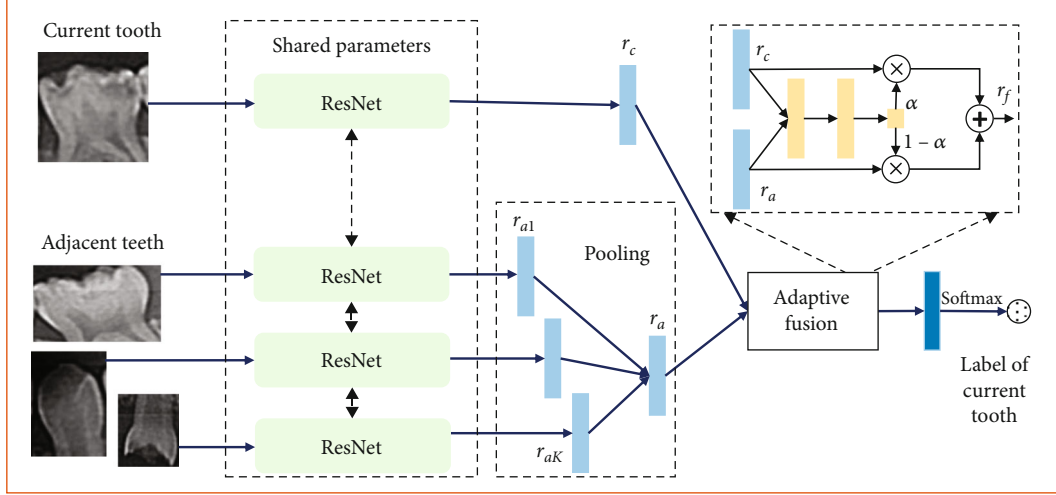


FIGURE 2: Overall framework of the proposed context aware CNN.

**2.6. Diagnostic Performance Evaluation.** Similar with previous works, five classical metrics are adopted for performance evaluation, i.e., accuracy, precision, recall,  $F1$ -score, and AUC. We use TP, FP, FN, and TN to represent classification true positive, false positive, false negative, and true negative, respectively; then, the metrics are calculated as

$$\text{Accuracy} = \frac{\text{TP} + \text{TN}}{\text{TP} + \text{TN} + \text{FP} + \text{FN}}, \quad (4)$$

$$\text{Precision} = \frac{\text{TP}}{\text{TP} + \text{FP}}, \quad (5)$$

$$\text{Recall} = \frac{\text{TP}}{\text{TP} + \text{FN}}, \quad (6)$$

$$F1 = \frac{2 \times \text{Precision} \times \text{Recall}}{\text{Precision} + \text{Recall}}. \quad (7)$$

As for the AUC, it is the area under the receiver operating characteristic (ROC) curve. Noted for all the metrics, higher values represent a better performance.

### 3. Results

**3.1. Diagnosis Performance.** Table 2 details the caries classification performance of the proposed context aware CNN model and the typical CNN baseline. Due to the consideration of context information, our method outperforms the typical CNN baseline for about 5 to 7 percentages in terms of accuracy, precision, recall, and  $F1$ . Figure 3 displays the ROC curves of the two methods with the area under the curve values, which again validates the helpfulness of utilizing context information for caries diagnosis.

To further verify the advantage of our proposed method, we show the classification accuracy for each tooth, as shown in Figure 4. It can be seen that our method outperforms the typical CNN baseline for most tooth positions. Specially, improvements against typical CNN baseline for teeth 54, 51, 63, 64, 65, and 81 are larger than 10 percentages, and up to about 17 percentage for tooth 71.

TABLE 2: Performance comparison between the proposed context aware CNN (CA-CNN) and the typical CNN baseline (CNN).

Methods	Accuracy	Precision	Recall	$F1$
CNN	0.7768	0.8056	0.8049	0.8052
CA-CNN	0.8272	0.8538	0.8770	0.8652

**3.2. Parameter Sensitivity.** In the proposed context aware CNN model, there is an important hyperparameter that controls how much context information is adopted. In this subsection, we change the neighbors selected to test the influence of this hyperparameter to the final performance. Table 3 displays the results with neighbors selected as 2, 3, and 5, respectively. Taking tooth position 51 as an example, when the number of neighbors is 2, teeth 52 and 61 are selected; when the number of neighbors is 3, teeth 52, 61, and 81 are considered; when the number of neighbors is 5, teeth 52, 61, 81, 82, and 71 are selected. According to the results and Table 2, we can draw the following conclusions: (1) by considering the context information, caries classification performance can be improved no matter what the numbers of neighbors are selected (see CNN results in Table 2), and (2) when the number of neighbors is 3, best performance can be obtained. This is because with less neighbors considered, not enough information is utilized, but with much more neighbors selected, such information may cause extra complications.

**3.3. Comparative Evaluation of the Abilities with Human.** The diagnosis performance of human evaluators (two five-years attending doctors) and the proposed context aware CNN is presented in Table 4. It can be seen that the average classification performance of human evaluators is higher than that of the proposed method and the currently mainstream CNN baseline (see CNN results in Table 2). However, the time used for a panoramic radiograph image diagnosis of the proposed method is much less than that of human evaluators.



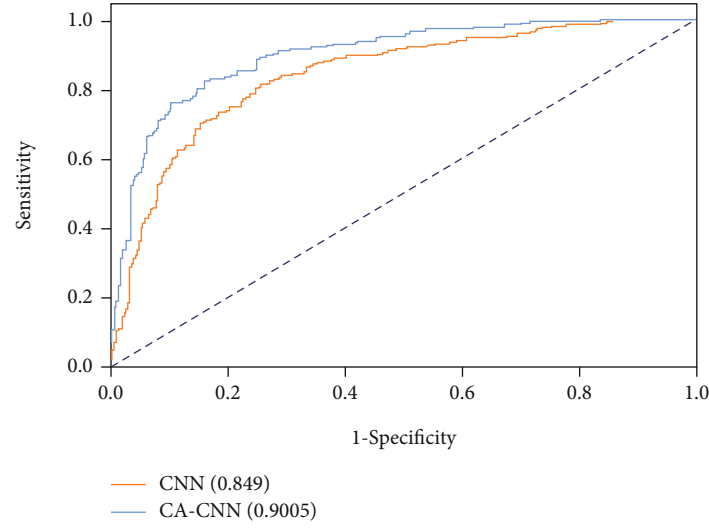


FIGURE 3: Receiver operating characteristic (ROC) curves of the proposed context aware CNN (CA-CNN) and the typical CNN baseline (CNN). Numbers in parentheses show the area under the curve (AUC) values.

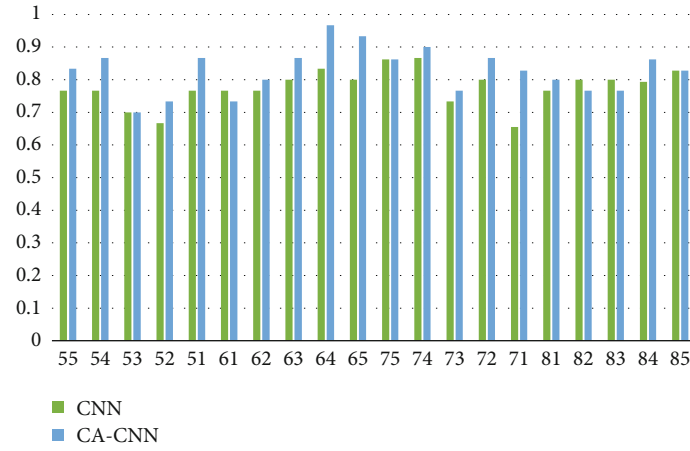


FIGURE 4: Classification accuracy of each tooth for our context aware CNN (CA-CNN) and the typical CNN baseline (CNN). Numbers in the horizontal ordinate denote the tooth positions.

TABLE 3: Influence of the numbers of neighbors selected in the proposed context aware CNN (CA-CNN). CA-CNN-X means X neighbors being selected.

Metrics	Accuracy	Precision	Recall	<i>F1</i>	AUC
CA-CNN-2	0.8020	0.8051	0.8155	0.8103	0.8537
CA-CNN-3	0.8272	0.8538	0.8770	0.8652	0.9005
CA-CNN-5	0.8104	0.8452	0.8738	0.8593	0.8725

TABLE 4: Comparison of the classification performance and average testing time of a dental panoramic radiograph image between the proposed context aware CNN (CA-CNN) and two five-year attending doctors (AD, average performance is reported).

Metrics	Accuracy	Precision	Recall	<i>F1</i>	Time (s)
CA-CNN	0.8272	0.8538	0.8770	0.8652	1.0619
AD	0.8842	0.8509	0.9417	0.8940	64.5000

TABLE 5: Classification accuracy of each tooth for the proposed context aware CNN (CA-CNN) and two five-year attending doctors (AD, average performance is reported).

Position	55	54	53	52	51
CA-CNN	0.8333	0.8667	0.7000	0.7333	0.8667
AD	0.7667	0.9000	0.9333	0.9333	0.9333
Position	61	62	63	64	65
CA-CNN	0.7333	0.8000	0.8667	0.9667	0.9333
AD	0.8333	0.9333	0.8667	0.8667	0.8333
Position	75	74	73	72	71
CA-CNN	0.8621	0.9000	0.7667	0.8667	0.8276
AD	0.8276	0.9000	0.8333	1.0000	0.9310
Position	81	82	83	84	85
CA-CNN	0.8000	0.7667	0.7667	0.8621	0.8276
AD	0.9333	0.9000	0.9000	0.9310	0.7241

Table 5 displays the diagnosis accuracy of each tooth position for the proposed method and the attending doctors. Even through the attending doctors perform better in most tooth positions, the model works much better on primary molars like tooth positions 55, 64, 65, 75, and 85. One possible reason is that mild caries on primary molars is hard to be detected by human due to the lower contrast.

#### 4. Discussion

With the breakthrough of deep learning, especially its outstanding performances in computer vision tasks based on CNN architecture, various advanced CNN approaches are developed. Benefited from the interdisciplinary study, researchers are borrowing the powerful CNN technology for stomatology imaging analysis. Very recently, CNN has been utilized for panoramic radiography caries detection, which is one of the most common diseases in oral health.

Various CNN methods have been tested for panoramic radiography caries classification, and relatively good performances have been obtained [12, 14, 27–29]. For example, Bui et al. [14] tested several typical CNN methods including the most famous Alexnet, Googlenet, VGG16, VGG19, Resnet18, Resnet50, Resnet101, and Xception networks. In their experimental results, values of accuracy, sensitivity, and specificity are 91.70%, 90.43%, and 92.67%, respectively. Based on the results, CNNs are promising for dentists and capable of wide-scale implementation caries detection in hospitals.

In this study, we aim to promote conventional CNN based methods for more accurate children caries diagnosis, so as to help clinical applications. The motivation lies in the observation that current deep learning based caries diagnosis approaches just copy the CNN methods designed for natural image analysis. We argue that the modality gap between natural image and dental panoramic radiographs image may cause performance degeneration, and most importantly, by properly considering general knowledge of caries classification may largely promote the diagnosis performance.

We propose context aware CNN by considering its adjacent teeth information when deciding whether a tooth is a car-

ies. Specifically, the information of adjacent teeth is extracted utilizing the same networks used for the current tooth information extraction, and a three-layer perception network is adopted calculating weights for their adaptive fusion. Accordingly, only a small number of network parameters are added compared with conventional CNN frameworks. Results in terms of accuracy, precision, recall,  $F1$ , and AUC exceed typical CNN baseline. More specifically, the improvements are up to 5 to 7 percentages. We also display the diagnosis accuracy for each teeth position. Apart from three positions (61, 82, and 83), the proposed context aware CNN obtains much better performance with six positions (54, 51, 63, 64, 65, and 71) having at least 10 percentage improvements. The results show potential to revise current CNN approaches instead of just copying typical CNN methods for direct dental panoramic radiographs analysis.

In this study, we further validate the effects of the numbers of neighbors selected to form the context information. As neighbors of a tooth, we choose the neighbors based on the tooth positions. Taking tooth position 51 as an example: 2 neighbors means its left and right sides (positions 52 and 61); 3 neighbors will add its facing tooth (positions 52, 61, and 81); 5 neighbors will consider another two diagonal teeth (positions 52, 61, 81, 82, and 71). The results show that the best performance corresponds to 3 neighbors. This is reasonable, because those 3 neighbors are most close to the current tooth, which will largely help its diagnosis based on common sense. More or fewer neighbors considered may bring in noise information or ignore useful information, respectively.

The diagnosis abilities of human (five-years attending doctors) and the proposed method are compared. Almost all the evaluation metrics of the proposed context aware CNN are lower than that of the professional attending doctors, but the diagnosis speed of a dental panoramic radiograph image is significantly faster. More specifically, it takes an average of 1.0619s for our context aware CNN model, but attending doctors need an average of 64.5000s for a diagnosis of a dental panoramic radiograph image, showing a significant difference. So, if a deep learning based model is utilized for assisting caries diagnosis, it would help shorten the

diagnosis time of clinicians especially for those with little experience. In the comparison of classification accuracy for each tooth, the proposed method outperforms professional attending doctors in the second primary molar. This is inspiring because it may provide a very useful auxiliary diagnosis for clinicians, such as to verify or improve the diagnosis accuracy on caries of the second primary molar.

This study also has some limitations. First, the proposed context aware CNN model is based on the extraction of each tooth from the dental panoramic radiographs, so extra human annotation is necessary, which limits its usage in clinical applications when performing computer aided diagnosis. Second, caries has different stages [28], so instead of making a binary classification of whether a tooth is a caries, it is more helpful to assist dentist to make an accurate diagnosis of what degree of the caries is. A follow-up study by considering different stages of caries and an end-to-end extraction and classification framework is necessary and will be studied in the future work.

## 5. Conclusions

By introducing general knowledge in the field to advance typical CNN model, a context aware CNN has been developed, which shows 5 to 7 percentage improvements compared with typical CNN baseline in terms of classification accuracy, precision, recall,  $F1$ , and AUC. The proposed model shows potential to revise typical CNN approaches instead of just copying them for direct dental panoramic radiographs analysis as in previous works. Furthermore, the results of this study are expected to help clinicians make decisions for children caries diagnosis on panoramic radiographs, especially for the second primary molar caries diagnosis, which shows higher accuracy than that of two five-year attending doctors.

## Data Availability

Data used in this study were obtained from Department of Stomatology, Beijing Children's Hospital, Capital Medical University, National Center for Children's Health and are available with the permission of the Institutional Review Board (IRB) of Beijing Children's Hospital, Capital Medical University, National Center for Children's Health.

## Ethical Approval

This study was conducted according to the guidelines of the Declaration of Helsinki, and approved by the Institutional Review Board (IRB) of Beijing Children's Hospital, Capital Medical University, National Center for Children's Health (approval number: [2022]-E-044-R).

## Consent

By the Institutional Review Board (IRB) of Beijing Children's Hospital, Capital Medical University, National Center for Children's Health, patient consent was waived for the need for individual informed consent as this study had a

noninterventional retrospective design, and all the data were analyzed anonymously; therefore, no written/verbal informed consent was obtained from the participants.

## Conflicts of Interest

The authors declare no conflicts of interest.

## References

- [1] H. Colak, C. T. Dülgergil, M. Dalli, and M. M. Hamidi, "Early childhood caries update: a review of causes, diagnoses, and treatments," *Journal of natural science, biology, and medicine*, vol. 4, no. 1, pp. 29–38, 2013.
- [2] M. S. Skeie, M. Raadal, G. V. Strand, and I. Espelid, "The relationship between caries in the primary dentition at 5 years of age and permanent dentition at 10 years of age - a longitudinal study," *International Journal of Paediatric Dentistry*, vol. 16, no. 3, pp. 152–160, 2006.
- [3] J. Lapidattanakul, R. Nomura, R. Okawa et al., "Oral lactobacilli related to caries status of children with primary dentition," *Caries Research*, vol. 54, no. 2, pp. 194–204, 2020.
- [4] O. Fejerskov and E. Kidd, *Dental Caries: The Disease and Its Clinical Management*, John Wiley & Sons, 2009.
- [5] P. H. Lira, G. A. Giraldo, and A. Neves, "Panoramic dental x-ray image segmentation and feature extraction," in *Proceedings of V workshop of computing vision*, Sao Paulo, Brazil, 2009.
- [6] B. Bergner, C. Rohrer, A. Taleb et al., "Interpretable and interactive deep multiple instance learning for dental caries classification in bitewing X-rays," <http://arxiv.org/abs/2112.09694>.
- [7] F. Schwendicke, M. Tzschoppe, and S. Paris, "Radiographic caries detection: a systematic review and meta-analysis," *Journal of Dentistry*, vol. 43, no. 8, pp. 924–933, 2015.
- [8] S. Mertens, J. Krios, A. G. Cantu, L. T. Arsiwala, and F. Schwendicke, "Artificial intelligence for caries detection: randomized trial," *Journal of dentistry*, vol. 115, p. 103849, 2021.
- [9] M. Nandeesh and B. Naveen, "A literature review on caries detection and classification in dental radiographs," *Industrial Engineering Journal*, vol. 13, no. 6, 2020.
- [10] K. J. Jeon, S. S. Han, C. Lee, Y. J. Choi, H. I. Jung, and Y. H. Kim, "Application of panoramic radiography with a multilayer imaging program for detecting proximal caries: a preliminary clinical study," *Dentomaxillofacial Radiology*, vol. 49, no. 8, p. 20190467, 2020.
- [11] M. Yurtta, Elik, and I. S. Bayrakdar, *Diagnostic Charting on Panoramic Radiography Using Deep- Learning Artificial Intelligence System*, Authorea, 2021.
- [12] A. HaghaniFar, M. M. Majdabadi, and S. B. Ko, "PaXNet: dental caries detection in panoramic x-ray using ensemble transfer learning and capsule classifier," 2020, <http://arxiv.org/abs/2012.13666v1>.
- [13] G. Jader, M. Fontineli, and M. Ruiz, "Deep instance segmentation of teeth in panoramic x-ray images," in *2018 31st SIB-GRAP conference on graphics, Patterns and Images*, 2018.
- [14] T. H. Bui, K. Hamamoto, and M. P. Paing, "Deep fusion feature extraction for caries detection on dental panoramic radiographs," *Applied Sciences*, vol. 11, no. 5, p. 2005, 2021.
- [15] M. Muresan, R. Barbura, and S. Nedevschi, "Teeth detection and dental problem classification in panoramic x-ray images using deep learning and image processing techniques," in

2020 IEEE 16th International Conference on Intelligent Computer Communication and Processing, Cluj-Napoca, Romania, 2020.

- [16] R. Kaur, R. S. Sandhu, A. Gera, and T. Kaur, "Edge detection in digital panoramic dental radiograph using improved morphological gradient and MATLAB," in *2017 International Conference On Smart Technologies For Smart Nation*, 2017.
- [17] A. Haghanifar, M. M. Majdabadi, and S. B. Ko, "Automated teeth extraction from dental panoramic x-ray images using genetic algorithm," in *2020 IEEE International Symposium on Circuits and Systems*, Seville, Spain, 2020.
- [18] B. Thanathornwong and S. Suebnukarn, "Automatic detection of periodontal compromised teeth in digital panoramic radiographs using faster regional convolutional neural networks," *Imaging Science in Dentistry*, vol. 50, no. 2, pp. 169–174, 2020.
- [19] J. H. Lee, S. S. Han, Y. H. Kim, C. Lee, and I. Kim, "Application of a fully deep convolutional neural network to the automation of tooth segmentation on panoramic radiographs," *Oral surgery, oral medicine, oral pathology and oral radiology*, vol. 129, no. 6, pp. 635–642, 2020.
- [20] M. Y. Chung, J. Lee, S. Park et al., "Individual tooth detection and identification from dental panoramic X-ray images via point-wise localization and distance regularization," *Artificial Intelligence in Medicine*, vol. 111, p. 101996, 2021.
- [21] T. Saravanan, M. S. Raj, and K. Gopalakrishnan, "Identification of early caries in human tooth using histogram and power spectral analysis," *Middle-East Journal of Scientific Research*, vol. 20, pp. 871–875, 2014.
- [22] G. Virupaiah and A. K. Sathyanarayana, "Analysis of image enhancement techniques for dental caries detection using texture analysis and support vector machine," *International Journal of Applied Science and Engineering*, vol. 17, no. 1, pp. 75–86, 2020.
- [23] G. E. Hinton and R. R. Salakhutdinov, "Reducing the dimensionality of data with neural networks," *Science*, vol. 313, no. 5786, pp. 504–507, 2006.
- [24] Y. LeCun, Y. Bengio, and G. E. Hinton, "Deep learning," *Nature*, vol. 521, no. 7553, pp. 436–444, 2015.
- [25] Z. W. Li, F. Liu, W. J. Yang, S. H. Peng, and J. Zhou, "A survey of convolutional neural networks: analysis, applications, and prospects," *IEEE Transactions on Neural Networks and Learning Systems*, 2021.
- [26] D. R. Sarvamangala and R. V. Kulkarni, "Convolutional neural networks in medical image understanding: a survey," *Evolutionary Intelligence*, vol. 15, no. 1, pp. 1–22, 2022.
- [27] S. Vinayahalingam, S. Kempers, L. Limon et al., "Classification of caries in third molars on panoramic radiographs using deep learning," *Scientific Reports*, vol. 11, no. 1, p. 12609, 2021.
- [28] L. Y. Lian, T. Zhu, F. D. Zhu, and H. H. Zhu, "Deep learning for caries detection and classification," *Diagnostics*, vol. 11, no. 9, p. 1672, 2021.
- [29] H. H. Zhu, Z. Cao, L. Y. Lian, G. Ye, H. Gao, and J. Wu, "CariesNet: a deep learning approach for segmentation of multi-stage caries lesion from oral panoramic X-ray image," *Neural Computing and Applications*, 2022.
- [30] K. M. He, X. Y. Zhang, S. Q. Ren, and J. Sun, "Deep residual learning for image recognition," in *2016 IEEE conference on computer vision and pattern recognition*, 2016.

## Research Article

# Investigation of Applying Machine Learning and Hyperparameter Tuned Deep Learning Approaches for Arrhythmia Detection in ECG Images

Kogilavani Shanmugavadivel<sup>1</sup>, V. E. Sathishkumar<sup>2</sup>, M. Sandeep Kumar,<sup>3</sup>  
V. Maheshwari,<sup>3</sup> J. Prabhu<sup>3</sup> and Shaikh Muhammad Allayear<sup>4</sup>

<sup>1</sup>Department of Computer Science Engineering, Kongu Engineering College, Perundurai, Erode, 638 060 Tamil Nadu, India

<sup>2</sup>Department of Industrial Engineering, Hanyang University, Seoul, Republic of Korea

<sup>3</sup>School of Information Technology and Engineering, Vellore Institute of Technology, Vellore, 632014 Tamil Nadu, India

<sup>4</sup>Department of Multimedia and Creative Technology, Daffodil International University, Daffodil Smart City, Khagan, Ashulia, Dhaka, Bangladesh

Correspondence should be addressed to V. E. Sathishkumar; [sathishkumar@hanyang.ac.kr](mailto:sathishkumar@hanyang.ac.kr)  
and Shaikh Muhammad Allayear; [headmct@daffodilvarsity.edu.bd](mailto:headmct@daffodilvarsity.edu.bd)

Received 28 May 2022; Revised 8 August 2022; Accepted 24 August 2022; Published 12 September 2022

Academic Editor: Laith Abualigah

Copyright © 2022 Kogilavani Shanmugavadivel et al. This is an open access article distributed under the Creative Commons Attribution License, which permits unrestricted use, distribution, and reproduction in any medium, provided the original work is properly cited.

The level of patient's illness is determined by diagnosing the problem through different methods like physically examining patients, lab test data, and history of patient and by experience. To treat the patient, proper diagnosis is very much important. Arrhythmias are irregular variations in normal heart rhythm, and detecting them manually takes a long time and relies on clinical skill. Currently machine learning and deep learning models are used to automate the diagnosis by capturing unseen patterns from datasets. This research work concentrates on data expansion using augmentation technique which increases the dataset size by generating different images. The proposed system develops a medical diagnosis system which can be used to classify arrhythmia into different categories. Initially, machine learning techniques like Support Vector Machine (SVM), Naïve Bayes (NB), and Logistic Regression (LR) are used for diagnosis. In general deep learning models are used to extract high level features and to provide improved performance over machine learning algorithms. In order to achieve this, the proposed system utilizes a deep learning algorithm known as Convolutional Neural Network-baseline model for arrhythmia detection. The proposed system also adopts a novel hyperparameter tuned CNN model to acquire optimal combination of parameters that minimizes loss function and produces better result. The result shows that the hyper-tuned model outperforms other machine learning models and CNN baseline model for accurate classification of normal and other five different arrhythmia types.

## 1. Introduction

Humans find object classification to be a relatively simple operation, but machines have found it to be a difficult problem; hence, image classification has become a critical task. Image classification is the process of categorizing images into one of several predetermined categories. A single image can be classified into an endless number of categories [1]. Manually evaluating and classifying these images can be time-consuming, especially when there are a big number of

them; therefore, automating the process using machine learning and deep learning techniques would be quite beneficial. Particularly, these algorithms are really helpful to get precise results in medical domain like COVID-19 detection [2]. According to the World Health Organization (WHO), Cardiovascular Disease (CVD) is the main reason for heart attack [3]. The World Heart Federation says that, by 2030, there may be more than 23 million CVD-related deaths per year. Any irregular abnormality from normal heart rhythms leads to a type of CVD disease known as



arrhythmia. A succession of arrhythmia heartbeats can be harmful, even though a single pulse may not have a substantial influence on one's life. The proposed work applies CNN with electrocardiogram (ECG) grayscale images to create an effective arrhythmia classification method in order to classify ECG images into six categories, one being normal and the other five being distinct types of arrhythmia like Left Bundle Branch Block (LBBB), Right Bundle Branch Block (RBBB), Premature Atrial Contraction (PAC), Premature Ventricular Contraction (PVC), and Ventricular Fibrillation (VF). The contribution of this research work is as follows:

- (i) A novel hyper-tuned CNN model is proposed for the detection of arrhythmia
- (ii) Data augmentation is performed generating a large dataset
- (iii) ECG grayscale images are collected from Kaggle, and UCI repository can be used as input
- (iv) Five different types of arrhythmia are detected by applying machine learning, CNN-Baseline model, and hyper-tuned model

Various solutions for high-class imbalance across data types are discussed in [4]. Recent reviews unveil that the accuracy of the learned models may be improved by data augmentation. Data warping-based image augmentation is used in LeNet-5 [5], and it is the first application in which CNN is applied for handwritten digit classification. In [6], dataset size is increased by augmentation by applying cropping, flipping, and changing the intensity using PCA. Image data augmentation is a technique for increasing the size of the dataset artificially by producing different images of the same dataset. This is a method of applying various transformations to original images in order to create many modified versions of the same image. Each duplicate, on the other hand, differs in various ways, based on the techniques applied such as shifting, rotating, and flipping. These transformed images are mainly used by the algorithms for classification.

A CNN-Transformer-based model is applied to detect three different arrhythmia types in [7], and the mentioned method is applied to MIT-BIH dataset. A clustering-based approach is adopted in [8] to predict four types of arrhythmia. In this work, statistical index based on phase-space analysis is carried out for both prediction and classification. In order to distinguish between healthy heartbeat and pathological rhythms, data analysis can be carried out on edge devices in [9] using deep CNN. Purely rhythm-based methodology is introduced in [10] by computing RR-interval sequences from ECG signals, and for arrhythmia classification, LSTM is utilized. In order to identify the origin of the focal arrhythmia wave front, prediction curves can be generated in [11]. The numbers of neurons, activation function, optimizer, learning rate, batch size, and epochs are all tuned via hyperparameters. Convolution neural networks are used in computer vision to develop models for image-related processes such as image categorization and object detection. A

CNN model is formed by combining multiple convolution layers, pooling layers, dropouts, and finally fully linked layers in image classification applications. However, hyper-parameters in the CNN model may be tuned in order to obtain best results.

The main findings of this research work are that in order to obtain better accuracy, the proposed system adopts data augmentation and novel hyper-tuned CNN model. We performed evaluation on five different types of arrhythmia types from the dataset collected from Kaggle and UCI repository. The ImageDataGenerator class in Keras library is used to produce augmented images. To determine the best parameters in the CNN hyper-tuned model, Keras Tuner library is used.

The organization of this research paper is presented here. The literature survey about arrhythmia detection is discussed in Section 2. The proposed methodology is explained in Section 3, and it also gives full description of classification models utilized. Section 4 describes performance analysis of all the proposed models. Finally, in Section 5, the conclusion and future work are specified.

## 2. Literature Survey

The recent research work that can be carried out for ECG image classification by various learning approaches, dataset utilized, and results obtained is presented in Table 1.

The most frequently occurring problem when working with machine learning and Deep Neural Networks is that there is insufficient amount of training data or class imbalance among the dataset. One way to deal with this problem is data augmentation. In [27], the image style transfer method is proposed to perform various image transformations. Basic image transformations like color, geometric, and mixing of images are discussed in [28]. New samples were created from an existing dataset by performing translation and rotation as mentioned in [29].

## 3. Proposed System

The proposed system collects ECG image data from Kaggle and UCI repository [30, 31]. In order to get the variant of dataset, data augmentation is performed. Initially, training data is applied to state-of-the-art learning methods like SVM, Naïve Bayes, and Logistic Regression. In addition to that, an augmented dataset is applied to deep learning models like baseline CNN and CNN with hyper-tuned parameters. A trained model is validated using validation data and tested using unseen data. The proposed models classify ECG-based image dataset into normal as well as five different arrhythmia types or classes like LBBB, PAC, PVC, RBBB, and VF. The proposed system workflow is represented in Figure 1.

**3.1. Dataset Description.** The dataset utilized for this work is collected from Kaggle and UCI repository. The dataset contains six classes which includes normal rhythm with abnormal heart activity known as arrhythmias. The shapes of

TABLE 1: Literature study.

Author	Model	Approach	Dataset	Evaluation
Acharya et al. [12]	Convolutional Neural Network	Deep CNN with 11 input layers and 4 output neurons	MIT-BIH	Accuracy—92.5%
Isin and Ozdalili [13]	Artificial Neural Network and transferred deep learning	Transferred deep CNN is used to extract features and then applied Artificial Neural Network (ANN)	MIT-BIH	Accuracy—92%
Zubair et al. [14]	Convolutional Neural Network and LSTM	Dropout regularization	MIT-BIH	Accuracy—91.8% Appl. Sci. 9, 14 (2019), 2921. DOI: 10.3390/app9142921
Ribeiro et al. [15]	Deep Neural Network	Stacked transformations	CODE	F1-Score—above 80%
Porumb et al. [16]	CNN	Multilayer perceptron for raw signal classification	MIT-BIH(250 samples)	Accuracy—97%
Khan et al. [17]	Deep Neural Network	MobileNet	Manual dataset	Accuracy—98%
Atal and Singh [18]	Deep CNN	Bat-Rider Optimization algorithm	MIT-BIH	Accuracy—93.19%
Zheng et al. [19]	Ensemble models	Hyper-tuned classification model	Manually generate dataset	F1-Score—97%
Mathunjwa et al. [20]	CNN	Hyperparameter tuning	MIT-BIH	Accuracy—95. 3%
Jun et al. [21]	CNN	AlexNet, VGGNet	MIT-BIH	Accuracy—99.05%
Hu et al. [7]	CNN-Transformer-based model	Classification and positioning	MIT-BIH	Accuracy—99.49%
Yıldırım et al. [22]	1D-CNN	ECG signal fragments based on one lead	MIT-BIH	Accuracy—91.33%
Li et al. [23]	SE-ResNet deep learning model	19-layer deep squeeze-and-excitation residual network	MIT-BIH	Accuracy—99.61%
Sharma et al. [10]	LSTM	Rhythm-based method	MIT-BIH	Accuracy—90.07%
Simonyan and Zisserman [24]	Deep learning	ConvNet	ILSVRC-2012	Accuracy—93.2%
Damaševičius et al. [25]	Machine learning	KNN	Time series dataset	Accuracy—86%
Naz et al. [26]	Deep learning	AlexNet, VGG-16, Inception-V3	MIT-BIH	Accuracy—97.6%

different types of arrhythmias that can be found in ECG images are shown in Figure 2.

**3.2. Data Augmentation Techniques.** Training datasets can be made larger and of higher quality by adding additional data. The ImageDataGenerator component of the Keras framework is used in the proposed system to apply various transformation functions to all of the original images at various epochs. The recently created images contain various iterations of the same image and are used in deep learning and machine learning techniques. At each epoch, Keras ImageDataGenerator class produces different images for analysis purpose. But these augmented images need not be included in the original dataset due to overfitting problem. Another benefit of ImageDataGenerator is that it consumes less memory. This is because if you did not utilize this class, all of the images would have loaded at the same time. However, when it is used, the images are loaded in batches, saving a lot of memory. Standardization, rotation, shifts, flips, brightness alteration, and many other augmentation techniques are

available in Keras. Before any subsequent processing, the data is multiplied by a value called rescale. Shear range is used to apply shearing transformations at random. A dataset obtained after applying data augmentation techniques is described in Table 2.

ECG images can be rotated freely between 0 and 360 degrees by using an image rotation data augmentation technique. As the image is rotated, certain pixels will move outside the image, creating an empty space that needs to be filled in. This value can be filled in a variety of ways, such with a constant value or by nearest pixel values. To make the object to be at the centre of the ECG image, the pixels can be relocated either in a horizontal or vertical way. This can be done using height shift range and width shift range parameters. Flipping ECG images is another wonderful enhancement technique that can be applied to a variety of objects. The ImageDataGenerator class offers arguments like horizontal flip and vertical flip. This technique, however, should be used in accordance with the object in the ECG image. The random brightness of the ECG image is changed

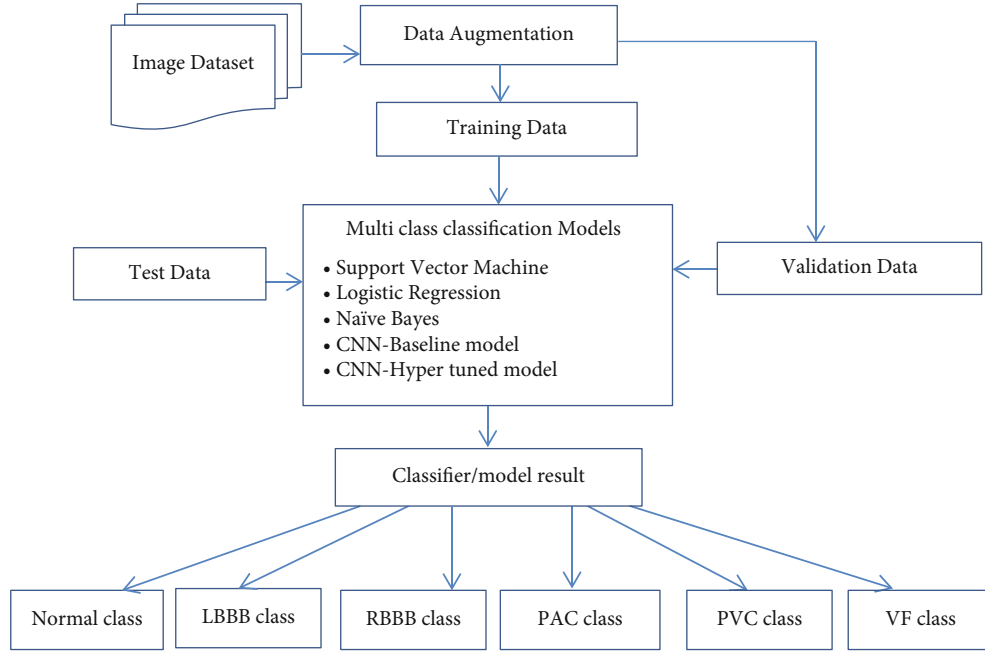


FIGURE 1: The proposed system work flow.




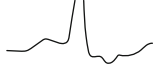
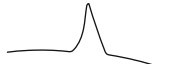

		
(1) Normal	(2) Ventricular Fibrillation (VF)	(3) Premature Atrial Contraction (PAC)
		
(4) Premature Ventricular Contractions (PVC)	(5) Left Bundle Branch Block (LBBB)	(6) Right Bundle Branch Block (RBBB)

FIGURE 2: Shape of ECG images with different arrhythmia types.

TABLE 2: Augmented ECG image dataset.

Class labels	Training data	Test data
Normal	7346	2179
LBBB	504	341
PAC	2054	1503
PVC	2759	1645
RBBB	2239	915
VF	439	242

at random. It is also a highly effective augmentation approach. The brightness range option in the ImageData-Generator class can be used to regulate the brightness. Values greater than 1.0 are used to brighten the ECG image. After applying the mentioned data augmentation techniques, sample ECG image is specified in Figure 3.

**3.3. Machine Learning Models.** A mathematical representation of the patterns concealed in data is represented through different machine learning models. When this model is trained on data, it develops some sort of controlling structure. This may be converted into rules that will be helpful for predicting new scenarios. So, if a model is trained on certain training data and then applied to fresh data, the model will be able to infer some sort of link. Various machine learning approaches, purpose, and advantages are discussed in [32]. Support Vector Machine is a supervised machine learning approach that may be applied to both regression and classification tasks. When used for classification, it uses a linear boundary to divide the classes. It creates a hyper-plane or a series of hyperplanes and is used to create good separation between the two classes [33]. The kernel function that is employed determines the algorithm's true power. The Naive Bayes algorithm adopts the Bayes theorem and works under the assumption that attributes are unrelated. Even




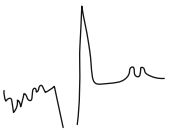


		
(1) Random Rotation 1	(2) Random Rotation 2	(3) Random Shift
		
(4) Vertical Flip	(5) Horizontal Flip	(6) Random Brightness

FIGURE 3: Sample augmented ECG image.

when other variables are available, it is impossible to know anything about other aspects [34]. So, the augmented dataset is applied to this algorithm to detect arrhythmia types without explicitly knowing about other parameters or attributes present in the dataset. Logistic regression is used to calculate the likelihood of a class [35]. The proposed system utilizes logistic regression to classify the given ECG images into five arrhythmia types.

**3.4. Deep Learning Models.** Deep learning is a subfield of machine learning that is becoming increasingly popular. Neural networks are used to create deep learning models. A neural network processes inputs by feeding them into hidden layers with weights that are adjusted during training. The model then issues a forecast. The weights are altered to discover patterns in order to produce better forecasts. Because the neural network learns on its own, the user does not need to define what patterns to look for. Keras is a Python-based neural network library that is easy to use. Each input image in a Convolutional Neural Network goes via two convolutional blocks, or two convolution layers, a pooling layer and a dropout layer for regularisation. Finally, each output is flattened and passed through a thick layer that sorts the image into one of six categories.

**3.4.1. CNN-Baseline Model.** A Convolutional Neural Network is a special category of the Artificial Neural Network which accepts images as inputs. The sequential model is developed as a baseline model by adding the convolution layer with filters and activation function. Then, the max pooling layer, hidden layer, and output layer are added. Then, the model is compiled and trained and evaluated. While the design of the Neural Network is vital for extracting information from input, updated rules based on the gradient of the loss function are used to improve everything. The optimizer determines the updating rules. Adam is a

well-known optimizer that is still in use in most neural networks. It uses an exponential declining average of the gradient, and it is squared to update the variables. The organization of CNN baseline model is shown in Figure 4.

The model type used in the CNN-Baseline model is sequential. During a model building process, multiple layers are added and ReLU is the activation function employed in the first two layers. Input shape is (64, 64, 1) with the value 1 indicating that the given images are in greyscale. A flatten layer is in between the Conv2D layers and the dense layer. It is used to connect the convolutional and dense layers. The output layer is dense, and it contains 6 nodes, one for each conceivable outcome (0–5). Softmax is the activation function to reduce the output to a single number. The CNN-Baseline model summary is specified in Table 3.

**3.4.2. CNN-Hyper-Tuned Model.** There are so many hyperparameters in neural networks that manually tuning them is nearly impossible. Keras Tuner makes tuning the hyperparameters of neural networks a breeze. Deep learning model development is an iterative process in which you start with a basic architecture and then tweak it until you have a model that can be trained efficiently in terms of both time and computing resources. To achieve this, adjust the settings of hyperparameters, and repeat the process until get the good performance. Hyperparameter tuning is the process of identifying a good collection of hyperparameters. For more complicated models, the number of hyperparameters might skyrocket, and manually tweaking them can be difficult. To address this issue, the proposed system utilizes Keras tuner. It is a library for tweaking the hyperparameters of a neural network that aids in the selection of ideal hyperparameters in a TensorFlow neural network. The model that utilizes Keras tuner is called a hyper-tuned model because it fine tunes the hyperparameters. The workflow of hyperparameter tuning process is represented in Figure 5.

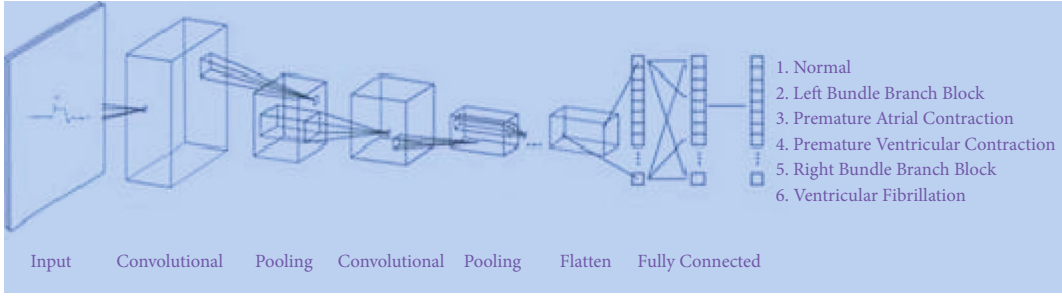


FIGURE 4: Convolutional neural network-baseline model.

TABLE 3: CNN-Baseline model summary.

Layer (type)	Output shape	Number of parameters
conv2d (Conv2D)	(None, 62, 62, 32)	320
max_pooling2d (MaxPooling2D)	(None, 31, 31, 32)	0
Flatten (flatten)	(None, 30752)	0
Dense (dense)	(None, 128)	3,936,384
Dense_1 (dense)	(None, 6)	774
Total params: 3,937,478	Trainable params: 3,937,478	Nontrainable params: 0

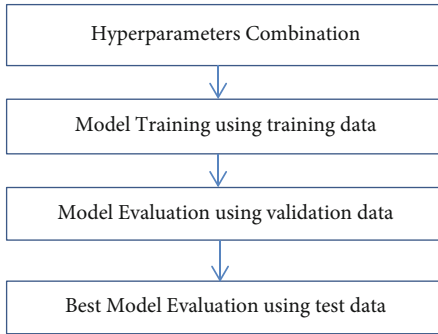


FIGURE 5: Hyperparameter tuning process workflow.

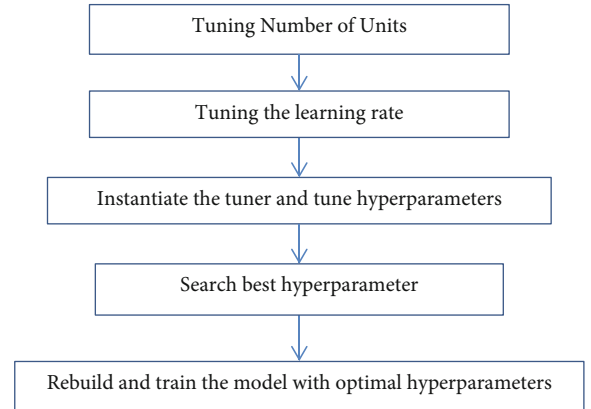


FIGURE 6: Hyper tuned Model Work Flow.

Randomly sampling hyperparameter combinations and testing them out is the most straightforward technique to undertake hyperparameter tweaking. First, choose an ideal value between 32 and 512 for the number of units in the first dense layer.

In order to specify the search space for dense units, minimum and maximum values, as well as the step size used to increment between them, are needed to be specified. Next, the optimizer's learning rate is adjusted by selecting an appropriate value from 0.01, 0.001, or 0.0001. During hyper tuning process, the selection of learning rate allows to designate discrete values to include in the search space. The process to be followed to obtain hyper tuned model is specified in Figure 6.

The tuner is then instantiated and the hyperparameters are tuned. The Hyper Band Tuner algorithm is used to optimize hyperparameters in this way. To swiftly converge on a high-performing model, it employs adaptive resource allocation and early-stopping. The number of models to run is determined by this procedure. The following step is to look

for the best hyperparameter. Finally, create the model using suitable hyperparameters, and train it. The CNN-hyper tuned model summary is specified in Table 4.

#### 4. Performance Evaluation

The precision score is a measure of how well the model predicted the positives out of all the positive predictions it generated. The accuracy score is a good predictor of prediction success when the classes are severely unbalanced. In mathematics, it displays the proportion of true positives to the total of true positives and false positives. By accurately calculating the number of true positives among all positive predictions, it is used to evaluate the model's performance. This value is calculated as mentioned in

$$\text{Precision} = \frac{\text{TP}}{\text{FP} + \text{TP}}. \quad (1)$$



TABLE 4: CNN-Hyper-tuned model summary.

Layer (type)	Output shape	Number of parameters
Conv2d_4 (Conv2D)	(None, 62, 62, 16)	448
Conv2d_5 (Conv2D)	(None, 60, 60, 16)	2320
Max_pooling2d_2 (MaxPooling 2D)	(None, 15, 15, 16)	0
Dropout (dropout)	(None, 15, 15, 16)	0
Conv2d_6 (Conv2D)	(None, 13, 13, 32)	4640
Conv2d_7 (Conv2D)	(None, 11, 11, 64)	18496
Max_pooling2d_3 (MaxPooling 2D)	(None, 5, 5, 64)	0
Dropout (dropout)	(None, 5, 5, 64)	0
Flatten_1 (flatten)	(None, 1600)	0
Dense_3 (dense)	(None, 128)	204928
Dropout_2 (dropout)	(None, 128)	0
Dense_3 (dense)	(None, 6)	774
Total params: 231,606	Trainable params: 231,606	Nontrainable params: 0

The recall score assesses the model's ability to accurately forecast positives from genuine positives. This is distinct from precision, which measures the proportion of accurate predictions a model makes among all accurate forecasts. It evaluates how effectively our machine learning model distinguishes between all genuine positives and all probable positives in a dataset. The recall score increases as the machine learning model becomes more adept at distinguishing between positive and negative data. Recall score is a good predictor of prediction success when the classes are severely unbalanced. In mathematics, it is the proportion of genuine positives to the total of true positives and false negatives. In terms of precisely counting true positives among all the real positive values, it is used to evaluate the model's performance. Recall value is calculated using

$$\text{Recall} = \frac{\text{TP}}{\text{FN} + \text{TP}}. \quad (2)$$

The accuracy metric for machine learning models is the proportion of true positives and true negatives to all positive and negative observations. In other words, accuracy represents the probability that, given the total number of predictions our machine learning model being made, it would correctly predict a result. It is the ratio of all mathematically accurate positive and negative predictions. By computing the ratio of true positives to true negatives over all forecasts, it is used to evaluate the model's performance. Accuracy is calculated using

$$\text{Accuracy} = \frac{\text{TP} + \text{TN}}{\text{TP} + \text{FN} + \text{TN} + \text{FP}}. \quad (3)$$

The F1-Score is a representation of the model score as a function of recall and precision. It is typically used as a single value that offers comprehensive information about the model's output quality. Mathematically, it can be written as the harmonic mean of the precision and recall score. When choosing either accuracy or recall score can lead to a model with significant false positives and false negatives, the F1-

TABLE 5: Performance evaluation.

Model	Precision	Recall	F1-Score	Accuracy
SVM	0.84	0.75	0.79	0.80
Naïve Bayes	0.77	0.79	0.78	0.73
Logistic Regression	0.67	0.80	0.73	0.70
CNN-Baseline model	0.88	0.90	0.89	0.91
CNN-Hyper-tuned model	0.92	0.90	0.91	0.94

Score, which is the harmonic mean of the two scores, is employed as a statistic. It is calculated using

$$\text{F1-Score} = \frac{2 * P * R}{P + R}. \quad (4)$$

The precision, recall, F1-Score, and accuracy for various machine learning algorithms and CNN algorithm baseline model and hyper-tuned model for validation dataset are shown in Table 5.

Optimizer, loss, and metrics are the three parameters used to build the model. The optimizer manages the learning rate. The CNN-Baseline model makes use of the Adam optimizer. Adam is a good optimizer to use, on the whole. For classification problems, the "categorical cross entropy" loss function is frequently employed. If the score is lower, the model is operating more effectively. Finally, the accuracy measure is utilized to determine the accuracy score on the validation set when we train the model. After each optimization iteration, a model's performance is shown by its loss value. Loss is defined as the difference between the problem's true values and the model's anticipated values. Model parameters are updated based on this loss value. A great accuracy with low loss means low errors on a dataset.

The precision, recall, F1-score, and accuracy values obtained by various machine learning models and deep learning models are shown in Figures 7–10. The result shows that with the help of hyperparameter tuning, the CNN-

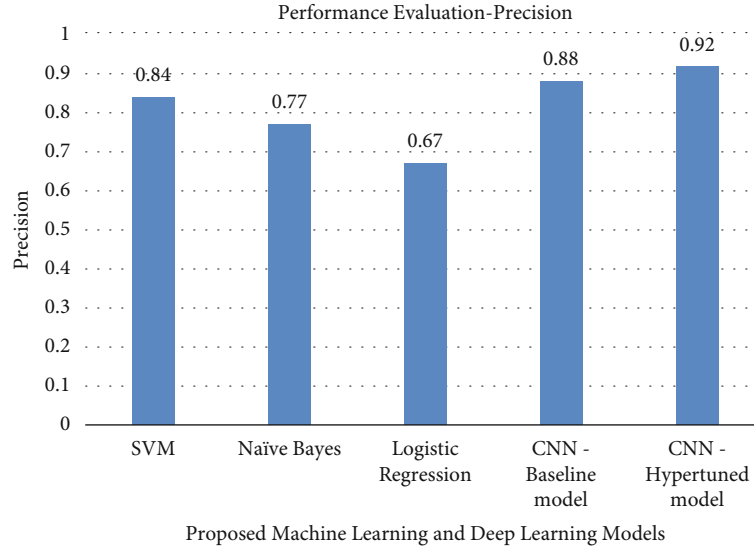


FIGURE 7: Performance evaluation of proposed models based on precision.

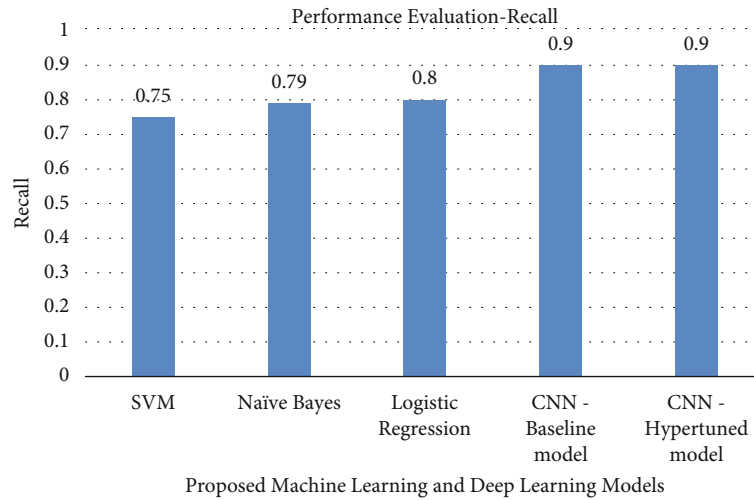


FIGURE 8: Performance evaluation of proposed models based on recall.

hyper-tuned model obtained the highest values compared to all other models.

Figure 11 shows accuracy and loss values of CNN-Baseline model for 20 epochs. The values show that training dataset loss is reduced from 1.0222 to 0.0889. Validation dataset loss is reduced from 0.8079 to 0.3438. Training dataset accuracy is improved from 0.6383 to 0.9724. Validation dataset accuracy is improved from 0.7163 to 0.9118 due to the fact that applying the CNN-Baseline model for 20 epochs in which each and every epoch the model automatically learn significant features from data.

Five different trials that output the trial summary and the best hyperparameters in the CNN-Hyper-tuned model are shown in Table 6. The result shows that at trail 4, the CNN-Hyper-tuned model obtained the best validation accuracy of 0.94375 using Random Search. With the help of Keras tuner, the proposed CNN-Hyper tuned model achieved 94% accuracy with a learning rate of 0.001. Each

trail runs for 20 epochs and each epoch took 180 seconds. Time taken to run each trail by the hyper tuned CNN model is about 3600 seconds.

**4.1. Error Analysis.** The confusion matrix obtained by machine learning model SVM to classify the ECG images into 6 classes like Normal, LBBB, PAC, PVC, RBBB, and VF is represented in Table 7. The correctly classified number of images is presented in diagonal elements of the confusion matrix. Out of 2179 images of the Normal category, 1743 images are correctly classified into the Normal category and remaining images are misclassified into different categories like LBBB, PAC, PVC, RBBB, and VF. Out of 6825 test images, 5460 images are correctly classified by the SVM machine learning model and obtained the highest accuracy among all the machine learning models.

Table 8 represents the confusion matrix obtained by the Naïve Bayes machine learning model. Out of 2179 images of

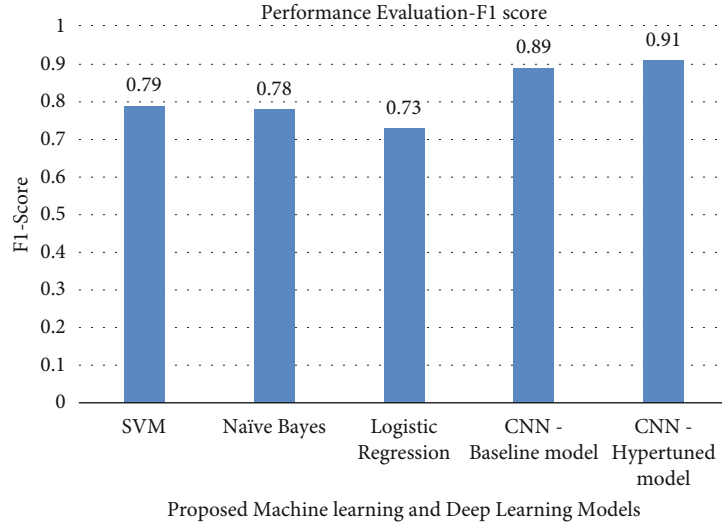


FIGURE 9: Performance evaluation of proposed models based on F1-Score.

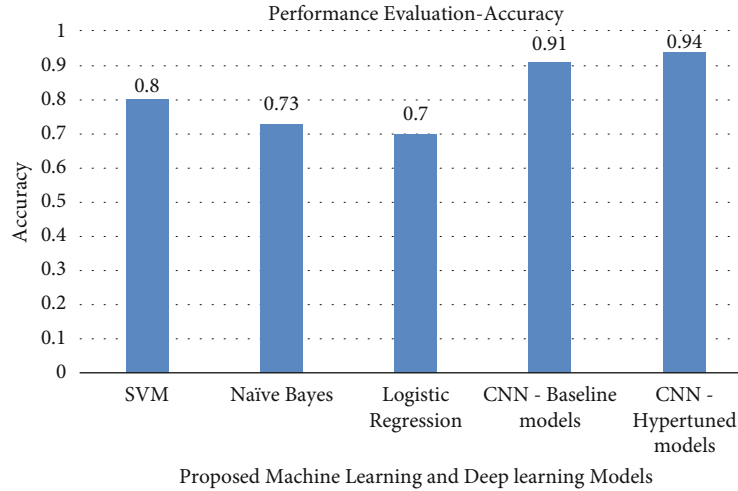


FIGURE 10: Performance evaluation of proposed models based on F1-Score.

the Normal category, 1590 images are correctly classified into the Normal category and remaining images are misclassified into different categories like LBBB, PAC, PVC, RBBB, and VF. Out of 6825 test images, 4816 images are correctly classified and this model obtained an accuracy of 0.73.

The confusion matrix obtained by the Logistic Regression machine learning model to classify the ECG images into 6 classes like Normal, LBBB, PAC, PVC, RBBB, and VF is represented in Table 9. Out of 2179 images of the Normal category, 1525 images are correctly classified into the Normal category and remaining images are misclassified into different categories like LBBB, PAC, PVC, RBBB, and VF. Out of 6825 images, 4775 test images are correctly classified by the Logistic Regression model and obtained the accuracy of 0.70.

The confusion matrix obtained by the deep learning model CNN-Baseline model to classify the ECG images into 6 classes like Normal, LBBB, PAC, PVC, RBBB, and VF is

represented in Table 10. Out of 2179 images of the Normal category, 1982 images are correctly classified into the Normal category and remaining images are misclassified into different categories like LBBB, PAC, PVC, RBBB, and VF. The developed CNN-Baseline model classifies 6005 images correctly out of 6825 images and obtained an accuracy of 0.91.

The confusion matrix obtained by deep learning model CNN-Hyper-tuned model to classify the ECG images into 6 classes like Normal, LBBB, PAC, PVC, RBBB, and VF is represented in Table 11. Out of 2179 images of the Normal category, 2048 images are correctly classified into the Normal category and remaining images are misclassified into different categories like LBBB, PAC, PVC, RBBB, and VF. Out of 6825 images, the proposed novel CNN-hyper tuned model correctly classifies 6413 images correctly and obtained an accuracy of 0.94.

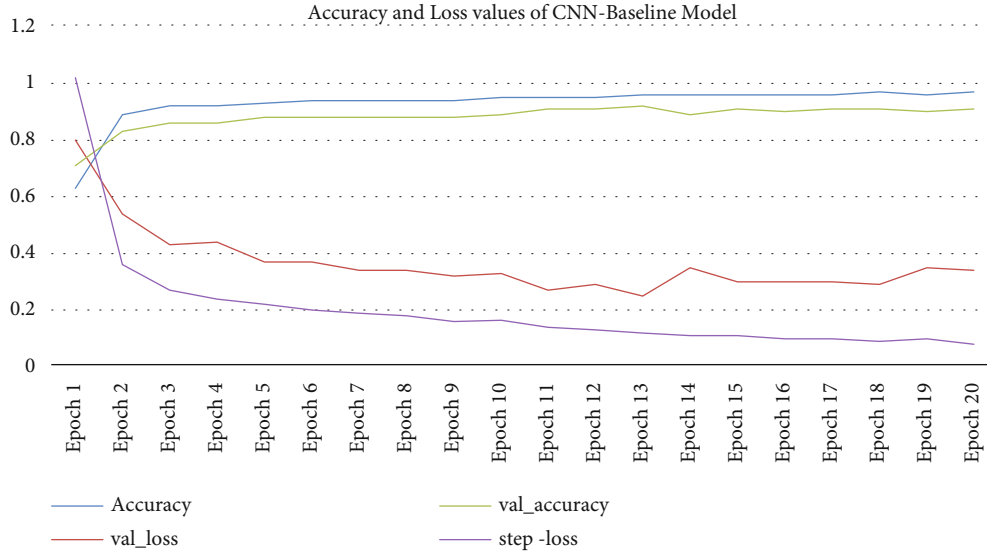


FIGURE 11: Accuracy and loss values of CNN-Baseline model.

TABLE 6: Hyperparameters and their values in the CNN-Hyper-tuned model.

Hyperparameters	Trail 1	Trail 2	Trail 3	Trail 4	Trail 5
conv_1_filter	80	80	112	96	64
conv_1_kernel	5	5	5	3	3
conv_2_filter	56	64	56	64	48
conv_4_filter	32	40	48	48	56
dense_1_units	80	80	128	64	64
dense_2_units	80	96	64	112	128
Learning_rate	0.01	0.001	0.01	0.001	0.01
Score	0.78123	0.83211	0.88993	0.94375	0.93531

TABLE 7: Confusion matrix-SVM.

	Normal	LBBB	PAC	PVC	RBBB	VF
Normal	1743	101	102	105	107	71
LBBB	11	273	17	15	11	14
PAC	52	218	1316	34	15	10
PVC	63	41	47	1202	106	44
RBBB	45	30	28	40	732	40
VF	9	15	7	10	7	194

TABLE 8: Confusion matrix-Naïve Bayes.

	Normal	LBBB	PAC	PVC	RBBB	VF
Normal	1590	182	101	93	113	100
LBBB	23	249	16	15	17	21
PAC	120	117	1200	98	63	47
PVC	56	153	76	1097	42	79
RBBB	23	39	87	44	667	55
VF	10	17	15	11	13	176

TABLE 9: Confusion matrix-Logistic Regression.

	Normal	LBBB	PAC	PVC	RBBB	VF
Normal	1525	203	63	159	178	51
LBBB	13	238	35	16	10	29
PAC	56	189	1151	83	153	13
PVC	51	73	67	1052	203	57
RBBB	98	58	23	62	640	34
VF	19	23	12	10	9	169

TABLE 10: Confusion matrix-CNN-Baseline model.

	Normal	LBBB	PAC	PVC	RBBB	VF
Normal	1982	18	46	52	63	18
LBBB	11	310	9	5	2	4
PAC	75	21	1496	11	26	16
PVC	13	25	34	1367	42	22
RBBB	13	11	19	23	832	12
VF	1982	18	46	52	63	18

TABLE 11: Confusion matrix-CNN-Hyper-tuned model.

	Normal	LBBB	PAC	PVC	RBBB	VF
Normal	2048	29	15	43	23	21
LBBB	1	320	3	4	2	11
PAC	26	14	1546	16	28	15
PVC	11	13	35	1412	25	7
RBBB	9	11	12	10	860	13
VF	2	1	3	4	5	227

## 5. Conclusion

This research work concentrates on developing an ECG-based image classification system that can be used to classify arrhythmia into different categories such as Normal, LBBB, PAC, PVC, RBBB, and VF using machine learning and deep learning models. ECG image-based heartbeat dataset collected from Kaggle and UCI repository is used for an analysis purpose. Initially, the data augmentation technique is used to enlarge the dataset. Then, machine learning models like Support Vector Machine, Naïve Bayes, and Logistic Regression are used for diagnosis. In order to extract high level features and to provide improved performance over machine learning algorithms, this research work utilizes deep learning-based Convolutional Neural Network approach called the CNN-Baseline model for arrhythmia detection. Further, to obtain optimal combination of parameters that minimizes loss function and produces better result in CNN, hyperparameter tuning is adopted in CNN and the CNN-Hyper-tuned model is developed. The proposed system utilizes the hyper-tuned model that employs Keras tuner to optimize hyperparameters used in the CNN-Baseline model. The result shows that the CNN-Hyper-tuned model applied on augmented dataset outperforms than other machine learning models and the CNN-Baseline model with 94% accuracy. Both machine learning and deep learning algorithms require long processing time and expensive also. In the future, transfer learning techniques like pretrained models will be utilized for classifying arrhythmia types.

## Data Availability

The data used to support the findings of this study are included within the article.

## Conflicts of Interest

The authors declare that there is no conflict of interest regarding the publication of this article.

## References

- [1] P. P. Fathimathul Rajeeana, R. Orban, K. S. Vadivel et al., "A novel method for the classification of butterfly species using pre-trained CNN models," *Electronics*, vol. 11, no. 13, p. 2016, 2022.
- [2] S. V. Kogilavani, J. Prabhu, R. Sandhiya et al., "COVID-19 detection based on lung CT scan using deep learning techniques," *Computational and Mathematical Methods in Medicine*, vol. 2022, Article ID 7672196, 13 pages, 2022.
- [3] World Health Organization, "Cardiovascular disease (CVDs)," 2021, [https://www.who.int/news-room/fact-sheets/detail/cardiovascular-diseases-\(cvds\)](https://www.who.int/news-room/fact-sheets/detail/cardiovascular-diseases-(cvds)).
- [4] M. S. Kumar, M. Z. Khan, S. Rajendran, A. Noor, A. S. Dass, and J. Prabhu, "Imbalanced classification in diabetics using ensembled machine learning," *Computers, Materials and Continua*, vol. 72, no. 3, pp. 4397–4409, 2022.
- [5] B. Subedi, V. E. Sathishkumar, V. Maheshwari, M. S. Kumar, P. Jayagopal, and S. M. Allayear, "Feature learning-based generative adversarial network data augmentation for class-based few-shot learning," *Mathematical Problems in Engineering*, vol. 2022, Article ID 9710667, 20 pages, 2022.
- [6] A. Krizhevsky, I. Sutskever, and G. E. Hinton, "Imagenet classification with deep convolutional neural networks," *Advances in Neural Information Processing Systems*, p. 25, 2012.
- [7] R. Hu, J. Chen, and L. Zhou, "A transformer-based deep neural network for arrhythmia detection using continuous ECG signals," *Computers in Biology and Medicine*, vol. 144, article 105325, 2022.
- [8] H. Chen, S. Das, J. M. Morgan, and K. Maharatna, "Prediction and classification of ventricular arrhythmia based on phase-space reconstruction and fuzzy c-means clustering," *Computers in Biology and Medicine*, vol. 142, article 105180, 2022.
- [9] H. D. M. Ribeiro, A. Arnold, J. P. Howard et al., "ECG-based real-time arrhythmia monitoring using quantized deep neural networks: a feasibility study," *Computers in Biology and Medicine*, vol. 143, article 105249, 2022.
- [10] A. Sharma, N. Garg, S. Patidar, R. San Tan, and U. R. Acharya, "Automated pre-screening of arrhythmia using hybrid combination of Fourier- Bessel expansion and LSTM," *Computers in Biology and Medicine*, vol. 120, article 103753, 2020.
- [11] D. Saluja, J. Kassotis, W. J. Kostis, and J. Coromilas, "A novel method for the prediction of focal wavefront origins in cardiac arrhythmias," *Computers in Biology and Medicine*, vol. 102, pp. 421–425, 2018.
- [12] U. R. Acharya, H. Fujita, O. S. Lih, Y. Hagiwara, J. H. Tan, and M. Adam, "Automated detection of arrhythmias using different intervals of tachycardia ECG segments with convolutional neural network," *Information Sciences*, vol. 405, pp. 81–90, 2017.
- [13] A. Isin and S. Ozdalili, "Cardiac arrhythmia detection using deep learning," *Procedia Computer Science*, vol. 120, pp. 268–275, 2017.
- [14] M. Zubair, J. Kim, and C. Yoon, "An automated ECG beat classification system using convolutional neural networks," in *2016 6th International Conference on IT Convergence and Security (ICITCS)*, pp. 1–5, Prague, Czech Republic, 2016.
- [15] A. H. Ribeiro, M. H. Ribeiro, G. M. Paixão et al., "Automatic diagnosis of the 12-lead ECG using a deep neural network," *Nature Communications*, vol. 11, no. 1, pp. 1–9, 2020.
- [16] M. Porumb, E. Iadanza, S. Massaro, and L. Pecchia, "A convolutional neural network approach to detect congestive heart failure," *Biomedical Signal Processing and Control*, vol. 55, article 101597, 2020.
- [17] A. H. Khan, M. Hussain, and M. K. Malik, "Cardiac disorder classification by electrocardiogram sensing using deep neural network," *Complexity*, vol. 2021, Article ID 5512243, 8 pages, 2021.
- [18] D. K. Atal and M. Singh, "Arrhythmia classification with ECG signals based on the optimization-enabled deep convolutional neural network," *Computer Methods and Programs in Biomedicine*, vol. 196, article 105607, 2020.
- [19] J. Zheng, H. Chu, D. Struppa et al., "Optimal multi-stage arrhythmia classification approach," *Scientific Reports*, vol. 10, no. 1, pp. 1–17, 2020.
- [20] B. M. Mathunjwa, Y. T. Lin, C. H. Lin, M. F. Abbod, and J. S. Shieh, "ECG arrhythmia classification by using a recurrence plot and convolutional neural network," *Biomedical Signal Processing and Control*, vol. 64, article 102262, 2021.
- [21] T. J. Jun, H. M. Nguyen, D. Kang, D. Kim, D. Kim, and Y. H. Kim, "ECG arrhythmia classification using a 2-D convolutional neural network," 2018, arXiv preprint arXiv:1804.06812.



- [22] Ö. Yıldırım, P. Pławiak, R. S. Tan, and U. R. Acharya, "Arrhythmia detection using deep convolutional neural network with long duration ECG signals," *Computers in Biology and Medicine*, vol. 102, pp. 411–420, 2018.
- [23] X. Li, F. Zhang, Z. Sun, D. Li, X. Kong, and Y. Zhang, "Automatic heartbeat classification using S-shaped reconstruction and a squeeze-and-excitation residual network," *Computers in Biology and Medicine*, vol. 140, article 105108, 2022.
- [24] K. Simonyan and A. Zisserman, "Very deep convolutional networks for large-scale image recognition," 2014, arXiv preprint arXiv:1409.1556.
- [25] R. Damaševičius, R. Maskeliūnas, M. Woźniak, and D. Połap, "Visualization of physiologic signals based on Hjorth parameters and Gramian angular fields," in *2018 IEEE 16th World Symposium on Applied Machine Intelligence and Informatics (SAMI)*, pp. 91–96, Kosice and Herlany, Slovakia, 2018.
- [26] M. Naz, J. H. Shah, M. A. Khan, M. Sharif, M. Raza, and R. Damaševičius, "From ECG signals to images: a transformation based approach for deep learning," *PeerJ Computer Science*, vol. 7, article e386, 2021.
- [27] A. Mikołajczyk and M. Grochowski, "Data augmentation for improving deep learning in image classification problem," in *2018 International Interdisciplinary PhD Workshop (IIPhDW)*, pp. 117–122, Poland, 2018.
- [28] C. Shorten and T. M. Khoshgoftaar, "A survey on image data augmentation for deep learning," *Journal of Big Data*, vol. 6, no. 1, pp. 1–48, 2019.
- [29] S. Rajendran, S. K. Mathivanan, P. Jayagopal et al., "Emphasizing privacy and security of edge intelligence with machine learning for healthcare," *International Journal of Intelligent Computing and Cybernetics*, vol. 15, no. 1, pp. 92–109, 2022.
- [30] <https://www.kaggle.com/datasets/shayanfazeli/heartbeat>.
- [31] <https://archive.ics.uci.edu/ml/datasets/arrhythmia>.
- [32] V. Jasti, G. K. Kumar, M. S. Kumar et al., "Relevant-based feature ranking (RBFR) method for text classification based on machine learning algorithm," *Journal of Nanomaterials*, vol. 2022, Article ID 9238968, 12 pages, 2022.
- [33] D. Pirova, B. Zaberzhinsky, and A. Mashkov, "Detecting heart 2 disease symptoms using machine learning methods," *Proceedings of the Information Technology and Nanotechnology*, vol. 2667, pp. 260–263, 2020.
- [34] S. K. B. Sangeetha, M. S. Kumar, H. Rajadurai, V. Maheshwari, and G. T. Dalu, "An empirical analysis of an optimized pre-trained deep learning model for COVID-19 diagnosis," *Computational and Mathematical Methods in Medicine*, vol. 2022, Article ID 9771212, 10 pages, 2022.
- [35] M. Subramanian, M. S. Kumar, V. E. Sathishkumar et al., "Diagnosis of retinal diseases Based on Bayesian optimization deep learning network using optical coherence tomography images," *Computational Intelligence and Neuroscience*, vol. 2022, Article ID 8014979, 15 pages, 2022.

## Research Article

# Medical Data Classification Assisted by Machine Learning Strategy

Lei Wang<sup>1</sup> and Keqiang Zuo<sup>2,3</sup> 

<sup>1</sup>Zhabei Center Hospital of Jing'an District of Shanghai, Jing'an, Shanghai 200070, China

<sup>2</sup>The Affiliated Hospital of Jiangangshan University, Ji'an 343000, China

<sup>3</sup>Shanghai 10th People's Hospital, Tongji University School of Medicine, Shanghai 200072, China

Correspondence should be addressed to Keqiang Zuo; 1805100@tongji.edu.cn

Received 17 June 2022; Revised 25 July 2022; Accepted 2 August 2022; Published 10 September 2022

Academic Editor: Hangjun Che

Copyright © 2022 Lei Wang and Keqiang Zuo. This is an open access article distributed under the Creative Commons Attribution License, which permits unrestricted use, distribution, and reproduction in any medium, provided the original work is properly cited.

With the development of science and technology, data plays an increasingly important role in our daily life. Therefore, much attention has been paid to the field of data mining. Data classification is the premise of data mining, and how well the data is classified directly affects the performance of subsequent models. In particular, in the medical field, data classification can help accurately determine the location of patients' lesions and reduce the workload of doctors in the treatment process. However, medical data has the characteristics of high noise, strong correlation, and high data dimension, which brings great challenges to the traditional classification model. Therefore, it is very important to design an advanced model to improve the effect of medical data classification. In this context, this paper first introduces the structure and characteristics of the convolutional neural network (CNN) model and then demonstrates its unique advantages in medical data processing, especially in data classification. Secondly, we design a new kind of medical data classification model based on the CNN model. Finally, the simulation results show that the proposed method achieves higher classification accuracy with faster model convergence speed and the lower training error when compared with conventional machine learning methods, which has demonstrated the effectiveness of the new method in respect to medical data classification.

## 1. Introduction

Disease diagnostic analysis is a highly specialized and time-consuming task, which is prone to inconsistencies between and within observers [1, 2]. Computer-aided diagnosis can reproduce the diagnostic process and reduce the subjectivity of observers to improve the reliability of results. Medical data classification is used to solve problems related to disease. The main goal is to extract clinically relevant pathological information or knowledge from medical data. Nowadays, with the development of technology, the huge amount of medical data generated by clinical practice makes data-driven high-precision computer-aided diagnosis possible [3].

How to mine valuable information from increasingly abundant data has become a research hotspot in the field of artificial intelligence. Data mining (DM) is one of the most powerful data analysis methods at present. Through

DM, it can extract the hidden but unknown and potentially useful information from data to discover rules or patterns [4]. In recent years, various DM techniques have been widely used in data analysis tasks. DM technology has been applied to medical data research since it was proposed. As the object of medical research gradually changes from clinical diagnostic data to bioinformatics data, medical data mining has increasingly become one of the most active research and application fields [5]. Clinical diagnostic data contain a large amount of valuable information. Data mining of clinical diagnostic data of patients with different diseases is helpful to discover the risk factors related to the disease and their interaction, which can provide reference for clinical diagnosis and treatment of the diseases [6].

With the increasing progress of science and technology, people now rely more and more on computers to obtain all kinds of information and use computer technology to solve

all kinds of classification problems encountered. In recent years, numerous statistical methods and disease risk factor analysis, including principal component analysis (PCA), logistic regression, linear discriminant analysis (LDA) and support vector machine (SVM), and many innovative research results have been obtained [7, 8]. However, since clinical data has the characteristics of high dimensional feature space, high redundancy, and strong correlation between data features, many classical classification algorithms are not ideal for the classification accuracy of medical datasets.

In recent years, deep learning models have made breakthroughs in data mining, artificial intelligence, data classification, and other fields. The deep learning model is generally a deep neural network composed of multiple processing layers, which can learn data representation and data features with multiple layers of abstraction [9]. Traditional machine learning classification methods are based on shallow structure algorithms, which cannot express complex function features in the case of limited data samples, and there is a problem of low model generalization ability in complex data classification [10, 11]. Deep neural network model can represent the deep nonlinear network structure and further approximate complex functions. It has the ability to learn the essential characteristics of data samples from a small number of data samples. The basic neural network model consists of many units that are simply interconnected called neurons, and a single neuron generates a single real-valued activation sequence [12]. Deep neural network generally adopts the gradient descent method to guide the updating of network parameters, which is used to represent the features obtained by the current layer from the previous layer and then passed down to the next layer. The neural parameters of each layer of the network model only affect the parameters of the next layer of the network model. The output results of the output layer are compared with the label, and the training error can be minimized by adjusting the connection weights of neurons in each layer of the network model [13, 14]. In practical applications, as most of the multilayer structures contain multiple nonlinear processing units, it often leads to the local minimum solution of the nonconvex cost objective function, and the final classification accuracy is lower than that of other machine learning algorithms. In view of this common problem, many new deep neural network models have been proposed through further research [15, 16].

In current studies, representative ones are recurrent neural network (RNN), long- and short-term memory (LSTM), CNN, restricted Boltzmann machine (RBM), etc., among which CNN is one of the most widely used deep learning models in recent years [17, 18]. Its main feature is that in the network model, the two layers are fully connected, and there is no connection within the layer. CNN is quite popular due to its excellent data feature extraction ability. Aiming at the complex characteristics of medical data and the advantages of CNN, this paper mainly studies the medical data classification algorithm based on the CNN model. While maintaining or improving the classification performance of the classification algorithm, the running time of the algo-

rithm is reduced, so that the data mining results have better transparency and understandability [19, 20]. This research belongs to the interdisciplinary research of computer science and biological information. The research results can not only enrich machine learning and data mining algorithms but also promote the application of data mining and machine learning technology in the medical field and provides scientific basis and decision support for medical experts to determine treatment plan and carry out medical research. The reminder of this paper is as follows: Section 2 gives the related work, and Section 3 is the machine learning-based medical data classification algorithm. And the experimental results and analysis are given in Section 4. Finally, Section 5 concludes the paper.

## 2. Related Work

Two important research directions of medical data mining are clinical data mining and biological information data mining. For clinical diagnostic datasets, data mining mainly uses feature selection and machine learning algorithms to explore disease risk factors, which affects the occurrence of certain diseases and provides decision support for doctors to make clinical diagnosis and reasonable treatment plans [21].

*2.1. Shallow Neural Network Classifier.* Machine learning has been widely used to analyze biomedical data and classification tasks [22, 23]. Classification is an important problem in supervised learning in machine learning. For nonlinear classification, the inner product between instances can be changed into kernel function, so that the problem can be transformed into a linear classification problem in a specific dimensional feature space, so that linear support vector machines can be learned in a high dimensional feature space. SVM has been widely used in neuroscience and bioinformatics because the algorithm can process high-dimensional data. The main disadvantage of this method is that it is easy to overfit due to the large amount of calculation. Logistic regression aims at a combination of variables to maximize the probability of predicting the expected outcome [24]. Maximum likelihood estimation is used for parameter estimation, and likelihood ratio test is used for significance test. In order to avoid overfitting and improve generalization ability, logistic regression and regularization are often used in combination by adding a penalty term to optimize the objective function, reducing the size of parameters corresponding to features. Logistic regression can get approximate probability prediction in addition to categories, which has the advantages of simple, efficient, easy to interpret, and easy to expand, and is widely used in the classification tasks of bioinformatics.

The random forest algorithm is based on the idea of ensemble learning to integrate multiple trees. Its basic unit is decision tree. For classification problems, each decision tree is a classifier that learns and makes predictions independently. The random forest algorithm integrates the results of all classification and then begins to vote to further obtain more accurate classification. The predicted variance is

inversely proportional to the number of independent trees in it. Random forest classifier has been widely used in bioinformatics [25]. One of its main advantages is that it can evaluate the importance of each feature in classification while determining categories. One of its disadvantages is its sensitivity to input parameters. Naive Bayes is a probability classifier based on Bayes theorem, which adopts the assumption of attribute condition independence. Naive Bayes builds conditional probabilities of features under each class and determines the most likely categories for features of test data. The advantage of naive Bayes is that it still has a fast running speed in the face of a large amount of training and test data. However, when the assumption is not met, there is no guarantee that it will perform well. This algorithm has many applications in bioinformatics. Multilayer perceptrons, also known as artificial neural networks (ANN), map multiple datasets of inputs to a single dataset of outputs [4]. Neurons make up an artificial neural network, each layer of which is connected by weight, also known as a synapse. The advantage of multilayer perceptron is that the number of neurons and hidden layers can be designed according to the complexity of the target dataset. Generally, the more complex the target dataset, the more hidden layers are needed for feature extraction. However, in the multilayer perceptron, the layers are fully connected, which makes it difficult to update parameters.

**2.2. Deep Neural Network Classifier.** Deep learning refers to the machine learning process in which a multilevel network structure representing the characteristics of the data is obtained by applying some specific training methods to the data samples. Deep learning network structure of the model is composed of a large number of neurons connected to each other, measured by weight connection strength between neurons connected to each other. Through the change of weight value in the process of model training so as to achieve the aim of function of the control model, the sizes of the neurons in essence are all in the neural network model which is for calculating the required minimum unit [26]. In recent years, deep learning methods have attracted extensive attention in the fields of pattern recognition and machine learning. The deep neural network model is a computing model composed of multiple processing layers, which extracts effective learning features from data [27]. As an important tool of artificial intelligence, the deep learning model has shown great potential. The theory and application of deep learning have attracted extensive attention in the international and domestic academic circles, and many famous enterprises in the world also attach great importance to the research and application of this aspect. For example, Tesla withdrew from self-driving cars based on deep learning, and Baidu, a Chinese Internet giant, set up a deep learning research institute to implement the technological research results of artificial intelligence.

Large-scale natural datasets have greatly promoted the development of deep learning technology. Deep learning can be used to complete the classification of medical image data [28]. However, its development is limited by data.

The scale of medical image data is often limited. When there is enough data, all parameters in the neural network can be randomly initialized and then trained. Another strategy is transfer learning. Another strategy is transfer learning, which fine-tunes the parameters of the network model trained in advance on external datasets. Most studies using transfer learning strategies replace and retrain the deepest layer of the network, while the shallow layer is a variation of the transfer learning strategy fixed after the initial training, which combines fine-tuning and deep feature methods. Fine-tune the pretrained network on new datasets to obtain deeper features [29]. Deep neural networks (DNN) are a discriminant model, which can be trained with the backpropagation algorithm, and weight updating can be solved by stochastic gradient descent. In a broad sense, DNN is the general term of deep learning, including a series of other neural network structures, such as convolutional neural network and recurrent neural network. Chivalrous DNN refers to a network structure with only full connections. Based on the above discussions, the main contributions of this work can be concluded as below:

- (1) The method in this paper is based on the depth model and can deal with the classification of large-scale medical data
- (2) Experimental results show the effectiveness and practicability of the proposed method. That is to say, the method in this paper has both theoretical and practical significance

### 3. The Machine Learning-Based Medical Data Classification Algorithm

The earliest feedforward neural network is also called multilayer perceptron (MLP), which is the simplest neural network model and given in Figure 1. From the figure, we know that the MLP contains the input layer, hidden layer, and output layer. And each neuron is arranged in layers. As the simplest neural network at that time, each neuron is connected to the upper layer, the output of the upper layer continues as the input of the lower layer, and there is no feedback between layers.

The MLP neural network is given in here, from which we can see that neural network can be divided into three parts: input layer, hidden layer, and output layer according to its different functions. Due to the shallow network layer and the use of linear activation units, the early fully connected neural network models are often unable to solve complex problems.

**3.1. Deep CNN Model for Medical Data Classification.** Based on the traditional full-connection layer neural network, CNN adds convolution layer and pooling layer to form the deep CNN model, which is shown in Figure 2.

The function of the convolution layer lies in the extraction of image features. The essence of the convolution kernel is a filter matrix, which can produce many different effects on

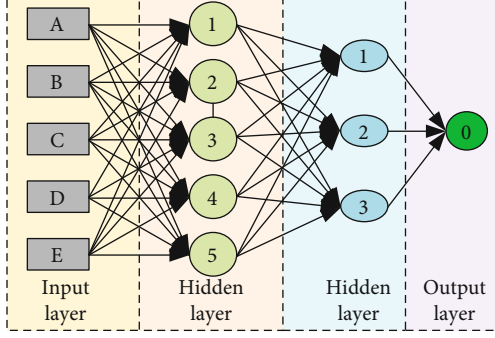


FIGURE 1: The conventional multilayer perceptron network.

the original image. The calculation process of convolution is shown below:

$$\text{CONV}_{(ij)} = \sum_i^{m-1} \sum_j^{n-1} u_{ij} \times w + b \quad (i = 1, 2 \dots m-1; j = 1, 2 \dots n-1), \quad (1)$$

where  $u_{ij}$  is the input image,  $m$  and  $n$  are the size of the input image,  $w$  is the size of the convolution kernel, and  $b$  is the bias constant of the convolution kernel.  $\text{CONV}_{(ij)}$  is the characteristic graph output after convolution operation.

CNN adds an activation function layer to the network and analyzes the model better by adopting the feature mapping method of nonlinear function.

$$f(x) = \frac{1}{1 + e^{-x}}. \quad (2)$$

The mathematical expression of tanh function is

$$f(x) = \frac{e^x - e^{-x}}{e^x + e^{-x}}. \quad (3)$$

The mathematical expression of ReLU function is

$$f(x) = \max(0, x). \quad (4)$$

The full name of ReLU function is rectified linear unit. The function is one of the commonly used activation functions, which is characterized by low computational complexity and no exponential operation. However, it is worth noting that although ReLU function has certain advantages, it also has some shortcomings in the actual calculation process. When the data passes through the negative range of ReLU function, the output value is equal to 0. The Leaky-ReLU function can solve the above problem.

$$f(x) = \begin{cases} x, & x \geq 0, \\ \alpha x, & x < 0. \end{cases} \quad (5)$$

Therefore, the efficiency of the entire network operation can be improved to a certain extent. The corresponding equations of  $\text{sig}$  and  $\text{tanh}$  are as follows:

$$\begin{cases} \text{sig}(x) = \frac{1}{1 + \exp(-x)}, \\ \tanh(x) = \frac{\exp(x) - \exp(-x)}{\exp(x) + \exp(-x)}, \end{cases} \quad (6)$$

$$h_{w,b}(x_i) = \begin{bmatrix} p(y_i = 1|x_i; w, b) \\ p(y_i = 2|x_i; w, b) \\ p(y_i = 3|x_i; w, b) \\ \dots \\ p(y_i = n|x_i; w, b) \end{bmatrix} = \frac{1}{\sum_{j=1}^n e^{w_j x_i + b_j}} \begin{bmatrix} e^{w_1 x_i + b_1} \\ e^{w_2 x_i + b_2} \\ e^{w_3 x_i + b_3} \\ \dots \\ e^{w_n x_i + b_n} \end{bmatrix}. \quad (7)$$

The output layer adopts softmax function to normalize, and the probability value  $h_{w,b}(x_i)$  in the corresponding category is shown in (7). In classification tasks, it is a common method to use crossentropy loss function to evaluate the gap between predicted value and true value. The crossentropy (CE) formula is as follows:

$$\text{loss} = -\frac{1}{m} \sum_{j=1}^m \sum_{i=1}^n y_{ji} \log(\hat{y}_{ji}). \quad (8)$$

The error calculated from the CE function needs to be calculated by back propagation, so as to realize the newer back propagation of model parameters. The original form of the gradient descent method is shown below:

$$\theta := \theta - \alpha \frac{\partial}{\partial \theta} J(\theta), \quad (9)$$

where the  $\theta$  is a parameter. In the experiments in the following chapters, this paper also verifies that the use of Adam has faster convergence than SGD. The mathematical expression of a common Adam optimizer is given as

$$\begin{aligned} m_t &= \beta_1 m_{t-1} + (1 - \beta_1) g_t, \\ v_t &= \beta_2 v_{t-1} + (1 - \beta_2) g_t^2. \end{aligned} \quad (10)$$

And the  $\beta_1$  and  $\beta_2$  are all parameters, and  $m_t$  and  $v_t$  are the wanted value. Therefore, the updating rule of gradient descent is as follows:

$$\theta_{t+1} = \theta_t - \frac{\alpha}{\sqrt{v_t} + \epsilon} m_t. \quad (11)$$

Based on the above discussions, the proposed medical data classification algorithm in this work is shown in Figure 3. It mainly includes data preprocessing, CNN model establishment, judgment of stop conditions, and final classification results.

## 4. Experimental Results and Analysis

**4.1. Experimental Data Introduction.** To verify the effectiveness of the proposed algorithm, three representative medical



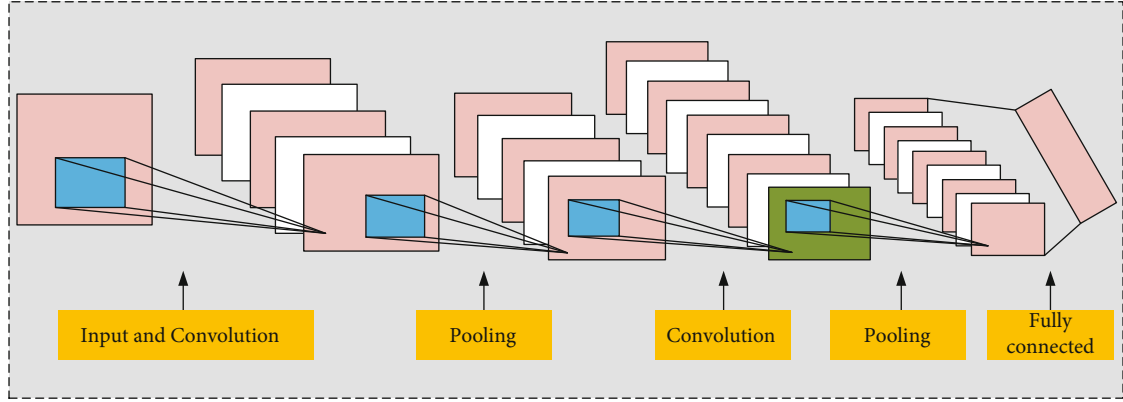


FIGURE 2: The typical schematic diagram of CNN neural network.

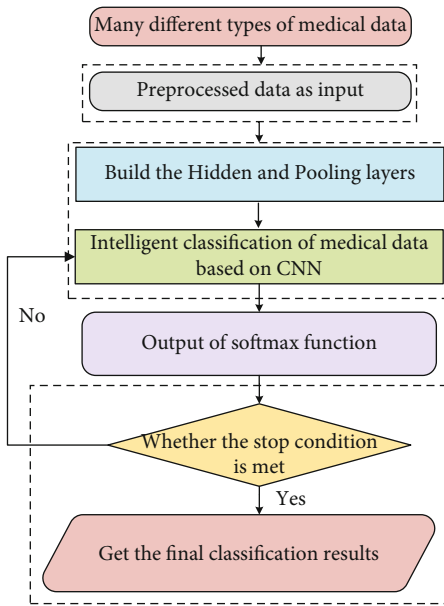


FIGURE 3: The overall process of the proposed method.

datasets were selected from the UCI dataset, which have been widely cited in the literature [29]. Among them, breast dataset is a breast cancer dataset from clinical cases, including 699 samples, 9 numerical variables, and 1 classification variable. The target variable is the category of samples: benign and malignant. Liver is a very different dataset with 395 samples, including 6 numerical variables and 1 target variable. Diabetes is a diabetes dataset, which is a constrained selection dataset consisting of 768 samples of descendants of Pima Indians older than 21 years, each containing 8 numerical variables and 1 categorical variable.

In addition, in order to better compare the test results, all the data were preprocessed, including noise removal, anomaly removal, and normalization processing, so as to obtain pure and directly usable data, which helped to improve the classification performance of the subsequent model.

**4.2. Experimental Result Analysis.** In order to demonstrate the universality of the proposed method, change curves of

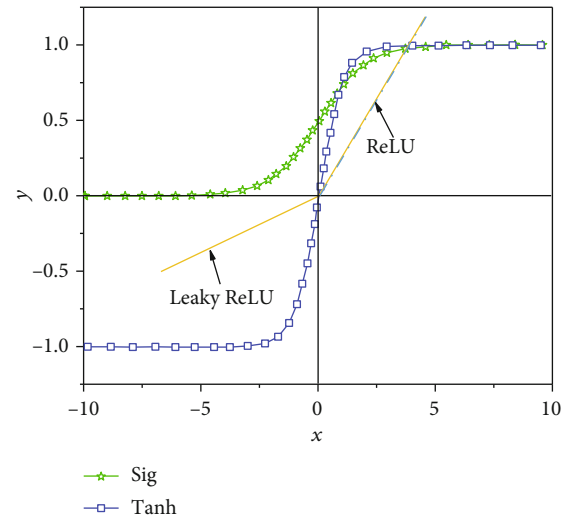


FIGURE 4: Different activation functions curves of the CNN model.

different activation functions of the CNN model are presented in Figure 4. As can be point out from the figure, under the dataset of this paper, different activation functions have different characteristics, but they all have the following common characteristics: (1) differentiability: this property is a prerequisite when using gradient-based optimization algorithms to optimize models and (2) monotonicity: when the activation function meets the monotonicity, the single-layer network is guaranteed to be convex, so that the subsequent convex optimization operations can be carried out. But in this case, the learning rate usually needs to be set to a small value, which inevitably increases the training time. Based on the above, the ReLU function is selected in this paper.

Apart from training errors, Figure 5 shows the effects of network layers on test accuracy and model testing time, the left is the effects on testing accuracy, and the right is the effects on model testing time: (a) test accuracy and (b) testing time. From the figure we know that with the increase of network layers, both test accuracy and test time show a normal distribution trend. In particular, when the number of network layers is 20, the test accuracy of the model

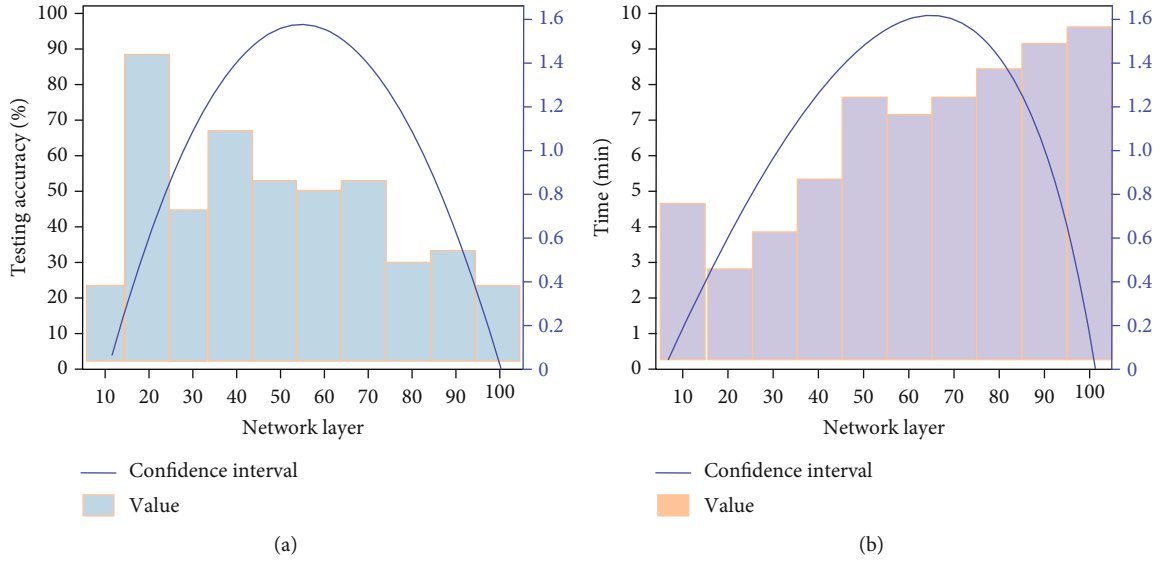


FIGURE 5: The influence of network layers on test accuracy and model testing time: (a) test accuracy and (b) testing time.

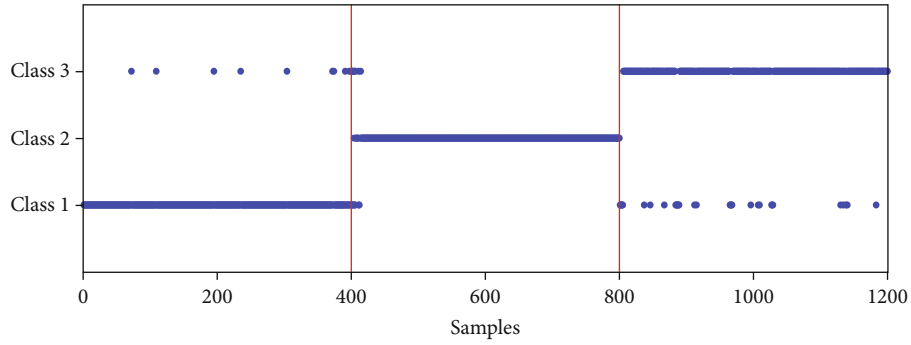


FIGURE 6: Classification results of the three kinds of disease by the CNN model.

reaches the highest, about 90%, while when the network layers is 100, the test accuracy reaches the lowest 18%. Similarly, when the number of network layers is 20, the test time of the model is the fastest 2.5 minutes. With the increase of the number of layers, the test time of the model becomes longer and longer. When the number of layers is 100, the test time of the model is the longest 9.3 minutes. From the above analysis, it can be seen that the selection of appropriate network structure is important.

Base on the above model setting, the classification results of three kinds of medical data by different methods are drawn as shown in Figure 6. Similarly, samples 1-400, 401-800, and 801-1200 on the abscissa are disease 1, disease 2, and disease 3, respectively, and the ordinate represents labels for medical data. From the figure, we know that the classification accuracy of the proposed CNN model method for disease data 1, 2, and 3 is 97.5%, 99.5%, and 92.25%, respectively. In addition, the average classification accuracy of CNN is much better than that of the SVM algorithm (96.42% compared with 65.92%, 68.83%, 76%), which also proves the effectiveness of the proposed method from another perspective.

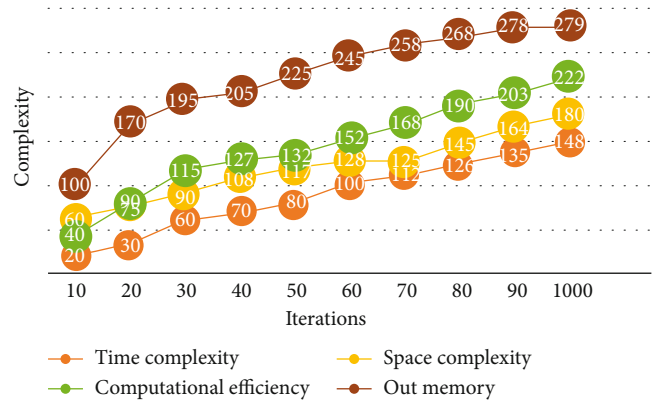


FIGURE 7: The relationship between model complexity and iteration times.

To further demonstrate the classification performance of the CNN approach, the relationship between model complexity and iteration times is given in Figure 7. Among them, the model has the fastest increase in memory requirements; so, the method proposed in this paper is based on the deep

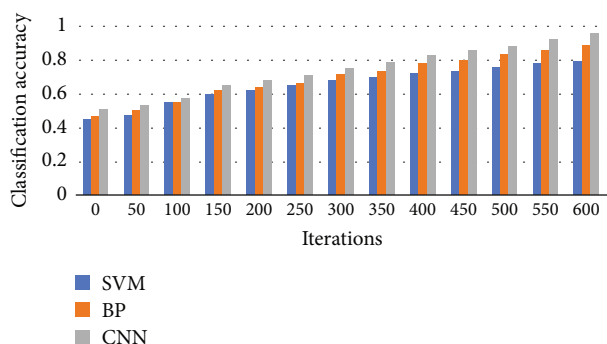


FIGURE 8: The relationship between classification accuracy and iteration times of different methods.

learning model, which has higher requirements on hardware computing capacity but can achieve better model performance. However, time complexity, space complexity, and computational efficiency all show a slow growth trend, which shows the practicality and reliability of the method presented in this paper.

Finally, Figure 8 shows the relationship between classification accuracy and iteration times of different methods. We can see from the figure that with the increase of iteration number, the classification performance of the three methods shows an increasing trend. When the iteration number is 600, the three models all reach the highest classification accuracy, which is 79%, 88%, and 97%, respectively. Therefore, the CNN model in this paper achieves the highest classification accuracy. In addition, even when the number of iterations is small, the proposed method also has the best model performance and achieves the highest classification accuracy throughout the training process, which demonstrates the effectiveness of the proposed method in medical data classification.

## 5. Conclusions

Data classification plays an important role in medical data processing and has been applied in many fields. Medical data classification problems are diverse and complex and are easily affected by noise and instrument defects in the process of data analysis, which will greatly affect the doctor's judgment of the lesion location. Therefore, how to improve the effect of medical data classification is conducive to the development of technology and practical application.

This paper introduces the background information of medical data classification and the development trend of classification technology at the present stage and introduces the relevant knowledge points. On this basis, the medical data classification method based on the CNN model is proposed in this paper, and the classification effect is good. Specifically, the method proposed in this paper achieved the best classification accuracy (97.5%, 99.5%, and 92.25% for disease data 1, 2, and 3, respectively) and fastest running speed. In addition, it can be seen that the parameters of the CNN algorithm are relatively high; so, the next step will focus on improving the operation effect of the CNN algorithm while

reducing parameters. And other physiological data about the patient can also be taken into account.

## Data Availability

The experimental data used to support the findings of this study are available from the corresponding author upon request.

## Conflicts of Interest

The authors declared that they have no conflicts of interest regarding this work.

## References

- [1] J. Lu, E. Song, A. Ghoneim, and M. Alrashoud, "Machine learning for assisting cervical cancer diagnosis: an ensemble approach," *Future Generation Computer Systems*, vol. 106, pp. 199–205, 2020.
- [2] B. Zhang, J. Tian, S. Pei et al., "Machine learning-assisted system for thyroid nodule diagnosis," *Thyroid*, vol. 29, no. 6, pp. 858–867, 2019.
- [3] K. Y. Ngiam and W. Khor, "Big data and machine learning algorithms for health-care delivery," *The Lancet Oncology*, vol. 20, no. 5, pp. e262–e273, 2019.
- [4] J. Latif, C. Xiao, A. Imran, and S. Tu, "Medical imaging using machine learning and deep learning algorithms: a review," in *2019 2nd international conference on computing, mathematics and engineering technologies (iCoMET)*, pp. 1–5, 2019.
- [5] H. J. Jang and K. O. Cho, "Applications of deep learning for the analysis of medical data," *Archives of Pharmacal Research*, vol. 42, no. 6, pp. 492–504, 2019.
- [6] S. Mohan, C. Thirumalai, and G. Srivastava, "Effective heart disease prediction using hybrid machine learning techniques," *IEEE access*, vol. 7, pp. 81542–81554, 2019.
- [7] Z. Zhang and E. Sejdić, "Radiological images and machine learning: trends, perspectives, and prospects," *Computers in Biology and Medicine*, vol. 108, pp. 354–370, 2019.
- [8] A. J. Hung, J. Chen, Z. Che et al., "Utilizing machine learning and automated performance metrics to evaluate robot-assisted radical prostatectomy performance and predict outcomes," *Journal of Endourology*, vol. 32, no. 5, pp. 438–444, 2018.
- [9] N. I. R. Yassin, S. Omran, E. M. El Houby, and H. Allam, "Machine learning techniques for breast cancer computer aided diagnosis using different image modalities: a systematic review," *Computer Methods and Programs in Biomedicine*, vol. 156, pp. 25–45, 2018.
- [10] E. Pellegrini, L. Ballerini, M. C. V. Hernandez et al., "Machine learning of neuroimaging for assisted diagnosis of cognitive impairment and dementia: a systematic review," *Alzheimer's & Dementia: Diagnosis, Assessment & Disease Monitoring*, vol. 10, no. 1, pp. 519–535, 2018.
- [11] G. Choy, O. Khalilzadeh, M. Michalski et al., "Current applications and future impact of machine learning in radiology," *Radiology*, vol. 288, no. 2, pp. 318–328, 2018.
- [12] M. Belić, V. Bobić, M. Badža, N. Šolaja, M. Đurić-Jovičić, and V. S. Kostić, "Artificial intelligence for assisting diagnostics and assessment of Parkinson's disease—a review," *Clinical Neurology and Neurosurgery*, vol. 184, article 105442, 2019.

- [13] M. J. Willeminck, W. A. Koszek, C. Hardell et al., "Preparing medical imaging data for machine learning," *Radiology*, vol. 295, no. 1, pp. 4–15, 2020.
- [14] A. Winkler-Schwartz, R. Yilmaz, N. Mirchi et al., "Machine learning identification of surgical and operative factors associated with surgical expertise in virtual reality simulation," *JAMA Network Open*, vol. 2, no. 8, pp. e198363–e198363, 2019.
- [15] P. R. Jeyaraj and E. R. Samuel Nadar, "Computer-assisted medical image classification for early diagnosis of oral cancer employing deep learning algorithm," *Journal of Cancer Research and Clinical Oncology*, vol. 145, no. 4, pp. 829–837, 2019.
- [16] A. Winkler-Schwartz, V. Bissonnette, N. Mirchi et al., "Artificial intelligence in medical education: best practices using machine learning to assess surgical expertise in virtual reality simulation," *Journal of Surgical Education*, vol. 76, no. 6, pp. 1681–1690, 2019.
- [17] P. Sun, "Wood quality defect detection based on deep learning and multicriteria framework," *Mathematical Problems in Engineering*, vol. 2022, Article ID 4878090, 9 pages, 2022.
- [18] K. G. Dinesh, K. Arumugaraj, K. D. Santhosh, and V. Mareeswari, "Prediction of cardiovascular disease using machine learning algorithms," in *2018 International Conference on Current Trends Towards Converging Technologies (ICCTCT)*, pp. 1–7, 2018.
- [19] C. J. Lynch and C. Liston, "New machine-learning technologies for computer-aided diagnosis," *Nature Medicine*, vol. 24, no. 9, pp. 1304–1305, 2018.
- [20] W. Chang, Y. Liu, Y. Xiao et al., "A machine-learning-based prediction method for hypertension outcomes based on medical data," *Diagnostics*, vol. 9, no. 4, p. 178, 2019.
- [21] J. Zhang, Y. Xie, Q. Wu, and Y. Xia, "Medical image classification using synergic deep learning," *Medical Image Analysis*, vol. 54, pp. 10–19, 2019.
- [22] M. Bakator and D. Radosav, "Deep learning and medical diagnosis: a review of literature," *Multimodal Technologies and Interaction*, vol. 2, no. 3, p. 47, 2018.
- [23] A. Esteva, K. Chou, S. Yeung et al., "Deep learning-enabled medical computer vision," *NPJ digital medicine*, vol. 4, no. 1, pp. 1–9, 2021.
- [24] K. K. Bressen, L. C. Adams, C. Erxleben, B. Hamm, S. M. Niehues, and J. L. Vahldiek, "Comparing different deep learning architectures for classification of chest radiographs," *Scientific Reports*, vol. 10, no. 1, pp. 1–16, 2020.
- [25] K. Chang, N. Balachandar, C. Lam et al., "Distributed deep learning networks among institutions for medical imaging," *Journal of the American Medical Informatics Association*, vol. 25, no. 8, pp. 945–954, 2018.
- [26] X. Zhou, Y. Li, and W. Liang, "CNN-RNN based intelligent recommendation for online medical pre-diagnosis support," *IEEE/ACM Transactions on Computational Biology and Bioinformatics*, vol. 18, no. 3, pp. 912–921, 2021.
- [27] W. N. Ismail, M. M. Hassan, H. A. Alsalamah, and G. Fortino, "CNN-based health model for regular health factors analysis in internet-of-medical things environment," *IEEE Access*, vol. 8, pp. 52541–52549, 2020.
- [28] M. Sajjad, S. Khan, K. Muhammad, W. Wu, A. Ullah, and S. W. Baik, "Multi-grade brain tumor classification using deep CNN with extensive data augmentation," *Journal of computational science*, vol. 30, pp. 174–182, 2019.
- [29] B. Amarnath, S. Balamurugan, and A. Alias, "Review on feature selection techniques and its impact for effective data classification using UCI machine learning repository dataset," *Journal of Engineering Science and Technology*, vol. 11, no. 11, pp. 1639–1646, 2016.

## Research Article

# Effect of Enhanced Recovery after Surgery (ERAS) Concept and Cluster Nursing on Psychological State and Pain of Oral Outpatients Undergoing Root Canal Therapy

Bei Liu,<sup>1</sup> Mao Xiong,<sup>1</sup> Feng Liu,<sup>1</sup> Wenyu Chen,<sup>1</sup> Shumei Jiang,<sup>1</sup> Meixiang Qu,<sup>2</sup>  
Lixiang Mao,<sup>1</sup> Genyun Yi,<sup>1</sup> Xiongwei Liu,<sup>1</sup> and Yuehui Wang<sup>1</sup> 

<sup>1</sup>Department of Stomatology, Hunan Provincial People's Hospital (The First Affiliated Hospital of Hunan Normal University, Changsha City, Hunan Province 410005, China)

<sup>2</sup>Outpatient Office, Hunan Provincial People's Hospital (The First Affiliated Hospital of Hunan Normal University, Changsha City, Hunan Province 410005, China)

Correspondence should be addressed to Yuehui Wang; wangyuehuicn@hunnu.edu.cn

Received 29 June 2022; Revised 18 July 2022; Accepted 4 August 2022; Published 10 September 2022

Academic Editor: Hangjun Che

Copyright © 2022 Bei Liu et al. This is an open access article distributed under the Creative Commons Attribution License, which permits unrestricted use, distribution, and reproduction in any medium, provided the original work is properly cited.

**Objective.** The effect of the concept of enhanced recovery after surgery (ERAS) and pain of patients undergoing root canal therapy in oral clinic. **Methods.** 200 participants in an oral clinic from March 2020 to March 2022 were enrolled in our study. The control group ( $n = 100$ ) accepted ERAS-based care and the research group ( $n = 100$ ) accepted ERAS concept and cluster nursing. Nursing satisfaction, comfort, self-efficacy, subjective well-being, self-rating anxiety scale (SAS), and self-rating depression scale (SDS) scores were compared. **Results.** The research group had 100% satisfaction rate; the control group had 87% satisfaction rate. After nursing, the scores of comforts and self-efficacy of the two groups increased and the scores of comforts and self-efficacy of the research group were higher than those of the control group. After nursing, the scores of subjective well-being of the two groups increased. Furthermore, the higher scores of life satisfaction, interpersonal harmony, and self-efficacy in the research group were found. There was no significant difference in the scores of SAS and SDS between the two groups before nursing ( $P > 0.05$ ), but after nursing, the scores of SAS and SDS in the two groups decreased, and the scores of SAS and SDS in the research group were lower than those in the control group, and there are statistically significant differences between the groups ( $P < 0.05$ ). The scores of visual analogue score (VAS) and numerical rating scale (NRS) following intervention decreased, and there are statistically significant differences between the groups ( $P < 0.05$ ). The less physiological, psychological, social functions, and health self-cognition in the research group were displayed, and there are statistically significant differences between groups ( $P < 0.05$ ). **Conclusion.** The adoption of the concept of ERAS and cluster nursing can effectively improve the psychological state and pain score of oral outpatients undergoing root canal therapy, improve comfort and self-efficacy, and enhance subjective well-being and quality of life. ERAS and cluster nursing is of great significance in relieving pain after root canal therapy in the outpatient department, reducing patients' pain and improving patients' quality of life.

## 1. Introduction

Periapical periodontitis is mainly characterized by the absorption of periapical bone tissue, which remains one of the common diseases in oral clinical work, seriously influencing the oral health and quality of life of patients. Oral health is one of the important indicators of human body health. In 1981, the World Health Organization (WHO) defined oral

health standards as follows: clean teeth, no caries, no pain, normal gingival color, and no bleeding [1]. Furthermore, pulpitis and periapical periodontitis are the pathological changes of inflammation, suppuration, and necrosis of dental pulp caused by bacterial infection, physical and chemical stimulation, and immune response and even spread to the periapical tissue, causing inflammation and absorption of periapical tissue [2]. Of note, infection control is the core principle for the



treatment of pulpitis and periapical periodontitis. Whitehouse supports this view for a long time and regards this view as the basic standard to guide clinical operation [3]. For more than one hundred years, there are two main ways to treat dental pulp disease and periapical disease: thorough debridement and harmless. Root canal therapy is a method developed based on the former as the basic principle. At present, the most ideal treatment for pulpitis and periapical periodontitis is root canal therapy, but in the process of root canal therapy, patients often have a certain degree of pain, intraoperative pain leads to patients being unable to cooperate with the doctor to complete the operation and even interrupts the treatment, and the patients refuse to see a doctor again. This kind of pain and discomfort can lead to anxiety, depression, irritability, and negative rebellious coping style; bad emotional state and coping strategies worsen doctor-patient relationship, reduce patients' trust in doctors, and patients evading treatment [4]. Therefore, the oral health condition is getting worse and worse, the quality of life cannot be guaranteed, and the well-being index of life is greatly reduced [5, 6]. Therefore, the purpose of this study was to investigate the effect of enhanced recovery after surgery (ERAS) concept and cluster nursing on the psychological state and pain of patients undergoing root canal therapy in dental clinics.

## 2. Patients and Methods

**2.1. Patient Clinical Data.** 200 patients of root canal therapies in oral clinic from Mar. 2020 to Mar. 2022 were selected.

The inclusive criteria were as follows: (1) patients who needed root canal therapy because of periapical periodontitis, pulpitis, and pulp necrosis (posterior molars), (2) patients had no systemic disease, (3) patients had no abnormal reaction and coping ability in normal life, (4) patients did not take painkillers and antibiotics within 1 month before treatment; and (5) those who volunteered to participate in this study and were able to return on time.

Exclusion criteria are as follows: (1) pregnant and breastfeeding patients; (2) patients whose oral pain could not be relieved due to periodontitis, periodontitis, pericoronitis of wisdom teeth, temporomandibular joint disorder syndrome, etc.; (3) those who could not complete the treatment and return on time as prescribed by the doctor; (4) those with a history of mental illness; (5) history of pain in other parts of the body and history of severe somatic diseases; and (6) inability to describe their feelings clearly and accurately. Seven cases of root canal filling showed that the overfilling was larger than that of 1 mm by X-ray.

**2.2. Treatment Methods.** The control group received routine nursing intervention. Since the control group, the research group used the concept of ERAS and cluster nursing. The designated initiatives were as follows: (1) take head nurse of oral clinic as the group leader and select the backbone nurses of the department as the group member according to the voluntary principle. When there are problems that nurses cannot solve or need to optimize and improve the process in clinical practice, (2) the team leader organized

thematic learning to train and assess the team members to ensure the ERAS cluster nursing strategy. At the same time, the head nurse organized for general practice nurses and obtained the recognition and support of other nurses to ensure the homogeneity of nursing measures. (3) Psychological nursing: actively and actively communicate with patients and tighten the distance between nurses and patients. Self-rating anxiety was used to evaluate the negative emotional state of patients and understand the causes of patients' worry and patiently guide them. The use of comfort, empathy, and other ways was analyzed to help patients with negative emotions, to introduce to patients the ideal quality of life of patients after dental root canal therapy, and to help patients to reconstruct their psychological balance. In strengthening health education, we introduce the related problems of postoperative recovery to the patients before the start of root canal therapy and explain the effect of the operation, so that the patients can rest assured. Before treatment, PPT was used to introduce postoperative nursing precautions to patients and to explain the effects of exercise, bath, diet, interpersonal communication and complications on prognosis, so as to let patients choose reasonably according to their own needs, evaluate their self-nursing ability, correct patients' misoperation in time, and continue until patients were discharged from hospital. We explain the postoperative diet and life matters needing attention, teach them how to keep the mouth clean, and enhance the patients' self-confidence. In pain nursing, when root canal therapy is carried out, gentle action is required to reduce stimulation. Patients are encouraged to supplement food properly before changing dressing in order to increase their pain threshold. When changing medicine, pay attention to the guidance of patients, divert their attention, and guide patients to cooperate in order to reduce pain. Adjust the temperature and humidity of oral clinic to improve the comfort of patients.

### 2.3. Evaluation Index

**2.3.1. Satisfaction.** After consulting the literature and experts' discussion, we designed patients' follow-up satisfaction [7]: Satisfaction rate = (very satisfied + common satisfied)/total number of cases  $\times$  100%.

**2.3.2. Comfort and Self-Efficacy Scores.** In comfort [8], we evaluate the comfort of patients, including treatment comfort, environmental comfort, temperature comfort, and nursing comfort. In self-efficacy, before and after the intervention, the Chinese version of the general self-efficacy scale [9] was used to evaluate the self-efficacy scale.

**2.3.3. Subjective Well-Being Score.** For subjective well-being, patients were assessed with Oxford well-being questionnaire (revised version) [10] before and after intervention. The scale included life satisfaction, interpersonal harmony, and self-efficacy with a total of 29 items.

**2.3.4. SAS and SDS Scoring.** (1) Self-rating anxiety scale (SAS), also known as Zung anxiety scale [11], was compiled by W.K. Zung in 1971. According to the results of the Chinese norm, the standard cut-off value of SAS was 50 points,

of which 50-59 points were mild anxiety, 60-69 points were moderate anxiety, and more than 69 points were severe anxiety. (2) Self-rating depression scale (SDS). [12] is a self-rating scale with 20 items, which is divided into 4 grades. The prototype is the depression scale compiled by W.K. Zung (1965). 53-62 was mild depression, 63-72 was moderate depression, and over 73 was severe depression.

**2.3.5. Pain Score.** In patient self-evaluation, the visual analogue score (VAS) [13] was used to evaluate pain. In nurse evaluation, the numerical rating scale (NRS) method [14] is the most common method to evaluate pain intensity. NRS method describes the strongest level of pain as the number 10 and painlessness as 0. If the pain symptoms are mild, between 1 and 3, the patient is mild pain; if the pain symptoms are severe, between 8 and 10, the patient is severe pain; and the pain symptoms between 5 and 7 are moderate pain symptoms.

**2.3.6. Quality of Life Scale.** The quality of life scale [15] consisted of four subscales with a total of 29 items. The scale was scored by 1-5 grades.

**2.4. Statistical Analysis.** IBM SPSS 24.0 software was applied for statistical analysis. The measurement data were expressed by mean  $\pm$  standard deviation. The counting data were expressed by frequency or rate. *t*-test was used when measurement data obey normal distribution, and rank sum test was used when it did not obey normal distribution.  $\chi^2$  test was used to compare the classified counting data. Repeated measurement data were analyzed by repeated measurement analysis of variance. Main effect test results were used when there was no interaction, and simple effect analysis was carried out when there was interaction.  $P < 0.05$  indicated that the difference between groups is statistically significant.

### 3. Results

**3.1. Comparison of Nursing Satisfaction.** The research group had 100% satisfaction rate; the control group had 87% satisfaction rate. The nursing satisfaction in the research group was higher than that in the control group ( $P < 0.05$ ). All results are shown in Figure 1.

**3.2. Comparison between Comfort and Self-Efficacy.** After nursing, the scores of comfort and self-efficacy were upregulated. The larger scores of comforts and self-efficacy were displayed in a studied cohort, and the difference was statistically significant, and there are statistically significant differences between groups ( $P < 0.05$ ). All results are shown in Table 1.

**3.3. Comparison of Subjective Well-Being Score.** The upregulated scores of life satisfaction, interpersonal harmony, and self-efficacy in the research group were shown statistically, and there are statistically significant differences between groups ( $P < 0.05$ ). All results are shown in Table 2.

**3.4. SAS and SDS Score Comparison.** Following care, the scores of SAS and SDS in the two groups reduced, and there

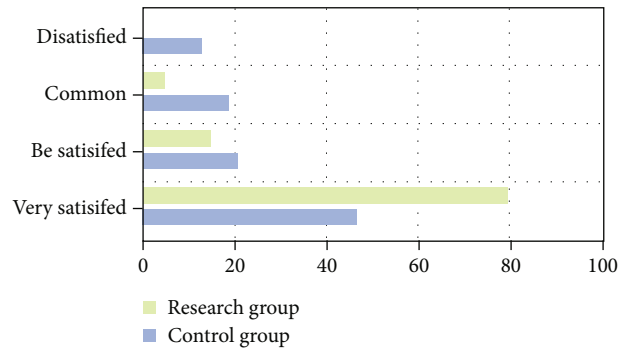


FIGURE 1: Nursing satisfaction between the two groups.

are statistically significant differences between groups ( $P < 0.05$ ). The downregulated scores of SAS and SDS in the study cohort were discovered, and there are statistically significant differences between groups ( $P < 0.05$ ). All results are shown in Table 3.

**3.5. Pain Score Comparison.** The scores of VAS and NRS in the two groups decreased following care, and there are statistically significant differences between groups ( $P < 0.05$ ). The lower scores of VAS and NRS in the study were displayed, and there are statistically significant differences between groups ( $P < 0.05$ ). All results are shown in Table 4.

**3.6. Comparison of Quality of Life Scores.** The lower scores of physiological, psychological, social functions, and health self-cognition in the research group were found, and the difference was statistically significant, and there are statistically significant differences between groups ( $P < 0.05$ ). All results are shown in Table 5.

### 4. Discussion

This study was to investigate the effect of enhanced recovery after surgery (ERAS) concept and cluster nursing on the psychological state and pain of patients undergoing root canal therapy in dental clinics. Periapical periodontitis, also known as periapical disease, is a common disease harmful to oral health. Inflammation occurs in periapical tissues, including periapical membrane, periapical cementum, and periapical alveolar bone; most of them are induced by the secondary pathogenesis of pulpitis, that is, infected dental pulp, bacteria, and other substances acting on the periapical tissue through the apical foramen [3]. Poor oral health behavior brings a lot of inconvenience to everyone's life, such as directly affecting masticatory function and also affecting speech, appearance, psychological activities, and even overall health [5]. In addition to dental caries and periodontitis, periapical periodontitis is also one of the most common oral diseases that interfere with oral health. Periapical periodontitis is an inflammatory disease that occurs around the apical tissue. Most of periapical periodontitis are the secondary diseases of dental pulp disease, which is mainly induced by the action of infectious substances in the root canal on the periapical tissue through the apical foramen, so it is also called periapical disease [16]. The range

TABLE 1: Comfort and self-efficacy scores ( $\bar{x} \pm s$ , points).

Grouping	Cases	Comfort degree		Self-efficacy	
		Before nursing	After nursing	Before nursing	After nursing
Control group	100	58.53 $\pm$ 3.42	76.81 $\pm$ 2.45 <sup>a</sup>	16.43 $\pm$ 2.69	26.48 $\pm$ 2.87 <sup>a</sup>
Research group	100	58.68 $\pm$ 3.64	84.52 $\pm$ 2.53 <sup>b</sup>	16.96 $\pm$ 2.86	36.81 $\pm$ 1.46 <sup>b</sup>
<i>t</i> value		0.300	21.891	1.349	32.080
<i>P</i> value		0.764	$P \leq 0.001$	0.178	$P \leq 0.001$

Note: the control group before and after nursing, <sup>a</sup> $P < 0.05$ ; the research group before and after nursing, <sup>b</sup> $P < 0.05$ .

TABLE 2: The subjective well-being scores ( $\bar{x} \pm s$ , points).

Grouping	Cases	Life satisfaction	Before nursing		After nursing	
			Interpersonal harmony	Sense of efficacy	Interpersonal harmony	Sense of efficacy
Control group	100	25.95 $\pm$ 3.91	29.73 $\pm$ 2.32	40.75 $\pm$ 3.91	34.91 $\pm$ 3.85	43.91 $\pm$ 2.55
Research group	100	25.82 $\pm$ 3.44	29.85 $\pm$ 2.91	40.81 $\pm$ 3.56	38.96 $\pm$ 3.81	48.96 $\pm$ 3.91
<i>t</i> value		0.249	0.322	0.322	7.477	10.818
<i>P</i> value		0.803	0.747	$P \leq 0.001$	$P \leq 0.001$	$P \leq 0.001$

TABLE 3: SAS and SDS scores between the two groups ( $\bar{x} \pm s$ , points).

Grouping	Cases	SAS		SDS	
		Before nursing	After nursing	Before nursing	After nursing
Control group	100	56.91 $\pm$ 3.42	43.66 $\pm$ 1.64 <sup>a</sup>	59.67 $\pm$ 1.53	47.71 $\pm$ 1.81 <sup>a</sup>
Research group	100	56.31 $\pm$ 3.43	38.42 $\pm$ 1.11 <sup>b</sup>	59.31 $\pm$ 1.12	39.43 $\pm$ 1.64 <sup>b</sup>
<i>t</i> value		0.113	26.460	1.898	33.899
<i>P</i> value		0.909	$P \leq 0.001$	0.059	0.031

Note: the control group before and after nursing, <sup>a</sup> $P < 0.05$ ; the research group before and after nursing, <sup>b</sup> $P < 0.05$ .

TABLE 4: VAS and NRS scores ( $\bar{x} \pm s$ , points).

Grouping	Cases	VAS		NRS	
		Before nursing	After nursing	Before nursing	After nursing
Control group	100	4.63 $\pm$ 0.89	3.76 $\pm$ 0.53 <sup>a</sup>	4.88 $\pm$ 1.22	3.42 $\pm$ 0.57 <sup>a</sup>
Research group	100	4.65 $\pm$ 0.81	2.44 $\pm$ 0.87 <sup>b</sup>	4.91 $\pm$ 1.27	2.06 $\pm$ 0.56 <sup>b</sup>
<i>t</i> value		0.166	12.957	0.170	17.019
<i>P</i> value		0.868	$P \leq 0.001$	0.864	0.031

Note: the control group before and after nursing, <sup>a</sup> $P < 0.05$ ; the research group before and after nursing, <sup>b</sup> $P < 0.05$ .

TABLE 5: Quality of life scores before nursing ( $\bar{x} \pm s$ , points).

Grouping	Cases	Physiological function		Psychological function		Social function		Healthy self-cognition	
		Before nursing	After nursing	Before nursing	After nursing	Before nursing	After nursing	Before nursing	After nursing
Control group	100	15.68 $\pm$ 4.56	13.96 $\pm$ 2.13 <sub>a</sub>	16.81 $\pm$ 3.58	14.66 $\pm$ 4.32 <sub>a</sub>	18.65 $\pm$ 3.52	16.53 $\pm$ 2.12 <sub>a</sub>	15.64 $\pm$ 3.56	13.12 $\pm$ 1.34 <sub>a</sub>
Research group	100	15.53 $\pm$ 4.51	10.56 $\pm$ 2.53 <sub>b</sub>	16.95 $\pm$ 3.92	10.56 $\pm$ 1.21 <sub>b</sub>	18.42 $\pm$ 3.23	10.68 $\pm$ 3.66 <sub>b</sub>	15.53 $\pm$ 3.67	10.45 $\pm$ 2.42 <sub>b</sub>
<i>t</i> value		0.233	10.280	0.263	9.139	0.481	13.830	0.215	9.652
<i>P</i> value		0.815	$P \leq 0.001$	0.792	$P \leq 0.001$	0.630	$P \leq 0.001$	0.829	$P \leq 0.001$

of periapical periodontitis includes inflammation of the periapical periodontal ligament, cementum, and alveolar bone [17]. Periapical periodontitis is one of the common dental hard tissue diseases. The etiology of periapical periodontitis includes not only bacterial factors, that is, infection factors, but also physical factors such as stimulation of chemicals such as phenols and aldehydes and trauma. According to its clinical manifestations and histopathological process, periapical disease can be divided into acute periapical periodontitis and chronic periapical periodontitis. The main symptoms of the former are severe tooth pain, dare not bite, and gingival and facial swelling, affecting the patient's work, study, and life [18]. Periapical inflammation can also spread to the jaw and surrounding tissue, when the resistance is low, which can form jaw osteomyelitis and cellulitis. If it is not treated in time, it may develop into septicemia and life-threatening. The latter is mostly chronic inflammation of periapical tissue promoted by chronic stimulation for a long time; that is, it often brings about different degrees of destruction of apical alveolar bone and occlusal discomfort. If it is not treated in time, it may become the focus of infection and results in diseases of distant organs of the body [19, 20]. In addition to the subjective factors of clinicians, the success rate of root canal therapy is also different, and the recovery time of apical bone defect after root canal treatment is different, which ultimately affects the recovery of tooth function. That is, the more periapical bone tissue damage defect (the larger the periapical transmission shadow on the X-ray film), the more complex the pathological process, the lower the success rate of root canal therapy, and the longer the postoperative recovery time. Therefore, early prevention, early diagnosis, early treatment, and regular follow-up are very indispensable in clinical work [21, 22].

The destruction degree of the apical alveolar bone of the teeth with periapical disease is different, the kinds of bacteria infected are different, the clinical pathological process is different, the clinical manifestations may be different, and the difficulty and complexity of root canal therapy are different. With the development of medical technology, cluster nursing based on evidence-based medicine has become one of the important nursing models, which takes scientific evidence as the main basis, attaches importance to human factors, and aims at fully understanding and respecting the wishes and needs of different patients. It is the most influential, most worthy of clinical application, and the worthiest of promotion and recognition of an effective measure [23]. Cluster nursing is a collection of measures, so it is systematic and holistic; each measure is based on evidence-based medicine, which is scientific and aimed at a certain problem, having pertinence and purpose, several measures influence and interact with each other, and the effect of coordinated implementation is far greater than that of a certain measure, with effectiveness and cooperation. It has been unanimously recognized by many clinical personnel [24, 25]. As a new evidence-based medicine concept, ERAS is not a new technology or method, but the optimization of existing perioperative management measures [26]. The clinical effect of ERAS regimen in a variety of operations has been verified. A number of randomized controlled trials and case-control studies

have confirmed that the application of ERAS regimen in surgery is safe and effective, which can contribute to the functional recovery of patients and shorten postoperative hospital stay and reduce medical expenses [27]. Meanwhile, our current study indicates that, compared with routine nursing, ERAS can be employed in oral outpatients, which can effectively relieve pain and improve negative emotion, indicating that the application of ERAS in oral outpatients is safe and effective.

The scores of comforts and self-efficacy in the research group were higher than those in the control group, the scores of SAS and SDS in the research group were lower than those in the control group, and the scores of VAS and NRS in the study, demonstrating that the concept of ERAS and cluster nursing can effectively relieve pain, reduce negative emotions, and improve patients' comfort, satisfaction, and self-efficacy. Root canal therapy is to remove the infectious substances in the pulp chamber and root canal by root canal preparation, then close the root canal in a three-dimensional space by root canal disinfection and strict root canal filling, cut off the infection pathway, and promote the healing of pulp disease and periapical lesions [28]. There are many causes of root canal pain, such as bacterial factors, iatrogenic factors, the patient's own physique, and the anatomical location of the affected teeth. Under the existing conditions, doctors have to take anesthetic injection to appease and comfort, but it is sometimes difficult to complete the whole course of root canal therapy. The pain feeling of root canal therapy has a certain impact on the patient's body and mind, resulting in the patient not returning to see the doctor on time and refusing to see a doctor when the affected tooth appears again in the oral cavity after seeing a doctor, which threatens the oral health condition and causes trouble to the patient's daily life [28]. In our study, the nursing satisfaction of the research group was higher than that of the control group.

As early as 1930, the theory of happiness was first put forward. Only with happy emotions can we have a healthy body and a harmonious life. Therefore, subjective well-being is used to describe the happiness of patients in this paper. With regard to the concept of subjective well-being (SWB), psychologists have different understandings of it according to their own research results. The overall evaluation of an individual's quality of life is according to the standards set by himself. Subjective well-being has the characteristics of subjectivity, stability, and integrity [29]. Combined with the results of the current study, the scores of life satisfaction, interpersonal harmony, and self-efficacy in the research group were higher than those in the control group, while the scores of physiological function, psychological function, social function, and health self-cognition in the research group were lower than those in the control group. In the research of Chinese scholars [30], words such as happiness, overall well-being, well-being, subjective quality of life, and happy life index are also utilized to express the concept of subjective well-being. Some studies have pointed out that SWB is an important attitude towards life, which can not only reflect the level of mental health but also measure the quality of life and psychological development. Through



the employment of the concept of ERAS and cluster nursing, we could effectively improve the SWB of oral outpatients with root canal therapy and further improve the quality of life. There are some limitations in this study. First, the sample size of this study is not large and it is a single-center study, so bias is inevitable. In future research, we will carry out multicenter, large-sample prospective studies, or more valuable conclusions can be drawn.

Collectively, the adoption of the concept of ERAS and cluster nursing can effectively improve the psychological state and pain score of oral outpatients undergoing root canal therapy, improve comfort and self-efficacy, and enhance subjective well-being and quality of life. ERAS and cluster nursing is of great significance in relieving pain after root canal therapy in outpatient department, reducing patients' pain, and improving patients' quality of life.

## Data Availability

No data were used to support this study.

## Conflicts of Interest

The authors declare that they have no conflicts of interest.

## References

- [1] R. Bharti, A. P. Tikku, A. Chandra, and P. Gupta, "Antimicrobial effectiveness of photodynamic therapy, 5% sodium hypochlorite and 2% chlorhexidine gluconate in root canal treated teeth: a clinical study," *Journal of Advanced Oral Research*, vol. 12, no. 2, pp. 193–199, 2021.
- [2] S. W. Kwak, J. H. Ha, Y. Shen, M. Haapasalo, and H. C. Kim, "Effects of root canal curvature and mechanical properties of nickel-titanium files on torque generation," *Journal of endodontics*, vol. 47, no. 9, pp. 1501–1506, 2021.
- [3] C. T. Rodrigues, R. Jacobs, K. F. Vasconcelos et al., "Influence of CBCT-based volumetric distortion and beam hardening artefacts on the assessment of root canal filling quality in isthmus-containing molars," *Dento Maxillo Facial Radiology*, vol. 50, no. 5, article 20200503, 2021.
- [4] J. C. Pinto, F. F. Torres, E. Lucas-Oliveira, T. J. Bonagamba, J. M. Guerreiro-Tanomaru, and M. Tanomaru-Filho, "Evaluation of curved root canals filled with a new bioceramic sealer: a microcomputed tomographic study using images with different voxel sizes and segmentation methods," *Microscopy Research and Technique*, vol. 84, no. 12, pp. 2960–2967, 2021.
- [5] L. D. Guimaraes, E. A. da Silva, F. G. Hespanhol, K. B. Fontes, L. A. Antunes, and L. S. Antunes, "Effect of photobiomodulation on post-operative symptoms in teeth with asymptomatic apical periodontitis treated with foraminal enlargement: a randomized clinical trial," *International Endodontic Journal*, vol. 54, no. 10, pp. 1708–1719, 2021.
- [6] D. P. Shilpa Jain, K. Jogikalmat, K. Dinesh, and N. Velmurugan, "Effect of cervical lesion centered access cavity restored with short glass fibre reinforced resin composites on fracture resistance in human mandibular premolars- an in vitro study," *Journal of the Mechanical Behavior of Biomedical Materials*, vol. 122, no. 85, p. 104654, 2021.
- [7] J. Wong, D. Manoil, P. Näsman, G. N. Belibasakis, and P. Neelakantan, "Microbiological aspects of root canal infections and disinfection strategies: an update review on the current knowledge and challenges," *Frontiers in Oral Health*, vol. 2, no. 51, pp. 149–156, 2021.
- [8] D. Weiqin, Z. Jianzhen, and Z. Yaqing, "Application of four-hand nursing cooperation technique in root canal therapy under oral microscope," *Qilu Journal of Nursing*, vol. 27, no. 12, pp. 61–63, 2021.
- [9] A. A. Ateş, B. Arican, E. Çiftçioğlu, and E. S. Küçükay, "Influence of different irrigation regimens on the dentinal tubule penetration of a bioceramic-based root canal sealer: a confocal analysis study," *Lasers in Medical Science*, vol. 36, no. 8, pp. 1771–1777, 2021.
- [10] Y. Zhao, Q. Zhao, M. Zheng et al., "Comparison of microstructural imaging of the root canal isthmus using propagation-based X-ray phase-contrast and absorption micro-computed tomography," *Journal of Microscopy*, vol. 284, no. 1, pp. 74–82, 2021.
- [11] T. Liu, A. Aman, M. Ainiwaer et al., "Evaluation of the anti-biofilm effect of poloxamer-based thermoreversible gel of silver nanoparticles as a potential medication for root canal therapy," *Scientific Reports*, vol. 11, no. 1, pp. 586–589, 2021.
- [12] S. Drukteinis, G. Bilvinaite, P. Tusas, H. Shemesh, and V. Peculiene, "Porosity distribution in single cone root canal fillings performed by operators with different clinical experience: a micro CT assessment," *Journal of Clinical Medicine*, vol. 10, no. 12, pp. 762–769, 2021.
- [13] Z. Jiani, L. Tingjun, and G. Lihong, "Effectiveness of XP-Endo finisher and passive ultrasonic irrigation on intracanal medication removal from root canals: a systematic review and meta-analysis," *BMC Oral Health*, vol. 21, no. 1, pp. 784–789, 2021.
- [14] K. Yağmur, K. Emrah, and K. M. Emin, "The effect of root canal preparation size and taper of middle mesial canals on fracture resistance of the mandibular molar teeth: an in vitro study," *Journal of Endodontics*, vol. 47, no. 9, pp. 185–190, 2021.
- [15] Y. Güven, A. D. Uygün, and H. Arslan, "Efficacy of EDDY, ultrasonic activation, XP-endo Finisher and needle irrigation on the removal of mTAP from artificially created grooves in root canals," *Australian endodontic journal*, vol. 47, no. 3, pp. 639–644, 2021.
- [16] M. I. Karobari, S. N. Basheer, F. R. Sayed et al., "An in vitro stereomicroscopic evaluation of bioactivity between Neo MTA plus, Pro Root MTA, BIODENTINE & glass ionomer cement using dye penetration method," *Materials*, vol. 14, no. 12, pp. 3159–3200, 2021.
- [17] R. Tingting, "Effect of knowledge, belief and practice health education on bad mood, compliance and coping style of older children undergoing root canal therapy," *International Journal of Nursing*, vol. 40, no. 8, pp. 1390–1393, 2021.
- [18] T. Qingmin, "Effect observation and value analysis of targeted nursing intervention in root canal therapy of patients with pulpitis," *Chinese Medicine Guide*, vol. 19, no. 8, pp. 165–166, 2021.
- [19] H. Min, L. Kai, and T. Daofang, "Analysis of the effect of four-hand operation combined with psychological nursing on the therapeutic effect of root canal therapy," *Journal of Lishui university*, vol. 43, no. 2, pp. 31–35, 2021.
- [20] T. von Arx, F. B. Kissling-Jeger, and S. F. Simone, "Through-and-through cystic lesion: spontaneous healing after needle aspiration and conventional root-canal therapy," *Swiss dental journal*, vol. 130, no. 1, pp. 49–56, 2020.



- [21] N. Andrejeva, D. Baumeister, Eich, and J. Tesarz, "Psychosoziale Faktoren in der Prävention von Schmerz [Psychosocial factors in the prevention of pain]," *Schmerz*, vol. 35, no. 1, pp. 21–29, 2021.
- [22] Z. Yaqing, L. Qin, and Z. Jianzhen, "The method of cooperative training between doctors and nurses was used to improve the practical ability of specialized nurses in root canal microtherapy," *Shanghai Stomatology*, vol. 28, no. 6, pp. 648–651, 2019.
- [23] Y. Junxing and H. Min, "Advances in the application of four-hand manipulation in root canal therapy in China," *PLA Journal of Nursing*, vol. 34, no. 20, pp. 53–56, 2017.
- [24] Y. Wu Lijuan and C. J. Fei, "Nursing care of patients with tooth defect after root canal treatment with rapid aesthetic porcelain system beside the chair," *Journal of Nursing*, vol. 31, no. 18, pp. 51–52, 2016.
- [25] T. Fangli, Z. Xiongqun, and L. Mei, "Application of PDCA cycle in root canal filling quality management," *Stomatology research*, vol. 31, no. 10, pp. 1029–1031, 2015.
- [26] G.-P. Bacteria, "Findings on *Enterococcus faecalis* reported by investigators at University of Freiburg (ultrasonic activation and chemical modification of photosensitizers enhances the effects of photodynamic therapy against *enterococcus faecalis* root-canal ...)," *Biotech Week*, vol. 45, no. 6, pp. 164–169, 2015.
- [27] C. Tennert, A. M. Drews, V. Walther et al., "Ultrasonic activation and chemical modification of photosensitizers enhances the effects of photodynamic therapy against *Enterococcus faecalis* root-canal isolates," *Photodiagnosis and Photodynamic Therapy*, vol. 12, no. 2, pp. 244–251, 2015.
- [28] Q. Haihong and L. Ling, "Cause analysis and preventive measures of instrument fracture in root canal therapy," *Journal of Modern Stomatology*, vol. 29, no. 2, p. 114, 2015.
- [29] Z. Changping, Z. Yun, and L. Rui, "Application status and problem analysis of four-hand operation and six-hand operation in dental diagnosis and treatment in China," *Chinese Journal of Nursing*, vol. 49, no. 11, pp. 1405–1408, 2014.
- [30] Z. Liwen, G. Yongbo, and Y. Ying, "Application effect of four-hand operation in dredging calcified root canals by microultrasound technique," *PLA Journal of Nursing*, vol. 31, no. 14, p. 61, 2014.

## Research Article

# Research on Medical Big Data Analysis and Disease Prediction Method Based on Artificial Intelligence

Fang Zhang, Zhen Zhang, and Hui Xiao 

Information Center, Zhongnan Hospital of Wuhan University, Hubei, Wuhan 430071, China

Correspondence should be addressed to Hui Xiao; xiaohui@znhospital.com

Received 20 June 2022; Revised 28 July 2022; Accepted 1 August 2022; Published 9 September 2022

Academic Editor: Hangjun Che

Copyright © 2022 Fang Zhang et al. This is an open access article distributed under the Creative Commons Attribution License, which permits unrestricted use, distribution, and reproduction in any medium, provided the original work is properly cited.

In recent years, the continuous development of big data, cloud services, Internet+, artificial intelligence, and other technologies has accelerated the improvement of data communication services in the traditional pharmaceutical industry. It plays a leading role in the development of my country's pharmaceutical industry, deepening the reform of the health system, improving the efficiency and quality of medical services, and developing new technologies. In this context, we make the following research and draw the following conclusions: (1) the scale of my country's medical big data market is constantly increasing, and the global medical big data market is also increasing. Compared with the global medical big data market, China's medical big data has grown at a faster rate. From the initial 10.33% in 2015, the proportion has reached 38.7% after 7 years, and the proportion has increased by 28.37%. (2) Generally speaking, urine is mainly slightly acidic, that is, the pH is around 6.0, the normal range is 5.0 to 7.0, and there are also neutral or slightly alkaline. 8 and 7.5 are generally people with some physical problems. In recent years, the pharmaceutical industry has continuously developed technologies such as big data, cloud computing, Internet+, and artificial intelligence by improving data transmission services. As an important strategic resource of the country, the generation of great medical skills and great information is of great significance to the development of my country's pharmaceutical industry and the deepening of the reform of the national medical system. Improve the efficiency and level of medical services, and establish forms and services. Accelerate economic growth. In this sense, we set out to explore.

## 1. Introduction

There is a growing need for an in-depth investigation of the application of logic in artificial intelligence and computer science. The Manual of Logic in Artificial Intelligence and Logic Programming and its companion The Manual of Logic in Computer Science were created to meet this need. A combination of comprehensive investigation and basic research explores underlying topics in various fields. We assume some mathematical complexity as background. Logicians and mathematicians will be interested in most of the material [1]. Constraint programming is currently successfully applied in many areas such as scheduling planning, vehicle routing, configuration, networking, and bioinformatics. But these necessarily focus on the main concepts and technologies and cannot cover extensions, applications, and languages at the same time.

The handbook provides a fairly complete coverage of all this work based on constraint programming so that the reader can get a fairly accurate picture of the entire field and its potential. Of course, each work is handled in a survey-like fashion, where some details may be omitted in favor of coverage [2]. Program computation guide artificial intelligence systems Michael Negnevitsky almost all literature on artificial intelligence is in the field of computer science, full of complex matrix algebra, and differential equations. The field of computational intelligence is presented, which includes rule-based expert systems, fuzzy expert systems, frame-based expert systems, artificial neural networks, evolutionary computing, hybrid intelligent systems, knowledge engineering, and data mining [3]. Among various uncertainties, randomness and ambiguity are the most important and fundamental. The relationship between randomness and ambiguity is discussed.

Uncertain states and their changes can be measured by entropy and hyperentropy, respectively. The uncertainties of various evolutions and differentiations of chaotic, fractal, and complex networks are studied. A simple and effective method is proposed to simulate uncertainty through knowledge representation, which provides a basis for the automation of logical thinking and image thinking with uncertainty [4]. It is not clear when to monitor the implementation. There is room for improvement, but if the data processing algorithm works, we can use the data processing algorithm outside the original algorithm. So, we cannot use it [5]. Large-scale medical data is a kind of data with large volume, rapid growth, complex structure, and high delay. Write big data machine learning technology applications and medical research progress, including regression analysis, decision trees, subtraction algorithms, low-level machine learning based on basic algorithms, neural network model analysis, and algorithms in big data analysis [6]. The number of outpatient visits in my country has increased significantly, which reduces outpatient time and improves the efficiency of outpatient care. A complementary model based on machine learning is proposed to support diagnosis of outpatients. Other diagnostic models use auxiliary vector machines (SVMs) and neural networks (NNs) to simultaneously classify hyperlipidemia based on clinical features obtained from a set of medical data. The results showed that the diagnostic model was 90% accurate in diagnosing hyperlipidemia [7]. Possible ways to monitor and analyze health conditions is through deep learning algorithms in collaboration with IoT-based medical big data. Recent research trends in related fields usually use traditional machine learning-based algorithms, which are not suitable for IoT-based big medical data due to manual feature extraction and low accuracy. IoT system for health monitoring based on deep learning helps to provide relevant results for different remote doctors in the field of IoT architecture to ensure the understanding of critically ill patients [8]. In the medical field, for the purpose of realizing personalized medicine, innovation has developed from the dissemination of electronic medical records to the accumulation of medical information to the integration of genomic information. However, there is a limit to the manual processing of these accumulated large amounts of information, so it is considered necessary to utilize technologies for medical big data that can be processed effectively and efficiently. Therefore, Fujitsu has developed medical big data analysis technology [9]. The rapid growth of medical data generated by hospital information systems marks the arrival of the era of big data in the medical field. This data has significant value for workflow management, patient care and treatment, scientific research, and education in the healthcare industry. However, the complex, distributed, and highly interdisciplinary nature of medical data highlights the limitations of traditional data analysis capabilities in terms of data access, storage, processing, analysis, distribution, and sharing [10]. The main advantage of the classification system is that, according to the rules of mining associations, they can evaluate multiple tasks at the same time. Association

classifiers are especially useful in programs where models help domain experts make decisions. A support system is proposed to predict cardiovascular disease in the Andhra Pradesh population. Experiments show that the accuracy of this set of rules is better than the current system [11]. A systematic review of biomonitoring models can predict the occurrence of disease events in selected drugs. We define pathological events as biological events of interest. These phenomena are characterized as infectious and pathological conditions. We looked at models that try to predict the prevalence of the disease, not just the dynamics of its spread, and models that refer to the national registry of selected factors are of interest in the United States [12]. The medical diagnosis process can be interpreted as a decision-making process in which a physician makes a diagnosis in a new, unknown case based on available medical knowledge and clinical experience. This process can be computerized to present medical diagnoses wisely, objectively, accurately, and efficiently. In recent decades, many researchers have worked to develop effective methods for predicting cardiovascular disease and decision-making systems. Accurate predictions are paramount in these systems [13]. Recent advances in genotyping techniques have allowed the use of large-scale genetic information to identify loci vulnerabilities, a successful discovery that has greatly improved our understanding of complex diseases. Despite these advances, the finding that most genetic effects are minimal for many complex diseases is a major hurdle in developing prognostic models of disease. We compare their accuracy by adapting to different complex diseases. Our results show that penalized regression is generally more stable than current methods and provides better accuracy, at least for the diseases in question [14]. Data mining is the process of extracting useful information from massive data. Data mining has broad application prospects in the medical field. Many researchers have proposed the use of  $K$ -nearest neighbors (KNN) algorithm for diabetes disease prediction. A different approach has been proposed by some researchers, using  $K$ -means clustering for preprocessing followed by KNN for classification. These methods result in poor classification accuracy or prediction. For a given dataset, we successfully achieve better results than existing methods. Our second method produces better results than the first method. Classification was performed using a ten-fold cross-validation technique [15]. The second part of the article discusses the application of big data and artificial intelligence technology in medicine. The third part introduces the intelligent model in artificial intelligence. The fourth part predicts the performance of diseases in big data of traditional Chinese medicine and optimizes intelligent methods.

## 2. AI-Based Medical Big Data Analysis

### 2.1. Medical System Application of Artificial Intelligence

**2.1.1. Outpatient Registration System.** The outpatient registration system is directly related to the current patient consultation process and is also the basis for its construction.

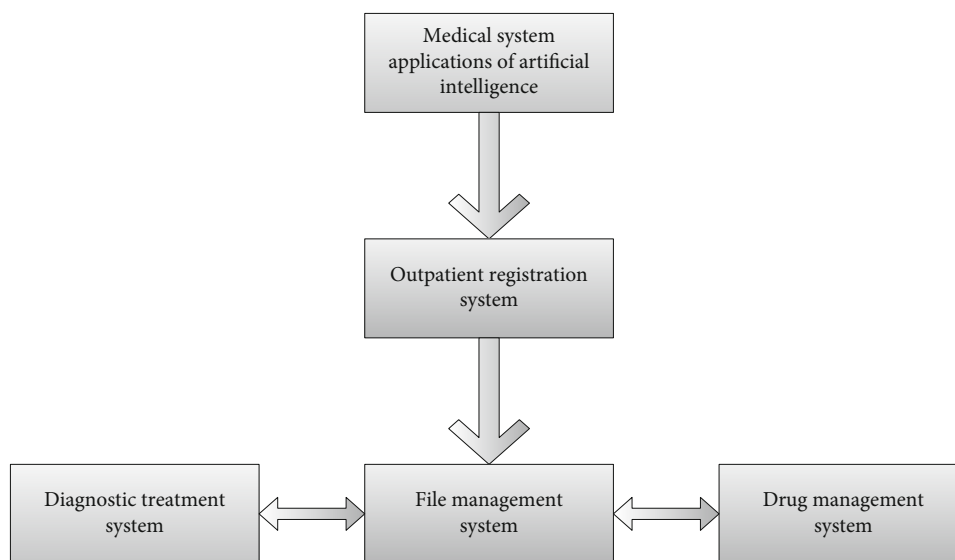


FIGURE 1: Medical system application of artificial intelligence.

The first thing to solve is the registration, which can be processed through the registration app and the medical portal. The outpatient registration system uses JSP technology to realize the intercommunication of related information by completing patient information entry, physician selection, or appointment management. In the process of setting up the system, lay the groundwork for it.

**2.1.2. Diagnosis and Treatment System.** The diagnosis and treatment system will be operated by physicians, and big data will be constructed based on the machine learning diagnosis and treatment system of big data. In the course of its research, it is analyzed through the collection of existing information, according to the mortality rate, discharge rate, and number of surgeries of existing patients in the hospital. The admission diagnostic criteria are imported; the compliance rate is analyzed; the specific coding value, upper limit value, and threshold value are determined; and then certain control is made. According to the establishment of the diagnosis management system, the existing medical history is analyzed, and then the diagnosis is entered for the patient based on the CT images, MRI, blood routine, and other test results taken by the patient. At the same time, the corresponding diagnosis results are issued to facilitate the continued use of control. And according to the input target to determine the specific standards, in the subsequent use process, do a good job of report analysis and basic maintenance.

**2.1.3. Medical Record Management System.** The medical record management system is a system that records the detailed information of patients. Based on the automatic concept of machine learning, in the process of model building, the decision tree algorithm is the core, and analysis is made according to the number of evaluations of the existing models. Get the computational status of its kernel model. The establishment of the system will analyze the relevant patient information, the accompanying information of the patient's family, the patient's own medical history, and the

patient's disease displacement status. Pay attention to the changing condition of the patient during use and continue to deal with it. This information will be input into the modules in the system, and automatic data generation can also be made according to the input status of the information. The main functions of the preview printing system include the management of daily data, the query of medical records, and the collection of relevant report data. In the maintenance process of dictionary data, medical record function data, and report data, it is managed.

**2.1.4. Drug Management System.** The drug management system is a kind of system that realizes drug classification as the management core. It integrates big data and can divide drugs into Chinese herbal medicines, western medicines, Chinese patent medicines, etc., realize the printing operation of drug functions, and complete the storage management and control of drugs. In terms of inventory management and preservation and drug functions, in view of the input control characteristics of drugs, medical treatment needs should be combined with big data diagnosis. During the establishment of the drug system, the management of warehousing, taking-out, loss reporting, inventory management, and drug application management is carried out. It is shown in Figure 1.

## 2.2. Current Shortcomings of Medical Big Data

**2.2.1. Problems in Data Analysis and Modeling.** Health information systems are generally not designed for data research and analysis. In terms of data analysis, medical data is often complex, and the modeling of medical data is closely related to medical business processes, requiring not only professional knowledge in various fields but also genetic experts. That is not possible at that dealership. In other words, how to coordinate experts in different fields to create an effective data model is very important.

**2.2.2. Medical Natural Language Processing Is Difficult and Affects Data Quality.** Because a lot of detailed patient data

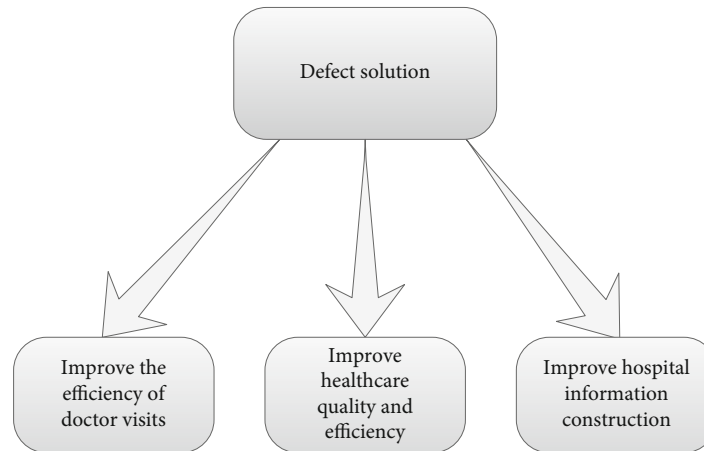


FIGURE 2: Solutions for medical big data deficiencies.

is stored in text, the data described in the text is often ambiguous, and there are many specific descriptions of how this structured data is transformed into coherent data: structured data is an important clinical dimensional data processing. One solution is to use natural language. Converting unstructured medical information to structured data requires many forms of medical natural language processing, such as identifying nominal medical topics, nominal auto coding of nominal objects, identifying language search variations of nominal objects, and retrieving temporal information, take data recovery as the core technology.

**2.2.3. Poor Quality of Medical Records.** Before data can be collected from a research server hub, it must be organized and standardized. This information is required on a case-by-case basis. Base units, time signals, and case data are organized and stored in open standard architectures such as HL7 and CDA to ensure availability and scalability. Offers flexible information retrieval options to help you find the right case. The print interface exports data in standard data formats that third-party platforms can handle. Clinical trials put forward higher requirements on the quality of medical records, and the poor quality of patient data directly leads to differences in clinical trial results, resulting in the precision and validation of data required to write medical records and the standardization of the meaning of each data.

**2.2.4. The Compliance of Patients to Provide Follow-Up Data Needs to Be Improved.** The follow-up implications of these data for medical research are obvious. During the internship, we learned that most patients with cardiovascular disease are elderly people, and the elderly do not know how to use electronic devices, which affects the speed and accuracy of data collection. In the future, wearables, teleconsultation, and integrity of information systems should be used in healthcare settings in different locations to improve access to healthcare, especially with patients from other countries.

### 2.3. Solutions to the Deficiencies of Medical Big Data

**2.3.1. Improve the Efficiency of Doctor Visits.** Data visualization can help clients, especially inexperienced clients, to con-

duct more targeted consultations, as some patients may have errors in their communication and descriptions with clients, resulting in differences in diagnosis and treatment. Systematic visualization of data analysis ensures perfect correlation, even as it helps clinicians learn more. Contact with doctors, especially with patients, becomes more practical and prevents diagnostic errors.

**2.3.2. Improve the Quality and Efficiency of Medical Data.** Hospital data is for reporting or clinical research purposes only. Due to inaccurate basic medical data standards and high data quality, the query efficiency of traditional database methods is low. Different types of medical data are processed and managed through the medical big data platform and processed through technical means such as word segmentation, structuring, and normalization to improve the quality of medical information. When viewing medical data, a clearer visual interface can be provided. Card checks by hospital staff increase the efficiency of medical information use from 10% to 30% to 80%. This means a significant increase in efficiency.

**2.3.3. Improve Hospital Informatization Construction.** Hospitals have to deal with standard information items. During the construction of the big data platform, medical data is integrated and processed, data visualization applications are developed, and decision-making, diagnosis and treatment support, and scientific support are provided for hospitals. Hospital data provide rvrf for academic research. It is shown in Figure 2.

## 3. Artificial Intelligence Computing Algorithms

**3.1. Quantized Convolution Calculation.** The quantized convolution calculation is a convolution calculation using the quantized low-bit value, and the quantized convolution calculation that does not require an inverse quantization operation will be introduced. Different from the numerical compression network that needs to perform inverse quantization operation during model inference, quantized convolution calculation only needs to perform sparse prediction



(whether it is zero) and does not require inverse quantization operation to restore numerical accuracy, so less computation is required. The amount and less computational complexity, the operation is faster. Formula (1) shows a classical convolution calculation process:

$$Y = \sum_i^N w_i \otimes x_i, \quad (1)$$

where the multiplication sign represents the convolution operation. For simplicity of description, the bias is ignored here. For a given quantization function  $f$ , the corresponding quantization convolution calculation process is shown in formula (2), where the plus sign represents the low-bit numerical quantization convolution operation.

$$f(Y) = f\left(\sum_i^N w_i \otimes x_i\right), \quad (2)$$

$$f(Y) = f\sum_i^N f(w_i \otimes x_i). \quad (3)$$

Since SeerNet only needs to predict the sparsity of the feature, that is, the spatial position of the zero value in the feature map after the ReLU layer and the max pooling layer, SeerNet does not need to perform inverse quantization. The quantization convolution calculation process is shown in the following formula:

$$\text{sign}(f(Y)) = \text{sign}\left(\sum_i^N (f_w(w_i) \oplus f_x(X_i))\right). \quad (4)$$

In many commonly used CNN models, Conv layers are usually followed by different combinations of batch normalization layers, ReLU layers, and max pooling layers. ReLU makes negative-valued features become zero-valued features, and the max pooling layer allows only one value with the largest absolute value in a subregion to be retained, and all other positions are discarded. Using the quantization network to predict the feature map sparsity after ReLU layer and max pooling layer can save more unnecessary computation compared to predicting only the feature map sparsity after ReLU layer. Depending on how the model experts design the model, the Conv layer, BatchNorm layer, and ReLU layer, the combination of max pooling layers is also different. Since the BatchNorm layer has the greatest impact on feature sparse prediction, SeerNet divides all combinations into the following two types with or without the BatchNorm layer:

$$B = \frac{\alpha \times (Y - \mu)}{\sqrt{\sigma^2 + \varepsilon}} + \beta, \quad (5)$$

$$B = \frac{\alpha \times \left(\sum_i^N W_i \otimes X_i + \text{bia} - \mu\right)}{\sqrt{\sigma^2 + \varepsilon}} + \beta. \quad (6)$$

By fusing the Conv layer and the BatchNorm layer, SeerNet reduces the computational burden and eliminates the accumulation of quantization errors. Kernel fusion is a common method to accelerate inference of DNN models.

$$f(B) = f\left(\frac{\sum_i^N \alpha W_i \otimes X_i + \alpha \times (\text{bias} - \mu)}{\sqrt{\sigma^2 + \varepsilon}} + \beta\right). \quad (7)$$

**3.2. Algorithms for AI Computing.** By sorting and examining this content, we can deepen our understanding of particle filtration algorithms and their artificial intelligence algorithms and their shortcomings, providing a good basis for further research and refinement of algorithms and to improve future research.

Improve the basic theoretical knowledge of artificial intelligence algorithms, and analyze the adaptive adjustment method at the same time. Through the sorting and learning of these contents, we can deepen the understanding of particle filter algorithm and artificial intelligence algorithm and understand their respective deficiencies, lay a good foundation for subsequent research and algorithm improvement, and improve the efficiency of subsequent research.

$$p(x|z) = \frac{p(x|z)p(z)}{p(z)}. \quad (8)$$

Using the posterior probability density function from the current moment to the next moment, the system model is used to predict, and the equation used for the prediction is as follows:

$$p(x_k|z_k) = \frac{p(z_k|x_k)p(x_k|z_k)}{\int p(z_k|x_k)p(x_k|z_k)dx_k}. \quad (9)$$

Let  $D$  be a random region in  $N$ -dimensional space, and let  $i$  be a multiple integral, expressed as

$$I = \int_D G(x)dx. \quad (10)$$

Then, its arithmetic mean is

$$g_m = \frac{1}{m} \sum_{i=1}^m g(x_i). \quad (11)$$

If these samples are distributed independently, the expectation is

$$E[i] = E[g(x)] = \frac{1}{m} \sum_{i=1}^m g(x_i). \quad (12)$$

Solve problems with random variables. A series of patterns in interstitial space, such as a segment of "particles," is an approximate distribution. Aggregation of these particles turns the aggregation problem into an aggregation problem, reducing computational complexity and time. If

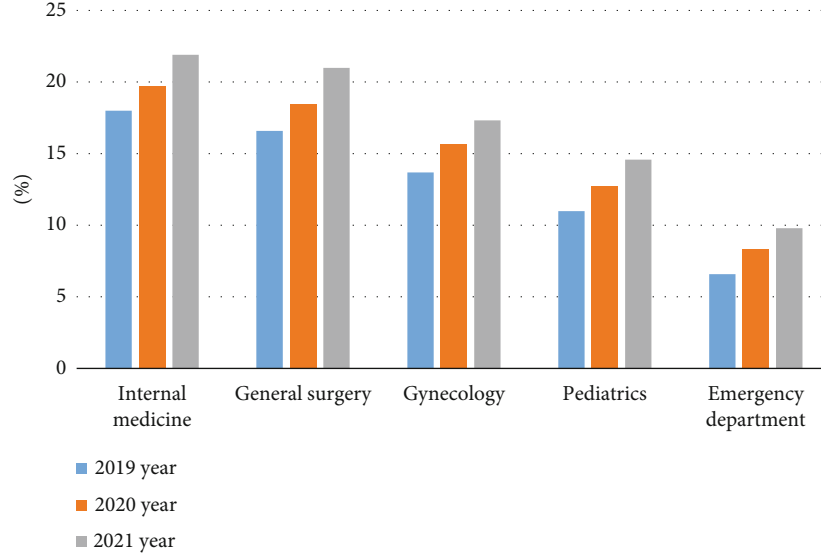


FIGURE 3: The proportion of the number of outpatient departments in tertiary hospitals.

the particle sample is large, the probability distribution may be overestimated.

It can be seen that the algorithm is the optimal filtering method. In practice, fundamental problems are solved with random variables. A set of spatial samples as “particles” are suitable for estimating the distribution. Adding these particles makes the integration problem more than just a summation problem, which reduces computational complexity and reduces computation time. When the particle sample is large, the posterior probability distribution of the problem can be approximated.

**3.3. Importance Sampling.** Assuming that, a random variable  $x \sim p(x)$  is estimated, it is difficult to directly extract the sample value in some cases, so an important density function  $q(x)$  can be used to replace the true distribution, and the expected estimated value is

$$E[i] = E[g(x)] = \frac{1}{m} \sum_{i=1}^m g(x_i), \quad (13)$$

where

$$w(x) = \frac{p(x)}{q(x)}. \quad (14)$$

Called the importance weight, the sample points are drawn from the proposed distribution function, and the estimated value can be approximated:

$$E\{h(x)\} = \frac{1}{n} \sum_{j=1}^n h(x^j) w(x^j). \quad (15)$$

TABLE 1: 2015-2021 medical big data market size and growth rate.

Years	Market size (100 million yuan)	Growth rate
2015 year	6.06	28.95%
2016 year	9.4	55.12%
2017 year	13.1	39.36%
2018 year	19	45.04%
2019 year	32.1	68.95%
2020 year	49.6	54.52%
2021 year	79.05	59.37%

Then, the posterior probability density is

$$p(x_t|z_t) \approx \sum_{i=1}^N w_i^t \delta(x_t - x_t^i). \quad (16)$$

According to the law of large numbers, when  $M$  is infinitely close to zero, the calculated posterior probability density can be approximately equal to the true posterior probability density. Therefore, the basic steps of the particle filter algorithm are summarized as follows: (1) initialization, including the initialization of parameters such as variance, simulation step size, number of particles, and evolutionary algebra. (2) Extract the particles. When  $t = 0$ , randomly select  $N$  particle points from the importance probability density function to form the initial particle set, and the weights are all  $1/N$ . (3) Body weight update. Grain weight is calculated using the latest calibration data. The closer the selected part is to the actual subject, the greater the weight given. Grain weight update formula:

$$w_t^i = \frac{1}{(2\pi\sigma^2)} \exp\left(-\frac{d_i^2}{2\sigma^2}\right). \quad (17)$$

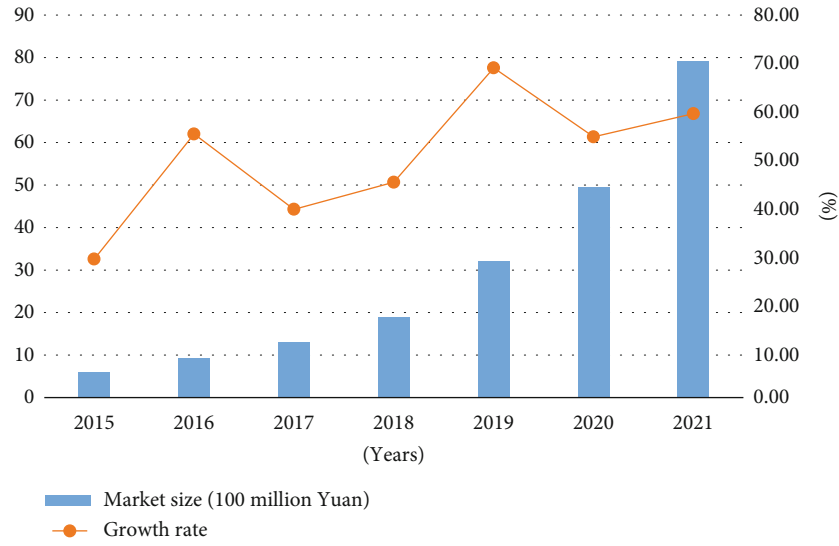


FIGURE 4: Scale and growth rate of my country's medical big data market from 2015 to 2021.

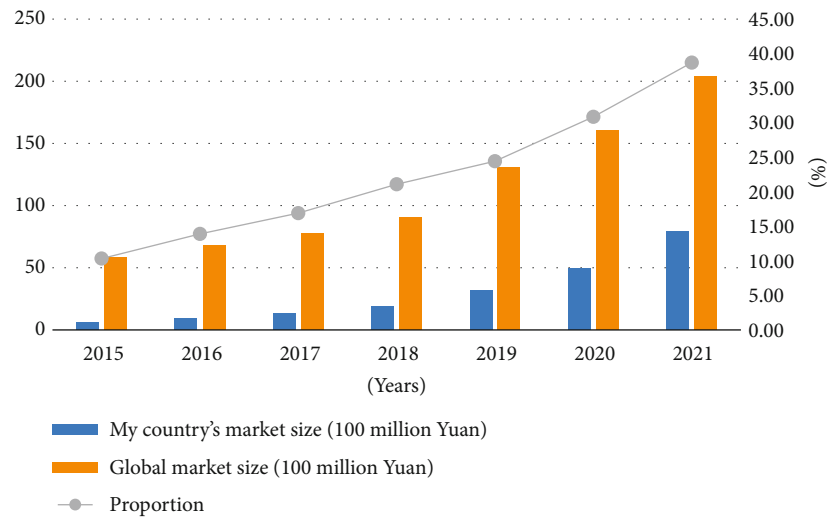


FIGURE 5: 2015-2021 my country and the global medical big data market scale.

TABLE 2: Combined disease datasets.

Features										Label
ID	Disease				D1	D2	D3	D4	D5	
1	D1	D2	D3	D4	D1	D2	D3	D4	D6	
2	D1	D2	D5	D6	D1	D2	D5	D6	D7	
3	D1	D5	D6	D7	D1	D5	D6	D7	D8	
4	D1	D5	D8	D9	D1	D5	D6	D7	D9	

TABLE 3: Prediction dataset.

Features				Label 1		Label 2
D1	D2	D3	D4	D5		0
D1	D2	D3	D4	D6		0
D1	D2	D5	D6	D7		1
D1	D5	D6	D7	D8		0
D1	D5	D6	D7	D9		0

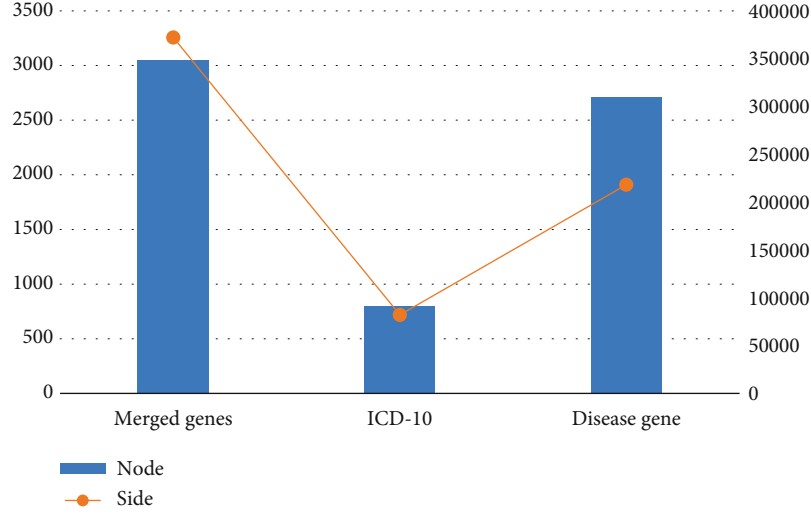


FIGURE 6: Disease network scale.

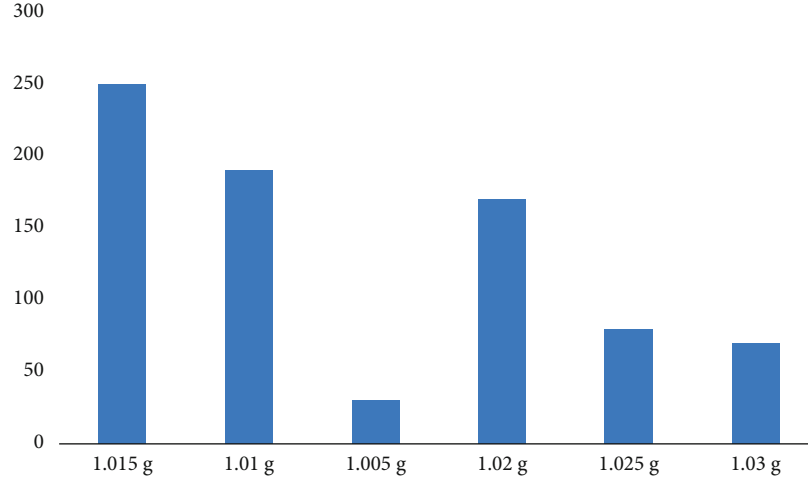


FIGURE 7: Distribution of SG value in urine test.

Normalized weights, normalized calculation of particle weights:

$$w_t^i = \frac{w_t^i}{\sum_{i=1}^N w_t^i}. \quad (18)$$

Status output is using a weighted method to determine the current target position of the tracking algorithm:

$$x \approx \sum_{i=1}^N x_m^i w_n^i. \quad (19)$$

Tracking performance is still inaccurate at some point. There is room for improvement. However, if the data processing algorithm is running, we can use the data processing algorithm outside the original algorithm, so we cannot use it.

It can be seen from the formula that the standard particle filter algorithm can track the target, but the tracking effect is

still inaccurate in some positions. There is room for improvement. After learning the whole process of the standard particle filter algorithm through the above part, you can have a deeper understanding of the particle filter algorithm, and at the same time, you can find the areas where the algorithm steps can be improved and prepare the relevant knowledge for subsequent algorithm improvements. In order to better improve the particle filter algorithm, the defect analysis is carried out to obtain

$$x_{id}(t+1) = x_{id}(t) + v_{id}(t). \quad (20)$$

#### 4. Research on Medical Big Data Analysis and Disease Prediction Methods Based on Artificial Intelligence

*4.1. Medical Data Analysis under Artificial Intelligence.* With the rapid growth of hospital outpatient business, outpatient diagnosis model based on big data analysis technology has

become a research hotspot. Researchers are collecting health information from higher-level hospital information systems (SIS). An analysis of data collected over three years shows that the number of outpatients is in the top five in terms of inpatient care is general surgery, gynecology, pediatrics, and emergency. Laboratory clinical trial production increased by 131%. This advancement in outpatient treatment has resulted in a significant increase in wait times for outpatient appointments, which even affects the normal functioning of hospitals under very difficult conditions. The increase in the number of outpatients has greatly increased the burden on outpatients. At its busiest, the average number of diagnoses per doctor increased from 13.2 to 27.6 times. Therefore, it is essential and cost-effective to develop an outpatient auxiliary diagnosis model to reduce the workload of physicians. The proportion of the number of outpatient departments in the top three hospitals is shown in Figure 3.

From the data in Figure 3, we can see that the number of outpatient clinics in internal medicine, department ranks among the top five in 2019-2021. The number of outpatient clinics in general surgery in 2019 was 16.59% and reached 20.99% in 2021; the department with the least number of outpatient clinics was the emergency department, which was only 6.58% in 2019, and increased to 9.97% in 2021. The market size and growth rate of medical big data from 2015 to 2021 are shown in Table 1.

From the data in Figure 4, we can see that the scale of the medical big data market in 2015-2021 shows a steady upward trend, from the initial 606 million yuan in 2015 to 7.905 billion yuan in 2021. From 28.95% in 2015, it increased to 59.37% after 7 years; the year with the highest growth rate was 68.95% in 2019, and the year with the lowest growth rate was only 28.95% in 2015. 2015-2021 my country and the global medical big data market scale is as shown in Figure 5.

**4.2. Research on Disease Prediction Methods.** Comorbidities usually refer to the development of a disorder caused by another disorder or symptom. For example, if a patient develops pneumonia from measles, new pneumonia may be understood as a comorbidity. Another disease or symptom may be due to the development of a disease, such as B. Patients who are prone to muscle pneumonia and new pneumonia can be understood as comorbidities. The combined disease dataset and prediction dataset are shown in Tables 2 and 3.

Take the patient diagnosis table as an example from Table 2. Compared with the first diagnosis, the second diagnosis of the patient is  $D5$  and  $D6$ , so  $D5$  and  $D6$  can be used as the patient's first diagnosis for future new diseases  $D1$ ,  $D2$ ,  $D3$ , and  $D4$ . Secondary diagnosis and two new disease data of  $D1$ ,  $D2$ ,  $D3$ , and  $D4 > > D5$  and  $D1$ ,  $D2$ ,  $D3$ , and  $D4 > > D6$  shown in Table 2.

As can be seen from the data in Table 3, if  $D7$  is a predictive disease, data for  $D7$  is added as a positive sample, and samples from other diseases (such as  $D6$ ) are added as a negative sample. The newly created disease record set is scanned, and the new disease records of severe pneumonia

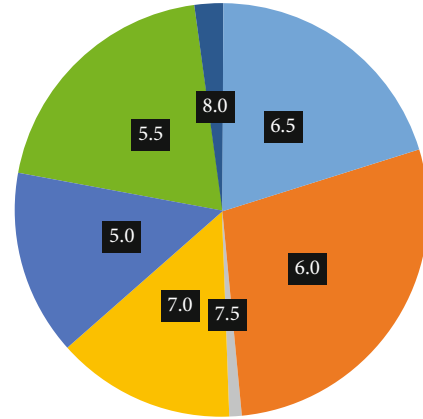


FIGURE 8: Distribution of pH indicators and disease occurrence.

are scanned, and the unique code is used as the positive sample to generate the research function, data for disease prediction. The network size of the disease is shown in Figure 6.

From the data in Figure 6, we can see that 77,640 disease genes were collected from MalaCards, UMLS, and other databases, covering 2,978 diseases and 9,012 genes. After analyzing the network nodes, only the prognosis data of severe pneumonia-related diseases were collected, the network was simplified, and finally, a disease co-occurrence network containing 2708 nodes and 218284 edges was constructed based on disease gene associations. The distribution of SG value in urine test generally predicts the occurrence of disease, and the distribution of SG index and disease occurrence is shown in Figure 7.

The data in Figure 7 show the distribution of SG according to urine specific gravity. The graph also shows that across the entire sample, the highest number of cases is 1,015, followed by 1.01 and finally 1.02. This indicates that many patients with pneumonia have an SG of 1.015. The distribution of each gear of pH value is shown in Figure 8.

From the data in Figure 8, we can understand the distribution of each level of pH value, normal urine is usually slightly acidic, so the pH value is 6.0, the normal range is 5.0 to 7.0, but urine below 5.0 is also neutral or slightly alkaline, and vegetarians over 7.0 are considered abnormal. So pH of 7.5 and 8 may be abnormal values in the body.

## 5. Conclusion

In recent years, technologies such as big data, cloud computing, Internet+, and artificial intelligence have continued to develop. As an important national strategic resource, accelerate the improvement of the data transmission service level of the traditional pharmaceutical industry. Implement and promote the deepening and improvement of the reform of the medical and health care system, improve the efficiency and quality of medical services, develop new formats and services, and accelerate economic growth. AI technology can now look for potential clues in patient cases to support a diagnosis, not only providing diagnostic clues and basics to inexperienced young doctors



but also helping those with more knowledge find more cost-effective prevention methods.

### Data Availability

The experimental data used to support the findings of this study are available from the corresponding author upon request.

### Conflicts of Interest

The authors declared that they have no conflicts of interest regarding this work.

### Authors' Contributions

Fang Zhang and Zhen Zhang contributed equally to this work.

### References

- [1] A. Ligeza, "Artificial intelligence: a modern approach," *Applied Mechanics & Materials*, vol. 263, no. 2, pp. 2829–2833, 2009.
- [2] F. Glover, "Future paths for integer programming and links to artificial intelligence," *Computers & Operations Research*, vol. 13, no. 5, pp. 533–549, 1986.
- [3] F. V. Jensen, "Bayesian artificial intelligence," *Pattern Analysis & Applications*, vol. 7, no. 2, pp. 221–223, 2004.
- [4] X. Zhu and A. B. Goldberg, "Introduction to semi-supervised learning (synthesis lectures on artificial intelligence and machine learning)," *Synthesis Lectures on Artificial Intelligence & Machine Learning*, vol. 3, no. 1, pp. 1–130, 2009.
- [5] M. Negnevitsky, "Artificial intelligence: a guide to intelligent systems," *Information & Computing Sciences*, vol. 48, no. 48, pp. 284–300, 2005.
- [6] M. Babar, M. U. Tariq, M. D. Alshehri, F. Ullah, and M. I. Uddin, "Smart teledentistry healthcare architecture for medical big data analysis using IoT-enabled environment," *Sustainable Computing: Informatics and Systems*, vol. 35, no. 3, article 100719, 2022.
- [7] T. Katsuda and H. Isshiki, "Contribution of medical big data analysis technology to medical innovations," *Fujitsu Scientific & Technical Journal*, vol. 54, no. 2, pp. 59–65, 2018.
- [8] Q. Chen and W. Wang, "Analysis on the application of big data technology in medical and health industry," *Journal of Physics: Conference Series*, vol. 1883, no. 1, article 012136, 2021.
- [9] S. G. Odaibo and D. G. Odaibo, "The way forward for big data analysis in ophthalmology and medicine," *Journal of Eye Science*, vol. 1, no. 1, p. 19, 2016.
- [10] A. T. Azar and A. E. Hassanien, "Dimensionality reduction of medical big data using neural-fuzzy classifier," *Soft Computing*, vol. 19, no. 4, pp. 1115–1127, 2015.
- [11] C. D. Corley, L. L. Pullum, D. M. Hartley et al., "Disease prediction models and operational readiness," *PLoS One*, vol. 9, no. 3, p. 91989, 2014.
- [12] S. Bashir, U. Qamar, F. H. Khan, and M. Y. Javed, "MV5: a clinical decision support framework for heart disease prediction using majority vote based classifier ensemble," *Arabian Journal for Science & Engineering*, vol. 39, no. 11, pp. 7771–7783, 2014.
- [13] S. M. Manemann, J. Sauver, and H. Liu, "Longitudinal cohorts for harnessing the electronic health record for disease prediction in a US population," *BMJ Open*, vol. 11, no. 6, article 044353, 2021.
- [14] R. H. Collier, "Pest and Disease Prediction Models," *Encyclopedia of Applied Plant Sciences*, vol. 3, pp. 120–123, 2017.
- [15] M. G. El-Shafiey, A. Hagag, and E. El-Dahshan, "A hybrid GA and PSO optimized approach for heart-disease prediction based on random forest," *Multimedia Tools and Applications*, vol. 81, no. 13, pp. 18155–18179, 2022.

## Research Article

# Analysis of Risk Factors and Surgical Strategy of Knee Traumatic Arthritis after Internal Plate Fixation in the Treatment of Tibial Plateau Fracture

Xingming Jin , Dengying Li, Lei Yang, Fuyuan Han, and Pinwu Jia

Department of Orthopaedics, Central Hospital of Jinchang City, Gansu Province 737100, China

Correspondence should be addressed to Xingming Jin; 631507020103@mails.cqjtu.edu.cn

Received 13 June 2022; Accepted 25 July 2022; Published 5 September 2022

Academic Editor: Hangjun Che

Copyright © 2022 Xingming Jin et al. This is an open access article distributed under the Creative Commons Attribution License, which permits unrestricted use, distribution, and reproduction in any medium, provided the original work is properly cited.

**Objective.** To explore the risk factors and surgical strategies of knee traumatic arthritis after internal plate fixation in the treatment of tibial plateau fracture. **Methods.** A total of 300 patients with tibial plateau fractures treated with internal plate fixation in our hospital from January 2019 to April 2021 were retrospectively analyzed. According to whether secondary knee traumatic arthritis occurred after operation, they were divided into control group and research group. The control group was nonsecondary knee traumatic arthritis ( $n = 231$ ), and the research group was secondary knee traumatic arthritis ( $n = 69$ ). Univariate and multivariate logistic regression analysis was used in this research. **Results.** There were significant differences in fracture classification, injury method, osteoporosis, and the time from injury to operation between the two groups, and there are statistically significant differences between groups ( $P < 0.05$ ). Fracture type, injury method, osteoporosis, and time from injury to operation were the influencing factors of tibial internal fixation, and there are statistically significant differences between groups ( $P < 0.05$ ). Platform fracture was an independent risk factor for postoperative knee joint traumatic arthritis, and there are statistically significant differences between groups ( $P < 0.05$ ). The HSS scores of both groups increased after operation, and there are statistically significant differences between groups ( $P < 0.05$ ). No loosening of the prosthesis was found in all 69 patients with postoperative X-ray examination. **Conclusion.** Fracture classification, injury mode, osteoporosis, and time from injury to operation are independent risk factors for knee traumatic arthritis in the treatment of tibial plateau fractures with internal plate fixation, incidence of knee trauma.

## 1. Introduction

Tibial plateau fractures are the most common fracture in knee trauma, accounting for 8 percent of fractures in the elderly [1]. Tibial plateau fractures are mostly caused by high-energy injuries, accounting for about 1% of systemic fractures. The incidence of posterolateral fractures is relatively low, accounting for 8%. Tibial plateau fracture is easy to be accompanied by different degrees of soft tissue injuries such as cruciate ligament and collateral ligament, which is relatively difficult to deal with [2]. Surgical methods are often used to treat tibial plateau fractures in order to restore the painless knee joint with stable structure, good line of force and good movement as far as possible. As most of the tibial plateau fractures are high-energy injuries in different directions, the injury mechanism

is very complex, and clinical surgical treatment is difficult [3]. Complex tibial plateau fractures are often accompanied by severe soft tissue injuries, which are difficult to treat in clinic. Improper treatment of soft tissue injuries associated with tibial plateau fractures can seriously affect the normal function of the knee joint, leading to traumatic arthritis and knee valgus deformity [4].

With the aging of population, the incidence of tibial fractures has risen sharply. The tibial plateau is one of the important load-bearing joints in the human body, and it is usually an intra-articular fracture [5]. With the development and progress of minimally invasive technology, minimally invasive methods have also been introduced into internal fixation technology. Minimally invasive percutaneous plate osteosynthesis (MIPPO) does not need to rely on the adhesion between the

plate and the fracture end. Keeping a certain distance between the two can significantly reduce soft tissue damage and provide sufficient blood to the fracture end to the greatest extent. It can promote the healing of fracture ends [6]. Foreign scholars have reported that the use of MIPPO technology combined with L-type and T-type plates in the treatment of patients of different ages has a satisfactory clinical effect and can minimize the pain of patients, which is beneficial to early rehabilitation exercise [7]. However, for elderly patients with degenerative joint disease, intra-articular fractures will be more serious and the clinical effect is not good. Minimally invasive internal fixation systems are not perfect, and there is a risk of secondary traumatic knee arthritis after surgery. In view of this, this study would investigate the risk factors affecting the secondary traumatic arthritis of the knee after the treatment of tibial plateau fractures with internal plate fixation.

## 2. Materials and Methods

**2.1. General Information.** A total of 300 patients with tibial plateau fracture treated by internal plate fixation in our hospital from January 2019 to April 2021 were retrospectively analyzed. According to whether secondary knee traumatic arthritis occurred after operation, they were divided into control group and research group. The control group was nonsecondary knee traumatic arthritis ( $n = 231$ ), and the research group was secondary knee traumatic arthritis ( $n = 69$ ). The general data of the two groups of patients were shown in Table 1. This study was approved by the Medical Ethics Association of our hospital.

Diagnostic criteria of tibial plateau fracture: the patient had a history of trauma such as falling. And there were symptoms such as pain, swelling, and limitation of movement of the affected knee joint. Combined with CT, X-ray, and other imaging examination, the diagnosis was in line with the relevant diagnostic criteria of tibial plateau fracture [8].

Selection criteria: (1) all the patients were simple tibial plateau fractures and were voluntarily treated with internal plate fixation; (2) freshly closed single limb fractures without vascular and nerve injury; (3) postoperative rehabilitation exercise according to the doctor's advice, regular reexamination, and complete follow-up.

Exclusion criteria: (1) patients with open fracture, pathological fracture, and old fracture; (2) complications such as osteofascial compartment syndrome and deep venous thrombosis of lower extremities; (3) patients with dysfunction of the affected limb, such as myasthenia gravis and paraplegia; (4) patients who could not cooperate with functional exercise and follow-up after operation; (5) patients with serious medical diseases, poor physique, and mental illness.

**2.2. Operation Methods.** All patients were treated by the same surgical team and were treated with continuous epidural anesthesia before operation. The healthy side was taken from the recumbent position, and the epidural catheter was placed in L1-2 or L2-3 lumbar intervertebral space. After seeing the reflux of cerebrospinal fluid, the anesthetic was injected slowly, and the anesthetic was 5 mg. The patient was changed to a supine position, and the procedure was performed under

the control of a balloon tourniquet. For patients with displaced fractures of type I according to Schatzker's classification [9], cannulated compression screw fixation was performed. Patients with type II and type III fractures were treated with lateral incision, patients with type IV fractures were treated with medial knee incision or a straight incision close to the midline, and type V fractures were treated with a lateral incision. Type VI fracture patients chose a straight incision close to the midline. Cut open the joint capsule and coronary ligament, check the injury of meniscus and ligament, show the tibial plateau from below the meniscus, retain the meniscus as far as possible during the operation, and remove the seriously injured meniscus. Expose the fracture end, observe the collapse of the platform, pry up the fracture block in the proximal tibia for the collapsed fracture of the articular surface, repair the articular surface, fix it temporarily, and insert the autogenous iliac bone into the defect of the proximal tibia to repair the bone defect and ligament repair. After satisfactory reduction by C-arm X-ray machine, the cancellous bone screws and anatomical plates selected in advance were fixed. Suture the coronal ligament and repair the injured meniscus and ligament. The ligament injury with avulsion bone mass was fixed in the first stage during the operation. For the patients with injury of the solid part of cruciate ligament, the primary repair or reconstruction could not be done during the operation, but the second-stage ligament reconstruction can be done. Negative pressure drainage and pressure bandaging were performed after operation.

### 2.3. Observation Index

**2.3.1. Incidence of Traumatic Knee Arthritis.** After the completion of the operation, 300 patients were followed up for 1 year, and the incidence of traumatic arthritis within 1 year after operation was calculated. Diagnostic criteria of knee traumatic arthritis [10]: (1) there was a history of trauma (surgery is also a history of external injury); (2) the early lesion was characterized by joint pain and discomfort, especially stiffness after exercise, which was improved after proper exercise massage, but did not overwork; (3) when the disease progresses to the later stage, there might be severe symptoms such as limitation of movement, repeated swelling of the joint, persistent pain and gradual aggravation, joint deformity, and effusion; (4) X-ray examination showed the narrowing of joint space and the formation of bone spur at the edge of subchondral articular surface sclerosis. For patients with severe condition, it could be characterized by irregular articular surface, bone end deformation, and loose body in the joint.

**2.3.2. General Information.** The age, sex, type of plate, meniscus injury, ligament injury, fracture classification, osteoporosis, mode of injury, time from injury to operation, weight bearing time after operation (5 kg) and whether to remove internal fixation were recorded in the two groups. (1) Determination of meniscus injury [11]: by asking the patient's symptoms, combined with freehand examination, imaging examination, and arthroscopy. If the patient has the symptoms of joint swelling and limitation of movement, the joint, joint space, and meniscus feel tenderness during physical

TABLE 1: Monofactor analysis of postoperative secondary knee traumatic arthritis.

Monofactor	Control group ( $n = 231$ )	Research group ( $n = 69$ )	$t/\chi^2$ value	$P$ value
Age	$55.19 \pm 2.31$	$55.14 \pm 2.44$	0.155	>0.05
Gender (male/female)	113/118	34/35	0.002	>0.05
Steel plate type				
Combined steel plate	105 (45.45%)	36 (52.17%)	0.967	>0.05
Anatomical plate	81 (35.06%)	21 (30.43%)		
Locking steel plate	45 (19.48%)	12 (17.39%)		
Fracture classification				
I	0	14 (20.29%)	67.188	<0.05
II	23 (9.96%)	15 (21.74%)		
III	115 (49.78%)	33 (47.83%)		
IV	93 (40.26%)	7 (10.14%)		
Mode of injury				
High energy	135 (58.44%)	12 (17.39%)	35.826	<0.05
Low energy	96 (41.56%)	57 (82.61%)		
Osteoporosis	41 (17.75%)	35 (50.72%)	30.542	<0.05
Meniscus injury	114 (49.35%)	27 (39.13%)	2.227	>0.05
Injury of collateral ligament	42 (18.18%)	18 (26.09%)	2.075	>0.05
Cruciate ligament injury	65 (28.14%)	23 (33.33%)	0.691	>0.05
Time from injury to operation				
$\leq 7$ d	157 (67.97%)	31 (44.93%)	12.052	<0.05
$> 7$ d	74 (32.03%)	38 (55.07%)		
Time from operation to weight-bearing				
$\leq 6$ months	34 (14.72%)	11 (15.94%)	0.062	>0.05
$> 6$ months	197 (85.28%)	58 (84.06%)		
Removal of internal fixation	77 (33.33%)	21 (30.43%)	0.202	>0.05

examination, MRI examination shows meniscus grade III signal changes; combined with arthroscopy, the existence of meniscus injury can be comprehensively determined. (2) Determination of ligament injury [12]: ligament injury can be divided into two types: collateral ligament injury and cruciate ligament injury. (3) Determination of osteoporosis [13]: the existence of osteoporosis was determined by whole body bone mineral density (BMD). If the bone mineral density was less than -2.5, it can be diagnosed as osteoporosis. (4) Determination of high-energy and low-energy injuries [14]: high-energy injuries referred to complex injuries caused by direct impact injury and changes in limb position at the same time. In addition to more combined injuries, limb fractures have a wide range of fractures and serious comminution. Local tissue was severely injured, generally accompanied by obvious soft tissue damage. The low-energy injury referred to the direct impact injury, the range of limb fracture was small, and the degree of local tissue trauma was low.

**2.3.3. Analysis of Risk Factors of Postoperative Knee Traumatic Arthritis.** Differences in the incidence of postoperative knee traumatic arthritis in patients with different clinical characteristics were included in a multivariate logistic regression model.

**2.3.4. Surgical Effect.** The knee function and acetabular bone healing of patients with secondary knee traumatic arthritis

after total knee arthroplasty and total knee joint surface placement were recorded. The improvement of knee joint function was evaluated by HSS score [15]. The total score of the scoring system was 100. The score was proportional to the function of hip joint.

**2.4. Statistical Analysis.** SPSS 22.0 statistical software was used to analyze the data. Measurement data are expressed as mean  $\pm$  standard deviation ( $\bar{x} \pm s$ ) using  $t$ -test or analysis of variance; those that do not conform to the normal distribution are represented by the median (quartile interval). Rank sum test was used, counting data was expressed by the number of cases and percentage,  $\chi^2$  test was used, and binary logistic regression analysis was used to screen the influencing factors of knee osteoarthritis. The difference was statistically significant, and the difference was statistically significant, and there are statistically significant differences between groups ( $P < 0.05$ ).

### 3. Results

**3.1. Incidence of Secondary Knee Traumatic Arthritis after Operation.** The incidence of knee traumatic arthritis after internal plate fixation in the treatment of tibial plateau fracture: 69 cases of knee traumatic arthritis occurred in 300 patients with tibial plateau fracture after internal plate fixation with an incidence of 23%. All results are shown in Figure 1.

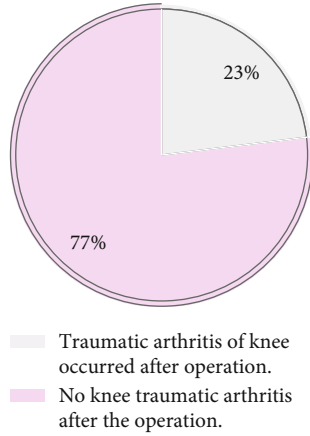


FIGURE 1: Incidence of secondary knee traumatic arthritis after operation.

**3.2. Monofactor Analysis of Knee Traumatic Arthritis after Internal Plate Fixation in the Treatment of Tibial Plateau Fracture.** There was no significant difference in age, sex, type of plate, meniscus injury, cruciate ligament injury, collateral ligament injury, weight bearing time, and internal fixation between the control group and the research group ( $P > 0.05$ ). There were significant differences in fracture classification, mode of injury, osteoporosis, and time from injury to operation between the two groups, and there are statistically significant differences between groups ( $P < 0.05$ ). All the data results are shown in Table 1.

**3.3. Logistic Regression Analysis of Multiple Factors Affecting Knee Traumatic Arthritis after Internal Plate Fixation in the Treatment of Tibial Plateau Fracture.** Internal plate fixation in the treatment of tibial plateau fracture after knee traumatic arthritis as a constant, fracture classification, mode of injury, osteoporosis, and injury to operation time as dependent variables are shown in Table 2. Multivariate logistic regression analysis showed that fracture classification, injury method, osteoporosis, and the time from injury to operation were the factors that led to the treatment of tibia with internal plate fixation. The independent risk factors of postoperative knee traumatic arthritis after platform fracture surgery were statistically different, and there are statistically significant differences between groups ( $P < 0.05$ ). All results are shown in Table 3.

**3.4. Curative Effect and Prognosis of Patients with Secondary Knee Traumatic Arthritis.** Treatment and prognosis of 69 cases of secondary knee traumatic arthritis: according to the investigation, 40 of 69 patients with secondary knee traumatic arthritis were treated with total knee arthroplasty, of which 29 cases were treated with biological fixation of acetabular cup. 11 cases were treated with bone cement acetabular cup fixation, and the other 29 cases were treated with total knee arthroplasty. The HSS scores of biological fixed acetabular cup fixation group, cement acetabular cup fixation group, and total knee arthroplasty group were compared. There was no significant difference among the three groups before and after operation ( $P > 0.05$ ). Comparison within groups, the HSS scores of

TABLE 2: Assignment table.

Dependent variable	Assignment
Fracture classification	I, II = 0, III, IV = 1
Mode of injury	Low energy = 0, high energy = 1
Osteoporosis	No = 0, yes = 1
Time from injury to operation	$>7d = 0$ , $\leq 7d = 1$

patients in each group increased pre- and postoperation, and there are statistically significant differences between groups ( $P < 0.05$ ). X-ray examination of 69 patients showed no loosening of prosthesis after operation. The average time between bone grafting and acetabular bony union was  $5.05 \pm 0.91$  months. All results are shown in Table 4.

## 4. Discussion

This study would investigate the risk factors affecting the secondary traumatic arthritis of the knee after the treatment of tibial plateau fractures with internal plate fixation. The structure of the tibial condyle is a spongy bone, which is prone to fracture under the impact of high-energy violence. Clinically, nonoperative treatment and surgical treatment can be selected for tibial plateau fractures. Nonoperative treatment is a conservative treatment. Its indications are incomplete fracture, no displacement, or displacement of the fracture piece  $< 3$  mm. The common treatment methods are plaster fixation, traction treatment, and reduction treatment. Nonsurgical treatment is less traumatic to patients and has a certain scope of application. Foreign scholars believe that nonsurgical treatment is suitable for nondisplaced fractures, and ultraknee splints can be used for external fixation for this type of fracture [16]. Other scholars believe that nonsurgical treatment can be applied to mildly displaced fractures, fracture reduction by manual reduction, and external fixation with an ultraknee splint [17]. Chinese scholars believe that nonsurgical treatment can also be applied to moderately displaced fractures [18].

In order to ensure that patients with tibial fractures can continue a healthy life, a variety of treatment methods have been developed clinically. Among them, the treatment effect of internal plate fixation is better, which has the characteristics of small trauma and high cure rate, and has been widely used in clinical practice. In addition to manual reduction, bone traction and extraknee splint external fixation should also be performed during treatment. When the tibial plateau is damaged by high energy, the articular surface usually collapses. If nonsurgical treatment methods such as traction or external fixation cannot solve the problem of articular surface collapse, it will lead to irreversible articular surface damage. The knee joint is thus affected, and its stability is greatly reduced, which can cause traumatic arthritis of the knee joint for a long time [19]. Surgery needs to meet certain surgical indications. If unstable fractures such as severe displacement of fracture, obvious collapse of articular surface, and ligament injury are found in the examination, surgical treatment must be adopted. The most common treatment is internal plate fixation [20, 21]. Some scholars pointed out that 60 patients with tibial plateau



TABLE 3: Logistic regression analysis of multiple factors affecting knee traumatic arthritis after internal plate fixation for tibial plateau fracture.

Constant	<i>b</i>	S. E	Chi-square value	<i>P</i> value	OR	95% CI for OR
Fracture classification	0.891	0.145	37.759	<0.05	2.438	1.835-3.239
Mode of injury	1.241	0.352	12.430	<0.05	3.459	1.735-6.896
Osteoporosis	1.692	0.592	8.188	<0.05	5.441	1.705-17.363
Time from injury to operation	-0.245	0.101	5.884	<0.05	0.783	0.642-0.954

TABLE 4: Therapeutic effect and prognosis of patients with secondary knee traumatic arthritis.

Grouping	<i>N</i>	HSS scoring		<i>t</i> value	<i>P</i> value
		Before operation	After operation		
Biological fixed acetabular cup fixation	29	36.53 ± 4.31	90.84 ± 1.55	63.854	<0.05
Cement fixation with acetabular cup fixation	11	36.40 ± 4.56	91.49 ± 2.35	35.617	<0.05
Total knee arthroplasty	29	36.19 ± 4.11	90.18 ± 2.45	60.763	<0.05
<i>F</i> value		0.046	1.725		
<i>P</i> value		>0.05	>0.05		

fractures suffered from low energy injury and were treated by internal plate fixation [22]. The patients were followed up for one year, and the results showed that the excellent and good rate of knee joint function recovery was only 85% and 15% of the patients had knee traumatic arthritis [23]. When observing the X-ray films of the patients' knee joints, it was found that different degrees of degeneration could be observed in the patients' knee joints, accounting for 30%. The possible reasons for the degeneration of knee joint function were as follows: firstly, the reduction by surgical treatment may lead to unsatisfactory reduction effect [24]. Secondly, the injured site of the fracture patients healed after treatment, but the weight-bearing line of the knee joint changed compared with that before the injury. Thirdly, because the knee joint was injured and complicated with soft tissue contusion, cartilage hyperplasia and heterotopic ossification appeared after recovery [25].

There are many complications of tibial plateau fractures, including early complications such as infection, vascular injury, soft tissue necrosis, and loss of internal fixation reduction, and late complications such as ankylosis, traumatic arthritis, fracture nonunion, and malunion. The occurrence of complications leads to the difficulty of clinical treatment [26, 27]. The key to the treatment of tibial plateau fracture is how to obtain a knee joint with normal movement, good alignment, painless, and stable. For patients with open tibial plateau fracture, emergency surgical treatment should be taken within 6-8 hours after operation. For patients with closed tibial plateau fracture, if the whole body and soft tissue are in good condition, open reduction and internal fixation should be performed as soon as possible to avoid local tension blisters and even induce osteofascial compartment syndrome, so as not to delay the disease and lose the best time for surgical treatment [28-30]. If the patient has soft tissue injuries, emergency treatment such as drainage and bone traction should be performed first. Open repositioning and internal fixation should be performed after the soft tissue swelling has subsided and the skin texture has returned to

normal. Compared with other treatments, the greatest advantage of internal plate fixation is its high stability and very low incidence of displacement [31-33]. Previous clinical studies showed that the operation time, blood loss, and the incidence of postoperative traumatic arthritis in the internal plate fixation group were lower than those in the intramedullary nail fixation group [34]. The postoperative healing rate was higher than that in the intramedullary nail fixation group. However, these methods have fatal shortcomings, which is easy to occur after operation [35, 36]. Therefore, it is very important to find the risk factors that can easily lead to traumatic arthritis after operation.

Combined with the results of this study, tibial plateau fracture is an intra-articular fracture. If the reduction effect is not ideal, it will cause unevenness of the articular surface. Once it exceeds the compensation and regeneration capacity of the knee joint, it will make one side excessive wear and degeneration, resulting in secondary arthritis. Because Schatzker IV is often associated with soft tissue injury and this type of fracture is difficult to achieve anatomical reduction because of more bone fragments, we often classify it as unstable fracture or complex fracture [37, 38]. This study also confirmed that fracture classification and injury mode were the independent risk factors of knee traumatic arthritis after internal plate fixation in the treatment of tibial plateau fracture. Our analysis shows that damage to the soft tissues surrounding the knee joint, or insufficient attention and protection during surgery, can compromise overall movement and coordination mechanisms [39]. In tibial plateau fracture with osteoporosis, the articular surface is prone to collapse and compression, resulting in varying degrees of bone loss. Because of osteoporosis, bone mass is significantly reduced especially in the process of reduction and bone graft. It is difficult to obtain strong fixation [40]. A retrospective analysis of 57 cases of poor reduction of tibial plateau fractures pointed out that strong fixation after anatomical reduction was the key to avoiding or delaying

traumatic osteoarthritis [41]. Severe osteoporosis is one of the reasons for the poor effect of fracture reduction. In this group, 69 cases developed secondary knee traumatic arthritis, of which 35 cases were associated with osteoporosis. Our findings were that osteoporosis and the time from injury to operation were independent risk factors, so we considered that osteoporosis was associated with osteoporosis. The main cause of long-term secondary knee traumatic arthritis was poor reduction of fracture. If there was no timely surgical treatment after injury, it might cause continuous damage of soft tissue, increase the difficulty of operation, and lead to traumatic arthritis after operation. After trauma or crush injury, relatively high energy injury can easily lead to joint compression and damage most blood vessels and nerves. And patients with crush injuries are more likely to develop arthritis after operation. This study still has some shortcomings. Firstly, the quality of this study is limited due to the small sample size we included in the study. Secondly, this research is a single-center study, and our findings are subject to some degree of bias. Therefore, our results may differ from those of large-scale multicenter studies from other academic institutes. This research is still clinically significant, and further in-depth investigations will be carried out in the future.

In conclusion, fracture classification, injury mode, osteoporosis, and time from injury to operation are independent risk factors for knee traumatic arthritis in the treatment of tibial plateau fractures with internal plate fixation, incidence of knee trauma.

## Data Availability

No data were unavailable in this study due to the patients' privacy.

## Conflicts of Interest

The authors declare that they have no conflicts of interest.

## References

- [1] T. Anita, S. A. Marit, A. Astrid et al., "Personally-generated quality of life outcomes in adults with juvenile idiopathic arthritis," *The Journal of Rheumatology*, vol. 13, no. 45, pp. 814–817, 2022.
- [2] F. Luke, A. G. Patrick, Z. Mingjun, and A. Lesley, "Using artificial intelligence to revolutionise the patient care pathway in hip and knee arthroplasty (ARCHERY): protocol for the development of a clinical prediction model," *JMIR research protocols*, vol. 11, no. 5, 2022.
- [3] M. B. Simonsen, K. Næsborg-Andersen, P. D. Leutscher et al., "The effect of foot orthoses on gait biomechanics and pain among people with rheumatoid arthritis: a quasi-experimental study," *Gait & Posture*, vol. 95, no. 55, pp. 121–128, 2022.
- [4] T. Ayako, I. Katsunori, Y. Koichiro et al., "Surgical intervention for patients with rheumatoid arthritis is declining except for foot and ankle surgery: a single-centre, 20-year observational cohort study," *Modern Rheumatology*, vol. 56, no. 441, 2022.
- [5] A. Rieke, M. Xavier, F. R. Marc et al., "Retention of subcutaneous abatacept for the treatment of rheumatoid arthritis: real-world results from the ASCORE study: an international 2-year observational study," *Clinical Rheumatology*, vol. 41, no. 8, pp. 2361–2373, 2022.
- [6] A. Adas Maryam, N. Sam, B. Sathiyaa et al., "Worse outcomes linked to ethnicity for early inflammatory arthritis in England and Wales: a national cohort study," *Rheumatology*, vol. 45, no. 44, 2022.
- [7] C. Yiran and S. Xu, "Rebuttal letter referring to the article "synergy of sarcopaenia and vitamin D deficiency in vertebral osteoporotic fractures in rheumatoid arthritis"," *Clinical Rheumatology*, vol. 41, no. 7, pp. 2275–2276, 2022.
- [8] P. R. Panduro, M. O. Rintek, S. A. M. Tetsche, D. Lene, B. Gunhild, and H. Annette, "Correction to: patient-controlled outpatient follow-up on demand for patients with rheumatoid arthritis: a 2-year randomized controlled trial," *Clinical Rheumatology*, vol. 41, no. 8, p. 2617, 2022.
- [9] Z. Zijun, F. Long, and T. Min, "Logistic regression analysis of risk factors and improvement of clinical treatment of traumatic arthritis after total hip arthroplasty (THA) in the treatment of acetabular fractures," *Computational and Mathematical Methods in Medicine*, vol. 2022, 10 pages, 2022.
- [10] K. W. Morse, N. K. Heinz, J. M. Abolade et al., "Factors associated with increasing length of stay for rheumatoid arthritis patients undergoing total hip arthroplasty and total knee arthroplasty," *HSS Journal®: The Musculoskeletal Journal of Hospital for Special Surgery*, vol. 18, no. 2, pp. 196–204, 2022.
- [11] Z. Xu, L. Xue, G. Shen et al., "The protective effect of ginsenoside Rg1 on apoptosis in human ankle joint traumatic arthritis chondrocytes," *Evidence-based Complementary and Alternative Medicine*, vol. 2022, 7 pages, 2022.
- [12] D. J. Cunningham, M. LaRose, G. Zhang et al., "Regional anesthesia associated with decreased inpatient and outpatient opioid demand in tibial plateau fracture surgery," *Analgesia*, vol. 134, no. 5, pp. 1072–1081, 2022.
- [13] Z. Xinlong, C. Wentao, Y. Shi et al., "Open reduction and internal fixation with plate via posteromedial approach of retaining pes anserinus tendon in the treatment of tibial plateau fracture," *Chinese journal of reparative and reconstructive surgery*, vol. 36, no. 2, pp. 5823–5825, 2022.
- [14] J. Xu, Y. Li, X. Zhao, H. Yang, and L. Wang, "Treatment activity and nursing values of a heterocyclic compound combined with aspirin on traumatic arthritis," *Journal of Structural Chemistry*, vol. 62, no. 10, pp. 1563–1568, 2021.
- [15] A. Cerlier, D. Guinard, A. M. Gay, and R. Legré, "Outcomes of secondary trapeziectomy after revision of trapeziometacarpal implants: a retrospective comparative matched study," *Journal of Hand Surgery (European Volume)*, vol. 46, no. 10, pp. 1096–1100, 2021.
- [16] L. Hao, Y. Y. Feng, and X. X. Liang, "A novel Zn (II) coordination polymer: inhibited the ROS content in the articular soft tissue and exerted treatment activity on the exercise induced traumatic arthritis," *Inorganic and Nano-Metal Chemistry*, vol. 51, no. 8, pp. 1060–1065, 2021.
- [17] P. Daniel, W. Jessica, K. S. Palmer et al., "Effects of hospital funding reform on wait times for hip fracture surgery: a population-based interrupted time-series analysis," *BMC Health Services Research*, vol. 21, no. 1, 2021.
- [18] R. Weiwei, L. Menglu, Q. Guo, and B. Lin, "Gastrocnemius muscle flap with vancomycin/gentamicin-calcium sulfate and autogenous iliac bone graft for the phase I treatment of localized osteomyelitis after tibial plateau fracture surgery," *Journal*

- of *Orthopaedic Surgery and Research*, vol. 16, no. 1, pp. 4941–4944, 2021.
- [19] L. Kai, P. Wang, N. Cheng, H. Luo, and D. Yu, “The effect of joint distraction osteogenesis combined with platelet-rich plasma injections on traumatic ankle arthritis,” *American Journal of Translational Research*, vol. 13, no. 7, article 8344, 2021.
  - [20] R. Henkelmann, M. Krause, L. Alm et al., “Correction to: effect of fracture surgery on the incidence of surgical site infections post tibial plateau fracture surgery,” *European Journal of Trauma and Emergency Surgery*, vol. 47, no. 1, p. 279, 2021.
  - [21] C. Zai, L. L. Zhang, and F. G. He, “Forensic analysis of 133 cases of knee injuries,” *Fa Yi Xue Za Zhi*, vol. 36, no. 5, pp. 688–690, 2020.
  - [22] J. Wan, L. Liu, Y. Zeng, H. Ren, and S. Zhang, “Comparison of different bone graft with arthroscopy-assisted arthrodesis for the treatment of traumatic arthritis of the subtalar joint,” *International orthopaedics*, vol. 44, no. 12, pp. 2719–2725, 2020.
  - [23] R. Henkelmann, M. Krause, L. Alm et al., “Effect of fracture surgery on the incidence of surgical site infections post tibial plateau fracture surgery,” *European journal of trauma and emergency surgery: official publication of the European Trauma Society*, vol. 46, no. 6, pp. 1249–1255, 2020.
  - [24] J. Sniderman and P. Henry, “Articular reductions – how close is close enough? A narrative review,” *Injury*, vol. 51, no. 42, pp. S77–S82, 2020.
  - [25] S. Anna, S. Nina, C. Mac Dermid Joy, and G. Ruby, “The natural history of scaphoid fracture malunion: a scoping review,” *Journal of wrist surgery*, vol. 9, no. 2, pp. 170–176, 2020.
  - [26] L. C. Junior, L. G. Brito, E. B. de Castro, S. Dertkigil, and C. R. Juliato, “Mid- to long-term magnetic resonance imaging results of two prolapse surgeries for apical defect: a secondary analysis of a randomized controlled trial,” *Revista Brasileira de Ginecologia e Obstetrícia*, vol. 43, no. 1, pp. 46–53, 2021.
  - [27] S. A. Callary, C. F. Jones, K. Kantar et al., “A new approach to surgical management of tibial plateau fractures,” *Journal of Clinical Medicine*, vol. 9, no. 3, p. 626, 2020.
  - [28] Z. Liu, K. Zhang, Y. Weng, J. Huang, and Y. Lu, “Resveratrol reduces cartilage matrix degradation and affects chondrocyte apoptosis in rats with traumatic arthritis,” *Journal of Biomaterials and Tissue Engineering*, vol. 10, no. 2, pp. 239–245, 2020.
  - [29] M. Jyothiprasanth, P. J. Venkatesh, P. S. Khan, and T. S. Gopakumar, “Arthroscopy-assisted tibial plateau fracture surgery - minimum 2 years follow up results,” *Journal of Arthroscopy and Joint Surgery*, vol. 7, no. 2, pp. 74–77, 2020.
  - [30] L. Sun, Z. Kong, and X. Ming, “Minimally invasive subtalar arthrodesis for traumatic subtalar arthritis,” *Journal of International Medical Research*, vol. 47, no. 12, pp. 6129–6138, 2019.
  - [31] K. Aubert, A. Germaneau, M. Rochette, P. Rigoard, and T. Vendevre, “Personalized finite element model for full weight-bearing after tibial plateau fracture surgery,” *Computer Methods in Biomechanics and Biomedical Engineering*, vol. 22, no. sup1, pp. S138–S140, 2019.
  - [32] Z. Wang and A. Yu, “Research progress of surgical treatment for lateral malleolus defect,” *Chinese journal of reparative and reconstructive surgery*, vol. 33, no. 9, pp. 195–196, 2019.
  - [33] J. Shelton, S. Dorman, A. Doorgakant, and E. Wood, “How well do we reduce ankle fractures intra-operatively: a retrospective 1 year review using Pettrone’s criteria,” *The Foot*, vol. 40, no. 52, pp. 46–53, 2019.
  - [34] Q. Xiao-Dong, Z. Jing-Jie, Z. Hong-Wei, C. Wei, and C. Xian-Hua, “Therapeutic effect of exercise acupuncture and osteopathy on traumatic knee arthritis,” *Zhongguo gu shang = China journal of orthopaedics and traumatology*, vol. 32, no. 6, pp. 493–497, 2019.
  - [35] J. Dušková, “Cytology of synovial fluid,” *Ceskoslovenska patologie*, vol. 55, no. 2, pp. 5941–5944, 2019.
  - [36] C. Lonza Geordie, G. Gardner-Morse Mack, M. Vacek Pamela, and B. D. Beynnon, “Radiographic-based measurement of tibiofemoral joint space width and magnetic resonance imaging derived articular cartilage thickness are not related in subjects at risk for post traumatic arthritis of the knee,” *Journal of orthopaedic research: official publication of the Orthopaedic Research Society*, vol. 37, no. 5, pp. 1052–1058, 2019.
  - [37] L. Peng, J. Zhu, Z. Wang et al., ““Rule of Spence” and Dickman’s classification of transverse atlantal ligament injury revisited,” *Spine*, vol. 44, no. 5, pp. E306–E314, 2019.
  - [38] C.-W. Kim, C.-R. Lee, K.-C. An et al., “Predictors of reduction loss in tibial plateau fracture surgery: focusing on posterior coronal fractures,” *Injury*, vol. 47, no. 7, pp. 1483–1487, 2016.
  - [39] U. Ozkaya and A. S. Parmaksizoglu, “Dual locked plating of unstable bicondylar tibial plateau fractures,” *Injury*, vol. 46, no. 9, pp. S9–S13, 2015.
  - [40] H. Huajun, H. Ming-Fa, Z. Guodong et al., “Improved accuracy of 3D-printed navigational template during complicated tibial plateau fracture surgery,” *Australasian physical & engineering sciences in medicine*, vol. 38, no. 1, pp. 109–117, 2015.
  - [41] P. Qing-Jiang, X. Yu, C. Xian-Jun, Y. Zhen-Chun, and G.-Z. He, “The management of acetabular malunion with traumatic arthritis by total hip arthroplasty,” *Pakistan journal of medical sciences*, vol. 29, no. 1, p. 191, 2013.

## Research Article

# Analysis of the Application Effect of Exercise Rehabilitation Therapy Based on Data Mining in the Prevention and Treatment of Knee Osteoarthritis

Wei Liu<sup>1,2</sup>, Congan Wang<sup>1</sup>, Gongchang Yu<sup>1</sup>, Bin Shi<sup>1</sup>, and Jingwen Wang<sup>2</sup>

<sup>1</sup>Department of Public Health, Neck-Shoulder and Lumbocrural Pain Hospital of Shandong First Medical University, Jinan, Shandong 250062, China

<sup>2</sup>School of Graduate Education, Shandong Institute of P.E. and Sports, Jinan, Shandong 250100, China

Correspondence should be addressed to Wei Liu; [liuwei1@sdpei.edu.cn](mailto:liuwei1@sdpei.edu.cn)

Received 31 May 2022; Revised 12 July 2022; Accepted 9 August 2022; Published 5 September 2022

Academic Editor: Shimin Wang

Copyright © 2022 Wei Liu et al. This is an open access article distributed under the Creative Commons Attribution License, which permits unrestricted use, distribution, and reproduction in any medium, provided the original work is properly cited.

**Objective.** To analyze the application effect of exercise rehabilitation therapy based on data mining in the prevention and treatment of knee osteoarthritis. **Methods.** Based on clinical data mining technology, that is, using complex network technology and association rules, the medical records of 1612 patients with KOA in the Department of Rheumatology and Immunology of our hospital were retrospectively analyzed, and they were divided into groups according to whether they used exercise rehabilitation therapy ( $n = 786$ ), and the control treatment group ( $n = 826$ ), the curative effect, the improvement of inflammatory factors and immune factors, the visual analogue scale (VAS), the knee joint function score (Lysholm), and the quality of life (WOMAC) scale were compared between the two groups score, analyze the relationship between VAS and Lysholm score and prognosis quality of life, and compare the recurrence within 12 months between the two groups. **Results.** The data mining results showed that the curative effect of the exercise rehabilitation therapy group was significantly higher than that of the control treatment group ( $P < 0.05$ ); the improvement of VAS and Lysholm scores of the exercise rehabilitation therapy group was significantly better than that of the control treatment group ( $P < 0.05$ ). The improvement effect of inflammatory indexes and immune cytokines was significantly better than that of the control treatment group ( $P < 0.05$ ); the improvement of WOMAC in the exercise rehabilitation therapy group was significantly better than that of the control treatment group ( $P < 0.05$ ); VAS and WOMAC scores were significantly positively correlated ( $r = 0.579$ ,  $P < 0.05$ ); Lysholm score was positively correlated with WOMAC score ( $r = -0.563$ ,  $P < 0.05$ ); the recurrence rate of exercise rehabilitation therapy group was 5.09%, which was significantly lower than that of control treatment group (17.63% ( $\chi^2 = 11.967$ ),  $P < 0.05$ ). **Conclusion.** Exercise rehabilitation therapy for KOA patients can effectively improve inflammatory and immune factors in patients, enhance knee joint function and prognosis quality of life, and reduce readmission rate, which is worthy of clinical application.

## 1. Background

The main contradiction facing medical treatment in China is that the current medical service capacity cannot meet people's increasing service demand, and the gap between supply and demand is very significant. In terms of demand, with the development of social economy, aging of population, and changes of disease spectrum, the demand for medical services increases, and problems such as insufficient overall health resources, concentration of high-quality medical

resources, and imbalance between supply and demand still exist in China [1]. In recent years, artificial intelligence technology has been widely applied in disease prediction, diagnosis, and treatment, drug research and development and other medical and health fields, which has significantly improved the level of medical services, effectively alleviated the above problems, and promoted the healthy development of medical reform policies [2]. Osteoarthritis (OA) is a common joint disease obviously related to aging. Its clinical characteristics are erosion of articular cartilage, subchondral



sclerosis, marginal osteophytic hyperplasia (osteophyte formation), and many biochemical and morphological changes of synovial membrane and joint capsule, among which the knee joint is most commonly affected. Knee osteoarthritis (KOA) is easy to form [3]. Clinically, the main manifestations are chronic joint pain, stiffness, swelling, and joint dysfunction. Knee joint is the most complex joint in the human body, and the joint with the largest load and shear force, which is also the main reason for the high incidence of OA in this part [4]. The incidence of OA increases with the increase of age. Therefore, with the aging of the world's population, osteoarthritis is an increasingly serious health problem [5]. In recent years, some healthy therapies have gradually become popular, such as exercise therapy, which can make patients combine muscles and bones, the whole and the local, with remarkable efficacy [6]. The role of sports rehabilitation therapy is the most recognized by evidence-based medicine, its role is to promote blood circulation, improve venous reflux and venous congestion, and increase range of motion, muscle strength, and joint stability, to accelerate the cartilage surface and synovial mesenchymal cell proliferation, and can stimulate the proliferation of cartilage cells around the lesion that support the degradation of cartilage regeneration; in KOA diagnosis and treatment, the application of artificial intelligence, computer gradually widely based on this, will be based on the movement of data mining the application result of rehabilitation therapy in the prevention and treatment of knee osteoarthritis, to provide theoretical basis for the prevention and treatment of knee osteoarthritis in China.

## 2. Materials and Methods

**2.1. Case Source.** A retrospective analysis was performed on 1612 KOA patients from the rheumatology department of our hospital from March 2016 to March 2020, including 893 males and 719 females, aged from 41 to 67 years, with an average age of  $(53.62 \pm 7.81)$  years.

**2.2. Diagnostic Criteria.** Using the diagnostic criteria for knee osteoarthritis revised by the American College of Rheumatology [7]: (1) clinical symptoms: knee pain most of the time in the previous month; (2) X-ray showed osteophytes at the joint edge; (3) laboratory tests of arthritis were consistent with osteoarthritis; (4) age > 40 years; (5) morning stiffness < 30 min; (6) bone sound during joint movement; conforming to (1)+(2) or (1)+(3)+(5)+(6) or (1)+(4)+(5)+(6) can diagnose knee OA.

**2.3. Inclusion and Exclusion Criteria.** Inclusion criteria: (1) sufferers who met the above diagnostic criteria and diagnosed with knee osteoarthritis; (2) aged 40-70 years old; (3) all sufferers gave informed consent; (4) voluntarily accepted this study and insisted on completing the course of therapy.

Exclusion criteria: (1) sufferers with severe knee osteoarthritis, notoriously narrowed joint space, and surgical indications; (2) sufferers with knee OA with severe knee valgus or knee varus; (3) rheumatism, rheumatoid, and knee joint diseases such as gout, bone tuberculosis, and bone

tumor; (4) sufferers with other diseases that seriously affect lower extremity function; (5) sufferers with severe heart, liver, kidney, and other organ diseases and blood diseases; (6) local skin infection, ulcers, or scars; (7) pregnant and lactating women.

Exclusion criteria: (1) subjects with poor compliance, complications, and unable to complete the entire course of therapy after inclusion; (2) those who do not meet the inclusion criteria; (3) those who cannot judge the efficacy or have incomplete data, which affect the judgment of efficacy.

### 2.4. Methods

**2.4.1. Intervention Methods.** SQL Server management tool was used to retrieve the inpatient data from the database of the rheumatology department of our hospital, to extract and convert the data, establish the database according to the requirements, and lock the data after checking errors and cleaning noise data.

Data were collected including efficacy and immune factors of two groups: ImmunoglobulinA (IgA), ImmunoglobulinM (IgM), ImmunoglobulinG (IgG), complement C3, and complement C4; inflammatory indicators: erythrocyte sedimentation rate (ESR), serum interleukin receptor-7(IL-7R), tumor necrosis factor alpha (TNF-alpha), erythrocyte sedimentation rate (ESR), serum interleukin receptor-7(IL-7R), TNF- $\alpha$ , insulin-like growth factor (IGF), visual simulation scoring (VAS), Knee function score, Lysholm, and WOMAC; the relationship between VAS and Lysholm score and prognostic quality of life was analyzed. The recurrence of 12 months was compared between the two groups.

**2.4.2. Data Mining Methods.** In this study, association analysis was used to find the correlation between the data of application effect of exercise rehabilitation therapy in the prevention and treatment of knee osteoarthritis. However, searching for correlation from large datasets may lead to lower efficiency, and the found correlation may be meaningless. Therefore, there are "support degree" and "confidence degree" in the research process. "Support degree" can delete those meaningless data based on grounds, while "confidence degree" can measure the possibility of setting rules. The main algorithms include Apriori algorithm, DHP algorithm, and DIC algorithm. Correlation analysis method to establish correlation pattern mining method, with the help of a variety of new optimization techniques, can effectively and efficiently reduce the application of exercise rehabilitation therapy in the prevention and treatment of knee osteoarthritis search space.

**2.4.3. Data Preprocessing.** After treatment, effective was "F"; ineffective was "T"; VAS, IL-7R, TNF- $\alpha$ , IGF, IgA, IgM, IgG, C3, C4, WOMAC, and elevated were set as "T"; normal and decreased were set as "F"; Lysholm descending value is set as "T"; normal and rising value is set as "F."

**2.5. Statistical Methods.** In this study, all the data were organized, and a corresponding database was established for it, and all the databases were entered into SPSS 26.0 for data processing, and the measurement data was tested for



normality. The test between multiple sets is  $F$ , the independent sample  $t$  test is used for the data between sets, the paired sample  $t$  test is used for the data within the set, and the Mann–Whitney  $U$  test is not consistent with normality; the rate is expressed as %, and the test is  $\chi^2$ ; sex; Kaplan–Meier test analyzed the cumulative readmission rate within one year; when  $P < 0.05$ , the disparity between the data was considered to be statistically extensive.

### 3. Results

**3.1. Contrast of General Data.** Using the data mining method, a total of 1612 sufferers were included. According to different therapy methods, they were divided into exercise rehabilitation therapy set ( $n = 786$ ) and contrast therapy set ( $n = 826$ ), as shown in Figure 1.

**3.2. Contrast of Clinical Efficacy of the Two Therapy Methods in Sufferers.** According to data mining, after therapy in different ways, there was a big disparity in the curative effect of the two therapy modes, mainly as the curative effect of the exercise rehabilitation therapy set was notoriously higher than that of the contrast therapy set ( $P < 0.05$ ), as shown in Table 1.

**3.3. Contrast of Joint Pain and Knee Function in Sufferers with Two Therapy Methods before and after Therapy.** According to data mining, before therapy, VAS joint pain and Lysholm score were lower in both sets, and the disparity was not statistically extensive ( $P > 0.05$ ). After therapy, VAS joint pain and Lysholm score in two sets were enhanced and exercised. The enhancement in the rehabilitation therapy set was notoriously better than that in the contrast therapy set ( $P < 0.05$ ) (see Table 2).

**3.4. Contrast of the Disparities in Laboratory Indicators before and after Therapy between the Two Sets of Sufferers with Different Therapy Methods.** According to data mining, before therapy, there was no extensive disparity in laboratory serum inflammatory indexes and immune cytokines between the two sets ( $P > 0.05$ ); after therapy, serum inflammatory indexes and immune cytokines in both sets were enhanced and exercised. The enhancement effect of the rehabilitation therapy set was notoriously better than that of the contrast therapy set ( $P < 0.05$ ), as shown in Table 3 and Table 4.

**3.5. Contrast of the Quality of Life of Sufferers with Different Therapy Methods in the Two Sets before and after Therapy.** According to data mining, before therapy, the WOMAC scores of quality of life in both sets were higher, and the disparity was not statistically extensive ( $P > 0.05$ ); after therapy, the WOMAC quality of life scores were enhanced in both sets, and the enhancement in the exercise rehabilitation therapy set was notoriously better than that in the contrast set ( $P < 0.05$ ), as shown in Table 5.

**3.6. Analysis of the Relationship between VAS and Lysholm Score and Prognosis Quality of Life.** According to data mining, VAS, Lysholm score, and WOMAC score of prognosis

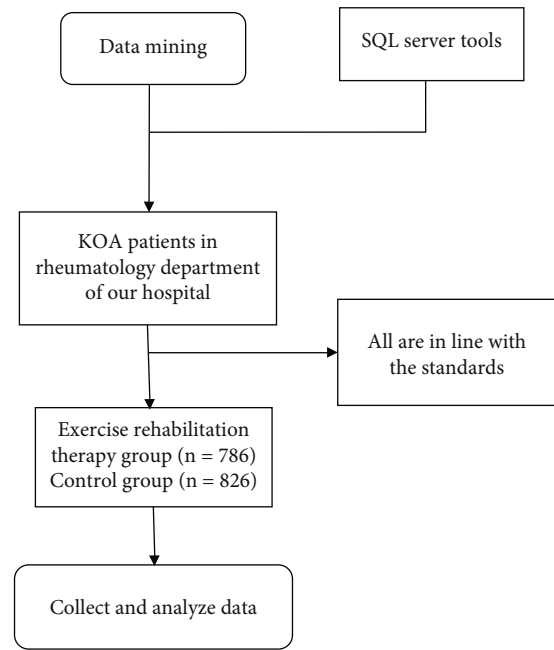


FIGURE 1: Flow chart of data mining literature selection.

quality of life were collected, and it was found that VAS score was notoriously positively correlated with WOMAC score ( $r = 0.579$ ,  $P < 0.05$ ); Lysholm score was notoriously positively correlated with WOMAC score ( $r = -0.563$ ,  $P < 0.05$ ) (see Figures 2 and 3).

**3.7. Contrast of Recurrence within 1 Year between the Two Therapy Sets.** According to data mining, the sufferers who completed the 12-month follow-up were recorded. During the follow-up period, 42 sufferers in the exercise rehabilitation therapy set were readmitted to the hospital for therapy, and the recurrence rate was 5.09%, which was notoriously lower than the 128 sufferers in the contrast therapy set, with a recurrence rate of 17.63%, and the disparity was statistically extensive. For academic significance ( $\chi^2 = 11.967$ ,  $P < 0.05$ ), see Figure 4.

### 4. Discussion

Modern medicine believes that the main pathological changes of KOA are articular cartilage degeneration, secondary bone hyperplasia and sclerosis, and subchondral bone cystic changes. However, the etiology and pathogenesis of KOA are not completely clear, and there is no effective therapy method [8]. Sports rehabilitation therapy breaks the traditional concept of rest therapy, is based on modern clinical fine anatomy, biomechanics, sports medicine, and rehabilitation medicine, focuses on scientific sports rehabilitation therapy, and focuses on the therapy of knee osteoarthritis [9]. However, there are few clinical application effects and situations of exercise rehabilitation therapy at present, and with the rapid development of the information age, the explosive growth of medical knowledge, and the continuous change of the disease spectrum, the clinical

TABLE 1: contrast of clinical efficacy between the two sets of sufferers [n (%)].

Set	Effective	Efficient	Invalid	Total efficiency
Exercise rehabilitation therapy set ( $n = 826$ )	563 (68.16)	203 (24.58)	60 (7.26)	766 (92.74)
Contrast therapy set ( $n = 786$ )	355 (45.17)	292 (37.15)	139 (17.68)	647 (82.32)
$\chi^2$				19.169
$P$				<0.001

TABLE 2: Contrast of joint pain and knee function in sufferers with two therapy methods before and after therapy ( $\bar{x} \pm s$ ).

Set	VAS score		Lysholm score	
	Before therapy	After therapy	Before therapy	After therapy
Exercise rehabilitation therapy set ( $n = 826$ )	7.85 $\pm$ 1.06	1.26 $\pm$ 0.23*	57.23 $\pm$ 8.51	87.63 $\pm$ 10.15*
Contrast therapy set ( $n = 786$ )	7.57 $\pm$ 1.09	2.57 $\pm$ 0.69*	57.63 $\pm$ 8.92	73.37 $\pm$ 9.81*
$t$	0.352	-12.216	-0.562	6.326
$P$	0.572	<0.001	0.524	<0.001

Note: \* indicates that contrast with before therapy in this set,  $P < 0.05$ , the disparity is statistically extensive.

TABLE 3: Contrast of inflammatory factors before and after therapy in two sets of sufferers with different therapy methods.

Set	IL-7R (ng/L)		TNF- $\alpha$ ( $\mu$ g/L)		IGF ( $\mu$ g/L)	
	Before therapy	After therapy	Before therapy	After therapy	Before therapy	After therapy
Exercise rehabilitation therapy set ( $n = 826$ )	173.56 $\pm$ 63.53	140.46 $\pm$ 35.33*	74.35 $\pm$ 18.56	50.69 $\pm$ 10.53*	75.63 $\pm$ 31.59	53.69 $\pm$ 31.57*
Contrast therapy set ( $n = 786$ )	173.93 $\pm$ 62.63	162.53 $\pm$ 39.57*	73.35 $\pm$ 17.36	73.57 $\pm$ 13.39*	74.69 $\pm$ 15.63	64.66 $\pm$ 14.65*
$t$	0.359	-3.303	0.433	-4.958	0.416	-4.607
$P$	0.412	0.001	0.512	<0.001	0.537	<0.001

Note: \* indicates that contrast with before therapy in this set,  $P < 0.05$ , the disparity is statistically extensive.

decision-making ability of doctors is facing severe challenges. Medication errors or misoperations caused by mistakes are one of the important causes of medical errors and even liability accidents [10]. Clinical decision support through massive objective reality data, medical guidance, literature, etc., with the help of computer's accurate and fast information storage, acquisition, and calculation capabilities, artificial intelligence technology, and computer logic, builds a knowledge base of various diseases and simulates the thinking of doctors in diagnosis and therapy. It can provide doctors with intelligent classification, disease inquiry, differential diagnosis, rational drug use, therapy evaluation, and other services, effectively solve the limitations of doctors' knowledge, reduce human errors and omissions, and enhance the efficiency of drug use, thereby improving the level of medical care, service capabilities, and efficiency, reducing medical errors to bring beneficial help; on this basis, the application of artificial intelligence technology and intelligent therapy intelligence will provide powerful solutions [11]. Based on this, in order to explain the mechanism of exercise rehabilitation therapy in KOA from a clinical perspective and verify its effectiveness, this study will provide a simple and effective set of clinical recovery and clinical symptom enhancement after

knee osteoarthritis therapy based on artificial intelligence data mining.

Among all kinds of rehabilitation therapy for arthritis, the role of exercise rehabilitation therapy is the most recognized by evidence-based medicine. Its functions promote blood circulation, enhance venous return and venous congestion, increase joint range of motion, muscle strength, and joint stability, promote the diffusion of synovial fluid to the cartilage surface and the intercellular substance, and can stimulate the proliferation of chondrocytes around the lesion area, supporting the regeneration of degenerated cartilage, and the strength of the sufferer's extensor muscles may increase the stability of the knee joint [12]. Clinical studies have shown that exercise rehabilitation is the most effective way to prevent and treat joint diseases and injuries and to support articular cartilage repair. Continuous passive movement of joints promotes the absorption of synovial fluid, which penetrates into articular cartilage, strengthens the metabolism of cartilage cells, and is beneficial to cartilage. The regeneration of functional quadriceps exercise in the therapy of knee osteoarthritis can effectively increase the stability of the knee joint and enhance the weight-bearing capacity of the knee joint [13]. The results of data

TABLE 4: Immune factors and metabolic indexes before and after therapy in two sets of sufferers with different therapy methods.

Set	IgA (g/L)		IgM (g/L)		IgG (g/L)		C3 (g/L)		C4 (g/L)	
	Before therapy	After therapy	Before therapy	After therapy	Before therapy	After therapy	Before therapy	After therapy	Before therapy	After therapy
Exercise rehabilitation therapy set ( <i>n</i> = 826)	2.39 ± 1.17	2.12 ± 0.91 *	1.19 ± 0.59	1.13 ± 0.52 *	12.56 ± 3.19	12.03 ± 2.02 *	113.25 ± 21.93	103.25 ± 19.47 *	26.89 ± 8.45	24.33 ± 6.42 *
Contrast therapy set ( <i>n</i> = 786)	2.41 ± 1.16	2.30 ± 1.02 *	1.20 ± 0.84	1.16 ± 0.81 *	12.58 ± 3.26	12.56 ± 2.36 *	117.25 ± 22.63	113.52 ± 21.53 *	27.83 ± 9.41	25.96 ± 6.88 *
<i>t</i>	0.569	11.589	0.693	12.646	0.891	10.513	0.953	11.527	0.838	10.972
<i>P</i>	0.512	0.001	0.473	<0.001	0.305	<0.001	0.217	0.001	0.349	<0.001

Note: \* indicates that contrast with before therapy in this set, *P* < 0.05, the disparity is statistically extensive.

TABLE 5: Contrast of knee joint function and quality of life before therapy and after 1 month of therapy.

Set	WOMAC	
	Before therapy	After therapy
Exercise rehabilitation therapy set ( $n = 826$ )	$66.37 \pm 8.94$	$28.55 \pm 4.89^*$
Contrast therapy set ( $n = 786$ )	$67.89 \pm 9.46$	$47.56 \pm 6.97^*$
$t$	0.893	17.836
$P$	0.221	<0.001

Note: \* indicates that contrast with before therapy in this set,  $P < 0.05$ , the disparity is statistically extensive.

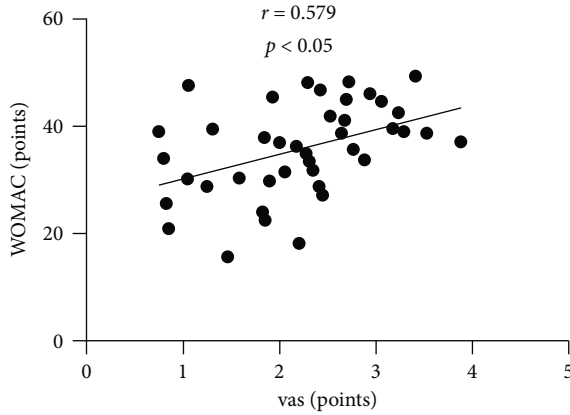


FIGURE 2: Analysis of the relationship between VAS and Lysholm scores and quality of life WOMAC score.

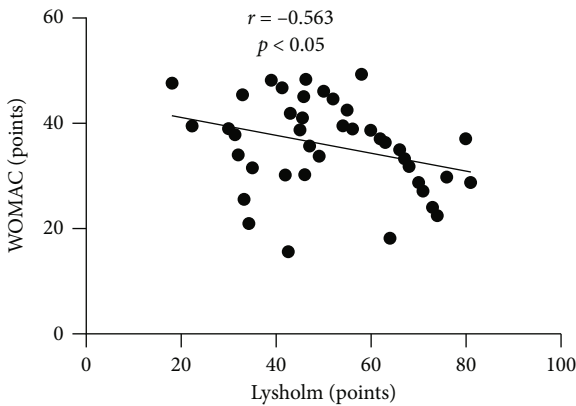


FIGURE 3: Analysis of the relationship between Lysholm score and prognosis quality of life WOMAC score.

mining showed that the therapeutic effect of the exercise rehabilitation group was significantly higher than that of the control group ( $P < 0.05$ ).

In addition, data mining results showed that VAS pain and Lysholm score were improved in both groups after treatment, and the improvement in the exercise rehabilitation therapy group was significantly better than that in the control group ( $P < 0.05$ ). The immune cytokines were enhanced, and the enhancement effect of the exercise rehabilitation therapy set was notoriously better than that of the contrast therapy set ( $P < 0.05$ ); for sufferers who are

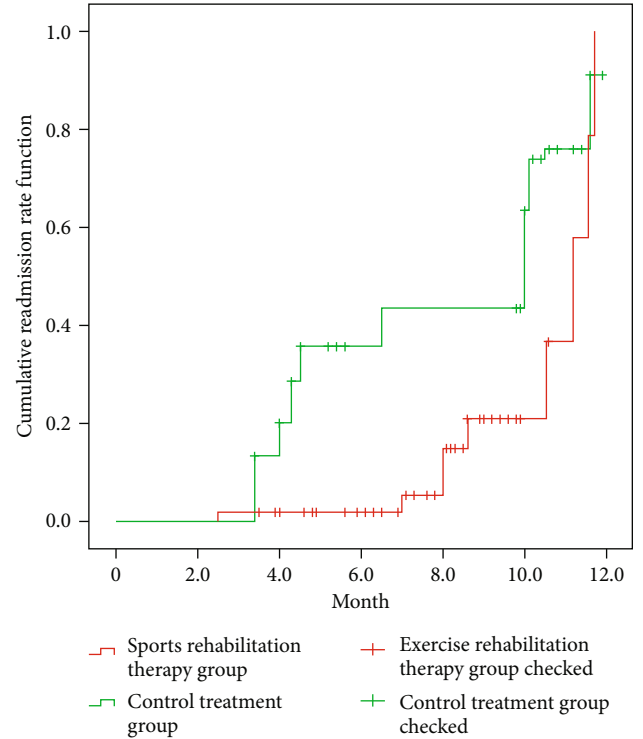


FIGURE 4: Cumulative readmission of sufferers in the two sets within 1 year.

unwilling to change behavior or have excessive pain and loss of joint function, KOA nondrug behavioral therapy is the first recommendation in terms of rehabilitation and prevention, while exercise rehabilitation therapy can enhance health-related symptoms and quality of life [14]. Physical rehabilitation is considered the basis for conservative disease management due to its extensive enhancement in sufferers with mild to severe KOA, whereas the main goals of exercise rehabilitation are pain relief, enhanced physiology, and effective participation in social activities, which can enhance physiological functions such as muscle strength, proprioception, range of motion, and cardiorespiratory function in sufferers with KOA to avoid abnormal body weight, mental status, and metabolism, as well as the risk of falling [15].

According to the data mining results, in this study, the sufferers who completed 12-month follow-up were recorded. During the follow-up period, 42 sufferers in the exercise

rehabilitation therapy set were readmitted to the hospital for therapy, with a recurrence rate of 5.09%, which was notoriously lower than that in the contrast set of 128 sufferers, with a recurrence rate of 17.63%. There was statistical significance ( $\chi^2 = 11.967$ ,  $P < 0.05$ ). Physical rehabilitation therapy is a cost-effective and acceptable approach in the therapy and prevention of KOA, and the updated OA therapy guidelines of the American Society of Clinical Rheumatology strongly recommend that KOA sufferers participate in aerobic, resistance, and aquatic interventions, help enhance functional limitations in KOA sufferers, and reduce the risk of recurrence. Although KOA sufferers can use various forms of exercise rehabilitation therapy, due to the extensive impact of muscle strength on pain and lower limb function in KOA sufferers, lower limb strength training is an important component of most knee and hip osteoarthritis exercise rehabilitation therapy section [16]. The combination of muscle strength training and aerobic training helps to enhance symptoms in most sufferers with KOA, but the type of exercise should be selected based on an assessment of the individual sufferer's condition, and the range of motion should be increased due to the reduced range of motion in sufferers with KOA [17]. Sufferers with KOA also have impaired neuromuscular contrast and an increased risk of falls, so for sufferers, balance training should be part of the exercise regimen, and the sufferer's balance should be assessed at the start of training to ensure safe movement, which is often as part of an overall KOA exercise program, KOA sufferers with overweight problems should also manage their KOA symptoms through diet and weight management [18].

To sum up, this study is based on data mining; combined with information network technology, exercise rehabilitation therapy for KOA patients can effectively improve inflammatory and immune factors in patients, enhance knee joint function and prognosis quality of life, and reduce readmission rate, which is worthy of clinical application.

## Data Availability

The datasets used in this paper are available from the corresponding author upon request.

## Conflicts of Interest

The authors declared that they have no conflicts of interest regarding this work.

## Acknowledgments

This work was supported by the Central Government Guides Local Science and Technology Development Project of Shandong Province (YDZX20203700002055), Natural Science Foundation of Shandong Province (grant number ZR2020QH318), and Shandong Province TCM Science and Technology Project (grant number 2021M149).

## References

- [1] G. Manogaran, N. Chilamkurti, and C. H. Hsu, "Special issue on advancements in artificial intelligence and machine learning algorithms for internet of things, cloud computing and big data," *International Journal of Software Innovation*, vol. 7, no. 2, pp. 335–337, 2019.
- [2] F. Qian and P. J. Schumacher, "Latest advancements in artificial intelligence-enabled technologies in treating type 1 diabetes," *Journal of Diabetes Science and Technology*, vol. 15, no. 1, pp. 195–197, 2021.
- [3] B. Kaufman, K. D. Allen, C. J. Coffman et al., "CC4 cost-effectiveness analysis of the stepped exercise program for patients with knee osteoarthritis (STEP-KOA) trial," *Value in Health*, vol. 23, no. 37, p. S2, 2020.
- [4] S. Shamsi, A. Alshehri, K. Amoudi, and S. Khan, "Effectiveness of physiotherapy management in knee osteoarthritis: a systematic review," vol. 11, no. 4, pp. 185–191, 2020.
- [5] L. O. Dantas, A. Jorge, P. R. M. da Silva Serrão, F. Aburquerque-Sendín, and T. de Fatima Salvini, "Cryotherapy associated with tailored land-based exercises for knee osteoarthritis: a protocol for a double-blind sham-controlled randomised trial," *BMJ Open*, vol. 10, no. 6, article e035610, 2020.
- [6] L. Wang, H. Chen, H. Lu, J. Chen, and S. Shang, "The effect of theory-led intervention for knee osteoarthritis in older adults: a cluster randomized trial," *Innovation in Aging*, vol. 33, no. 19, pp. 1256–1258, 2020.
- [7] J. Damen, R. M. Van Rijn, P. J. Emans et al., "Prevalence and development of hip and knee osteoarthritis according to American College of Rheumatology criteria in the CHECK cohort," *Arthritis Research & Therapy*, vol. 21, no. 1, pp. 362–365, 2019.
- [8] C. M. Xiao, L. I. Jing Jing, Y. Kang, and Y. C. Zhuang, "Follow-up of a Wuqinxin exercise at home programme to reduce pain and improve function for knee osteoarthritis in older people: a randomised controlled trial," *Age and Ageing*, vol. 50, no. 2, pp. 570–575, 2021.
- [9] P. M. Holm, H. M. Schröder, M. Wernbom, and S. T. Skou, "Low-dose strength training in addition to neuromuscular exercise and education in patients with knee osteoarthritis in secondary care - a randomized controlled trial," *Osteoarthritis and Cartilage*, vol. 28, no. 6, pp. 744–754, 2020.
- [10] E. Head, "Intelligent black boxes: advancements in artificial intelligence hold great promise for autonomous aircraft—but how do you certify a system you can't fully explain?," *Vertiflite*, vol. 63, no. 5, pp. 18–21, 2017.
- [11] S. Yongping, W. Li, and H. Liang, "Clinical observation of active exercise therapy for knee osteoarthritis and its influence on X-ray indicators," *Guizhou Medicine*, vol. 44, no. 2, pp. 3–6, 2020.
- [12] L. Wang, H. Chen, H. Lu et al., "The effect of theory-lead intervention for knee osteoarthritis in older adults: a cluster randomized trial," *BioMed Central*, vol. 25, no. 18, pp. 256–259, 2020.
- [13] A. Jorge, L. O. Dantas, P. R. M. S. Serrão, F. Alburquerque-Sendín, and T. F. Salvini, "Photobiomodulation therapy associated with supervised therapeutic exercises for people with knee osteoarthritis: a randomised controlled trial protocol," *BMJ Open*, vol. 10, no. 6, article e035711, 2020.
- [14] A. Lalbakhsh, R. Simorangkir, N. Bayat-Makou, A. A. Kishk, and K. P. Esselle, "Artificial intelligence and data



- science in environmental sensing,” in *Advancements and Artificial Intelligence Approaches in Antennas for Environmental Sensing*, pp. 19–38, 2022.
- [15] Y. Yalan, J. Xue, Z. Ying, L. Man, X. Ruishan, and Z. Lanshan, “Efficacy analysis of diamond block combined with intracavitary ozone injection and exercise rehabilitation in the therapy of knee osteoarthritis,” *China Journal of Modern Medicine*, vol. 31, no. 4, p. 67, 2021.
- [16] Y. Yan, L. Shuwei, and S. Chaojiang, “Discussion on the effect of combined exercise therapy and comprehensive rehabilitation therapy in the therapy of knee osteoarthritis,” *Guizhou Medicine*, vol. 45, no. 10, p. 225, 2021.
- [17] L. Huijun, W. Meng, and Y. Haixia, “Research progress on exercise therapy for knee osteoarthritis,” in *Journal of Inner Mongolia University: Natural Science Edition*, Art Intellig Data Sci Envir, 2020.
- [18] “Knee osteoarthritis exercise therapy clinical practice guideline writing set,” *National Medical Journal of China*, vol. 100, no. 15, pp. 26–29, 2020.

## Research Article

# Survey on Mental Health Status and Quality of Life and Correlation among Patients with Permanent Stoma of Colorectal Tumor

Yanlei Zou,<sup>1</sup> Qiu Yang,<sup>2</sup> Bi Guan,<sup>1</sup> Xiaoyu Fu,<sup>1</sup> Jia Wang,<sup>1</sup> and Yan Li<sup>3</sup> 

<sup>1</sup>Department of General Surgery, Chengdu Fifth People's Hospital, Chengdu, Sichuan 611130, China

<sup>2</sup>Center for Medical Research and Translation, Chengdu Fifth People's Hospital, Chengdu, Sichuan 611130, China

<sup>3</sup>Nursing Department, Chengdu Fifth People's Hospital, Chengdu, Sichuan 611130, China

Correspondence should be addressed to Yan Li; [edwin\\_foland@stu.centralaz.edu](mailto:edwin_foland@stu.centralaz.edu)

Received 4 July 2022; Accepted 17 August 2022; Published 5 September 2022

Academic Editor: Hangjun Che

Copyright © 2022 Yanlei Zou et al. This is an open access article distributed under the Creative Commons Attribution License, which permits unrestricted use, distribution, and reproduction in any medium, provided the original work is properly cited.

**Background.** Colorectal cancer is one of the malignant tumors of the digestive system relatively hidden onset with unobvious early clinical symptoms. Most patients have developed into middle and late stages when they were diagnosed, missing the best period of operation. Advanced colorectal cancer has strong diffusion and metastasis with short survival time, which seriously threatens the life safety of patients. **Objective.** To investigate the mental health status and quality of life and the relationship between them in patients with permanent stoma of colorectal cancer. **Methods.** In this study, a case-control study was conducted to select 80 patients (stoma group) with colorectal cancer treated by permanent stoma surgery in our hospital from January 2020 to June 2021 and 80 patients (control group) with colorectal cancer treated by sphincter-preserving surgery at the same time. The psychological health degree and quality of life of the two groups of patients were evaluated by the psychological resilience scale (CD-RISC), the positive psychological capital questionnaire (PPQ), and the cancer patient quality of life-specific scale (QOL-LC), and a linear correlation model was used to analyze the correlation of CD-RISC score, PPQ score, and QOL-LC score. **Results.** The total scores of tenacity, optimism, self-improvement, and resilience of the patients in the stoma group were significantly lower than those in the control one, and the difference between them was statistically significant ( $P < 0.05$ ); the four dimensions of self-efficacy, optimism, hope, and resilience and the total score of PPQ of patients in the stoma group were significantly lower than those in the control group, and all of the differences were statistically significant ( $P < 0.05$ ); the somatic function, psychological function, symptoms of side effects, social function, and the total QOL-LC score of patients in the stoma one were significantly lower than those in the control one, and all of the differences were statistically significant ( $P < 0.05$ ); the total QOL-LC score of patients in the stoma group showed a significant positive correlation with PPQ score and CD-RISC score ( $r = 0.511$  and  $r = 0.608$ ,  $P < 0.01$ ). **Conclusion.** The overall level of mental health and life quality of patients with permanent stoma of colorectal cancer was worse than that of patients without stoma measures, and there was a certain correlation between patients' mental health and quality of life.

## 1. Introduction

Colorectal cancer is a common clinical malignant tumor of the digestive system, among which rectal cancer is the most common one, accounting for about 50%–60%, and low rectal cancer is more common in rectal cancer [1]. According to the World Health Organization, the incidence of colorectal cancer ranks third in the incidence of malignant tumors [2]. Colorec-

tal cancer can cause changes in stool traits, abdominal pain, diarrhea, bloody stool, and other symptoms. In severe cases, intestinal obstruction, intestinal perforation, and other complications could also occur [3]. At present, the preferred method of clinical treatment for colorectal cancer is radical surgery, which can completely remove the lesion and save the lives of patients. However, postoperative complications can seriously affect the quality of life of patients [4].

A considerable proportion of patients with colorectal cancer needs to undergo permanent colostomy, which can lead to changes in defecation pathways and decreased defecation control ability. Improper care may also cause complications such as enterostomy infection, local dermatitis, stoma stenosis, and anastomotic fistula, which can lead to a serious decrease in the quality of life of patients. Patients are prone to anxiety, depression, inferiority, and other negative emotions, which adversely affects their mental health and leads to a decrease in treatment compliance, so as to affect their return to society [5, 6]. This study investigated the mental health status and quality of life and the relationship between them in patients with permanent colostomy of colorectal cancer.

Core tips: in this study, psychological resilience scale (CD-RISC) and positive psychological capital questionnaire (PPQ) were used to evaluate the psychological state of patients, and the quality of life of patients with colorectal cancer was evaluated by quality of life-specific scale (QOL-LC). It was found that colorectal cancer patients undergoing colostomy can have adverse effects on mental health and quality of life. This study also analyzed the relationship between them and found that the QOL-LC scores of stoma patients were positively correlated with PPQ scores and CD-RISC scores.

## 2. Materials and Methods

**2.1. General Information.** In this study, a case-control study was conducted to select 80 patients with colorectal cancer (stoma group) treated by permanent colostomy in our hospital from January 2020 to June 2021 and 80 patients with colorectal cancer (control group) treated by sphincter-preserving surgery in the same period. For the selection of research subjects, a table of random number was used.

Inclusion criteria: (1) patients were from 18 to 79 years old; (2) the diagnosis of colorectal cancer patients was based on postsurgical pathological examination results; (3) all patients underwent surgery in our hospital; (4) patients were with normal hearing, speaking, and comprehension abilities; (5) the research scheme met the basic requirements of Medical Ethics for Human Experimentation and Medical Ethics, and the informed consent was signed with the patient and his family before the operation.

Exclusion criteria: (1) combination of cancer in other sites, (2) combination of major diseases in other sites that affect the quality of survival, (3) history of mental illness, and (4) previous history of cranial surgery.

**2.2. Scale Measurement.** Resilience scale (CD-RISC) [7] consists of 25 questionnaire items and 3 questionnaire dimensions, which are assessed in terms of the patient's resilience, optimism, and self-improvement, respectively, and each questionnaire item is rated on a 5-point scale ranging from "never" to "almost always," with a rating range of 0 to 4. With a total score of 100, the higher the score the better the patient's resilience level.

The positive psychological capital questionnaire (PPQ) [8] was compiled by Professor Zhang Kuo of Tianjin Nankai

University in 2009. The scale contained 26 questionnaire items and 4 survey dimensions. The scale was scored from the four dimensions of patients' self-efficacy, optimism, hope, and resilience on a 7-point Likert scale, with a total scale score range of 26 to 182, and the scores are positively correlated with the psychological capital level of patients.

The quality of life-specific scale for cancer patients (QOL-LC) [9] was compiled by Wan Chonghua and other experts, which consists of four dimensions: physical function (six questionnaire items), psychological function (six questionnaire items), symptoms and side effects (five questionnaire items), and social function (five questionnaire items), with a total score of 220 and a significant positive correlation between the scores and the life quality of patients.

All patients were investigated by CD-RISC, PPQ, and QOL-LC and other three scales, which were completed independently by patients within a specified time frame, with a 100% recall rate. The scales were scored by two caregivers and the average values of the two results were taken.

**2.3. Statistical Processing.** Statistical software SPSS 21.0 was used for data statistics. The measurement indexes such as resilience, optimism, self-improvement, and total psychological resilience scores collected from the two groups in this study were tested by normal distribution, which were in line with approximate normal distribution or normal distribution, expressed as  $(\bar{x} \pm s)$ . The  $t$ -test was used for comparison between the two groups; the  $\chi^2$  test was used for comparison between groups for nonhierarchical count data such as adjuvant chemotherapy, health insurance mode, and tumor site; the relationship between life quality and PPQ score and CD-RISC score was studied by Pearson linear correlation analysis; the test level was  $\alpha = 0.05$ .

## 3. Results

**3.1. Comparison of Baseline Data between the Two Groups of Patients.** There was no significant difference in age, gender, BMI, years of education, adjuvant chemotherapy, medical insurance, and tumor location between the two groups ( $P > 0.05$ ) (Table 1).

**3.2. Comparison of Resilience Scores between the Two Groups.** The total scores of tenacity, optimism, self-improvement, and resilience of the patients in the stoma group were significantly lower than those in the control group, and the difference between them was statistically significant ( $P < 0.05$ ) (Table 2).

**3.3. Comparison of PPQ Scores between the Two Groups.** The four dimensions of self-efficacy, optimism, hope, and resilience and the total score of PPQ of patients in the stoma group were significantly lower than those in the control group, and all of the differences were statistically significant ( $P < 0.05$ ) (Table 3).

**3.4. Comparison of Quality of Life Scores between the Two Groups.** The somatic function, psychological function, symptoms of side effects, social function, and the total QOL-LC score of patients in the stoma group were significantly lower

TABLE 1: Comparison of baseline data between the two groups.

Group	<i>n</i>	Age (years)	Gender (%)		BMI (kg/m <sup>2</sup> )	Years of education (years)	Adjuvant chemotherapy (%)	Medical insurance mode (%)		Tumor site (%)	
			Male	Female				Urban workers	Urban and rural residents	Rectal cancer	Colon cancer
Stoma group	80	53.66 ± 8.03	48 (60.00)	32 (40.00)	22.77 ± 2.16	8.55 ± 2.01	70 (87.50)	32 (40.00)	48 (60.00)	64 (80.00)	16 (20.00)
Control group	80	51.70 ± 7.94	40 (50.00)	40 (50.00)	22.48 ± 1.95	8.14 ± 1.68	66 (82.50)	39 (48.75)	41 (51.25)	69 (86.25)	11 (13.75)
<i>t</i> / $\chi^2$		1.552		1.616	0.891	1.400	0.784		1.241		1.114
<i>P</i>		0.123		0.204	0.374	0.164	0.376		0.265		0.291

TABLE 2: Comparison of psychological elasticity scores between the two groups ( $\bar{x} \pm s$ , points).

Group	<i>n</i>	Tenacity	Optimistic	Self-improvement	Total score of psychological elasticity
Stoma group	80	28.48 ± 6.41	8.64 ± 2.00	19.50 ± 4.47	56.62 ± 7.05
Control group	80	32.50 ± 5.84	9.44 ± 2.15	26.03 ± 6.15	67.97 ± 8.55
<i>t</i>		-4.146	-2.437	-7.682	-9.161
<i>P</i>		0.000	0.016	0.000	0.000

TABLE 3: Comparison of PPQ scores between the two groups ( $\bar{x} \pm s$ , points).

Group	<i>n</i>	Self-efficacy	Optimistic	Hope	Toughness	PPQ total score
Stoma group	80	30.76 ± 5.94	30.78 ± 5.84	27.58 ± 5.20	31.01 ± 4.98	120.13 ± 11.64
Control group	80	34.66 ± 5.50	33.75 ± 4.92	33.04 ± 6.16	34.58 ± 6.03	136.03 ± 14.58
<i>t</i>		-4.309	-3.479	-6.058	-4.083	-7.623
<i>P</i>		0.000	0.001	0.000	0.000	0.000

TABLE 4: Comparison of quality of life scores between the two groups ( $\bar{x} \pm s$ , points).

Group	<i>n</i>	Somatic function	Psychological function	Symptomatic side effects	Social function	QOL-LC total score
Stoma group	80	36.95 ± 5.70	31.03 ± 6.02	33.51 ± 7.46	26.33 ± 5.03	127.82 ± 13.76
Control group	80	41.14 ± 6.33	35.76 ± 7.50	38.64 ± 7.92	34.28 ± 6.05	149.82 ± 15.00
<i>t</i>		-4.400	-4.399	-4.217	-9.038	-9.667
<i>P</i>		0.000	0.000	0.000	0.000	0.000

than those in the control group, and all of the differences were statistically significant ( $P < 0.05$ ) (Table 4).

**3.5. Correlation of Quality of Life with PPQ Score and CD-RISC Score.** Simple linear correlation analysis showed that the total score of QOL-LC was positively correlated with PPQ score ( $r = 0.511$ ,  $P < 0.01$ ) and CD-RISC score ( $r = 0.608$ ,  $P < 0.01$ ) (Figures 1 and 2).

#### 4. Discussion

Epidemiological survey found that the incidence of colorectal cancer in China was 13.29:100 000. Although this ratio was lower than that in Western European and American countries, the total number of colorectal cancer cases is still considerable due to the large population base in China [10–12]. In recent years, the incidence rate of colorectal can-

cer has shown a gradual increasing trend with the improvement of the living standard [13]. Surgery is the cornerstone of various treatments for colorectal cancer, but the surgical trauma is large, and patients suffer great physical and mental pain during perioperative period [14–16]. Although the current implementation of neoadjuvant therapy has reduced the recurrence rate of local lesions and increased the possibility of anus preservation, a considerable number of patients still have local recurrence due to the particularity of the physiological and anatomical location of the colorectal part and the lymphatic drainage pathway [17, 18].

Enterostomy, also known as artificial anus, is a section of intestinal opening artificially flipped and sewn to the abdominal wall incision after resection of the intestinal lesion to replace the function of the anus in order to solve the defecation problem of colorectal cancer patients [19, 20]. However, enterostomy causes great inconvenience to

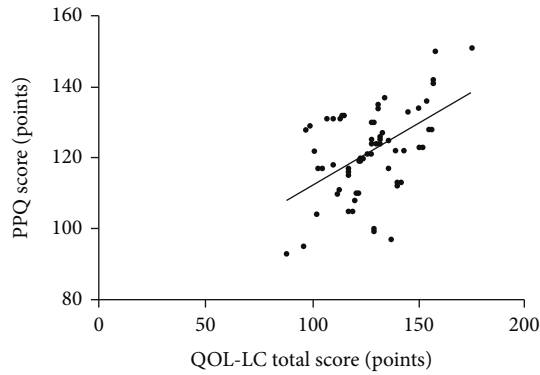


FIGURE 1: Scatter diagram of correlation between total QOL-LC score and PPQ score.

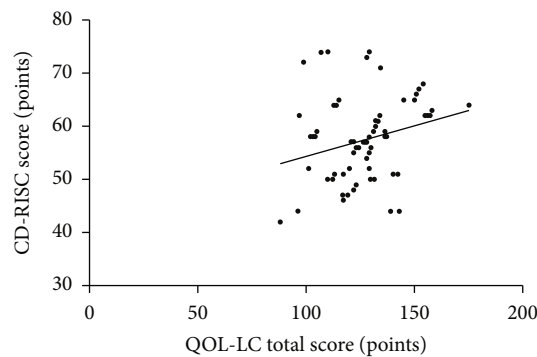


FIGURE 2: Scatter diagram of correlation between total QOL-LC score and CD-RISC score.

patients' life, resulting in great physical and psychological pain, and even affects their compliance with subsequent treatment [21]. CD-RISC scale is a tool to evaluate the resilience of patients. Hope and optimism represent positive attitudes towards life and the hope for rehabilitation and future life. Resilience refers to the confidence to deal with difficulties, not easily abandoned, go away from the plight and negative state as soon as possible [22, 23]. Q scale is the basis for evaluating the psychological capital level of patients, including four dimensions of self-efficacy, optimism, hope, and resilience [24, 25]. This study found that the total scores of resilience, optimism, self-improvement, and psychological resilience as well as the four dimensions of self-efficacy, optimism, hope, and resilience and the total score of PPQ were significantly lower in patients with stoma than in patients without stoma, which was due to the fact that colorectal cancer disease itself and the pain caused by treatment could lead to great psychological stress, and patients often had negative psychological emotions due to concerns about their condition, prognosis, and treatment costs [26, 27]. Stomatostomy has changed the normal defecation pathway, which may lead to problems such as decreased defecation control ability, odor, and infection, thereby reducing psychological resilience and self-efficacy, and unable to get out of the dilemma quickly [28, 29].

One of the current treatment goals for malignant tumors is to improve the survival quality of patients, and the QOL-

LC is a common tool for evaluating the survival quality of patients with good reliability and validity. The scale can comprehensively reflect the survival quality of patients from four dimensions, including physical function, psychological function, symptoms of side effects, and social function [30, 31]. This study found that the physical function, psychological function, symptoms of side effects, social function, and QOL-LC scores of stoma patients were significantly lower than those of nonstoma patients, which suggested that the overall survival quality of patients with colorectal cancer undergoing permanent colostomy was worse than that of patients without colostomy. This is due to the change in the defecation mode of patients with enterostomy, the loss of the control function of the sphincter, and the failure to control the excretion behavior. It is necessary to wear the stoma bag for life to collect the excreta, which not only changes the body shape but also produces odors and sounds. Patients are afraid of being found and abandoned, which has a negative impact on the daily life and social activities of patients [32, 33].

The simple linear correlation analysis was also used in this study. The QOL-LC total score of colostomy patients was significantly positively correlated with PPQ score and CD-RISC score. This result suggested that there was a certain correlation between the mental health status and life quality of colorectal cancer patients with permanent colostomy. Mental health is an important part of life quality. Negative emotions can affect sleep quality, cause the body to be under stress, reduce self-efficacy, and have certain adverse effects on physical function, symptoms of side effects, and social function [34, 35].

In conclusion, the overall level of mental health and life quality of patients with colorectal cancer undergoing permanent colostomy was worse than that of patients without colostomy, and there was a certain correlation between mental health and life quality of patients.

## Data Availability

The datasets used and analyzed during the current study are available from the corresponding author upon reasonable request.

## Conflicts of Interest

The authors declare that they have no conflicts of interest.

## Authors' Contributions

Yanlei Zou and Qiu Yang contributed equally to this work and share first authorship.

## Acknowledgments

This work was funded by the Chengdu Health Commission 2022, Chengdu Medical Research Project "Application of Plasticity Chassis in Patients with Permanent Colorectal Tumors and Enterostomy and Health Economics Analysis" No. 509.



## References

- [1] R. Delahunty, M. Lee, H. L. Wong et al., "Utilisation of systemic therapy options in routine treatment of metastatic colorectal cancer in Australia," *Internal Medicine Journal*, vol. 50, no. 2, pp. 165–172, 2020.
- [2] Z. J. Jia, Z. H. Yang, C. X. Jia et al., "A systematic review and meta-analysis of randomized controlled trials on treating ulcerative colitis by the integration method of heat-clearing, damp-excreting, spleen-strengthening, and stasis-removing of traditional Chinese medicine with western medicine," *World Journal of Traditional Chinese Medicine*, vol. 6, no. 1, pp. 74–82, 2020.
- [3] C. Y. S. Lim, R. C. Laidsaar-Powell, J. M. Young, S. C. H. Kao, Y. Zhang, and P. Butow, "Colorectal cancer survivorship: a systematic review and thematic synthesis of qualitative research," *European Journal of Cancer Care*, vol. 30, no. 4, p. e13421, 2021.
- [4] A. Anderson, K. Barnett, M. Bhagat, and R. Steele, "A qualitative evaluation of the impact of a training programme on colorectal cancer risk reduction for specialist screening practitioners on health promotion, knowledge and practice," *European Journal of Cancer Care*, vol. 30, no. 1, article e13350, 2021.
- [5] A. Bartoszek, J. Fichna, A. Tarasiuk et al., "Free fatty acid receptors as new potential targets in colorectal cancer," *Current Drug Targets-The International Journal for Timely In-Depth Reviews on Drug Targets*, vol. 21, no. 14, pp. 1397–1404, 2020.
- [6] H. Kim, K. Wang, M. Song, and E. L. Giovannucci, "A comparison of methods in estimating population attributable risk for colorectal cancer in the United States," *Cancer*, vol. 148, no. 12, pp. 2947–2953, 2021.
- [7] M. S. Khoshouei, "Psychometric evaluation of the Connor-Davidson resilience scale (CD-RISC) using Iranian students," *International Journal of Testing: Official Journal of the International Test Commission*, vol. 9, no. 1, pp. 60–66, 2009.
- [8] K. Zhang, S. Zhang, and Y. H. Dong, "Positive psychological capital: measurement and its relationship with mental health," *Psychological and Behavioral Research*, vol. 8, no. 1, pp. 58–64, 2010.
- [9] M. Qiong, W. Chonghua, and L. Jiahong, "Application of EORTC QLQ-C30," *Chinese Behavioral Medicine*, vol. 14, no. 3, pp. 273–274, 2005.
- [10] J. Malmqvist, V. Siersma, M. S. Hestbech, D. R. Nicolaisdóttir, C. W. Bang, and J. Brodersen, "Psychosocial consequences of invitation to colorectal cancer screening: a matched cohort study," *Journal of Epidemiology and Community Health*, vol. 75, no. 9, pp. 867–873, 2021.
- [11] W. Rozpędek, D. Pytel, A. Wawrzynkiewicz et al., "Use of small-molecule inhibitory compound of PERK-dependent signaling pathway as a promising target-based therapy for colorectal cancer," *Current Cancer Drug Targets*, vol. 20, no. 3, pp. 223–238, 2020.
- [12] M. Rouyer, E. François, A. Sa Cunha et al., "Effectiveness of first-line cetuximab in wild-type RAS metastatic colorectal cancer according to tumour BRAF mutation status from the EREBUS cohort," *British Journal of Clinical Pharmacology*, vol. 87, no. 3, pp. 1120–1128, 2021.
- [13] V. Hanicinea, V. Brynychova, J. Rosendorf et al., "Gene expression of cytokinesis regulators *PRC1*, *KIF14* and *CIT* has no prognostic role in colorectal and pancreatic cancer," *Oncology Letters*, vol. 22, no. 2, p. 598, 2021.
- [14] M. Gilfoyle, A. Chaurasia, J. Garcia, and M. Oremus, "Perceived susceptibility to developing cancer and screening for colorectal and prostate cancer: a longitudinal analysis of Alberta's Tomorrow Project," *Journal of Medical Screening*, vol. 28, no. 2, pp. 148–157, 2021.
- [15] L. M. Sabik, K. Y. Eom, B. Dahman et al., "The impact of Massachusetts health reform on colorectal and breast cancer stage at diagnosis," *Medical Care*, vol. 58, no. 2, pp. 183–191, 2020.
- [16] P. P. Coll, B. Korc-Grodzicki, B. T. Ristau et al., "Cancer prevention and screening for older adults: part 1. lung, colorectal, bladder, and kidney cancer," *Journal of the American Geriatrics Society*, vol. 68, no. 10, pp. 2399–2406, 2020.
- [17] C. Antoniotti, W. M. Korn, F. Marmorino et al., "Original research tumour mutational burden, microsatellite instability, and actionable alterations in metastatic colorectal cancer: next-generation sequencing results of tribe2 study," *European Journal of Cancer*, vol. 15, no. 5, pp. 73–84, 2021.
- [18] R. Moradi-Marjaneh, F. Asgharzadeh, E. Khordad, and M. M. Marjaneh, "The clinical impact of quantitative cell-free DNA, KRAS, and BRAF mutations on response to anti-EGFR treatment in patients with metastatic colorectal cancer," *Current Pharmaceutical Design*, vol. 27, no. 7, pp. 942–952, 2021.
- [19] A. Kuchel, E. Ahern, S. Collins et al., "Trends in epidemiology, treatment and molecular testing of metastatic colorectal cancer in a real-world multi-institution cohort study," *Asia-Pacific Journal of Clinical Oncology*, vol. 17, no. 1, pp. 84–93, 2021.
- [20] J. E. Lambert, L. D. Hayes, T. J. Keegan, D. A. Subar, and C. J. Gaffney, "The impact of prehabilitation on patient outcomes in hepatobiliary, colorectal, and upper gastrointestinal cancer surgery," *Annals of Surgery*, vol. 274, no. 1, pp. 70–77, 2021.
- [21] C. Kirana, E. Smith, D. T. Ngo et al., "High preoperative levels of circulating SFRP5 predict better prognosis in colorectal cancer patients," *Future Oncology*, vol. 16, no. 31, pp. 2499–2509, 2020.
- [22] B. Heritage, A. A. Al Asadi, and D. G. Hegney, "Examination of the Connor-Davidson resilience scale 10 (CD-RISC-10) using the polytomous Rasch model," *Psychological Assessment*, vol. 33, no. 7, pp. 672–684, 2021.
- [23] S. Bezdjian, K. G. Schneider, D. Burchett, M. T. Baker, and H. N. Garb, "Resilience in the United States Air Force: psychometric properties of the Connor-Davidson resilience scale (CD-RISC)," *Psychological Assessment*, vol. 29, no. 5, pp. 479–485, 2017.
- [24] D. Collins, H. M. Paterson, R. J. Skipworth, and D. Speake, "Implementation of the Versius robotic surgical system for colorectal cancer surgery: first clinical experience," *Colorectal Disease*, vol. 23, no. 5, pp. 1233–1238, 2021.
- [25] N. Murphy, P. T. Campbell, and M. J. Gunter, "Are sugar-sweetened beverages contributing to the rising occurrence of colorectal cancer in young adults?," *Gastroenterology*, vol. 70, no. 12, pp. 2222–2223, 2021.
- [26] E. Travis, L. Ashley, M. Pownall, and D. B. O'Connor, "Barriers to flexible sigmoidoscopy colorectal cancer screening in low uptake socio-demographic groups: a systematic review," *Psycho-Oncology*, vol. 29, no. 8, pp. 1237–1247, 2020.
- [27] A. Delpla, T. de Baere, E. Varin, F. Deschamps, C. Roux, and L. Tselikas, "Role of thermal ablation in colorectal cancer lung metastases," *Cancers*, vol. 13, no. 4, p. 908, 2021.

- [28] H. Tanaka, C. Saigo, Y. Iwata et al., “Human colorectal cancer-associated carbohydrate antigen on annexin A2 protein,” *Journal of Molecular Medicine*, vol. 99, no. 8, pp. 1115–1123, 2021.
- [29] J. P. Väyrynen, M. C. Lau, K. Haruki et al., “Prognostic significance of immune cell populations identified by machine learning in colorectal cancer using routine hematoxylin and eosin-stained sections,” *Clinical Cancer Research*, vol. 26, no. 16, pp. 4326–4338, 2020.
- [30] C. S. Bonhof, L. V. van de Poll-Franse, D. K. Wasowicz, L. V. Beerepoot, G. Vreugdenhil, and F. Mols, “The course of peripheral neuropathy and its association with health-related quality of life among colorectal cancer patients,” *Journal of Cancer Survivorship: Research and Practice*, vol. 15, no. 2, pp. 190–200, 2021.
- [31] P. Wieszczy, E. Waldmann, M. Løberg et al., “Colonoscopist performance and colorectal cancer risk after adenoma removal to stratify surveillance: two nationwide observational studies,” *Gastroenterology*, vol. 160, no. 4, pp. 1067–1074.e6, 2021.
- [32] K. Ishimaru, K. Kawai, H. Nozawa et al., “Hazard function analysis of metastatic recurrence after colorectal cancer surgery—a nationwide retrospective study,” *Journal of Surgical Oncology*, vol. 123, no. 4, pp. 1015–1022, 2021.
- [33] Q. Wang, P. Liao, Y. Wu, Y. Huang, Y. Wu, and X. Xu, “Studies on apoptosis and mechanism of curcumin chitosan induced human colon cancer cells in colorectal cancer,” *Journal of Biomaterials and Tissue Engineering*, vol. 10, no. 7, pp. 987–991, 2020.
- [34] J. Han, K. Y. Lee, N. K. Kim, and B. S. Min, “Metachronous metastasis confined to isolated lymph node after curative treatment of colorectal cancer,” *International Journal of Colorectal Disease*, vol. 35, no. 11, pp. 2089–2097, 2020.
- [35] P. Weimers, D. Vedel Ankersen, S. Lophaven et al., “Disease activity patterns, mortality, and colorectal cancer risk in microscopic colitis: a Danish nationwide cohort study, 2001 to 2016,” *Journal of Crohn’s & Colitis*, vol. 15, no. 4, pp. 594–602, 2021.

## Research Article

# Detection Method of Athlete Joint Injury Based on Deep Learning Model

Jianjia Liu,<sup>1,2</sup> Xin Yang ,<sup>1</sup> Tiannan Liao,<sup>1</sup> and Yong Huang<sup>1</sup>

<sup>1</sup>Department of Orthopedics, Hospital of Chengdu University of Traditional Chinese Medicine, Chengdu 610072, China

<sup>2</sup>School of Public Affairs & Law, Southwest Jiaotong University, Chengdu, 610000, China

Correspondence should be addressed to Xin Yang; [stella19830116yx@126.com](mailto:stella19830116yx@126.com)

Received 1 July 2022; Revised 9 August 2022; Accepted 16 August 2022; Published 2 September 2022

Academic Editor: Hangjun Che

Copyright © 2022 Jianjia Liu et al. This is an open access article distributed under the Creative Commons Attribution License, which permits unrestricted use, distribution, and reproduction in any medium, provided the original work is properly cited.

The research on accurate and intelligent segmentation of knee joint MRI images is of great significance to reduce the work intensity of clinical doctors and nurses. In order to solve the problem that knee joint MRI image segmentation model needs a large number of high-quality tagged images and excessive labeling workload, a semisupervised learning segmentation network model based on 3D scSE-UNet is proposed. The model adopts a self-training semisupervised learning framework and adds a cSE-block+ module on the basis of the 3D UNet model. This module can enhance the effective features of the feature image from two aspects of space and channel, while suppressing irrelevant features and preserving image edge information more completely. In order to solve the problem of rough edge of pseudolabel caused by model segmentation, a fully connected conditional random field is added to refine the edge of pseudolabel in the process of model training. The effectiveness of the model is verified by open source MRNet dataset and OAI dataset. The results show that the proposed model can achieve the segmentation effect of fully supervised learning through a small number of labeled images and effectively reduce the dependence of knee joint MRI image segmentation on expert labeling data.

## 1. Introduction

Knee joint is one of the most important composite joints in human body [1]. Most of the complex human movements are inseparable from the knee joint, and it is also the most important load-bearing joint [2]. For athletes who take various sports as their professions, the health of knee joints and the early detection and treatment of injuries are particularly important [3]. After knee joint injury caused by exercise, timely and accurate professional evaluation of anterior cruciate ligament injury is of great significance for medical staff to choose the best treatment and to prevent the impact of injury on athletes' career [4]. In medicine, the examination of knee joint injury and lesion usually depends on magnetic resonance imaging (MRI). The advantage of MRI over arthroscopy is that it can clearly display articular cartilage and bone areas [5]. Theoretically, the knee joint history of

patients and the pathological changes occurred during the occurrence of knee joint abnormalities can play a very important role in the diagnosis of specific knee joint problems. However, in the actual operation, there is still a case of low diagnostic sensitivity. The doctor will inevitably touch the pain point of the patient's knee joint in the clinical examination, which will increase the pain of the patient. This problem hinders clinical examination [6].

Knee arthroscopy is one of the commonly used methods in the diagnosis of knee joint diseases. However, since the introduction of MRI technology, this relatively noninvasive diagnostic tool has gradually replaced invasive arthroscopy [7]. It visualizes the abnormal problems of the knee joint by presenting a high-resolution image of the interior of the knee joint. The application of MRI provides reference and guidance for orthopedic experts in the preliminary diagnosis, treatment, and prognosis of meniscus, ligament, and

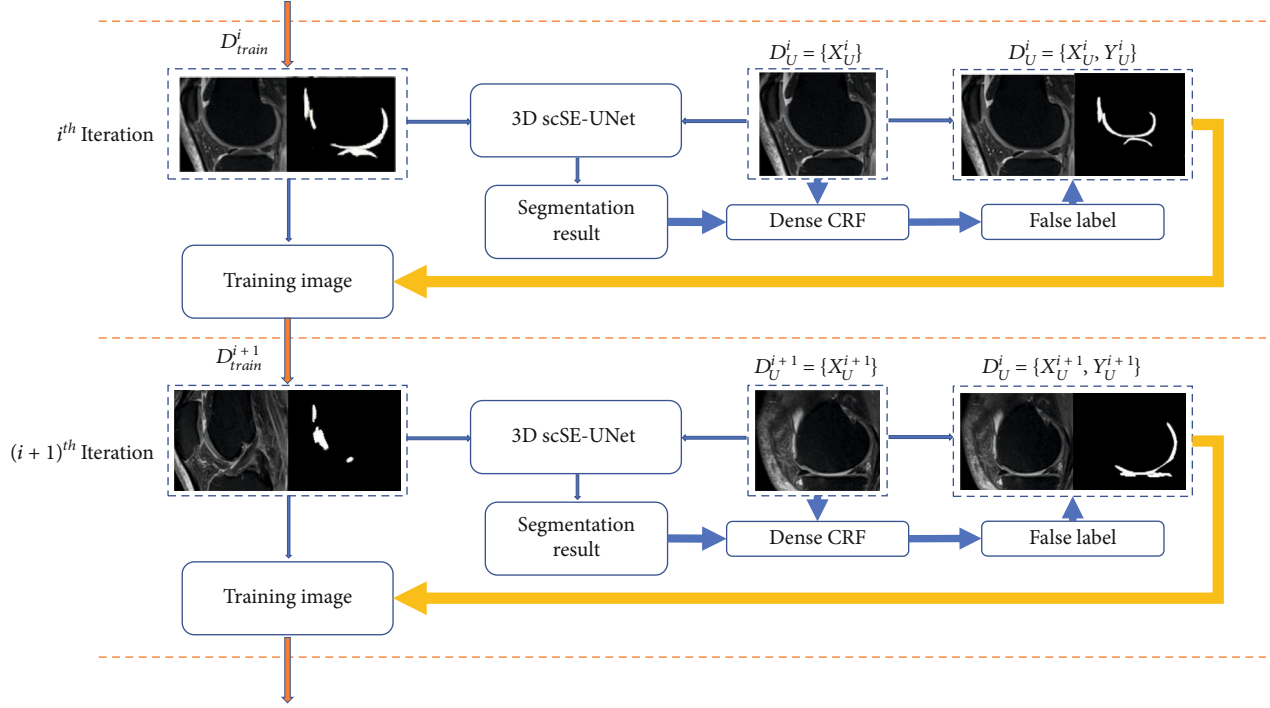


FIGURE 1: Training method of 3D scSE-UNet network model.

tendon-related problems. At the same time, the cost of MRI of the knee joint is also slowly falling. Coupled with its non-invasive advantages, the current medical diagnosis and treatment is not only in the preoperative MRI examination of patients but also began to be used as an auxiliary diagnosis in the preliminary diagnosis of knee joint diseases.

In recent years, deep learning methods have made great progress in the field of computer vision, such as object detection [8], human posture estimation [9], or semantic segmentation [10]. Similarly, in the field of medical images, deep learning has achieved excellent results in disease classification [11, 12], cancer detection [13, 14], organ segmentation [15], and image reconstruction [16]. The application of deep learning in knee joint MRI image analysis is becoming a hot research content. Li et al. [17] used the multimode feature fusion model in deep learning to diagnose the injury of knee joint MRI images. The results show that the prediction accuracy of the model in knee joint tear is 96.28%, and it is proved that the MRI image classification model based on depth learning can accurately classify the type of anterior cruciate ligament injury. Chaudhari et al. [18] compared deep learning super resolution (DLSR) with conventional knee MRI and found that conventional MRI was 92% accurate in evaluating knee cartilage, meniscus, bones, ligaments, extensors, and synovium, while DLSR was consistent with its accuracy. This shows that DLSR can simplify the diagnosis of knee joint MRI. Yang et al. [19] applied the conditioned adversarial network to 30 groups of clinical MRI images and successfully carried out automatic cartilage segmentation through model training. The results show that transfer learning can achieve the same segmentation accuracy as

human when the number of samples is small. Iqbal et al. [20] aimed at automatically monitoring the health degree of human knee synovial fluid and adopted the transfer learning model to solve the problem that it is difficult to label data sets on a large scale in medical images. At the same time, it is also proved that the model has a good recognition of human knee joint synovial fluid.

The above research has made some progress in knee joint MRI image segmentation, but still does not solve a common problem. On the one hand, for MRI images, it is difficult for a medical institution or imaging center to have enough tagged and untagged data. However, the MRI images from different image centers will be affected by imaging equipment, imaging protocols, and operating technicians, which makes it difficult for the model to train well. The main reason for this effect is that the resolution of MRI image is different due to the difference of imaging equipment and imaging protocol. Different levels of operators easily lead to differences in the degree of presentation of lesions on MRI images. On the other hand, well-trained models should be more robust to adapt to different sources of data.

Based on the above problems, we use two open knee joint MRI data sets from different sources, namely, MRNet and OAI datasets for semisupervised learning. The main difference between the two datasets is that each sample is marked with an exception in the MRNet dataset, while the OAI dataset is untagged. In this paper, the semisupervised learning knee joint segmentation method of self-training 3D scSE-UNet segmentation network is used to train part of the MRI dataset as tagged data and the other part as untagged data. In the process of self-training, a fully

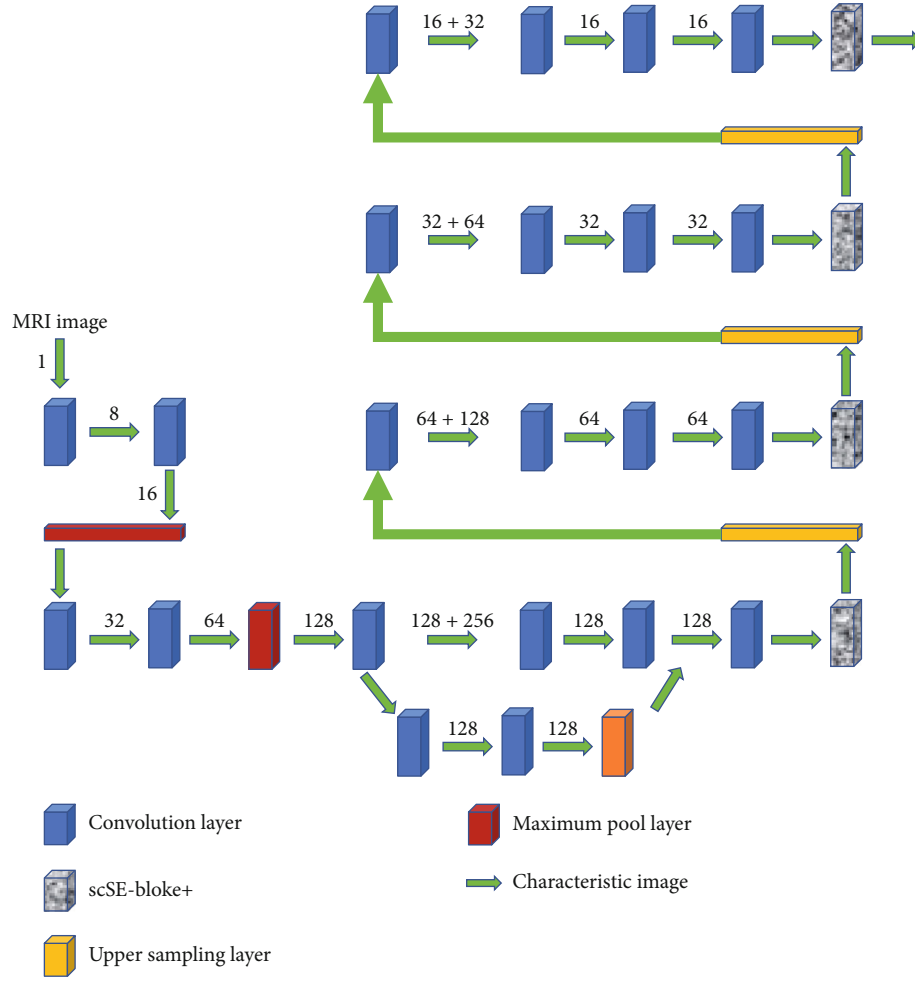


FIGURE 2: Outline of the structure of 3D scSE-UNet network model.

connected conditional random field is added to refine the predicted pseudolabel edge to improve the accuracy. After training, the model can achieve the purpose of effectively training 3DscSE-UNet with a small amount of labeled data and a large number of unlabeled data, so as to improve the accuracy of knee joint segmentation (abnormalities, ACL tears, and meniscus tears) and reduce the dependence of deep learning image segmentation methods on label data.

## 2. Methods

**2.1. Self-Training Semisupervised Learning Segmentation.** Reasonable and effective use of the effective information in MRI images is helpful to improve the segmentation accuracy of the target region. Therefore, the self-training method is used to segment the image. Self-training is a representative method in semisupervised learning. It trains the untagged data through a small amount of tagged data to produce pseudotags. Combined with true tags to pseudotags, the segmentation model is trained. In the process of segmentation, a small amount of tagged data is input into the segmented

network while a large amount of untagged data is input to carry out cyclic iterative training of the network.

In this study, the self-training semisupervised segmentation method is shown in Figure 1. In the figure,  $X$  represents the MRI image, and  $Y$  tags it. In self-training semisupervised learning, two datasets are used, which are shown in the following formula.

$$\text{Tagged data : } D_L = \{X_L, Y_L\}, \quad (1)$$

$$\text{Untagged dataset : } D_U = \{X_U\}. \quad (2)$$

Among them, the label in the tagged data set comes from the expert, hereinafter, referred to as the truth label. The untagged dataset contains only grayscale images. The goal of this training is to predict the untagged data set and get pseudotags by training the 3D scSE-UNet model. Finally, the pseudotag is extended to the untagged dataset.

The specific training steps can be subdivided into 5 steps: (1) using tagged  $D_L$  of partial data in MRNet dataset to train 3D scSE-UNet model. (2) The untagged dataset is randomly divided into several subdatasets. Input the subdataset into



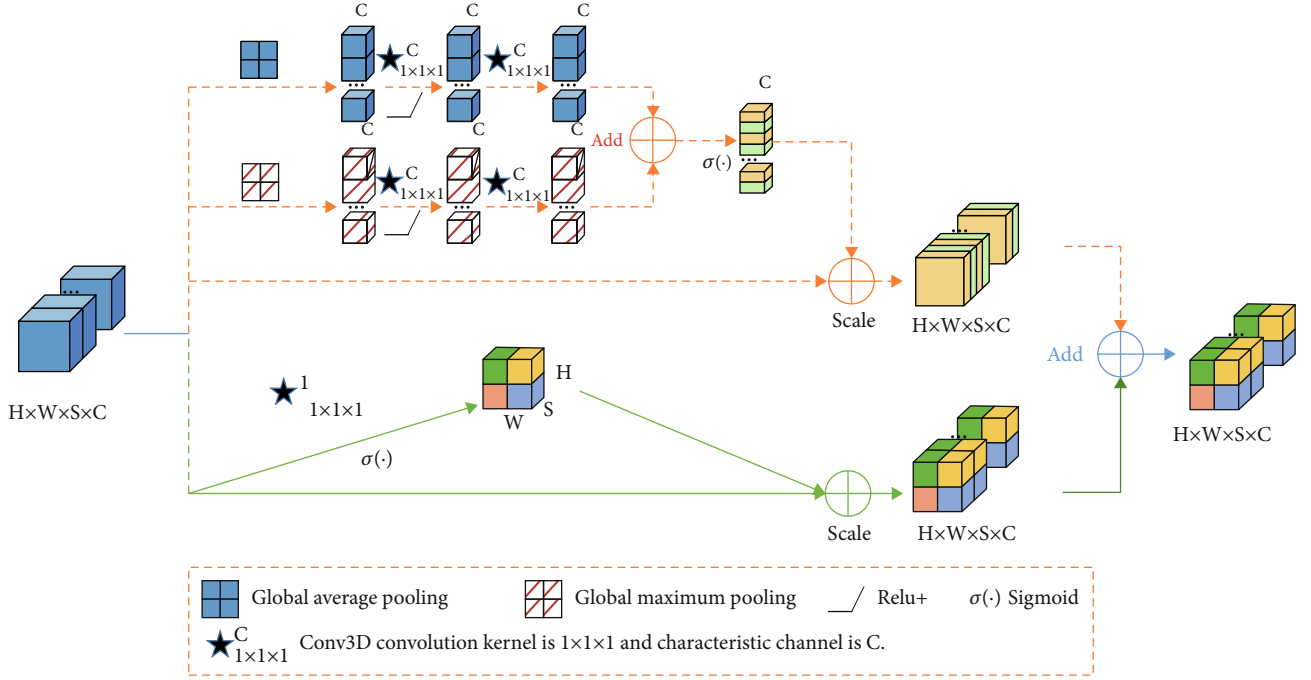


FIGURE 3: Schematic diagram of scSE-block+ structure of additional processing layer.

the 3DscSE-UNet model for prediction, and the prediction result of the response can be obtained. It is important to note that the subdataset contains tagged data from MRNet and untagged dataset from OAI. (3) Inputting the segmentation result into dense CRF for edge refinement to make it closer to the true value label. Finally, the refined pseudotags are added to equation (3) to build a new dataset, namely, equation (4). (4) Adding equation (5) to  $D_{trian}^{i+1}$  to build equation (6). Use  $X$  for the next round of training. (5) Inputting the updated training set into 3DscSE-UNet model for training again. After the training is completed, enter the next batch of untagged data and repeat the above steps until all untagged data produces false tags. In the process of training, because the pseudotag is extended to the training set, the model can continuously obtain new features and enhance the robustness of the model.

$$D_U^i = \{X_U^i\}, \quad (3)$$

$$D_U^i = \{X_U^i, Y_U^i\}, \quad (4)$$

$$D_U^i = \{X_U^i, Y_U^i\}, \quad (5)$$

$$D_{trian}^{i+1} = D_{trian}^i + D_U^i. \quad (6)$$

In the formula,  $i$  represents the  $i$  iteration,  $i+1$  represents the  $i+1$  iteration,  $U$  represents unlabeled data,  $D$  represents the data set, and  $trian$  represents the training set.

**2.1.1. DscSE-UNet Segmentation Network.** In the self-training learning segmentation method involved in this study, scSE-block+ is combined with 3D UNet. ScSE is an

attention module which integrates channel dimension and spatial dimension. Its main function is to enhance the meaningful features and suppress the useless features, so as to improve the accuracy. The two constitutes the 3DscSE-UNet segmentation network model. The schematic diagram of its structure is shown in Figure 2. The structure design of the network model is similar to that of 3DUNet, which adopts U-shaped structure. In the figure, the arrows represent the connection mode of different processing layers and the input direction of the feature map. The text above the arrow represents the number of channels of the feature map.

The difference between the new model and the 3D UNet model structure is that a scSE-block+ is added at the end of each hop connection layer in the 3D UNet decoding part, that is, the red square in the figure. The processing layer resets the weight of the feature channel of the input image to strengthen the effective features while weakening the useless features, so as to improve the ability of self-training semi-supervised learning network to learn effective features and improve the accuracy.

The decoding layer of the model performs the operations of generating feature maps and extracting features from MRI images of the input model by up/downsampling techniques, respectively. Among them, four lower sampling layers are designed in the coding layer, and each lower sampling layer is composed of two convolution layers. The convolution layer is responsible for extracting different levels of image features and activating them through the ReLU function. After two convolution layers, a maximum pool layer with a step size of 2 is connected to compress the features and reduce the dimension. In the decoding layer, each layer

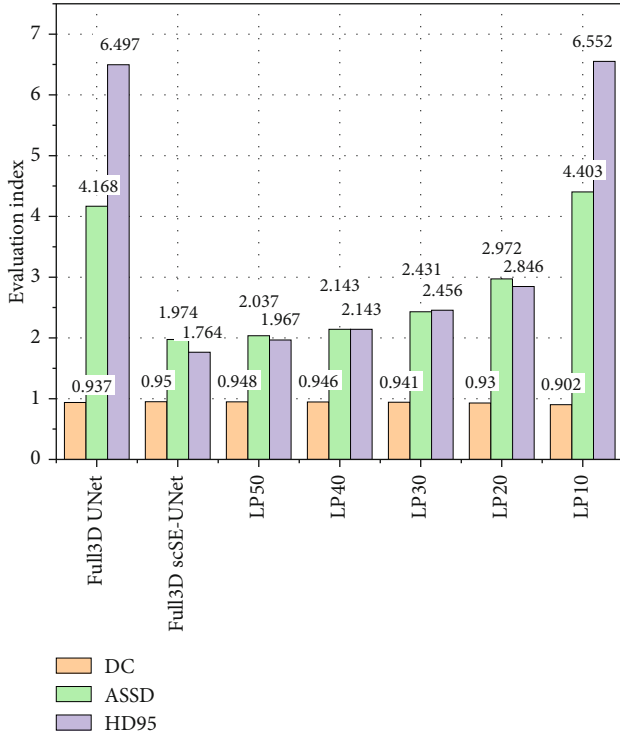


FIGURE 4: Performance comparison of prediction results of training sets with different ratios of labeled data (full 3D UNet refers to fully supervised 3D UNet model, full 3D scSE-UNet refers to fully supervised 3D scSE-UNet model, LP50 refers to semisupervised 3D scSE-UNet model and training set with 50% of tagged data, and the following labels are synonymous).

consists of an upper sampling layer with a step size of 2 and 2 convolution layers with a step size of  $3 \times 3 \times 3$ . After each convolutional layer, a ReLU function is set to activate it. Through the way of jump connection, the model combines the feature images obtained by the coding layer and the feature images obtained by the decoding layer with the same resolution. The combination of shallow and deep features to refine the image allows more texture information of the original image to spread in the high-resolution layer. Finally, the fused features are input into the scSE-block+ module to suppress the unimportant features and improve the accuracy of the segmentation results.

**2.2. scSE-Block+ Module.** In the proposed self-training semi-supervised learning model, a total of 4 scSE-block+ modules are used, and their structure is shown in Figure 3. The main reason for setting up four scSE-block+ modules is that the module can perform its function better in front of the upper sampling layer. This module can calculate the feature space domain and feature channel domain at the same time. By learning the importance of each feature, the feature graph is recalibrated. ScSE-block+ is the weight of channel SE module and spatial SE module.

As can be seen in Figure 3, we have improved the cSE-block, that is, the part of the figure marked as a dotted line. On the basis of the original cSE-block module, the model

adds a global maximum pool layer, which is marked as a red square in the figure. The newly added pooling layer is parallel to the original global average pooling layer of cSE-block. In the process of compressing spatial information, the selection of spatial feature tensor is different between the maximum pool layer (MPL) and the average pool layer (APL), which makes up for the problem that the original cSE-block module is not comprehensive.

The essence of MPL is to calculate the maximum value of the whole feature graph. Because the edge of the feature graph may produce the largest eigenvalue, MPL can retain the texture and edge features of the image to the maximum extent. The essence of APL is to calculate the average value of the whole feature graph and pay more attention to the downsampling of the whole feature. Therefore, APL can better retain the background of the feature map. MPL and APL are visible. In the task of extracting image edge information, MPL is more effective than APL. If the two are processed in parallel, the dual characteristics of edge and background can be retained. It plays a significant role in improving the performance of the model. Specifically, cSE-block evaluates the importance of channels by compressing spatial information. The module inputs the feature graph of  $H \times W \times S \times C$  into a MPL and an APL in parallel. Among them,  $H \times W \times S \times C$  represents the length, width, depth, and number of channels of the feature graph, respectively. MPL and APL compress the global spatial information in the lattice channel to a tensor value, respectively. The eigenvalue produced by this process is  $1 \times C$ . Then, these eigenvalues are convoluted in three dimensions. The convolution kernel size is  $1 \times 1 \times 1$  and the number of channels is  $C$ . Finally, the features obtained by convolution operation are activated by ReLU function, respectively. After the above convolution operation, two tensors of  $1 \times 1 \times 1 \times C$  with different values but with the same dimension are obtained. After the two tensors are added, the input sigmoid layer is normalized. By multiplying the normalized value with the original eigenmatrix, the unimportant information in the channel can be suppressed obviously, and the information in the important channel can be preserved losslessly. The important information mentioned here, in this study, refers to the information related to the purpose of model training.

In image segmentation, the spatial information of each pixel will provide more information. Therefore, the parallel sSE-block module is introduced into the research. This module can evaluate the importance of spatial location by compressing channel information. For the feature map of an input module, the module realizes space extrusion through convolution operation. Then, it is normalized by sigmoid. Finally, it is multiplied by the original characteristic tensor.

**2.3. Fully Connected Conditional Random Field.** In the self-training model, the unlabeled samples segmented by the algorithm are prone to missegmentation. After the missegmented samples are generated, they will still be extended to the training set to participate in the new round of training as the mark of the next round of samples. This causes the model to learn the wrong labels and make the errors accumulate, even magnify the errors.

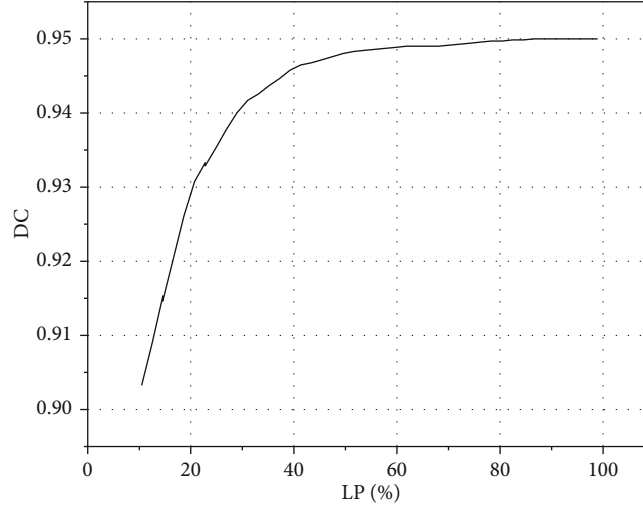


FIGURE 5: Dice score curve of 3D scSE-UNet with different proportions of labels.

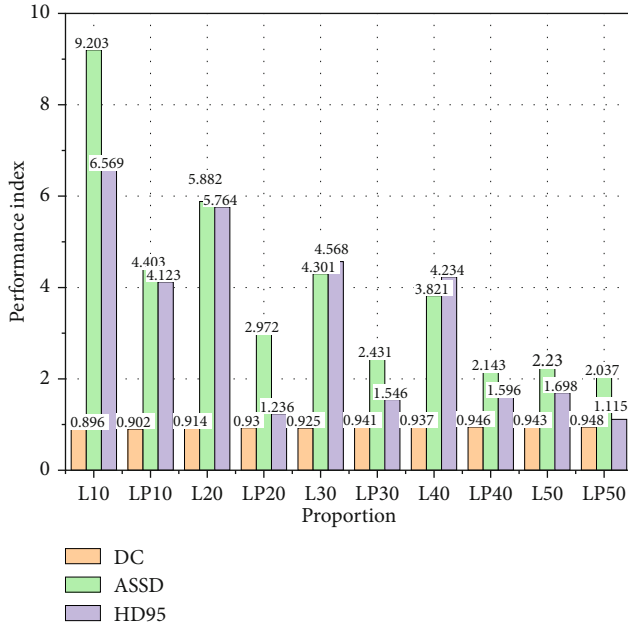


FIGURE 6: Performance comparison of fully supervised and semisupervised segmentation under different label ratios (L10 reference training set uses only 10 cases of tagged data, no untagged data, and the following labels are synonymous).

In order to solve the above problems, it is necessary to improve the accuracy of pseudotags to the maximum extent. The fully connected conditional random field can optimize the rough and uncertain tags in the pseudotags, correct the missegmented regions, improve the positioning characteristics of the network, and then get more accurate and detailed pseudotags. In this study, we introduce fully connected conditional random field (dense CRF) in the self-training process to refine the pseudotags obtained in each iteration of the self-training process.

The core of dense CRF algorithm is to calculate the relationship between pixels and pixels. The two pixels with high degree of similarity are assigned the same label, and the

probability of being segmented is low. However, when different labels are assigned between the two pixels with lower similarity, the probability of being segmented increases. The energy function of dense CRF algorithm is shown in the following formula:

$$E(x) = \sum_i \psi_u(f_i) + \sum_{i < j} \psi_p(f_i, f_j), \quad (7)$$

$$\psi_u(f_i) = -\log P(f_i). \quad (8)$$

$\psi_u(f_i)$  represents the unary potential energy, and it is mainly used to calculate the classification probability of pixel points, as shown in equation (8), and  $f_i$  represents the prediction result of pixel  $i$  by the segmentation model.  $P(f_i)$  represents the probability that the predicted result of pixel  $i$  is  $f$ .  $\psi_p(f_i, f_j)$  represents the binary potential energy between pixel  $i$  and the predicted result  $f_i, f_j$  on pixel  $j$ , which can describe the relationship between the two pixels

$$\psi_p(f_i, f_j) = \mu(f_i, f_j) \left[ \begin{array}{c} \omega_1 \exp \left( -\frac{\|x_i - x_j\|^2}{2\sigma_\alpha^2} - \frac{\|y_i - y_j\|^2}{2\sigma_\beta^2} \right) + \\ \omega_2 \exp \left( -\frac{\|x_i - x_j\|^2}{2\sigma_\gamma^2} \right) \end{array} \right]. \quad (9)$$

In the formula,  $\omega_1$  and  $\omega_2$  are linear combination weights;  $\mu$  is the label compatibility function, and  $\mu(f_i, f_j)$  is the label compatibility item, which restricts the condition of conduction between pixels, when  $f_i \neq f_j$ ; it has the value 0; the proximity and similarity between pixels are controlled by coefficients  $\sigma_\alpha$  and  $\sigma_\beta$ ;  $\sigma_\gamma = 1$ , which can remove small independent regions.  $X_i$  and  $X_j$  are the position information of pixel  $i$  and pixel  $j$ , respectively, and  $y_i$  and  $y_j$  are the intensity

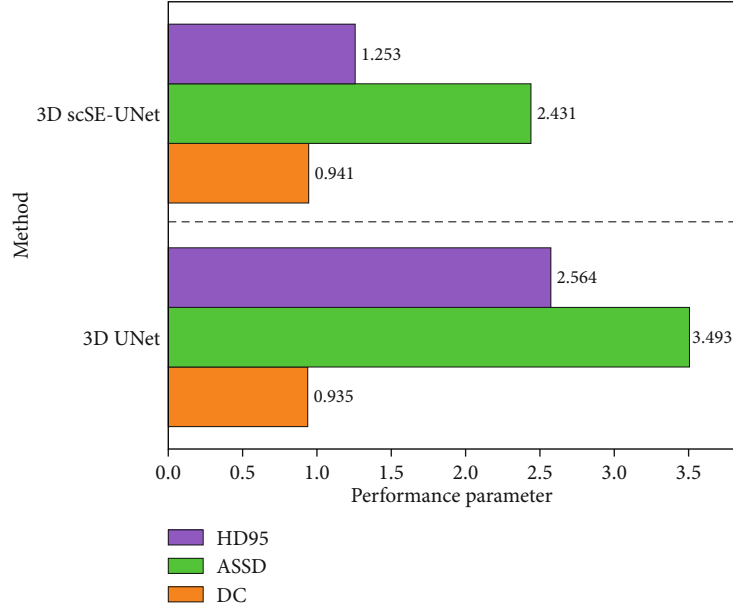


FIGURE 7: Performance comparison of 3D UNet and 3D scSE-UNet segmentation results.

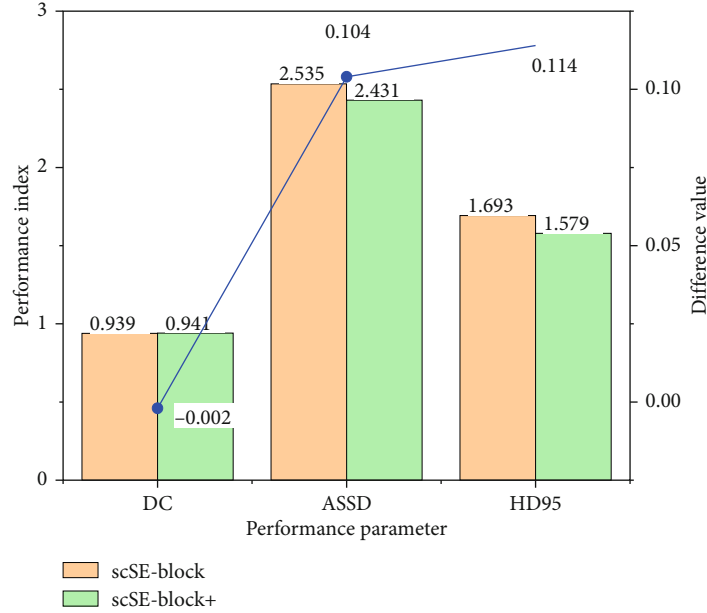


FIGURE 8: Comparison of segmentation results between scSE-block and scSE-block+.

values of pixel  $i$  and pixel  $j$ , respectively. The binary potential energy function will pay more attention to the pixels with similar position  $x$  and similar intensity  $y$  but with different marks  $f$ . The smaller the energy  $E(x)$  is, the more accurate the predicted category label  $x$  is.

In the process of segmenting MRI image by dense CRF module, the unary potential can represent the probability distribution map. Specifically, it is the result obtained by the input softmax function of the characteristic graph output of the model. The position information and gray information extracted from the original image are assigned to the binary potential energy. With the combination of unitary potential

energy and binary potential energy, the relationship between pixels can be comprehensively evaluated, and the results can be optimized. In this study, the model uses the iterative energy function  $E(x)$  to find the minimum solution of each image through five iterations to identify the most likely category of each pixel in the MRI image. Finally, each optimized prediction result is added to the self-training learning as a pseudotag.

### 3. Model Training and Evaluation Method

**3.1. Model Training Parameter Setting.** In the aspect of model parameter setting, the unlabeled data set is divided

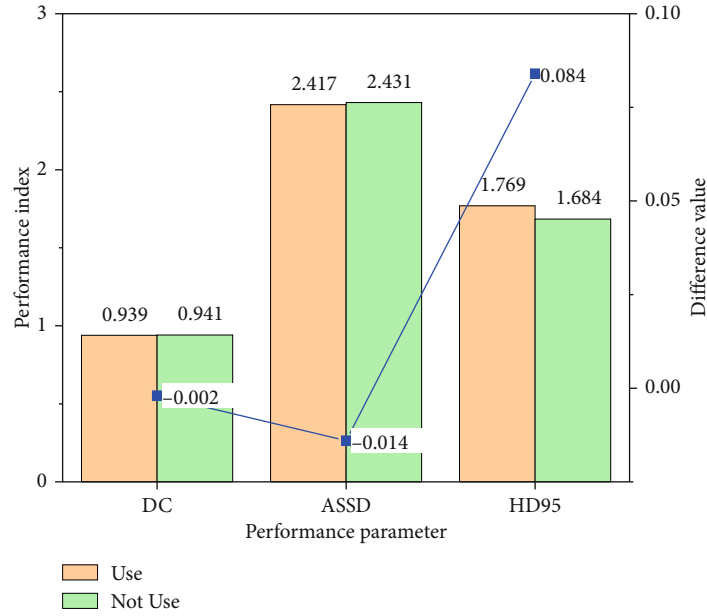


FIGURE 9: Performance comparison of segmentation results between using and unusing dense CRF.

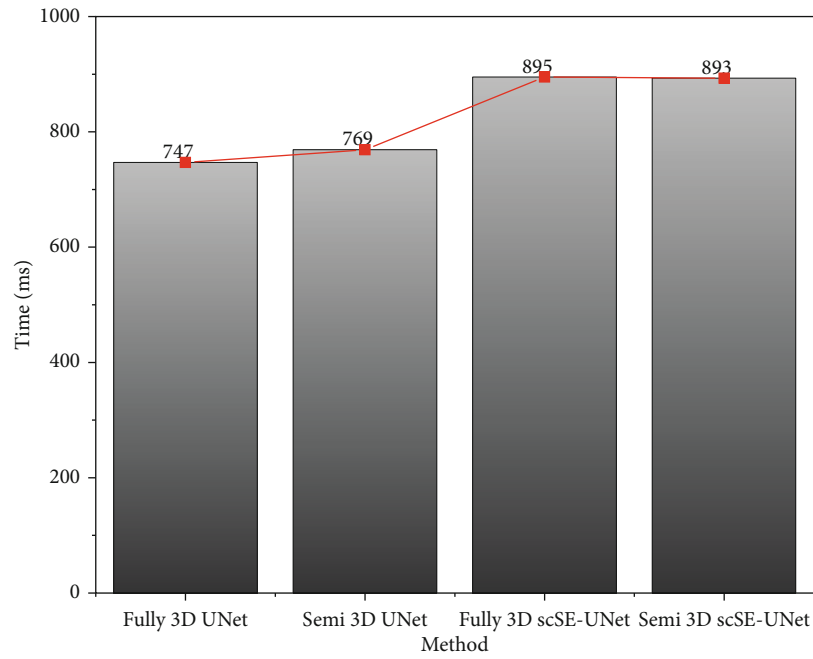


FIGURE 10: Average image processing time of different models.

into 5 subdata sets. Each data set is input into the model in turn for prediction, and the corresponding prediction results (segmentation results) are produced. In the process of training, the gradient descent algorithm built into Adam optimizer is used to find the minimum value of network parameter error function. Set the network learning rate of the model to 0.0001 epoch; set the training number (epoch) to 150; set the batchsize to 1; and stop training after reaching

the maximum number of cycles. The setting of training cycle, training times, and batch size is mainly based on the experience of previous studies. All data set processing, model training, verification, and evaluation are done on the same computer.

**3.2. Evaluation Index.** The quantitative indexes for evaluating the semisupervised 3DscSE-UNet model are average



symmetrical surface distance (ASSD), 95 percentile Hausdorff distance (HD95), and disc coefficient (DC), respectively. ASSD is used to calculate the average surface difference between segments. Hausdorff distance calculates the maximum point distance between segments. DC focuses on evaluating the degree of overlap between the two groups of segmentation results. Therefore, these three indicators are complementary and trinity.

ASSD calculates the overall average of the distance from  $\partial G$  to the point on  $\partial S$  and the distance from the boundary of  $S(\partial S)$  to the point on  $G(\partial G)$  boundary, as shown in the following formulas:

$$\text{ASSD}(G, S) = \frac{\sum_{g \in \partial G} \min_{s \in \partial S} \|s - g\| + \sum_{s \in \partial S} \min_{g \in \partial G} \|g - s\|}{|\partial G| + |\partial S|}, \quad (10)$$

$$\|\vec{a}\| = \sqrt{\sum_{i=1}^n (a_i)^2} = \sqrt{(a_1)^2 + (a_2)^2 + \dots + (a_n)^2}. \quad (11)$$

In the formulas,  $G$  is the segment of basic facts, and  $S$  is the segment to be predicted.  $|\cdot|$  represents the cardinality of the set. The smaller the calculation result of ASSD is, the better the split boundaries are consistent with each other.

The Hausdorff distance is calculated by the following formula:

$$\text{HD}(G, S) = \max(h(G, S), h(S, G)). \quad (12)$$

Among them, the calculation method of  $h(G, S)$  is

$$h(G, S) = \max_{g \in G} \min_{s \in S} \|g - s\|. \quad (13)$$

HD is the module for calculating the maximum segmentation error. Because HD is highly sensitive to outliers, and outliers in HD are replaced with 95% of the maximum in HD95.

The calculation model of DC is

$$\text{DC} = \frac{2|G \cap S|}{|G| + |S|}. \quad (14)$$

DC is a widely recognized index in the research of knee joint MRI image segmentation. Its scope is  $[0, 1]$ , where 0 means undivided, and 1 indicates that the segmentation is completely consistent.

## 4. Results and Analysis

**4.1. Results.** In order to avoid the chance of the training results of the model, five experiments were carried out based on the model proposed in the study, and the average value of the five experiments was taken as the result. The model involved in this study is trained on NVIDIA RTX3090 GPU, and the training time of one model is about 26 hours. Once the model is trained, the average segmentation time of each test image is less than 2 s.

In each experiment, 20 images from the tagged MRNet dataset and 26 images from the OAI dataset were randomly selected as the test set. The number of randomly selected images from both datasets is 1/5 of the labeled images in the dataset. 100 images were selected from MRNet data set, and 50, 40, 30, 20, and 10 MRI images and their truth tags were randomly selected as tagged data. The remaining 50, 60, 70, 80, and 90 MRI images were used as untagged data to form five training sets with different proportion of tagged data. The model obtained under five kinds of training conditions was used to predict the test set, and the segmentation results were compared with those obtained by 3D UNet fully supervised learning. Full-supervised and semisupervised methods show different performance in knee joint MRI image segmentation, as shown in Figure 4.

As can be seen from Figure 4, when the proportion of label data in knee joint segmentation reaches 30%, ASSD = 2.431, HD95 = 1.596 mm, and DC = 0.941. The prediction result of full supervision method is ASSD = 1.974, HD95 = 2.697 mm, and DC = 0.950. It can be seen that when the labeled data accounts for 30% of the training set, the evaluation index of semisupervised learning segmentation result is better than that of fully supervised learning method.

In order to compare the segmentation performance of the model under different percentages of labeled data in the training set, based on the study of the proposed model, the DC values under different conditions are obtained through training, and the DC changes under different ratios are drawn, as shown in Figure 5. As can be seen in the figure, the DC value increases with the increase of the proportion, and the growth rate decreases gradually. When the proportion is less than 40%, the DC value increases with the increase of the proportion, and the rising speed increases from 0.902 to 0.946. When the proportion is more than 40%, the growth rate slows down. Until the proportion reaches 100%, the fully supervised model DC = 0.950.

**4.2. Performance Comparison between Semisupervised Learning and Fully Supervised Learning.** Comparing the performance of the self-training semisupervised model with the full-supervised model, we can better verify the effectiveness of the self-trained semisupervised model. For this reason, the 3D scSE-UNet segmentation network model is used to train the semisupervised model and the full-supervised model, respectively, and the performance of the semisupervised model and the full-supervised model is compared. The comparison results are shown in Figure 6.

As can be seen in the figure, when the network model is segmented by 3DscSE-UNet at the same time, and the label data are the same, the performance of the semisupervised learning model is better than the fully supervised learning model. The main reason is that the semisupervised learning model can improve the segmentation performance through the effective use of unlabeled data, especially in the case of less tagged data. In the case of more tagged data, the segmentation accuracy of semisupervised learning model is not significantly higher than that of fully supervised learning, especially when the proportion of tagged data is 50%.

The main reason for this phenomenon is that when there are a lot of labeled data, the fully supervised learning model can segment the image more accurately through training, and there is little room for semisupervised learning to improve.

**4.3. Comparison of Segmented Networks with scSE-Block+.** In order to understand the improvement effect of the scSE-block+ module added in this study on the self-training semisupervised learning network model, the model is used to compare the segmentation ability of the model before and after adding. The training adds 30% of the training set with tagged data, and the result is shown in Figure 7. As can be seen in the figure, the ASSD value, HD95 value, and DC value of the model are significantly improved after the addition of scSE-block+ module. It can be seen that the scSE-block+ module can make more full use of the channel and spatial information in the feature graph.

Because the global maximum pool layer is added to the scSE-block module in the study, it is necessary to verify and compare the performance of the module before and after the addition and evaluate the impact of the improved module on the segmentation results. This verification uses a training set with a 30% proportion of labeled data, and the verification result is shown in Figure 8. As can be seen in the figure, the effect of image segmentation is better after adding the global maximum pool layer. In the process of feature extraction, using the global maximum pool layer can retain more abundant edge information and optimize the segmentation effect of the segmentation model on the target region.

**4.4. Dense CRF Performance Comparison.** In order to refine the segmentation results of pseudo tags, a dense CRF module is added to the research model. In order to analyze the thinning effect of pseudotags, the segmentation effects of pseudotags before and after thinning are compared, as shown in Figure 9. The training set used in the comparative study is 30% of the labeled data.

As can be seen in the figure, the performance index of the segmentation result optimized by dense CRF module has been improved compared with that before optimization. From the point of view of the segmentation results, the optimized segmentation results are closer to the truth label at the edge and even overlap with the truth label. For the part of the segmentation result with poor edge, the dense CRF module can modify it to make it closer to the truth label.

By calculating the relationship between a single pixel and all other pixels, the dense CRF module establishes a dependency on all pixel pairs in the image and then finely processes the probability map of the segmentation network prediction. Although the overall segmentation accuracy is not greatly improved by adding dense CRF module to the self-training semisupervised learning model, the edge thinning effect of the segmentation result is better.

**4.5. Comparison of Time Performance of Models.** In this study, the average image processing time of the four models

involved in the study was compared. The four models are fully supervised 3DUNet model, semisupervised 3DUNet model, fully supervised 3DscSE-UNet model, and semisupervised 3DscSE-UNet model. One hundred untagged MRI images were randomly selected from OAI datasets to test the average processing time of the four models, and the results are shown in Figure 10. As can be seen from the figure, due to the addition of the scSE-block+ module, the average processing time of the 3DscSE-UNet segmentation model is longer than that of the 3DUNet model, but there is little difference between the two models, which is only 150 ms. Under the same segmentation model, the effect of semisupervised learning or fully supervised learning on the average image processing time can be ignored.

The improved training model can segment MRI images more accurately and can basically achieve automatic segmentation of MRI images. This study has some significance to reduce the workload of medical workers and reduce the misdiagnosis of knee lesions.

## 5. Conclusion

In order to solve the problem that MRI image segmentation needs large labeling data and time-consuming experts in the field of knee joint depth learning, this study proposes a semisupervised learning segmentation model of 3DscSE-UNet knee joint MRI image based on scSE-block+, which reduces the dependence on labeled data in knee joint depth learning research and draws the following conclusions.

The fully connected conditional random field improves the detail processing ability of the semisupervised 3DscSE-UNet model and improves the accuracy of generating pseudotags in the segmented network. The addition of pseudotags to the semisupervised learning model significantly improves the segmentation performance of the model and achieves the purpose of making a large number of predictions from a small amount of label data. Through the verification of the model, it is found that the segmentation effect of the model is similar to that of the fully supervised learning model in the case of learning a small amount of labeled data.

By learning the relationship between different features, the semisupervised 3DscSE-UNet model can enhance the useful features while suppressing the irrelevant features and improve the accuracy of knee joint MRI image segmentation. The addition of scSE-block+ module in the semisupervised 3D scSE-UNet model increases the average image processing time of the model. No matter which supervision method is adopted, the image processing time of the 3D scSE-UNet model is 17.94% higher than that of the 3DUNet model, with a difference of 150 ms. However, under the same supervision mode, the segmentation performance of 3D scSE-UNet model is significantly better than that of 3D UNet model.

The main disadvantage of the self-training semisupervised learning model is that if the unlabeled data is mistakenly segmented in the initial segmentation, the problem will be magnified in the subsequent model training process. The main reason for the amplification is that the initial error

marker has the potential to act as a trusted label, allowing subsequent errors to accumulate. In this study, the dense CRF module is used to alleviate the problem. In the follow-up study, we will work to improve this problem.

## Data Availability

The experimental data used to support the findings of this study are available from the corresponding author upon request.

## Conflicts of Interest

The authors declared that they have no conflicts of interest regarding this work.

## References

- [1] J. A. Gustafson, S. Gorman, G. K. Fitzgerald, and S. Farrokhi, "Alterations in walking knee joint stiffness in individuals with knee osteoarthritis and self-reported knee instability," *Gait & Posture*, vol. 43, pp. 210–215, 2016.
- [2] N. Bien, P. Rajpurkar, R. L. Ball et al., "Deep-learning-assisted diagnosis for knee magnetic resonance imaging: development and retrospective validation of MRNet," *Plos Medicine*, vol. 15, no. 11, article 1002699, 2018.
- [3] L. Tognolo, M. C. Maccarone, S. De Trane, A. Scanu, S. Masiero, and P. Fiore, "Therapeutic exercise and conservative injection treatment for early knee osteoarthritis in athletes: a scoping review," *Medicina*, vol. 58, no. 1, article 69, 2022.
- [4] Y. C. Chen, Y. L. Tian, and M. Y. He, "Monocular human pose estimation: a survey of deep learning-based methods," *Computer Vision and Image Understanding*, vol. 192, article 102897, 2020.
- [5] X. Dong, Y. Lei, T. H. Wang et al., "Automatic multiorgan segmentation in thorax CT images using U-net-GAN," *Medical Physics*, vol. 46, no. 5, pp. 2157–2168, 2019.
- [6] A. Garcia-Garcia, S. Orts-Escolano, S. Oprea, V. Villena-Martinez, P. Martinez-Gonzalez, and J. Garcia-Rodriguez, "A survey on deep learning techniques for image and video semantic segmentation," *Applied Soft Computing*, vol. 70, pp. 41–65, 2018.
- [7] K. Hammernik, T. Klatzer, E. Kobler et al., "Learning a variational network for reconstruction of accelerated MRI data," *Magnetic Resonance in Medicine*, vol. 79, no. 6, pp. 3055–3071, 2018.
- [8] Z. L. Hu, J. S. Tang, Z. M. Wang, K. Zhang, L. Zhang, and Q. L. Sun, "Deep learning for image-based cancer detection and diagnosis – a survey," *Pattern Recognition*, vol. 83, pp. 134–149, 2018.
- [9] X. W. Wu, D. Sahoo, and S. C. H. Hoi, "Recent advances in deep learning for object detection," *Neurocomputing*, vol. 396, pp. 39–64, 2020.
- [10] T. Jo, K. Nho, and A. J. Saykin, "Deep learning in Alzheimer's disease: diagnostic classification and prognostic prediction using neuroimaging data," *Frontiers in Aging Neuroscience*, vol. 11, article 220, 2019.
- [11] J. N. Katz, K. R. Arant, and R. F. Loeser, "Diagnosis and treatment of hip and knee osteoarthritis," *Jama-journal of the American Medical Association*, vol. 325, no. 6, pp. 568–578, 2021.
- [12] S. L. Kolasinski, T. Neogi, M. C. Hochberg et al., "2019 American College of Rheumatology/Arthritis Foundation guideline for the management of osteoarthritis of the hand, hip, and knee," *Arthritis & Rheumatology*, vol. 72, no. 2, pp. 220–233, 2020.
- [13] Y. X. Li and L. L. Shen, "Skin lesion analysis towards melanoma detection using deep learning network," *Sensors*, vol. 18, no. 2, article 556, 2018.
- [14] A. Premkumar, D. A. Kolin, K. X. Farley et al., "Projected economic burden of periprosthetic joint infection of the hip and knee in the United States," *Journal of Arthroplasty*, vol. 36, no. 5, pp. 1484–1489.e3, 2021.
- [15] F. Liu, Z. Y. Zhou, H. Jang, A. Samsonov, G. Y. Zhao, and R. Kijowski, "Deep convolutional neural network and 3D deformable approach for tissue segmentation in musculoskeletal magnetic resonance imaging," *Magnetic Resonance in Medicine*, vol. 79, no. 4, pp. 2379–2391, 2018.
- [16] J. Liu and X. W. Wang, "Plant diseases and pests detection based on deep learning: a review[J]," *Plant Methods*, vol. 17, no. 1, pp. 1–18, 2021.
- [17] Z. Li, S. Ren, R. Zhou et al., "Deep learning-based MRI image features for diagnosis of anterior cruciate ligament injury," *Journal of Healthcare Engineering*, vol. 2021, article 4076175, 9 pages, 2021.
- [18] A. S. Chaudhari, M. J. Grissom, Z. Fang et al., "Diagnostic accuracy of quantitative multicontrast 5-minute knee MRI using prospective artificial intelligence image quality enhancement," *American Journal of Roentgenology*, vol. 216, no. 6, pp. 1614–1624, 2021.
- [19] M. R. Yang, C. Colak, K. K. Chundru et al., "Automated knee cartilage segmentation for heterogeneous clinical MRI using generative adversarial networks with transfer learning," *Quantitative Imaging in Medicine and Surgery*, vol. 12, no. 5, pp. 2620–2633, 2022.
- [20] I. Iqbal, G. Shahzad, N. Rafiq, G. Mustafa, and J. W. Ma, "Deep learning-based automated detection of human knee joint's synovial fluid from magnetic resonance images with transfer learning," *IET Image Processing*, vol. 14, no. 10, pp. 1990–1998, 2020.

## Research Article

# Effect of Multichannel Convolutional Neural Network-Based Model on the Repair and Aesthetic Effect of Eye Plastic Surgery Patients

YixinQu,<sup>1</sup> BingyingLin,<sup>1</sup> ShuilingLi,<sup>1</sup> XianchaiLin,<sup>1</sup> ZhenMao,<sup>1</sup> XingyiLi,<sup>1</sup> RongxinChen<sup>ID</sup>,<sup>1</sup> and DanpingHuang<sup>ID</sup><sup>2</sup>

<sup>1</sup>Zhongshan Ophthalmic Center, Sun Yat-Sen University, Department of Oculoplastic, Guangzhou, Guangdong 510060, China

<sup>2</sup>State Key Laboratory of Ophthalmology, Zhongshan Ophthalmic Center, Sun Yat-Sen University, Guangzhou, Guangdong 510060, China

Correspondence should be addressed to DanpingHuang; [hdanp@mail.sysu.edu.cn](mailto:hdanp@mail.sysu.edu.cn)

Received 31 May 2022; Revised 1 August 2022; Accepted 8 August 2022; Published 1 September 2022

Academic Editor: Hangjun Che

Copyright © 2022 YixinQu et al. This is an open access article distributed under the Creative Commons Attribution License, which permits unrestricted use, distribution, and reproduction in any medium, provided the original work is properly cited.

**Objective.** This study is aimed at exploring the impact of eye model based on multichannel convolutional neural network (CNN) on eye plastic surgery and aesthetic effect, thus formulating methods to improve the effect of eye plastic surgery. **Methods.** A total of 64 patients who underwent pouch plastic surgery from January 2020 to March 2021 were selected as the research objects and were divided into observation group and control group by random number table method. The subjects in the observation group were evaluated by multichannel CNN-based eye model and doctors' experience, while those in the control group were evaluated by doctors' experience only, with 32 cases in both groups. Blepharoplasty, lower eyelid skin wrinkles, skin luster, and aesthetic scores were compared between the two groups. **Results.** The similarity between the multichannel CNN model detected shape and the actual eye shape (98.78%) was considerably higher than that of the CNN model detected shape (78.65%) ( $P < 0.05$ ). After treatment, the indexes of pouch degree, lower eyelid skin wrinkle, eyelid lacrimal sulcus, skin gloss, and aesthetic score in the observation group were better than those in the control group ( $P < 0.05$ ). The incidence of complications in the observation group (13%) was considerably lower than that in the control group (28%) ( $P < 0.05$ ). **Conclusion.** The eye model based on the multichannel CNN model was helpful to improve the surgical repair and aesthetic effect of patients and can improve the occurrence of postoperative complications.

## 1. Introduction

With the gradual improvement of people's living standards, people's focus has gradually shifted from the original problem of food and clothing to the external image, so that cosmetic surgery has become a demand of people nowadays, especially when there are external defects in the human body [1]. Eyes, as a window to convey people's feelings, have a great influence on the overall image of the individual. Having an appropriate eye shape is very meaningful to the personal appearance and temperament. At present, eye plastic surgery is very common in medical cosmetic surgery, including double eyelid plastic surgery [2], canthus opening surgery [3], ptosis correction [4], and pouch surgery [5].

Among them, pouch surgery, as one of the surgeries for eye rejuvenation, is very common in the cosmetic industry, and the surgical method is based on the principle of fat removal and skin removal [6]. The formation of bags under the eyes is related to the skin of the eyelid and the connective tissue under the skin. Skin relaxation, atrophy, or edema of the connective tissue will all cause bags under the eyes, resulting in aging around the eyes and affecting people's external image [7]. Therefore, many beauty lovers pay attention to eye plastic surgery. Pouch surgery has substantial effect in the early stage, but there are many problems in the later stage, which is closely related to the formulation of the surgical plan, and the design of the surgical method needs to be determined according to the patient's own eye



structure. To better understand the tissue structure of patients' eyes, we will use stereoscopic imaging technology to establish a three-dimensional (3D) model for evaluation in this study.

With the rapid development of artificial intelligence technology, people explore more and more deeply in the 3D world, and 3D technology today is more and more widely used. At present, 3D technology has been applied in the film industry [8], medical image processing [9], high-precision map [10], and intelligent detection [11]. Image feature extraction is relatively important in the process of 3D image establishment, and the convolutional neural network (CNN) algorithm is one of the common methods of 2D image recognition and information extraction at the present stage [12]. Studies showed that the application of CNN in deep learning is very mature and has been widely used in image feature extraction, classification, and other fields with excellent performance [13]. However, when there is a large amount of data to be processed, there will be a large error in the image processing of CNN. Therefore, someone proposed the three-channel CNN algorithm [14], that is, to process three sets of data at one time. However, there is a lack of research on the application of multichannel CNN model in ocular plastic surgery. Based on this, a multichannel CNN algorithm was established to analyze the three-dimensional model effect of reconstructing the eyelid tissue structure and used to assist the formulation of pouch surgery plan.

A three-dimensional model of eyelid tissue was established based on multichannel CNN algorithm to assist ophthalmologists to develop a reasonable pouch surgery plan, and its auxiliary effect was evaluated by surgical results, aesthetic scores, and complications. It is aimed at obtaining methods to improve the effect of ocular plastic surgery and reduce the occurrence of postoperative adverse reactions in patients, so that patients are more satisfied.

## 2. Methods

**2.1. The Research Object.** 64 patients who underwent blepharoplasty in XXX Hospital from January 2019 to March 2022 were studied. Among them, there were 26 male patients and 38 female patients, aged 28~60 years old, with mean age of  $44.02 \pm 6.27$  years. 64 patients were randomly divided into observation group and control group. The patients in the observation group were evaluated by the ocular model based on multichannel CNN and the experience of the doctor to develop the surgical method, while the patients in the control group were evaluated only according to the experience of the doctor to develop the surgical method. The patients in a group were 32 cases. The auxiliary effect of multichannel CNN ocular model was evaluated by comparing the surgical effect and aesthetic score between the two groups. This study had been approved by the relevant medical ethics committee.

Inclusion criteria are as follows: (I) All patients had obvious pouch due to loose and bloated skin of lower eyelid. (II) All patients voluntarily underwent pouch surgery. (III) All patients had normal mental cognition and clear consciousness. (IV) All patients can cooperate with the normal operation. (V) All patients signed informed consent.

Exclusion criteria are as follows: (I) patients with visual impairment; (II) patients with dry eye; (III) patients with other heart diseases; (IV) patients with a history of ocular and periocular tissue surgery; (V) patients who took drugs affecting the experiment before surgery; and (VI) women in pregnancy or lactation.

**2.2. Feature Extraction Based on CNN Algorithm.** The feature extraction of CNN algorithm is carried out in the volume base, and feature extraction is carried out by convolution kernel. When the size of the image is large, it is necessary to slice the image, and the specific processing is as follows:

It is assumed that the size of the image is  $A \times B$ , and the size of the image block is set to  $a \times b$ ; then, the number of image blocks  $N$  is

$$N = \frac{A \times B}{a \times b}. \quad (1)$$

When  $N$  is not an integer,  $N$  is set to an integer by adding 0 to the image matrix. Then, the image is normalized to make the pixel values of image blocks more similar. The processing functions are as follows:

$$\hat{O}(x, y) = \frac{[(O - J)(x, y)]}{[\sigma(x, y) + z]}, \quad (2)$$

$$J(x, y) = \frac{\left[ \sum_{\Theta \in (k, l)} J(x + k, y + l) \right]}{[a' \times b']}, \quad (3)$$

$$\sigma(x, y) = \frac{\left[ \sqrt{\sum_{\Theta \in (k, l)} ((x + k, y + l) - J(x, y))} \right]}{[a' \times b']}. \quad (4)$$

In the above equations,  $(x, y)$  represents the pixel point of the image,  $O$  represents the pixel value at  $(x, y)$ ,  $J$  represents the mean value of the area block,  $\sigma$  represents the standard deviation of the area block,  $z$  represents any extremely small positive number (avoiding  $[\sigma(x, y) + z] = 0$ ),  $\Theta$  represents the local area of the calculation of  $J$  and  $\sigma$ ,  $(k, l)$  represents the area block size,  $(a', b')$  represents the length and width of  $\Theta$ , and  $\hat{O}$  represents the pixel value of  $(x, y)$  after normalization. At this point, the mean value of the original image is 0, and the variance is 1.

After that, feature extraction is carried out on the image. The convolution layer of CNN is composed of many feature graphs, which are obtained by convolution kernel and upper input image through convolution operation. All the elements in the convolution kernel belong to the weight parameters, and the corresponding pixel value of the image needs to be multiplied and added by the convolution kernel and the pixel value of the input image and then obtained through the calculation of the activation function. Then, the matrix  $W_v^m$  calculation expression corresponding to the first feature graph of the first layer is as follows:



$$W_v^m = f\left(\int_{i \in S_v} W_v^{m-1} \cdot l_{vi}^m + d_v^m\right). \quad (5)$$

In the above equation,  $f(\int_{i \in S_v} W_v^{m-1} \cdot l_{vi}^m + d_v^m)$  represents the activation function,  $S_v$  represents the combination of feature graphs,  $W_v^{m-1}$  represents the feature graph matrix of the upper layer,  $\cdot$  represents the convolution processing,  $l_{vi}^m$  represents the weight, and  $d_v^m$  represents the bias.

**2.3. CNN 3D Reconstruction Based on Multichannel.** To reconstruct the image more carefully, the image is divided into blocks to the minimum range, which may lead to a large increase in image data. Therefore, it is necessary to suggest multichannel image processing to improve the processing efficiency and increase the similarity of image reconstruction.

The multichannel system is used to extract features from images. The multichannel CNN model is improved by the three-channel CNN model. The obtained feature images are combined to form a 3D image. Before reconstruction, it is necessary to estimate the probability of 3D images obtained from 2D feature images, mainly through threshold calculation. After input of image information, binarization threshold is obtained. Then, this value is applied to the probability model, and every pixel value is binarized to obtain the final 3D model. The specific process is as follows:

$$T = t(I), \quad (6)$$

$$P = p(I), \quad (7)$$

$$U = \int_{1, P_{i,j,k} \leq T}^{0, P_{i,j,k} > T} P_{i,j,k} \in P. \quad (8)$$

In the above equations,  $I$  represents the characteristic image of input,  $t$  is the threshold calculation,  $T$  is the output threshold,  $P$  is the probability model,  $p$  is the basic network,  $P_{i,j,k}$  is the model probability of threshold calculation  $P$ , and  $(i, j, k)$  is the spatial coordinates of the model.

**2.4. Evaluation Methods.** The established three-dimensional model of the eye overlapped with the actual ocular structure of the patient to obtain similarity, and its reconstruction effect was evaluated by similarity and model reconstruction efficiency (the required time). The specific algorithm for similarity is as follows.

$$S = \left[ \frac{V_{\text{coi}}}{V_{\text{total}}} \right] \times 100\%. \quad (9)$$

In the above equation, similarity is represented by  $S$ , overlapping volume is represented by  $V_{\text{coi}}$ , and total volume is represented by  $V_{\text{total}}$ .

**2.5. Observation Indicators.** The effect of surgical treatment was evaluated by observing and comparing the changes of pouch degree, skin wrinkle depth of lower eyelid, lacrimal groove depth of eyelid, and skin gloss before and after treatment in the two groups. The assessment method of pouch

degree is shown in Table 1, which was graded into mild 1 point, moderate 2 points, and severe 3 points. Fitzpatrick wrinkle grading method [15] was used to score skin wrinkles of lower eyelid, with scores ranging from 1 to 9. The lacrimal sulcus was evaluated by the degree of lacrimal sulcus filling [16], and the score was 0 ~ 10. Skin glossiness was detected by gloss meter glossiness meter [17], and the mean value was taken twice. The lower the Fitzpatrick wrinkle grading score, the higher the lacrimal filling degree and skin gloss, the better the treatment effect.

Aesthetic score [18] was used for aesthetic analysis of the eyes of patients in the two groups. Skin color, eye bag shape, eye contour, eye bag volume, and overall aesthetic feeling were analyzed. The score of each item was rated as 0, 1, or 2, and the total score was 10. The higher the score, the better the aesthetic effect.

The incidence of complications during treatment in the two groups was recorded and analyzed.

**2.6. Statistical Methods.** The SPSS 22.0 software was used for statistical analysis of the data in this study. The measurement data was expressed as mean  $\pm$  standard deviation ( $\bar{x} \pm s$ ), and the counting data was expressed as percentage (%).  $T$ -test was used to analyze eye related indicators and aesthetic scores, and  $\chi^2$  test was used to analyze clinical efficacy and incidence of complications. 0.05 was taken as the test level, and  $P < 0.05$  indicated statistically significant difference.

### 3. Results

**3.1. Comparison of Reconstruction Effects.** In this study, the multichannel CNN reconstruction algorithm was compared with the traditional CNN algorithm, and the reconstruction efficiency and similarity of the two stereo graphics were compared. The results showed that the reconstruction efficiency of the multichannel CNN algorithm was 3.41 s, which was basically consistent with the traditional CNN algorithm's reconstruction efficiency of 4.02 s, and there was no substantial statistical difference ( $P > 0.05$ ). The similarity between the multichannel CNN model and the actual eye shape was 98.78%, which was considerably higher than that of the traditional CNN model (78.65%), and there was substantial statistical difference ( $P < 0.05$ ) (Figures 1 and 2).

**3.2. Comparison of General Clinical Data.** Through the statistics of the general data (gender, age, weight, education, etc.) of the two groups, in the control group, there were 14 male patients (45%) and 18 female patients (55%), with an average age of  $42.21 \pm 5.11$  years, an average body mass index (BMI) of  $28.02 \pm 1.43 \text{ kg/m}^2$ , and 4 patients (12.5%) with below junior high school diploma, 5 patients (15%) with junior high school ~ senior high school diploma, 16 patients (50%) with senior high school ~ specialist/undergraduate diploma, and 7 patients (22.5%) with above specialist/undergraduate diploma. In the observation group, there were 13 male patients (40%) and 19 female patients (60%), with an average age of  $45.45 \pm 3.66$  years, an average BMI of  $28.77 \pm 1.31 \text{ kg/m}^2$ , 3 patients (10%) with below junior high school diploma, 6 patients (17.5%) with junior high

TABLE 1: Evaluation criteria of pouch degree.

Degree	Manifestations	Score
Mild	The adipose bulge was located in the medial orbit without skin laxity	1
Moderate	Fat swelling was found in the medial and medial orbitals, with slight fine lines and basically no skin laxity	2
Severe	In, inside, and lateral adipose all bulge, and wrinkle and skin flabby phenomenon appears	3

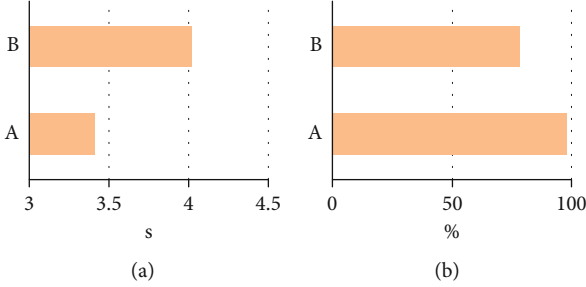


FIGURE 1: Reconstruction efficiency and similarity comparison. A, multichannel CNN algorithm; B, CNN algorithm. (a) Reconstruction efficiency; (b) similarity. Note: “\*” indicates that eye models based on multichannel CNN are more similar compared to traditional CNN models ( $P < 0.05$ ).

school ~ senior high school diploma, 17 patients (52.5%) with senior high school ~ specialist/undergraduate diploma, and 6 patients (20%) with above junior high school diploma. There were no statistically substantial differences in gender distribution, mean age, mean BMI, and educational background distribution between the two groups ( $P > 0.05$ ) (Figure 3).

**3.3. Comparison of Surgical Results.** Figure 4 shows the statistical results of pouch degree, skin wrinkles of lower eyelid, eyelid lacrimal sulcus, and skin gloss of the two groups before and after surgical treatment. Before treatment, the ocular scores in the control group were  $2.89 \pm 0.03$  points,  $6.39 \pm 0.43$  points, and  $3.84 \pm 0.21$  points, respectively, and the scores in the observation group were  $2.83 \pm 0.04$  points,  $6.27 \pm 0.42$  points, and  $3.76 \pm 0.23$  points, respectively. After comparison, there were no statistically substantial differences in pouch degree, lower eyelid skin wrinkle, eyelid lacrimal sulcus, and skin gloss score between the two groups before treatment ( $P > 0.05$ ). After treatment, the results of ocular scores in the control group were  $1.83 \pm 0.18$  points,  $4.85 \pm 0.23$  points, and  $5.76 \pm 0.75$  points, respectively, and the results of ocular scores in the observation group were  $1.01 \pm 0.08$  points,  $3.03 \pm 0.14$  points, and  $7.12 \pm 0.72$  points, respectively. After comparison, the degree of pouch under the eyes, skin wrinkles of lower eyelid, eyelid lacrimal sulcus, and skin gloss scores of patients in the two groups were improved after treatment, and the improvement degree of various scores in the observation group was considerably better than that in the control group ( $P < 0.05$ ).

**3.4. Aesthetic Score Results.** Before treatment, the aesthetic score was  $4.33 \pm 1.17$  points in the control group and  $4.34 \pm 1.15$  points in the observation group. There was no significant difference in the aesthetic score between the two

groups before treatment ( $P > 0.05$ ). The aesthetic score was  $7.09 \pm 1.33$  points in the control group and  $8.68 \pm 1.05$  points in the observation group. After treatment, the ocular aesthetic score of the two groups was higher than that before treatment, and the aesthetic score of the observation group after treatment was higher than that of the control group ( $P < 0.05$ ) (Figure 5).

**3.5. Comparison of Complication Rates.** Through observation, the two groups of patients had postoperative complications such as lower eyelid eversion, lower eyelid retraction, and hematoma. The control group had 3 cases of lower eyelid eversion, 3 cases of lower eyelid retraction, and 3 cases of hematoma; the observation group had 1 case of lower eyelid eversion, 1 case of lower eyelid retraction, and 2 cases of hematoma; after analysis, the incidence rate of complications in the observation group (13%) was significantly lower than that in the control group (28%) ( $P < 0.05$ ) (Figure 6).

## 4. Discussion

Due to the increasingly extensive pursuit of beauty today, it has greatly promoted the development of cosmetic and plastic surgery industry. Although successful cosmetic surgery has helped many people regain confidence in their appearance, there are still many cases of plastic surgery failure in clinical practice, which is more related to unreasonable surgical plans [18, 19]. To improve the effect of plastic surgery, CNN algorithm based on multichannel was adopted to establish 3D images of patients' eye structures to assist patients in making surgical plans.

The results showed that the efficiency of the multichannel CNN reconstruction algorithm (3.41 s) was basically consistent with that of the traditional CNN algorithm (4.02 s) ( $P > 0.05$ ), while the reconstructed similarity (98.78%) was considerably higher than that of the traditional CNN algorithm (78.65%) ( $P < 0.05$ ). According to the results, under the condition of the same reconstruction efficiency, the reconstruction algorithm based on multichannel CNN had a better effect, indicating that the multichannel system can improve the algorithm processing efficiency. This was consistent with the research results of Mughal and Ross [20]. Hu et al. [21] also mentioned in their study that multichannel CNN has good performance in processing multiple data parameters.

Abundant studies have shown that different pouch surgery methods have different therapeutic effects [22]. Therefore, it is very important to select reasonable and effective surgical methods to improve the aesthetic degree of patients' eyes. The degree of pouch, skin wrinkles of lower eyelid, skin gloss, and aesthetic score were compared to analyze the

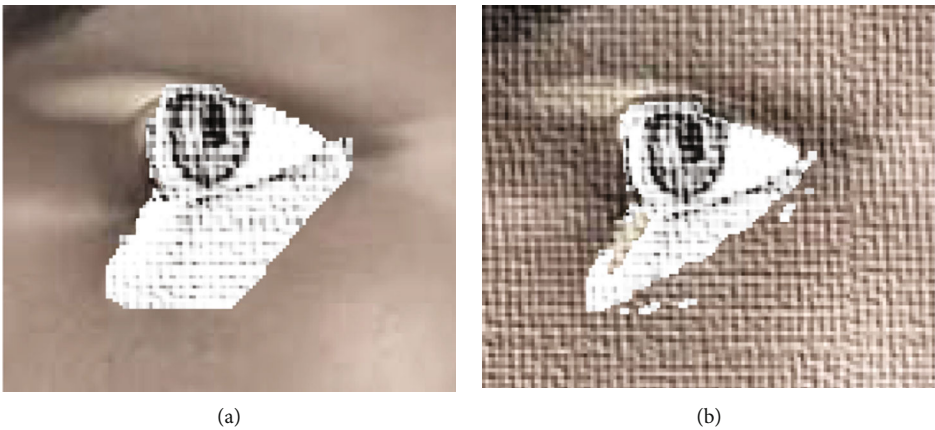


FIGURE 2: Overlap area correlation: (a) multichannel CNN algorithm; (b) CNN algorithm.

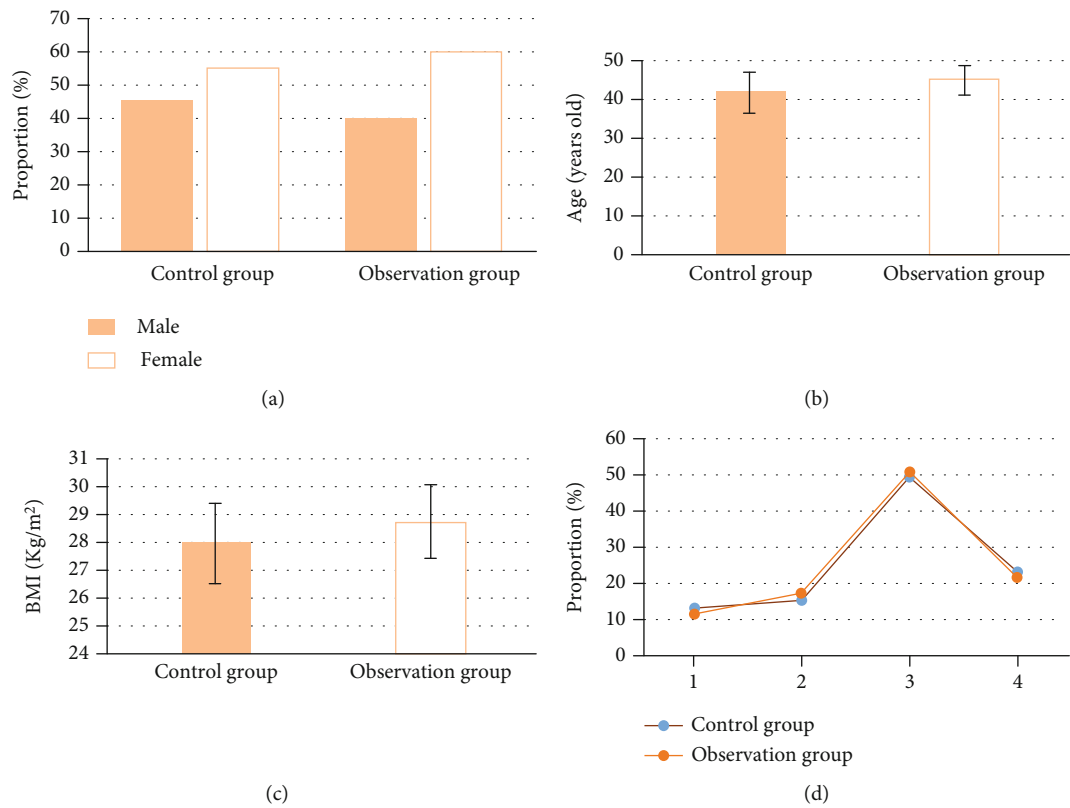


FIGURE 3: Comparison of general data: (a) gender; (b) age; (c) BMI; (d) educational attainment. 1, junior high school or below; 2, junior to senior high school; 3, high school ~ junior college/bachelor degree; 4, college/bachelor degree or above.

effect of surgical treatment, and the auxiliary effect of multi-channel CNN eye model in pouch plastic surgery was evaluated. The results showed that, after treatment, the degree of pouch under the eyes, skin wrinkles of lower eyelid, skin gloss, and aesthetic score in the two groups were improved compared with before treatment, and the improvement degree of scores in observation group was considerably better than that in the control group ( $P < 0.05$ ). It was suggested that the selection of surgical method and the formulation of surgical plan with the help of eye model can improve the

effect of plastic surgery. Relevant studies have shown that to improve the symptoms of eye bags, canthus wrinkles, the rational release of orbital septal fat is relatively important [23, 24]. Different surgical methods have different therapeutic targets, such as orbital septal release surgery for the release of fat in the lower eyelid [25] and lateral canthus anchoring technology for the improvement of fullness and elasticity of the lower eyelid [26]. Therefore, the establishment of a model and the simulation of the surgical process are conducive to the improvement of the pertinence of the

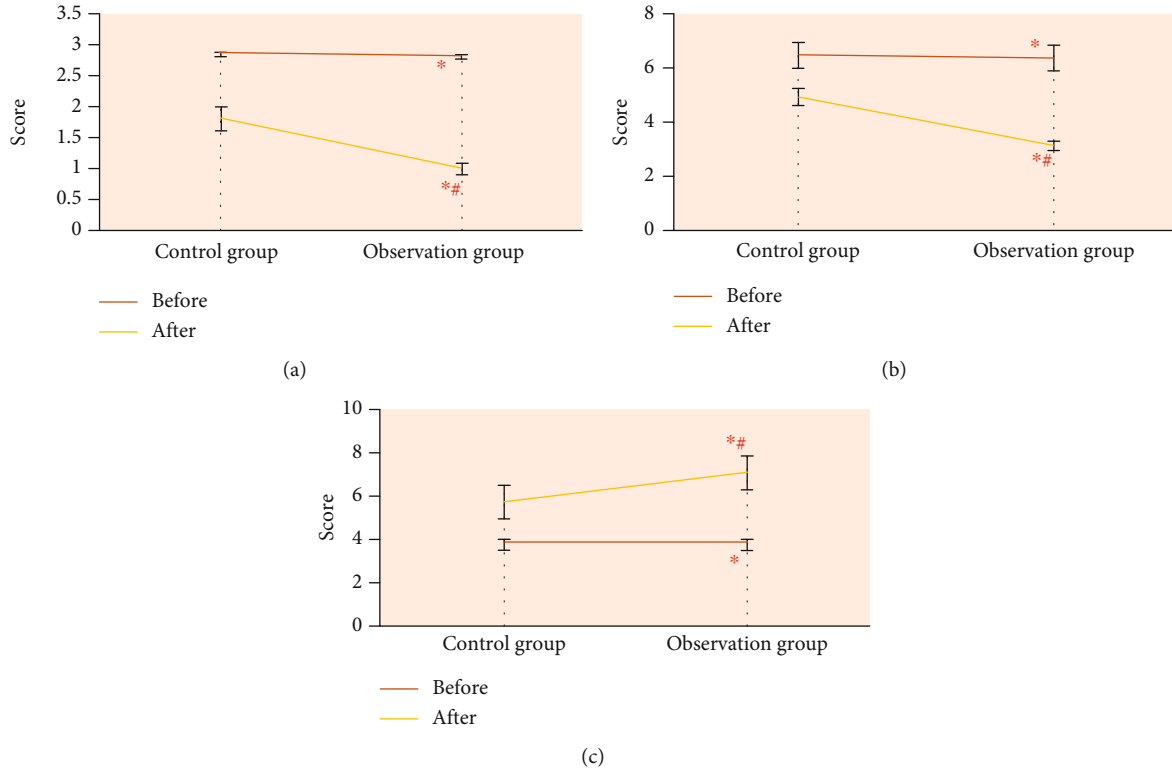


FIGURE 4: Comparison of scores of treatment indicators: (a) degree of eye bags; (b) skin wrinkles of lower eyelid; (c) skin gloss. Note: “\*” indicates that the pouch degree, lower eyelid skin wrinkles, and skin gloss score of patients in the two groups were significantly improved compared with those before operation ( $P < 0.05$ ); “#” indicates that the pouch degree, lower eyelid skin wrinkles, and skin gloss score of patients in the observation group were better improved after treatment compared with those in the control group ( $P < 0.05$ ).

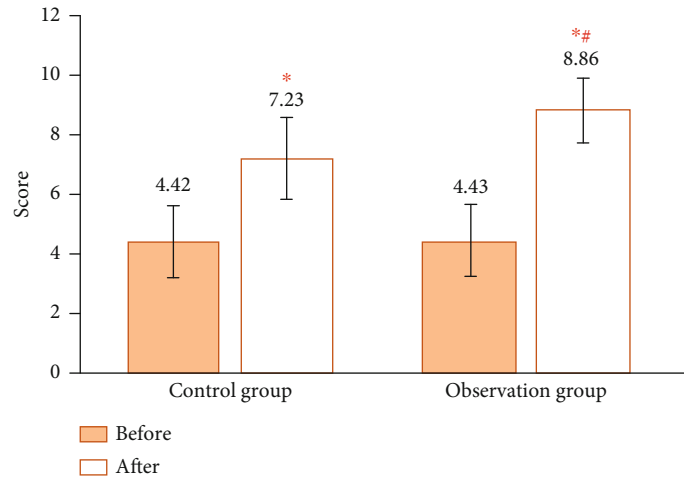


FIGURE 5: Comparison of aesthetic score between the two groups before and after treatment. Note: “\*” indicates that the aesthetic score of patients in the two groups was significantly improved compared with that before operation ( $P < 0.05$ ); “#” indicates that the aesthetic score of patients in the observation group was better improved after treatment compared with that in the control group ( $P < 0.05$ ).

surgical plan. In addition, the incidence of complications was considerably lower in the observation group (13%) than in the control group (28%) ( $P < 0.05$ ), indicating that reasonable and effective pouch surgery can alleviate the occurrence of complications after surgical treatment and improve the safety of surgery. This was consistent with a

number of clinical research results, and the symptomatic degree of surgical method has a certain impact on the outcome of surgical treatment and the occurrence of postoperative complications [27–29]. Therefore, accurate examination and surgical method design is the pursuit of various clinical surgical treatment and is also very important to improve

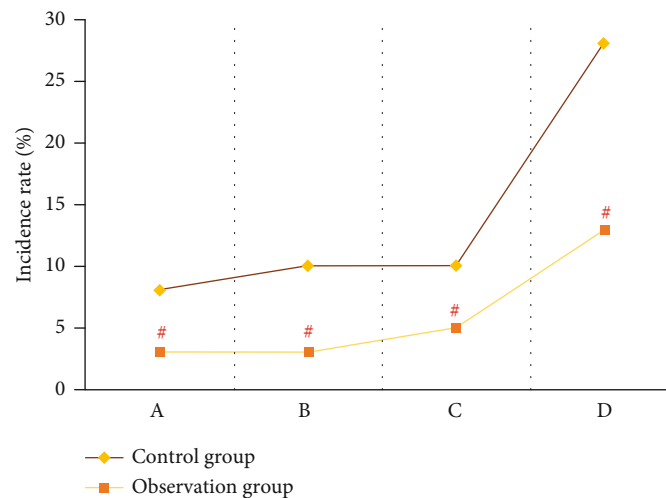


FIGURE 6: Comparison of complication rates: (a) lower eyelid ectropion; (b) lower eyelid retraction; (c) hematoma; (d) total complication rate. Note: “#” indicates that the incidence rate of complications in the observation group was lower than that in the control group ( $P < 0.05$ ).

patient satisfaction, especially in the cosmetic and plastic surgery industry.

## 5. Conclusion

The effect of the 3D eye model based on the multichannel CNN algorithm in the formulation of reasonable pouch surgery plan by cosmetic surgeons was evaluated. The results showed that the eye model based on the multichannel CNN model could help improve the surgical repair and aesthetic effect of patients and could improve the occurrence of postoperative complications. However, there is no targeted comparative analysis of specific surgical methods in this study, which lacks certain comprehensiveness. Further treatment will be carried out later. Through this study, it is concluded that the development prospect of intelligent algorithm in the medical field is very considerable, worthy of further exploration and promotion of clinical research.

## Data Availability

The datasets used in this paper are available from the corresponding author upon request.

## Conflicts of Interest

The authors declared that they have no conflicts of interest regarding this work.

## Authors' Contributions

Yixin Qu and Bingying Lin contributed equally to this work. They are co-first authors.

## Acknowledgments

This study was supported by the Guangdong Provincial Natural Science Foundation(2021A1515010467).

## References

- [1] M. Chopan, L. Sayadi, E. M. Clark, and K. Maguire, “Plastic surgery and social media,” *Plastic and Reconstructive Surgery*, vol. 143, no. 4, pp. 1259–1265, 2019.
- [2] L. S. Khoo, Y. C. Hsiao, J. J. Huang et al., “Simultaneous orthognathic surgery with Asian double eyelid suture blepharoplasty,” *Journal of Craniofacial Surgery*, vol. 32, no. 8, pp. 2592–2596, 2021.
- [3] C. Lavia, L. Dallorto, M. Maule, M. Ceccarelli, and A. M. Fea, “Minimally-invasive glaucoma surgeries (MIGS) for open angle glaucoma: a systematic review and meta-analysis,” *PLoS One*, vol. 12, no. 8, article e0183142, 2017.
- [4] E. Pan, W. L. Chen, S. C. Zhang, Y. Chen, and J. G. Yu, “Mild to moderate blepharoptosis correction: outcomes of levator aponeurosis posterior layer plication,” *Medicine (Baltimore)*, vol. 99, no. 12, article e19038, 2020.
- [5] Y. Jin, W. Gao, H. M. T. Teo, and X. Lin, “Transconjunctival lower blepharoplasty using midcheek spaces for orbital fat transposition (S.O.F.T.),” *Annals of Plastic Surgery*, vol. 86, no. 6, pp. 620–626, 2021.
- [6] B. K. Jung, Y. S. Kim, W. K. Jung, J. M. Kim, Y. H. Jung, and T. S. Roh, “Septo-capsulopalpebral fascial recession flap technique in lower blepharoplasty: an experience of 453 consecutive cases and a review of the literature,” *Journal of Plastic, Reconstructive & Aesthetic Surgery*, vol. 73, no. 1, pp. 156–165, 2020.
- [7] H. P. Peng and J. H. Peng, “Treating the tear trough-eye bag complex: treatment targets, treatment selection, and injection algorithms with case studies,” *Journal of Cosmetic Dermatology*, vol. 19, no. 9, pp. 2237–2245, 2020.
- [8] W. Gan, Y. Wang, S. Xiao et al., “Magnetically driven 3D cellulose film for improved energy efficiency in solar evaporation,” *ACS Applied Materials & Interfaces*, vol. 13, no. 6, pp. 7756–7765, 2021.
- [9] Z. Wan, Y. Dong, Z. Yu, H. Lv, and Z. Lv, “Semi-supervised support vector machine for digital twins based brain image fusion,” *Frontiers in Neuroscience*, vol. 15, p. 802, 2021.



- [10] X. Tu, J. Zhang, R. Luo et al., "Reconstruction of high-precision semantic map," *Sensors (Basel)*, vol. 20, no. 21, p. 6264, 2020.
- [11] J. Yin, J. Han, R. Xie et al., "MC-LSTM: real-time 3D human action detection system for intelligent healthcare applications," *IEEE Transactions on Biomedical Circuits and Systems*, vol. 15, no. 2, pp. 259–269, 2021.
- [12] X. Zhou, Y. Li, and W. Liang, "CNN-RNN based intelligent recommendation for online medical pre-diagnosis support," *IEEE/ACM Transactions on Computational Biology and Bioinformatics*, vol. 18, no. 3, pp. 912–921, 2021.
- [13] C. ShanWei, S. LiWang, N. T. Foo, and D. A. Ramli, "A CNN based handwritten numeral recognition model for four arithmetic operations," *Procedia Computer Science*, vol. 192, pp. 4416–4424, 2021.
- [14] W. Gong, H. Chen, Z. Zhang et al., "A novel deep learning method for intelligent fault diagnosis of rotating machinery based on improved CNN-SVM and multichannel data fusion," *Sensors (Basel)*, vol. 19, no. 7, p. 1693, 2019.
- [15] Z. D. Draelos and R. S. Peterson, "A double-blind, comparative clinical study of newly formulated retinol serums vs tretinoin cream in escalating doses: a method for rapid retinization with minimized irritation," *Journal of Drugs in Dermatology*, vol. 19, no. 6, pp. 625–631, 2020.
- [16] Z. Liu, X. Li, Y. Wu et al., "Functional nasolacrimal duct decompression for chronic dacryocystitis," *Lin Chuang er bi yan hou tou jing wai ke za zhi= Journal of Clinical Otorhinolaryngology, Head, and Neck Surgery*, vol. 34, no. 7, pp. 651–654, 2020.
- [17] S. S. Al-Angari, S. Meaigel, N. Almayouf, S. Quwayhis, A. Aldahash, and N. S. Al-Angari, "The effects of a coffee beverage and whitening systems on surface roughness and gloss of CAD/CAM lithium disilicate glass ceramics," *Journal of Applied Biomaterials & Functional Materials*, vol. 19, 2021.
- [18] J. Monton, N. Kenig, L. Chang-Azancot, J. Jordan, and R. Insausti, "A free tool for breast aesthetic scale computation," *Annals of Plastic Surgery*, vol. 86, no. 4, pp. 458–462, 2021.
- [19] G. Zucchelli, L. Tavelli, M. K. McGuire et al., "Autogenous soft tissue grafting for periodontal and peri-implant plastic surgical reconstruction," *Journal of Periodontology*, vol. 91, no. 1, pp. 9–16, 2020.
- [20] M. Mughal and D. Ross, "Management of the post-pregnancy abdomen: the plastic surgical perspective," *Hernia*, vol. 25, no. 4, pp. 929–938, 2021.
- [21] J. Hu, Y. Kuang, B. Liao, L. Cao, S. Dong, and P. Li, "A multi-channel 2D convolutional neural network model for task-evoked fMRI data classification," *Computational Intelligence and Neuroscience*, vol. 2019, Article ID 5065214, 9 pages, 2019.
- [22] A. K. Singh, I. R. Khan, S. Khan, K. Pant, S. Debnath, and S. Miah, "Multichannel CNN model for biomedical entity reorganization," *BioMed Research International*, vol. 2022, Article ID 5765629, 11 pages, 2022.
- [23] H. Carpenter, A. Hotouras, W. J. English, F. G. M. Taylor, and S. Andreani, "Revisional ileoanal pouch surgery: a systematic literature review assessing outcomes over the last 40 years," *Colorectal Disease*, vol. 23, no. 1, pp. 52–63, 2021.
- [24] S. Masket, N. R. Fram, A. Cho, I. Park, and D. Pham, "Surgical management of negative dysphotopsia," *Journal of Cataract and Refractive Surgery*, vol. 44, no. 1, pp. 6–16, 2018.
- [25] J. L. Chen, C. H. Liu, and C. G. Yi, "Transconjunctival orbital septum fat release and preservation for orbitopalpebral sulcus in lower eyelid blepharoplasty," *Aesthetic Plastic Surgery*, vol. 41, no. 3, pp. 568–572, 2017.
- [26] L. Jiang, Y. Deng, and W. Li, "Application of orbital septum fat flap stuffing to correct inferior orbital sulcus deformities," *Plastic and Reconstructive Surgery. Global Open*, vol. 7, no. 12, article e2561, 2019.
- [27] S. O. Baek, J. W. Kim, J. Y. Lee, and H. Kwon, "Traction applying technique on bicanalicular crawford silicone tube to overcome the notching deformity after lacrimal canalicular repair," *Journal of Craniofacial Surgery*, vol. 32, no. 2, pp. 719–722, 2021.
- [28] E. Nielsen, L. M. Andras, T. J. Anesi, N. Lightdale-Miric, and P. J. Lee, "Operative fixation of medial epicondyle fractures: complication rates based on mode of fixation," *Medicine (Baltimore)*, vol. 99, no. 21, article e20015, 2020.
- [29] D. S. Wendling-Keim, M. Binder, H. G. Dietz, and M. Lehner, "Timing of osteosynthesis of fractures in children changes the outcome," *European Journal of Trauma and Emergency Surgery*, vol. 25, no. 1, 2020.

## Research Article

# Correlation Analysis and Application of Respiratory and Lung Diseases in Pediatrics of Traditional Chinese Medicine Based on Factor Analysis Method

Shengnan Sun, Lingling Zhuang , and Ming Cao

*Traditional Chinese Medicine Academy of Science of Jilin Province, Changchun Jilin 130021, China*

Correspondence should be addressed to Lingling Zhuang; 2016123783@jou.edu.cn

Received 18 June 2022; Revised 20 July 2022; Accepted 25 July 2022; Published 31 August 2022

Academic Editor: Hangjun Che

Copyright © 2022 Shengnan Sun et al. This is an open access article distributed under the Creative Commons Attribution License, which permits unrestricted use, distribution, and reproduction in any medium, provided the original work is properly cited.

Many scholars have studied the influencing factors of children's lung infection, whether it is the region or the environment, or the living air quality of the mother during pregnancy. Western medicine is the most frequently used medicine, but Chinese medicine has more remarkable characteristics in treating children's lung diseases. For viral invasive diseases, people often use antibiotics to treat them. Children's lung conditions are too fragile, and taking antibiotics will lead to the damage of *Staphylococcus* in the lungs, resulting in pulmonary respiratory insufficiency. Although the conditioning time of traditional Chinese medicine is longer than that of western medicine, traditional Chinese medicine will not cause secondary damage to the lungs. In this paper, we introduce factor analysis and principal component analysis and compare the performance of the three analysis methods by using data such as cure rate, improvement rate, mortality rate, and drug taking frequency as evaluation indexes. In the model comparison, the accuracy rate of factor analysis method is over 97%, while the error rate is below 5%. Compared with the other two analysis methods, this method has a better application effect. Finally, we compare the comprehensive scores of eigenvalues of the three analysis methods. From 2016 to 2021, the comprehensive scores of factor analysis gradually increased.

## 1. Introduction

Children's lungs are easily infected by viruses, and circulating diseases such as pneumonia have great influence on children's lungs, which may cause irreversible damage [1]. By analyzing the blood gas performance of children, we can get some children's lung diseases related to clinical analysis, and the study can find different clinical manifestations and injury degrees of children [2]. Children's lung disease is one of the most common and complicated diseases in pediatric medicine. Before the Soviet Union was decomposed, good achievements were made in the treatment and effective control of children's lung disease [3]. The question why children's lungs are most susceptible to diseases has also attracted the attention of many researchers. Is it related to geography and environment? We statistically analyzed the number of children infected with lung diseases in various regions and found that geographical environment is one of the important pathological reasons [4]. Generally, we can

take antibiotics to treat viral infections. However, studies have found that in children's lung diseases, taking antibiotics will lead to the damage of *Staphylococcus* in children's lungs, which will lead to pulmonary respiratory insufficiency [5]. The complication principle of children's lung diseases may lie in the air quality of mothers during lactation. We should pollute the living air quality of pregnant women, which is beneficial to the development of children's lungs [6, 7]. MRI findings of pneumonia caused by mycoplasma pneumoniae, *Streptococcus pneumoniae*, and other pathogens in children and abnormalities of lung parenchyma, pleura, and lymph nodes have good features on MRI. Contrast enhancement may be useful in distinguishing active inflammatory and noninflammatory changes, and MRI is especially useful in the follow-up of chronic lung diseases in children [8, 9]. Comparing the pathological conditions of two children, it is particularly difficult to determine the causes of these lesions and distinguish tumor process from infection. Patients with intrathoracic myopathy should be

considered in the differential diagnosis of pulmonary and mediastinal mass lesions [10]. The parameters of traditional factor model are different among regulator variables, so a semiparametric moderation factor modeling method is proposed, which is feasible in parameter recovery and ability to distinguish different measurement invariance models [11]. This paper selects the relevant financial data of 10 listed real estate companies, such as Xiangjiang Holdings, Yunnan Chengtong, and Wantong Real Estate, evaluates their financial indicators and nonfinancial indicators by factor analysis, and makes quantitative and qualitative analysis [12–14]. The incidence and spread speed of the Novel Coronavirus are predicted and classified by machine learning algorithms [15]. It is very important to analyze the soil quality factors and quantitatively evaluate the soil quality in karst rocky desertification areas for providing the living conditions [16]. In selecting excellent genes of plants, the relationship between complex factors and variables can also be studied by factor analysis, and finally, seeds with good fruit quality can be selected [17–20]. Using different ultraviolet spectra, factor analysis was adopted to measure some antibacterial drugs [21]. The correlation among carcass was used as false phenotypes in genetic evaluation, and principal component method and variable rotation algorithm were used to extract factors [22]. In enterprise application, exploratory and confirmatory factor analysis is used to verify employees' self-leadership ability [23, 24]. This method studies the factors of the formation of dandruff in adolescents and uses principal component analysis to find out the main factors affecting dandruff in normal people [25].

## 2. Development Trend of Traditional Chinese Medicine

**2.1. Development of Chinese Medicine Abroad.** Chinese medicine has spread abroad for more than 2,000 years. As early as Qin and Han Dynasties, Chinese medicine spread to Japan, Korea, Vietnam, and other neighboring countries. Subsequently, the medical exchanges between Southeast Asian countries and China continued to deepen, and traditional Chinese medicine began to spread widely in Arab countries. Later, infectious diseases such as smallpox broke out, which made vaccination spread to five continents and four oceans. Once, the president of the United States also told his own experience of receiving acupuncture treatment after the operation of broad tail inflammation in China, which made acupuncture spread quickly throughout the United States and western countries. Chinese acupuncture has become a major treatment measure for medical health in the world. Nowadays, Chinese medicine has spread to more than 100 countries and regions in the world and has gradually become one of the important ways for people in the world to choose medical care.

**2.2. Trends in Chinese Medicine Trade.** The outbreak of COVID-19 pandemic in recent years has made the supply of drugs even more cramped. Studies have shown that Lianhua Qingpo Capsule has a protective effect on Novel Coronavirus, which makes the export of traditional Chinese

medicine reach the peak in recent years. The average annual growth rate of Chinese medicine export has reached more than 10% in recent five years, and the number of Chinese medicines exporting countries has reached nearly 200 countries or regions. At the same time, some ready-for-use traditional Chinese medicine trademarks and brands with international influence have been formed, such as Compound Danshen Dropping Pills, Compound Banlangen, Huoxiang Zhengqi Liquid, Kanglaite Capsule, Kanglaite Injection, and Lianhua Qingpo Capsule. The total drug exports in China from 2016 to 2021 are shown in Figure 1.

## 3. Different Analysis Algorithms

**3.1. Principal Component Analysis Algorithm.** Principal components of the influence of traditional Chinese medicine on children's lungs are

$$F_i = a_1X_1 + a_2X_2 + \dots + a_iX_i. \quad (1)$$

Eigenvalues and eigenvectors of principal components of the influence of traditional Chinese medicine on children's lungs are

$$A = (a_{ij})_{p \times m} = (a_1, a_2, \dots, a_m), \quad (2)$$

$$Ra_i = \lambda_i a_i.$$

The correlation of  $\lambda_i$  is  $\lambda_1 \geq \lambda_2 \geq \dots \geq \lambda_p \geq 0$ , and  $\lambda_i$  is different from each other.

Calculate orthogonal matrices:

$$A' A = I. \quad (3)$$

Calculate the covariance:

$$\begin{aligned} \text{cov}(F_i, F_j) &= \lambda_i \delta_{ij}, \\ \delta_{ij} &= \begin{cases} 0 & i \neq j \\ 1 & i = j. \end{cases} \end{aligned} \quad (4)$$

Set the principal components of the influence of TCM on children's lungs as functions:

$$(F_1, F_2, \dots, F_m)' = A' X. \quad (5)$$

Calculate the sum of squares of  $X$  coefficients in the principal components of TCM's influence on children's lungs:

$$\sum_{k=1}^p a_{ki}^2 = 1. \quad (6)$$

Combine principal component functions:

$$F = \sum_{i=1}^m (\lambda_i/p) F_i. \quad (7)$$

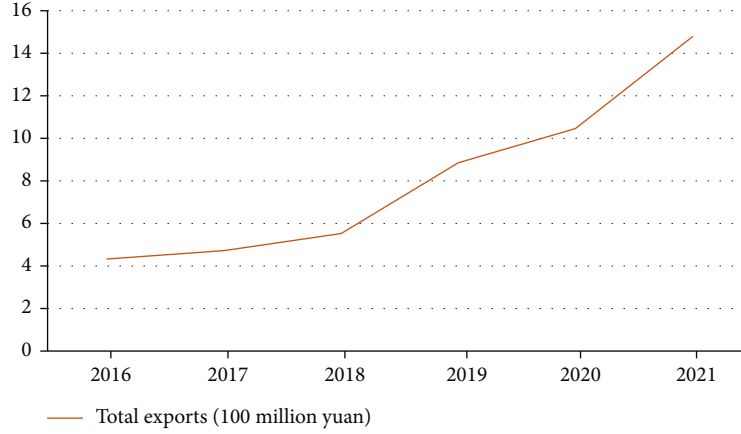


FIGURE 1: Total exports of traditional Chinese medicine in China from 2016 to 2021.

TABLE 1: Standardization and unification of Chinese medicine names.

Drug serial number	Before specification	After specification
1	Panax notoginseng powder	Panax notoginseng
2	Yunling	Poria cocos
3	Polygonatum sibiricum	Polygonatum sibiricum
4	Patchouli	Agastache rugosa
5	Rhizoma Rehmanniae	Rehmannia glutinosa
6	Whole insect	Scorpion
7	Dismiss Rhizoma Atractylodis	Atractylodes lancea
8	Grass nut	Tsaoko
9	Grass river cart	Paris polyphylla
10	Xiaoyaozhu	Xu Changqing
11	White ginseng	Ginseng

TABLE 2: KMO test results.

Drug name	Degree of freedom	Significance
Poria cocos	4755	0
Xu Changqing	3782	0
Ginseng	4003	0
Atractylodes lancea	3431	0
Rehmannia glutinosa	2546	0

Firstly, it uses dimension reduction technology to replace the original multiple variables with a few comprehensive variables, which concentrate most of the information of the original variables. Secondly, it evaluates the objective economic phenomena scientifically by calculating the score of the comprehensive principal component function. Thirdly, it focuses on the comprehensive evaluation of information contribution and influence in application.

The analysis steps of principal component analysis are defined as follows:

Step 1: select initial variables

Step 2: choose whether to use covariance matrix or correlation matrix to find principal components according to the characteristics of initial variables

Step 3: calculate the eigenvalues and eigenvectors of the covariance matrix or correlation matrix

Step 4: determine the number of principal components

Step 5: the economic meaning of principal component is determined by several indexes with greater weight in each linear combination

**3.2. Factor Analysis Algorithm.** Variables of the influence of traditional Chinese medicine on children's lungs are as follows:

$$X_j = b_{j1}Y_1 + b_{j2}Y_2 + \cdots + b_{jm}Y_m + \epsilon_j, \quad (8)$$

$$\text{cov}(\epsilon_j, Y_i) = 0,$$

where  $\epsilon_j$  and  $Y_i$  represent special factors. The covariance between them is 0, and the formula is  $\text{cov}(\epsilon_j, Y_i) = 0$ .

The variable factor load matrix is

$$B = (b_{ij})_{p \times m} = \hat{B}C, \quad (9)$$

$$\hat{B} = (\sqrt{\lambda_1}a_1, \sqrt{\lambda_2}a_2, \dots, \sqrt{\lambda_m}a_m).$$

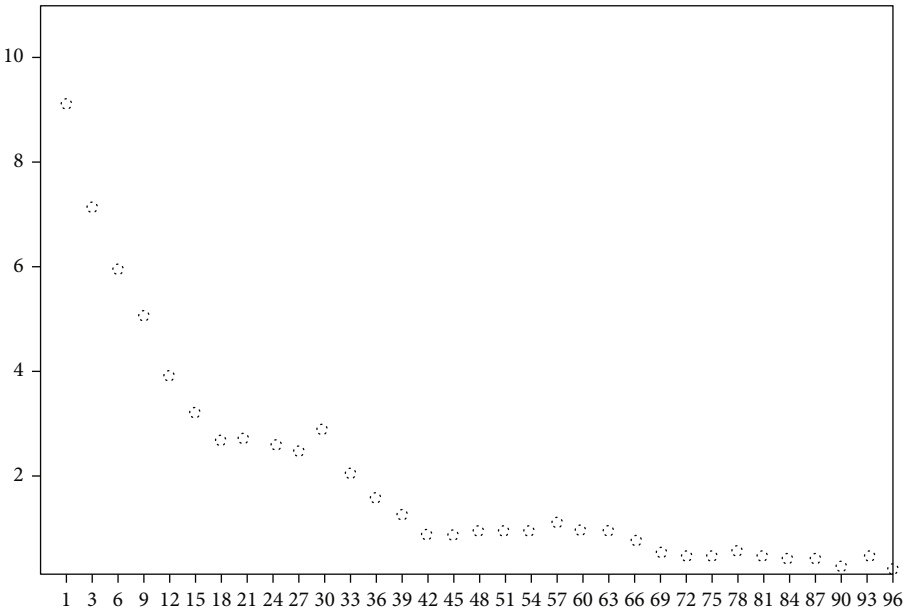


FIGURE 2: Lithotripsy diagram of medication frequency factor of lung diseases.

TABLE 3: Application data of factor analysis in pediatric treatment of lung.

Evaluation index	Accurate value	Error value	F1	Recall rate	ROC
Cure rate	97.89%	3.57%	78.56%	76.54%	80.54%
Rate of improvement	96.57%	4.21%	77.92%	75.83%	82.34%
Mortality rate	98.34%	4.45%	79.65%	75.52%	81.49%
Drug use rate	96.39%	3.86%	78.97%	78.48%	81.78%

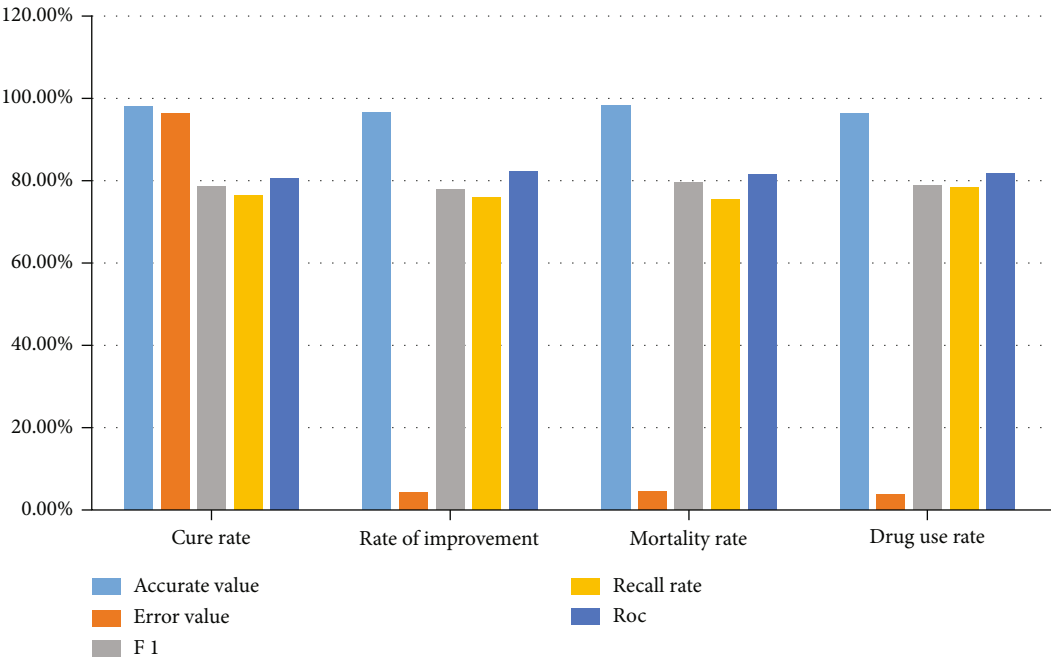


FIGURE 3: Performance comparison of evaluation indexes of children's lung treatment.



TABLE 4: Application data of ratio analysis in pediatric treatment of lung.

Evaluation index	Accurate value	Error value	F1	Recall rate	ROC
Cure rate	73.45%	12.68%	56.55%	46.54%	60.54%
Rate of improvement	78.65%	13.21%	57.82%	45.88%	52.34%
Mortality rate	72.76%	12.25%	58.49%	47.54%	51.89%
Drug use rate	74.58%	14.51%	57.25%	52.48%	55.78%

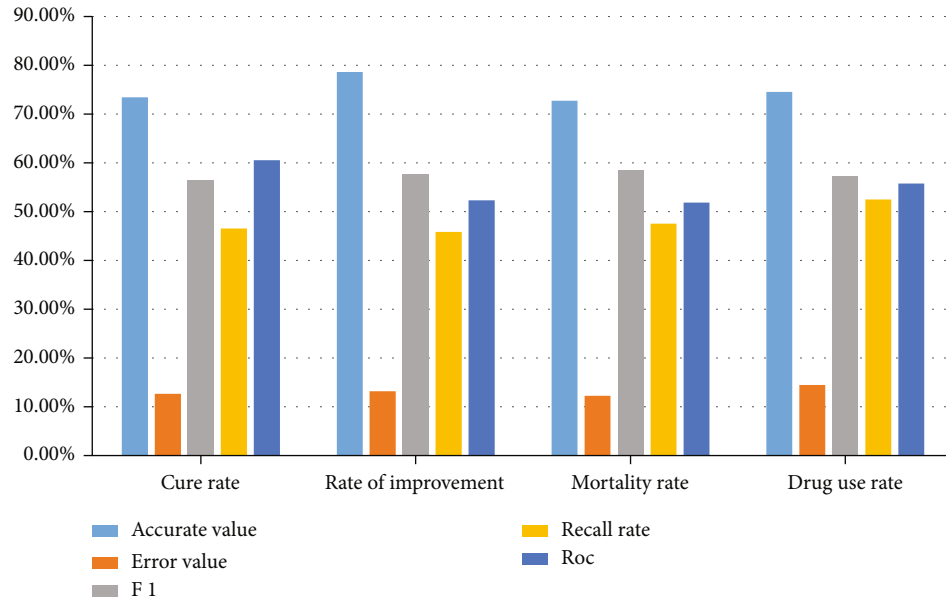


FIGURE 4: Performance comparison of evaluation indexes of children's lung treatment.

TABLE 5: Application data of trend analysis method in pediatric treatment of lung.

Evaluation index	Accurate value	Error value	F1	Recall rate	ROC
Cure rate	53.47%	32.66%	39.55%	36.59%	40.44%
Rate of improvement	58.66%	33.25%	41.82%	37.67%	42.74%
Mortality rate	62.76%	32.28%	40.46%	40.04%	43.86%
Drug use rate	54.56%	34.54%	39.23%	38.58%	42.38%

Its matrix relationship is

$$B'B \neq I. \quad (10)$$

The correlation of variables is

$$X_i Y_j = b_{ij}. \quad (11)$$

Calculate the covariance:

$$\begin{aligned} \text{cov}(Y_i, Y_j) &= \delta_{ij}, \\ \delta_{ij} &= \begin{cases} 0 & i \neq j \\ 1 & i = j. \end{cases} \end{aligned} \quad (12)$$

The contribution value of factor  $Y_i$  to  $X$  is

$$v_i = \sum_{k=1}^p b_{ki}^2 (\neq \lambda_i). \quad (13)$$

The expression for calculating the score value of variable factor is

$$(Y_1, Y_2, \dots, Y_m)' = B'R^{-1}X. \quad (14)$$

The factor similarity function is

$$\sum_{i=1}^m b_{ij}^2 + \sigma_j^2 = h_j^2 + \sigma_j^2 = 1, \quad (15)$$

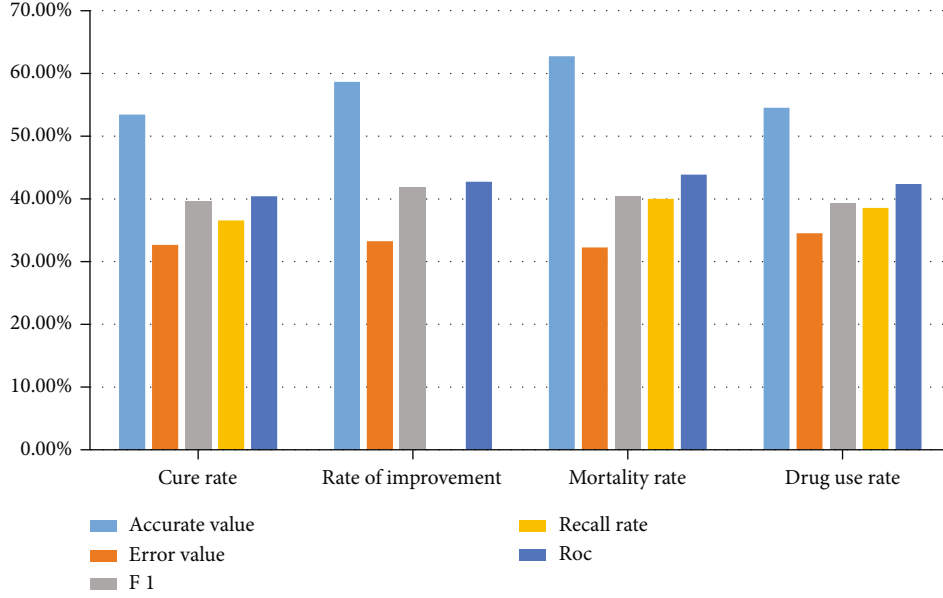


FIGURE 5: Performance comparison of evaluation indexes of children's lung treatment.

where  $h_j^2$  stands for common degree and  $\sigma_j^2$  stands for special variance. Commonality refers to the sum of squares of the loads of each variable in each common factor.

The factor covariance expression is

$$\text{cov}(\epsilon_i, \epsilon_j) = \delta_{ij} \delta_j^2. \quad (16)$$

Synthesize the score function expression of each factor:

$$Y = \sum_{i=1}^m (v_i/p) Y_i, \quad (17)$$

$$\frac{v_i}{p} = \frac{v_i}{v_1 + v_2 + \dots + v_m}.$$

The standardized formulas of various indicators of the influence of traditional Chinese medicine on children's lungs are as follows:

Inverse indicator:

$$x_i' = 1/x_i \quad (18)$$

Moderate indicators:

$$x_i' = 1/(1 + |a_i - x_i|) \quad (19)$$

Therefore, the unified standardization of indicators is

$$Y_{ij} = \frac{x_{ij} - x_i}{s_j}. \quad (20)$$

Test the index:

$$\frac{1}{N-1} \sum_{j=1}^N x_{ij}' x_{ij}, R = \{r_{ij}\}. \quad (21)$$

The analysis steps of factor analysis is defined as follows:

Step 1: choose the variables for analysis

Step 2: calculate the correlation coefficient matrix of the selected original variables

Step 3: put forward common factors

Step 4: factor rotation

Step 5: calculate factor scores

Find out the factor score of each sample. If you have the factor score value, you can use these factors in many analyses, such as using the factor score as a variable in cluster analysis and a regression factor in regression analysis.

## 4. Experiment

**4.1. Data Processing.** Traditional Chinese medicine has the phenomenon of multiple names, abbreviations, and different places of origin, which has a great impact on the later statistics. Therefore, before formal analysis, we need to preprocess the data and unify the drug names, as shown in Table 1.

Standardize and unify the names of traditional Chinese medicines for treating lung diseases, and make a preliminary analysis of the frequency of medication. Select high-frequency drugs to test whether they meet the conditions of factor analysis. KMO test is carried out on lung traditional Chinese medicine with high-frequency medication. If the KMO value is greater than 0.6, it has a good linear relationship and is also suitable for factor analysis in Table 2.

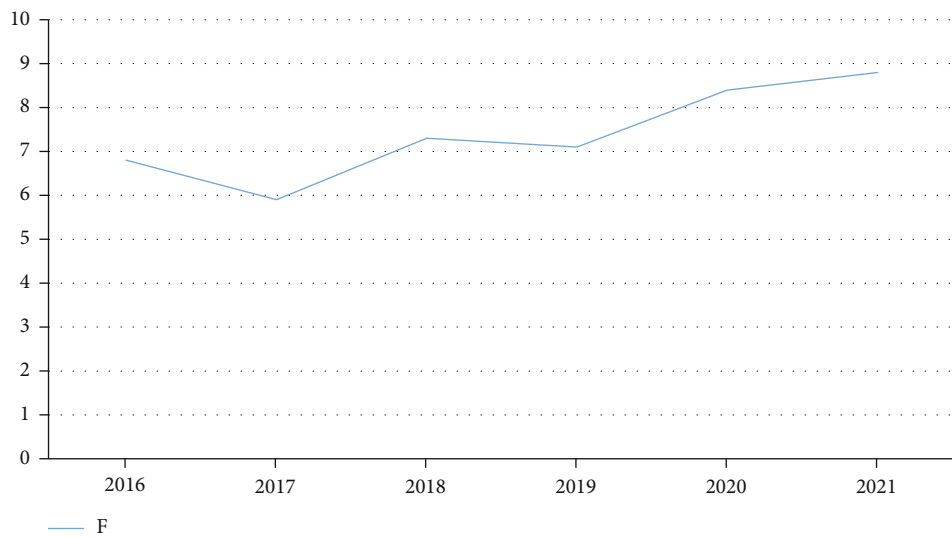


FIGURE 6: Comprehensive scores of factor analysis in recent years.

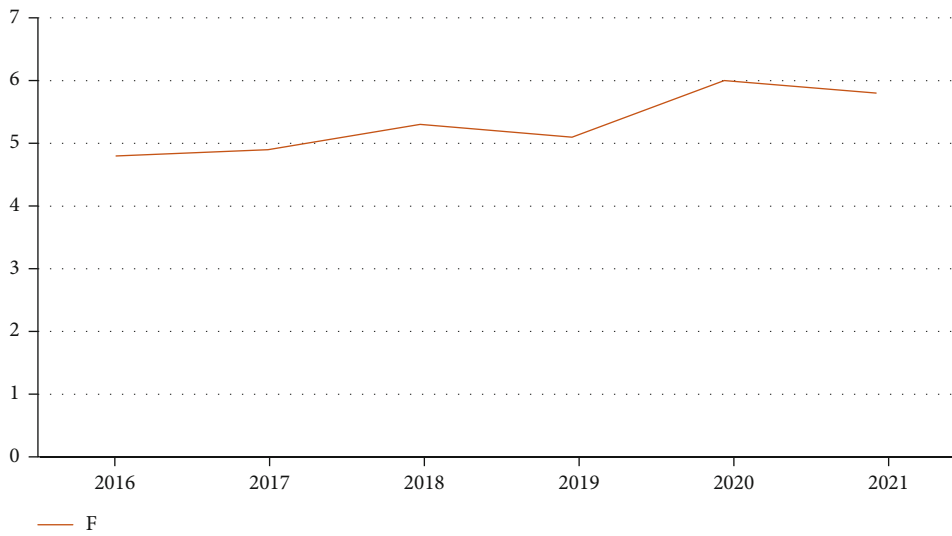


FIGURE 7: Comprehensive scores of ratio analysis in recent years.

The covariance is calculated by factor analysis, and the gravel diagram composed of each factor variable is shown in Figure 2.

It can be seen in Figure 2 that 72-75 factors are the most stable, that is, 72-75 factors are the most appropriate.

**4.2. Model Comparison.** There are many analytical methods for TCM treatment of children’s lung diseases. In order to find the best analytical method, we compare the performance of various analytical methods on the cure rate, improvement rate, mortality rate, drug taking frequency, and other indicators of lung pediatrics.

The data analysis and statistics of pediatric lung diseases by factor analysis are shown in Table 3.

The application data of pulmonary pediatric treatment evaluation index are counted into a bar chart as shown in Figure 3.

The data analysis and statistics of pediatric lung diseases by ratio analysis method are shown in Table 4.

The application data of pulmonary pediatric treatment evaluation index are counted into a bar chart as shown in Figure 4.

The data analysis and statistics of pediatric lung diseases by trend analysis method are shown in Table 5.

The application data of pulmonary pediatric treatment evaluation index are counted into a bar chart as shown in Figure 5.

**4.3. Contrast Experiment.** By comparing the performance of three kinds of analysis methods, we can get the index data of children’s lung treatment. Using the factor analysis method, we can get better statistical results. In order to further verify the best effect of this method, we use the factor analysis and other two analysis methods to compare the comprehensive

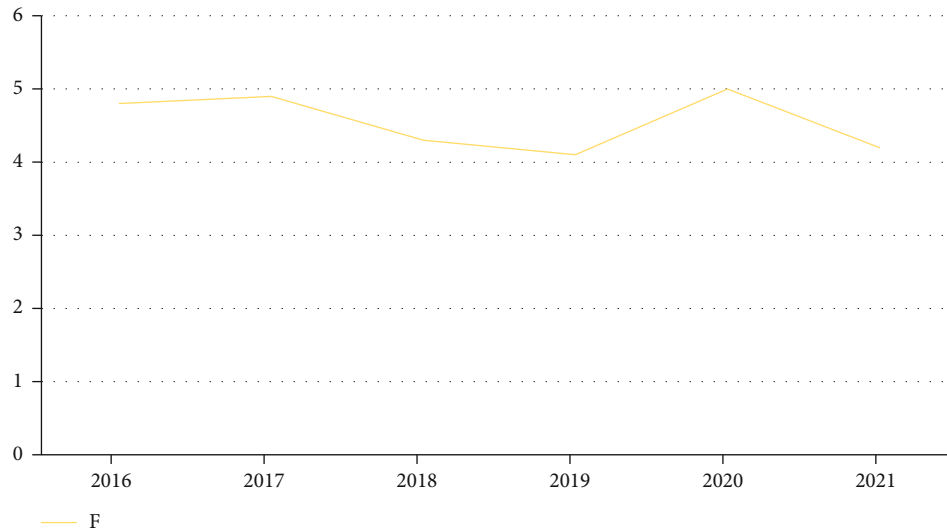


FIGURE 8: Comprehensive scores of trend analysis in recent years.

scores of eigenvalues from 2016 to 2021, as shown in Figures 6–8.

Comprehensive evaluation refers to the method of using systematic and standardized methods to evaluate multiple indicators and units at the same time. The comprehensive score is the final index to measure the advantages and disadvantages of each evaluation object, and through ranking the comprehensive score, find out the best scheme.

## 5. Conclusion

Children's pathological conditions have always been a concern for parents. In recent years, western medicine treatment is still popular because of its quick effect and short time. However, people ignore that traditional Chinese medicine is a radical medicine for human body conditioning. Children's lung disease is a common kind of children's disease. We put forward factor analysis to analyze the correlation of pediatric respiratory lung disease in traditional Chinese medicine. The conclusions are as follows:

- (1) Factor analysis has good data analysis ability for complex pathological factors, and the data accuracy of traditional Chinese medicine for children's lung diseases is high
- (2) Comparing the performance of the three data analysis methods mentioned in this paper, the accuracy of factor analysis method reaches more than 90%, far exceeding the other two analysis methods
- (3) In the contrast experiment, the comprehensive score of the eigenvalues of the three analysis methods is carried out, and the comprehensive score of factor analysis method gradually increases, while the trend analysis method can only see one trend, which cannot reach a higher accuracy

## Data Availability

The experimental data used to support the findings of this study are available from the corresponding author upon request.

## Conflicts of Interest

The authors declared that they have no conflicts of interest regarding this work.

## Acknowledgments

We acknowledge the analysis and application of Chinese medicine in pediatric respiratory and pulmonary diseases based on the factor analysis method.

## References

- [1] G. H. McCracken, R. F. Jacobs, and J. A. Margenthaler, "Effects of pneumonia on lungs of children," *Clinical Pediatrics: Open Access*, vol. 6, no. 9, pp. 1-2, 2021.
- [2] R. Kraemer, "Clinical relevance of blood gas analysis in children with lung disease," *Revue Suisse De Medecine Praxis*, vol. 71, no. 11, pp. 459-462, 1982.
- [3] S. I. Kaganov, "Achievements in the control of diseases of the lungs in children during the years of Soviet power," *Voprosy Okhrany Materinstva i Detstva*, vol. 12, no. 11, pp. 68-73, 1967.
- [4] O. Wasz-Höckert, "Geomedical problems in pulmonary diseases in childhood," *Praxis der Pneumologie*, vol. 30, no. 9, pp. 544-546, 1976.
- [5] N. L. Kushch, G. A. Sopov, and A. A. Lykov, "Use of antibiotics in staphylococcal destruction of the lungs in children," *Sovetskaia Meditsina*, vol. 34, no. 8, pp. 69-72, 1971.
- [6] B. Nemery and P. de Marie Katoto, "Protecting children's lungs by providing clean air during pregnancy?," *The Lancet Planetary Health*, vol. 1, no. 8, pp. e309-e310, 2017.

- [7] O. Sommerburg, J. P. Schenk, and M. A. Mall, "Lung diseases in children," *Der Radiologe*, vol. 55, no. 7, pp. 545–553, 2015.
- [8] A.-M. Waleed, "Is systemic inflammatory response syndrome relevant to pulmonary complications and mortality in multiply injured children," *Journal of Pediatric Orthopedics*, vol. 40, no. 1, pp. 1–7, 2020.
- [9] P. Ville, R. Olli, and S. Erkki, "Magnetic resonance imaging of lung infections in children," *Pediatric Radiology*, vol. 38, no. 11, pp. 1225–1231, 2008.
- [10] S. M. Spinola, R. A. Bell, and F. W. Henderson, "Actinomycosis. A cause of pulmonary and mediastinal mass lesions in children," *American Journal of Diseases of Children*, vol. 135, no. 4, pp. 336–339, 1981.
- [11] M. Dylan, "A flexible moderated factor analysis approach to test for measurement invariance across a continuous variable," *Psychological Methods*, vol. 26, no. 6, pp. 660–679, 2021.
- [12] W. Li, "Comprehensive evaluation of the performance of listed real estate companies in my country– based on factor analysis," *Frontiers in Economics and Management*, vol. 2, no. 12, pp. 160–165, 2021.
- [13] J. Jolanta and J. Grzegorz, "Application of factor analysis in company management – selected examples related to competitiveness and market success," *Engineering Management in Production and Services*, vol. 13, no. 3, pp. 25–36, 2021.
- [14] J. Chen, "Identification of key risk factors in port service supply chain based on factor analysis method," *Academic Journal of Business & Management*, vol. 3, no. 5, 2021.
- [15] A. K. Dubey, "Performance estimation of machine learning algorithms in the factor analysis of COVID-19 dataset," *Computers, Materials, & Continua*, vol. 66, no. 2, pp. 1921–1936, 2021.
- [16] Y. Deng, "Soil quality assessment via the factor analysis of karst rocky desertification areas in Hunan, China," *Soil Use and Management*, vol. 38, no. 1, pp. 248–261, 2021.
- [17] D. Gizem and G. Atila, "Estimation of Effective Spatial Variables When Visiting Public Squares through Factor Analysis Model," *Journal of Urban Planning and Development*, vol. 148, no. 3, pp. 25–36, 2022.
- [18] C. Kong, M. Feng, and S. Tian, "Dynamic thinking on the construction and development of hydrogen stations: research on influencing factors based on factor analysis method," *IOP Conference Series: Earth and Environmental Science*, vol. 702, no. 1, 2021.
- [19] A. Abordán and N. P. Szabó, "Uncertainty reduction of interval inversion estimation results using a factor analysis approach," *GEM-International Journal on Geomathematics*, vol. 11, no. 1, pp. 87–97, 2020.
- [20] F. S. Moslemi, M. Dianati, J. A. Olfati, and Y. Hamidoghli, "Selection of elite F3 lines in cucumber using factor analysis method," *International Journal of Vegetable Science*, vol. 26, no. 5, pp. 498–505, 2020.
- [21] M. Esteki, E. Dashtaki, Y. V. Heyden, and J. Simal-Gandara, "Application of rank annihilation factor analysis for antibacterial drugs determination by means of pH gradual change-UV spectral data," *Antibiotics*, vol. 9, no. 7, 2020.
- [22] J. T. Paiva, H. R. Oliveira, M. Nascimento et al., "Genetic evaluation for latent variables derived from factor analysis in broilers," *British Poultry Science*, vol. 61, no. 1, pp. 3–9, 2020.
- [23] R. Wu, J. Chen, J. Zhao, J. Chen, and S. Chen, "Identifying geochemical anomalies associated with gold mineralization using factor analysis and spectrum–area multifractal model in Lao-wan District, Qinling-Dabie Metallogenic Belt, Central China," *Minerals*, vol. 10, no. 3, pp. 229–229, 2020.
- [24] K. Na-Nan and S. Saribut, "Validation of employees' self-leadership using exploratory and confirmatory factor analysis," *The International Journal of Quality & Reliability Management*, vol. 37, no. 4, pp. 552–574, 2020.
- [25] S. Y. Wei, H. Y. Zhang, Y. T. Yin et al., "Factor analysis approach unveils the influencing factors of dandruff in the normal teenage population," *Dermatologic Therapy*, vol. 33, no. 4, article e13690, 2020.



## Research Article

# Efficacy and Mechanisms of Oleuropein in Postmenopausal Osteoporosis

Huilan Liu,<sup>1,2</sup> Aiguo Zhao,<sup>3</sup> Yulu Huang,<sup>4</sup> Anli Hou,<sup>2</sup> Wenbin Miao,<sup>2</sup> Lu Hong,<sup>2</sup> Nina Deng,<sup>2</sup> and Yujuan Fan <sup>1,2</sup>

<sup>1</sup>Jinan University, China

<sup>2</sup>Department of Gynaecology, University of Chinese Academy of Sciences Shenzhen Hospital, Shenzhen 518106, China

<sup>3</sup>Department of Medical Administration, University of Chinese Academy of Sciences Shenzhen Hospital, Shenzhen 518106, China

<sup>4</sup>Department of Gynaecology, Wuzhou Red Cross Hospital, Wuzhou 543002, China

Correspondence should be addressed to Yujuan Fan; yjfan530@163.com

Received 21 July 2022; Accepted 3 August 2022; Published 25 August 2022

Academic Editor: Hangjun Che

Copyright © 2022 Huilan Liu et al. This is an open access article distributed under the Creative Commons Attribution License, which permits unrestricted use, distribution, and reproduction in any medium, provided the original work is properly cited.

**Background.** Postmenopausal osteoporosis (PMOP) has a supernal morbidity rate in elderly females. **Objective.** To appraise the effects of oleuropein on bone densitometry, bone metabolic index, oxidative stress, and inflammatory index in PMOP. In addition, the mechanism of olive bittersweet preventing bone loss was explored. **Methods.** We grouped 80 salubrious female Sprague-Dawley rats into four teams: (1) sham operation team (sham,  $N = 20$ ), (2) ovariectomy (OVX,  $N = 20$ ), (3) castrated mice fed with oleuropein (OVX+ole,  $N = 20$ ), and (4) castrated mice fed with estrogen (OVX+E2,  $N = 20$ ). The ovariectomized SD rats were continuously raised with 200  $\mu\text{g/kg/dose}$  of oleuropein. Bone mineral density and bone metabolism indexes were recorded. In order to assess the effectiveness of oleuropein on osteopenia, an enzyme-linked immunosorbent assay (ELISA) was devoted to examining the bone marrow indexes. The bone metabolism standards of PMOP rats were appraised by assessing serum levels of calcium, alkaline phosphatase (ALP), phosphorus, malondialdehyde (MDA), and nitrate content by experimental detection methods and levels of osteoclastogenesis inhibitory factor (OPG) and receptor activator for nuclear factor- $\kappa\text{B}$  ligand (RANKL) by ELISA. The OPG-RANK-RANKL signal passage was examined by Western blot (WB). We measured bone mineral density using dual-energy X-rays. **Results.** Our animal experimental results indicated that oleuropein could significantly improve the bone mineral density of ovariectomized SD rats. In the meantime, it could reduce ending interleukin-6 (IL-6), malondialdehyde (MDA), nitrate, alkaline phosphatase (ALP), and phosphorus (P) serum concentration and would not affect  $\text{Ca}^{2+}$  concentration. In cell experiments, oleuropein also can promote the proliferation of osteoblasts. Furthermore, it can promote the expression of OPG protein and mRNA. In reverse, it inhibits the expression of RANKL protein and mRNA. **Conclusion.** Oleuropein can not only improve the inflammatory and oxidative indexes of castrated rats but also prevent osteoporosis. Oleuropein avoids bone resorption by regulating OPG/RANKL expression.

## 1. Introduction

Postmenopausal osteoporosis (PMOP) is a systemic disease in women, which is mainly manifested as the loss of bone mass and increased risk of bone mass caused by the significant decline of estrogen in the clinic [1]. According to relevant data, more than 200 million women worldwide have osteoporosis. At the same time, the number of fracture patients caused by osteoporosis will double by 2050, which will impose a huge

medical and economic burden on the global health system [2]. Currently, estradiol and bisphosphonates are the main methods to prevent PMOP in most hospitals. However, the literature showed that antiosteoporosis drugs have decreased in recent years, especially bisphosphonates [3], because it was highly probable that the drug would increase the incidence of cancer and the risk of osteonecrosis in the patient over the long term [4]. In addition, postmenopausal women could use raloxifene and hormone replacement therapy to prevent

osteoporosis [5]. Therefore, due to various side effects of the drug, most postmenopausal women look for natural plant drugs to replace traditional drug therapy.

Components extracted from natural plants are an important origin of new drugs for treating multiple human diseases, including PMOP. Many researchers have demonstrated that the prevalence of carcinoma, coronary artery disease, and osteoporosis [6] is prominently low in the Mediterranean basin [7–9]. People like to eat olive oil on Mediterranean coastal. However, the main component of olive oil is oleuropein, which has been extensively utilized in clinical medicine to resist inflammation, antioxidation [10], and anticarcinogenic effects [11]. Postmenopausal osteoporosis can be alleviated by anti-inflammatory and antioxidant therapy. The Mediterranean diet mainly includes the consumption of olive oil, which includes hydroxytyrosol and oleuropein. The researcher's former experiment displayed that olive oil can delay bone loss, but its functional components are not clear [12].

In this experiment, we fed ovariectomized SD rats with oleuropein to research the resist inflammation, antioxidant, and antiosteoporosis effects of oleuropein. In addition, we also concluded that oleuropein could prevent osteoporosis by regulating the OPG/RANK/RANKL signalling pathway. The results provided a theoretical basis for the effect of oleuropein on preventing osteoporosis and help oleuropein to be widely used in clinical practice in the future.

## 2. Methods and Materials

**2.1. Medical Ethics.** The Medical Ethics Committee approved all animal and cell experimental protocols of the University of Chinese Academy of Sciences Shenzhen Hospital. All SD rats were anesthetized by intraperitoneal injection of 5.2% ketamine for surgery. Animals were managed and raised according to methods provided by the Institutional Animal Care and Use Committee (IACUC).

**2.2. Animal Experiment Modelling Approach and Treatments.** Eighty healthy Specific Pathogen Free (SPF) female Sprague-Dawley (SD) rats were 3 months old. All experimental SD rats were raised at the University of Chinese Academy of Sciences Shenzhen Hospital in ventilated, dry, fixed lighting, and quiet environment. Experimental SD rats were reared in a room with an environmental temperature of 18°C–25°C and humidity of 50%–60%, and they were allowed to eat water freely. After a week of acclimation, 80 SD rats were divided into the sham operation group (20 cases) and the castration group (60 cases). The SD rats were intraperitoneally annotated with 5.2% amiodarone. After the onset of anesthesia, the Y-shaped uterus was found by vertically cutting the middle of the lower abdomen with a scalpel and entering the abdominal cavity. After the bilateral ovaries were found in the abdominal cavity, which was removed, the wound surface of the incision was sutured for hemostasis. Sham surgery was performed to remove bilateral perioophorectomy adipose tissue of the same size as the ovary.

**2.3. Grouping and Processing of Experimental SD Rats.** We grouped 80 salubrious female Sprague-Dawley rats into four teams: (1) sham operation team (sham,  $N = 20$ ), (2) ovariec-

tomy (OVX,  $N = 20$ ), (3) castrated mice fed with oleuropein (OVX+ole,  $N = 20$ ), and (4) castrated mice fed with estrogen (OVX+E2,  $N = 20$ ). The ovariectomized SD rats were continuously raised with 200  $\mu\text{g/kg}$ /dose of oleuropein or 25  $\mu\text{g/kg}$  of estrogen. All experimental SD rats were fed consecutively for 12 weeks according to subgroups.

## 3. Measurement

**3.1. Bone Metabolism Index in Serum.** The blood of the left ventricle of the experimental SD rats was measured, which was centrifuged at 4°C and 2500 rpm for 10 minutes. After centrifugation, the supernatant was placed in Eppendorf tubes and kept at -20°C. The serum should be cooled to room temperature when the automatic biochemical indicator detector was used to detect serum indicators. The serum levels of calcium, phosphorus, malondialdehyde (MDA), and alkaline phosphatase (ALP) were measured by traditional experimental methods. Serum IL-6 values were measured using the ELISA method following the steps of the kit. The contents of osteoclastogenesis inhibitory factor (OPG) and receptor activator for nuclear factor- $\kappa\text{B}$  ligand (RANKL) in serum of the four groups were detected by ELISA. The specific operation steps follow the instructions of each kit.

**3.2. Bone Mineral Density.** Measurement of the lumbar spine and left femur bone mineral density (BMD) in SD rats uses dual-energy X-ray (Hologic, Bedford, MA, USA) (S/N806409).

**3.3. Isolation, Culture, and Passage of Osteoblasts.** Three newborn SD suckling rats were taken from the same litter for 48 h to clean the body surface and sacrificed with cervical dislocation. The cranial bone was removed and cleaned with PBS balance solution (at least 3 times) to remove the periosteum, blood vessels, and other connective tissues until the skull became bright and white. The cranial bones were placed in a sterile beaker containing low sugar DMEM and cut into 1 mm  $\times$  1 mm pieces with sterile scissors. Add 1 mg/ml of type 2 collagenase into the beaker and digest it for 2 hours at 37°C for 3 times. After digestion, it forms a cell suspension. The cell suspension was centrifuged at 1000 r/min for 10 min, and the supernatant was sucked with a pipette. The precipitated cell clumps were cultured in a culture medium at 5%  $\text{CO}_2$  and 37°C. After the monolayer of cells was covered with a culture flask, digestion was performed with 1 ml 0.25% trypsin, and digestion was terminated with a 10% FBS culture medium. Vials were divided and subcultured, and cells of the third generation were taken for the experiment (Figure 1(a)).

**3.4. Identification of Osteoblasts.** After discarded culture medium was washed with PBS, osteoblasts were fixed with 2.5% glutaraldehyde at room temperature for 10 min. Alkaline phosphatase staining was performed with the NBT/BCIP kit after PBS washing. The morphology, nucleus, and cytoplasm of osteoblasts were observed under an inverted phase contrast microscope (Figure 1(b)).

**3.5. Drugs Treat Osteoblasts.** The osteoblasts were cultured for an alternative time (24 h, 48 h, and 72 h), and the concentrations of 50, 100, 200, and 400  $\mu\text{g/ml}$  oleuropein were added,

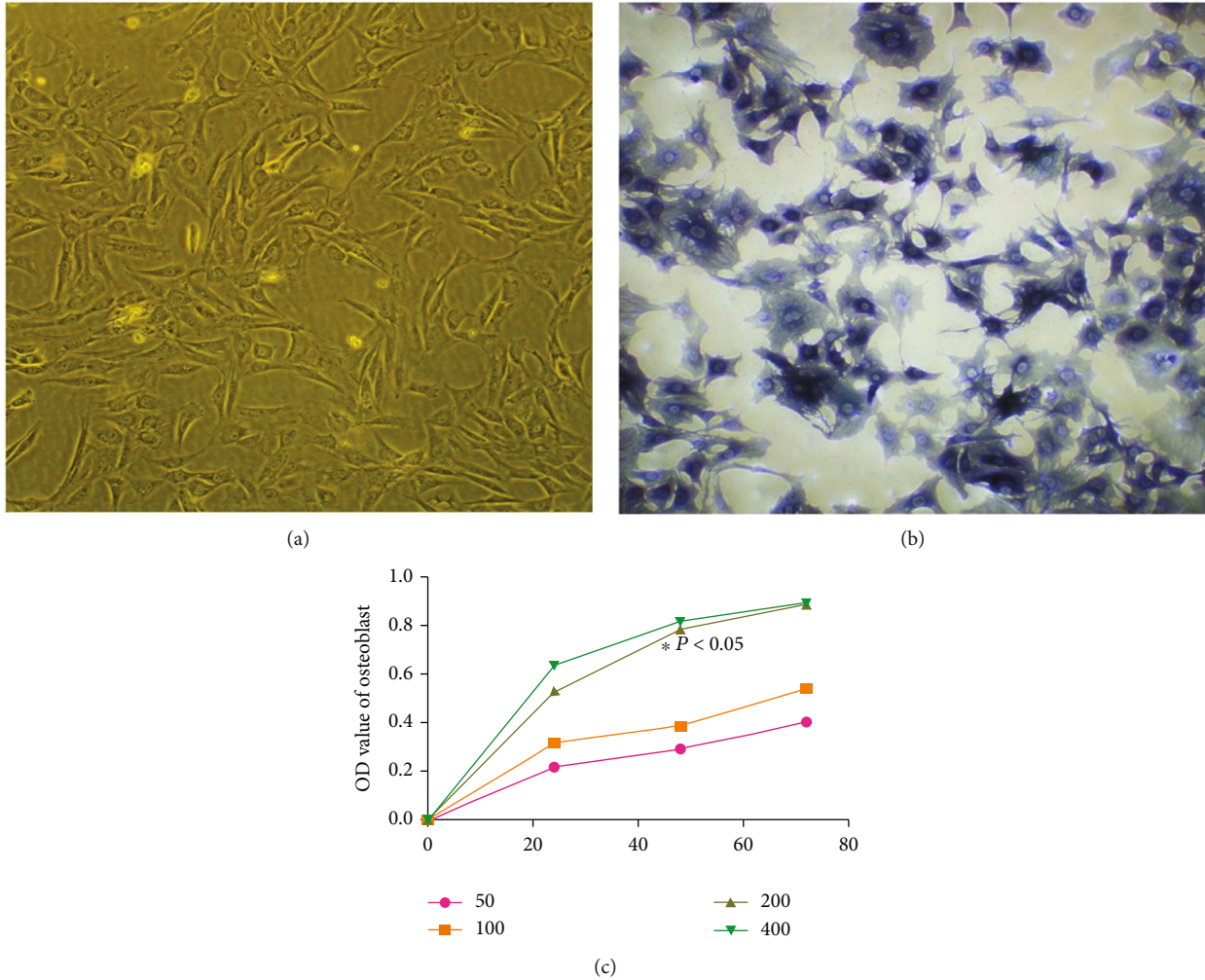


FIGURE 1: (a) The third generation of osteoblasts. (b) Osteoblasts stained with alkaline phosphatase. (c) Effects of oleuropein on osteoblast proliferation at different time points and concentrations. After 48 h, the concentration of 200  $\mu\text{g/ml}$  of oleuropein had the strongest effect on osteoblast proliferation ( $*P < 0.05$  vs. blank control group (c)).

respectively. The OD value of osteoblasts was detected by the MTT method, and the optimal oleuropein solubility and action time were obtained. The osteoblasts were separated into the blank group (A) and oleuropein group (B) for 48 h culture. The effects of oleuropein on protein and mRNA expression of OPG and RANKL in the compound culture system were measured in groups A and B. The specific operation steps follow the instructions of each kit.

**3.6. Data Analysis.** SPSS 23.0 was used for statistical analysis, and GraphPad Prism 7 (GraphPad Software, CA, USA) was used to visualize the data into required figures. All data were expressed as the mean  $\pm$  standard deviation (SD). Comparisons between groups were made using an analysis of variance or the LSD method for statistical differences. The comparison between the two groups in accordance with the normal distribution was examined by the  $t$ -test. The use of  $P < 0.05$  stands for statistical difference.

## 4. Results

**4.1. Changes in Serum Metabolic Indexes and Bone Mineral Density in Experimental SD Rat  $\text{Ca}^{2+}$  and P.** We examined the  $\text{Ca}^{2+}$  of 4 different groups of mice. We found that the discrepancy had no statistical meaning in  $\text{Ca}^{2+}$ . That implied that  $\text{Ca}^{2+}$  values in each group did no significant changes (Figure 2(a)). Completely contradictory, compared to the sham group, the P level significantly declined in the OVX+ole group, the OVX group, and OVX+E2 ( $P < 0.05$ , Figure 2(b)). However, there was no statistical difference in the three groups ( $P > 0.05$ , Figure 2(b)).

**4.2. ALP and IL-6.** Compared with the other three groups, In the OVX group, the serum interleukin-6 (IL-6) and ALP levels of SD rats were significantly increased ( $P < 0.05$ , Figures 2(c) and 2(d)). The OVX+ole group and the OVX+E2 group indicated no marked differences between the two indexes, which

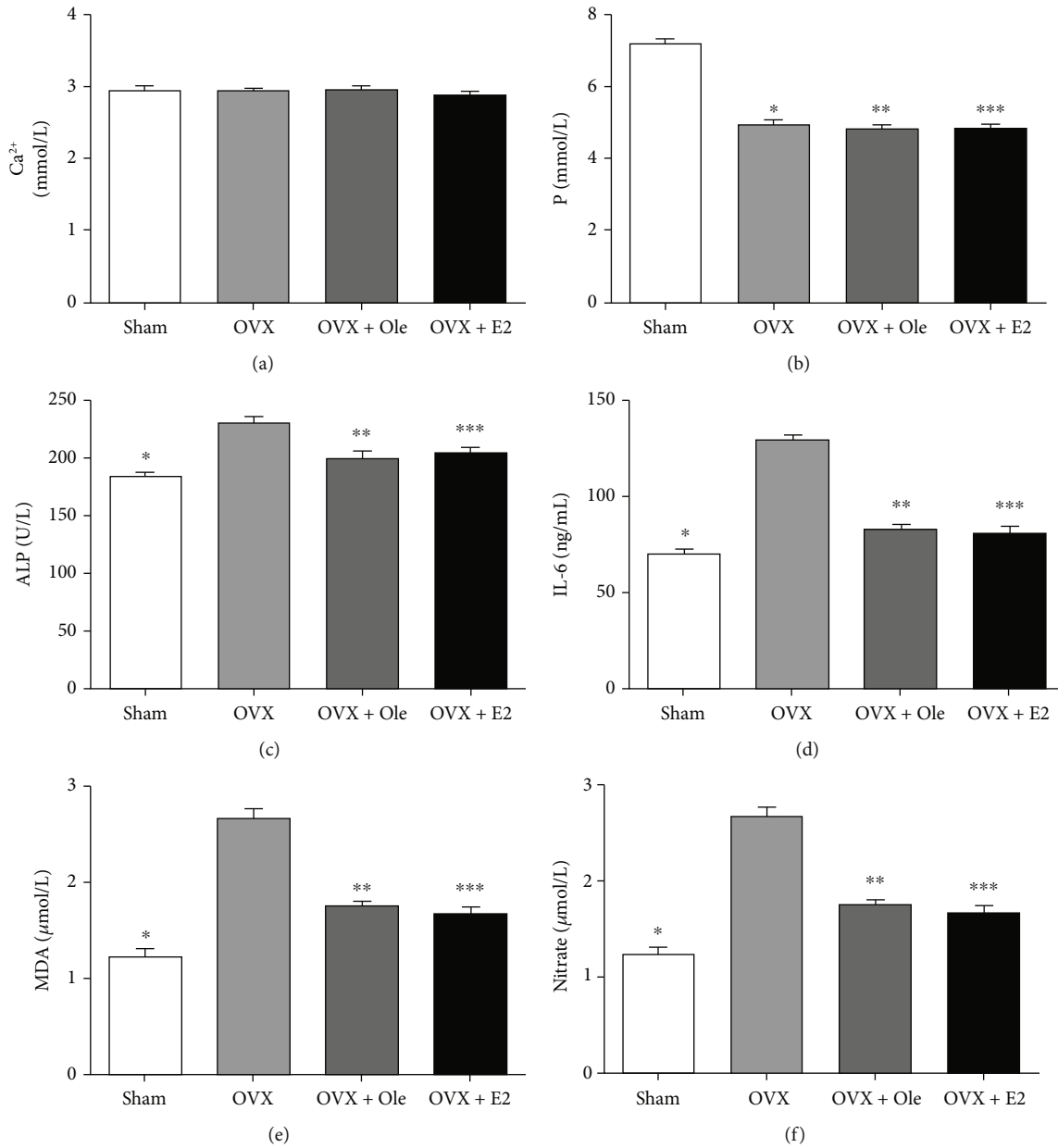


FIGURE 2: Serum metabolite indexes of different groups at 12 weeks postoperation: (a) comparison of  $\text{Ca}^{2+}$  level; (b) comparison of P level; (c) comparison of ALP level; (d) comparison of IL-6 level; (e) comparison of MDA level; (f) comparison of nitrate level. Data express the means  $\pm$  SD ( $n = 20$ ) (\* $P < 0.05$ , \*\* $P < 0.05$ , \*\*\* $P < 0.05$  vs. OVX group).

showed that oleuropein and estrogen probably had the same impact on osteogenesis ( $P > 0.05$ , Figures 2(c) and 2(d)).

**4.3. MDA and Nitrate.** In the OVX group, MDA and nitrate levels ascended notably. However, in the OVX+ole group, MDA decreased slightly ( $P < 0.05$ , Figure 2(e)), and nitrate notably decreased. These results exhibited that oleuropein possibly significantly influences antioxidation to avoid bone absorption ( $P < 0.05$ , Figure 2(f)).

**4.4. Change of Bone Mineral Density in Experimental SD Rats aft Three Months.** The mean bone mineral density of the lumbar vertebra and left femur in the OVX group was

lower than that in the other three groups, and the difference was marked dissimilarity ( $P < 0.05$ ). Compared with the OVX+E2 and sham groups, the bone mineral density of the OVX+ole group was no different. It demonstrated that oleuropein had a good effect on maintaining bone mineral density (Figures 3(a) and 3(b)).

**4.5. Serum OPG/RANKL Indexes.** Compared with the other three groups, the serum OPG level in the OVX group was lower ( $P < 0.05$ , Table 1). Compared with the sham group, OPG levels in the OVX+ole and OVX+E2 groups were decreased, and the differences were statistically significant ( $P < 0.05$ , Table 1); nevertheless, OPG levels in the latter two



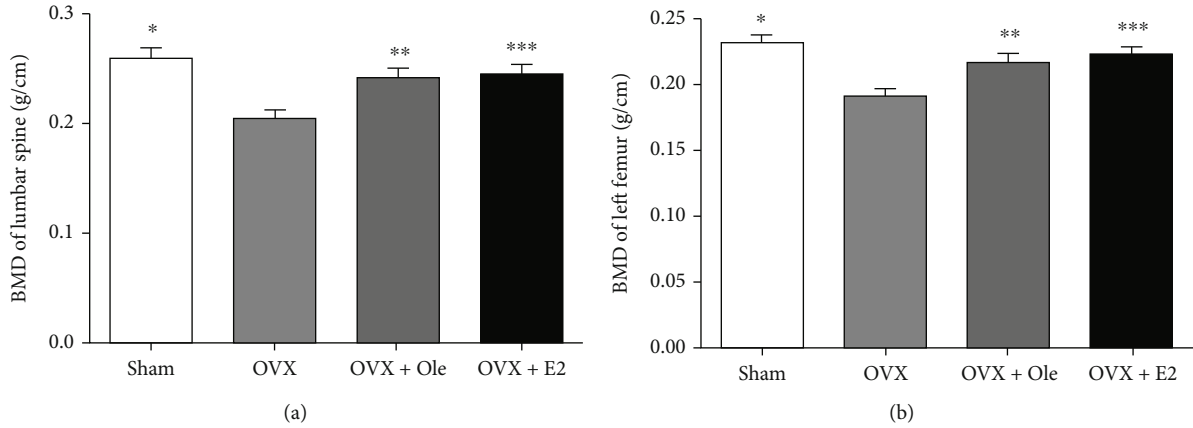


FIGURE 3: Change of BMD in experimental SD rats after three months. (a) Bone density of the lumbar spine. (b) Bone density of left femur. Data represent the means  $\pm$  standard deviation (SD) ( $n = 20$ ) (\* $P < 0.05$ , \*\* $P < 0.01$ , \*\*\* $P < 0.001$  vs. OVX group).

TABLE 1: Comparison of OPG/RANKL levels in four groups (mean  $\pm$  SD).

	<i>n</i>	OPG (pmol/l)	RANKL (pmol/l)
Sham	20	0.55 $\pm$ 0.05*	0.53 $\pm$ 0.07*
OVX	20	0.18 $\pm$ 0.06 <sup>#</sup>	0.79 $\pm$ 0.1
OVX+ole	20	0.45 $\pm$ 0.05* <sup>#</sup>	0.43 $\pm$ 0.13* <sup>Δ</sup>
OVX+E2	20	0.47 $\pm$ 0.04* <sup>#</sup>	0.55 $\pm$ 0.11*

\* $P < 0.05$  vs. OVX group; <sup>#</sup> $P < 0.05$  vs. sham group; <sup>Δ</sup> $P < 0.05$  vs. OVX+E2 group.

groups were not different ( $P > 0.05$ , Table 1). In contrast with the OVX group, serum RANKL of the sham, OVX+E2, and OVX+ole groups decreased significantly, and the differences were statistically significant ( $P < 0.05$ , Table 1). In relation to the OVX+E2 group, the RANKL level was lower in the OVX+ole group ( $P < 0.05$ , Table 1).

**4.6. Effects of Oleuropein on Osteoblast Proliferation at Different Time Points and Concentrations.** Compared with the blank control group, 50, 100, 200, and 400  $\mu\text{g/ml}$  oleuropein had a proliferation effect on osteoblasts, and the dissimilarity was memorably important ( $P < 0.05$ , Figure 1(c)). After 48 h of treatment, 200  $\mu\text{g/ml}$  oleuropein had the strongest proliferation effect on osteoblasts ( $P < 0.05$ , Figures 1(a)–1(c)). There was no distinguished distinction in the OD value of osteoblasts after 72 h treatment ( $P > 0.05$ , Figures 1(a)–1(c)).

**4.7. Effects of Oleuropein on Protein and mRNA Expression of OPG and RANKL in Osteoblasts.** After 200  $\mu\text{g/ml}$  oleuropein was used to culture osteoblasts for 48 h, compared with the blank control group, the expression of OPG protein and mRNA was significantly increased in the experimental group ( $P < 0.05$ , Figures 4(a) and 4(c)), while the expression of RANKL protein and mRNA was significantly decreased ( $P < 0.05$ , Figures 4(a) and 4(c)).

## 5. Discussion

The regulation and balance of hormone levels are very important for women's health. An estrogen level that changes dramatically throughout life determines the development of women's age-associated diseases. The hormonal imbalance and estrogen deficiency, resulting in obesity, autoimmune disease, and osteoporosis, greatly increased the risk of fractures during the perimenopausal period. Osteoporosis is a systematic bone disease featured by osteopenia and degeneration of bone microarchitecture, which easily leads to the occurrence of bone fragility and increases the risk of fracture [13]. Osteoporosis and its complications place a huge economic burden on society and, at the same time, pose an unprecedented challenge to the health system as the majority of patients with osteoporosis go untreated [14]. In addition, since the number of drug treatments for osteoporosis has decreased as a side effect of drugs for osteoporosis, many women are looking for natural plant drugs as alternative therapy [1]. Olive oil is an important part of the Mediterranean diet, which is known for its protective effects on human health. Oleuropein, the most common phenolic compound in olive oil, has a good therapeutic effect on humans' multifarious diseases [15–17]. The result has been clarified in a lot of shown mechanisms and has indicated promising consequences in animal and human studies, especially in PMOP, breast carcinoma, oophoroma, and other disorders [18–20]. Oleuropein is a phenolic compound extracted from natural olive oil, which belongs to iridoids. Currently, there are few studies on the use of oleuropein to prevent postmenopausal osteoporosis.

Our experiment results on animals suggested that oleuropein could significantly avoid BMD descent of ovariectomized SD rats. Besides, it could reduce the levels of serum IL-6, MDA, nitrate, ALP, and P but does not affect the level of  $\text{Ca}^{2+}$ . In osteoblast experiments, oleuropein also can promote the proliferation of osteoblasts. At the same time, it can promote the expression of OPG protein and mRNA. On the contrary, it inhibits the expression of RANKL protein and mRNA.

$\text{Ca}^{2+}$  and P are essential elements of the skeleton. 99% of calcium is stored in bone tissue in the form of hydroxyapatite crystals, and 1% of calcium is distributed in body fluids and



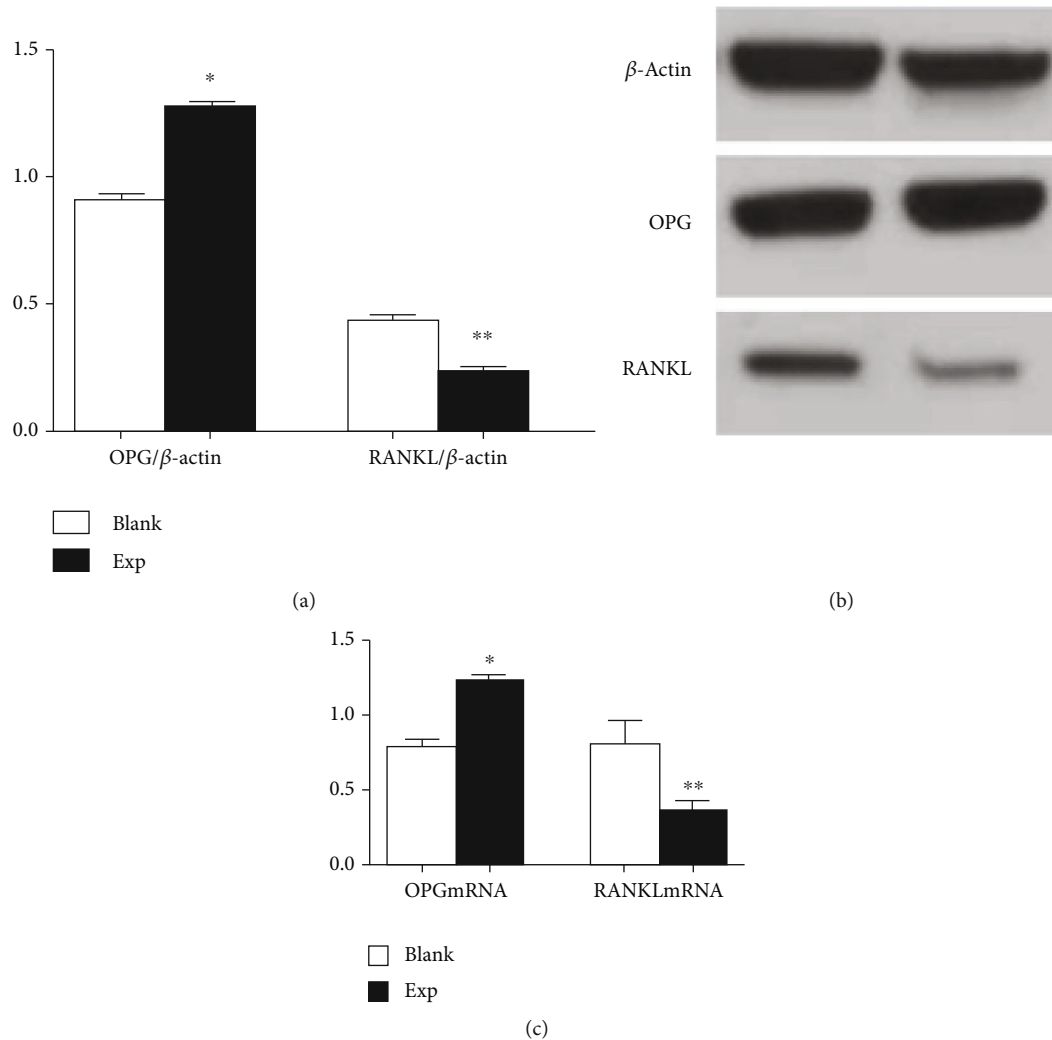


FIGURE 4: (a) Effects of oleuropein on the expression of OPG and RANKL proteins in osteoblasts; (b) representative figure of OPG and RANKL proteins; (c) effects of oleuropein on the expression of OPG and RANKL mRNA in osteoblasts. (\* $P < 0.05$ , \*\* $P < 0.05$  vs. blank control group).

soft tissues, which are in a dynamic balance [21, 22]. Phosphorus is also an essential element of the human body. 86% of phosphorus is stored in bone tissues in the form of calcium phosphate, and 14% of phosphorus is distributed in important parts of bones and other tissues, which can avoid bone loss and reduce the danger of bone fractures [23]. A lot of studies have also confirmed the important position of calcium and phosphorus in the prevention and treatment of osteoporosis. This study showed that serum phosphorus levels in the OVX group and sham operation group were significantly different ( $P < 0.05$ ). There was no notable dissimilarity in serum phosphorus levels between the OVX group and the OVX+oleuropein group ( $P > 0.05$ ). There was no significant difference in serum calcium levels between the two groups ( $P > 0.05$ ). These results are inconsistent with Saleh and Saleh's research [24], The data showed that the serum P level of SD rats was significantly reduced after OVX, but the serum phosphorus level of OVX rats was not significantly changed after the appli-

cation of oleuropein. A research study confirmed our view [24]. There were no significant changes in serum calcium levels after OVX in SD rats or in serum calcium solubility after OVX in OVX rats. We consider that such results may be related to the fluctuation of blood calcium content over time during the development of osteoporosis [25].

Stable proliferation between osteoblasts and osteoclasts maintains stable bone metabolism. Osteoblast mineralization plays an essential part in osteoporosis formation of osteoporosis, and ALP activity is very important in the bone formation of osteoblasts because ALP promotes the formation of mineralization matrix proteins of osteoblasts through the hydrolysis of pyrophosphate and inorganic phosphate [26, 27]. This study showed that there were significant differences in serum ALP levels between the OVX group and the OVX+oleuropein group. With significance ( $P < 0.05$ ), the use of oleuropein can significantly reduce the serum ALP level of ovariectomized SD rats. We hypothesized that oleuropein might inhibit mineralization

matrix protein formation in osteoblasts by decreasing ALP levels. This mechanism needs further study in our later experiments.

Oxidative stress is also significant pathogenesis of postmenopausal osteoporosis. Reactive oxygen species, for example, MDA, are produced during cell metabolism [28]. Hence, the detected amount of MDA can often reflect the degree of lipid peroxidation in vivo and cell injury. Its level also indirectly reflects the severity of the free radical attack on body cells [29]. The occurrence and development of osteoporosis are often accompanied by oxidative stress and osteoblast apoptosis, whose mechanism is to increase the activity of osteoclasts and promote the apoptosis of osteoblasts and the degradation of bone organic matter [1]. The results of this experiment showed that the serum MDA level of the OVX group had a statistically significant increase ( $P < 0.05$ ). While in the OVX+oleuropein group, the serum MDA level significantly declined. We speculated that oleuropein might reduce the degree of lipid oxidation in vivo by reducing the serum MDA content of ovariectomized SD rats, thereby indirectly reducing the apoptosis of osteoblasts and the degradation of bone organic matter and thus achieving the effect of preventing and treating osteoporosis. Oleuropein had been reported that the viability and dissolvability of nitrate in the blood plasma of ovariectomized rats declined notably after receiving oleuropein [30]. The experimental data showed that the serum nitrate level was significantly reduced after oleuropein treatment ( $P < 0.05$ ). The conclusions reached in this study were consistent with those reported above, but there were no relevant reports explaining the reason, so this result needs to be further explored in our later experiments. Our research results are consistent with the report, but the reason is unclear, and further research is needed.

Our experiment showed that the level of IL-6 in the OVX group was significantly higher than in other groups. The secretion of lymphocytes is the main source of IL-6. Transgenic rats with interleukin-6 overexpression have bone loss and increased bone absorption [31]. Recently, according to relevant literature, IL-6 promotes bone resorption by inducing the proliferation of osteoclasts along the RANKL/RANK/OPG axis [32]. IL-6 can raise the expression of RANKL in osteoblasts [33]. The literature indicated that oleuropein in olive oil could prevent osteoporosis by inhibiting the expression of IL-6 in osteoblasts and decreasing the expression of RANKL in osteoblasts [34, 35]. This view is consistent with the results of this experiment.

The OPG-RANKL-RANK signal system plays an important role in bone remodelling. The proliferation and differentiation mechanism of osteoblasts are affected by the OPG-RANKL-RANK signalling system [36]. Research has shown that anti-RANKL therapy can improve the mechanical properties of bones [37]. High-affinity binding of OPG to RANK acts as an inhibitor of RANK activation, which blocks osteoclast differentiation and inhibits osteoclast function, thereby preventing bone resorption. Therefore, the OPG/RANKL ratio is a lever that modulates the balance between bone resorption and osteogenesis. In postmenopausal women, sudden descent in estrogen secretion results in improved RANKL secretion, declined OPG synthesis, and increased osteoclasts, leading to increased bone resorption and dynamic imbalance of bone remodelling [1]. Data from our animal and cellular

experiments indicated that oleuropein could upregulate OPG expression and downregulate RANKL expression, preventing and treating bone loss. At the same time, oleuropein also promoted the proliferation of osteoblasts in a time-dependent manner. Moreover, it is necessary to study a large number of experiments, and there will be more convincing results in the future.

## 6. Conclusion

Oleuropein can not only improve the inflammatory and oxidative indexes of castrated rats but also prevent osteoporosis. Oleuropein avoids bone resorption by regulating OPG/RANKL expression.

## Data Availability

The datasets used and analyzed during the current study are available from the corresponding author upon reasonable request.

## Conflicts of Interest

The authors declare that they have no conflicts of interest.

## Authors' Contributions

Huilan Liu, Aiguo Zhao, and Yulu Huang contributed equally to this work as first authors.

## Acknowledgments

This project is supported by the Shenzhen Guangming District Science and Technology Innovation Research Project, No. 2020R01113.

## References

- [1] T. Zhou, Z. Gai, X. Gao, and L. Li, "The potential mechanism of exercise combined with natural extracts to prevent and treat postmenopausal osteoporosis," *Journal of Healthcare Engineering*, vol. 2021, 2852669 pages, 2021.
- [2] P. Paola, R. M. Daniela, F. Conversano et al., "Major osteoporotic fragility fractures: risk factor updates and societal impact," *World Journal of Orthopedics*, vol. 7, no. 3, pp. 171–181, 2016.
- [3] W. Słupski, P. Jawień, and B. Nowak, "Botanicals in postmenopausal osteoporosis," *Nutrients*, vol. 13, no. 5, p. 1609, 2021.
- [4] J. A. Kanis, C. Cooper, R. Rizzoli, and J. Y. Reginster, "Correction to: European guidance for the diagnosis and management of osteoporosis in postmenopausal women," *Osteoporosis International: A Journal Established As Result of Cooperation Between the European Foundation for Osteoporosis and the National Osteoporosis Foundation of the USA*, vol. 31, no. 4, p. 801, 2020.
- [5] J. Kanis, C. Cooper, R. Rizzoli, J. Y. Reginster, and On behalf of the Scientific Advisory Board of the European Society for Clinical and Economic Aspects of Osteoporosis (ESCEO) and the Committees of Scientific Advisors and National Societies of the International Osteoporosis Foundation (IOF), "European guidance for the diagnosis and management of

- osteoporosis in postmenopausal women,” *Osteoporos International*, vol. 30, pp. 3–44, 2019.
- [6] A. Cano, S. Marshall, I. Zolfaroli et al., “The Mediterranean diet and menopausal health: an EMAS position statement,” *Maturitas*, vol. 139, pp. 90–97, 2020.
  - [7] V. Izadi, H. Tehrani, F. Haghighatdoost, A. Dehghan, P. J. Surkan, and L. Azadbakht, “Adherence to the DASH and Mediterranean diets is associated with decreased risk for gestational diabetes mellitus,” *Nutrition*, vol. 32, no. 10, pp. 1092–1096, 2016.
  - [8] C. Assaf-Balut, N. G. de la Torre, A. Durán et al., “A Mediterranean diet with additional extra virgin olive oil and pistachios reduces the incidence of gestational diabetes mellitus (GDM): a randomized controlled trial: the St. Carlos GDM prevention study,” *PLoS ONE*, vol. 12, p. e0185873, 2017.
  - [9] L. Schwingshackl, C. Schwedhelm, C. Galbete, and G. Hoffmann, “Adherence to Mediterranean diet and risk of cancer: an updated systematic review and meta-analysis,” *Nutrients*, vol. 9, no. 10, p. 1063, 2017.
  - [10] J. G. Fernández-Bolaños and C. Alarcón-de-la-Lastra, “Oleuropein down regulated IL-1 $\beta$ -induced inflammation and oxidative stress in human synovial fibroblast cell line SW982,” *Food and Function*, vol. 8, pp. 1890–1898, 2017.
  - [11] S. Rahiman, T. H. El-Metwally, D. Shrivastava, M. N. Tantry, and B. A. Tantry, “Oleuropein and oleic acid: a novel emerging dietary target for human chronic diseases,” *Indian Journal of Biochemistry and Biophysics*, vol. 56, pp. 263–268, 2019.
  - [12] H. Liu, H. Huang, B. Li et al., “Olive oil in the prevention and treatment of osteoporosis after artificial menopause,” *Clinical Interventions in Aging*, vol. 9, pp. 2087–2095, 2014.
  - [13] R. Bartl and C. Bartl, “Epidemiology of osteoporotic fractures,” in *In The Osteoporosis Manual*, pp. 231–232, Springer International Publishing, Cham, Switzerland, 2019.
  - [14] S. Mohapatra, A. Iqbal, M. J. Ansari et al., “Benefits of black cohosh (*Cimicifuga racemosa*) for women health: an up-close and in-depth review,” *Pharmaceuticals (Basel)*, vol. 15, no. 3, p. 278, 2022.
  - [15] A. Foscolou, E. Critselis, and D. Panagiotakos, “Olive oil consumption and human health: a narrative review,” *Maturitas*, vol. 118, pp. 60–66, 2018.
  - [16] C. La Lastra, M. Barranco, V. Motilva, and J. Herrerias, “Mediterranean diet and health biological importance of olive oil,” *Current Pharmaceutical Design*, vol. 7, no. 10, pp. 933–950, 2001.
  - [17] L. Abenavoli, M. Milanović, N. Milić, F. Luzzza, and A. M. Giuffrè, “Olive oil antioxidants and non-alcoholic fatty liver disease,” *Expert Review of Gastroenterology & Hepatology*, vol. 13, no. 8, pp. 739–749, 2019.
  - [18] R. Owen, R. Haubner, G. Würtele, W. Hull, B. Spiegelhalder, and H. Bartsch, “Olives and olive oil in cancer prevention,” *European Journal of Cancer Prevention*, vol. 13, no. 4, pp. 319–326, 2004.
  - [19] C. Nocella, V. Cammisotto, L. Fianchini et al., “Extra virgin olive oil and cardiovascular diseases: benefifits for human health,” *Endocrine, Metabolic & Immune Disorders-Drug Targets (Formerly Current Drug Targets-Immune, Endocrine & Metabolic Disorders)*, vol. 18, pp. 4–13, 2018.
  - [20] P. Ditano-Vázquez, J. D. Torres-Peña, F. Galeano-Valle et al., “The fluid aspect of the Mediterranean diet in the prevention and management of cardiovascular disease and diabetes: the role of polyphenol content in moderate consumption of wine and olive oil,” *Nutrients*, vol. 11, no. 11, p. 2833, 2019.
  - [21] K. Zhu and R. L. Prince, “Calcium and bone,” *Clinical Biochemistry*, vol. 45, no. 12, pp. 936–942, 2012.
  - [22] V. Vaishali, W. Ran, P. Dhawan, Y. H. Jeon, and S. Christakos, “Vitamin D, calcium homeostasis and aging,” *Bone Research*, vol. 4, p. 16041, 2016.
  - [23] M. S. Calvo and K. L. Tucker, “Is phosphorus intake that exceeds dietary requirements a risk factor in bone health?,” *Annals of the New York Academy of Sciences*, vol. 1301, pp. 29–35, 2013.
  - [24] N. K. Saleh and H. A. Saleh, “Olive oil effectively mitigates ovariectomy-induced osteoporosis in rats,” *BMC Complementary and Alternative Medicine*, vol. 11, no. 1, p. 10, 2011.
  - [25] W. Z. Wang, O. Douglas, G. Liang et al., “Collagen XXIV(-col24 $\alpha$ 1) pro-motes osteoblastic differentiation and mineralization through TGF- $\beta$ / smads signaling pathway,” *International Journal Of Biological Sciences*, vol. 645, no. 8, pp. 1310–1322, 2012.
  - [26] L. Ma, F. Kong, Y. Gong, Q. Wang, J. Liu, and L. Sui, “Combined effects of proton radiation and simulated microgravity on the cell viability and ALP activity of murine osteoblast cells,” *Frontiers in Public Health*, vol. 9, p. 759236, 2021.
  - [27] Proliferation, “ALP activity and photocatalytic activity on sintered anatase and rutile titanium dioxide,” *Materials (Basel)*, vol. 14, no. 16, p. 4414, 2021.
  - [28] J. Jasieczek, M. Trocha, A. Derkacz, E. Szahidewicz-Krupska, and A. Doroszko, “Effect of the renin-angiotensin-aldosterone system reactivity on endothelial function and modulative role of valsartan in male subjects with essential hypertension,” *Journal of Clinical Medicine*, vol. 10, no. 24, p. 5816, 2021.
  - [29] J. Lu, B. Ma, X. Qiu, Z. Sun, and K. Xiong, “Effects of resistant starch supplementation on oxidative stress and inflammation biomarkers: a systematic review and meta-analysis of randomized controlled trials,” *Asia Pacific Journal of Clinical Nutrition*, vol. 30, no. 4, pp. 614–623, 2021.
  - [30] R. De la Puerta, E. Martinez-Dominguez, and V. Ruiz-Gutierrez, “Effect of minor components of virgin olive oil on topical antiinflammatory assays,” *Zeitschrift für Naturforschung. Section C*, vol. 55, no. 9–10, pp. 814–819, 2000.
  - [31] T. Hioki, H. Tokuda, G. Kuroyanagi et al., “Olive polyphenols attenuate TNF- $\alpha$ -stimulated M-CSF and IL-6 synthesis in osteoblasts: suppression of Akt and p44/p42 MAP kinase signaling pathways,” *Biomedicine & Pharmacotherapy*, vol. 141, p. 111816, 2021.
  - [32] O. N. Austah, K. V. Lillis, A. N. Akopian, S. E. Harris, R. Grinceviciute, and A. Diogenes, “Trigeminal neurons control immune-bone cell interaction and metabolism in apical periodontitis,” *Cellular and Molecular Life Sciences*, vol. 79, no. 6, p. 330, 2022.
  - [33] K.-Y. Chin and S. Ima-Nirwana, “Olives and bone: a green osteoporosis prevention option,” *International Journal of Environmental Research and Public Health*, vol. 13, no. 8, p. 755, 2016.
  - [34] J. M. Lean, J. T. Davies, K. Fuller et al., “A crucial role for thiol antioxidants in estrogen-deficiency bone loss,” *The Journal of Clinical Investigation*, vol. 112, no. 6, pp. 915–923, 2003.
  - [35] O. García-Martínez, E. De Luna-Bertos, J. Ramos-Torrecillas et al., “Phenolic compounds in extra virgin olive oil stimulate human osteoblastic cell proliferation,” *PLoS One*, vol. 11, no. 3, article e0150045, 2016.

- [36] H. Tao, W. Li, W. Zhang et al., “Urolithin A suppresses RANKL-induced osteoclastogenesis and postmenopausal osteoporosis by, suppresses inflammation and downstream NF- $\kappa$ B activated pyroptosis pathways,” *Pharmacological Research*, vol. 174, p. 105967, 2021.
- [37] H. Dounia, M. Laetitia, P. B. Antoine et al., “An anti-RANKL treatment reduces muscle inflammation and dysfunction and strengthens bone in dystrophic mice,” *Human Molecular Genetics*, vol. 28, no. 18, pp. 3101–3112, 2019.

## Research Article

# Design of Association Application System of Face Recognition and Test-Tube Barcode Based on CNN

Zhangning Zhou,<sup>1,2</sup> He Shi,<sup>3</sup> and Xuemin Niu<sup>2,4</sup> 

<sup>1</sup>General Practice Department, Huzhou Central Hospital, Huzhou 313003, China

<sup>2</sup>Affiliated Central Hospital Huzhou University, Huzhou 313000, China

<sup>3</sup>Zhejiang Health Technology Co., Ltd., Hangzhou 311100, China

<sup>4</sup>Clinical Laboratory, Huzhou Central Hospital, Huzhou 313003, China

Correspondence should be addressed to Xuemin Niu; 60525@zjhu.edu.cn

Received 16 June 2022; Revised 18 July 2022; Accepted 29 July 2022; Published 24 August 2022

Academic Editor: Hangjun Che

Copyright © 2022 Zhangning Zhou et al. This is an open access article distributed under the Creative Commons Attribution License, which permits unrestricted use, distribution, and reproduction in any medium, provided the original work is properly cited.

In order to improve the standardization and accuracy of business process management of laboratory department in hospitals, combined with convolutional neural networks (CNN) and face recognition technology, an association application system of laboratory face recognition and test-tube barcode is designed by inputting patient's face and blood test-tube barcode into the system for storage. When the patient logs into the system again, the system uses the patient's face to automatically search for a matching test-tube barcode to obtain the test results. The simulation results show that the system can accurately recognize the face and match the corresponding test-tube barcode, and the accuracy and ROC of face recognition are 0.85 and 0.94, respectively. In addition, when the patient's face is within 5 m from the system camera, the accuracy of face recognition can reach 100%. It can be seen that the system designed in this paper shows good performance.

## 1. Introduction

With the continuous development of computer vision and image processing technology, face recognition technology began to be applied to many fields, and it gradually becomes a hot topic. At present, many technologies are applied to face recognition, such as Haar feature matching and BP neural network [1–14]. These technologies play an important role in face recognition and detection. In specific studies, Ghazal and Ghazal proposed the Fisherface algorithm, which has attracted more attention [15]. In addition to this method, Abratenko et al. designed Haar-like, which has also achieved certain effects in face recognition scenes [10]. With the application of face recognition in various fields, how to apply it to the medical field has become a hotspot of current research. For example, Lyanpen and others applied face recognition to patient admission management, which greatly saved the time of admission [16]; Mamata and Ninad combined face recognition with voice assistance to help patients call nursing services [17]; Jenifa et al. applied face recogni-

tion to patients' expression evaluation, which can assist in the evaluation of patients' emotions [18]. However, it has been found in practice that the application of face recognition technology in medical institutions is increasing, but there are not many studies on the application of bar codes in laboratory departments. Therefore, it is necessary to strengthen the research in this field. It is hoped that through this application, the obstacle between face recognition and test results can be broken through, so that patients can obtain the report results only through the face instead of through the conventional QR code. This is the problem that has not been solved or is trying to be solved in the previous research. With the help of such new technology, the business process of the laboratory can be simplified, so as to improve efficiency and gradually realize the goal of paperless office.

## 2. Face Target Detection Based on SSD

The SSD algorithm is used to realize face detection. The core part of the algorithm is the anchor mechanism, which takes



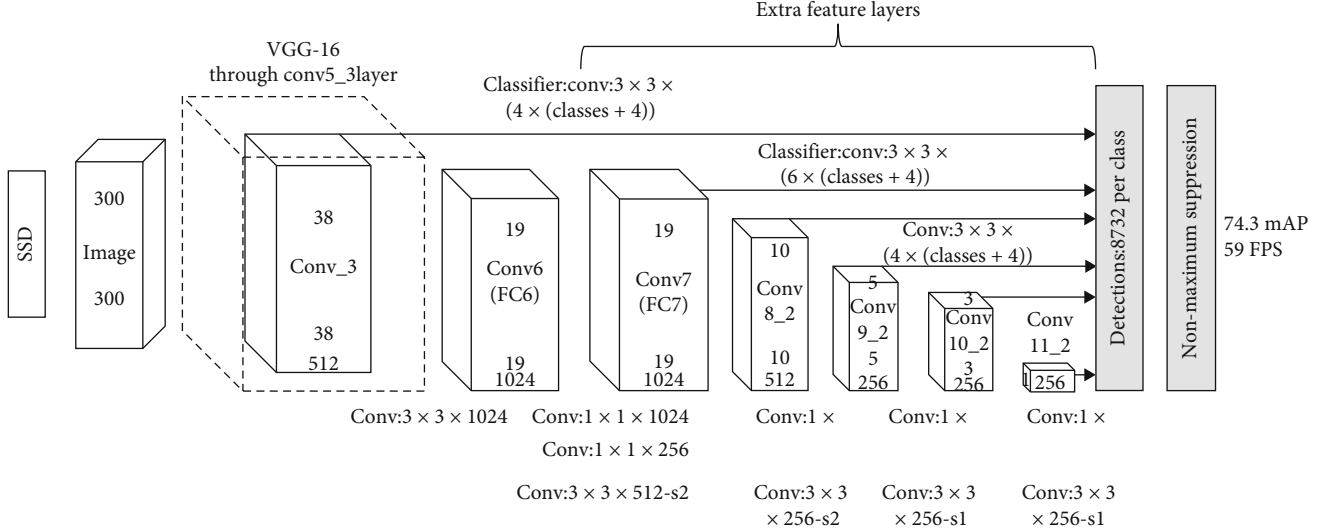


FIGURE 1: Principle of the SSD model.

each point as the center point of candidate area and makes regression for location and target category. Moreover, the multiscale feature map is utilized in the detection process, which is helpful to improve the accuracy of detection results. In general, this algorithm belongs to a method based on deep learning, in which there is no need to extract candidate box, the operation is relatively simple, and the application prospect is broad. However, the SSD algorithm also faces some challenges in application, especially for different fields, its requirements for image detection and recognition are different, and its image processing is also different. This research is mainly aimed at patients' face recognition. In the image detection method, the requirement for accuracy is higher. Therefore, in this article, how to use the SSD algorithm to accurately identify patients is an important challenge. SSD is chosen because it is a new convolutional neural network face detection framework. Its face detection mechanism is different from the network using candidate frame mechanism. Different convolution layers of convolution neural network have different receptive fields and different feature dimensions. The receptive fields of shallow neurons are small, the output feature map is large, the receptive fields of deep neurons are large, and the output feature map is small. Therefore, in the SSD convolution network, different levels of feature maps are not only used as the input of the lower convolution layer to extract features but also as the input of the detection and prediction network to output the face category score and accurately locate the face. The basic principle of the algorithm is shown in Figure 1 [19–22].

As can be seen from Figure 1, this algorithm model can be divided into several parts, among which the initial part is VGG16, the backbone networks are VGGNet, Inception, etc. Conv4\_3 and Conv6 are all convolution layers. Then, the full connection layer is FC6, and FC7 is converted into the convolution layer. In addition, the recognition layer is after Conv7, which requires continuous downsampling until (1×1). The structure and function of each layer

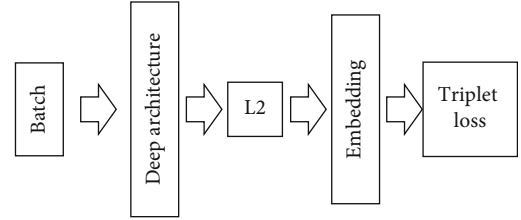


FIGURE 2: FaceNet network structure.

are different. There is a special classifier layer in Conv4\_3 layer, through which feature map can be extracted. This convolution layer also exists in other layers, such as Conv8\_2 and Conv11\_2. The corresponding feature map can also be extracted.

The extracted feature map is input into the detection layer to obtain location and category information. During this process, default boxes need to be defined to obtain the target offset and category score.

The basic form of loss function is as follows [23–25]:

$$L(x, c, l, g) = \frac{1}{N} (L_{\text{conf}}(x, c) + \alpha L_{\text{loc}}(x, l, g)), \quad (1)$$

where  $L_{\text{loc}}$  and  $L_{\text{conf}}$  are regression and classification loss functions, respectively, and smooth and softmax functions are used for them, respectively.  $N$  is the number of positive samples in the prediction box,  $c$  is the category confidence prediction value,  $l$  is the position prediction value corresponding to the prediction box,  $g$  is the position marked by GT, and  $\alpha$  is the weight coefficient of position loss and confidence loss.

In this design, the backbone network is ResNet, and feature learning can be carried out in combination with feature map. However, in order to obtain high-precision detection results, it is generally necessary to use multiple feature maps. For the SSD algorithm, six feature maps can meet the requirements of detection.

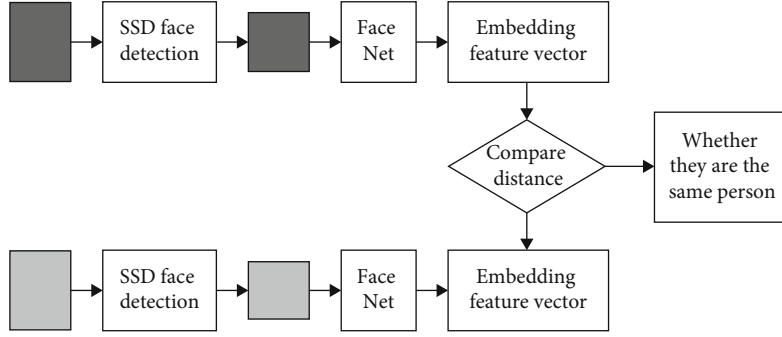


FIGURE 3: FaceNet recognition.

### 3. Face Recognition Based on FaceNet

The FaceNet algorithm is used to map images to the multi-dimensional space, and the similarity of face is calculated and compared. Specifically, face similarity needs to be quantitatively compared according to the size of the spatial distance; that is, the image of a person is generally small in the spatial distance, and the image between different  $g$  individuals will maintain a high spatial distance. In this way, the detection of the face can be realized, and then the identity of the person is determined.

For the FaceNet algorithm, triplet loss function and image mapping method are adopted in the training process, so as to obtain the corresponding vector space. The specific network structure is shown in Figure 2 [26–28].

As can be seen from Figure 2, batch represents training data, which includes more triples. Then, the process of feature extraction is carried out, and the image transformation and normalization operations are successively carried out; thus, vector embedding can be obtained. Then, it is input into the triplet loss function. On the basis of obtained feedback, the update of embedding is achieved. After completing training, the triplet loss is transformed, and the similarity measurement results are obtained through extracting embedding and calculating Euclidian distance.

In the last part of the FaceNet model, triplet loss function is required to complete the training process, in which the input feature vectors are negative feature vector, positive feature vector, and anchor feature vector. Feature vectors 1 and 3 belong to the different type of samples. Feature vectors 2 and 3 belong to the same type of samples, which needs to perform feature optimization, so as to ensure that the different type of samples can keep a large distance, while the same type of samples has a small distance. Triplet loss is shown as follows:

$$\|f(x_i^a) - f(x_i^p)\|_2^2 + \alpha < \|f(x_i^a) - f(x_i^n)\|_2^2, \quad (2)$$

where  $f(x_i^p)$  and  $f(x_i^n)$  represent the different or same types of sample pairs,  $f(x_i^a)$  stands for anchor vector, and  $\alpha$  stands for interval, which is used to adjust the sample distance.

The basic form of loss function is as follows:

$$L_i = \sum_i^N \left[ \|f(x_i^a) - f(x_i^p)\|_2^2 + \|f(x_i^a) - f(x_i^n)\|_2^2 + \alpha \right], \quad (3)$$

where  $N$  represents the number of sample pairs. Based on this function, sample similarity can be measured, and Euclidean distance is generally adopted in the specific calculation.  $L_i$  represents the triplet loss function.

The basic flow of the FaceNet algorithm is shown in Figure 3.

As can be seen from Figure 3, SSD face recognition is divided into two parts. One part is to train the pictures to obtain the trained SSD network, and then the trained network is used to test the pictures, which are compared with the correct face features, so as to judge whether they are the same person. Finally, the purpose of face recognition is achieved.

### 4. Business System Construction of Laboratory Department Based on Face Recognition

**4.1. Design of Overall System Architecture.** The purpose of this paper is to try to apply face recognition to the business of laboratory departments, so that patients can log in system to query test reports through face. Therefore, based on this particular scenario, and combined with the specific business of the laboratory department, the system is divided into several parts, including the client, server, and database part, in which detailed analysis and design are made for each part. The specific architecture is shown in Figure 4.

In Figure 4, http protocol is used for communication between the server and the client. When the client needs to obtain resources from the server, get method can be adopted, and when the client transfers resources to the server, post method can be adopted.

**4.2. Construction of System Network Architecture.** The overall network architecture of system is shown in Figure 5.

In the overall architecture, each system of the hospital is included, which is connected through a unified network, so as to obtain various data of the hospital system and finally achieve the purpose of data sharing of the whole hospital.

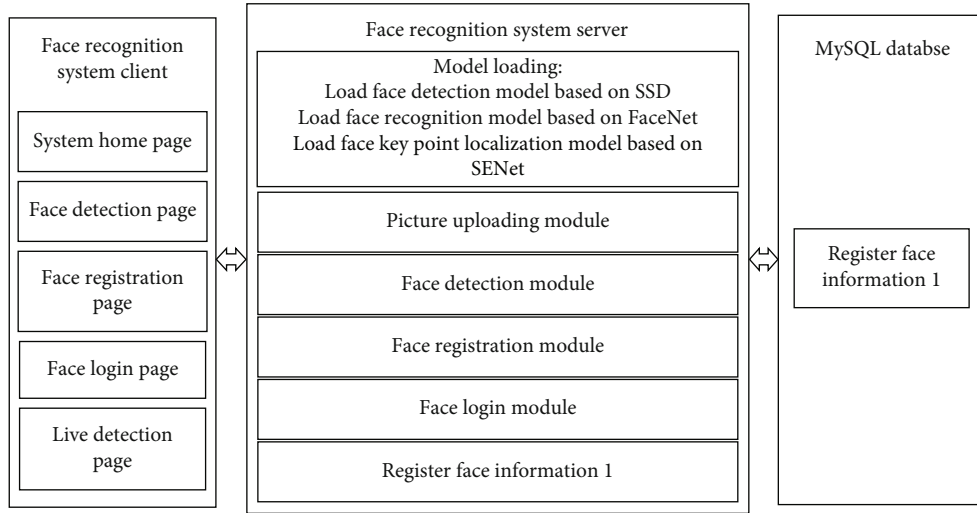


FIGURE 4: Design of overall system architecture.

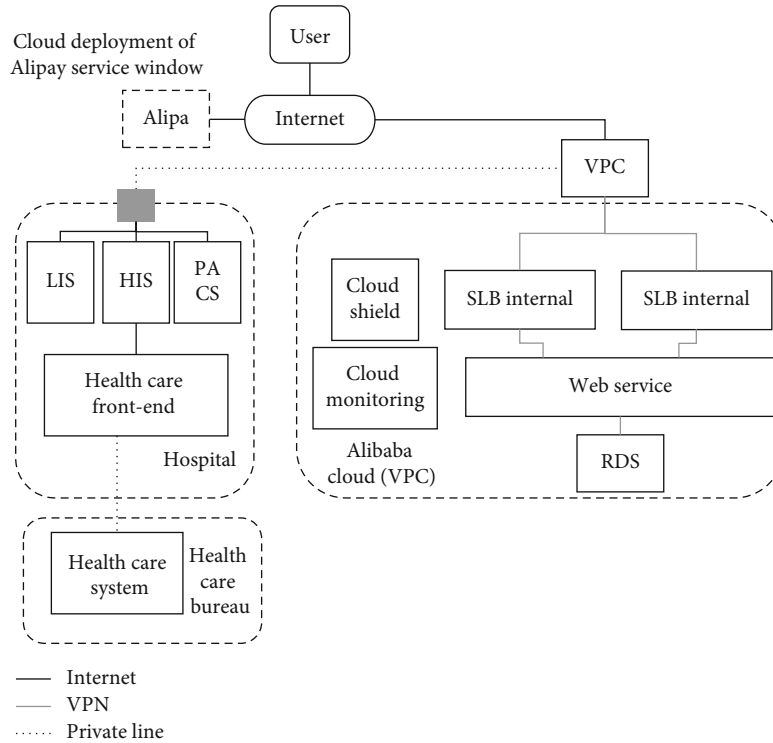


FIGURE 5: Overall architecture of the system.

In other words, face recognition can not only realize the query of report results of inspection department but also lay the foundation for other queries and applications.

#### 4.3. Process of Some Functions of the System

**4.3.1. Face Swiping Detection Process.** The face swiping detection process is shown in Figure 6.

When patients are collecting specimens, they are verified by the face recognition system in the cloud, and the face features are compared with the comparison source

through the background. After verification, the results are returned.

**4.3.2. Process of “Face Recognition+Preplacement Bar Code.”** The identification process is shown in Figure 7.

The detailed steps in Figure 7 are as follows:

- (a) Firstly, carry out the user identity authentication process. In the specimen collection process, set the mode of “face swiping” and then select the face

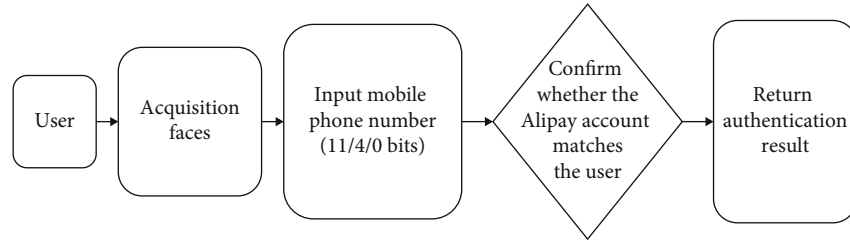


FIGURE 6: Face swiping detection process.

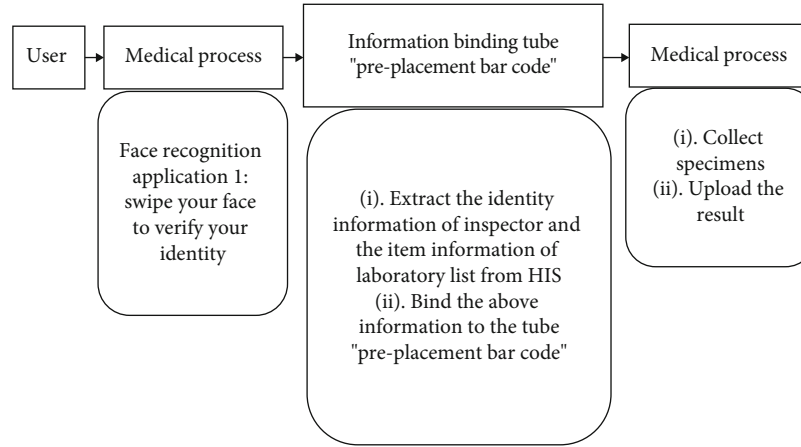


FIGURE 7: Process of “face recognition+pre-placement bar code.”

meeting the requirements to realize the identity authentication

- (b) Secondly, set the mode of bar code and check the label of preplacement bar code of disposable vacuum tube using the equipment provided by the manufacturer
- (c) Moreover, select Confirm key. The user's information can be extracted from HIS, and it can be associated with the “pre-placement bar code” test tube
- (d) Finally, upload the obtained results by inspectors

**4.3.3. Process of Printing Report by Swiping Face.** The process is shown in Figure 8.

As can be seen from the figure, users need to swipe their faces through the self-service machine first and then compare the collected face images. After verifying the user's identity, the corresponding laboratory sheet is queried, and it can be printed out.

## 5. Method and System Verification

### 5.1. Face Detection and Verification Based on SSD

**5.1.1. Data Processing of WIDER FACE.** The data set of this study is the public wide face dataset. WIDER FACE dataset is utilized to test the designed SSD model, which has rich face samples and is widely used in face recognition and detection [21–25], where it contains a total of 32,203 face

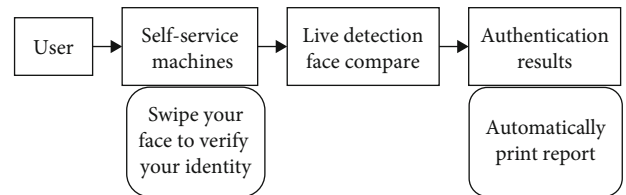


FIGURE 8: Process of printing report by swiping face.

images under different conditions such as illumination, occlusion, and scale. This data set is actually extracted from 61 event category videos, which are extracted and divided according to each event category. Thus, there are three parts obtained, which are, respectively, used for training, testing, and crossverification, and the ratio of the three part is 4:5:1. Partial images of this dataset are shown in Figure 9.

The first is to convert the format of this dataset; thus, PASCAL VOC format is obtained. After the conversion, three directories, namely, annotations, image sets, and JPEG images, are obtained. The information stored in each directory has certain differences, namely, picture interpretation, image collection, and picture.

**5.1.2. Face Detection Model Training Based on SSD.** TensorFlow is mainly used for training. After the completion of model construction, the code is adjusted according to the requirements of face detection, and then the training process



FIGURE 9: Partial images in WIDER FACE dataset.

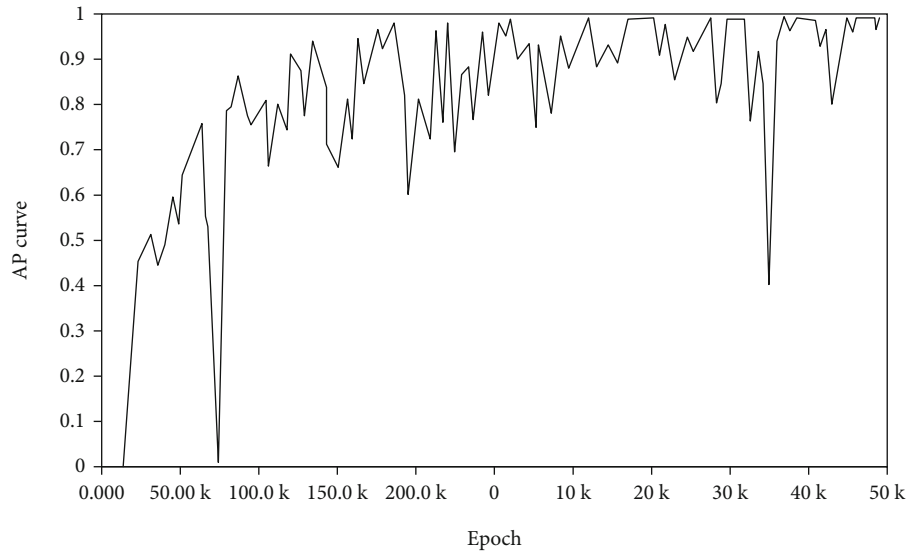


FIGURE 10: AP curve of target detection.

is completed by invoking the relevant interface according to the data set.

After the preprocessing, test.txt and train.txt can be generated, and data sets in PASCAL VOC format are obtained. The create\_pascal\_tf\_Record.py file is then packaged to obtain the TFRecord format and the corresponding file. The specific packaging information involves path, file name, and image size information. Once the information is packed, training can be carried out.

In the training process, the SSD algorithm is mainly adopted, and the model\_main.py file is directly utilized in this process, which is located in the source code of the SSD algorithm. After modifying the configuration file and relevant parameters, all can be used in the process of model training.

TensorFlow is used in this experiment. The configuration files of the SSD algorithm model are all located in configs in the sample directory. However, face detection cannot be performed directly in general, so it needs to be modified appropriately, where `ssd_resnet50_v1_fpn_`



FIGURE 11: Target detection results of SSD.

`shared_box_predictor_640×640_COCO14_sync.config` is modified as follows:

Here, train.record and test.record are used as training data and test data, respectively. The parameters are set reasonably; that is, `image_resizer` is `256*256`, `numclass` = 1,



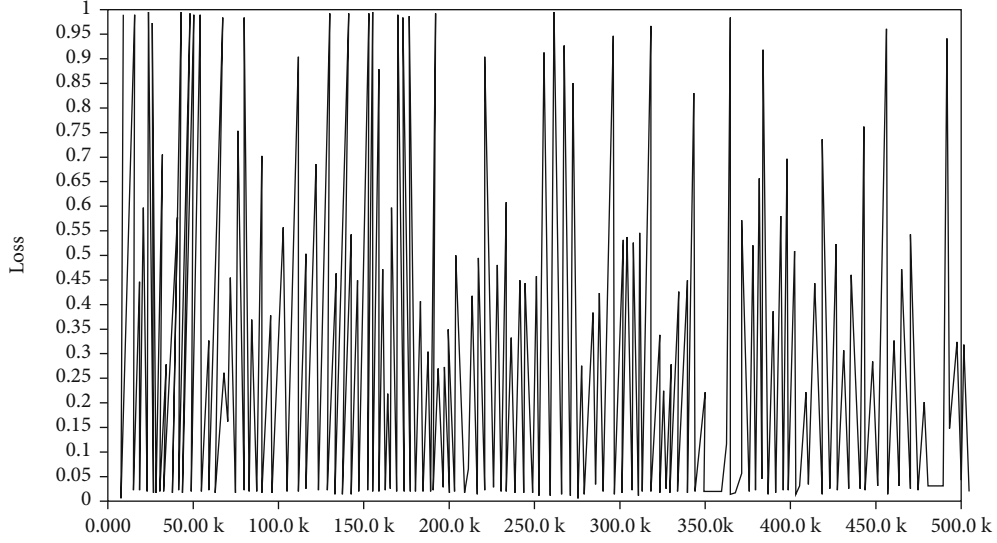


FIGURE 12: Loss diagram of training set WebFace.

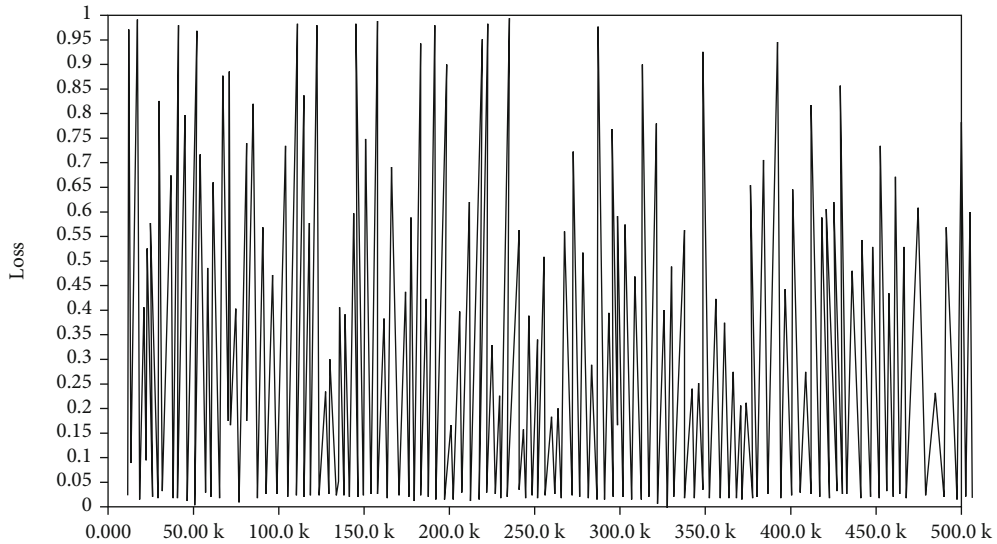


FIGURE 13: Loss diagram of training set CelebA.

batch\_size = 24, and num\_steps = 100000. In addition, sigmoid and smooth functions are used for classification and regression loss, respectively.

After the configuration file is set, the Python script program is executed in the terminal, and the name of file is model\_main.py. And then the relevant interface is called for metatraining, and the formed information is displayed in the terminal. The AP curve of detection is shown in the following Figure 10.

AP values can be obtained, including three IoU ratios, namely, small, medium, and large. Among them, the AP values of large, medium, and small targets are different, which are 0.626, 0.28, 7 and 0.038, respectively.

The training set used in the experiment includes CelebA, CASIA-facev5, and CASIA-WebFace, while the test set is LFW dataset.

**5.1.3. Model Test.** Test the trained model, restore graph in combination with the obtained model file, and then perform the forward calculation process. In addition to this method, graph of the model can be restored first, and then pb files containing network structure and parameters can be generated. On this basis, forward calculation can be performed. The advantage of this method is high efficiency and convenient for system design and testing.

In TensorFlow, the integrated export\_inference\_graph.py file is used to convert graph to pb files. This file can be called directly from the terminal, and then the conversion can be achieved; thus, the corresponding pb file is obtained. However, the obtained model file at this time cannot be used directly, in which parameters need to be adjusted, and the specific parameter setting is shown as follows: the input\_type needs to be set to image\_tensor.

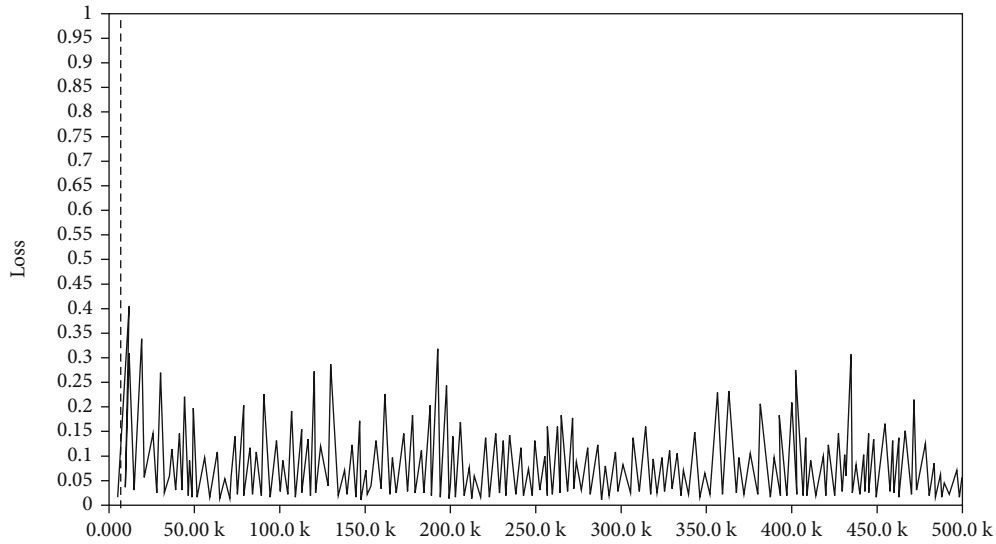


FIGURE 14: Loss diagram of training set WebFace-CelebA.

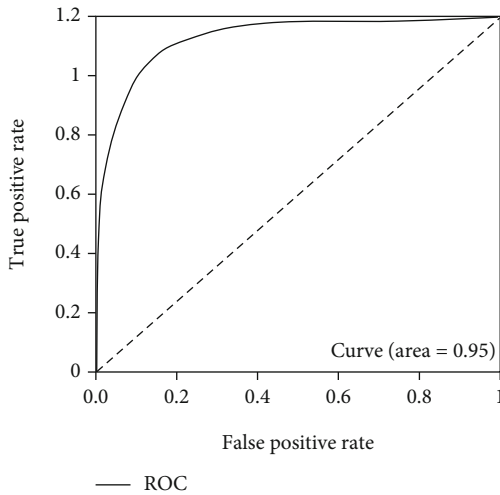


FIGURE 15: ROC diagram of training set WebFace.

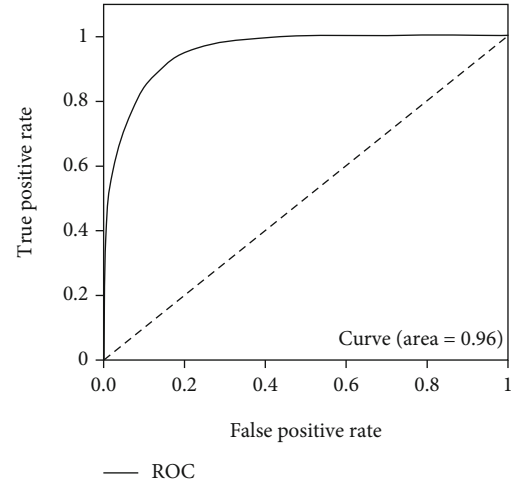


FIGURE 16: ROC diagram of training set CelebA.

Then, add the path of `ssd_resnet50_v1_fpn_shared_box_predictor_640640_coco14_sync_face.config` to this file. After all the information is modified and verified correctly, `export_inference_graph.py` can be called at the terminal. After parameters such as pb file name and storage path are set well, the corresponding `face_detection_model.pb` file can be obtained.

It can be seen that a `test_model.py` script is written to call the previously generated `face_detection_model.pb` file. After the test set data is input, face detection is carried out, and the detected faces are marked, including certain differences in posture, skin color, and other aspects of a variety of face images.

The final processed results are shown in the following Figure 11.

As can be seen from the test results, the model achieves good results in face detection, realizing multiface detection. In addition to the detection of the positive face, the side

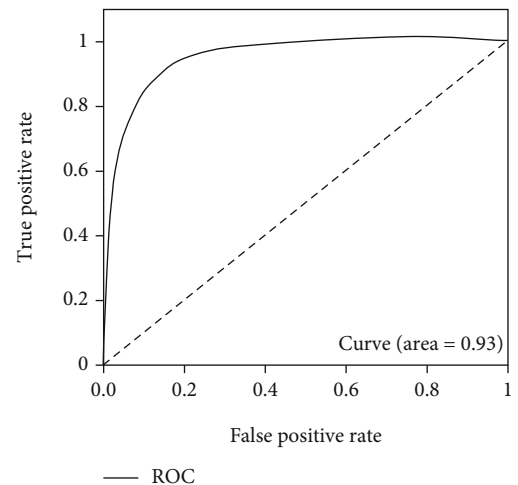


FIGURE 17: ROC diagram of training set WebFace-CelebA.

TABLE 1: Test table of face detection.

Test project	Distance < 5 m (front face)	5 m < distance < 10 m (front face)	Front face (distance < 5 m)	Side face (distance < 5 m)
Detection rate	100%	86.7%	100%	100%
Average time	398 ms	473 ms	395 ms	414 ms

and each color of the face can be effectively detected, which has high robustness and is suitable for the design of actual face detection function.

## 5.2. Face Recognition Model Training Based on FaceNet

**5.2.1. Data Set Preprocessing.** It is necessary to use appropriate data sets during algorithm testing. In this study, multiple data sets are selected, including CelebA, CASIA-faceV5, CASIA-WebFace, and LFW data sets, so as to verify the validity of FaceNet algorithm.

**5.2.2. Face Recognition Model Training Based on FaceNet.** The train\_tripletloss.py script file can be directly used during training, which is located in the FaceNet source code. This file needs to be adjusted according to the requirements of specific applications. Here, epoch\_size, batch\_size, and max\_nrof\_epochs are set to 1000, 30, and 500, respectively. At the same time, adjust\_brightness and adjust\_contrast methods need to be added to improve the robustness of the model. After the modification is complete, enter the four data sets described previously for training.

In the training, the data sets are combined appropriately to verify the training effect of using different data sets, so as to determine the optimal model. Firstly, CelebA\_160 and CASIA-WebFace\_160 are merged into a new dataset Web-face-CelebA\_160. Then, start the training process and input the merged data sets and the previous three data sets, respectively, for training. Thus, four models can be obtained. Then, input test set and verify the application effect of each model, and on this basis, it can determine the optimal model. The loss diagram in training is shown as following Figures 12–14.

Through the comparison of loss functions in Figures 12–14, it can be seen that in the identification of FaceNet, the value of loss function in the combined data set is the smallest, indicating that FaceNet is more suitable for the mixed picture data sets.

**5.2.3. Model Test.** In this test process, the validate\_on\_lfw.py file is used, and it is also located in the FaceNet source code. The test set is LFW, from which 6000 sample pairs are extracted, specifically divided into positive and negative sample pairs, and the number of the two is 5700 and 300, respectively. Tests are carried out for each training model, and the difference of each model is clarified through ROC diagram analysis. The ROC curve is drawn according to FPR and TPR, while FPR and TPR are calculated as follows [26–28]:

$$\text{FPR} = \frac{\text{FP}}{\text{FP} + \text{TN}}, \quad (4)$$

TABLE 2: Face recognition test table.

Tester	No. 1 (registered)	No. 2 (registered)	No. 3 (unregistered)
Login success rate	100%	100%	0%
Average time	623 ms	618 ms	0 ms

$$\text{TPR} = \frac{\text{TP}}{\text{TP} + \text{FN}}. \quad (5)$$

Thus, the optimal model is determined, and the final test results are shown as following Figures 15–17.

As can be seen, the test result accuracy of the model trained by CelebA and CASIA-WebFace data set is high, where accuracy and ROC are higher than 0.85 and 0.94, respectively. In addition, after the training set is merged, the obtained model also can achieve good results in the test, and its accuracy is basically consistent with CelebA and CASIA-WebFace. The model trained based on this data set can be used for face recognition, and it has higher robustness. Therefore, this model is finally selected in this paper.

## 5.3. System Test

**5.3.1. Function Test of Face Detection.** Tests are carried out under normal lighting conditions to detect the effect of face recognition. During the experiment, face posture and test distance are adjusted to analyze whether the detection effect can be achieved.

There are three testers, all of whom need to be tested 60 times, namely, 15 times for the front and side faces, 15 times for the test distance between 5 m and 10 m, and below 5 m. After the setup is completed, the test is carried out, and the final results are shown in Table 1.

**5.3.2. Function Test of Face Recognition.** Face recognition is divided into two parts, namely, registration part and login part. During the test, face images are collected from the front, and the distance from the camera is within 5 m. The test is carried out under normal lighting conditions, so as to verify the effect of face recognition and the login time.

There are three testers. Both tester 1 and tester 2 need to register. After registration, the login test will be conducted. Tester 3 performs the login test directly without registration and records the test results. The specific information is shown in the following Table 2.

## 6. Conclusion

In conclusion, the application of face recognition in the laboratory department can effectively improve the recognition accuracy of patients. Through the deep learning algorithm,

the recognition accuracy can reach 100% within a distance of less than 5 m, which shows that the application of the deep learning algorithm to the QR code association system of the inspection department has a certain accuracy. At the same time, the identification system can effectively establish the relationship between patients and test results in the test department, so as to greatly improve the information and intelligence level of test department. The innovation of this study is to apply face recognition to the QR code recognition of the laboratory department, so as to connect the patients with the test results of the laboratory department, so that the patients can query the results through face recognition.

However, the focus of this study is only to apply deep learning to face recognition and test tube bar code association system. The main direction of next step of this research should be how to apply deep learning to query the test results.

## Data Availability

The experimental data used to support the findings of this study are available from the corresponding author upon request.

## Conflicts of Interest

The authors declared that they have no conflicts of interest regarding this work.

## Acknowledgments

This work is supported by the Medical and Health Science and Technology Program Fund of Zhejiang Province, China: Project Name "Design of face recognition combined with bar code technology in laboratory information system" (2020PY070).

## References


- [1] X. Wang, X. Kuang, J. Li, J. Li, X. Chen, and Z. Liu, "Oblivious transfer for privacy-preserving in VANET's feature matching," *IEEE Transactions on Intelligent Transportation Systems*, vol. 22, no. 7, pp. 1–8, 2020.
- [2] T. Mahmood, M. Shah, J. Rashid, T. Saba, M. W. Nisar, and M. Asif, "A passive technique for detecting copy-move forgeries by image feature matching," *Multimedia Tools and Applications*, vol. 79, no. 43–44, pp. 31759–31782, 2020.
- [3] MHuang Xu and Wan Xue and Peng Daifeng, "Robust feature matching with spatial smoothness constraints," *Remote Sensing*, vol. 12, no. 19, pp. 3158–3158, 2020.
- [4] S. Chen, L. Liang, J. Ouyang, and Y. Yuan, "Accurate 3D motion tracking by combining image alignment and feature matching," *Multimedia Tools and Applications*, vol. 79, no. 29–30, pp. 21325–21343, 2020.
- [5] Y. Du, Z. Weng, C. Liu, and D. Wu, "Dynamic pavement distress image stitching based on fine-grained feature matching," *Journal of Advanced Transportation*, vol. 2020, Article ID 5804835, 15 pages, 2020.
- [6] MXin Wang and He Pan, "Multi-view face recognition based on BP neural network and KPCA," *Advanced Materials Research*, vol. 1030, pp. 1737–1740, 2014.
- [7] "Robust feature matching using guided local outlier factor," *Pattern Recognition*, vol. 117, p. 107986, 2021.
- [8] MChao Zhang and Na Song and Yudun Li, "Incipient fault identification of distribution networks based on feature matching of power disturbance data," *Electrical Engineering*, vol. 103, no. 5, pp. 2447–2457, 2021.
- [9] L. Guo, T. Wang, Z. Wu et al., "Portable food-freshness prediction platform based on colorimetric barcode combinatorics and deep convolutional neural networks," *Advanced Materials*, vol. 32, no. 45, p. 2004805, 2020.
- [10] P. Abratenko, M. Alrashed, R. An et al., "Convolutional neural network for multiple particle identification in the Micro-BooNE liquid argon time projection chamber," *Physical Review D*, vol. 103, no. 9, article 092003, 2021.
- [11] Z. Khodaverdian, H. Sadr, and S. A. Edalatpanah, "A shallow deep neural network for selection of migration candidate virtual machines to reduce energy consumption," in *2021 7th International Conference on Web Research (ICWR)*, pp. 191–196, Tehran, Iran, 2021.
- [12] X. Lu, W. Liao, W. Huang, Y. Xu, and X. Chen, "An improved linear quadratic regulator control method through convolutional neural network-based vibration identification," *Journal of Vibration and Control*, vol. 27, no. 7–8, pp. 839–853, 2021.
- [13] Z. Khodaverdian, H. Sadr, S. A. Edalatpanah, and M. N. Solimandarabi, "Combination of convolutional neural network and gated recurrent unit for energy aware resource allocation," 2021, <http://arXiv:2106.12178>.
- [14] A. Panda and S. Muniz, "Smart home with neural network based object detection," *Big Data and Computing Visions*, vol. 2, no. 1, pp. 40–48, 2022.
- [15] M. T. Ghazal and K. Abdullah, "Face recognition based on curvelets, invariant moments features and SVM," *TELKOMNIKA (Telecommunication Computing Electronics and Control)*, vol. 18, no. 2, pp. 733–733, 2020.
- [16] W. Lyanpen, O. G. Petrosyan, and D. Jianming, "Face recognition based on the coefficient tree for three scale wavelet transformation," *Automatic Control and Computer Sciences*, vol. 53, no. 8, pp. 995–1005, 2019.
- [17] P. Mamata and M. Ninad, "Face recognition-based automatic hospital admission with SMS alerts," *Science*, vol. 2, no. 2, 2021.
- [18] G. Jenifa, N. Yuvaraj, B. Karthikeyan, and K. R. S. Preethaa, "Deep learning based voice assistance in hospitals using face recognition," *Journal of Physics: Conference Series*, vol. 1916, no. 1, p. 012159, 2021.
- [19] L. Chen, X. M. Me, N. Zhu et al., "Facial expression recognition with machine learning and assessment of distress in patients with cancer," *Oncology Nursing Forum*, vol. 48, no. 1, pp. 81–93, 2021.
- [20] W. Wang, M. He, X. Wang, and W. Yao, "Sewing gesture image detection method based on improved SSD model," *Electronics Letters*, vol. 57, no. 8, pp. 321–323, 2021.
- [21] J. Yang, W. Y. He, T. L. Zhang, C. L. Zhang, L. Zeng, and B. F. Nan, "Research on subway pedestrian detection algorithms based on SSD model," *IET Intelligent Transport Systems*, vol. 14, no. 11, pp. 1491–1496, 2020.
- [22] G. Yu, H. Fan, H. Zhou, T. Wu, and H. Zhu, "Vehicle target detection method based on improved SSD model,"

- Journal on Artificial Intelligence*, vol. 2, no. 3, pp. 125–135, 2020.
- [23] L. Lv and Y. Tan, “Detection of cabinet in equipment floor based on AlexNet and SSD model,” *The Journal of Engineering*, vol. 2019, no. 15, pp. 605–608, 2019.
  - [24] T. Zhao, J. Liu, S. Dian, R. Guo, and S. Li, “Sliding-mode-control-theory-based adaptive general type-2 fuzzy neural network control for power-line inspection robots,” *Neuro-computing*, vol. 401, no. preublish, pp. 281–294, 2020.
  - [25] C. Shen, X. Pan, X. Wu, J. Xu, F. Dong, and Y. Zheng, “Ecological risk assessment for difenoconazole in aquatic ecosystems using a web-based interspecies correlation estimation (ICE)-species sensitivity distribution (SSD) model,” *Chemosphere*, vol. 289, pp. 133236–133236, 2022.
  - [26] S. Liu, M. Zhang, M. Fang, J. Zhao, K. Hou, and C. C. Hung, “Speech emotion recognition based on transfer learning from the FaceNet framework,” *The Journal of the Acoustical Society of America*, vol. 149, no. 2, pp. 1338–1345, 2021.
  - [27] W. Chunming and Y. Zhang, “MTCNN and FACENET based access control system for face detection and recognition,” *Automatic Control and Computer Sciences*, vol. 55, no. 1, pp. 102–112, 2021.
  - [28] Z. Ying, Y. AiPing, and X. DanTong, “Person recognition based on FaceNet under simulated prosthetic vision,” *Journal of Physics: Conference Series*, vol. 1437, no. 1, pp. 12012–12012, 2020.



## Research Article

# A Cohort Study of the Effects of Integrated Medical and Nursing Rounds Combined with AIDET Communication Mode on Recovery and Quality of Life in Patients Undergoing Percutaneous Coronary Intervention

Lan Li,<sup>1</sup> Yongheng Li,<sup>2</sup> Tao Yin,<sup>2</sup> Jinglin Chen,<sup>3</sup> and Fengjiao Shi <sup>1</sup>

<sup>1</sup>Department of Cardiovascular Medicine II, The Fourth Hospital of Changsha City, No. 70 Lushan South Road, Yuelu District, Changsha City, Hunan Province, China 410006

<sup>2</sup>Nursing Department, The Fourth Hospital of Changsha City, No. 70 Lushan South Road, Yuelu District, Changsha City, Hunan Province, China 410006

<sup>3</sup>Respiratory Medicine Ward II, The Fourth Hospital of Changsha City, No. 70 Lushan South Road, Yuelu District, Changsha City, Hunan Province, China 410006

Correspondence should be addressed to Fengjiao Shi; 631607010621@mails.cqjtu.edu.cn

Received 21 June 2022; Accepted 28 July 2022; Published 24 August 2022

Academic Editor: Hangjun Che

Copyright © 2022 Lan Li et al. This is an open access article distributed under the Creative Commons Attribution License, which permits unrestricted use, distribution, and reproduction in any medium, provided the original work is properly cited.

**Objective.** To explore the influence of the communication mode of “Acknowledge, Introduce, Duration, Explanation, and Thanks (AIDET)” on the postoperative recovery and quality of life of patients undergoing percutaneous coronary intervention. **Methods.** Sixty patients with percutaneous coronary intervention in our hospital from April 2019 to April 2021 were selected. The patients were randomly divided into a control group ( $n = 30$ ) and research group ( $n = 30$ ). The control group received integrated medical and nursing rounds, and the research group received integrated medical and nursing rounds combined with AIDET communication mode. The scores of nursing satisfaction, cardiac function, self-nursing ability, short-term prognosis, and quality of life were compared between the two groups. **Results.** In the comparison of nursing satisfaction between the two groups, the satisfaction of the research group was low in 1 case, moderate in 6 cases, and high in 27 cases, with a satisfaction rate of 96.67%. In the control group, there were 7 cases with low satisfaction, 10 cases with moderate satisfaction, and 13 cases with high satisfaction, with a satisfaction rate of 76.67%. The nursing satisfaction of the research group was higher than that of the control group, and the difference was statistically significant, and the difference was statistically significant ( $P < 0.05$ ). After intervention, the cardiac function of the two groups was improved. The LVEF and LVESVI of the research group were higher than those of the control group, while the WMSI of the research group was lower than that of the control group ( $P < 0.05$ ). In the comparison of self-nursing ability, the self-nursing maintenance, self-nursing management, self-nursing confidence, and total score of self-nursing in the research group were significantly higher than those in the control group, and the difference was statistically significant ( $P < 0.05$ ). The incidence rates of acute myocardial infarction (AMI), revascularization, arrhythmia, heart failure, cardiogenic shock, and cardiac death in the research group were obviously lower than those in the control group, and the difference was statistically significant ( $P < 0.05$ ). After intervention, the scores of quality of life of the two groups decreased, and the scores of physiological function, psychological function, social function, and health self-cognition in the research group were lower than those in the control group ( $P < 0.05$ ). **Conclusion.** Medical and nursing integrated ward rounds combined with AIDET communication mode can effectively improve the prognosis of patients undergoing percutaneous coronary intervention to promote the establishment of a harmonious nurse-patient relationship. The patients’ self-care ability is able to be effectively enhanced.

## 1. Introduction

With the development of economy, society, and medical technology, the disease-centered traditional medical model has been gradually replaced by the “bio-psycho-social” medical model. “Bio-psycho-social” is a person-centred medical model. At this time, there is an urgent need for hospital management to use the spirit of innovation to explore a new working mode to adapt to the gradual transformation of the health care relationship from the initial dominant-subordinate model to the juxtaposition-complementary model [1]. In the past, the working mode was that doctors instructed nurses to work and nurses carried out medication orders. Therefore, there was a lack of comprehensive communication between doctors and nurses. In the 1950s, the nursing activities of senior practical nurses were carried out in Britain, the United States, and other developed countries. The work mode of combining medical and nursing assistance has been applied in clinical work, which can well improve the quality and efficiency of medical and nursing service to meet the expectations of each other's roles between doctors and nurses. The integration model of medical and nursing assistance has sprung up and has been gradually promoted [2]. The mode of integration of medical care and assistance is different from the previous way in which doctors make medical plans and nurses carry out doctor's orders, which breaks the original parallel lines of doctors and patients and nurses and patients [3]. In 2003, the American Nursing Association defined the health care integration model as a reliable cooperation model between doctors and nurses [4]. At the same time, there is a reasonable division of labor, close contact, information exchange, and mutual cooperation between doctors and nurses [5]. It is an important part of the continuous improvement of medical quality. The studies have shown that good cooperation between doctors and nurses can shorten the days of hospitalization, reduce the incidence of mortality and complications, and improve nursing satisfaction [6–8].

The quality of communication not only affects patients' medical experience but also can be used as one of the important reference indicators to evaluate and judge the quality of medical services [9]. The use of certain tools or skills will help to improve the efficiency of communication and solve clinical practical medical and nursing problems. Since the 1990s, foreign scholars have begun to study the mode of doctor-patient communication. Studer Group was founded in 1999, which provided guidance, teaching, evidence-based tools, and strategies to health care organizations and rural hospitals in the United States to help medical organizations achieve cultural transformation [10]. In AIDET communication mode, A (acknowledge) is indicated as greetings. I (introduce) is indicated as introduction, in which your name, professional title, qualification, and working hours are introduced. D (duration) is indicated as process. In view of the following operational matters and how much time it will take, the patients have an expectation of the operation to ease their anxiety about unknown things and to better cooperate with our work. E (explanation) means letting patients know that our services represent their interests. T

(thanks) means thank you. At the end of the operation, the patients will be grateful for their cooperation and understanding, which not only shows the good professionalism of the medical staff but also allows the patients to get rid of their helplessness as a patient and restore their sense of self-worth. Finally, they are informed that if they need help, they can contact us at any time. The use of AIDET communication mode helps to communicate clearly and improve the patient experience [11, 12].

Percutaneous coronary intervention (PCI) refers to the treatment of cardiac catheterization to dredge the narrow or even occluded coronary artery lumen so as to improve myocardial perfusion. Although the clinical application of PCI has been mature, there is still a risk of postoperative complications, affecting the outcome of postoperative disease. Good nursing measures can play the effect of adjuvant therapy. At present, the nursing interventions of patients after PCI at home and abroad mainly include community nursing, collaborative nursing, home nursing, continuous nursing, and so on. China has also carried out some research in this area, but there are still some shortcomings [13]. Most of them only carry out health education for diseases, the form of intervention is single, and targeted guidance is lacking. The participants are only nurses; with lack of medical cooperation and good communication, patients passively receive health education given by medical staff. Medical staff do not know the relevant knowledge of patients after PCI. The duration of good self-care behavior established in life is limited [14]. At present, medical and nursing integration mode and AIDET communication mode have been used in peritoneal dialysis, wound treatment, outpatient examination, chronic disease management, and other fields and have achieved good results [15]. In this study, the impact of integrated medical and nursing rounds combined with AIDET communication mode was explored on the recovery and quality of life of patients after percutaneous coronary intervention.

## 2. Materials and Methods

**2.1. General Information.** Sixty patients with percutaneous coronary intervention in our hospital from April 2019 to April 2021 were selected. The patients were randomly divided into two groups: the control group ( $n = 30$ ) and research group ( $n = 30$ ). The control group received routine nursing, and the research group received medical and nursing care combined with AIDET communication mode. The age of control cases ranged from 43 to 80 years with an average of  $63.35 \pm 3.42$  years, including 18 males and 12 females. The course of coronary heart disease ranged from 5 to 8 years with an average of  $6.15 \pm 1.44$  years. The age of study cases was 44–76 years with an average of  $63.55 \pm 3.91$  years, including 17 males and 13 females. The course of coronary heart disease ranged from 4 years to 8 years with an average of  $6.11 \pm 1.48$  years. There was no statistical significance in the general data of the two groups. This study was approved by the Medical Ethics Association of our hospital, and all patients signed informed consent.

Inclusion criteria: (1) in accordance with the diagnostic criteria of coronary heart disease established by the interventional cardiology group of the Cardiology Branch of Chinese Medical Association [16], those who underwent PCI; (2) those who were more than 18 years old and less than 80 years old; (3) those who could understand and answer the questionnaire; and (4) those who have informed consent and voluntary participation in this study were included in the study.

Exclusion criteria: (1) those with mental illness, (2) those with other serious diseases, and (3) those who were accompanied by professional or temporary caregivers were excluded from the study.

Elimination standard: (1) those who died for any reason; (2) those who stopped participating in the research for various reasons; (3) those who failed to complete the questionnaire due to the loss of follow-up for various reasons; and (4) those who were hospitalized again during the intervention period were eliminated.

**2.2. Methods.** The control group accepted the traditional medical work mode. The patients received integrated medical and nursing rounds. The specific process of the integrated medical and nursing rounds mode is as follows. (1) During the morning meeting, all medical staff would turn over at the nurses' station to report the condition of patients in the ward. (2) Ward rounds were jointly attended by attending physicians, bed-in-charge residents, responsible nurses, therapists, and patients. The nurses reported the changes of their condition, the completion of treatment and the problems that need to be solved, and the bed-attendant supplement and put forward the next diagnosis and treatment plan. Finally, the attending physician put forward measures to solve the problems encountered and cooperated with nurses and therapists to evaluate the current diagnosis, treatment, nursing, and rehabilitation plan. The corresponding improvement methods were put forward. The nursing effect was observed after 3 months.

The research group carried out nursing intervention based on AIDET communication mode based on integrated medical and nursing assistance. The specific process of integrated medical and nursing rounds was the same as that of the control group. The AIDET communication mode was applied on this basis: (1) before the intervention, the relevant nurses formed an AIDET communication group to train the group staff on relevant knowledge, mainly for PCI-related knowledge and specific implementation measures of AIDET. (2) Implement AIDET and carry out nursing intervention around 5 main aspects of AIDET communication mode. A (greeting): take the initiative to greet patients, use honorific titles, take a positive attitude, learn about patients' knowledge about the disease and their physical condition, ask if they are not feeling well and need help, and always maintain a patient and understanding attitude. I (introduction): introduce yourself to patients, such as "Hello, I am your responsible nurse, my professional title is .... My working life is...." This paper introduces the development history of hospital cardiology and the level of specialist team, so as to eliminate strangeness and enhance trust. (3) Introduce the nursing

measures in many aspects, such as postoperative diet, rehabilitation exercise, disease and medicine, and the importance of taking medicine on time and according to the doctor's advice, and emphasize the importance of postoperative nursing in promoting prognosis. D (process): let patients understand the postoperative nursing process and the problems that may be encountered in the postoperative rehabilitation process, the treatment methods currently used, and the examination, rehabilitation training, and drug taking methods that need to be carried out in the recovery phase, so as to enhance treatment confidence. E (explanation): patiently answer patients' questions, such as "Why should they take drugs for a long time" and "Why should they carry out postoperative rehabilitation training, such as respiratory function exercise," so as to alleviate their doubts and fears and enhance their sense of trust. T (thanks): thank the patients for their support after the nursing work is completed, and ask the patients if they have any other needs. The nursing effect was observed after 3 months.

### 2.3. Observation Index

**2.3.1. Satisfaction.** Evaluation of patient satisfaction: (1) evaluation tool: a patient satisfaction questionnaire was used. This questionnaire was a satisfaction questionnaire of discharged patients designed by Zhang Huizhi referring to the North American Hospital Consumer Evaluation Health Service and Service System (HCAHPS). The Cronbach's  $\alpha$  coefficient of the internal consistency of the questionnaire was 0.84, the CVI of each item was 0.8-1.0, and the average CVI of all items was 0.98 [17]. (2) Assessment content: this questionnaire was divided into 5 dimensions with a total of 12 items, all of which are closed-ended questions, including 3 items for service attitude (questions 1, 2, and 5) and 1 item for business level (question 12), 2 items of caring for patients (items 3 and 4), 1 item of nursing management (item 6), and 5 items of health education (items 7, 8, 9, 10, and 11). (3) Evaluation method: the survey of patient satisfaction was conducted by the members of the research group trained in the AIDET communication mode course to distribute the questionnaire on the spot and take it back. (4) Evaluation standard: the Likert 5-level scoring method was used, which was expressed according to the degree of satisfaction, from "very satisfied" to "very dissatisfied" and from very satisfied to very dissatisfied. Five to 1 point was assigned, respectively. The score range was 12-60:  $\leq 35$  as low satisfaction, 36-53 as medium satisfaction, and  $\geq 54$  as high satisfaction. Satisfaction rate = (medium satisfaction + high satisfaction) / total number.

**2.3.2. Cardiac Function Index.** The indexes of cardiac function, including left ventricular ejection fraction (LVEF), left ventricular end-systolic volume index (LVESVI), and wall motion integral index (WMSI), were evaluated before and 3 months after nursing.

**2.3.3. Self-Care Behavior.** The self-nursing behavior ability was evaluated before nursing and 3 months after nursing. The SCHFI scale was developed from the University of Pennsylvania Reigel in 2004 by the self-management scale

[18]. The scale had 22 items, including 3 subscales as self-nursing maintenance (10 items), self-nursing management (6 items), and self-nursing confidence (6 items). Each subscale can be used separately. Except for the two items of self-nursing management using the Likert 5-point score (0—unaware, 1—slow, 2—faster, 3—fast, and 4—very fast), the rest were rated using the Likert 4-point score (1—never, 2—occasionally, 3—often, and 4—always or daily). The standard score of each subscale can be calculated according to the formula. And the conversion formula of the standard score was as follows:  $\text{standard score} = (\text{actual score} - \text{the lowest score of the item}) / (\text{the highest score of the item} - \text{the lowest score of the item}) \times 100$ . The score of each scale can be converted into 100 points. The total score of the scale was 300 points. More than 70 points in each scale indicated that the patient has better self-care ability.

**2.3.4. Short-Term Prognosis.** Major adverse cardiovascular events (MACE) were recorded as poor prognosis, including recurrent acute myocardial infarction (AMI), revascularization, arrhythmia, heart failure, cardiogenic shock, and cardiogenic death.

**2.3.5. Quality of Life Scale.** The quality of life scale consisted of four subscales, including physical, psychological, social, and health self-awareness with a total of 29 items [19]. Cronbach's  $\alpha$  coefficient of the scale is 0.79 to 0.91. The scale was scored by 1-5 grades.

**2.4. Statistical Analysis.** SPSS23.0 statistical software was adopted to process the data. The measurement data were presented as  $\bar{x} \pm s$ . The group design  $t$ -test was adopted for the comparison, and the analysis of variance was adopted for the comparison between multiple groups. The Dunnett  $t$ -test was adopted for comparison with the control group. The counting data were presented in the number of cases and the percentage, the  $\chi^2$  test was adopted for comparison between groups, and the bilateral test was employed for all statistical tests.

### 3. Results

**3.1. Comparison of Nursing Satisfaction.** In the comparison of nursing satisfaction between the two groups, the satisfaction of the research group was low in 1 case, moderate in 6 cases, and high in 27 cases, with a satisfaction rate of 96.67%. In the control group, there were 7 cases with low satisfaction, 10 cases with moderate satisfaction, and 13 cases with high satisfaction, with a satisfaction rate of 76.67%. The nursing satisfaction of the research group was largely higher than that of the control group, and the difference was statistically significant ( $P < 0.05$ ). All results are shown in Figure 1.

**3.2. Comparison of Cardiac Function.** After the intervention, the cardiac function of the two groups was improved. Comparison between the two groups showed that the LVEF and LVESVI in the research group were obviously higher than those in the control group. The WMSI was remarkably lower

than that in the control group, and the difference was statistically significant ( $P < 0.05$ ). All results are shown in Table 1.

**3.3. Comparison of Self-Nursing Ability.** Compared with the self-nursing ability, the self-nursing maintenance, the self-nursing management, the self-nursing confidence, and the total score of self-nursing in the research group were significantly higher than those in the control group, and the difference was statistically significant ( $P < 0.05$ ). All results are shown in Table 2.

**3.4. Comparison of Short-Term Prognosis.** In the comparison of recent prognosis, the incidences of AMI, revascularization, arrhythmia, heart failure, cardiogenic shock, and cardiac death in the research group were considerably lower than those in the control group, and the difference was statistically significant ( $P < 0.05$ ). All results are shown in Figure 2. The meaning of the data in Figure 2 is the quantity. The indicators in the figure are commonly used indicators to observe the short-term prognosis of the two groups.

**3.5. Comparison of Quality of Life Scores.** After intervention, the scores of quality of life of the two groups decreased, and the scores of physiological function, psychological function, social function, and health self-cognition in the research group were markedly lower than those in the control group, and the difference was statistically significant ( $P < 0.05$ ). All results are shown in Table 3.

### 4. Discussion

Coronary atherosclerotic heart disease is a kind of heart disease caused by myocardial ischemia, hypoxia, or necrosis caused by coronary atherosclerosis, which is called coronary heart disease. According to the World Health Organization, cardiovascular disease is the leading cause of death from noncommunicable diseases [20, 21]. The number of acute myocardial infarction in China in 2016 is about 4 million, and it is estimated that the number of acute myocardial infarction in 2030 will reach about 6.1 million [22]. PCI is one of the most effective methods for the treatment of coronary heart disease, including intracoronary stent implantation, percutaneous transluminal coronary angioplasty (PTCA), and rotational grinding of atherosclerotic plaques [23]. PCI can quickly dredge the blocked coronary artery, reduce the risk of myocardial infarction, and improve the prognosis of patients. More than 500,000 patients are treated with PCI each year in the United States. Early studies have shown that the total number of cases of interventional therapy in China exceeded 660,000 in 2016. Patients with acute ST segment elevation myocardial infarction received direct PCI in more than 50,000 cases as high as 38.9% [24]. With the continuous development and maturity of PCI, the mortality rate of coronary heart disease has been continuously reduced. Previous studies have shown that PCI in the treatment of coronary heart disease can reduce surgical trauma, improve the success rate of surgery, shorten the length of hospital stay, accelerate disease recovery, and alleviate the advantages of clinical symptoms, and restoration of myocardial blood supply can effectively improve the physiological



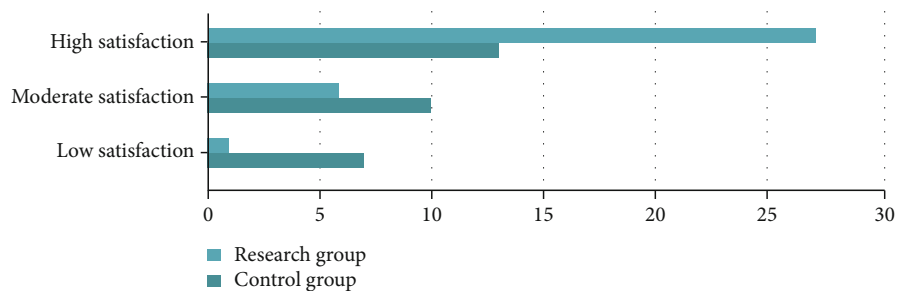


FIGURE 1: Comparison of nursing satisfaction between the two groups.

TABLE 1: Comparison of cardiac function between the two groups ( $\bar{x} \pm s$ ).

Grouping	N	LVEF (%)		LVESVI (ml·m <sup>-3</sup> )		WMSI	
		Before intervention	After intervention	Before intervention	After intervention	Before intervention	After intervention
Control group	30	51.92 ± 3.84	55.49 ± 5.66*	44.91 ± 5.32	47.14 ± 4.31*	1.85 ± 0.44	1.68 ± 0.34*
Research group	30	51.35 ± 3.31	59.39 ± 4.34*	44.95 ± 5.44	49.19 ± 3.42*	1.81 ± 0.42	1.52 ± 0.11*
t value		0.615	2.994	0.028	2.040	0.360	2.452
P value		>0.05	<0.05	>0.05	<0.05	>0.05	<0.05

Note: \* represents the comparison before and after nursing in this group ( $P < 0.05$ ).

TABLE 2: Comparison of self-care ability between the two groups ( $\bar{x} \pm s$ , points).

Grouping	N	Self-care maintenance	Self-nursing management	Self-care confidence	Total score
Control group	30	43.29 ± 9.32	50.39 ± 6.56	39.19 ± 4.34	135.96 ± 5.92
Research group	30	48.49 ± 5.34	58.39 ± 4.66	44.96 ± 4.10	148.65 ± 6.34
t value		2.651	5.445	5.293	8.012
P value		<0.05	<0.05	<0.05	<0.05

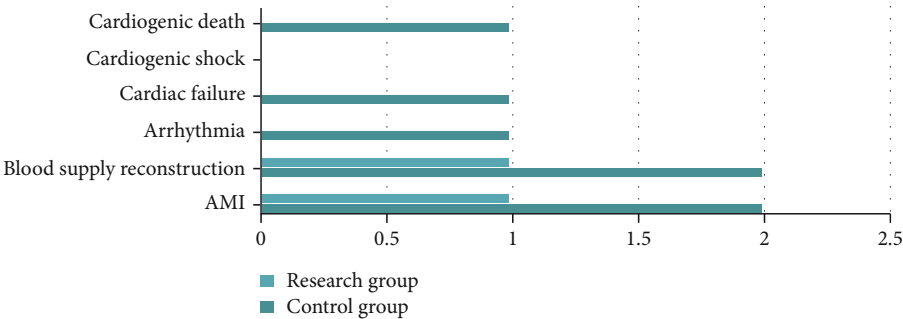


FIGURE 2: Comparison of short-term prognosis between the two groups.

indicators of patients, thereby improving the quality of life of patients [25, 26].

PCI has the advantages of less trauma, rapid recovery, and good prognosis and can quickly dredge the occlusive or narrow lumen under special circumstances. However, PCI is also an invasive operation, and the negative emotions such as tension, fear, anxiety, and postoperative complications will affect the therapeutic effect and prognosis of patients. Therefore, strengthening the postoperative nursing care of patients undergoing PCI is the key to save the

patients' lives and improve the prognosis. With the change of the medical model, communication is becoming more and more important in nursing. A public survey has shown that higher professional skills account for only 25% of the success factors in the process of communicating with patients, while good communication skills account for 75% [27–29]. Therefore, our nursing services emphasize not only professional skills but also high emotion and high EQ. At present, there are more in-depth studies on improving the communication mode and promoting the healthy



TABLE 3: Comparison of quality of life scores between the two groups ( $\bar{x} \pm s$ , points).

Grouping	N	Physiological function		Psychological function		Social function		Healthy self-cognition	
		Before nursing	After nursing	Before nursing	After nursing	Before nursing	After nursing	Before nursing	After nursing
Control group	30	15.75 $\pm$ 4.42	13.20 $\pm$ 2.54*	16.54 $\pm$ 3.11	14.36 $\pm$ 4.66*	18.84 $\pm$ 3.98	16.64 $\pm$ 2.44*	15.56 $\pm$ 3.82	13.64 $\pm$ 1.55*
Research group	30	15.44 $\pm$ 4.66	11.84 $\pm$ 2.31*	16.45 $\pm$ 3.53	11.94 $\pm$ 1.45*	18.44 $\pm$ 3.53	12.74 $\pm$ 3.42*	15.75 $\pm$ 3.64	10.67 $\pm$ 2.42*
t value		0.264	2.169	0.104	2.715	0.411	5.084	0.197	5.660
P value		>0.05	<0.05	>0.05	<0.05	>0.05	<0.05	>0.05	<0.05

Note: \* represents the comparison before and after nursing in this group ( $P < 0.05$ ).

development of nurse-patient relationship at home and abroad, in which AIDET communication mode is first developed by the Studer Group team and widely used by American medical institutions. It is often used to communicate between nurses and patients, helping them to achieve good results in the adjustment of patient satisfaction [30]. The model includes procedures and standard terms for communication between nurses and patients. This model consists of the initials of five very important keywords that make up the communication framework. Through this standardized communication procedure to choose the correct language to communicate effectively with patients, it is helpful to reduce the psychological pressure of patients and their stress reaction to achieve a relaxed and pleasant state.

In the United States, the communication mode of AIDET was first used in Baptist Memorial hospitals in the late 1990s. Through the survey, it was found that patient satisfaction increased from 40% to 90% [31]. AIDET communication mode was first applied to anesthetic pain management in China. In 2010, Bor et al. applied AIDET communication mode to orthopedic pain management, which not only made the pain well controlled but also enhanced the mutual trust between nurses and patients and the enthusiasm of doctors and patients to participate in pain management [32]. In 2012, the pain management team first applied the AIDET communication model to the management of postoperative analgesia [33]. The patients have high compliance and satisfaction with postoperative analgesia services. In 2014, Ji et al. reported that the application of AIDET communication model to patients undergoing gastrointestinal surgery not only improved patient compliance and satisfaction in a short period of time but also improved the efficiency of communication between nurses and patients and maximized the efficiency of communication [34]. Through AIDET communication mode, a harmonious and trusting nurse-patient relationship can be gradually established [35]. AIDET communication mode is also successfully used in maternal care (giving psychological support to parturients). Through the combination of preoperative education and postoperative rehabilitation, maternal anxiety can be alleviated [36]. After a large number of related literature review, there are no reports about the application of AIDET communication follow-up model to patients after PCI [37].

In recent years, doctors and nurses have gradually changed into a working relationship of mutual assistance and cooperation. Effective cooperation between doctors and nurses can shorten the average length of stay of patients, reduce hospitalization costs, and improve hospitalization satisfaction [38]. The integrated medical and nursing model was applied to the discharge follow-up of patients with type 2 diabetes [39]. The specific method is for doctors to establish electronic files and electronic reminders for patients. Nurses carry out health education and consultation to patients. These studies show that the integrated model of health care can improve the quality of health care without increasing economic investment. Klancik et al. pointed out that the new type of health care integration refers to a kind of interpersonal relationship in which doctors and nurses communicate and cooperate with each other in 2005 [40]. The “prehospital-in-hospital-posthospital” integrated and innovative ward of Massachusetts General Hospital is established on the basis of “relationship-based care” (RBC). Attending doctors, rehabilitation doctors, nursing specialists, head nurses, and responsible nurses participate in daily rounds to discuss patients’ condition and treatment, formulate nursing and rehabilitation priorities, and extend services after discharge. It can emphasize the relationship between nurses and patients, family members, doctors, and other medical staff. This model has become a nursing work mode recognized and recommended by the American Medical Association [41]. The research on the integration of health care in China started relatively late. In 1992, Zhang et al. applied the concept of “integration of health care” to nursing teaching [42]. The integrated teaching of health care can embody the holistic view of health care, which focuses on the organic connection between treatment and nursing, avoids the disconnection and repetition of the content, and strengthens students’ understanding of the integrity of health care. Since then, the concept of health care integration has been introduced into clinical work to describe health care cooperation. At present, many hospitals have begun to explore a new integrated cooperation model of health care, which is mainly used in nursing personnel training, specialist disease nursing, nursing quality management, home nursing service, and so on. The implementation of the health care integration model is mainly realized through the establishment of a health care integration team, optimization of

work flow, and joint health education between doctors and nurses. According to the actual situation, the weak links of the work flow are reformed and perfected and continuously optimized, so as to effectively avoid medical and nursing risks in treatment and nursing work to improve the satisfaction of patients and the degree of cooperation between doctors and nurses. With in-depth discussion of the details of high-quality nursing services, nurses become more consultants, decision-makers, and leaders. Medical and nursing cooperation strengthens the communication among doctors to improve the work efficiency of both doctors and nurses [43]. Doctors, nurses, and patients can all benefit from the integrated work mode of health care. Therefore, the implementation of medical and nursing integration model in general hospitals is an effective means to realize the sustainable development strategy of nursing management.

Related studies pointed out that self-care ability is the premise and basis of carrying out the above-mentioned activities, such as self-examination of symptoms and signs, taking medicine according to doctor's advice, healthy diet, and proper exercise after PCI [44]. The implementation of AIDER communication mode nursing in multiple departments can improve patients' experience, relieve anxiety, and harmonize nurse-patient relationship. The reason is that most PCI patients have a long course of disease before operation and suffer from pain for a long time. Some patients are accompanied by other basic diseases, which have a great impact on the daily activities of patients, resulting in poor self-care awareness and self-care ability. At the same time, the disease will lead to self-doubt and affect the prognosis of patients. In this study, integrated medical and nursing rounds combined with AIDET communication mode were used to intervene patients after PCI in order to strengthen health education on disease-related knowledge, which make patients master postoperative nursing-related knowledge and skills. The AIDET model will pay more attention to nurses' communication attitude and skills. Through AIDET mode communication, an effective process of inertia operation is formed. The implementation of nursing measures is optimized. Integrated medical and nursing rounds combined with AIDET communication mode are effective in the intervention of patients after PCI. The reason is that integrated medical and nursing rounds can effectively avoid problems such as inconsistent medical records and disjointed medical and nursing services. Doctors and nurses should strengthen communication between the two sides and jointly understand the changes of patients' conditions and problems existing in the process of treatment and nursing. In addition, in the process of integrated medical and nursing rounds, patients' participation is also conducive to deepening their understanding of their own condition and mastering basic nursing knowledge and skills, so as to reduce the incidence of complications. Our study still has some shortcomings. Firstly, the quality of this study is limited due to the small sample size we included in the study. Secondly, this research is a single-center study, and our findings are subject to some degree of bias. Therefore, our results may differ from those of large-scale multicenter studies from other academic institutes. Our research is still clinically sig-

nificant, and further in-depth investigations will be carried out in the future.

In conclusion, medical and nursing integrated ward rounds combined with AIDET communication mode can effectively improve the prognosis of patients undergoing percutaneous coronary intervention to promote the establishment of a harmonious nurse-patient relationship. The patients' self-care ability is able to effectively enhance and further improve cardiac function.

## Data Availability

The datasets used and analyzed during the current study are available from the corresponding author upon reasonable request.

## Conflicts of Interest

The authors declare that they have no conflicts of interest.

## References

- [1] H. H. Hwa, C. L. K. Fung, L. J. Bang et al., "TCTAP A-012 first report on 30-day outcomes of patients treated with DynamX Bioadaptor drug-eluting stent in primary percutaneous coronary intervention," *Journal of the American College of Cardiology*, vol. 79, no. 15, p. S7, 2022.
- [2] K. Jumpei, I. Yoshihiro, F. Atsushi, T. Kobayashi, and S. Nakamura, "TCTAP A-015 acute and mid-term results of percutaneous coronary intervention for severely calcified coronary artery lesions with orbital atherectomy system (OAS)," *Journal of the American College of Cardiology*, vol. 79, no. 15, p. S8, 2022.
- [3] K. Hironobu, K. Tatsuya, H. Kazutoshi et al., "TCTAP A-018 safety, feasibility, and compatibility of percutaneous coronary intervention (PCI) via distal radial approach (dRA) in daily practice," *Journal of the American College of Cardiology*, vol. 79, no. 15, p. S11, 2022.
- [4] S. Mugilan, J. Q. Wy, G. K. Guruparan et al., "TCTAP A-025 "do women truly have worst outcomes?" Comparison of outcome differences for percutaneous coronary intervention in unprotected left main disease - a propensity matched analysis," *Journal of the American College of Cardiology*, vol. 79, no. 15, pp. S17-S19, 2022.
- [5] B. Khuyag, G. Gankhulug, B. Bum-Erdene et al., "TCTAP A-029 SYNTAX II score predicted and real life observed mortality in patients with left main coronary artery stenosis who treated by percutaneous coronary intervention," *Journal of the American College of Cardiology*, vol. 79, no. 15, p. S21, 2022.
- [6] I. A. Waliul, M. Shams, A. Q. M. Reza et al., "TCTAP A-033 percutaneous coronary intervention of saphenous vein graft in post-CABG patient - outcome experiences at our center - SVG to OM are more likely to develop occlusion," *Journal of the American College of Cardiology*, vol. 79, no. 15, p. S23, 2022.
- [7] P. Yusra, H. L. Yan, and E. Romi, "TCTAP A-035 the success rate of chronic total occlusions percutaneous coronary intervention in rural area," *Journal of the American College of Cardiology*, vol. 79, no. 15, pp. S23-S24, 2022.

- [8] J. Rafał, W. Wojciech, S. Zbigniew et al., "TCTAP A-036 annual operator volume among patients treated using percutaneous coronary interventions with rotational atherectomy and procedural outcomes - analysis based on a large national registry," *Journal of the American College of Cardiology*, vol. 79, no. 15, p. S24, 2022.
- [9] N. Xu, J. Sida, Y. Deshan et al., "TCTAP A-040 big endothelin-1 and five-year long-term all-cause death in patients with coronary artery disease and prediabetes or diabetes after percutaneous coronary intervention," *Journal of the American College of Cardiology*, vol. 79, no. 15, pp. S27–S28, 2022.
- [10] P. Wang, Y. Deshan, and Y. Jinqing, "TCTAP A-041 prognostic value of fibrinogen-to-albumin ratio in patients with coronary artery disease and diabetes following percutaneous coronary intervention," *Journal of the American College of Cardiology*, vol. 79, no. 15, p. S28, 2022.
- [11] P. J. G. Ngurah, L. N. Toding, P. P. K. A. Aditya, and Y. Pintaningrum, "TCTAP A-051 early and long-term outcome of intravascular ultrasonography-guided primary percutaneous coronary intervention in ST-elevation myocardial infarction: a network meta-analysis," *Journal of the American College of Cardiology*, vol. 79, no. 15, pp. S32–S33, 2022.
- [12] J. Q. Wy, S. Mugilan, and K. Jayakhanthan, "TCTAP A-065 percutaneous coronary intervention in elderly population: Asian perspective," *Journal of the American College of Cardiology*, vol. 79, no. 15, pp. S40–S41, 2022.
- [13] M. Shaban, A. A. Rahman, A. Dina et al., "TCTAP A-069 cost-effectiveness analysis of high-potency versus low-potency statins for reducing mortality in coronary artery disease patients on dual antiplatelet therapy post percutaneous coronary intervention," *Journal of the American College of Cardiology*, vol. 79, no. 15, p. S44, 2022.
- [14] W. Xinlei, P. L. Renkens Mick, K. Laura et al., "TCTAP A-072 immediate effect of percutaneous coronary intervention by bioresorbable scaffold or drug-eluting stent on superficial wall strain of stenotic coronary arteries," *Journal of the American College of Cardiology*, vol. 79, no. 15, pp. S45–S46, 2022.
- [15] Y. A. Romero, M. Ariel, and G. Roy, "TCTAP A-079 comparison between one versus multiple brand stents on in-stent restenosis events during percutaneous coronary intervention (COMBINED PCI Study)," *Journal of the American College of Cardiology*, vol. 79, no. 15, pp. S49–S50, 2022.
- [16] The Cardiology Branch of Chinese Medical Association is involved in Cardiology Group, the Thrombosis Prevention and treatment Professional Committee of Cardiovascular Physicians Branch of Chinese Medical Association, and the editorial Committee of Chinese Journal of Cardiovascular Diseases, "Guidelines for percutaneous coronary intervention in China (2016)," *Chinese Journal of Cardiovascular Diseases*, vol. 44, no. 5, pp. 382–400, 2016.
- [17] W. J. Lim, H. S. Loh, T. Y. Beh, and B. Kandasamy, "TCTAP C-012 stormy primary percutaneous coronary intervention during COVID-19 pandemic," *Journal of the American College of Cardiology*, vol. 79, no. 15, pp. S79–S81, 2022.
- [18] G. Suhashni, K. S. Kooi, and L. Hounghang, "TCTAP C-014 successful transradial percutaneous coronary intervention in dextrocardia," *Journal of the American College of Cardiology*, vol. 79, no. 15, pp. S83–S85, 2022.
- [19] H. K. Bali and D. Amreen, "TCTAP C-044 percutaneous coronary intervention in a complex left main trifurcation lesion using two guide catheters," *Journal of the American College of Cardiology*, vol. 79, no. 15, pp. S143–S145, 2022.
- [20] C. M. Wah and R. A. Irawan, "TCTAP C-054 chronic total occlusion percutaneous coronary intervention in anomalous right coronary artery arising from left coronary cusp," *Journal of the American College of Cardiology*, vol. 79, no. 15, pp. S163–S165, 2022.
- [21] A. N. Henry, H. T. Lu, K. Gobal, V. Kulasingham, H. S. Kim, and C. K. Tee, "TCTAP C-084 percutaneous coronary intervention in an occluded saphenous vein graft," *Journal of the American College of Cardiology*, vol. 79, no. 15, pp. S220–S221, 2022.
- [22] Y. A. Romero, Y. S. Azmi, G. K. Gurupparan et al., "TCTAP C-102 management and retrieval of undelatable non-compliant coronary balloon during percutaneous coronary intervention," *Journal of the American College of Cardiology*, vol. 79, no. 15, pp. S252–S253, 2022.
- [23] T. C. Keong, G. Mahadevan, K. H. Shee et al., "TCTAP C-108 septal artery perforation during wire advancement for percutaneous coronary intervention of proximal left anterior descending artery calcified lesion - how we persevere till the end," *Journal of the American College of Cardiology*, vol. 79, no. 15, pp. S263–S265, 2022.
- [24] Chinese Medical Association and Editorial Board of Chinese Journal of Cardiology, "Chinese guideline for percutaneous coronary intervention in patients with left main bifurcation disease," *Zhonghua Xin Xue Guan Bing Za Zhi*, vol. 50, no. 4, 2022.
- [25] L. Ewelina, S. Konrad, N. Karol et al., "Optical coherence tomography-guided percutaneous coronary intervention in a myocardial infarction patient. One more argument for a wider use of now reimbursed optical coherence tomography," *Kardiologia Polska*, vol. 80, no. 5, pp. 616–618, 2022.
- [26] S.-H. Zhou, S.-T. Huang, N. Xu, L.-W. Chen, and Q. Chen, "Application of the wechat platform to implement continuous nursing for patients after percutaneous coronary intervention," *Medical Science Monitor*, vol. 26, p. e925444, 2020.
- [27] O. Kaishi, F. Atsuki, H. Takuro, T. Matsuo, T. Isimatsu, and K. Oku, "A case of mediastinal hematoma due to pericardiophrenic artery injury after percutaneous coronary intervention," *Cardiovascular Intervention and Therapeutics*, 2022.
- [28] M. Tetsuji, U. Hiroyasu, M. Yasuhiko, and T. Hiroshi, "Relationship of body mass index to clinical outcomes after percutaneous coronary intervention," *European Journal of Clinical Investigation*, vol. 52, no. 8, article e13789, 2022.
- [29] Z. Zhang, J. Bai, Y. Huang, and L. Wang, "Implementation of a clinical nursing pathway for percutaneous coronary intervention," *Medicine*, vol. 99, no. 43, p. e22866, 2020.
- [30] A. Z. Omer, B. Loulia, M. Shaaban et al., "Effect of CYP2C19 genetic variants on bleeding and major adverse cardiovascular events in a cohort of Arab patients undergoing percutaneous coronary intervention and stent implantation," *Pharmacogenetics and Genomics*, vol. 32, no. 5, pp. 183–191, 2022.
- [31] B. Gorav, A. Suleman, W. Lars et al., "Data standards for acute coronary syndrome and percutaneous coronary intervention: the European Unified Registries for Heart Care Evaluation and Randomised Trials (Euro Heart)," *European Heart Journal*, vol. 43, no. 24, pp. 2269–2285, 2022.
- [32] Y.-L. Lu, L. Zhu, G.-H. Hou et al., "Expert consensus on nursing management for patients undergoing primary percutaneous coronary intervention during the COVID-19 pandemic," *Cardiology Plus*, vol. 5, no. 2, pp. 81–88, 2020.
- [33] W. S. Chew Nicholas, N. C. Han, K. Gwyneth et al., "Meta-analysis of percutaneous coronary intervention versus

- coronary artery bypass grafting for left main narrowing,” *The American Journal of Cardiology*, vol. 173, pp. 39–47, 2022.
- [34] R. J. Woong, K. Yongcheol, L. OhHyun, I. Eui, D.-K. Cho, and D. Choi, “Successful primary percutaneous coronary intervention without stenting: insight from optimal coherence tomography,” *Yonsei Medical Journal*, vol. 63, no. 4, pp. 399–404, 2022.
  - [35] T. Yang, P. Fu, J. Chen et al., “Increased risk of adverse cardiovascular events by strict glycemic control after percutaneous coronary intervention (HbA1c < 6.5% at 2 years) in type 2 diabetes mellitus combined with acute coronary syndrome: a 5-years follow-up study,” *Current medical research and opinion*, vol. 37, no. 9, pp. 1517–1528, 2021.
  - [36] Y. Farah, K. Sumeet, S. Manjeet et al., “Gender-based differences in primary percutaneous coronary intervention in patients with myocardial infarction from a developing country: a retrospective cohort study,” *Annals of Medicine and Surgery*, vol. 76, article 103532, 2022.
  - [37] I. A. Maria, H. Thomas, B. Hakim et al., “Angiographic predictors of septal collateral tracking during retrograde percutaneous coronary intervention for chronic total occlusion: anatomical analysis or rolling the dice?,” *The Journal of Invasive Cardiology*, vol. 34, no. 4, pp. E286–E293, 2022.
  - [38] C. Yashasvi, B. Rupinder, K. Tak et al., “Outcomes of intravascular ultrasound-guided versus angiography-guided percutaneous coronary interventions in chronic total occlusions: a systematic review and meta-analysis,” *The Journal of Invasive Cardiology*, vol. 34, no. 4, pp. 310–318, 2022.
  - [39] C. Nicola, F. Paolo, M. Alberto et al., “Alex plus versus Xience drug-eluting stents for percutaneous coronary intervention in routine clinical practice: a propensity score-matched analysis,” *The Journal of Invasive Cardiology*, vol. 34, no. 4, pp. 319–325, 2022.
  - [40] K. Viktor, P. Ladislav, N. Marek, P. Tousek, and V. Kocka, “Long-term follow-up in patients with ST-segment elevation myocardial infarction who underwent primary percutaneous coronary intervention,” *Cardiology*, vol. 24, Supplement\_B, pp. B16–B22, 2022.
  - [41] K. Y. Jeong, L. B. Ki, P. K. Woo et al., “Prasugrel-based de-escalation of dual antiplatelet therapy after percutaneous coronary intervention in patients with STEMI,” *Korean circulation journal*, vol. 52, no. 4, pp. 304–319, 2022.
  - [42] R. Zhang, S. Wu, S. Yuan et al., “Effects of diabetes mellitus on post-intervention coronary physiological assessment derived by quantitative flow ratio in patients with coronary artery disease underwent percutaneous coronary intervention,” *Diabetes Research and Clinical Practice*, vol. 186, article 109839, 2022.
  - [43] B. Aslan, M. Özbek, A. Aktan, B. Boyraz, and E. Tenekecioğlu, “Factors associated with all-cause mortality in patients with coronary artery chronic total occlusions undergoing revascularization (percutaneous coronary intervention or surgery) or medical treatment,” *Kardiologiia*, vol. 62, no. 3, pp. 49–55, 2022.
  - [44] A. Mohammad Moman, P. Jonas, B. Sergio et al., “Trends in clinical practice and outcomes after percutaneous coronary intervention of unprotected left main coronary artery,” *Journal of the American Heart Association*, vol. 11, no. 7, article e024040, 2022.



## Research Article

# Clinical Efficacy, Survival, and Adverse Reaction Evaluation of Immune Checkpoint Inhibitor in Advanced Gastric Cancer: A Systematic Review and Meta-Analysis

Ping Zhang,<sup>1</sup> Xiaomeng Zhang,<sup>2</sup> Na Zhu,<sup>1</sup> Feifei Zhuang,<sup>1</sup> Dongmei Zhou <sup>1</sup>,  
and Ping Wang <sup>1</sup>

<sup>1</sup>Department of Medical Oncology, Yantaishan Hospital, Yantai 264003, China

<sup>2</sup>Public Health Division, Yantaishan Hospital, Yantai 264003, China

Correspondence should be addressed to Ping Wang; 631607040429@mails.cqjtu.edu.cn

Received 6 July 2022; Revised 15 July 2022; Accepted 23 July 2022; Published 23 August 2022

Academic Editor: Hangjun Che

Copyright © 2022 Ping Zhang et al. This is an open access article distributed under the Creative Commons Attribution License, which permits unrestricted use, distribution, and reproduction in any medium, provided the original work is properly cited.

**Objective.** To systematically assess the clinical effect and survival time of immune checkpoint inhibitor (ICIs) in advanced gastric cancer (GC) and adverse reactions to provide evidence-based medicine for its enhancement and adoption. **Methods.** PubMed, EMBASE, ScienceDirect, Cochrane Library, China Knowledge Network database (CNKI), China VIP database, Wanfang database, and China Biomedical Literature Database (CBM) online database were searched for randomized controlled trials (RCT) of immuno-checkpoint inhibitors in advanced GC therapy. Retrieval time was limited to the period from the date the database was established to present. Separately, two researchers gathered the data. Statistical software RevMan5.4 was used to estimate bias risk according to the Cochrane Handbook 5.3 standard. **Results.** The computer database retrieved 1723 articles, and 465 articles were eliminated when repeated studies were removed. After screening the titles and abstracts of 287 articles, 124 articles were contained after eliminating irrelevant studies, reviews, case reports, and no control literature. After carefully reading 108 studies with insufficient data and no major outcome markers, 6 RCTs were eventually contained. 4 articles compared the levels of carcinoembryonic antigen (CEA) and carbohydrate antigen 199 (CA199) after treatment. The result indicated that the levels of serum CEA and CA199 in the study group were notably lower, and the difference was statistically significant ( $P < 0.05$ ). The immune function indexes after treatment were compared, suggesting that the improvement of immune function indexes in the study group was notably better, and the difference was statistically significant ( $P < 0.05$ ). Three clinical trials reported the median progression-free survival (PFS). The PFS of the study group was notably longer after treatment, and the difference was statistically significant ( $P < 0.05$ ). The occurrence of adverse reactions after treatment was analyzed by meat, and all the literatures were analyzed. No notable differences were observed in the incidence of adverse reactions. **Conclusion.** ICIs associated with chemotherapy is effective when treating GC, which can effectively promote the disease control rate of patients, enhance immune function, reduce the level of tumor markers, and prolong survival time. The safety is controllable, which is worth popularizing in clinical practice. However, more studies and follow-up with higher methodological quality and longer intervention time are needed to further verify it.

## 1. Introduction

The most common malignant tumor of the digestive tract in China is gastric cancer (GC), which is highly prevalent and has a poor prognosis. GC ranked second in incidence and mortality among malignant tumors in China, right behind

lung cancer, according to the results of a tumor epidemiological survey. GC is a type of malignant tumor of the digestive tract that is highly morbid and highly lethal. With the application of new treatment methods, like surgery, neoadjuvant radiotherapy, neoadjuvant chemotherapy, and targeted therapy, the treatment of GC has changed to



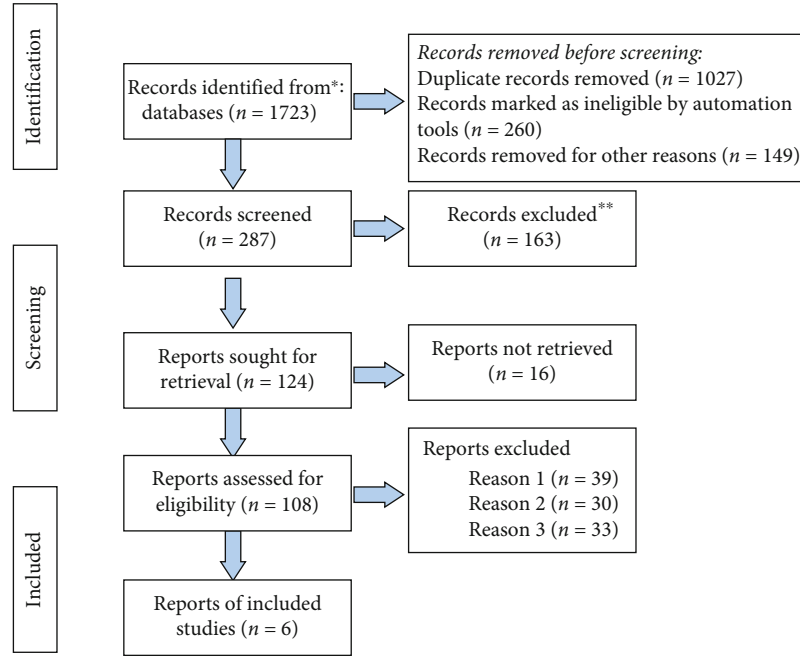


FIGURE 1: Illustration of literature screening.

TABLE 1: Basic characteristics of literature.

Include the literature	Year of publication	N (C/T)	Intervention method		Outcome index	Course of treatment	Whether it is random or not	Whether it is blind or not
			C	T				
Zheng Guili [17]	2021	40/40	FOLFOX4Chemotherapy regimen	FOLFOX4Chemotherapy regimen+PD-1Inhibitor	①②③	6 courses of treatment	Yes	No
Liang Lijun [18]	2022	43/43	Irinotecan/paclitaxel + tigio + apatinib mesylate	Irinotecan/paclitaxel + tigio + apatinib mesylate + Carrell monoclonal antibody	①④⑤	24 weeks	Yes	No
Shen Wang [19]	2022	45/43	Alotinib	Alotinib + Carrilizu monoclonal antibody	①②⑤	4 courses of treatment	Yes	No
Zhang Lianhua [20]	2021	40/40	Docetaxel + irinotecan hydrochloride + tigio	Docetaxel + irinotecan hydrochloride + tigio + Carrell monoclonal antibody	①③⑤	3 cycles	No	No
Tu Huiyang [21]	2021	38/38	XELOX/FOLFOX chemotherapy regimen	XELOX/FOLFOX chemotherapy regimen + pablizumab	①②③	3 cycles	Yes	No
Wang Junsong [22]	2022	40/42	Oxaliplatin + capecitabine	Oxaliplatin + capecitabine + Pabolizhu monoclonal antibody	①④⑤	To the progress of the disease	Yes	No

Note: C: control group; T: study group; ①: clinical efficacy; ②: immune function index; ③: tumor marker level; ④: survival time; ⑤: adverse reactions.

individualized and comprehensive treatment. The short-term survival rate of patients has been improved, but the 5-year survival rate is still low [1]. East Asia is a high incidence area of GC. The morbidity and mortality of GC are high in China, especially in rural areas [2]. From clinical practice, the symptoms of early GC are often atypical with only mild epigastric discomfort, which is difficult to attract people's attention. At the time of the initial diagnosis, more

than 60% of the patients had locally advanced or metastatic GC. The prognosis is often poor and the median survival time is about 1 year [3].

To treat advanced GC, the first-line treatment is platinum and 5-fluorouracil-based chemotherapy [4]. A first-line treatment for patients with GC who have HER-2 positivity has been approved for trastuzumab [5]. HER-2-positive patients with advanced first-line therapy can be

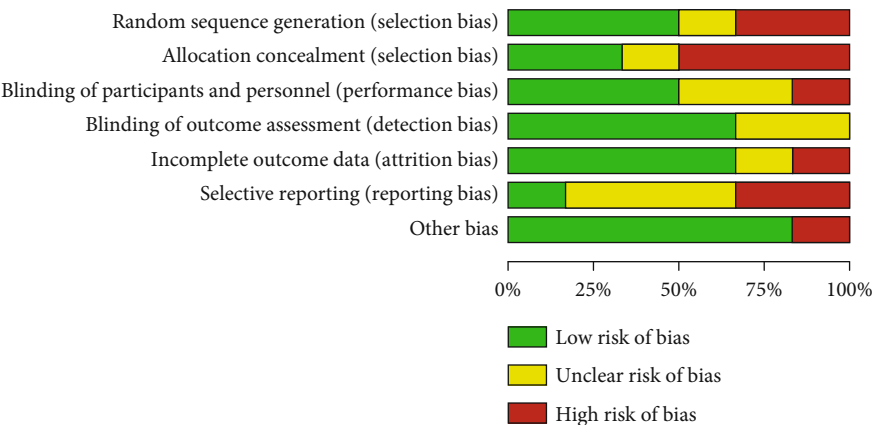


FIGURE 2: Risk of bias chart.



FIGURE 3: Summary chart of risk bias.

treated with trastuzumab and antivascular endothelial growth factor receptor 2 antibody Amatumixab or associated with paclitaxel, while HER-2-negative patients can choose second-line therapy with docetaxel, paclitaxel, or irinotecan alone [6]. Even though chemotherapy for advanced GC patients is constantly improving and gradually diversifying, the five-year survival rate is only 20%-30% [7]. With the emergence of molecular targeted therapy and immunotherapy, especially the advent of immune checkpoint inhibitor (ICIs), the pattern of third-line therapy for advanced GC may change notably.

The antitumor mechanism of traditional chemotherapeutic drugs may regulate the immune model. In combination with PD-1, PD-L1 inhibits T cell function, inhibiting tumor immunity and promoting tumor growth. In light of the study of this mechanism, blocking the PD-1/PD-L1 signal pathway makes sense for treating patients with GC. For example, chemotherapeutic drugs such as cyclophosphamide, platinum, and paclitaxel can enhance the antigenicity of tumor cells, while paclitaxel, cisplatin, and doxorubicin enhance the sensitivity of tumor cells to immune effector cells [8, 9]. PD-1 and programmed cell death ligand 1 (PD-L1) inhibitors revolutionize the treatment of advanced solid cancer [10]. In the study of the comprehensive molecular characteristics of gastric adenocarcinoma, Min and Zhang found that the overexpression of PD-L1 was observed in 65% of GC tissues [11].

The occurrence of GC is related to unhealthy diet, Helicobacter pylori infection and Epstein-Barr virus infection. Cancerous cells evade host immune defense and attack through high expression of immune checkpoint proteins to facilitate tumor growth. ICIs block the immunosuppressive signal pathway activated by cancer cells through antibodies, to enhance the body's antitumor immunity and kill tumor cells [12, 13]. Chemotherapeutic drugs can also affect the patient's immune system, such as paclitaxel, doxorubicin, and cisplatin directly act on cytotoxic lymphocytes, paclitaxel, gemcitabine, and 5-Fu eliminate immunosuppressive cells. When immunosuppressants are used in combination with chemotherapy, in one sense, chemotherapeutic drugs enhance the patient's antitumor immune response. Antitumor immunity can be enhanced by ICIs, and subsequently, drug-resistant tumor cells can be further eradicated after chemotherapy with ICIs. In this way, ICIs may provide clinical benefits when combined with chemotherapy in antitumor therapy. Current clinical trials have also studied ICIs combined chemotherapy [14]. Based on randomized clinical trials, ICIs have shown antitumor activity and good safety when compared with chemotherapy or placebo in advanced GC. In spite of this, there exhibits no consensus on whether PD-1/PD-L1 inhibitors are successful in treating advanced GC. It is proved that the clinical efficacy of ICIs is not accurate by the effectiveness of a literature or the improvement of

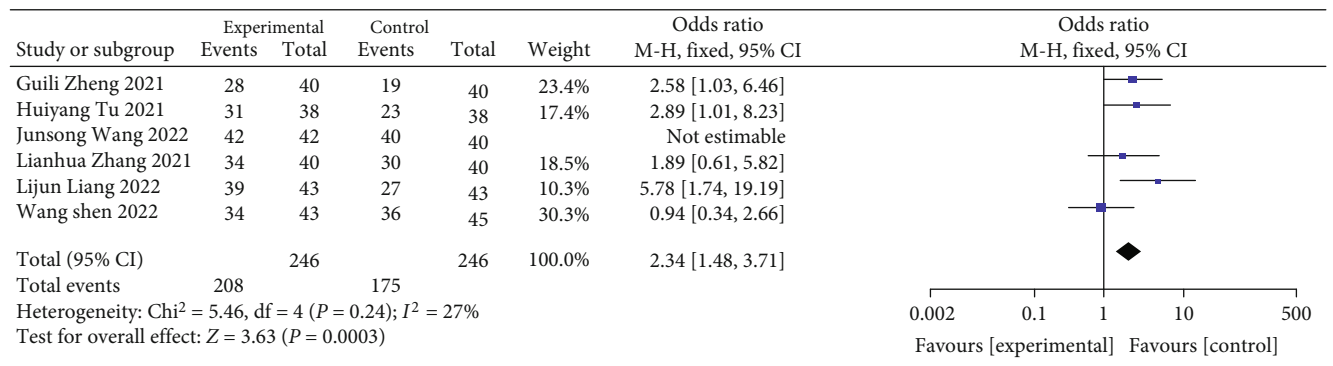


FIGURE 4: Forest plot of meta-analysis of disease control rate.

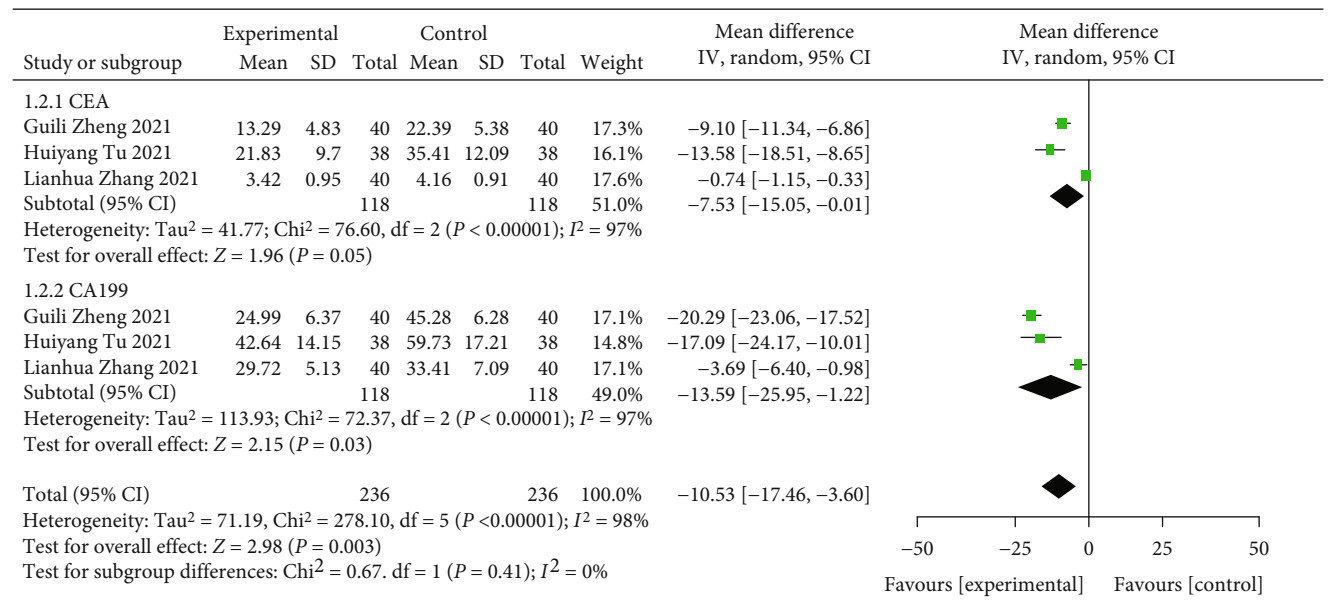


FIGURE 5: Forest plot of meta-analysis of levels of serum tumor markers.

an evaluation index. In this context, it is very necessary to systematically, quantitatively and comprehensively analyze the results of similar independent studies through meta-analysis. This paper was to systematically assess the clinical effect and survival time of immune checkpoint inhibitor (ICIs) in advanced gastric cancer (GC) and adverse reactions to provide evidence-based medicine for its enhancement and adoption.

2. Research Contents and Methods

2.1. Sources and Retrieval Methods of Documents. Search PubMed, EMBASE, ScienceDirect, CochraneLibrary, China Journal Full-Text Database (CNKI), VIP full-text Database (VIP), Wanfang Database and Chinese Biomedical Literature data (CBM), related journals, conference papers, and degree papers were searched and collected relevant data about the use of immuno-checkpoint inhibitors when treating patients with advanced GC. Searching literatures were conducted with free words + subject words, with the key

words of ICIs; GC; progression; survival time; therapeutic effect; adverse reactions; meta-analysis, from January 2010 to May 2022.

2.2. Inclusion and Exclusion Criteria of Literature

2.2.1. Literature Inclusion Criteria. (1) Type of study: all controlled trials (CT) using immunosuppressive agents to treat patients with advanced GC. (2) Participants: all patients with advanced GC were diagnosed as GC by gastroscopy/laparoscopy. The diagnostic criteria were referred to the relevant literature [15]. The TNM stage was stage III B-IV. (3) Intervention: the study group was associated with ICIs on the basis of the control group, and the control group only received chemotherapy. Indications for the use of ICIs: there were differences in the indications of different drugs, as detailed in the relevant reference [16].

2.2.2. Document Exclusion Criteria. (1) The data report was incomplete and the data could not be used; (2) the research

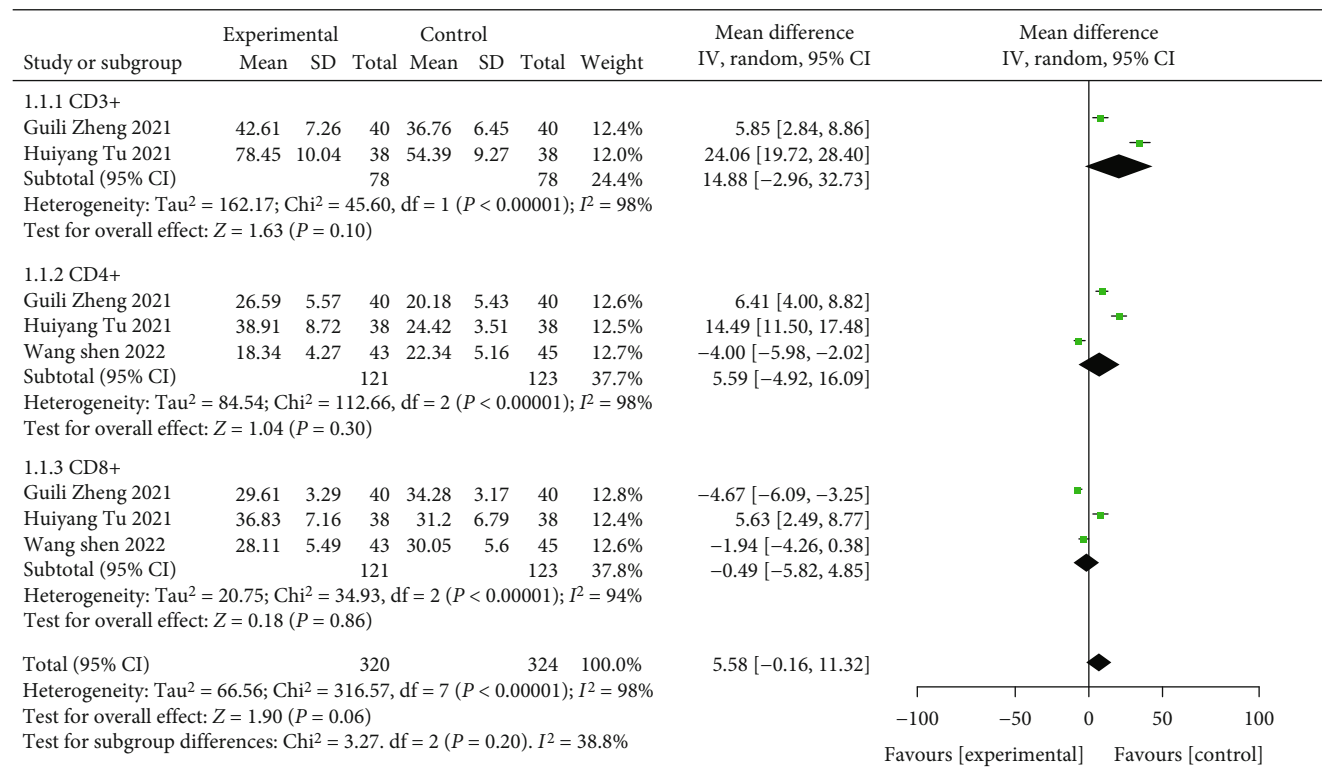


FIGURE 6: Forest plot of meta-analysis of immune function index level.

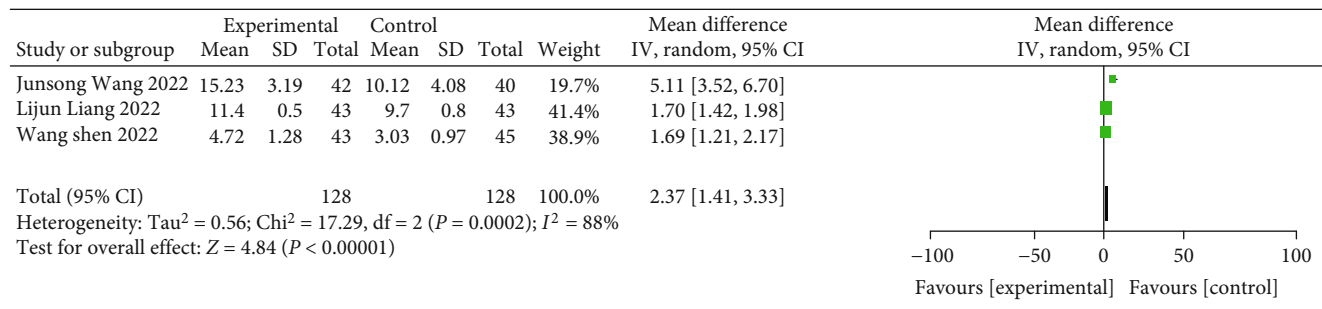


FIGURE 7: Forest plot of meta-analysis of survival.

was repeated to select the most recent studies; (3) the evaluation of the curative effect of the study was not notable.

2.3. Quality Evaluation and Data Extraction

- (1) Bias risk assessment contained in the study: for the evaluation, a bias risk assessment tool recommended by Cochrane System Review Manual 5.4 was used
- (2) Literature screening and data extraction: independently, two researchers screened literature, gathered data, assessed quality, and cross-checked results. A disagreement should be discussed and resolved, or a third researcher should be invited to contribute to the judgement. Note: Express document management software and Excel office software were used

to manage and extract research data. If the data contained in the literature was incomplete, the author of this article would be contacted to supplement it. The content of data extraction contained (1) basic information: author, publication time, and number of cases; (2) intervention: plan, course of treatment; and (3) outcome index

2.4. Statistical Processing. The RevMan5.4 software originated from Cochrane collaboration network for meta-analysis. The mean and standard deviation of the net change difference of serum albumin, prealbumin, and hemoglobin in the experiment, and the control cohorts were input into RevMan5 for analysis. Because the index is a continuous variable, the weighted mean difference (WMD) is used as the effect scale, and 95% confidence interval is selected. First,

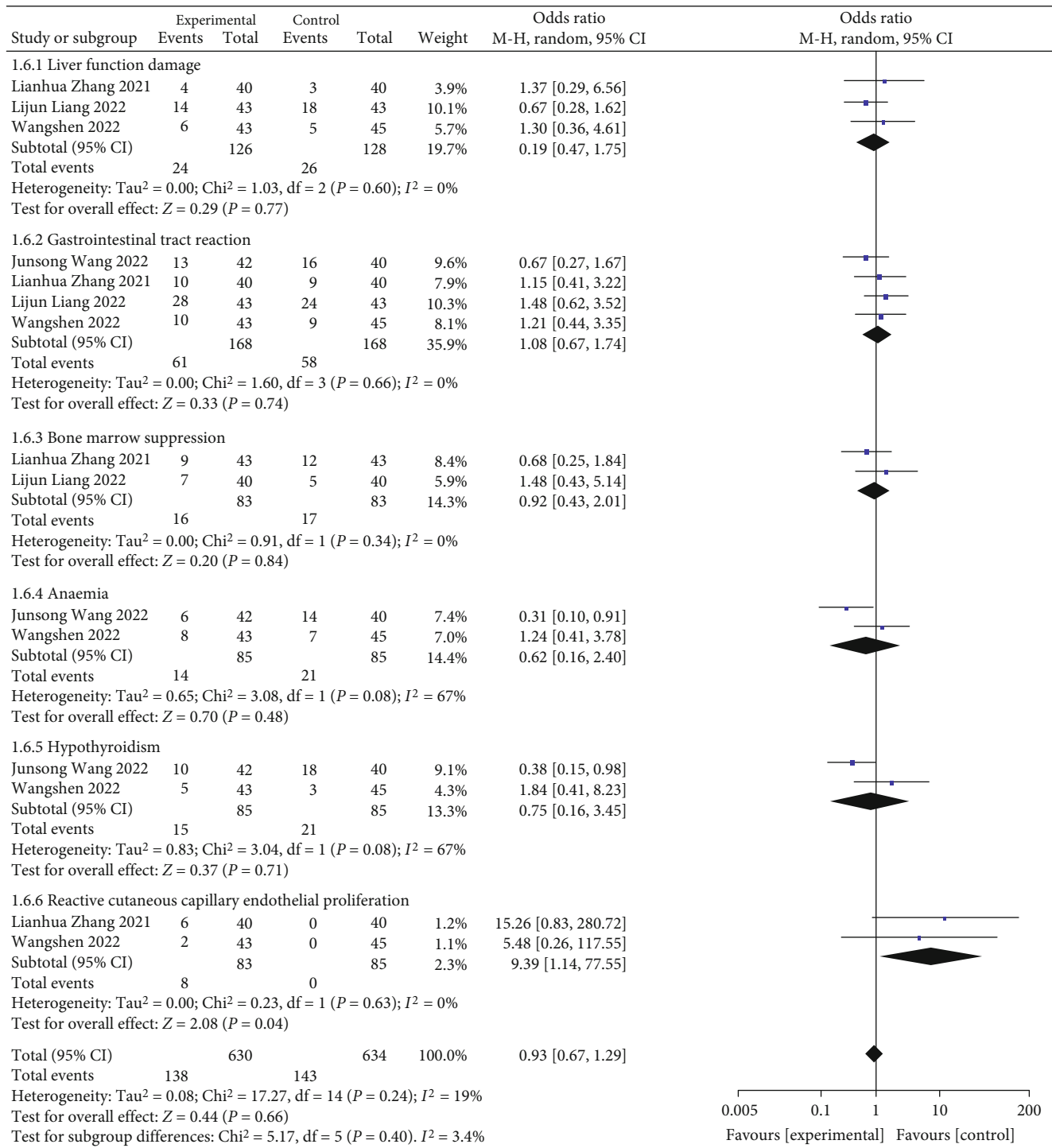


FIGURE 8: Forest plot of meta-analysis of adverse reactions.

$\chi^2$  test is used to determine whether there is heterogeneity between the studies, if  $P > 0.05$  and  $I^2 < 50\%$ , it is considered that the included study is homogeneous, and the modified impact model can be collected for meta-analysis; if  $P < 0.05$  and  $I^2 \geq 50\%$ , when judging the homogeneity of the included study, the combined effect is needed, then choose the random effect model; if  $P < 0.05$ , and the source of het-

erogeneity could not be judged, meta-analysis was not performed, and descriptive analysis was used.

### 3. Results and Analysis

3.1. The Results of Literature Retrieval and the Basic Situation of Literature Inclusion. The computer database



retrieved 1723 articles, and 465 articles were eliminated when repeated studies were removed. After screening the titles and abstracts of 287 articles, 124 articles were contained after eliminating irrelevant studies, reviews, case reports, and no control literature. After carefully reading 108 studies with insufficient data and no major outcome markers, 6 RCTs were eventually contained [15–21]. The meta-analysis covered 492 samples in total. Illustration of literature screening was shown in Figure 1. Basic characteristics of literature was shown in Table 1.

**3.2. Evaluation of the Quality of the Methodology Contained in the Literature.** The six CT articles contained in this meta-analysis reported the baseline health status of the patients. The six studies contained all gave detailed intervention measures and treatment time. None of the 6 articles described in detail the number and reasons of the blind method and those who lost follow-up or withdrew. According to the Jadad scale, all the 6 articles were less than 2 points (Figures 2 and 3).

### 3.3. Results of Meta-Analysis

**3.3.1. Disease Control Rate.** There were 492 samples from 6 studies contained in this study. The disease control rates were analyzed by meta. The results of heterogeneity test indicated that the research data contained in the study showed distinct heterogeneity.  $\chi^2 = 5.46$ ,  $df = 4$ ,  $P = 0.24$ , and  $I^2 = 27\%$ , without obvious heterogeneity among the contained data. The analysis of random effect model (Figure 4) indicated that the disease control rate of the study group was notably better, and the difference was statistically significant ( $P < 0.05$ ). It is suggested that the use of ICIs when treating patients with advanced GC can notably enhance the disease control rate.

**3.3.2. Levels of Serum Tumor Markers.** Four of them compared the levels of CEA and CA199 after treatment. The results of heterogeneity test indicated that: CEA:  $\chi^2 = 76.60$ ,  $df = 2$ ,  $P < 0.00001$ ,  $I^2 = 97\%$ ; CA199:  $\chi^2 = 72.37$ ,  $df = 2$ ,  $P < 0.00001$ ,  $I^2 = 97\%$ . Based on the summary analysis of all the literatures, the heterogeneity test results indicated that  $\chi^2 = 278.10$ ,  $df = 5$ ,  $P < 0.00001$ ,  $I^2 = 98\%$ , indicating that the research data contained in the study showed distinct heterogeneity. The analysis of random effect model (Figure 5) indicated that the levels of serum CEA and CA199 in the study group were notably lower after treatment, and the difference was statistically significant ( $P < 0.05$ ). It has suggested that the treatment of patients with advanced GC with ICIs can better inhibit tumor progression and alleviate the disease.

**3.3.3. Immune Function Index Level.** There were 492 samples from 6 studies contained in this study. The immune function indexes after treatment were compared. The results of heterogeneity test indicated that CD3+:  $\chi^2 = 45.60$ ,  $df = 1$ ,  $P < 0.00001$ ,  $I^2 = 98\%$ ; CD4+:  $\chi^2 = 112.66$ ,  $df = 2$ ,  $P < 0.00001$ ,  $I^2 = 98\%$ ; CD8+:  $\chi^2 = 34.93$ ,  $df = 2$ ,  $P < 0.00001$ ,  $I^2 = 94\%$ . It indicated that the research data contained in

the study showed distinct heterogeneity. The analysis of random effect model (Figure 6) indicated that the improvement of immune function indexes in the study group was notably better after treatment, and the difference was statistically significant ( $P < 0.05$ ). It has suggested that ICIs therapy can protect and enhance the immune function and reshape the antitumor immune system.

**3.3.4. Survival Period.** This study contained 6 studies with a total of 492 samples, of which 3 clinical trials reported post-operative median PFS. The results of heterogeneity test indicated that the research data contained in the study showed distinct heterogeneity ( $\chi^2 = 17.29$ ,  $df = 2$ ,  $P = 0.0002$ ,  $I^2 = 88\%$ ). The analysis of random effect model (Figure 7) indicated that the PFS of the study group was notably longer after treatment, and the difference was statistically significant ( $P < 0.05$ ). It has suggested that immuno-checkpoint inhibitor therapy can notably prolong the survival time of patients with advanced GC.

**3.3.5. Adverse Reactions.** The common adverse reactions contained liver function injury, myelosuppression, gastrointestinal reactions, anemia, hypothyroidism, and reactive capillary hyperplasia. The results of heterogeneity test indicated that  $\chi^2 = 17.27$ ,  $df = 14$ ,  $P = 0.24$ , and  $I^2 = 19\%$ . No obvious heterogeneity was found among the contained research data. The analysis of random effect model (Figure 8) indicated that there exhibited no notable difference in the incidence of adverse reaction ( $P > 0.05$ ). It has suggested that routine chemotherapy associated with immuno-checkpoint inhibitor therapy would not notably increase the adverse reactions of patients with advanced GC.

## 4. Analysis and Discussion

The ICIs can restore the immune response by blocking the process of immune escape. At present, immunotherapy has been successfully applied in solid cancers such as advanced head and neck squamous cell carcinoma, non-small-cell lung cancer, and malignant melanoma, and gratifying results have been obtained in the early study of GC [23]. For patients with advanced GC, two or three kinds of drugs associated with chemotherapy and targeted therapy are the main means of drug therapy at present, but long-term use of highly toxic chemotherapeutic drugs can cause drug accumulation and cause severe discomfort in patients. In clinical practice, some patients often refuse chemotherapy due to adverse reactions or other reasons, resulting in rapid tumor progression. There is limited evidence that targeted therapy can improve the prognosis of patients with GC, so it is necessary to explore new treatment models. Immunotherapy has gradually attracted medical attention. It is a landmark development in the field of immune oncology that ICIs were developed [24]. At present, the most studied ICIs are PD-1 inhibitors. Many kinds of malignant tumors have been shown to benefit from PD-1 inhibitors in terms of enhancing antitumor immunity, promoting immune-mediated tumor cell elimination, and improving overall survival rates [25]. This paper was to systematically assess the clinical

effect and survival time of immune checkpoint inhibitor (ICIs) in advanced gastric cancer (GC) and adverse reactions to provide evidence-based medicine for its enhancement and adoption.

Tumor cells mainly escape the monitoring of immune response through the coinhibitory signal pathway mediated by immune checkpoint [26]. It has aroused great interest in the application of immunotherapy in patients with advanced GC, thus triggering several key clinical trials. In view of this theory, scholars began to try to develop and apply ICIs. PD-1 is the main inhibitory molecule on the surface of T cells and attaches importance to the negative regulation of immune response [27]. It has been confirmed that tumor microenvironment can induce the expression of PD-1 on tumor surface. PD-1 inhibitors, as common clinical ICIs, can induce and enhance antitumor immune response. Camrelizumab is a PD-1 inhibitor independently developed in China, which has been officially permitted by the State Drug Administration in May 2019 [28]. Cytotoxic T lymphocyte associated antigen-4 and PD-1 are the most concerned immune checkpoints. PD-1 is mainly expressed on the surface of tumor infiltrating lymphocytes, B cells, natural killer cells, and dendritic cells and binds to PD-L1, which can make activated T cells become nonreactive T cells [29, 30]. Associated with the results of this study, the disease control rate of the study group was notably better. It is suggested that the use of ICIs when treating patients with advanced GC can notably enhance the disease control rate, indicating that ICIs has obvious therapeutic effect on patients with GC. In addition, the drug can inhibit tumor progression and reduce the volume of tumor. PFS of the study group was notably longer after treatment. It is suggested that the treatment with ICIs can notably prolong the survival time of patients with advanced GC. The prolongation of survival time also reflects the exact effect of the drug, indicating that ICIs can fundamentally improve the condition of the patients. The short-term and long-term effects are reliable and can effectively prolong the survival time of patients. In tumor immunity, the immune system can recognize and get rid of tumor cells to prevent the progression of cancer. Nevertheless, tumor cells can avoid recognition and killing by immune system through immune escape, thus developing into malignant proliferation. During the period of malignant proliferation of tumor cells, they can escape immune surveillance by constantly changing the antigen phenotype and then suppress the antitumor immune response through various immunosuppression and immunosuppressive factors in the tumor microenvironment to form immune escape.

At present, clinical trials of camrelizumab when treating many kinds of tumors have been carried out. The results show that camrelizumab can increase the CR rate of relapsed/refractory classical Hodgkin's lymphoma and the objective remission rate of advanced non-small-cell lung cancer, advanced esophageal squamous cell carcinoma, and advanced GC. Clinical studies have confirmed that the immune system can enhance the immune response to tumor, to enhance the ability of autoimmune system to clear tumor cells by strengthening the inhibition of PD-1/PD-L1 pathway to achieve the purpose of antitumor. The improve-

ment of immune function indexes in the study group was notably better after treatment. It is fully proved that immunotherapy associated with chemotherapy can improve the synergism. On the one hand, chemotherapy can obviously damage the normal cell function of the body while killing tumor cells, resulting in low immunity of patients. Immunotherapy can protect and improve the immune function of the body, reshape the antitumor immune system, enhance the antitumor effect, prolong the survival time, and improve the quality of life. Therefore, the immunity of patients has been greatly improved after the application of ICIs, which is of positive significance to the treatment and rehabilitation of the disease. Four articles in this study compared the levels of CEA and CA199 after treatment. It is suggested that the use of ICIs when treating patients with advanced GC can better inhibit tumor progression and alleviate the disease. It is considered that PD-1 inhibitors can better reduce immunosuppression, enhance antitumor immune response, and effectively prevent the progression of disease. As important tumor markers, the levels of serum CEA and CA199 can accurately reflect the disease control of patients. In this study, the levels of serum CEA and CA199 in the study group decreased notably, indicating that ICIs have a good effect on advanced GC.

No notable difference was discovered in the incidence of adverse reactions. It is suggested that routine chemotherapy associated with ICIs will not notably increase the adverse reactions of patients with advanced GC, indicating that immuno-checkpoint inhibitors are safe and suitable for patients with severe conditions. Patients are well tolerated and can be safely used. The limitations of the study are as follows: (1) the inclusion and exclusion criteria are relatively strict, and the final number of included literature is relatively small; (2) the source of heterogeneity cannot be found through subgroup analysis, which needs to be followed up by scholars, and the results of this study need to provide more support. More high-quality randomized controlled trials are needed to verify.

## 5. Conclusion

To sum up, ICIs have high clinical application value in advanced GC. Combined chemotherapy can successfully enhance the level of T lymphocytes, regulate the function of immune system, and prolong the survival time of patients. In addition, the adverse reactions are within a controllable range.

## Data Availability

The datasets used and analyzed during the current study are available from the corresponding author upon reasonable request.

## Conflicts of Interest

The authors declare that they have no conflicts of interest.

## References

- [1] A. P. Thrift and H. B. El-Serag, "Burden of gastric cancer," *Clinical Gastroenterology and Hepatology*, vol. 18, no. 3, pp. 534–542, 2020.
- [2] S. S. Joshi and B. D. Badgwell, "Current treatment and recent progress in gastric cancer," *CA: a Cancer Journal for Clinicians*, vol. 71, no. 3, pp. 264–279, 2021.
- [3] M. Alipour, "Molecular mechanism of *Helicobacter pylori*-induced gastric cancer," *Journal of Gastrointestinal Cancer*, vol. 52, no. 1, pp. 23–30, 2021.
- [4] R. E. Sexton, M. N. Al Hallak, M. Diab, and A. S. Azmi, "Gastric cancer: a comprehensive review of current and future treatment strategies," *Cancer Metastasis Reviews*, vol. 39, no. 4, pp. 1179–1203, 2020.
- [5] K. Shitara, Y. J. Bang, S. Iwasa et al., "Trastuzumab deruxtecan in previously treated HER2-positive gastric cancer," *The New England Journal of Medicine*, vol. 382, no. 25, pp. 2419–2430, 2020.
- [6] H. C. Chung, Y. J. Bang, S. Fuchs et al., "First-line pembrolizumab/placebo plus trastuzumab and chemotherapy in HER2-positive advanced gastric cancer: KEYNOTE-811," *Future Oncology*, vol. 17, no. 5, pp. 491–501, 2021.
- [7] Y. Y. Janjigian, S. B. Maron, W. K. Chatila et al., "First-line pembrolizumab and trastuzumab in HER2-positive oesophageal, gastric, or gastro-oesophageal junction cancer: an open-label, single-arm, phase 2 trial," *The Lancet Oncology*, vol. 21, no. 6, pp. 821–831, 2020.
- [8] C. Dolladille, S. Ederhy, M. Sassier et al., "Immune checkpoint inhibitor rechallenge after immune-related adverse events in patients with cancer," *JAMA Oncology*, vol. 6, no. 6, pp. 865–871, 2020.
- [9] A. Pellino, E. Riello, F. Nappo et al., "Targeted therapies in metastatic gastric cancer: current knowledge and future perspectives," *World Journal of Gastroenterology*, vol. 25, no. 38, pp. 5773–5788, 2019.
- [10] H. Bukamur, H. Katz, M. Alsharedi, A. Alkrekhshi, Y. R. Shweihat, and N. J. Munn, "Immune checkpoint inhibitor-related pulmonary toxicity: focus on nivolumab," *Southern Medical Journal*, vol. 113, no. 11, pp. 600–605, 2020.
- [11] T. Min and J. Zhang, "PD-1/PD-L1 signal pathway and its research progress when treating GC J," *Modern Medicine and Health*, vol. 36, no. 13, pp. 2021–2025, 2020.
- [12] M. Tokunaga, Y. Sato, M. Nakagawa et al., "Perioperative chemotherapy for locally advanced gastric cancer in Japan: current and future perspectives," *Surgery Today*, vol. 50, no. 1, pp. 30–37, 2020.
- [13] H. C. Chung, Y.-J. Bang, C. S. Fuchs et al., "First-line pembrolizumab/placebo plus trastuzumab and chemotherapy in HER2-positive advanced gastric cancer: KEYNOTE-811," *Future Oncology*, vol. 17, no. 5, pp. 491–501, 2021.
- [14] Y. Jiang, J. Xie, W. Huang et al., "Tumor immune microenvironment and chemosensitivity signature for predicting response to chemotherapy in gastric cancer," *Cancer Immunology Research*, vol. 7, no. 12, pp. 2065–2073, 2019.
- [15] G. Yan and P. Qingwen, "Clinical characteristics and diagnostic experience of GC in young people," *Chinese Medicine Guide*, vol. 7, no. 3, pp. 38–39, 2009.
- [16] Y. Xing, W. Qing, and Y. Jier, "Research progress of ICIs when treating advanced GC," *Zhejiang Medicine*, vol. 42, no. 14, pp. 1545–1550, 2020.
- [17] Z. Guili, L. Xiuju, D. Min, S. Yanlong, W. Yan, and Z. Chen, "Efficacy of PD-1 inhibitor associated with FOLFOX4 chemotherapy when treating advanced GC," *China Medical Herald*, vol. 18, no. 8, pp. 98–101, 2021.
- [18] L. Lijun, "Efficacy and progression-free survival of apatinib mesylate associated with carelizumab when treating stage III/IV GC," *Journal of Practical Cancer*, vol. 37, no. 5, pp. 851–854, 2022.
- [19] W. Shen, D. Fengyi, L. Mingying, X. Zhiji, and P. Liming, "Efficacy and short-term prognosis of carilizumab associated with amlotinib when treating advanced GC," *Evaluation and Analysis of Drug use in Chinese Hospitals*, vol. 22, no. 1, pp. 32–37 +42, 2022.
- [20] Z. Lianhua, T. Mingcai, and T. Guoying, "Clinical study of carilizumab associated with chemotherapy when treating advanced GC," *Study on Drug Evaluation*, vol. 44, no. 7, pp. 1502–1507, 2021.
- [21] T. Huiyang, X. Chao, and Z. Lingzhi, "Observation on the effect of immunotherapy associated with chemotherapy when treating GC," *Shenzhen Journal of Integrated Traditional Chinese and Western Medicine*, vol. 31, no. 15, pp. 131–133, 2021.
- [22] W. Junsong and L. Xiupeng, "Efficacy and safety of capecitabine, oxaliplatin associated with parbolizumab when treating advanced GC," *Practical Drugs and Clinical Practice*, vol. 25, no. 3, pp. 217–220, 2022.
- [23] Z. Yangting, L. Yanli, M. Hongbo, and X. Bin, "Progress of paclitaxel when treating advanced GC," *Chinese Journal of Gerontology*, vol. 42, no. 6, pp. 1524–1527, 2022.
- [24] PET Group, "Nuclear medicine branch of Chinese Medical Association. Expert consensus on PET/CT evaluation of ICIs when treating malignant tumors (version 2020)," *Chinese Journal of Oncology*, vol. 42, no. 9, pp. 697–705, 2020.
- [25] Q. Wu, L. Jiang, S. C. Li, Q. J. He, B. Yang, and J. Cao, "Small molecule inhibitors targeting the PD-1/PD-L1 signaling pathway," *Acta Pharmacologica Sinica*, vol. 42, no. 1, pp. 1–9, 2021.
- [26] J. Li, X. H. Zhang, S. H. Bei, and L. Feng, "PD-1/PD-L1 antagonists in gastric cancer: current studies and perspectives," *World Journal of Meta-Analysis*, vol. 7, no. 3, pp. 101–109, 2019.
- [27] A. Saeed, R. Park, and W. Sun, "The integration of immune checkpoint inhibitors with VEGF targeted agents in advanced gastric and gastroesophageal adenocarcinoma: a review on the rationale and results of early phase trials," *Journal of Hematology & Oncology*, vol. 14, no. 1, pp. 1–11, 2021.
- [28] D. B. Doroshov, S. Bhalla, M. B. Beasley et al., "PD-L1 as a biomarker of response to immune-checkpoint inhibitors," *Nature Reviews. Clinical Oncology*, vol. 18, no. 6, pp. 345–362, 2021.
- [29] R. Park, S. Williamson, A. Kasi, and A. Saeed, "Immune therapeutics in the treatment of advanced gastric and esophageal cancer," *Anticancer Research*, vol. 38, no. 10, pp. 5569–5580, 2018.
- [30] N. Koizumi, S. Kashiwagi, S. Ogino, Y. Kamada, H. Fujiki, and C. Sakakura, "A case of initially unresectable advanced gastric cancer radically resected by conversion surgery after nivolumab immunotherapy," *Cancer & Chemotherapy*, vol. 47, no. 11, pp. 1624–1626, 2020.

## Research Article

# Effect of Psychological Nursing Intervention on Abnormal-Induced Labor of Fetus during Puerperium: Study on the Effects of Anxiety, Depression, and Life Events

Yanjuan He,<sup>1</sup> Huiwen He,<sup>2</sup> and Cai Tang<sup>3</sup> 

<sup>1</sup>Department of Obstetrics, Changsha Hospital for Maternal and Child Health Care, Changsha 410000, China

<sup>2</sup>Department of Neurology, Hunan Children's Hospital, Changsha, Hunan 410000, China

<sup>3</sup>Department of Gynecology, Hunan Provincial People's Hospital (The First Affiliated Hospital of Hunan Normal University), Changsha, Hunan 410000, China

Correspondence should be addressed to Cai Tang; 2016124117@jou.edu.cn

Received 13 July 2022; Accepted 4 August 2022; Published 23 August 2022

Academic Editor: Hangjun Che

Copyright © 2022 Yanjuan He et al. This is an open access article distributed under the Creative Commons Attribution License, which permits unrestricted use, distribution, and reproduction in any medium, provided the original work is properly cited.

**Objective.** To study the effects of psychological nursing intervention on anxiety, depression, and life events in puerperal women with fetal abnormalities. **Methods.** From January 2020 to January 2022, eighty women with abnormal fetal induction and puerperium-treated were selected in our hospital as the subjects. The research group ( $n = 40$ ) and control group ( $n = 40$ ) were arbitrarily selected from 80 women with abnormal fetal induction and puerperium. The research group was given psychological nursing intervention based on routine nursing, and the control cases were given routine nursing. The scores of Generalized Anxiety Scale (GAD-7), Patient Health Questionnaire (PHQ-9), Event Impact Scale (IES-R), Life Events Scale (LES), and Newcastle Nursing Satisfaction Scale (NSNS) were studied before nursing and 4 weeks after discharge. **Results.** Four weeks after discharge, the score of GAD-7 in the research group was lower, and the difference was statistically significant ( $P < 0.05$ ). The score of PHQ-9 in the research group was lower, and the difference was statistically significant ( $P < 0.05$ ). The IES-R score of the research group was lower, and the difference was statistically significant ( $P < 0.05$ ). The LES score of the research group was lower, and the difference was statistically significant ( $P < 0.05$ ). And the NSNS score of the research group was higher, and the difference was statistically significant ( $P < 0.05$ ). **Conclusion.** The value of psychological care interventions in women with abnormally induced labor is more remarkable, contributing to the reduction of anxiety and depression and increasing the satisfaction of care for women with abnormally induced labor.

## 1. Introduction

Fetal abnormalities include congenital malformations and stillbirths [1]. Fetal congenital malformation refers to the abnormal development of fetal morphology, structure, and physiological function caused by various internal and external factors in the process of embryonic development [2]. Stillbirth refers to fetal death in the womb after 20 weeks of pregnancy [3]. The progress of prenatal diagnosis technology has greatly improved the diagnosis rate of fetal developmental abnormalities. The current intrauterine treatment techniques are still very limited. Once the fetus is diagnosed

with serious developmental abnormalities, we must face the cruel reality and fierce emotional struggle to terminate the pregnancy [4, 5]. Termination of pregnancy is necessary when fetal malformations are detected during pregnancy. This is a strong psychological shock and emotional blow to the pregnant woman and can bring about devastating psychosocial problems [6]. Previous studies have shown that such events can cause posttraumatic stress disorder (PTSD) in women with abnormal fetal induction of labor, as well as strong negative emotions such as anxiety, depression, helplessness, fear, and dissatisfaction [7, 8]. In addition, the symptoms of PTSD and depression caused by abnormal-



induced labor indicated a persistent pattern, which persisted for 2-7 years after induced labor [9]. In recent years, a number of studies have found that women have negative psychological experiences after the traumatic event of an abnormal fetal induction. The psychological torment of women with abnormal fetal induction is so severe that they may even be suicidal [10, 11]. From placenta delivery to the maternal body organs (except breast) to restore to the normal nonpregnant state of a period (generally 6 weeks) is called puerperal period [2]. Puerperium is a critical period for the physical and psychological recovery of pregnant women. Previous studies have shown that postpartum 3-7 days is the peak period of anxiety and depression in puerperal women [12, 13]. Most women with induced labor have a short hospitalization time and can be discharged from hospital 2-3 days after induced labor. There are few social support resources available during puerperal period after discharge. Physical and mental rehabilitation and nursing are weak links at this stage. Psychological nursing intervention has become a widely concerned field of maternal and obstetrical health care in China. A few studies have shown that psychological nursing intervention model can fully meet the health needs of puerperal women, reduce the occurrence of postpartum depression, increase self-care ability, successfully complete the role transformation, and promote the physical rehabilitation of parturients [14, 15]. Therefore, this paper formulated the intervention program for the puerperal psychology of women with fetal abnormal-induced labor and verified the effects of the intervention program on puerperal anxiety, depression, and life events.

## 2. Patients and Methods

**2.1. General Information.** During January 2020 to January 2022, eighty women with abnormal fetal induction and puerperium-treated were selected in our hospital as the subjects. The research group ( $n = 40$ ) and control group ( $n = 40$ ) were arbitrarily selected from 80 women with abnormal fetal induction and puerperium. In the former group, the age distribution ranged from 29 to 38 years old with an average of  $(31.48 \pm 2.16)$  years. The gestational age was between 14 and 35 weeks with an average of  $(25.74 \pm 3.12)$  weeks. In the latter group, the age distribution was from 28 to 39 years old with an average of  $(31.15 \pm 2.33)$  years. The gestational weeks were between 14 and 34 weeks with an average of  $(25.69 \pm 3.19)$  weeks. Inclusion criteria were as follows: (1) pregnant women were diagnosed as fetal malformations or stillbirths by prenatal diagnosis; (2) hospitalized for induced labor, the gestational week at the time of induced labor was  $\geq 14$  weeks; (3) the individual had not received psychotherapy or counseling recently; and (4) a pregnant woman and her family are voluntarily participating in this study and signed an informed consent form. Exclusion criteria were as follows: (1) previous patients with severe mental disorders (including schizophrenia, mania, severe depression, anxiety disorders and other psychotic disorders), history of mental illness, and unable to complete; (2) people with hearing and expression disorders; (3) those who could not understand the contents of the questionnaire, such as illiteracy and low education level; (4) previous history of

fetal malformation and stillbirth; and (5) pregnancy termination was performed due to other reasons.

## 2.2. Treatment Methods

**2.2.1. Technical Route.** The technical route of this study was shown in Figure 1.

**2.2.2. Intervention Program.** The protocol for the control group was for patients to receive routine diagnosis, treatment, and care. Routine admission education was then given, and invitations to join the control group's microgroup were made. The researcher established a good nurse-patient relationship with the subjects on the day of admission and conducted admission health education and discharge education. Interaction and feedback were always maintained with the mother via WeChat during the puerperium. Follow-up visits were made two weeks after discharge and 42 days after delivery to remind and inform women about the hospital review and the process. The whole intervention consists of 4 weeks.

The scheme of the research group is as follows: psychological nursing intervention was carried out on the basis of routine nursing. The researchers established a good nurse-patient relationship with the subjects on the day of admission. The woman's anxiety and depression were assessed. Patients expressing their current worries and concerns were encouraged, and targeted admission health education (e.g., basic concepts and diagnosis of fetal abnormalities, methods and precautions for termination of pregnancy, and family support education) was given. In addition, the individualized instruction time was 30-50 min. One-to-one postnatal health education (what to do after termination of pregnancy) for the subject at the bedside 24 hours was performed after induction of labor. Yoga instruction and evaluation of the subject's practice were needed for 30-40 min. Yoga was required to practice yoga once a day before discharge. Pregnancy-related knowledge and health education were enhanced. Similar success stories of women having second pregnancies were shared to guide women to understand the disease properly to reduce guilt and alleviate negative emotions. The subjects' yoga practice was evaluated and guides them to write a record of the intervention topics. After discharge, the patients were intervened for 4 weeks through the online WeChat platform with the theme course 30 min every week. Pregnancy and childbirth science was regularly promoted through the online WeChat platform, which provided an opportunity for mothers and their spouses to exchange information and emotions. Invite pregnant women who have had another successful pregnancy to enhance their faith in another successful pregnancy. The content of family support is reinforced, and patients give positive feedback to their families through practical actions expressing gratitude. The patients were guided to explore available social support resources and write weekly intervention themes. During the intervention, pregnant women were urged to complete their homework via WeChat to improve intervention compliance. The intervention should be timed to avoid the subject's treatment and daily care time. The whole intervention process included 4 weeks.



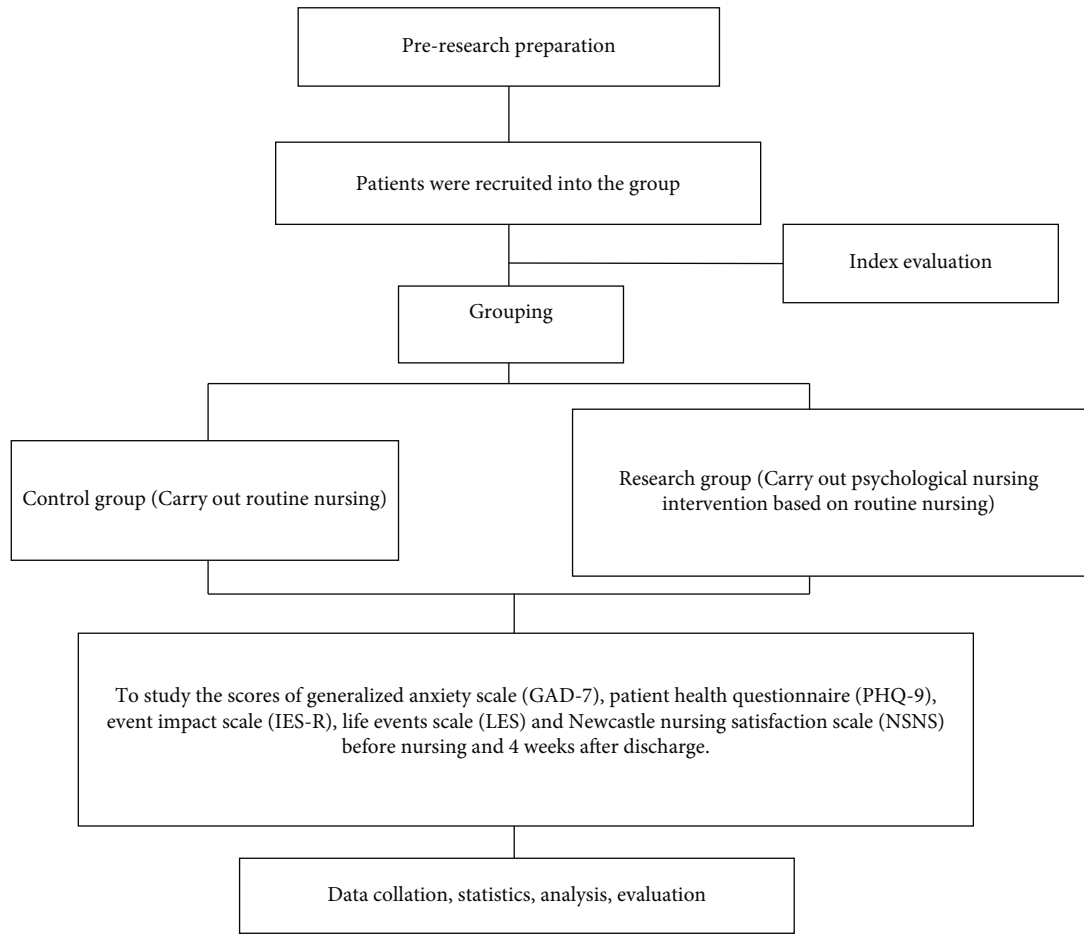


FIGURE 1: Technology roadmap.

### 2.3. Observation Indicators

- (1) The scores of GAD-7 before nursing and 4 weeks after discharge: the GAD-7 scale [16] was used to evaluate the anxiety state of parturients with fetal abnormality-induced labor. There were 7 items in the scale, and each item was scored according to 0-3. The total score of the scale was 0-21, including 0-4 as no anxiety, 5-9 as mild anxiety, 10-14 as moderate anxiety, and  $\geq 15$  as severe anxiety. Cronbach's  $\alpha$  coefficient of the scale was 0.92 [17]
- (2) The scores of PHQ-9 before nursing and 4 weeks after discharge: the PHQ-9 scale was used to evaluate the depression status of parturients with fetal abnormality-induced labor [18]. There were 9 items in the scale. The total score of the scale was 0-27. Depression levels increase as the score increases. There was no depression in score that ranges 0-4, mild depression was 5-8, moderate depression was 9-10, severe depression was 15-19, and extremely severe depression was 20-27. Cronbach's  $\alpha$  coefficient of the scale was 0.89 [19]
- (3) The scores of IES-R before nursing and 4 weeks after discharge: the revised version of the IES-R scale was

a commonly used tool to assess the performance and severity of posttraumatic stress response in the world [20]. A total of 22 items were divided into three dimensions, including intrusion, escape, and arousal, including 8 entries in intrusion dimension (1, 2, 3, 6, 9, 14, 16, 20), 8 items in escape dimension (5, 7, 8, 11, 12, 13, 17, 22), and 6 entries in arousal dimension (4, 10, 15, 18, 19, 21). Using the 5-level scoring method, from "no impact" to "especially many" represented the "0~4" score with a total score of 0~88. Foreign studies have found that people with a total score of more than 19 points were regarded as the standard of clinical attention [21]. The scale had good reliability and validity, and Cronbach's  $\alpha$  coefficient was 0.89 [22]

- (4) The scores of LES before nursing and 4 weeks after discharge: the LES [23] included family life (28 items), work and study (13 items), and social and other aspects (7 items). There were 2 blank items, and the degree of influence was divided into 5 grades. 0, 1, 2, 3, and 4 points were scored from no influence to extremely serious influence
- (5) The scores of NSNS before nursing and 4 weeks after discharge: the total score of NSNS scale ranged from

0 to 95 [24]. Each item was evaluated with a score of 1 to 5, of which 1: very displeased, 2: displeased, 3: general satisfaction, 4: pleased, and 5: very pleased

**2.4. Statistical Analysis.** SPSS23.0 statistical software was adopted to process the data. The measurement data were presented as ( $\bar{x} \pm s$ ). The group design *t*-test was adopted for the comparison, and the analysis of variance was adopted for the comparison between multiple groups. Dunnett's *t*-test was adopted for comparison with the control group. The counting data were presented in the number of cases and the percentage,  $\chi^2$  test was adopted for comparison between groups, and bilateral test was employed for all statistical tests.

### 3. Results

**3.1. Comparison of General Data.** There exhibited no remarkable difference in demographic data such as age, gestational week, education level, bad pregnancy history, with or without children, pregnancy type, and fetal abnormality type ( $P > 0.05$ ), as shown in Table 1.

**3.2. The Scores of GAD-7 Scale before Nursing and 4 Weeks after Discharge.** Before nursing, there exhibited no remarkable difference in the score of the GAD-7 scale ( $P > 0.05$ ). Four weeks after discharge, the score of GAD-7 in the research group was lower, and the difference was statistically significant ( $P < 0.05$ ), as shown in Table 2.

**3.3. The Scores of PHQ-9 before Nursing and 4 Weeks after Discharge.** Before nursing, there exhibited no remarkable difference in the score of the PHQ-9 scale ( $P > 0.05$ ). Four weeks after discharge, the score of PHQ-9 in the research group was lower, and the difference was statistically significant ( $P < 0.05$ ), as shown in Table 3.

**3.4. The IES-R Score of Two Groups before Nursing and 4 Weeks after Discharge.** Before nursing, there exhibited no remarkable difference in the score of the IES-R scale ( $P > 0.05$ ). Four weeks after discharge, the IES-R score of the research group was lower, and the difference was statistically significant ( $P < 0.05$ ), as shown in Table 4.

**3.5. The Score of LES Scale before Nursing and 4 Weeks after Discharge.** Before nursing, there exhibited no remarkable difference in the score of the LES scale ( $P > 0.05$ ). Four weeks after discharge, the LES score of the research group was lower, and the difference was statistically significant ( $P < 0.05$ ), as shown in Table 5.

**3.6. NSNS Scale Score before Nursing and 4 Weeks after Discharge.** Before nursing, there exhibited no remarkable difference in the score of the NSNS scale ( $P > 0.05$ ). Four weeks after discharge, the NSNS score of the research group was higher, and the difference was statistically significant ( $P < 0.05$ ), as shown in Table 6.

### 4. Discussion

China's "second child" policy has led to a sharp increase in the number of elderly pregnant women. The development

of prenatal diagnosis techniques has greatly increased the rate of prenatal diagnosis of fetal defects. The number of women with induced labor due to fetal congenital defects or stillbirth will be increasing year by year [25]. Termination of pregnancy can lead to severe posttraumatic stress disorder and strong psychological sadness response, which is common and lasting and may continue to affect the next pregnancy [26]. Giving appropriate psychological interventions before therapeutic induction of labor and during the puerperium can improve the patient's psychological well-being and build confidence to conceive again. At the same time, it is also conducive to promote the development of eugenics and the construction of mental health service system for this kind of population.

In this study, puerperal women carried out body relaxation and relaxation through yoga practice, so as to promote postpartum physical recovery, reduce the occurrence of postpartum complications, and alleviate the fear of poor postpartum physical recovery. It can help women better realize the meaning and self-value of life, improve the postpartum growth level of women with abnormal induced labor, and improve the quality of life. Previous studies have shown that 3-7 days after delivery are the peak period of anxiety and depression in puerperal women [27]. Compared to women with normal births, women with fetal abnormalities are 4 times more likely to suffer from depression, as well as 7 times more likely to suffer from PTSD. Intervention research on the psychological problems of women with fetal abnormalities in induced labor has also become a major topic in the world. The main psychological care intervention models include the provision of information support, supportive psychotherapy, grief counselling, and integrated clinical support services. The results indicated that after psychological nursing intervention, the scores of GAD-7, PHQ-9, IES-R, and LES were lower than those of routine nursing, while the score of NSNS was higher compared to routine nursing. The value of psychological care interventions in women with abnormal induction of labor has proved to be more remarkable. It is more helpful in reducing patients' anxiety and depression, improving the quality of life and increasing the satisfaction of care for women with abnormally induced labor. This is mainly due to the fear and worry of women who are induced with fetal abnormalities and their own low level of coping. In addition, these pregnant women do not have good control over the physical and emotional changes that occur during the puerperium. According to the psychological experience of puerperal women, we should formulate the theme of intervention, give positive guidance, and correct disease cognitive guidance to pregnant women. The disease-related information and emotional support should be provided, and postpartum continuous care should be supplied to support for women. It can help women better deal with fetal abnormal events, relieve anxiety and depression, and increase confidence in second pregnancy [28]. The earlier study found that relaxation training could increase the release of  $\alpha$  brain waves and enkephalin in the human body to reduce the excitability of sympathetic nerve and relieve patients' negative emotions [29]. Sensible postnatal exercise can enhance a woman's sense of self-worth and self-confidence, thereby alleviating negative emotions. Postnatal

TABLE 1: The general data of two groups.

Group	Age (years)	Gestational week (week)	Educational level		Bad pregnancy history		With or without children		Type of conception		Fetal abnormality type	
			Senior high school and below (example/%)	Senior high school or above (example/%)	Yes (example/%)	None (example/%)	Yes (example/%)	None (example/%)	Natural conception (example/%)	Involuntary pregnancy (example/%)	Fetal malformation (case/%)	Stillbirth (example/%)
C group ( $n = 40$ )	$31.15 \pm 2.33$	$25.69 \pm 3.19$	20/50.00	20/50.00	20/50.00	20/50.00	17/42.50	23/57.50	20/50.00	20/50.00	17/42.50	23/57.50
R group ( $n = 40$ )	$31.48 \pm 2.16$	$25.74 \pm 3.12$	18/45.00	22/55.00	18/45.00	22/55.00	16/40.00	24/60.00	18/45.00	22/55.00	16/40.00	24/60.00
$t/\chi^2$	0.657	0.071	0.201		0.201		0.052			0.201		0.052
$P$	0.513	0.944	0.654		0.654		0.820			0.654		0.820

TABLE 2: The scores of GAD-7 before nursing and 4 weeks after discharge.

Grouping	Before nursing (points)	4 weeks after discharge (points)
Control group	15.28 ± 3.44	9.15 ± 2.27*
Research group	15.31 ± 3.37	5.19 ± 1.04*
<i>t</i> value	0.039	10.030
<i>P</i> value	0.968	<0.01

Note: \* represents the comparison before nursing and 4 weeks after discharge in this group,  $P < 0.05$ .

TABLE 3: The score of the PHQ-9 scale before nursing and 4 weeks after discharge.

Grouping	Before nursing (points)	4 weeks after discharge (points)
Control group	16.38 ± 3.23	8.77 ± 2.32*
Research group	16.41 ± 3.21	5.72 ± 1.12*
<i>t</i> value	0.041	7.487
<i>P</i> value	0.966	<0.01

Note: \* represents the comparison before nursing and 4 weeks after discharge in this group,  $P < 0.05$ .

TABLE 4: The score of the IES-R scale before nursing and 4 weeks after discharge.

Grouping	Before nursing (points)	4 weeks after discharge (points)
Control group	67.12 ± 7.39	47.29 ± 5.15*
Research group	66.14 ± 7.27	28.25 ± 2.14*
<i>t</i> value	0.597	21.592
<i>P</i> value	0.551	<0.01

Note: \* represents the comparison before nursing and 4 weeks after discharge in this group,  $P < 0.05$ .

TABLE 5: LES score before nursing and 4 weeks after discharge from hospital.

Grouping	Before nursing (points)	4 weeks after discharge (points)
Control group	78.59 ± 9.17	57.18 ± 5.39*
Research group	78.63 ± 9.14	31.53 ± 3.11*
<i>t</i> value	0.019	26.069
<i>P</i> value	0.985	<0.01

Note: \* represents the comparison before nursing and 4 weeks after discharge in this group,  $P < 0.05$ .

exercise can also increase interpersonal and social resources and gain support from friends and/or family. This can reduce social isolation and therefore reduces the level of depression [30, 31]. This study still has some shortcomings. Firstly, the quality of this study is limited due to the small sample size we included in the study. Secondly, this research is a single-

TABLE 6: The score of the NSNS scale before nursing and 4 weeks after discharge.

Grouping	Before nursing (points)	4 weeks after discharge (points)
Control group	58.44 ± 1.44	81.59 ± 2.11*
Research group	58.12 ± 1.41	90.15 ± 3.36*
<i>t</i> value	1.004	13.645
<i>P</i> value	0.318	<0.01

Note: \* represents the comparison before nursing and 4 weeks after discharge in this group,  $P < 0.05$ .

center study, and our findings are subject to some degree of bias. Therefore, our results may differ from those of large-scale multicenter studies from other academic institutes. This research is still clinically significant, and further in-depth investigations will be carried out in the future.

To sum up, the value of psychological care interventions in women with abnormally induced labor is more remarkable, contributing to the reduction of anxiety and depression and increasing the satisfaction of care for women with abnormally induced labor.

## Data Availability

The datasets used and analyzed during the current study are available from the corresponding author upon reasonable request.

## Conflicts of Interest

The authors declare that they have no conflict of interest.

## Acknowledgments

This study is supported by the Scientific Research Program of Hunan Provincial Health Commission (202114031150) and Science and Technology Program of Changsha (KQ2014017).

## References

- [1] L. Yanfen, "Application of NT ultrasonography in fetal abnormality screening in early pregnancy," *Chinese Practical Medicine*, vol. 16, no. 14, pp. 85–87, 2021.
- [2] Z. Xiaoli, *Study on puerperal psychological experience and intervention of women with fetal abnormality induced labor*, Zhejiang University, 2020.
- [3] N. Ping, Y. Weitao, and P. Jing, "Analysis of causes and preventive measures of 202 cases of stillbirth in obstetrics," *Chinese Journal of Modern Medicine*, vol. 24, no. 3, pp. 85–88, 2022.
- [4] C. Luchi, M. Schifano, C. Sacchini et al., "Detailed fetal anatomy assessment in the first trimester at 11, 12 and 13 weeks of gestation," *The Journal of Maternal-Fetal & Neonatal Medicine*, vol. 25, no. 6, pp. 675–678, 2012.
- [5] B. Huilian, "Investigation and study on the depression level of pregnant women with stillbirth and fetal malformation induced labor," *The latest Medical Information Abstracts in the World*, vol. 18, no. 84, pp. 195–202, 2018.

- [6] C. L. Westby, A. R. Erlandsen, S. A. Nilsen, E. Visted, and J. C. Thimm, "Depression, anxiety, PTSD, and OCD after stillbirth: a systematic review," *BMC Pregnancy and Childbirth*, vol. 21, no. 1, pp. 1–17, 2021.
- [7] P. Ludwig-Beymer, B. Vottero, A. Coates, N. Blodgett, J. Rogers, and M. McGonigal-Kenney, "Nursing faculty workload: Balancing fiscal responsibility and faculty satisfaction," *Nurse Educator*, vol. 47, no. 3, pp. 174–179, 2022.
- [8] M. Kicia, A. Skurzak, K. Wiktor, G. Iwanowicz-Palus, and H. Wiktor, "Anxiety and stress in miscarriage," *Polish Journal of Public Health*, vol. 125, no. 3, pp. 162–165, 2015.
- [9] A. Kersting, M. Dorsch, C. Kreulich et al., "Trauma and grief 2–7 years after termination of pregnancy because of fetal anomalies – a pilot study," *Journal of Psychosomatic Obstetrics and Gynecology*, vol. 26, no. 1, pp. 9–14, 2005.
- [10] D. J. Krosch and J. Shakespeare-Finch, "Grief, traumatic stress, and posttraumatic growth in women who have experienced pregnancy loss," *Psychological Trauma: Theory, Research, Practice, and Policy*, vol. 9, no. 4, pp. 425–433, 2017.
- [11] C. Lafarge, K. Mitchell, and P. Fox, "Posttraumatic growth following pregnancy termination for fetal abnormality: the predictive role of coping strategies and perinatal grief," *Anxiety, Stress, & Coping*, vol. 30, no. 5, pp. 536–550, 2017.
- [12] G. Xin, C. Danling, and Z. Jing, "Clinical investigation and nursing study of postpartum depression," *Chinese Journal of Maternal and Child Health*, vol. 4, no. 4, pp. 32–33, 2013.
- [13] N. K. Özcan, N. E. Boyacıoğlu, and H. Dinç, "Postpartum depression prevalence and risk factors in Turkey: a systematic review and meta-analysis," *Archives of Psychiatric Nursing*, vol. 31, no. 4, pp. 420–428, 2017.
- [14] R. Chunying, H. Zhanyun, and G. E. Jinxia, "Effect of psychological intervention on pregnancy outcome and postpartum depression," *Psychological Monthly*, vol. 16, no. 18, pp. 143–144, 2021.
- [15] H. Wenying and Z. Liyan, "Effect of postpartum visit nursing intervention on mental state and quality of life of puerperal women," *Heilongjiang Medicine*, vol. 35, no. 2, pp. 472–474, 2022.
- [16] Q. S. Victory, "Diagnostic test of generalized anxiety scale in screening generalized anxiety disorder in psychological outpatient department of general hospital," *Chinese Journal of Mental Health*, vol. 29, no. 12, pp. 939–944, 2015.
- [17] S. M. Moyer, "Work-life balance of nursing faculty: A scoping review," *Nursing Education Perspectives*, vol. 43, no. 4, pp. 211–216, 2022.
- [18] W. Wang, Q. Bian, Y. Zhao et al., "Reliability and validity of the Chinese version of the Patient Health Questionnaire (PHQ-9) in the general population," *General Hospital Psychiatry*, vol. 36, no. 5, pp. 539–544, 2014.
- [19] C. Manman and Q. S. Shengli, "Diagnostic test of patient health questionnaire in screening depressive disorder in psychiatric outpatient department of general hospital," *Chinese Journal of Mental Health*, vol. 29, no. 4, pp. 241–245, 2015.
- [20] S. Christianson and J. Marren, "The impact of event scale-revised (IES-R)," *Medsurgery Nursing*, vol. 21, no. 5, pp. 321–322, 2012.
- [21] K. Erlandsson, P. Avelin, K. Säflund, R. Wredling, and I. Rådestad, "Siblings' farewell to a stillborn sister or brother and parents' support to their older children: a questionnaire study from the parents' perspective," *Journal of Child Health Care*, vol. 14, no. 2, pp. 151–160, 2010.
- [22] G. Suran, X. Ziqiang, and G. L. Na, "Analysis of reliability and validity of the revised version of event impact scale," *Chinese Journal of Clinical Psychology*, vol. 15, no. 1, pp. 15–17, 2007.
- [23] R. R. S. Clark, M. E. Peele, and E. T. Lake, "Nursing resources by type of maternity unit across regions of the United States," *Journal of Obstetric, Gynecologic & Neonatal Nursing*, vol. 51, no. 3, pp. 290–301, 2022.
- [24] M. Piredda, E. Vellone, G. Piras et al., "Psychometric evaluation of the Newcastle satisfaction with nursing scales," *Journal of Nursing Care Quality*, vol. 30, no. 1, pp. 84–92, 2015.
- [25] H. Cho, K. Sagherian, L. D. Scott, and L. M. Steege, "Occupational fatigue, workload and nursing teamwork in hospital nurses," *Journal of Advanced Nursing*, vol. 78, no. 8, pp. 2313–2326, 2022.
- [26] T. Carlsson, V. Starke, and E. Mattsson, "The emotional process from diagnosis to birth following a prenatal diagnosis of fetal anomaly: a qualitative study of messages in online discussion boards," *Midwifery*, vol. 48, pp. 53–59, 2017.
- [27] N. Asplin, H. Wessel, L. Marions, and S. Georgsson Öhman, "Pregnancy termination due to fetal anomaly: Women's reactions, satisfaction and experiences of care," *Midwifery*, vol. 30, no. 6, pp. 620–627, 2014.
- [28] C. Lafarge, K. Mitchell, A. C. Breeze, and P. Fox, "Pregnancy termination for fetal abnormality: are health professionals' perceptions of women's coping congruent with women's accounts?," *BMC Pregnancy and Childbirth*, vol. 17, no. 1, pp. 1–12, 2017.
- [29] B. Y. Sim, Y. W. Lee, H. Kim, and S. H. Kim, "Post-traumatic growth in stomach cancer survivors: Prevalence, correlates and relationship with health-related quality of life," *European Journal of Oncology Nursing*, vol. 19, no. 3, pp. 230–236, 2015.
- [30] J. Knapen, D. Vancampfort, Y. Moriën, and Y. Marchal, "Exercise therapy improves both mental and physical health in patients with major depression," *Disability and Rehabilitation*, vol. 37, no. 16, pp. 1490–1495, 2015.
- [31] R. Poyatos-León, A. García-Hermoso, G. Sanabria-Martínez, C. Álvarez-Bueno, I. Cavero-Redondo, and V. Martínez-Vizcaino, "Effects of exercise-based interventions on postpartum depression: a meta-analysis of randomized controlled trials," *Birth*, vol. 44, no. 3, pp. 200–208, 2017.



## Research Article

# MRI Evaluation of Indomethacin Suppositories in the Prevention of Complications of Pancreatitis and Hyperamylasemia after Choledocholithiasis ERCP Based on Image Denoising Algorithm

Fusheng Gao, Chuan Zhang, Yue Feng, and Yutao Zhan 

Department of Gastroenterology, Beijing Tongren Hospital, Capital Medical University, Beijing 100176, China

Correspondence should be addressed to Yutao Zhan; yutaozhan0508@sina.com

Received 7 June 2022; Revised 6 July 2022; Accepted 6 August 2022; Published 23 August 2022

Academic Editor: Shimin Wang

Copyright © 2022 Fusheng Gao et al. This is an open access article distributed under the Creative Commons Attribution License, which permits unrestricted use, distribution, and reproduction in any medium, provided the original work is properly cited.

**Objective.** To explore the value of MRI evaluation of indomethacin suppositories in the prevention of pancreatitis and hyperamylasemia in patients with common bile duct calculi after endoscopic retrograde cholangiopancreatography (ERCP) based on image denoising algorithm. **Methods.** A retrospective analysis in August 2020 to December 2021. Because of the common bile duct calculi hospitalized parallel ERCP operation, 89 cases of patients, according to the different postoperative treatments, were divided into group A ( $n = 44$ ) and group B ( $n = 45$ ), in which A set of separate application inhibits the pancreatic enzyme secretion after surgery drug treatment, and B group on the basis of group A linked with indole beauty Xinshuan treatment. The incidence of postoperative pancreatitis and hyperamylasemia was compared between the two groups. The levels of serum amylase were compared between the two groups. Patients in group B were diagnosed with pancreatitis by conventional MRI and MRI with denoising algorithm, respectively, and the imaging characteristics and diagnosis rate differences of the two methods were observed. ROC curve was drawn to evaluate the diagnostic efficacy of MRI denoising algorithm for postoperative pancreatitis and serum amylase level detection for hyperamylasemia. **Results.** The incidence of postoperative pancreatitis and hyperamylasemia in group B was significantly lower than that in group A ( $P < 0.05$ ). There were 6 cases of postoperative pancreatitis in group B, 2 cases (33.33%) were diagnosed by conventional MRI, and 5 cases (83.33%) were diagnosed by MRI based on denoising algorithm. Although there was no significant difference in diagnosis rate between the two methods, the number of cases of pancreatitis diagnosed by MRI based on denoising algorithm was slightly higher than that by conventional MRI. Compared with conventional MRI images, MRI images with denoising algorithm showed that the number of cases with pancreatic swelling, the number of cases with pancreatic duct/bile duct dilation, and the number of cases with abdominal effusion were all high (all  $P < 0.05$ ). ROC results showed that the area under the curve of MRI with denoising algorithm for the diagnosis of postoperative pancreatitis was 0.855, and the sensitivity was 89.40%. The specificity was 83.20%, and the area under the curve of serum amylase for postoperative hyperamylasemia was 0.893, the sensitivity was 89.80%, and the specificity was 85.20%, all of which had high diagnostic efficacy. **Conclusion.** MRI results of denoising algorithm suggest that indomethacin suppositories can effectively reduce the incidence of postoperative pancreatitis and hyperamylasemia after ERCP, which is worthy of clinical application.

## 1. Introduction

As the most common disease in the digestive system, choledocholithiasis can be divided into primary and secondary stones according to different sources, and the incidence of choledocholithiasis has been increasing year by year with

the development of social economy and the change of dietary structure [1]. At present, there has not been a unified conclusion on the causes of choledocholithiasis in clinical practice, and most studies show that it is closely related to age, hypothyroidism, gastrointestinal dysfunction, and Oddi sphincter dysfunction [2]. The main clinical symptoms of

such diseases are abdominal pain, jaundice, chills, and high fever. If medical treatment is not timely, it is highly likely to cause secondary infection and cholangitis and then induce systemic infection, endangering the life and health of patients [3]. Endoscopic retrograde cholangiopancreatography (ERCP) is widely used in the diagnosis and treatment of clinical hepatobiliary and pancreatic diseases and also has high clinical efficacy in the treatment of choledocholithiasis. However, some scholars have pointed out that pancreatitis and hyperamylaseemia caused by ERCP are inevitable in the long-term clinical application process. Therefore, it is of great significance to seek a treatment that can effectively reduce postoperative complications of ERCP to improve the prognosis of patients with choledocholithiasis [4, 5]. In the past clinical practice, doctors usually give patients indomethacin before surgery to reduce the incidence of postoperative complications, but the drug delivery way will be complicated by gastric mucosal injury after surgery, so this study by adopting indomethacin suppositories in anus to medicine way, the effect of postoperative complications in patients with lower ERCP was observed, and the denoising algorithm of magnetic resonance imaging (MRI) to evaluate the specific efficacy is presented as the following reports [6].

## 2. General Information and Methods

**2.1. General Information.** A retrospective analysis was performed on 89 patients admitted for choledocholithiasis and undergoing ERCP from August 2020 to December 2021, who were divided into group A ( $n=44$ ) and group B ( $n=45$ ) according to different postoperative treatment methods. The baseline data of the two groups are shown in Table 1, which were comparable ( $P > 0.05$ ). All the patients included in the study signed informed consent before surgery. In addition, we have the right to know the treatment and detection methods adopted in this study. The clinical data and general information obtained in this study are kept confidential and will not be used for other purposes. This study was approved by the Ethics Committee.

Inclusion criteria are as follows: (1) it met the clinical diagnostic criteria for common bile duct calculi [7]. These include biliary colic caused by bile duct obstruction, cholangitis caused by secondary bacterial infection, abdominal pain, jaundice, chills, and high fever; (2) signed the informed consent before surgery; (3) ERCP operation was used in all cases; and (4) complete clinical data and general information.

Exclusion criteria are as follows: (1) accompanied by mental diseases, (2) intolerant to surgery, (3) congenital immune dysfunction or coagulation disorder, (4) deviation of study results caused by private use of other drugs during treatment; and (5) people who have allergic contraindications to the drugs used in the treatment process.

## 2.2. Methods

**2.2.1. MRI Detection of Image Denoising Algorithm.** MRI images of patients in group B were detected by conventional

TABLE 1: The baseline data ( $n(\%)$ )/( $\bar{x} \pm s$ ).

	A group ( $n=44$ )	B group ( $n=45$ )	$t/\chi^2$	$P$
Age (years)	46.55 $\pm$ 5.31	45.98 $\pm$ 4.86	0.527	0.610
Gender			0.096	0.756
Man	21 (47.73%)	20 (44.44%)		
Woman	23 (52.27%)	25 (55.56%)		
BMI (kg/m <sup>2</sup> )	23.21 $\pm$ 1.89	23.18 $\pm$ 2.05	0.080	0.937
Level of education			0.087	0.541
Primary and below	9 (20.45%)	11 (24.44%)		
Junior to senior high	23 (52.27%)	20 (44.44%)		
University and above	12 (27.27%)	14 (31.11%)		

MRI and denoising algorithm, respectively. The operation contents of each detection are as follows:

MRI was examined using a superconducting magnetic resonance imaging scanner (purchased from GE Corporation; Model: Discovery 750); before the test, it is required to fast and forbid water for 12 h and hold your breath for 20 seconds. It is forbidden to wear any metal jewelry during the test. The abdominal coil was a 32-channel phased array, and the cross-sectional unit first fired a single fast spin echo T2WI scan sequence. The scan sequence was set as layer thickness (5 mm), matrix (320  $\times$  256), layer spacing (1 mm), field of vision (340  $\times$  340) mm, and repeat time (TR)/echo time (TE) 4500/120 ms. The scan sequence was set as layer thickness (5 mm), matrix (224  $\times$  180), layer spacing (1 mm), field of vision (340  $\times$  340) mm, and TR/TE 2500/110 ms. T1WI fat suppression sequence scanning was performed by rapid volumetric imaging of liver (TR/TE3.6/1.7 ms), layer thickness (5 mm), matrix (224  $\times$  180), and field of vision (360  $\times$  360) mm. Contrast agent was injected at a rate of 2~3 mL/s with a special dual-tube high-pressure syringe for MR, and 20 mL 0.9% sodium chloride solution was injected with the same flow rate group. Continuous scanning was performed for 40 times.

The denoising model is constructed as follows. The MRI image obtained above is given a noisy MRI  $Y$ , and the image is obtained by partitioning block set  $RY = (R_1 Y, R_2 Y, \dots, R_m Y)$ ,  $RY$  was divided into class  $K$  by GMM prior, and  $R_K Y = [R_{K1}, R_{K2}, \dots, R_{Kd(k)}]$  was used to represent the moment blocks composed of all image blocks in class  $K$  and decomposed according to the formula  $\bar{R}_K Y = Z_K + N_X$  ( $Z_K$  and  $N_X$  are low-rank matrices and noise matrices, respectively). Assuming that the noise at each pixel in the image is independently distributed, the value of  $Z_K$  can be obtained according to the following formula:

$$E(Z_K) = \tau \|Z_K\| + \frac{1}{\sigma^2} \bar{R}_K Y - Z_K \Bigg|_F^2, \quad (1)$$

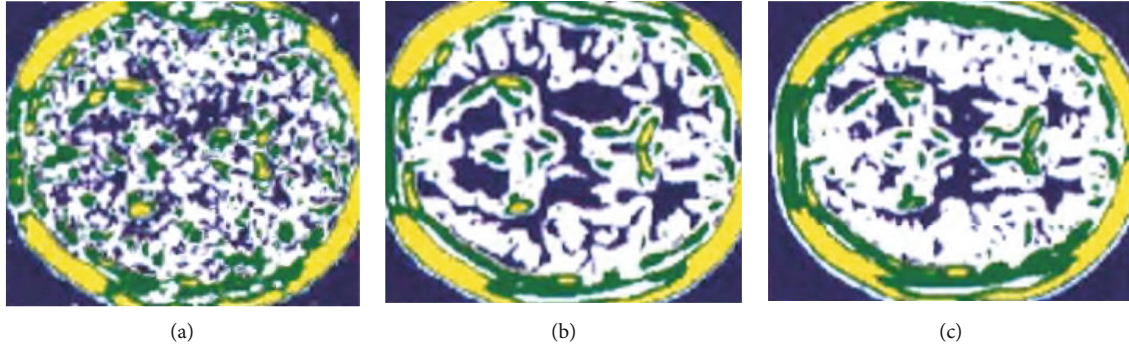


FIGURE 1: Denoising image processing process. Note: (a) the obtained original noise image, (b) the clustering result after 10 cycles, and (c) the clustering result of denoised MRI.

TABLE 2: Comparison of postoperative complications ( $n(\%)$ ).

Group	$n$	Hyperamylasemia	Mild pancreatitis	Moderate pancreatitis
A group	44	10 (22.73%)	9 (20.45%)	5 (11.36%)
B group	45	3 (6.67%)	4 (8.89%)	2 (4.44%)
$\chi^2$		4.601		4.363
$P$		0.032		0.037

where  $\tau$  is constant and  $\sigma$  is noise standard deviation. By summarizing the given noisy MRI  $Y$ , the denoised MRI  $X$  is reconstructed by the following formula:

$$(\hat{X}, \hat{C}, \{\hat{Z}_K\}) = \underset{X, C, \{Z_K\}}{\operatorname{argmin}} \frac{\lambda}{\sigma^2} \|Y - X\|_2^2 - \log p(RY, C|\Theta) + \sum_{k=1}^K E(Z_K), \quad (2)$$

where  $\lambda$  is a constant and  $\sigma$  is the noise standard deviation, and the clustering visualization result under GMM prior in Figure 1 can be obtained. The result shows that with the increase of the number of cycles, the MRI image can be effectively close to the denoised MRI.

**2.2.2. Serum Amylase Detection.** 5 ml of fasting venous blood was extracted from the two groups in the morning and put into a centrifuge with centrifuge parameters of 3500 r/min and centrifuge radius of 13.5 cm. After centrifugation for 10 min, the blood was placed under low temperature to be tested. A dry chemical automatic biochemical analyzer was used (purchased from Johnson & Johnson, USA, Model: VITROS950), serum amylase level was detected by dry biochemical assay, and the normal value was  $<200$  U/L.

**2.2.3. Treatment Methods.** ERCP was performed by the same team in both groups. Diazepam 10 mg (manufacturer: Dubeite Pharmaceutical Co., Ltd., National Drug Approval H41020631, specification: 10 mg), scopolamine 20 mg (purchased from Henan Furen Huaiqingtang Pharmaceutical Co., Ltd., National Drug Approval H19994038, specification: 1 ml:0.3 mg), and 0.3 mg octreotide were given to group A

TABLE 3: Comparison of serum amylase levels ( $\bar{x} \pm s$ ).

Group	$n$	Amylase (U/L)
A group	44	$298.35 \pm 13.19$
B group	45	$256.42 \pm 12.05$
$t$		15.658
$P$		$<0.001$

TABLE 4: MRI observation of pancreatic imaging characteristics with denoising algorithm ( $n(\%)$ ).

	Conventional MRI detection ( $n = 45$ )	MRI detection with denoising algorithm ( $n = 45$ )	$t/\chi^2$	$P$
The pancreas swelling			4.686	0.030
Y	14 (31.11%)	5 (11.11%)		
N	31 (68.89%)	40 (88.89%)		
Whether the pancreatic duct/bile duct is dilated			3.902	0.048
Y	17 (37.78%)	8 (17.78%)		
N	28 (62.22%)	37 (82.22%)		
Combined with peritoneal effusion			5.099	0.024
Y	13 (28.89%)	4 (8.89%)		
N	32 (71.11%)	41 (91.11%)		
T1WI signal			4.994	0.025
High	21 (46.67%)	31 (68.89%)		
Low	24 (53.33%)	14 (31.11%)		
T2WI signal			5.756	0.016
High	19 (42.22%)	8 (17.78%)		
Low	26 (57.78%)	37 (82.22%)		

(purchased from Beijing Baiao Pharmaceutical Co., Ltd., National Drug Approval H20061309, specification: 1 ml:0.1 mg), and continuous intravenous infusion was performed 6h before surgery. Group B was combined with indomethacin suppository (purchased from Beijing Shuangji



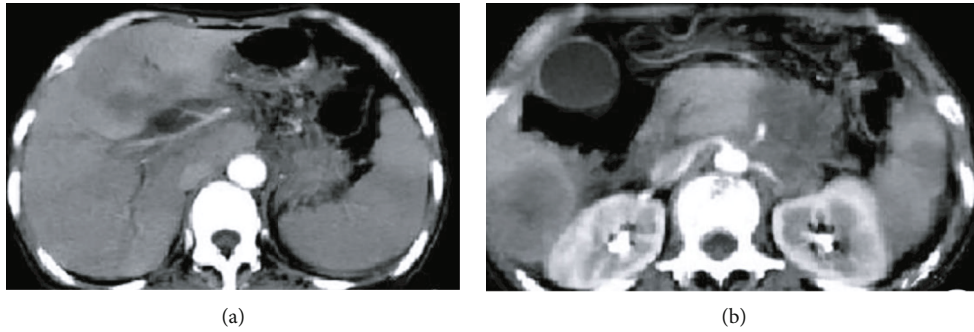


FIGURE 2: Conventional MRI image. Note: (a, b) conventional MRI images, showing poorly defined boundaries of the pancreas.

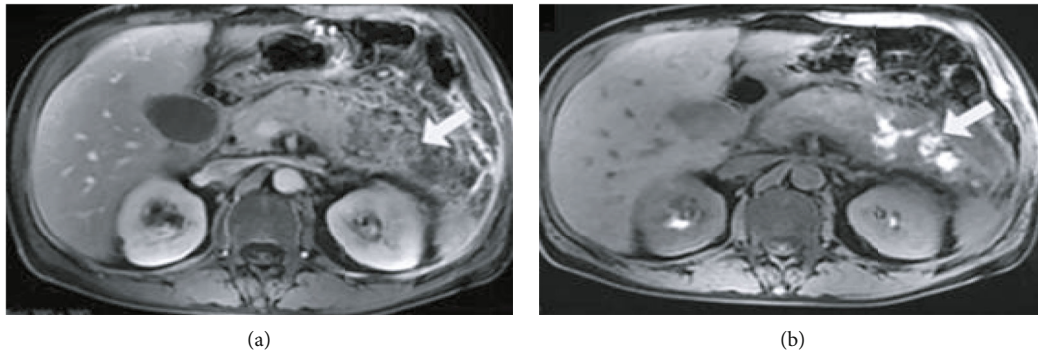


FIGURE 3: Denoised MRI image of a postoperative pancreatitis patient. Note: the figure shows denoised MRI images of patients with postoperative pancreatitis, in which the arrow in (a) shows large nonenhanced manifestations of pancreas and surrounding area, and the arrow in (b) shows T1WI image, with high shadow at the site indicated by the arrow, indicating the possibility of bleeding.

Pharmaceutical Co., Ltd., H11021391, specifications: 100 mg) on the basis of group A, and anal plug was performed 30 min before surgery. Both groups were given the same anti-infection operation after surgery and observed.

**2.2.4. Diagnostic Criteria for Pancreatitis.** Diagnostic criteria for acute pancreatitis was divided into three, specified as follows: first, the pain symptoms: pancreatitis, typical pain symptoms are severe, mainly located in the upper abdomen, generally will appear early in the abdomen to the left or on the entire abdominal pain, have serious pain even when it appears late in the abdomen, all of them, and will start from light to heavy. Second, changes in blood amylase: the value of blood amylase exceeds more than three times the normal value, the general blood amylase will increase in the initial 2-12 hours of acute pancreatitis attack, and if the increase is more than three times, it represents the positive diagnostic criteria. Third, imaging examination: this includes B ultrasound, CT, and other examinations; there are typical changes in peripheral necrosis of pancreatitis, which suggest acute pancreatitis. If two of the three criteria are positive, the condition is often diagnosed as acute pancreatitis.

**2.3. Statistical Treatment.** The SPSS 25.0 statistical software was used for data analysis. (1) Measurement data: If the data followed normal distribution and homogeneity of variance after normality test, it was represented by mean  $\pm$  standard deviation. Paired sample  $t$  was used for intragroup test,

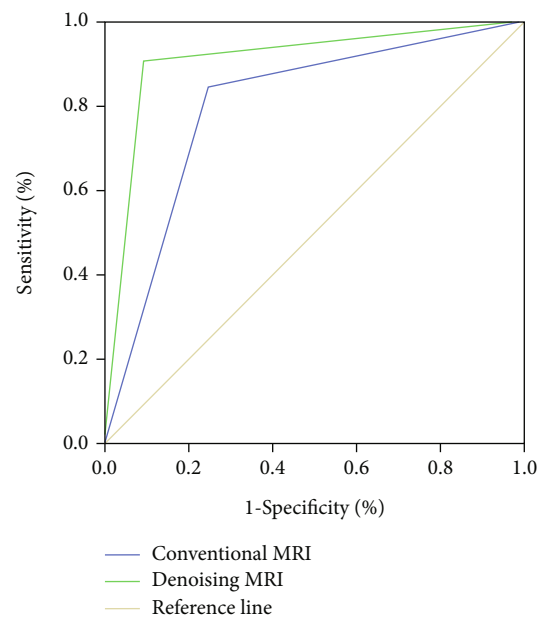


FIGURE 4: ROC image of pancreatitis on denoised MRI.

and variance comparison was used between groups. (2) Count data: Descriptive statistical analysis was conducted by percentage, and  $\chi^2$  test was performed. (3) ROC curve was drawn to evaluate the diagnostic efficacy of MRI denoising algorithm for postoperative pancreatitis and serum

TABLE 5: Diagnostic efficacy of denoised MRI.

	95% CI	Sensitivity (%)	Specificity (%)	AUC	Cutoff value
Denoising MRI	0.774~0.925	89.40%	83.20%	0.855	–
Conventional MRI	0.704~0.873	84.50%	78.60%	0.787	–

amylase level detection for hyperamylasemia. All the above data showed significant differences with  $P < 0.05$ .

### 3. Results

**3.1. To Compare the Incidence of Postoperative Pancreatitis and Hyperamylasemia.** The incidence of postoperative pancreatitis and hyperamylasemia in group B was significantly lower than that in group A ( $P < 0.05$ ), as shown in Table 2.

**3.2. Serum Amylase Levels Were Compared after Operation.** The postoperative serum amylase level in group B was significantly lower than that in group A ( $P < 0.05$ ), as shown in Table 3.

**3.3. Comparison of Imaging Characteristics and Diagnosis Rates of Different MRI Detection Methods.** There were 6 cases of postoperative pancreatitis in group B, 2 cases (33.33%) were detected by conventional MRI, and 5 cases (83.33%) were detected by MRI based on denoising algorithm. Although there was no significant difference in diagnosis rates between the two methods, the number of cases of pancreatitis detected by MRI based on denoising algorithm was slightly higher than that of conventional MRI. The differences in imaging characteristics of the two detection methods are shown in Table 4 and Figures 2 and 3. The results showed that compared with conventional MRI images, MRI images with denoising algorithm showed higher cases of pancreatic swelling, dilatation of pancreatic duct/bile duct, and combined with abdominal effusion (all  $P < 0.05$ ).

**3.4. ROC Evaluation of MRI Diagnostic Value of Denoising Algorithm for Postoperative Pancreatitis.** ROC curve (Figure 4) showed that denoised MRI had high diagnostic value for postoperative pancreatitis in patients with ERCP, and its area under the curve was significantly higher than that of conventional MRI. The diagnostic efficacy is shown in Table 5.

**3.5. ROC Evaluation of Serum Amylase Detection in the Diagnosis of Postoperative Hyperamylasemia.** ROC curve (Figure 5) showed that serum amylase had high diagnostic value in patients with hyperamylasemia after ERCP surgery, with a line area of 0.893 and high specificity and sensitivity. The diagnostic efficacy is shown in Table 6.

### 4. Discussion

As an important way of clinical diagnosis and treatment of biliopancreatic diseases, ERCP has become the preferred treatment for choledocholithiasis in the application history of more than 30 years. However, some scholars pointed out that post-

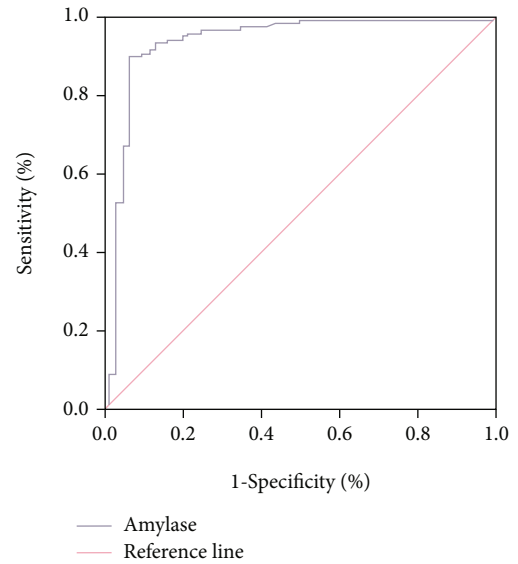


FIGURE 5: Diagnostic value of serum amylase in postoperative hyperamylasemia.

operative complications of ERCP are still unavoidable at present, especially the common postoperative acute pancreatitis and hyperamylasemia. Therefore, it is of great significance to seek a way to effectively reduce postoperative complications of ERCP for such patients [8, 9]. Indomethacin suppositories, as a commonly used drug in ERCP, can reduce the incidence of postoperative pancreatitis and hyperamylasemia to a certain extent, but its gastrointestinal irritation may cause complications related to the digestive system [10]. Therefore, indomethacin suppositories were adopted in this study to avoid gastrointestinal irritation by anal insertion, and its influence on reducing the incidence of postoperative complications in ERCP patients was further observed. In addition, MRI imaging technology with denoising algorithm was used to further evaluate the clinical efficacy of the drug. Lay a theoretical foundation for improving the prognosis of patients with choledocholithiasis in clinic [11].

The results of this study showed that indomethacin suppositories were given to patients 30 min before surgery, which could significantly reduce the incidence of postoperative pancreatitis and hyperamylasemia, and the serum amylase expression in group B was significantly lower than that in group A ( $P < 0.05$ ). To analyze the mechanism of action of these results may after the author thinks that due to trigger factors including intraoperative ERCP postoperative pancreatitis mechanical injury, infection, and related inflammation, so by taking a certain means to control inflammation factor to reduce inflammation plays an important role to reduce the incidence of postoperative ERCP pancreatitis



TABLE 6: Diagnostic efficacy of serum amylase.

	95% CI	Sensitivity (%)	Specificity (%)	AUC	Cutoff value
Amylase	0.773~0.912	89.80%	85.20%	0.893	201.31 U/L

[12]. Indomethacin suppositories, as a kind of nonsteroidal anti-inflammatory drugs (NSAIDs), through the rectum can inhibit PLA2 activity after the treatment and prevent neutrophil leads to the organization, further blocking mediated by phospholipase A2 a large release of proinflammatory factor, secretion, thereby reducing the body's inflammatory response and reduce the incidence of postoperative pancreatitis and high blood amylase [13]. Li et al. [14] also showed in the study that indomethacin suppositories, as a phospholipase A2 antagonist, can inhibit prostaglandin activity and regulate inflammatory factor-related transmitters such as platelet active factor and interleukin, which can block the expression activity of inflammatory cytokines in the early stage of inflammation so as to prevent the inflammatory waterfall reaction. Thus, it can reduce postoperative complications, which is consistent with the results of this study.

In addition, MRI with denoising algorithm was used to further evaluate the specific efficacy of indomethacin suppositories. Since ordinary MRI is prone to noise pollution in the imaging process, there is a certain deviation in the evaluation of image results. Therefore, in order to obtain high-quality MRI images and evaluate the specific efficacy of indomethacin suppositories, in this study, GMM was used to conduct the prior of noise images and low-rank rectangular decomposition algorithm was used for denoising [15, 16]. After denoising processing, MRI images showed A group of patients with postoperative swelling; the number of cases of pancreas and pancreatic duct/bile duct expansion in the number of cases occurred, and merger of peritoneal effusion was significantly higher than that of group B; prompt after denoising MRI images can be various and multidimensional imaging; high-resolution display of pancreatic necrosis area, at the same time, is under the condition of noninvasive assessment of the change of the bile duct, which clearly shows whether there are complications in local areas [17]. In addition, the ROC curve showed that MRI images of the denoising algorithm had a high diagnostic efficiency for the diagnosis of acute pancreatitis after ERCP, with an area of 0.855 under the curve. Meanwhile, timely detection of serum amylase level in patients after ERCP could also predict the occurrence of hyperamylasemia and take relevant measures to prevent the occurrence of adverse prognosis in time [18].

To sum up, indomethacin suppositories can significantly reduce the common bile duct calculi patient pancreatitis and the probability of high blood amylase after ERCP, and the denoising algorithm of postoperative pancreatic imaging features of MRI image display of group B was significantly better than that of group A, further illustrating indomethacin suppositories for improving the prognosis of patients with common bile duct calculi ERCP postoperative outcome have high clinical curative effect. However, due to the small sample size of this study, the results lack a certain degree of

rigor. Therefore, the sample size can be expanded in the next study, and cluster analysis of the results can be carried out to further observe the improvement effect of indomethacin suppositories on postoperative complications of ERCP, so as to make the results more rigorous and accurate.

## Data Availability

The dataset used in this paper are available from the corresponding author upon request.

## Conflicts of Interest

The authors declared that they have no conflicts of interest regarding this work.

## References

- [1] M. E. Bosley, I. J. Zamora, and L. P. Neff, "Choledocholithiasis—a new clinical pathway," *Translational Gastroenterology and Hepatology*, vol. 6, no. 6, p. 35, 2021.
- [2] J. Zhang and X. Ling, "Risk factors and management of primary choledocholithiasis: a systematic review," *ANZ Journal of Surgery*, vol. 91, no. 4, pp. 530–536, 2021.
- [3] M. Kuwatani and N. Sakamoto, "Asymptomatic choledocholithiasis that causes a dilemma between treatment and observation," *JMA Journal*, vol. 4, no. 2, pp. 176–177, 2021.
- [4] P. Cianci and E. Restini, "Management of cholelithiasis with choledocholithiasis: endoscopic and surgical approaches," *World Journal of Gastroenterology*, vol. 27, no. 28, pp. 4536–4554, 2021.
- [5] H. Neuhaus, "Choledocholithiasis in pregnancy: when and how to perform ERCP?," *Endoscopy International Open*, vol. 8, no. 10, pp. E1508–E1510, 2020.
- [6] G. Iccan, E. Onalan, and M. Yucesoy, "Comparison of stent and indomethacin suppositories suppository efficacy in the prevention of acute pancreatitis after ERCP," *Acta Biomed*, vol. 92, no. 4, 2021.
- [7] S. Reddy, N. Jagtap, R. Kalapala et al., "Choledocholithiasis in acute calculous cholecystitis: guidelines and beyond," *Annals of Gastroenterology*, vol. 34, no. 2, pp. 247–252, 2021.
- [8] G. Iccan, E. Onalan, and M. Yucesoy, "Comparison of stent and indomethacin suppository efficacy in the prevention of acute pancreatitis after ERCP," *Acta Biomed*, vol. 92, no. 4, 2021.
- [9] M. Jalili, F. Shirani, P. Entezari, M. Hedayatshodeh, V. Baigi, and H. Mirfazaelian, "Desmopressin/indomethacin combination efficacy and safety in renal colic pain management: a randomized placebo controlled trial," *The American Journal of Emergency Medicine*, vol. 37, no. 6, pp. 1009–1012, 2019.
- [10] J. D. Machicado, R. Mounzer, P. Paragomi et al., "Rectal indomethacin does not mitigate the systemic inflammatory response syndrome in acute pancreatitis: a randomized trial," *Clinical and Translational Gastroenterology*, vol. 12, no. 11, 2021.

- [11] A. Sadeghi, M. Abbasinazari, H. Asadzadeh Aghdai et al., “Does melatonin addition to indomethacin decrease post endoscopic retrograde cholangiopancreatography pancreatitis? A randomized double-blind controlled trial,” *European Journal of Gastroenterology & Hepatology*, vol. 31, no. 11, pp. 1350–1355, 2019.
- [12] Z. L. Smith, B. J. Elmunzer, G. S. Cooper, and A. Chak, “Real-world practice patterns in the era of rectal indomethacin for prophylaxis against post-ERCP pancreatitis in a high-risk cohort,” *The American Journal of Gastroenterology*, vol. 115, no. 6, pp. 934–940, 2020.
- [13] Y. Y. Qian, N. Ru, H. Chen et al., “Rectal indometacin to prevent pancreatitis after extracorporeal shock wave lithotripsy (RIPEP): a single-centre, double-blind, randomised, placebo-controlled trial,” *The Lancet Gastroenterology & Hepatology*, vol. 7, no. 3, pp. 238–244, 2022.
- [14] L. Li, M. Liu, T. Zhang et al., “Indomethacin down-regulating HMGB1 and TNF- $\alpha$  to prevent pancreatitis after endoscopic retrograde cholangiopancreatography,” *Scandinavian Journal of Gastroenterology*, vol. 54, no. 6, pp. 793–799, 2019.
- [15] M. Moreno López, J. M. Frederick, and J. Ventura, “Evaluation of MRI denoising methods using unsupervised learning,” *Frontiers in Artificial Intelligence*, vol. 4, no. 4, article 642731, 2021.
- [16] C. J. Zhang, X. Y. Huang, and M. C. Fang, “MRI denoising by NeighShrink based on chi-square unbiased risk estimation,” *Artificial Intelligence in Medicine*, vol. 97, no. 1, pp. 131–142, 2019.
- [17] D. Xie, Y. Li, H. Yang et al., “Denoising arterial spin labeling perfusion MRI with deep machine learning,” *Magnetic Resonance Imaging*, vol. 68, no. 1, pp. 95–105, 2020.
- [18] P. L. Bazin, A. Alkemade, W. van der Zwaag, M. Caan, M. Mulder, and B. U. Forstmann, “Denoising high-field multi-dimensional MRI with local complex PCA,” *Frontiers in Neuroscience*, vol. 13, no. 13, p. 1066, 2019.

## Research Article

# Effects of Different Surgical Procedures on the Therapeutic Effects, Prognosis, and Major Complications of Acetabular Fractures in the Elderly of China: A Systematic Review and Meta-Analysis

Lei Wen,<sup>1</sup> Kun Liu ,<sup>2</sup> Ge Chen,<sup>1</sup> Jianhua Ji,<sup>1</sup> Changshun Chen,<sup>1</sup> and Zhong Chen<sup>1</sup>

<sup>1</sup>Department of Orthopaedic and Trauma Surgery, Affiliated Hospital of Yunnan University, Kunming, Yunnan Province 650000, China

<sup>2</sup>Department of Anesthesiology, The First Affiliated Hospital of Kunming Medical University, Kunming City, Yunnan Province 650000, China

Correspondence should be addressed to Kun Liu; [chencs666@ynu.edu.cn](mailto:chencs666@ynu.edu.cn)

Received 10 June 2022; Accepted 20 July 2022; Published 18 August 2022

Academic Editor: Hangjun Che

Copyright © 2022 Lei Wen et al. This is an open access article distributed under the Creative Commons Attribution License, which permits unrestricted use, distribution, and reproduction in any medium, provided the original work is properly cited.

**Objective.** Different surgical approaches were systematically evaluated to provide an evidence-based medical rationale for the application and promotion of acetabular fractures in the elderly of China. **Methods.** Randomized controlled trials (RCT) of different surgical methods in the treatment of elderly acetabular fractures were searched in the PubMed, EMBASE, ScienceDirect, Cochrane Library, China Knowledge Network Database (CNKI), China VIP Database, Wanfang Database, and China Biomedical Literature Database (CBM). The search time threshold was set from the time the database was created to the current time. Investigators obtained data independently, and the bias risk of each included writing was reviewed using the Cochrane Manual 5.1.0 criterion. The meta data was analyzed using RevMan 5.4 statistical package. **Results.** 6 RCT articles were included in the end. A total of 445 samples were analyzed by meta. All the six RCT literatures included in this meta-analysis reported the baseline status of patients, only 3 RCT mentioned “random assignment” without any explanation, and the rest did not mention “random” information. The five studies included all gave detailed intervention measures. The number and reasons of blind method and lost follow-up or withdrawal were not described in detail in 6 RCT articles. Through the meta-analysis excellent and good rate between the experimental group and the control group through 6 RCT studies, the heterogeneity test results were  $\chi^2 = 6.11$ ,  $df = 4$ ,  $P = 0.19 > 0.05$ , and  $I^2 = 35\%$ , without obvious heterogeneity at  $Z = 2.68$  and  $P = 0.007$ . These results suggested that the total hip arthroplasty application has the same excellent rate as other surgical treatment methods, indicating that total hip arthroplasty has a significant effect on the treatment of elderly acetabular fractures. Through the meta-analysis hip-joint function score, the heterogeneity test results were  $\chi^2 = 56.16$ ,  $df = 4$ ,  $P < 0.00001$ , and  $I^2 = 93\%$ , with obvious heterogeneity. The great difference was discovered in hip function score between total hip arthroplasty and other surgical methods, showing that total hip arthroplasty can greatly improve hip-joint function. Then, the incidence of hip complications between the experimental cases and the control cases was calculated by meta. The heterogeneity test results were  $\chi^2 = 3.17$ ,  $df = 4$ ,  $P = 0.53 > 0.05$ , and  $I^2 = 0\%$ , without remarkable heterogeneity at  $Z = 3.05$  and  $P = 0.002$ . This demonstrated that a significant difference was observed in the complication incidence, indicating that total hip arthroplasty displayed a lower incidence of hip-joint functional complications. **Conclusion.** Total hip arthroplasty has a good prognosis and a low complication rate in the treatment of acetabular fractures in the elderly. However, more studies and longer follow-ups are needed to further validate the findings of this study.

## 1. Introduction

An acetabular fracture is a break in the socket portion of the “ball-and-socket” hip joint. In the past, acetabular fractures were treated conservatively. Conservative treatment involves prolonged bed rest and many complications (e.g., early joint degeneration or avascular necrosis of the femoral head). It often fails to restore the matching relationship between the femoral head and the acetabulum and therefore has a very poor outcome. With the continuous improvement of diagnosis and treatment technology and the emergence of new internal fixation equipment, open reduction and internal fixation have become the gold standard for the treatment of displaced acetabular fractures [1]. As there are many factors that affect the effect of treatment, even if treated by experienced specialists, there may still be some postoperative complications, affecting the long-term effect. The common complications affecting joint function after acetabular fracture are traumatic arthritis, osteonecrosis of the femoral head, heterotopic ossification, nerve injury, and so on.

Traumatic arthritis is the most common complication after operation of medullary acetabular fracture with an incidence of 12%-57% [2], which occurs in all types of acetabular fractures. Poor reduction is the main factor leading to traumatic arthritis [3]. When traumatic arthritis progresses with severe pain and dysfunction, surgical treatment is often needed. The popular surgical approaches are hip arthroplasty and hip replacement, which are often not accepted by patients because of the problems of hip fixation after hip fusion [4]. Total hip arthroplasty (THA) is an ideal method for the treatment of acetabular fractures, but whether fresh acetabular fractures need one-stage total hip replacement is still controversial [5, 6]. Its indications should be strictly grasped. Petohazi et al. used one-stage total hip arthroplasty to treat acetabular posterior column fractures with femoral head and neck fractures with satisfactory results [7–9]. At present, there are few articles on meta-analysis of acetabular fractures in the elderly with different surgical methods. In view of the small number of patients included in the individual articles and their age, the meta-analysis is again carried out in this paper, taking into account the high-quality relevant literature published in recent years, both nationally and internationally. In this paper, meta-analysis was used to compare the treatment effects, prognosis, and main complications of different surgical methods in the treatment of acetabular fractures in the elderly, in order to provide options for clinicians to choose a more optimized and more suitable treatment plan for patients.

## 2. Research Content and Methods

**2.1. The Sources and Retrieval Methods of Documents.** Randomized controlled trials (RCT) of different surgical methods in the treatment of elderly acetabular fractures were searched in the Cochrane Library, PubMed, Embase, OVID, China Knowledge Network Database (CNKI), Wanfang Database, China Biomedical Literature Database (CBM), and VIP Central Database (VIP). Chinese search words were

“total hip arthroplasty, traditional surgery, pelvic fracture, acetabular fracture, randomized controlled trial,” etc.; manual search was conducted of references and grey literature included in the literature in order to find potential studies that meet the inclusion criteria of this system evaluation. The search time threshold was set from the time the database was created to the current time and the language is limited to Chinese.

### 2.2. Literature Inclusion Criteria and Exclusion Criteria

**2.2.1. Literature Inclusion Criteria.** The literature inclusion criteria are as follows: (1) the type of research was a randomized controlled trial (RCT) and the language is Chinese only; (2) the intervention subjects were patients with pelvic and acetabular fractures diagnosed clearly, regardless of age, sex, race, or region; (3) the intervention measures were total hip arthroplasty and other operations; (4) the observation indexes included operation time, intraoperative blood loss, postoperative complications, hospital stay, clinical effect, incision length, drainage volume, extubation time, blood transfusion volume, Matta score, Harris score, imaging results, Merled score, and so on.

**2.2.2. Literature Exclusion Standard.** The literature exclusion criteria are as follows: (1) retrospective studies, cohort studies, case reports, etc.; (2) the studies with incomplete results; (3) the research with a too small sample size (less than 20 cases); (4) repeated studies: repeated reports from the same team.

**2.3. Quality Evaluation and Data Extraction.** The quality was evaluated by two scholars with reference to the bias risk assessment criteria of the Cochrane Collaboration Network, including the following aspects: the generation of random methods, the concealment of allocation schemes, whether participants are blind, data integrity of results, selective reporting, and other sources of bias [10]. The documents were independently extracted and cross-checked by two evaluators. When there were differences between the two, an agreement was reached through consultation. It included the author(s), published time, sample size, treatment method, curative effect evaluation method, and so on.

**2.4. Statistical Processing.** The standardized mean difference (SMD) with Hedges'  $g$  was chosen as the measure of the effect. The effect size was calculated using a random-effect model with a restricted maximum-likelihood (REML) and considered a large, moderate, and small effect with respect to the SMD values of 0.8, 0.5, and 0.2, respectively. The heterogeneity among the studies included in a meta-analysis was assessed using Cochrane's  $Q$ , tau-squared, and  $I$ -squared ( $I^2$ ). Cochrane's  $Q$  test quantifies total variance and generates a  $P$  value that determines that heterogeneity is present. Tau-squared indicates the true variance that is the between-study variance, while  $I^2$  represents the percentage of the total variance that is due to the true variance. The degree of heterogeneity is said to be low, moderate, and high, with  $I^2$  values of 25%, 50%, and 75%. RevMan 5.4 software was adopted for meta-analysis. HR and its 95% CI were employed

TABLE 1: Basic characteristics of literature.

Include the literature	Year of publication	N (C/T)	Treatment method	C	Outcome index	Whether it is random or not	Whether it is blind or not
Zhao Fuwen	2021	23/23	Open reduction and fixation	Total hip arthroplasty	①②③	Yes	No
Zhang Yong	2012	30/31	Surface replacement of hip joint	Total hip arthroplasty	①②③	Yes	No
Wang Yong	2014	35/30	Open reduction and fixation	Total hip arthroplasty	①②③	Yes	No
Li Xiangxiang	2018	50/50	Hemiarthroplasty	Total hip arthroplasty	②③	No	No
Liu Zhengmin	2020	43/50	Open reduction and fixation	Total hip arthroplasty	①②③	No	No
Xie Min	2014	40/40	Conservative treatment	Total hip arthroplasty	①	No	No

Note: ①: excellent and good rate; ②: hip-joint function score; ③: incidence of complications.

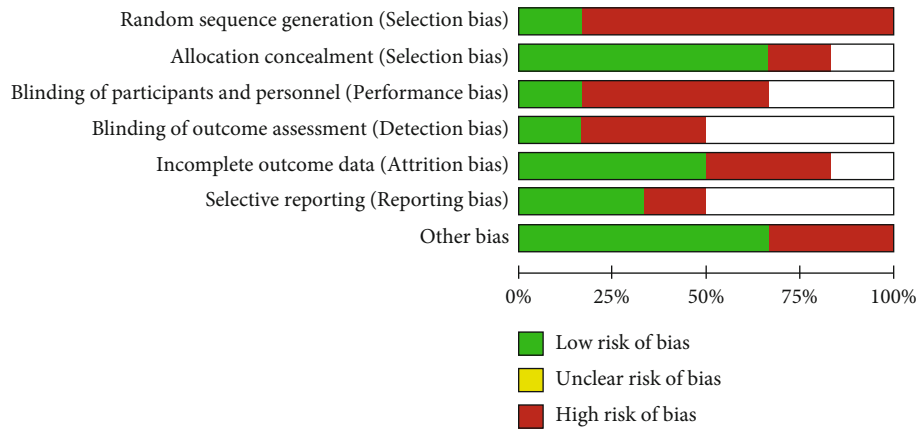


FIGURE 1: Risk of bias.

as effect analysis statistics for OS and PFS, and risk ratio and 95% CI were employed as effect analysis statistics for binary variables.  $P$  and  $I^2$  values in heterogeneity test results were adopted to determine whether there was statistical heterogeneity among the results.  $P > 0.10$  and  $I^2 < 50\%$  indicated that there was no statistical heterogeneity among the research results, and a fixed-effect model was used for combined analysis.  $P \leq 0.10$  and  $I^2 \geq 50\%$  indicated statistical heterogeneity among the research results, and a random-effect model was adopted for combined analysis. The test level of meta-analysis was set as  $\alpha = 0.05$ . Eggers' test was used to examine the funnel plot asymmetry. Whenever this test was significant with a  $P$  value of less than 0.1, we used the trim and fill method to correct the funnel plot and adjust the effect size for potential publication bias.

### 3. Results and Analysis

**3.1. The Results of Literature Retrieval and the Basic Situation of Literature Inclusion.** 2431 papers were retrieved through computer database retrieval; 242 papers were obtained after excluding duplicate studies; 105 papers were obtained by preliminary reading of the titles and abstracts of the papers, excluding unrelated studies, reviews, case reports, and noncontrol literatures; 21 articles were initially included; and then, 15 articles with incomplete data and no main outcome indicators were read carefully. In the end, 6 RCT [11–16] were included in the current analysis (Table 1).

**3.2. Evaluation of the Methodology Quality Included in the Literature.** All the six RCT literatures included in this meta-analysis reported the baseline status of patients, only 3 RCT mentioned “random assignment” without any explanation, and the rest did not mention “random” information. The five studies included all gave detailed intervention measures. The number and reasons of blind method and lost follow-up or withdrawal were not described in detail in 6 RCT articles. The proportion of various biases included in the study is shown in Figure 1, and the study quality evaluation and risk assessment are included in Figure 2.

### 3.3. Meta-Analysis Result

**3.3.1. Excellent and Good Rate.** Through the meta-analysis excellent and good rate among 6 RCT studies, heterogeneity tests were  $\chi^2 = 6.11$ ,  $df = 4$ ,  $P = 0.19 > 0.05$ , and  $I^2 = 35\%$ , without no obvious heterogeneity at  $Z = 2.68$  and  $P = 0.007$ . The results were considered that the total hip arthroplasty has the same excellent rate as other surgical treatment methods. Significant difference was found, indicating that total hip arthroplasty in the treatment of elderly acetabular fractures was effective (Figure 3).

**3.3.2. Hip-Joint Function Score.** Through the meta-analysis hip-joint function score between the experimental group and the control group of 6 RCT studies, the heterogeneity test suggested  $\chi^2 = 56.16$ ,  $df = 4$ ,  $P < 0.00001$ , and  $I^2 = 93\%$ , with obvious heterogeneity. The results implied there was obvious



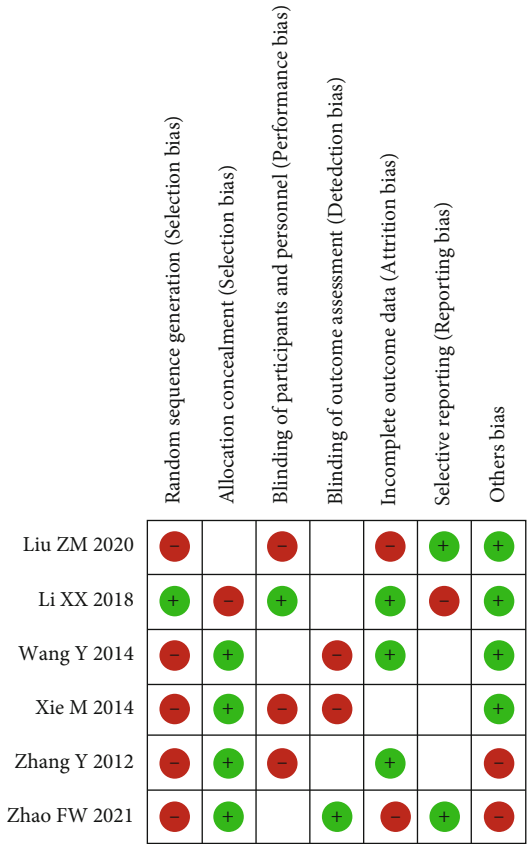


FIGURE 2: Risk of bias summary.

differences in the hip-joint function score, meaning that total hip arthroplasty was able to greatly enhance the hip-joint function (Figure 4).

**3.3.3. Complication Incidence.** Overall, 445 samples from 6 RCT studies were included. The incidence of hip complications between the experimental group and the control group was analyzed by meta-analysis. The heterogeneity test results were  $\chi^2 = 3.17$ ,  $df = 4$ ,  $P = 0.53 > 0.05$ , and  $I^2 = 0$  without obvious heterogeneity at  $Z = 3.05$  and  $P = 0.002$ . This meant there were markable differences in the complication incidence, indicating that total hip arthroplasty has less incidence of hip-joint functional complications. Due to the small number of literatures included in the analysis, it was not suitable to make a funnel chart, but the analysis may have a certain degree of publication bias (Figure 5).

4. Discussion

The hip joint is the largest and most important weight-bearing joint in the human body. The treatment of acetabular fractures is a great challenge for orthopedic surgeons due to the special anatomical position of the acetabulum, its irregular anatomical form, and changing fracture types [17, 18]. With the average life expectancy of human beings having increased significantly, the proportion of the elderly population has greatly increased [19]. A few studies have shown that the proportion of elderly people over 60 years old in

patients with acetabular fractures increased by 1.4 times from 1980 to 2007 [20]. In elderly patients with acetabular fractures, the difficulty of treatment is magnified by the complex fracture pattern, the poor biomechanical properties of the bone, and the number of underlying diseases [21, 22]. In the past, due to the limitations of the development of medical technology, many elderly patients with acetabular fractures had to undergo conservative treatment, which often required long-term brake or bed rest, which would lead to the decline of the function of the bone and muscle system [23].

In the 1860s, Yu et al. [24] took the lead in proposing surgical treatment of acetabular fractures in the elderly, which was supported and imitated by many scholars, and achieved good results. The scholars performed statistical classification on 120 elderly patients with acetabular fractures [25]. As the patients' age increased, their prognosis became worse and worse, but they still had a high excellent and good rate. Ali et al. reported 21 cases of elderly acetabular fractures involving the tetragonal area [26]. Although the anatomic reduction rate was only 52.4%, the SF-12PCS and Harris scores were satisfactory after an average follow-up of 4.2 years. ElSherif and Abonnour reported that 18 elderly patients with acetabular fractures were treated with open reduction and internal fixation [27]. The average follow-up was 31 months. The results showed that the Harris score was 90. Only one patient needed two-stage total hip arthroplasty because of aseptic necrosis of the femoral head. Many studies have demonstrated that although the rate of anatomical repositioning in elderly patients with acetabular fractures is lower than that in younger patients, long-term functional outcomes remain satisfactory and only a minority of patients require a repeat total hip replacement. Therefore, for elderly patients with acetabular fractures with obvious displacement, except for some special types of fractures that need one-stage total hip arthroplasty, open reduction and internal fixation should be the first choice [28]. In order to reduce the incidence of postoperative hip pain, traumatic osteoarthritis, and failure of internal fixation, acetabular fracture surgery should achieve hip white anatomical reconstruction and maintain concentric reduction of the hip joint [29].

Acetabular fractures are generally poor, and the emergency surgery is not recommended [30]. The delayed operation easily forms heterotopic ossification and fixation deformity, and fixation is difficult. Therefore, when the vital signs permit, the fracture should be treated as soon as possible, in which the best time is 3-7 days [31]. For old acetabular fractures that have been more than 3-4 months, the opportunity for surgical reduction is basically lost and total hip arthroplasty may be more effective [32, 33]. Acetabular fractures are intra-articular fractures, which should follow the principles of anatomical reduction, effective internal fixation, and early functional exercise. For acetabular fracture with posterior dislocation of the hip joint, closed reduction of the hip joint should be performed first, followed by acetabular reduction. The acetabulum is a complex geometry with various curves and radians. In order to achieve strong internal fixation, there are different internal fixation

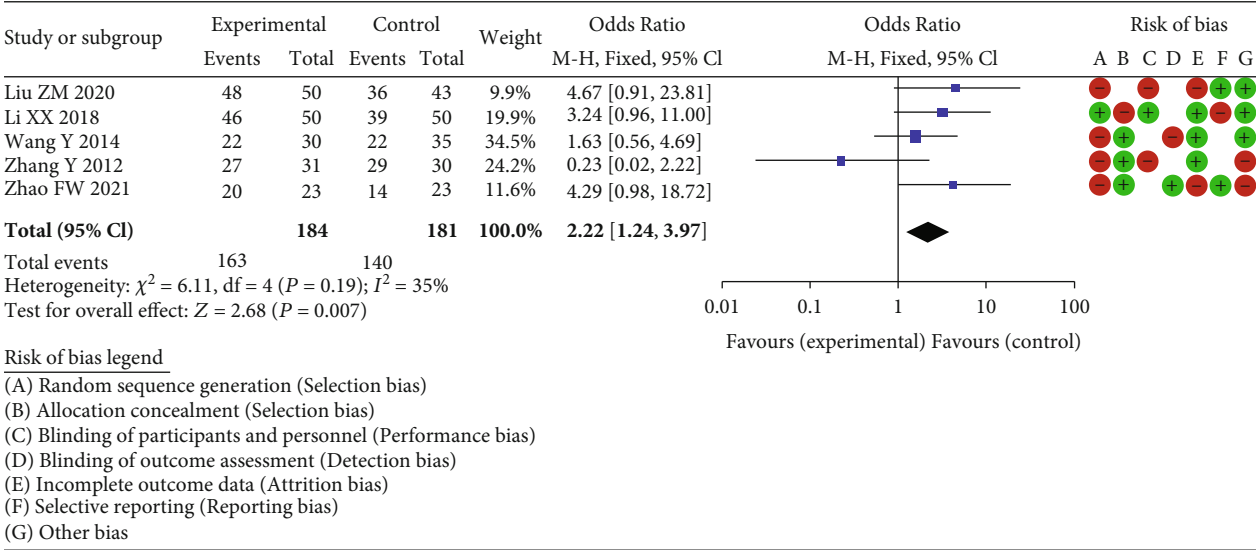


FIGURE 3: Forest plot of meta-analysis of excellent and good rate.

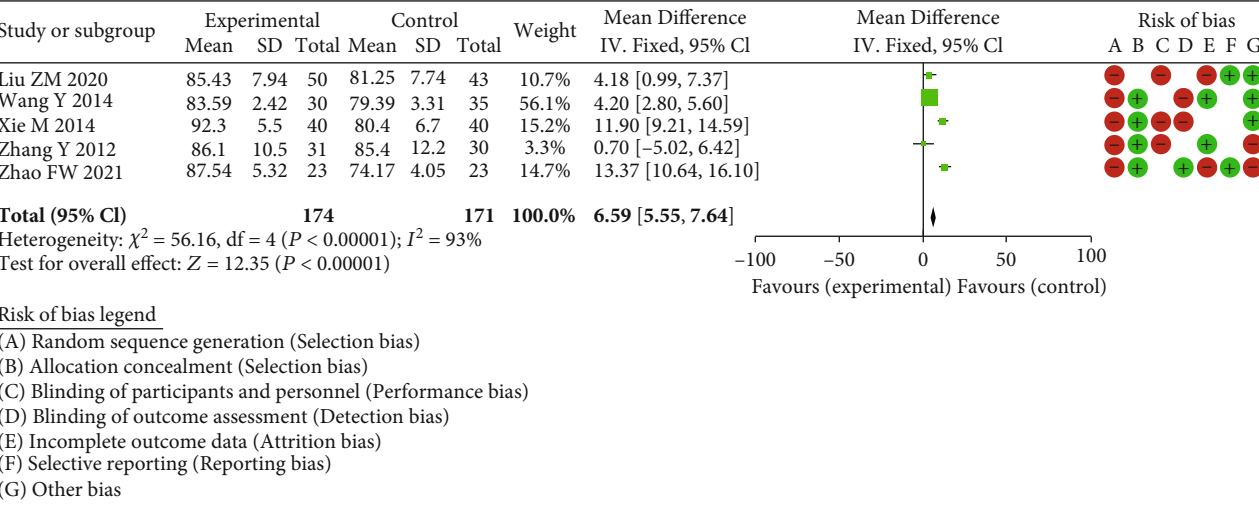


FIGURE 4: Forest plot of meta-analysis of hip-joint function score.

methods and internal fixation devices for different types of fractures [34, 35]. The main results are as follows: (1) Steel wire internal fixation is suitable for fractures in which the fracture line extends to the large notch of the ischium, including partial posterior column, horizontal, and double column fractures, especially for elderly patients with osteoporosis; the operation is relatively simple, but the strength is poor; it is often used in combination with other internal fixation methods. (2) Reconstruction plate internal fixation: the reconstruction plate can be well molded according to the anatomical morphology of the acetabulum, and the biomechanics is stable, but accurate prebending is needed. There is a possibility of postoperative traumatic arthritis caused by screw penetration into the joint cavity and fracture displacement during screw compression. (3) Locking compression plate internal fixation system: the overall stability between the plates and nails of the locking compression plate internal fixation system is equivalent to the internal fix-

ation bracket, with high fixation strength, low shaping requirements, and simple fixation of the posterior wall, and it allows the steel plate to leave the bone surface for fixation. There is no need to peel off the periosteum or expose more soft tissue during the operation, which can effectively protect the blood flow of the fracture end and reduce the occurrence of heterotopic ossification after operation. (4) Memory alloy three-dimensional internal fixation system for acetabular fractures. (5) Percutaneous screw fixation: percutaneous screw fixation is often combined with fluoroscopic navigation. This new method combines computer image processing and visualization technology with clinical surgery in the form of interactive image navigation. Using infrared devices on the patient and surgical instruments, the position of the patient's bones and the position of the surgical instruments can be determined, providing real-time spatial position and movement of the surgical instruments and visualising this information to the operator to complete the

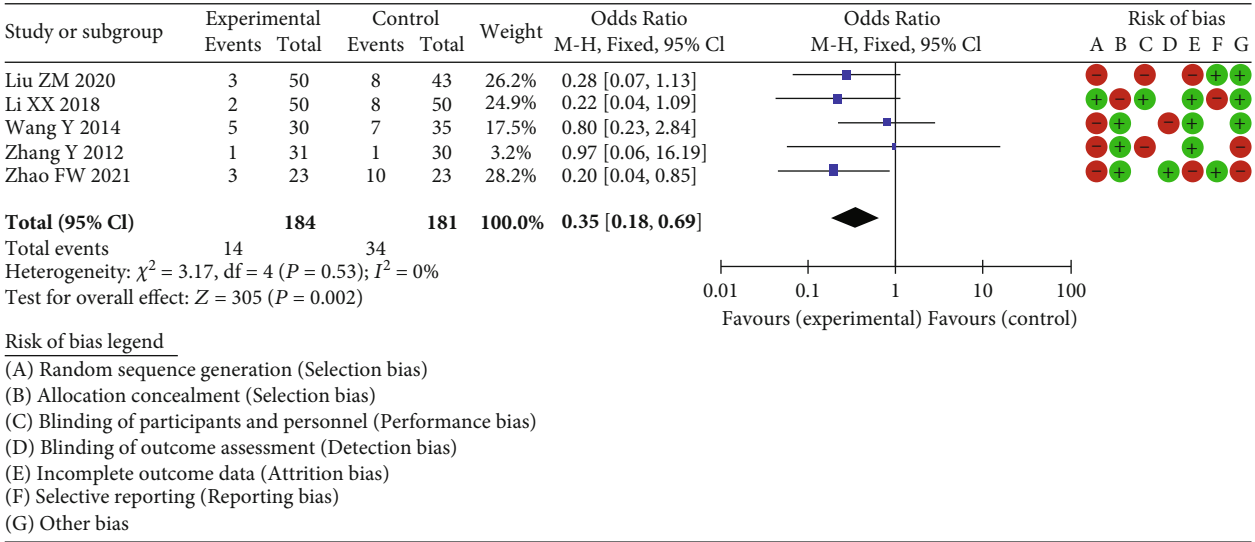


FIGURE 5: Forest plot of meta-analysis of incidence of complications.

operation accurately. At present, there are two-dimensional perspective navigation and three-dimensional perspective navigation. Percutaneous screw fixation under the guidance of two-dimensional perspective navigation for the treatment of acetabular fractures has been accepted by more and more orthopedic surgeons and has been popularized in a certain range. The more visual and intuitive three-dimensional perspective navigation is a new technology, which can display images of the hip joint on the sagittal, coronal, and cross-sections at the same time on the display. Although it is still in the exploratory stage, it has broad application prospects [36].

Artificial hip replacement began in the 1940s [37]. According to the different materials of artificial femoral head and acetabular cup lining, it can be divided into metal to metal, metal to polyethylene, ceramic to polyethylene, ceramic to ceramic, and so on. Hemiarthroplasty was reported for the first time in “Artificial Femoral Head Summary of Femoral Neck Fracture” published in 1963 in China. The prosthesis used was the Judette femoral head, made of polymethyl methacrylate. The excellent and good rate of treatment was 4/7 [38]. Total hip arthroplasty was reported for the first time in the reference material of Orthopaedic Trauma in 1975, and the surgical procedures of artificial joint were introduced in detail. After 80 years of continuous development and improvement, THA has been mastered by more and more orthopedic surgeons. More and more elderly patients with acetabular fracture choose artificial hip replacement to improve the life quality after operation [39].

6 RCT articles were included in the end. A total of 445 samples were analyzed by meta-analysis. All the six RCT literatures included in this meta-analysis reported the baseline status of patients, only 3 RCT mentioned “random assignment” without any explanation, and the rest did not mention “random” information. The five studies included all gave detailed intervention measures. The number and reasons of blind method and lost follow-up or withdrawal were not described in detail in 6 RCT articles. Through the meta-analysis excellent and good rate between the experimental

group and the control group through 6 RCT studies, the heterogeneity test results were  $\chi^2 = 6.11$ ,  $df = 4$ ,  $P = 0.19 > 0.05$ , and  $I^2 = 35\%$ , without obvious heterogeneity at  $Z = 2.68$  and  $P = 0.007$ . These results suggested that the total hip arthroplasty application has the same excellent rate as other surgical treatment methods, indicating that total hip arthroplasty has a significant effect on the treatment of elderly acetabular fractures. Through the meta-analysis hip-joint function score, the heterogeneity test results were  $\chi^2 = 56.16$ ,  $df = 4$ ,  $P < 0.00001$ , and  $I^2 = 93\%$ , with obvious heterogeneity. The great difference was discovered in the hip function score between total hip arthroplasty and other surgical methods, showing that total hip arthroplasty can greatly improve hip-joint function. Then, the incidence of hip complications between the experimental cases and the control cases was calculated by meta-analysis. The heterogeneity test results were  $\chi^2 = 3.17$ ,  $df = 4$ ,  $P = 0.53 > 0.05$ , and  $I^2 = 0\%$ , without remarkable heterogeneity at  $Z = 3.05$  and  $P = 0.002$ . This demonstrated that a significant difference was observed in the complication incidence, indicating that total hip arthroplasty displayed a lower incidence of hip-joint functional complications. The same idea can be found in the study put forward by other scholars [40–42]. They have applied new methods in the study, and the conclusions drawn can also give some support to this study. There are some limitations in this study. First of all, the sample size of the references included in this study is small, and they all belong to single-center research; there is a certain deviation. In the future research, we will carry out a large sample of prospective studies and hopefully draw more valuable conclusions.

5. Conclusion

Total hip arthroplasty has a good prognosis and a low complication rate in the treatment of acetabular fractures in the elderly of China. However, more studies and longer follow-ups are needed to further validate the findings of this study.

## Data Availability

No data were used to support this study.

## Conflicts of Interest

The authors declare that they have no conflicts of interest.

## References

- [1] H. Nico, D. Julius, M. Matthias et al., "Biomechanical analysis of fixation methods in acetabular fractures: a systematic review of test setups," *European Journal of Trauma and Emergency Surgery*, vol. 43, no. 41, pp. 841–845, 2022.
- [2] J. C. Giunta, C. Tronc, G. Kerschbaumer et al., "Outcomes of acetabular fractures in the elderly: a five year retrospective study of twenty seven patients with primary total hip replacement," *International Orthopaedics*, vol. 43, no. 10, pp. 2383–2389, 2019.
- [3] K. Kanakaris Nikolaos and D. Amit, "Classification of acetabular fractures: how to apply and relevance today," *Orthopaedics and Traumatology*, vol. 56, no. 35, pp. 3943–3948, 2022.
- [4] M. Albrektsson, O. Wolf, A. Enocson, and M. Sundfeldt, "Validation of the classification of surgically treated acetabular fractures in the Swedish Fracture Register," *Injury*, vol. 56, no. 52, pp. 94–96, 2022.
- [5] M. Ali, G. Justin, W. J. Eric, C. Jon, and B. Hartley, "Immediate outcomes of early versus late definitive fixation of acetabular fractures: a narrative literature review," *Injury*, vol. 53, no. 3, pp. 931–935, 2022.
- [6] I. M. Heimke, N. R. Scarcella, N. M. Simske, R. Furdock, and H. A. Vallier, "Surgical versus nonsurgical management of acetabular fractures with associated patterns in elderly patients: factors affecting outcomes," *JAAOS: Global Research and Reviews*, vol. 6, no. 3, pp. 967–969, 2022.
- [7] A. Petohazi, O. Musbahi, O. Akilapa, M. Gee, and P. Harnett, "412 operative fixation for acetabular fractures in the elderly: a prospective cohort study from a UK major trauma centre," *British Journal of Surgery*, vol. 109, Supplement\_1, pp. 3939–3941, 2022.
- [8] A. S. Monteleone, P. Feltri, M. N. Molina, J. Müller, G. Filardo, and C. Candrian, "Quality of life from return to work and sports activities to sexual dysfunction after surgical treatment of acetabular fractures," *Archives of Orthopaedic and Trauma Surgery*, vol. 45, no. 31, pp. 391–395, 2022.
- [9] Y. Yun, Z. Chang, F. Yue, and S. Sujun, "Clinical efficacy and its influencing factors of surgical treatment for T-shaped associated with posterior wall acetabular fractures & using combined surgical approaches," *BMC Surgery*, vol. 22, no. 1, pp. 955–958, 2022.
- [10] M. Stavarakis Ioannis, I. Kritsotakis Evangelos, V. Giannoudis Peter et al., "Sciatic nerve injury after acetabular fractures: a meta-analysis of incidence and outcomes," *European Journal of Trauma and Emergency Surgery*, vol. 75, no. 41, pp. 951–956, 2022.
- [11] Z. Fuwen, "Clinical analysis of total hip arthroplasty in the treatment of displaced acetabular fractures in the elderly," *Grass-roots Medical Forum*, vol. 25, no. 28, pp. 4034–4036, 2021.
- [12] L. Xiangxiang, "Analysis of the medium-and long-term effect of total hip arthroplasty and hemiarthroplasty in the treatment of traumatic hip arthritis and osteonecrosis of femoral head secondary to acetabular fracture," *The latest Medical Information Abstracts in the World*, vol. 18, no. 65, pp. 28–29, 2018.
- [13] Z. Yong, "Study on the efficacy of total hip arthroplasty and hip surface replacement in the treatment of osteoarthritis after acetabular fracture," *Medical review*, vol. 18, no. 21, pp. 3717–3719, 2012.
- [14] W. Yong, "Study on the effect and prognosis of different fixation combined with total hip arthroplasty in elderly patients with acetabular fracture," *Asia-Pacific Traditional Medicine*, vol. 10, no. 21, pp. 65–67, 2014.
- [15] L. Zhengmin and S. Xiaoshu, "Medium-and long-term effect of total hip arthroplasty in the treatment of traumatic hip arthritis and osteonecrosis of femoral head secondary to acetabular fracture," *Guizhou Medicine*, vol. 44, no. 1, pp. 73–74, 2020.
- [16] X. Min, L. Minqiang, and M. Jigang, "Analysis of the efficacy of artificial total hip replacement in the treatment of old acetabular fractures with traumatic arthritis in the elderly," *Chinese and Foreign Medical Treatment*, vol. 33, no. 18, pp. 36–38, 2014.
- [17] S. Tian, R. Zhang, S. Liang et al., "Is plating fixation through the Kocher–Langenbeck approach for associated posterior wall fragment indispensable in both-column acetabular fractures?," *Orthopaedic Surgery*, vol. 14, no. 3, pp. 977–979, 2022.
- [18] Z. Yifan, C. Jianan, Y. Siyu et al., "Application of computerized virtual preoperative planning procedures in comminuted posterior wall acetabular fractures surgery," *Journal of Orthopaedic Surgery and Research*, vol. 17, no. 1, pp. 193–199, 2022.
- [19] H. Guixiong, C. Kaifang, W. Yulong, and X. Guo, "Finite element analysis of the union plate in treating elderly acetabular fracture patients," *Journal of Orthopaedic Surgery and Research*, vol. 17, no. 1, pp. 195–199, 2022.
- [20] D. P. Luc, A. Thomas, M. Véronique, P. Upex, P. Jouffroy, and G. Riouallon, "Identification and treatment of atypical acetabular fractures having an independent acetabular roof fragment: three-column fractures," *Orthopaedics & Traumatology, Surgery & research: OTSR*, vol. 3, no. 5, pp. 196–199, 2022.
- [21] S. Tomonori, M. Yasuaki, Y. Yohei, Y. Shiratani, H. Hamano, and Y. Wada, "Comparison between ilioinguinal approach and modified Stoppa approach for the treatment of acetabular fractures: an updated systematic review and meta-analysis," *Orthopaedics & Traumatology: Surgery & Research*, vol. 33, no. 66, pp. 134–138, 2022.
- [22] W. Lisa, S. Sabrina, G. Claudio et al., "Biomechanical comparison of acetabular fracture fixation with stand-alone THA or in combination with plating," *European Journal of Trauma and Emergency Surgery*, vol. 44, no. 31, pp. 197–199, 2022.
- [23] L. Hoehmann Christopher, D. V. Michael, S. Osborn Nathan et al., "Excessively long interfragmentary screws for posterior wall acetabular fractures can predict intraarticular penetration," *Orthopaedics & Traumatology: Surgery & Research*, vol. 44, no. 55, pp. 14–18, 2022.
- [24] Y. Yi-Hsun, C. Ying-Chao, Y. Bo-Yan, Y. H. Hsu, I. Chen, and L. C. Wei, "Intentional fallers with complex pelvic and acetabular fractures do not have worse radiological and functional outcomes than accidental fallers," *BioMed Research International*, vol. 2022, Article ID 8292345, 6 pages, 2022.
- [25] V. K. Mousafeiris, G. D. Chloros, M. Panteli, and P. V. Giannoudis, "Management and outcomes of bilateral acetabular fractures: a critical review of the literature," *Journal of Orthopaedics*, vol. 56, no. 5, pp. 752–761, 2022.



- [26] A. Fergany, A. A. Khalifa, A. Mohamedean, F. F. Adam, and O. Farouk, "Management of anterior associated types of acetabular fractures utilizing the modified Stoppa and the pararectus approaches: a prospective cohort study and early experience from a level one Egyptian trauma centre," *International Orthopaedics*, vol. 46, no. 4, pp. 897–909, 2022.
- [27] E. S. Mahmoud and A. Mostafa, "Role of combined brim and spring plates in the treatment of acetabular fractures involving quadrilateral plates: a retrospective study," *Current Orthopaedic Practice*, vol. 15, no. 55, pp. 385–389, 2022.
- [28] W. Liu, H. Yang, Z. Yu et al., "Comparison of therapeutic outcomes of transabdominal pararectus approach and modified Stoppa approach in treating pelvic and acetabular fractures," *Journal of Orthopaedics*, vol. 56, no. 5, pp. 829–836, 2022.
- [29] S. Khakpour, A. Esrafilian, P. Tanska, M. E. Mononen, R. K. Korhonen, and T. Jämsä, "Effect of osteoporosis-related reduction in the mechanical properties of bone on the acetabular fracture during a sideways fall: a parametric finite element approach," *PLoS one*, vol. 17, no. 2, pp. 197–199, 2022.
- [30] M. Sarasa-Roca, M. C. Angulo-Castaño, J. Gómez-Vallejo, A. Torres-Campos, J. M. Laserra-SanRomán, and J. Albareda-Albareda, "Artroplastia total de cadera primaria en fractura de acetabulo en el paciente anciano," *Revista Española de Cirugía Ortopédica y Traumatología*, vol. 66, no. 1, pp. T52–T59, 2022.
- [31] P. Masionis, T. Vileikis, P. Giedrius, I. Šatkauskas, V. Uvarovas, and G. Kvederas, "Management of complex pelvic ring and acetabular fracture associated with open tibia fracture in severe polytrauma patient: a case report," *Cureus*, vol. 14, no. 1, pp. 134–138, 2022.
- [32] B. A. Butler, R. S. Selley, C. K. Cantrell et al., "Algorithm improves acetabular fracture radiograph interpretation among inexperienced practitioners," *Cureus*, vol. 14, no. 1, pp. 1977–1979, 2022.
- [33] G. Ashwini, K. Kaushlendra, and S. Ranjit, "Spring plate for fixation of comminuted posterior wall acetabular fractures," *Journal of Orthopaedic Diseases and Traumatology*, vol. 5, no. 1, pp. 595–599, 2022.
- [34] C. Gianluca, D. M. Domenico, R. Giuseppe et al., "Anterior intrapelvic approach and suprapectineal quadrilateral surface plate for acetabular fractures with anterior involvement: a retrospective study of 34 patients," *BMC Musculoskeletal Disorders*, vol. 22, no. 42, pp. 845–849, 2021.
- [35] C. Cibura, E. Yilmaz, D. Straeter, T. A. Schildhauer, and C. Kruppa, "Femoral neck osteotomy: a salvage procedure for unstable and locked acetabulum fractures in selected frail patients," *Indian Journal of Orthopaedics*, vol. 55, no. 31, pp. 319–321, 2021.
- [36] S. Bonhomme, C. Ostrowka, K. Belaifa et al., "Screening for venous thrombotic events in patients presenting with pelvis and acetabular fractures: a new practice based on a prospective study," *Thrombosis Update*, vol. 5, no. 41, pp. 100091–100399, 2021.
- [37] S. Oide, M. Banno, A. Saitsu, and N. Saka, "Letter regarding "open reduction and internal fixation alone versus open reduction and internal fixation plus total hip arthroplasty for displaced acetabular fractures in patients older than 60 years: a prospective clinical trial," *Injury*, vol. 53, no. 3, pp. 19–23, 2021.
- [38] K. Mathew Kevin, B. Marchand Kevin, M. Tarazi John et al., "Heterotopic ossification prophylaxis following operative fixation of acetabular fractures: a systematic review," *Surgical Technology International*, vol. 40, no. 55, pp. 394–396, 2022.
- [39] S. Amit, R. R. Kumar, K. Prasoon, R. U. Haq, and I. K. Dhammi, "Ilioinguinal versus modified Stoppa approach for open reduction and internal fixation of displaced acetabular fractures: a systematic review and meta-analysis of 717 patients across ten studies," *Archives of Orthopaedic and Trauma Surgery*, vol. 55, no. 24, pp. 195–199, 2022.
- [40] F. Zhang, Y. Ye, W. Yu, D. Yin, and K. Xu, "Treatment of tibia avulsion fracture of posterior cruciate ligament with total arthroscopic internal fixation with adjustable double loop plate: a retrospective cohort study," *Injury*, vol. 53, no. 6, pp. 2233–2240, 2022.
- [41] X. Song, X. Zhang, Y. Weng et al., "Effects of early acupuncture combined with rehabilitation training on limb function and nerve injury rehabilitation in elderly patients with stroke: based on a retrospective cohort study," *BioMed Research International*, vol. 2022, Article ID 8557936, 9 pages, 2022.
- [42] A. Saghadzadeh and N. Rezaei, "Vascular endothelial growth factor levels in tuberculosis: a systematic review and meta-analysis," *PLoS One*, vol. 17, no. 5, article e0268543, 2022.



## Retraction

# Retracted: A Retrospective Analysis of Internet-Based Sharing Nursing Service Appointment Data

### Computational and Mathematical Methods in Medicine

Received 19 September 2023; Accepted 19 September 2023; Published 20 September 2023

Copyright © 2023 Computational and Mathematical Methods in Medicine. This is an open access article distributed under the Creative Commons Attribution License, which permits unrestricted use, distribution, and reproduction in any medium, provided the original work is properly cited.

This article has been retracted by Hindawi following an investigation undertaken by the publisher [1]. This investigation has uncovered evidence of one or more of the following indicators of systematic manipulation of the publication process:

- (1) Discrepancies in scope
- (2) Discrepancies in the description of the research reported
- (3) Discrepancies between the availability of data and the research described
- (4) Inappropriate citations
- (5) Incoherent, meaningless and/or irrelevant content included in the article
- (6) Peer-review manipulation

The presence of these indicators undermines our confidence in the integrity of the article's content and we cannot, therefore, vouch for its reliability. Please note that this notice is intended solely to alert readers that the content of this article is unreliable. We have not investigated whether authors were aware of or involved in the systematic manipulation of the publication process.

Wiley and Hindawi regrets that the usual quality checks did not identify these issues before publication and have since put additional measures in place to safeguard research integrity.

We wish to credit our own Research Integrity and Research Publishing teams and anonymous and named external researchers and research integrity experts for contributing to this investigation.

The corresponding author, as the representative of all authors, has been given the opportunity to register their agreement or disagreement to this retraction. We have kept a record of any response received.

### References

- [1] Y. Fan, Y. Ma, Y. Zhang, and C. Sun, "A Retrospective Analysis of Internet-Based Sharing Nursing Service Appointment Data," *Computational and Mathematical Methods in Medicine*, vol. 2022, Article ID 8735099, 7 pages, 2022.

## Research Article

# A Retrospective Analysis of Internet-Based Sharing Nursing Service Appointment Data

Yuchen Fan <sup>1</sup>, Yuezhen Ma,<sup>2</sup> Yong Zhang,<sup>2</sup> and Changjian Sun <sup>3</sup>

<sup>1</sup>Department of Hepatobiliary Surgery, Shandong Provincial Third Hospital, Jinan 250000, China

<sup>2</sup>Intensive Care Unit, Shandong Provincial Third Hospital, Jinan 250000, China

<sup>3</sup>College of Electronic Science and Engineering, Jilin University, Changchun 130012, China

Correspondence should be addressed to Changjian Sun; [suncj15@mails.jlu.edu.cn](mailto:suncj15@mails.jlu.edu.cn)

Received 21 June 2022; Accepted 4 August 2022; Published 18 August 2022

Academic Editor: Hangjun Che

Copyright © 2022 Yuchen Fan et al. This is an open access article distributed under the Creative Commons Attribution License, which permits unrestricted use, distribution, and reproduction in any medium, provided the original work is properly cited.

**Aims.** To investigate the historical data of the “Internet+ Nursing” service platform and provide a theoretical basis to optimize the “Internet+ Nursing” service model by analyzing a population in need of nursing care services, service prices, services in demand, willingness to place orders, and feedback on use. **Methods.** A retrospective analysis of data related to home care services on the “Jiuzhou Nursing Care” platform from April 2020 to August 2021, a total of 279 person-times, relevant information about the research subjects, and the status of home care services was conducted. SPSS 24.0 software was used for data analyses, such as calculating frequencies and percentages and conducting chi-square tests. **Results.** The “Jiuzhou Online Nurse” primarily serves elderly patients, and the majority of these patients have lost their ability to care for themselves. The average cost of nursing services was ¥183.45, and the unit cost of services had no effect on the number of service items. This particular internet-based home nursing service has a high level of satisfaction. Patients aged 60 to 74 have the highest number of Internet-based home care service orders ( $\chi^2 = 11.791$ ,  $P < 0.05$ ). Patients who reuse the platform are more willing to assign people to provide services ( $\chi^2 = 238.078$ ,  $P < 0.05$ ). Patients who were unable to care for themselves had a higher rate of repeat order ( $\chi^2 = 10.877$ ,  $P < 0.05$ ). **Conclusion.** The “Internet+ Nursing” service platform specifically meets the individual needs of elderly patients, provides them with home nursing services, and improves local medical treatment and door-to-door services. This platform also provides convenience for elderly individuals who cannot care for themselves so that they can receive prompt treatment and assistance to improve their quality of life.

## 1. Introduction

As the world population continues to age, rapidly growing numbers of elderly people are exposed to risk factors for a long period of time. Due to the deterioration of organs in elderly people, physical decline, and other factors, the prevalence of chronic disease has increased. The care of discharged patients and elderly people with chronic diseases in the community have gradually become a problem that cannot be ignored [1], and growing numbers of family members have become informal caregivers, bearing large burdens of care and considerable pressure [2–4]. In this context, home care has shown positive effects, and the use of home-based long-term care services is beneficial to the health of patients with chronic diseases, especially elderly patients [5]. Home care resources may provide a

more flexible and proactive approach to maintain functional status, maximize symptom relief, and prevent avoidable hospitalizations [6, 7]. Additionally, it may reduce care burden, family pressure [4, 8, 9], and medical expenditure [10]. Furthermore, home care can provide short-term care services as well as long-term healthcare services such as health exercises [11]. Professional and medically qualified family nurses can establish a harmonious relationship with the family while providing service. While providing home care services, services can be customized according to the unique needs of the family to support the effects of home care services [12–14].

In recent years, electronic and information technology have developed quickly, and a new form of “Internet +” has emerged. Medical services, including home care services, have gradually become electronic, digital, and platform-based,

which has supported the integration of online and offline medical services. In developed countries, electronic and information technology are commonly used in home care. To reduce the costs of service and labor experienced as part of in-home rehabilitation, South Korea has studied the use of network-based vision and wearable device home rehabilitation systems to improve the quality of home care [15]. The United States developed internet-based care enhancement tools in the early years to build a communication bridge between consumers and medical providers [16]. Sweden uses applications as useful information and communication technology innovations that can improve communication and accessibility for older people that need home-based healthcare [17]. The Norwegian internet-based personalized online care communication platform has been successfully exposed to research on lifestyle, behavior changes, and childbirth [18–20]. Initially, China provided health guidance and online Q&A for patients with chronic diseases discharged from the hospital through mobile medical follow-up calls and official WeChat accounts [21]. In 2019, the National Health Commission announced that it would launch a pilot project with nurses [22]. As part of the “Internet +” plan, China launched the “Internet+ Nursing” service and actualized an online nursing service platform (or “online nurse appointment” platform) that allowed registered nurses to visit patients to provide home care services [23]. The online nursing service platform first started in Jinan in 2016. It has successfully expanded from Shandong Province to first-tier cities such as Beijing, Shanghai, Guangzhou, and Shenzhen [24]. The popularity of Internet in foreign countries is earlier, and the development of “Internet + nursing” platform is also earlier. For example, an Internet care platform for children with attention deficit and hyperactivity disorder (ADHD) was planned abroad in 2002 [25]. There is a platform system for a particular disease, and the platform will make personal risk reports and personal care recommendations based on the patient’s daily state [26]. Although we are late in developing Internet nursing services, our platform system realizes electro-nization, digitization, and platformization, supporting the integration of online and offline medical services. Experience feedback is the great advantage of “Internet+ nursing” service platform. Experiential feedback helps the platform identify service deficiencies and improve the quality of home care services for patients in the community who need continuous care.

All telenurses in China are professional nursing technicians approved by medical institutions (hospitals, community healthcare centers, and private clinics). Telenurses complete personal information registration by logging into the nursing terminal of the platform. Patients can complete information registration through the client portal, apply for nursing care service, and after a shared nurse grabs (or claims) the order, the reservation is confirmed. Patients can also invite specific nurses to provide services, and the appointment is confirmed after the invitees agree. Subsequently, the shared nurse arrived at the designated place on time with the required nursing materials to complete the nursing service. After the service, the patient provides feedback regarding the nursing service.

Exploration of the patient group, service need, experience, and feedback of home care service are key roles in the “Internet+ Nursing” service for elderly patients. This research can

encourage sharing of accurate information among patient groups and improve the quality of home care services for patients discharged from hospitals and patients who need continuous care in the community. On the other hand, traditional nursing care services consume considerable manpower and financial resources [27, 28]. Telenurses can meet patients’ home care needs while reducing the pressure on nursing staff and appropriately allocating human resources. It determines the direction of nurses’ future professional development and skill training. However, there are still few studies on patients’ demand for telenurses (that is, group composition, service needs, willingness to place orders, and satisfaction). The current study is aimed at addressing the practice gap, providing a basis for improving the quality of home care, and further optimizing the shared governance model.

## 2. Materials and Methods

**2.1. Design and Participants.** The research subjects were selected patients from April 2020 to August 2021 who were discharged from hospitals, medical consortium units, and communities in Jinan City who used the “Jiuzhou Nursing Care” platform to place orders. The total number of order samples collected is 279 person-times. The inclusion criteria were as follows: register the patient’s real-name information and provide a diagnosis certificate from a second-level or higher medical institution assessed by the health department.

**2.2. Measurements.** Sociodemographic information included sex, age, and self-care ability. The current status of home care services includes the itemized list of home care services, total charges, service times, order mode, order frequency, and satisfaction. The survey data come from the “Jiuzhou Nursing Care” management platform and are uniformly coded. SPSS 24.0 statistical software was used to establish a database for descriptive analysis. Statistical methods included frequency, percentage, and chi-square test.  $P < 0.05$  indicates that the difference is statistically significant.

**2.3. Quality Control.** The researcher contacted the person in charge of the Jinan City “Jiuzhou Nursing Care” platform, obtained agreement, and exported relevant data content through the system. In cases of missing data, the system will prompt feedback and supplement the data in a timely manner.

## 3. Results

**3.1. Demographic Characteristics of the Participants.** The age of the study subjects was between 49 and 95 years old, with an average age of 70.96 years old. Among them, 92.8% were aged  $\geq 60$  years old, 62.0% were aged 60 to  $< 75$  years old, 29.0% were aged 75 to  $< 90$  years old, and 1.8% were aged  $\geq 90$  years old. A total of 60.6% of patients were male, and 39.4% of patients were female, as shown in Table 1.

**3.2. “Internet+ Nursing” Home Care Service Status.** The total cost of home care services in this study was ¥51183, and the number of different services for all patients was 279 person-times. The average price of the service is ¥183.45. The home care services with high demand are catheterization care,

TABLE 1: Relevant situation of research subjects ( $n = 279$ ).

		Count ( $n$ )	Percent (%)
Gender	Male	169	60.6%
	Female	110	39.4%
Age group (years)	<60	20	7.2%
	60 to <75	173	62.0%
	75 to <90	81	29.0%
	$\geq 90$	5	1.8%

gastric tube care, and peripherally inserted central catheter (PICC) maintenance. Oral care and tracheotomy care services were the least common. The project with the highest average price is pressure ulcer wound care, and the price is ¥258. The lowest average price item is venous blood collection, and the price is ¥162. Table 2 shows the payment status of home care service orders for research subjects.

The satisfaction with home care services was as high as 100%, and 98.6% of patients who received home care services were very satisfied, as shown in Table 3.

Differences in order mode selection among patients of different ages include the following: patients between the ages of 60 and 74 have the largest number of home care orders and patients over 90 years old have the least number of home care orders. The home care service order mode in this study is divided into two modes: grab order mode and designated mode. Most of the order modes were grabbing orders. For patients aged 60 to 89, the proportion of designated orders increases gradually with the increase of age. There was a significant correlation between age and order mode ( $P < 0.05$ ), as shown in Table 4.

The home care service order frequency in this study includes multiple orders and a single order. As shown in Table 5, the same registered user places 37.99% of orders multiple times. Differences in order mode selection among patients with different order frequencies include a total of 97.7% of patients who ordered only one home care service with the same registered account chose the order-grabbing mode, while 94.3% of patients who ordered home care services with the same registered account multiple times chose the designated service provider for nursing care. Patients who only seek home care are more inclined to designate personnel to provide onsite services.

There was a significant correlation between order frequency and order mode ( $P < 0.05$ ), as shown in Table 6. The Pearson between order frequency and order mode is 0.385, and the  $P$  value is less than 0.05, the positive correlation between order frequency and order mode is significant. This indicates that users with more orders tend to prefer the specified order mode.

As shown in Table 7, patients with total loss of self-care ability placed orders the most frequently, accounting for 65.9% of the total number of orders. Patients with partial loss of self-care ability accounted for 26.2% of the total, and patients with self-care ability placed the least orders. Additionally, patients with total loss of self-care ability had the highest proportion of multiple orders, accounting for 75.5%.

TABLE 2: Payment status of home care service orders for research subjects ( $n = 279$ ).

Service items	Service charge (¥)	Service times ( $n$ )	Average price (¥)
PICC maintenance	7378	31	238
Bladder irrigation	334	2	167
Catheterization care	18512	104	178
Enema care	609	3	203
Venous blood collection	810	5	162
Oral care	178	1	178
Tracheostomy care	218	1	218
Surgical wound dressing	344	2	172
Stomach tube care	19040	112	170
Sputum suction care	1008	6	168
Pressure ulcer wound care	2064	8	258
Stoma care	688	4	172

TABLE 3: Research subjects' home care service orders and satisfaction ( $n = 279$ ).

Satisfaction degree	Count ( $n$ )	Percent (%)
Very dissatisfied	0	0.0%
Dissatisfied	0	0.0%
Generally	0	0.0%
Satisfy	4	1.4%
Very satisfied	275	98.6%

There was no significant correlation between order frequency and self-care ability ( $P > 0.05$ ), as shown in Table 8. The Pearson between order frequency and self-care ability is only -0.061;  $P$  value is greater than 0.05, so the correlation between order frequency and self-care ability is not significant.

#### 4. Discussion

The composition of family nursing service demand groups is the research object of this study. The analysis and discovery of service groups will optimize the nursing service mode in the next step. In order to better study the difference of the elderly, the age was grouped according to the new age segmentation of the World Health Organization [29]. As shown in Table 1, the average age of patients with chronic diseases in this survey was 70.96 years old, of which 92.8% were aged  $\geq 60$  years old, indicating that elderly patients with chronic diseases are the main group demanding home care services, and they are not excluded from accepting internet appointments for home care services because they are not familiar with the internet. Although some elderly patients are unable to operate their mobile phones proficiently [30, 31], they still have the opportunity to reserve care services via the internet with the help of their family members.

Analyzing the popularity of different services from the perspective of home care services can provide data support for medical institutions in the cultivation of professional talent



TABLE 4: Comparison of ordering modes among patients of different age groups ( $n = 279$ ).

Group	Order mode				Chi-square	P value
	Grab an order, <i>N</i> (%)		Specify, <i>N</i> (%)			
Age (years)					11.791	0.006
<60	19	95.0%	1	5.0%		
60 to <75	107	61.8%	66	38.2%		
75 to <90	46	56.8%	35	43.2%		
≥90	3	60.0%	2	40.0%		
Total	175	62.7%	104	37.3%		

TABLE 5: Comparison of patient ordering modes with different ordering frequencies ( $n = 279$ ).

Group	Order mode				Total	Chi-square	P value
	Grab an order, <i>N</i> (%)		Specify, <i>N</i> (%)				
Frequency						238.078	0.001
Single	169	97.7%	4	2.3%	173	62.01%	
Multiple	6	5.7%	100	94.3%	106	37.99%	
Total	175	62.7%	104	37.3%	279	100%	

TABLE 6: Correlation analysis between order frequency and order mode ( $n = 279$ ).

	Order mode	
	Pearson	0.385**
	Significant difference	0.000
Order frequency	Total	279

\*\*\* $P < 0.01$ , \*\* $P < 0.05$ , and \* $P < 0.1$ .

and the deployment of medical resources. As shown in Table 2, the services with high demand in this study are catheterization care, gastric tube care, and PICC catheter maintenance, followed by pressure ulcer wound care, sputum suction care, and venous blood sampling, which indicates that the most frequently requested home care services are medical services. On the one hand, high-demand services require highly skilled professionals, and while nursing materials are difficult to obtain, families experience difficulty in providing care independently. Therefore, support from professional and technical personnel is required. Second, high-demand services are common for diseases that require long-term treatment and recovery, which increases the frequency of patients' needs. Especially in the context of shortened hospital stays and improved community health services, communities and family homes have become the main places for the treatment and rehabilitation of most chronic diseases, and the demand for professional nursing care services is increasing among elderly patients. This has increased the urgency of seamless connection between home care and hospital care. Providing professional and appropriate treatment and nursing care technology is the basis for satisfactory home care services for elderly patients with chronic diseases [32].

Economic pressure is a factor that affects home care services. Patients with chronic disease have a long course of illness and a high treatment costs, which increases the financial

burden on the family and affects the patient's ability and willingness to pay their bills. This study analyzes the relationship between the average price of a single service and the number of services to identify whether the patient group has a low willingness to pay for home care, which restricts the development of home care services. As shown in Table 2, the average price of the services in this study is RMB 183.45. At present, home care services are not included in medical insurance and but are instead paid at the patients' expense. It is worth noting that after comparing and analyzing the service times and prices of different projects, we found that the times of different services did not have a positive correlation with service prices. This may depend on two reasons: first, because home care does not need to occupy the space of a medical institution and can flexibly occupy other locations, the price is much lower than the cost of nursing care in a medical institution [33]; second, because most medical services are necessary expenses for families, the development of home care services is not restricted. However, improving the "Internet+ Nursing" service platform, reducing service costs to provide professional and appropriate nursing care services, reducing the burden of care for family members, and meeting home care service needs for elderly patients with chronic diseases are still important goals for this service model.

The service satisfaction data reveal that patients are highly satisfied with online appointment care. As shown in Table 3, 98.6% of patients reported that they were very satisfied with the service. High levels of satisfaction encourage patients to make repeat appointments on the platform. As shown in Tables 3 and 4, when analyzing order frequencies, repeat orders accounted for 37.99%, and the number of elderly patients with chronic diseases between age 60 and 74 who placed home care orders was the largest. This shows that "young elderly" individuals [34] have a higher demand for home care services, which indicates that young elderly individuals are better at accepting and applying via medical websites,



TABLE 7: Comparison of ordering frequencies of patients with different self-care abilities ( $n = 279$ ).

Group	Self-care, $N$ (%)		Self-care ability Partial loss, $N$ (%)		Complete loss, $N$ (%)		Chi-square	$P$ value
Frequency							10.877	0.004
Single	12	6.9%	57	32.9%	104	60.1%	173	
Multiple	10	9.4%	16	15.1%	80	75.5%	106	
Total	22	7.9%	73	26.2%	184	65.9%	279	

TABLE 8: Correlation analysis between order frequency and self-care ability ( $n = 279$ ).

		Self-care ability
Order frequency	Pearson	-0.061
	Significant difference	0.307
	Total	279

apps, hospital WeChat public accounts, and other service platforms to obtain relevant medical service information. From the order mode perspective, there is a significant correlation between age and order mode. As shown in Tables 4 and 5, the older people are, the higher the proportion of making orders. As they grow older, they become more isolated and require customized nursing care services. Appointing people who are more familiar with their condition to make an appointment for nursing care services will be more beneficial to their care. In addition, people who repeatedly place orders are more likely to choose a dedicated service provider, indicating their demand for and affirmation of the professional skills of nursing staff.

The home care appointment model is of great significance to patients who lack total self-care ability. As shown in Table 7, patients with chronic diseases who have lost their ability to care for themselves place the most frequent orders, and the proportion of multiple orders is the highest [35]. The proportion of people who could not care for themselves was 92.1%. As age increases, physical functions decline, and the demand for home care services increases. Elderly people who cannot care for themselves need targeted care services [36]. This shows that the home care service model has significantly improved the convenience of nursing care for this group. This portion of the population does not require hospital care; they can easily receive home care instead.

### 5. Limitations

This study has limitations. First, the research subjects included in this study were all from hospitals, medical union units, and communities in Jinan, which limits the generalizability of the results. Second, this study only performed a descriptive analysis of the current status of the use of services for people who have ordered home care services and did not identify the factors that influence home care services and the nurses using the platform. These two limitations can be addressed in future studies to provide sufficient evidence to improve practice.

### 6. Conclusion

The “Internet+ Nursing” service based on the online nurse appointment platform is a new intelligent nursing care model. Through a retrospective analysis of the order data of “Jiuzhou Nursing”, including the patient’s gender, age, self-care ability, home care service items, cost, order method, order time, and satisfaction, this study found that the platform can provide personalized services to patients’ needs. Through resource integration, information sharing, and convenient use, this platform provides seamless connection between home care and hospital care. Elderly patients are the main group demanding home care service, especially elderly patients who are unable to care for themselves. The demand is mainly for professional nursing care, and the price of service is lower than the price of hospital care. Feedback regarding services indicate a high level of satisfaction, and patients are more willing to allow the people they are familiar with to provide care services. On the other hand, through the “Internet+ nursing” service, the pressure on nursing staff can be reduced, and human resources can be appropriately allocated. Research on the current status of services from the patients’ perspective provides theoretical guidance to optimize service models.

### Data Availability

The data used to support the findings of this study are included in the article.

### Ethical Approval

This retrospective study was conducted following the approval from the Ethics Committee of Shandong Provincial Third Hospital, with the approval number KYLL-2022014. The ethical approval document and English translation version are in Supplementary Materials.

### Disclosure

The authors are accountable for all aspects of the work in ensuring that questions related to the accuracy or integrity of any part of the work are appropriately investigated and resolved.

### Conflicts of Interest

The authors declare no conflict of interest.

## Authors' Contributions

Yuchen Fan used statistical techniques to analyze the experimental data and wrote the initial draft. Yuezhen Ma completed the discussion and summary of the analysis results with the team based on her medical experience. Yong Zhang obtained the required data in the service platform database and converted and unified the data format for data analysis. As the framework designer of the manuscript, Changjian Sun devised the methodology for the experimental analysis and edited the draft. Yuchen Fan and Yuezhen Ma contributed equally to this work.

## Supplementary Materials

The ethical approval document and English translation version. (*Supplementary Materials*)

## References

- [1] H. Wang, K. Li, J. Li et al., "Moderate chronic kidney disease and left atrial enlargement independently predict thromboembolic events and mortality in elderly patients with atrial fibrillation: a retrospective single-center study," *Journal of International Medical Research*, vol. 47, no. 9, pp. 4312–4323, 2019.
- [2] R. D. Adelman, L. L. Tmanova, D. Delgado, S. Dion, and M. S. Lachs, "Caregiver burden," *Journal of the American Medical Association*, vol. 311, no. 10, p. 1052, 2014.
- [3] Y. Arai, S. Zarit, M. Sugiura, and M. Washio, "Patterns of outcome of caregiving for the impaired elderly: a longitudinal study in rural Japan," *Aging & Mental Health*, vol. 6, no. 1, pp. 39–46, 2002.
- [4] M. Lee, E. Yoon, and N. Kropf, "Factors affecting burden of south Koreans providing care to disabled older family members," *International Journal of Aging & Human Development*, vol. 64, no. 3, pp. 245–262, 2007.
- [5] M. Chen, C. Kao, L. Chiu et al., "Effects of home-based long-term care services on caregiver health according to age," *Health & Quality of Life Outcomes*, vol. 15, no. 1, p. 208, 2017.
- [6] G. Næss, M. Kirkeveld, W. Hammer, J. Straand, and T. B. Wyller, "Nursing care needs and services utilised by home-dwelling elderly with complex health problems: observational study," *BMC Health Services Research*, vol. 17, no. 1, p. 645, 2017.
- [7] M. Nakanishi, J. Niimura, and A. Nishida, "Factors associated with end-of-life by home-visit nursing-care providers in Japan," *Geriatrics & Gerontology International*, vol. 17, no. 6, pp. 991–998, 2017.
- [8] J. Huang, D. Barzallo, S. Rubinelli, N. Münzel, M. Brach, and A. Gemperli, "Professional home care and the objective care burden for family caregivers of persons with spinal cord injury: cross sectional survey," *International Journal of Nursing Studies Advances*, vol. 3, article 100014, 2021.
- [9] J. Roldán-Merino, I. C. García, J. D. Ramos-Pichardo, A. Foix-Sanjuan, J. Quilez-Jover, and M. Montserrat-Martinez, "Impact of personalized in-home nursing care plans on dependence in ADLs/IADLs and on family burden among adults diagnosed with schizophrenia: a randomized controlled study," *Perspectives in Psychiatric Care*, vol. 49, no. 3, pp. 171–178, 2013.
- [10] S. Szanton, Y. Alfonso, B. Leff et al., "Medicaid cost savings of a preventive home visit program for disabled older adults," *Journal of the American Geriatrics Society*, vol. 66, no. 3, pp. 614–620, 2018.
- [11] L. Teri, S. McCurry, and R. Logsdon, "A home health care approach to exercise for persons with Alzheimer's disease," *Care Management Journals*, vol. 6, no. 2, pp. 90–97, 2005.
- [12] H. Weiss, "Home visits: necessary but not sufficient," *The Future of Children*, vol. 3, no. 3, p. 113, 1993.
- [13] N. Beer, "The role of the home visiting nurse in the total education programme of spinal cord injured persons," *Paraplegia*, vol. 22, no. 5, pp. 311–315, 1984.
- [14] E. Burton, K. Farrier, R. Galvin et al., "Physical activity programs for older people in the community receiving home care services: systematic review and meta-analysis," *Clinical Interventions in Aging*, vol. 14, pp. 1045–1064, 2019.
- [15] S. H. Chae, Y. Kim, K. S. Lee, and H. S. Park, "Development and clinical evaluation of a web-based upper limb home rehabilitation system using a smartwatch and machine learning model for chronic stroke survivors: prospective comparative study," *JMIR mHealth and uHealth*, vol. 8, no. 7, article e17216, 2020.
- [16] M. P. Metcalf, T. B. Tanner, M. B. Coulehan, and M. Mooney, "Internet based care enhancement tools: two examples from the real world," in *Proceedings of the AMIA Symposium*, p. 975, Washington, DC, 2001.
- [17] C. Göransson, I. Eriksson, K. Ziegert et al., "Testing an app for reporting health concerns—experiences from older people and home care nurses," *International Journal of Older People Nursing*, vol. 13, no. 2, article e12181, 2018.
- [18] M. R. Van Dijk, N. A. Huijgen, S. P. Willemsen, J. S. E. Laven, E. A. P. Steegers, and R. P. M. Steegers-Theunissen, "Impact of an mHealth platform for pregnancy on nutrition and lifestyle of the reproductive population: a survey," *JMIR mHealth and uHealth*, vol. 4, no. 2, article e5197, 2016.
- [19] T. Probst, R. C. Pryss, B. Langguth et al., "Outpatient tinnitus clinic, self-help web platform, or mobile application to recruit tinnitus study samples?," *Frontiers in Aging Neuroscience*, vol. 9, p. 113, 2017.
- [20] L. E. Dahlberg, D. Grahm, J. E. Dahlberg, and C. A. Thorstenson, "A web-based platform for patients with osteoarthritis of the hip and knee: a pilot study," *JMIR Research Protocols*, vol. 5, no. 2, article e5665, 2016.
- [21] K. Chiang and H. Wang, "Nurses' experiences of using a smart mobile device application to assist home care for patients with chronic disease: a qualitative study," *Journal of Clinical Nursing*, vol. 25, no. 13–14, pp. 2008–2017, 2016.
- [22] The State Council, "China pilots an internet plus nursing program," 2019, [http://english.www.gov.cn/state\\_council/ministries/2019/02/13/content\\_281476520056360.htm](http://english.www.gov.cn/state_council/ministries/2019/02/13/content_281476520056360.htm).
- [23] World Health Organization, "Global observatory for eHealth series, volume 3 [EB/OL]," <http://www.Who.int/goedpublications/ehealth.series-vol3/en>.
- [24] M. M. Bujnowska-Fedak and A. Mastalerz-Migas, "Usage of medical internet and E-health services by the elderly," *Environment Exposure to Pollutants*, vol. 834, pp. 75–80, 2014.
- [25] C. Foss, "Gender bias in nursing care? Gender-related differences in patient satisfaction with the quality of nursing care," *Scandinavian Journal of Caring Sciences*, vol. 16, no. 1, pp. 19–26, 2002.

## Research Article

# Big Data Analysis and Application of Liver Cancer Gene Sequence Based on Second-Generation Sequencing Technology

Chaohui Xiao,<sup>1</sup> Fuchuan Wang,<sup>2</sup> Tianye Jia,<sup>3</sup> Liru Pan,<sup>1</sup> and Zhaohai Wang<sup>1</sup> 

<sup>1</sup>Faculty of Hepato-Biliary-Pancreatic Surgery, Chinese People's Liberation Army (PLA) General Hospital, Beijing 100853, China

<sup>2</sup>Faculty of Hepatology Medicine, Chinese People's Liberation Army (PLA) General Hospital, Beijing 100039, China

<sup>3</sup>Department of Laboratory, Fifth Medical Center, Chinese People's Liberation Army (PLA) General Hospital, Beijing 100039, China

Correspondence should be addressed to Zhaohai Wang; 161849064@masu.edu.cn

Received 24 May 2022; Revised 3 July 2022; Accepted 14 July 2022; Published 16 August 2022

Academic Editor: Shimin Wang

Copyright © 2022 Chaohui Xiao et al. This is an open access article distributed under the Creative Commons Attribution License, which permits unrestricted use, distribution, and reproduction in any medium, provided the original work is properly cited.

In big data analysis with the rapid improvement of computer storage capacity and the rapid development of complex algorithms, the exponential growth of massive data has also made science and technology progress with each passing day. Based on omics data such as mRNA data, microRNA data, or DNA methylation data, this study uses traditional clustering methods such as kmeans, K-nearest neighbors, hierarchical clustering, affinity propagation, and nonnegative matrix decomposition to classify samples into categories, obtained: (1) The assumption that the attributes are independent of each other reduces the classification effect of the algorithm to a certain extent. According to the idea of multilevel grid, there is a one-to-one mapping from high-dimensional space to one-dimensional. The complexity is greatly simplified by encoding the one-dimensional grid of the hierarchical grid. The logic of the algorithm is relatively simple, and it also has a very stable classification efficiency. (2) Convert the two-dimensional representation of the data into the one-dimensional representation of the binary, realize the dimensionality reduction processing of the data, and improve the organization and storage efficiency of the data. The grid coding expresses the spatial position of the data, maintains the original organization method of the data, and does not make the abstract expression of the data object. (3) The data processing of nondiscrete and missing values provides a new opportunity for the identification of protein targets of small molecule therapy and obtains a better classification effect. (4) The comparison of the three models shows that Naive Bayes is the optimal model. Each iteration is composed of alternately expected steps and maximal steps and then identified and quantified by MS.

## 1. Introduction

Next-generation sequencing (NGS), also known as high-throughput sequencing or massively parallel sequencing, is a technology that can sequence thousands to billions of DNA fragments simultaneously and independently. The dideoxynucleoside end-termination sequencing method began in the 1970s. In the follow-up continuous improvement, the Sanger method caused a sequencing boom and became the mainstream due to its simplicity and rapidity. In order to meet the increasingly complex research needs, next-generation sequencing technology emerges from time to time [1–3]. Using NGS technology to detect a variety of cancers, and compared the results with the Sanger method, it was found that in addition to common gene mutations,

NGS technology can also detect many gene mutations that were ignored by real-time quantitative PCR detection technology. It may play a prompting and guiding role in the occurrence and development of cancer and the diagnosis and treatment of patients and also reflects the value of using NGS technology in clinical work. There are currently three mainstream NGS platforms: Roche454, Ion Torrent, and Illumina platforms. The Roche454 platform is based on the pyrosequencing method, that is, bases are incorporated in the order of T, A, C, and G during sequencing, and pyrophosphate is released after pairing. The Ion Torrent platform is the semiconductor sequencing technology. The ion sensor can detect the pH change caused by proton release during the synthesis process and then judge the sequence of the base. NGS technology detection programs have

different focuses, including whole genome sequencing (WGS), which can detect all genetic changes and conduct a comprehensive analysis of tumor-related genes, but it is costly and time-consuming. Whole exome sequencing (WES), which only detects the coding gene regions, is more economical and can detect already known mutant coding genes and discover new gene mutations in cancer. Whole transcriptome sequencing, based on cDNA sequence sequencing, can detect information about the overall transcriptional activity [4]. Targeted target sequencing can select some genes required for disease research for higher sequencing efficiency, but it is not suitable for detecting unknown mutations [5–7]. The techniques of experimental manipulation (wet experiment) and bioinformatics analysis (dry experiment) have been developed continuously. NGS technology is widely used in solid tumors, and more new gene mutations have been discovered, providing new ideas for the detection of genetic susceptibility and the guidance of individualized precision medicine, and have played an extremely important role in the study of the genetic pathways of human malignant tumor mutations effect. Liver cancer is one of the most common cancers in cancer patients today [8–10]. According to the 2020 report by the American Cancer Society, there are an estimated 42,810 new cases and 30,160 deaths from the liver and intrahepatic cholangiocarcinoma in the United States throughout the year. Statistics at home and abroad show that liver cancer is an important cause of cancer death worldwide, and the treatment of liver cancer is also an urgent problem to be solved. Liver cancer is divided into two types: primary and secondary. Primary liver cancer (PLC) is the most common. From a histological point of view, primary liver cancer can be divided into different subtypes according to the cell origin, hepatocellular carcinoma (HCC) (about 75-85% of all cases), intrahepatic cholangiocarcinoma (ICC) (about 75% of all cases), intrahepatic cholangiocarcinoma (ICC) (10-15%), and other rare forms. Hepatocellular carcinoma has become the main type of liver cancer research. The main known carcinogens of liver cancer are hepatotropic virus: mainly chronic infection with hepatitis B (HBV) and hepatitis C (HCV) virus; chemical stimulation: such as alcohol abuse and aflatoxin; metabolic abnormalities: diabetes and nonalcoholic fatty liver disease, hereditary hemochromatosis, etc.; immune-related causes: such as cirrhosis-related immune dysfunction syndrome (CAID) and autoimmune hepatitis; etc. Among them, viral infection is the main factor causing liver cancer [11–13]. Hepatocellular carcinoma cells have extensive heterogeneity from undesired lesions caused by a small number of mutations to eventually develop into an advanced form of the disease. Because the factors that induce liver cancer are diverse and the distribution in different countries and regions is different, the molecular mechanism of liver cancer is complicated. In a broad sense, liver cancer is divided into two categories: proliferative and nonproliferative. The proliferative type is common in HBV-induced liver cancer, with low degree of differentiation, high alpha-fetoprotein (AFP) expression, more vascular invasion, and worse prognosis; this type of liver cancer is characterized by increased inactivating mutations in TP53 and AXIN1, and at the same time,

cell cycle, mTOR, RAS-MAPK, and MET signaling pathways that promote survival are all activated. The nonproliferative class is commonly seen in HCV and alcohol-related hepatocellular carcinoma, with moderate or high differentiation, low AFP expression, less aggressiveness, and chromosomal stability. This type of hepatocellular carcinoma is characterized by more heterogeneity, higher frequency of CTNNB1 ( $\beta$ -catenin) activating mutations, and TERT promoter mutations, as well as activation of WNT and IL6/JAK-STAT signaling pathways. However, these commonly mutated genes TP53, AXIN1, CTNNB1, and TERT in liver cancer proved to be difficult to target [14, 15]. At present, liver resection and liver transplantation have become the main treatment methods for patients with early-stage liver cancer, and patients with intermediate-stage liver cancer are often treated with hepatic arterial chemoembolization and radioembolization, which can greatly prolong the survival of patients. However, due to the lack of specific symptoms and tumor biomarkers, most HCC patients are diagnosed at an advanced stage, so these curative treatments are not suitable. Sorafenib, a multi-receptor tyrosine kinase inhibitor, was identified as a therapeutic drug with survival benefits for patients with advanced liver cancer. Multiple drugs have since been shown to have clinical efficacy, including other RTK inhibitors such as lenvatinib, regorafenib, and cabozantinib. The liver is an important organ that removes toxins and regulates blood sugar, fat, and amino acid uptake. Similar to all cancers, the gradual accumulation of genetic and epigenetic changes in the liver, accompanied by a large number of metabolic changes, leads to abnormal proliferation of mature hepatocytes and the evolution of liver cancer.. Due to the high heterogeneity of liver cancer cells and the complex pathogenic factors caused by the involvement of various signaling pathways, it is clinically found that using a unified treatment regimen to treat all patients may have different curative effects and may even exacerbate symptoms. Therefore, “personalized medicine” is the development direction of contemporary treatment of liver cancer, and different therapeutic methods based on molecular and cell therapy have also been developed. The emerging molecular-level therapeutic strategies include molecular targeted therapy, targeted radionuclide therapy, and epigenetic modification-based therapy, which provide new strategies for the treatment of liver cancer.

## 2. Big Data Analysis of Liver Cancer

**2.1. Disease Diagnosis of Omics Big Data.** Cancer subtype classification methods based on omics data mainly include subtype classification methods based on single omics data and subtype classification methods based on multiomics data fusion. The former is based on an omics data such as mRNA data, microRNA data, or DNA methylation data and uses traditional clustering methods such as kmeans, K-nearest neighbors, hierarchical clustering, affinity propagation, and nonnegative matrix decomposition to classify samples. The results of subtype classification of cancer are obtained, as shown in Figure 1. With the development of related technologies, the collection of omics data has



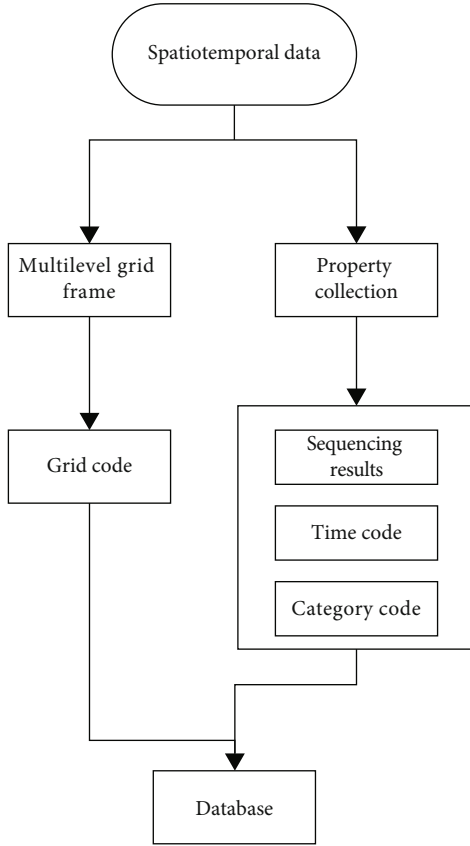


FIGURE 1: Conceptual model.

shown an explosive trend, and its acquisition cost has been greatly reduced. A large number of genomics, transcriptomics, proteomics, and other data of different cancer patients are given in the database headed by TCGA omics data. Since different omics data can describe the complex life process in cancer cells and the interactions between various molecules from different perspectives, the information is complementary, and the integrated analysis of multiomics data can identify more accurate and reasonable subtype results. In recent years, research has mainly focused on the field of multiomics data integration analysis methods. Most existing integrative analysis methods need to address problems closely related to biological data. The data sample size is small, and the dimensionality is high (the so-called curse of dimensionality problem). When the data scope and data type are not consistent, the underlying omics-specific and between-group data structures are easily overlooked in multi-omics data. Divided from the data supported by integrative analysis methods, existing integrative analysis methods include general methods that can analyze any multiomics data and specialized methods designed only for specific data types. The former can be applied to any multiomics data and can be easily extended to the analysis of more omics data, while the latter requires the use of known biological relationships (such as the association between copy number changes and gene expression profiles), which can only be analyzed specific data types.

**2.2. Epigenetics of Liver Cancer.** Abnormal epigenetic changes are important etiologies for the occurrence, development, and metastasis of liver cancer. Epigenetics, the heritable modification of gene function without altering the DNA sequence, is caused by many different factors. Epigenetic alterations are often present in liver cancer. The screening process is shown in Figure 2. Epigenetic processes include, but are not limited to, chromatin remodeling, histone modification, DNA methylation, and expression of noncoding RNAs. Unlike the irreversible nature of genomic alterations, epigenetic changes are reversible, opening a promising avenue for the development of new therapeutic modalities. Therefore, epigenetic changes associated with cancer and liver cancer are gradually being widely used in the development of biomarkers. Hepatocellular carcinoma (HCC) is one of the most common liver tumors and has become the leading cause of cancer-related death in many regions and countries. Although many measures have been taken to prevent, early screen, diagnose, and treat liver cancer, the current situation of liver cancer in my country is still not optimistic.

### 3. Algorithm Model

#### 3.1. Naive Bayes [16–20]. Semiconductor sequencing

$$\begin{aligned} X' &= \left\{ \left( x'_1, y'_1 \right), \left( x'_2, y'_2 \right), \dots, \left( x'_n, y'_n \right) \right\} X' \\ &= \left\{ \left( x'_1, y'_1 \right), \left( x'_2, y'_2 \right), \dots, \left( x'_n, y'_n \right) \right\}, \end{aligned} \quad (1)$$

$$x_{\text{new}} = x_i + \text{rand}(0, 1) \times (x'_j - x_i).$$

Ion sensor,  $D$  is the matrix reconstruction function,  $x$  is the group sparse constraint function, and  $y$  is the weight of the group sparse constraint term.

$$\begin{aligned} D &= \{(x_1, y_1), (x_2, y_2), \dots, (x_m, y_m)\}, \\ h_i &= \varepsilon(N, m). \end{aligned} \quad (2)$$

Unknown genome sequence

$$\begin{aligned} H(x) &= \arg \max_{y \in Y} \sum_{t=1}^T (I(h(x) = y)), \\ P_i &= (x_i, y_i, z_i) \quad i = 1, 2, 3, 4 \dots \end{aligned} \quad (3)$$

Nucleic acid fragments are sequenced,  $Row$  is the number of clusters,  $y_i$  is the index of the sample belonging to the  $i$ th category, and  $r$  is the sparse constraint function.

$$\begin{aligned} Row &= \frac{2y_i}{r}, \\ Column &= \frac{2x_i}{r} \quad i = 1, 2, 3, 4 \dots, \\ Z &= \sum_{i=1}^n z_i. \end{aligned} \quad (4)$$



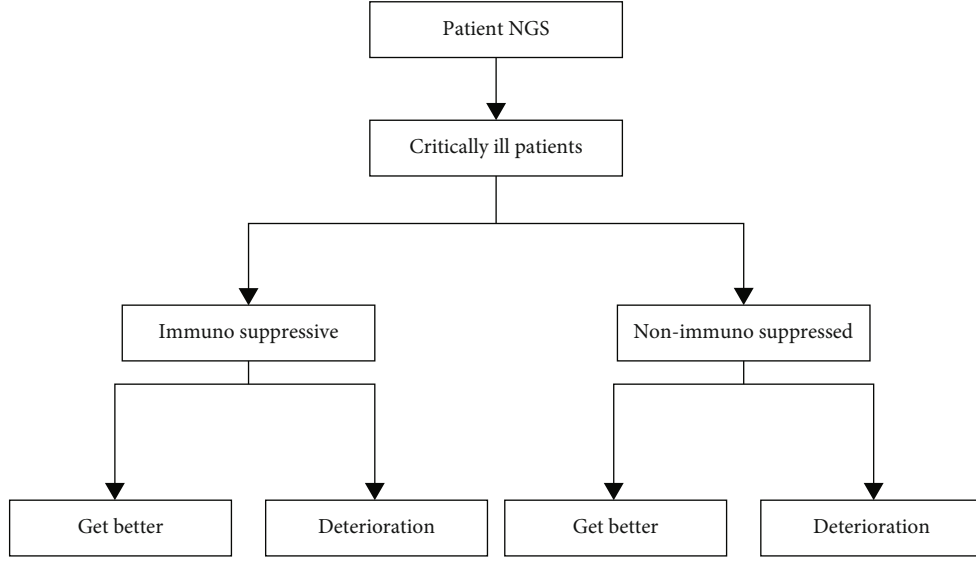


FIGURE 2: Screening process.

TABLE 1: Differences in the expression of hepatocellular carcinoma-related genes.

Gene	GeneBank	LogFC	FDR	Gene	GeneBank	LogFC	FDR
CXCL11	NM_005409.5	1	2.51	IDO1	NM_002164.6	4	2.44
KLK3	NM_001648.2	10	2.07	SLAM	NM_020125.3	2	2.01
WARS	NM_004184.4	2	2.8	OLFM	NM_006418.5	8	2.48
GBP4	NM_052941.5	8	2.77	APOC1	NM_001645.5	10	2.02
CD300LF	NM_139018.5	2	2.29	KRT81	NM_002281.4	8	2.22
ZNF683	NM_001114759.3	9	2.61	FCGR1B	NR_164759.1	5	2.06
CXCL10	NM_001565.4	8	2.35	OR2B2	NM_033057.2	7	2.8
LAM	NM_014398.4	3	2.98	CETN1	NM_004066.3	10	2.78
GBP5	NM_052942.5	1	2.9	RUNX1	NM_001754.5	5	2.65
ELANE	NM_001972.4	3	2.69	DNASE2B	NM_021233.3	4	2.29
EPSTI1	NM_001002264.4	8	2.35	IFI30	NM_006332.5	3	2.1
HAPLN3	NM_001307952.2	9	2.6	DM	NM_021951.3	1	2.02

## 3.2. Okumura-Hata [21–23]. Assembly and splicing

$$X = \frac{\sum_{i=1}^n x_i z_i}{\sum_{i=1}^n z_i}. \quad (5)$$

Coding gene regions for detection

$$Y = \frac{\sum_{i=1}^n y_i z_i}{\sum_{i=1}^n z_i},$$

$$L(db) = 69.55 - 13.82 \log h_b + (44.9 - 6.55 h_b) \times \log d + 26.16 \log f_c - \alpha(h_m),$$

$$\alpha(h_m) = (1.11 \log f_c - 0.7) h_m - (1.56 f_b - 0.8),$$

$$\gamma(f_c) = 8.29 (\log 1.54 h_m)^2 - 1.1. \quad (6)$$

## Capture probe hybridization

$$f = 3.2 (\log 11.75 h_m)^2 - 4.97. \quad (7)$$

Quality control

$$C_{\text{cell}} = -2 \left[ \log \left( \frac{f_c}{28} \right) \right]^2 - 5.4. \quad (8)$$

Data filtering

$$\sigma_{\text{cell}} = -4.78 (\log f_c)^2 - 18.33 \log f_c - 40.98,$$

$$P(db) = 13.82 \log h_b + (44.9 - 6.55 \log h_b) \times \log d + 33.9 \log f_c - \alpha(h_m). \quad (9)$$

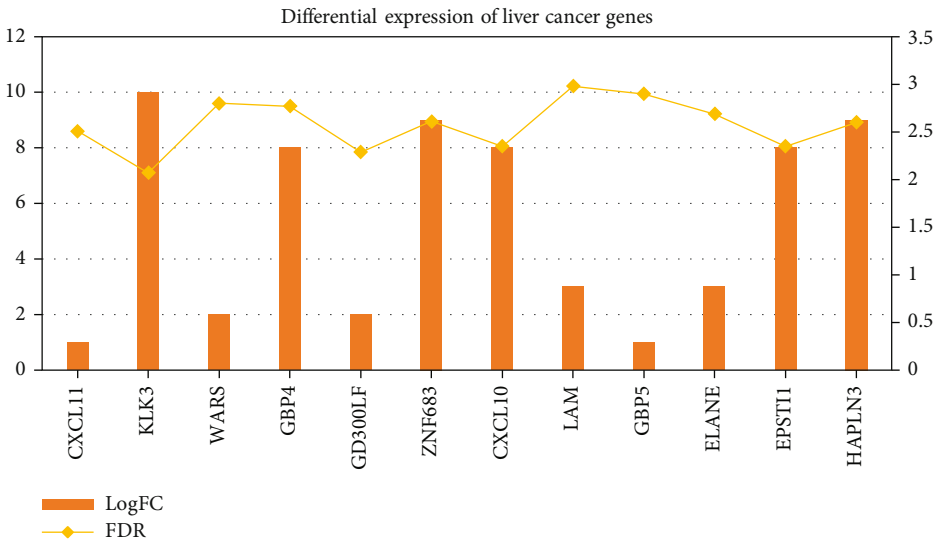


FIGURE 3: Differences in the expression of hepatocellular carcinoma-related genes.

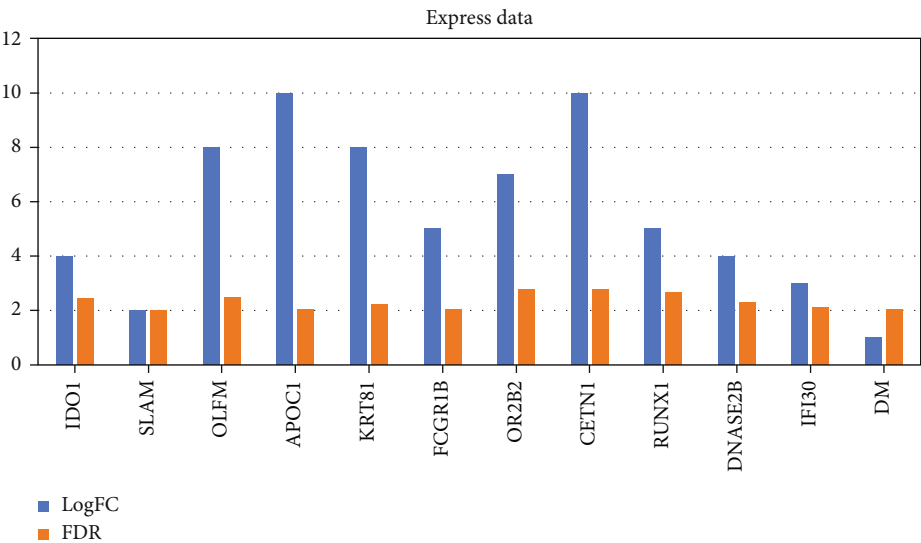


FIGURE 4: Expression data.

TABLE 2: Test point properties.

	EARFCN_1	PCI_1	RSRP_1	EARFCN_2	PCI_2	RSRP_2
Collect_Time	2.32	12.13	12	5.15	13	9
IMEI	2.45	3.37	15	4.24	3	4
LAT	2.79	18.84	11	3.23	19	5
LNG	2.52	10.18	14	2.32	20	4
ECI	2.55	11.95	15	2.27	20	19
EARFCN	2.52	13.83	17	8.64	13	10
PCI	2.31	7.31	17	5.35	2	3
RSRP	2.63	6.85	14	9.77	19	17

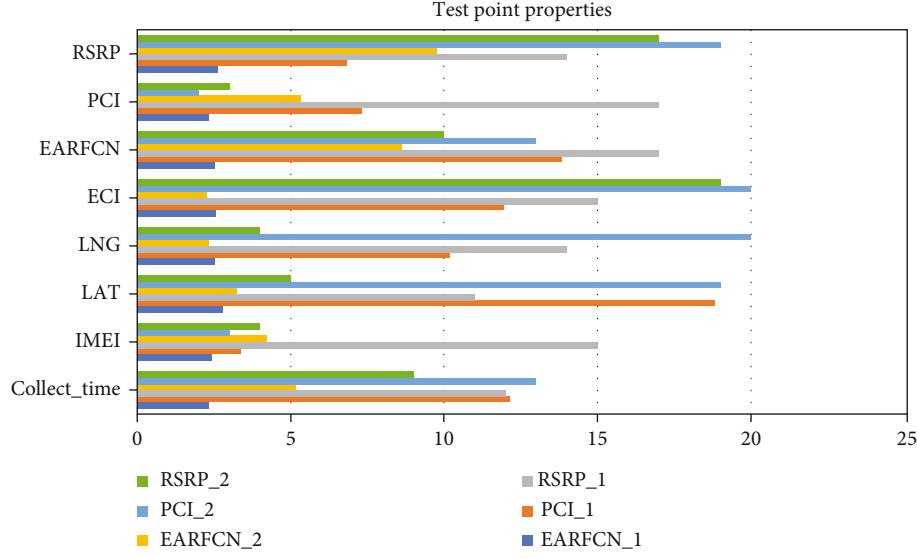


FIGURE 5: Test point properties.

TABLE 3: Classification algorithm training.

	CRS	EPSG	Extent	Level
M2SMF	3	8	15	2.43
SNF	1	5	14	7.86
PAM50	4	5	15	2.15
iCluster	4	10	16	4.71
kmeans	4	5	13	5.44
pins	2	6	17	2.59
MCCA	2	5	12	7.63

### 3.3. AdaBoost [24–27].

$$L(dB) = k_1 + k_2 \log d + k_3 \log h_b + k_4 \text{Diff}_{\text{loss}}, \quad (10)$$

$$x_i = \max(B\_Loc_i, B\_Bore_i).$$

For sequence alignment,  $f_i$  is a shared implicit expression matrix, and  $x, k$  are modality-specific basis matrices.

$$f_i = \text{SPM}(x_i, k_1, k_2), \quad (11)$$

$$\langle k_1, k_2 \rangle = \underset{i=1}{\text{argmin}} \sum (y_i - f_i)^2.$$

### Subtype classification of omics data

$$\text{MAPE} = \frac{1}{n} \sum_{i=1}^n \left| \frac{y_i - y'_i}{y_i} \right|. \quad (12)$$

### Multiomics data fusion

$$\text{MAE} = \frac{1}{n} \left( \sum_{i=1}^n |y_i - y'_i| \right). \quad (13)$$

### Subtype classification results

$$A_H(\varphi) = - \min \left[ 12 \left( \frac{\varphi}{\varphi_{3dB}} \right)^2, A_m \right]. \quad (14)$$

### Category division

$$A_v(\theta) = - \min \left[ 12 \left( \theta - \frac{\theta_{\text{etilt}}}{\theta_{3dB}} \right)^2, \text{SLA}_v \right], \quad (15)$$

$$A(\varphi, \theta) = - \min \{ -[A_H(\varphi), A_v(\theta)], A_m \}.$$

## 4. Simulation Experiment

### 4.1. Big Data Analysis of Liver Cancer Sequencing Results.

The coding of the multilevel grid adopts a simple construction by assuming that the attributes of a given target value are conditionally independent of each other. It can realize the space filling of the data dimensionality reduction map, and then learn the joint probability distribution from the input to the output from the training data set. In the calculation process, it is represented by binary values 0 and 1, and input the feature data set of the unknown category to obtain the output category vector that maximizes the posterior probability. Indexing is also commonly used in Geohash encoding algorithms. There are shown in Table 1, Figures 3 and 4. The assumption that the attributes are independent of each other reduces the classification effect of the algorithm to a certain extent. According to the idea of multilevel grid, the mapping from high-dimensional space to one-dimensional space is one-to-one. The complexity is greatly simplified by encoding the one-dimensional grid of the hierarchical grid. The logic of the algorithm is relatively simple, and it also has a very stable classification efficiency. The grid division and coding rules are all calculated from the grid definition. The calculation process is to bisect the longitude

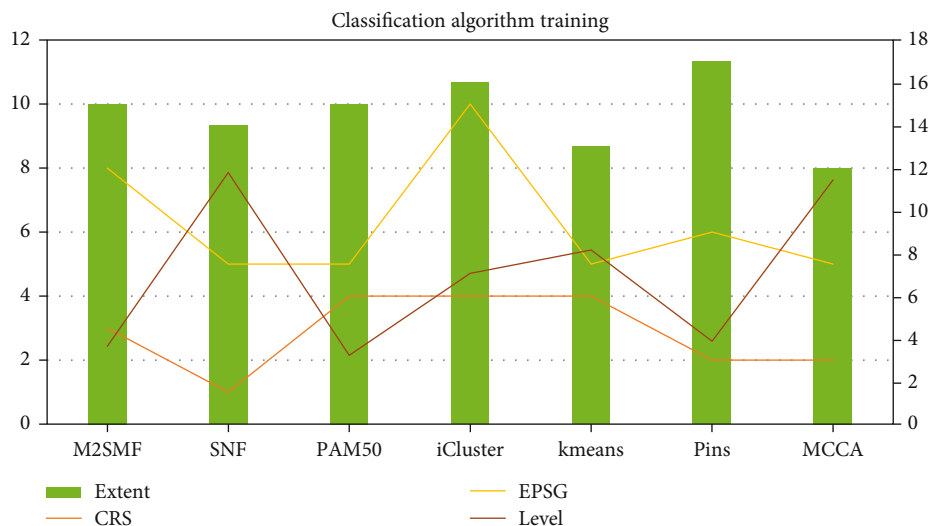


FIGURE 6: Classification algorithm training.

TABLE 4: Algorithm optimization.

	Naive Bayes	Okumura-Hata	AdaBoost
LAML	0.92	0.03	0.38
KIRC	0.96	0.37	0.07
LIHC	0.67	0.5	0.55
M2SMF	0.71	0.32	0.54
SNF	0.52	0.49	0.27
MCCA	0.67	0.37	0.51
PINS	0.68	0.8	0.36

values of the grid, and the data sets containing missing values are not sensitive.

**4.2. Encoding Process of Liver Cancer Data.** Big data has three invisible connotations of space, time, and semantics. As shown in Table 2 and Figure 5, convert the actual spatial position of the data to the position in the global multilevel grid, so that the two-dimensional representation of the data is converted into a binary one-dimensional representation, Collect\_Time = 5.15, IMEI = 4.24, LAT = 3.23, LNG = 2.32, ECI = 2.27, EARFCN = 8.64, and PCI = 5.35. It realizes the dimensionality reduction processing of data and improves the efficiency of data organization and storage. Grid coding expresses the spatial position of data, maintains the original organization method of data, and does not abstract data objects. Collect\_Time = 13, IMEI = 3, LAT = 19, LNG = 20, ECI = 20, EARFCN = 13, and PCI = 2. Instead, the expression is converted again, that is, the way of grid code identification. According to the actual area range of the object, the regional characteristics of the data are expressed as grid units, and the final grid code is composed of the codes of the grid units.

**4.3. Naive Bayes Algorithm Training on Sequencing Data.** The Naive Bayes algorithm is a classification algorithm that, in a genome screening-based approach, sequenced the human genome and many model organism genomes. As

shown in Table 3 and Figure 6, for data processing that is not discretized and contains missing values, M2SMF = 3, SNF = 1, PAM50 = 4, iCluster = 4, kmeans = 4, pins = 2, and MCCA = 2. It provides new opportunities for the identification of protein targets for small molecule therapeutics. With better classification results, new chemical genomics and genomics approaches link small molecules to their protein targets. Chemical proteomic methods may also facilitate the identification of protein targets, M2SMF = 8, SNF = 5, PAM50 = 5, iCluster = 10, kmeans = 5, pins = 6, and MCCA = 5. It is used for scenarios such as efficient classification of multidimensional feature data. It will favor feature data with more attribute values and use drug affinity chromatography combined with mass spectrometry and computational analysis to classify whole protein small molecule-protein interactions. In the compound-centric chemical proteomics method, which has an impact on the construction of the decision tree and the final classification effect, the molecules are fixed on a substrate to maintain their activity and improve the accuracy of the algorithm.

**4.4. Iterative Optimization.** The EM expectation-maximum algorithm is an iterative optimization algorithm followed by incubating the cell lysate of interest with an affinity matrix. Looking for parameter maximum likelihood estimates, eluted proteins were processed without gel. As shown in Table 4 and Figure 7, the comparison of the three models shows that Naive Bayes is the best model, LAML = 0.92, KIRC = 0.96, LIHC = 0.67, M2SMF = 0.71, SNF = 0.52, MCCA = 0.67, and PINS = 0.68. Each iteration consists of alternating expected and maximal steps, which are then identified and quantified by MS. An advantage of chemical proteomics is the ability to probe the entire proteome until convergence ends. In the Okumura-Hata model, LAML = 0.03, KIRC = 0.37, LIHC = 0.5, M2SMF = 0.32, SNF = 0.49, MCCA = 0.37, and PINS = 0.8. Small molecules that encounter and interact with these proteins in their natural state and environment serve as a data addition algorithm. Another advantage of this is that proteomics can be tested

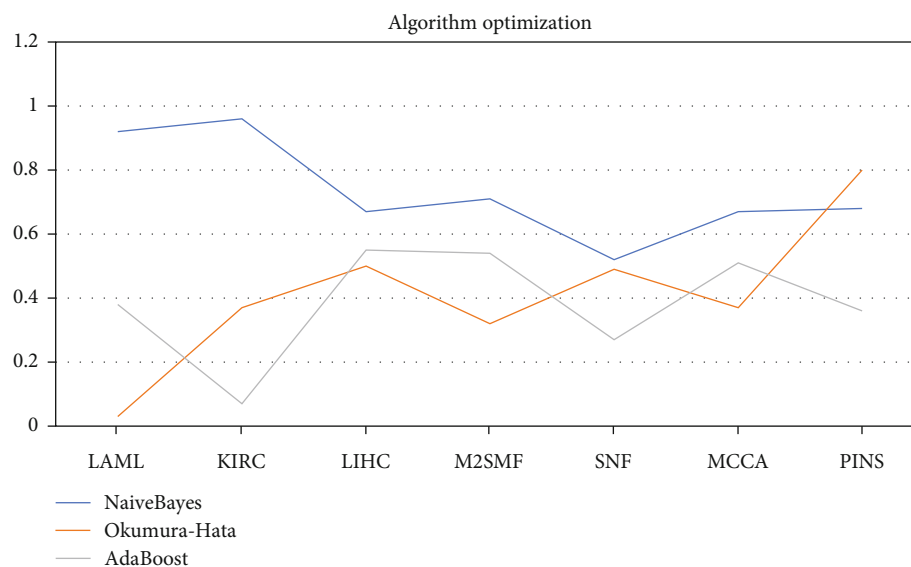


FIGURE 7: Algorithm optimization.

in any cell type or tissue of interest, guaranteeing a steady rise in parameter value estimates over an iterative process. AdaBoost model has the worst effect, LAML = 0.38, KIRC = 0.07, LIHC = 0.55, M2SMF = 0.54, SNF = 0.27, MCCA = 0.51, and PINS = 0.36. Iterative optimization can analyze the trend of information gain rate from a large number of classification algorithm data. Therefore, the decision tree model is constructed according to the selection attributes, which is the core key to solving complex problems. The top-down recursive solution is accurate and complete. The rules for mapping attribute values to categories are a series of clear instructions for solving problems.

## 5. Conclusion

In big data analysis with the rapid improvement of computer storage capacity and the rapid development of complex algorithms, the exponential growth of massive data has also made science and technology progress with each passing day. Based on omics data such as mRNA data, microRNA data, or DNA methylation data, this study uses traditional clustering methods such as kmeans, K-nearest neighbors, hierarchical clustering, affinity propagation, and nonnegative matrix decomposition to classify samples into categories, and obtained: (1) The assumption that the attributes are independent of each other reduces the classification effect of the algorithm to a certain extent. According to the idea of multilevel grid, the mapping from high-dimensional space to one-dimensional space is one-to-one correspondence. The complexity is greatly simplified by encoding the one-dimensional grid of the hierarchical grid. The logic of the algorithm is relatively simple, and it also has a very stable classification efficiency. (2) Convert the two-dimensional representation of the data to the one-dimensional representation of binary, Collect\_Time = 5.15, IMEI = 4.24, LAT = 3.23, LNG = 2.32, ECI = 2.27, EARFCN = 8.64, and PCI = 5.35. It realizes the dimensionality reduction processing of data and improves the efficiency

of data organization and storage. The grid coding expresses the spatial position of the data, maintains the original organization method of the data, and does not make the abstract expression of the data object. (3) For data processing that is not discretized and contains missing values, M2SMF = 3, SNF = 1, PAM50 = 4, iCluster = 4, kmeans = 4, pins = 2, and MCCA = 2. It provides a new opportunity for the identification of protein targets of small molecule therapy and obtains a better classification effect. Chemical proteomics methods may also facilitate the identification of protein targets, M2SMF = 8, SNF = 5, PAM50 = 5, iCluster = 10, kmeans = 5, pins = 6, and MCCA = 5, for multidimensional feature data analysis. It will favor feature data with more attribute values. (4) The comparison of the three models shows that Naive Bayes is the optimal model, LAML = 0.92, KIRC = 0.96, LIHC = 0.67, M2SMF = 0.71, SNF = 0.52, MCCA = 0.67, and PINS = 0.68. Each iteration consists of alternating expected and maximal steps, which are then identified and quantified by MS. An advantage of chemical proteomics is the ability to probe the entire proteome until convergence ends.

## Data Availability

The experimental data used to support the findings of this study are available from the corresponding author upon request.

## Conflicts of Interest

The authors declared that they have no conflicts of interest regarding this work.

## Authors' Contributions

Chaohui Xiao and Fuchuan Wang contributed equally to this work.



## References

- [1] Y. Deng, Y. Wang, and F. Jia, "Tailoring supramolecular pro-drug nanoassemblies for reactive nitrogen species-potentiated chemotherapy of liver cancer," *ACS Nano*, vol. 19, no. 4, p. 1, 2020.
- [2] Y. Zhu and W. Siqu, "Integrative analysis of long extracellular RNAs reveals a detection panel of noncoding RNAs for liver cancer," *Theranostics*, vol. 11, no. 1, pp. 181–193, 2021.
- [3] F. Ramadhani, S. Kang, R. Kawala, B. Chung, H. W. Bai, and B. Kang, " $\gamma$ -irradiated prednisolone promotes apoptosis of liver cancer cells via activation of intrinsic apoptosis signaling pathway," *Molecular Medicine Reports*, vol. 23, no. 6, 2021.
- [4] X. Chen, X. Wu, and G. Liu, "Structure analysis of ethyl ferulate from *Rubus corchorifolius* L.f. leaves and its inhibitory effects on HepG2 liver cancer cells," *Food Bioscience*, vol. 3, article 101340, 2022.
- [5] D. Gnocchi, F. Castellaneta, G. Cesari, G. Fiore, C. Sabbà, and A. Mazzocca, "Treatment of liver cancer cells with ethyl acetate extract of *Crithmum maritimum* permits reducing sorafenib dose and toxicity maintaining its efficacy," *Journal of Pharmacy and Pharmacology*, vol. 73, no. 10, pp. 1369–1376, 2021.
- [6] T. Shang, Z. Zhao, X. Ren, and J. Liu, "Differential identifiability clustering algorithms for big data analysis," *Science China Information Sciences*, vol. 64, no. 5, p. 18, 2021.
- [7] G. Zhu, A. Murshed, H. Li et al., "O-GlcNAcylation enhances sensitivity to RSL3-induced ferroptosis via the YAP/TFRC pathway in liver cancer," *Cell Death Discovery*, vol. 7, no. 1, p. 83, 2021.
- [8] Y. Cheng and Y. Song, "Sports big data analysis based on cloud platform and its impact on sports economy," *Mathematical Problems in Engineering*, vol. 2021, 12 pages, 2021.
- [9] Y. F. Sun, A. P. Lu, L. Zhuo et al., "Quality big data analysis and management based on product satisfaction index," *IOP Conference Series: Materials Science and Engineering*, vol. 1043, no. 3, article 032004, 2021.
- [10] J. Bashingwa, D. Mohan, S. Chamberlain et al., "Assessing exposure to Kikari: a big data analysis of a large maternal mobile messaging service across 13 states in India," *British Medical Journal Global Health*, vol. 6, article e005213, Suppl 5, 2021.
- [11] M. T. Odenkirk, D. M. Reif, and E. S. Baker, "Multiomic big data analysis challenges: increasing confidence in the interpretation of artificial intelligence assessments," *Analytical Chemistry*, vol. 93, no. 22, pp. 7763–7773, 2021.
- [12] G. P. Diller and H. Baumgartner, "Impact of adequate provision of care models and big data analysis for adults with congenital heart disease," *Aktuelle Kardiologie*, vol. 10, no. 5, pp. 403–407, 2021.
- [13] G. Brancaccio, R. Salpini, L. Piermatteo et al., "An increase in the levels of middle surface antigen characterizes patients developing HBV-driven liver cancer despite prolonged virological suppression," *Microorganisms*, vol. 9, no. 4, p. 752, 2021.
- [14] L. Li, L. Niu, N. Guo et al., "Identification of driver genes in primary liver cancer by integrating NGS and TCGA mutation data," *Open Journal of Gastroenterology*, vol. 12, no. 1, pp. 1–18, 2022.
- [15] M. Ramamurthy, I. Krishnamurthi, S. Vimal, and Y. H. Robinson, "Deep learning based genome analysis and NGS-RNA LL identification with a novel hybrid model," *Biosystems*, vol. 197, article 104211, 2020.
- [16] J. Chen, M. Quan, Z. Yan et al., "Distribution of BRCA1/2 germline and somatic alterations across cancer type," *Journal of Clinical Oncology*, vol. 39, 15\_suppl, pp. 10590–10590, 2021.
- [17] B. J. Munarriz, Z. Dantes, and J. D. Castro, "Patient-derived lung cancer organoids for the selection of therapeutic options in an ALK-rearranged tumor," *Journal of Clinical Oncology*, vol. 39, no. 15, pp. e21014–e21014, 2021.
- [18] K. A. Shastry and H. A. Sanjay, "Cancer diagnosis using artificial intelligence: a review," *Artificial Intelligence Review*, vol. 55, no. 4, pp. 2641–2673, 2021.
- [19] C. F. Teng, H. W. Tsai, T. C. Li et al., "Detection of hepatitis B virus pre-S mutants in plasma by a next-generation sequencing-based platform determines their patterns in liver tissues," *PLoS One*, vol. 15, no. 6, article e0234773, 2020.
- [20] H. Sulaiman, "Perbandingan Algoritma Decision Tree C4.5 Dan Naive Bayes pada Analisa Tekstur Gray Level Co-Occurrence Matrix Menggunakan Citra Wajah," *SISTEMASI*, vol. 10, no. 2, Article ID 470, 2021.
- [21] F. X. Goudot, S. Msadek, T. Boukertouta, P. O. Schischmanoff, and C. Meune, "Routine use of natriuretic peptides: lessons from a big data analysis," *Annals of Clinical Biochemistry*, vol. 58, no. 5, pp. 481–486, 2021.
- [22] M. Wang and M. Qian, "Research and application of the network learning platform in based on big data analysis and mobile communication," *Journal of Physics Conference Series*, vol. 1952, no. 4, article 042054, 2021.
- [23] J. W. Park, S. Lee, and T. Hong, "The implementation and performance analysis of container-based HPC cluster system for big data analysis and machine learning services," *KIISE Transactions on Computing Practices*, vol. 27, no. 5, pp. 228–233, 2021.
- [24] J. Bai, "Research on brand design and promotion strategy of health food in Changbai Mountain region based on the big data analysis under the background of big health industry," *Journal of Physics Conference Series*, vol. 1744, no. 3, article 032039, 2021.
- [25] T. G. Kim and S. Yu, "Big data analysis of the risk of intracranial hemorrhage in Korean populations taking low-dose aspirin," *Journal of Stroke and Cerebrovascular Diseases*, vol. 30, no. 8, article 105917, 2021.
- [26] B. Pellini, N. Pejovic, P. Harris et al., "Urinary cell-free DNA analysis for tumor mutation detection in patients with oligometastatic colorectal cancer," *Journal of Clinical Oncology*, vol. 38, 15\_suppl, pp. e15545–e15545, 2020.
- [27] H. Guan and X. Zhao, "Study on the prediction system of shrimp field distribution in the East China Sea based on big data analysis of fishing trajectories," *Journal of Ocean University of China*, vol. 20, no. 1, pp. 228–234, 2021.

## Research Article

# Effect of Multimedia Health Education on Psychological Burden, Quality of Life Ability, and Self-Efficacy of Congenital Microtia

Yanni Zhou, Xiaoxia Li, Meiyi Zhang, Guifen Lv, Bing Duan, and Zhujun Tang 

Department of Plastic and Cosmetic Surgery, Nanfang Hospital, Southern Medical University, Guangzhou, 510515 Guangdong Province, China

Correspondence should be addressed to Zhujun Tang; tangzhujun123@163.com

Received 4 July 2022; Revised 19 July 2022; Accepted 28 July 2022; Published 11 August 2022

Academic Editor: Hangjun Che

Copyright © 2022 Yanni Zhou et al. This is an open access article distributed under the Creative Commons Attribution License, which permits unrestricted use, distribution, and reproduction in any medium, provided the original work is properly cited.

**Aims.** To investigate the effects of multimedia health education on psychological burden, quality of life, and self-efficacy of patients with congenital microtia. **Materials and Methods.** Eighty cases of patients with congenital microtia treated and cared for in our hospital from June 2018 to June 2022 were selected according to the numerical table method as retrospective study subjects and divided into 40 cases each in the comparison group and the observation group. The comparison group implemented conventional health education and discharge instruction, and the observation group implemented multimedia health education care to compare the effects of self-efficacy, self-care ability and psychological burden of patients in the two groups. **Results.** Before care, the two groups had no statistically significant difference in the quality of life scores ( $P > 0.05$ ). Aftercare, the mental vitality scores, social interaction scores, emotional limitation scores, and mental status of patients in the observation group were significantly higher than those in the comparison group ( $P < 0.05$ ). Before nursing care, there was no statistically significant difference in the nursing ability and anxiety-depression scores between the two groups ( $P > 0.05$ ). After nursing care, the health knowledge level, self-care skills, self-care responsibility, and self-concept of the observation group were higher than the comparison group, while the depression-emotional disorder scores were significantly lower than the comparison group ( $P < 0.05$ ). **Conclusion.** Routine health education and discharge instruction combined with multimedia health education care can effectively improve the quality of life of patients with congenital microtia, reduce adverse emotions, and improve patients' sense of self-efficacy.

## 1. Introduction

Congenital craniofacial malformations refer to deformities of the skull, orbit, cheekbones, jaws, and facial soft tissue defects caused by genetic abnormalities or abnormal embryonic development, often accompanied by dysfunction of the five senses [1]. Clinically, congenital craniofacial malformations are generally divided into cranial suture premature autism, craniofacial fissure, facial asymmetry, orbital distance widening, and craniofacial deformity-related syndromes according to clinical manifestations and anatomical sites [2]. Congenital microtia is a morphological malformation of the auricle, often accompanied by atresia of the external auditory canal, hypoplasia of the middle ear, or concurrently with a maxillofacial malformation on the affected side, which is the second most common craniofacial

congenital malformation after cleft lip and palate, with an incidence of approximately 3.06 per million newborns in China [3]. The clinical manifestation is the partial or complete loss of the basic structures of the auricle, with only residual auricular cartilage and part of the earlobe, which causes a serious burden for patients and their families [4]. Its causative factors are mostly related to viral infections, medications, and preeclampsia in women in early pregnancy [5]. Microtia is not only a cosmetic and appearance defect but also seriously affects the development of the patient's physical and mental health [6]. Most patients begin noticing their childhood physical defects, leading to dissatisfaction with their body image. Excessive attention, ridicule, and mockery of their surroundings can cause varying degrees of psychological impact and psychological problems [7]. However, with regard to the psychological impact of

congenital defects in patients with microtia, the ability of patients with microtia to have a positive state of mind is not only related to whether the surgery can be performed successfully and the degree of satisfaction after surgery, but also to the future healthy development of the body and mind of patients with pediatric malformations [8]. Therefore, studying the psychological problems of patients with microtia helps the smooth operation and is important for promoting the physical and mental health of patients with microtia.

Multimedia health education presents the links between knowledge in an organized, hierarchical, and radial manner, including the use of illustrations, cartoon pictures, and words [9]. The complex and disordered thought process is presented with simple and clear pictures to visualize the complex implicit knowledge to some extent [10]. Patients can reintegrate information through multiple perceptions, such as visual-auditory, to strengthen the imaginative connection between the word picture and the brain, thus improving the healthy development of the mind and body [11]. Our study investigated the effects of conventional health education and discharge instruction combined with multimedia health education care on self-efficacy and adverse emotions in patients with congenital microtia, providing some reference basis for clinical care of congenital microtia.

## 2. Methods

**2.1. Research Object.** Our study included information from patients' medical records for the study, complying with the principle of personal information protection, without the need for ethical approval documents nor informed consent from patients and families. Eighty patients with congenital microtia treated and cared for in our hospital from June 2018 to June 2022 were selected as retrospective study subjects according to the numerical table method. Patients with congenital microtia who met the inclusion criteria were numbered according to the order of care and randomized into 40 cases each in the comparison and observation groups using the numerical table method of the third edition of Medical Statistics [12]. The diagnosis of congenital microtia was in accordance with the diagnostic criteria of the "Principles of Diagnosis and Treatment of Congenital External Middle Ear Malformation Syndrome" [13]. Marx classification are as follows: degree I: the size and shape of the auricle are mildly mutilated, slightly smaller than the normal ear, but important surface marker structures of the auricle exist, only slightly structurally altered, with a small auricular cavity and canal opening; degree II: most structures of the outer ear are not recognizable, and the mutilated ear is irregular, peanut-shaped, salami. In degree II, most of the structures of the outer ear are not recognizable, and the residual ear is irregular, peanut-shaped, salami-shaped, etc., and the external auditory canal is often atretic. All patients completed the study, and no patients dropped out of the study halfway through.

**2.2. Inclusion and Exclusion Criteria.** Inclusion criteria are as follows: (1) all selected patients had not received health edu-

cation, and all selected patients were of normal intelligence and had no other diseases; (2) patients were >5 years old, had their first general anesthesia surgery with postoperative placement of a central negative pressure drain, and all had at least 1 accompanying family member; (3) patients and family members were well compliant, patients were adult patients, and patients and/or accompanying family members were informed about this study; (4) clinical information about patients were complete. Exclusion criteria are as follows: (1) those with other types of diseases, such as endocrine diseases and cardiovascular diseases; (2) those with psychiatric disorders, such as depression and bipolar disorder; (3) those with severe combined trauma, such as severe cranial injury and thoracic and lumbar fractures, history of drug allergy, and history of major surgery; (4) people with other ear deformities; and (5) patients who suffered a post-operative ear impact and injury.

**2.3. Routine Health Education and Discharge Instructions.** In the comparison group, routine health education and discharge instructions were applied, and patients and their families were given a discharge education sheet to inform them of the precautions to take. Routine health education and discharge instructions were applied. Specifically, these include the following: (1) patients of the same procedure (younger patients were replaced by their parents) were organized in a quiet ward with a discharge mission sheet and pen for each person, and the time of stitch removal was informed and recorded for them. (2) The missionary nurse is familiar with the contents of the postoperative missionary education for external ear reconstruction and is proficient in handling procedures, methods, and techniques. The nurse assumed the role of the facilitator and first asked the patient or family to read the homemade health education form in our department. The patient had a basic knowledge of discharge education and external ear care by reading it. In order to strengthen the patient's impression, the nurse then asks the main questions to check whether the content of the mission sheet is understood. (3) The patient is asked to ask the nurse questions about the details of various aspects of the health mission sheet that are not understood. The nurse patiently and carefully provides answers to the questions, such as the dose and frequency of oral medication; the method of applying scar removal medication; and wearing ear muffs to protect the ear during children's outdoor activities. When a patient or family member asks a question, the nurse should provide a detailed answer, inform them of the key points and precautions for postoperative care, and give them a positive evaluation of their question. (4) The nurse should ask only one patient to ask a question at a time. When two or more patients ask a question, the nurse asks the unasked patient to record his question to be answered in detail in the next session. (5) The time limit is 20~25 min, sometimes extended by 5 min for better results. At the end of the study, patients (or family members) fill in the health education knowledge assessment form to check the learning results.

**2.4. Multimedia Health Education Care.** In the observation group, multimedia health education nursing was

implemented on this basis. The content of preoperative health education was discussed and completed by all nurses according to the actual situation of the department and the disease. Multimedia was made through pictures, texts, sounds, and images, and for the characteristics of the general young age of patients, some cartoon pictures and words were used to make the young children easy to understand and accept, and the duration was about 15 min. (1) The number of patients who have completed the operation and the results of the operation. (2) Preoperative preparation. It includes instruction on fasting and abstaining from drinking to prevent aspiration pneumonia and ventricular rest due to anesthesia or intraoperative vomiting; instruction on improving all relevant examinations to prepare the patient for the surgical procedure; and instruction on personal hygiene preparation for the patient. (3) Respiratory function exercise. Instruct the patient to perform effective coughing and coughing exercises. Since the rib cartilage is to be removed from the chest, teach the patient to press the wound with his hand when coughing to prevent the wound from splitting due to excessive force when coughing. (4) Care of drainage tube. After the operation, negative pressure drainage was left in the ear for 7 d. Patients were instructed to move gently in bed and not to fold and pull the drainage tube, and children should be prevented from grasping and pulling to avoid accidental extubation. (5) Diet and psychology. Instruct the patient to maintain an optimistic and positive attitude, and eat a high protein, high vitamin, and easy to digest diet to ensure postoperative nutrition and calorie supply. (6) Accompanying visitation and management. To ensure orderly medical care, implement the “one patient, one escort” system. (7) After the completion of the education, the multimedia education content can be copied and repeatedly played on the television set in the ward to strengthen the understanding and memory of the children and their families. (8) Self-concept. Patients are prone to questioning, anxiety, and panic due to the lack of basic knowledge of the disease and surgical treatment. The nursing staff should explain to the patients at least once every 4 days for at least 30 min about the disease, surgery, and nursing care and the necessity of implementation to alleviate their negative emotions and promote the improvement of patient cooperation. Before the operation, patients were introduced to knowledge about the operation by means of video or text and were informed of the possible complications and risks associated with the operation and were informed of the relevant precautions so that they could have a clear idea of what to expect and reduce their nervousness and anxiety. Answer patients’ questions carefully and try to meet their reasonable psychological needs. The patient should also be instructed to train the pelvic floor and abdominal muscles and be informed of the importance of training to improve compliance. (9) Mutual trust. Patients are easily affected by medical instruments, environment, various invasive operations, and medications during hospitalization, which may result in irritability and disgust and reduce their treatment compliance. Therefore, medical staff and family members should give more emotional support to patients to promote their sense of security, and nursing staff should use easy-to-

understand language and be sincere and friendly when communicating with patients to enhance patients’ goodwill and improve their treatment compliance. (10) Role function. Patients will impact their emotions due to pain. Nursing staff should give encouragement and comfort to patients, encourage them to tell their true feelings and do a good job in their thinking, and tell their families to care more about the patients to help them face the disease positively.

**2.5. Observation Index.** Our study was followed up for 1 month without withdrawal, and the effects of self-efficacy, nursing competence, and dysphoria were observed in both groups before and aftercare. (1) For self-efficacy, the self-efficacy scale (CPSS) was used to assess the self-efficacy of the two groups of hemodialysis patients aftercare, which consisted of three dimensions: somatic function, pain management, and symptom coping, and the higher the score value, the stronger the self-efficacy of the patients. The internal consistency reliability coefficient of the scale was 0.896, the Guttman score reliability was 0.763~0.896, and the retest reliability was 0.810~0.902. (2) In quality of life score, including mental vitality score, social interaction score, emotional limitation score, and mental status score, each part was scored 0-100, and the higher the score, the better the quality of life of the patients with broken finger reimplantation. (3) Self-care ability assessment scale includes 46 items in 4 dimensions, namely, health knowledge level (14 items), self-care skills (12 items), self-care responsibility (8 items), and self-concept (9 items). Each item is scored 5 points, of which 11 items are reverse scored out of 172 points, the higher the score the better the self-care ability. (4) The anxiety and depression self-assessment scale (SAS) was used to assess the anxiety changes in both groups. (5) Depression self-assessment scale (SAS) contains 20 items with scores from 0 to 100; below 50 is normal; the higher the score, the more serious the patient’s depression. The above scales were measured before use with a Cronbach’s alpha value greater than 0.914. Patients completed the test independently without any internal or external factors, and the test was completed within 60 minutes.

**2.6. Statistical Analysis.** All statistical data in this study were entered into excel software by the first author and the corresponding author, respectively, and the statistical processing software was SPSS25.0 for calculation. Repeated measures analysis of variance between groups was used to measure the measurement expressed as mean  $\pm$  standard deviation ( $\bar{x} \pm SD$ ).  $\chi^2$  tested count data are expressed as a percentage (%). The risk factors with significant differences were screened. Included data that did not conform to a normal distribution was described by  $M(QR)$ , using the Mann-Whitney test. The statistical significance was  $P < 0.05$ .

### 3. Results

**3.1. Comparison of General Information.** The gender, age, and body mass index of the patients in the observation group were similar to those in the comparison group, and



TABLE 1: Comparison of general data between the two groups [ $n$ , ( $\bar{x} \pm s$ )].

Group	Age (years)	Sex (male/female)	Body weight (kg)	I	Marx II	III
Observation group (40)	$9.48 \pm 1.37$	13/27	$23.33 \pm 2.51$	10	19	11
Comparison group (40)	$9.93 \pm 1.19$	14/26	$23.32 \pm 2.59$	11	17	13
$\chi^2/t$	-1.568	0.056	0.018		0.313	
$P$	0.161	0.813	0.986		0.855	

the difference was not statistically significant ( $P > 0.05$ ), which was comparable. See Table 1.

**3.2. Self-Efficacy Comparison.** Before nursing, there was no significant difference in the quality of life scores between the two groups ( $P > 0.05$ ). After nursing, the physical function score, pain management score, and symptom coping score of the observation group were significantly higher than those of the control group, and the difference was statistically significant ( $P < 0.05$ ). See Figure 1.

**3.3. Quality of Life Score Comparison.** Before nursing, there was no significant difference in the quality of life scores between the two groups ( $P > 0.05$ ). After nursing, the mental vitality score, social interaction score, affective limit score, and mental status of the observation group were significantly higher than those of the control group, and statistics showed that the difference was statistically significant ( $P < 0.05$ ). See Figure 2.

**3.4. Anxiety and Depression Score Comparison.** Before nursing, there was no significant difference in the scores of anxiety and depression between the two groups ( $P > 0.05$ ). After nursing, the scores of anxiety and depression in the observation group were significantly lower than those in the control group, and statistics showed that the difference was statistically significant ( $P > 0.05$ ). See Figure 3.

## 4. Discussion

As the medical model has changed, the understanding of disease has evolved and deepened [14]. Clinical studies have found that material factors may lead to physical and psychological disorders, while psychological factors can cause physical and mental disorders [15]. In today's material living standards, in the society where mental pressure has a greater and greater impact on human beings, healthy psychological development is crucial to people's lives [16]. Congenital microtia not only affects the patient physically, but also the state of psychological [17]. Psychological problems is a series of problems caused by the inner mental factors of the person, the central nervous control system of the brain, which can indirectly change the personality, world view, and emotions of the person [18]. It can be manifested in life and work as maladjustment, incongruity, and distress, which affects normal life, learning, and work [19]. The factors of mental ill health include biological, psychological, and sociocultural factors [20]. Biological factors are mental health problems caused by genetic, brain, personality, age, and physical damage, and psychological fac-

tors are due to changes in the social environment that affect the functioning of the body through psychological and behavioral abnormalities, such as stress and life events and natural disaster factors [21]. Psychologists have shown that biological factors determine the occurrence and existence of psychological phenomena and social factors and the direction of occurrence, development, and change of psychological phenomena [22]. Social factors include environmental, cultural, economic, moral, and educational levels [23].

In our study, patients were first informed about the causes of their negative emotions such as anxiety and depression, and then stimuli favorable and unfavorable to recovery were identified. In the intervention phase, specific interventions such as health education, diversified communication activities, and targeted counseling were carried out according to the different characteristics of the patients in order to achieve a good psychological state and improve depressive symptoms [24]. The nursing staff assessed the main psychological and physiological cognitive interventions of the patients, identified the influencing factors associated with them, and developed a targeted care plan for the patients, thus helping them to alleviate their psychological condition and promote their psychological adaptation [25]. The use of multimedia health education in the treatment of many diseases has been reported to have positive implications for improving patients' attitudes and treatment outcomes [26].

In our study, the somatic function score, pain management score, and symptom response score of self-efficacy of patients in the observation group were significantly higher than those in the comparison group aftercare, indicating that conventional health education and discharge instructions combined with multimedia health education care can effectively improve the self-efficacy of patients with congenital microtia. The reasons for this are as follows: self-efficacy is related to the individual's psychological expressions of self-confidence, anxiety, depression, helplessness, and fear when facing various external environments [27]. Self-efficacy is the judgment and speculation of an individual about his or her ability to perform a certain behavior and is a determinant of the human body's ability to perform certain behaviors [28]. A person with a strong sense of self-efficacy is confident in all difficulties, i.e., the stronger the patient's sense of self-efficacy, the better his or her confidence in disease treatment, and the higher his or her compliance with treatment and care implementation [29]. By strengthening communication and exchange with patients, patiently listening to what they have to say, carefully answering their questions,



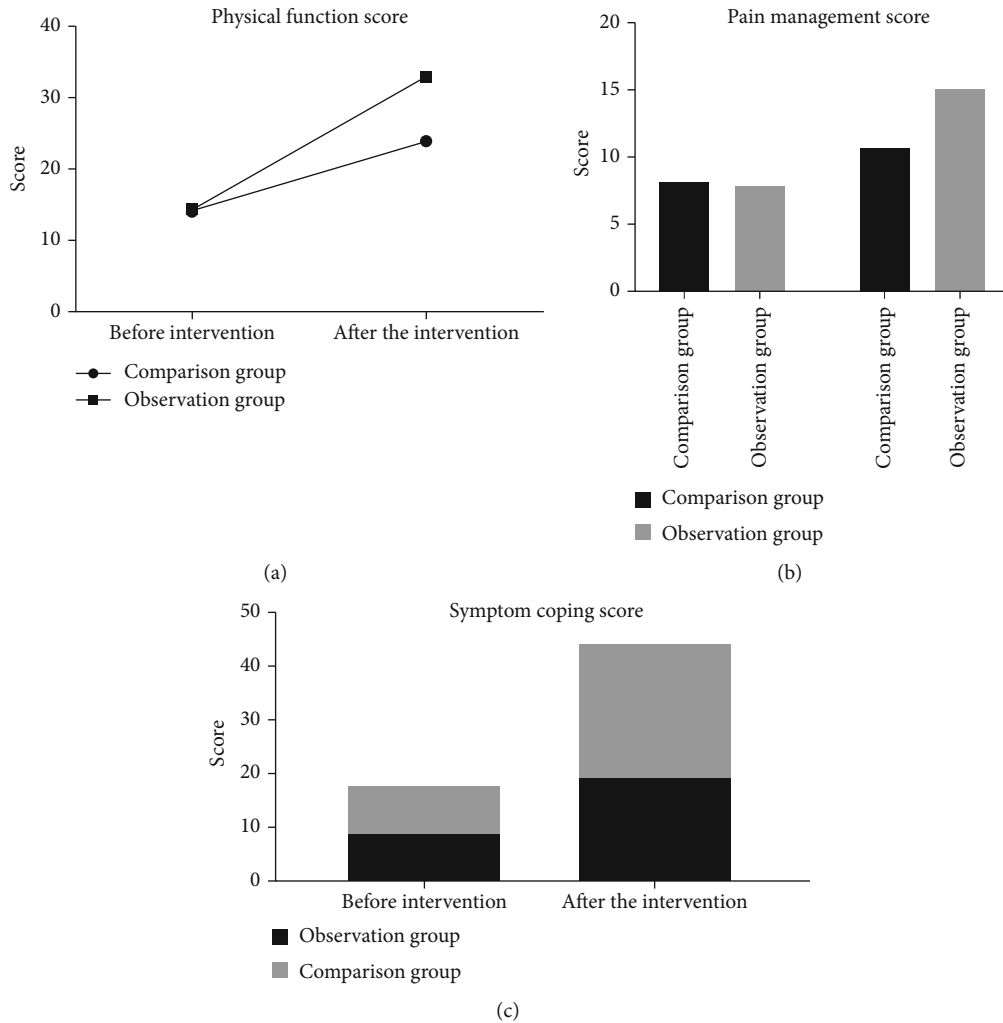


FIGURE 1: Self-efficacy comparison. (a). Physical function score; (b) pain management score; (c) symptom coping score (values expressed as mean  $\pm$  standard deviation). \*  $P < 0.05$  vs. control group.

and providing correct guidance, nursing staff promote a cordial nurse-patient relationship and relieve patients' psychological burden [30]. The encouraging language was adopted to enhance their confidence in overcoming the disease, explain their condition to the patients carefully, explain patiently, correct the patients' previous misconceptions of cognition, and guide how to carry out the correct way of coping [31]. Successful clinical cases were used to encourage patients and instruct them to adjust their lifestyle, develop good habits, and perform regular exercise routines, thereby improving their sense of self-efficacy [32]. It can be seen that improving patients' self-efficacy is extremely crucial to accelerate their recovery.

The mental vitality score, social interaction score, emotional limitation score, and mental status of patients in the observation group were significantly higher than those in the comparison group after our study care, indicating that conventional health education and discharge instruction combined with multimedia health education care can effectively improve the quality of life of patients with congenital microtia. By carrying out conventional health education

and discharge instruction combined with multimedia health education nursing intervention, the patients' poor cognition was changed, and cognitive reconstruction was carried out [33]. Patients were made to consciously discard unstable factors in their daily life, adopt relaxation techniques to effectively cope with stress in all aspects, and then establish a healthy behavior and psychological approach to effectively improve the quality of life of patients [34].

The level of health knowledge, self-care skills, sense of self-care responsibility and self-concept in the observation group were higher than those in the comparison group after our study care, while the depressive mood disorder scores were significantly lower than those in the comparison group, indicating that conventional health education and discharge instruction combined with multimedia health education care can effectively improve the self-care ability of patients with congenital microtia. This may be related to the following advantages of multimedia health education: patients' physiological and psychological adaptation mechanisms are strengthened, their adaptation range is expanded, and their tolerance to stimuli is subsequently increased [35,

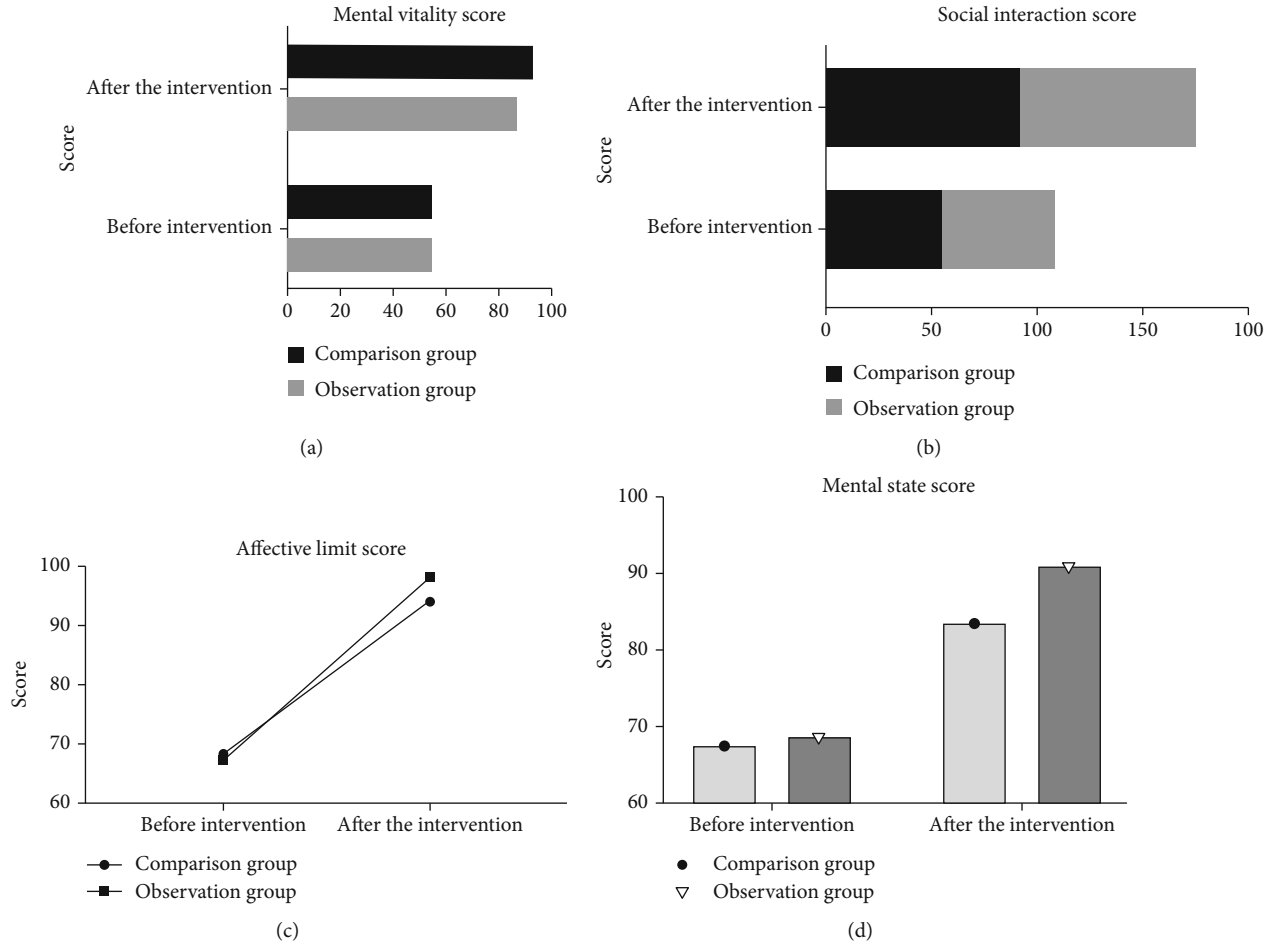


FIGURE 2: Quality of life score. (a) Mental vitality score; (b) social interaction score; (c) affective limit score; (d) mental status scores (values expressed as mean  $\pm$  standard deviation). \* $P < 0.05$  vs. control group.

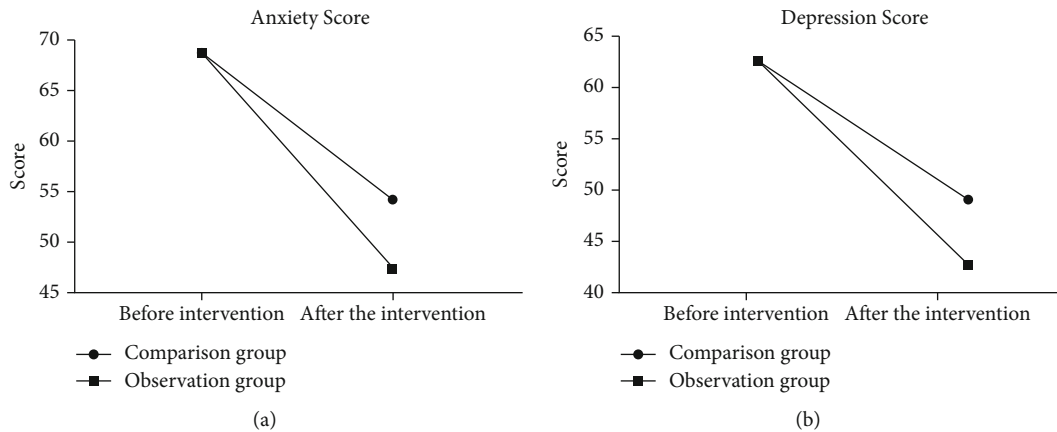


FIGURE 3: Anxiety and depression score. (a) Anxiety scores; (b) depression scores (values expressed as mean  $\pm$  standard deviation). \* $P < 0.05$  vs. control group.

36]. Multimedia health education is good control of the primary and secondary stimuli relevant to the patient, keeping the adaptation of the patient's body within its acceptable range and thus avoiding or minimizing the impact of adverse stimuli on the organism [37]. Individual support and encour-

agement mechanisms implemented during care can help patients to face the stimuli correctly so that individual adaptive responses can be enhanced and maintained, thus promoting the improvement of patients' dysphoria and enhancing self-care and self-efficacy [38].

Our study is innovative and has some limitations. First, our study included congenital microtia patients without routine health education and discharge instruction combined with multimedia health education care to assess self-efficacy and poor mood in congenital microtia patients. Second, the selected patients were all from patients treated or cared for in our hospital, so the selection of included and excluded patients was subjective, and the study results may not be representative or biased. Finally, our study only investigated the effect of conventional health education combined with multimedia health education care on self-efficacy and poor emotion in patients with congenital microtia and failed to study patients with congenital microtia in depth and follow up their recovery after congenital microtia care for a long time.

## 5. Conclusion

Conventional health education and discharge instruction combined with multimedia health education care can effectively improve the quality of life of patients with congenital microtia, reduce adverse emotions, and improve patients' self-efficacy, which has certain reference value for the care of patients with congenital microtia.

## Data Availability

The datasets used and analyzed during the current study are available from the corresponding author upon reasonable request.

## Conflicts of Interest

The authors declare that they have no conflicts of interest.

## References

- [1] Y. L. Huang and L. Teng, "Research progress in craniofacial malformations genetics," *Journal of Tissue Engineering and Reconstructive Surgery*, vol. 16, no. 5, pp. 415–441, 2020.
- [2] J. L. Zhen, "Coding analysis of congenital craniofacial malformations ICD-10," *Chinese Medical Record*, vol. 23, no. 1, pp. 37–39, 2022.
- [3] Y. Zhang, H. Jiang, Q. Yang et al., "Microtia in a Chinese specialty clinic population: clinical heterogeneity and associated congenital anomalies," *Plastic and Reconstructive Surgery*, vol. 142, no. 6, pp. 892e–903e, 2018, PMID: 30489530.
- [4] S. Q. Xu, X. L. Jia, Y. Choi et al., "Three-dimensional scanning technique in the congenital microtia reconstruction with tissue expander," *Chinese Medical Journal*, vol. 134, no. 7, pp. 842–844, 2020.
- [5] K. B. Cywka, B. Król, and P. H. Skarżyński, "Effectiveness of bone conduction hearing aids in young children with congenital aural atresia and microtia," *Medical Science Monitor*, vol. 27, no. 27, article e933915, 2021.
- [6] L. J. Ren, Y. S. Duan, J. C. Yu, Y. Z. Xie, and T. Y. Zhang, "Instant auditory benefit of an adhesive BCHD on children with bilateral congenital microtia," *Clinical Otolaryngology*, vol. 46, no. 5, pp. 1089–1094, 2021.
- [7] V. H. Ramprasad, A. D. Shaffer, and N. Jabbour, "Utilization of diagnostic testing for renal anomalies and congenital heart disease in patients with microtia," *Otolaryngology-Head and Neck Surgery*, vol. 162, no. 4, pp. 554–558, 2020.
- [8] A. Paul, S. Achard, F. Simon et al., "Congenital abnormalities associated with microtia: a 10-years retrospective study," *International Journal of Pediatric Otorhinolaryngology*, vol. 146, article 110764, p. 11, 2021.
- [9] Y. Y. Fu, C. L. Li, J. L. Zhang, and T. Y. Zhang, "Autologous cartilage microtia reconstruction: complications and risk factors," *International Journal of Pediatric Otorhinolaryngology*, vol. 116, pp. 1–6, 2019.
- [10] Y. Zhu, Y. Zhou, Q. Zhao, Y. Ma, and Y. Lu, "3D technique-based nonsurgical correction of deformational congenital auricular deformities," *ORL J Otorhinolaryngol Relat Spec*, vol. 83, no. 2, pp. 59–64, 2021.
- [11] M. Shirazi, E. Abbariki, R. Pirjani, S. Akhavan, and E. Dastgerdy, "Congenital microtia in a neonate due to maternal isotretinoin exposure 1 month before pregnancy: case report," *The Journal of Obstetrics and Gynaecology Research*, vol. 41, no. 6, pp. 975–978, 2015.
- [12] X. Yongyong, S. Zhenqiu, and Y. Hong, *Medical Statistics (Third Edition)/Higher School Textbook*, Higher Education Press, 2019.
- [13] Z. Tianyu and C. Ying, "Principles of diagnosis and treatment of congenital external and middle ear malformation syndrome," *Journal of Clinical Otolaryngology Head and Neck Surgery*, vol. 32, no. 12, pp. 883–885, 2018.
- [14] Y. Y. Fu, C. L. Li, Y. Z. Xie, Y. Y. Zhu, and T. Y. Zhang, "Functional ear reconstruction strategies for microtia with congenital aural stenosis in seventy-six patients," *Clinical Otolaryngology*, vol. 45, no. 4, pp. 611–615, 2020.
- [15] P. Guo, Z. Ji, H. Jiang, X. Huang, C. Wang, and B. Pan, "Identification of a novel CYP26A1 mutation in a Chinese family with congenital microtia," *International Journal of Pediatric Otorhinolaryngology*, vol. 139, article 110488, 2020.
- [16] M. M. Alsebayel, F. A. Abaalkhail, F. M. Alsebayel, D. A. Alissa, A. H. Al-Jedai, and H. Elsiey, "Congenital esophageal atresia and microtia in a newborn secondary to mycophenolate mofetil exposure during pregnancy: a case report and review of the literature," *The American Journal of Case Reports*, vol. 19, no. 19, pp. 523–526, 2018.
- [17] Z. Ding, J. Chen, and Y. Wang, "Clinical analysis of congenital microtia complicated with retroauricular subperiosteal abscess in 7 cases," *Journal of Clinical Otorhinolaryngology, Head, and Neck Surgery*, vol. 35, no. 11, pp. 1014–1017, 2021.
- [18] J. M. Dou, D. N. Wang, S. Q. Zhao et al., "Congenital microtia with aural atresia or stenosis accompany with first branchial cleft anomaly: report of 5 cases," *Chinese Journal of Otorhinolaryngology Head and Neck Surgery*, vol. 54, no. 5, pp. 349–354, 2019.
- [19] N. Bitterman, O. Ben-Nun, S. Movshovich, N. Calderon, and A. Barak, "Total reconstruction of congenital microtia-our experience with 150 patients," *Harefuah*, vol. 159, no. 8, pp. 565–569, 2020.
- [20] S. Q. Zhao, "Strategies for hearing reconstruction of congenital microtia and atresia," *Chinese journal of otorhinolaryngology head and neck surgery*, vol. 56, no. 4, pp. 409–413, 2021.
- [21] F. Guo, L. Lin, X. Yu et al., "Congenital heart defects in patients with isolated microtia: evaluation using colour Doppler

- echocardiographic image,” *Cardiology in the Young*, vol. 31, no. 2, pp. 260–263, 2021.
- [22] N. Ogasawara, S. Jitsukawa, N. Takahashi, K. Takano, and T. Himi, “Congenital microtia treated at Sapporo Medical University Hospital: clinical characteristics and associated anomalies,” *Excellence in Otolaryngology*, vol. 77, pp. 12–16, 2016.
- [23] T. Cao, Q. Chen, B. Wang, J. Hu, M. Zou, and Q. Zhang, “Epidemiological research of microtia combined with congenital heart disease,” *The Journal of Craniofacial Surgery*, vol. 32, no. 3, pp. 920–924, 2021.
- [24] P. P. Schnurr, M. J. Friedman, and N. C. Bernardy, “Research on posttraumatic stress disorder: epidemiology, pathophysiology, and assessment,” *Clinical Psychologist*, vol. 58, no. 8, pp. 877–889, 2002.
- [25] D. C. Tu, M. L. Batten, K. Palczewski, and R. N. Van Gelder, “Nonvisual photoreception in the chick iris,” *Science*, vol. 196, no. 4811, pp. 129–131, 2004.
- [26] F. C. Macgregor, “Ear deformities: social and psychological implications,” *Clinics in Plastic Surgery*, vol. 5, no. 3, article 347350, 1978.
- [27] N. M. Sperling and N. Patel, “A patient-benefit evaluation of unilateral congenital conductive hearing loss presenting in adulthood: should it be repaired?,” *Laryngoscope*, vol. 109, no. 9, pp. 1386–1391, 1999.
- [28] B. Brent, “The team approach to treating the microtia atresia patient,” *Otolaryngologic Clinics of North America*, vol. 33, no. 6, pp. 1353–1365, 2000.
- [29] S. A. Wolchik, C. E. Schenck, and I. N. Sandier, “Promoting resilience in youth from divorced families: lessons learned from experimental trials of the new beginnings program,” *Journal of Personality*, vol. 77, no. 6, pp. 1833–1868, 2009.
- [30] S. Turan Kavrak and Ö. Z. Canli, “The effect of education and telephone follow-up intervention based on the Roy adaptation model after myocardial infarction: randomised controlled trial,” *Scandinavian Journal of Caring Sciences*, vol. 34, no. 1, pp. 247–260, 2020.
- [31] B. S. Buckner and E. B. Buckner, “Post-revolution Egypt: the Roy adaptation model in community,” *Nursing Science Quarterly*, vol. 28, no. 4, pp. 300–307, 2015.
- [32] V. T. Armenti, J. A. Daller, S. Constantinescu et al., “Report from the National Transplantation Pregnancy Registry: outcomes of pregnancy after transplantation,” *Clinical Transplants*, pp. 57–70, 2006.
- [33] S. Azarmi and Z. Farsi, “Roy’s adaptation model-guided education and promoting the adaptation of veterans with lower extremities amputation,” *Iranian Red Crescent Medical Journal*, vol. 17, no. 10, article e25810, 2015.
- [34] M. Ichikawa, “Protection of the surgical wound following plastic surgery and nursing care to maintain cleanliness of the regions—protection and preservation of the surgical wound following plastic surgery of cleft lip and palate and microtia,” *[Kango Gijutsu]: [Nursing Technique]*, vol. 31, no. 9, pp. 1176–1182, 1985.
- [35] F. E. Ursavaş, Ö. Karayurt, and Ö. İşeri, “Nursing approach based on Roy adaptation model in a patient undergoing breast conserving surgery for breast cancer,” *The Journal of Breast Health*, vol. 10, no. 3, pp. 134–140, 2014.
- [36] Y. Lv, G. Ren, X. Ren, and X. Ren, “Changes of intestinal flora and lymphocyte subsets in patients with chronic renal failure,” *Evidence-Based Complementary and Alternative Medicine*, vol. 2021, Article ID 4288739, 2021.
- [37] F. Erol Ursavaş and Ö. Karayurt, “Effects of a Roy’s adaptation model-guided support group intervention on sexual adjustment, body image, and perceived social support in women with breast cancer,” *Cancer Nursing*, vol. 44, no. 6, pp. E382–E394, 2021.
- [38] Y. Chen, L. J. Ren, N. Gao et al., “Long-term hearing performance and soft tissue outcomes of the Baha® Attract system in patients with bilateral congenital microtia in a single centre,” *Clinical Otolaryngology: Official Journal of ENT-UK; Official Journal of Netherlands Society for Oto-rhino-laryngology & Cervico-facial Surgery*, vol. 47, no. 2, pp. 357–363, 2022.

## Research Article

# Diagnostic Value and Prognostic Significance of Procalcitonin Combined with C-Reactive Protein in Patients with Bacterial Bloodstream Infection

Yan Zhang,<sup>1</sup> Mei La<sup>1,2</sup> ,<sup>2</sup> Jihong Sun,<sup>2</sup> Mimi Chen,<sup>2</sup> Dandan Liu,<sup>2</sup> Xiaolin Liu,<sup>2</sup> and Yating Kang<sup>2</sup>

<sup>1</sup>Clinical Laboratory Northwest A&F University Hospital, Yangling 721000, China

<sup>2</sup>Yan'an University Xianyang Hospital, Clinical Laboratory, Xianyang, 712000, China

Correspondence should be addressed to Mei La; 1764100122@e.gzhu.edu.cn

Received 14 June 2022; Accepted 19 July 2022; Published 11 August 2022

Academic Editor: Hangjun Che

Copyright © 2022 Yan Zhang et al. This is an open access article distributed under the Creative Commons Attribution License, which permits unrestricted use, distribution, and reproduction in any medium, provided the original work is properly cited.

**Objective.** To study the clinical values and implications for the prognosis of procalcitonin (PCT) combined with C-reactive protein (hs-CRP) in patients with bacterial bloodstream infection. **Methods.** One hundred and twenty patients with infection hospitalized from Mar. 2020 to Jun. 2021 were chosen as subjects. All participants were tested for serum PCT, hs-CRP, and blood culture. According to the types of pathogenic bacteria, they were divided into the gram-negative bacteria bloodstream infection group ( $n = 53$ ) and the gram-positive bacteria bloodstream infection group ( $n = 31$ ). Depending on the prognostic outcome of the participants after 28 days, they were categorized into survival and fatality cohorts. The PCT and hs-CRP levels were compared to explore diagnostic value implications for the prognosis of the cases with bacterial bloodstream infection. **Results.** Serum PCT and hs-CRP values in the positive cohort were higher than those in the negative cohort. The levels of serum PCT and hs-CRP in pulmonary infection were higher than those in the group with negative cases, and the difference was statistically significant ( $P < 0.05$ ). There were 27 gram-positive participants and 9 gram-negative cases in the positive cohort. The serum PCT value of gram-negative bacterial infection was greater than that of gram-positive bacterial infection. The value of serum PCT in the gram-negative bacterial infection group was higher than that in the gram-positive bacterial infection group, and the difference was statistically significant ( $P < 0.05$ ). The areas under the curve (AUCs) of PCT, combination of hs-CRP and PCT, and hs-CRP were 0.946, 0.783, and 0.991, respectively. The combined examination of PCT and hs-CRP was the largest, PCT was the second, and hs-CRP was the lowest. These results indicated that the accuracy of combined detection of PCT and hs-CRP in the diagnostic bloodstream infection was the highest (0.991), followed by PCT (0.946) and the lowest (0.783). The PCT and hs-CRP levels of the survival cohort were lower than those in the death cohort. AUCs of PCT, hs-CRP and PCT, and hs-CRP were 0.848, 0.826, and 0.934, respectively. The combined examination of PCT and hs-CRP was the largest, followed by PCT and hs-CRP. The accuracy of the combination of PCT and hs-CRP was the highest (0.934), followed by PCT (0.848), and the diagnostic accuracy of hs-CRP was the lowest (0.826). **Conclusion.** There were significant differences in the levels of PCT and CRP between the gram-positive bacteria group and the gram-positive bacteria group. PCT and CRP have high diagnostic values in predicting the short-term prognosis of patients. PCT and CRP assist clinical diagnosis and guide treatment and play a positive role in early treatment and prognosis evaluation of patients.

## 1. Introduction

Bloodstream infection is one of the severe infectious diseases in clinic, which seriously threatens the life and health of patients [1]. Bloodstream infection is one of the main factors leading to an increase in morbidity and mortality worldwide

[2–5]. In 2002, the number of deaths caused by bloodstream infections in the United States exceeded 30000, and the incidence of bloodstream infections continues to increase [6]. Between 2000 and 2010, the mortality rate of septicemia increased by 17% [7]. Recent reports have suggested that septicemia mortality ranges from 34% to 52% [8]. In 2009,



TABLE 1: Comparison of PCT and hs-CRP levels between the two groups.

Grouping	N	PCT (ng/ml)	hs-CRP (mg/l)
Blood culture negative group	84	$0.48 \pm 0.43$	$24.72 \pm 5.36$
Blood culture positive group	36	$4.93 \pm 0.87$	$35.38 \pm 10.54$
<i>t</i>		37.516	7.340
<i>P</i>		<0.05	<0.05

the data from a US study showed that one in 23 hospitalized patients in the United States was affected by bloodstream infection, accounting for 4.2%. In the ranking of hospitalization factors, bloodstream infection ranked sixth.

The incidence of BSI has been increasing year by year. Given the high mortality rate of BSI, the length of stay in hospital is longer and the cost of hospitalization is more expensive, to the extent that patients' lives are seriously threatened. Various invasive diagnostic and testing techniques, like trauma and scald, can disrupt the integrity of the body's barrier function, cause a decrease in immune function, and increase the risk of bloodstream infection. In addition, diverse factors, such as prolonged coma, malnutrition, and advanced age, can also increase the prevalence of bloodstream infections. It therefore becomes important and urgent to identify early, rapidly, and accurately the pathogens causing BSI and then to select the appropriate antibiotic treatment.

With the rapid development of biomedical engineering technology, blood culture technology is widely used in clinic and is regarded as the "gold standard" for the diagnosis of BSI. However, this technique still has some limitations, such as the relatively long cycle of detection of pathogenic microorganisms (usually 24-48 hours), which often leads to the loss of the best opportunity for diagnosis and treatment of BSI patients. Therefore, it is of great clinical significance to find reliable and sensitive biomarkers for early diagnosis of BSI.

At present, the main biomarkers that can be used to diagnose BSI are blood routine test (BRE), procalcitonin (PCT), and C-reactive protein (CRP) [8, 9]. Among them, BRE mainly calculates the changed number of blood cells and related parameters, comprehensively analyzes the morphological distribution of blood cells, and judges the blood condition of the body, so as to screen diseases. PCT is the precursor protein of serum calcitonin, which can hardly be detected under normal conditions. The concentration of PCT increases significantly when patients suffer from pathogenic microbial infections (such as bacterial, fungal, and parasite infections) and sepsis, and when there are some autoimmune reactions and viruses, serum PCT levels do not suddenly increase rapidly. When a local bacterial infection, fungal infection, viral infection, or other chronic inflammation occurs in a certain part of the body, it will not cause an increase in the level of PCT [10–12]. CRP is a nonspecific inflammatory protein synthesized through the liver, and its expression is significantly increased when patients are invaded by bacteria or tissue damage. Previous

studies have focused on exploring the expression of PCT and CRP between gram-negative bacteria and gram-positive bacteria, but there are few reports on the diagnosis and prognosis of bloodstream infections by PCT and CRP. Therefore, this study analyzed the clinical data of 120 patients to study the diagnostic value of procalcitonin (PCT) combined with high-sensitivity C-reactive protein (hs-CRP) in the diagnosis of bacterial bloodstream infection and its prognostic significance.

## 2. Materials and Methods

**2.1. General Information.** One hundred and twenty patients with infection hospitalized from March 2020 to June 2021 were selected as the objects of study. All patients were tested for serum PCT and hs-CRP and blood culture. Among the 120 patients with infection, there were 62 males and 58 females with ages from 19 to 85 years (mean  $45.83 \pm 4.23$ ). Our clinic's Professional Conduct Association gave their approval towards this experiment. Every participant provided written informed consent.

**2.1.1. Selection Criterion.** (1) There was no limitation to the sex of the patient, and the initial disease was caused by pulmonary infection, urinary tract infection, suppurative meningitis, bacillary dysentery, and other infections. Blood culture samples and serum samples were sent for examination at the same time; (2) without cognitive, language, and intellectual impairment and with basic reading and writing ability; (3) the diagnostic criteria of bloodstream infection met the following requirements: fever, chills, and other symptoms; hematological tests find antigenic substances of pathogens; and/or when pathogenic bacteria or fungi were isolated by blood culture, any of the following requirements can be met: (a) the strains of pathogenic bacteria isolated from many times of blood culture are the same, and the results of the drug sensitivity test are the same; (b) the strains of pathogenic bacteria isolated from other infected sites are the same as those of blood culture, and the results of drug sensitivity test are the same; and (c) it was effective to use sensitive antimicrobial agents for the isolated pathogenic bacteria. (4) The clinical data are complete, (5) there was no history of surgery or trauma within 3 months, and (6) there were no autoimmune diseases and hematological diseases.

**2.1.2. Exclusion Criteria.** The exclusion criteria are (1) patients with severe heart, liver, and renal insufficiency and malignant tumors, (2) patients who had been treated with corticosteroids for a long time, (3) patients with hematological diseases, (4) patients who had a history of taking antibiotics and hormones within 3 months before entering the group, and (5) patients with a history of organ transplantation and immunosuppressant use.

**2.2. Methods.** The levels of serum PCT and hs-CRP were detected in all patients, and blood culture was performed. The sensitivity, specificity, and diagnostic accuracy of three kinds of detection of bloodstream infection were compared to determine their value in early clinical diagnosis and

TABLE 2: Comparison of the serum PCT and hs-CRP values between the two groups ( $\bar{x} \pm s$ ).

Grouping	N	PCT (ng/ml)	hs-CRP (mg/l)
Pulmonary infection in patients with negative blood culture	53	$0.53 \pm 0.47$	$24.56 \pm 5.55$
Pulmonary infection in patients with positive blood culture	31	$5.09 \pm 0.93$	$35.48 \pm 10.66$
<i>t</i>		29.848	6.178
<i>P</i>		<0.05	<0.05

TABLE 3: The serum PCT and hs-CRP values in patients with bloodstream infection caused by gram-positive bacteria and gram-negative bacteria ( $\bar{x} \pm s$ ).

Grouping	N	PCT (ng/ml)	hs-CRP (mg/l)
Gram-positive bacteria	27	$1.67 \pm 0.46$	$37.29 \pm 9.48$
Gram-negative bacteria	9	$6.54 \pm 1.26$	$34.98 \pm 11.67$
<i>t</i>		17.292	0.598
<i>P</i>		<0.05	>0.05

TABLE 4: The bacterial species and serum PCT and hs-CRP values between gram-positive bacteria and gram-negative bacteria ( $\bar{x} \pm s$ ).

Grouping	N	PCT (ng/ml)	hs-CRP (mg/l)
Gram-positive bacteria	27		
Staphylococcus epidermidis	14	$1.61 \pm 0.42$	$37.51 \pm 9.23$
Staphylococcus aureus	9	$1.68 \pm 0.44$	$37.83 \pm 9.45$
Streptococci	2	$1.68 \pm 0.03$	$39.45 \pm 4.12$
Enterococci	2	$1.65 \pm 0.02$	$36.69 \pm 3.87$
Gram-negative bacteria	9		
Klebsiella pneumoniae	4	$6.35 \pm 1.62$	$34.28 \pm 11.95$
Acinetobacter baumannii	3	$6.15 \pm 1.72$	$35.05 \pm 11.59$
Pseudomonas aeruginosa	2	$6.61 \pm 1.03$	$34.88 \pm 3.41$

prognosis evaluation of bloodstream infection. The PCT determination kit (electrochemiluminescence) is from Roche Diagnostic products (Shanghai) Co., Ltd., using the Roche automatic electrochemiluminescence immunoassay system. The hs-CRP determination kit (scatter turbidimetry) comes from Shenzhen Pumen Technology Co., Ltd., using the PA-990P specific protein analyzer. The blood culture instrument comes from Bact/ALERT3D automatic Mycobacterium culture and identification system (Merieux). For the identification and drug sensitivity of gram-positive bacteria, VITEKGP was used, with drug sensitivity VITEKAST-GP67. For the identification and drug sensitivity of gram-negative bacteria, VITEKGN was used, with drug sensitivity VITEKAST-GN09.

**2.2.1. Observation Index.** On the day of admission and 28 days after the patient's admission, the cubital venous blood was drawn in the early morning on an empty stomach and centrifuged at 3000 r/min for 15 min. The upper serum was separated for testing. The PCT value was detected by the chemiluminescence method, and the kit was purchased from

Zhengzhou Antu Bioengineering Co., Ltd. The hs-CRP level was detected by immunoturbidimetry, and the kit was purchased from Shenzhen Pumen Technology Co., Ltd. Analyzer Roche 411.

**2.3. Statistical Analysis.** The SPSS22.0 statistical program was used for data analysis. The chi-squared test ( $\chi^2$  test) was applied to compare the counting data. The measured data were expressed by  $\bar{x} \pm s$ , the *t*-test was used, and analysis of variance was used to compare multiple-group data. The difference was statistically significant, and the difference was statistically significant ( $P < 0.05$ ). The area under the receiver operating characteristic (ROC) curve was used to evaluate the clinical diagnostic value of PCT, hs-CRP, and combined detection in bloodstream infection and prognosis of patients.

### 3. Results

**3.1. Comparison of PCT and hs-CRP Levels between the Two Groups.** The values of serum PCT and hs-CRP in the group with positive blood culture were higher than those in the group with negative blood culture, and the difference was statistically significant ( $P < 0.05$ ). See Table 1.

**3.2. The Serum PCT and hs-CRP Values between the Two Groups of Pulmonary Infection by Blood Culture.** In the positive blood culture group, the serum PCT value and hs-CRP value of the patients with pulmonary infection were larger than those in the negative blood culture group, and the difference was statistically significant ( $P < 0.05$ ). See Table 2.

**3.3. The Serum PCT and hs-CRP Values in Patients with Bloodstream Infection Caused by Gram-Positive Bacteria and Gram-Negative Bacteria.** In the blood culture positive group, there were 27 cases of gram-positive bacterial infection and 9 cases of gram-negative bacterial infection. The value of serum PCT in the gram-negative bacterial infection group was higher than that in the gram-positive bacterial infection group ( $P < 0.05$ ). See Table 3.

**3.4. The Bacteria Species and Serum PCT and hs-CRP Values between Gram-Positive Bacteria and Gram-Negative Bacteria.** Among the infections of gram-positive bacteria, there were 14 cases of Staphylococcus epidermidis infection, 9 cases of Staphylococcus aureus infection, 2 cases of Streptococcus infection, and 2 cases of Enterococcus infection. Among the patients infected with gram-negative bacteria, there were 4 cases of Klebsiella pneumoniae infection, 3 cases of Acinetobacter baumannii infection, and 2 cases of Escherichia coli infection, and the serum PCT value of

TABLE 5: Diagnostic efficacy of PCT, hs-CRP, and combined blood culture in patients with bloodstream infection.

Index	AUC (95% CI)	Truncation value	Sensitivity (%)	Specificity degree (%)	Youden index
PCT (ng/ml)	0.946 (0.911~0.974)	1.283	88.61	94.02	0.818
hs-CRP (mg/l)	0.783 (0.681~0.892)	31.684	63.75	92.54	0.557
PCT+hs-CRP	0.991 (0.972~1.000)	304.39	94.18	98.73	0.921

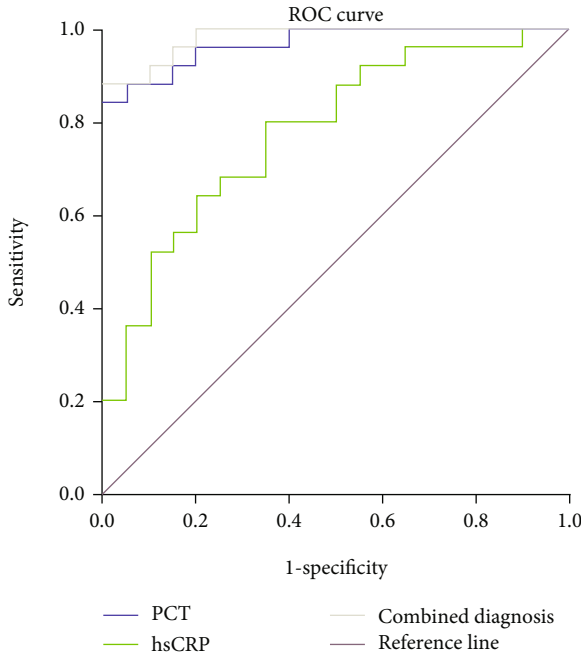


FIGURE 1: ROC curve of PCT and hs-CRP in the diagnosis of bloodstream infection. Note: the AUCs of PCT, hs-CRP and PCT, and hs-CRP were 0.946, 0.783, and 0.991, respectively (all  $P < 0.05$ ). The area under the joint detection curve of PCT and hs-CRP was the largest, PCT was the second, and hs-CRP was the lowest.

TABLE 6: The serum PCT and hs-CRP levels between the survival group and the death group.

Grouping	N	PCT (ng/ml)	hs-CRP (mg/l)
Survival group	29	$1.63 \pm 0.76$	$73.28 \pm 30.11$
Death group	7	$4.18 \pm 2.04$	$117.54 \pm 44.83$
$t$		5.505	3.167
$P$		$<0.05$	$<0.05$

gram-negative bacterial infection was greater than that of gram-positive bacterial infection, and the difference was statistically significant ( $P < 0.05$ ). There was no significant difference in serum hs-CRP between gram-negative bacteria and gram-positive bacteria ( $P > 0.05$ ). There was no statistical significance in the comparison of serum PCT and hs-CRP values in patients infected with gram-negative bacteria ( $P > 0.05$ ). There was no statistical significance in the comparison of serum PCT and hs-CRP values in patients infected with gram-positive bacteria ( $P > 0.05$ ). See Table 4.

**3.5. Diagnostic Value of PCT, hs-CRP, and Their Combination in Bloodstream Infection.** The AUCs of PCT, hs-CRP and PCT, and hs-CRP were 0.946, 0.783, and 0.991, respectively (all  $P < 0.05$ ). The area under the joint detection curve of PCT and hs-CRP was the largest, PCT was the second, and hs-CRP was the lowest. The accuracy of combined detection of PCT and hs-CRP in the diagnosis of bloodstream infection was the highest (0.991), followed by PCT (0.946), and hs-CRP was the lowest (0.783). See Table 5 and Figure 1.

**3.6. The Serum PCT and hs-CRP Levels between Survival Group and Death Group.** Of the 36 patients with bacterial bloodstream infection, 29 survived and 7 died. The serum PCT and hs-CRP values in the survival group were lower than those in the death group, and the difference was statistically significant ( $P < 0.05$ ). See Table 6.

**3.7. The Value of PCT and hs-CRP in Diagnosing the Prognosis and Survival of Patients.** ROC curve analysis showed that the AUCs of PCT, hs-CRP and PCT, and hs-CRP were 0.848, 0.826, and 0.934, respectively (all  $P < 0.05$ ). The AUC of combined detection of PCT and hs-CRP was the largest, followed by PCT, and the lowest was hs-CRP. The accuracy of combined detection of PCT and hs-CRP was the highest (up to 0.934), followed by PCT (0.848), and the diagnostic accuracy of hs-CRP was the lowest (0.826). See Table 7 and Figure 2.

## 4. Discussion

Bloodstream infection (BSI) is a general term for septicemia and bacteremia. Septicemia is when bacteria enter the bloodstream and grow, producing large amounts of toxins and metabolites, causing systemic severe infection syndrome. Bacteremia is toxemia in which bacteria enter the bloodstream temporarily but do not cause obvious symptoms of systemic infection. Under certain conditions, bacteremia and septicemia can be converted into each other [13]. The disease lacks characteristic clinical manifestations in the early stage, so it is difficult to be detected. Because of the high specificity of blood culture, it is often used as the first choice for the diagnosis of bloodstream infection. However, blood culture has the following disadvantages: (1) the blood should be collected before medication, and the blood is easy to be contaminated, (2) the positive rate is easily affected by the number of bacteria, and (3) the culture takes a long time, resulting in the lag of the results. Previous studies have shown that C-reactive protein and procalcitonin play an important role in the occurrence and development of bloodstream infection [14, 15].

TABLE 7: The value of PCT and hs-CRP in the diagnosis of prognosis and survival of patients.

Index	AUC (95% CI)	Truncation value	Sensitivity (%)	Specificity degree (%)	Youden index
PCT (ng/ml)	0.848 (0.733~0.963)	2.406	91.83	80.65	0.736
hs-CRP (mg/l)	0.826 (0.708~0.944)	74.833	88.94	53.57	0.429
PCT+hs-CRP	0.934 (0.854~1.000)	81.421	88.92	94.27	0.647

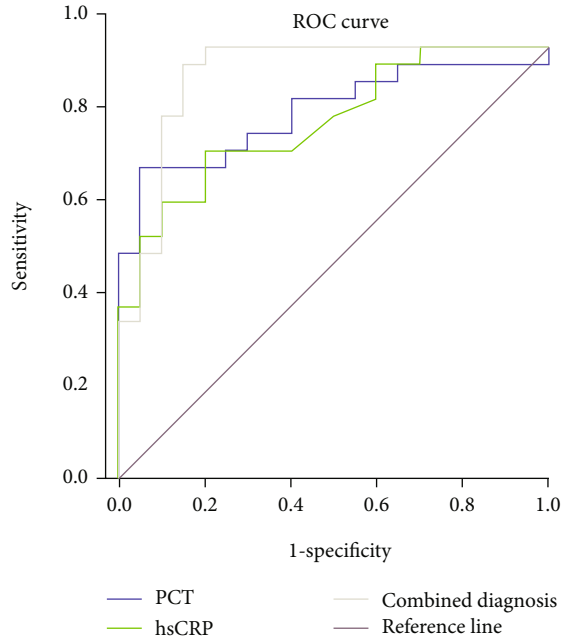


FIGURE 2: ROC curve of prognosis and survival of patients diagnosed by PCT and hs-CR. Note: the AUCs of PCT, hs-CRP and PCT, and hs-CRP were 0.848, 0.826, and 0.934, respectively (all  $P < 0.05$ ). The AUC of combined detection of PCT and hs-CRP was the largest, followed by PCT, and the lowest was hs-CRP.

Recently, a large number of broad-spectrum antibiotics, hormone drugs, and immunosuppressants have been widely used in clinic with the continuous development of invasive diagnosis and treatment technology. C-reactive protein is an acute phase reactive protein, which is mainly released from the liver under the stimulation of interleukin-6 and other cytokines [16]. When the body is infected, CRP can play both anti-inflammatory and proinflammatory effects, mainly because it can mediate the elimination of pathogens and inhibit the interaction between endothelial cells and white blood cells. Therefore, CRP is often used for the early diagnosis of infectious diseases. Studies have shown that CRP can improve the early diagnosis rate of pneumonia [17, 18]. For patients after surgery, CRP can help distinguish acute appendicitis from other noninfectious abdominal pain and predict infection complications after colorectal surgery [19, 20]. However, some studies have shown that the diagnostic value of CRP alone in sepsis is only moderate, and the predicting positive blood culture and disease prognosis are lower than that of procalcitonin and sTREM-1 [21]. In general, CRP levels decrease within 48 hours after anti-infective treatment [22]. Baruah et al. investigated 891

patients with community-acquired septicemia, showing that CRP levels of most patients decreased within 48 hours and serum CRP levels of all patients decreased within 5 days after anti-infection treatment [23].

Procalcitonin, a propeptide of calcitonin, has no hormonal activity and is usually produced by thyroid C cells. In healthy people, almost all calcitonin is converted to calcitonin, so its content in serum is generally lower than that of 0.05 ng/ml. When infection occurs, the content of serum procalcitonin changes at any time [24]. When the symptoms of sepsis are severe, the content of procalcitonin released into the blood is high. When the symptoms of sepsis are mild, the amount of procalcitonin released into the blood is relatively low. Assicot and his colleagues first proposed PCT as a potential biomarker of sepsis and infection in 1993. Some scholars have shown that the advantage of PCT as a biomarker to predict infection lies in its high stability in vitro, and the serum level can increase within 2-3 hours after infection [25]. The study of Wallihan et al. showed that the areas under the ROC curve of PCT predicting sepsis positive blood culture and negative blood culture were 0.96 and 0.89, respectively [26], indicating that PCT can early predict, so as to take effective diagnosis, treatment, and nursing measures in time. Although PCT is closely related to infection, its specificity for infection is not complete [27]. There is evidence that when patients suffer from trauma or other diseases, the value of PCT can also slightly increase [28]. Therefore, it is impractical to use PCT concentration alone to diagnose sepsis. Generally speaking, when the serum PCT content is higher than 2.0 ng/ml, the risk of sepsis or septic shock increases significantly. When the PCT content is between 0.5 and 2.0 ng/ml, the risk rate is at a medium level. When the PCT content is less than 0.5 ng/ml, the risk rate of sepsis is very low. According to the results of a meta-analysis conducted by Jiaqiong et al., the sensitivity and specificity of PCT in the diagnosis of sepsis are 77% and 79%, respectively, and the diagnostic value is poor [29]. Therefore, when using PCT to predict sepsis or diagnose sepsis, it is necessary to make a comprehensive judgment combined with the clinical characteristics of patients and other experimental indicators. CRP is often used in the early diagnosis of infectious diseases [30, 31]. Therefore, this paper studies the diagnostic value of procalcitonin (PCT) combined with C-reactive protein (hs-CRP) in the diagnosis of bacterial bloodstream infection and its significance for the prognosis of patients. There are some limitations to this study. First, the sample size of this study is not large, and it is a single-center study, so bias is inevitable. In future research, we will carry out multicenter, large-sample prospective studies, or more valuable conclusions can be drawn.



In conclusion, there were significant differences in the levels of PCT and CRP between gram-positive bacteria and gram-negative bacteria. PCT and CRP have high diagnostic value in predicting the short-term prognosis of patients. PCT and CRP assist clinical diagnosis and guide treatment and play a positive role in early treatment and prognosis evaluation of patients.

## Data Availability

No data were used to support this study.

## Conflicts of Interest

The authors declare that they have no conflicts of interest.

## References

- [1] W. V. Kern and S. Rieg, "Burden of bacterial bloodstream infection—a brief update on epidemiology and significance of multidrug-resistant pathogens," *Clinical Microbiology and Infection*, vol. 26, no. 2, pp. 151–157, 2020.
- [2] D. J. Diekema, P. R. Hsueh, R. E. Mendes et al., "The microbiology of bloodstream infection: 20-year trends from the SENTRY antimicrobial surveillance program," *Antimicrobial Agents and Chemotherapy*, vol. 63, no. 7, article e00355-19, 2019.
- [3] P. K. Patel, A. Gupta, V. M. Vaughn, J. D. Mann, J. M. Ameling, and J. Meddings, "Review of strategies to reduce central line-associated bloodstream infection (CLABSI) and catheter-associated urinary tract infection (CAUTI) in adult ICUs," *Journal of Hospital Medicine*, vol. 13, no. 2, pp. 105–116, 2018.
- [4] V. G. Fowler, A. F. Das, J. Lipka-Diamond et al., "Exebacase for patients with *Staphylococcus aureus* bloodstream infection and endocarditis," *The Journal of Clinical Investigation*, vol. 130, no. 7, pp. 3750–3760, 2020.
- [5] M. Falcone, M. Bassetti, G. Tiseo et al., "Time to appropriate antibiotic therapy is a predictor of outcome in patients with bloodstream infection caused by KPC-producing *Klebsiella pneumoniae*," *Critical Care*, vol. 24, no. 1, pp. 1–12, 2020.
- [6] Y. L. Li, L. C. Zhai, J. H. Ji, and L. Y. Liu, "Detection of combined procalcitonin and c-reactive protein applied in the diagnosis of bacterial infections," *Journal of Biological Regulators and Homeostatic Agents*, vol. 31, no. 1, pp. 177–181, 2017.
- [7] S. M. Aloush and F. A. Alsaraireh, "Nurses' compliance with central line associated blood stream infection prevention guidelines," *Saudi Medical Journal*, vol. 39, no. 3, pp. 273–279, 2018.
- [8] Y. Leng, C. Chen, Y. Zhang, C. Luo, and B. Liu, "Ability of serum procalcitonin to distinguish focus of infection and pathogen types in patients with bloodstream infection," *Annals of Translational Medicine*, vol. 7, no. 7, p. 135, 2019.
- [9] N. M. Kargaltseva, V. I. Kotcherovets, A. Y. Mironov, O. Y. Borisova, and A. T. Burbello, "Inflammation markers and bloodstream infection (review of literature)," *Klinicheskaia Laboratornaia Diagnostika*, vol. 64, no. 7, pp. 435–442, 2019.
- [10] P. Liang and F. Yu, "Value of CRP, PCT, and NLR in prediction of severity and prognosis of patients with bloodstream infections and sepsis," *Frontiers in Surgery*, vol. 9, no. 1, p. 34, 2022.
- [11] S. Xiaolei, Z. Rui, and F. Kaiyu, "The value of IL-17, PCT/ALB and mHLA-DR in evaluating the condition and prognosis of elderly patients with multi-drug resistant *Acinetobacter baumannii* infection," *People's Liberation Army Medical Journal*, vol. 33, no. 11, pp. 72–75, 2021.
- [12] W. H. Hahn, J. H. Song, H. Kim, and S. Park, "Is procalcitonin to C-reactive protein ratio useful for the detection of late onset neonatal sepsis?," *The Journal of Maternal-Fetal & Neonatal Medicine*, vol. 31, no. 6, pp. 822–826, 2018.
- [13] H. H. Liu, M. W. Zhang, J. B. Guo, J. Li, and L. Su, "Procalcitonin and C-reactive protein in early diagnosis of sepsis caused by either Gram-negative or Gram-positive bacteria," *Irish Journal of Medical Science (1971-)*, vol. 186, no. 1, pp. 207–212, 2020.
- [14] B. Gutiérrez-Gutiérrez, I. Morales, S. Pérez-Galera et al., "Predictive value of the kinetics of procalcitonin and C-reactive protein for early clinical stability in patients with bloodstream infections due to gram negative bacteria," *Diagnostic Microbiology and Infectious Disease*, vol. 93, no. 1, pp. 63–68, 2019.
- [15] M. Bassetti, A. Russo, E. Righi et al., "Role of procalcitonin in bacteremic patients and its potential use in predicting infection etiology," *Expert Review of Anti-Infective Therapy*, vol. 17, no. 2, pp. 99–105, 2019.
- [16] Y. Bamba, H. Moro, N. Aoki et al., "Increased presepsin levels are associated with the severity of fungal bloodstream infections," *PLoS One*, vol. 13, no. 10, article e0206089, 2018.
- [17] M. F. Lin, B. Sun, Z. Y. Liu, P. Tang, L. J. Zhang, and Y. Y. Wang, "Evaluation of the clinical diagnostic value of traditional inflammatory markers and novel biomarkers in intracellular bacterial bloodstream infections," *Cytokine*, vol. 136, article 155238, 2020.
- [18] Q. Shukun, L. Jianhua, and L. Rui, "The value of serum PCT, CRP and NLR in evaluating the bacterial types of patients with bloodstream infection and its effect on prognosis," *Labelled Immunoassay and Clinical Application*, vol. 29, no. 1, pp. 11–14+18, 2022.
- [19] H. Dengju and X. Saiping, "Significance of serum IAP and CRP levels in patients with acute appendicitis," *Continuing Medical Education in China*, vol. 13, no. 30, pp. 130–134, 2021.
- [20] C. T. Lin, J. J. Lu, Y. C. Chen, V. C. Kok, and J. T. Horng, "Diagnostic value of serum procalcitonin, lactate, and high-sensitivity C-reactive protein for predicting bacteremia in adult patients in the emergency department," *PeerJ*, vol. 5, p. 4094, 2017.
- [21] R. F. Shan, Y. A. Zhu, J. Qin, and J. P. Chen, "Traditional Chinese medicine for septic patients undergoing ulinastatin therapy," *Medicine*, vol. 100, no. 38, p. e27151, 2021.
- [22] J. F. Jones, J. Le, and K. C. Lee, "Effect of antidepressant use on length of hospitalization in patients on anti-infective therapy," *Journal of Psychiatric Research*, vol. 134, pp. 97–101, 2021.
- [23] A. Baruah and N. Paul, "Abnormal platelet count as a prognostic indicator in community-acquired pneumonia in children," *Indian Journal of Child Health*, vol. 8, no. 2, pp. 84–89, 2021.
- [24] F. H. Obaid, M. M. Ahmed, M. S. Ali, and A. A. Jasim, "The role of procalcitonin and neutrophil CD64 in non culture-based diagnosis of neonatal and infantile septicemia," *International Journal*, vol. 3, no. 6, p. 574, 2020.
- [25] O. B. Ojuawo, A. E. Fawibe, O. O. Desalu et al., "Clinical utility of serum procalcitonin in adult patients admitted with community-acquired pneumonia in Ilorin, Nigeria," *Journal of the Pan African Thoracic Society*, vol. 2, no. 2, pp. 77–84, 2021.



- [26] R. G. Wallihan, N. M. Suárez, D. M. Cohen et al., “Molecular distance to health transcriptional score and disease severity in children hospitalized with community-acquired pneumonia,” *Frontiers in Cellular and Infection Microbiology*, vol. 8, p. 382, 2018.
- [27] R. Méndez, R. Menéndez, C. Cillóniz et al., “Initial inflammatory profile in community-acquired pneumonia depends on time since onset of symptoms,” *American Journal of Respiratory and Critical Care Medicine*, vol. 198, no. 3, pp. 370–378, 2018.
- [28] H. Nishikawa, M. Shirano, Y. Kasamatsu et al., “Comparison between procalcitonin and C-reactive protein in predicting bacteremias and confounding factors: a case-control study,” *Clinical Chemistry and Laboratory Medicine (CCLM)*, vol. 55, no. 7, pp. 1043–1052, 2017.
- [29] L. Ljungström, A. K. Pernestig, G. Jacobsson, R. Andersson, B. Usener, and D. Tilevik, “Diagnostic accuracy of procalcitonin, neutrophil-lymphocyte count ratio, C-reactive protein, and lactate in patients with suspected bacterial sepsis,” *PloS one*, vol. 12, no. 7, p. 0181704, 2017.
- [30] L. Ying, R. Lin, and C. Hongfei, “Application of combined test of whole blood C-reactive protein and blood routine in the diagnosis of bacterial infectious diseases,” *Quality Safety and Inspection*, vol. 32, no. 1, pp. 103–104, 2022.
- [31] Y. Ting, “Expression and clinical significance of serum PCT, CRP and WBC in patients with severe bacterial infectious diseases,” *Chinese Medical Engineering*, vol. 29, no. 12, pp. 132–134, 2021.

## Research Article

# Extraction and Analysis of Foot Bone Shape Features Based on Deep Learning

Yue Ma<sup>1,2</sup> and Zhuangzhi Zhi<sup>3</sup> 

<sup>1</sup>School of Forensic Science, Criminal Investigation Police University of China, Shenyang 110854, China

<sup>2</sup>Key Laboratory of Impression Evidence Examination and Identification Technology, Ministry of Public Security, Shenyang 110854, China

<sup>3</sup>School of Medical Instrument, Shenyang Pharmaceutical University, Shenyang 110016, China

Correspondence should be addressed to Zhuangzhi Zhi; 106040101@syphu.edu.cn

Received 10 June 2022; Revised 14 July 2022; Accepted 21 July 2022; Published 10 August 2022

Academic Editor: Hangjun Che

Copyright © 2022 Yue Ma and Zhuangzhi Zhi. This is an open access article distributed under the Creative Commons Attribution License, which permits unrestricted use, distribution, and reproduction in any medium, provided the original work is properly cited.

With the rapid development of artificial intelligence, more and more researchers and research institutions begin to pay attention to the bone feature recognition field. Human bone movement is very complex, and human bone shape recognition technology can be widely used in medical treatment, sports, and other fields. At present, there are mainly two kinds of methods for extracting the shape features of human foot bone based on optical image acquisition technology and sensor information perception technology. However, due to the interference factors such as target posture change, camera shake, and individual behavior differences, it is still a very challenging task to design a robust algorithm for extraction and analysis of foot bone shape features. In recent years, convolutional neural network- (CNN-) based foot contour feature recognition methods emerge one after another and have made breakthrough progress. How to use and how to fully explore the potential relationship of various characteristics contained in the foot bone data and how to enhance the robustness of view changes and other aspects need to be further studied. In this context, this paper proposed an improved CNN model, which not only has the capability of deep feature extraction of the CNN model but also can obtain the optimal model parameters with the combination of particle swarm optimization algorithm. The effectiveness of the proposed method in the extraction and analysis of foot bone shape features is verified in the simulation experiment.

## 1. Introduction

With the development of science and technology, human body skeleton recognition in the field of artificial intelligence has been a very hot research topic, and the position of the human skeleton is extracted and identified in the image, so as to track the human body and identify, analyze, and judge the human actions. Human motion recognition is a subject involving many fields [1, 2]. Nowadays, people can sense and capture movement information through the eyes, head, ears, and other organs, extract the obtained information in the brain, and finally input it into the computer for movement recognition and judgment. The human action recognition algorithm imitates the human action recognition process, automatically detects the human action from the

action sequence data collected by various sensors, analyzes the human action, and deduces its semantic information. However, the law of human movement is highly complex, especially the simulation of human movement coordination mechanism being very difficult, so the development of science and technology is still unable to generate very realistic movement data based on algorithms or other ways [3]. Motion capture technology still plays a very important role in medical film and television scenes and can overcome the problems of high complexity and high nonlinear simulation mechanisms.

Motion recognition technology based on human bone points can be widely used in public security, intelligent home, wisdom classroom, and other fields. (1) Public security: this includes airports, stations, and other crowded

public areas, for the installation of monitoring equipment systems [4, 5]. Once suspected criminals are found and some unconventional behaviors are identified by the system, the public security organs can get alarm information and immediately send police to control criminals, avoid the spread of criminal activities, and protect people's personal and property safety. Human motion monitoring technology based on bone recognition can expand the early warning range of public monitoring and relieve the pressure of public security. (2) Smart home: human motion recognition systems can also be combined with the Internet of Things devices, becoming a basic technology in smart homes. Intelligent control of household equipment can be realized by recognizing human movement. It also can realize home monitoring; once the elderly and children fall, it will immediately send a message to inform the family to deal with it. Once there is an intruder, it can also carry out intelligent alarm tracking, to ensure the safety of the family property. (3) Intelligent class: students' performance and behaviors in class can be classified and counted to analyze the teaching state and classroom atmosphere in each period of class. Schools and teachers take it as a reflection of teaching quality and then carry out teaching policy improvement to improve teaching quality.

Among them, the traditional target detection algorithm, the recognition, detection, and tracking of human bone movement belongs to the low-level processing mode of machine vision, and this kind of algorithm does not need to carry out a large number of training data sets. The recognition of human bone movement is a more advanced stage. The detection of the action of the testee is the key to visual processing. Many scholars have proposed mature algorithms for the solution of action recognition and detection. In the traditional field, human target detection methods include background subtraction, frame difference, and optical flow. These methods are mainly used for tracking through matching and motion characteristics. Using deep learning, the method of human-computer interaction is in the advanced processing stage. The human motion detection and motion analysis-related technologies of this kind of algorithm are in the hot spot of exploration and research [6]. In the traditional field, human target detection methods include background subtraction, frame difference, and optical flow. These methods are mainly used for tracking through matching and motion characteristics. In using deep learning, the method of human-computer interaction is in the advanced processing stage. The core technology hidden behind this kind of human motion detection and analysis method is the hot spot and difficult point of academic and industrial research. Researchers collect bone characteristics from smart devices to monitor human health and physical training and track the lives of older adults. Intelligent devices to detect bone features have been widely used in people's daily life and social production. Using deep learning, the human-computer interaction method for bone feature detection and analysis of the relevant technology is the focus of exploration and research [7].

In human life activities, walking is the most common behavior of the human body, and the body posture change presented in the process of walking is called gait. It is decep-

tively simple but involves the precise coordination of multiple tissues and organs throughout the body [8]. Among them, the brain generates the intention to walk, and the central nervous system decomposes the intention and transmits control information to the muscle tissues involved in the movement. Each muscle tissue generates joint torques through contraction, thus driving the limb bones to complete the walking action. Obviously, in this series of information transmission and drive control process, gait contains abundant mechanism characteristics and life system mystery of the human body. The in-depth analytical study of human foot bone movement and the discovery of useful characteristic information have important guiding significance for the development of lower limb exoskeleton robot project and the application based on foot bone characteristics. For a long time, people are constantly exploring and studying their own foot bone movement [9]. Humans have been studying their own walking movements for centuries, but due to the limitations of science at the time, the earliest studies of foot bone characteristics were only a few lines of written records. Subsequently, with the advent of sensors, computers, and other modern instruments, the research on foot bone characteristics has gradually become scientific. At the same time, the in-depth study of foot bone also promotes the rapid development of information science, which is closely related to human biology. Based on the previous theoretical research and coupled with advanced instruments and equipment, now, the study of foot bone characteristics can be more and more in-depth [10].

As a key technology in artificial intelligence, feature fusion technology has great innovation space and application value, attracting more and more enterprises and research institutions. From the perspective of motion recognition, human skeleton recognition can be roughly divided into posture data acquisition, skeleton dynamic data acquisition, and key posture mining. To meet the requirements of personal information security, the foot bone movement in posture characteristics is regarded as a collection of hard connected segments between the nodes of the human physiological skeleton. At present, various organizations and well-known universities have spent a lot of energy and time on the research of this technology [11, 12]. In order to give full play to the advantages of depth image and bone data, the depth feature is combined with the foot bone feature for human behavior recognition. The method of human behavior extraction based on feature fusion is studied to capture behavioral cues in depth images and extract the combined features of human behavior. Then, using skeletal data to extract various features of foot bone shape achieves results only related to behavioral distribution, but it takes a long time. Some scholars also proposed the iterative learning control algorithm to track human foot bone joint and knee feature extraction method, combined with human lower limb structure analysis, to establish the dynamic model of lower limb exoskeleton robot [13]. Therefore, how to use the deep learning model to extract and analyze the shape features of human foot bone has important theoretical value and practical application prospect. Here, the layout of this paper is the following: Section 2 gives the related works;

then, the proposed method is shown in Section 3. After that, the simulation results are introduced in Section 4. Finally, Section 5 concludes the article.

## 2. Related Work

Under the guidance of image processing and machine vision technology, the development of foot bone feature recognition technology not only has universal market value and huge economic value in medical monitoring, elderly monitoring, and motion analysis but also has academic research significance [14, 15]. Due to the high research value of human skeleton recognition in many aspects, a large amount of investment has been stimulated at home and abroad. In recent years, whether the government or enterprises, people from all walks of life in the field of human behavior identification investment in a large number of human, financial, and material resources so far have made rich achievements. Human motion recognition can extract the key features of human motion by obtaining the video sequence of human motion. After years of research, researchers have conducted an in-depth exploration of human motion recognition algorithms, formed a number of research directions, and achieved a lot of valuable results. According to the different human motion features adopted by the algorithm, human motion recognition can be divided into the following categories. The following is a brief introduction based on the existing research results.

(1) Foot bone feature recognition is based on human body structure features. The human body structure can be expressed as the trunk and limbs connected by joints. An action video sequence can be seen as the combination of different human poses generated by the relative displacement of different body parts in a certain time range. The motion representation features are extracted from the three-dimensional bone point information of the human body. The common steps include human motion detection, bone point information extraction, bone point information description, extraction of relevant features, and classification of human motion. (2) Foot motion recognition is based on global features. Global feature refers to the feature that represents the action in the whole sequence, which is usually the spatial change of the whole sequence with spatiotemporal information. The first is to identify the region of interest, the use of target detection, and other ways to identify the human body region, and then, through the region of the posture trajectory and other related information, the human movement of the region of interest is described and finally realizes the human bone movement recognition. (3) Human foot bone motion recognition is based on local structural features. Local features of the human body refer to the local parts of the body that change significantly, such as the arm and neck, through the characteristics of these parts to characterize the whole movement. The motion recognition algorithm based on local structural features firstly extracts the human motion features from video sequences, then describes the feature points with appropriate descriptors, calculates the local body features, and finally establishes a classifier to recognize human actions [16, 17].

Motion captures data in animation; film production has the real nature of the task action, can make the movie role more vivid, and is the basis of high-quality animation and special effects. And the motion data in this application field will still be an important part, but motion capture equipment is expensive, the motion capture process is complex and tedious, and there is motion data processing workload and other shortcomings. In order to improve the utilization of motion capture data, in recent years, human motion data prediction, motion sequence fragment transition, and other technologies emerged. The main prediction methods of human movement data include deep learning models based on adversarial neural network and recurrent neural network as well as traditional methods [18]. The transition technology models of motion sequence fragments mainly include probability statistics, motion graph, and deep learning. For the transition model of motion sequence fragments, in order to make full use of the reusability of motion data, several short or moving sequence fragments can be spliced together to generate a long moving sequence with complex semantics. If the sequence of walking and running, which have different postures and semantics, is directly spliced together, there will be a very stiff sliding step and space jump of movement track, and the human eye is very sensitive to this difference. Compared with foreign countries, domestic research on human behavior recognition started a little later, but many domestic universities and research institutions have made some achievements in this area [19]. At present, domestic research institutions have gradually reached the development level of the foreign research field, and some of them can be used as commercial systems. Some famous conferences and international authoritative journals have opened relevant columns on human bone behavior recognition, which provides a platform for communication for the majority of enthusiasts and will greatly promote the rapid development of behavior recognition. Major conferences and journals include PAMI (IEEE Transactions on Pattern Analysis and Machine Intelligence), Image and Vision Computing (IVC), and Computer Vision and Image Understanding (CVIU). Although the above methods have achieved a lot in the extraction and analysis of foot bone shape features, these methods are all shallow models, and the relevant research on the deep learning model will be introduced next.

The deep learning method is the preferred model for image processing, image recognition, and classification system [19]. Neural networks are widely used in recognition systems, natural language processing, and recognition. Compared with traditional detection methods, the main advantage of the neural network is that it can be detected automatically without any human supervision and it also has high computational efficiency. Its algorithm using the convolution layer and pooling layer is very simple and can be applied to other instances only by adjusting its parameters appropriately. This enables the neural network model to run on other devices, which makes the neural network have universal applicability. However, the convolutional neural network (CNN) algorithm cannot deal with continuous time series, which greatly increases the limitations of the convolutional neural network algorithm. Among deep learning

algorithms, the most mature algorithm at present is the CNN algorithm, which is widely used and can be said to be the most popular deep learning architecture at present, which greatly improves the huge popularity and effectiveness of deep learning [20]. At present, human skeleton motion detection is most widely used by machine vision technology and digital image processing technology. Deep learning can directly learn two-dimensional images without changing the structure of image nodes, which can greatly reduce a lot of manual processing of image input and can achieve comprehensive automation without excessive human participation, and the learning process is completely completed by the system itself. Deep learning has been widely used in various fields of image recognition, such as target line recognition of license plate recognition of face recognition of wood and so on. The deep learning method not only has good learning ability but also can accurately extract the recessive features that reflect the essence of input sequence and accurately identify detection objects [21]. Therefore, it has the characteristics of fast discrimination, high cost performance, simple operation, and safety, which greatly improves the process of automatic recognition of human movements. Therefore, it can be applied to the research of foot bone feature extraction and recognition.

At present, the traditional bone feature recognition methods include the optical flow method and frame difference method, but these methods cannot complete the detection and recognition of complex actions, and their low efficiency and high misjudgment rate cannot meet the needs of the market. In order to enable intelligent equipment to efficiently identify human movements and check the standardization of movements, deep learning can be used for processing [22]. The combination of human behavior recognition and human movement detection methods will greatly improve the accurate recognition of human bone movement, promote the development of factory movement detection related fields, and ultimately improve the economic benefits of enterprises. Human bone feature recognition and analysis of human activities have always been the field of computer vision, machine learning, and artificial intelligence. Human motion analysis is a complex video-based processing process that captures both single frame position information and dynamic motion features. It can realize automatic understanding and analysis of data by computer through human-computer interaction and establish relationships between data related to low-level and high-level semantic operations. However, in real-world application scenarios, surveillance cameras usually have multiple perspectives, which will result in great differences for intelligent devices such as computers to understand and process scene content from different perspectives. At the same time, it is urgent to evaluate the mobile status of equipment with secure and real-time performance [23]. Therefore, the robustness, accuracy, and effectiveness of the method to evaluate human skeletal state are important challenges for future research. In order to realize the spatial information analysis of the skeleton by computer, some scholars proposed the ST-GCN network. ST-GCN represents the skeleton array of the spatiotemporal graph network (ST-GCN) on the spatiotemporal graph network (ST-GCN) and

designs the motion recognition model by extending the graph network. The model is based on the skeleton diagram, and each node is associated with the joints of the human body. This model is mainly divided into two types, and each model has an edge structure. An edge corresponds to the natural connection of every two bone nodes in the spatial domain, and a temporary edge is connected to each other in a continuous time step. On this basis, the author constructs the graph convolution of multilayer space and time to combine the length information of the graph with the time information, which greatly improves the recognition rate of the network [24]. Some scholars proposed an end-to-end framework called the memory network as the center to enhance the spatial and temporal features of foot bone feature recognition. In the framework of the model, the module is temporarily modified to redefine the time focus of the bone wheel of the action line, and the powerful space-time convolution module of CNN is used to redefine the space-time relationship of human activities. It can obviously improve the accuracy of skeleton-based action recognition. Based on the above discussions, we give the main contributions of this work.

- (1) In this paper, the deep learning model is applied to the extraction and analysis of foot bone features for the first time, and good experimental results have been achieved
- (2) In this paper, the multiobjective optimization algorithm is used to select the optimal model parameters and further improve the performance of the model, so it has good theoretical value and application prospect

### 3. Optimized CNN for Extraction and Analysis of Foot Bone Shape Features

**3.1. Deep CNN Model Introduction.** CNN adds the convolution layer and pooling layer to form the deep CNN model, which is shown in Figure 1.

The calculation process of convolution is shown below:

$$\text{CONV}_{(ij)} = \sum_i^{m-1} \sum_j^{n-1} u_{ij} \times w + b \quad (i = 1, 2 \dots m-1, j = 1, 2 \dots n-1), \quad (1)$$

where  $u_{ij}$  is the input image,  $m$  and  $n$  are the size of the input image,  $w$  is the size of the convolution kernel, and  $b$  is the bias constant of the convolution kernel.  $\text{CONV}_{(ij)}$  is the characteristic graph output after convolution operation.

CNN adds an activation function layer to the network and analyzes the model better by adopting the feature mapping method of nonlinear function. Then, the mathematical expression of common activation function is introduced one by one as

$$f(x) = \frac{1}{1 + e^{-x}}. \quad (2)$$



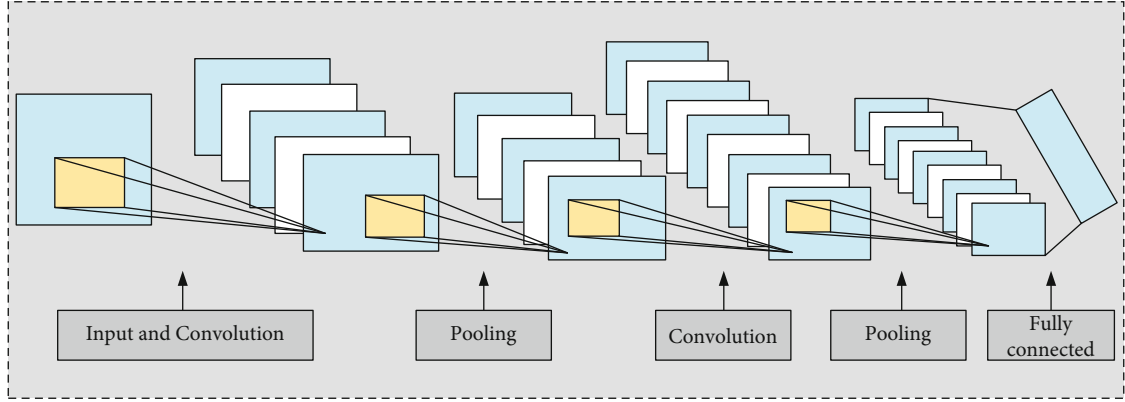


FIGURE 1: The typical schematic diagram of CNN neural network.

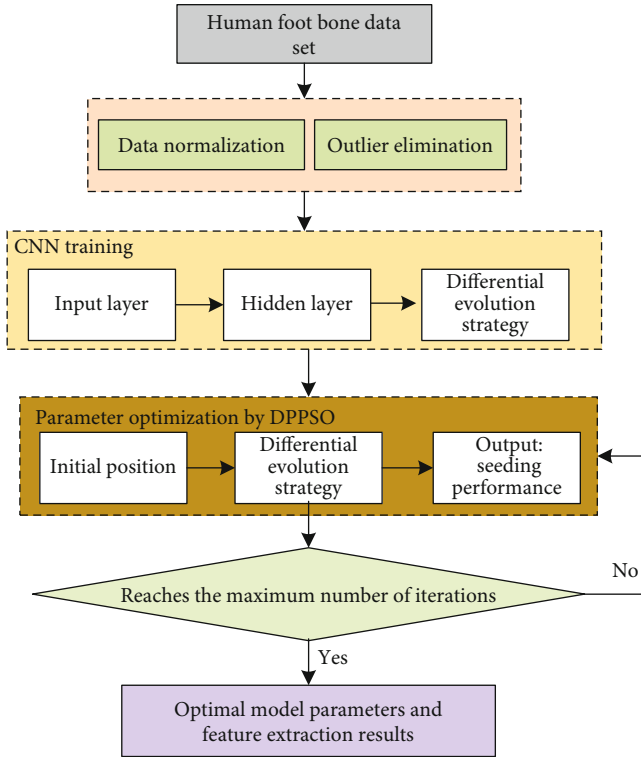


FIGURE 2: The framework of the CNN-based foot bone shape feature extraction and analysis method.

In addition to the above activation functions, other common activation functions are as follows: the mathematical expression of tanh function is

$$f(x) = \frac{e^x - e^{-x}}{e^x + e^{-x}}. \quad (3)$$

The mathematical expression of ReLU function is

$$f(x) = \max(0, x). \quad (4)$$

The full name of the ReLU function is the rectified linear

unit. The function is one of the commonly used activation functions, which is characterized by low computational complexity and no exponential operation. However, it is worth explaining that ReLU function has certain defects in the calculation process. When the data passes through the negative range of ReLU function, the output value is equal to 0. The Leaky-ReLU function can solve the above problem:

$$f(x) = \begin{cases} x, & x \geq 0, \\ \alpha x, & x < 0. \end{cases} \quad (5)$$

The corresponding equations of sig and tanh are as follows:

$$\begin{cases} \text{sig}(x) = \frac{1}{1 + \exp(-x)}, \\ \tanh(x) = \frac{\exp(x) - \exp(-x)}{\exp(x) + \exp(-x)}, \end{cases}$$

$$h_{w,b}(x_i) = \begin{bmatrix} p(y_i = 1|x_i; w, b) \\ p(y_i = 2|x_i; w, b) \\ p(y_i = 3|x_i; w, b) \\ \vdots \\ p(y_i = n|x_i; w, b) \end{bmatrix} = \frac{1}{\sum_{j=1}^n e^{w_j x_i + b_j}} \begin{bmatrix} e^{w_1 x_i + b_1} \\ e^{w_2 x_i + b_2} \\ e^{w_3 x_i + b_3} \\ \vdots \\ e^{w_n x_i + b_n} \end{bmatrix}. \quad (6)$$

The cross-entropy (CE) formula is as follows:

$$\text{loss} = -\frac{1}{m} \sum_{j=1}^m \sum_{i=1}^n y_{ji} \log(\hat{y}_{ji}). \quad (7)$$

The original form of the gradient descent method is shown below:

$$\theta := \theta - \alpha \frac{\partial}{\partial \theta} J(\theta). \quad (8)$$

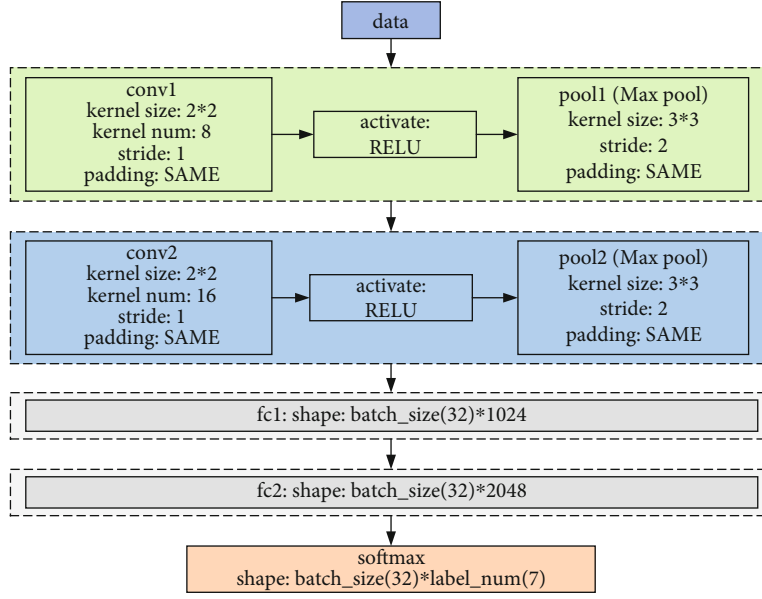


FIGURE 3: The CNN model setting in this paper.

The mathematical expression of a common Adam optimizer is given as

$$\begin{aligned} m_t &= \beta_1 m_{t-1} + (1 - \beta_1) g_t, \\ v_t &= \beta_2 v_{t-1} + (1 - \beta_2) g_t^2. \end{aligned} \quad (9)$$

**3.2. Optimized CNN Model.** Since conventional CNNs are prone to local optimality, particle swarm optimization (PSO) is simple and easy to solve, but it is prone to local extreme points, low accuracy, slow convergence, and stagnation. In this section, the differential perturbation is introduced into the PSO to form the differential perturbation particle swarm optimization (DPPSO) algorithm, which makes use of the advantages of fast convergence speed and good global performance of difference, overcomes the shortcomings of low precision and local optimality caused by the use of PSO, and builds an optimized CNN model. The multiobjective optimization model is

$$\begin{aligned} &\min f_1(x_1, x_2), \\ &\max f_2(x_1, x_2) \\ &\text{s.t. } p_1 < g_1(x_1, x_2) < q_1 \\ &\quad p_2 < g_2(x_1, x_2) < q_2 \\ &\quad p_3 < g_3(x_1, x_2) < q_3 \\ &\quad p_4 < g_4(x_1, x_2) < q_4, \\ &120 < x_1 < 180, \\ &120 < x_2 < 180, \end{aligned} \quad (10)$$

where  $f_1$  represents energy consumption target,  $f_2$  represents the output target, and  $g_1, g_2, g_3, g_4$  represent the packaging quality of 4 indicators: crushing strength, wear

strength, drop strength, and compressive strength, respectively. It is worth noting the fusion mechanism of deep learning and differential perturbation particle swarm optimization (DPPSO) algorithm can be seen in Figure 2.

Based on the above discussions, the optimized deep neural network and its application in extraction and analysis of foot bone shape features are shown in Figure 2. It mainly includes data preprocessing, CNN model training and testing, and DPPSO algorithm design, finally getting the optimal model performance.

## 4. Experimental Results and Analysis

**4.1. Experimental Data Introduction.** In recent years, human bone recognition technology has developed rapidly. Many researchers at home and abroad have carried out the research and application of human behavior recognition in different scenarios. Although there are differences in database and behavior recognition model, human behavior recognition technology is similar. The database in this paper mainly comes from depth sensors. The pixel value in the depth data represents the depth value, which is used to represent the distance between the camera and the object. The larger the value, the darker the distance will appear in the image. The smaller the value, the smaller the distance, and the brighter the display.

Firstly, the motion sequence is obtained by a sensor and then preprocessed by a computer (such as gray-scale morphological processing and denoising). Then, some coding mode is used to write the preprocessed data to describe its action characteristics. Finally, a classifier is used to train and test behavior categories, among which data acquisition and data pretreatment belong to the category of data pretreatment, and feature extraction behavior classification and understanding belong to the category of pattern recognition. In this paper, bone data from MSR-

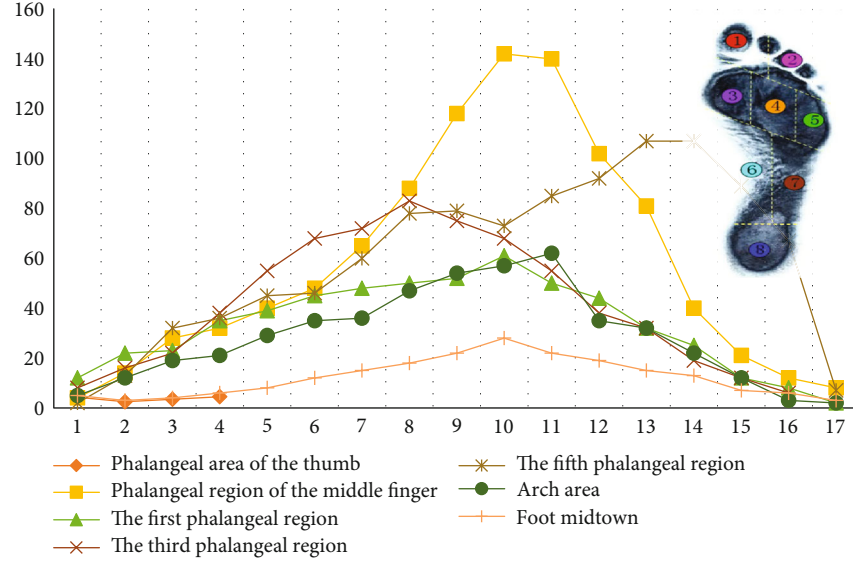


FIGURE 4: Multisensor foot bone pressure acquisition signal.

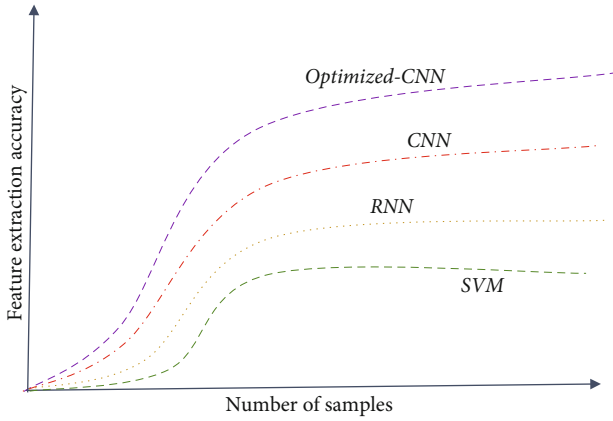


FIGURE 5: Comparison of feature extraction accuracy of CNN before and after optimization.

Action3D, UTkinect-Action, and Flerence3D-Action databases were used in the experiment. It is worth noting that the framework system of the CNN model applied in this paper is shown in Figure 3.

**4.2. Experimental Result Analysis.** In order to obtain more comprehensive information on foot bone, according to the human anatomy and the distribution of foot pressure, the human sole was divided into regions, and flexible pressure measuring units were placed in these regions to form a multisensor foot pressure detection system. Within a gait cycle, the statistical variation of pressure signals in different areas is shown in Figure 4.

In a complete gait detection cycle, the pressure sensor of the multipoint array can only collect the foot pressure signals of local corresponding regions in different gait periods due to the influence of the special touch form of the foot. For example, the sensor in the heel area can only record

the pressure signal during the gait touching the ground, but when the heel leaves the ground, it cannot continue to collect the pressure signal effectively. A similar situation exists in other sensors. At the same time, the overlap between the signal and redundancy also increases the detection system in the burden of data transmission, processing, and storage; for the foot, eight areas of the pressure sensor have optimized configuration and are made with the best sensor array location with the least number of sensors, to maximize the amount of information limited to collect signals and finally get the ideal detection results.

This paper also compares the graph convolutional network (GCN) before and after optimization, and the experimental database and sample selection are consistent with the previous section. The optimized GCN network contains 10 layers, including 64 convolutional kernels in layers 1 to 4, 128 convolutional kernels in layers 5 to 7, and 256 convolutional kernels in the last three layers. The stride of the five and eight layers is 2, and the default value of the other layers is 1. Finally, a whole office mean pooling was connected to softmax for classification, and the learning rate was set to 0.001, and the equal interval descent method was adopted to adjust the learning rate gamma value to 0.1. The dropout value was set to 0.5, the random loss information source was prevented from overfitting, and the batch size was set to 16. Cross-entropy was still selected as the loss function evaluation, and the random gradient descent (SGD) method was used for learning optimization. Figure 5 shows the trend of feature extraction accuracy of the CNN model before and after optimization with the number of cycles. It can be seen from Figures 5(a) and 5(b) that the network reaches saturation accuracy at about 60 cycles, and the final accuracy is higher than that of the improved CNN.

Figure 6 shows the confusion matrix diagram of feature classification of the optimized CNN model in the data sets MSR-Action3D and UTkinect-Action. As can be seen from

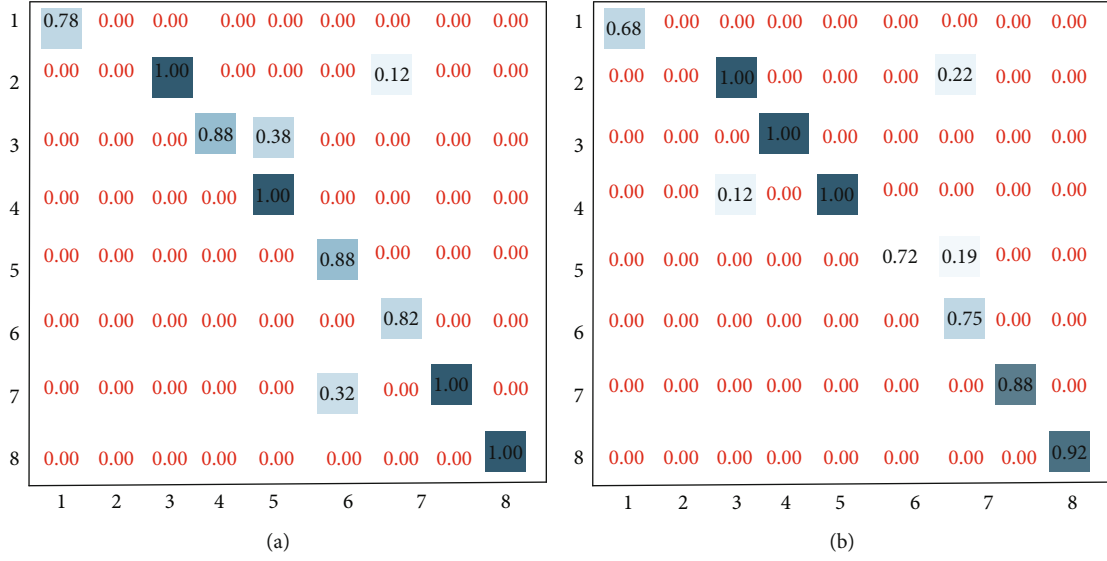


FIGURE 6: The confusion matrix diagram of feature classification of the optimized CNN model in different data sets: (a) MSR-Action3D; (b) UTkinect-Action.

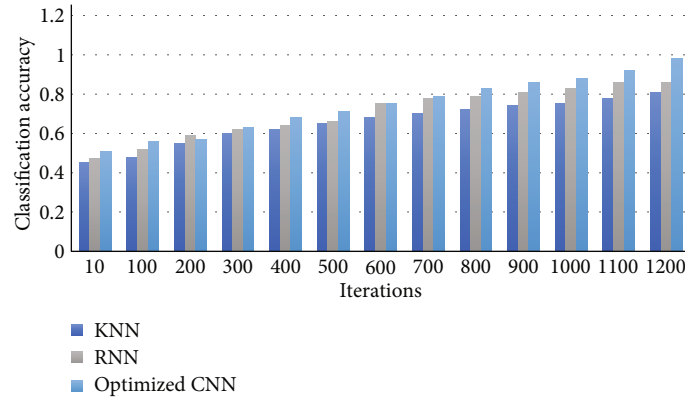


FIGURE 7: The relationship between the feature extraction accuracy and iteration times of different methods.

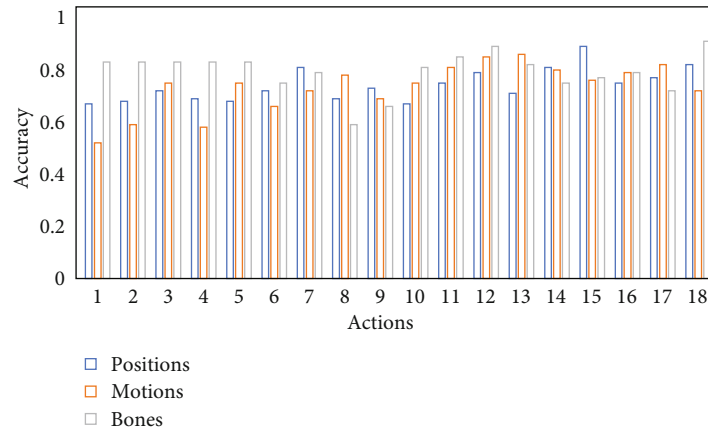


FIGURE 8: Multifeature histogram comparison.

the figure, the feature classification accuracy of the model is different for different action subsets. However, no matter in which data set, the method proposed in this paper can achieve higher accuracy of feature classification. Thus, the

stability and effectiveness of the proposed method for foot bone feature extraction are verified.

In order to further demonstrate the feature extraction accuracy of the proposed method, Figure 7 shows the

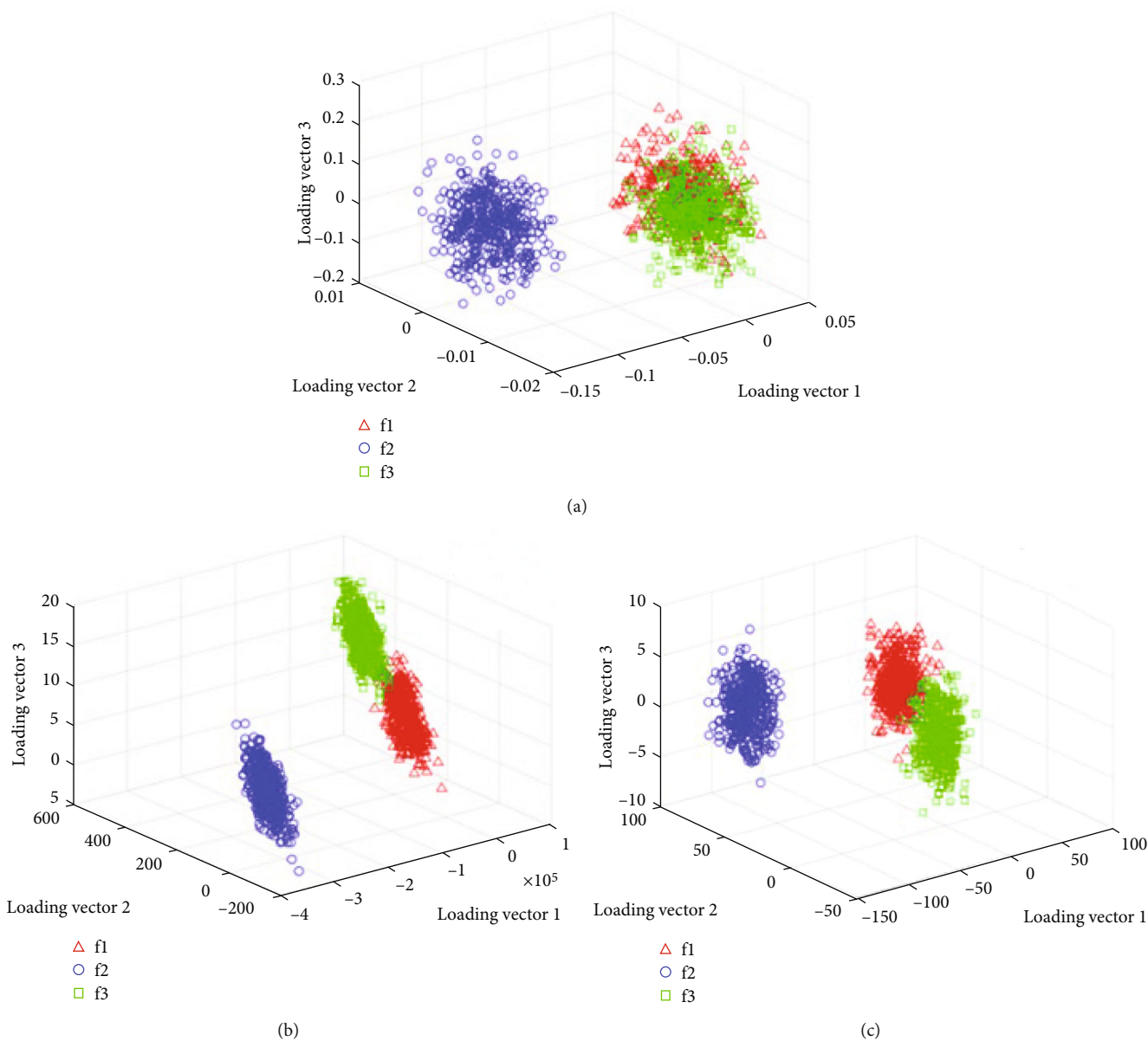


FIGURE 9: Continued.



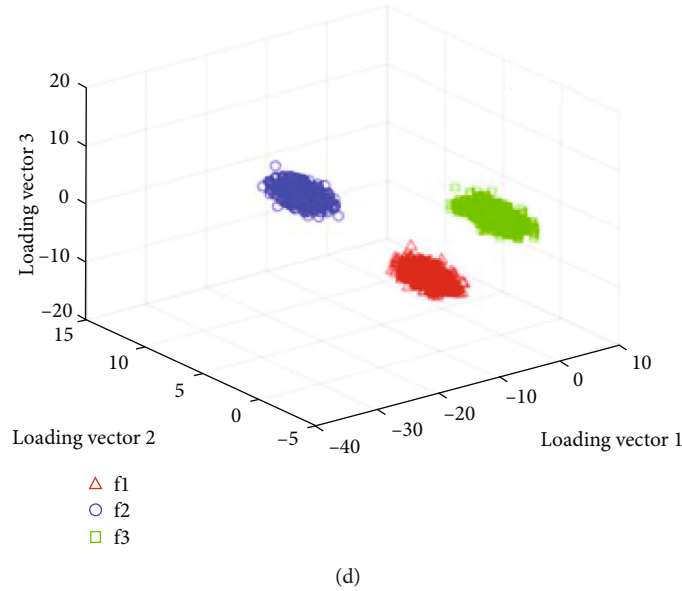


FIGURE 9: Feature classification accuracy by (a) SVM, (b) BP, (c) CNN, and (d) optimized CNN.

relationship between classification accuracy and iteration times of different methods. We can figure out from the figure, with the increase in the iteration number, that the classification performance of the three methods shows an increasing trend. When the iteration number is 1200, the three models all reach the highest classification accuracy, which is 81%, 86%, and 98%, respectively. Therefore, the improved CNN model in this paper achieves the highest feature extraction accuracy. In addition, even when the number of iterations is small, the proposed method also has the best model performance throughout the training process, which demonstrates the effectiveness of the proposed method in the foot bone feature extraction field.

In order to further show the characteristics of various features, Figure 8 shows the change of recognition accuracy of the proposed method in 18 action categories with respect to three features. The abscissa is 18 action categories, and the ordinate is the recognition accuracy. It can be found from the bar chart that different features in different action categories have good and bad recognition results. From the above observation, it can be found that motions with small amplitude and local concentration can be better discriminated by feature positions, motion tracks the bone node and motion lasting for a long time, and motions with feature motions can provide better representation. Feature bones have a relatively good recognition effect when it comes to local joint changes. The above experimental structures indicate that different bone structures may be represented by different features, and diversified features will provide richer information for bone structure discrimination. It also indicates the complementarity between different characteristics. Therefore, the above experimental results verify that it is reasonable to extract multiple features to comprehensively characterize a skeletal action in this paper.

To be noted, the classification results obtained by different methods are shown in Figures 9(a)–9(d). Specifically, there are plenty of overlaps between feature 1 (f1), feature 2 (f2), and

feature 5 (f5) in Figure 9(a), which means the SVM cannot separate the three features well. And the similar situation happens in Figures 9(b) and 9(c). In contrast, from the visual results in Figure 9(d), we know that the optimized CNN method shows no overlaps in separating the three features, which means the optimized CNN achieves the best classification performance with the least misclassification points.

## 5. Conclusions

Nowadays, artificial intelligence and computer vision technology are widely developed, and bone feature extraction, as an important branch of computer vision, is widely used in intelligent video surveillance, robot vision, and other fields. Previous work is either based on static image of human skeleton recognition, or based on the continuous motion recognition of traditional video, each frame of image background segmentation manual extraction of human backbone, and then to identify and learn, the process is too complicated, and large amount of calculation.

In view of the above problems, this paper conducted in-depth research on the extraction and analysis of human foot bone features and proposed the foot bone feature and extraction model based on the improved CNN model. This method not only has good extraction ability of foot bone features but also achieves high fault classification accuracy. The feasibility of the proposed method in human motion monitoring is verified by experiments. Future research may need to add factors such as the individual body structure and dietary habits of research subjects, so as to further improve the accuracy of foot bone feature extraction and recognition.

## Data Availability

The experimental data used to support the findings of this study are available from the corresponding author upon request.

## Conflicts of Interest

The authors declared that they have no conflicts of interest regarding this work.

## Acknowledgments


The study was funded by the following: (1) project source: University-Industry Collaborative Education Program, project name: the Training Simulation Base Construction Program for the Public Security (project number: 202102126049), and (2) project source: Special Program for Innovation Methodology of the Ministry of Science and Technology, project name: the Research and Demonstration of Innovative Approaches of Nurturing Talents with Higher Education (project number: 2020IM030100).

## References

- [1] F. Zhang, T. Y. Wu, J. S. Pan, G. Ding, and Z. Li, "Human motion recognition based on SVM in VR art media interaction environment," *Human-centric Computing and Information Sciences*, vol. 9, no. 1, pp. 1–15, 2019.
- [2] M. Wang, Y. D. Zhang, and G. Cui, "Human motion recognition exploiting radar with stacked recurrent neural network," *Digital Signal Processing*, vol. 87, pp. 125–131, 2019.
- [3] P. Wang, W. Li, P. Ogunbona, J. Wan, and S. Escalera, "RGB-D-based human motion recognition with deep learning: a survey," *Computer Vision and Image Understanding*, vol. 171, pp. 118–139, 2018.
- [4] L. Guo, Z. Lu, and L. Yao, "Human-machine interaction sensing technology based on hand gesture recognition: a review," *IEEE Transactions on Human-Machine Systems*, vol. 51, no. 4, pp. 300–309, 2021.
- [5] M. T. Wu, "Confusion matrix and minimum cross-entropy metrics based motion recognition system in the classroom," *Scientific Reports*, vol. 12, no. 1, pp. 1–10, 2022.
- [6] H. Wang, J. Shi, and X. Luo, "Swimmer's posture recognition and correction method based on embedded depth image skeleton tracking," *Wireless Communications and Mobile Computing*, vol. 2022, 12 pages, 2022.
- [7] A. Huang and J. Wang, "Wearable device in college track and field training application and motion image sensor recognition," *Journal of Ambient Intelligence and Humanized Computing*, vol. 7, pp. 1–14, 2021.
- [8] S. Bohm, R. Marzilger, F. Mersmann, A. Santuz, and A. Arampatzis, "Operating length and velocity of human vastus lateralis muscle during walking and running," *Scientific Reports*, vol. 8, no. 1, pp. 1–10, 2018.
- [9] T. Nakamura, Y. Kita, J. Fujimoto, K. Ayuzawa, and H. Ozawa, "Hyoid bone movement during swallowing and mechanism of pharyngeal residue in patients with profound intellectual and multiple disabilities," *International Journal of Pediatric Otorhinolaryngology*, vol. 149, article 110849, 2021.
- [10] M. H. Tsai, R. M. A. Wahab, and F. Yazid, "Timing of orthodontic tooth movement in bone defects repaired with synthetic scaffolds: a scoping review of animal studies," *Archives of Oral Biology*, vol. 132, article 105278, 2021.
- [11] D. Lee, W. H. Lee, H. G. Seo, B. M. Oh, J. C. Lee, and H. C. Kim, "Online learning for the hyoid bone tracking during swallowing with neck movement adjustment using semantic segmentation," *IEEE Access*, vol. 8, pp. 157451–157461, 2020.
- [12] K. P. Klein, F. P. S. Guastaldi, H. S. G. Pereira, Y. He, and S. E. Lukas, "Dronabinol inhibits alveolar bone remodeling in tooth movement of rats," *American Journal of Orthodontics and Dentofacial Orthopedics*, vol. 161, no. 3, pp. e215–e222, 2022.
- [13] Y. Zheng, Y. Wang, and J. Liu, "Analysis and experimental research on stability characteristics of squatting posture of wearable lower limb exoskeleton robot," *Future Generation Computer Systems*, vol. 125, pp. 352–363, 2021.
- [14] S. K. Das, P. Roy, and A. K. Mishra, "Recognition of ischaemia and infection in diabetic foot ulcer: a deep convolutional neural network based approach," *International Journal of Imaging Systems and Technology*, vol. 32, no. 1, pp. 192–208, 2022.
- [15] M. A. R. Ahad, M. Ahmed, A. das Antar, Y. Makihara, and Y. Yagi, "Action recognition using kinematics posture feature on 3D skeleton joint locations," *Pattern Recognition Letters*, vol. 145, pp. 216–224, 2021.
- [16] H. Wang, B. Yu, J. Li, L. Zhang, and D. Chen, "Multi-stream interaction networks for human action recognition," *IEEE Transactions on Circuits and Systems for Video Technology*, vol. 32, no. 5, pp. 3050–3060, 2022.
- [17] A. Nadeem, A. Jalal, and K. Kim, "Automatic human posture estimation for sport activity recognition with robust body parts detection and entropy markov model," *Multimedia Tools and Applications*, vol. 80, no. 14, pp. 21465–21498, 2021.
- [18] M. Liu, B. Peng, and M. Shang, "Lower limb movement intention recognition for rehabilitation robot aided with projected recurrent neural network," *Complex & Intelligent Systems*, vol. 12, pp. 1–12, 2021.
- [19] C. Y. Luo, S. Y. Cheng, H. Xu, and P. Li, "Human behavior recognition model based on improved EfficientNet," *Procedia Computer Science*, vol. 199, pp. 369–376, 2022.
- [20] S. Dong, P. Wang, and K. Abbas, "A survey on deep learning and its applications," *Computer Science Review*, vol. 40, article 100379, 2021.
- [21] F. Pérez-Hernández, S. Tabik, A. Lamas, R. Olmos, H. Fujita, and F. Herrera, "Object detection binary classifiers methodology based on deep learning to identify small objects handled similarly: application in video surveillance," *Knowledge-Based Systems*, vol. 194, article 105590, 2020.
- [22] S. Z. Gurbuz and M. G. Amin, "Radar-based human-motion recognition with deep learning: promising applications for indoor monitoring," *IEEE Signal Processing Magazine*, vol. 36, no. 4, pp. 16–28, 2019.
- [23] S. Mei, Y. Hu, X. Wu et al., "Health risks of mobile phone addiction among college students in China," *International Journal of Mental Health and Addiction*, vol. 5, pp. 1–16, 2022.
- [24] K. Tan, W. Huang, X. Liu, J. Hu, and S. Dong, "A hierarchical graph convolution network for representation learning of gene expression data," *IEEE Journal of Biomedical and Health Informatics*, vol. 25, no. 8, pp. 3219–3229, 2021.

## Research Article

# A Case Study of Multiple Maintenance Efficacy in Gynaecological Surgery Assessed by Deep Learning

Yanmei Zheng<sup>1,2</sup> and Qi Yuan <sup>1,2</sup>

<sup>1</sup>Department of Operating Room Nursing, West China Second University Hospital, Sichuan University/West China School of Nursing, Sichuan University, Chengdu, Sichuan 610000, China

<sup>2</sup>Key Laboratory of Birth Defects and Related Diseases of Women and Children, Ministry of Education, Sichuan University, Chengdu, Sichuan 610000, China

Correspondence should be addressed to Qi Yuan; [zqwang1029@stu.suda.edu.cn](mailto:zqwang1029@stu.suda.edu.cn)

Received 14 June 2022; Revised 18 July 2022; Accepted 22 July 2022; Published 8 August 2022

Academic Editor: Hangjun Che

Copyright © 2022 Yanmei Zheng and Qi Yuan. This is an open access article distributed under the Creative Commons Attribution License, which permits unrestricted use, distribution, and reproduction in any medium, provided the original work is properly cited.

Deep learning is a new learning concept and a highly effective way of learning, which is still being explored in the field of nursing education. This paper analyses the effectiveness of interventions in perioperative gynaecological care using humanised care in the operating theatre and the impact of this model of care on patients' psychological well-being and sleep quality. A deep learning-based vision robot was designed to provide higher quality of care for our human care and simplify our approach to gynaecological surgery. The anxiety and depression scores of the two groups were significantly improved after and before care, and the scores of the observation group were lower than those of the control group, with a statistically significant difference ( $P < 0.05$ ). The humanised care for gynaecological surgery patients in the perioperative period is more conducive to the improvement of their negative emotions and at the same time can improve the sleep quality of patients, so it can be further promoted.

## 1. Introduction

As a source of stress, gynaecological surgery does not reduce the psychological disturbance and adverse effects on patients, which requires nursing interventions in parallel with the surgery, in the hope of improving the psychological state of patients and their sleep quality [1].

Humanised care is a model of care based on conventional care, which pays more attention to the physical and mental health of the patient, formulating a care plan that is tailored to each patient's specific physical and mental state, and which also shows respect for the differences in gynaecological surgery patients [2].

In addition, the use of humanised care in gynaecological surgery has brought patients and nurses closer together and provided an important guarantee of safety in the operating theatre, which has positive implications for the health and long-term development of the doctor-patient relationship [3]. The results of this study suggest that the

anxiety and depression of the patients who received humanised care in the operating theatre improved significantly, suggesting that this model of care is conducive to improving the psychological well-being of the patients. At the same time, patients with humanised care services in the operating theatre slept longer after surgery, which indicates that this model of care has a positive impact on prolonging patients' sleep time and improving sleep quality and that the improved sleep quality of patients also ensures the nutrition supply of the body to a large extent, which is also important for postoperative recovery [4].

Operating theatre nursing is characterised by high workload, long working hours, high technical requirements, and high risks, especially in gynaecological operating theatres [5]. Therefore, for gynaecological surgery patients, it is important to strengthen clinical perioperative nursing interventions for patients. Humanised care reflects respect for individual differences, and this model of care is therefore recognised and supported by the majority of patients [6].

With the addition of vision, the robot is able to observe the external environment, process the information from the camera, and obtain information about the object to be grasped based on the information from the camera [7]. Similarly, vision robots are able to locate objects, and with the combination of object recognition and vision positioning, the exact coordinates of the object to be grasped can be obtained. The advent of artificial intelligence has not only brought about ideas but also many technological changes that are leading the way in vision robots [8]. Deep learning has not only allowed vision robots to shed their bulky shells but has also made them smarter than ever, and some have even developed ideas and minds of their own. Artificial intelligence has also become a technology hit now and is now being used in a variety of fields, changing traditional production processes and habits. The artificial intelligence robotics industry is now driving business growth [9].

Faced with the negative impact of informing nursing, the use of an in-depth learning approach in gynaecological nursing guides gynaecological patients in evaluating evidence of practice and encourages gynaecological patients to engage in self-directed learning, thereby developing nurses' meta-cognitive skills and critical thinking. This paper examines the use of an in-depth learning model in clinical nursing to train nurses in emergency clinical skills [10].

## 2. Related Work

The results of the survey indicate that nursing students have some awareness of deep learning but are at a low to moderate level and need to be improved. A number of studies have shown that the educational environment is positively correlated with the level of deep learning and that a good educational support environment is an important prerequisite for the creation of a learning environment and access to learning resources [11]. A semistructured interview to explore nurses' perceptions of the teaching and learning environment showed that effective classroom teaching and learning environment is a catalyst for nurses' use of deeper learning [12]. The survey identified that medical students generally adopted three learning styles, in-depth learning, surface learning, and strategic learning, and that they were able to adapt their learning methods to the changing teaching environment in a timely manner. [13] pointed out that nurses' sense of self-efficacy in online learning is an important influence on deep learning, and that a good sense of self-efficacy among nurses can positively predict and guide the development of deep learning, and that level of education, network skills, and self-directed learning also have an impact on the level of deep learning. However, some studies suggest that there is disagreement about the impact of general demographic characteristics such as gender, grade, and profession on the production of deeper learning styles, and further research is needed [14, 15].

The study reported that the use of clinical nursing experience alone is not effective in facilitating the development of advanced learning and that only trainee nurses engaged in advanced learning can take the initiative to develop the creative and participatory skills to master the whole-patient

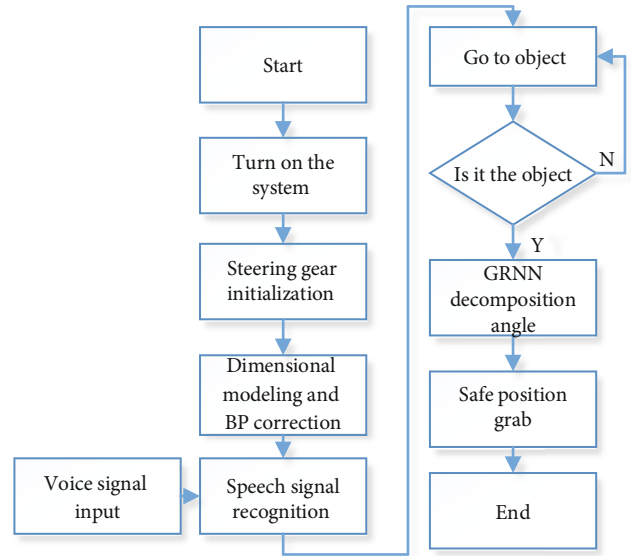


FIGURE 1: Flow of a care robot grasping an object.

model of care [16, 17]. Lectures on human anatomy and physiology are based on an in-depth learning pathway that takes full advantage of the learning community to teach students to solve complex problems to complete the transfer of knowledge. In [18], an online postclinical pilot study was conducted in which nurse educators guided students through a complex clinical environment. Students were able to structure conversations in a face-to-face or online environment to successfully deal with complex or acute clinical patients, developing their integrative skills such as clinical scenarios and guided discussions.

## 3. Binocular Vision System for Nursing Robots

**3.1. The Overall Process of the Care Robot.** The main work of this paper is to build a set of deep learning-based vision servo system for nursing robots; the main function of the system is to complete some basic actions of the home robot and to autonomously complete the tasks assigned to it by the master, for example, a simple operation like grasping a cup; the master just needs to issue a voice command to grasp the cup, and the nursing robot can autonomously find the cup in the field of view and can autonomously grab the cup. To design such a care robot, it is important to have an overview of the whole system, to understand the types of signals and the sequence of the various stages [19]. As voice control is used, there must be recognition of speech. There is the grasping of the cup, so there is the creation of a three-dimensional coordinate system for vision, as well as object recognition. All these technologies are key to researching nursing robots today.

The main purpose of designing this care robot is to play a role in caring for people who are inconvenienced and to help them with the daily operations of life. The workflow of the care robot for grasping objects in a practical application is described here, as shown in Figure 1.





FIGURE 2: Coordinate transformation.

TABLE 1: Intergroup comparison of pre- and postcare adverse psychological scores ( $\bar{x} \pm s$ , scores).

Group	Anxiety score	Depression score
Observation group ( $n = 100$ )		
Before nursing	$15.23 \pm 2.26$	$16.89 \pm 2.33$
After nursing	$7.41 \pm 0.15$	$7.32 \pm 0.52$
Control group ( $n = 100$ )		
Before nursing	$15.43 \pm 2.28$	$16.78 \pm 2.54$
After nursing	$12.42 \pm 0.22$	$12.49 \pm 0.48$

As shown in Figure 1, the main steps in its mode of operation are as follows.

In the first step, the care robot acquires an external voice signal, which is a specific human voice signal, not only for convenience but also to prevent interference from other people's voices and for greater security.

In the second step, the PC processes the voice signal, analyses the voice commands, and makes the care robot act accordingly, which is much faster.

The third step is to accept the acquired voice commands, capture the image with the binocular camera, find the target object in the image, and obtain the coordinates of the object.

In the fourth step, a neural network is used to correct the coordinate information of the target and then perform the grasping action.

**3.2. Human-Specific Speech Recognition for Care Robots.** The original intention of the deep learning-based care robot design was to have artificial intelligence, so to be as flexible and the control signals as simple as possible, and after comparing other control signals, the one chosen was the voice signal. There are three main advantages.

Firstly, the use of a voice signal also ensures that the person giving the command only needs to wear a wireless headset and send voice commands within a certain range. Traditional command outputs often require the user to be right next to the machine, and the use of voice input solves this problem.

Secondly, the functions that can be added by using voice signals are often more than those of hardware input, and it is not necessary to consider the number of voice commands, but traditional hardware is different; after all, more signals require more hardware to distinguish the type of signal, using voice input solves this problem and is also more convenient for us to control.

Thirdly, the choice of specific human voice recognition can also play a major role in preventing interference from other people's voices and can increase the stability of the input signal.

The advantage of choosing a headset plus a computer processing method is mainly to determine the distance

TABLE 2: Comparison of sleep duration between groups ( $\bar{x} \pm s$ , h).

Group	One day after operation	Three days after operation	Seven days after operation
Observation group ( $n = 100$ )	$6.88 \pm 0.12$	$7.49 \pm 0.56$	$8.11 \pm 0.27$
Control group ( $n = 100$ )	$5.23 \pm 0.26$	$5.85 \pm 0.22$	$6.01 \pm 0.22$
$T$ value	57.621	27.256	60.295
$P$ value	0	0	0

between the sound source and the receiver, which can effectively control the decibel level of the sound, thus allowing better recognition and reducing recognition errors. As this experimental platform uses a one-to-one service, the recognition of the voice signal must be person specific so as to ensure that the care robot has as little influence on the outside world as possible [20].

The main method used to acquire the speech signal is the recognition of isolated words for person-specific speech recognition. The training of the person-specific speech is carried out, and the specific process includes the following steps.

*Step 1.* The acquired person-specific speech signal sequence  $X(n)$  is preprocessed to obtain a new speech sequence  $Y_{\text{oum}}(n)$  after which a Fourier transform is applied to it:

$$X(i, k) = \text{FFT}[X_m(n)]. \quad (1)$$

Universal line energy:

$$E(i, k) = [X(i, k)]^2. \quad (2)$$

*Step 2.* Filtered by  $H_m(k)$  filter phantom,

$$H_m(k) = \begin{cases} \frac{k - f(m-1)}{f(m) - f(m-1)}, & f(m-1) \leq k \leq f(m), \\ \frac{f(m+1) - k}{f(m+1) - f(m)}, & f(m) \leq k \leq f(m+1), \\ 0, & 0 \leq k \leq f(m-1), \quad f(m+1) < k. \end{cases} \quad (3)$$

In equation (3),  $0 \leq m \leq M$ ,  $M$  is the number of filters  $H_m(k)$ .

Energy after  $H_m(k)$  filter:

$$S(i, k) = \sum_{k=0}^{N-1} E(i, k) H_m(k), \quad 0 \leq m \leq M. \quad (4)$$

*Step 3.* Calculate the characteristic parameters of MFCC:

$$\text{mfcc}(i, n) = \sqrt{\frac{2}{M}} \sum_m^{M-1} \log[S(i, m)] \cos\left(\frac{\pi n(2m-1)}{2M}\right). \quad (5)$$



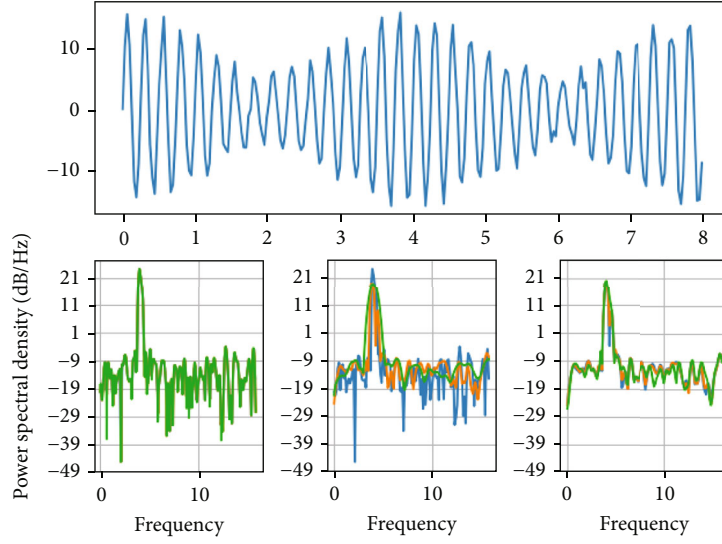


FIGURE 3: Deep learning training and care outcomes.

*Step 4.* The feature matrix calculated is saved with the command in the form of a file name, which is matched when a speech signal is received to determine the speech command and obtain the object to be grasped.

The main idea of using the DTW algorithm is to use the global minimum method, comparing the template calculated by the DTW algorithm with the implementation of the saved template, if the shortest distance from one of the templates, the corresponding content is the command of that saved template.

**3.3. Vision Coordinate System Establishment for the Nursing Robot.** After the care robot receives the voice signal, the computer matches the corresponding command, and then, it enters the vision part, which needs to make corresponding actions to the voice signal, identify the object to be grasped, and grasp the object to be grasped and needs to get the 3D coordinates of the grasped object, where the 3D coordinates are obtained by establishing a binocular vision coordinate system, modelling the visual space to facilitate the later identification and grasping action of the robot arm.

The images captured using a single camera are two-dimensional and lack depth information. The addition of a camera is also used to calculate the depth information by comparing the difference in coordinates of the same point in two images through a parallax map. (Based on observations and experiments, it was found that the  $X$  coordinate of the object in the right view is different from the left view, but the  $F$  coordinate is the same, and the parallax is set to  $Z$ .) The coordinates of point  $P$  in the left and right camera are different, but in practice, it is just a point, and the coordinates of this point are set to  $p(x, y, z)$ . The following conclusions can be drawn from the triangulation.

$$A(x, y) = f \frac{x}{z}, \quad (6)$$

$$B(x, y) = f \left( \frac{x - d}{z} \right), \quad (7)$$

$$A(x, y) = B(x, y) = f \frac{y}{z}, \quad (8)$$

$$D = A(x, y) - B(x, y). \quad (9)$$

After calculation, we get

$$x = \frac{B \cdot A(x, y)}{D}, \quad (10)$$

$$y = \frac{B \cdot A(x, y)}{D} = \frac{B \cdot B(x, y)}{D}, \quad (11)$$

$$Z = \frac{B \cdot f}{D}. \quad (12)$$

The coordinates of the object calculated by the above formula are the coordinates under the camera; if you want to get the image coordinates, you need to do the following process.

As shown in Figure 2, the process of establishing a 3D coordinate system with the binocular camera is actually the process of transforming the coordinate system to obtain the real coordinates of the object in reality. After establishing the 3D coordinates, the experimental verification was carried out on the same platform as the voice platform, both being MFC projects under Windows.

## 4. Case Studies

**4.1. General Information.** From October 2019 to June 2020, 200 patients who underwent gynaecological surgery in the operating room of our hospital were selected as the subjects of the study and were divided into a control group and an observation group according to the random number table method, with 100 patients in each group. The average age of the control group was 22-68 years,  $46.26 \pm 1.82$  years

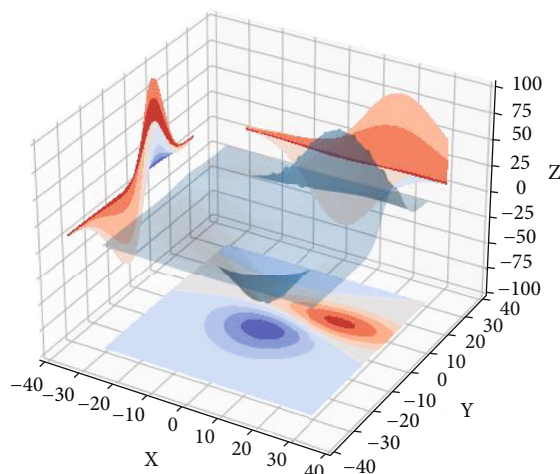


FIGURE 4: Nursing robot gripping effect.

old; the average age of the observation group was 23-69 years old,  $46.29 \pm 1.87$  years old. The general data of the two groups were not statistically significant ( $P > 0.05$ ) and were comparable. The study was approved by the ethics committee of the hospital, and the patients gave their informed consent.

**4.2. Results.** The negative emotions of both groups improved after care, and the negative psychological scores of patients in the observation group were significantly lower than those in the control group after care, with statistically significant differences ( $P < 0.05$ ) (see Table 1).

The sleep time of the two groups was counted at 1 d, 3 d, and 7 d postoperatively, and the results showed that the sleep interval of the observation group was significantly longer than that of the control group at each time point (see Table 2).

As can be seen from Figure 3, the function fitness value reaches its optimal value after almost 35 iterations, and in subsequent iterations, the function fitness value does not fluctuate or jump massively and basically tends to be stable. The genetic algorithm optimises the BP neural network to a certain extent to avoid the difficulties of tuning the parameters and on the other hand to find better parameters more quickly.

The application of CNN to a nursing robot not only solves the problem of object recognition when the robot arm grasps an object but also allows this to be combined with the grasping state of the robot arm. The role of object recognition in a nursing robot is not only to mark the object but also to give the robot arm advice on how to grasp the object by recognising it. This increases the gripping stability of the nursing robot, as shown in Figure 4.

## 5. Conclusion

This paper describes the overall structure of the deep learning-based nursing robot vision system and provides an in-depth study of the control strategy of the deep learning-based nursing robot vision system. The human-

specific speech recognition part of the nursing robot was completed, mainly using the DTW algorithm, and experimental validation was carried out to demonstrate the accuracy of the DTW algorithm used on speech-isolated word signals. The theoretical derivation of the 3D coordinate system established by the binocular camera and the elaboration of the specific operation steps were carried out, and the upper computer was programmed to experimentally verify the application of the 3D coordinate system established by the binocular vision in the nursing robot.

## Data Availability

The dataset used in this paper are available from the corresponding author upon request.

## Conflicts of Interest

The authors declared that they have no conflicts of interest regarding this work.

## References

- [1] B. E. Bejnordi, M. Veta, P. J. Van Diest et al., "Diagnostic assessment of deep learning algorithms for detection of lymph node metastases in women with breast cancer," *JAMA*, vol. 318, no. 22, pp. 2199–2210, 2017.
- [2] H. C. Dong, H. K. Dong, M. H. Yu, Y. H. Lin, and C. C. Chang, "Using deep learning with convolutional neural network approach to identify the invasion depth of endometrial cancer in myometrium using MR images: a pilot study," *International Journal of Environmental Research and Public Health*, vol. 17, no. 16, p. 5993, 2020.
- [3] H. Jung, C. Shen, Y. Gonzalez, K. Albuquerque, and X. Jia, "Deep-learning assisted automatic digitization of interstitial needles in 3D CT image based high dose-rate brachytherapy of gynecological cancer," *Physics in Medicine & Biology*, vol. 64, no. 21, p. 215003, 2019.
- [4] P. Lakhani and B. Sundaram, "Deep learning at chest radiography: automated classification of pulmonary tuberculosis by using convolutional neural networks," *Radiology*, vol. 284, no. 2, pp. 574–582, 2017.
- [5] M. A. Bartek, R. C. Saxena, S. Solomon et al., "Improving operating room efficiency: machine learning approach to predict case-time duration," *Journal of the American College of Surgeons*, vol. 229, no. 4, pp. 346–354e3, 2019.
- [6] J. A. Golden, "Deep learning algorithms for detection of lymph node metastases from breast cancer: helping artificial intelligence be seen," *JAMA*, vol. 318, no. 22, pp. 2184–2186, 2017.
- [7] A. Akselrod-Ballin, M. Chorev, Y. Shoshan et al., "Predicting breast cancer by applying deep learning to linked health records and mammograms," *Radiology*, vol. 292, no. 2, pp. 331–342, 2019.
- [8] D. S. W. Ting, C. Y. L. Cheung, G. Lim et al., "Development and validation of a deep learning system for diabetic retinopathy and related eye diseases using retinal images from multi-ethnic populations with diabetes," *JAMA*, vol. 318, no. 22, pp. 2211–2223, 2017.
- [9] C. T. Strömblad, R. G. Baxter-King, A. Meisami et al., "Effect of a predictive model on planned surgical duration accuracy,

- patient wait time, and use of presurgical resources,” *JAMA Surgery*, vol. 156, no. 4, pp. 315–321, 2021.
- [10] S. Borsci, G. Lawson, and S. Broome, “Empirical evidence, evaluation criteria and challenges for the effectiveness of virtual and mixed reality tools for training operators of car service maintenance,” *Computers in Industry*, vol. 67, pp. 17–26, 2015.
  - [11] B. Norgeot, B. S. Glicksberg, L. Trupin et al., “Assessment of a deep learning model based on electronic health record data to forecast clinical outcomes in patients with rheumatoid arthritis,” *JAMA Network Open*, vol. 2, no. 3, pp. e190606–e190606, 2019.
  - [12] A. Zemmar, A. M. Lozano, and B. J. Nelson, “The rise of robots in surgical environments during COVID-19,” *Nature Machine Intelligence*, vol. 2, no. 10, pp. 566–572, 2020.
  - [13] S. H. Cho, Y. M. Sung, and M. S. Kim, “Missed rib fractures on evaluation of initial chest CT for trauma patients: pattern analysis and diagnostic value of coronal multiplanar reconstruction images with multidetector row CT,” *The British Journal of Radiology*, vol. 85, no. 1018, pp. e845–e850, 2012.
  - [14] F. Amato, S. Marrone, V. Moscato, G. Piantadosi, A. Picariello, and C. Sansone, “HOLMeS: EHealth in the big data and deep learning era,” *Information*, vol. 10, no. 2, p. 34, 2019.
  - [15] M. G. Hanna, V. E. Reuter, M. R. Hameed et al., “Whole slide imaging equivalency and efficiency study: experience at a large academic center,” *Modern Pathology*, vol. 32, no. 7, pp. 916–928, 2019.
  - [16] X. Wang, H. Chen, C. Gan et al., “Weakly supervised deep learning for whole slide lung cancer image analysis,” *IEEE transactions on cybernetics*, vol. 50, no. 9, pp. 3950–3962, 2020.
  - [17] G. Moawad, P. Tyan, and M. Louie, “Artificial intelligence and augmented reality in gynecology,” *Current Opinion in Obstetrics and Gynecology*, vol. 31, no. 5, pp. 345–348, 2019.
  - [18] R. Mohammadi, I. Shokatian, M. Salehi, H. Arabi, I. Shiri, and H. Zaidi, “Deep learning-based auto-segmentation of organs at risk in high-dose rate brachytherapy of cervical cancer,” *Radiotherapy and Oncology*, vol. 159, pp. 231–240, 2021.
  - [19] J. Haverinen, N. Keränen, P. Falkenbach, A. Maijala, T. Kolehmainen, and J. Reponen, “Digi-HTA: health technology assessment framework for digital healthcare services,” *Finnish Journal of eHealth and eWelfare*, vol. 11, no. 4, pp. 326–341, 2019.
  - [20] P. Guo, Z. Xue, Z. Mtema et al., “Ensemble deep learning for cervix image selection toward improving reliability in automated cervical precancer screening,” *Diagnostics*, vol. 10, no. 7, p. 451, 2020.

## Research Article

# Study on the Effect of Positive Psychological Intervention Based on PERMA Model on Perioperative Patients with AIDS Complicated with Breast Cancer

Lingmei Luo , Ying Li, Zhou Zhou, Saifen Yang, Yao Qin, Hua Peng, Yirong Wang, Zhe Li, and Tianqin Yin

Department of Infectious Diseases Surgery, The First Hospital of Changsha, Changsha, Hunan Province 410000, China

Correspondence should be addressed to Lingmei Luo; 631507010411@mails.cqjtu.edu.cn

Received 10 June 2022; Accepted 8 July 2022; Published 8 August 2022

Academic Editor: Hangjun Che

Copyright © 2022 Lingmei Luo et al. This is an open access article distributed under the Creative Commons Attribution License, which permits unrestricted use, distribution, and reproduction in any medium, provided the original work is properly cited.

**Objective.** To study the effect of positive psychological intervention based on PERMA model on perioperative AIDS patients complicated with breast cancer. **Methods.** A total of 120 perioperative patients with AIDS complicated with breast cancer treated in our hospital from January 2021 to December 2021 were randomly divided into research group ( $n = 60$ ) and control group ( $n = 60$ ). The research group received positive psychological intervention based on PERMA model, while the control group received routine nursing. The scores of disease uncertainty scale (MUIS), Frankl treatment compliance scale, cancer-related fatigue scale, self-rating anxiety scale (SAS), self-rating depression scale (SDS), and quality of life scale EORTCQLQ-C30 (v3.0) were studied. **Results.** After 12-week nursing, the MUIS score of the research group was lower than that of the control group, and the difference was statistically significant ( $P < 0.05$ ). After 12 weeks of nursing, the score of Frankl treatment compliance scale in the research group was higher than that in the control group, and the difference was statistically significant ( $P < 0.05$ ). Following 12-week nursing, the scores of SAS and SDS in the research group were lower than those in the control group, and the difference was statistically significant ( $P < 0.05$ ). After 12 weeks of nursing, the score of cancer-related fatigue scale in the research group was lower than that in the control group, and the difference was statistically significant ( $P < 0.05$ ). The EORTCQLQ-C30 (v3.0) scale-symptom domain score in the research group was lower than that in the control group following 12-week nursing, and the difference was statistically significant ( $P < 0.05$ ). After 12 weeks of nursing, the EORTCQLQ-C30 (v3.0) scale-overall health domain score and functional domain score in the research group were higher than those in the control group, and the difference was statistically significant ( $P < 0.05$ ). **Conclusion.** The application value of positive psychological intervention based on PERMA model in perioperative patients with AIDS complicated with breast cancer is more significant. It contributes more to treatment compliance and improves negative feelings of anxiety and depression.

## 1. Introduction

Acquired immunodeficiency syndrome (AIDS) is a highly contagious infectious disease caused by human immunodeficiency caused by human infection with human immunodeficiency virus (HIV) [1]. AIDS cannot be cured, because HIV specifically invades human CD4<sup>+</sup> cells, causing serious damage to the human immune system. By the end of 2017, there

were 36.9 million people living with HIV worldwide, of which 1.8 million were new HIV infections [2]. In China, as a country with a large population, the number of new AIDS patients is also very staggering. From 2012 to 2017, the number of new cases of HIV/AIDS in China increased from 82434 to 134512 every year and there is still an upward trend [3, 4]. According to the latest data of the Chinese Center for Disease Control and Prevention, there were 445716



cases of HIV infection and 323456 cases of AIDS in China by the end of January 2018 with 241519 reported deaths [5]. The widespread spread of AIDS has become a serious social problem.

AIDS patients with depression need effective psychological intervention and support to ensure the effectiveness and health of nursing measures. A large number of foreign studies have examined the effect of psychological intervention on AIDS patients from an empirical point of view, which is effective in immune function, emotional regulation, compliance, and high-risk sexual transmission blocking. According to clinical studies, a large number of AIDS patients suffer from malignant tumors. Before 1995, AIDS-related malignant tumors such as Kaposi's sarcoma, non-Hodgkin's lymphoma, and invasive cervical cancer accounted for 80% of the total cancer burden of AIDS patients [6, 7]. In recent years, due to the improvement of the level of antiretroviral therapy and the level of minimally invasive breast surgery, the survival rate of AIDS patients with breast cancer has also been effectively improved [8]. However, AIDS patients with breast cancer still need to face various problems such as social discrimination, economic, and mental pressure. AIDS combined with breast cancer not only seriously damages the life and health of patients but also brings more serious psychological trauma to patients [9, 10]. Numerous studies have pointed out that psychological intervention can play an important and positive role in the maintenance of AIDS and mental health [11–13]. With the popularization of treatment, the proportion of malignant tumors in AIDS patients has changed greatly and the proportion of non-HIV-related malignant tumors such as breast cancer has increased significantly [14–17]. PERMA model is a happiness model proposed by Seligman, which consists of five elements such as positive emotion, input, interpersonal relationship, meaning, and achievement. The theory holds that having these five elements can overcome negative emotions and have a happy life [18]. At present, PERMA model has been used in stroke disabled patients [19], AIDS hospitalized patients [20], disabled college students [21], and achieved good results, but it is not known whether this model is suitable for perioperative AIDS patients with breast cancer in China. Therefore, this paper studied the effect of positive psychological intervention based on PERMA model on perioperative patients with AIDS complicated with breast cancer.

## 2. Materials and Methods

**2.1. General Information.** A total of 120 perioperative AIDS patients with breast cancer treated in our hospital from January 2021 to December 2021 were selected. 120 perioperative AIDS patients with breast cancer were randomly divided into research group ( $n = 60$ ) and control group ( $n = 60$ ). In the research group, the age ranged from 25 to 67 years old with an average of  $54.48 \pm 5.16$  year old. In the control group, the age ranged from 25 to 68 years old with an average of  $54.15 \pm 5.33$  years old. There was no significant difference in general data between the two groups ( $P > 0.05$ ).

Inclusion criteria are as follows: (1) female patients with primary breast cancer who met the indications for surgical

treatment; (2) hospitalized patients diagnosed with AIDS; (3) those who had access to the Internet and were proficient in using WeChat; (4) their condition was basically stable and can basically take care of themselves. No special hobbies such as drug use and alcohol abuse; (5) normal spirit and intelligence and normal communication skills such as listening, speaking, reading, and writing; and (6) volunteer to participate in this study.

Exclusion criteria are as follows: (1) with other cancers or serious basic diseases such as heart, liver, and kidney; (2) mental illness or disturbance of consciousness; (3) cases with low intelligence did not have basic listening, speaking, reading, and writing skills; (4) patients who were unable to care for themselves; (5) cases with mental illness, paranoid personality, drug addicts, and alcoholics; and (6) cases without Internet access and will not use WeChat, QQ, and other chat tools.

## 2.2. Methods

**2.2.1. Technical Route.** Figure 1 shows the technology roadmap.

**2.2.2. Intervention Scheme.** Control group scheme: routine care: from the first week of hospitalization, the responsible nurse conducted 8 consecutive health education interviews with the patients, including the following: (1) introduction and prevention of AIDS and breast cancer, (2) introduction and countermeasures of common complications of AIDS, (3) introduction of common programs for antiviral treatment of AIDS, (4) introduction of breast cancer operation plan, (5) medication guidance and common adverse drug reactions of AIDS complicated with breast cancer, (6) dietary guidance, (7) compliance education of antiviral drugs, (8) the significance and indication of perioperative prophylactic medication, and (9) the present situation and prospect of antiretroviral therapy and minimally invasive breast surgery. The WeChat group was established to keep in touch with patients and to encourage patients to continue to participate in the study. If the patient was discharged, the patient would be interviewed through WeChat voice chat, message, or phone.

Research group plan: the research group was given positive psychological intervention based on PERMA model. One phase was 3 weeks, 4 phases, a total of 12 weeks. The first three stages were intervened twice, and the last stage intervention only needed once with a total of 7 times. Every time 30–50 min, the intervention place was the breast surgery demonstration room. The intervention methods were interviews and exercises, including on-site guidance and home-based exercises. The specific contents included (1) the first time: Interviews were conducted with patients around their feelings after the illness. The patient was asked to talk about his negative thoughts and to guide the patient to think dialectically about the idea. (2) The second time is as follows: to introduce positive emotion. The patients were guided to understand and familiarize themselves with the relevant knowledge of positive emotions and to conduct preliminary exercises on positive emotions. Through the



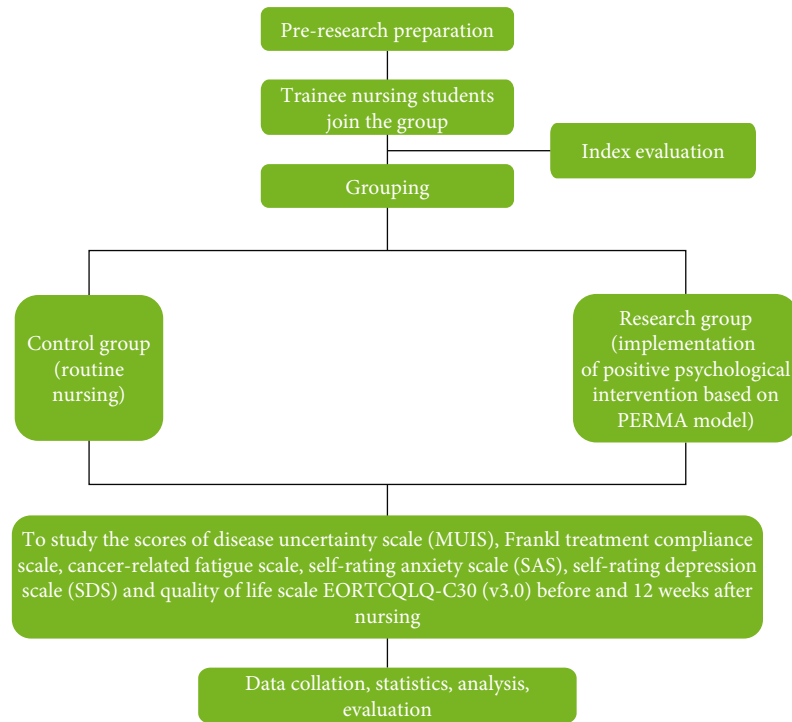


FIGURE 1: Technology roadmap.

combination of slides and videos, the famous experiments of positive psychology were introduced to patients in an easy-to-understand language. The interviews with patients would be conducted around people or things that needed to be grateful during illness. (3) The third time is as follows: to establish positive emotion. The patients were guided to cultivate positive thinking and interviewed around positive events in life. (4) The fourth time is as follows: to input. The patients were guided to understand and familiarize themselves with the relevant knowledge of input and flow experience. The patients were encouraged to conduct preliminary exercises on flow experience interview content. (5) The fifth time is as follows: relationship. The patients were guided to understand and be familiar with the relevant knowledge of interpersonal communication methods and skills. (6) The sixth time is as follows: meaning. Guided patients were asked to understand and familiarize themselves with the relevant knowledge of the meaning of life. The patients should find and determine their own meaning of life interview content through the combination of slides and videos to introduce real examples of meaningful life to patients. (7) The 7th time is as follows: goals and achievements. The patients were informed and familiarized with goals and achievements. The patients were guided to set goals that are of interest to them. The patients were presented with real-life examples of discharged patients' achievements through a combination of slides and videos.

### 2.3. Observation Index

- (1) *Mishel Uncertainty in Illness Scale (MUIS)*. The total score of MUIS ranged from 320 to 160.

- (2) *Frankl Treatment Compliance Scale*. The scoring criteria of Frankl compliance scale were as follows: 1: refusal, pain; 2: uncooperation, reluctance; 3: use, indifference; and 4: active cooperation and enjoyment.
- (3) The scores of self-rating anxiety scale (SAS) and self-rating depression scale (SDS) were studied. Anxiety was defined as the standard score of  $SAS \geq 50$ . With the increase of the score, the degree of anxiety was more serious. The standard score of  $SDS \geq 53$  points was seen as depression.
- (4) *The Score of Cancer-Related Fatigue Scale*. The scale of cancer-related fatigue includes behavioral fatigue, cognitive fatigue, physical fatigue, and emotional fatigue with a full score of 10.
- (5) The EORTCQLQ-C30 (v3.0) score of the quality-of-life measurement scale was studied. The EORTCQLQ-C30 (v3.0) scale included a total of 15 evaluation dimensions and 30 items. The functional areas were included: 5 items of body, 2 items of role, 2 items of cognition, 4 items of emotion, and 2 items of social function; general health status is as follows: 1 item of general health and 1 item of quality of life. The domain (12 items for fatigue, pain, nausea, and vomiting and 1 item for health-related economic conditions) had a total of 30 items. Among them, items 29 and 30 were scored on the scale of 1-7 points, while the others were scored on the order of 1-4 points.

TABLE 1: MUIS score ( $\bar{x} \pm s$ , points).

Grouping	N	Before nursing (points)	After 12 weeks of nursing (points)
Control group	60	59.53 $\pm$ 6.14	41.15 $\pm$ 3.27*
Research group	60	59.45 $\pm$ 6.23	36.19 $\pm$ 2.04*
<i>t</i> value		0.071	9.968
<i>P</i> value		0.945	<0.01

Note: \* represented the comparison of this group before nursing and 12 weeks after nursing, and the difference was statistically significant ( $P < 0.05$ ).

TABLE 2: Frankl treatment adherence scale scores ( $\bar{x} \pm s$ , points).

Grouping	N	Before nursing	After 12 weeks of nursing
Control group	60	1.24 $\pm$ 0.31	2.69 $\pm$ 0.28*
Research group	60	1.21 $\pm$ 0.32	3.69 $\pm$ 0.08*
<i>t</i> value		0.522	26.599
<i>P</i> value		0.603	<0.01

Note: \* represented the comparison of this group before nursing and 12 weeks after nursing, and the difference was statistically significant ( $P < 0.05$ ).

TABLE 3: The score of SAS and SDS ( $\bar{x} \pm s$ , points).

Grouping	N	SAS scoring		SDS scoring	
		Before nursing	After 12 weeks of nursing	Before nursing	After 12 weeks of nursing
Control group	60	66.34 $\pm$ 5.32	57.66 $\pm$ 4.08*	72.45 $\pm$ 7.26	62.23 $\pm$ 6.14*
Research group	60	66.29 $\pm$ 5.45	50.44 $\pm$ 3.25*	72.38 $\pm$ 7.34	50.29 $\pm$ 2.03*
<i>t</i> value		0.051	10.722	0.053	14.302
<i>P</i> value		0.959	<0.01	0.958	<0.01

Note: \* represented the comparison of this group before nursing and 12 weeks after nursing, and the difference was statistically significant ( $P < 0.05$ ).

**2.4. Statistical Analysis.** The IBMSPSS24.0 software was applied for statistical analysis. The measurement data were expressed by mean  $\pm$  standard deviation. The counting data were expressed by frequency or rate. *t*-test was used when measurement data obey normal distribution, and rank sum test was used when it did not obey normal distribution.  $\chi^2$  test was used to compare the classified counting data. Repeated measurement data were analyzed by repeated measurement analysis of variance. Main effect test results were used when there was no interaction, and simple effect analysis was carried out when there was interaction.  $P < 0.05$  indicated that the difference between groups is statistically significant.

### 3. Results

**3.1. The Score of MUIS.** Before nursing, there was no significant difference in the MUIS score between the two groups ( $P > 0.05$ ). After 12 weeks of nursing, the MUIS score in the research group was lower than that in the control group, and the difference was statistically significant ( $P < 0.05$ ) (see Table 1).

**3.2. Study Frankl Scale Score.** Before nursing, there was no significant difference in the scores of Frankl scale between the two groups ( $P > 0.05$ ). After 12 weeks of nursing, the

scores of Frankl scale in the research group were higher than those in the control group, and the difference was statistically significant ( $P < 0.05$ ) (see Table 2).

**3.3. The Score of SAS and SDS.** Before nursing, the SAS and SDS scores of the two groups were not statistically significant ( $P > 0.05$ ). After 12 weeks of nursing, the SAS and SDS scores of the research group were lower than those of the control group, and the difference was statistically significant ( $P < 0.05$ ) (see Table 3).

**3.4. The Score of Cancer-Related Fatigue Scale.** Before nursing, there was no significant difference in the score of cancer-related fatigue scale between the two groups ( $P > 0.05$ ). However, the score of cancer-related fatigue scale in the research group was lower than that in the control group following 12-week nursing, and the difference was statistically significant ( $P < 0.05$ ) (see Table 4).

**3.5. Study the Score of EORTC QLQ-C30 (v3.0) Scale.** Before nursing, there was no statistical difference in the scores of EORTCQLQ-C30 (v3.0) between the groups ( $P > 0.05$ ). After 12 weeks of nursing, the EORTCQLQ-C30 (v3.0) scale-symptom domain score of the research group exhibited lower than the control group, and the difference was statistically significant ( $P < 0.05$ ). After 12 weeks of nursing, the EORTCQLQ-C30 (v3.0) scale-general health domain score

TABLE 4: The score of cancer-related fatigue scale ( $\bar{x} \pm s$ , points).

Grouping	N	Before nursing	After 12 weeks of nursing
Control group	60	8.59 $\pm$ 1.17	6.36 $\pm$ 0.25*
Research group	60	8.63 $\pm$ 1.14	4.02 $\pm$ 0.12*
<i>t</i> value		0.189	65.362
<i>P</i> value		0.849	<0.01

Note: \* represented the comparison of this group before nursing and 12 weeks after nursing, and the difference was statistically significant ( $P < 0.05$ ).

and functional domain score of the research group were higher than those of the control group, and the difference was statistically significant ( $P < 0.05$ ) (see Table 5).

#### 4. Discussion

Clinical studies have shown that HIV mainly invades host CD4<sup>+</sup> cells (T cells, mononuclear macrophages, dendritic cells, etc.). It can bind to the CD4 molecule on the surface of the target cell membrane through the glycoprotein gp120 of its outer membrane. In addition, gp120-CD4 is able to bind to the chemokine receptor CXCR4 or CCR5 expressed on the surface of the target cell membrane to form a trimolecular complex of CD4-gp120-CCR5 (or CCR4), which will result in the conformational change of gp120 and exposes the masked gp41. gp41 is capable of inserting directly into the target cell membrane. The hydrophobic effect of the membrane itself mediated the fusion of the virus envelope and the cell membrane, which makes the virus enter the target cells and directly damage the immune defense and immune surveillance function [22]. CXCR4 receptor not only exists on the surface of CD4<sup>+</sup> T cells but also highly expressed on the surface of breast cancer cells. A large number of studies have proved that the combination of breast cancer cell CXCR4 and its ligand CXCL12 can promote the proliferation of primary tumor and distant metastasis of liver, lung, and brain, which will aggravate the patient's condition and increase the difficulty of treatment [23]. Therefore, there is a certain association between AIDS breast cancer. Many patients are suffering from these two diseases at the same time.

The treatment of breast cancer has the characteristics of diversity and combination, and local treatment includes surgical resection, local radiotherapy, systemic therapy including chemotherapy, endocrine therapy, and targeted therapy [24]. AIDS patients with breast cancer are more likely to have serious mental and psychological problems such as anxiety and depression. Applying positive psychological intervention based on PERMA model to breast cancer patients can reduce the fear of cancer recurrence in breast cancer patients [25].

Due to the chronic incurability of AIDS and public panic and discrimination against AIDS, people with AIDS are more likely to suffer from many psychological problems, such as anxiety, depression, discrimination, guilt, and suicidal tendencies [26]. Shurong conducted a questionnaire survey on 321 newly diagnosed HIV infections and found that the positive rates of depressive symptoms, anxiety

symptoms, and suicidal ideation were 41.1% (132/321), 31.5% (101/321), and 27.7% (89/321), respectively [27]. Early findings have shown that AIDS patients with depression need additional psychological intervention and support from health care interventions [28]. However, the nurses in our country have a low mastery of psychological nursing knowledge, and the application of psychological nursing in AIDS patients is very rare [29]. The only psychological nursing research is only in the exploratory stage [30–34]. Thus, the current psychological care cannot meet the psychological needs of AIDS patients. Some studies have shown that the application of positive psychological intervention based on PERMA model to AIDS patients can improve the subjective well-being of AIDS patients [35]. Among AIDS patients, there is no lack of patients with low BMI and poor nutritional status. The immune function is impaired, and the adverse reactions caused by chemotherapeutic drugs are more obvious. As a result, the cancer progression of AIDS patients is faster than that of the general population, so the prognosis of AIDS patients with breast cancer is poor, which not only requires our active treatment [36, 37]. Therefore, this study introduced positive psychological intervention based on PERMA model into perioperative nursing care of AIDS patients with breast cancer.

The results of this study proved that the application value of positive psychological intervention based on PERMA model in perioperative patients with AIDS complicated with breast cancer is more significant. It is more helpful to reduce the uncertainty of disease and the degree of cancer-related fatigue. This is mainly because the incidence of anxiety and depression in AIDS is high [37]. Some studies have shown that the ability of emotion adjustment plays a very important role in controlling the occurrence and development of anxiety and depression in AIDS patients. It is also an important index to evaluate mental health [38]. In the PERMA model, clinical medical staff should include positive psychological factors such as emotion, input, interpersonal relationship, meaning, and achievement in the health guidance management system of AIDS patients with breast cancer [39, 40]. In the guidance of propaganda and education, more attention should be paid to the psychological status of patients. Furthermore, their negative emotions such as anxiety and depression should be reduced through the training of positive explanation and optimistic explanation style in the interview. It can increase the positive emotion through gratitude practice, the establishment of positive emotion file, and the improvement of interpersonal relationship by active response, so as to guide patients to express their negative

TABLE 5: EORTC QLQ-C30 (v3.0) scale score ( $\bar{x} \pm s$ , points).

Grouping	N	Symptom field		Functional area		General health field	
		Before nursing	After 12 weeks of nursing	Before nursing	After 12 weeks of nursing	Before nursing	After 12 weeks of nursing
Control group	60	36.44 $\pm$ 3.28	29.59 $\pm$ 2.32*	15.54 $\pm$ 2.09	25.39 $\pm$ 4.13*	3.15 $\pm$ 0.25	4.03 $\pm$ 0.45*
Research group	60	36.12 $\pm$ 3.34	24.36 $\pm$ 1.14*	15.65 $\pm$ 2.02	40.77 $\pm$ 5.12*	3.16 $\pm$ 0.08	7.12 $\pm$ 0.11*
t value		0.529	15.672	0.293	18.111	0.295	51.668
P value		0.598	<0.01	0.769	<0.01	0.768	<0.01

Note: \* represented the comparison of this group before nursing and 12 weeks after nursing, and the difference was statistically significant ( $P < 0.05$ ).

emotion towards the disease. Specific negative psychological aspects of the patient are identified, and counselling and thought-transformation exercises are given to help patients change their negative perceptions of the illness, reduce their uncertainty about the illness, and enhance their positive emotions and experiences. In addition, the patients are made to understand that their current negative emotions are related to misperceptions through the principles of cognitive intervention. Through the further understanding of the disease, the patients will learn to explain the current physical problems and challenges from a positive point of view, which greatly increases their confidence in resisting the disease. There are some limitations in this study. First, the sample size of this study is not large, and it is a single-center study, so bias is inevitable. In future research, we will carry out multicenter, large-sample prospective studies, or more valuable conclusions can be drawn.

In conclusion, the application value of positive psychological intervention based on PERMA model in perioperative patients with AIDS complicated with breast cancer is more significant. It is more helpful to reduce disease uncertainty and cancer-related fatigue and, in the meanwhile, to improve treatment compliance and quality of life.

## Data Availability

No data were used to support this study.

## Conflicts of Interest

The authors declare that they have no conflicts of interest.

## References

- [1] L. Koski, M. J. Brouillette, N. E. Mayo, S. C. Scott, L. K. Fellows, and D. Sookman, "A short-term psychological intervention for people living with HIV during the first wave of COVID-19," *International Journal of Cognitive Therapy*, vol. 15, no. 1, pp. 21–41, 2022.
- [2] A. I. Ajayi, E. Mudefi, O. V. Adeniyi, and D. T. Goon, "Achieving the first of the joint United Nations Programme on HIV/AIDS (UNAIDS) 90-90-90 targets: understanding the influence of HIV risk perceptions, knowing one's partner's status and discussion of HIV/sexually transmitted infections with a sexual partner on uptake of HIV testing," *International Health*, vol. 11, no. 6, pp. 425–431, 2019.
- [3] L. Ruijuan, "The value of high quality nursing when nursing breast cancer patients with arm TIVAP," *Chinese community physician*, vol. 36, no. 15, pp. 129–130, 2020.
- [4] STD Control Center of Chinese Center for Disease Control and Prevention, "National AIDS/STD epidemic situation in December 2017," *AIDS and sexually transmitted diseases in China*, vol. 24, no. 2, p. 5, 2018.
- [5] STD Control Center of China Center for Disease Control and Prevention, "January 2018 national AIDS and STD epidemic situation," *AIDS and sexually transmitted diseases in China*, vol. 24, no. 3, p. 219, 2018.
- [6] L. N. Foschiera, M. F. Dupont, and L. F. Habigzang, "Follow-up evaluation of psychotherapy protocols for women with a history of intimate partner violence: scoping review," *Trends in Psychology*, vol. 30, no. 2, pp. 261–282, 2022.
- [7] X. Hong, "Self-confidence group psychological intervention of college students based on EEG test technology-take patients with social anxiety disorder as an example," *Neuro Quantology*, vol. 16, no. 6, pp. 33–38, 2018.
- [8] P. F. Rebeiro, T. D. Mcpherson, K. M. Goggins et al., "Health literacy and demographic disparities in HIV care continuum outcomes," *AIDS and Behavior*, vol. 22, no. 8, pp. 2604–2614, 2018.
- [9] S. Pramod, "A soft silicone foam dressing that aids healing and comfort in oncology care," *British journal of nursing (Mark Allen Publishing)*, vol. 30, no. 1, pp. 40–46, 2021.
- [10] J. Fei, F. Xiuling, and Z. Ruiyin, "Effects of preservation of anterior thoracic nerve and intercostobrachial nerve on post-operative recovery and incidence of complications in patients undergoing radical mastectomy," *Clinical Medicine*, vol. 41, no. 11, pp. 41–43, 2021.
- [11] J. L. Glick, R. Russo, B. Jivapong et al., "The PrEP care continuum among cisgender women who sell sex and/or use drugs globally: a systematic review," *AIDS and Behavior*, vol. 24, no. 5, pp. 1312–1333, 2020.
- [12] J. D. Emery, P. Nguyen, J. Minshall, K. L. Cummings, and J. Walker, "Chemoprevention: a new concept for cancer prevention in primary care," *Australian journal of general practice*, vol. 47, no. 12, pp. 825–828, 2018.
- [13] L. Habert, F. Audebert, C. Feiterna-Sperling et al., "Not recommended, but done: breastfeeding with HIV in Germany," *AIDS Patient Care and STDs*, vol. 35, no. 2, pp. 33–38, 2021.
- [14] B. S. Kristin, E. R. Begnel, M. R. Golden, A. Moore, M. Ramchandani, and J. C. Dombrowski, "'It's me as a person, not me the disease': patient perceptions of an HIV care model designed to engage persons with complex needs," *AIDS Patient Care and STDs*, vol. 34, no. 6, pp. 267–274, 2020.
- [15] R. Haque, R. T. Chlebowski, and L. H. Chen, "Sleep medication use and risk of fractures in breast cancer survivors," *Breast Cancer Research and Treatment*, vol. 190, no. 3, pp. 541–548, 2021.
- [16] F. Camacho, R. Anderson, and G. Kimmick, "Investigating confounders of the association between survival and adjuvant radiation therapy after breast conserving surgery in a sample of elderly breast cancer patients in Appalachia," *BMC Cancer*, vol. 19, no. 1, pp. 1228–1228, 2019.
- [17] N. Zdenkowski, P. Butow, A. Spillane et al., "Single-arm longitudinal study to evaluate a decision aid for women offered neo-adjuvant systemic therapy for operable breast cancer," *Journal of the National Comprehensive Cancer Network: JNCCN*, vol. 16, no. 4, pp. 378–385, 2018.
- [18] L. P. Howell, S. J. DeNardo, N. B. Levy, J. Lund, and G. L. Denardo, "Immunohistochemical staining of metastatic ductal carcinomas of the breast by monoclonal antibodies used in imaging and therapy: a comparative study," *The International Journal of Biological Markers*, vol. 10, no. 3, pp. 129–135, 2018.
- [19] J. P. Gao, Y. H. Jin, S. F. Yu, W. F. Wu, and S. F. Han, "Evaluate the effectiveness of breast cancer decision aids: a systematic review and meta-analysis of randomized clinical trials," *Nursing Open*, vol. 8, no. 5, pp. 2091–2104, 2021.
- [20] J. Si, R. Guo, X. Lu et al., "Decision aids on breast conserving surgery for early stage breast cancer patients: a systematic review," *BMC Medical Informatics and Decision Making*, vol. 20, no. 1, p. 275, 2020.
- [21] L. Yu, P. Li, S. Yang et al., "Web-based decision aids to support breast cancer screening decisions: systematic review and meta-



- analysis," *Journal of Comparative Effectiveness Research*, vol. 9, no. 14, pp. 985–1002, 2020.
- [22] K. Yao, J. Belkora, C. Lee et al., "An in-visit decision aid for surgeons to address decision making for bilateral mastectomy for newly diagnosed breast cancer patients," *Annals of Surgical Oncology*, vol. 26, no. 13, pp. 4372–4380, 2019.
  - [23] X. Gocko, M. Fondacci, C. Dibi, and C. Plotton, "Information around organized breast cancer screening. Do INCa and Cancer Rose meet criteria for decision aids?," *Revue d'épidémiologie et de sante publique*, vol. 68, no. 1, pp. 33–36, 2020.
  - [24] A. B. Anbari, P. Ostby, and P. K. Ginex, "Breast cancer-related lymphedema: personalized plans of care to guide survivorship," *Current Breast Cancer Reports*, vol. 12, no. 4, pp. 237–243, 2020.
  - [25] A. D. Kimmel, S. P. Masiano, R. S. Bono et al., "Structural barriers to comprehensive, coordinated HIV care: geographic accessibility in the US south," *AIDS Care*, vol. 30, no. 11, pp. 1459–1468, 2018.
  - [26] L. Yudan, "Study on the application of cognitive behavioral therapy combined with sleep intervention nursing in postoperative chemotherapy of breast cancer patients," *World Journal of Sleep Medicine*, vol. 5, no. 5, pp. 604–606, 2018.
  - [27] Y. Shurong, "To explore the clinical application of surgical rapid rehabilitation concept in nursing perioperative patients with breast cancer after modified radical mastectomy," *Intelligence and health*, vol. 7, no. 30, pp. 186–188, 2021.
  - [28] G. V. Hal and P. D. Garcia, "Lung cancer screening: targeting the hard to reach—a review," *Translational Lung Cancer Research*, vol. 10, no. 5, pp. 2309–2322, 2021.
  - [29] S. Lin, "To explore the effect of rapid rehabilitation surgery in nursing perioperative patients with breast cancer after modified radical mastectomy," *Chinese Medicine Guide*, vol. 18, no. 20, pp. 210–211, 2020.
  - [30] H. Lijun, "Observation on the perioperative clinical effect of psychological nursing for patients with breast cancer," *Chinese Medicine Guide*, vol. 17, no. 19, pp. 225–226, 2019.
  - [31] A. D. Mccrorie, A. M. Begley, J. J. Chen, N. K. McCorry, G. Paget, and S. A. McIntosh, "Improving preparedness prior to reconstructive breast surgery via inclusion of 3D images during pre-operative counselling: a qualitative analysis," *BMC Women's Health*, vol. 21, no. 1, pp. 323–325, 2021.
  - [32] Z. Zhili, "Application of rapid rehabilitation surgery concept in nursing perioperative patients with breast cancer after modified radical mastectomy," *Everyone's Health (mid-edition)*, vol. 12, no. 7, pp. 99–100, 2018.
  - [33] W. Jianping, "Improvement of blood hypercoagulable state of patients with breast cancer after radical mastectomy by comprehensive rehabilitation nursing of traditional Chinese medicine," *Thrombus and hemostasis*, vol. 24, no. 1, pp. 122–123, 2018.
  - [34] C. Lixiang, "Observation on the effect of standardized skin care on skin lesions of breast cancer after radiotherapy," *Bethune Medical Journal*, vol. 16, no. 1, pp. 108–110, 2018.
  - [35] M. L. Kern, L. E. Waters, A. Adler, and M. A. White, "A multidimensional approach to measuring well-being in students: Application of the PERMA framework," *The journal of positive psychology*, vol. 10, no. 3, pp. 262–271, 2015.
  - [36] M. Vishnuteja, S. S. Rout, and P. K. Sahoo, "A prospective study of triple assessment in evaluation of breast lump," *International Journal of Advanced Research*, vol. 9, no. 3, pp. 65–71, 2021.
  - [37] X. Chunhao, "Effect of intervention nursing on cancer-related fatigue and quality of life in breast cancer patients undergoing chemotherapy," *Chinese and foreign medical research*, vol. 16, no. 13, pp. 108–110, 2018.
  - [38] X. Weina and P. Lin, "Explore the effect of routine nursing and aerobic exercise combined with music therapy in postoperative nursing of breast cancer," *Contemporary medicine*, vol. 24, no. 2, pp. 142–144, 2018.
  - [39] M. Sadeghi, T. Farajkhoda, M. Khanabadi, and M. Eftekhari, "PERMA model vs. integrative-behavioral couple therapy for fertility problems: a randomized clinical trial protocol," *International Journal of Reproductive BioMedicine (IJRM)*, vol. 19, no. 12, pp. 1105–1116, 2022.
  - [40] N. Zdenkowski, P. Butow, S. Tesson, and F. Boyle, "A systematic review of decision aids for patients making a decision about treatment for early breast cancer," *The Breast*, vol. 26, pp. 31–45, 2016.

## Research Article

# Expression of TNF- $\alpha$ and IL-1 $\beta$ in Peripheral Blood of Patients with T2DM Retinopathy

Jin Qian and Ying Huang 

Medical Laboratory Center, Jiangsu Taizhou People's Hospital, Taizhou, 225300 Jiangsu Province, China

Correspondence should be addressed to Ying Huang; 2111817015@e.gzhu.edu.cn

Received 16 June 2022; Accepted 13 July 2022; Published 8 August 2022

Academic Editor: Hangjun Che

Copyright © 2022 Jin Qian and Ying Huang. This is an open access article distributed under the Creative Commons Attribution License, which permits unrestricted use, distribution, and reproduction in any medium, provided the original work is properly cited.

**Aims.** The expression and clinical significance of tumor necrosis factor- $\alpha$  (TNF- $\alpha$ ) and interleukin 1- $\beta$  (IL-1 $\beta$ ) in retinal cells of patients with type 2 diabetes (T2DM) retinopathy were detected by flow cytometry. **Materials and Methods.** Fifty patients with T2DM who attended our ophthalmology clinic between May 2021 and May 2022 were selected as the observation group. Another 50 healthy individuals who were examined at our hospital during the same period were selected as the comparison group. Tear film rupture time (BUT), fluorescein staining (FL), basal tear secretion (Schirmer I) test, and conjunctival impression cytology (CIC) were detected in both groups, and the expression of TNF- $\alpha$  and IL-1 $\beta$  in retinal cells was observed by immunohistochemical staining. **Results.** The levels of IL13 and TNF- $\alpha$  in the two groups were not exactly the same. The serum levels of IL13 and TNF- $\alpha$  in the observation group were significantly higher than those in the control group, and there was a statistically significant difference ( $P < 0.05$ ). TNF- $\alpha$  and IL-1 $\beta$  expressions in the observation group were positively correlated with the fluorescence staining, and the expression of TNF- $\alpha$  and IL-1 $\beta$  in the observation group was significantly negatively correlated with the BUT test and Schirmer I test. **Conclusion.** Serums TNF- $\alpha$  and IL-1 $\beta$  are significantly elevated in patients with T2DM retinopathy and gradually increase with disease progression. Combined detection of serums TNF- $\alpha$  and IL-1 $\beta$  can help determine the severity of the disease and assess the prognosis.

## 1. Introduction

Diabetic patients often complain of dryness, burning, and foreign body sensations in the eye and other symptoms such as reduced corneal perception and edema. This brings inconvenience to the life of diabetic patients, so diabetic ocular surface disease has attracted great clinical attention [1]. Recent experimental studies in foreign animal models have reported that the P38 mitogen-activated protein kinase (MAPK) signaling pathway is mainly involved in the inflammatory response under stress, and a variety of inflammatory stockiness and some stress responses can activate the signaling pathway and regulate many inflammatory expressions, for which the inflammatory factor tumor necrosis factor- $\alpha$  (TNF- $\alpha$ ) and interleukin 1- $\beta$  (IL-1 $\beta$ ) are key factors. Another important signaling pathway is phosphatidylinositol 3-kinase (PI3K)/protein kinase B (Akt), which plays a role in cell growth,

proliferation, proliferation, and inflammation. Another important instruction pathway is PI3K/Akt, which plays an important role in cell growth, proliferation, survival, and apoptosis [2]. Therefore, by interfering with the expression of key signaling molecules in the P38/MAPK and PI3K/Akt signaling pathways in clinical treatment, it is possible to block the signaling pathways of their associated inflammatory pathways and block the inflammatory response [3]. Retinopathy in type 2 diabetes (T2DM) is a common complication of T2DM, and the main pathological manifestations are retinal microvascular damage, basement membrane thickening, and regularization [4]. Both hyperglycemia and long-term stimulation of late coagulation end products (Age) can lead to local aerodynamic abnormalities of the eye, leading to hypoxia of retinal tissue, vascular epithelial damage and inflammatory cytosine activation, disruption of the blood retinal barrier, and ultimately diabetic retinopathy (DR) [5].

In the inflammatory loop of T2DM homoeopathy, two factors, TNF- $\alpha$  and IL-1 $\beta$ , also occupy an important position, among which TNF- $\alpha$  tumor necrosis factor, which functions to cause tumor chemise necrosis and tumor cell death, has a wide range of biological activity [6]. Epithelial and epithelial cells activated by TNF- $\alpha$  can produce IL-1 $\beta$ , which can act as an immune mediator in inflammation development [7]. This shows that the two factors play complementary roles in the inflammatory loop of T2DM homoeopathy and together promote the formation of ocular surface inflammation [8]. TNF- $\alpha$  and IL-1 $\beta$  are two factors with inflammatory significance in the P38MAPK and PI3K/Akt signaling pathway in T2DM patients with induced T2DM homoeopathy, which can reflect the inflammatory state of the ocular surface [9]. Our study analyzed the expression of TNF- $\alpha$  and IL-1 $\beta$  in the peripheral blood of patients with T2DM homoeopathy, aiming to provide more references for the clinical treatment of patients.

## 2. Material and Methods

**2.1. Research Object.** Fifty patients with T2DM who attended our ophthalmology clinic between May 2021 and May 2022 were selected as the observation group, and 50 healthy people who underwent physical examination in our hospital during the same period were selected as the comparison group. The diagnosis of T2DM was based on the diagnostic criteria of T2DM established by WHO [10] (fasting blood glucose greater than or equal to 7.0 mole/L, or two-hour postprandial blood glucose greater than or equal to 11.1 mole/L); T2DM homoeopathy conforms to the international clinical DR severity grading criteria in 2002 [11], i.e., the patient's fundus shows characteristic retinal micromanage, hemorrhages, hard extenuates, soft extenuates, oracular edema, retinal regularization, etc. DR proliferation stage: regularization appears on the retinal surface or in front of the retina, or there is vitreous hemorrhage, fiber proliferation, and retinal detachment. Patients in the healthy comparison group were required to have no disorders of Coolidge metabolism, no family history of T2DM, and no abnormalities in fundus examination.

**2.2. Inclusion and Exclusion Criteria.** Inclusion criteria are as follows: observation group: (1) the selected patients were in the nonproliferation stage of DR; (2) the history of T2DM reached more than 8 years and had good hypoglycemic control; (3) there was a clear history of type 2 T2DM, meeting the diagnostic criteria of T2DM homoeopathy, and the diagnosis of nonproliferation stage by fundus fluorescence bibliography, aged from 40 to 80 years old, both sexes were eligible. Comparison group: no ocular medication, no corneal contact lens, no ocular laser surgery, no ocular surface-related ocular trauma, no ocular-related surgery, no systemic diseases, and no other ocular diseases within the last three weeks.

Exclusion criteria are as follows: (1) pregnancy, air breast women, abnormal liver function, T2DM telepathy kidney failure (toxaemia phase, uremic phase), history of allergies, unsuitable for fluoroscope, psychiatric patients, combined

with cardiovascular, liver, kidney, and hematologist system and other serious primary diseases; (2) other eye diseases combined (such as glaucoma, cataracts that significantly affect the fundus examination, non-T2DM Homoeopathy, and ileitis); (3) patients with other eye diseases (such as glaucoma, cataract that significantly affects fundus examination, non-T2DM homoeopathy, and ileitis), those who have worn corneal contact lenses, laser eye surgery, ocular surface-related eye trauma, and ocular-related surgery; and (4) patients with T2DM, T2DM during pregnancy, and other special types of T2DM, combined with connective tissue disease or other autoimmune diseases, those who have used hormones and noninflammatory drugs within the last 3 months, combined with severe liver and kidney insufficiency, malignant tumors, or acute and chronic patients with acute and chronic infections.

## 3. Methods

**Tear film rupture time measurement (BUT):** use sterile forceps to take saline-soaked and then lightly touch the florescent sodium test paper of the patient's lower lid instructing the patient to blink sometimes, lightly touch the patient's lower face conjunct sac, instruct the patient to blink a number of times, and then look flatly ahead, live microscope cobalt blue light under wide slit light band observation, stopwatch timing, open the eyes after the last blink until the first black spot appears in the cornea, and record the average value after 3 times when the BUT value < 10 s was considered abnormal. **Florescent staining (FL):** aseptic forceps were used to take sodium fluorescent test paper after wetting with physiological saline, lightly touching the patient's lower lid conjunct capsule, asking the patient to blink several times, and then looking flatly ahead, cobalt in vivo microscopy, and wide slit light band observation under blue light. **Scoring:** the cornea was divided into 4 quadrants, grade 0: no staining (-), grade 1: scattered dot staining (+), grade 2: dense dot staining (++), and grade 3: Bellamy staining (+++). The scores 3, 2, 1, and 0 were recorded, respectively.

**Basic tear secretion test:** without surface anesthetic, reverse-fold the tear detection filter paper strip at the 0-point blank and gently place it in the conjunct membrane of the lower third of the outer and outer eyelid, put it down and ask the patient to gently close the eyes to avoid stimulating excessive tear production, remove the tear detection filter paper strip 5 minutes after starting the timing, and read the wetting (discoloration) length of the filter paper from the reverse-folded 0-point, and the wetting length < 10 m is abnormal.

**Blot cytology:** 3 mm  $\times$  3 mm square nitrocellulose filter paper was disinfected by UV light irradiation before the experiment. **Anesthesia:** procaine hydrochloride binocular solution was dabbed in the right eye of both groups of patients, and surface anesthesia was performed for about 5 min, and any excess tears or anesthetics were removed by aspiration with the filter paper. **Collection and fixation:** the edges of the nitrocellulose filter paper sheets were gently clamped with flat forceps and pressed firmly against the ha side of the conjunct surface of the right eye, and

TABLE 1: Comparison of baseline information of patients in the two groups.

Group	Average age (years)	Sex (M/F)	Body mass index (kg/m <sup>2</sup> )	Body weight (kg)
Comparison group (50)	60.90 ± 1.71	24/26	23.05 ± 2.23	54.35 ± 1.29
Observation group (50)	61.10 ± 1.62	23/27	23.40 ± 2.03	54.10 ± 1.31
$\chi^2/t$	-0.600	0.040	-0.821	0.962
$P$	0.550	0.841	0.414	0.339

the filter paper was removed after 10 seconds of gentle pressure and fixed in 95% ethanol to correspond to the markings. Staining: periodic acid-Schiff (PAS) staining was applied. Gradient alcohol was dehydrated, ethylene was transparent, and the number and status of scapular cells were observed and recorded under light microscope at 400x.

Photochemical staining: nitrocellulose films were cut into 3 mm × 3 mm squares and sterilized for use. Antidepletion slides were prepared. In both groups, procaine hydro chloride eye solution was spotted in the right eye, and surface anesthesia was performed for about 5 min, and any excess tears or anesthetics were removed using filter paper. The edge of the nitrocellulose filter paper sheet should be gently clamped by a flat regent and pressed tightly against the right eye conjunct surface after the title side, and the filter paper was removed after 10 seconds of gentle pressure, and the specimen was fixed on the slide and marked. The nitrocellulose film blot slides were fixed in 95% ethanol. Anhydrous alcohol was dehydrated and then rinsed with water for microwave repair. 0.3% H<sub>2</sub>O<sub>2</sub> was incubated for 10 min at room temperature to drive off the endogenous peroxide enzyme reaction. Distilled water rinsing is followed by 0.01% PBS drops washing for 5 min three times. Add a nonstaining blocking solution for 60 min at room temperature to remove nonspecific staining, add monoclonal antibody and incubate overnight at 4°C, and rinse with PBS for 5 min for a total of three times. Add horseradish-labeled secondary antibody and place in a 37 degree Celsius incubator for 1 hour, and rinse with PBS for 5 minutes 3 times. DAB horseradish hydroxide staining: 0.5 mL each of DAB staining solutions A and B, 1 dab staining working solution (ration at any time of the experiment) at room temperature and protected from light for 30 in. Distilled water wash for 5 minutes to terminate the reaction. Bayer hematology staining for 2 minutes, rinse with tap water for 10 minutes. Specimens were rinsed with tap water for 10 min. The blotted pieces were fixed in 95% alcohol, dried in anhydrous alcohol, and homogeneously transparent in ethylene, and the blotted pieces were sealed with treacle. The following criteria judged IL-1B and TNF- $\alpha$  staining results: observed by light microscope, clear cytologist boundary, no cytoplasmic staining was recorded as negative (-); light cytoplasmic staining, showing light brown color was recorded as weakly positive (+); and moderate cytoplasmic staining, showing brown color was recorded as moderate positive (++). Significant cytoplasmic staining with a dark brown color was recorded as a strong positive (++++).

**3.1. Statistical Methods.** All data of our study were checked using Excel double entry and SPSS 28.0 for statistical analysis, setting the test level  $\alpha = 0.05$  and considering  $P < 0.05$  as

a statistically significant difference. Statistical descriptions of measurement data that obeyed normal distribution were described by mean ± standard deviation, and those not obeying normal distribution were described by median (inter-quartile spacing), and count data were described by frequency and composition ratio. General patient data were analyzed: categorical data were analyzed by chi-square test, continuity-corrected chi-square test, and Fisher's exact probability method; measurement data were analyzed by  $t$ -test. Obedience to a normal distribution, paired-sample  $t$ -test was used for within-group comparisons and two-independent sample  $t$ -test for between-group comparisons; disobedience to normal distribution, nonparametric constellation signed-rank test was used for within-group comparisons, and rank-sum test was used for between-group comparisons for analysis.

## 4. Results

**4.1. Baseline Data Comparison.** The mean age, gender, body mass index, and weight of the patients in the observation group were not statistically significant compared with the comparison group ( $P > 0.05$ ) (see Table 1).

**4.2. Comparison of IL-1 $\beta$  and TNF- $\alpha$  Levels.** A one-way ANOVA comparison of the two groups showed that the levels of IL-1 $\beta$  and TNF- $\alpha$  were not identical between the two groups. Further comparison showed that the serum IL-1 $\beta$  and TNF- $\alpha$  levels of patients in the observation group were significantly higher than those in the comparison group, with statistically significant differences ( $P < 0.05$ ) (see Figure 1).

**4.3. The Relationship between TNF- $\alpha$  and IL-1 $\beta$  Cytokines.** The expressions of TNF- $\alpha$  and IL-1 $\beta$  in the observation group were positively correlated with fluorescence staining, and the expressions of TNF- $\alpha$  and IL-1 $\beta$  in the observation group were significantly negatively correlated with the BUT test and Schemer I test. The results indicated that fluorescent staining, BUT, and Schemer I experiments reflected the patient's progress (see Figure 2).

**4.4. Comparison of the Expression of TNF- $\alpha$  and IL-1 $\beta$  in Retinal Cells.** Comparing the expression rates of stockiness between the two groups, the expressions of TNF- $\alpha$  and IL-1 $\beta$  in retinal cells in the observation group were significantly increased compared with those in the control group, with a statistically significant difference ( $P < 0.05$ ) (see Figure 3).



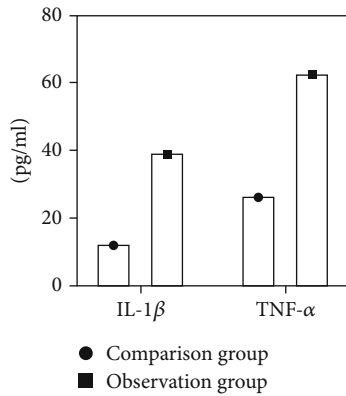


FIGURE 1: Comparison of IL-1 $\beta$  and TNF- $\alpha$  levels. In our study, all data were checked by double entry in Excel, and SPSS 28.0 was used for statistical analysis. The statistical descriptive measurement data obeyed the normal distribution. They were described by the mean  $\pm$  standard deviation. Paired sample *t*-test was used for intragroup comparison, and two-independent sample *t*-test was used for intergroup comparison. It was found that a one-way ANOVA comparison of the two groups showed that the levels of IL-1 $\beta$  and TNF- $\alpha$  were not identical between the two groups. Further comparison showed that the serum IL-1 $\beta$  and TNF- $\alpha$  levels of patients in the observation group were significantly higher than those in the comparison group, with statistically significant differences ( $P < 0.05$ ), \* $P < 0.05$ .

## 5. Discussion

The results of early animal model studies of T2DM showed a large number of white blood cell aggregates in retinal macular cells and a significant increase in several inflammatory factors, including interleaves and TNF- $\alpha$  [12]. A comparative study of T2DM patients undergoing hysterectomy found that IL-1 $\beta$  and TNF- $\alpha$  were significantly elevated in vitreous bodies without proliferative homeopathy, confirming the role of inflammatory factors in developing DR [13]. There are two types of IL-1, IL-1 $\alpha$ , and IL-1 $\beta$ , and IL-1 in the blood is mainly IL-1 $\beta$  secreted by monocyte and esophageal. IL-1 $\beta$  binds to its receptor and is involved in the inflammatory response through G protein coupling for signal instruction [14]. IL-1 $\beta$  can cause intramural infiltration and diffusion of serum proteins and erythrocytes, leading to local exudation, edema, inflammation, widening of the vascular epithelial space, and destruction of the blood retinal barrier [15]. IL-1 $\beta$  can regulate immune cells and induce epithelial cells to express cell-free adhesion factors, is a strong chemotactic agent that enhances nutrition, and plays an important role in leukocyte adhesion and activation [16]. In addition, IL-1 $\beta$  is involved in the formation of nonproliferation homeopathy by acting on retinal pigment epithelial cells and promoting collagen synthesis and deposition [17]. One study found that serum IL-1 $\beta$  was elevated in patients with T2DM homeopathy compared to the comparison group, suggesting that elevated IL-1 $\beta$  levels are an important factor in DR. TNF- $\alpha$  is mainly secreted by denuclearize esophageal and is an inflammatory cytosine with multiple biological functions [18]. First, TNF- $\alpha$  is involved in developing insulin resistance and promotes the progression of

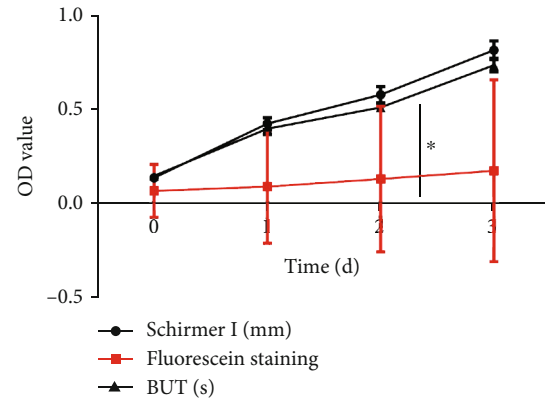


FIGURE 2: The relationship between TNF- $\alpha$  and IL-1 $\beta$  stockiness. In our study, all data were checked by double entry in Excel, and SPSS 28.0 was used for statistical analysis. The statistical descriptive measurement data obeyed the normal distribution. The mean  $\pm$  standard deviation described them. Paired sample *t*-test was used for intragroup comparison, and two-independent sample *t*-test was used for intergroup comparison. It was found that the expressions of TNF- $\alpha$  and IL-1 $\beta$  in the observation group were positively correlated with fluorescence staining, and the expressions of TNF- $\alpha$  and IL-1 $\beta$  in the observation group were significantly negatively correlated with the BUT test and Schermer I test. The results indicated that fluorescent staining, BUT, and Schermer I experiments reflected the patient's progress.

T2DM and its complications [19]. TNF- $\alpha$  induces activation of the NFL pathway by acting on receptors on vascular epithelial cells, causing the appearance of retinal vascular cells, increasing vascular permeability, stimulating the proliferation of additional vascular stromal and vascular cells, and promoting binocular normalization [20]. TNF- $\alpha$  can also increase the activity of eyeglasses and promote abnormal expression of adhesion factors, which enhances the local adhesion and aggregation of inflammatory cells and releases radioactive mediators in the retina, stimulating the local inflammatory response to form a vicious circle [21]. Studies have shown that TNF- $\alpha$  is significantly correlated with the severity of the disease, and that inhibition of TNF- $\alpha$  expression reduces retinal vascular epithelial cell apoptosis by about 80% [22].

It is currently believed that the P38MAPK and PI3K/Akt instruction system triggers inflammatory responses by enhancing TNF- $\alpha$  expression to promote cellular regulation. Conversely, TNF- $\alpha$  factors can act as triggering factors to stimulate signaling pathways [23]. In recent research trials, signaling pathway inhibitory drugs have become a hot issue in treating chronological and inflammatory diseases, with little relevant research on T2DM homeopathy [24]. Our experiment indirectly responded to the activation level of the P38MAPK and PI3K/Akt instruction system by detecting TNF- $\alpha$  and IL-1 $\beta$  stockiness, formulators of signaling pathways, to provide a basis for subsequent therapeutic studies in ocular surface diseases [25]. TNF- $\alpha$  has a wide range of biological activities, and crucially, it can also direct the production of IL-1 $\beta$  by inflammatory cells [26]. The detection factor IL-1 $\beta$  in our experiments is precursor, which has similar biological activities, multifunctional biological roles, and potent inducers of TNF- $\alpha$  [27].



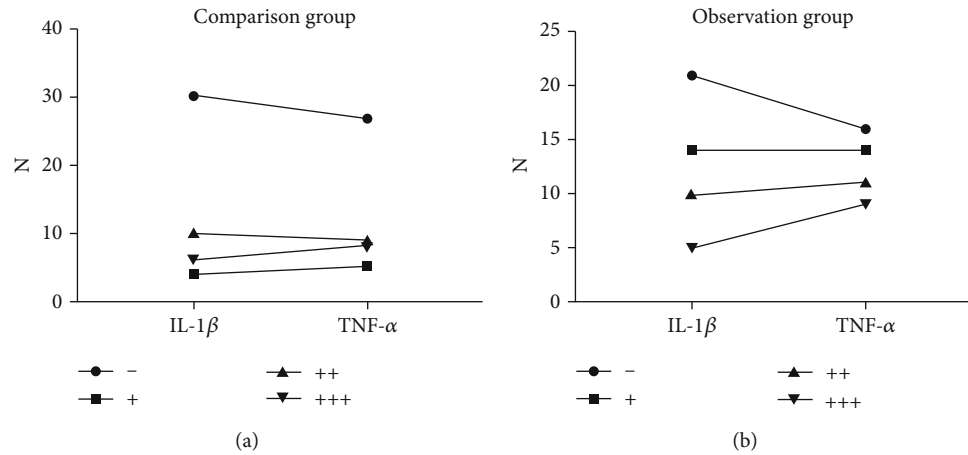


FIGURE 3: Comparison of the expression of TNF- $\alpha$  and IL-1 $\beta$  in retinal cells. In our study, all data were checked by a double entry in Excel, and SPSS 28.0 was used for statistical analysis. The statistical descriptive measurement data obeyed the normal distribution. The mean  $\pm$  standard deviation described them. Paired sample  $t$ -test was used for intragroup comparison, and two-independent sample  $t$ -test was used for intergroup comparison. It was found that comparing the expression rates of stockiness between the two groups, the expressions of TNF- $\alpha$  and IL-1 $\beta$  in retinal cells in the observation group were significantly increased compared with those in the control group, with a statistically significant difference ( $P < 0.05$ ).

We used a photochemical staining assay to detect the levels of TNF- $\alpha$  and IL-1 $\beta$  production and thus analyze the inflammatory mechanisms of T2DM homoeopathy caused by T2DM patients. The results showed that when the level of inflammation of the retinal epithelium was higher than normal, the ocular surface condition of patients with T2DM was in a state of increased inflammatory activity, which may lead to abnormal changes in the normal tear film on the surface of the eye, thus aggravating the progression of homeopathy in T2DM. The results of related studies have shown that impregnation of TNF- $\alpha$  and IL-1 $\beta$  in the retina affects the normal release of transmitters in transmissible [28]. To study the epidemiological changes in the ocular surface of mice with T2DM homoeopathy, a model of increased production of inflammatory factors TNF- $\alpha$  and IL-1 $\beta$  in the conjunctiva of mice was made by inhibiting the general function of choleric receptors in the lackey gland. The results showed that this model could cause a decrease in tear secretion [29]. In contrast, it was found that rat corneal epithelial cell lines produce inflammatory stockiness derived from inflammatory mediators and that TNF- $\alpha$  production may be due to inflammation rather than due to dryness per SE [30]. It was demonstrated that nourishing Yin and eye pill inhibit the inflammatory response of the ocular surface by interfering with the signaling molecules that are key to the P38MAPK signaling pathway by detecting the P38MAPK protein content in the rat conjunct skin [31]. The triggering factors of our experiment were different from the above study, but the results obtained were consistent.

Our experimental results showed that the expression of TNF- $\alpha$  and IL-1 $\beta$  in T2DM patients was significantly and negatively correlated with BUT and chimeric. The corneas of patients with various types and severity of T2DM homoeopathy were compared and observed in detail using laser confocal corneal microscopy, and it was found that the severity of disease in patients with T2DM homoeopathy correlated with the distribution of inflammatory cells in the corneal epithelium and

whether they were activated or not [32]. The values of Schemer II experiment were significantly reduced in patients with T2DM, while Schemer I experiment and BUT experiment values did not show significant differences compared to the comparison group [33]. This is inconsistent with the results of the present experiment, considering that Goebbels' experimental subjects were T2DM patients related. The experimental results showed that there was also a significant impregnation of inflammatory factors in milder than T2DM homoeopathy, suggesting that inflammation occurs early in T2DM homoeopathy, indicating that this unnoticeable inflammation predates the epithelial damage visible to the naked eye. Therefore, the inflammatory response may be a cause of epithelial damage [34]. Therefore, whether inflammation is the initiating factor could be a new starting point for further studies. Therefore, appropriate prophylaxis is given to T2DM patients at the beginning of T2DM homoeopathy, i.e., when epithelial damage has not occurred. The severity of T2DM homoeopathy varies, and their expression varies, reflecting the course of disease development, i.e., as the inflammatory response gradually increases, the extent of the conjunct area it affects becomes more extensive [35]. The experimental results showed that the expression of TNF- $\alpha$  and IL-1 $\beta$  in retinal cells of T2DM patients was negatively correlated with the values of BUT test and Schemer I test, so it is possible to initially assess the level of inflammation in the ocular surface based on clinical examination results, and it is crucial to select the timing of inflammatory treatment relatively accurately [36].

There are some deficiencies in this study. We found that the serums TNF- $\alpha$  and IL-1 $\beta$  in patients with T2DM homoeopathy were significantly higher than those in normal people, and the serums TNF- $\alpha$  and IL-1 $\beta$  in patients with T2DM homoeopathy were higher than those in ordinary diabetic patients. Serum levels of TNF- $\alpha$  and IL-1 $\beta$  were highest in patients with nonproliferation of T2DM homoeopathy. Correlation analysis showed that serums TNF- $\alpha$  and IL-1 $\beta$  were significantly positively correlated. The above all

suggest that the two play a synergistic role in the occurrence and development of patients with T2DM homoeopathy, but the two belong to the upstream and downstream relationship or the same level relationship, which needs further discussion. In addition, we found that both serums TNF- $\alpha$  and IL-1 $\beta$  were related to body mass index and disease course, while T2DM homoeopathy patients had higher body weight, which further confirmed that serums TNF- $\alpha$  and IL-1 $\beta$  were significantly related to DR progression.

In summary, serums TNF- $\alpha$  and IL-1 $\beta$  are significantly elevated in patients with T2DM homoeopathy and gradually increase with disease progression. Combined detection of serums TNF- $\alpha$  and IL-1 $\beta$  can help determine the severity of the disease and assess prognosis. Our study is expected to provide a basis for preventing and diagnosing T2DM homoeopathy.

## Data Availability

No data were used to support this study.

## Conflicts of Interest

The authors declare that they have no conflicts of interest.

## References

- [1] W. Wang, J. Bhang, H. Wang, X. Wang, and S. Li, "Vitamin D deficiency enhances insulin resistance by promoting inflammation in type 2 diabetes," *International journal of clinical and experimental pathology*, vol. 12, no. 5, pp. 1859–1867, 2019.
- [2] S. D. Aspergilliosis, A. Lizzie, G. Tiresias et al., "Diabetes associated periodontitis: differences between type 1 and type 2 diabetes mellifluous," *Journal of periodontal research*, vol. 46, no. 2, pp. 164–169, 2011.
- [3] S. I. Hater, A. A. Mohamed, A. H. Aisha et al., "Stabilized-chitosan selenium nanoparticles efficiently reduce renal tissue injury and regulate the expression pattern of aldose reductase in the diabetic-nephropathy rat model," *Life Sciences*, vol. 279, article 119674, 2021.
- [4] K. Rehman, K. Haider, K. Jabeen, and M. S. H. Akash, "Current perspectives of oleic acid: regulation of molecular pathways in mitochondrial and endothelial functioning against insulin resistance and diabetes," *Reviews in Endocrine & Metabolic Disorders*, vol. 21, no. 4, pp. 631–643, 2020.
- [5] J. Feng, H. Wang, Z. Jing et al., "Relationships of the trace elements zinc and magnesium with diabetic nephropathy-associated renal functional damage in patients with type 2 diabetes mellitus," *Frontiers in Medicine*, vol. 8, article 626909, 2021.
- [6] T. Chen, J. Yu, J. Wang, Q. Chang, and C. Qian, "Elevated serum levels of Lp-PLA2 and IL-18 are associated with progression of diabetic foot ulcers," *Clinical Laboratory*, vol. 66, no. 10/2020, 2020.
- [7] H. Zhang, Y. Zhang, X. Chen, J. Li, Z. Zhang, and H. Yu, "Effects of statins on cytokines levels in gingival crevicular fluid and saliva and on clinical periodontal parameters of middle-aged and elderly patients with type 2 diabetes mellitus," *PLoS One*, vol. 16, no. 1, article e0244806, 2021.
- [8] Y. Yang, Y. Wang, Y. Kong et al., "Carnosine prevents type 2 diabetes-induced osteoarthritis through the ROS/NF- $\kappa$ B pathway," *Frontiers in Pharmacology*, vol. 9, p. 598, 2018.
- [9] H. Li, Q. Xu, C. Xu et al., "Bicyclol regulates hepatic gluconeogenesis in rats with type 2 diabetes and non-alcoholic fatty liver disease by inhibiting inflammation," *Frontiers in Pharmacology*, vol. 12, article 644129, 2021.
- [10] L. F. Li, L. L. Ding, Z. L. Zhan, and M. Qiu, "Meta-analysis on the safety and cardiorenal efficacy of SGLT2 inhibitors in patients without T2DM," *Frontiers in Cardiovascular Medicine*, vol. 8, article 690529, 2021.
- [11] C. P. Wilkinson, F. L. Ferris, R. E. Klein et al., "Proposed international clinical diabetic retinopathy and diabetic macular edema disease severity scales," *Ophthalmology*, vol. 110, no. 9, pp. 1677–1682, 2003.
- [12] M. Lin, D. Song, S. Zhang, and P. Li, "Dysregulation of miR-638 in diabetic nephropathy and its role in inflammatory response," *Diabetology and Metabolic Syndrome*, vol. 13, no. 1, p. 122, 2021.
- [13] O. C. Martínez-Ramírez, D. A. Salazar-Piña, R. M. de Lorena et al., "Association of NF $\kappa$ B, TNF $\alpha$ , IL-6, IL-1 $\beta$ , and LPL polymorphisms with type 2 diabetes mellitus and biochemical parameters in a Mexican population," *Biochemical Genetics*, vol. 59, no. 4, pp. 940–965, 2021.
- [14] M. S. Rabelo, G. H. Gomes, A. M. Foz et al., "Short-term effect of non-surgical periodontal treatment on local and systemic cytokine levels: role of hyperglycemia," *Cytokine*, vol. 138, article 155360, 2021.
- [15] N. Kotagale, S. Rahangdale, A. Borkar et al., "Possible involvement of agmatine in neuropharmacological actions of metformin in diabetic mice," *European Journal of Pharmacology*, vol. 907, article 174255, 2021.
- [16] X. Li, J. He, X. Li, Y. Li, Y. Zhou, and S. Cai, "Neu-P11- a novel melatonin receptor agonist, could improve the features of type-2 diabetes mellitus in rats," *Endokrynologia Polska*, vol. 72, no. 6, pp. 634–642, 2021.
- [17] M. Sun, J. Yang, J. Wang et al., "TNF- $\alpha$  is upregulated in T2DM patients with fracture and promotes the apoptosis of osteoblast cells in vitro in the presence of high glucose," *Cytokine*, vol. 80, pp. 35–42, 2016.
- [18] J. Banerjee, Y. Dhas, and N. Mishra, "Middle-aged Indians with type 2 diabetes are at higher risk of biological ageing with special reference to serum CDKN2A," *Journal Diabetes Research*, vol. 2020, article 7569259, pp. 1–10, 2020.
- [19] D. Mo, S. Liu, H. Ma et al., "Effects of acarbose and metformin on the inflammatory state in newly diagnosed type 2 diabetes patients: a one-year randomized clinical study," *Drug Design, Development and Therapy*, vol. Volume 13, pp. 2769–2776, 2019.
- [20] D. C. D. Santos, I. S. Ribeiro, D. P. S. Lopes et al., "Gender-related differences in the modulation of anthropometric, biochemical, and immune markers by physical activity in hypertensive and diabetic individuals," *Anais da Academia Brasileira de Ciências*, vol. 93, article e20201905, suppl 4, 2021.
- [21] A. H. Dyer, L. McKenna, I. Batten et al., "Peripheral inflammation and cognitive performance in middle-aged adults with and without type 2 diabetes: results from the ENBIND study," *Frontiers in Aging Neuroscience*, vol. 12, article 605878, 2020.
- [22] N. E. Doody, M. M. Doweiko, E. C. Akam et al., "The role of TLR4, TNF- $\alpha$  and IL-1 $\beta$  in type 2 diabetes mellitus

- development within a north Indian population,” *Annals of Human Genetics*, vol. 81, no. 4, pp. 141–146, 2017.
- [23] G. Tsuji, A. Hashimoto-Hachiya, V. H. Yen et al., “Metformin inhibits IL-1 $\beta$  secretion via impairment of NLRP3 inflammasome in keratinocytes: implications for preventing the development of psoriasis,” *Cell death discovery*, vol. 6, no. 1, pp. 1–11, 2020.
  - [24] W. Ding, Z. Xiao, C. Wen et al., “Correlation between salivary developmental endothelial locus-1, interleukin 17 expression level and severity of periodontal disease in patients with type 2 diabetes mellitus,” *American Journal of Translational Research*, vol. 13, no. 10, pp. 11704–11710, 2021.
  - [25] T. Reinehr and C. L. Roth, “Inflammation markers in type 2 diabetes and the metabolic syndrome in the pediatric population,” *Current Diabetes Reports*, vol. 18, no. 12, p. 131, 2018.
  - [26] X. Yang, Y. Chen, W. Zhang et al., “Association between inflammatory biomarkers and cognitive dysfunction analyzed by MRI in diabetes patients,” *Diabetes, Metabolic Syndrome and Obesity: Targets and Therapy*, vol. Volume 13, no. 13, pp. 4059–4065, 2020.
  - [27] L. Borges, M. E. P. Passos, M. B. B. Silva et al., “Dance training improves cytokine secretion and viability of neutrophils in diabetic patients,” *Mediators of Inflammation*, vol. 2019, Article ID 2924818, 8 pages, 2019.
  - [28] O. Azmy Nabeh, M. Ishak Attallah, and N. El-Sayed El-Gawhary, “The pivotal relation between glucagon-like peptides, NF $\kappa$ B and inflammatory bowel disease,” *Clinical and Experimental Pharmacology & Physiology*, vol. 47, no. 10, pp. 1641–1648, 2020.
  - [29] Y. Dhas, J. Banerjee, G. Damle, and N. Mishra, “Serum 25(OH) D concentration and its association with inflammation and oxidative stress in the middle-aged Indian healthy and diabetic subjects,” *Steroids*, vol. 154, article 108532, 2020.
  - [30] J. Liu, Q. Zuo, Z. Li, J. Chen, and F. Liu, “Trelagliptin ameliorates IL-1 $\beta$ -impaired chondrocyte function via the AMPK/SOX-9 pathway,” *Molecular Immunology*, vol. 140, pp. 70–76, 2021.
  - [31] L. Zhu, L. Sha, K. Li et al., “Dietary flaxseed oil rich in omega-3 suppresses severity of type 2 diabetes mellitus via anti-inflammation and modulating gut microbiota in rats,” *Lipids in Health and Disease*, vol. 19, no. 1, p. 20, 2020.
  - [32] M. J. Carranza-Naval, M. Vargas-Soria, C. Hierro-Bujalance et al., “Alzheimer’s disease and diabetes: role of diet, microbiota and inflammation in preclinical models,” *Biomolecules*, vol. 11, no. 2, p. 262, 2021.
  - [33] S. Yu, Y. Cheng, L. Zhang et al., “Treatment with adipose tissue-derived mesenchymal stem cells exerts anti-diabetic effects, improves long-term complications, and attenuates inflammation in type 2 diabetic rats,” *Stem Cell Research & Therapy*, vol. 10, no. 1, p. 333, 2019.
  - [34] C. Liu, X. Feng, Q. Li, Y. Wang, Q. Li, and M. Hua, “Adiponectin, TNF- $\alpha$  and inflammatory cytokines and risk of type 2 diabetes: a systematic review and meta-analysis,” *Cytokine*, vol. 86, pp. 100–109, 2016.
  - [35] K. Karstoft and B. K. Pedersen, “Exercise and type 2 diabetes: focus on metabolism and inflammation,” *Immunology and Cell Biology*, vol. 94, no. 2, pp. 146–150, 2016.
  - [36] B. K. Pedersen, “Anti-inflammatory effects of exercise: role in diabetes and cardiovascular disease,” *European Journal of Clinical Investigation*, vol. 47, no. 8, pp. 600–611, 2017.

## Research Article

# Antistroke Network Pharmacological Prediction of Xiaoshuan Tongluo Recipe Based on Drug-Target Interaction Based on Deep Learning

Yongfu Zhou 

*School of Chemistry and Pharmaceutical Engineering Chongqing Industry Polytechnic College, Chongqing 401120, China*

Correspondence should be addressed to Yongfu Zhou; [zhouyf@cqipc.edu.cn](mailto:zhouyf@cqipc.edu.cn)

Received 16 June 2022; Revised 14 July 2022; Accepted 21 July 2022; Published 2 August 2022

Academic Editor: Hangjun Che

Copyright © 2022 Yongfu Zhou. This is an open access article distributed under the Creative Commons Attribution License, which permits unrestricted use, distribution, and reproduction in any medium, provided the original work is properly cited.

Stroke is a common cerebrovascular disease that threatens human health, and the search for therapeutic drugs is the key to treatment. New drug discovery was driven by many accidental factors in the early stage. With the deepening of research, disease-related target discovery and computer-aided drug design constitute a more rational drug discovery process. The deep learning model was constructed by using recurrent neural network, and then, the classification and prediction of compound-protein interactions were studied. In this study, the network pharmacological prediction of stroke based on deep learning is obtained. (1) In the case of discrete time, a distributed optimization algorithm with finite time convergence is applied. A distributed exact first-order algorithm for the case where the objective function is smooth. On the basis of the DGD algorithm, an additional cumulative correction term is added to correct the error caused by the fixed step size of DGD. Solve multiple optimization problems with equality constraints by using Lagrangian functions. Alternately update the original variable and the dual variable to get the solution of a large global problem. It converges to the optimal solution in an asymptotic or exponential way; that is, the node can reach the optimal solution more accurately when the time tends to infinity. (2) Deep learning, also sometimes called representation learning, has a set of algorithms that can automatically discover the desired classification or detection by feeding it into a machine using raw datasets. Multiple levels of abstraction are abstracted through the use of nonlinear models. This simplifies finding solutions to complex and nonlinear functions. Based on the automatic learning function, it provides the functions of modularization and transfer learning. Deep architectures, which usually contain hidden layers, differ from traditional machine learning, which requires a large amount of data to train the network. There are many levels of modules that are nonlinear and transform the information present on the first level into higher levels which are more abstract in nature and are basically used for feature extraction and transformation. (3) The accuracy rate of the framework based on the multitask deep learning algorithm is 91.73%, and the recall rate reaches 96.13%. The final model was predicted and analyzed using real sample data. In the inference problem, it has the advantages of fast training and low cost; in the generation problem, it also has the advantages of fast training, high stability, high diversity, and high quality of image reconstruction.

## 1. Introduction

Stroke, commonly known as “stroke,” is a common type of cerebrovascular disease that threatens human health. It has the characteristics of high morbidity, high mortality, high disability rate, and high recurrence rate. After stroke, the cortical swallowing center is damaged, namely, pseudobulbar palsy, which mainly affects the first two phases of the swallowing process—oral preparation phase and oral phase.

Damage to the cortical swallowing center will cause severe swallowing disorders, and it will be impossible to control the swallowing intensity. Strokes are mostly due to internal injury accumulation, coupled with loss of work and rest, depression, uncontrolled diet, or invasion of external pathogens, resulting in the imbalance of yin and yang of the internal organs of the human body. Qi machine disorder, internal movement of liver wind, phlegm fire, channeling meridians, blocking the mind orifices, and thus sudden



syncope eventually lead to brain tissue death; that is, the proportion of ischemic stroke is as high as 80%. Stroke disorders, including inhibitory neuronal circuits, will also be affected. The medulla oblongata swallowing center is damaged, that is, true bulbar palsy. After trauma to the medulla oblongata swallowing center, there will be abnormalities in the pharyngeal stage, pharyngeal muscle paralysis, levator laryngeal muscle weakness, pharyngeal dyskinesia, tongue muscle tremor, atrophy, slurred speech, prolonged swallowing reflex initiation, and difficulty swallowing. Food retention in the pharynx can easily cause asphyxia. Decreased input of sensory information will result in a delay in the initiation of swallowing, resulting in dysphagia. Stroke may cause extensive brain tissue damage leading to cognitive impairment. In inflammatory mechanism, cerebral ischemia causes blood-brain barrier diffusion dysfunction, inflammatory reaction, edema of brain cells, and neuronal death under the action of cytokines, chemokines, and reactive oxygen species. For the changes in neurotransmitter levels, when the levels of neurotransmitters associated with cognition are abnormal after stroke, cognitive impairment can also be caused. Abnormal levels of dopamine can lead to executive control impairment. Visual-spatial attention and working memory are innervated by cholinergic and dopaminergic pathways involving frontoparietal and frontostriatal networks [1–3]. Application of traditional Chinese medicine and acupuncture in the treatment of phlegm and blood stasis blocking collaterals type arrhythmia, to resolve phlegm and dissipate stagnation, *Salvia*, *Dilong* to promote blood circulation to remove blood stasis and dredging collaterals, licorice tablets to detoxify and reconcile various medicines, the whole formula clears phlegm and opens orifices, activates blood and dredges collaterals. The results show that Ditan Decoction combined with acupuncture in the treatment of poststroke dysphagia patients with phlegm and blood stasis blocking collaterals can effectively reduce the symptoms of dysphagia and the risk of aspiration and significantly reduce complications. As one of the complications after stroke, swallowing dysfunction has no specific name in ancient Chinese medicine books, but it is based on the causes of swallowing dysfunction (esophageal disease, throat disease, cerebrovascular accident, etc.). Traditional Chinese medicine decoction is a common treatment method in traditional Chinese medicine. Because of its advantages of simple preparation and rapid curative effect, it is often used for the treatment of dysphagia after stroke. The patients were treated with Bushen-Liyan Decoction and their symptoms were evaluated. The results showed that the total effective rate was 83.33% [4–6]. Qiyan Decoction can effectively treat patients with dysphagia after stroke with internal obstruction of blood stasis. This method is effective and safe. Acupuncture provides valuable practical experience in the treatment of dysphagia after stroke. Whether the swallowing function is normal or not is related to the tongue, pharynx, larynx, and other parts. Therefore, from the perspective of TCM meridians, swallowing function is related to the Ren meridian, the spleen meridian of the foot Taiyin, the stomach meridian of the foot Yangming, the kidney meridian of the foot Shaoyin, and foot Jueyin liver meridian. Acupunc-

ture and moxibustion can effectively regulate the brainstem neuron network and the higher cortical center, make the cerebral cortex more active, restore the normal blood supply to the brain, and improve the level of central nervous system function; in addition, it can also allow the normal activities of the swallowing muscles. The research data of acupuncture treatment of poststroke dysphagia patients were collected and sorted, and a meta-analysis was carried out on this basis. The results showed that this treatment can improve the level of swallowing function. When dealing with a neural network, a loss function is preset, and then, an optimization algorithm can be used to minimize the loss value of the loss function. In the optimization algorithm, the set loss function is generally called the objective function of the optimization problem. Even if the optimization algorithm is used, it may not be guaranteed that all neural networks have good generalization errors. Therefore, in the process of neural network training, it is necessary to pay attention to problems such as overfitting and underfitting, so as to obtain the numerical solution of the objective function. It is necessary to choose suitable values to update the independent variables in the reverse direction along the gradient to reduce the value of the objective function. KEGG pathway enrichment of signaling pathways describe gene regulation [7–9]. Deep learning techniques define and design model inputs according to some principles, such as data packets, PCAP files, and flow statistical feature files. Second, models and algorithms are purposefully selected according to the features of the model and the purpose of the classifier. Finally, a deep learning classifier is trained to associate the inputs with the corresponding class labels. The training of deep learning models requires a large number of labeled samples, which are difficult to collect in real network environments. A flow feature extraction algorithm based on the concept of bidirectional flow is used to preprocess the malicious traffic dataset. It solves the problem of low recognition accuracy of traditional feature extraction algorithms and proposes a multitask-based deep learning model, which is more efficient than the single-task-based deep learning model on the public CIC-IDS2017 dataset and CIC-DDoS2019 dataset. For better performance, a data preprocessing scheme was proposed to construct a feature extraction algorithm based on the concept of bidirectional flow and a malicious traffic monitoring system with a multitask deep learning CNN model. The experiment is a subset of the public CIC-IDS2017 dataset and the CIC-DDoS2019 dataset. The malicious traffic of some malicious traffic categories in all the datasets is less than the malicious traffic of the malicious traffic category selected in this paper [10–12]. Class imbalance is an important problem in malicious traffic classification, and how to eliminate the training impact brought by this class imbalance is a valuable research in the future. In the multitask-based deep learning training experiment, we found that if the loss weights of different tasks are correctly combined for the three tasks, the accuracy of each task recognition is also different. So how to set the most appropriate combination of loss weights to achieve the best learning accuracy is a valuable research. There are only a dozen types of malicious traffic identified by the malicious traffic monitoring system



based on multitask deep learning, so capturing and collecting enough malicious traffic types is an important part of our next work. The deep learning model was constructed by using recurrent neural network, and then, the classification and prediction of compound-protein interactions were studied. Complete the collection and preprocessing of experimental data. Postconditions are related to the initial and final states, assuming that all other threads obey the dependency constraints [13–15]. The key to achieving compositionality is to reformulate interference-free tests.

## 2. Drug Target Prediction

**2.1. Predicting Drug-Target Interactions.** “Drug discovery,” as a research direction at the intersection of biology, chemistry, and informatics, represents the unremitting efforts of human beings to contribute to survival and health. As shown in Figure 1, drug discovery was driven by many accidental factors in the early stage. With the deepening of research, the two links of disease-related target discovery and computer-aided drug design together constitute a more rational drug discovery process. Systems pharmacology is derived from presystems biology and emphasizes the integration of multilevel and multiomics information. The latter is often compared to the “design key,” which takes structural biology and analytical chemistry as the source of thought, and derives structure-based drug design, usually referring to LBDD with clear binding site structure information and ligand-based drug design. Traditional drug discovery mostly follows the assumption of “single target-local antagonism”; that is, it is assumed that the mechanism of action of a drug is that a certain single component acts on a certain single target, and then through the downstream signaling pathway, and finally affects the phenotype, that is, from the drug molecule to the phenotype. From molecular target to final phenotype, it goes through a linear “mechanical process.” Such assumptions have profoundly affected the whole process of drug discovery from methodology and preclinical research system to clinical trial design, including computer-aided drug design usually targeting a certain target or binding site; research based on systems pharmacology or network medicine is often attributed to finding a molecule that conforms to the characteristics of the network structure or a molecule on the core link of the key mechanism as a target.

**2.2. Drug-Disease Relationship Prediction Algorithm.** Under the assumption of low rank, the bounded kernel norm regularization method (BNRR) was used to complete the drug-disease matrix. BNRR is performed on adjacency matrices of heterogeneous drug-disease networks integrating drug-drug, drug-disease, and disease-disease networks. But integrating all similar networks can introduce noise into the data, as shown in Figure 2. Matrix factorization and matrix completion techniques have been applied to drug relocation in recent years. Including the interaction network among genes, a matrix decomposition model was established. Using the information in the gene network, the relationship between drugs and diseases can be predicted, and new indications of known drugs can be obtained. The

drug-drug relationship network, disease-disease relationship network, and drug-disease relationship network were integrated to construct a heterogeneous network, and then, the dominant singular value and the corresponding singular vector of the association matrix were efficiently calculated using R4SVD. Based on the singular value threshold (SVT) algorithm, a drug relocation recommendation system (DRRS) is proposed to rank the potential associations between drugs and diseases by complementing the drug-disease association matrix. The loss function, also known as the cost function, is used as a learning criterion for optimizing the parameters of the neural network. The loss function is used to measure the degree of difference between the predicted value of the model and the real value. It is a non-negative real-valued function. The better the model fits the real value, the smaller the loss function. The worse the model fits the true value, the larger the value of the loss function. Similar to the choice of activation function, the types of loss functions used by different models and problems are also different. The loss functions are generally divided into empirical risk loss functions and structural risk loss functions.

## 3. Deep Learning Algorithms

### 3.1. LDAP [16–20].

$$\min f(x) + g(z). \quad (1)$$

Classifier:

$$\begin{aligned} \text{s.t. } Ax + Bz &= c, \\ p^* &= \inf \{f(x) + g(z) | Ax + Bz = c\}. \end{aligned} \quad (2)$$

Marked samples:

$$\begin{aligned} L_\rho(x, y, z) &= f(x) + g(z) + y^T(Ax + Bz - c) + \frac{\rho}{2} \|Ax + Bz - c\|_2^2, \\ x^{k+1} &= \arg \min_x L_\rho(x, z^k, y^k). \end{aligned} \quad (3)$$

Dataset:

$$\begin{aligned} z^{k+1} &= \arg \min_z L_\rho(x^{k+1}, z, y^k), \\ y^{k+1} &= y^k + \rho(Ax^{k+1} + Bz^{k+1} - c). \end{aligned} \quad (4)$$

**3.2. NSSQL [21–23].** Feature extraction algorithm for bidirectional flow concept:

$$\sum_{i=1}^n f_i(x) + g(x). \quad (5)$$

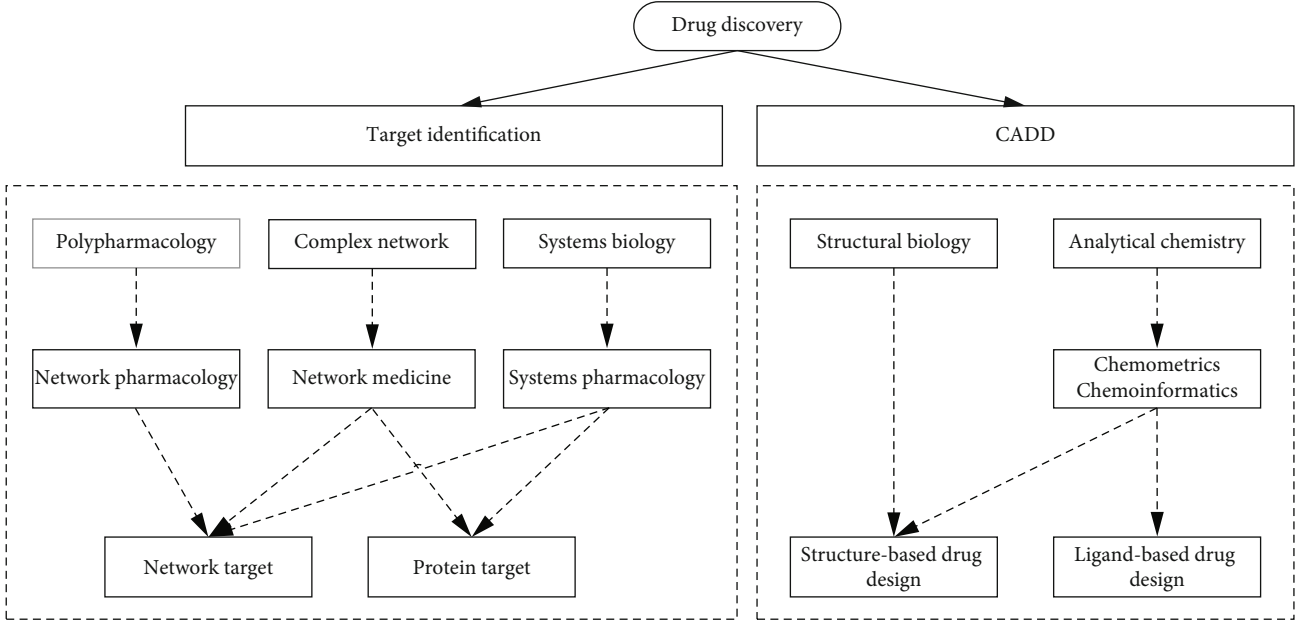


FIGURE 1: Schematic diagram of network target.

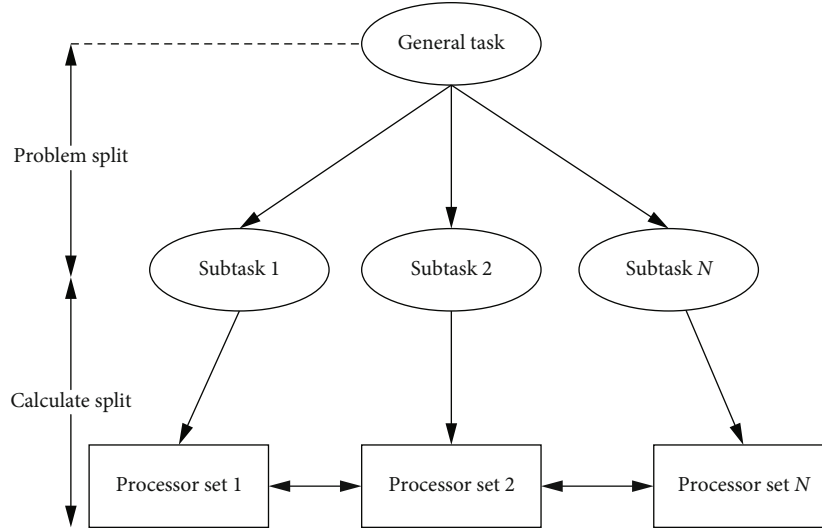


FIGURE 2: Distributed learning framework.

Loss function:

$$\begin{aligned} \min \sum_{i=1}^n f_i(x_i) + g(z) \\ \text{s.t. } x_i - z = 0, i = 1, \dots, n. \end{aligned} \quad (6)$$

Multitask deep learning:

$$L_p(\{x_i\}, z, \{y_i\}) = \sum_{i=1}^n \left( f(x_i)_i + y_i^T (x_i - z) + \frac{\rho}{2} \|x_i - z\|_2^2 \right) + g(z). \quad (7)$$

TABLE 1: Experimental results of autoencoder.

Test set	Accu. (%)	Prec. (%)	Sen. (%)	MCC (%)	AUC (%)
1	41.43	59.13	48.04	73.83	72.12
2	42.82	85.9	43.96	66.69	75.94
3	61.88	60.22	84.56	70.2	88.81
4	74.26	43.75	82.02	83.36	86.93
5	75.39	63.51	49.35	51.89	83.8
6	65.15	68.77	77.3	62.52	75.77

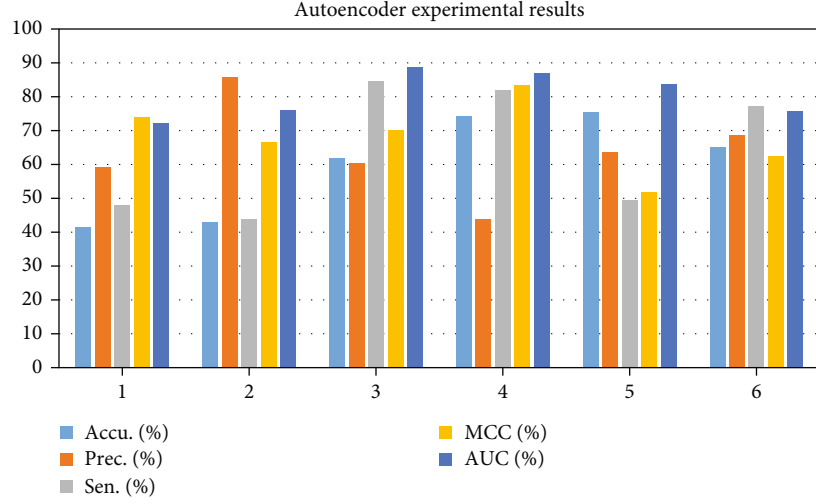


FIGURE 3: The experimental results of the autoencoder.

TABLE 2: Model performance comparison.

	BF-Alg Accu	BF-Alg Recall	BF-Alg F1-score	T-Alg Accu	T-Alg Recall	T-Alg F1-score
LDAP	82.4	97.31	87.86	98.82	90.21	81.15
NSSQL	91.11	82.53	88.61	86.47	96.25	90.91
NetBIOS	96.61	89.38	92.28	98.08	82.48	82.75
SYN	84.95	85.93	90.61	82.83	92.77	97.04
TFTP	95.94	87.95	90.74	83.91	98.53	98.91

Monitoring system identification:

$$\begin{aligned}
 x_i^{k+1} &= \arg \min f_i(x_i)_i + y_i^{kT} (x_i - z^k) + \frac{\rho}{2} \|x_i - z^k\|_2^2, \\
 z^{k+1} &= \arg \min \left( g(z) + \sum_{i=1}^n \left( -y_i^{kT} z + \frac{\rho}{2} \|x_i^{k+1} - z\|_2^2 \right) \right).
 \end{aligned} \tag{8}$$

Compound-protein interactions:

$$y_i^{k+1} = y_i^k + \rho (x_i^{k+1} - z^{k+1}). \tag{9}$$

Activation function:

$$\min \sum_{i=1}^n f_i(x_i) + g \left( \sum_{i=1}^n x_i \right). \tag{10}$$

Multiomics information integration:

$$\begin{aligned}
 L_p(\{x_i\}, \{z_i\}, \{y_i\}) &= \sum_{i=1}^n \left( f_i(x_i)_i + y_i^T (x_i - z_i) + \frac{\rho}{2} \|x_i - z_i\|_2^2 \right) \\
 &+ g \left( \sum_{i=1}^n z_i \right).
 \end{aligned} \tag{11}$$

3.3. NetBIOS [24–26]. Systems pharmacology:

$$\begin{aligned}
 x_i^{k+1} &= \arg \min \left( f_i(x_i) + \frac{\rho}{2} \|x_i - z_i^k + u_i^k\|_2^2 \right), \\
 z_i^{k+1} &= \arg \min \left( g \left( \sum_{i=1}^n z_i \right) + \sum_{i=1}^n \left( \frac{\rho}{2} \|z_i - x_i^k - u_i^k\|_2^2 \right) \right).
 \end{aligned} \tag{12}$$

Single target:

$$\begin{aligned}
 u_i^{k+1} &= u_i^k + x_i^{k+1} - z_i^{k+1}, \\
 \min g(n\bar{z}) &+ \frac{\rho}{2} \left( \sum_{i=1}^n \|z_i - \alpha_i\|_2^2 \right).
 \end{aligned} \tag{13}$$

Downstream signaling pathway:

$$\bar{z} = \frac{1}{n} \sum_{i=1}^n z_i. \tag{14}$$

Molecular target:

$$x_i^{k+1} = \arg \min \left( f_i(x_i) + \frac{\rho}{2} \|x_i - x_i^k + \bar{x}^k - \bar{z}^k + u_i^k\|_2^2 \right). \tag{15}$$

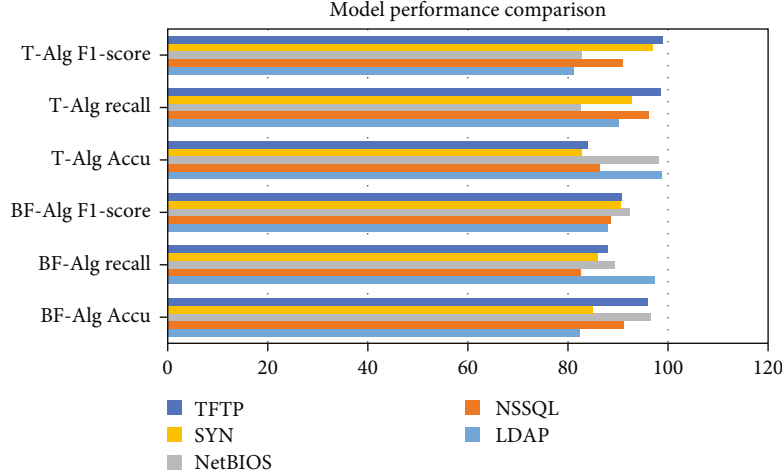


FIGURE 4: Model performance comparison.

Regularization method:

$$z^{k+1} = \arg \min \left( g(n\bar{z}) + \frac{n\rho}{2} \left\| \bar{z} - x^{k+1} - u^k \right\|_2^2 \right). \quad (16)$$

Drug-disease matrix:

$$s(i, j) = (X * W)(i, j) = \sum_m \sum_n x(i + m, j + n) w(m, n). \quad (17)$$

Predicting drug-disease relationships:

$$\begin{aligned} \min \sum_{i=1}^n f_i(w_i) + g(w), \\ \min \sum_{i=1}^n f_i(w_i) + \frac{\lambda}{2} \|w_i - w\|^2. \end{aligned} \quad (18)$$

## 4. Simulation Experiment

**4.1. Distributed Algorithm.** The ADMM algorithm can decompose a complex problem into a simple subproblem, so as to solve the problem in parallel. Early distributed optimization algorithms were distributed subgradient algorithms. DGD is a simple distributed first-order gradient descent algorithm suitable for solving nonsmooth convex functions. Distributed optimization algorithms that converge in finite time can be divided into discrete and continuous. In the discrete-time case, a distributed optimization algorithm with finite-time convergence is applied. Each agent performs its own consensus step and then descends along the local subgradient of its own convex objective function. As shown in Table 1 and Figure 3, the experimental results are shown in data 1, Accu.(%) = 41.43, Prec.(%) = 59.13, Sen.(%) = 48.04, MCC (%) = 73.83, and AUC (%) = 72.12. But this algorithm only works for balanced graphs. In dataset 6, Accu.(%) = 65.15, Prec.(%) = 68.77, Sen.(%) = 77.3, MCC (%) = 62.52, and AUC (%) = 75.77.

TABLE 3: Experimental results of network parameter tuning.

	2	3	4
F1-score	92.12	82.43	88.56
Accuracy	80.92	85.27	91.06
AUC	95.23	86.24	93.88
AUPR	84.94	98.92	88.93
Loss	96.49	89.19	95.65
Precision	95.19	85.07	82.03
Recall	97.54	86.09	93.03
Specificity	83.33	80.4	89.41

**4.2. ADMM General Form.** It is shown in Table 2 and Figure 4. The problem of selectivity and invariance is the main difficulty of conventional machine learning; therefore, the ability of these methods to deal with data in raw form is limited. In the LDAP category, BF – Alg Accu = 82.4, BF – Alg Recall = 97.31, BF – Alg F1 – score = 87.86, T – Alg Accu = 83.91, T – Alg Recall = 98.53, and T – Alg F1 – score = 98.91. Each layer takes the output of the previous layer as input and applies nonlinear transformations to extract useful features for classification. Selectivity versus invariance means selecting those features that contain more information and ignoring those features that contain less information about the parameters; i.e., the selected features should be different from each other. In the TFTP category, BF – Alg Accu = 95.94, BF – Alg Recall = 87.95, BF – Alg F1 – score = 90.74, T – Alg Accu = 83.91, T – Alg Recall = 98.53, and T – Alg F1 – score = 98.91. Deep learning, sometimes called representation learning, has a set of algorithms that can automatically discover desired classifications or detections by feeding them into machines using raw datasets. Deep learning methods abstract multiple levels of abstraction by using nonlinear models. This simplifies finding solutions to complex and nonlinear functions. Deep learning is based on the automatic learning function and provides the function of modularization and transfer learning. Deep learning usually includes deep

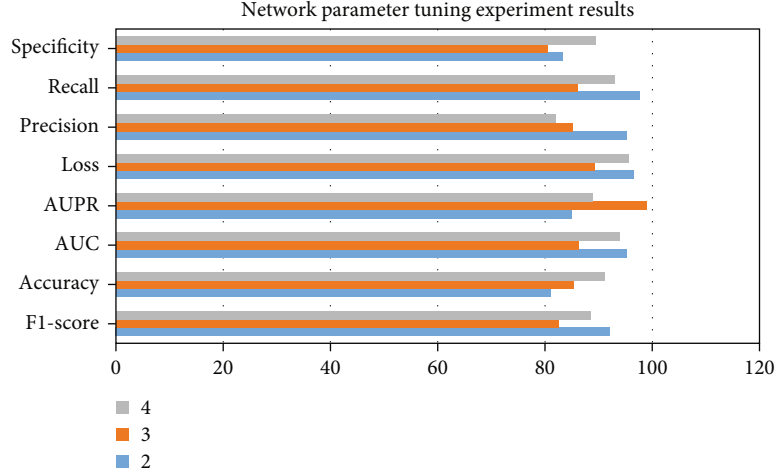


FIGURE 5: The experimental results of network parameter tuning.

architectures with hidden layers, and unlike traditional machine learning, deep learning requires a large amount of data to train the network. There are many levels of modules in deep learning which are nonlinear and transform the information present on the first level into higher upper levels which are more abstract in nature and are basically used for feature extraction and transformation.

**4.3. Autoencoders.** The encoder operation converts the input vector into a compressed representation, while the decoder operation attempts to reconstruct from input variables. The sizes of the input and output layers are equal, and the size of the hidden layer must be smaller than the size of the input layer. The acquired information will inevitably contain a lot of noise, or the information is very rich and diverse. Whether it is noise information or other information irrelevant to the subsequent tasks, it is not helpful for subsequent tasks such as classification and recognition. The dimension of the original data feature space is reduced to obtain a set of classification samples with low probability of classification error and no redundancy. The scale of data information grows very fast, and linear discriminant analysis, autoencoder, isometric mapping, local linear embedding, and traditional autoencoders have developed many improved models based on autoencoders through continuous development. As shown in Table 3 and Figure 5, the tuning results are F1 – score = 92.12, Accuracy = 80.92, AUC = 95.23, AUPR = 84.94, Loss = 96.49, Precision = 95.19, Recall = 97.54, and Specificity = 83.33. Since the vector output by the traditional autoencoder is unknown and disordered, the autoencoder can only learn data but cannot actively generate data. At the same time, the feature vector of the hidden layer lacks continuity, that is, under small disturbances, the generated data will be very strange and very deviating from the input data of the original model. The hidden layer obtained in the traditional autoencoder coding network is changed to obtain the mean and variance, and then, from the normal distribution satisfying the mean and variance, the mean and variance are uniquely determined. The output of both the encoder and the decoder in the variational autoencoder are probability density distributions,

TABLE 4: Model prediction results.

Method	Dataset	Recall (0.9)	Samplesa	Recall (0.5)
DNN EDTPs1	3216	13.62	18	40.67
DNN EDTPs2	3827	9.09	14	71.98
DNN EDTPs	7043	23.46	14	88.36
HN EDTPs1	3216	21.89	17	76.88
HN EDTPs2	3827	31.59	19	58.29
HN EDTPs	7043	12.37	19	55.39
RNN EDTPs1	3216	24.64	20	43.58
RNN EDTPs2	3827	45.67	17	46
RNN EDTPs	7043	14.54	10	52.5
RF EDTPs1	3216	24.79	15	47.17
RF EDTPs2	3827	24.8	16	47.84
RF EDTPs	7043	25.44	17	81.09
SVM EDTPs1	3216	32.19	17	58.06
SVM EDTPs2	3827	31.76	18	59.54
SVM EDTPs	7043	37	13	67.21

and the variables in the probability distribution are constrained by parameters. For common data such as pictures, videos, and audios, it is often assumed that they are generated by some lower-level variables, and these variables satisfy some specific distributions, which are called latent variables or latent variables. These hidden variables represent the internal structure of the data or some kind of abstraction. In order to solve the inference problem, the main methods are Monte Carlo Markov chain and variational inference. Because Monte Carlo Markov chains require large batches of data at each step in training, the training cost is very high. Compared with the inference problem, it has the advantages of fast training and low cost. In the generation problem, it also has the advantages of fast training, high stability, high diversity, and high image reconstruction quality. The disadvantages are low definition and so on.

**4.4. Deep Learning Model Training.** Its input is preserved due to the deep learning modulo internal memory. Just like



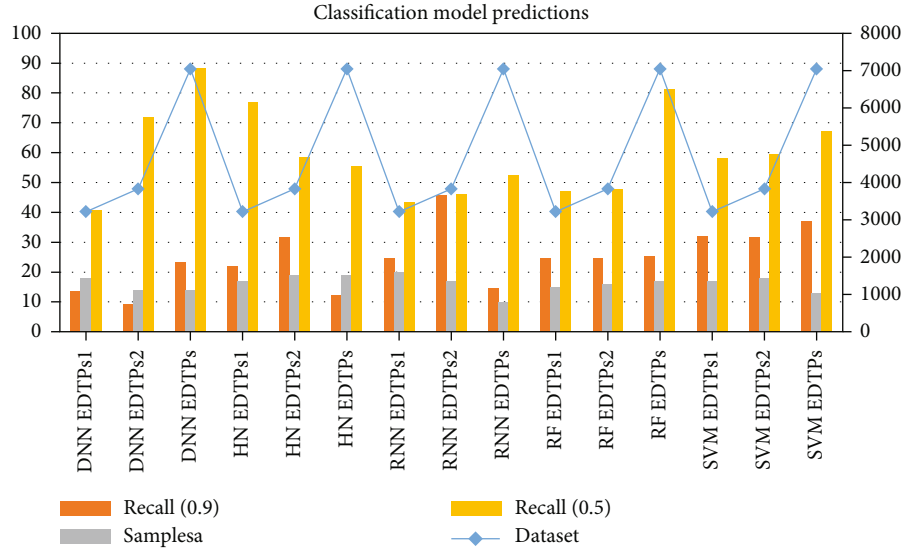


FIGURE 6: Classification model prediction results.

human behavior, it takes into account the information it currently has as well as previous experience gained through loops when making a decision. The most popular implementation is long short-term memory, which backpropagates errors through layers, learning in a circular fashion. According to these characteristics of network traffic, identification techniques in data mining can be used to achieve good traffic identification through machine learning. In network traffic identification, this prior knowledge can be different characteristics of network traffic and personnel supervision information. Choosing an appropriate machine learning algorithm can make full use of prior knowledge to complete traffic identification. As shown in Table 4 and Figure 6, in DNN EDTPs1 prediction, Dataset = 3216, Recall (0.9) = 13.62, Samplesa = 18, and Recall (0.5) = 40.67. When the traffic characteristics are easily outdated quickly, there are many observation samples, and the learning efficiency is not very high. A framework based on multitask deep learning algorithms is included. Separate and purify the PCAP files of the public datasets according to traffic categories. In view of the fact that the packets are captured at the link layer, some data packets may be ARP protocol, etc., and there is no upper layer information, so these data packets are regarded as invalid packets. In addition, some data packets have no port information, and an exception will be thrown. These packets are discarded. Using timestamp, source ip, source port, destination ip, and destination port, the data packets of the PCAP file are purified into a new PCAP file according to the malicious traffic type according to the collection information of malicious traffic. The prediction results of SVM EDTPs1 are Dataset = 3216, Recall (0.9) = 32.19, Samplesa = 17, and Recall (0.5) = 58.06. The data fed into the model training needs to be detected outliers; otherwise, the recognition performance of the model may be degraded. The outliers in the flow features are eliminated and normalized. The label data needs to be labeled according to the classification rules of the task to form a label

file with the same sample size as the dataset. It also helps the classification task to converge faster during model training after the label file is formed. The dataset is divided into three parts before model training, which are used as the input of the main task, auxiliary task, and model test, respectively; after the model is constructed, the test data is used to test the model, and finally, the three parts of the multitask deep learning model are output. Each task recognition result outputs the confusion matrix of the main task and four performance evaluation indicators: precision, recall, F1-Score and accuracy.

## 5. Conclusion

Stroke is a common cerebrovascular disease that threatens human health, and the search for therapeutic drugs is the key to treatment. New drug discovery is driven by many accidental factors in the early stage. With the deepening of research, the two links of disease-related target discovery and computer-aided drug design together constitute a more rational drug discovery process. The deep learning model was constructed by using recurrent neural network, and then, the classification and prediction of compound-protein interactions were studied. Complete the collection and preprocessing of experimental data. Postconditions are related to the initial and final states, assuming that all other threads obey the dependency constraints. The key to achieving compositionality is to reformulate interference-free tests. (1) In the discrete-time case, a distributed optimization algorithm with finite-time convergence is applied. Each agent performs its own consensus step and then descends along the local subgradient of its own convex objective function. Under the assumption that the subgradient is bounded, the distributed subgradient descent algorithm with gradually decreasing step size can gradually converge to a domain of the optimal solution. When the objective function is smooth, a distributed exact first-order algorithm can be obtained. The central idea is to add an additional cumulative

correction term based on the DGD algorithm to correct the error caused by the fixed step size of DGD. The experimental results are shown in data 1, Accu.(%) = 41.43, Prec.(%) = 59.13, Sen.(%) = 48.04, MCC (%) = 73.83, and AUC (%) = 72.12. But this algorithm only works for balanced graphs. It is allowed to use its local continuous state arbitrarily to obtain the optimal value within a limited time step. The optimal value is obtained when the network topology graph is a directed graph and is strongly connected. Alternating direction multiplier method is to solve multiple optimization problems with equality constraints through Lagrangian functions. Alternately update the original variable and the dual variable to get the solution of a large global problem. In dataset 6, Accu.(%) = 65.15, Prec.(%) = 68.77, Sen.(%) = 77.3, MCC (%) = 62.52, and AUC (%) = 75.77. Most of the algorithms converge to the optimal solution in an asymptotic or exponential manner, that is, the nodes can reach the optimal solution more accurately when the time tends to infinity. (2) The problem of selectivity and invariance is the main difficulty of conventional machine learning; therefore, the ability of these methods to deal with data in raw form is limited. In the LDAP category, BF – Alg Accu = 82.4, BF – Alg Recall = 97.31, BF – Alg F1 – score = 87.86, T – Alg Accu = 98.82, T – Alg Recall = 90.21, and T – Alg F1 – score = 81.15. Each layer takes the output of the previous layer as input and applies nonlinear transformations to extract useful features for classification. Selectivity versus invariance means selecting those features that contain more information and ignoring those features that contain less information about the parameters; i.e., the selected features should be different from each other. In the TFTP category, BF – Alg Accu = 95.94, BF – Alg Recall = 87.95, BF – Alg F1 – score = 90.74, T – Alg Accu = 83.91, T – Alg Recall = 98.53, and T – Alg F1 – score = 98.91. (3) Traditional autoencoders such as autoencoder, isometric mapping, and local linear embedding have been developed continuously, and many models based on autoencoder improvement have been developed. As shown in Table 3 and Figure 5, the tuning results are F1 – score = 92.12, Accuracy = 80.92, AUC = 95.23, AUPR = 84.94, Loss = 96.49, Precision = 95.19, Recall = 97.54, and Specificity = 83.33. Since the vector output by the traditional autoencoder is unknown and disordered, the autoencoder can only learn data but cannot actively generate data. At the same time, the feature vector of the hidden layer lacks continuity; that is, under small disturbances, the generated data will be very strange and very deviating from the input data of the original model. (4) Selecting an appropriate machine learning algorithm can make full use of prior knowledge to complete traffic identification. As shown in Table 4 and Figure 6, in DNN EDTPs1 prediction, Dataset = 3216, Recall (0.9) = 13.62, Samples = 18, and Recall (0.5) = 40.67. When the traffic characteristics are easily outdated quickly, there are many observation samples, and the learning efficiency is not very high. A framework based on multitask deep learning algorithms is included. Separate and purify the PCAP files of the public datasets according to traffic categories. The prediction results of SVM EDTPs1 are Dataset = 3216, Recall (0.9) = 32.19, Samples = 17, and Recall (0.5) = 58.06.

## Data Availability

The experimental data used to support the findings of this study are available from the corresponding author upon request.

## Conflicts of Interest

The authors declared that they have no conflicts of interest regarding this work.

## References

- [1] J. Lee, "Integration of digital twin and deep learning in cyber-physical systems," *Towards Smart Manufacturing*, vol. 38, no. 8, pp. 901–910, 2020.
- [2] L. H. Zhang, W. Y. Zhang, J. M. Xiong et al., "Mechanisms of compound Kushen injection for the treatment of bladder cancer based on bioinformatics and network pharmacology with experimental validation," *Chinese Journal of Natural Medicines*, vol. 20, no. 1, p. 11, 2022.
- [3] D. K. Jain, Z. Zhang, and K. Huang, "Multi angle optimal pattern-based deep learning for automatic facial expression recognition," *Pattern Recognition Letters*, vol. 139, pp. 157–165, 2020.
- [4] H. An, S. Kim, and Y. Choi, "Sportive fashion trend reports: a hybrid style analysis based on deep learning techniques," *Sustainability*, vol. 13, no. 17, p. 9530, 2021.
- [5] G. Weng, C. Pei, J. Ren et al., "Modeling and forecasting of wind power output of urban regional energy internet based on deep learning," *Journal of Physics Conference Series*, vol. 1732, no. 1, article 012190, 2021.
- [6] U. Matthias, R. Karl-Philipp, and K. Karl-Patrik, "Deep learning detects heart failure with preserved ejection fraction using a baseline electrocardiogram," *European Heart Journal-Digital Health*, vol. 4, p. 4, 2021.
- [7] Q. Li, T. Lan, S. He et al., "A network pharmacology-based approach to explore the active ingredients and molecular mechanism of Lei-gong-gen formula granule on a spontaneously hypertensive rat model," *Chinese Medicine*, vol. 16, no. 1, p. 99, 2021.
- [8] J. Q. Guo, Y. Li, and J. L. Fan, "Study on the mechanism of Renshen Gansong herb in the treatment of paroxysmal atrial fibrillation based on network pharmacology," *Journal of Hainan Medical University*, vol. 27, no. 20, p. 6, 2021.
- [9] A. D. Waterman, W. Shannon, and M. Boechler, "Validation of clinical classification schemes for predicting stroke," *JAMA : The Journal of the American Medical Association*, vol. 285, no. 22, pp. 20–21, 2001.
- [10] H. Zhang, M. Hao, H. Wu et al., "Protein residue contact prediction based on deep learning and massive statistical features from multi-sequence alignment," *Tsinghua Science and Technology*, vol. 27, no. 5, pp. 843–854, 2022.
- [11] D. Tian, Q. Gao, J. Lin et al., "Uncovering the mechanism of the Shenzhi Jiannao formula against vascular dementia using a combined network pharmacology approach and molecular biology," *Phytomedicine*, vol. 90, p. 153637, 2021.
- [12] J. Jonnalagadda and M. Hashemi, "Feature selection and spatial-temporal forecast of oceanic Niño index using deep learning," *International Journal of Software Engineering and Knowledge Engineering*, vol. 32, no. 1, pp. 91–107, 2022.

- [13] Q. Chen, Y. Zhao, M. Li et al., "HPLC-MS and network pharmacology analysis to reveal quality markers of Huo-Xue-Jiang-Tang Yin, a Chinese herbal medicine for type 2 diabetes mellitus," *Evidence-based Complementary and Alternative Medicine*, vol. 2021, Article ID 1072975, 12 pages, 2021.
- [14] R. Jiang, J. Shen, X. Li, R. Gao, Q. Zhao, and Z. Su, "Detection and recognition of veterinary drug residues in beef using hyperspectral discrete wavelet transform and deep learning," *International Journal of Agricultural and Biological Engineering*, vol. 15, no. 1, pp. 224–232, 2022.
- [15] S. Agarwal, "Deep learning-based sentiment analysis: establishing customer dimension as the lifeblood of business management," *Global Business Review*, vol. 23, no. 1, pp. 119–136, 2022.
- [16] D. Hirahara, E. Takaya, M. Kadowaki, Y. Kobayashi, and T. Ueda, "Effect of the pixel interpolation method for down-sampling medical images on deep learning accuracy," *Journal of Computer and Communications*, vol. 9, no. 11, pp. 150–156, 2021.
- [17] W. G. Members, D. Mozaffarian, and E. J. Benjamin, "Executive summary: heart disease and stroke statistics–2016 update: a report from the American Heart Association," *Circulation*, vol. 127, pp. 143–152, 2016.
- [18] R. G. Hart, L. A. P. Ms, and A. M. I. Aguilar, "Meta-analysis: antithrombotic therapy to prevent stroke in patients who have nonvalvular atrial fibrillation," *Annals of Internal Medicine*, vol. 146, no. 12, pp. 857–867, 2007.
- [19] W. G. Members, D. Mozaffarian, and E. J. Benjamin, "Heart disease and stroke statistics-2016 update: a report from the American Heart Association," *Circulation*, vol. 133, no. 4, article e38, 2016.
- [20] X. Li, S. Feng, and H. Zhang, "Research progress of acupuncture and moxibustion in treating constipation after stroke," *Stroke*, vol. 5, no. 4, pp. 139–143, 2021.
- [21] A. Ranjan, S. Shukla, D. Datta, and R. Misra, "Generating novel molecule for target protein (SARS-CoV-2) using drug-target interaction based on graph neural network," *Network Modeling Analysis in Health Informatics and Bioinformatics*, vol. 11, no. 1, p. 6, 2022.
- [22] D. Rohmantor, B. G. Purnomo, M. Amiruddin, and S. Mahendra, "Analysis of the effect of a catalyst hydrocarbon crack system spiral pipe against the 4-stroke motorcycle engine power," *Journal of Physics: Conference Series*, vol. 1823, no. 1, p. 012047, 2021.
- [23] A. J. Obaidullah, M. M. Alanazi, N. A. Alsaif et al., "Deeper insights on Cnesmone javanica Blume leaves extract: chemical profiles, biological attributes, network pharmacology and molecular docking," *Plants*, vol. 10, no. 4, p. 728, 2021.
- [24] B. Yu, F. Lin, H. Ning, and B. Ling, "Network pharmacology study on the mechanism of the Chinese medicine Radix Isatidis (Banlangen) for COVID-19," *Medicine*, vol. 100, no. 32, article e26881, 2021.
- [25] L. Zhu, A. Damianou, and E. D. Daniel, "Inflammasome activation controlled by the interplay between post-translational modifications: emerging drug target opportunities," *Cell Communication and Signaling: CCS*, vol. 19, no. 1, 2021.
- [26] P. M. Wadanambi and U. Mannapperuma, "Computational study to discover potent phytochemical inhibitors against drug target, squalene synthase from *Leishmania donovani*," *Helicon*, vol. 7, no. 6, article e07178, 2021.

## Research Article

# Analysis and Recognition of Clinical Features of Diabetes Based on Convolutional Neural Network

Rui Wang<sup>1</sup>, Ping Li<sup>2</sup>, and Zhengfei Yang<sup>1</sup>

<sup>1</sup>Institute of Traditional Chinese Medicine, Ningxia Medical University, Yinchuan 750000, China

<sup>2</sup>Weifang Engineering Vocational University, Weifang, Shandong Province 262500, China

Correspondence should be addressed to Zhengfei Yang; [yangzhengfei@nxmu.edu.cn](mailto:yangzhengfei@nxmu.edu.cn)

Received 14 June 2022; Revised 4 July 2022; Accepted 9 July 2022; Published 29 July 2022

Academic Editor: Hangjun Che

Copyright © 2022 Rui Wang et al. This is an open access article distributed under the Creative Commons Attribution License, which permits unrestricted use, distribution, and reproduction in any medium, provided the original work is properly cited.

Diabetes mellitus is a common chronic noncommunicable disease, the main manifestation of which is the long-term high blood sugar level in patients due to metabolic disorders. However, due to excessive reliance on the clinical experience of ophthalmologists, our diagnosis takes a long time, and it is prone to missed diagnosis and misdiagnosis. In recent years, with the development of deep learning, its application in the auxiliary diagnosis of diabetic retinopathy has become possible. How to use the powerful feature extraction ability of deep learning algorithm to realize the mining of massive medical data is of great significance. Therefore, under the action of computer-aided technology, this paper processes and analyzes the retinal images of the fundus through traditional image processing and convolutional neural network-related methods, so as to achieve the role of assisting clinical treatment. Based on the admission records of diabetic patients after data analysis and feature processing, this paper uses an improved convolutional neural network algorithm to establish a model for predicting changes in diabetic conditions. The model can assist doctors to judge the patient's treatment effect by using it based on the case records of inpatient diagnosis and treatment and to predict the risk of readmission of inpatients after discharge. It also can help to judge the effectiveness of the treatment plan. The results of the study show that the model proposed in this paper has a lower probability of misjudging patients with poor recovery as good recovery, and the prediction is more accurate.

## 1. Introduction

Diabetes is a common chronic noncommunicable disease. Metabolic disturbances in patients can lead to chronically high blood sugar levels in patients. Since the disease is not easy to cure, the long-term high blood sugar level of the patient has brought serious harm to the patient's kidney, cardiovascular, and nervous system, resulting in many complications, which has brought great harm to the patient's physical and mental health [1, 2]. However, according to the World Health Statistics Report released by the World Health Organization in 2017, about 40 million people died of chronic noncommunicable diseases in 2015. Among them, diabetes is the fourth leading cause of death in humans. According to the report, about 80% of people with diabetes are in low- and middle-income countries. Therefore, it is beneficial for diabetic patients, especially those in low- and middle-income countries, to carry out diabetes pre-

vention and control work and help patients improve treatment efficiency [3, 4].

However, there are many problems in the prevention and treatment of diabetes. The traditional treatment of diabetes is based on the medical experience and medical knowledge of doctors [5, 6]. However, according to statistics, by the end of 2017, the total number of health personnel in China was 11.749 million, including 3.39 million practicing (assistant) doctors and 901,000 rural doctors. Although there are a large number of practitioners, compared with the goals in the "Healthy China 2030" plan proposed by China, the number of doctors is far from enough, and some doctors in areas with limited medical resources have a low level of education, although the number of rural doctors is limited [7, 8]. Therefore, some patients in areas with limited medical resources cannot obtain efficient treatment plans or long-term follow-up treatment. Physicians may not be able to monitor the treatment effect of patients in place and



cannot adjust treatment plans in a timely and effective manner, thus delaying the treatment opportunity of some patients. However, physicians hope to improve the efficiency of treatment in various ways, so that more patients can receive better treatment and improve the quality of patients' lives [9, 10]. The treatment effect and condition monitoring of diabetic patients are mainly focused on changes in blood sugar levels. Few studies have focused on predicting treatment outcomes for hospitalized patients; however, information on patients' hospitalizations is crucial for patient recovery.

The incidence of diabetic retinopathy in diabetic patients is relatively high. The patients have no obvious symptoms of discomfort in the early stage, and the patients' vision will be affected in the middle stage of the disease course, and there will be transient blurred vision during this period. It will soon return to normal, but patients are often unusual, so that long-term blurred vision, blood shadows, and floating mosquitoes appear in the later stage, resulting in irreversible vision damage and gradually causing vision loss [11, 12]. If diabetic patients have regular fundus examinations and treatment at the early stage of the disease, it may completely eliminate the risk of blindness. Therefore, early screening of diabetic retinopathy and timely treatment for diabetic patients are very necessary [13, 14]. Therefore, it is of great significance to explore the potential medical laws in medical data to assist doctors in understanding the treatment effect and disease trend of patients.

In recent years, due to the advancement of medical informatization and the development of information technology, it is possible to realize the above-mentioned target of diabetes treatment. Due to the realization and popularization of electronic medical records, patients who go to the hospital will leave detailed records such as diagnostic reports at various stages of their diagnosis and treatment in the electronic medical records, physical examination indicators, and other detailed records [15, 16]. These records hide a large number of rules for the diagnosis and treatment of diabetes. These rules can assist some inexperienced or limited medical practitioners in the diagnosis and treatment work and help doctors to formulate accurate and effective treatment plans for patients. The treatment effect of the disease is tracked [17, 18].

In the past, retinal image processing required many stages, and at each step, retinal image processing required at least one computer vision technique. At the same time, the complexity of retinal samples and the influence of various lesions increase the difficulty of their processing. Force majeure external factors make the processing of retinal images cumbersome and require further judgment based on original medical knowledge. In retinal processing, errors in one process or unsatisfactory results can increase the difficulty of the next step and reduce the accuracy of image classification tests. In developed countries with a high incidence of diabetes, many universities and research institutes have been studying how to conduct diabetic retinopathy (DR) screening. The current research is mainly limited by the following aspects: (1) the quality of fundus retinal images. Since the resolution, contrast, saturation, brightness,

and other indicators of the acquired image are easily affected by some conditions such as sunlight, camera, hardware, and the experience of the imaging operator, the image quality of the completed retinal images will be uneven. The current situation is uneven, and the quality of some images is quite different. (2) The grading of retinal images is not very clear, and some small changes may affect the judgment of grading, which makes it difficult to label the image grading. (3) The structure of the fundus retina is complex, and the use of traditional machine learning algorithms has high requirements for feature extraction, and information extraction is difficult. All in all, the researchers have achieved good empirical results by examining the existing diabetes data.

Retinal pathological images play an important role in medical diagnosis. Doctors can use this to determine the stage of the disease, and accurate classification of retinal images plays an important role in the treatment of DR. Therefore, researchers at home and abroad have devoted themselves to the research of DR classification with great enthusiasm and developed a variety of classification and diagnosis methods. However, when the severity of the disease is different, there is not much difference between the DR images, and the feature extraction and classification work are difficult to perform well [19].

As a multidomain interdisciplinary subject, machine learning has been greatly developed in recent years. Deep learning can be used to mine deep features of data due to its powerful feature extraction capabilities. At present, many scholars use machine learning algorithms to study the data of diabetic patients to improve the treatment effect and condition of diabetic patients. Generally speaking, these research methods can be divided into mathematical statistics methods and machine learning methods. However, in order to achieve the purpose of using diabetes data mining to realize the purpose of auxiliary diagnosis and treatment with practical value, more in-depth research is needed.

Computer is used to classify the image, the pixel points of the image are converted into features, the neural network is used to analyze the characteristics of the image, and the target image is classified according to the feature information. The use of computer technology can perform automatic diagnostic analysis and rapid processing of fundus images, which can greatly reduce the workload of professional ophthalmologists. Doctor can not only obtain the classification result according to the model, but also can remove the influence of the photograph of the environment through the preprocessing method and obtain a clearer fundus image. The doctor can further improve the accuracy of the diagnosis by combining the results given by the computer. Image classification is a hot topic recently. It is meaningful to study the use of intelligent methods to automatically analyze medical images to assist doctors in achieving efficient diagnosis of diseases [20].

All in all, with the continuous development of image processing, convolutional neural network, and other technologies, medical image processing has shown broad development prospects and plays an important role in the rapid and accurate diagnosis and treatment of certain diseases. DR data processing by computer, combined with traditional



image processing and deep learning methods to screen and diagnose data, can greatly improve the efficiency and accuracy of DR diagnosis, which is of great significance to doctors and patients. Using this method can adjust the treatment plan for the patient in time; it is a subject worth studying, and the research on this subject has certain practical significance and scientific research value.

## 2. Convolutional Neural Network

With the continuous deepening of the network structure, its ability to express features is gradually strengthened. The deep convolutional neural network model, which is based on the traditional neuron model, has been widely used in the field of image processing. Convolutional neural networks reduce the number of parameters by using local receptive fields for weight sharing. Each neuron only perceives the data of this layer, and the higher perception layer combines the underlying data to obtain global data, greatly reducing the number of parameters. This part mainly introduces the convolutional neural network and the classic convolutional neural network model in image classification. A neural network is formed by connecting neurons one by one. The difference between a convolutional neural network and a traditional neural network is that the convolutional neural network contains a feature extractor composed of convolutional layers and subsampling layers. As shown in Figure 1, a convolutional neural network consists of an input layer, a convolutional layer, a fully connected layer, and an output layer.

**2.1. Convolutional Layer.** In convolutional neural networks, the process of feature extraction is carried out in convolutional layers. The features extracted by low-level convolution and high-level convolution are different. Low-level features such as edges, lines, corners, and textures are usually extracted by low-level convolution layers. Complex information of images is often extracted by high-level convolution layers, which is obtained by layer extraction, so as to complete the extraction of the global information of the image. The image is passed to the convolution kernel through the input layer to perform the convolution operation, and then the excitation function is used to process the result of the convolution operation to obtain the feature map. The calculation formula of the convolutional layer is:

$$y_n^l = f_l \left( \sum_{m \in V_n^l} y_m^{l-1} w_{m,n}^l + b_n^l \right). \quad (1)$$

Among them,  $y$  is the  $n$ th feature map in the  $l$ th layer of the convolutional neural network,  $f$  represents the activation function,  $b$  is the bias term, and  $V$  is the input feature map set.

Activation function is used to increase the nonlinear factor of the convolutional neural network. The widely used activation functions are the sigmoid function, tanh function, and ReLU function. The expression for the sigmoid function

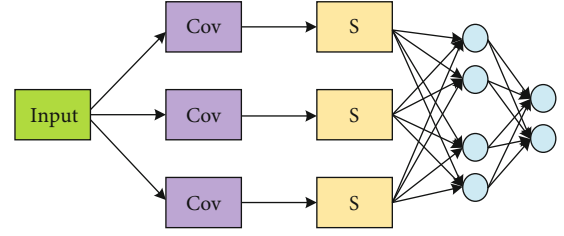


FIGURE 1: Convolutional neural network.

is

$$f(z) = \frac{1}{1 + e^{-z}}. \quad (2)$$

It can be known from the sigmoid function that its value is between (0, 1), and the output can be mapped to between (0, 1), which is shown in Figure 2. It is usually used in binary classification problems. The disadvantage of this function is that the derivation is complex, and the amount of calculation is large when backpropagation is performed. And the derivatives at both ends of the function are close to 0, which will cause the gradient to disappear in the backpropagation of the deep network.

The expression of the tanh function is

$$f(z) = \tanh(z) = \frac{e^z - e^{-z}}{e^z + e^{-z}}, \quad (3)$$

$$\tanh(z) = 2\text{sigmoid}(2z) - 1. \quad (4)$$

It can be known from the tanh function that the value range of the tanh function is between (-1, 1), which is shown in Figure 2. Compared to sigmoid, the output of the tanh function is centered at 0 and has a wider output range. However, after the derivation of both ends of the same function, it is close to 0. It is easy to cause the gradient to disappear, which is not conducive to the training of deep network.

The expression of the ReLU function is

$$f(z) = \max(0, z). \quad (5)$$

**2.2. Pooling Layer.** Pooling layers are also known as down-sampling layers. Adding a pooling layer after the convolution operation can effectively reduce the parameters and avoid the computer computing pressure caused by the large amount of parameter data. This reduces the amount of data processing while retaining useful information and also speeds up the training of the network. Generally, pooling is divided into max pooling and average pooling. Maximum pooling is generally used when reducing dimensions and can extract the main features, while average pooling averages the features and does not contribute to the extraction of the main features. The feature calculation formula of the pooling layer is as follows:

$$y_n^l = f_l \left( z_n^{l-1} w_n^l + b_n^l \right). \quad (6)$$

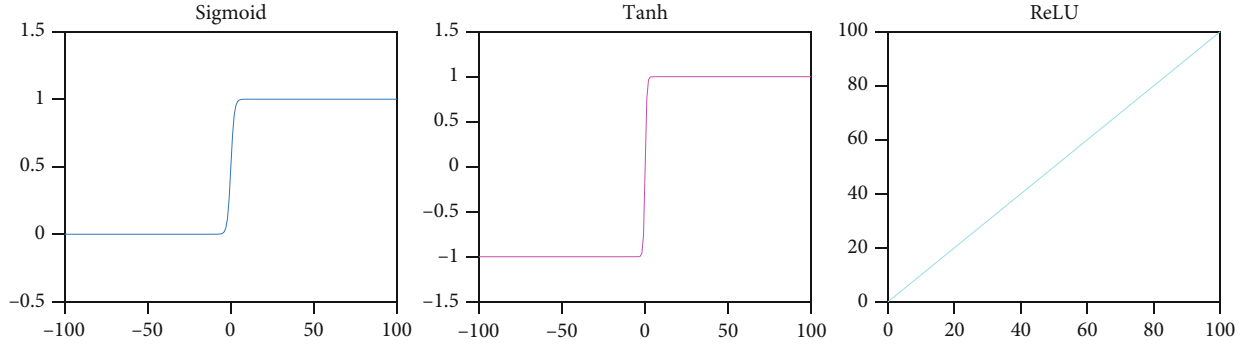


FIGURE 2: Figures of the functions.

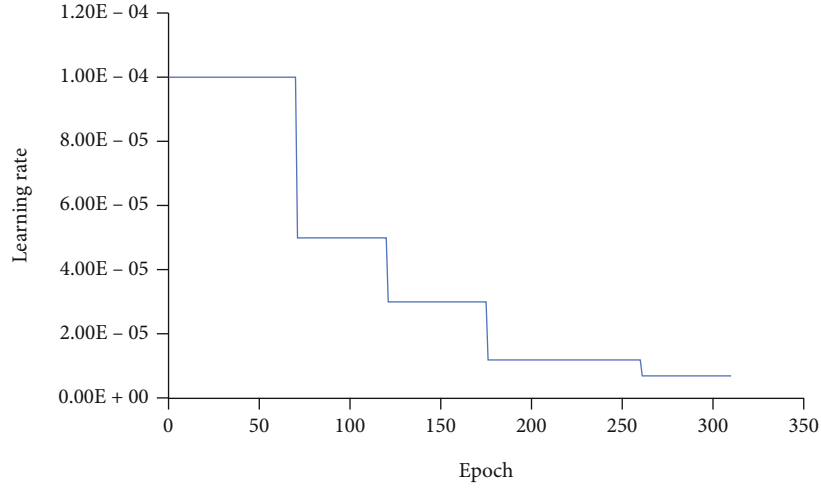


FIGURE 3: Learning rate change curve in experiment 1.

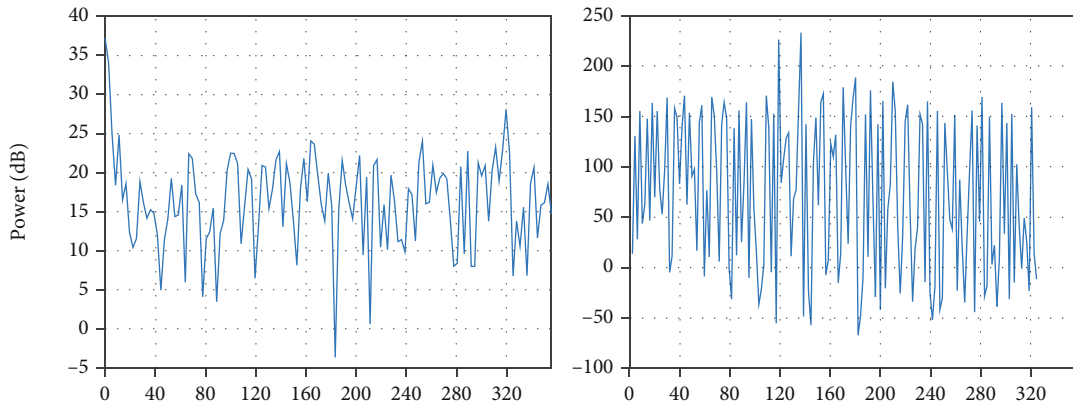


FIGURE 4: Accuracy and loss rate curves.

**2.3. Fully Connected Layer.** In the convolutional neural network, the role of “classifier” is usually played by the fully connected layer, which can be classified according to the combination of features. It usually exists in the later layers of the convolutional neural network. The feature position brings the accuracy of classification. The adverse effects can be effectively reduced by the fully connected layer. It can be regarded as a conventional artificial neural network

introduced in the previous section and works in the same way as the artificial neural network. The output formula of the fully connected layer neuron is shown below.

$$y_n^l = f_l \left( \sum_{m=1}^{N_l-1} y_m^{l-1} w_{m,n}^l + b_n^l \right). \quad (7)$$

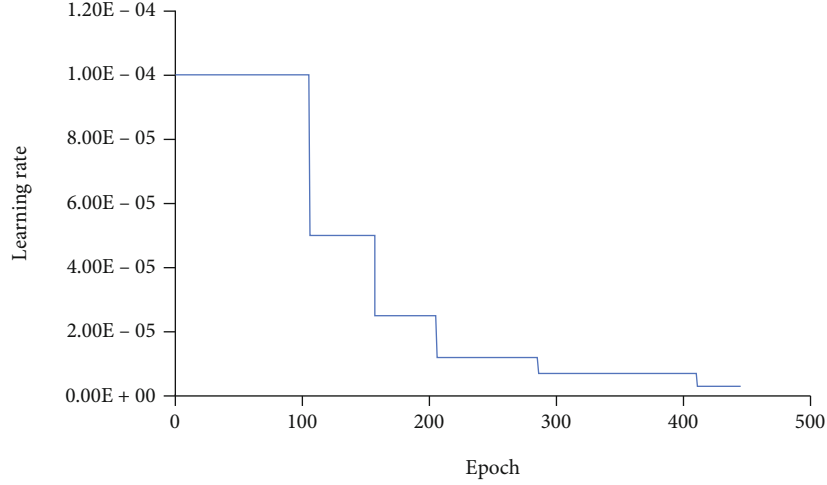


FIGURE 5: Learning rate change curve in experiment 2.

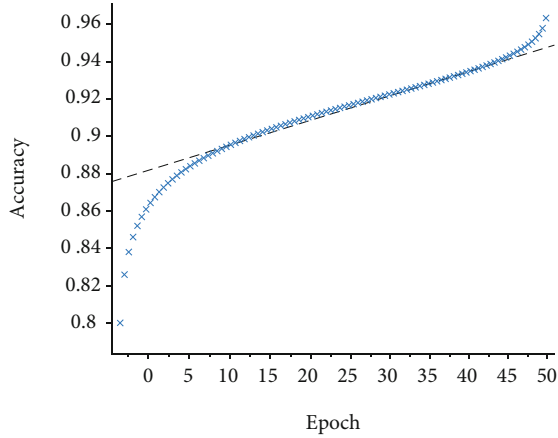


FIGURE 6: The comparison with different preprocessing methods.

**2.4. Training of Convolutional Neural Networks.** Convolutional neural networks often use the backpropagation method to learn and optimize parameters. The loss function is used to judge the gap between the actual value and the predicted value, and different optimizers are selected to update and calculate the network parameters of the model to make it approximate or reach the optimum value.

The loss function is used to represent the error between the actual calculation result and the expected output result. The smaller the loss function, the better the model learning data. Often, the distance between the predicted value and the true value can be estimated simply by using the mean squared error (MSE), which is given by

$$MSE = \frac{\sum_{i=1}^n (y_i - \hat{y}_i)^2}{n}. \quad (8)$$

Taking a single sample as an example,  $z$  is the real value,  $b$  is the activation value  $\partial(z)$ , and  $z$  is the neural network output  $wx + b$ . The mean square error loss function can be

written as

$$MSE = C = \frac{(y - a)^2}{2}. \quad (9)$$

In the training of the convolutional neural network, the weight parameters are updated by taking the partial derivatives of  $w$  and  $b$ , and the results are

$$\frac{\partial C}{\partial w} = a\sigma'(z), \quad (10)$$

$$\frac{\partial C}{\partial b} = a\sigma'(z). \quad (11)$$

If it is a convolutional layer, for each convolution kernel, the weights and biases are updated as follows:

$$W^l = W^l - \alpha \sum_{i=1}^m \delta^{i,l} a^{i,l-1}, \quad (12)$$

$$b^l = b^l - \alpha \sum_{i=1}^m \sum_{\mu,v} \delta^{i,l}. \quad (13)$$

### 3. Diabetes Data Analysis and Processing

The experimental data for this research topic were case data from 10 years of admission records of diabetic patients in 130 hospitals across the United States. Due to the huge amount of data in this dataset, the first thing to do in this research for such a dataset is to perform basic analysis and data screening on the dataset to gain a preliminary understanding of the content of the dataset. The dataset has a total of 10766 samples, 49 attribute columns, and 2 label variables. The label variable 0 means the patient was not readmitted within 30 days of discharge, and 1 means the patient was readmitted within 30 days. The label of the patient's admission record is used to judge whether the patient is likely to be readmitted in a short period of time, so as to judge the effect of this treatment. Among them, each

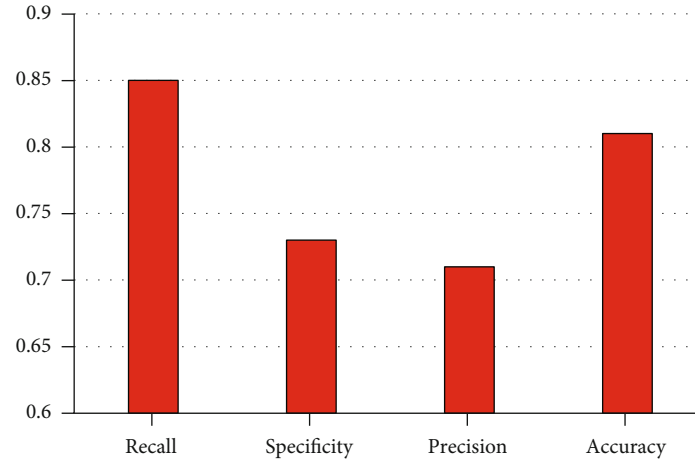


FIGURE 7: Prediction of short-term readmission risk of diabetes mellitus without data balancing.

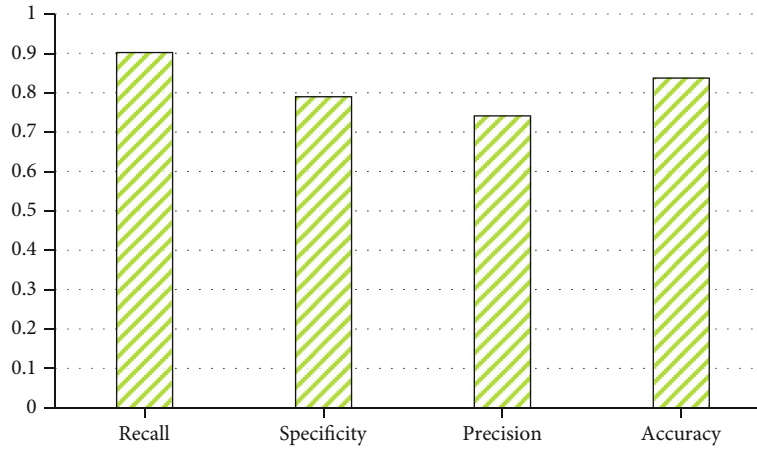


FIGURE 8: Predicting short-term readmission risk in diabetes by data balancing processing datasets.

sample includes 49 attributes, such as patient number, race, gender, and age. This study divides these attributes into four dimensions: (1) the patient's basic physiological information, including weight, race, and gender; (2) the patient's basic admission registration information, including the patient's admission number and admission time; (3) the patient's condition diagnosis records; and (4) records of patients' medication information. This paper uses machine learning algorithms to mine the hospitalization records of diabetic patients. Then this paper explores the potential treatment experience and predicts the development of the patient's condition, so as to improve the treatment efficiency and treatment effect of the patient.

With reference to the opinions of hospital physicians, this study firstly performed manual classification of the features in the dataset. In this dataset, the age, gender, weight, and other information of patients have been fully confirmed to have an impact on diabetes. Through observation of the dataset, it is found that the patients admitted to the hospital include different races. Considering that race may be a potential factor for the onset of diabetes, so add it to the data dimension. Secondly, this study selected biochemical indica-

tors related to diabetes, which mainly include fasting blood glucose value, glycosylated hemoglobin value, and insulin release test. Among them, the blood sugar level can be reflected and is an important criterion for judging the changes in the condition of diabetic patients. Glycated hemoglobin is formed by the combination of hemoglobin in red blood cells and sugars in serum, and its content depends on the blood glucose concentration and the contact time between blood glucose and hemoglobin. Therefore, it can be used as an important indicator for diabetes monitoring; the insulin release experiment can reflect whether the function of the insulin-secreting  $\beta$  cells in the patient's pancreatic islets is normal. These biochemical indicators can provide important reference for doctors to diagnose the disease and also have important value for the experimental purpose of this study. In attribute selection, this study also selected doctors' diagnostic records and medication records as key attributes.

Since the dataset used in this experiment is the original dataset recorded by the hospital, there are problems such as inconsistent data format, incomplete data, and data recording errors in the dataset. Since the quality of the data

determines the upper limit of the analytical performance of the model, this section focuses on data cleaning.

An important task of data cleaning is to deal with missing values in the original dataset. The main reasons for the lack of data in the medical records are that the medical staff misses the records or does not obtain a certain record of the patient. Generally, there are three main methods for dealing with missing values: delete records, data imputation, and no processing.

If only a small number of records can be deleted to achieve the set goal, the method of deleting missing values is effective, but this method has great limitations, wastes a lot of data resources, and discards a large number of records hidden in these records. The methods of data interpolation mainly include the use of fixed values for interpolation; the use of known points to establish appropriate interpolation functions for interpolation; and the use of mean/median for interpolation. Since some models can treat missing values as a special value and allow modeling on missing values, missing values are not handled.

#### 4. Simulation Analysis

A total of 307 epochs were trained in the experiment, and the learning rate change curve during the whole training process is shown in Figure 3. The accuracy and loss curves for training and validation sets are shown in Figure 4. By comparing the quasi-curvature curve and the loss curve, it can be found that the simulation has 200-300 epochs after training, the accuracy on the training set and the accuracy on the validation set gradually become stable, and the accuracy on the training set after 250 epochs is stable. The rate is basically stable, and the accuracy rate on the validation set also oscillates within the stable range. At the same time, during the whole training process, the training loss curve kept a steady decline, and the validation set loss curve oscillated and decreased. After 200 epochs, the oscillation amplitude became larger, and after approaching 300 epochs, the oscillation amplitude increased especially obviously, and there was a certain increase in trend. In summary, it can be considered that the model gradually stabilizes in fitting ability after epoch is 200. For this reason, in this experiment, the model with epoch in the range of 200-305, which performed well in the accuracy and loss rate of the validation set, was tested on the final 53575 test set.

Experiment 2 trains a total of 445 epochs, and the learning rate changes during the training process, as shown in Figure 5. By comparing the quasi-curvature curve and the loss curve, it can be found that after the simulation has 350-450 epochs after training, the accuracy on the training set and the accuracy on the validation set gradually become stable, and the accuracy on the training set after 400 epochs is basically stable, and the accuracy rate on the validation set also oscillates in the stable range. At the same time, during the whole training process, the training loss curve keeps decreasing steadily, and the validation set loss curve oscillates and decreases. At about 350 epochs, the oscillation amplitude still stays stable.

In summary, it can be concluded that the model gradually stabilizes in fitting ability when epoch is bigger than 350. For this reason, the epoch around 350-450 was selected for this experiment, and the model has good accuracy and loss rate in the validation set. The obtained specificity, sensitivity, and accuracy rate turns out that it is the best model.

In this paper, a data preprocessing method based on CNN is proposed, which is compared with the traditional normalization preprocessing method. After Gaussian filtering, it is fused with the original image to eliminate noise information, and the gamma correction method is used to eliminate the influence of high exposure and underexposure. The experimental chart is shown in Figure 6. It can be seen from the figure that the data of the preprocessing methods gradually increases with the training accuracy of the 0~20 generation model and then tends to be flat, and the results fluctuate around the final value. At the beginning, because the network model is preprocessed, the accuracy of the model changes greatly when verifying the preprocessing method proposed in this paper, the graph shows an upward trend, the slope is large, and the accuracy increases rapidly. Compared with the original method, the accuracy rate of the method is small, but the final accuracy rate is higher than the original single method. That is, the accuracy rate is increased by 0.7% compared with the previous method. The results show that the various preprocessing methods proposed in this paper can improve the classification accuracy.

In addition, in order to further verify the effectiveness of the proposed model, the images were processed by traditional matched filtering, morphological methods, proposed improved matching filtering, and morphological fusion scheme. The result is also compared with the expert manual segmentation results. For the retinal blood vessel segmentation of the fundus, the retinal blood vessel segmentation method given in this paper has a certain improvement in effect compared with the morphological method and the matched filtering method, and the accuracy and sensitivity are improved, and specificity, the retinal vessel segmentation method in this paper performs better, and its value is also improved. In order to intuitively compare the effects of various methods on blood vessel segmentation in retinal images, three retinal images were selected from two publicly available DRIVE and STARE datasets, which are commonly used in retinal blood vessel segmentation, and processed with three methods, respectively. The algorithm proposed in this paper has a good segmentation effect, can segment most of the tiny blood vessels, and can restore the blood vessel feature information better. This is because the Hessian matrix is used to obtain the direction of the blood vessels in the retinal blood vessel segmentation scheme given in this paper, so as to guide the filtering angle of the matched filter, so the accuracy of the segmentation is improved, and the multiscale operation can better improve the blood vessel details, so that most of the tiny blood vessels can be segmented.

*4.1. No Data Balance Predicts Short-Term Readmission Risk for Diabetes.* In order to verify the effectiveness of hospital



case data balancing, this study tested the classification prediction method proposed in this study by observing the experimental results and using the data without data balancing processing. The experimental results are shown in Figure 7. The experimental classification model with the dataset and no data balance has a prediction accuracy of 0.81, a recall of 0.84, a specificity of 0.73, and a precision of 0.71.

**4.2. Predicting Short-Term Readmission Risk in Diabetes by Data Balancing Processing Datasets.** In order to verify the necessity of data balance, this study conducted training on the data after data balance. In this study, CNN was used to predict color patches of  $6 * 6$  pixels, with a total of 180,818 pieces of data. Figure 8 shows that the classification accuracy of the CNN model is 0.837. It can be seen that the model predicts the trend of diabetes more accurately, and the variance value of the algorithm is small, indicating that the algorithm has good stability. The recall of the algorithm was 0.902, the accuracy of the model was 0.741, and the specificity of the model was 0.79. Combining these indicators, it can be seen that the performance of the model is good and the recall rate is high. The results showed that the model had a lower probability of misjudging patients with poor recovery as good recovery, and the prediction was more accurate.

## 5. Conclusion

In this paper, a convolutional neural network is used to establish a diabetes prediction model. In the model, there are mainly four parts: data collection, data analysis and processing, initial feature selection, classification prediction, and algorithm validity test. The conclusions are drawn as follows:

- (1) First of all, the dataset can be used as a representative of the diabetes dataset. It is not only rich in features, but also has a large number of experimental samples, which has the characteristics of good representativeness
- (2) Combined with the opinions of the doctors in the hospital, the dataset was classified and analyzed filled with data. The abnormal data was detected, and the features were sorted by contribution degree. The features that are irrelevant to the experimental purpose were eliminated after combining with the doctor's opinion, and the data features were preliminarily processed
- (3) The processed data is fed into a CNN model for training, and classification results are obtained. However, since the research purpose of this study is to assist physicians in the diagnosis and treatment of diabetic patients in areas with limited medical resources, the prediction results of this model are still in the research stage, and there is still a certain distance from practical application

## Data Availability

The experimental data used to support the findings of this study are available from the corresponding author upon request.

## Conflicts of Interest

The authors declared that they have no conflicts of interest regarding this work.

## Acknowledgments

This work was sponsored in part by the Ningxia Natural Science Foundation (2022AAC03145) and the Ningxia Key Research and Development Program (Special Talent Introduction) (2021BEB04037).

## References

- [1] S. A. Alex, J. Nayahi, H. Shine, and V. Gopirekha, "Deep convolutional neural network for diabetes mellitus prediction," *Neural Computing and Applications*, vol. 34, no. 2, pp. 1319–1327, 2021.
- [2] S. K. Jangir, N. Joshi, M. Kumar, D. K. Choubey, S. Singh, and M. Verma, "Functional link convolutional neural network for the classification of diabetes mellitus," *International Journal for Numerical Methods in Biomedical Engineering*, vol. 37, no. 8, article e3496, 2021.
- [3] J. Guan, G. Liu, F. Fu, Y. Lai, and Z. Lin, "Prediction and analysis of diabetes based on convolution neural network," *International Journal of Higher Education Teaching Theory*, vol. 2, no. 1, pp. 21–27, 2021.
- [4] V. Parshva and S. Sudhir, "Detecting diabetic retinopathy using embedded computer vision," *Applied Sciences*, vol. 10, no. 20, pp. 7274–7274, 2020.
- [5] A. C. S. Reyes, G. R. C. Milan, J. M. M. Quilaton, B. E. G. Sique, S. V. E. Arellano, and K. C. Karamihan, "SBC-based diabetic retinopathy and diabetic macular edema classification system using deep convolutional neural network," *International Journal of Recent Technology and Engineering (IJRTE)*, vol. 9, no. 3, pp. 9–16, 2020.
- [6] D. Wen, P. Li, Y. Zhou et al., "Feature classification method of resting-state EEG signals from amnesic mild cognitive impairment with type 2 diabetes mellitus based on multi-view convolutional neural network," *IEEE Transactions on Neural Systems and Rehabilitation Engineering*, vol. 28, no. 8, pp. 1702–1709, 2020.
- [7] H. A. Hassan, M. Yaakob, S. Ismail et al., "Detection of proliferative diabetic retinopathy in fundus images using convolutional neural network," *IOP Conference Series Materials Science and Engineering*, vol. 769, no. 1, article 012029, 2020.
- [8] E. P. Özmen and T. Özcan, "Diagnosis of diabetes mellitus using artificial neural network and classification and regression tree optimized with genetic algorithm," *Journal of Forecasting*, vol. 39, no. 4, pp. 661–670, 2020.
- [9] D. Harri, "Identification of diabetic retinopathy from color fundus images using deep convolutional neural network," *International Journal of Recent Technology and Engineering*, vol. 9, no. 1, pp. 878–884, 2020.

- [10] H. V. Yadavalli, "Convolution neural network for diabetic retinopathy detection," *International Journal of Recent Technology and Engineering (IJRTE)*, vol. 9, no. 1, pp. 2436–2440, 2020.
- [11] B. B. Narhari, K. M. Bakwad, and A. D. Sayyad, "Identification of diabetic retinopathy from color fundus images using deep convolutional neural network," *International Journal of Recent Technology and Engineering (IJRTE)*, vol. 9, no. 1, pp. 878–884, 2020.
- [12] L. I. U. Yang, "Research on diabetes prediction model based on BP neural network," *International Journal of Neural Systems Engineering*, vol. 1, no. 2, pp. 21–28, 2017.
- [13] A. M. Pour, H. Seyedarabi, S. H. A. Jahromi, and A. Javadzadeh, "Automatic detection and monitoring of diabetic retinopathy using efficient convolutional neural networks and contrast limited adaptive histogram equalization," *IEEE Access*, vol. 8, pp. 136668–136673, 2020.
- [14] R. Agarwal, A. Mahamuni, N. Gautam, P. Awachar, and P. Sagar, "Detection of diabetic retinopathy using convolutional neural network," *International Journal of Recent Technology and Engineering (IJRTE)*, vol. 8, no. 4, pp. 1957–1959, 2019.
- [15] J. H. Wu, J. Li, J. Wang et al., "Risk prediction of type 2 diabetes in steel workers based on convolutional neural network," *Neural Computing and Applications*, vol. 32, no. 13, pp. 9683–9698, 2019.
- [16] Y. Sun, "The neural network of one-dimensional convolution—an example of the diagnosis of diabetic retinopathy," *IEEE Access*, vol. 7, pp. 69657–69666, 2019.
- [17] X. Zeng, H. Chen, Y. Luo, and W. Ye, "Automated diabetic retinopathy detection based on binocular Siamese-like convolutional neural network," *IEEE Access*, vol. 7, pp. 30744–30753, 2019.
- [18] A. Kori, S. S. Chennamsetty, and V. Alex, "Ensemble of convolutional neural networks for automatic grading of diabetic retinopathy and macular edema," <http://arxiv.org/abs/1809.04228>.
- [19] H. Khastavaneh and H. Ebrahimpour-Komleh, "Segmentation of diabetic retinopathy lesions in retinal fundus images using multi-view convolutional neural networks," *Iranian Journal of Radiology*, vol. 16, 2019.
- [20] C. Raja and L. Balaji, "An automatic detection of blood vessel in retinal images using convolution neural network for diabetic retinopathy detection," *Pattern Recognition and Image Analysis*, vol. 29, no. 3, pp. 533–545, 2019.

## Research Article

# Humanistic Spirit Training of Medical Students Based on Multisource Medical Data Fusion

Jie Bai 

*College of Nursing and Rehabilitation, Xi'an Medical University, Xi'an 710021, China*

Correspondence should be addressed to Jie Bai; [baijie@xiyi.edu.cn](mailto:baijie@xiyi.edu.cn)

Received 13 June 2022; Revised 1 July 2022; Accepted 8 July 2022; Published 29 July 2022

Academic Editor: Hangjun Che

Copyright © 2022 Jie Bai. This is an open access article distributed under the Creative Commons Attribution License, which permits unrestricted use, distribution, and reproduction in any medium, provided the original work is properly cited.

Medical colleges need to strengthen the cultivation of medical students' humanistic and spiritual literacy. First of all, schools need to change the current educational concept and the cultivation mode of humanistic quality. In educational work, schools should pay attention to the social cognitive skills of medical students, and at the same time pay attention to the cultivation of students' basic qualities. Schools need to find problems in time, and schools need to take corresponding measures to deal with these problems. Medical colleges need to strengthen the training of medical students' comprehensive quality and incorporate humanistic education into the goal of all-round development of medical students. Specifically, schools need to adopt a work method of distributed implementation and distributed guidance to fully mobilize the enthusiasm and initiative of school leaders, teachers, and students themselves. Schools need to strengthen inspection and supervision and summarize the experiences and lessons that students have learned in their learning. On this basis, schools need to improve the quality and efficiency of students' humanities education work. Through the analysis of multisource medical data, this paper conducts research on the working mode of humanistic quality cultivation in medical colleges. Specifically, school education will be people-centered. Schools need to cultivate the humanistic spirit of medical students in the ideological and political education work. This paper conducts mathematical statistical analysis based on multisource medical data and analyzes the differences in the effect of different teaching modes and training methods on the cultivation of medical students' humanistic spiritual literacy. Based on this, the research proposes recommendations for the future development of medical schools. First of all, schools need to build a humanized classroom, combine skills education with moral education, and improve the learning efficiency of student groups. In addition, schools need to teach students to feel respected and valued. Secondly, schools need to implement human-oriented teaching work to give full play to students' own talents and personalities. During school education work, schools need to organically combine classroom education and social practice. Schools need to link teaching and real society and link students' learning process with real life. Schools need to organically combine reading and learning with life, so as to promote the all-round development of students' humanistic quality.

## 1. Introduction

Hospital culture is a hospital's long-term development of values and codes of conduct that all employees agree and abide by. The internship stage plays an important role in the cultivation of medical students' humanitarian spirit, medical ethics, values, and philosophy of life. Hospital culture education is also an important part of medical school education. In the existing research, the medical school's hospital culture education mainly adopts the survey method,

and the questionnaires are distributed to the teachers and interns of the medical university, respectively. The hospital explores the influence of culture and medical students' humanistic education through questionnaires, in order to improve the ideological and moral sentiments of medical students and cultivate outstanding medical talents [1, 2]. In the current environment, the doctor-patient relationship in China is relatively tense [3]. Violence in medical institutions such as hospitals occurs from time to time. Faced with such a severe situation, medical institutions need to actively find

countermeasures. The cultivation of the humanistic spirit of medical students helps to create a good medical environment and strengthen the effective communication between doctors and patients [4].

The original intention of every medical student entering a medical school is to protect life and save the wounded. A qualified doctor should not only have the professional skills to save lives, but also have professional ethics full of humanistic spirit [5, 6]. Therefore, the important responsibility of medical schools at the current stage is to cultivate and inherit the medical humanistic spirit to the majority of medical and nursing practitioners. Medical students are the future doctors and the main body of future medical activities [7, 8]. The cultivation of the humanistic spirit of medical students is directly related to the cultivation of the comprehensive quality of medical talents. The shaping of the humanistic spirit of medical students is directly related to the improvement of the doctor-patient relationship and the transformation of the medical model [9]. The medical profession is a profession that combines theory and practice very closely. Every medical staff needs to have complete theoretical knowledge and excellent practical operation skills at the same time. Medical humanistic spirit is the moral standard for medical workers to engage in daily medical service work. At present, all medical colleges and universities have gradually begun to pay attention to the cultivation of medical students' humanistic spirit. However, there are relatively few effective training methods and systematic research results that medical schools can propose. This study discusses the importance and urgency of the cultivation of humanistic spirit of medical students, trying to find the point of convergence between the cultivation of humanistic spirit and ideological and political education [10, 11]. The research results of this paper try to find a new way to cultivate the humanistic spirit of medical students from the aspects of the renewal of medical students' ideological and political education concept, the enrichment of content, and the expansion of form [12, 13].

In recent years, medical schools have debated the concept of humanistic spirit of medical students, and there is still no clear definition. However, the discussion of humanistic spirit at the current stage is always inseparable from the two key contents of "humanities" and "humanistic education." Some scholars believe that humanistic education is the education that cultivates the humanistic spirit. The original intention of humanistic education is to cultivate and improve personality through education [14, 15]. The focus of humanistic education research and attention is the law of world development and change. In the research content of humanistic education, we have continuously enriched our thinking on the development stages and development priorities of the world. In the research system, the ideological value system has become the focus of attention. Medical staff need to strengthen communication with patients. Medical staff need to respect the patient's personality and opinions as much as possible. The process of communication between medical staff and patients' needs to focus on methods. In general, the humanistic ideology and social governance concepts involved in ancient Chinese culture have deepened. As

an important support for the continuous cultivation and development of contemporary Chinese humanistic spirit, humanistic education also covers a very strong spirit. The term humanistic spirit mainly derived from western textbooks. The cultivation of humanistic concepts has accompanied by the continuous development of modern education in China in the past three decades [16]. The inheritance and development of the humanistic spirit and humanistic concept require the joint efforts of people of insight from all lifestyles [17, 18]. In the process of cultivating traditional medical humanistic spirit, medical schools pay attention to effective information transmission to students. Information transmission involves multiple subjects such as the source of information, the medium of information, the mode of information transmission, and the recipient of information. In the current environment, the mode of information transmission is constantly updated, and the process of information transmission includes multiple links such as potential language, cultural traditions, and interpersonal influence. The effectiveness of information delivery also involves the ability of the recipient to understand the information [19]. The communication model for the cultivation of medical humanistic spirit based on multisource data support is shown in Figure 1.

## 2. The Focus of Cultivating the Humanistic Spirit of Medical Students

*2.1. The Concept of Medical Humanistic Spirit.* Humanistic spirit belongs to the category of spiritual culture, and humanistic spirit specifically refers to the concept of life contained in the humanities. This philosophy is a concern for the meaning and value of human existence. This concept is also a kind of thought with people as the object and people as the main body. This idea mainly embodied in philosophy, religion, and art. In a narrow sense, humanistic spirit refers to a trend of thought in the Renaissance. However, the current education on ideological and political courses is still dominated by traditional classroom "cramming" teaching. In practice, many colleges and universities mainly reform the teaching objectives of ideological and political courses. This reform model is difficult to accomplish the task of medical humanities education. In the process of reform, the school lacks the cultivation of medical students' personality and professional ethics. The core idea of this spirit is the sustainable development of humanity and the harmonious coexistence of man and the environment. The humanistic spirit attaches great importance to the value of human beings and opposes the repression of human nature by theology. Secondly, the humanistic spirit represents rational thinking and people's pursuit of truth. Humanistic spirit can show to a broad scientific spirit. In addition, the humanistic spirit has a certain transcendence of ideas, which is the pursuit of the meaning of life [20, 21]. The humanistic spirit is the concern for the living environment of human beings, especially the respect for the spiritual life of human beings. The basis for the continuous development of the humanistic spirit is to respect the value of each person as a spiritual existence. The definition of the concept of humanistic spirit

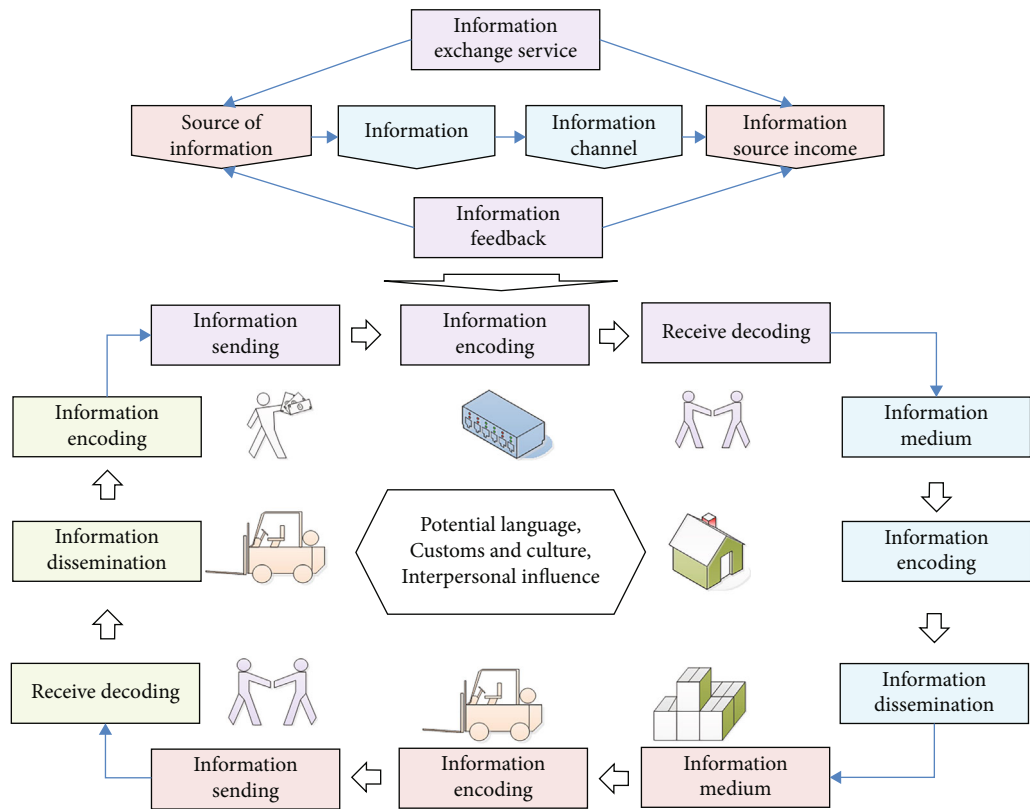


FIGURE 1: The communication model for the cultivation of medical humanistic spirit based on multisource data support.

includes the following aspects. First, the humanistic spirit is people’s pursuit and concern for the value and meaning of life, and the humanistic spirit is the rational understanding of the rise and fall of national culture. Humanism is concern for others, for the country, for society, and for nature. Humanistic spirit specifically includes values, morality, ideological realm, and other nonintellectual causes. Compared with the characteristics of seeking “truth” in scientific spirit, humanistic spirit mainly based on seeking “goodness” and seeking “beauty” as the core content [22].

Medical students are future doctors, and medical students are the main body of medical activities. Due to the particularity of the profession, the humanistic spirit of medical students has its special performance and special significance. The humanistic spirit of medical students mainly manifested in the following aspects [23]. Therefore, schools cannot replace humanities courses with ideological and political courses. The teaching content of humanities courses needs to further enriched. At present, the school’s overly simple humanistic spirit teaching content cannot achieve the purpose of cultivating the humanistic quality of medical students. At the same time, the simple teaching of humanistic spirit cannot make medical students obtain the correct values of unity of body and mind. The first is the humanitarian spirit of caring for life and saving the wounded. Secondly, the humanistic spirit is a sense of morality and responsibility. Third, the humanistic spirit is a concrete manifestation of the spirit of benevolence and the benignity

of human beings. Fourth, humanistic spirit is the expression of equality, communication, cooperation, and personality consciousness. If humanistic education neglected in medical education and medical activities, major teaching accidents will easily occur. If the medical teaching work lacks human development and the reshaping of the humanistic spirit of medical students, there will be systematic risks in teaching. The knowledge system of humanistic quality education in medical colleges is shown in Figure 2.

**2.2. The Importance of Medical Humanistic Spirit.** At the current stage, the construction of medical ethics and medical style in hospitals at all levels in China has made significant progress compared with previous years. However, the attitude of the patients to the medical service is still not very satisfied, and the patients still have great dissatisfaction with the doctor’s diagnosis and treatment process. Overall, it is closely related to the general lack of humanistic spirit of current doctors. Technology cannot represent everything, and medical workers with high technology are not necessarily competent or excellent doctors in the minds of patients. Numerous examples from ancient and modern times at home and abroad have proved that medical research and medical work require medical practitioners to have a high level of cultivation and medical workers to have a high humanistic quality. Medical students are the doctors of the future. This situation has also led to a significant decline in the frequency of use of the school library system by the



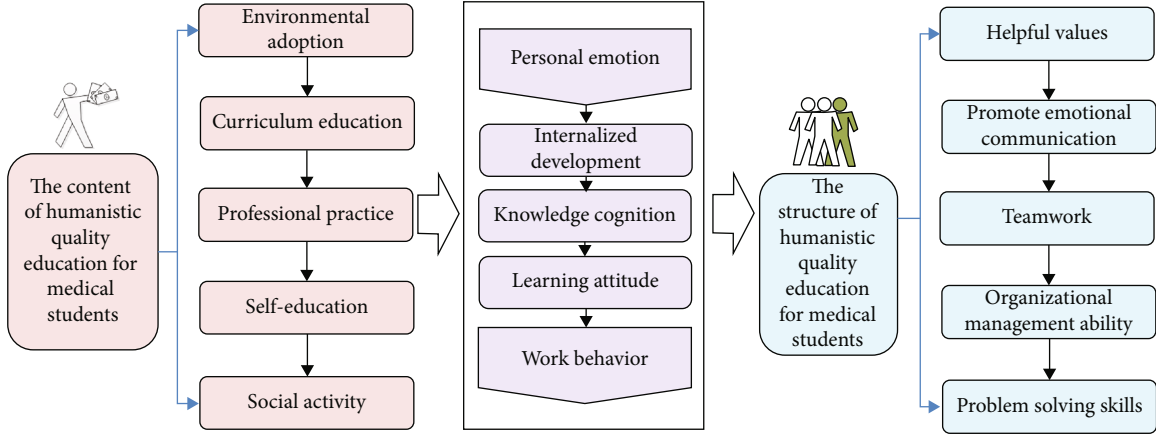


FIGURE 2: The knowledge system of humanistic quality education in medical colleges.

medical student population. In addition, the existing books in the library are relatively old, the layout of the books is old, and the update speed of the books is slow. The degree of humanistic accomplishment of medical students determines their values.

People with good humanistic qualities are often good at choosing and sticking to correct values. Medical students with good values are more discerning in comparing the true, the good, the beautiful, and the false, the ugly, and the ugly. In view of this situation, this requires us to change the educational thought and educational concept in the process of medical education. In the specific teaching process, medical schools should not only impart medical professional knowledge and skills to students, but also strengthen the education of students' knowledge of humanities and social sciences. A correct teaching environment can enable students to receive the edification of humanities and the guidance of correct values while learning professional knowledge. To sum up, the connotation of humanistic spirit needs to closely link with society and the times. The humanistic spirit is constantly developing, and we should view the humanistic spirit in the new era with a developing and open mind. In the current stage of historical development, humanistic spirit has become a concept with rich content. Only the combination of professional education and humanistic quality education can contribute to the all-round development of medical students.

This paper analyzes the influence of multisource medical data on the cultivation of medical students' humanistic spirit. The premise of model analysis is to unify the dimensions of multisource data. This paper normalizes the study data prior to model analysis. There are many ways to normalize data, but one common goal is to make data dimensionless between data. This paper summarizes the following data standardization methods based on several literatures:

Range transformation formula of cost index. In the formula,  $x_{ij}$  refers to the training effect of individual literacy of medical students, and  $y_{ij}$  refers to the training effect of humanistic quality education in medical colleges. Formula

(1) refers to the professional value training model of medical schools in the process of humanistic cultivation:

$$y_{ij} = \frac{x_{ij} - \min_{i \in \{1,2,\dots,n\}} x_{ij}}{\max_{i \in \{1,2,\dots,n\}} x_{ij} - \min_{i \in \{1,2,\dots,n\}} x_{ij}}. \quad (1)$$

Formula (2) refers to the work attitude cultivation model of medical schools in the process of humanistic cultivation. The transformation formula of fixed indicators is as follows:

$$y_{ij} = \begin{cases} \frac{\min |x_{ij} - a_j|}{|x_{ij} - a_j|} x_{ij} & x_{ij} \neq a_j \\ 1 & x_{ij} = a_j \end{cases}. \quad (2)$$

Formula (3) refers to the work of medical schools in the process of humanistic cultivation literacy training model interval transformation formula and is as follows:

$$y_{ij} = \begin{cases} 1 - \frac{q_1^j - x_{ij}}{\max \left\{ q_1^j - \min_{i \in \{1,2,\dots,n\}} x_{ij}, \max_{i \in \{1,2,\dots,n\}} x_{ij} - q_2^j \right\}} & x_{ij} < q_1^j \\ 1 & x_{ij} \in [q_1^j, q_2^j] \\ 1 - \frac{x_{ij} - q_1^j}{\max \left\{ q_1^j - \min_{i \in \{1,2,\dots,n\}} x_{ij}, \max_{i \in \{1,2,\dots,n\}} x_{ij} - q_2^j \right\}} & x_{ij} > q_2^j \end{cases}. \quad (3)$$

### 3. Main Problems in the Cultivation of Humanistic Spirit in Medical Schools

Generally speaking, the campus environment is conducive to the cultivation of good personality and spirit of medical

students, and medical schools need to offer relevant courses to cultivate the spirit and personality of medical students. At present, some medical schools have adopted a series of methods in personnel training. The effect of talent training in schools is still not obvious enough, and there are many problems in talent training.

**3.1. The Traditional Curriculum Training Mode Is Relatively Simple.** In China, most medical colleges offer courses in humanities and social sciences. Medical schools also take it as the main course and subject to cultivate the humanistic spirit of medical students. However, the humanities and social science courses in our country are mainly composed of courses related to Marxist theory. At the current stage, we cannot ignore the cultivation of the humanistic spirit of medical students. The lack of humanistic spirit may cause medical students to deviate from the value orientation of truth, goodness, and beauty. The lack of basic concepts of medical students may develop into medical behaviors that lose their rationality and humanity. The content of the course is mainly ideological and political education. Ideological and political courses play an important role in promoting the spirit of Marxism and adhering to the development path of socialism with Chinese characteristics. Ideological and political theory can also establish a correct outlook on life, world outlook, and values for college students. In general, ideological and political education plays an irreplaceable and important role in the quality training of college students. However, there are essential differences between the goals of ideological and political education and the cultivation of humanistic spirit. At the same time, in the current stage of the teaching of ideological and political courses, different colleges and universities have adopted various teaching methods, and colleges and universities have generally reformed and innovated the teaching forms of ideological and political courses.

**3.2. Insufficient Resources Available to Schools.** In addition to traditional classroom teaching, the cultivation of students' humanistic spirit in medical schools mainly achieved by creating a good campus environment. At the same time, medical schools often carry out a variety of teaching practice activities inside and outside the school. Medical students can also participate in a variety of practical activities during their stay in school. Students can use the teaching resources provided by the school to improve their humanistic quality. However, at present, the most direct learning channel that medical students can access in colleges and universities is still the school library system. Multisource data also provides a new field for medical humanities educators, allowing schools to continuously expand the scope of ideological and political education with the power of data. In the process of changing times, the cultivation of humanistic literacy in medical colleges will face many opportunities and challenges. Medical colleges are specialized medical colleges. At present, most of the library collections of medical colleges are mainly specialized books. This situation can lead to a lack of sufficient study materials for medical students in the humanistic spirit. At present, there are relatively insuffi-

cient books on philosophy, social sciences, and medical humanities in medical schools, which hinder the improvement of medical students' humanistic quality and the cultivation of humanistic spirit.

A research in China has shown that when medical colleges conduct student surveys, it found that less than 3% of students read more than 2 hours a day outside of class. Sixty percent of medical students read less than five hours a week outside of class. Among the students surveyed, the reason why most of the students lacked long-term reading is the lack of schoolbook resources. Among them, the shortage of humanities and social science book resources is more serious. Medical schools also lack the procurement of humanities and social science books. The library's current book search function is not perfect, which is one of the main reasons why students are reluctant to borrow humanities books. The library is an important place for medical students to cultivate their humanistic spirit. Libraries need to continuously optimize the structure of books. Libraries need to use the Internet and high-tech means to open a variety of lending channels. Medical colleges need to strengthen the cultivation of medical students' humanistic and spiritual literacy. First of all, schools need to change the current educational concept and the cultivation mode of humanistic quality. In educational work, schools should pay attention to the social cognitive skills of medical students and at the same time pay attention to the cultivation of students' basic qualities. The library needs to understand the reading needs of students as much as possible and meet the needs of students to the greatest extent possible. In addition, medical schools need to cultivate the humanistic spirit of students in many aspects. Under the current situation, it is far from enough for schools to rely on the library to cultivate the humanistic quality of medical students. Schools should also open a variety of channels and platforms to provide students with the most abundant resources and the broadest learning space.

Medical colleges adopt a variety of modes for students' quality education. In this paper, the model analysis of different training modes is carried out, and the MAE model is specifically used to measure the humanistic mental state of medical students. The smaller the MAE value is, the higher the prediction quality is. Suppose there are  $n$  items in the system, the score set predicted by the algorithm is  $\{p_1, p_2, \dots, p_n\}$ , and the corresponding actual score set is  $\{r_1, r_2, \dots, r_n\}$ , and the MAE calculation formula is as follows:

$$\text{MAE} = \frac{\sum_{i=1}^N |p_{ui} - q_{ui}|}{N}. \quad (4)$$

Coverage index calculates the ratio of predicted items to all unscored items, so as to measure the comprehensiveness of prediction. Cov refers to the actual effect model of the humanistic quality cultivation project. Assuming that  $h$  items are predicted, the calculation method of coverage is as follows:

$$\text{Cov} = \frac{h}{n}. \quad (5)$$

Recall index is also used to evaluate the system effect in the field of information retrieval. The larger recall value is, the better the recommendation quality of the algorithm is.

$$\text{recall} = \frac{\text{Hits}}{|\text{test}|} = \frac{|\text{test} \cap \text{Top} - N|}{|\text{test}|}. \quad (6)$$

In order to verify the clustering effect of user attributes, the contour coefficient  $S$  is used to evaluate the clustering result, and the specific expression is:

$$S(i) = \frac{b(i) - a(i)}{\max \{a(i), b(i)\}}. \quad (7)$$

**3.3. The Learning Efficiency of the Student Group Is Not High.** At present, the main channels for medical students to improve their humanistic spirit involve several aspects. The teaching mode of medical colleges mainly includes two parts: teacher teaching and after-class autonomous learning. Medical students often have a heavy academic load, and students study a wide range of subjects. Schools need to find problems in time, and schools need to take corresponding measures to deal with these problems. Medical colleges need to strengthen the training of medical students' comprehensive quality and incorporate humanistic education into the goal of all-round development of medical students. In the intense study life of medical students, college students conduct full self-learning in their spare time. Medical students will use their spare time to prepare for various professional course exams. In addition, medical students also need to use this time to rest, and it is difficult for students to study humanities and social science courses at the same time. The evaluation index system of medical humanistic literacy training of practicing physicians is shown in Figure 3.

According to the results of our questionnaire survey on some medical colleges in China, more than 85% of college students choose the Internet as a platform for leisure and relaxation. About half of these students choose to watch movies and TV series. 20% of the students choose to obtain news information through the Internet. 11.9% of the students chose online games for leisure and relaxation. 10.6% of the students chose to relax by chatting online. Finally, less than 15% of the students will choose other leisure and entertainment methods. Specifically, schools need to adopt a work method of distributed implementation and distributed guidance to fully mobilize the enthusiasm and initiative of school leaders, teachers, and students themselves. Schools need to strengthen inspection and supervision and summarize the experiences and lessons that students have learned in their learning. In terms of the choice of extracurricular reading materials, the survey results show that medical students are more inclined to choose novels, magazines, and books with entertainment themes. In addition, medical students need to deal with the college foreign language test for CET-4 and CET-6, as well as various medical professional qualification examinations. At the same time, medical students need to read a large number of professional subject books to prepare for the final exam. Therefore, this paper uses a machine

training model to conduct a vectorized analysis of the effect of medical students' humanistic quality training.  $re$ ,  $we$ , and  $pe$  refer to the main factors designed in the cultivation of humanistic quality of medical students under the multi-source data integration environment.

$$re = we + pe, \quad (8)$$

$$Q = X \times W^Q. \quad (9)$$

Specifically, this paper uses the self-attention level in the model for analysis. Taking the self-attention calculation in the encoder model as an example, three vectors, query vector  $Q$ , key vector  $K$ , and value vector  $V$ , are used to describe the calculation of the self-attention mechanism. The corresponding formula is as follows:

$$K = X \times W^K, \quad (10)$$

$$V = X \times W^V. \quad (11)$$

However, general humanities books are not among the students' main choices and less than 20% of them selected. Humanities and social science books can cultivate students' humanistic literacy, but their proportion in students' daily reading is very limited. In terms of the form of reading humanities books, students are more likely to take extensive reading, skimming and other methods. On this basis, schools need to improve the quality and efficiency of students' humanities education work. Through the analysis of multi-source medical data, this paper conducts research on the working mode of humanistic quality cultivation in medical colleges. Specifically, school education will be people-centered. In addition, less than 10% of the students who use intensive reading can conscientiously summarize and reflect and take good reading notes. It said that the students' enthusiasm for learning in the cultivation of humanistic spirit is not high, and the learning efficiency is relatively low. At the same time, there are also major problems in the arrangement of the students' spare time. On the one hand, network resources have become an important part of the students' daily life. Therefore, medical schools need to rely on new media platforms to stimulate students' enthusiasm for learning and to improve the learning efficiency of student groups. In addition, schools also need to enhance students' humanistic literacy through the promotion of humanities books.

#### 4. The Humanistic Literacy Training Strategy of Medical Students Based on Multisource Medical Data

**4.1. Strengthen the Construction of Campus Culture and Build a Good Humanistic Environment.** At present, the speed of talent training is accelerating, and the focus of medical colleges on the training of student groups is constantly tilting towards natural sciences. However, medical students still need a relatively complete humanistic quality training mechanism. However, the current construction of

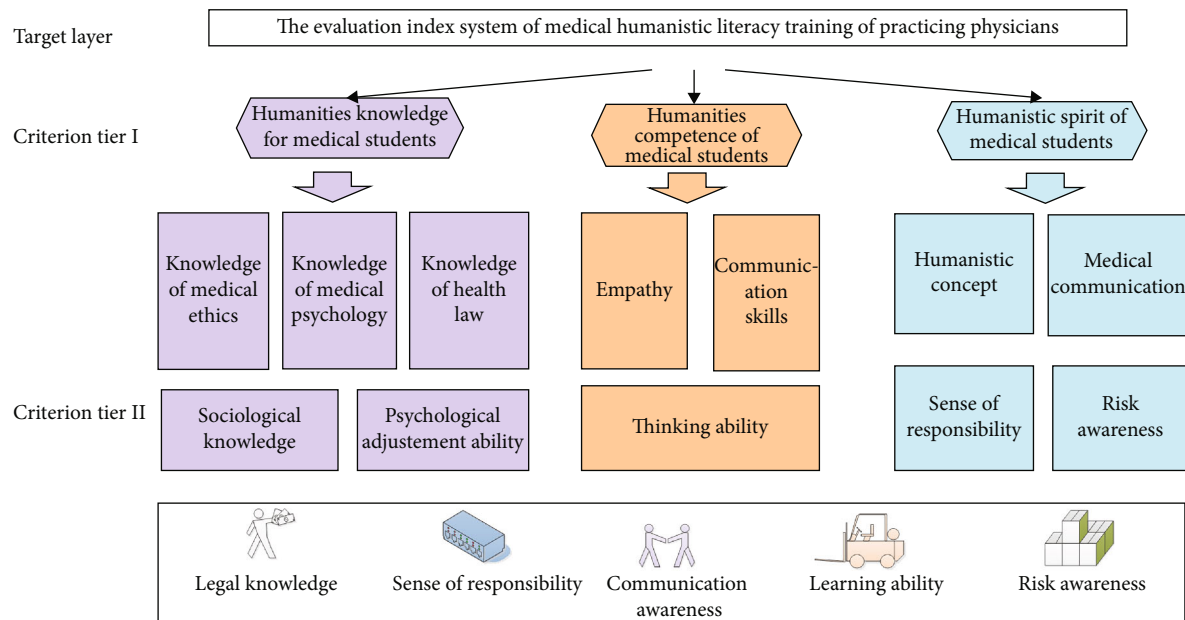


FIGURE 3: The evaluation index system of medical humanistic literacy training of practicing physicians.

humanities and humanities education in some colleges and universities is slow or even stagnant. This situation directly leads to the relatively weak humanistic atmosphere of the school. In modern medical education, the construction of campus cultural environment is of great significance for cultivating qualified and excellent doctors. The humanistic education that medical students receive in colleges and universities is very important to their own future development. The cultivation of humanistic quality in colleges and universities also has a nonnegligible impact on the future work of students. Schools need to cultivate the humanistic spirit of medical students in the ideological and political education work. First of all, schools need to build a humanized classroom, combine skills education with moral education, and improve the learning efficiency of student groups. In addition, schools need to teach students to feel respected and valued. A strong campus humanistic environment can not only improve students' humanistic quality, but also enable students to form correct values and worldviews in a subtle way. A good humanistic education in schools can exercise the spirit of medical students who are not afraid of hardships and have the courage to innovate. Therefore, medical schools should pay attention to the cultivation of humanistic quality of students and strengthen the construction of campus culture. On this basis, the school needs to build a very strong medical humanistic spiritual environment. Such an environment can provide guarantees for cultivating excellent doctors. In addition, schools also need to optimize their own humanistic education resources and create excellent courses for humanistic learning. The schools need to carry out various activities to promote the humanistic spirit of medicine. These activities not only enhance students' humanistic knowledge, but also guide students actively participate in the construction of the school's humanistic environment. The schools need to implement human-oriented teaching

work to give full play to students' own talents and personalities. During school education work, schools need to organically combine classroom education and social practice. Schools need to link teaching and real society and link students' learning process with real life. Schools need to organically combine reading and learning with life, so as to promote the all-round development of students' humanistic quality. Under the current environment, medical colleges use multisource heterogeneous data to cultivate the humanistic quality of medical students. The school adopts a single-model training method, and the training effect of medical students' humanistic spirit presents a significant linear change. When the school adopts a comprehensive training method of multiple models, the humanistic quality of medical students will show a typical wave-like progressive change. The training effect produced by the direct or indirect training mode adopted by medical schools will have great differences. The direct or indirect training effect of medical students' humanistic level is shown in Figure 4.

**4.2. Improve the Humanistic Quality of Teachers and Improve the Teaching Mode of Classroom Teaching.** With the continuous development of medical technology, the current educational model is gradually becoming diversified and open. However, some humanities teachers in colleges and universities still use traditional teaching methods. At the same time, the humanities quality of teachers in some medical colleges and universities is relatively poor, which makes the humanities courses in colleges and universities less attractive to students. Humanistic quality training courses need to be more attractive to students. A good course attractiveness is conducive to improving students' interest in independent learning. At the same time, the school's requirements for face-to-face teaching mode are also increasing. The actual effect of the traditional classroom-



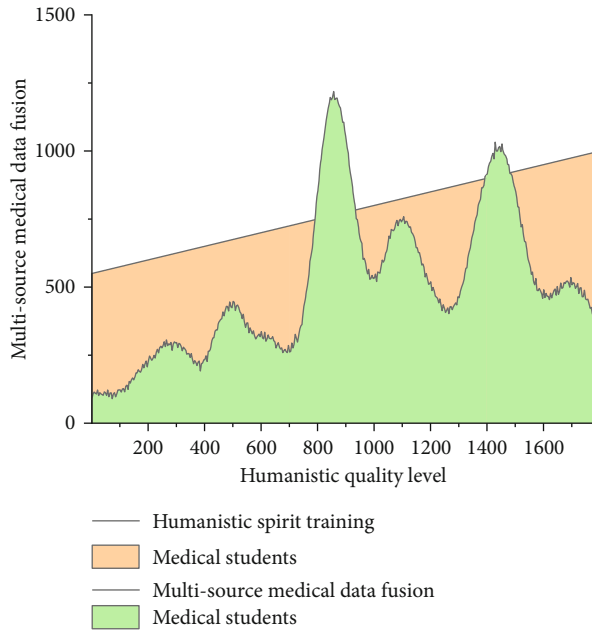


FIGURE 4: The direct or indirect training effect of medical students' humanistic level.

teaching mode is relatively weak, and scholars generally resist this kind of classroom teaching method. The school needs to have a group of teachers with high humanistic quality and appropriate teaching methods. This high-quality teacher team is conducive to improving the overall humanistic quality of medical schools. The traditional medical teaching mode based on face-to-face teaching and students can better understand the classroom content. Schools also need to use important ideas such as Deng Xiaoping theory as a guiding basis. Schools need to strengthen the inheritance and promotion of Chinese traditional excellent culture. The cultivation of the humanistic spirit of the school needs to learn from the excellent cultural achievements of other countries, and the school needs to actively advocate the promotion of humanistic education. However, the current medical discipline is developing very fast, and students need to master a lot of knowledge. The traditional rhythm of classroom teaching is difficult to improve students' interest in learning, and it is difficult to mobilize students' enthusiasm for learning. The traditional teaching mode also makes it impossible for students to fully understand the teaching content of the whole set of medical humanities. This teaching mode is also relatively inefficient. Under the current environment, different medical colleges adopt different education and training models, and medical colleges also have differences in the cultivation of students' humanistic spirit. Schools have a variety of ways to cultivate cultural courses and students' humanistic literacy, and there are differences in the effects of different training modes on medical students. The comparison of the effects of different training modes for medical students is shown in Figure 5.

In the process of classroom teaching, the teaching team can combine a variety of teaching methods and teaching

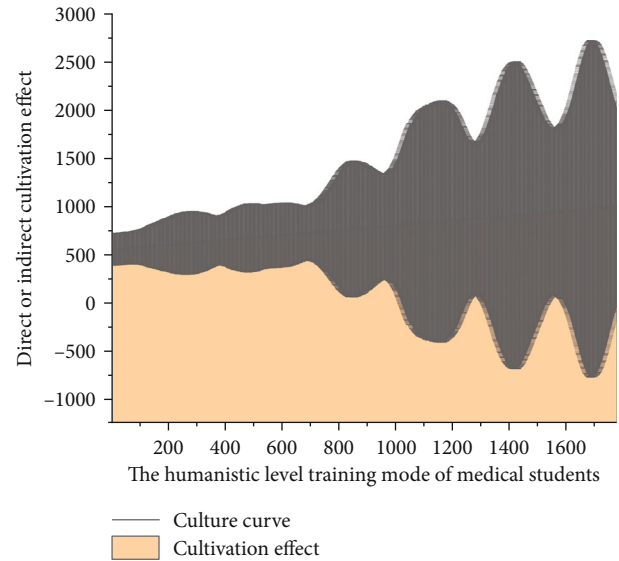


FIGURE 5: The comparison of the effects of different training modes for medical students.

methods. Through the innovation of teaching mode, the teaching team makes the blunt, obscure, and difficult knowledge simple, visualized, and interesting. In addition, according to the characteristics of medical schools, the teaching team can also offer special courses combining medical professional courses and humanities in a planned way. The school increases students' interest in learning by offering relevant courses. The setting of professional courses enables students subtly increase their cognition of humanistic spirit while learning professional courses. After classroom teaching, schools can organize student groups to carry out more practice that is social. The practice of these courses involves many aspects. For example, student groups can go to hospitals, nursing homes, hospice institutions, and other institutions to carry out social practice in their spare time. Student groups need to strengthen the study of humanistic knowledge, to continuously improve their ideological awareness and moral quality in practice, and to deepen their understanding of humanistic spirit and humanistic knowledge.

**4.3. Change Original Ideas and Focus on the Cultivation of Humanistic Spirit.** In the current social environment, the continuous progress of science and technology can effectively enhance social productivity and construction capacity. Contemporary college students have an intuitive feeling about the progress of science and technology. In particular, a large number of medical students begin to engage in medical work, mainly because medical work can bring stable income and relatively high social status. Medical students generally have a high pursuit of medical technology. Medical students also have relatively high expectations for the development of current medical technology. However, the cultivation of humanistic quality of medical students in medical schools is relatively insufficient, and most medical students themselves are not active enough to learn about humanistic



quality. Medical students in school need to combine noble medical spirit with down-to-earth and rigorous work style.

Medical students need to treat illness and save lives as the key to self-improvement and need to treat lifesaving as an important part of their work. While dealing with medical technology work, medical workers also need to strengthen their care and care for patients. Everyone has own independent personality and thoughts. Human beings are not cold-blooded polar weapons. The way humans deal with problems needs to be continuously optimized and improved. The humanistic care that patients receive from medical workers also affects the actual treatment effect to a certain extent. This requires medical workers to have a certain humanistic quality and sufficient humanistic knowledge reserve. However, the foundation of this series of work is based on medical workers' cognition and understanding of humanistic spirit. If doctors do not pay attention to the cultivation of their own humanistic spirit, even if doctors themselves have consummate medical skills, it is difficult for doctors to achieve a high level of professional development. Generally speaking, different medical students' humanistic quality training will produce differentiated medical students' humanistic quality education effect. The current medical training mode mainly includes professional quality training, humanistic spirit training, and social activity training. At different stages, different teaching modes will have different effects on the training results of individual humanistic literacy of medical students. The effect of humanistic quality education for medical students is shown in Figure 6.

*4.4. Diversified Educational Concepts and Integrate Various Educational Models.* With the rapid development of multimedia technology and information technology, major universities in the world are facing the cultivation of all-round talents. Facing the rapidly developing medical technology and the increasingly complex doctor-patient relationship, Chinese medical institutions need more comprehensive medical technical. The all-round training and quality education of medical talents have become the general trend of medical students training in colleges and universities. Hospitals attach great importance to the ability of medical students to solve practical problems. This situation makes the organic integration of science, technology, engineering, humanities, mathematics, and other disciplines becomes the general trend of future development. In addition, medical institutions pay special attention to students' ability to solve problems, which requires schools continuously improve the cultivation of humanistic quality of students. Medical colleges attach great importance to the cultivation of medical students' abilities. Medical colleges need to flexibly use the existing teaching mode and combine teaching activities with the actual situation of colleges and universities. The new teaching mode requires colleges and universities to adopt a more flexible way to carry out teaching activities, combining teaching activities with the actual needs of medical institutions. Different teaching modes of medical school will have different effects on the cultivation of medical students' humanistic quality. Specifically, the training mode of humanistic quality of medical students includes individual

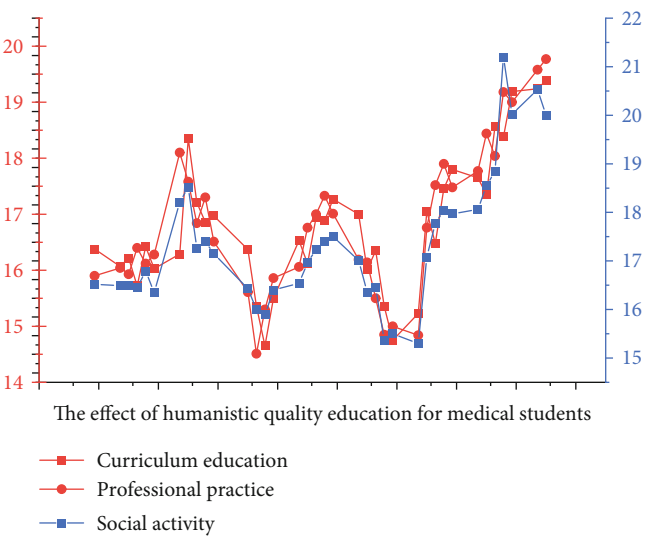


FIGURE 6: The effect of humanistic quality education for medical students Module.

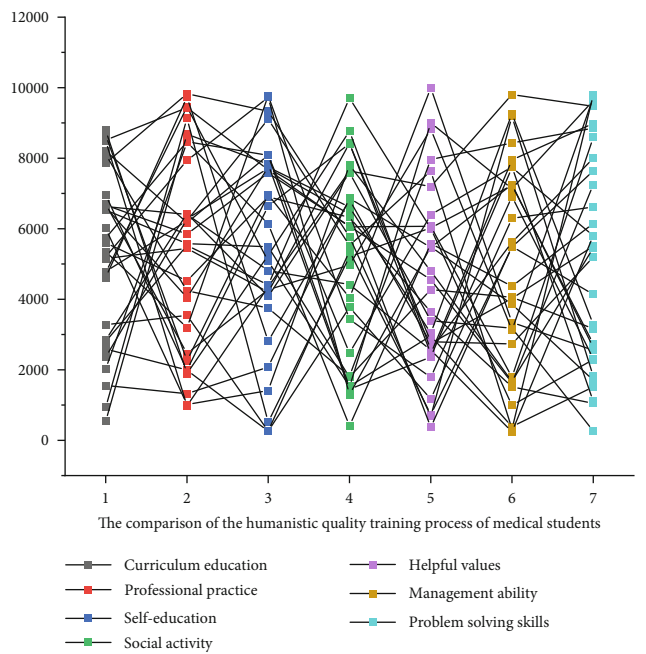


FIGURE 7: The effect of humanistic quality education for medical students.

education, professional education, self-cultivation mode, social activity mode, management ability training, and social mode training. Through different teaching stages, the training level of medical students' humanistic quality will change. The teaching comparison of different modes is shown in the figure below. The effect of humanistic quality education for medical students is shown in Figure 7.

The innovation of this teaching mode can make the process of cultivating medical students' humanistic quality more flexible, easier to understand, and more in line with the

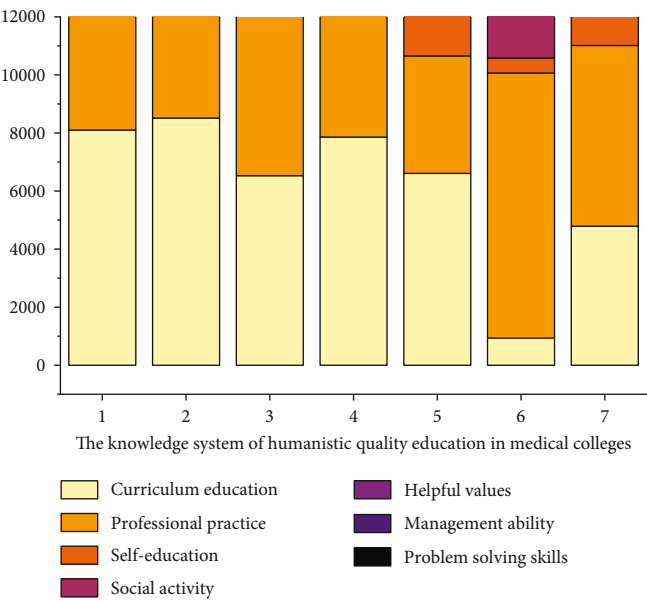


FIGURE 8: The knowledge system of humanistic quality education in medical colleges.

development requirements of the times. At the same time, the World Medical Student Education Conference has given clear requirements for the cultivation of medical students' comprehensive ability. In addition to professional technical training, medical students also need to strengthen the training in the five aspects of science, technology, engineering, mathematics, and art. Among them, art courses include the content of art, humanities, history, and philosophy. The essence of teaching in the field of art is the organic combination of natural science knowledge and humanistic spirit. This teaching method pursues the comprehensive training of talents. The educational concept of diversity and inclusion is especially suitable for the humanistic and spiritual education of medical schools in the current environment. Medicine is an integrative discipline in which the natural sciences and the humanities intertwined. The common core of the discipline is people-oriented, which embodied by superb clinical skills and doctors' care and respect for patients. This advanced educational concept can fully take into account the comprehensive development of medical technology and humanistic spirit. This teaching mode is also conducive to the improvement of medical students' technical and moral literacy. This teaching mode enables medical students to have a certain humanistic quality, while medical technology grows. This training model can effectively alleviate the tense doctor-patient relationship in medical institutions. The knowledge system of humanistic quality education in medical colleges involves many aspects, and we compare and analyze the teaching effect. The results of the study found that social and humanistic education carried out through various channels such as social education, personal self-education, and medical schools will achieve differentiated effects. The knowledge system of humanistic quality education in medical colleges is shown in Figure 8.

5. Conclusion

In general, the rapid development of multisource data fusion technology is inseparable from the support of the concept of healthy humanities. Big data is a new type of strategic resource in China. Big data can innovate the human thinking system and bring a new methodology to scientific research. However, under the current environmental system, the process of using and developing big data in medical schools is complicated. In this process, medical schools cannot ignore the humanistic care for the health of medical students and constantly deepen the concept of big data application in the process of humanistic education for medical students. Schools need to look at the impact of big data on the development of human society objectively, and schools need to clarify the threat of rapid development of big data and technological progress to students' ideological systems. Schools need to practice the concept of healthy humanities and promote the harmonious development of human society on the basis of rational use of big data. The arrival of the era of big data provides new development ideas for the ideological and political education of various medical colleges.

Multisource data fusion technology is the trend of the times, and medical schools need to closely combine multisource data fusion technology with ideological and political education. School education also needs to pay attention to preventing educational risks and deficiencies, so as to comprehensively improve the effect of ideological and political education of students. Schools need to give full play to the positive role of big data, further improve the comprehensive quality of medical college students, and promote more professional and comprehensive development of medical college students. Medical colleges need to cultivate comprehensive

and practical talents for China's medical and health services. Medical schools need to strengthen the humanistic spirit training of medical students in ideological and political education. The cultivation of this kind of humanistic quality not only contributes to the all-round development of students, but also promotes the development and construction of the ideological and political education system in colleges and universities. Colleges and universities need to strengthen the cultivation of humanistic spirit in the process of ideological and political education. Schools need to focus on the needs of their students. Schools need to combine teaching activities with practical activities and comprehensively cultivate the humanistic quality of medical students. At the same time, the school also needs to internalize the humanistic spirit in the specific practical work and continuously strengthen the education of the spiritual and cultural aspects of the student group. Schools need to jointly strengthen the cultivation of medical students' humanistic quality from various aspects, so that they can better adapt to the complex and changing working environment in the future.

### Data Availability

The experimental data used to support the findings of this study are available from the corresponding author upon request.

### Conflicts of Interest

The authors declared that they have no conflicts of interest regarding this work.

### References

- [1] C. Shieuming and L. Chen, "Outcomes study on improving professional identity and humanistic care literacy of nursing students through implementing life education in Taiwan," *Journal of Nursing Administration*, vol. 6, no. 13, pp. 45–47, 2018.
- [2] S. Wang, R. Whitlock, J. C. Lai et al., "Response to: relevance of population-based cut-offs to define frailty in clinical studies," *Hepatology*, vol. 32, no. 3, pp. 17–23, 2022.
- [3] B. Ramotowski, W. J. Forys, and A. Budaj, "Misleading qualification of active smokers based on carbon monoxide measurement of exhaled air," *European Journal of Preventive Cardiology*, vol. 29, Supplement\_1, pp. 36–47, 2022.
- [4] P. Zilundu, F. Chibhabha, G. Yu, R. Fu, and L. H. Zhou, "Pre-clinical medical students' use of motivational and cognitive study strategies during anatomy learning: a three-year cross-sectional survey," *Anatomical Sciences Education*, vol. 4, no. 31, pp. 45–57, 2021.
- [5] A. McCormick, P. Jenkins, and C. Roobottom, "Medical app minefield: radiologists use of medical apps for education and reporting and do they require regulation?," *Clinical Radiology*, vol. 76, no. 10, pp. 774–778, 2021.
- [6] Y. Ulfa, Y. Igarashi, K. Takanawa, E. Shishido, and S. Horiuchi, "A comparison of team-based learning and lecture-based learning on clinical reasoning and classroom engagement: a cluster randomized controlled trial," *BMC Medical Education*, vol. 21, no. 1, pp. 78–89, 2021.
- [7] C. Chan and K. Lee, "Reflection literacy: a multilevel perspective on the challenges of using reflections in higher education through a comprehensive literature review," *Educational Research Review*, vol. 32, no. 2, article 100376, 2021.
- [8] J. I. Vousden, A. J. Cunningham, H. Johnson et al., "Decoding and comprehension skills mediate the link between a small-group reading programme and English national literacy assessments," *British Journal of Educational Psychology*, vol. 92, no. 1, pp. 105–130, 2022.
- [9] K. Jacob, C. Paulickthiel, J. Teebken, S. Veit, and M. Singer-Brodowski, "Change from within: exploring transformative literacy in public administrations to foster sustainability transitions," *Sustainability*, vol. 13, no. 9, p. 4698, 2021.
- [10] M. Demiroren, B. Atilgan, G. T. Teker, and S. Turan, "From the lens of the clinical residents: undergraduate to postgraduate medical education and the transition process," *Postgraduate Medical Journal*, vol. 97, no. 1151, pp. 547–555, 2020.
- [11] H. Humphreys, N. Stevens, D. Leddin et al., "Pathology in Irish medical education," *Journal of Clinical Pathology*, vol. 73, no. 1, pp. 47–50, 2020.
- [12] J. D. Katz and D. T. George, "Reclaiming magical incantation in graduate medical education," *Clinical Rheumatology*, vol. 39, no. 3, pp. 1–5, 2019.
- [13] J. Jackson, "Clinical case-based image portfolios in medical histopathology," *Anatomical Sciences Education*, vol. 18, no. 3, pp. 8–23, 2019.
- [14] A. J. Grace and S. A. Fields, "The power of patient engagement: implications for clinical practice and medical education," *The International Journal of Psychiatry in Medicine*, vol. 53, no. 5–6, pp. 345–349, 2018.
- [15] S. L. Carpenter and C. M. E. Questions, "Continuing medical education questions: April 2018: ACG clinical guideline: diagnosis and management of pancreatic cysts," *Official journal of the American College of Gastroenterology* | ACG, vol. 113, no. 4, pp. 480–491, 2018.
- [16] C. Cuerda, S. M. Schneider, and A. Van Gossum, "Reply, letter to the editor—clinical nutrition education in medical schools—comment on the ESPEN survey," *Clinical Nutrition*, vol. 37, no. 3, p. 1083, 2018.
- [17] J. P. Koller, K. A. Cochran, and L. A. Hedrick, "Practical strategies to enhance resident engagement in clinical quality improvement," *BMC Medical Education*, vol. 22, no. 1, pp. 1–9, 2022.
- [18] B. Brickley, L. T. Williams, M. Morgan, A. Ross, K. Trigger, and L. Ball, "Patient-centred care delivered by general practitioners: a qualitative investigation of the experiences and perceptions of patients and providers," *BMJ Quality & Safety*, vol. 31, no. 3, pp. 191–198, 2022.
- [19] T. M. D. Silva, K. H. J. F. Sousa, A. D. D. S. Oliveira, F. C. M. Amorim, and C. A. P. L. Almeida, "Obstetric violence: theme approach in the training of certified nurse-midwives," *Acta Paulista de Enfermagem*, vol. 33, no. 3, 2020.
- [20] T.-S. G. Wood, F. Smith, and C. Chaib, "The humanistic burden of advanced non-small cell lung cancer (NSCLC) in Europe: a real-world survey linking patient clinical factors to patient and caregiver burden," *Quality of Life Research*, vol. 28, no. 7, pp. 1849–1861, 2019.
- [21] W. Yan, L. Xie, and W. U. Tiejun, "The construction of training mode of intercultural communicative competence of minority college students: dimension of humanistic quality," *Journal of Higher Education*, vol. 7, no. 3, pp. 63–72, 2018.

- [22] C. Shieuming and L. Chen, "Thoughts on developing nursing staff's humanistic care abilities through life education," *Journal of Nursing Administration*, vol. 9, no. 4, p. 79, 2018.
- [23] Y. Yang, "Selection method of cross-border e-commerce export logistics mode based on collaborative filtering algorithm," *Journal of Mathematics*, vol. 2022, no. 3, p. 11, 2022.

## Research Article

# Health Effects of Probiotics on Nonalcoholic Fatty Liver in the Life Cycle Based on Data Analysis

Jia Wang,<sup>1</sup> Yanfei Hao ,<sup>1</sup> Xiao Jin,<sup>2</sup> Xiaoyue Li,<sup>1</sup> Yi Liu,<sup>1</sup> Li Zhang,<sup>1</sup> Jing Wang,<sup>1</sup> and Mingxin Hu<sup>1</sup>

<sup>1</sup>Department of Health Management, Aerospace Center Hospital, Beijing 10089, China

<sup>2</sup>China Aerospace Academy of Systems Science and Engineering, Beijing 100037, China

Correspondence should be addressed to Yanfei Hao; haoyanfei@asch.net.cn

Received 20 April 2022; Revised 10 July 2022; Accepted 13 July 2022; Published 29 July 2022

Academic Editor: Shimin Wang

Copyright © 2022 Jia Wang et al. This is an open access article distributed under the Creative Commons Attribution License, which permits unrestricted use, distribution, and reproduction in any medium, provided the original work is properly cited.

**Objective.** To observe the effect of intestinal probiotics in the treatment of nonalcoholic fatty liver disease (NAFLD) and the effect on liver function and inflammatory factors. **Methods.** 34 healthy rats were selected for the study and divided into 10 rats in the control group, 12 rats in the model group, and 12 rats in the treatment group according to the random number table method. The control group was given behavioral and lifestyle interventions, and the treatment group was given Bifidobacterium minus Black enteric capsules 5 g/(kg-d) by strong feeding method on the basis of the control group. The fatty liver index (FLI), liver ultrasound examination results, liver function, and inflammatory factor levels were compared among the three groups. After 8 weeks of treatment, there were statistically significant differences between the FLI values and liver ultrasound results of the three groups, and the serum alanine aminotransferase (ALT), aspartate aminotransferase (AST), triacylglycerol (TG), and total cholesterol (TC) levels of the observation group were lower than those of the control group and the model group. The levels of serum high molecular weight lipocalin (HMW-APN) and interleukin 22 (IL-22) in the observation group were higher than those in the control group, and the levels of tumor necrosis factor- $\alpha$  (TNF- $\alpha$ ) were lower than those in the control and model groups, and the differences were statistically significant ( $P < 0.05$ ). **Conclusion.** Intestinal probiotics can improve the clinical efficacy of patients with NAFLD, improve liver function, and alleviate the inflammatory response, in order to provide a theoretical basis for the clinical treatment of patients with NAFLD.

## 1. Introduction

NAFLD is a clinicopathological syndrome characterized by diffuse hepatocellular steatosis, excluding alcohol and other definite hepatoprotective factors, and is classified into simple fatty liver, NAFLD, and associated cirrhosis based on the presence of inflammation and fibrosis [1]. The prevalence of NAFLD is as high as 57% and 98% in overweight and obese populations, respectively [2], and in recent years, as overweight and obesity rates in the Chinese population and obesity rates have been rising, the prevalence of NAFLD has been increasing rapidly and at a younger age.

The pathogenesis of NAFLD is currently considered to be the hepatic manifestation of the metabolic syndrome and has not been fully elucidated, but recent studies have shown that its development is closely related to changes in

the intestinal flora and that disturbances in the intestinal flora and increased intestinal wall permeability play an important role in the development of NAFLD, mediated by an immune response [3]. Probiotics, represented by Lactobacillus and Bifidobacterium, have been shown to be directly associated with cholesterol metabolism, gastrointestinal infections, and bacterial translocation [4]. The use of probiotic preparations in NAFLD is currently uncommon, and the therapeutic effects and mechanisms of NAFLD are unknown [5]. In addition, common pharmacological treatments include vitamin E, pioglitazone, metformin, capsaicin, cloacenamides, and statins, of which the most effective pharmacological treatment is uncertain [6].

The pathogenesis of NAFLD is not fully understood. Recent theories suggest that because simple steatosis is a benign process in many patients, whereas NASH is a



progressive process, NASH may have a unique pathogenesis in which the liver is exposed to a combination of insulin resistance, oxidative stress, enteric-derived endotoxins, bacterial endotoxins, altered adipocytosine profile, and reduced bile secretion, leading to an inflammatory response [7]. The traditional “second strike” theory suggests that the first strike, including hepatic fat accumulation and insulin resistance, leads to hepatic steatosis, which increases the release of inflammatory factors, adipocytosine, oxidative stress, and mitochondrial dysfunction (second strike) and ultimately leads to NASH and even liver fibrosis [8].

The human intestinal flora contains more than 1000 species of bacteria with a total of  $1 \times 10^{14}$  species, a mass of 1–2 kg, and a total number of genes exceeding 150 times the total number of host genes [9]. The intestinal flora may be influenced by multiple factors such as diet, lifestyle, age, host genotype, and drug use and is a dynamic combination of quantitative and species changes [10]. According to reports, increased intestinal mucosal permeability and SIBO are common in patients with NAFLD and correlate with the severity of hepatic steatosis [11]. Studies have shown that the bacterial endotoxin lipopolysaccharide (LPS) is hepatotoxic, is increased in the plasma of patients with diabetes, metabolic syndrome, and NAFLD, and plays an important role in the progression of NASH [12]. In addition, ecological dysbiosis of the intestinal flora can lead to an increase in bacterial synthesis of endogenous alcohol, resulting in the production of large amounts of reactive oxygen species during alcohol metabolism, which further increases intestinal mucosal permeability and promotes liver inflammation [13].

Nonalcoholic fatty liver disease (NAFLD) is a metabolic disease characterized by diffuse steatosis of hepatocytes, except for excessive alcohol consumption or other diseases based on fatty degeneration of hepatic parenchymal cells, which can progress to steatohepatitis, cirrhosis, and liver cancer [14]. The pathogenesis of NAFLD is still unclear, but it is currently considered to be related to lipid metabolism, insulin resistance, and inflammatory factor release, and it has been found that the “enterohepatic axis” of intestinal flora plays an important role in its pathogenesis. On the other hand, the endotoxin produced by the flora can cause high expression of inflammatory factors, which can lead to liver damage [15]. We used probiotics in the treatment of NAFLD in mice and observed the effect of intestinal probiotics on the treatment of NAFLD and the effect on liver function and inflammatory factors, in order to provide reference for clinical treatment.

## 2. Materials and Methods

**2.1. Animals.** We used 34 SD male rats (Beijing Weitong Lihua Laboratory Animal Technology Co., Ltd.), SPF grade, production license number SCXK (Zhejiang, China) 2016-0006, age about 8 weeks, weight about 300 g. TNF, IL-6 radioimmunoassay kits were provided by Wuhan Dr. Biotechnology Co. Basic feed formulation is as follows: 35% standard meal, 15.5% bran, 20% soybean meal, 20% corn meal, 0.5% soybean oil, 5% fish meal, 2.5% bone meal, and 1% yeast; high-fat feed formulation is as follows: 60% basal

feed, 15% cooked lard, 10% egg yolk powder, 8% skim milk powder, 5% casein, and 2% white sugar. Japan Hitachi U2200 double-beam spectrophotometer, 7170 automatic biochemical analyzer, vortex mixer, low-temperature high-speed centrifuge, and Olympus IX71 inverted microscope were used. The animal room environment and cages were kept clean during the experimental period. During the experimental period, animals were provided with humane care according to the “3R” principle. The study was approved by the Animal Ethics Committee.

## 2.2. Methods

**2.2.1. Drug Interventions.** Thirty-four rats were divided into 3 groups, 10 in the control group, 12 in the model group, and 12 in the treatment group, and continued to be fed a high-fat diet. The control group continued to be fed a basal diet. The treatment group was given *Lactobacillus bifidum* triple solution (4 tablets mixed with 20 mL distilled water) 5 g/(kg·d), 1 time/d by the strong feeding method, and 1 time/d; the same volume of saline was given to the model group by the strong feeding method. At the end of week 16, at 8 weeks, healthy subjects were performed and blood was collected for testing.

**2.2.2. Collection and Processing of Specimens.** At the end of 8 weeks of dosing, rats are fasted for 12 hours. The abdominal cavity is rapidly opened, and blood is drawn from the abdominal aorta at 12,000 r/min. The serum is isolated and stored at  $-80^{\circ}\text{C}$  to detect adipokines, lipids, and liver function. The rest of the liver is immediately frozen in liquid nitrogen and transferred to  $-80^{\circ}\text{C}$  for freezing and storage.

**2.2.3. Indicator Testing.** The liver index was calculated by weighing the wet mass of the liver and the body mass of the liver, and the liver/body ratio was calculated as the liver index. The fasting blood-glucose (FBG) was measured by a fully automated biochemical analyzer. Fasting insulin (FINS) was determined by the immunoassay method, and the insulin resistance index (HOMA-IR) was calculated as  $\text{FPG} \times \text{FINS} / 22.5$ . TNF- $\alpha$ , lipocalin, and IL-6 were determined by ELISA. Each section was examined under light microscopy for  $5 \times 400$  fields of view to grade the degree of hepatic steatosis and inflammatory cell infiltration. The diagnosis was made by an experienced pathology faculty member who read the slides blindly.

Statistical analysis data were described as mean  $\pm$  SD. The SPSS 16.0 statistical software was used for analysis, *t*-test was used for comparison between two groups, and one-way ANOVA was used for comparison between groups, and  $P < 0.05$  was considered statistically significant.

## 3. Results

**3.1. Comparison of Blood Lipids, Liver Function, and Liver Index.** Serum triglycerides (TGs), total cholesterol (TC), alanine aminotransferase (ALT) and aspartate aminotransferase (AST), and liver index were significantly higher in the model group rats compared with the normal control group ( $P < 0.01$ ); compared with the model group, TG,

TABLE 1: Lipid, liver function, and liver index concentrations in rats (mean  $\pm$  SD).

Group	<i>n</i>	TC (mmol/L)	TG (mmol/L)	ALT (U/L)	AST (U/L)	Liver index
Control group	10	1.72 $\pm$ 0.16	0.48 $\pm$ 0.09	41.2 $\pm$ 0.09	145.8 $\pm$ 3.1	2.45 $\pm$ 0.24
Model group	12	2.3 $\pm$ 0.11	0.90 $\pm$ 0.08	88.4 $\pm$ 4.3	223.6 $\pm$ 4.9	3.78 $\pm$ 0.33
Treatment group	12	2.24 $\pm$ 0.13	0.52 $\pm$ 0.03	55.1 $\pm$ 5.9	157.6 $\pm$ 2.7	2.58 $\pm$ 0.19

Note: the meaning of all abbreviations, group (control, model, and treatment), and the statistical test used.

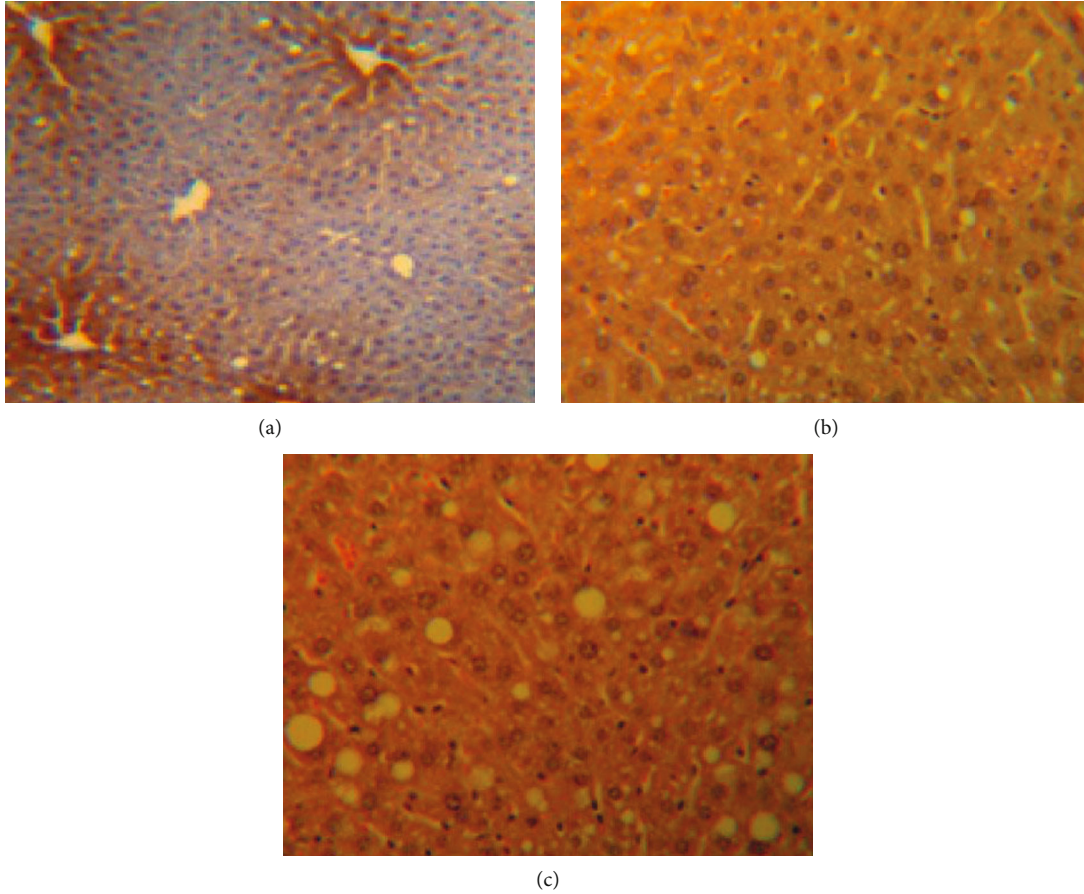


FIGURE 1: Hepatic steatosis in each group of rats (HE  $\times$ 400). (a) Control group; (b) model group; (c) treatment group.

transaminases, and liver index were significantly lower in the treated group rats ( $P < 0.05$ ); however, compared with the normal control group, they remained elevated ( $P < 0.05$ ); TC levels in the treated group were not significantly reduced compared with the model group ( $P > 0.05$ , Table 1).

**3.2. Changes in Liver Pathology in All Groups of Rats.** The hepatocytes were radially distributed around the central vein without lipid infiltration, and there was no inflammatory cell infiltration in the confluent area and lobules (Figure 1(a)). In the NAFLD model group, the hepatocytes were disorganized and sparse, with poorly defined borders. Inflammatory cells were mainly lymphocytes (Figures 1(b) and 2(b)), which were significantly different from the normal control group ( $P < 0.01$ ). Compared with the control group, steatosis was

still present in the treated group, and the hepatocytes were sparsely arranged; however, the lipid droplets were smaller and more restricted, and the number of inflammatory cells infiltrating the confluent area was significantly lower compared with the model group ( $P < 0.01$ , Figures 1(c) and 2(c)).

**3.3. Comparison of Serum Inflammatory Factors and Insulin Resistance in Rats.** At the end of 16 weeks, serum IL-6, TNF- $\alpha$ , and HOMA-IR levels were significantly higher in the model group than in the normal control group, while lipocytin levels were significantly lower ( $P < 0.01$ ). After 8 weeks of probiotic treatment, serum HOMA-IR, IL-6, and TNF- $\alpha$  levels decreased significantly ( $P < 0.05$ ), while lipocytin levels increased but did not return to normal serum levels ( $P > 0.05$ , Table 2).

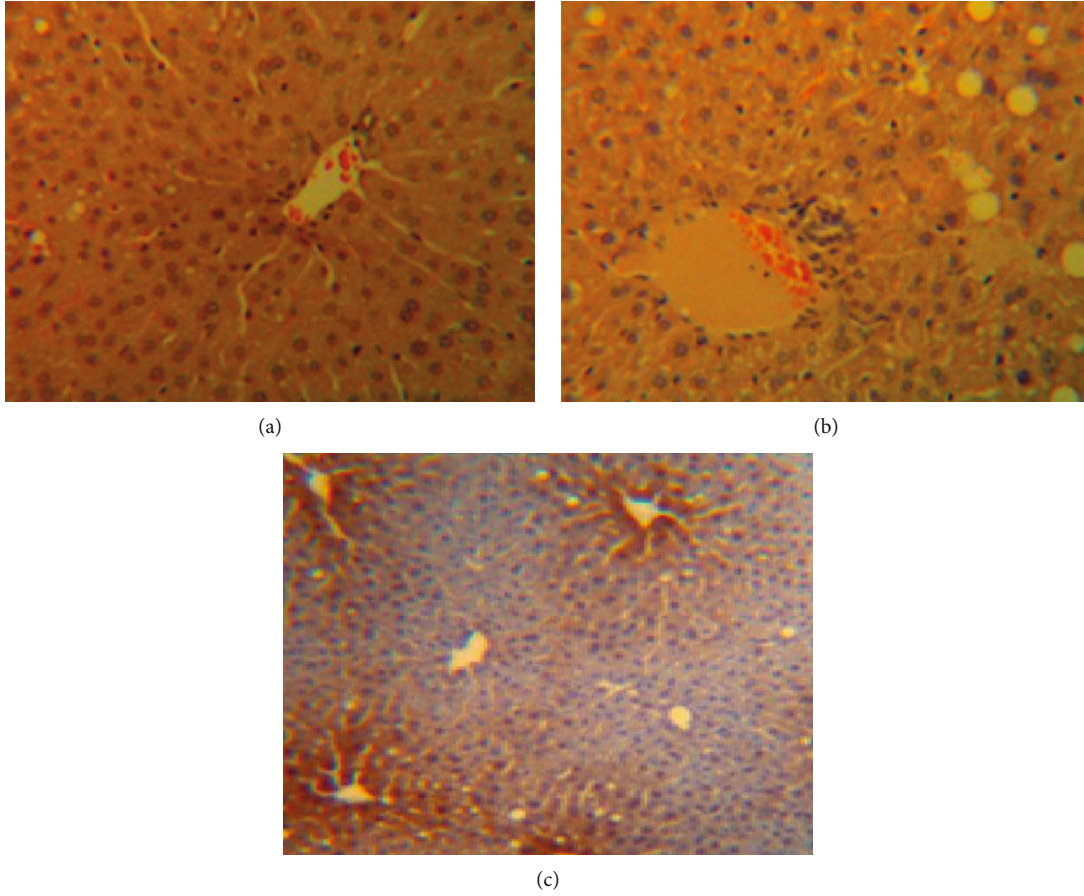


FIGURE 2: Infiltration of inflammatory cells in the liver of rats in each group (HE  $\times 400$ ). (a) Control group; (b) model group; (c) treatment group.

TABLE 2: Serum inflammatory factor concentrations and insulin resistance index in the healthy group (mean  $\pm$  SD).

Group	$n$	IL-6 (ng/L)	Adiponectin ( $\mu\text{g/L}$ )	TNF- $\alpha$ (ng/L)	HOMA-R
Control group	10	$0.45 \pm 0.18$	$2.18 \pm 0.39$	$1.92 \pm 0.21$	$5.38 \pm 1.12$
Model group	12	$1.13 \pm 0.11$	$1.42 \pm 0.08$	$2.47 \pm 0.13$	$10.16 \pm 0.29$
Treatment group	12	$0.64 \pm 0.13$	$2.03 \pm 0.13$	$2.09 \pm 0.36$	$6.26 \pm 1.23$

Note: the meaning of all abbreviations, group (control, model, and treatment), and the statistical test used.

#### 4. Discussion

In recent years, the incidence of NAFLD in China has been increasing year by year with the improvement of living standards. There is no definite mechanism for the pathogenesis of NAFLD, but the “second strike” theory, which is based on insulin resistance and lipid oxidative stress, has been widely accepted in previous studies [16]. However, this theory is still controversial. Based on anatomical and functional correlations, the concept of the “intestine-liver axis” suggests that the liver and intestine interact in multiple ways to provide for each other’s immune integrity [17]. The role of intestinal barrier function in the pathogenesis of NAFLD is becoming an important aspect of research. The intestinal mucosal barrier is the sum of the structures and functions of the intestine that prevent harmful substances such as bac-

teria and toxins in the intestinal lumen from crossing the intestinal mucosa into other tissues and organs of the body and the blood circulation [18].

The intestinal barrier is functionally classified into mechanical, chemical, immune, and biological barriers. Specifically, the mechanical barrier is the normal anatomical structure of the intestine, including the mucus layer, intestinal epithelial cells, and the tight junctions between epithelia; the chemical barrier mainly includes gastric acid, various digestive enzymes, and bile; the immune barrier mainly consists of lymphocytes and immunoglobulin A secreted by the intestinal mucosa; the biological barrier consists of the balance of normal flora, which is an important environmental factor for energy absorption and storage. Impairment of intestinal barrier function is mainly manifested by dysbiosis of intestinal flora, excessive growth of small intestinal



bacteria, and increased permeability of intestinal mucosa. The intestinal biological barrier maintains a dynamic balance. Experiments in humans [19] showed that the composition of the intestinal flora varied between individuals within a short period of time in response to a change in diet. Normal human intestinal flora ferment undigested food from the digestive organs, increasing the efficiency of energy metabolism and thus providing more energy to the host.

When the balance of intestinal flora is disturbed, the number of conditionally pathogenic bacteria increases and the corresponding normal flora decreases, resulting in impaired energy metabolism. Of course, NAFLD also contributes to the dysbiosis of the intestinal flora. The development of NAFLD is accompanied by the production of various inflammatory mediators. IL-1 and interferon inhibit the feeding centre, reducing appetite and reflexively weakening gastrointestinal motility; prostaglandin 2 and platelet-activating factor cause abnormal intestinal motility, gastrointestinal dysfunction, and reduced or absent migratory motor complexes, with the most important consequence of stagnation of the contents of the small intestine, leading to dysbiosis [20].

The intestinal flora is a complex symbiotic system in the human body, and probiotics can regulate the intestinal microecological balance and play the role of protecting intestinal mucosa, anti-inflammation, and improving lipid metabolism. The dysbiosis of intestinal flora causes acute immune response, and thus, TNF- $\alpha$  is expressed in large amounts, which activates the expression of genes with lipid synthesis function, such as SREBP-1c gene fragment, through sensitization, thus promoting hepatocyte steatosis. Probiotics can inhibit the nuclear factor  $\kappa$ B pathway in intestinal epithelial cells, thereby increasing IL-22 expression, which plays an important role in stabilizing the internal environment and tissue repair and affecting cellular value-added, differentiation, apoptosis, and immune effects by regulating the tyrosine protein kinase-1 (JAK1)/signal transduction-activated transcription factor-3 (STAT3) signaling pathway and down-regulating TG synthesis-related genes; the expression of fatty acid transporter protein (FATP) was downregulated to inhibit hepatocyte steatosis. Therefore, probiotics have significant anti-inflammatory and antistatogenic effects and can also reduce TG synthesis [21]. The results of the study showed that probiotic treatment increased serum HMW-APN levels and thus promoted fat metabolism, which is consistent with the findings of Owaga et al. [22]. By anti-inflammatory, promote lipid metabolism and inhibit lipid synthesis, thus restoring liver enzymatic indexes to positive levels, lowering blood lipids, and promoting the improvement of patients' conditions.

There is no ideal drug for the treatment of NAFLD, but recent studies have found that probiotic preparations are effective in the treatment of NAFLD. The therapeutic principle is to use the interaction between the intestine and liver to promote the growth and reproduction of normal microorganisms in order to inhibit the growth of pathogenic bacteria, reduce the production of bacterial endotoxins, inflammatory factors, and other harmful substances, rapidly establish the microecological balance of the gastrointestinal

tract and maintain the stability of the intestinal biomucosal barrier. For this reason, more and more physicians tend to use probiotics and other intestinal barrier modulating drugs in clinical practice for the prevention and treatment of NAFLD, but the results are still controversial due to the small number of large-scale clinical studies and ethical issues [23].

## 5. Conclusions

The probiotic preparation used in this study is a live preparation of *Bifidobacterium longum*, *Lactobacillus bulgaricus*, and *Streptococcus thermophilus*. All three form a combined flora that grows under different conditions and has a fast and long-lasting effect.

This study demonstrated that the probiotic preparation improved liver function and dyslipidemia in a healthy population with NADLD and significantly improved hepatocyte steatosis, possibly by regulating the intestinal flora and thereby reducing inflammatory factors and improving insulin resistance. The role of intestinal dysbiosis in the pathogenesis of NAFLD should not be overlooked, and probiotic preparations have many advantages such as less adverse effects and good tolerability, but in terms of the prevention and treatment of fatty liver, its long-term efficacy and the causal relationship with insulin resistance need to be studied more thoroughly.

## Data Availability

The experimental data used to support the findings of this study are available from the corresponding author upon request.

## Conflicts of Interest

The authors declared that they have no conflicts of interest regarding this work.

## References

- [1] Y. Tang, J. Huang, W. Y. Zhang et al., "Effects of probiotics on nonalcoholic fatty liver disease: a systematic review and meta-analysis," *Therapeutic Advances in Gastroenterology*, vol. 12, p. 175628481987804, 2019.
- [2] S. R. Sharpton, B. Maraj, E. Harding-Theobald, E. Vittinghoff, and N. A. Terrault, "Gut microbiome-targeted therapies in nonalcoholic fatty liver disease: a systematic review, meta-analysis, and meta-regression," *The American Journal of Clinical Nutrition*, vol. 110, no. 1, pp. 139–149, 2019.
- [3] Y. Y. Ma, L. Li, C. H. Yu, Z. Shen, L. H. Chen, and Y. M. Li, "Effects of probiotics on nonalcoholic fatty liver disease: a meta-analysis," *World Journal of Gastroenterology: WJG*, vol. 19, no. 40, pp. 6911–6918, 2013.
- [4] A. Hadi, H. Mohammadi, M. Miraghajani, and E. Ghaedi, "Efficacy of synbiotic supplementation in patients with nonalcoholic fatty liver disease: a systematic review and meta-analysis of clinical trials: synbiotic supplementation and NAFLD," *Critical Reviews in Food Science and Nutrition*, vol. 59, no. 15, pp. 2494–2505, 2019.

- [5] B. R. Loman, D. Hernández-Saavedra, R. An, and R. S. Rector, "Prebiotic and probiotic treatment of nonalcoholic fatty liver disease: a systematic review and meta-analysis," *Nutrition Reviews*, vol. 76, no. 11, pp. 822–839, 2018.
- [6] H. Koutnikova, B. Genser, M. Monteiro-Sepulveda et al., "Impact of bacterial probiotics on obesity, diabetes and non-alcoholic fatty liver disease related variables: a systematic review and meta-analysis of randomised controlled trials," *BMJ Open*, vol. 9, no. 3, article e017995, 2019.
- [7] X. Pan, S. W. Wen, A. C. Kaminga, and A. Liu, "Gut metabolites and inflammation factors in non-alcoholic fatty liver disease: a systematic review and meta-analysis," *Scientific Reports*, vol. 10, no. 1, pp. 1–11, 2020.
- [8] K. Sridharan, G. Sivaramakrishnan, R. P. Sequeira, and A. Elamin, "Pharmacological interventions for non-alcoholic fatty liver disease: a systematic review and network meta-analysis," *Postgraduate Medical Journal*, vol. 94, no. 1116, pp. 556–565, 2018.
- [9] J. Du, Y. Y. Ma, C. H. Yu, and Y. M. Li, "Effects of pentoxifylline on nonalcoholic fatty liver disease: a meta-analysis," *World Journal of Gastroenterology: WJG*, vol. 20, no. 2, pp. 569–577, 2014.
- [10] N. Bazar and M. Parohan, "The effects of curcumin supplementation on body mass index, body weight, and waist circumference in patients with nonalcoholic fatty liver disease: a systematic review and dose-response meta-analysis of randomized controlled trials," *Phytotherapy Research*, vol. 34, no. 3, pp. 464–474, 2020.
- [11] H. Li, D. Zeng, L. Chen, Q. Chen, M. Wang, and C. Zhang, "Immune multipath reliable transmission with fault tolerance in wireless sensor networks," in *International Conference on Bio-Inspired Computing: Theories and Applications*, pp. 513–517, Singapore, October 2016.
- [12] H. Jin, X. Xu, B. Pang et al., "Probiotic and prebiotic interventions for non-alcoholic fatty liver disease: a systematic review and network meta-analysis," *Beneficial Microbes*, vol. 12, no. 6, pp. 517–529, 2021.
- [13] S. Khalesi, D. W. Johnson, K. Campbell et al., "Effect of probiotics and synbiotics consumption on serum concentrations of liver function test enzymes: a systematic review and meta-analysis," *European Journal of Nutrition*, vol. 57, no. 6, pp. 2037–2053, 2018.
- [14] C. Buss, C. Valle-Tovo, S. Miozzo, and A. A. de Mattos, "Probiotics and synbiotics may improve liver aminotransferases levels in non-alcoholic fatty liver disease patients," *Annals of Hepatology*, vol. 13, no. 5, pp. 482–488, 2014.
- [15] J. P. Mann, G. Y. Tang, V. Nobili, and M. J. Armstrong, "Evaluations of lifestyle, dietary, and pharmacologic treatments for pediatric nonalcoholic fatty liver disease: a systematic review," *Clinical Gastroenterology and Hepatology*, vol. 17, no. 8, pp. 1457–1476.e7, 2019.
- [16] J. Chen and L. Vitetta, "Bile acids and butyrate in the effects of probiotics/synbiotics on nonalcoholic fatty liver disease," *European Journal of Gastroenterology & Hepatology*, vol. 31, no. 11, pp. 1475–1476, 2019.
- [17] S. M. Ferolla, G. N. de Almeida Armiliato, C. A. Couto, and T. C. A. Ferrari, "Probiotics as a complementary therapeutic approach in nonalcoholic fatty liver disease," *World Journal of Hepatology*, vol. 7, no. 3, pp. 559–565, 2015.
- [18] M. H. Rouhani, A. Hadi, E. Ghaedi, M. Salehi, A. Mahdavi, and H. Mohammadi, "Do probiotics, prebiotics and synbiotics affect adiponectin and leptin in adults? A systematic review and meta-analysis of clinical trials," *Clinical Nutrition*, vol. 38, no. 5, pp. 2031–2037, 2019.
- [19] A. F. Cicero, A. Colletti, and S. Bellentani, "Nutraceutical approach to non-alcoholic fatty liver disease (NAFLD): the available clinical evidence," *Nutrients*, vol. 10, no. 9, p. 1153, 2018.
- [20] C. Thongprayoon, W. Kaewput, S. T. Hatch et al., "Effects of probiotics on inflammation and uremic toxins among patients on dialysis: a systematic review and meta-analysis," *Digestive Diseases and Sciences*, vol. 64, no. 2, pp. 469–479, 2019.
- [21] G. Tarantino and C. Finelli, "Systematic review on intervention with prebiotics/probiotics in patients with obesity-related nonalcoholic fatty liver disease," *Future Microbiology*, vol. 10, no. 5, pp. 889–902, 2015.
- [22] E. Owaga, R. H. Hsieh, B. Mugendi, S. Masuku, C. K. Shih, and J. S. Chang, "Th17 cells as potential probiotic therapeutic targets in inflammatory bowel diseases," *International Journal of Molecular Sciences*, vol. 16, no. 9, pp. 20841–20858, 2015.
- [23] G. Tarantino, S. Costantini, C. Finelli et al., "Is serum Interleukin-17 associated with early atherosclerosis in obese patients?," *Journal of Translational Medicine*, vol. 12, no. 1, pp. 1–10, 2014.



## Research Article

# Expression and Clinical Significance of Serum Krüppel-Like Factor 7 (KLF7) in NSCLC Patients

Huigai Song,<sup>1</sup> Jingjing Sun,<sup>1</sup> Zhiming Xu,<sup>1</sup> Xinru Liu,<sup>2</sup> and Na Liu <sup>1</sup>

<sup>1</sup>Pathology Department, Hebei Chest Hospital, Shijiazhuang, Hebei 050000, China

<sup>2</sup>Department of Immunization Planning, Chengde Center for Disease Control and Prevention, Chengde, Hebei 067000, China

Correspondence should be addressed to Na Liu; 2016150296@jou.edu.cn

Received 20 June 2022; Accepted 9 July 2022; Published 27 July 2022

Academic Editor: Hangjun Che

Copyright © 2022 Huigai Song et al. This is an open access article distributed under the Creative Commons Attribution License, which permits unrestricted use, distribution, and reproduction in any medium, provided the original work is properly cited.

Nonsmall cell lung cancer (NSCLC) is a serious threat to the life and health of patients with high incidence rate and mortality. The present research was to assess the relationship between the serum Krüppel-like factor 7 (KLF7) level and the recurrence and metastasis of NSCLC patients. 150 patients with NSCLC treated by thoracoscopic radical resection of lung cancer in our hospital from January 2016 to February 2017 were selected. As the control group, 148 healthy people who went to the hospital for physical examination in the same period were screened. The expression levels of serum KLF7 in the observation group and the control group were compared and analyzed. According to the level of KLF7 expression, the patients in the observation group were divided into KLF7 high expression group ( $\geq 258.6$  ng/L,  $n=75$ ) and KLF7 low expression group ( $<258.6$  ng/L,  $n=75$ ). The 3-year recurrence and metastasis rate of patients in each group was compared and analyzed. It was found the concentration of serum KLF7 in peripheral blood of NSCLC ( $2.25 \pm 0.65$ ) ng/ml was significantly higher than that in healthy population ( $1.42 \pm 0.38$ ) ng/ml ( $P < 0.05$ ). The expression level of serum KLF7 was not related to gender, age, smoking history, and tumor diameter of NSCLC patients ( $P > 0.05$ ), but related to the degree of differentiation and TNM stage of NSCLC patients ( $P < 0.05$ ). Univariate analysis showed that the degree of differentiation, TNM stage, and KLF7 were significantly correlated with 3-year recurrence and metastasis of NSCLC patients ( $P < 0.05$ ). Cox regression analysis showed that low degree of differentiation, TNM stage IIIa, and KLF7 were independent risk factors for recurrence and metastasis in NSCLC patients in 3 years ( $P < 0.05$ ). Taken together, the expression level of serum KLF7 in patients with NSCLC is significantly increased, which is an independent risk factor for recurrence and metastasis in 3 years, and is worthy of clinical application.

## 1. Introduction

Lung cancer is the leading cause of death worldwide, with high incidence rate and mortality [1–5]. Nonsmall cell lung cancer (NSCLC) refers to all epithelial cell lung cancer except small cell lung cancer. At present, it is mainly treated by surgical resection, radiotherapy, and chemotherapy, with good clinical efficacy. However, some patients can still have distant metastasis and recurrence, which seriously affects the prognosis [6–8]; therefore, timely assessment of the risk of recurrence and metastasis after treatment can formulate a reasonable clinical treatment plan in advance, so as to significantly improve the prognosis of patients [9, 10]. Therefore, it is particularly important to study the biological characteristics of lung cancer and find the method of early detection

of lung cancer to improve the cure rate and prognosis of lung cancer.

Krüppel-like factor 7 (KLF7) is a member of specificity protein/Krüppel-like factor (SP/KLF) family. It is widely expressed at low and medium levels in adult tissues. Functional studies show that KLF7 plays an important role in the development of the nervous system and adipogenesis and is a gene related to many diseases [11–13]. Recent studies have shown that KLF7 is also involved in many new biological processes, such as sciatic nerve regeneration [14, 15], mediating tissue inflammatory response [16], participating in cancer radiotherapy [17] and chemotherapy rehabilitation, regulating oxidative phosphorylation pathway [18], and so on. Furthermore, it has been reported that KLF7 can enhance the ability of tumor migration and invasion,

which is related to tumor recurrence and metastasis [19, 20], whereas there are few studies on its expression in the serum of patients with NSCLC. Based on this, this study explored the relationship between the expression level of serum KLF7 and the recurrence and metastasis of NSCLC patients, in order to provide reference for predicting the recurrence and metastasis of NSCLC in advance. The report is as follows.

## 2. Clinical Data

150 patients with NSCLC treated by thoracoscopic radical resection of lung cancer in our hospital from January 2016 to February 2017 were selected as the observation group, including 100 males and 50 females; the age ranged from 47 to 74 years, with an average of  $(56.25 \pm 8.42)$  years; 72 cases had tumor diameter  $\geq 4$  cm and 78 cases had tumor diameter  $< 4$  cm; 60 cases were poorly differentiated and 90 cases were moderately well differentiated; TNM stages were stage I in 50 cases, stage II in 35 cases, and stage IIIa in 65 cases. The informed consent form was signed with the patients before the clinical study and approved by the ethics committee of the hospital. The serum of the healthy control group was taken from 148 healthy subjects in the same period in the physical examination center of our hospital, including 101 males and 47 females; The age ranged from 46 to 74 years, with an average of  $(56.32 \pm 8.25)$  years. There was no significant difference in gender and age between pathological group and healthy control group. Inclusion criteria: (1) no specific treatment for lung cancer, including surgery, radiotherapy, chemotherapy, targeted drug therapy, and biotherapy, was received before admission; (2) patients with lung cancer confirmed by fiberscope biopsy, percutaneous needle aspiration biopsy, or postoperative pathology were classified according to the classification standard of lung cancer tissue issued by the World Health Organization (WHO) in 2015, and the lung cancer was staged according to the 8<sup>th</sup> edition of lung cancer primary tumor lymph node metastasis (TNM) staging system issued by the International Anti Cancer Alliance in 2017.

## 3. Methods

The fasting peripheral blood of NSCLC patients and healthy controls was collected with Ethylenediamine tetraacetic acid (EDTA) anticoagulant tube, stored in 4°C refrigerator for temporary storage, and sent to the laboratory within 24h. After low-temperature and high-speed centrifugation, the serum was sub-packed and tested in -80°C refrigerator. The double antibody sandwich enzyme-linked immunosorbent assay (ELISA) was used to detect KLF7, which was operated in strict accordance with the instructions of ELISA Kit (R&D, USA).

The standard curve was drawn through the solution of standard KLF7 protein concentration and its OD<sub>450</sub>, and the serum OD<sub>450</sub> of healthy people and lung cancer patients was detected, respectively, so as to calculate the serum KLF7 concentration, and the serum KLF7 levels of healthy people and lung cancer patients were compared, respectively; in

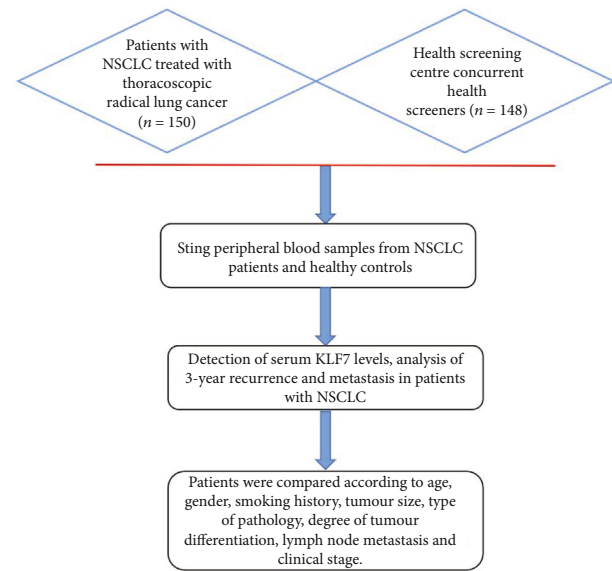


FIGURE 1: Summary images.

patients with NSCLC, they were compared according to their age, gender, smoking history, tumor size, pathological type, degree of tumor differentiation, lymph node metastasis, and clinical stage.

## 4. Observation Index

All patients were treated with thoracoscopic radical resection of lung cancer. They were followed up for 3 years by outpatient and telephone. The starting time of follow-up was the recurrence and metastasis of CT examination or the last follow-up was the end of follow-up. All patients were followed up successfully. (1) The expression levels of serum KLF7 in the observation group and the control group were compared and analyzed. (2) To analyze the relationship between the expression level of serum KLF7 and the clinicopathological features of NSCLC patients. (3) According to the level of KLF7 expression in the observation group (taking the average value of its expression level as the dividing line), they were divided into KLF7 high expression group ( $\geq 258.6$  ng/L,  $n=75$ ) and KLF7 low expression group ( $< 258.6$  ng/L,  $n=75$ ). The 3-year recurrence and metastasis rate of patients in NSCLC was compared and analyzed. (4) To analyze the influencing factors of 3-year recurrence and metastasis in patients with NSCLC (Figure 1).

## 5. Results

**5.1. Comparison of Serum KLF7 Concentration in Peripheral Blood.** The serum KLF7 concentration in peripheral blood of NSCLC ( $2.25 \pm 0.65$ ) ng/ml was markedly higher than that in healthy population ( $1.42 \pm 0.38$ ) ng/ml, and the divergence was statistically prominently ( $P < 0.05$ ).

**5.2. Single Factor Analysis of Serum KLF7 in Patients with NSCLC.** The expression level of serum KLF7 was not related to gender, age, smoking history, and tumor diameter of

TABLE 1: Single factor analysis of serum KLF7 in patients with NSCLC ( $\bar{x} \pm s$ ).

Characteristic	Cases ( <i>n</i> )	KLF7	<i>t</i>	<i>P</i>
Gender			0.145	0.885
Male	100	2.15 ± 0.32		
Female	50	2.13 ± 0.52		
Age			0.870	0.386
≥60	78	2.25 ± 0.42		
<60	72	2.32 ± 0.56		
Smoking history			0.443	0.658
Have	80	2.12 ± 0.23		
No have	70	2.14 ± 0.32		
Tumor diameter			0.698	0.486
≥4 cm	68	2.32 ± 0.54		
<4 cm	82	2.26 ± 0.51		
Degree of differentiation			5.134	0.001
Low differentiation	55	2.41 ± 0.41		
Medium and high differentiation	95	2.15 ± 0.21		
TNM staging			5.274	0.001
Phase I~II	85	2.04 ± 0.42		
Phase IIIa	65	2.38 ± 0.35		

Note: *P* value represents the difference with statistical significance.

TABLE 2: Univariate analysis of 3-year recurrence and metastasis rate in patients with NSCLC (*n*, %).

Characteristic	3-year recurrence and metastasis rate ( <i>n</i> , %)	$\chi^2$	<i>P</i>
Gender		0.240	0.624
Male	68 (68)		
Female	32 (64)		
Age		0.366	0.545
≥60	45 (57.69)		
<60	38 (52.77)		
Smoking history		2.228	0.135
Have	56 (70)		
No have	36 (51.43)		
Tumor diameter		2.636	0.104
≥4 cm	50 (73.53)		
<4 cm	50 (60.97)		
Degree of differentiation		6.981	0.008
Low differentiation	45 (81.82)		
Medium and high differentiation	58 (60.05)		
TNM staging		6.803	0.009
Phase I~II	48 (56.47)		
Phase IIIa	50 (76.92)		
KLF7		8.466	0.003
≥258.6 ng/L	62 (82.67)		
<258.6 ng/L	45 (61.33)		

Note: *P* value represents the difference with statistical significance.

NSCLC patients ( $P > 0.05$ ) but significantly related to the degree of differentiation and TNM stage of NSCLC patients ( $P < 0.05$ ) (see Table 1).

**5.3. Analysis of 3-Year Recurrence and Metastasis in Patients with NSCLC.** Univariate analysis showed that the degree of differentiation, TNM stage, and KLF7 were significantly correlated with 3-year recurrence and metastasis of NSCLC patients ( $P < 0.05$ ). TNM stage IIIa and KLF7 were independent risk factors for recurrence and metastasis of NSCLC patients in 3 years was Cox regression analysis clarified ( $P < 0.05$ ) (see Tables 2 and 3).

## 6. Discussion

With the change of living environment and air quality, the number of lung cancer patients has a high trend. According to relevant data, the number of new lung cancer patients worldwide is more than 1.8 million every year, while China's lung cancer data in 2015 shows 733000 new cases and more than 610000 deaths. Lung cancer is the most common malignant tumor in the clinic [21–23], and the most common pathological type is NSCLC, which mainly includes squamous cell carcinoma (SCC), adenocarcinoma (LAC), and large cell carcinoma (LCC) [24–26]. With the development of precision medicine, chemotherapy, radiotherapy, targeted therapy, and immunotherapy have prolonged the survival of some patients with advanced lung cancer, but the 5-year survival rate is still less than 21% [27–30]. Therefore, it is of great clinical significance to find a simple and easy to operate prognostic evaluation index. So far, the immune function has attracted attention of patients with lung cancer. Studies have shown that the occurrence,

TABLE 3: COX regression analysis of 3-year recurrence and metastasis rate in patients with NSCLC.

Influence factor	$\beta$	SE	Wald $X^2$	$P$	HR (95% CI)
The degree of differentiation is low	0.396	0.207	3.856	0.043	1.472 (1.012~2.225)
TNM stage is IIIa stage	0.368	0.202	3.821	0.048	1.485 (1.325~2.684)
KLF7	0.725	0.206	7.815	0.004	2.084 (1.396~3.105)

Note:  $P$  value represents the difference with statistical significance.

development, metastasis, and recurrence of malignant tumors are related to the defects of immune function [31–33]. Patients with lung cancer have a certain degree of abnormal immune function [34, 35]. In recent years, with the rise and development of molecular biology, tumor drug therapy has shown a diversified trend. Among them, molecular targeted drugs have become a hot spot in the clinical treatment of nonsmall cell lung cancer because of their strong pertinence and high safety. Moreover, the continuous development of multidisciplinary comprehensive treatment methods such as molecular targeted therapy and immunotherapy has provided a new direction for the clinical treatment of lung cancer and enriched the means of lung cancer treatment [36–38]. With the in-depth study of the immune tolerance mechanism of lung cancer, the interaction of KLF7 in the occurrence and development of lung cancer has attracted more and more attention of scholars at home and abroad.

The research on KLF7 in the serum of cancer patients is not uncommon. The research shows that the research on KLF7 in the serum of cancer patients is not uncommon. At present, a research has found that the serum KLF7 level of breast cancer patients is higher than that of healthy people [39]; furthermore, a study has found that the level of serum KLF7 has diagnostic significance for gastrointestinal cancer [11]. The research on the correlation between KLF7 and NSCLC is mainly concentrated in lung cancer tissues and cells [40], and its research in the serum of lung cancer patients is relatively few. The research results mostly suggest that KLF7 has a positive correlation with the malignant degree of NSCLC, which is consistent with the findings of this study. The mechanism of KLF7 promoting tumor may be related to KLF7 promoting the invasion of tumor cells into microvessels and promoting the formation of neovascularization.

At present, the study has found that the expression of serum KLF7 in patients with lung cancer is significantly higher than that in healthy people [41], suggesting that KLF7 is expected to become a new tumor marker. In patients with lung cancer, the expression level of serum KLF7 had nothing to do with the gender, age, smoking history, and tumor diameter of patients with NSCLC. However, the level of serum KLF7 in patients with low differentiation was higher than that in patients with high differentiation. The concentration of serum KLF7 in patients with clinical stage IIIa was significantly higher than that in patients with stage I~II, suggesting that KLF7 may have a positive correlation with the degree of malignancy of patients and may have a certain value for the prognosis of lung cancer. The 3-year

recurrence and metastasis rate of KLF7 high expression group was significantly higher than that of KLF7 low expression group, and KLF7 was an independent risk factor for recurrence and metastasis 3 years after operation. The results showed that the expression level of KLF7 increased and participated in the recurrence and metastasis of NSCLC. The study also found that TNM stage IIIa was an independent risk factor for 3-year recurrence and metastasis of NSCLC patients. It is considered that the cancer at this stage may have spread outside the lung and it is difficult to completely eliminate the cancer by surgical treatment. In conclusion, the expression level of serum KLF7 in patients with NSCLC is significantly increased, which is an independent risk factor for recurrence and metastasis in 3 years. It has a high efficiency in predicting recurrence and metastasis in 3 years after operation, which is worthy of clinical application. However, this study is a single-center study. Only NSCLC patients treated with thoracoscopic radical resection of lung cancer and NSCLC patients not treated with radiotherapy and chemotherapy may have selection bias in the results. At the same time, the follow-up time is short, and further research is needed in the follow-up.

The advantages of molecular targeted therapy are targeting safety and convenience. Compared with traditional chemotherapy, molecular targeted therapy can reduce the pain of patients' clinical treatment as much as possible [42]. At present, targeted therapy has gradually completed the development goal of individualized and accurate treatment. At the same time, it is committed to carrying out comprehensive treatment with multiple disciplines. Its application in clinical treatment is also gradually popularized, avoiding the pain of patients caused by chemotherapy to the greatest extent. The emergence of molecular targeted therapy has opened up a new field for the clinical treatment of lung cancer. It has the advantages comparable to traditional chemotherapy and is an important link in the clinical standard treatment of modern medical lung cancer. How to maximize the benefits of molecular targeted therapy in tumor treatment and give the most effective "one-to-one" clinical treatment scheme to individual patients has become a hot topic in medical tumor treatment. With the development of molecular targeted therapy, there are still many problems to be solved. In a word, with the continuous exploration of molecular targeted therapy, the mechanism of molecular targeted therapy will be more and more clear. How to formulate a targeted plan for the treatment based on the actual situation and tolerance of patients and how to use molecular targeted therapy to prolong the survival time of patients are a subject of continuous medical research.



## Data Availability

The datasets used and analyzed during the current study are available from the corresponding author upon reasonable request.

## Conflicts of Interest

The authors declare that they have no conflicts of interest.

## References

- [1] R. Nooreldeen and H. Bach, "Current and future development in lung cancer diagnosis," *International Journal of Molecular Sciences*, vol. 22, no. 16, p. 8661, 2021.
- [2] H. A. Hamann, E. S. Ver Hoeve, L. Carter-Harris, J. L. Studts, and J. S. Ostroff, "Multilevel opportunities to address lung cancer stigma across the cancer control continuum," *Journal of Thoracic Oncology*, vol. 13, no. 8, article S1556086418306270, pp. 1062–1075, 2018.
- [3] H. Abolfathi, M. Sheikhpour, S. S. Shahraeini, S. Khatami, and S. A. Nojoumi, "Studies in lung cancer cytokine proteomics: a review," *Expert Review of Proteomics*, vol. 18, no. 1, pp. 49–64, 2021.
- [4] J. C. Martin, "Genetic biomarkers: implications of increased understanding and identification in lung cancer management," *Clinical Journal of Oncology Nursing*, vol. 24, no. 6, pp. 648–656, 2020.
- [5] J. U. Lim, "Update on adjuvant therapy in completely resected NSCLC patients," *Cancer*, vol. 13, no. 3, pp. 277–283, 2022.
- [6] J. Fuchs, M. Früh, A. Papachristofilou et al., "Resection of isolated brain metastases in non-small cell lung cancer (NSCLC) patients - evaluation of outcome and prognostic factors: a retrospective multicenter study," *PLoS One*, vol. 16, no. 6, article e0253601, 2021.
- [7] C. A. Welch, M. J. Sweeting, P. C. Lambert et al., "Impact on survival of modelling increased surgical resection rates in patients with non-small-cell lung cancer and cardiovascular comorbidities: a VICORI study," *British Journal of Cancer*, vol. 123, no. 3, pp. 471–479, 2020.
- [8] M. Peer, S. Azzam, A. Cyjon et al., "Major pulmonary resection after neoadjuvant chemotherapy or chemoradiation in potentially resectable stage III non-small cell lung carcinoma," *Scientific Reports*, vol. 11, no. 1, p. 20232, 2021.
- [9] R. Xu, X.-R. Cao, B.-Q. Zhang, J. L. Wang, L. Wang, and W. Q. Sun, "BLACAT1 is negatively associated with prognosis in patients with NSCLC and inhibits cell progression, metastasis and epithelial-mesenchymal transition through down-regulating Wnt/ $\beta$ -catenin signaling pathway," *European Review for Medical and Pharmacological Sciences*, vol. 23, no. 14, pp. 6217–6225, 2019.
- [10] D. Chen and Y. Jinming, "Effectiveness of postoperative or preoperative radiotherapy on prognosis in patients with stage II resectable non-small cell lung cancer: a retrospective study based on the SEER database," *Medicina (Kaunas, Lithuania)*, vol. 57, no. 11, article medicina57111202, p. 1202, 2021.
- [11] Y. Li, Q. Wang, D. W. Wang, and W. Fu, "KLF7 promotes gastric carcinogenesis through regulation of ANTXR1," *Cancer Management and Research*, vol. 13, pp. 5547–5557, 2021.
- [12] Y. Guo, B. Chai, J. Jia et al., "KLF7/VPS35 axis contributes to hepatocellular carcinoma progression through CCDC85C-activated  $\beta$ -catenin pathway," *Cell & Bioscience*, vol. 11, no. 1, p. 73, 2021.
- [13] F. Guan, Z. Kang, J.-T. Zhan et al., "KLF7 promotes polyamine biosynthesis and glioma development through transcriptionally activating ASL," *Biochemical and Biophysical Research Communications*, vol. 514, no. 1, article S0006291X19307648, pp. 51–57, 2019.
- [14] W.-Y. Li, G.-Y. Zhu, W.-J. Yue, G.-D. Sun, X.-F. Zhu, and Y. Wang, "KLF7 overexpression in bone marrow stromal stem cells graft transplantation promotes sciatic nerve regeneration," *Journal of Neural Engineering*, vol. 16, no. 5, article 056011, 2019.
- [15] Y. Wang, W.-Y. Li, H. Jia et al., "KLF7-transfected Schwann cell graft transplantation promotes sciatic nerve regeneration," *Neuroscience*, vol. 340, pp. 319–332, 2017.
- [16] L. Jiang, M. Wang, R. Sun et al., "Methylation of miR-19b-3p promoter exacerbates inflammatory responses in sepsis-induced ALI via targeting KLF7," *Cell Biology International*, vol. 45, no. 8, pp. 1666–1675, 2021.
- [17] M. De Donato, G. Babini, S. Mozzetti et al., "KLF7: a new candidate biomarker and therapeutic target for high-grade serous ovarian cancer," *Journal of Experimental & Clinical Cancer Research*, vol. 39, no. 1, article 1775, p. 265, 2020.
- [18] R. van der Lee, R. Szklarczyk, J. Smeitink, H. J. Smeets, M. A. Huynen, and R. Vogel, "Transcriptome analysis of complex I-deficient patients reveals distinct expression programs for subunits and assembly factors of the oxidative phosphorylation system," *BMC Genomics*, vol. 16, no. 1, pp. 1–13, 2015.
- [19] R. Gupta, P. Malvi, K. R. Parajuli et al., "KLF7 promotes pancreatic cancer growth and metastasis by up-regulating ISG expression and maintaining Golgi complex integrity," *Proceedings of the National Academy of Sciences of the United States of America*, vol. 117, no. 22, pp. 12341–12351, 2020.
- [20] Y.-X. An, Y.-J. Shang, X. Zhi-Wei et al., "STAT3-induced long noncoding RNA LINC00668 promotes migration and invasion of non-small cell lung cancer via the miR-193a/KLF7 axis," *Biomedicine & Pharmacotherapy*, vol. 116, article 109023, 2019.
- [21] M. Evison and A. Z. U. K. Limited, "The current treatment landscape in the UK for stage III NSCLC," *British Journal of Cancer*, vol. 123, Supplement 1, pp. 3–9, 2020.
- [22] Y. K. Chae, S. Chang, T. Ko et al., "Epithelial-mesenchymal transition (EMT) signature is inversely associated with T-cell infiltration in non-small cell lung cancer (NSCLC)," *Scientific Reports*, vol. 8, no. 1, p. 2918, 2018.
- [23] V. Relli, M. Trerotola, E. Guerra, and S. Alberti, "Abandoning the notion of non-small cell lung cancer," *Trends in Molecular Medicine*, vol. 25, no. 7, pp. 585–594, 2019.
- [24] S. S. Lee and Y. K. Cheah, "The interplay between microRNAs and cellular components of tumour microenvironment (TME) on non-small-cell lung cancer (NSCLC) progression," *Journal of Immunology Research*, vol. 2019, Article ID 3046379, 12 pages, 2019.
- [25] E. N. Imyanitov, A. G. Iyevleva, and E. V. Levchenko, "Molecular testing and targeted therapy for non-small cell lung cancer: current status and perspectives," *Critical Reviews in Oncology/Hematology*, vol. 157, article 103194, 2021.
- [26] J.-C. Liu, S. Narva, K. Zhou, and W. Zhang, "A review on the antitumor activity of various nitrogenous-based heterocyclic compounds as NSCLC inhibitors," *Mini Reviews in Medicinal Chemistry*, vol. 19, no. 18, pp. 1517–1530, 2019.



- [27] M. Nagasaka and S. M. Gadgeel, "Role of chemotherapy and targeted therapy in early-stage non-small cell lung cancer," *Expert Review of Anticancer Therapy*, vol. 18, no. 1, pp. 63–70, 2018.
- [28] N. Gaj-Levra, P. Borghetti, A. Bruni et al., "Current radiotherapy techniques in NSCLC: challenges and potential solutions," *Expert Review of Anticancer Therapy*, vol. 20, no. 5, pp. 387–402, 2020.
- [29] L. Osmani, F. Askin, E. Gabrielson, and Q. K. Li, "Current WHO guidelines and the critical role of immunohistochemical markers in the subclassification of non-small cell lung carcinoma (NSCLC): moving from targeted therapy to immunotherapy," *Seminars in Cancer Biology*, vol. 52, Part 1, pp. 103–109, 2018.
- [30] M. J. Grant, R. S. Herbst, and S. B. Goldberg, "Selecting the optimal immunotherapy regimen in driver-negative metastatic NSCLC," *Nature Reviews. Clinical Oncology*, vol. 18, no. 10, pp. 625–644, 2021.
- [31] D. Satgé, "A tumor profile in primary immune deficiencies challenges the cancer immune surveillance concept," *Frontiers in Immunology*, vol. 9, p. 1149, 2018.
- [32] G. Liao, Z. Jiang, Y. Yang et al., "Combined homologous recombination repair deficiency and immune activation analysis for predicting intensified responses of anthracycline, cyclophosphamide and taxane chemotherapy in triple-negative breast cancer," *BMC Medicine*, vol. 19, no. 1, p. 190, 2021.
- [33] J. Friedrich, L. Heim, D. I. Trufa et al., "STAT1 deficiency supports PD-1/PD-L1 signaling resulting in dysfunctional TNF $\alpha$  mediated immune responses in a model of NSCLC," *Oncotarget*, vol. 9, no. 98, pp. 37157–37172, 2018.
- [34] P. A. Ott, S. Hu-Lieskovan, B. Chmielowski et al., "A phase Ib trial of personalized neoantigen therapy plus anti-PD-1 in patients with advanced melanoma, non-small cell lung cancer, or bladder cancer," *Cell*, vol. 183, no. 2, pp. 347–362.e24, 2020.
- [35] R. Li, R. Salehi-Rad, W. Crosson et al., "Inhibition of granulocytic myeloid-derived suppressor cells overcomes resistance to immune checkpoint inhibition in LKB1-deficient non-small cell lung cancer," *Cancer Research*, vol. 81, no. 12, pp. 3295–3308, 2021.
- [36] G. Liang, W. Meng, X. Huang et al., "miR-196b-5p-mediated downregulation of TSPAN12 and GATA6 promotes tumor progression in non-small cell lung cancer," *Proceedings of the National Academy of Sciences of the United States of America*, vol. 117, no. 8, pp. 4347–4357, 2020.
- [37] D.-B. Luo, H.-B. Lv, X.-H. Sun, Y. Wang, J. H. Chu, and A. L. Salai, "LncRNA TRERNA1 promotes malignant progression of NSCLC through targeting FOXL1," *European Review for Medical and Pharmacological Sciences*, vol. 24, no. 3, pp. 1233–1242, 2020.
- [38] S. Xiao-Hong, Y.-R. Zhu, Y.-J. Hou, K. Li, and N. H. Dong, "PVT1 induces NSCLC cell migration and invasion by regulating IL-6 via sponging miR-760," *Molecular and Cellular Probes*, vol. 54, article 101652, 2020.
- [39] X. Daoping Zhang and M. P. Ding, "LncRNA SNHG14 accelerates breast cancer progression through sponging miR-543 and regulating KLF7 expression," *Archives of Gynecology and Obstetrics*, vol. 305, no. 6, pp. 1507–1516, 2022.
- [40] K. Li and C. Yuan, "MicroRNA-103 modulates tumor progression by targeting KLF7 in non-small cell lung cancer," *International Journal of Molecular Medicine*, vol. 46, no. 3, pp. 1013–1028, 2020.
- [41] R. Niu, Y. Tang, Y. Xi, and D. Jiang, "High expression of Kruppel-like factor 7 indicates unfavorable clinical outcomes in patients with lung adenocarcinoma," *The Journal of Surgical Research*, vol. 250, pp. 216–223, 2020.
- [42] H. Petrek, P. Y. Ho, N. Batra et al., "Single bioengineered ncRNA molecule for dual-targeting toward the control of non-small cell lung cancer patient-derived xenograft tumor growth," *Biochemical Pharmacology*, vol. 189, article 114392, 2021.

## Research Article

# Prediction of Metabolic Characteristics of Cardiovascular and Cerebrovascular Diseases Based on Convolutional Neural Network

Zhengfei Yang<sup>1</sup>, Ping Li<sup>2</sup> and Rui Wang<sup>1</sup>

<sup>1</sup>Institute of Traditional Chinese Medicine, Ningxia Medical University, Yinchuan 750000, China

<sup>2</sup>Weifang Engineering Vocational University, Weifang, Shandong Province, 262500, China

Correspondence should be addressed to Rui Wang; [ruiwang@nxmu.edu.cn](mailto:ruiwang@nxmu.edu.cn)

Received 13 June 2022; Revised 29 June 2022; Accepted 6 July 2022; Published 27 July 2022

Academic Editor: Hangjun Che

Copyright © 2022 Zhengfei Yang et al. This is an open access article distributed under the Creative Commons Attribution License, which permits unrestricted use, distribution, and reproduction in any medium, provided the original work is properly cited.

As a typical disease, cardiovascular and cerebrovascular diseases cause great damage to the human body. In view of the problem that the existing models failed to describe and represent the characteristics of cardiovascular and cerebrovascular indicators, convolution neural network was used to analyze the metabolic factors of cardiovascular and cerebrovascular. Based on convolutional neural network theory, feature extraction was carried out on the relevant parameters of the model, and the change trend of different cardiovascular and cerebrovascular indicators was studied by model optimization, theoretical analysis, and experimental verification. Relevant studies show that the value of neurons increases slowly at first and then rapidly with the increase of bias term  $b$ . And with the increase of computing time, the corresponding nonlinear characteristics are gradually reflected; so, the influence of computing time on neuron results should be considered when selecting bias term  $b$ . The gradient changes under different functions have typical symmetry, which indicates that the effects of functions on model parameters have certain cyclic characteristics. Among them, ReLU function has the largest variation range, tanh function has a relatively small curve variation range, and sigmoid function has the smallest variation range. Five indicators are selected to describe the metabolic characteristics of the disease through characteristic analysis of cardiovascular and cerebrovascular diseases. The onset signs have the greatest impact on cardiovascular and cerebrovascular diseases, while the corresponding metabolic characteristics have the least impact on cardiovascular and cerebrovascular diseases. The study showed that the influence of different indicators on the model had typical stage characteristics, and relevant data were used to verify the accuracy of the model. Finally, the optimization model based on convolutional neural network was used to predict the metabolic characteristics of cardiovascular and cerebrovascular diseases. Relevant studies show that the optimization model can better analyze the metabolic characteristics of cardiovascular and cerebrovascular diseases. This research can provide theoretical support for the application of convolutional neural networks in other fields.

## 1. Introduction

Convolutional neural network has a wide application prospect in different fields, and its application directions mainly include video anomaly detection [1], vehicle tracking [2], photovoltaic product detection [3], lime structure calculation [4], and high-speed train [5]. In view of the low accuracy of robust time series, the optimization model under convolutional neural network was used to conduct a targeted analysis of genetic algorithm [6]. First, the characteristic parameters of the model were extracted. The corresponding

optimization parameters were obtained by parameter extraction, and then the model features in the time series parameters were further modified to obtain the optimization algorithm that can characterize the model sequence. Finally, the accuracy of the model was verified by relevant experimental data. In view of the problems existing in the original convolutional neural network model in the study of prostate cancer and other symptoms, the revised convolutional neural network model was adopted to further analyze the data of relevant symptoms [7], so as to obtain the corresponding optimization results, which can be verified by the model. In

biomedicine, based on the relevant theories of convolutional neural network, the feature insertion method was adopted to analyze the relevant features of organisms [8], and the corresponding optimization results were finally obtained. Finally, relevant data was used to prove the model.

The above studies mainly focus on the application of convolutional neural network in engineering and other aspects, but there were relatively few studies on cardiovascular and cerebrovascular diseases; so, it was necessary to carry out studies on the metabolic characteristics of cardiovascular and cerebrovascular diseases. Based on the relevant theory of convolutional neural network, this paper conducts targeted research on the related problems in cardiovascular and cerebrovascular diseases by means of feature extraction, model insertion, and experimental verification. Studies have found that different indicators can describe metabolic characteristics of cardiovascular and cerebrovascular diseases, indicating that the correlation optimization model based on convolutional neural network can carry out correlation analysis and prediction of metabolic characteristics of cardiovascular and cerebrovascular diseases, and provide support for the application of convolutional neural network in different fields.

## 2. Basic Theory of Convolutional Neural Networks

The genetic algorithm is a kind of random search algorithm, which regards a biological individual as a solution in the optimization algorithm, and the population composed of many individuals is the solution set of the algorithm [9, 10]. Then, through genetic operations such as selection crossover and mutation of the population, the poor individuals are constantly eliminated, and the individual genes with favorable mutation are passed on to the next generation through probabilistic selection, after continuous iteration and update. When the termination condition is reached, the output individual is the optimal one that survives after screening. The genetic algorithm is easy to operate and can be applied to both continuous optimization problems and discrete problems. Its multidirectional global optimization performance has a good theoretical value for solving complex optimization problems today.

*2.1. Basic Knowledge of Neural Network.* Machine learning, as one of the ways to achieve artificial intelligence, has been revived in recent years with the development of high-performance computer hardware such as image processors and mobile Internet [11, 12]. Deep learning is a kind of nonlinear neural network with multiple hidden layers. It imitates the working mechanism of human brain neurons and constantly extracts features for learning and analysis under the training of a large amount of data. It has strong generalization. It has been widely used in machine vision, natural language processing, autodriving, semantics, speech recognition, and other fields.

Traditional learning model and deep learning model have many shortcomings in theoretical practice and relevant calculation methods. Deep learning is using more data

or better algorithms to improve the results of a learning algorithm. For some applications, deep learning works better on large data sets than other machine learning methods. Moreover, deep learning is more suitable for unlabeled data; so, it is not limited to the field of natural language processing mainly based on entity recognition. In order to further illustrate the differences between the two models, we drew the model performance curves of the traditional learning model and the deep learning model based on relevant experimental data, as shown in Figure 1. It can be seen from the figure that with the continuous increase of data, the performance of corresponding curves shows different trends. From the perspective of traditional learning model, this model has typical two-stage characteristics. In the first stage, with the gradual increase of test data, the corresponding model performance values show a gradually increasing trend, but the slope of the increasing curve gradually decreases. When the corresponding data reaches 75 or so, the slope of the corresponding curve is zero. When it exceeds 75, the model performance data of the corresponding traditional learning model shows a constant change trend with the gradual increase of data, indicating that the gradual increase of data has no influence on the model performance. The curve of the deep learning model can be divided into three stages according to the different characteristics of changes. In the first stage, the curve shows a slow rise. With the gradual increase of data, the corresponding model performance parameters gradually improve, and the corresponding curve slope also shows a trend of slow decline. However, the slope of the corresponding curve is higher than that of the traditional learning model of the same period. The second stage of the curve is the stage of steady increase, in which the slope of the corresponding curve shows an approximately constant trend, indicating that the model performance of this stage gradually improves with the increase of data. When it exceeds the critical value of the second stage, the curve enters the third stage. In the third stage, the performance of the deep learning model gradually improves with the increase of experimental data, and the slope of the corresponding curve increases rapidly. This indicates that the slope of the curve shows a typical nonlinear increasing trend at this stage. Therefore, it can be seen from the above analysis that the deep learning model can describe two stages of nonlinear increase and nonlinear attenuation, while the traditional model can only describe the nonlinear attenuation stage and cannot give a good description of the nonlinear acceleration stage.

Artificial neural network (ANN) is a kind of neural network that simulates the process from activation to signal sending of brain neurons and organizes many neurons according to certain hierarchical structure to form multilayer neural network [13, 14]. At first, the neural network in biology was abstracted into a simple linear model based on threshold logic algorithm, called MP (McCulloch-Pitts) neuron model. The MP neuron model has a wide range of applications in different fields. The MP neuron model has the following capabilities: (1) Each neuron is an information processing unit with multiple inputs and single

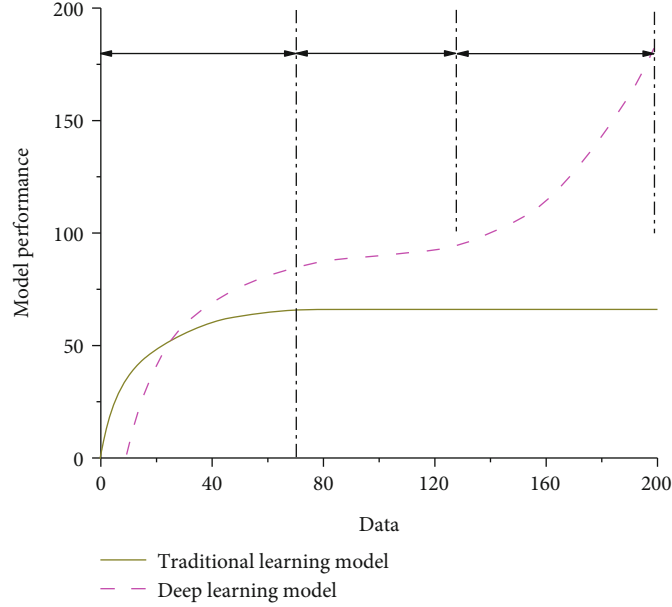


FIGURE 1: Performance comparison diagram of two models.

outputs; (2) Neuron input can be divided into excitatory input and inhibitory input. (3) Neurons have spatial integration characteristics and threshold characteristics. (4) There is a fixed time delay between the input and output of neurons, mainly due to synaptic delay.

It can be seen from the above analysis that the MP model, as one of the convolution neural network models, can calculate different types of data. In order to analyze the calculation principle of this MP model, the corresponding MP model is summarized as shown in Figure 2. It can be seen from the figure that the calculation of MP model first requires crossreplacement of different types of data corresponding to  $x$  and  $w$ , so that the corresponding data can have typical characteristics. Then, these representative parameters are imported into the corresponding  $b$  module, through which parameters are extracted, analyzed, and optimized, so that the obtained neuron data can further reflect the optimal value and corresponding parameter characteristics of the  $b$  model. Then, the obtained parameter characteristics are further calculated and output. Finally, the optimized data are further verified by the targeted model verification method, and finally, the optimized model data is output.

Corresponding neurons can be expressed as follows:

$$y_i = f \times \left( \sum_i w_i x_i + b \right), \quad (1)$$

where  $(x_1, x_2, x_3, \dots, x_n)$  and  $(y_1, y_2, y_3, \dots, y_n)$  are the input and output values of the network, respectively.  $I$  represents the input or output of the  $i$ -th neuron,  $(w_1, w_2, w_3, \dots, w_n)$  is the connection weight value of the network, and  $b$  is the bias term.

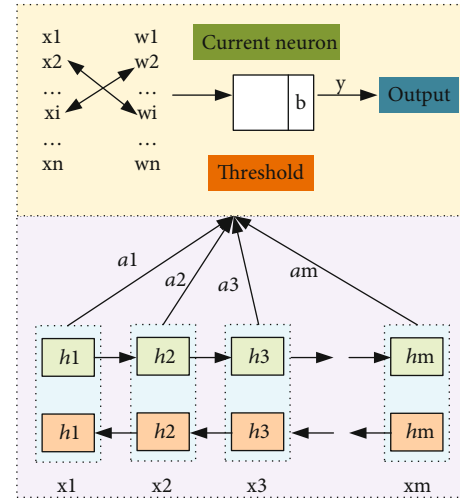


FIGURE 2: MP model.

In order to further analyze the influence of bias term  $b$  on neuron parameters, we obtained the corresponding neuron calculation data according to the calculation formula and theory of bias term  $b$  and obtained the contour diagram of neuron changes under the action of bias term  $b$ , as shown in Figure 3. It can be seen from the figure that with the increase of bias term  $b$ , the corresponding neuron value increases slowly at first, and then when the bias term  $b$  reaches about 20, the corresponding curve shows a rapid increase trend, and the corresponding slope also shows a nonlinear increase. When the bias term  $b$  exceeds about 27, the slope of the corresponding curve drops rapidly, indicating that the effect of bias term  $b$  on neuron

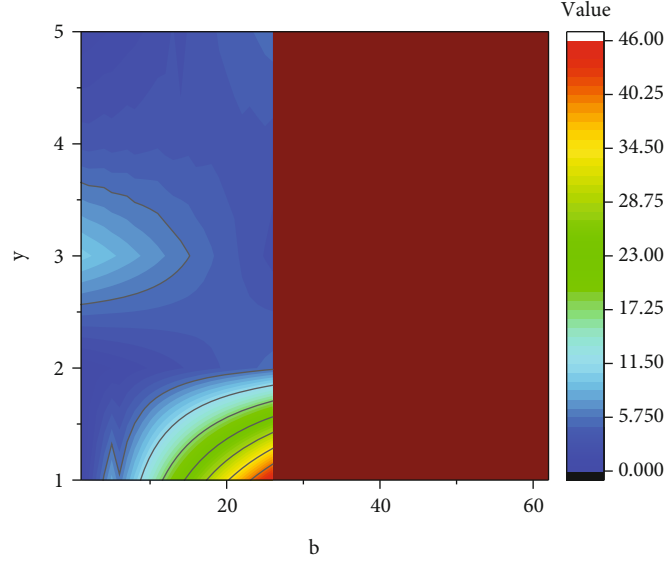


FIGURE 3: Contour variation diagram of offset term.

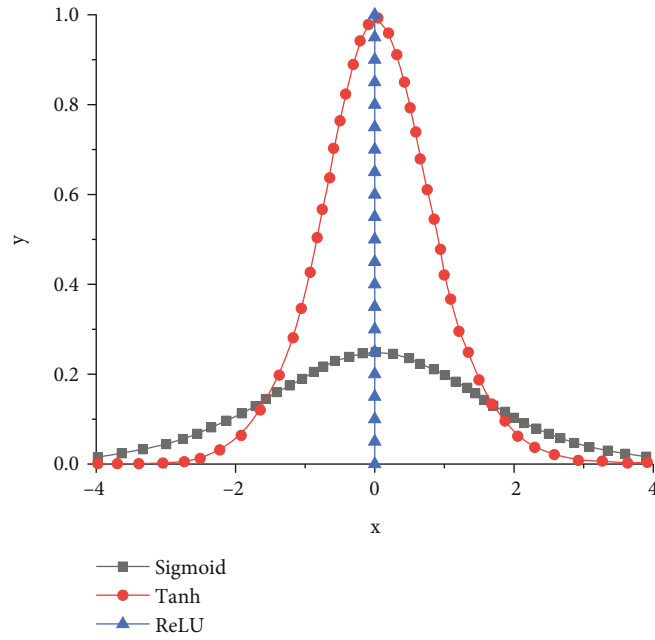


FIGURE 4: Gradient diagram of different functions.

parameters has typical nonlinear characteristics. Therefore, it is necessary to comprehensively consider the variation range of bias term  $b$  in computational neurons, so as to obtain accurate computational parameters of neurons.

Activation function is an indispensable nonlinear mapping function in convolutional neural network. The use of activation function in neural network is equivalent to introducing nonlinear factors into neurons, so that they have nonlinear fitting ability and can be applied to various non-

linear models and increase the richness of neural network expression ability.

The sigmoid logic function is the earliest and most commonly used activation function. The corresponding function expression is as follows:

$$\text{sigmoid}(x) = \frac{1}{1 + e^{-x}}. \quad (2)$$



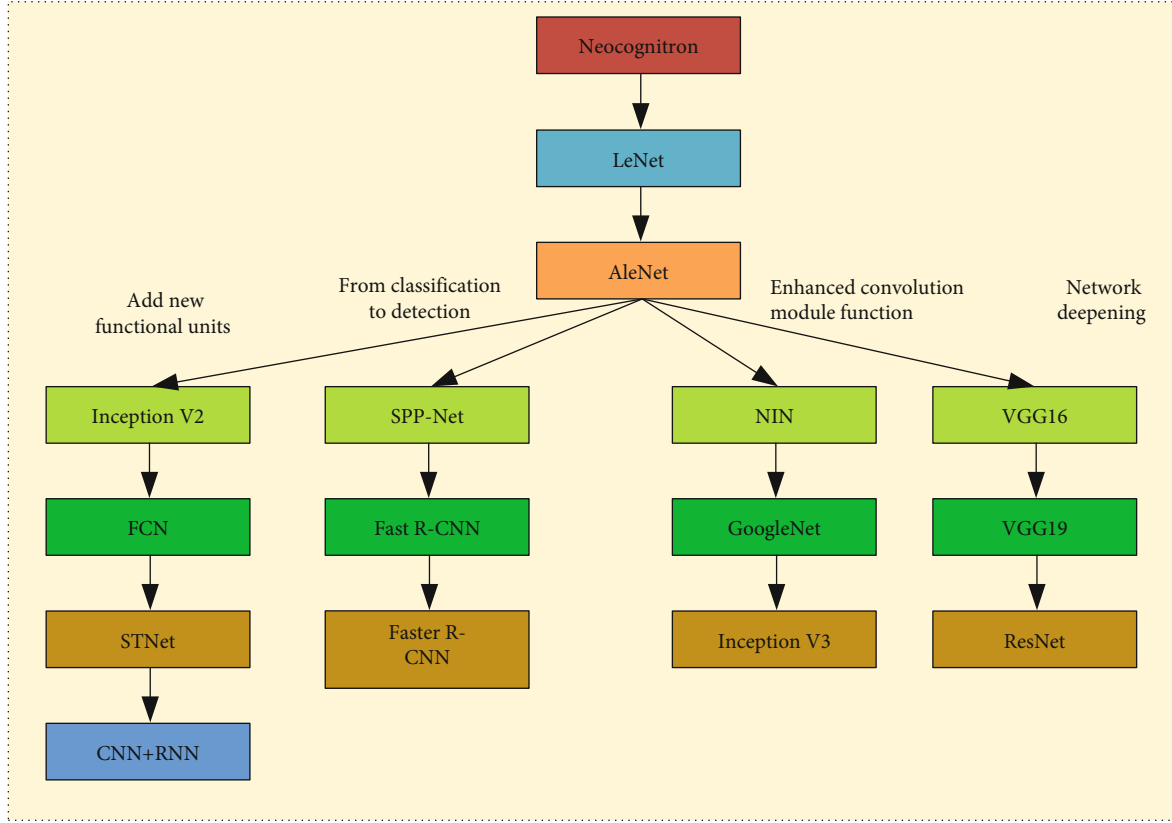


FIGURE 5: Development history of convolutional neural network.

Tanh function is the deformation of the above functions, and the mathematical expression is as follows:

$$\tanh(x) = \frac{e^x - e^{-x}}{e^x + e^{-x}}. \quad (3)$$

The curves of tanh function and sigmoid function are very similar. The difference is that the output interval expands from (0, 1) to (-1, 1), and zero is taken as the output center.

ReLU activation function is also called modified linear unit, and the formula is as follows:

$$f(x) = \begin{cases} x, & x \geq 0, \\ 0, & x < 0. \end{cases} \quad (4)$$

ReLU is a piecewise linear function that can prevent some neurons from being activated, thus enhancing the sparsity and learning accuracy of the network and avoiding the overfitting phenomenon. When the input value is positive, only linear operation is needed, the calculation speed and convergence speed are much faster than the above two functions, and the problem of gradient disappearance is solved.

Through the above formula and theoretical analysis, it can be seen that different functions have different trends of

change. In order to qualitatively analyze this change trend, we use gradient graph to analyze three different functions and draw corresponding gradient graph under different functions. The specific change curve is shown in Figure 4. It can be seen from the figure that three different functions have three different changing trends. However, it can be seen from the figure that the three different functions have typical symmetric characteristics, and the axis of symmetry is  $x = 0$ . It can be seen from the sigmoid function that, with the gradual increase of parameter  $x$ , the corresponding  $y$  value first presents a slow increase trend, and the corresponding slope also presents a gradual increase change. When it reaches the highest point, the corresponding  $y$  value is only 0.24. When it exceeds the maximum value, the corresponding curve declines gradually, and the slope also shows a trend of gradually approaching zero. It can be seen from the curve of tanh function that in the first stage, the curve shows a slow and approximately constant change, while when  $x$  is -2, the corresponding curve increases rapidly. The slope of the corresponding curve also shows a nonlinear increasing trend. When it reaches the maximum value of 0.95, the corresponding  $x$  is also 0. When the curve exceeds the highest point, the corresponding curve shows a rapid decline. From the change curve of ReLU function, we can see that the corresponding curve shows a change trend parallel to the  $y$ -axis. Through the above analysis, we can see that the curves corresponding to three different functions have different characteristics of change; so, we need to analyze the specific

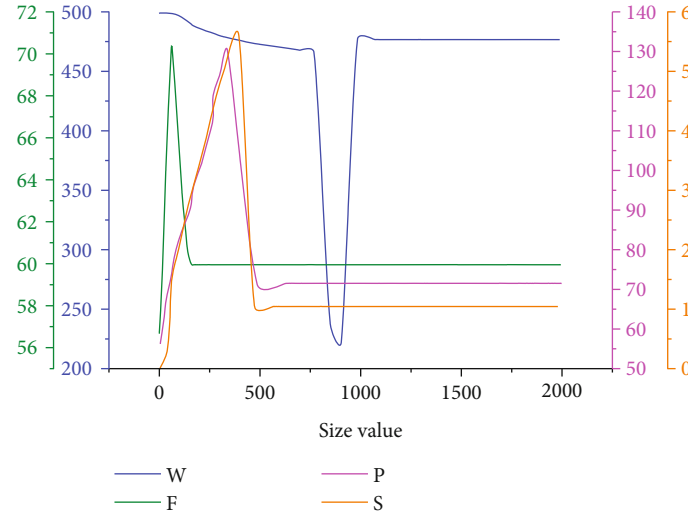


FIGURE 6: Influence curve of different coefficients on convolution layer.

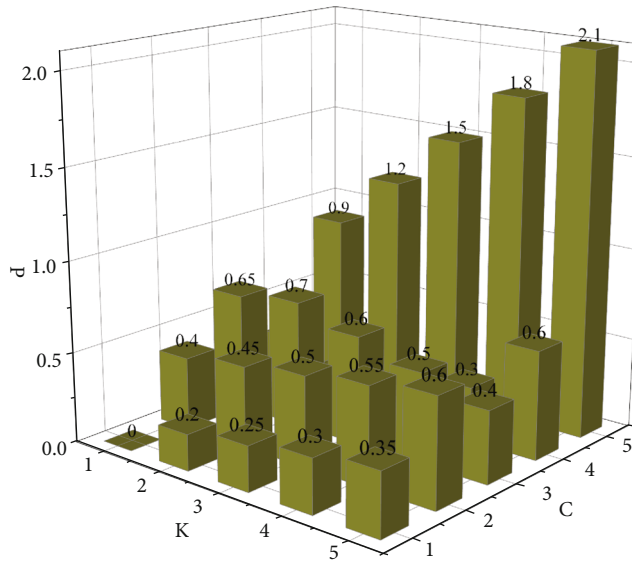


FIGURE 7: Influence of size and channel on the number of parameters.

situation qualitatively and then select different functions to solve and verify the parameters.

**2.2. Convolutional Neural Network.** Convolutional neural network is a kind of multilayer feedforward neural network, which is also one of the important forms of deep neural network [15, 16]. It is specially used to process data with network topology.

Convolutional neural network models have different changing characteristics in the process of calculation and development. In order to further analyze convolutional neural network models, the corresponding development flow chart is obtained by summarizing the development history of some models, as shown in Figure 5. It can be seen

from the figure that the convolutional neural network model can be divided into four different types of variable modules: first, new functional unit modules are added, which can further improve the calculation accuracy and operation range of the model. The second is to make a breakthrough from two aspects of detection and classification. The third is to enhance the relevant functions of the convolution module and improve the operation effect of the corresponding model. Fourth, network deepening is carried out for the model.

The convolution layer of the convolutional neural network is composed of one or more convolution kernels and feature graphs [17, 18]. The size of the convolution kernel is usually odd, and the features of the feature graph of the

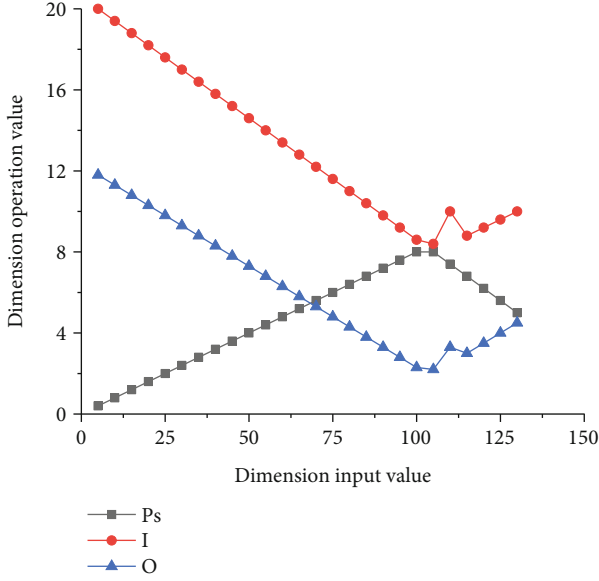


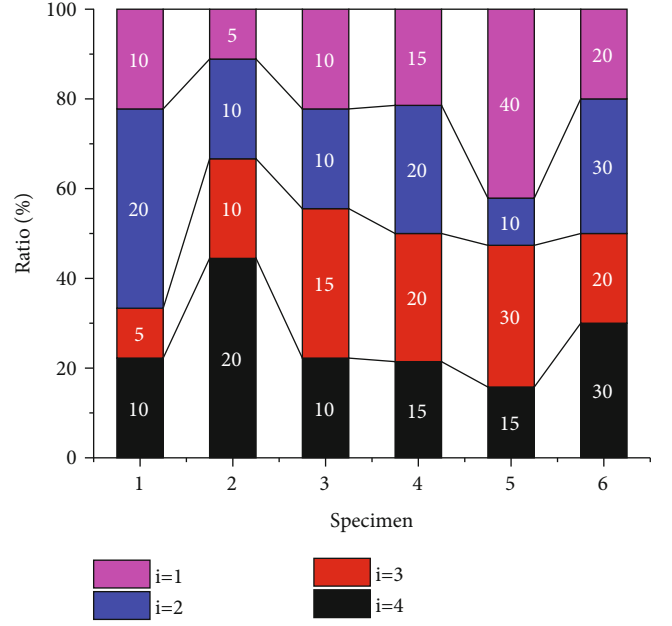
FIGURE 8: Image size output value after pooling.

upper layer are extracted through the convolution operation of the convolution kernel to output the feature graph of the next layer. The specific calculation formula is as follows:

$$N = \frac{W-F+2P}{S} + 1, \quad (5)$$

where  $N$  is the size of the output image,  $W$  is the size of the input image,  $F$  is the size of the convolution kernel,  $P$  is the filling number of the image edge, and  $S$  is the sliding step. The influence of sliding steps  $S$  on the convolution kernel in the convolutional neural network is mainly reflected in the following aspects: The larger the moving step  $S$  of the sliding window is, the smaller the size of the output feature graph is, and the fewer image features it carries.

Through the above analysis, it can be seen that the convolution layer is composed of parameters of different types and characteristics, among which the most influential ones are input image size  $W$ , convolution size  $F$ , image filling edge  $P$ , and step size  $S$ . In order to further analyze the specific rules of the size of the output image, the change curves of the size of the convolution running image under different parameters are drawn, as shown in Figure 6. It can be seen from the figure that with the gradual increase of the size value, the corresponding curve has typical nonlinearity and diversity. As can be seen from the change process of parameter  $W$ , with the gradual increase of graph size value, the corresponding curve first presents a slow increase trend. Then, when the size value is 825, the corresponding curve drops rapidly to the lowest value. When the curve reaches the lowest point, the curve rises rapidly with an approximate constant slope, and then the corresponding curve shows a gentle change when it immediately reaches the local maximum value. It can be seen from the change curve of parameter  $F$  that with the gradual increase of size value, the corresponding curve increases rapidly, and the slope also

FIGURE 9: Proportion of predicted value of parameter  $i$  to different samples.

reaches the maximum value and then gradually decreases. When it reaches the lowest value, the curve gradually tends to be gentle with the increase of the size, which indicates that the influence of parameter  $F$  on the size of the graph only remains at a relatively low value. It can be seen from the curve change of parameter  $P$  that with the gradual increase of the size value, the corresponding curve increases rapidly first, but the slope of the curve is lower than that of the corresponding parameter  $F$ . When it reaches the maximum value, the curve also shows a downward trend, but the corresponding downward value is also less than the parameter  $F$  and then tends to gentle. It can be seen from the curve corresponding to  $S$  value that the overall trend of the curve of this parameter is basically the same as that of the curve of parameter  $P$ , except that the specific value is slightly different. Therefore, it can be seen that the curves of parameters  $F$ ,  $P$ , and  $S$  have obvious variation characteristics: In other words, the corresponding influence is more obvious in the small size, and with the gradual increase of size, the corresponding calculation value of size output is more constant. Therefore, through comprehensive consideration, we can see that the corresponding output image size  $W$  has the greatest influence on the convolution layer.

The corresponding operation formula of the convolution layer of the convolutional neural network is shown as follows:

$$f[x, y] * g[x, y] = \sum_{n_1=-a}^a \sum_{n_2=-a}^a f[n_1, n_2] \times g[x-n_1, y-n_2], \quad (6)$$

where  $f[n_1, n_2]$  is the input image,  $g[n_1, n_2]$  is the convolution kernel, and  $n_1$  and  $n_2$  represent pixel points.  $P$  is the number of parameters of the convolution layer.

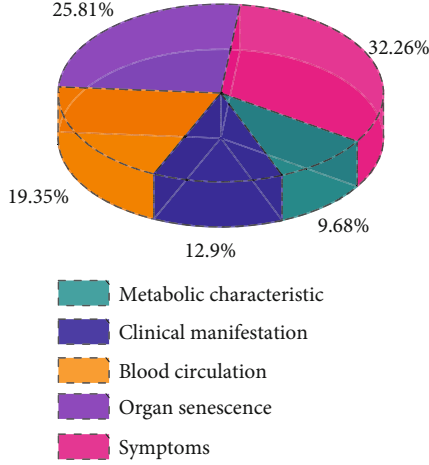


FIGURE 10: Distribution diagram of different characteristic indexes.

Parameter  $P$  is obtained by multiplying the dimensions of the convolution kernel  $K_w$  and  $K_h$ , the number of input channels  $C_1$ , and the number of input channels  $C_2$ , and the corresponding formula is expressed as

$$P = K_w \times K_h \times C_1 \times C_2. \quad (7)$$

In order to further analyze the influence of size and channel on parameter quantity, the quantitative change diagram of parameter quality under two different parameters was drawn, as shown in Figure 7. It can be seen from the figure that with the increase of parameter  $K$ , the corresponding curve histogram shows a trend of gradual increase. Especially when parameter  $C$  is constant at the maximum value, the value of the corresponding parameter  $K$  increases the most. When the parameter  $K$  is constant, the curve corresponding to parameter  $C$  shows an obvious fluctuation trend. This indicates that the influence of parameter  $K$  on the number of parameters is more obvious, while the influence of parameter  $C$  on the number of parameters is more volatile. Therefore, it is necessary to comprehensively consider the proportion of parameter  $K$  and parameter  $C$  in the specific operation process, so as to obtain the accurate number of parameters. The size of convolution check is mainly represented by parameter  $K$ , while the corresponding channel is mainly described by the number of input channels  $C$ . The research methods and contents of the two different parameters are different, resulting in different influences on the convolution parameter  $P$ .

**2.3. Parameter Optimization of Convolutional Neural Network.** Currently, the main pooling operations are maximum pooling, average pooling, and random pooling [19, 20]. Maximum pooling compares the values of pixels in each region and selects the maximum value within the pixel region as the output of this pixel region. Average pooling takes the average of pixels in each region as the output of the pixel region. Random pooling randomly selects pixels in the region according to their probability as the output of the pixel region, which improves the generalization ability.

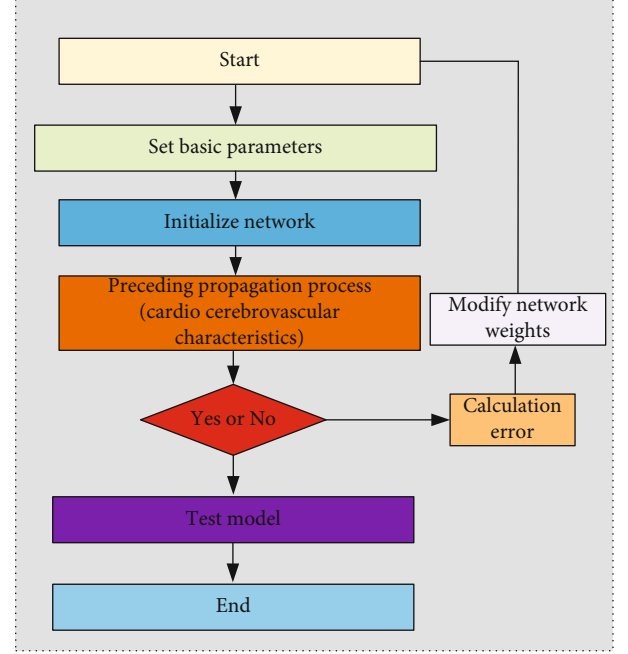


FIGURE 11: Cardio-cerebrovascular metabolic flow chart based on convolutional neural network.

After the pooling operation, the output image size calculation formula is as follows:

$$O = \frac{I - P_s}{S} + 1, \quad (8)$$

where  $O$  is the size of the pooled output image,  $I$  is the size of the input image,  $P_s$  is the size of the pooled layer, and  $S$  is the moving step. For maximum pooling, the default step is  $S = 2$ .

In order to further analyze the specific influencing factors of the size of the pooled output image, we drew the output curves of the pooled size image under several different influencing factors, as shown in Figure 8. It can be seen from the curve that the effects of different parameters on the pooling of convolutional neural networks have different performance characteristics. The curve as a whole can be divided into two phases. In the first stage, with the gradual increase of  $P_s$  and size output and input values, the corresponding curve shows an approximately constant linear change, while the corresponding parameter  $I$  shows a linear decline in the first stage, and the slope of the corresponding curve is higher than that of  $P_s$ . This indicates that in the first stage, the influence of parameter  $P_s$  on the output value  $O$  is higher than that of parameter  $I$ . And the corresponding curve of the output image size after pooling also shows a trend of gradual decline. In the second stage, as the corresponding parameter  $P_s$  increases with the input value, the corresponding size output value shows a trend of gradual decline, while the corresponding parameter  $I$  curve shows a trend of fluctuation

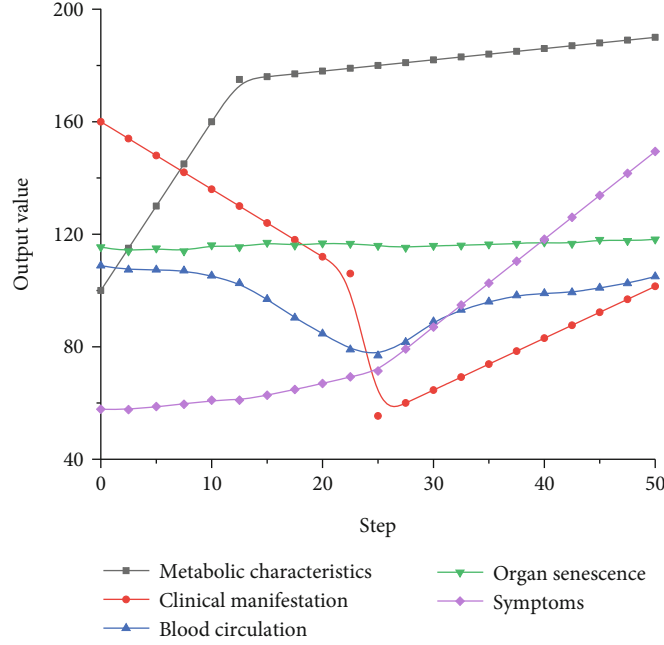


FIGURE 12: Summary diagram of metabolic characteristics of cardiovascular and cerebrovascular diseases based on convolutional neural network.

first and then gradually rising. Finally, the data of parameter  $O$  shows a trend of gradual increase with the increase of the input value.

The full connection layer usually appears at the end of the convolutional neural network. Since the fully connected layer can only accept 2D matrix, it is necessary to convert the 3D feature tensor of the image extracted by the previous convolution layer into a long vector. Then, the full connection layer performs classification or regression tasks. For the output of the  $i$ -th neuron of layer  $L$ , the calculation formula of the full connection layer is as follows:

$$x_i^l = f \left( \sum_{j=1}^n x_j^{l-1} w_{ij}^{l-1} + b_i^{l-1} \right), \quad (9)$$

where  $x_j^{l-1}$  is the output value of the  $j$ -th neuron in layer  $l-1$ ,  $w_{ij}^{l-1}$  is the connection weight between the  $j$ -th neuron in layer  $l-1$  and the  $i$ -th neuron in layer  $l$ ,  $n$  is the number of neurons in layer  $l-1$ , and  $b_i^{l-1}$  is the corresponding bias quantity of the  $i$ -th neuron in layer  $l$ .

The sigmoid, also known as the squeeze function, is a very common dichotomy method that squeezes input values that fluctuate over a wide range into an output interval of (0, 1). The advantages of this function are as follows: (1) the function curve is smooth, and (2) the function is continuous everywhere and easy to differentiate. Disadvantages of sigmoid function are as follows: (1) easy to saturate and (2) large amount of calculation, both forward and back propagation involves division and power operation, which increases

the training time. The mathematical expression of softmax function is as follows:

$$\text{softmax}(z_i) = \delta(z_i) = \frac{\exp(z_i)}{\sum_{j=1}^m \exp(z_j)}, \quad (10)$$

$$\text{loss} = y \log_2 \hat{y}, \quad (11)$$

where  $i$  is the node,  $j$  is the category index,  $m$  is the number of output nodes, and  $\hat{y}$  is the output predictive value of the neural network for cardio-cerebrovascular. The change of the result of category index  $j$  will have a great influence on softmax function, and the range of category index  $j$  is (1,  $m$ ). The sum of all output values of the softmax function is as follows:

$$\sum_{i=0}^j \delta(z_i) = 1. \quad (12)$$

The change of parameter  $i$  will lead to the change of model prediction parameters. In order to further analyze the influence rule of parameter  $i$  on sample prediction value, the model prediction proportion curves under different parameters are drawn, as shown in Figure 9. As can be seen from the figure, as the number of samples increases gradually, the proportion of the predicted value corresponding to parameter  $i = 1$  shows a fluctuating trend of increasing first, then stabilizing and finally increasing again, indicating that parameter  $i = 1$  has a great influence on the parameter. The reason is that parameter  $i$  further affects the proportion of the model by changing the specific value and calculation



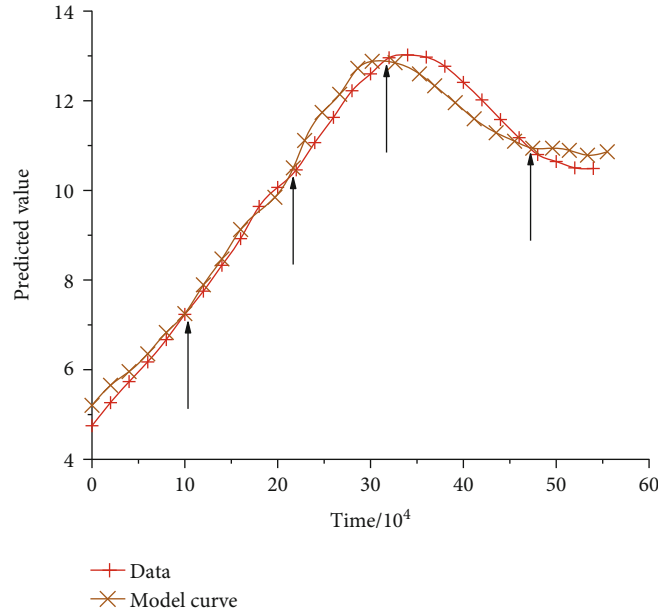


FIGURE 13: Model prediction diagram.

method of the output function. When parameter  $i = 2$ , the proportion of the corresponding model shows a trend of gradual increase. When the parameter is increased to 3, the proportion curve of the corresponding model shows a relatively stable trend as the number of samples increases. This indicates that parameter  $i = 3$  has a limited influence on the model. Finally, when parameter  $i = 4$ , the volatility of corresponding model parameters is more obvious than that when parameter  $i = 1$ . Based on the above analysis, we can see that parameter  $i$  has different influences on parameters of different samples, and the specific value and basis of parameter sample number should be considered comprehensively in sample analysis. Thus, a clear calculation process and accurate calculation results are obtained.

### 3. Application and Prediction of Convolutional Neural Networks in Cardiovascular and Cerebrovascular Diseases

**3.1. Main Features of Metabolism of Cardiovascular and Cerebrovascular Diseases.** As a relatively common disease, cardiovascular and cerebrovascular diseases do great harm to the human body. In order to further quantitatively analyze the changing rules and characteristics of cardiovascular and cerebrovascular diseases in the metabolic process, five different characteristic parameters are selected to describe the cardiovascular and cerebrovascular diseases. The five characteristic parameters were metabolic characteristics, clinical manifestations, blood circulation, organ senescence, and symptom of disease. As an indirect manifestation of cardiovascular and cerebrovascular diseases, metabolic characteristics can reflect the related characteristics of cardiovascular and cerebrovascular diseases. Therefore, metabolic characteristics of patients need to be analyzed in

daily life, so as to obtain more accurate results. As the direct manifestation of cardiovascular and cerebrovascular diseases, clinical manifestations can improve the precise treatment for patients with cardiovascular and cerebrovascular diseases and provide a strong guarantee for the rehabilitation of cardiovascular and cerebrovascular diseases. Blood circulation is a very complex index, which can not only reflect the related content of cardiovascular and cerebrovascular but also judge the physical health of patients through relevant tests. Organ aging is a complication of cardiovascular and cerebrovascular diseases. We can further improve the precision of relevant treatment schemes for cardiovascular and cerebrovascular diseases by delaying organ aging. As an important indicator of cardiovascular and cerebrovascular diseases, symptoms can provide strong guarantee and support for clinical treatment and rehabilitation. Through the statistics and analysis of a large number of clinical data, the characteristic indexes of the influence of different characteristic parameters on cardiovascular and cerebrovascular diseases were obtained, as shown in Figure 10. According to the proportion in the figure, it can be seen that metabolic characteristics have the least influence on cardiovascular and cerebrovascular diseases, only 9.68%. Clinical manifestations accounted for about 13%. The proportion of blood circulation is about 20%. Organ senescence accounted for 25.8%. The proportion of symptoms was the highest, about 32.3%.

**3.2. Application of Convolutional Neural Network in Metabolic Features of Cardiovascular and Cerebrovascular Diseases.** Through the above analysis and research, we can see that convolutional neural network has good application in different fields [21, 22]. In view of the problems related to metabolic characteristics in cardiovascular and cerebrovascular diseases, in order to better analyze the influence of

the characteristics of cardiovascular and cerebrovascular diseases on the disease, relevant theories of convolutional neural network are introduced to build the corresponding optimization model. Furthermore, the optimized convolutional neural network model was used to further analyze the metabolic characteristics of cardiovascular and cerebrovascular diseases and to make targeted prediction of cardiovascular and cerebrovascular diseases.

In order to further apply convolutional neural network to metabolic analysis of cardiovascular and cerebrovascular diseases, a calculation method of cardiovascular and cerebrovascular diseases based on convolutional neural network was obtained through model optimization and theoretical analysis. In order to further explain this calculation process accurately, a characteristic flow chart of cardio-cerebrovascular metabolism based on convolutional neural network was drawn, as shown in Figure 11. It can be seen from the figure that the basic parameters of cardiovascular and cerebrovascular diseases need to be set first, and then the metabolic characteristics of cardiovascular and cerebrovascular diseases are analyzed by using the initialization grid in the convolutional neural network and then imported into the pretransmission process. In this way, the related cardiovascular and cerebrovascular characteristic parameters are further elaborated and extracted, and then the calculation process is discriminated by the judgment equation. If it does not meet the relevant requirements, the error calculation and network weight modification shall be carried out, and the obtained results shall be further iterated. Finally, the optimized results shall be imported into the test model for further analysis, and finally, the optimized characteristics of cardiovascular and cerebrovascular diseases shall be derived.

The above methods can be used to further analyze the metabolic characteristics of cardiovascular and cerebrovascular diseases, so as to obtain the corresponding metabolic results and index curves, as shown in Figure 12. From the curve changes in the figure, we can see that metabolic indicators at different steps have different output results, which indicates that the selection of different indicators has a wide range of descriptions, which can be used to describe different aspects of cardiovascular and cerebrovascular diseases. As the number of iterations increases, the metabolic characteristics of cardiovascular and cerebrovascular diseases first show a trend of rapid increase, and the constant slope of the corresponding curve indicates that the change conforms to the change of linear characteristics. However, with the further increase of iteration steps, the corresponding index output value shows a slow increase trend. And the slope is going to be lower than the first step. It can be seen from the clinical performance indicators that the curve has obvious fluctuation characteristics, which firstly drops rapidly to the lowest point, and then shows a slow increase trend with the increase of the number of iterations, indicating that the clinical performance can well describe the linear changes of cardiovascular and cerebrovascular output values at different stages. Blood circulation has a typical symmetry, indicating that its description of cardiovascular and cerebrovascular can have obvious regularity. The blood circulation curve showed a slow decline at first and then a rapid decline

to the lowest point, followed by a significant improvement with the increase of iteration steps. The characteristic indexes of organ senescence of cardiovascular and cerebrovascular diseases have a relatively constant change trend under different steps; that is, organ senescence does not change with the change of iterative steps, which is an inherent attribute of cardiovascular and cerebrovascular diseases. The curve of the corresponding symptom increases slowly at first, and with the increase of iteration number, the curve has a significant increase range, indicating that the curve corresponding to the symptom has a significant change to the higher iteration number. The reason for the changes in metabolic indicators of cardiovascular and cerebrovascular diseases is that metabolic characteristic parameters are calculated by different change functions. The obtained results are imported into the convolutional neural network for optimization of corresponding parameters, so that the obtained results have different change characteristics, which can describe different types of cardiovascular and cerebrovascular diseases.

#### 4. Discussion

The above analysis carried out targeted analysis on the metabolic characteristics of cardiovascular and cerebrovascular diseases under different indicators, indicating that the metabolic characteristics of cardiovascular and cerebrovascular diseases based on convolutional neural network can well describe the specific conditions of patients with cardiovascular and cerebrovascular diseases. In order to further analyze and predict the changing trend of cardiovascular and cerebrovascular diseases and provide better medical services for patients, convolutional neural network was adopted to analyze the relevant data and indicators of cardiovascular and cerebrovascular diseases, so as to obtain the model prediction curves of cardiovascular and cerebrovascular diseases at different times, as shown in Figure 13. Through the specific changes of the test curve and model curve, it can be seen that the cardio-cerebrovascular indicators based on convolutional neural network can well reflect the real cardio-cerebrovascular data, and there are overlapping indicators in different time periods. This also shows the accuracy of model index selection from another aspect. And it can be seen from the prediction that cardiovascular and cerebrovascular diseases show an obvious trend of improvement with the increase of time. However, when it reaches a certain time, the curve shows a slow decline, which indicates that cardiovascular and cerebrovascular diseases have different characteristics of change at different times. We need to take different measures according to the actual situation to carry out targeted evaluation and evaluation of cardiovascular and cerebrovascular diseases. The selection of the corresponding parameters of cardiovascular and cerebrovascular diseases is uncertain, and the corresponding parameters will show a complex change process with the difference of time and samples, which will lead to the deviation between the calculated results and the actual results.

## 5. Conclusion

- (1) The traditional learning model is a typical two-stage change feature, which can describe the attenuation and stability stages of characteristic parameters. However, it cannot describe the nonlinear increase stage because it does not consider the factor of nonlinear increase. However, due to the introduction of nonlinear factors, the deep learning model can not only represent the attenuation and constant stage of feature parameters but also reflect the nonlinear increase stage of feature parameters
- (2) The change curve of input image size  $W$  has obvious fluctuation characteristic, while the curve corresponding to convolution size  $F$ , image filling edge  $P$ , and step size  $S$  is basically the same. It shows that these three parameters have basically the same influence on the graph output, and the graph size  $W$  has the largest influence. Therefore, we need to consider the influence of various factors comprehensively when selecting different parameters
- (3) The output image size after pooling can be divided into two different change stages according to different influencing factors. Relevant studies show that parameter  $I$  has a positive influence on the output size, while parameter  $P_s$  has a negative influence on the output value  $O$

## Data Availability

The experimental data used to support the findings of this study are available from the corresponding author upon request.

## Conflicts of Interest

The authors declared that they have no conflicts of interest regarding this work.

## Acknowledgments

This work was sponsored in part by the Ningxia Natural Science Foundation (2022AAC03145) and Ningxia Key Research and Development Program (Special Talent Introduction) (2021BEB04037).




## References

- [1] P. Reinartz, "Multiple pedestrians and vehicles tracking in aerial imagery using a convolutional neural network," *Remote Sensing*, vol. 13, no. 5, pp. 720–742, 2021.
- [2] N. V. Sridharan and V. Sugumaran, "Convolutional neural network based automatic detection of visible faults in a photovoltaic module," *Energy Sources Part A Recovery Utilization and Environmental Effects*, vol. 10, no. 2, pp. 1–16, 2021.
- [3] J. Wang, R. Wang, M. Yang, and D. Xu, "Understanding zinc-doped hydroxyapatite structures using first-principles calculations and convolutional neural network algorithm," *Journal of Materials Chemistry B*, vol. 10, no. 8, pp. 1281–1290, 2022.
- [4] F. M. Philip, V. Jayakrishnan, and F. Ajesh, "Corrigendum to: video anomaly detection using the optimization-enabled deep convolutional neural network," *The Computer Journal*, vol. 18, no. 5, pp. 57–69, 2021.
- [5] Z. Wang, J. Peng, and W. Song, "A convolutional neural network-based classification and decision-making model for visible defect identification of high-speed train images," *Journal of Sensors*, vol. 12, no. 53, pp. 1–17, 2021.
- [6] J. Wu, Y. Ji, and S. Li, "Genetic-algorithm-based convolutional neural network for robust time series classification with unreliable data," *Sensors and Materials*, vol. 33, no. 4, pp. 1149–1157, 2021.
- [7] B. Yang and Z. Xiao, "A multi-channel and multi-spatial attention convolutional neural network for prostate cancer ISUP grading," *Applied Sciences*, vol. 11, no. 10, pp. 4321–4330, 2021.
- [8] T. Zhu, Y. Qin, Y. Xiang, B. Hu, Q. Chen, and W. Peng, "Distantly supervised biomedical relation extraction using piecewise attentive convolutional neural network and reinforcement learning," *Journal of the American Medical Informatics Association*, vol. 28, no. 12, pp. 2571–2581, 2021.
- [9] B. Feizizadeh, M. K. Garajeh, T. Lakes, and T. Blaschke, "A deep learning convolutional neural network algorithm for detecting saline flow sources and mapping the environmental impacts of the Urmia Lake drought in Iran," *Catena*, vol. 207, no. 10, article 105585, 2021.
- [10] Y. Kimura, N. Kadoya, Y. Oku, T. Kajikawa, S. Tomori, and K. Jingu, "Error detection model developed using a multi-task convolutional neural network in patient-specific quality assurance for volumetric-modulated arc therapy," *Medical Physics*, vol. 48, no. 9, pp. 4769–4783, 2021.
- [11] G. Li, J. Wu, and C. Deng, "Convolutional neural network-based Bayesian Gaussian mixture for intelligent fault diagnosis of rotating machinery," *IEEE Transactions on Instrumentation and Measurement*, vol. 62, no. 9, pp. 1–15, 2021.
- [12] T. Li, Y. Xu, and J. Luo, "A method of amino acid terahertz spectrum recognition based on the convolutional neural network and bidirectional gated recurrent network model," *Scientific Programming*, vol. 10, no. 5, pp. 752–764, 2021.
- [13] X. Li, J. Xia, and L. Cao, "Driver fatigue detection based on convolutional neural network and face alignment for edge computing device," *Proceedings of the Institution of Mechanical Engineers, Part D: Journal of Automobile Engineering*, vol. 235, no. 10, pp. 2699–2711, 2021.
- [14] Y. Liu, S. Zhou, W. Han et al., "Detection of adulteration in infant formula based on ensemble convolutional neural network and near-infrared spectroscopy," *Food*, vol. 10, no. 4, p. 785, 2021.
- [15] M. Sad, L. Xavier, and F. Giudice, "Breast cancer detection in digital mammography with convolutional neural network: retrospective study in Belgium," *International Journal of Computer Assisted Radiology and Surgery*, vol. 76, no. 12, pp. 15236–15248, 2021.
- [16] Y. M. Chen, Y. J. Chen, Y. K. Tsai, W. H. Ho, and J. T. Tsai, "Classification of human electrocardiograms by multi-layer convolutional neural network and hyperparameter optimization," *Journal of Intelligent and Fuzzy Systems*, vol. 40, no. 4, pp. 7883–7891, 2021.
- [17] M. Cullell-Dalmau, S. Noé, and M. Otero-Vias, "Convolutional neural network for skin lesion classification: understanding the fundamentals through hands-on learning," *Frontiers in Medicine*, vol. 8, no. 10, pp. 6443–6467, 2021.

- [18] P. Deepan and L. R. Sudha, “Comparative analysis of scene classification methods for remotely sensed images using various convolutional neural network,” *EAI Endorsed Transactions on Cognitive Communications*, vol. 20, no. 16, pp. 168–194, 2021.
- [19] J. Zhang, X. Guo, B. Wang, and W. Cui, “Automatic detection of invasive ductal carcinoma based on the fusion of multi-scale residual convolutional neural network and SVM,” *IEEE Access*, vol. 9, no. 6, pp. 40308–40317, 2021.
- [20] N. Brili, M. Ficko, and S. Klannik, “Automatic identification of tool wear based on thermography and a convolutional neural network during the turning process,” *Sensors*, vol. 21, no. 5, pp. 1917–1926, 2021.
- [21] Y. Zhou, H. Chen, Y. Li, S. Wang, L. Cheng, and J. Li, “3D multi-view tumor detection in automated whole breast ultrasound using deep convolutional neural network,” *Expert Systems with Applications*, vol. 168, no. 12, article 114410, 2021.
- [22] Y. Ding, Z. Ma, S. Wen et al., “AP-CNN: weakly supervised attention pyramid convolutional neural network for fine-grained visual classification,” *IEEE Transactions on Image Processing*, vol. 30, no. 99, pp. 2826–2836, 2021.

## Research Article

# Study on the Mechanism of Action of Different Acupuncture Regimens on Premature Ovarian Failure Model Rats

Yonghao Yuan,<sup>1</sup> Qingchang Xia,<sup>1</sup> Wenzhe Cui,<sup>1</sup> Wen Cao,<sup>1</sup> Ziyang Zhou ,<sup>1</sup> Jian Peng,<sup>2</sup> Hailiang Huang ,<sup>1</sup> Zhifei Song,<sup>3</sup> Shuying Xie,<sup>3</sup> Runjie Geng,<sup>2</sup> Ran Li,<sup>1</sup> Xiaohua Yu,<sup>1</sup> and Jing Zhang <sup>1</sup>

<sup>1</sup>School of Acupuncture and Tuina, Shandong University of Traditional Chinese Medicine, Jinan, Shandong 250355, China

<sup>2</sup>School of Traditional Chinese Medicine, Shandong University of Traditional Chinese Medicine, Jinan, Shandong 250355, China

<sup>3</sup>School of Pharmacy, Shandong University of Traditional Chinese Medicine, Jinan, Shandong 250355, China

Correspondence should be addressed to Jing Zhang; 202111114611001@zcmu.edu.cn

Received 10 June 2022; Accepted 15 July 2022; Published 25 July 2022

Academic Editor: Hangjun Che

Copyright © 2022 Yonghao Yuan et al. This is an open access article distributed under the Creative Commons Attribution License, which permits unrestricted use, distribution, and reproduction in any medium, provided the original work is properly cited.

**Objective.** To study the mechanism of acupuncture on premature ovarian failure (POF) through the apoptosis pathway mediated by Bcl-2/Bax. **Methods.** POF rats were successfully obtained by cyclophosphamide. They were divided into five groups. After that, acupuncture was performed. The blank group and model group were not treated. The routine acupuncture group was acupuncture at Guanyuan, Sanyinjiao, Zhongji, and Guilai four points. The Neck-seven-acupuncture group was selected from Fengchi, Fengfu, Tianzhu, and Wangu four acupoints; the three-viscera simultaneous treatment group selected Guanyuan, Shenshu, Sanyinjiao, Taichong, and Baihui five points; and the data mining group selected Guanyuan and Sanyinjiao two points for 14 days of treatment. During the treatment, some rats were shed one after another due to the side effects of bone marrow suppression caused by mold-making. After treatment, serum estradiol (E2), follicle forming hormone (FSH), and luteinizing hormone (LH) were detected by radioimmunoassay, Bcl-2 and Bax proteins were analyzed by Western blot method, and Bcl-2 and Bax RNA were analyzed by PCR method. **Results.** Bcl-2 increased and Bax decreased in rats with premature ovarian failure treated with acupuncture. It shows that acupuncture can affect the secretion of ovarian-related hormones and the expression of apoptosis-related proteins, which is more significant in the conventional acupuncture point group. **Conclusion.** Acupuncture can inhibit the apoptosis of granulosa cells in ovarian tissue of rats with premature ovarian failure and improve ovarian function. The mechanism of its effect is to promote Bcl-2 gene expression and protein synthesis and inhibit Bax gene expression and protein synthesis. The conventional treatment group works best. This provides an experimental basis for the clinical use of acupuncture to intervene in the treatment of premature ovarian failure.

## 1. Introduction

Premature ovarian failure (POF) is a general term for a series of symptoms such as amenorrhea before the age of 40 in modern medicine [1]. In ancient China, there was no name of “premature ovarian failure.” According to its performance, it can be classified into categories such as “amenorrhea,” “blood depletion,” and “infertility” [2]. It is a common disease in the field of gynecological endocrinology, with an incidence of 1-3.8% at home and 1% abroad [3]. Premature ovarian failure is characterized by primary or secondary amenorrhea, infertility, low menstrual flow, etc., accompanied by changes in some

hormone levels, such as increased blood sex-stimulating hormone (FSH) and decreased estrogen level (E2). At the same time, it will be accompanied by different degrees of symptoms, such as hot flashes, sweating, and facial flushing, which seriously damages the fertility of women of childbearing age and is not conducive to coping with the current pattern of population aging. Generally speaking, the average age of normal amenorrhea in women is 50 to 52 years old, and the age of amenorrhea in patients with premature ovarian failure is much earlier. There are many causes of premature ovarian failure, and the modern and diversified lifestyle further complicates its etiology. Among them, improper weight loss,



mental stress, and cold and humid environment, the influence of chemotherapy drugs may cause premature ovarian failure. As a result, premature ovarian failure has become the focus and difficulty of reproductive medicine research. Modern medicine has not made a breakthrough in the prevention and treatment of POF. Hormone replacement therapy has poor efficacy and many side effects, so it is not easy to be accepted by patients [4]. Therefore, it is an urgent problem to seek suitable POF control technology. As a nondrug therapy, acupuncture has fewer side effects and a higher safety factor than the use of hormones. And in the long-term clinical practice, the clinical effect of acupuncture on premature ovarian failure has been fully proved, which has been widely concerned by the medical community. Bcl-2/Bax-mediated apoptosis pathway is involved in the progress of POF. Therefore, this experiment started with Bcl-2/Bax, combined with the data indicators related to the hypothalamic-pituitary-gonadal axis function of endocrine hormones, follicle forming hormone (FSH), luteinizing hormone (LH), etc., to study the mechanism of acupuncture intervention on premature ovarian failure, so as to provide traditional acupuncture technology for treatment. Premature ovarian failure provides new ideas and more reasonable and effective acupoint prescriptions for clinical practice.

## 2. Materials and Methods

### 2.1. Materials

**2.1.1. Experimental Animal.** There were seventy 8-week-old SPF female Wistar rats (provided by Beijing Weitong Lihua Laboratory Animal Technology Co., Ltd., license number SCXK (Beijing) 2016-0011) with a body weight of  $200 \pm 20$  g. The animals were fed adaptively for a week in the SPF observation room of the Animal Experimental Center of Shandong University of Traditional Chinese Medicine. The room temperature is 22–26°C, and the relative humidity is 60%. Maintain indoor ventilation and natural day and night light.

**2.1.2. Experimental Materials and Instruments.** Experimental materials and instruments are as follows: sterile acupuncture needle (produced by Suzhou Medical Supplies Co., Ltd., 0.3 mm  $\times$  15 mm); cyclophosphamide for injection (Jiangsu Shengdi Pharmaceutical Co., Ltd., product batch number is 18060125); hematoxylin staining solution (Nanchang Yulu Experimental Equipment Co., Ltd., product batch number 181001); 0.9% saline (Shandong Qilu Pharmaceutical Company); methanol, acetone, alcohol, SDS (China Solarbio Co., Ltd., analytical purity); ELISA, Western blot, and PCR kits (China Biyantian Company, UK Abcam Company, US Thermo Fisher Company, US BD Company); 1/10,000 electronic balance (Osho Instruments (Changzhou) Co., Ltd.); microscope (ZEISS Co., Ltd.); ultralow temperature refrigerator and medical refrigerator (China Haier Company); manual micropipette (Germany Eppendorf Company); overspeed centrifuge (Thermo Fisher Company, USA); constant temperature metal bath (Shanghai Jingxin Industrial Development Co., Ltd.); TY-8013 Decolorization Shaker (Jiangsu Science and Technology Instrument Co., Ltd.); cryogenic benchtop centrifuge (Thermo Fisher Company of the United States);

automatic water purifier (Millipore Company of the United States); Western blotting vertical electrophoresis apparatus (Bio-PAD, USA); Western blotting transfer membrane apparatus (Bio-PAD, USA); desktop calcium flow detection workstation (American Molecular instrument Co., Ltd.); full-wavelength enzyme labeling instrument (American BioTek Company); multicolor fluorescence imaging system (automatic chemiluminescence gel imaging analysis, American GE Company); ultramicro spectrophotometer (American GE Company); and biochemical incubator (Shanghai Longyue Instrument Equipment Co., Ltd.). The above are used in strict accordance with the instructions.

### 2.2. Experimental Method

**2.2.1. Animal Modeling Method.** The POF model was prepared by continuous intraperitoneal injection of cyclophosphamide in experimental rats [2]. This method of modeling has a high success rate, is simple and reliable, requires no special apparatus, and is easy to operate. The specific scheme is that after 1 week of adaptive feeding, the rats were fixed in 12 h intervals in the morning and evening twice a day to expose their vaginal opening, and their vulva was first cleaned with a cotton swab dipped in distilled water, after which a cotton swab moistened with saline was slowly inserted into the rat's vagina for 0.8–1 cm and gently rotated and removed, and the secretion was evenly applied to the slide, which was allowed to dry naturally and then fixed with 95% alcohol for 1 min and washed away. The next step was hematoxylin staining for 3 min, followed by washing the slide until there was no hematoxylin discoloration, and after drying, the morphology of rat vaginal cells was observed under a microscope to determine the stage of the animal's motility cycle. From which rats with regular cycles (with an estrous cycle of about 4–5 days, predominantly nucleated epithelium in the preestrous phase, predominantly keratinized epithelium in the estrous phase, predominantly leukocytes in the late estrous phase, and uniform distribution of the three cells in the interestrous phase [2], as shown in Figures 1–4), 7 of the 61 animals were selected by random number table method as blank control group and fed routinely. The rest were modeled by intraperitoneal injection of cyclophosphamide at 8:00 every morning for 14 days. The injection dose was 50 mg/kg on the first day and 8 mg/kg every day thereafter [2]. 42 rat POF models were successfully established. The successful rats were randomly divided into model group (without treatment), routine acupuncture group, item seven-needle group, three-viscera cotreatment group, and data mining core acupoint group.

**2.2.2. Acupuncture Treatment.** After successful modeling, the normal group and model group ate and drank normally and grabbed once a day. The rats in the three Zang-organs treatment group, routine acupuncture group, data mining core acupoint group, and item seven acupuncture group were treated with acupuncture once a day, one day off every six days, and continuous treatment for 14 days. Twist (a TCM acupuncture technique) once every five minutes for one minute each time. The needle is left in place for twenty minutes. The acupoints were positioned by referring to the "Experimental Guidance

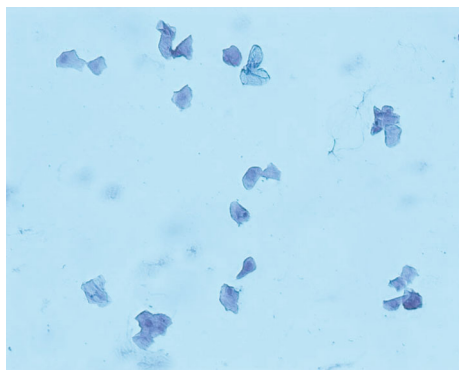


FIGURE 1: Preestrus vaginal smear.

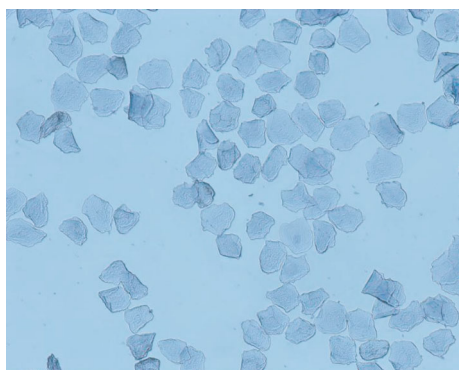


FIGURE 2: Vaginal smear during estrus.

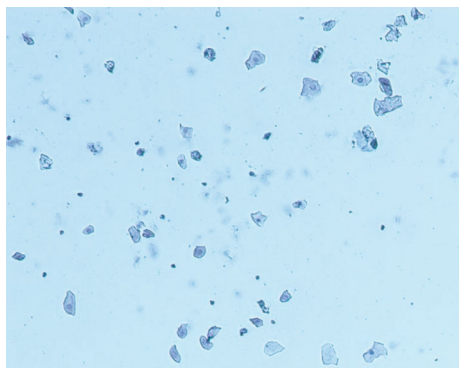


FIGURE 3: Postestrus vaginal smear.

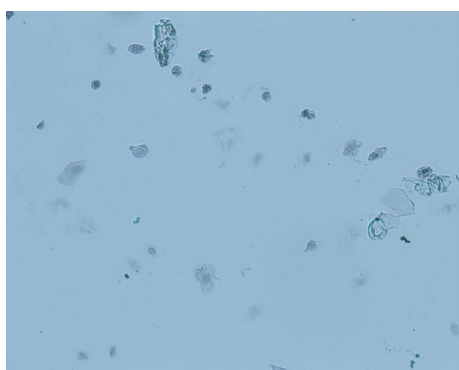


FIGURE 4: Interestrus vaginal smear.

for Experimental Acupuncture and Moxibustion” combined with anatomy and analogous to the method of measuring the bone size of the human body. Guanyuan was selected in the routine acupuncture group (because the navel of the rats was not obvious after weaning, so the navel was taken as the navel from the xiphoid process to the superior edge of the pubic symphysis, and the downward 25 mm was used to determine the acupoints), Sanyinjiao (the upper 10 mm of the medial malleolus of the hind limb), the middle pole (the intersection of the upper 4 × 5 and the lower 1 pm 5 of the above position of the navel and the upper edge of the pubic symphysis), and return (at the middle extreme level, 5 mm was separated on both sides). For routine disinfection, Guanyuan, Zhongji, and Huilai were injected with 5 mm acupuncture points, and the acupoints on both sides were used for Sanyinjiao and Huilai. In the treatment group, Guanyuan, Shenshu (both sides of the second lumbar vertebra), Sanyinjiao, Taichong (the 1st and 2nd intermetatarsal depressions of the hind limbs of rats), and Baihui (the center of parietal bone) were selected. After routine disinfection, they were treated with stainless steel filiform acupuncture of 0.30 × 15 mm, Guanyuan needling 5 mm, twirling and tonifying method. Shenshu needling 2 mm, twirling and tonifying method; Sanyinjiao needling 2 mm, tonifying and reducing method; Taichong needling 1 mm, twirling and reducing method; Baihui needling 1 mm, tonifying and reducing method. Each technique is designed to give a tight feeling under the needle. After the prone position of the rats in the item seven acupuncture group was fixed, the bilateral wind cistern (under the occipital bone, the depression between the upper end of the sternocleidomastoid muscle and the upper end of the trapezius muscle) was obliquely punctured into 5 mm. Fengfu (the back depression of the occipital atlantoid joint behind the occipital ridge), bilateral Tianzhu (beside Fengfu, in the depression of the outer edge of the trapezius muscle), and Wanggu (the depression behind the posterior auricular mastoid) were punctured directly into 3 mm, and the acupuncture was performed with the method of tonifying and relieving. The core acupoint group was determined by data mining, and only two acupoints Guanyuan and Sanyinjiao were selected, and the acupuncture method was the same as the abovementioned acupuncture groups.

**2.2.3. Material Method.** After the treatment, the rats were weighed. The rats were killed at 60 mg/kg injection using pentobarbital sodium (2% diluted in saline). The blood samples were collected by celiac vein puncture, and the blood samples were placed in 3000 r/min centrifugation 15 min. The supernatant, namely, serum, was stored in the refrigerator at -20°C in the Animal Experimental Center of Shandong University of Traditional Chinese Medicine. Then, disinfect the abdominal skin with ethanol and take aseptic samples. The uterus and ovary on the left side of the abdominal cavity were dissected, cleaned with filter paper, and preserved with liquid nitrogen. After the tissue was precisely weighed, it was placed in the homogenate tube, and normal saline was added in proportion at 1 : 9 to homogenate. The homogenate was placed in EP tube, 3500 r/min centrifugal 15 min, and stored in the negative 80-degree refrigerator on the third floor of the Animal Experimental Center of Shandong University of Traditional Chinese

Medicine for follow-up index detection. In the right segment of the uterus and ovary, fat was removed, and after weighing, the ovaries and uterus were immersed in a frozen tube filled with 10% paraformaldehyde solution and fixed.

### 2.3. Detection Method

**2.3.1. Analysis of E2, FSH, and LH by ELISA Method.** Blood samples were collected by celiac vein puncture; blood samples were placed static and centrifuged, and serum was taken. The contents of E2, FSH, and LH were determined by ELISA kit. According to the principle of double antibody sandwich method, the reagents in the kit were prepared and diluted, and then, the purified antibodies were coated with microwell plates, and the solid phase antibodies were prepared and incubated at 37°C. The antibody-antigen-enzyme-labeled antibody complex was formed by combining it with the labeled antibody. After washing for 5 times, add color developing agent, and finally, convert to yellow after blue color. At this time, adding stop solution, you can measure the absorbance according to the curve and calculate the index concentration according to the difference of color depth, and there is a positive correlation between the two. The entire operation needs to be carried out as soon as possible within 5 minutes to avoid inactivation. After using, it should be stored in the -20°C refrigerator in room 314 of the experimental center. Since room temperature needs to be equilibrated before use, repeated freezing and thawing should be avoided in multiple use projects. Avoid cross-contamination and contact with other irrelevant reagents during the whole process.

**2.3.2. Analysis of Bcl-2 and Bax by Western Blot.** The protein was extracted from the ice-thawed homogenate of ovarian tissue, and the protein concentration was determined by BCA protein quantitative kit. The parameters for the electrophoretic transfer of the membrane were 150mA steady flow for 2 hours. Prepare 5% nonfat milk powder blocking solution and block overnight, incubate with primary antibody (Bcl-21: 5000, Bax1: 1000,  $\beta$ -actin1: 3000) at room temperature for 2 hours, add secondary antibody (1: 2000) for 2 hours, and develop with SuperEclPlus ultrasensitive luminescent solution. X-film was exposed and scanned and processed by the Quantity One gel analysis software, the integral absorbance A of each histone band was measured, and the IA ratio of the target band and the  $\beta$ -actin band was used as the expression level of Bcl-2 and Bax proteins.

**2.3.3. Determination of mRNA of Bcl-2 and Bax by PCR.** Total RNA was extracted from rat ovarian tissues. The purity of total RNA was determined on the basis of absorbance A260/A280, between 1.9 and 2.1, with good purity. And calculate the RNA concentration. Take PCR tube, add the amount of RNA template containing 2  $\mu$ g as template for reverse transcription, reaction conditions 42°C, hold for 60 min, and inactivate reverse transcriptase by holding at 80°C for 5 min after the end. PCR amplification reaction conditions are as follows: pre-denaturation at 95°C for 10 min, denaturation at 95°C for 15 s, and extension at 60°C for 1 min, total 40 cycles. The results were sorted by the  $\Delta\Delta$ Ct method, and GAPDH was used as the internal reference to calculate the relative mRNA expres-

sion levels of Bcl-2 and Bax, which were expressed as 2- $\Delta\Delta$ Ct. The primer sequences are as follows: Bcl-2-F (5'-CTTCGCCGAGATGTCCAG-3'), Bcl-2-R (5'-GGCTCAGATAGGCACCCA-3'); Bax-F (5'-CCCACCAGCTCTGAACAGTTC-3'), Bax-R (5'-CCAGCCACAAAGATGGTCAC-3'); and GAPDH-F (5'-GCACCGTCAAGGCTGAGAAC-3'), GAPDH-R (5'-TGGTGAAGACGCCAGTGGA-3').

**2.3.4. Analysis of the Number of Ovarian Follicles and Corpus Luteum by He Staining on Paraffin Sections.** The uterus and ovary of rats were removed, fat was removed, and the ovaries and uterus were immersed in 10% paraformaldehyde solution for fixation, routine sampling, dehydration, paraffin embedding, slice preparation, HE staining, sealing, reading under light microscope, and counting the number of follicles and corpus luteum in the ovary.

**2.3.5. SPSS 26.0 Statistical Analysis.** The data were analyzed and processed by the SPSS 26.0 statistical software, the measurement data were expressed by  $\bar{X} \pm S$ , the analysis of variance was used for comparison among groups, the LSD method was used for variance, and the Dunnett's T3 method was used for variance discrepancy. Paired *t*-test was used for pairwise comparison, and  $p < 0.05$  indicated that the difference was statistically significant.

## 3. Result

**3.1. Ovarian Index.** There was no significant relationship between ovarian index and intervention mode ( $p > 0.05$ ), which may be related to the complex factors affecting the size of ovary (organ mass and body weight of rats are shown in Table 1). And the organ index is generally a toxicological index, which has little to do with the treatment and intervention of premature ovarian failure. The relationship of each group was as follows: neck-seven-acupuncture group > three-viscera simultaneous treatment group > normal group > model group > data mining group > routine acupuncture group; the ovarian index of the three-viscera simultaneous treatment group was similar to that of the normal control group.

**3.2. Hormone Levels.** There were significant differences in the regulation of estrogen in the neck-seven-acupuncture group, follicle-stimulating hormone in the same treatment group, and luteinizing hormone in any group (the sex hormone indicators are shown in Table 2). However, the specific mechanism is not clear, and the hypothalamus and pituitary will be further studied in the future. This is in line with the previous literature that the decrease of FSH and the increase of E2 are more closely related to premature ovarian failure, while the fluctuation of LH may not be closely related to the occurrence and intervention process of premature ovarian failure [5–9].

**3.3. Bcl-2/Bax.** There were significant differences among the groups (the Western blot results are shown in Figure 5, and the PCR results are shown in Table 3). The Bcl-2 mRNA level in the model group was lower than that in the normal group, and the Bcl-2 mRNA level in each treatment group was higher than that in the model group, with the highest level in the



TABLE 1: Ovarian mass, body mass, and ovarian index.

Group	Ovarian weight/mg	Body weight/g	Ovarian index
Normal control group	188.242 ± 36.672	258.000 ± 19.698	1.442 ± 0.294
Model group	180.600 ± 29.715	252.444 ± 10.393	1.427 ± 0.210
Item seven stitches group	168.211 ± 21.626	235.111 ± 22.855	1.537 ± 0.324
Three internal organs treatment group	184.750 ± 16.525	265.125 ± 23.613	1.446 ± 0.191
Data mining group	189.438 ± 29.119	253.625 ± 23.415	1.354 ± 0.143
Routine acupuncture group	183.300 ± 12.056	242.125 ± 20.629	1.323 ± 0.1021

TABLE 2: Difference of hormone levels in each group to the average value of the model group.

Group	E2/(pg/mL)	FSH/(mIU/mL)	LH/(mIU/mL)
Normal control group	0.329687	-0.52283	0.277500
Item seven stitches group	3.659333	-0.377583	-0.441083
Three internal organs treatment group	1.387833	-0.826167	0.006917
Data mining group	0.584625	-0.128083	-1.224937
Routine acupuncture group	0.765875	-0.123458	-1.636062

conventional acupuncture group. The relationship of each group was as follows: routine acupuncture group > data mining group > three-viscera treatment group > normal group > neck-seven-acupuncture group > model group; three-viscera treatment group and neck-seven-acupuncture group were close to the normal group. Bax mRNA in the model group was higher than that in the normal group, and all treatment groups were lower than those in the model group, among which the routine acupuncture group was the lowest. Routine acupuncture group < data mining group < normal group < three-viscera treatment group < neck-seven-acupuncture group < model group, the three-viscera treatment group was close to the normal group. It can be seen that acupuncture can intervene in the treatment of premature ovarian failure by regulating Bcl-2/Bax. The routine acupuncture group has the best effect, followed by the data mining group. Compared with the routine acupuncture group, more acupoints in the lower abdomen and closer to the surface of the ovary were selected, which may indicate that selecting relevant acupoints will obtain better results [10]. However, there is no significant difference about Bax between the neck-seven-acupuncture group and the model group, which may indicate that neck-seven-acupuncture is not effective for reducing Bax.

**3.4. Paraffin Section.** The number of follicles in each group was lower than that in the normal group, and the number in the model group was the most (the pathological section of ovary in each group is shown in Figure 6, and the number of follicles in each group is shown in Table 4). The three groups of routine group, data mining group, and neck-seven-acupuncture group were all 0, which was significantly different from that of the model group, which may mean that the follicles of the model group stopped developing and remained in the initial stage because of premature ovarian failure. In addition to the model group, the medium-term follicles in each group were more than the normal group, the conventional group was

the highest, and the model group was not obvious, indicating that acupuncture has a promoting effect on follicular development. There was no significant difference in the number of late follicles in each group [11–14], but less than the normal group. The number of corpus luteum was significantly different between the conventional group and each group and was less than that of the normal group, and all other groups were more than the normal group. Although the pathological section is the gold standard, the estrous cycle is not differentiated among the groups, and the comparison of the number of follicles and corpus luteum at all levels may lack significance.

#### 4. The Rationality of Acupuncture Point Selection

In traditional Chinese medicine, it is believed that the kidney is in charge of reproduction, the liver is in charge of dredging and excretion, it is also in charge of storing blood, and the spleen is in charge of controlling blood, which is closely related to female development. The syndromes of premature ovarian failure in traditional Chinese medicine are also based on this, which is roughly divided into liver-kidney yin deficiency type, heart-kidney noncommunication type, spleen-kidney yang deficiency type, kidney deficiency and liver stagnation type, and kidney deficiency and blood stasis type. Therefore, in terms of syndrome differentiation and treatment, traditional Chinese medicine mainly focuses on restoring the sea of blood, invigorating the kidney qi, regulating the functions of the zang-fu organs, and achieving the purpose of improving symptoms [15]. Based on the analysis of the characteristics and rules of the selection of acupoints in the treatment of infertility by acupuncture and moxibustion in ancient literature, the scheme of simultaneous treatment of three Zang organs pays attention to the selection of acupoints of Ren meridian and foot Shaoyin kidney meridian, highlighting the combined use of acupoints

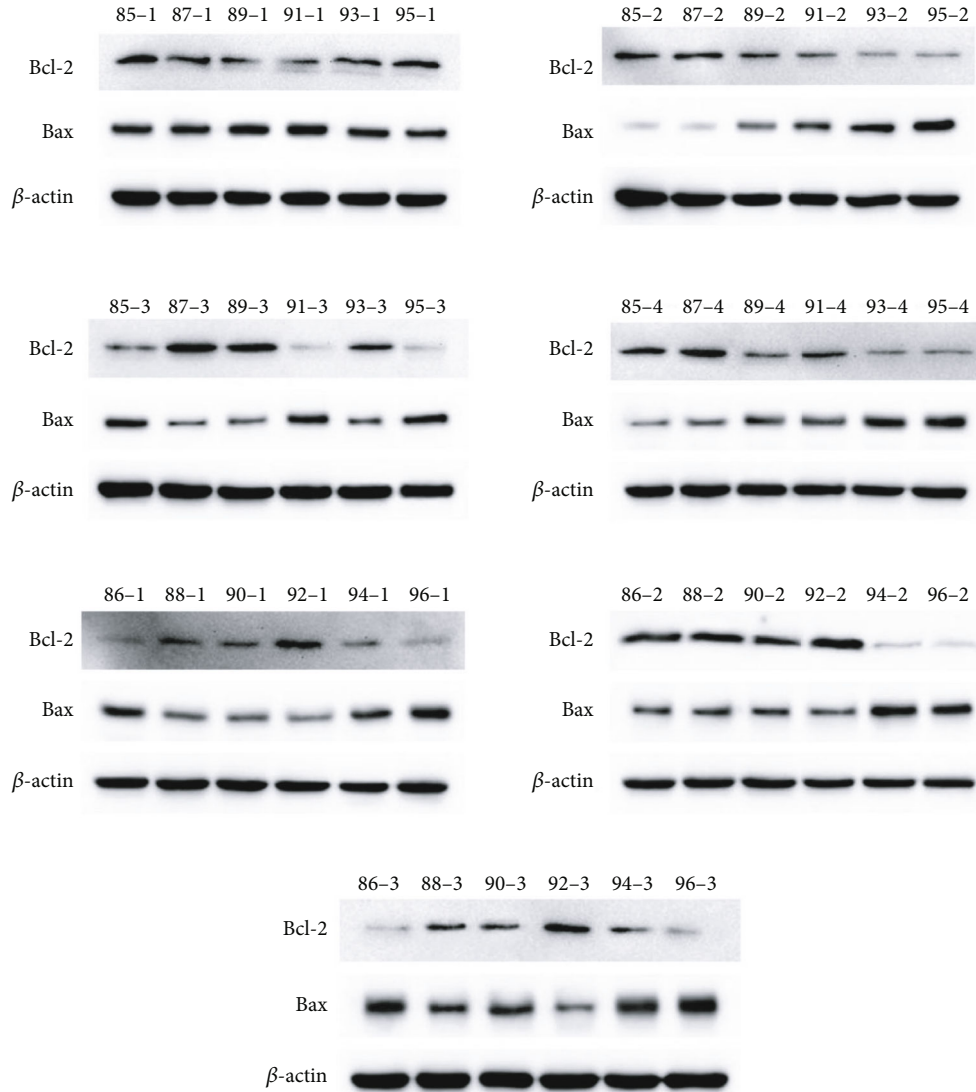


FIGURE 5: Expression of Bcl-2, Bax, and  $\beta$ -actin in each group. Note: 85 and 86 are normal groups; 87 and 88 are model groups; 89 and 90 are three-viscera treatment groups; 91 and 92 are seven-needle groups; 93 and 94 are data groups; 95 and 96 are routine groups.

TABLE 3: mRNA of Bcl-2 and Bax.

Group	Bcl-2	Bax
Normal control group	$22.3529 \pm 0.74651$	$22.1696 \pm 0.82631$
Model group	$20.1352 \pm 0.33802$	$22.9024 \pm 0.26619$
Item seven-needle group	$20.6405 \pm 0.64202$	$22.7505 \pm 0.62806$
Three internal organs treatment group	$20.9581 \pm 0.19195$	$22.2971 \pm 0.26982$
Data mining group	$21.6252 \pm 0.64202$	$21.6376 \pm 0.23624$
Routine acupuncture group	$22.3529 \pm 0.74651$	$21.1390 \pm 0.43992$

and attaching importance to the application of meridian intersection acupoints, Wushu acupoints, and mu acupoints. The method of selecting acupoints based on syndrome differentiation and syndrome differentiation is emphasized [16]. In the textbook *Acupuncture Therapeutics* of the 13th five-year plan of higher education in the national traditional

Chinese medicine industry, the main acupoints for the treatment of amenorrhea are Guanyuan, Zhongji, Sanyinjiao, return, and other acupoints. Guanyuan acupoint is located in Renmai, and it is the intersection of foot Sanyin meridian and Renmai. Zhongji acupoint is located in Renmai, which is the intersection of foot Sanyin and Renmai and the mu



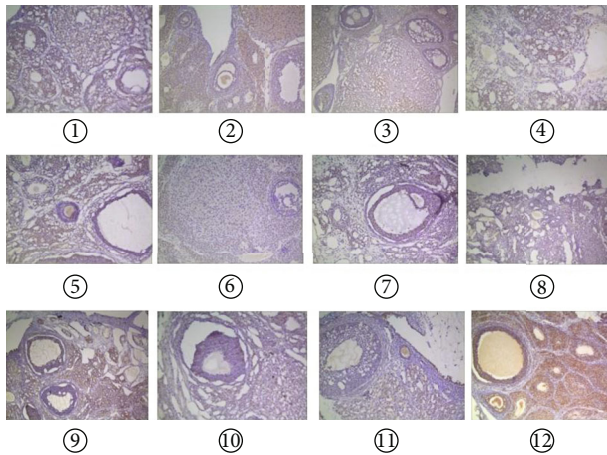


FIGURE 6: (a) Paraffin sections of routine group. (b) Model group paraffin sections. (c) Paraffin sections of the three-viscera treated. (d) Paraffin sections of data mining. (e) Paraffin section of the seven-needle. (f) Paraffin sections of normal. (g) Paraffin section of routine. (h) Paraffin sections of model group. (i) Paraffin sections of three-viscera treated group. (j) Paraffin sections of data mining group. (k) Paraffin section of the seven-needle. (l) Paraffin sections of normal group.

acupoint of bladder. Sanyinjiao is located in the foot Taiyin spleen meridian, which is the intersection point of the foot Sanyin meridian. The return acupoint is located in the stomach meridian of foot Yangming, and its name is related to the adjustment of the main function under the menstrual zone. The above acupoints can be used to treat diseases of the female reproductive system. The data mining technology was used to screen the effective literature to find the acupoints with the highest frequency in the effective treatment of premature ovarian failure. The results showed that the most frequently selected meridians were Ren meridian, bladder meridian, spleen meridian, stomach meridian, and kidney meridian, and the most frequently used acupoints were Guanyuan acupoint, Sanyinjiao acupoint, Zusanli acupoint, Shenshu acupoint, and uterus acupoint. To some extent, this also reflects the Chinese medicine in the treatment of syndrome differentiation from the overall point of view, advocating congenital, complementary to make the blood sea restore vitality, so as to improve a series of symptoms of premature ovarian failure. The purpose of this experiment is to study the mechanism of acupuncture on premature ovarian failure model rats, taking into account the experimental process; in line with the concept of complexity and simplicity, select the two most critical points obtained from data mining, and set up the conventional acupuncture group. The results of each group show that acupuncture can change the content of related hormones and proteins and improve the ovarian function of model rats to a certain extent. However, this study has shortcomings; this study is from the rat experimental exploration. There is still controversy about the distribution of acupoints in experimental animals, and their generalizability may be poor. Based on this, we will study the positioning of acupoints in experimental animals

in our subsequent work, and strive to be able to extend the experimental findings to the extent that they can guide clinical applications.

## 5. Discussion

A large number of experiments have proved that the content of FSH and E2 in the serum of the core standard animal successfully established by the POF model has changed; that is, the content of FSH is significantly increased, and the content of E2 is significantly decreased. Changes in serum sex hormone levels are important indicators for evaluating ovarian function in POF models. Due to the decrease of serum E2 content caused by pathological low ovarian function, when effective treatment is given and ovarian function gradually recovers, it will naturally rise to close to the normal level, which is an ideal detection index for this experiment. Follicle-stimulating hormone (FSH) can promote the proliferation and differentiation of follicular granulosa cells, tend to mature, and then make the ovary grow. When the ovarian function is damaged, the concentration will increase in feedback and can fall back to the normal level with the recovery of ovarian function, which is a commonly used detection index [17–21]. In this experiment, the above three endocrine hormones are used as reference analysis indicators to judge the success of modeling and the degree of onset of the treatment process. Due to unavoidable cross-reaction and other influencing factors or changes in enzyme activity and pH value due to contamination of impurities and poor storage conditions of tissue samples, some experimental data are also unsatisfactory. At the same time, Bcl-2 (apoptosis inhibitory gene) and Bax (apoptosis promoting gene) were selected as the research indexes at the molecular biological level. Overexpression of Bax can antagonize the inhibitory effect of Bcl-2 and make cells tend to die. Premature ovarian failure is the premature aging of the ovary, and the process of aging is the process of apoptosis. Bcl-2 and Bax were selected as the research indexes on the molecular biological level of apoptosis. Bcl-2 has a decisive role in significantly inhibiting apoptosis, and Bax inhibits the protective effect of Bcl-2 by forming heterodimers and promotes apoptosis. Specifically, in the premature ovarian failure rats modeled by the chemotherapeutic drug cyclophosphamide, Bcl-2 can inhibit ovarian cell apoptosis by enhancing the resistance of cells to DNA damage factors. Although apoptosis may be mediated by some specific pathways, it is not sensitive to Bcl-2/Bax. Or because Bax belongs to Bcl-2 family, both homology, molecular weight, and other properties are close, and Bax expression is far more extensive than Bcl-2, resulting in the impact of experimental data; it may also be due to cross-contamination, primer dimerization, and other factors leading to the accuracy of the experimental results. With regard to the solution of this problem, we will continue to carry out more specific index selection and other related research through network pharmacology analysis in the follow-up plan, follow up the mastery of cutting-edge technology, and strive to get more objective and reasonable experimental conclusions.

TABLE 4: Number of follicles and corpus luteum at all levels.

Group	Early follicle ( <i>n</i> )	Metaphase follicle ( <i>n</i> )	Late follicle ( <i>n</i> )	Corpus luteum ( <i>n</i> )
Normal control group	$2.25 \pm 2.667$	$2.08 \pm 4.010$	$0.92 \pm 1.240$	$2.50 \pm 1.784$
Model group	$1.87 \pm 1.995$	$1.67 \pm 1.291$	$0.73 \pm 0.884$	$2.80 \pm 3.342$
Seven-needle group	$0 \pm 0$	$3.07 \pm 1.438$	$0.27 \pm 0.458$	$2.87 \pm 1.506$
Three internal organs treatment group	$1.12 \pm 1.799$	$2.53 \pm 1.328$	$0.65 \pm 1.115$	$3.76 \pm 1.348$
Data mining group	$0 \pm 0$	$2.92 \pm 3.095$	$0.31 \pm 0.855$	$2.85 \pm 2.267$
Conventional acupuncture group	$0 \pm 0$	$3.56 \pm 2.007$	$0.33 \pm 0.500$	$0.44 \pm 1.014$

In recent years, there have been many studies on the treatment of premature ovarian failure by acupuncture. Kong Suping started from the liver and kidney and took Guanyuan, Sanyinjiao, Taixi, Taichong, and other acupoints, and the research confirmed the rationality of the method of tonifying the kidney and soothing the liver. One of the functional axes of ovarian regulation is hypothalamus-pituitary-ovary axis. Therefore, most scholars believe that acupuncture-related acupoints can stimulate hypothalamus to secrete GnRH, then regulate pituitary gonadotropin secretion, and then regulate ovarian function. The mechanism of premature ovarian failure is not clear. Modern medical treatment believes that premature ovarian failure is closely related to the apoptosis of ovarian granulosa cells. Hormone replacement therapy is often used in clinic. Although this treatment is effective quickly, it is not ideal for the complete recovery of ovarian function. Therefore, some researchers are committed to starting from the root, improve ovarian function to make hormones back to normal, and then make the symptoms of premature ovarian failure disappear. In the field of traditional Chinese medicine, the treatment of related prescriptions has also made great progress, but the specific treatment mechanism is still not clear; the effect of drugs is more complex; different drugs may have different mechanisms. For the time and efficiency of treatment, acupuncture treatment of premature ovarian failure is currently one of the more ideal programs. Several studies have shown that acupuncture can reduce the content of Bcl-2 protein and increase the content of Bax protein, thereby inhibiting ovarian cell apoptosis and improving ovarian function. From the aspect of apoptosis inhibitory genes, the mechanism of premature ovarian failure is also studied on the caspase family and the study on Apaf-1. The above genes, including Bcl family, are the determinants of ovarian granulosa cell apoptosis. Previous studies have shown that endoplasmic reticulum stress proteins can downregulate Bcl-2 and promote cell apoptosis and at the same time lead to the activation of a series of genes related to the caspase family, resulting in cell apoptosis. Related studies have shown that estrogen has an inhibitory effect on endoplasmic reticulum stress proteins. Therefore, we can speculate that the mechanism of acupuncture treatment of premature ovarian failure may be through the upregulation of estrogen and then inhibit the endoplasmic reticulum stress response, so as to achieve the purpose of inhibiting ovarian granulosa cell apoptosis. However, whether other hormones are involved in this regulation process needs further study. In this way, increasing the content of related hormones can indeed improve ovarian function; this

regulatory axis forms a closed loop, and the improvement of ovarian function can affect the secretion of related hormones. The mechanism of acupuncture must be more than that, and our hypothesis lays a foundation for further experimental research [22, 23].

In this experiment, the data obtained from the experimental study showed that acupuncture can reduce the FSH content and increase the E2 content in POF model rats and improve the ovarian function of POF rats. However, due to lack of experience in this experiment, there were some inevitable small errors in rat modeling and acupoint positioning. The results of Bcl-2/Bax index were not particularly ideal, but to a certain extent, it proved that acupuncture at acupoints could upregulate the expression of Bcl-2 and inhibit the expression of Bax, thereby inhibiting the apoptosis of ovarian granulosa cells [24–26]. Although there are some omissions in the experiment, after analyzing the problem and finding a feasible solution, it still lays the foundation for our future research. In the future, to further improve the experimental design and carry out more in-depth research on the mechanism of acupuncture in the treatment of premature ovarian failure, it is still expected to provide new ideas and methods for the clinical search for appropriate prevention and treatment techniques for premature ovarian failure [27]. As a clinical practical technology that is easy to learn, promote, and master, it is conducive to solving the technical problems of grass roots and community health service institutions and can further reduce medical costs and improve the quality of medical services [28, 29]. However, this study has shortcomings. At present, the effect and mechanism of electroacupuncture on POF have been explored from the rat level. Clinical experiments need to further confirm the mechanism of electroacupuncture in POF. In addition, the treatment of POF by electroacupuncture involves the Bcl-1/Bax-mediated apoptosis pathway. Whether there are other pathways mediated needs to be further explored in the next experiment.

## 6. Conclusions

In this experiment, POF rat model was built; it was found that Bcl-2 increased and Bax decreased in rats with premature ovarian failure treated with acupuncture. It shows that acupuncture can affect the secretion of ovarian-related hormones and the expression of apoptosis-related proteins, which is more significant in the routine acupuncture group. This indicates that acupuncture can inhibit the apoptosis of

granulosa cells in ovarian tissue of rats with premature ovarian failure and improve ovarian function. The mechanism of its effect is to promote Bcl-2 gene expression and protein synthesis and inhibit Bax gene expression and protein synthesis. The routine acupuncture group works best. This provides an experimental basis for the clinical use of acupuncture to intervene in the treatment of premature ovarian failure.

## Data Availability

No data were used to support this study.

## Conflicts of Interest

The authors declare that they have no conflicts of interest.

## Acknowledgments

This work was supported by the following fund projects: the Shandong Provincial Natural Science Foundation Key Project “Study on the Molecular Mechanism of Acupuncture on Ovarian Protection in POF Rats from PI3K/AKT To Regulate Ovarian Granulocyte Autophagy” (No. ZR2020KH027), the Shandong Provincial Key R&D Program Project (No. 2018GSF119025), and the Shandong Province Traditional Chinese Medicine Science and Technology Development Program Project (No. 2017-010).

## References






- [1] D. Gao, “Construction of acupuncture and moxibustion diagnosis and treatment plan for premature ovarian insufficiency: a mixed methods study,” *Chinese Academy of Chinese Medical Sciences*, 2018.
- [2] M. Yu, Q. Liuqiao, C. Jiming et al., “Effects of Dihuang Cuscuta Tiaojing granule on stem cell factors in cyclophosphamide-induced premature ovarian failure rats,” *Chinese Medicine Science and Technology*, vol. 23, no. 1, pp. 25–27, 2016.
- [3] F. Cheng, *Association between Finger-Length Ratio and AR Gene and SHBG Gene Polymorphism in Premature Ovarian Failure*, Ningxia Medical University, 2015.
- [4] C. Zheng and H. Guangying, “Understanding of Chinese and Western medicine on premature ovarian failure,” *Integrative Medicine*, vol. 4, no. 3, pp. 150–155, 2012.
- [5] L. M. Nelson, “Clinical practice. Primary ovarian insufficiency,” *The New England Journal of Medicine*, vol. 360, no. 6, pp. 606–614, 2009.
- [6] A. Kokcu, “Premature ovarian failure from current perspective,” *Gynecological Endocrinology*, vol. 26, no. 8, pp. 555–562, 2010.
- [7] M. L. Shelling and R. S. Kirsner, “Failure to counsel patients with psoriasis to decrease alcohol consumption (and smoking),” *Archives of Dermatology*, vol. 146, no. 12, p. 1370, 2010.
- [8] C. Wilson, “Autoimmunity: autoimmune Addison disease and premature ovarian failure,” *Nature Reviews. Endocrinology*, vol. 7, no. 9, p. 498, 2011.
- [9] P. B. Hoyer and I. G. Sipes, “Assessment of follicle destruction in chemical-induced ovarian toxicity,” *Annual Review of Pharmacology and Toxicology*, vol. 36, no. 1, pp. 307–331, 1996.
- [10] F. Penghui, Z. Liao, Y. Huacheng et al., “Research progress on the occurrence, diagnosis and treatment of premature ovarian failure,” *China Maternal and Child Health*, vol. 33, no. 20, pp. 4795–4797, 2018.
- [11] D. Guémené and J. B. Williams, “LH responses to chicken luteinizing hormone-releasing hormone I and II in laying, incubating, and out of lay Turkey hens,” *Domest Anim Endocrinology*, vol. 17, no. 1, pp. 1–15, 1999.
- [12] J. P. Moore Jr. and S. Wray, “Luteinizing hormone-releasing hormone (LHRH) biosynthesis and secretion in embryonic LHRH neurons,” *Endocrinology*, vol. 141, no. 12, pp. 4486–4495, 2000.
- [13] J. J. Eppig, “Oocyte control of ovarian follicular development and function in mammals,” *Reproduction*, vol. 122, no. 6, pp. 829–838, 2001.
- [14] Y. Chen, Y. Fang, J. Yang, F. Wang, Y. Wang, and L. Yang, “Effect of acupuncture on premature ovarian failure: a pilot study,” *Evidence-based Complementary and Alternative Medicine*, vol. 2014, Article ID 718675, 6 pages, 2014.
- [15] X. Fang, Y. Chen, F. Wang, and L. Yang, “Pre-acupuncture intervention on 24 cases of premature ovarian failure,” *Chinese Acupuncture*, vol. 37, no. 3, pp. 256–258, 2017.
- [16] Z. Jing, F. Weisen, L. Yunsheng, Z. Ruqi, Z. Yongchen, and Z. Jiwei, “Analysis of the application rules of acupuncture and moxibustion in the treatment of infertility meridians in ancient literature based on data mining technology,” *Fujian Traditional Chinese Medicine*, vol. 50, no. 6, pp. 1–4, 2019.
- [17] J. Cheng, D. Lijun, and Y. Hu, “Research progress on animal model preparation of premature ovarian failure,” *Chinese Journal of Comparative Medicine*, vol. 4, pp. 66–70, 2013.
- [18] J. Xiaochen, Z. Lu, M. Wenjing, and S. Yehui, “Reparative effect of human umbilical cord mesenchymal stem cells combined with goserelin on premature ovarian failure,” *Tianjin Medicine*, vol. 45, no. 1, pp. 25–29, 2017.
- [19] W. Xu, *Study on the Relationship between Sno N Expression Level and Follicular Development in Mouse Ovary*, Shandong normal University, 2009.
- [20] C. Yingru, F. Dong, L. Chunhua, C. Hong, and X. Tao, “Effects of acupuncture at different times on central and peripheral hormone levels in rats with premature ovarian failure,” *Shanghai Journal of Acupuncture*, vol. 39, no. 2, pp. 220–225, 2020.
- [21] X. Jieting, X. Wang, and T. Sheng, “AMH and FSH/LH combined with gynecological ultrasound in early diagnosis of premature ovarian failure,” *Contemporary Medicine*, vol. 25, no. 35, pp. 147–148, 2019.
- [22] A. Falorni, S. Laureti, P. Candeloro et al., “Steroid-cell autoantibodies are preferentially expressed in women with premature ovarian failure who have adrenal autoimmunity,” *Fertility and Sterility*, vol. 78, no. 2, pp. 270–279, 2002.
- [23] R. K. Naz, D. Thurston, and N. Santoro, “Circulating tumor necrosis factor (TNF)-alpha in normally cycling women and patients with premature ovarian failure and polycystic ovaries,” *American Journal of Reproductive Immunology*, vol. 34, no. 3, pp. 170–175, 1995.
- [24] C. Xiaoping, “Clinical factors and experimental study of ovarian dysfunction,” *Guangzhou University of Traditional Chinese Medicine*, vol. 12, 2014.
- [25] F. Lanying, S. Xu, and F. Yizhong, “Expression and significance of Beclin-1, Bcl-2 and Bax in endometrioid adenocarcinoma,” *Chinese Community Physician*, vol. 30, no. 35, pp. 133–136, 2014.
- [26] T. Lei, L. Jinli, S. Linlin, H. Jiafu, F. Yu, and Y. Gao, “Preventive effects of Zuogui pills and Yougui pills on ovarian senescence

- in mice with premature ovarian failure,” *Proprietary Chinese Medicine*, vol. 39, no. 2, pp. 260–265, 2017.
- [27] D. Li, Y. Chen, L. Qi, X. Ju, H. Liu, and G. Wang, “Differentially expressed genes in cisplatin-induced premature ovarian failure in rats,” *Animal Reproduction Science*, vol. 137, no. 3–4, pp. 205–213, 2013.
- [28] W. Xu, H. Gao, L. Yang, and L. Ze, “Effect of Heyankuntai capsule on sex hormone level and expression of VEGF and bFGFmRNA in rats with premature ovarian failure,” *Chongqing Medicine*, vol. 46, no. 6, pp. 738–741, 2017.
- [29] Q. Jiajia, Q. Wu, J. Yang, and J. Liang, “Experimental study on tonifying kidney and nourishing yin combined with stem cell transplantation in the treatment of premature ovarian failure after chemotherapy,” *Journal of Beijing University of traditional Chinese Medicine*, vol. 38, no. 11, pp. 735–739, 2015.



## Research Article

# Expression of DNA Helicase Genes Was Correlated with Homologous Recombination Deficiency in Breast Cancer

Mengping Long <sup>1</sup>, Hongjun Liu,<sup>2</sup> Jinbo Wu,<sup>2</sup> Shu Wang <sup>2</sup>, Xin Liao <sup>2</sup>, Yiqiang Liu <sup>1</sup>, and Taobo Hu <sup>2</sup>

<sup>1</sup>Department of Pathology, Peking University Cancer Hospital, Beijing, China

<sup>2</sup>Department of Breast Surgery, Peking University People's Hospital, Beijing, China

Correspondence should be addressed to Xin Liao; [dongliao@pku.edu.cn](mailto:dongliao@pku.edu.cn), Yiqiang Liu; [victor.liu76@163.com](mailto:victor.liu76@163.com), and Taobo Hu; [thuac@bjmu.edu.cn](mailto:thuac@bjmu.edu.cn)

Mengping Long and Hongjun Liu contributed equally to this work.

Received 2 May 2022; Accepted 22 June 2022; Published 9 July 2022

Academic Editor: Shimin Wang

Copyright © 2022 Mengping Long et al. This is an open access article distributed under the Creative Commons Attribution License, which permits unrestricted use, distribution, and reproduction in any medium, provided the original work is properly cited.

Homologous recombination deficiency which is currently measured by the homologous recombination deficiency (HRD) score including score of telomeric allelic imbalance (TAI), large-scale transition (LST), and loss of heterozygosity (LOH) is highly related with sensitivity to platinum-containing drug and PARP inhibitors. DNA helicases are essential components for the homologous recombination repair process in which DNA helicases unwind double-strand DNA utilizing ATP hydrolysis. In our study, the correlation between the expression of DNA helicase genes and HRD score in breast cancer was analyzed. The overexpression in half of the DNA helicase genes was found to be highly correlated with a high HRD score both in BRCA-mutated and BRCA wild-type breast cancer. Moreover, HRD score can be predicted by a linear function contributed by five DNA helicase genes. In conclusion, our study revealed a close relation between the overexpression of certain DNA helicase genes and the deficiency of homologous recombination repair in breast cancer.

## 1. Introduction

DNA helicases are proteins that unwind DNA into single-strand structure utilizing the energy produced by ATP hydrolysis. They are also indispensable components in the repair process of DNA double-strand break (DSB) by homologous recombination repair (HRR) where the production of a single-strand DNA was essential [1]. Germline mutations in certain DNA helicase genes can cause cancer predisposition syndromes including the Bloom syndrome caused by *BLM* mutation [2] and the Werner syndrome caused by *WRN* mutation [3]. Moreover, the loss of function in DNA helicase genes including *RECQL*, *BLM*, *WRN*, *RECQL5*, and *BRIP1* are also known to be highly correlated with the carci-

nogenesis of breast cancer and the BRCAness phenotype in breast cancer [4–8].

In breast cancer, the deficiency in homologous recombination repair pathway is called “BRCAness phenotype” and can be measured by the presence of genomic scar including telomeric allelic imbalance (TAI), large-scale transition (LST), and loss of heterozygosity (LOH) via single nucleotide polymorphism (SNP) profile. The numeric sum of the TAI, LST, and LOH is called HRD score, and a HRD score greater than or equal to 42 is defined as BRCAness phenotype. BRCAness phenotype in breast cancer has been shown to be highly correlated with the response to platinum-based chemotherapy and PARP inhibitors in *BRCA1* and *BRCA2* germline wild-type triple negative breast cancer (TNBC)



[9, 10]. Importantly, in BRCA wild-type TNBC, the percentage of BRCAness phenotype was shown to be over 50% [9] even though the mechanism for the specific cause of HRD was unclear in those samples. Thus, it is important to characterize the molecular features of breast cancer with BRCAness phenotype in order to understand the detailed mechanism and to develop a more convenient biomarker for the evaluation of HRD.

Previous studies have focused on the mutation of targeted genes in the HRR pathway, while numerous recent papers have shown that the altered expression in DNA helicase genes including *BLM*, *RECQL5*, *SLFN11*, and *ATM* have impact on the HRR efficiency and consequently sensitivity on platinum-based chemotherapy and PARP inhibitors [11–14]. Also, studies showed that small molecules inhibiting DNA helicases including *BLM* and *WRN* could induce DNA damage and sensitivity to PARP inhibitor [15, 16]. Thus, it provides the rationale for us to look at the effect of the expression of DNA helicases which are essential components in the HRR pathway on the measured HRD status in breast cancer. In this study, we comprehensively analyzed the correlation between the expression of DNA helicase genes participated in HR and the HR status in breast cancer defined by the HRD score using TCGA data. A strong correlation between the overexpression of DNA helicase genes and HRD was found both in *BRCA1/2*-mutated breast cancer as well as in *BRCA1/2* wild-type breast cancers. A gene signature composed of five DNA helicase genes was identified that can predict the HRD score with high accuracy.

## 2. Materials and Methods

**2.1. Data Collection.** Data acquisition and analysis were conducted using R software (version 3.5.1 or above) unless otherwise mentioned. RNA-seq and clinical data were downloaded from the TCGA dataset [17] using the TCGA-biolinks R/Bioconductor package (version 2.10.5) [18]. The three genetic signature scores and HRD score of breast cancers from TCGA were derived from previous study, together with the germline mutation status of *BRCA1/2* genes [10]. The genetic signature score is calculated using algorithms developed by researchers using the Affymetrix SNP6 data downloaded from TCGA.

Fragments per kilobase of transcript per million mapped reads upper quartile (FPKM-UQ) is used for the normalization of RNA transcript reads. FPKM-UQ RNA-seq data were downloaded and prepared using the GDCquery, GDCdownload, and GDCprepare functions, as described in our previous publications [19–21].

**2.2. Correlation Heatmap Generation.** Unsupervised hierarchical clustering and heatmap generation was performed using “ComplexHeatmap” package. Comparison of HRD scores and gene expression values between different groups was performed by Student’s *t*-test. *P* values were calculated as two-sided, with statistical significance declared for *P* less than 0.05.

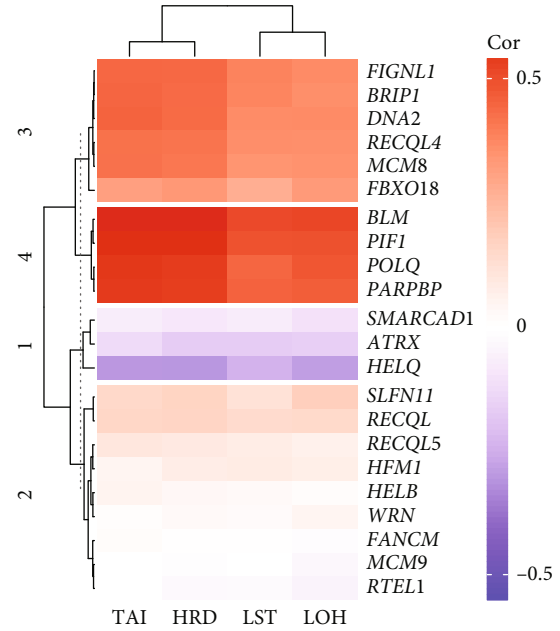


FIGURE 1: Correlation heatmap between the expression of DNA helicase gene and the score of genomic scars. The correlation efficiency between the expression of DNA helicase genes and the score of genomic scars are presented in a color scale ranging from red for positive correlation to blue for negative correlation.

**2.3. Correlation Analysis and Model Building.** The best multivariate model was generated using the “bess” function from “BeSS” R package. The “BeSS” package uses primal dual active set (PDAS) algorithm to solve the best subset selection problem under the general convex loss setting. The algorithms can be used for variable selection in a linear model. The correlation analysis between predicted HRD and actual HRD score was evaluated with Pearson’s correlation coefficient.

## 3. Results

**3.1. The Expression of DNA Helicase Genes Was Positively Correlated with HRD Score in Breast Cancer.** 871 cases of breast cancer patients were included in the study, and the scores of genomic scars including TAI, LST, and HRD-LOH were obtained from previous study [10]. *BRCA1* or *BRCA2* germline mutation was found in 43 of them with 23 patients harboring pathogenic mutations and the others harboring nonpathogenic mutations [10]. The threshold for defining HRD score high and low was based on the average HRD score in *BRCA* pathogenic mutation population which was 58.9. Thus, a HRD score  $\geq 59$  was considered HRD high and a score smaller than 59 was considered to be HRD low. This HRD threshold score is set higher than the conventional threshold of 42. Twenty-two DNA helicase genes participating in homologous recombination were analyzed in the study. The correlation between the expression of DNA helicase genes and HRD score was calculated and a correlation heatmap was generated (Figure 1). The scores of TAI, LST, and LOH were highly correlated with each

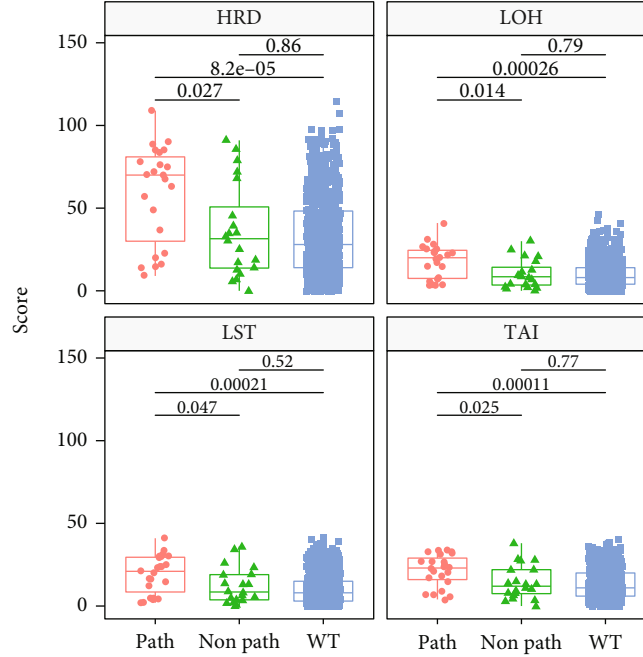


FIGURE 2: Box plot of HRD score in BRCA1/2 germline mutated and wild-type breast cancer. The scores for HRD and each type of genomic scar were plotted in three groups of breast cancer patients. Breast cancers patients harboring germline pathogenic were named as “Path” group presented in red. Patients harboring nonpathogenic germline BRCA1/2 mutation were named as “NonPath” group represented in green, while those with germline wild-type BRCA1/2 were named as “WT” group represented in blue.

other as they show very similar correlation with each gene. The 22 DNA helicase genes were clustered by K-means algorithm and can be divided into 4 groups according to their correlation with HRD score (Figure 1). Among them, the expression of *BLM*, *PIF1*, *POLQ*, and *PARPBP* showed highly positive correlation with HRD score which was included in group 4. Six out of the 22 genes were included in group 3 which showed modest positive correlation with HRD score, and three of them in group 1 showed modest negative correlation with HRD score. No significant correlation was observed between the other nine genes and HRD score. Among the 22 selected DNA helicase genes, the expression of *SLFN11* has been previously shown to be correlated with homologous recombination efficiency and drug sensitivity to PARP inhibitor in non-small-cell lung cancer [11–13], while no correlation was detected between *SLFN11* expression and HRD score in breast cancer by this study.

**3.2. Overexpression of DNA Helicase Genes Contributed to Both BRCA-Related and -Unrelated HRD.** Next, the correlation between gene expression and HRD score was analyzed in BRCA-mutated and nonmutated patients. Breast cancer with pathogenic germline BRCA mutation harbored high HRD score when compared with BRCA wild-type and nonpathogenic mutation group (Figure 2). No difference was identified between nonpathogenic mutation group and wild-type group. However, for BRCA wild-type breast cancer, there were also 17.5% (145/828) of them having a HRD score above the average of BRCA mutated breast cancer, while no specific genetic mutation can be attributed to explain the mechanism. When the correlated DNA helicase

genes identified above were analyzed, it was found that all of the positively correlated genes except *RECQL4* showed higher expression in HRD high patients regardless of BRCA mutation status (Figure 3), whereas for the three negatively correlated genes, lower expression was noticed in HRD high group only in BRCA wild-type cases. No difference in expression was identified between BRCA-mutated group and HRD low group. The above results indicated a shared mechanism behind HRD-high groups caused regardless of BRCA mutation status.

**3.3. Gene Signature of DNA Helicase Genes Can Predict the Status of HRD in Breast Cancer.** We next further explored the possibility of predicting HRD score using the expression of DNA helicase genes. A linear regression model was built to predict the HRD score of each breast cancer using the above DNA helicase genes. The model was represented as following:

$$\text{HRD} = 4.52 \times \text{BLM} + 5.40 \times \text{FIGNL1} + 4.72 \times \text{PIF1} + 10.31 \times \text{FBXO18} - 8.78 \times \text{HELQ} - 227.56. \quad (1)$$

Using this model, the predicted HRD score has a correlation score of 0.64 with the actual HRD score (Figure 4). Thus, our study built a new model for the prediction of PARP inhibitor efficiency in breast cancer as shown in Figure 5. In breast cancer patients with germline pathogenic BRCA1/2 mutations, cancer cells harbor homologous recombination repair deficiency (HRD) due to malfunction of BRCA1 or BRCA2 protein in DNA damage repair. The application of

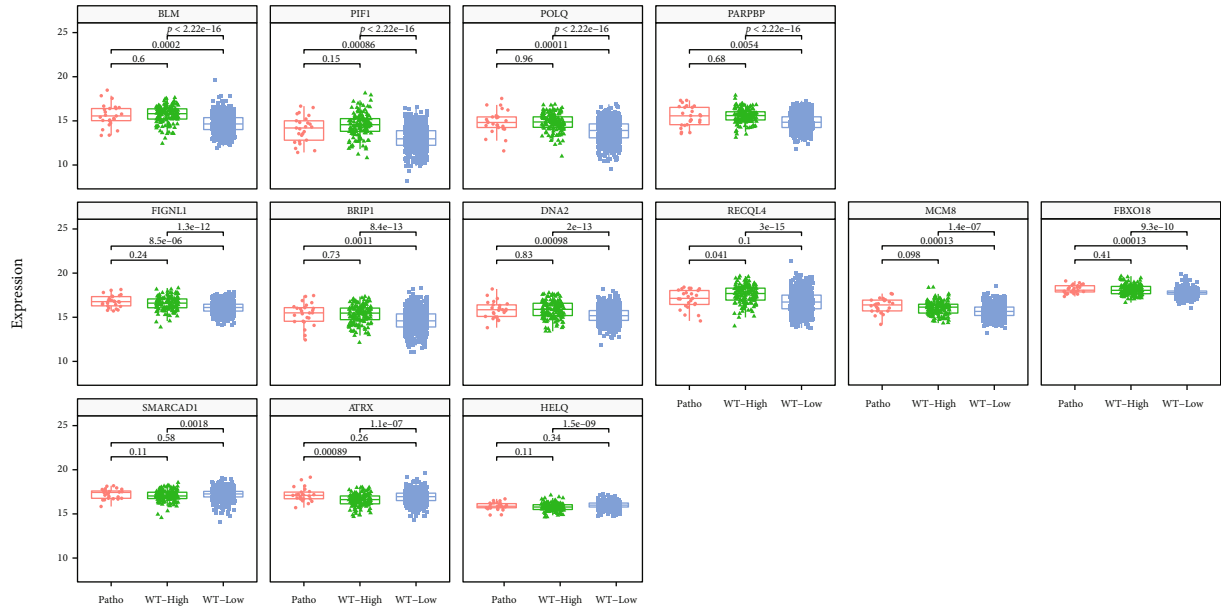


FIGURE 3: The expression of correlated DNA helicase genes in BRCA1/2 germline mutated breast cancer and in BRCA1/2 wild-type breast cancer with high and low HRD score, respectively. The expression of thirteen significantly correlated genes identified in Figure 1 was plotted in three groups of breast cancer patients. Patients with germline BRCA1/2 mutation were included in the “Patho” group, while patients with germline wild-type BRCA1/2 genes were divided into “WT-High” and “WT-Low” groups according to the score of HRD score.

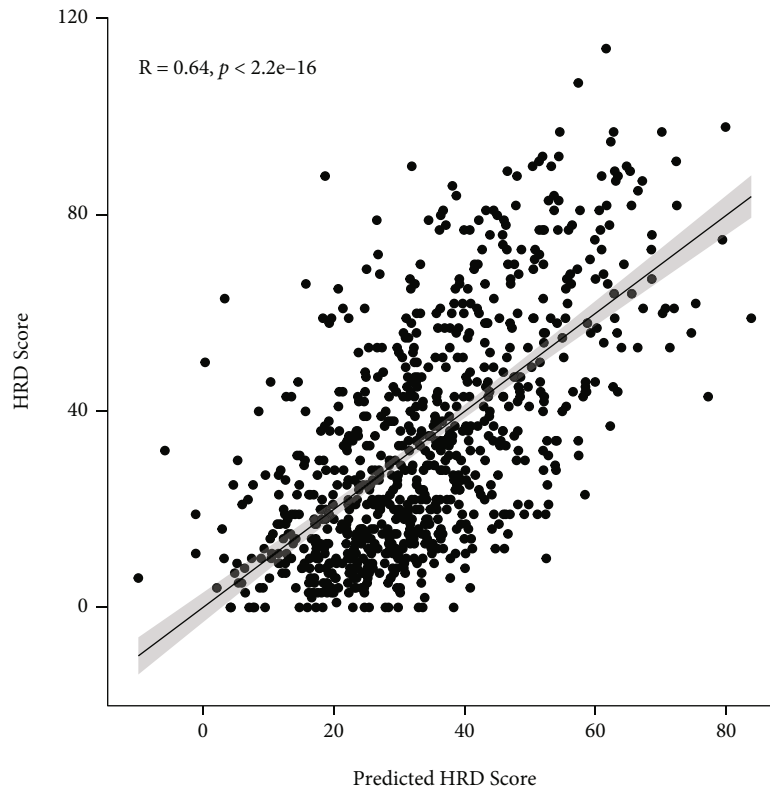


FIGURE 4: Correlation plot between the predicted HRD score using linear model of DNA helicase genes and the actual HRD score. The horizontal axis displays the HRD score of each individual patients calculated with the expression value of five DNA helicase genes using algorithms developed above, while the vertical axis displays the original HRD score calculated through DNA SNP data.

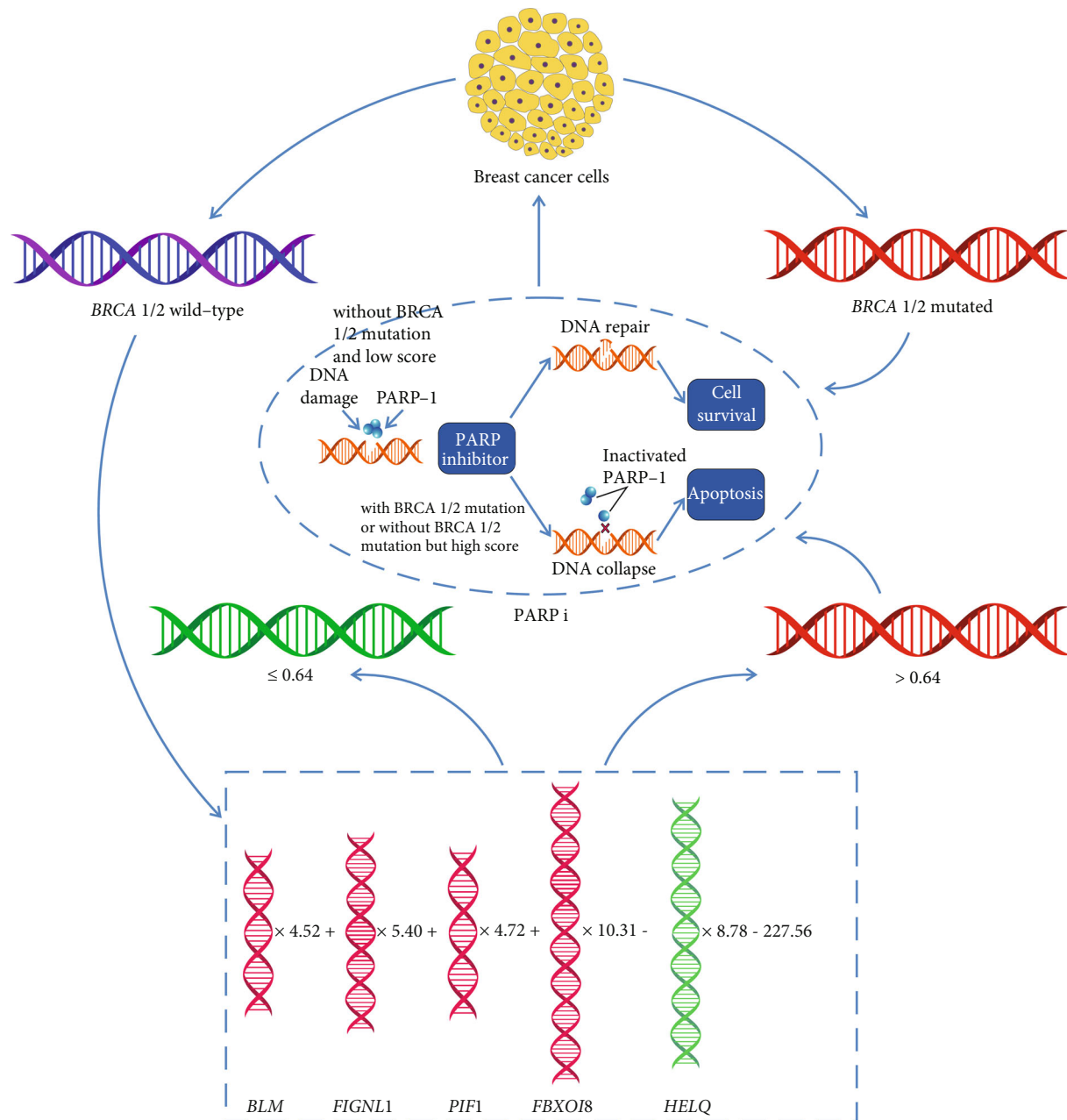


FIGURE 5: Model for the prediction of HRD phenotype in breast cancer. In breast cancer patients with germline pathogenic BRCA1/2 mutations, cancer cells harbor homologous recombination repair deficiency (HRD) due to malfunction of BRCA1 or BRCA2 protein in DNA damage repair. The application of PARP inhibitors in these patients causes defect in single-strand DNA damage repair due to inhibition of PARP-1 protein. The block of both repair pathways promotes the apoptosis of tumor cells, which is called the “synthetic lethal” mechanism of PARP inhibitors, while for breast cancer patient without pathogenic BRCA1/2 mutations, HRD score can be predicted with gene expression of five DNA helicase genes using the linear regression model to further select breast cancer patients with HRD phenotype. When the predicted score is greater than 0.64, the possibility of HRD should be considered and this part of breast cancer could possibly benefit from the treatment of PARP inhibitors.

PARP inhibitors in these patients causes defect in single-strand DNA damage repair due to inhibition of PARP-1 protein. The block of both repair pathways promotes the apoptosis of tumor cells, which is called the “synthetic lethal” mechanism of PARP inhibitors, while for breast cancer patient without pathogenic BRCA1/2 mutations, HRD score

can be predicted with gene expression of five DNA helicase genes using the linear regression model to further select breast cancer patients with HRD phenotype. When the predicted score is greater than 0.64, the possibility of HRD should be considered and this part of breast cancer could possibly benefit from the treatment of PARP inhibitors.

## 4. Discussion

In this study, the correlation between the expression of DNA helicase genes and the HRD score was analyzed. A strong correlation between the overexpression of DNA helicase genes and HRD was found both in *BRCA1/2*-mutated breast cancer as well as in *BRCA1/2* wild-type breast cancers. And a linear model was built to predict the HRD score using the mRNA expression of five DNA helicase genes with high accuracy. The correlation between the overexpression of DNA helicase genes and HRD in breast cancer has been reported before. Previous studies found that overexpression of *BLM* can promote the occurrence of DNA damage and the knockdown or deficiency of *BRCA1* induced the overexpression of *BLM*, indicating the role of *BLM* in both *BRCA1*-related and -unrelated homologous recombination repair [22]. However, our study reported for the first time that the overexpression in multiple DNA helicase genes was highly correlated with HRD indicating a shared mechanism among them. Further studies need to be conducted to reveal the exact molecular mechanism.

PARP inhibitors including olaparib, rucaparib, niraparib, and talazoparib have shown robust efficiency in breast cancer patients with germline *BRCA1/2* mutation both as second-line therapy and as first-line therapy [23–25]. Moreover, molecular and early clinical study demonstrated that PARP inhibitor was also effective in *BRCA1/2* wild-type cells with HRD phenotype [26, 27]. However, the measurement of HRD score was currently expensive and inconvenient compared with measurement of gene expression. Our study showed that HRD score in breast cancer can be effectively predicted by the expression of DNA helicase genes which provided a tool for assessing BRCAness phenotype in breast cancer. Despite PARP inhibitors, other small molecules targeting the HRR pathway through DNA helicase proteins in breast cancer have been developed as potential therapeutics. A small molecule which binds specifically to DNA helicase RECQL5 and stabilizes the interaction between RECQL5 and RAD51 could inhibit the proliferation of breast cancer cells in a RECQL5-dependent manner [28]. Noticeably, the above study is performed in MCF-7 cell line which has wild-type *BRCA1/2* gene, suggesting that the HRR pathway could also be a target in *BRCA1/2* wild-type breast cancer. Also, study showed that using CHK1 inhibitor in WRN-deficient cancer cells could produce synergic killing effect [29, 30]. Together with the results in our study, the expression of DNA helicase could be a tool of measuring HRR status as well as a therapeutic target in breast cancer.

Our study is limited by the fact that the developed model has only been tested in a single database. Validation in other breast cancer database should be performed in future work. Besides, this model may be experimentally validated to show HR deficiency in cancer, as mentioned by various methods in many recent reports, for instance, a recent study evaluated response of PARP inhibitor using autophagy-proficient and -defective breast cancer cells and xenograft SCID-mice model [31]. Future validation of our work could be performed by constructing breast cancer cell lines overexpressing DNA helicases *BLM*, *FIGL1*, *PIF1*, or *FBXO18* and

cell lines downregulating *HELQ*. Efficiency of HRR in the constructed cell lines should be evaluated by assays including H2Agamma foci quantification. Sensitivity to PAPR inhibitor should be evaluated.

## Data Availability

Previously reported data were used to support this study and are available at the TCGA database (<https://portal.gdc.cancer.gov/>). Other data generated or analyzed during this study are available from the corresponding author upon reasonable request.

## Ethical Approval

Ethical review and approval were waived for this study, due to the use of open-accessed data.

## Consent

Patient consent was waived due to the deidentification in the TCGA database.

## Conflicts of Interest

The authors declare no competing interests.

## Authors' Contributions

XL, TH, and ML contributed to the conception of the study; TH, SW, YL, and ML performed the data analyses; JW, HL, YL, and GZ contributed to the methodology; YL, HL, and SW helped the manuscript writing with constructive discussion; XL, TH, and ML wrote the final manuscript. Mengping Long and Hongjun Liu contributed equally to this work.

## Acknowledgments

The authors disclose the receipt of the following financial support for the research, authorship, and/or publication of this article: this work was supported by the National Natural Science Foundation of China (Grant No. 82002979), the National Key Research and Development Program of China (Grant No. 2021YFE0203200), the Research and Development Funds of Peking University People's Hospital (Grant Nos. RDX2021-05 and RDY2020-16), and the Young Investigator Program of Peking University Health Science Center (Grant No. BMU2021PYB013).

## References

- [1] E. Huselid and S. F. Bunting, "The regulation of homologous recombination by helicases," *Genes*, vol. 11, no. 5, 2020.
- [2] N. A. Ellis and J. German, "Molecular genetics of Bloom's syndrome," *Human Molecular Genetics*, vol. 5, Supplement\_1, pp. 1457–1463, 1996.
- [3] J. C. Shen and L. A. Loeb, "The Werner syndrome gene: the molecular basis of RecQ helicase-deficiency diseases," *Trends in Genetics*, vol. 16, no. 5, pp. 213–220, 2000.



- [4] Z. Wang, Y. Xu, J. Tang et al., "A polymorphism in Werner syndrome gene is associated with breast cancer susceptibility in Chinese women," *Breast Cancer Research and Treatment*, vol. 118, no. 1, pp. 169–175, 2009.
- [5] T. Banerjee and R. M. Brosh Jr., "RECQL: a new breast cancer susceptibility gene," *Cell Cycle*, vol. 14, no. 22, pp. 3540–3543, 2015.
- [6] S. Seal, D. Thompson, A. Renwick et al., "Truncating mutations in the Fanconi anemia J gene *BRIP1* are low-penetrance breast cancer susceptibility alleles," *Nature Genetics*, vol. 38, no. 11, pp. 1239–1241, 2006.
- [7] A. Tavera-Tapia, M. de la Hoya, O. Calvete et al., "RECQL5: another DNA helicase potentially involved in hereditary breast cancer susceptibility," *Human Mutation*, vol. 40, no. 5, pp. 566–577, 2019.
- [8] E. R. Thompson, M. A. Doyle, G. L. Ryland et al., "Exome sequencing identifies rare deleterious mutations in DNA repair genes *FANCC* and *BLM* as potential breast cancer susceptibility alleles," *PLoS Genetics*, vol. 8, no. 9, article e1002894, 2012.
- [9] M. L. Telli, K. M. Timms, J. Reid et al., "Homologous recombination deficiency (HRD) score predicts response to platinum-containing neoadjuvant chemotherapy in patients with triple-negative breast cancer," *Clinical Cancer Research*, vol. 22, no. 15, pp. 3764–3773, 2016.
- [10] A. M. Marquard, A. C. Eklund, T. Joshi et al., "Pan-cancer analysis of genomic scar signatures associated with homologous recombination deficiency suggests novel indications for existing cancer drugs," *Biomarker Research*, vol. 3, no. 1, p. 9, 2015.
- [11] C. Allison Stewart, P. Tong, R. J. Cardnell et al., "Dynamic variations in epithelial-to-mesenchymal transition (EMT), ATM, and SLFN11 govern response to PARP inhibitors and cisplatin in small cell lung cancer," *Oncotarget*, vol. 8, no. 17, pp. 28575–28587, 2017.
- [12] B. H. Lok, E. E. Gardner, V. E. Schneeberger et al., "PARP inhibitor activity correlates with SLFN11 expression and demonstrates synergy with temozolomide in small cell lung cancer," *Clinical Cancer Research*, vol. 23, no. 2, pp. 523–535, 2017.
- [13] V. Nogales, W. C. Reinhold, S. Varma et al., "Epigenetic inactivation of the putative DNA/RNA helicase SLFN11 in human cancer confers resistance to platinum drugs," *Oncotarget*, vol. 7, no. 3, pp. 3084–3097, 2016.
- [14] Y. Hu, X. Lu, G. Zhou, E. L. Barnes, and G. Luo, "Recql5 plays an important role in DNA replication and cell survival after camptothecin treatment," *Molecular Biology of the Cell*, vol. 20, no. 1, pp. 114–123, 2009.
- [15] M. Aggarwal, J. A. Sommers, R. H. Shoemaker, and R. M. Brosh Jr., "Inhibition of helicase activity by a small molecule impairs Werner syndrome helicase (WRN) function in the cellular response to DNA damage or replication stress," *Proceedings of the National Academy of Sciences of the United States of America*, vol. 108, no. 4, pp. 1525–1530, 2011.
- [16] S. R. Hengel, M. A. Spies, and M. Spies, "Small-molecule inhibitors targeting DNA repair and DNA repair deficiency in research and cancer therapy," *Cell Chemical Biology*, vol. 24, no. 9, pp. 1101–1119, 2017.
- [17] The Cancer Genome Atlas Network, "Comprehensive molecular portraits of human breast tumours," *Nature*, vol. 490, no. 7418, pp. 61–70, 2012.
- [18] A. Colaprico, T. C. Silva, C. Olsen et al., "TCGAbiolinks: an R/Bioconductor package for integrative analysis of TCGA data," *Nucleic Acids Research*, vol. 44, no. 8, article e71, 2016.
- [19] T. Hu, Y. Chen, Y. Liu, D. Zhang, J. Pan, and M. Long, "Classification of PR-positive and PR-negative subtypes in ER-positive and HER2-negative breast cancers based on pathway scores," *BMC Medical Research Methodology*, vol. 21, p. 108, 2021.
- [20] T. Hu, G. Zhao, Y. Liu, and M. Long, "A machine learning approach to differentiate two specific breast cancer subtypes using androgen receptor pathway genes," *Technology in Cancer Research & Treatment*, vol. 20, 2021.
- [21] M. Long, W. Hou, Y. Liu, and T. Hu, "A histone acetylation modulator gene signature for classification and prognosis of breast cancer," *Current Oncology*, vol. 28, pp. 928–939, 2021.
- [22] N. J. Birkbak, Y. Li, S. Pathania et al., "Overexpression of BLM promotes DNA damage and increased sensitivity to platinum salts in triple-negative breast and serous ovarian cancers," *Annals of Oncology*, vol. 29, no. 4, pp. 903–909, 2018.
- [23] M. E. Robson, N. Tung, P. Conte et al., "OlympiAD final overall survival and tolerability results: olaparib versus chemotherapy treatment of physician's choice in patients with a germline BRCA mutation and HER2-negative metastatic breast cancer," *Annals of Oncology*, vol. 30, no. 4, pp. 558–566, 2019.
- [24] J. K. Litton, S. A. Hurvitz, L. A. Mina et al., "Talazoparib versus chemotherapy in patients with germline BRCA1/2-mutated HER2-negative advanced breast cancer: final overall survival results from the EMBRACA trial," *Annals of Oncology*, vol. 31, no. 11, pp. 1526–1535, 2020.
- [25] V. Dieras, H. S. Han, B. Kaufman et al., "Veliparib with carboplatin and paclitaxel in BRCA -mutated advanced breast cancer (BROCADE3): a randomised, double-blind, placebo-controlled, phase 3 trial," *The Lancet Oncology*, vol. 21, no. 10, pp. 1269–1282, 2020.
- [26] N. McCabe, N. C. Turner, C. J. Lord et al., "Deficiency in the repair of DNA damage by homologous recombination and sensitivity to poly (ADP-ribose) polymerase inhibition," *Cancer Research*, vol. 66, no. 16, pp. 8109–8115, 2006.
- [27] P. G. Pilie, C. M. Gay, L. A. Byers, M. J. O'Connor, and T. A. Yap, "PARP inhibitors: extending benefit beyond BRCA-mutant cancers," *Clinical Cancer Research*, vol. 25, no. 13, pp. 3759–3771, 2019.
- [28] S. Chakraborty, K. Dutta, P. Gupta et al., "Targeting RECQL5 functions, by a small molecule, selectively kills breast cancer in vitro and in vivo," *Journal of Medicinal Chemistry*, vol. 64, no. 3, pp. 1524–1544, 2021.
- [29] P. Gupta, A. G. Majumdar, and B. S. Patro, "Enigmatic role of WRN-RECQL helicase in DNA repair and its implications in cancer," *Journal of Translational Genetics and Genomics*, vol. 6, no. 2, pp. 147–156, 2022.
- [30] P. Gupta, B. Saha, S. Chattopadhyay, and B. S. Patro, "Pharmacological targeting of differential DNA repair, radio-sensitizes WRN-deficient cancer cells in vitro and in vivo," *Biochemical Pharmacology*, vol. 186, p. 114450, 2021.
- [31] G. Pai Bellare, B. Saha, and B. S. Patro, "Targeting autophagy reverses de novo resistance in homologous recombination repair proficient breast cancers to PARP inhibition," *British Journal of Cancer*, vol. 124, no. 7, pp. 1260–1274, 2021.